MINERALOGICAL COMPARISON OF NORTHWEST AFRICA 7317 AND TAFASSASSET: TWO EQUILIBRATED ROCKS RELATED TO CR CHONDRITES.

D. Abe[1,2] and T. Mikouchi[1,2], [1]Dept. of Earth and Planet. Sci., University of Tokyo, Hongo, Tokyo 113-0033, Japan (d_abe@um.u-tokyo.ac.jp), [2]University Museum, University of Tokyo, Hongo, Tokyo 113-0033, Japan.

Introduction: Most CR chondrites show evidence for aqueous alteration and classified into petrologic types 1 and 2 [1,2]. However, in recent years, CR samples experiencing thermal metamorphism (e.g., CR6) have been known [3]. Furthermore, there are more "differentiated" samples known such as Tafassasset and NWA 6704 whose O, Cr, and Ti isotopic compositions are plotted within the CR chondrite field [e.g., 4-6]. Therefore, it is of great interest to explore the petrogenetic relationship among these "CR-related" meteorites to better understand thermal evolution of the CR chondrite parent body [e.g., 3]. To begin with, we studied NWA 7317 CR6 chondrite and Tafassasset to compare their mineralogy and petrology.

Samples and Methods: 1 polished thin section (PTS) of NWA 7317 and 2 PTSs of Tafassasset were observed with optical microscope and mineral compositions were analyzed by FE-EPMA (JEOL JXA 8530F @Univ. of Tokyo).

Results and Discussions: NWA 7317 shows a poikioblastic texture dominated by homogeneous olivine (Fa_{35-36}). Remnants of barred olivine chondrules are present. Accessory minerals are high-Ca pyroxene ($Fs_{11-13}Wo_{42-45}$), low-Ca pyroxene ($Fs_{27-29}Wo_{2-3}$), plagioclase ($An_{45-54}Or_{1-2}$), Fe-Ni metal, chromite and troilite. Tafassasset has a similar texture and mineral assemblages to NWA 7317, but two different Tafassasset PTSs show slightly different mineral abundances and textural heterogeneity is observed even in a single PTS. It is noted that the size of Fe-Ni metal in one of the PTSs are much larger (~2 mm) than that in the other (~0.8 mm, mostly 0.2 mm). In our Tafassasset PTSs, no relict chondrules are present. The olivine and pyroxene compositions of Tafassasset are mostly homogeneous in major elements: olivine (Fa_{26-28}), high-Ca pyroxene ($Fs_{9-13}Wo_{37-44}$), and low-Ca pyroxene ($Fs_{21-24}Wo_{2-12}$), but plagioclase ($An_{21-57}Or_{1-8}$) and Fe-Ni metal show wide compositional ranges.

NWA 7317 and Tafassasset have homogeneous major element compositions of olivine and pyroxene, but it is clear that Tafassasset has more magnesian olivine-pyroxene compositions than NWA 7317 (Fig. 1). This implies that the source materials of these two meteorites were different. Closer look of other mineral compositions also exhibits difference between NWA 7317 and Tafassasset, probably reflecting their distinct cooling histories. Al and Ti contents in low-Ca pyroxene are homogeneous in NWA 7317 (Al_2O_3: 0.6-0.9 wt%, TiO_2: 0.1-0.2 wt%), but those in Tafassasset show some variations (Al_2O_3: 0.2-0.7 wt%, TiO_2: 0.1-0.3 wt%) (Fig. 2). Similarly, Fe-Ni metal has different compositions between two meteorites. In NWA 7317, Fe-Ni metal is independently present as kamacite (6-7 wt% Ni) and taenite (17-25 wt% Ni). On the other hand, Fe-Ni metal in Tafassasset exhibits extensive chemical zoning (Ni content: 5-28 wt%). Such differences suggest that NWA 7317 cooled more rapidly than Tafassasset.

Conclusion: NWA7317 and Tafassasset are classified as equilibrated meteorites with CR chondrite affinities. However, their distinct mineral compositions indicate that their source mineral compositions were different. Furthermore, relatively faster cooling of Tafassasset as well as its heterogeneous texture compared to NWA 7317 suggests that Tafassasset is more "unequilibrated" than CR6 although there are several classifications proposed [e.g., 7].

References: [1] Weisberg M. K. et al. (1993) *Geochimica et Cosmochimica Acta* 57: 1567-1586 [2] Schrader D. L. et al. (2011) *Geochimica et Cosmochimica Acta* 75: 308–325 [3] Irving A. J. et al. (2014) *LPS XLV*, Abstract #2465. [4] Sanborn M. E. et al. (2019) *Geochimica et Cosmochimica Acta* 245: 577–596. [5] Gardner-Vandy K. G. et al. (2012) *Geochimica et Cosmochimica Acta* 85: 142–159. [6] Breton T.et al. (2015) *Earth and Planetary Science Letters* 425: 193-203. [7] Nehru C. E. et al. (2014) Annual Meeting of 77th Meteoritical Society, Abstract #5382. [8] Gardner-Vandy K. G. et al. (2013) *Geochimica et Cosmochimica Acta* 122: 36–57.
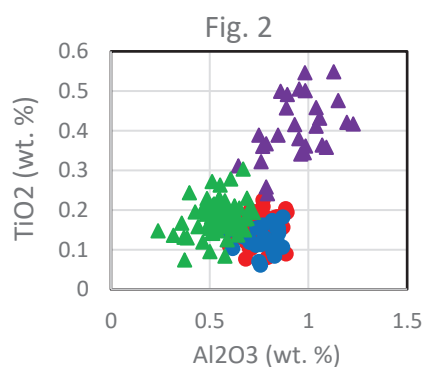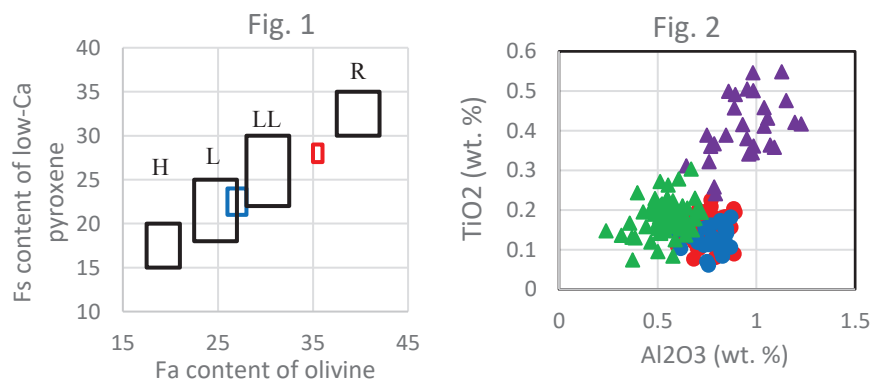

Fig. 1. Fa in olivine vs Fs in low-Ca pyroxene for ordinary chondrites [8], R chondrite [8] and this study. Red square is NWA 7317 and blue one is Tafassasset.

Fig. 2. Al_2O_3 vs. TiO_2 for pyroxene in NWA 7317 and Tafassasset. Red circles are high-Ca pyroxene and blue ones are low-Ca pyroxene in NWA 7317. Purple triangles are high-Ca pyroxene and green ones are low-Ca pyroxene in Tafassasset.

TEXTURES AND CHEMICAL COMPOSITIONS OF EXPERIMENTAL CHONDRULE SYNTHESIS BY A RADIATIVE HEATING MODEL.

K. Abe[1], J. P. Greenwood[1], and W. Herbst[2], [1]Dept. of Earth and Environmental Sciences, Wesleyan University, Middletown, CT 06459 USA (kabe01@wesleyan.edu) [2]Dept. of Astronomy, Wesleyan University, Middletown, CT 06459 USA.

Introduction: A radiative heating model recently proposed may explain chondrite formation as well as chondrule formation [1]. According to this model, chondrules and chondrites formed together during a brief radiative heating event caused by the close encounter of a small (m to km-scale), primitive planetesimal with incandescent lava on the surface of a large (100 km-scale) differentiated planetesimal. In this study, we performed chondrule synthesis experiments under the condition predicted by the radiative heating model and compared synthesized chondrules with natural Type I chondrules.

Experimental: We prepared three starting materials as chondrule analog; (1) Globe mix, (2) Type IA chondrule composition, (3) Type IAB chondrule composition. Globe mix consists of natural peridotite xenolith from Globe, AZ that was picked, cleaned and sieved to <20 μm and mixed with similar grain size of plagioclase feldspars (Miyake anorthite and Salva Tierra oligoclase) and graphite. We prepared the bulk compositions of Type IA [2] and IAB [3] chondrule by oxide regents and Fe^0, respectively. Chondrule synthesis experiment was conducted for four thermal trajectories predicted by the radiative heating model (Fig. 1) using a Deltech furnace with gaseous mixtures of CO and CO_2 to control fO_2 to IW-1. Experimental charges were analyzed using Hitachi SU5000 FEG-SEM equipped with EDAX Apollo 10/X/Octane Pro SiDD for observation and chemistry.

Result and Discussion: The Globe mix charges are mainly composed of porphyritic olivine (Fo_{98-99}) with a size of 30–50 μm in diameter, glass, and small amount of low-Ca pyroxene. There is little difference of texture and chemical composition among thermal trajectories. The IA charges have numerous smaller porphyritic olivines (Fo_{97-98}) with ~10 μm in diameter for NG4a, 5a and 6a and ~20 μm in diameter for 7a. The olivines often include tiny chromite. Chromite outside olivines are larger and sometimes form aggregate. Chemical compositions of glass in Globe mix and IA match well with average composition of glass in Semarkona Type I chondrule. The IAB charges are variable in texture among thermal trajectories. Olivine grains in NG4a, 5a and 6a has a massive shape with ~100 μm in diameter and cylindrical shape with various width and length, whereas olivines in NG7a show barred shape. Pyroxenes grow from olivines as dendritic. The dendritic pyroxenes in NG4a are coarser than those in NG5a and 6a. Chromite grains are attached to pyroxenes. The chromites in NG6a and NG7a are dendritic. Chemical compositions of glass in IAB charges are slightly depleted in MgO, Al_2O_3 and CaO. A lot of tiny bubbles exist into glass in NG6a and 7a.

Porphyritic olivines in IA charges seem to be slightly smaller than those of natural Type I PO chondrule because of small grain size of starting materials [4]. It infers that it might be difficult to produce porphyritic olivines with similar size to natural PO chondrule directly from fine grains such as matrix materials by the single heating event. In spite of fine grain size of starting materials, IAB charges have similar grain size of natural Type IAB chondrule though our pyroxenes are dendritic.

References: [1] Herbst W. and Greenwood J. P. (2019) *Icarus* Accepted, in press. [2] Jones R. H. and Scott E. R. D. (1989) *Proc. Lunar Planet. Sci. Conf. 19th*, pp. 523–536. [3] Jones R. H. (1994) *Geochim. Cosmochim. Acta*, 58, 5325–5340. [4] Fox G. E. and Hewins R. H. (2005) *Geochim. Cosmochim. Acta*, 69, 2441–2449.
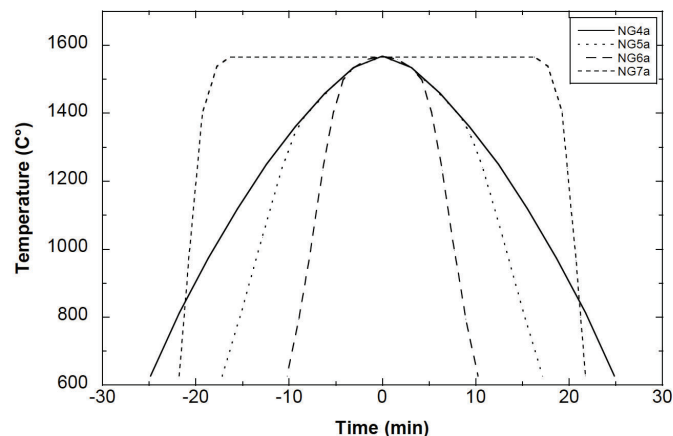
Fig. 1 Thermal trajectories predicted by the radiative heating model [1] used in this study.

ONSET OF MAGMATISM ON A CARBONACEOUS CHONDRITE PLANETESIMAL

J. Aléon[1], A. Aléon-Toppani[2], B. Platevoet[3], J.M. Bardintzeff[3], K. D. McKeegan[4], F. Brisset[5], [1]IMPMC, UMR 7590, Sorbonne Univ., MNHN, CNRS, IRD, 61 rue Buffon, 75005 Paris, France, (jerome.aleon@mnhn.fr), [2]IAS, UMR 8617, CNRS, Univ. Paris-Saclay, 91405 Orsay cedex, France, [3]GEOPS, CNRS UMR 8148, Univ Paris-Saclay, 91405 Orsay cedex, France, [4]Dept of Earth, Planet., & Space Sci., UCLA, Los Angeles, CA 90095-1567, USA, [5]ICMMO, CNRS UMR 8182, Univ. Paris-Saclay, 91405 Orsay cedex, France.

Introduction: Chondritic meteorites and differentiated achondrites were long assumed to sample solar system objects with different planetary evolution. However, paleomagnetic studies and magma ocean models indicate that some carbonaceous chondrite parent-bodies may have undergone core-mantle differentiation at depth, while keeping a surficial chondritic crust [e.g. 1,2]. High precision isotopic analysis of heavy elements such as Cr, Mo, W unambiguously demonstrated the link between some differentiated materials including iron meteorites and carbonaceous chondrites [e.g. 3,4]. However, direct evidence of magmatic activity testifying of the onset of partial melting and partial differentiation is extremely rare and has not previously been reported for carbonaceous chondrites. Here we report the mineralogy, petrography, O and Mg isotopic study of a differentiated clast enclosed in the CR chondrite El Djouf 001 and evaluate its relationship with carbonaceous chondrites.

Methods: UH154-11 was found in a thin section of El Djouf 001 from the University of Hawaii. Its mineralogy and petrography were studied using various Scanning Electron Microscopes (SEM) including Field-Emission-Gun SEMs in UCLA, GEOPS, ICCMO and ENS Paris and Electron Probe MicroAnalysis at the CAMPARIS facility in Paris. O and Mg isotopes were measured in-situ by IMS 1270 SIMS in UCLA and NanoSIMS 50 in the National Museum of Natural History in Paris, respectively.

Results: UH154-11 has a fine-grained doleritic texture typical of magmatic dykes. It is dominantly composed of andesine plagioclase laths (plag, An_{40-50}) about 10 μm in width and up to 100 μm in length, approximately equant sometimes skeletal Fe-rich olivine (ol, Fo_{40-50}) less than 10 μm in size and augitic clinopyroxene (cpx) of variable shape, typically 5 μm in size or less. Plag crystals have skeletal rims enclosing tiny cpx and ol. Shards of cpx are found enclosed in plag and ol enclosed small cpx and minute melt inclusions. UH154-11 is almost completely crystallized but still contains interstitial melt pockets with glassy areas too tiny for analysis, dendritic sub-μm Ca-phosphates and minute nm-sized Fe-sulfides and Ti-oxides. Its highly silica-undersaturated bulk composition is consistent with that of an Fe-rich trachybasalt having 5.8 wt% Na_2O and 15.1 wt% FeO at the limit with the tephrite field. The bulk Na/K wt% ratio (Na/K = 17.5) and O isotopic composition ($\Delta^{17}O$ = -2.8 ± 0.7 ‰, 2σ) are comparable to those of CV chondrites from the oxidized subgroup (CVox). No ^{26}Mg excesses resulting from the decay of ^{26}Al were found in plag, yielding a crystallization age younger than 3.3 My after Ca-Al-rich inclusions (2σ upper limit).

Discussion and conclusion: The skeletal rims of plagioclase are indicative of crystallization during cooling at an increasing cooling rate as observed in ascending magmas on Earth and opposite to that expected for impact melts. Additionally, the bulk chemical composition is close to those of melts produced during partial melting experiments of chondritic materials [5,6] indicating that UH154-11 is not an impact melt but a partial melt from a chondritic body. The best match between experiments and UH154-11 is obtained for partial melts produced at ~1100°C, near the IW buffer. However, the enrichment in Na and depletion in Si relative to these compositions point to very low degree of melting, problably down to 5% or less. Being unfractionated during partial melting, the high Na/K ratio relative to most chondrites but similar to some CVox, CO and CK chondrites suggests that the initial chondrite source was previously enriched in Na by metasomatism. The ^{16}O-rich isotopic composition, identical to that of the Mokoia CV chondrite, further link the source of UH154-11 with carbonaceous chondrites and more specifically with CVox chondrites. UH154-11 therefore formed by a very low degree partial melting at ~1100°C of a carbonaceous chondrite, most likely from the CV parent body, at a depth, where previous metasomatism/metamorphism occurred. It subsequently crystallized during ascent through the carbonaceous chondrite crust with a degree of supercooling induced by the thermal difference between the magma and host rock. It was finally excavated by an impact and incorporated to the regolith of the CR parent-body, which has to be located in a close nebular region. UH154-11 can thus be considered representative of the first partial melts produced at the onset of planetary differentiation in a large carbonaceous chondrite body.

References: [1] Carporzen, L. et al. (2011) *Proc. Natl. Acad. Sci. USA* 108:6386–6389. [2] Elkins-Tanton, L. T., Weiss, B. P. & Zuber, M. T. (2011) *Earth Planet. Sci. Lett.* 305:1–10. [3] Warren, P. H. (2011) *Earth Planet. Sci. Lett.* 311:93–100. [4] Kruijer, T. S., Burkhardt, C., Budde, G. & Kleine, T. (2017) *Proc. Natl. Acad. Sci. USA* 114:6712–6716. [5] Usui, T., Jones, J. H. & Mittlefehldt, D. W. (2015) *Meteorit. & Planet. Sci.*, 1–23, doi: 10.1111/maps.12392. [6] Lunning, N. G. et al. (2017) *Geochim. Cosmochim. Acta* 214:73-85.

FINE-GRAINED CAIS AT THE NANOMETER SCALE: DISCOVERY OF A PRISTINE AGGREGATE OF SUB-µM CONDENSATES

A. Aléon-Toppani[1], J. Aléon[2], F. Brisset[3], IAS, UMR 8617, CNRS, Univ. Paris-Saclay, 91405 Orsay cedex, France, (alice.aleon@ias.u-psud.fr), [2]IMPMC, UMR 7590, Sorbonne Univ., MNHN, CNRS, IRD, 75005 Paris, France, [3]ICMMO, CNRS UMR 8182, Univ. Paris-Saclay, 91405 Orsay cedex, France.

Introduction: Based on equilibrium thermodynamic calculations, the first solar system rocks are believed to have formed by gas-solid condensation from a gas of solar composition [1,2]. The refractory Ca-Al-rich inclusions (CAIs) from chondritic meteorites, the oldest rocks formed in the solar system, thus formed from high temperature condensate precursors having experienced a subsequent complex thermal history including multiple reheating events up to partial melting. In that respect, fine-grained CAIs with aggregate nodular textures, are widely believed to be preserved aggregates of early solar system condensates [3]. However, their fine grain size render them sensitive to secondary modifications by reheating or late fluid circulations on the parent-body. In order to better understand the nature of the first solar system condensates and to confront natural samples with the predictions of thermodynamics, we initiated a Transmission Electron Microscopy (TEM) study of several fine-grained CAIs from the barely meta-morphosed reduced CV3 chondrite Efremovka. Here we report the discovery and the mineralogical characterization of an unusual fine-grained CAI E045-V.

Methods: High-resolution BSE images and X-ray maps of E045-V were obtained with field emission gun scan-ing electron microscopes (IMPMC Paris, ICMMO, Orsay). Several FIB sections (about 5 to 15 µm) were extracted from the CAI and thinned down to ~100 nm for TEM characterization using the 30 keV focused gallium ion beam at IEMN (Lille, France). Using a 200keV TEM (IMPMC, Paris), chemical analyses, X-ray mapping, Z-contrast imaging and conventional TEM imaging has been performed in order to characterize the CAI sections.

Results: E045-V is about 1.5 mm by 500 µm. It is composed of three different lithologies: (1) a compact ex-tremely fine-grained core, (2) a mantle enriched in volatiles including Fe, Na and Si and (3) local inclusions of clas-sical core-mantle spinel-melilite nodules. The compact fine-grained core is an extremely complex aggregate of 1 to 2 µm concentrically-zoned polymineralic nodules showing grains with sizes from 10 to 200 nm. Some crystals have perfectly euhedral shape while others have rounded shape. Triple junctions were sometimes observed. From core to rim the mineralogical sequence of individual nodules includes spinel, melilite, Ca-rich clinopyroxene and a Mg-Si-rich amorphous layer. The composition of pyroxene is extremely heterogeneous and varies from almost pure diop-side to Ti-Al-rich fassaite at a sub-µm scale. Some nodules can be Ti-free while other could contain Al-Ti rich fassaite. Melilite contains up to 20 at% Mg. Fe content of the spinels can be up to 2 wt% independently of the spinels location. Fe-rich spinels and Fe-free spinels can be found at the center of nodules sometimes within a µm from each other. The nodules are cemented by interstitial anorthite. Euhedral crystals of zoned olivine with Fe-enriched rim are interspersed between the nodules. It is noticeable that some nodules contain multiple cores.

Discussion and conclusion: None of these observations have previously been reported in the literature. All crys-tals properties are very similar to those reported in experimental condensation [4], including crystal sizes, shapes and chemistry. This indicates that the E045-V CAI core is the most pristine condensate assemblage reported to date and can be used to shed light on the conditions of condensation. (1) The mineralogical sequence is close to that expected by equilibrium condensation with the exception of spinel, which appears to be the first phase to condense, most likely as a result of a kinetic control. (2) The amorphous rim observed around the nodules is an additional indication of incomplete equilibrium process. Its preservation testifies of a minimal secondary alteration of the nodules. (3) The presence of Fe-rich spinel inside unaltered nodules suggests either disequilibrium during condensation or more oxidizing conditions than expected in the inner disk [e.g. 1]. (4) Finally, the presence of multiple cores within single nodules indicates that coagulation of grains occurred as condensation proceeds. As a result, a thorough investigation of growth rates should give informations about the grain density in the inner protoplanetary disk.

References: [1] Grossman L. (2010) *Meteorit. Planet. Sci.* 45:7-20. [2] Ebel, D.S. and Grossman L. (2000) *Geochim. Cosmochim. Acta* 64:339-366. [3] Krot, A.N. (2004) *Meteorit. Planet. Sci.* 39:1517-1553. [4] Toppani A. et al. (2006) *Geochim. Cosmochim. Acta* 70:5035-5060.

A CHONDRULE EARTH?

C.M.O'D. Alexander. DTM, Carnegie Institution of Washington, 5241 Broad Branch Road, NW, Washington, DC 20015, USA (calexander@carnegiescience.edu).

Introduction: The chondrites formed at about the time when the embryo building blocks of the terrestrial building blocks would have been growing. As a result, it is generally assumed that the chondrites are representative of the building blocks' compositions, or at the least the elemental and isotopic fractionations amongst the chondrites provide clues to the processes that controlled the compositions of the terrestrial planets. Recently, it has been suggested that the dichotomy in the isotopic compositions of the non-carbonaceous (non-CC) and carbonaceous (CC) chondrites is a consequence of the formation of Jupiter isolating the inner (non-CC) from the outer (CC) Solar System. Since the Earth and Mars formed in the inner Solar System, it might be expected that they more closely resemble the non-CCs than the CCs. Indeed, the Earth is almost identical isotopically to the ECs. As a result, many researchers have suggested that the building blocks of the Earth were dominated by EC-like objects and/or their differentiated counterparts (aubrites). However, estimates of the Earth's lithophile element composition (i.e., little modified by core formation) more closely resembles those of the CCs. The mixed chemical and isotopic affinities of the Earth's composition is a conundrum that has yet to be resolved. To better understand the fractionations amongst the chondrites, quantitative models of the fractionations in the chondrites are briefly described, and how they might be used to reconcile the conflicting affinities of the Earth's elemental and isotopic compositions are discussed.

The models: While the chondrites were all modelled as mixtures of refractory material, chondrules, matrix and water, it proved necessary to treat the CCs and non-CCs separately. The average compositions of the components in the two models were determined by least squares fitting to the bulk compositions of the respective chondrite groups. The matrix was assumed to be anhydrous and reduced (i.e., its pre-alteration condition), but otherwise CI-like in its elemental composition. The chondrules or their precursors were also assumed to have formed from the same CI-like material, but were subject to loss of moderately volatile elements and metal without fractionating the common and refractory lithophiles. The Mg/Si and Al/Si ratios of the refractory components were fixed by where the two best fit lines to the CC and non-CC groups intersect an AOA-CAI mixing line.

The CCs were reproduced to within the uncertainties of their bulk compositions, with (i) the refractory component abundances controlling the refractory element enrichments and the nucleosynthetic anomalies, (ii) the chondrule abundances controlling the moderately volatile element and metal-silicate fractionations, and (iii) matrix controlling the abundances of elements with condensation temperatures below ~800 K. All components contributed to the bulk O isotopes. For the non-CCs, there is very little fractionation amongst the lithophiles, and this is reflected in the average compositions of the chondrules and the nominally refractory component (alkali/Al ratios, for instance, are not very different from CI. In addition, to reproduce the non-CC isotopic compositions, the CI-like material that made up the matrix in the non-CCs and from which their chondrules formed cannot have had CI-like or Earth-like nucleosynthetic isotope anomalies. The same is true for the non-CC refractory component.

Implications for Earth: Estimates of the bulk Earth composition have higher than CI Al/Si and depleted moderately volatile element fractions that correlate with their condensation temperatures. Any volatility trends amongst the siderophile and chalcophile elements have been obscured by core formation. Producing the enhanced Al/Si by enriching the proto-Earth in the non-CC refractory component would result in a composition with abundances of volatile lithophiles that are much too high. On the other hand, a combination of the CC chondrule and refractory components can reproduce the bulk Earth lithophile abundances remarkably well, especially if 2 wt.% of CI material is added to account for the highly volatile element budgets of the Earth.

However, the CC component model cannot explain the Earth's lithophile isotopic composition. Here it is suggested that the fractionations amongst the CCs, rather than the non-CCs, reflect the dominant processes acting in the early Solar System, including in the region where the Earth's building blocks formed. The CC vs. non-CC isotopic dichotomy demonstrates that there was spatial and/or temporal isotopic heterogeneity in or evolution of the nebula. It seems possible that because he Earth's precursors formed at a different time and place from the chondrites their isotopic compositions were also slightly different. Indeed, estimates suggest that there may have been a linear variation between ^{48}Ca, ^{50}Ti, Δ^{17}O and possibly ^{54}Cr in the nebula.

RELICT FORSTERITE IN UNEQUILIBRATED ENSTATITE CHONDRITES

N. V. Almeida[1], P. F Schofield[1], K. Geraki[2] and S. S. Russell[1], [1]Planetary Materials Group, Natural History Museum (London, SW7 5BD, U.K., n.almeida@nhm.ac.uk), [2]Diamond Light Source Ltd. (Chilton, OX11 0DE, U.K.)

Introduction: Enstatite chondrites are notable for their reduced mineralogy [1] and chemical similarity to the inner Solar System; indeed, they are considered isotopic twins of the Earth [2]. Solar and cosmogenic noble gas compositions also support heliocentric distances of EC parent bodies at 1-1.4 AU [e.g. 3]. While most authors have assumed that the ECs formed from material condensed at high C/O [e.g. 4], recent trace element work suggests that EC chondrule precursors may have formed in a more oxidising environment and were later reduced by exposure to a reducing Si- and S-rich gas [5]. This gas reduced the olivine to Mg-rich pyroxene and formed sulphides, thus EC chondrules record an evolving nebular composition from oxidising to reducing conditions. We have made a detailed study of relict olivine in primitive enstatite meteorites in order to test this model.

Methods: Sections of Kota Kota (EH3; BM. 1905,105; P22810), MAC 88136 (EL3; 106) and Qingzhen (EH3; BM.1999,M27; P22813 & P22814) were studied. Element mapping by EDS (Zeiss EVO 15LS SEM) was used to locate olivine, followed by cathodolumines ece (CL) imaging and EPMA (Cameca SX100 microprobe) for mineral compositions. Synchrotron XRF maps and Ti-XANES data were acquired at beamline I18, Diamond Light Source.

Findings: Relict forsterite grains were identified in all three meteorites, appearing as anhedral to subhedral cores in chondrules surrounded by enstatite. The grains exhibit different CL properties across the UEC in this study, broadly fitting into four groups: i) consistently red throughout; ii) red interiors rimmed by strong blue CL; iii) mixed CL appearing purple; iv) consistently blue throughout. Blue olivine differs from red olivine with lower Ca, Mn, and Cr, and higher Fe, Al and Ni concentrations. An example is included in *Figure 1*: chondrule C2 contains an almost intact forsterite grain and two others that are more progressively altered, all showing bright red CL. The grains are surrounded by enstatite with blue CL (Ca, Al, Ti, Cr, Mn-poor) and the whole central relict is surrounded by a later generation of chondrule growth – enstatite grains with red CL (Ca, Al, Ti, Cr, Mn-bearing). Consistent differences in Ti-XANES spectra are observed between the relict forsterite and surrounding enstatite.
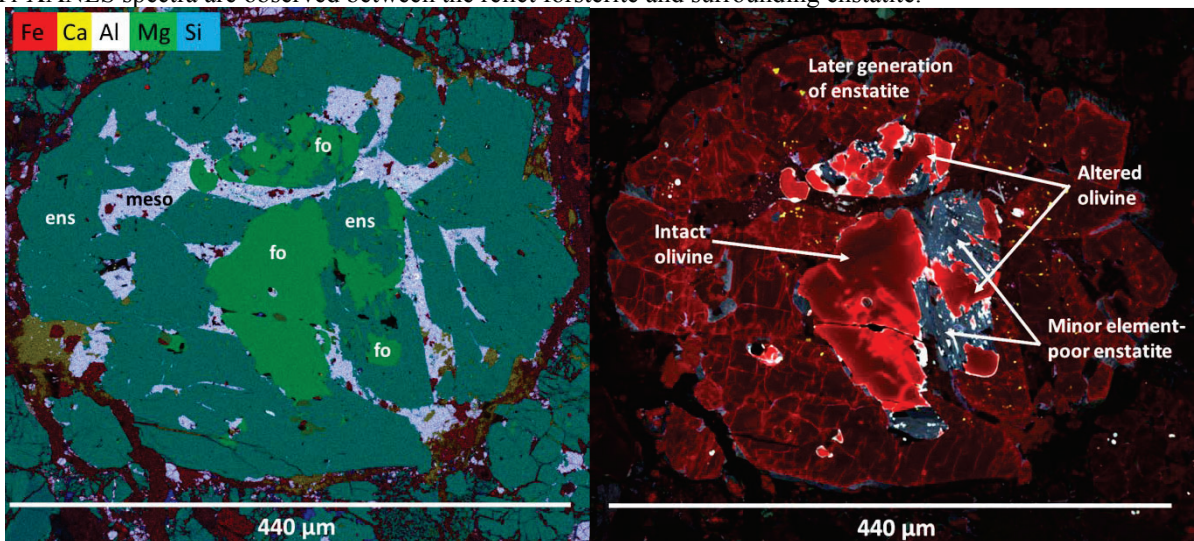

Figure 1: Composite element map (left) and CL image (right) of chondrule C2 in Kota Kota (P22810).

Implications: The model of evolving nebular compositions is supported by our petrological observations, suggesting the chondrules were once more similar to those in carbonaceous and ordinary chondrites. If the enstatite chondrules did indeed originally form under more oxidising conditions, they could plausibly be more closely related to the Earth and other terrestrial planets on the one hand, and to other chondrite groups on the other, than previously thought.

Next steps: Our work on relict forsterite will advance to oxygen and chromium isotopic analyses to constrain the formation region of the relict material, and dating via the Al-Mg system.

References: [1] Keil, K. (1989) *Meteoritics* 24:195-208. [2] Javoy M. et al. (2010) *Earth and Planetary Science Letters* 293:259-268. [3] Nakashima D. et al. (2006) *Meteoritics & Planetary Science* 41:851-862. [4] Weisburg M. & Kimura M. (2012) *Chem. der Erde* 72:101 [5] Jacquet E. et al. (2015) *Meteoritics & Planetary Science* 50:1 [6] Steele, I. M. (1986) *Geochimica et Cosmochimica Acta*, 50:1379-1395.

THE PETROLOGY OF OPAQUE ASSEMBLAGES IN UNEQUILIBRATED ORDINARY CHONDRITES

S. P. Alpert[1,2] (salpert@amnh.org), D. S. Ebel[1,2,3], M. K. Weisberg[1,2,3], N. T. Kita[4], G. Siron[4], and K. Fukuda[4]. [1]Dept. of Earth and Planetary Sci., American Museum of Natural History, New York, NY 10024, USA, salpert@amnh.org. [2]Earth and Environmental Sci., CUNY Graduate Center, New York, NY 10016, USA. [3]Dept. Physical Sci., Kingsborough Community College, CUNY, Brooklyn, NY 11235, USA. [4]WiscSIMS, Dept. of Geoscience, University of Wisconsin-Madison, Madison, WI 53706, USA

Introduction: Variations in iron content among chondrites suggest that metal-silicate fractionation was a key process in the early protoplanetary disk. Previous work [1] on CR chondrites determined relationships between FeNi metal textural setting (in chondrules or isolated in matrix) and concentrations of trace siderophile elements, concluding that some metal nodules were expelled from chondrule melts and partially vaporized/recondensed, while others follow no interpretable trend. To understand and constrain such processes, we began a study of the opaque assemblages (OAs) in ordinary chondrites (OC). OAs range from nearly pure to variable mixtures of metals, sulfides, oxides, and in rare cases silicates [2, 3, 4, 5]. Here we provide detailed petrologic descriptions, modal abundances, and mineral compositions of 37 OAs in the unequilibrated OC, Semarkona (LL3.01).

Methods: Element x-ray intensity maps were collected in WDS stage mapping mode using the Cameca SX100 electron microprobe (EMP) at the AMNH on four polished sections and a suite of standards at 1µm/pixel resolution, 15ms dwell, 40nA current. Maps were run through a machine learning algoritm which identifies the mineral phase of each pixel based on standards [6]. Quantitative point analysis was conducted on the EMP for Mg, Fe, Cr, Si, S, Na, Co, Ti, Al, P, Ni, Mn, and Ca at 20nA and 15kV, with a 1µm spot size. Oxygen isotope analyses of olivine grains were obtained using ~12 µm spot size accoding to the method similar to [8]

Results: OAs occur in matrix (sharply bound, 300 to >2000 µm in size, generally round, often mineralogically layered) and associated with chondrules (either completely interior to chondrules or as full or partial rims). Rim OAs range from matrix OA size down to micron size. OAs are dominantly kamacite with avg. wt. % 85 Fe, 7.5 Ni; taenite 45 Fe, 49 Ni; magnetite; troilite or mono-sulfide solution (MSS). Chondrule interior OAs are similar to matrix, but some matrix OAs contain fine-grained silicates: either matrix-like olivine or olivine-rich microchondrules as in [7]. We measured oxygen isotopes in 5 microchondrules in one OA, finding $\Delta^{17}O$ from $-1.4\pm0.3‰$ to $+0.3\pm0.2‰$. Negative $\Delta^{17}O$ values are most similar to ^{16}O-rich relict grains in PO chondrules in LL3's [8]. OAs in both textural settings have a range of mineral abundances (Fig. 1). Matrix OAs exhibit a higher abundance of oxides (75%) than chondrule OAs with nearly pure metal or pure sulfide OAs only being found associated with chondrules.

Discussion: The OAs exhibit a wide range in both structure and mineralogy, suggesting different histories and varying degrees of oxidation/sulfidation. OAs enclosed in chondrules (Fig. 2) were likely shielded from both nebular and parent body oxidation. Matrix OAs within a few µm proximity exhibit wide composition ranges, suggesting each formed as an independent object prior to lithification. OAs in chondrules and matrix must have a close relationship. Either matrix OAs were immiscible droplets expelled from chondrule melts, or OAs formed as pre-existing solid nodules, some of which were then incorporated into chondrule melts. Unmelted OAs will be examined in the future by field emission scanning electron microscopy to resolve their fine-grained mineralogy and determine whether they exhibit textures indicative of direct condensation from a gas.

 References: [1] Connolly H. C. Jr. et al. (2001) *Geochim. Cosmochim. Acta 65*:4567-4588. [2] Zanda B. et al. (1994) *Science 265*:1846-1849. [3] Rubin A. (2005) *Geochim. Cosmochim. Acta 69*:4907-4918. [4] Campbell A. et al. (2005) In *Chondrites & the Protoplanetary Disk, ASP Conf. Ser. 431*, 407-431. [5] Schrader D and Lauretta D (2010) *Geochim. Cosmochim. Acta 74*:1719-1733 [6] Alpert S. P. et al. (2019) *QMA 2019*. [7] Bigolski J. et al. (2016) *Meteoritics & Planet. Sci. 51*: 235-260. [8] Kita N. T. et al. (2010) *Geochim. Cosmochim. Acta 74*:6610–6635.
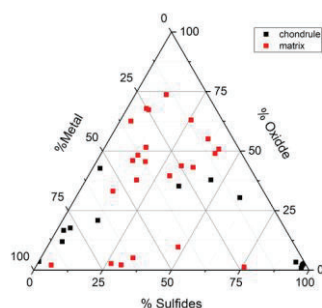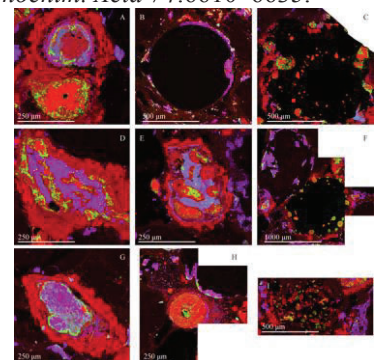

Fig. 1 (left) Normalized percentage of the most abundant mineral phases counted by the modal algorithm for OAs in Semarkona (AMNH #4128). **Fig. 2** (right) Elemental map (Fe-Ni-S; Red-green-blue) of OAs showing their structures and distribution of mineral phases (FeS is purple, Ni-rich phases green, Fe metal bright red, Fe oxide dull red).

SODIUM-22 PRODUCTION IN SUPERNOVAE.

Sachiko Amari[1] and Marco Pignatari[2], [1]McDonnell Center for the Space Sciences and Physics Department, Washington University, St. Louis, MO 63130, USA (sa@physics.wustl.edu), [2]E.A. Milne Centre for Astrophysics, School of Mathematics and Physical Sciences, University of Hull, HU6 7RX, United Kingdom.

Presolar grains are stardust that formed in stellar outflow or stellar ejecta, and were contained in extraterrestrial materials. The study of presolar grains in the laboratory has yielded a wealth of information about nucleosynthesis in stars, mixing in stellar ejecta and the Galactic chemical evolution [e.g., 1]. Mineral types of presolar grains include diamonds [2], SiC [3, 4], graphite [5], oxides [6, 7], and silicates [8-11]. Presolar graphite is the carrier of an exotic ^{22}Ne-rich component, Ne-E(L) [5]. Bulk (= aggregates of grains) noble gas analysis has shown that Ne-E(L) mostly consists of ^{22}Ne from ^{22}Na ($T_{1/2}$ = 2.6 a) with a small amount of ^{22}Ne from asymptotic giant branch stars [12]. Sodium-22 was traditionally attributed to novae because ONe novae produce ^{22}Na along with ^{26}Al [e.g., 13].

Many SN grains, mostly populated in low-density fractions, show Si isotopic anomalies (mostly ^{28}Si excesses, but, in a few cases, ^{29,30}Si excesses), the initial presence of ^{44}Ti, and high ^{26}Al/^{27}Al ratios [14, 15]. Helium and Ne analyses of individual graphite grains have shown that a few SN grains contain ^{22}Ne from ^{22}Na [16-19].

Isotopic abundances of SN models give us a diagnostic tool to probe stellar physics and nuclear physics uncertainties affecting the simulations. The radioactive isotope ^{22}Na, in a 15M_{sun} model (s15a28c) by Rauscher et al. [20], is produced in the O/Ne zone during hydrostatic burning with the maximum yield of 2.2×10^{-6} by mass fraction. It is hard, if not impossible, to explain ^{22}Ne-rich SN graphite grains by ^{22}Na from the O/Ne zone because 1) ^{22}Na is produced in the inner O-rich zone where the C abundance is very low ($< 1 \times 10^{-2}$), and 2) the abundance of ^{22}Na is only at a few ppm level. Recently, Pignatari et al. [21] have proposed supernova models including the effect of high shock velocities, and the H injection in the He/C zone. In these models explosive H burning produces large abundances of ^{22}Na. The largest production obtained is in the model 25T-H, with a mass fraction of $\sim 5 \times 10^{-2}$ in the O/nova zone, which is adjacent to the C-rich He/C zone. These models produce a significant amount of ^{22}Na by the explosive H burning in the outer zone of supernovae. Therefore, it would be much easier to explain the trapping of ^{22}Na into graphite grains.

Explosive H burning in supernovae [21] has been invoked to explain the isotopic signatures of ^{15}N-rich SiC A+B grains [22] and those of a few ^{14}N-rich A+B grains [23]. A+B grains comprise a few percent of the total SiC grains [24]. It is estimated that 27% of the total graphite grains originated from supernovae [15]. There are uncertainties in the estimation for the fraction of ^{22}Ne-rich grains among SN graphite grains because the detection of the noble gases depends on the conditions of the analyses prior to noble gas analysis [19]. However, if we take the number of ^{22}Ne-rich grains (86%) obtained from one of the Orgueil mounts [19], it is concluded that many SN graphite grains contain ^{22}Ne from ^{22}Na. Considering that many presolar grains show signatures of explosive H burning, a significant portion of the SN population may explosive H burning.

References: [1] Lodders K. and Amari S. (2005) *Chem. Erde* 65:93-166. [2] Lewis R. S. et al. (1987) *Nature* 326:160-162. [3] Bernatowicz T. et al. (1987) *Nature* 330:728-730. [4] Tang M. and Anders E. (1988) *Geochim. Cosmochim. Acta* 52:1235-1244. [5] Amari S. et al. (1990) *Nature* 345:238-240. [6] Nittler L. R. et al. (1994) *Nature* 370:443-446. [7] Huss G. R. et al. (1994) *Astrophys. J.* 430:L81-L84. [8] Messenger S. et al. (2003) *Science* 300:105-108. [9] Nguyen A. N. and Zinner E. (2004) *Science* 303:1496-1499. [10] Nagashima K. et al. (2004) *Nature* 428:921-924. [11] Mostefaoui S. and Hoppe P. (2004) *Astrophys. J.* 613:L149-L152. [12] Amari S. et al. (1995) *Geochim. Cosmochim. Acta* 59:1411-1426. [13] José J. and Hernanz M. (1998) *Astrophys. J.* 494:680-690. [14] Jadhav M. et al. (2013) *Geochem. Cosmochim. Acta* 113:193-224. [15] Amari S. et al. (2014) *Geochem. Cosmochim. Acta* 133:479-522. [16] Amari S. (2009) *Astrophys. J.* 690:1424-1431. [17] Heck P. R. et al. (2009) *Astrophys. J.* 701:1415-1425. [18] Meier M. M. M. et al. (2012) *Geochem. Cosmochim. Acta* 76:147-160. [19] Heck P. R. et al. (2018) *Meteorit. Planet. Sci.* 53:2327-2342. [20] Rauscher T. et al. (2002) *Astrophys. J.* 576:323-348. [21] Pignatari M. et al. (2015) *Astrophys. J. Lett.* 808:L43:6pp. [22] Liu N. et al. (2017) *Astrophys. J. Lett.* 842:L1:8pp. [23] Hoppe P. et al. (2019) In *Nuclei in the Cosmos XV (Springer Proceedings in Physics 219),* (Formicola A., Junker M., Gialanella L. and Imbriani G.) Springer, New York, in press. [24] Hoppe P. and Ott U. (1997) In *Astrophysical Implications of the Laboratory Study of Presolar Materials,* (Bernatowicz T. J. and Zinner E.) AIP, New York 27-58.

SILICA-RICH VESTAN CRUSTAL TERRANES? INTERMEDIATE COMPOSITIONS REVEALED BY AN INHOMOGENEOUS IMPACT SPHERULE IN NORTHWEST AFRICA 12231.

C. Anderkin, University of Florida Department of Geological Sciences, Gainesville, FL 32612, USA (anderkinc@ufl.edu)

Introduction: The HED suite of meteorites (howardites, eucrites, and diogenites) is generally believed to originate from the both the outer crustal layers of 4 Vesta (howardites and eucrites) as well as the solidified Vestan mantle (diogenites) [1]. Howardites are polymict breccias whose lithic constitution is composed primarily of fragmental eucrites and diogenites, dispersed throughout the Vestan regolith by impactors and subsequently lithified under the force of Vesta's gravity [2]. This work will focus on the compositions derived from an impact spherule in a howardite, Northwest Africa 12231.

Methods: Oxide wt. percentages were determined with EDAX energy-dispersive x-ray spectroscopy (EDS). A probe current of 1.9nA was employed, as well as a voltage of 15kV. A spot size of 4 μm was employed.

Results: Analysis of a glassy impact spherule in Northwest Africa 12231 has yielded inhomogeneous compositions, ranging from 53-58 wt% SiO_2, with most analyses yielding 'andesitic' compositions. Summary of the average data is presented in Table 1. The compositions analyzed here are intermediate between eucritic bulk compositions (EBC) and proposed Vestan felsic terrranes [3] (VFT), as evidenced by mixing lines between EBC and VFT. Here, it is proposed that the felsic composition of the glass is attributable to the mixing of the two compositions by an impactor. To verify that the compositions were not a result of impact-induced vapor fractionation, the compositions have been plotted on an Al_2O_3/CaO vs. K_2O/CaO and K_2O/CaO vs. FeO/CaO diagram (Fig. 1). Due to the differences in volatility of K_2O and more refractory oxides (FeO, CaO, Al_2O_3), the enrichment could be resultant of the selective volatilization and condensation of less refractory oxides [4]. This effect was ruled out, as the behavior of K_2O in the analyzed glass systematically varies with FeO, CaO, and Al_2O_3 (Fig. 1). Due to the linear trend of the data (Fig. 2), it is possible that the values observed here could be obtained by impact melting and subsequent mixing of two compositionally heterogeneous materials, namely the eucritic bulk composition and another more felsic endmember.

Figures:

SiO2	Na2O	MgO	Al2O3	P2O5	MnO	SO2	K2O	CaO	TiO2	FeO
54.90477	1.726446	10.73421	14.58807	0.169584	0.398883	0.195203	0.912947	7.195977	0.150333	8.842365

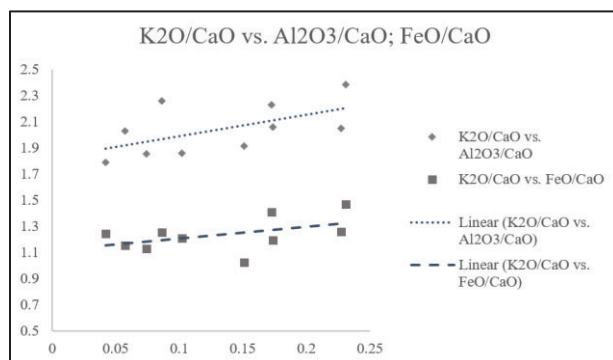*Table 1: Average wt% oxide compositions of the glass spherule analyzed here.*

Figure 1: Diagram controlling for volatility of K2O during impact induced vapor fractionation. Here, the K2O content varies systematically with more refractory oxides, and thus, enrichment attributable to impact fractionation can be ruled out.
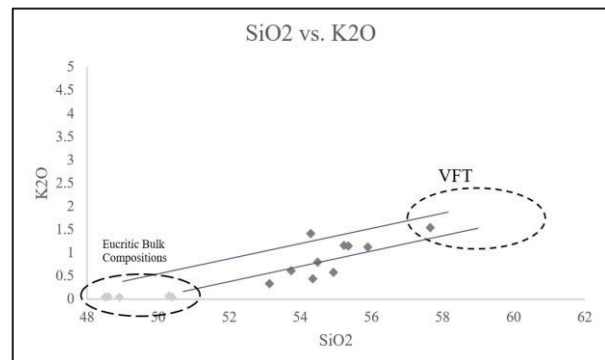

Figure 2: Diagram indicating possible mixing lines between EBC and a more felsic material, possibly a proposed Vestan felsic terrane. Compositions here are 'andesitic', and range from 53-58% SiO2.

References: [1] Binzel R. P. and Xu S. 1993. Chips off of asteroid 4 Vesta: Evidence for the parent body of basaltic achondrite meteorites. Science 5105:186–191 [2] TAKEDA, H. (1997), Mineralogical records of early planetary processes on the howardite, eucrite, diogenite parent body with reference to Vesta. Meteoritics & Planetary Science, 32: 841-853. doi:10.1111/j.1945-5100.1997.tb01574.x [3] Barrat, Jean-Alix & Bohn, Michael & Gillet, Philippe & YAMAGUCHI, A. (2009). Evidence for K-rich Terranes on Vesta from impact spherules. Meteoritics & Planetary Science. 44. 359 - 374. 10.1111/j.1945-5100.2009.tb00738.x. [4] Delano, J. W., Pristine lunar glasses; criteria, data, and implications. In Proceedings of the 16th Lunar Planet. Sc. Conf.; (eds. Ryder, G. & Schubert, G.). J. Geophys. Res. B. 91, 4, D201-D213 (1986).

IMPROVED PRECISION FOR THE *CHEMISTRY AND DATING EXPERIMENT* USING FS-LASER ABLATION.

F. S. Anderson[1], A. Alexander[1], C. Crow[2], T. J. Whitaker[1], and J. Levine[3], [1]Southwest Research Institute, Department of Space Operations, Southwest Research Institute, 1030 Walnut St., Boulder, Colorado 80302, USA (anderson@boulder.swri.edu), [2]University of Colorado Boulder, Geological Sciences, Boulder, CO 80309, USA, [3]Department of Physics and Astronomy, Colgate University, Hamilton, New York 13346, USA.

Introduction: We have developed a portable Rb-Sr and Pb-Pb dating instrument called the Chemistry and Dating EXperiment (CDEX) to address billion year uncertainties in inner solar system chronology [1-3]. CDEX uses laser ablation resonance ionization mass spectrometry (LARIMS) to produce isochrons, test concordance, and map geochemistry of samples. We have demonstrated Pb-Pb dates with an average precision of ~±50 Ma years, and Rb-Sr dates with an average precision of ~±180 Ma. We hypothesized that the difference in precision between Rb-Sr and Pb-Pb dates originates with time dependent elemental fractionation caused by low intensity (~60 GW/cm^2) 213-nm nanosecond laser ablation. Thus, elemental fractionation limits the Rb-Sr precision, but not the Pb-Pb precision. In order to test this hypothesis, we have replaced our ablation laser with a femtosecond laser with intensities up to ~400 PW/cm^2. Using this fs-laser, we have made new measurements of the Zagami meteorite that show the CDEX measurement precision has improved by ~5X, resulting in a Rb-Sr date of 191±56 Ma, (^{87}Sr/^{86}Sr)$_i$ of 0.725, and MSWD of 1.17 with 415 spot measurements. These results are consistent with previous laboratory measurements [4], and suggest that increasing ablation intensity can improve Rb-Sr precision to the instrumental limits consistent with our intra element Pb-Pb measurements.

Relevance: The chronology of the inner solar system is based on models relating the crater densities of planetary surfaces to calibrated radiometric dates of well-provenanced lunar samples that primarily constrain the era between 3.5 and 4.2 Ga, as well as the very recent past. These results have been extrapolated to Mars, and throughout the solar system. However, recent work comparing the numerous lunar chronology models in the literature [e.g., 5, 6], illustrates differences between the models of up to one billion years for the period between ~2.8 to 3.3 Ga [7]. Improving CDEX measurements opens the door to rapid, simple, and precise chronology measurements on rocky bodies throughout the inner solar system. CDEX dates with a precision of ±50 Ma are more than sufficient to address the billion year uncertainties in solar system history from 1-3 Ga. Furthermore, because CDEX can produce dates in as little as 5 hours, it can be used to produce measurements on multiple samples thought to be from comagmatic lithologies, potentially improving precision sufficiently to constrain the age of large impact basins.

Laser Ablation: The laser ablation literature is replete with demonstrations of how higher intensity (>1 GW/cm^2 [e.g., 8]), shorter wavelength (<266 nm [9, 10]), and shorter pulse duration improve ion and particulate production [11-13]. Based on these observations, high intensity, nanosecond pulse length, UV ablation lasers with TRL of 6+ are being developed for spaceflight. Recent technological developments enable the potential for shorter pulses in flight systems [14, 15]. Our new ablation laser is capable of producing 266, 400, and 800-nm wavelengths, pulse durations of 40-1000+ femtoseconds, and power of up to 3.5W. After careful studies of measurement reproducibility [16], we have identified optimal measurement conditions at 150-fs and 250 TW/cm^2. Current measurements have only used the 800-nm capability, with shorter wavelength measurements to be completed in the near future.

Conclusion: In addition to new measurements of Zagami, we are currently making new measurements of Sudbury impact lapilli, and expanding our understanding lunar Pb reservoirs to improve our ability to derive lunar Pb-Pb dates. We are also developing methods to improve isotopic measurements while reducing instrument size, complexity, and cost, using new approaches like using photon momentum for isotopic separation.

References: [1] Anderson, F.S., J. Levine, and T.J. Whitaker, (2015) *RCMS*. [2] Anderson, F.S., J. Levine, and T.J. Whitaker, (2015) *RCMS*, 2015. [3] Anderson, F.S., et al., *LPSC*, 2017. [4] Borg, L.E., J.E. Edmunson, and Y. Asmerom, *GCA*, 2005. [5] Hartmann, W.K., C. Quantin, and N. Mangold, *Icarus*, 2007. [6] Marchi, S., et al., *The Astronomical Journal*, 2009. [7] Robbins, S.J., *EPSL*, 2014. [8] Elsila, J.E., N.P. de Leon, and R.N. Zare, *Analytical Chemistry*, 2004. [9] Gonzalez, J., et al., *J. Anal. At. Spectrom.*, 2002. [10] Guillong, M., I. Horn, and D. Günther, *J. Anal. At. Spectrom.*, 2003. [11] Riedo, A., et al., *PSS*, 2013. [12] Zhang, B., et al., *Analytical Chemistry*, 2013. [13] Bao, Z., et al., *Int. J. Mass Spectrom.*, 2016. [14] Anderson, F.S., J. Levine, and T. Whitaker, Dating the Martian Meteorite Zagami by the^{87}Rb-^{87}Sr Isochron Method with a Prototype In-situ Resonance Ionization Mass Spectrometer. Rapid Comm. Mass Spectrom., 2014. [17] Riedo, A., et al., *CHIMIA International Journal for Chemistry*, 2016. **70**(4): p. 268-273. [16] Anderson, F.S., T.J. Whitaker, and J. Levine, *LPSC*, 2019.

STUDY OF THE FRACTAL PROPERTIES OF CERES

A. O. Andreev[1] , E. N. Akhmedshina[1], Y. A. Nefedyev[1], R. Hudec[2]
[1]Kazan Federal University, Russia, Kazan, Kremlyovskaya st., 18. E-mail: alexey-andreev93@mail.ru
[2]Czech Technical University, Prague 6, Czech Republic

Introduction: Currently, Ceres is one of the most studied small celestial bodies. It is believed that the analysis of material composition of Ceres surface allows studying its internal structure and constructing a theory of Ceres's evolution. The "Dawn" spacecraft defined and matched an element base with the geological structure, which allowed comparing chemical parameters of the small planet with physical processes occurring there [1]. As a result, it was established that the composition of the dwarf planet represents a silicate body filled with water; in the course of evolution Ceres was heated and structurally modified, and geological process are still going on [2]. It should be noted, in order to create a complete picture of both the modern state and evolution of Ceres the knowledge of material composition must be integrated with the physical parameters of its surface [2]. In this work, fractal properties of Ceres asteroid were analyzed using the data from "Dawn" space mission.

Methods: The 3D model of Ceres constructed by us confirms the conclusion that the structure of Ceres surface (SCS) is a complex fractal system. The study of such objects requires the use of harmonic multi-parametric methods. When analyzing SCS, the Weierstrass-Mandelbrot fractal simulation method was used. According to this approach, models of complex fractal structures cannot represent a separate fractal and are described by multifractals – interrelated system of fractals [3]. These compound fractals are recursive, since they are invariant to the entire model of complex structure by both scale and symmetry [4]. Thus, multi-parametric fractal analysis allows representing systems similar to SCS as a fractal estimates spectrum. An advantage of fractal analysis is that local areas of the physical surface can also be investigated. In this work, the calculation algorithm by Minkowski was used. The surface model of Ceres asteroid was built by expanding altitude function into a regression harmonic series [5]. The order of the expansion of altitude function depends on the number of reference points. The latter must exceed the planned accuracy of the model from 5 to 15 times. At the final stage, an overdetermined system for various local areas of topocentric information was solved with an aim of postulating the model accounting the external measures.

Results: Using the harmonic expansion of altitude function into spherical functions the 3D model of Ceres was developed in order to carry out its fractal analysis. The fractal dimensions D for local areas and the whole model of SCS were determined. The variations of D ranging from 1.37 to 1.92 depending on Ceres's longitude and latitude were calculated. The main conclusion are as follows: 1) structure of Ceres surface varies more significantly in longitude; 2) in latitude the structure of Ceres is smoother; 3) the self-similarity coefficient varies in longitude rather quickly.

Discussion: It should be noted that the produced fractal dimensions are considerably scattered in both longitude and latitude of Ceres. This fact confirms the presence of complex structure in the spatial model of the small planet. This also applies to the real physical surface of Ceres.

Conclusions: Analyzing structure and evolution of celestial bodies includes various methods of statistical multiparametric analysis [6]. This also refers to planetary systems [7]. At the present time one of the promising directions of studying heterogeneous natural objects' structure is fractal geometry. For instance, the fractal analysis of the Solar system bodies' parameters has been conducted in the works [8]. The fundamental property of fractal objects is similarity or scaling when zooming. Investigations of fractal dimensions allow studying not only the structure, but the connection between structure and its formation processes as well [9]. The results of the work allow concluding that fractal simulation may provide independent values of fractal dimension for both the whole model of Ceres asteroid and its local macrostructural areas. The further development of the presented method of comparative fractal analysis will permit astronomers to investigate more local chemical and physical parameters and anomalies of SCS.

References: [1] McCord, T.B., et al. (2019) *Icarus* 318: 1. [2] Thomas B. McCord and Francesca Zambon (2019) *Icarus* 318: 2-13. [3] Nefedyev Y.A., et al. (2018) *Meteoritics & Planetary Science* 53/S1: 6192. [4] Demin S.A. (2018) *Journal of Physics: Conference Series* 1038/1: N 012020I. [5] Andreev A.O. (2018) *Journal of Physics: Conference Series* 1038/1. N 012003. [6] Nefedyev Y. (2012) *Advanced in Space Research* 50: 1564-1569. [7] Varaksina N.Y. (2015) *Journal of Physics: Conference Series*, 661/1: N 012014, 2015. [8] Nefedyev Y. (2018) *Astronomy Reports* 62/12: 1015–1019. [9] Turcotte D.L. (1987) *Journal of Geophysical Research* 92/B4: 597-601.

MULTI-FACTOR ANALYSIS OF ASTROPHYSICAL PARAMETERS FOR CIRCUMLUNAR AND CIRCUMSOLAR METEOROIDS AND STUDY OF THEIR GENETIC CONNECTIONS

A. O. Andreev[1] , Y. A. Nefedyev[1], R. Hudec[2] , N. Y. Demina[1], S. A. Demin[1]
[1]Kazan Federal University, Russia, Kazan, Kremlyovskaya st., 18. E-mail: alexey-andreev93@mail.ru
[2]Czech Technical University, Prague 6, Czech Republic

Introduction: The analysis of meteoroid dynamics is an important direction in the study of evolutionary processes in the Solar System. The majority of NEOs reach the orbits with small perihelion distance, and this also applies to the near-Moon objects (NMO). The evolution of asteroids in the solar neighborhood is supposed to play a significant role in the formation of physical properties, distribution for size, and dynamic features of NEOs [1]. Near-Sun objects (NSO) may achieve equilibrium temperatures high enough to change surface as a result of thermal breaks, drying, and decomposition of hydrated silicates. When an NSO moves near the Sun, it is exposed to significant tidal and thermal influences and also interacts with the solar atmosphere at rather small heliocentric distances [2]. These physical phenomena must change the surface of the NSO substantially and probably lead to its disintegration or full collapse. The study of these processes is considered in the paper.

Methods: The study of activity of NMO allows investigating the subtle structure of meteor showers. Currently, various aspects of meteoroids' collisions with the Moon are being intensively analyzed. Falls of meteorites lead to the increase in alkaline metals (Na and K) content in the lunar exosphere [3]. When the main meteor showers are at the stage of activity, the dust particle content in the lunar atmosphere increases [4]. It means at least a part of the dust particles are brought to the lunar atmosphere when meteoroids fall. The processing of the observations of dust clouds generated at meteoroid falls on the Moon is going to be carried out with standard methods used for plotting light curves of optical flashes on the Moon. When constructing a model of equilibrium composition of impact steam formed after large meteoroids collide with the Moon, the method based on using the maximum entropy principle is planned to be applied [5]. The study of MHD-formations was conducted using flicker-noise spectroscopy and the new method of multi-parametric analysis [6].

Results: To analyze and simulate the dynamic processes related to NMO, the interrelated tasks on the study of meteoroid environment, its influence on physical and chemical properties of the Moon using the seismic data, determination of lunar meteorite bombardment intensity, and investigation of subtle effect of the lunar spin-orbital dynamics were solved. NSO include objects that are located or have been moving on orbits with perihelion distances $q < 0.1$ AU. To study NSO, MHD-formations were analyzed and a method of constructing a simulation model of NSO accounting astrophysical parameters of these objects, their distribution for size, and dynamic behavior in space was developed [7].

Discussion: It should be noted that the Moon acts as a huge meteoroid detector [8]. This allows studying the distribution of large impactors for size and collisions with the Moon rate. Besides, the study of NMO activity also allows investigating the subtle structure of meteor showers. On the other hand, properties of NSO are related to solar wind influence, and its parameters at distances greater than 0.3 AU would significantly further understanding of the influence of the varying solar magnetic field on the structure and dynamics of corona and solar wind. However, the corona's heating and acceleration resulting in the generation of solar wind are still unexplained.

Conclusions: The results obtained in the paper will allow creating and analyzing physical models and long-term processes caused by tidal evolution and meteoroids' interaction with planets and other small bodies using the new parameters [9]. The produced methods and software are going to be in demand for the reduction of both existing and new data obtained in space missions [10].

References: [1] Jewitt D. (2013) *The Astronomical Journal* 145:133. [2] Vokrouhlický D. and Nesvorný D. (2012) *Astronomy & Astrophysics* 541: A109. [3] Colaprete A., et al. (2016) *Science* 351/6270: 219-252. [4] Szalay J. R. and Horányi M. (2016) *Icarus* 275. 221-231. [5] Demin S.A. (2014) *Kinematics and Physics of Celestial Bodies* 30: 63-69. [6] Demin S.A. , et al. (2018) *Advances in Space Research* 61/2: 639-644. [7] Sokolova M.G. (2018) *Advances in Space Research* 62/8: 2355-2363. [8] Nefedyev Y.A. (2017) *SGEM* 17/62: 961-966 [9] Sokolova M.G., et al. (2014) *Advances in Space Research* 54/ 11: 2415-2418. [10] Sokolova M., et al. (2016) *Advances in Space Research* 58/4: 541-544.

DESTINY+: FLYBY OF ASTEROID (3200) PHAETHON AND IN-SITU DUST ANALYSES.

T. Arai[1], M. Kobayashi[1], K. Ishibashi[1], F. Yoshida[1], H. Kimura[1], T. Hirai[1], P. Hong[1], K. Wada[1], H. Senshu[1], M. Yamada[1], O. Okudaira[1], S. Kameda[2], R. Srama[3], H. Krüger[4], M. Ishiguro[5], H. Yabuta[6], T. Nakamura[7], J. Watanabe[8], T. Ito[8], K. Ohtsuka[8,21], S. Tachibana[9], T. Mikouchi[9], M. Komatsu[10], K. Nakamura-Messenger[11], S. Messenger[11], S. Sasaki[12], T. Hiroi[13], S. Abe[14,] S. Urakawa[15,] N. Hirata[16], H. Demura[16], G. Komatsu[1, 17], T. Noguchi[18], T. Sekiguchi[19], T. Inamori[20], T. Yanagisawa[22], T. Okamoto[22], H. Yano[22], M. Yoshikawa[22], T. Ohtsubo[22], T. Okada[22], T. Iwata[22], H. Toyota[21], K. Nishiyama[22], , Y. Kawakatsu[21] and T. Takashima[21], [1]Planetary Exploration Research Center (PERC), Chiba Institute of Technology, Chiba 275-0016, Japan (tomoko.arai@it-chiba.ac.jp), [2]Rikkyo University, Japan, [3]Institut für Raumfahrtsysteme, Stuttgart University. [4]Max Planck Institute for Solar System Research, [5]Seoul National University, South Korea, [6]Hiroshima University, Japan, [7]Tohoku University, Japan, [8]National Astronomical Observatory of Japan, [9]The University of Tokyo, Japan, [10]The Graduate University for Advanced Studies, Japan, [11]NASA Johnson Space Center, TX, U.S.A, [12]Osaka University, Japan, [13]Brown University, RI, U.S.A, [14]Nihon University, Japan, [15]Japan Spaceguard Association, Japan, [16]Aizu University, Japan, [17]Università d'Annunzio, Italy, [18]Kyushu University, Japan, [19]Hokkaido University of Education, [20]Nagoya University, [21]Tokyo Meteor Network, [22]ISAS, JAXA.

DESTINY[+] (Demonstration and Experiment of Space Technology for INterplanetary voYage, Phaethon fLyby and dUst Science) was proposed for JAXA/ISAS small-class program in 2015 and was selected in 2017 [1]. It is currently in the pre-project phase (Phase-A) with a launch targeted for 2022. It is a joint mission of technology demonstration and scientific observation. It will test high performance electric propelled vehicle technology and high-speed flyby of asteroid (3200) Phaethon and possibly asteroid 2005UD, which is a likely break-up body from Phaethon [2] as an extended mission. Engineering challenges include an up-close encounter at a distance of 500 km from Phaethon with radio-optical hybrid navigation guidance and control, and autonomous imaging based on optical information for target tracking during a high-speed flyby of 33km/sec. The science goal is to understand the nature and origin of cosmic dust brought onto the Earth, in the context of exogenous contribution of carbon and organics for possible prebiotic seeds of the terrestrial life. Phaethon is a parent body of Geminid meteor shower, and thus a known source to periodically provide dust to the Earth, via the dust stream. Phaethon is a B-type, active asteroid which ejects dust only at the perihelion passage [e.g. 3,4]. The science objectives are: (1) in-situ analyses of velocity, arrival direction, mass and chemical composition of interplanetary and interstellar dust particles around 1 au, the dust trail, and nearby Phaethon, and (2) flyby imaging of Phaethon to study its geology, for understanding dust ejection mechanism of active asteroid and the surface compositional variation. Planned science observation is illustrated in Fig. 1. Phaethon approached the Earth as close as 10,000,000 km in December 2017. International observation campaign, including photometric, spectroscopic, polarimetric and radar observation were successfully conducted. These observation data are crucial to better characterize Phaethon for mission planning of DESTINY[+].

References: [1] Arai T. et al. (2018) LPSC 49th, abstract#2570. [2] Ohtsuka K. et al. (2006) A&A 450, L25. [3] Jewitt D. and Li J. (2010) AJ, 140, 1519. [4] Jewitt D. et al. (2013) Astrophys. J. Lett. 771, L36.
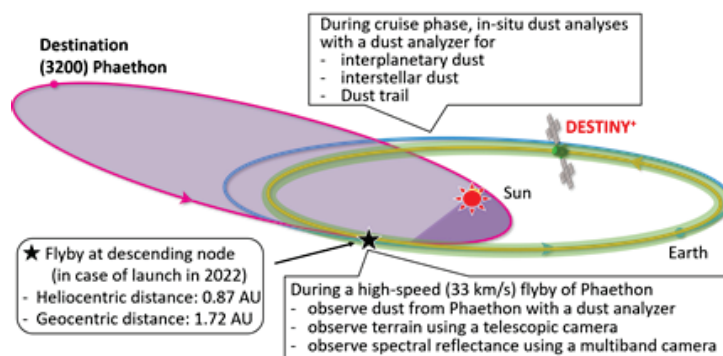

Fig. 1. Overview of DESTINY+ science observation.

METEOR: TWO-YEAR METEOR OBSERVATION FROM THE INTERNATIONAL SPACE STATION.

Tomoko Arai[1], M. Kobayashi[1], M. Yamada[1], H. Senshu[1], K. Maeda[1], K. Wada[1], S. Ohno[1], K. Ishibashi[1], R. Ishimaru[1], T. Matsui[1], M. Fortenberry[2], Planetary Exploration Research Center, Chiba Institute of Technology, Chiba 275-0016, Japan (tomoko.arai@it-chiba.ac.jp), [2]Southwest Research Institute, San Antonio, TX 78238 U.S.A.

Introduction: Meteor showers occur when the Earth crosses streams of dust derived from specific comets or asteroids. Based on the dynamical link, parent bodies of major annual meteor showers are specified. Since velocity of dust for meteor showers are known, the size of dust can be estimated from the brightness and light curve of meteors. Major element composition of the dust can be constrained from the visible emission spectra of meteors. Photometric and spectroscopic observations of meteor showers provide clues to understand physical and chemical properties for the meteoroids and their parent bodies. METEOR is two-year meteor observation project onboard the International Space Station (ISS) [1], conducting photometric observation for the first year and spectroscopic observation for the second year. ISS is an ideal platform for continuous meteor observation without distortion caused by weather and atmospheric disturbances. The flux data collected allow better comparison of physical and chemical data among major meteor showers and their parent bodies. After two launch failures in October 2014 and June 2015, METEOR was delivered to the ISS in March 26, 2016 and started nominal operation on July 7, 2016. Since planned photometric and spectroscopic observation was not complete in the nominal two-year period due to variable constraints, such as the Moon condition, the ISS high-beta condition, hardware failures, and etc., extra observation was conducted for another half year. All the observation was complete on March 5, 2019 and the METEOR instruments were de-installed on March 31, 2019. Initial results were presented [2, 3] and further data analyses are currently underway.

Method: The ISS orbits the Earth at the altitude of about 400 km, while meteors generally starts to illuminate at the altitude of 100 km. Because a distance to a meteor is three time greater from the ISS than from the ground, a meteor looks darker by one order of magnitude on the ISS than on ground. METEOR consists of a high sensitive, high definition TV (HDTV) color camera equipped with a wide-angle, extremely bright lens (F0.95, f=10.5mm, diagonal FOV=57.8 deg) [2]. METEOR is installed in the Window Observational Research Facility (WORF) rack of the US Lab module (Destiny). It observes meteors through the US Lab window facing toward the Earth during orbital night when the Sun is beneath the horizon viewed from the ISS. The ISS orbits the Earth for 90 minutes and each orbital night is about 35 minutes except high beta periods when orbital night is shorter. Observation schedule is uploaded to the onboard PC one or two weeks in advance of observation based on the orbital prediction using two-line elements. Activation/deactivation of the camera and the encoder, data recording and processing are autonomously conducted with uploaded batch file commands. Observation is done in visible wavelength, as the METEOR camera has an IR cut filer, allowing visible light only, up to 700 nm. A transmitted blazed diffraction grating (300 grooves/mm) is used for spectroscopic observation. It is manually installed by ISS crew in front of the lens. Target atomic emission lines are Fe I (370nm), Ca I (393nm), Mg I (518nm), Na I (589nm), which are key elements of dominant silicate minerals, such as olivine, pyroxene and plagioclase in meteorites and interplanetary dust. A software to detect meteors in the recorded video data and extract the portion including meteors was developed utilizing deep learning, in collaboration with the Software Technology and Artificial Intelligence Research Laboratory of Chiba Institute of Technology.

Results: Video data for a single orbital night recorded at 20 Mbps is about 5.5 GB. With allowable data downlink rate (max. 4 Mbps) and 9 hours' daily command window, 6-9 GB is the maximum downlinkable data volume per day. All the recorded data of 20 Mbps are stored in a 750 GB HDD installed in the onboard PC. Thirty five HDDs were launched with METEOR in March, 2016 and another ten HDDs were delivered to ISS on Dec. 17, 2017. The used HDD is swapped with a new HDD by the ISS crew and periodically returned by Space-X Dragon vehicles. The HDDs used for the observation in 2019 and the METEOR instruments will be returned by Space-X #17 Dragon by June this year. Photometric and spectroscopic data for twelve meteor showers were successfully captured. Photometric data are analyzed to study the number of meteors, the luminosity variation, and the arrival direction, in order to understand the dust flux for each meteor shower. Spectral data of meteor showers are analysed to understand compositional variation within each meteor shower and among meteor showers, and thus their parent bodies. Some of the captured meteor images are available at the METEOR project website: http://www.perc.it-chiba.ac.jp/project/meteor/.

References: [1] Arai T. et al. (2014) LPSC 45th abstract #1610. [2] Arai T. et al. (2017) LPSC 48th, abstract# 3034 [3] Arai T. et al. (2018) LPSC 49th, abstract# 2525.

COMPOUND CHONDRULE FORMATION VIA HIGH-SPEED COLLISION OF SUPERCOOLED DROPLETS IN OPTICALLY THIN SHOCK WAVES.

S. Arakawa[1] and T. Nakamoto[1], [1]Department of Earth and Planetary Sciences, Tokyo Institute of Technology, 2-12-1 Ookayama, Meguro, Tokyo 152-8551, Japan. Email: arakawa.s.ac@m.titech.ac.jp.

Introduction: Chondrules are millimeter-sized spherules contained within chondrites as a major component and some chondrules, referred to as compound chondrules, are composed of two or more chondrules stick together. Although the formation mechanism of compound chondrule is still under debate, most of the previous studies interpreted the presence of compound chondrules as the result of collisions [e.g., 1−4]. The ubiquitous existence of cratered chondrules also suggests that some of the chondrules have experienced collisions before the accretion onto parent bodies [1]. Wasson et al. [5] classified each constituent chondrules as primary or secondary. Primary chondrules keep their spherical shape while secondary chondrules are deformed. Compound chondrules with blurred boundaries are rare within ordinary chondrites [5], indicating that compound chondrules are formed by collisions between crystallized and non-crystallized precursors [3].

The textures of compound chondrules have noteworthy features. Wasson et al. [5] reported that ~ 80% of primaries and ~ 90% of secondaries are nonporphyritic chondrules while only 15% of all chondrules in ordinary chondrites are nonporphyritic [1]. Therefore, compound chondrules are selectively formed from the precursors of nonporphyritic chondrules. Crystallization experiments [6] revealed that completely molten precursors turn into supercooled droplets as they are cooled below their liquidus temperature, and they crystallize immediately once these supercooled droplets collide with other particles [7]. Then we can imagine that compound chondrules are formed when crystallized chondrules and supercooled precursors collide and stick together [3].

Numerous ideas are proposed as chondrule formation mechanisms, including shock-wave heating [e.g., 8], planetesimal collisions [e.g., 9], and radiative heating by lightning [e.g., 10], and shock-wave heating within the solar nebula is one of the leading candidates. In this study, we examine the possibility of compound chondrule formation via collisions of supercooled precursors in shock waves.

Results and discussion: We calculated the velocity and the temperature of chondrules in one-dimensional normal shocks. For the case of optically thick shock waves, chondrules are thermally coupled with gas in post-shock regions [11], and collisions of chondrules would occur when the temperature is above their liquidus temperature. In this case, molten chondrules cannot avoid collisional destruction [12] and compound chondrules might not be formed.

In contrast, chondrule precursors can maintain their supercooling until the fine dust grains condense and accrete onto supercooled droplets in optically thin shock waves. Using a viscosity-temperature relation of chondrule melts [13], the critical velocity for collisional sticking would be higher than 1 km s^{-1} when the temperature of supercooled droplets is lower than ~ 1400 K. Therefore, compound chondrules can be formed in post-shock regions of optically thin shock waves.

Bow shocks caused by 100−1000 km-sized planetary bodies with eccentric orbits [e.g., 14] may be potent candidates for the sources of optically thin shock waves because the optical depth of the chondrule-forming region is lower than or on the order of unity when the dust-to-gas mass ratio is the solar metallicity [15]. The collision frequency between crystallized chondrules and supercooled precursors is also consistent with the fraction of compound chondrules in nonporphyritic chondrules [15].

References: [1] Gooding J. L. and Keil K. (1981) *Meteoritics* 16:17−43. [2] Ciesla F. J. (2006) *Meteoritics and Planetary Science* 41:1347−1359. [3] Arakawa S. and Nakamoto T. (2016) *Icarus* 276:102−106. [4] Bogdan T. et al. (2019) *Icarus* 319:133−139. [5] Wasson J. T. et al. (1995) *Geochimica et Cosmochimica Acta* 59:1847−1869. [6] Nagashima K. et al. (2008) *Journal of Mineralogical and Petrological Sciences* 103:204−208. [7] Connolly Jr. H. C. et al. (1994) *Meteoritics* 29:458. [8] Iida A. et al. (2001) *Icarus* 153:430−450. [9] Johnson B. C. et al. (2015) *Nature* 517:339−341. [10] Desch S. J. and Cuzzi J. N. (2000) *Icarus* 143:87−105. [11] Morris M. A. and Desch S. J. (2010) *The Astrophysical Journal* 722:1474−1494. [12] Jacquet E. and Thompson C. (2014) *The Astrophysical Journal* 797:30. [13] Hubbard A. (2015) *Icarus* 254:56−61. [14] Nagasawa M. et al. (2019) *The Astrophysical Journal* 871:110. [15] Arakawa S. and Nakamoto T. *The Astrophysical Journal* (in press).

THERMAL CONDUCTIVITY OF BIFRACTAL AGGREGATES: THEORETICAL INTERPRETATION.

S. Arakawa[1], M. Takemoto[1], and T. Nakamoto[1], [1]Department of Earth and Planetary Sciences, Tokyo Institute of Technology, 2-12-1 Ookayama, Meguro, Tokyo 152-8551, Japan. Email: arakawa.s.ac@m.titech.ac.jp.

Introduction: Understanding the thermal conductivity of dust aggregates is important for numerous topics in planetary science: for example, the thermal evolution of planetesimals is controlled by the thermal conductivity of dust aggregates [e.g., 1], the near-surface temperature distribution of comets and asteroids also depends on the thermal conductivity of surface dust layers [e.g., 2]. The thermal conductivity of dust aggregates depends on many physical parameters (e.g., the temperature, porosity, composition, radius of monomer grains), and there are many experimental [e.g., 3] and numerical [e.g., 4−6] studies on the thermal conductivity of dust aggregates. Recently, we revealed that the thermal conductivity through the solid network of dust aggregates is approximately proportional to the square of the filling factor [5,6]. However, the reason why the thermal conductivity is given by the power-law function of the filling factor was not yet revealed.

Theoretical prediction: Here we investigate the geometric structure of highly porous and fractal dust aggregates. We study the graph structure of fractal aggregates formed by the ballistic cluster-cluster aggregation process (hereafter BCCA; [7]) to understand the origin of this power-law dependence. It is known that the fractal dimension of BCCA aggregates is approximately 1.9 [e.g., 8] and the graph structure of BCCA aggregates is classified as a tree. Therefore the gyration radius R_{gyr} and the filling factor ϕ must be connected by the equation, $R_{\mathrm{gyr}} \sim \phi^{-1/(3-1.9)}$, and the number of the heat conduction path per unit area, σ, would be given by $\sigma \sim \phi^{2/(3-1.9)}$ for BCCA aggregates. The internal structure of compressed BCCA aggregates is bifractal: the fractal dimension is 3 for a large-scale structure but is 1.9 for a small-scale structure [9]. Therefore, we can predict the filling factor dependence of the thermal conductivity of compressed BCCA aggregates if we know the relation between the mean geodesic distance and the gyration radius of a BCCA aggregate.

Results. We calculated the geodesic distances of monomer grains within a BCCA aggregate. We found that the root mean square of the geodesic distance D_{rms} is given by $D_{\mathrm{rms}} \sim R_{\mathrm{gyr}}^{1.3}$ (Figure 1). The thermal conductivity of BCCA aggregates is inversely proportional to the geodesic distance per the gyration radius, $D_{\mathrm{rms}}/R_{\mathrm{gyr}}$, and is proportional to the number of the heat conduction path per unit area, σ. Therefore, the thermal conductivity of compressed BCCA aggregates f is proportional to $f \sim \phi^{2.1}$, as shown in Figure 2.
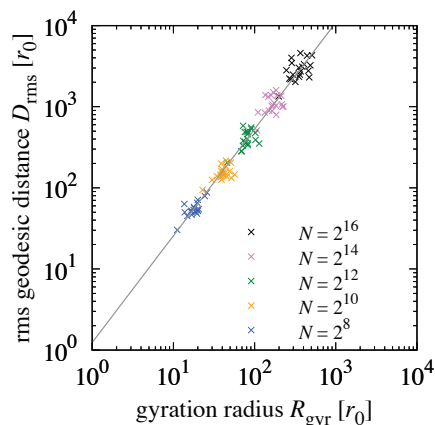

Figure 1. The mean geodesic distance D_{rms} and the gyration radius R_{gyr}. The number of monomer grains is $N = 2^8 - 2^{16}$.
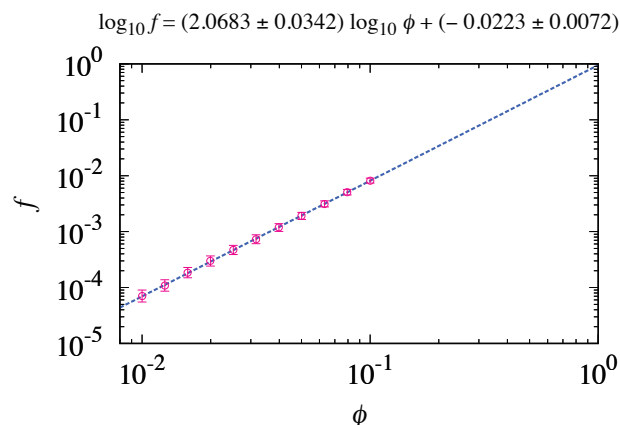
Figure 2. The normalized thermal conductivity f and the filling factor ϕ. The definition of f is described in Arakawa *et al.* [5,6].

References: [1] Henke S. et al. (2016) *Astronomy & Astrophysics* 589:A41. [2] Blum J. et al. (2017) *Monthly Notices of the Royal Astronomical Society* 469:S755−S773. [3] Sakatani N. et al. (2017) *AIP Advances* 7:015310. [4] Sirono S.-i. (2014) *Meteoritics & Planetary Science* 49:109−116. [5] Arakawa S. et al. (2017) *Astronomy & Astrophysics* 608:L7. [6] Arakawa S. et al. (2019) *Icarus* 324:8−14. [7] Meakin P. (1991) *Reviews of Geophysics* 29:317−354. [8] Okuzumi S. et al. (2009) *The Astrophysical Journal* 707:1247−1263. [9] Kataoka A. et al. (2013) *Astronomy & Astrophysics* 554:A4.

EXPERIMENTAL EVIDENCE FOR HIGH-PRESSURE TRANSFORMATION OF MERRILLITE AND Na-BEARING PHOSPHATES.

A. V. Arefiev[1], K. D. Litasov[1], A. Shatskiy[1], S. Greaux[2], and T. Irifune[2] [1]Sobolev Institute of Geology and Mineralogy SB RAS, 3 Koptyuga Ave, Novosibirsk, 630090, Russia (klitasov@igm.nsc.ru); [2]Geodynamic Research Center, Ehime University, 2-5 Bunkyo-cho, Matsuyama, Ehime, 790-8577, Japan.

Introduction: Merrillite and apatite are most important phosphate minerals in meteorites [1]. In the shock-melt veins of the heavily shocked chondrite and martian meteorites, apatite is often transformed to high-pressure polymorph tuite [2, 3], stable in static high-pressure experiments at pressures above 12 GPa [4]. Surprizingly, merrillite is also transformed to tuite-structured phase according to Raman spectroscopy and synchrotron X-ray diffraction [5, 6]. However, compositions of merrillite and apatite are different and no synthetic high-pressure phase of merrillite composition was obtained. In this work, we provide data on the synthesis of merrillite and some other Na-bearing phosphates at 15-20 GPa and show their relevance to high-pressure phosphates in meteorites.

Methods: Starting merrillite $Ca_9NaMg(PO_4)_7$ was synthesized from a mixture of phosphates in the experiment at 1 atm and 1450 °C for 3 hours. This merrillite, as well as a mixture of phosphates with the addition of Na-carbonate flux, was studied at pressures of 6, 15 and 20 GPa and 1400-1600 °C using multianvil technique at GRC, Ehime University.
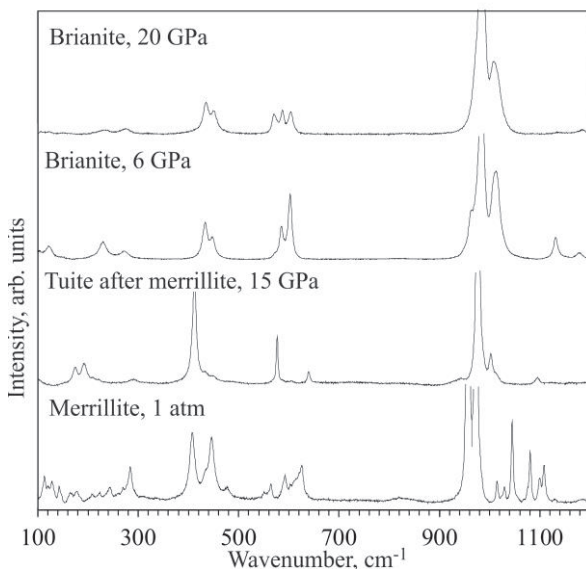

Fig.1. Raman spectra of synthesized merrillite and brianite at high-pressures.

Results and discussion: Examination of the obtained samples using Raman spectroscopy show that, at 15 and 20 GPa, merrillite has a spectrum similar to tuite (Fig.1), which is consistent with observations in chondrite and iron meteorites [5, 6]. Most likely, these phases are isostructural, and Mg and Na play the role of impurities in the $Ca_3(PO_4)_2$ tuite. Unfortunately, in these experiments, it was not possible to obtain large crystals of the high-pressure phase of merrillite. An additional phase in the experiments was phosphate with the composition of buchwaldite $Na(Ca_{0.75}Mg_{0.25})PO_4$. The Raman spectrum of this phosphate differs from the spectrum of buchwaldite at 1 atm and has poor quality. In runs with a mixture of phosphates and carbonate flux at 15 and 20 GPa, merrillite did not crystallize. The products of the experiments were tuite and Na-phosphate with composition corresponding to brianite $Na_2MgCa(PO_4)_2$ (Fig.1). The Raman spectrum of this phase at 15 and 20 GPa correspond to brianite at 1 atm and 6 GPa, which indicates its strong stability at high pressures at least up to 20 GPa.

The solvent in the form of alkaline carbonatite melt was not formed since all Na was bound to phosphates. The carbonate phase was represented by magnesite. As a result of the experiments, it was found that the Na-carbonate melt is not a reasonable flux for the crystallization of high-pressure phosphates. Perhaps an appropriate solvent is potassium carbonate, which is planned to be used in subsequent experiments.

References: [1] Rubin A. E. and Ma C. (2017) *Chemie der Erde Geochem.* 77: 325-385. [2] Xie X. et al. (2003) *Eur. J. Mineral.* 15: 1001-1005. [3] Tomioka N. and Miyahara, M. (2017) *Met. Planet. Sci.* 52: 2017-2039. [4] Murayama J. K. et al. (1986) *Phys. Earth Planet. Inter.* 44: 293-303. [5] Xie X. et al. (2013) *Met. Planet. Sci.* 48: 1515-1523. [6] Litasov K. D. and Podgornykh N. M. (2017) *J. Raman Spectr.* 48: 1518-1527.

INVESTIGATING VOLCANISM WITHIN IMBRIUM AND SERENITATIS BASINS: A SYSTEMATIC STUDY OF BASALTIC REGOLITH FRAGMENTS.

V. Assis Fernandes[1,2], P. Czaja[2], L. Fawcett[1], R.O.C. Fonseca[3], A. Khan[4], C. Liebske[4], A. Nemchin[5], J. Sliwinski[4], J. Snape[6], M. Whitehouse[7] & M. Willbold[8], [1]SEES, Univ. Manchester, Oxford Rd., M13 9PL Manchester, U.K., veraafernandes@yahoo.com, [2]Museum für Naturkunde-Berlin, Invalidenstr. 43, 10115 Berlin, Germany, [3]Inst. Geologie und Mineralogie, Univ. Cologne, [4]ETH-Zürich, Switzerland, [5]Curtin Univ., Perth, Australia, [6]VU-Amsterdam, The Netherlands, [7]NordSIM, Naturhistoriska riksmuseet, Stockholm, Sweden, [8]Geowissenschaftliches Zentrum, Göttingen Univ., Göttingen, Germany.

Introduction: From remote sensing data obtained by different lunar orbiters, there is a clear dichotomy between a KREEP-enriched terrain (containing heat-producing elements and covering most of the nearside of the Moon) and a KREEP-depleted terrain (the remainder of the Moon). Most lunar volcanism ocurred within the KREEP-rich terrain where the lunar crust is also thinner. Imbrium Basin is located within the KREEP-enriched terrain, whereas most of Serenitatis Basin is outside of it. Visible and spectral images of the interior of the Imbrium and Serenitatis Basins reaveal 30 and 29 spectrally different lava flows, respectively. Considering the continuous "gardening" of the lunar surface resulting from the continued cratering, it is conceivable that ejecta material formed by small craters on different lava flows travelled to where the Apollo 15 and 17 landing sites are located, enabling access to "rocks" (2-4 mm, ~50 mg, basaltic fragments) that formed 100-1000 kms from the landing site. Small craters in the vicinity of the landing sites excavated both the local stratigraphy and potentially also exposed some of this distant material.

Samples and Methods: In this presentation will be reported results from the systematic study of Apollo 15 and Apollo 17 basaltic regolith fragments (2-4 mm Ø) collected along the ejecta of small craters. Each fragment was characterized petrographically (SEM), geochemically (EMPA), chronologically ($^{40}Ar/^{39}Ar$ step-heating & in-situ U-Pb), and for its trace-element composition (LA-ICP-MS). Figure 1A shows phase identification and vol% determination used for estimation of bulk composition; Figure 1B shows a 30 heating steps $^{40}Ar/^{39}Ar$ age spectrum corresponding to an age of 3659±35 Ma.
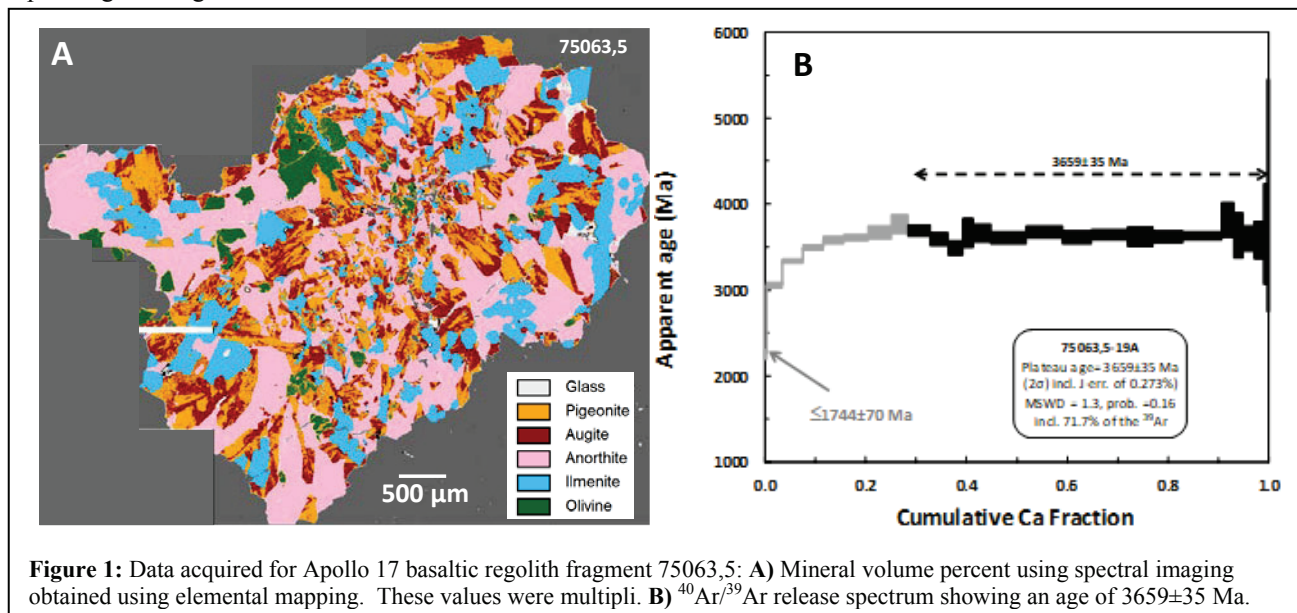

Figure 1: Data acquired for Apollo 17 basaltic regolith fragment 75063,5: **A)** Mineral volume percent using spectral imaging obtained using elemental mapping. These values were multipli. **B)** $^{40}Ar/^{39}Ar$ release spectrum showing an age of 3659±35 Ma.

Results: Data show that the regolith basalts comprise an array of compositions, the age of Apollo 17 fragments ranges between 3.66 Ga and 4.01 Ga extending the known range towards older ages, whereas Apollo 15 fragments range between 3.16 and 3.90 Ga. Mineral trace-element data suggest compositions outside the known range.

Preliminary findings: Using thermobarometry, estimated pressure (depth) and temperature of basaltic magma generation were similar to those calculated when using Apollo 15 and 17 bulk compositions reported in the literature. This suggests that it is possible to have lithic-representability out of 2-4 mm Ø regolith basaltic fragments.

THE INFLUENCE OF INCLUSIONS ON THE FORMATION OF METAL STRUCTURE IN ATAXITES

K.A. Badekha[1,2], V. I. Grokhovsky[1] and G.A Yakovlev[1], [1]Institute of Physics and Technology, Ural Federal University, Ekaterinburg, 620002, Russian Federation, e-mail: Ksenia_uimina@mail.ru, [2] Vernadsky Institute of Geochemistry, Kosigina str., 19, Moscow, 119991, Russian Federation.).

Introduction: Plessite microstructure is formed from taenite: γ (fcc) $\rightarrow$ α_2(bcc)+γ(fcc) $\rightarrow$ α(bcc)+γ(fcc) at different temperature and Ni concentration in accordance with Fe-Ni phase diagram [1]. There are four morphological types of martensitic structure: lath (packet); butterfly; lenticular and thin plate martensite[2]. It is observed in Fe-Ni artificial and meteorite alloys. Nearby nonmetallic inclusions in high-Ni meteorites (15-20 wt.% Ni) is in focus of our interest. Chemical composition revealed that the metal surrounding FeS-$FeCr_2S_4$ inclusions contain higher Ni concentration and small inclusions of $(FeNi)_3P$ that altogether influences the temperature of bainite transformation in the region and forwards the nucleation of the oriented structure of plessite. EBSD method was applied to reveal crystallographic orientations in plessite.

Experimental: Seven meteorites were studied in the current work: Hoba (16,56 wt.% Ni, 0,07 wt.% P), Cape of Good Hope* (16,3 wt.% Ni, 0,12 wt.% P), Tawallah Valley (17,6 wt.% Ni, 0,10 wt.% P) and Iquique (16 wt.% Ni, 0,09 wt.% P) IVB members and also some close relative to the group ataxites: Chinga (16,58 wt.% Ni, 0,05 wt.% P) and Gebel Kamil (20,7 wt.% Ni, 0,16 wt.%P), El Qoseir (14,0%Ni, 0,7% Co, 0,16%P) [3]. The meteoritic metal microstructure was examined using Zeiss Axiovert 40 MAT inverted microscope and FE-SEM $\sum$IGMA VP electron microscope with EBSD and EDS units.

Results and Discussion: Meteorites sections demonstrated the various amount of inclusions. The sections of Hoba and Iquique meteorite demonstrated quite rare small (50x5 μm and 3x2 μm) inclusions of troilite FeS and daubréelite $(FeNi)_3P$ of comparable size with irregular shape rarely in the intergrowth but no laths. Several large (0,5-3 mm) troilite-daubréelite inclusions of rectangular and rounded shape in Hoba were surrounded by oriented plessite. Numerous inclusions of troilite FeS and Cr_2FeS_4 appear to be the nucleus for the α-spindeles (Fig. 1 a,b). Schlieren bands [3, 4] cross the whole samples of the meteorites and are not disturbed by the inclusions, even in Hoba, where plessite structure differs nearby large inclusions.

Schlieren bands in Chinga are well defined [3, 5] with rare inclusions. The authors [5] gave us a few examples of the troilite-daubréelite intergrowth in the form of laths with enrichment of V and Mn – the same we observed in Cape of Good Hope (Fig. 1 c,d). Plessite surrounding the inclusions and the embryos of the α-phase is well distinguished with an optical microscope in Hoba and Iquique meteorites, is well distinguished and grossly structural in Gebel Kamil, Tawallah Valley and El Qoseir meteorites (Fig. 1 a), poorly soluble in Chinga [4].
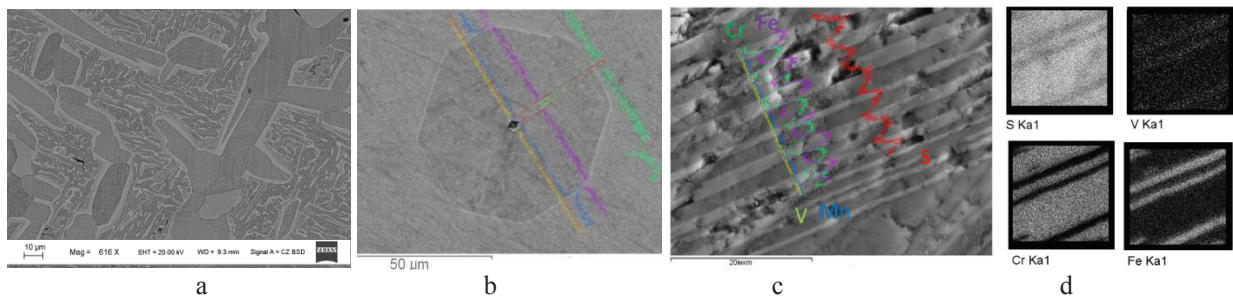

Figure 1 – FeS-$FeCr_2S_4$ inclusions in the ataxites: a - SEM-images El Qoseir (14,0%Ni, 0,7% Co, 0,16%P), b - An example of the growth of the α-phase embryo around the inclusion of daubreelite in the cross section in Cape of Good Hope, c - troilite and daubreelite lamela with elements profiles: Fe, Cr ,S, Mn, V in Cape of Good Hope, d- elements distribution in the inclusion (c).

The largest α-spindeles are stretched parallel to the border of the Schlieren bands. EDS –analysis proved that about 30% of the α-phase nuclei of Gebel Kamil and Tavallah Valley and Hoba nearby the large inclusions of FeS-$FeCr_2S_4$, $(FeNi)_3P$ contain micro-inclusions of schreibersite, and also chromites and troilite [3].

References: [1] Yang C.-W. et al. 1996. *Phase Equilibria 17*: 522–531. [2] Cahn R. W. and Haasen P. (2014) *Physical Metallurgy (Fifth Edition)* 9: 1021–1072. [3] Buchwald V.F., 1975. *University of California Press*, Berkley, CA. [4] Grokhovsky V. I. et al. 2014 *Meteoritics & Planetary Science* 49: A5364. [5] Buchner E. et al. 2012. *Meteoritics & Planetary Science*. 47: 1491–1501.

OXYGEN ISOTOPE SYSTEMATICS OF ORDINARY CHONDRITE CHONDRULES AND THEIR MAIN CHONDRULE POPULATION

L. Baeza[1], T. R. Ireland[1], J. N. Ávila[1], G. Mallmann[1]. [1] Research School of Earth Sciences, The Australian National University. email: leonardo.baeza@anu.edu, trevor.ireland@anu.edu.au

Introduction: Chondrites are cosmic breccias with well defined bulk O-isotope compositions on the triple-O diagram [1]. However, it appears that each chondrite contains specific groups of chondrules with distinct $\Delta^{17}O$ ratios (= $\delta^{17}O-0.52\times \delta^{18}O$) and 'chondrule populations' have been suggested but never statistically assessed [2]. We focus on the *in situ* O-isotope of chondrule olivine from unequilibrated ordinary chondrites (OCs) of the different iron groups (H, L, and LL) and performed high precision ion microprobe O-isotope analysis using the Sensitive High Resolution Ion Microprobe – Stable Isotopes (SHRIMP-SI) at The Australian National University. Nine unequilibrated OCs were studied: WSG95300 (H3.3), QUE93030 (H3.6), ALHA77299 (H3.7), GRO06054 (L3.05), DOM10556 (L3.1), MIL 05050 (L3.1), LAR06279 (LL3.8), LAR06301 (LL3.8), and LAR12034 (LL3.8). A statistical treatment of chon-drule populations in OCs, and chondrites in general, would provide further insight about chondrule formation envi-ronments, the processes involved in those regions, and the solid dynamics of the protoplanetary disk [3, 4].

Results and discussion: 794 olivine grains from 537 chondrules were analyzed. Most of the measurements plot above the terrestrial fractionation (TF) line in the $\delta^{18}O$ vs. $\delta^{17}O$ diagram (Fig. 1A). This distinctive feature is clearer when exploring the probability density function (PDF) of the $\Delta^{17}O$ value of the studied chondrules showing a unimodal bell-shaped distribution peaking between 0‰ and 2‰ no matter the host chondrite group (Fig. 1B). This suggests that OCs accreted one main chondrule population, in agreement with the assertion of [4]. To statistically evaluate that OCs sampled the same population(s) of chondrules, a Kolmogorov-Smirnov test was applied to the chondrule $\Delta^{17}O$ distri-butions. The test confirms that the samples have the same continuous distribution at the 95% confidence interval ($\sigma_{95\%}$), meaning that the probability for the $\Delta^{17}O$ chondrule distribution to be different between the H, L, and LL samples is 5%. Therefore, OCs incorporated chondrules into their parental bodies that are statistically the same, in terms of their oxygen isotope composition.
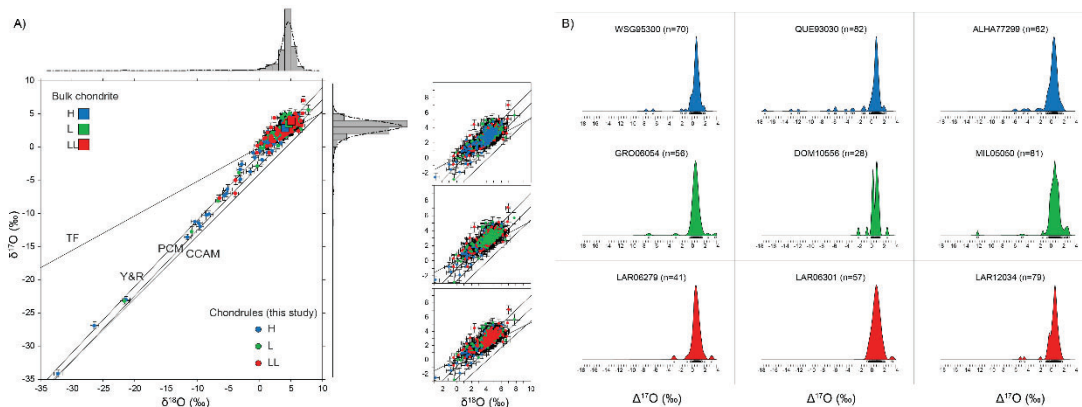

Fig. 1. A) O-isotope ratios of chondrules per OC group. PDFs of $\delta^{18}O$ and $\delta^{17}O$ and a zoom in are shown. TF, Y&R [6], PCM [7], and CCAM [8] lines are shown for reference. Bulk equilibrated OCs compositions are from [5]. B) PDFs of chondrule $\Delta^{17}O$ per meteorite sample.

In order to constrain the boundaries of the main chondrule population, all $\Delta^{17}O$ data from H, L, and LL chondrites were merged into one database. This allows to exploit the sample size on behalf of finer statistics for the population. The preferred method to estimate the mean of this population is the weighted mean at $\sigma_{95\%}$. After this analysis, the MSWD statistic of the sample is 1.12, allowing to infer that the chondrule sample was drawn from a single population, ergo the main chondrule population of OCs. The main chondrule population is characterized by a $\Delta^{17}O$ weighted mean of 0.72 ± 0.08‰ (external error, $\sigma_{95\%}$) with a variability of 0.50‰ (2SD, $\sigma_{95\%}$). It is stated then that OCs accreted a majority of chondrules that formed in a location of the protoplanetary disk dominated by an oxygen isotope gaseous reservoir of $\Delta^{17}O$ ~0.7‰. The consequences of having such a sample distribution of $\Delta^{17}O$ chondrule compositions in OCs is relevant considering its predictive power. This will be discussed at the conference.

References: [1] R. N. Clayton (1993). *Ann. Rev. Earth Planet. Sci* 21:15–149. [2] Tenner T. et al. (2018). *Chondrules: Records of Protoplanetary Disk Processes*, pp. 196-246. [3] Kita N. T. et al. (2017) Chondrules as Astrophysical Objects, Abstract#1975. [4] Jones R. et al. (2018) *Chondrules: Records of Protoplanetary Disk Processes*, pp. 57-90. [5] Clayton R. N. et al. (1991). *Geochimica et Cosmochimica Acta* 55(8): 2317–2337. [6] Young E. D. and Russell S. S. (1998). *Science*, 282, 5388:452-455 [7] Ushikubo T. et al. (2012). *Geochimica et Cosmochimica Acta* 90: 242–264. [8] R. N. Clayton et al. (1977). *Earth and Planetary Science Letters* 34(2):209-224.

SUPERIMPOSED PROCESSES IN CHONDRULES OF THE OCHANSK METEORITE

A.I. Bakhtin[1], R.Kh. Sungatullin[1], A.V. Gusev[1], A.A. Eskin[1], D.M. Kuzina[1]
[1]Kazan Federal University, Institute of Geology and Petroleum Technologies, Russia, Kazan, Kremlyevskaya st., 18.
E-mail: Rafael.Sungatullin@kpfu.ru

Introduction: The Ochansk meteorite belong to group of olivine-bronzite H-chondrites [1-3]. It is intensively brecciated and is represented by a disorderly mixture of silicate chondrules, their breaks and their fine-grained matrix enclosed by silicate minerals, interstitial silicate glass and ore minerals (kamacite, troilite). The chondrules fill about one third of the meteorite volume. Their size is usually 0.2-0.9 mm. They consist of olivine, bronzite, diopside, plagioclase. Often they contain silicate glass.

Methods: In study of the Ochansk meteorite we used following methods and instruments: 1) microprobe analysis on scanning electron microscope XL-30 from Philips with EDAX; 2) X-ray fluorescence analysis on the Bruker S8 Tiger analyzer; 3) X-ray diffraction analysis on P2 Phaser diffractometer from Bruker; 4) crystal-optical study of petrographic sections on microscope from Zeiss; 5) ThermoGravimetry (TG) - Differential Scanning Colorimetry (DSC) Analyser STA/TG-DSC NETZSCH STA 449F3.

Results: The following processes were identified that participated in formation of chondrules: 1) cooling and recrystallization of melts formed during melting of ProtoSolar Nebula substance as result of Supernova explosion in its vicinity; 2) collisions of chondrules and initial melts with each other; 3) high-temperature autometasomatic transformations in chondrules; 4) superimposed low-temperature processes: hydrocarbonization, carbonatization, silicification, serpentinization, chloritization.

Discussion: The stationary cooling mode of chondrite melts caused formation of the dominant granular structures for chondrules in the Ochansk meteorite. Less common are the radiant, grate and glassy structures of chondrules, indicating their formation from supercooled silicate melts. When a chondrules collide, oval dents are noted on their surface, and cracks appear inside the chondrules, which are sometimes filled with residual melts of the impacting chondrules, causing glassy and microgranular veinlets and nests in chondrules. The residual silicate melts cause high-temperature autometasomatic transformations in chondrules: orthopyroxene develops on olivine, and clinopyroxene (diopside) develops on orthopyroxene. Low-temperature superimposed processes in chondrules were expressed in formation of calcite, magnesite, quartz, serpentine, chlorite, and accumulations of hydrocarbons. The latter showed effect of "boiling" - gas emission under the action of microscope electron beam, and in thermal analysis of bitumen accumulation generated an exothermic peak on DSC curve and weight loss on TG curve at 330ºC. The thermograms also show the effects of serpentine dehydration (150°C), dissociation of magnesite, chlorite (595°C), and calcite (870°C).

Conclusions: The chondrules and Ochansk meteorite substance underwent secondary low-temperature (hydrothermal) transformations. It can be assumed that the substance of future Ochansk meteorite was located in near-surface zone of parent body, in which the processes of internal differentiation of its substance took place, and in its near-surface part they were expressed in development of hydrothermal processes with addition of H_2O, CO_2, CO, Si, Ca, Mg, K, Na and hydrocarbons. These processes led to the hydrocarbonization, carbonatization, silicification, serpentinization, chloritization.

References: [1] Bakhtin A.I. et al. 2017. Meteoritics & Planetary Science. 52(S1): A15. [2] Kaushal S.K., Wetherill G.W. 2016. J. Geophys. Res. 158: 569-582. [3] Marakushev A.A. et al. 1992. Space Petrology, M. MGU. 325p.

A MULTI-TECHNIQUE ANALYSIS OF THE PARIS METEORITE TO CHARACTHERIZE ITS ORGANIC CONTENT *"IN SITU"*, WITHIN ITS MINERAL MATRIX

D. Baklouti[1], M. Noun[2,3], R. Brunetto[1], F. Borondics[4], T. Calligaro[5], Z. Dionnet[1], and S. Della-Negra[2], [1]Institut d'Astrophysique Spatiale, CNRS/Université Paris-Sud, Université Paris-Saclay, bâtiment 121, 91405 Orsay Cedex, France. (donia.baklouti@ias.u-psud.fr), [2]Institut de Physique Nucléaire d'Orsay, CNRS/Université Paris-Sud, Université Paris-Saclay, 91405 Orsay Cedex, France, [3]Lebanese Atomic Energy Commission, CNRSL, Beirut, Lebanon, [4]Synchrotron Soleil, L'Orme des Merisiers, BP48, Saint Aubin, F91192 Gif sur Yvette, France, [5]Centre de Recherche et de Restauration des musées de France, UMR 171, Palais du Louvre, 75001 Paris, France.

Introduction: The Paris meteorite is the least altered CM2 classified so far [1], and thus, a good witness of the Solar System early history. The first objective of this study is to analyze the mineral and organic composition of a raw chunk of the Paris chondrite without any preliminary preparation or extraction of the sample. The aim is to obtain simultaneous chemical characterization of organic and mineral phases while preserving their spatial distribution within the meteorite fragment. The second objective is to obtain laboratory spectroscopic measurements which can be compared to data obtained by space missions as well as by remote observations of cometary dust and asteroid surfaces.

Materials and methods: This study is carried out by coupling typical remote sensing tools (IR and visible reflectance spectroscopies) to TOF-SIMS (Time-Of-Flight Secondary Ion Mass Spectrometry), a high spatial resolution technique that was embarked on the Rosetta space mission (the COSIMA instrument [2,3,4]), and that is planned to be performed on future collected asteroidal samples [5,6]. Both mid-IR spectroscopy and TOF-SIMS are performed in imaging mode with a spatial resolution of a few micrometers for the first and 1 to 2 μm for the latter. We also add micro-Raman and micro-PIXE measurements of the same sample area as an independent confirmation or clarification of the mineral composition, in order to have a better understanding of the mineralogical context of the organic moieties and components found by TOF-SIMS and IR. The depths of analysis of these different methods are: from a few hundreds of nm to a few μm for the IR and Raman spectroscopies depending on material absorptivity, from 10 to 20 μm for micro-PIXE, the first 10 nm from the surface for static SIMS, and up to a few 100 nm for dynamic SIMS (3D imaging using argon cluster gun).

Results and discussion: The matrix of Paris is found to be as dark as the very dark asteroids Ryugu and Bennu currently visited by Hayabusa2 and OSIRIS-REx [7,8]. By combining the results given by micro-PIXE, TOF-SIMS and IR and Raman micro-spectroscopies, we are able to show the different stages of hydration and amorphization of the amorphous silicate phase dominating the matrix of the analyzed Paris fragment. The infrared signatures of water and hydroxyl groups mapped for a chosen large area (500 x 500 μm²) of the meteorite fragment give a good idea of the circulation of the fluid that partially altered the amorphous silicate phase. TOF-SIMS, one of the rare techniques allowing the simultaneous and micrometric analysis and mapping of organic and mineral mixed phases, gives an interesting insight on the organic matter composition and its systematic spatial association with the partially hydrated amorphous silicate phase and iron under different states. This latter result illustrated in previous studies of other carbonaceous chondrites [9,10] together with the detection by TOF-SIMS of metal-containing organic moieties, emphasizes the important and specific interaction that must take place between the mineral phase and the organic material.

References: [1] Hewins, R. et al. (2014) *Geochimica et Cosmochimica Acta*, 124:190–222. [2] Kissel, J. et al. (2007) *Space Science Reviews*, 128:823-867. [3] Hilchenbach, M. et al. (2016) *The Astrophysical Journal Letters*, 816:L32. [4] Bardyn, A., Baklouti D. et al. (2017) *Monthly Notices of the Royal Astronomical Society,* 469:S712-S722. [5] Uesugi, M. et al. (2014) *Earth, Planets and Space*, 66:102. [6] Naraoka, H. et al. (2015) *Earth, Planets and Space*; 67:67. [7] Kitazato, K. et al. (2019) *Science,* 364:6437:272-275. [8] Hamilton, V.E. et al. (2019) *Nature Astronomy*, 3:332-340. [9] Le Guillou, C. et al. (2014) *Geochimica et Cosmochimica Acta*, 131:344–367. [10] Le Guillou, C. et al. (2014). *Geochimica et Cosmochimica Acta*, 131:368–392.

MINERALOGY AND SPECTROSCOPY (VNIR AND FTIR) OF MUKUNDPURA CM2:MORE INSIGHTS INTO THE AQUEOUS ACTIVITY AND POST ACCRETION HISTORY

S. Baliyan[1], H. Moitra[2], S. Sarkar[3], D. Ray[1], D.K. Panda[1], A.D. Shukla[1], S. Bhattacharya[3] and S. Gupta[2] [1]Physical Research Laboratory, Ahmedabad 380009, India (shivanib@prl.res.in). [2]Indian Institute of Technology, Kharagpur 721302, India, [3]Space Application Centre, Ahmedabad 380015, India.

Introduction: The mineralogy of CM2 chondrites is very intriguing due to the higher phyllosilicate content (~70-80 vol%) in their matrix. Additionally, with the fine-grained nature of the matrix and difficulty in identifying crystalline and amorphous phases, the mineralogy of CM2 chondrites remains poorly constrained. Thus, using XRD for identification and quantification of phases is very useful for precise mineralogical characterisation. The VNIR and FTIR studies further facilitate proper identification of hydrous phases and therefore provide insights into the aqueous process occuring in the parent asteroids of the early Solar System. Laboratory studies of CM chondrites have further applications in linking remotely acquired spectra from the primitive asteroid targets during Hyabusa 2 (Ryugu) and OSIRIS REx (Bennu) missions. In this study, we examine the mineralogy and spectral characters of a newly fallen meteorite Mukundpura CM2 (June 6, 2017) and conduct phase identification, quantification and precise characterisation of the hydrated minerals vis-a-vis the extent and mineralogy of the alteration.

Results and Discussion: Preliminary petrography of Mukundpura CM2 has been previously described elsewhere [1]. The most striking features of the matrix are occurrences of variegated clasts with distinct FeO-enriched rims. Otherwise, flaky serpentine is also common and appears to grow either from the clast boundary or within the clast interior. The matrix serpentine includes Mg-rich (with more or less stoichiometric composition), intermediate Fe (FeO ~22-30 wt%) and high Fe (FeO ~38-45 wt%) types. The Mukundpura matrix corresponds well within the known field of CM phyllosilicate. However, there is a slight deviation in serpentine solid solution probably due to lack of crystallinity of many phases in the matrix. The calculated MAI (Mineralogical Alteration Index) is 0.42 [2]. The FeO/SiO_2 and S/SiO_2 of high-Fe bearing clasts range between 1.46-2.42 and 0.08-0.53 respectively [3]. XRD of bulk samples reveal majority of Mg and Fe serpentine and minor calcite in the marix. The Visible Near Infrared (VNIR) spectrum of Mukundpura CM2 shows distinct absorption bands near 0.72, 0.91, 1.12, 1.94 and 2.24 μm. Mixed-valence serpentine-group phyllosilicates are the strongest contributors to the absorption band around 0.72 μm [4]. This serpentine-group along with their Fe rich varieties is likely to be responsible for the absorption near 0.91 μm. The broad absorption band centered at 1.12 μm may be related by the presence of forsteritic olivine in chondrules or within the matrix [1]. The broad absorption feature centered at around 1.94 μm is attributed to the combination of H-O-H bend with the OH stretches of the water molecules attached to the phyllosilicates [5]. The absorption feature around 2.24 μm is related to the presence of serpentine minerals. The prominent absorption features of the FTIR spectrum of the Mukundpura CM2 shows a sharp absorption band around 1000 cm^{-1}, peaking at 985 cm^{-1}, an absorption band centred at about 633 cm^{-1}, followed by a small peak at 579 cm^{-1}; a broad absorption band around 450 cm^{-1} with distinct peaks at 445 cm^{-1}, 454 cm^{-1} and 461 cm^{-1} and shoulders at 406 cm^{-1}, 419 cm^{-1}, 502 cm^{-1}, 546 cm^{-1} and 564 cm^{-1}; two separate absorption bands centred at 1629 cm^{-1} and 1423 cm^{-1} and a broad absorption band between 2900-3700 cm^{-1}. The sharp, single-peak nature of the absorption around 1000 cm^{-1} suggests that the Si-O stretch vibrations primarily represent saponite [6]. This, along with the lower frequency of the peak centred at 985 cm^{-1}, shows the lack of any signature of highly crystalline phases like olivine or pyroxene in this band. The absorption band between 600 and 700 cm^{-1}, centred at 633 cm^{-1}, can be attributed to the OH-librations of the phyllosilicates. The narrow absorption band centred at 1423 cm^{-1} can be attributed to υ3 asymmetric stretch of calcite. The υ2 and υ4 IR active bands of calcite are supposed to be at 879 and 680 cm^{-1}, respectively [7]. The other narrow absorption band centred at 1629 cm^{-1} can be assigned to the bending vibrations in H_2O attached to the phyllosilicates. The broad absorption band between 2900 cm^{-1} and 3700 cm^{-1} is due to the OH-stretch in the H_2O molecules attached to the minerals as well as in the hydroxyl ions of the phyllosilicates.

Summary: Our integrated mineralogic and spectroscopic data suggests Mukundpura CM2 experienced modest degree of aqueous alteration. Matrix clasts suffered varied extents of aqueous alteration inducing formation of crystalline and amorphous phyllosilicates in matrix. The intermix of Mg-Fe serpentine and "Fe-rimed" clasts suggests pervasive aqueous alteration is likely achieved locally. However, presence of anhydrous silicate clasts and relict chondrules suggest that the alteration is incomplete or possibility of incorporation of variously altered clast and correspond to the variability of geochemical conditions during the aqueous alteration preferably aftermath the accretion of the parent body.

References: [1] Ray, D. R. and Shukla, A.D. (2018) *PSS* 151:149–154. [2] Browning L. B. et al. (1996) *GCA* 60:2621-2633. [3] Rubin A. E. et. al. (2007) *GCA* 71:2361-2382. [4] Cloutis E.A. et al. (2011) *Icarus* 216:309-346. [5] Clark R. N. (1999) *Remote sensing for the Earth Sciences*, 3:3-58. [6] Beck P. et. al. (2014) *Icarus* 229:263-277. [7] Farmer V.C. (1974) *The Infrared spectra of minerals*. Mineralogical Society, London.

DIAMOND METEORITES BETWEEN SCIENCE AND LEGENDS

Aly A. Barakat
Sukari Gold Mines, Egypt- email: alybarakat20000@gmail.com

Introduction: Much early human beings speculated that diamonds connect with extraterrestrial sources. The native folklore version regarding the origin of the Vaal diamonds of South Africa reflects these speculations, as it says [1, pp. 47]: "after the passing of many moons, and when there was great sorrow in the land, a spirit, pitying the wants and miseries of men, descended from heaven with a huge basket filled with diamonds. The spirit flew over the Vaal, starting beyond Delpoort's Hope, sowing diamonds as be flew on, past Barkly West, Klipdam, and on towards Kimberley, throwing out handful after handful from the huge basket all the while. On reaching Kimberley, where at the time large trees were growing, his toe got caught in the branches of a high kameeldoorn tree, and, tripping, be upset the basket, emptying out all the diamonds; thus forming the Kimberley mines!". Realization the terrestrial volcanic pipes as a source of diamonds after the discovery of the South Africa diamonds in 1867, did not rule against the assumptions that heavenly processes contribute to the terrestrial diamonds.

Extraterrestrial Diamonds: Haidinger in 1846 described a cubic form of graphite crystals in Arva, Hungary, iron meteorite, which Gustave Rose suggests that the crystals are pseudo morphs after diamond [2]. Discovery of tiny grains of diamond in Nova Yori meteorite in 1888 followed by reporting micro grains of diamond in the Canyon Diablo meteoritic iron fragments, in 1891[2], reintroduced the legends regarding the extraterrestrial sources of diamonds, e.g. the legend of the "blazing star", to the scientific community. Therefore, in 1912, a group of scientists and financiers organized a syndicate for locating the "blazing star", believed to be one solid diamond, which according to the legend, fell ages ago in the Arizona Desert [1] in the fall site of Canyon Diablo meteorite. In the meantime, A. Meydenbauer [3] suggests that the diamond of the earth is of cosmic origin, having fallen as a meteorite at later periods of the earth's formation. In his comment on this hypothesis, Sir William Crookes [4, pp. 135-136] states: "according to this hypothesis, the so-called volcanic pipes are simply holes bored in the solid earth by the impact of monstrous meteors the larger masses boring the holes, while the smaller masses, disintegrating in their fall, distributed diamonds broadcast. Bizarre as such a theory appears, I am bound to say there are many circumstances which show that the notion of the heavens raining diamonds is not impossible".

On the other hand, researchers, e.g., L. Nikolaev [5] denies the occurrence of diamond meteorites, considering diamond in meteorites is quite rare and only a few diamond-containing meteorites are known. Nevertheless, the scientific research indicates that diamonds is one of the solid minerals made by stars, [e.g. 6-7].

The First Identified Diamond Meteorite: The first solid evidence of the possible common existence of diamond meteorites may come from the discovery of diamond-rich carbonaceous pebble, in 1996 from the Libyan glass area southwestern Egypt [8], which studies [e.g., 9] indicate that it is of extraterrestrial origin with tendency to consider it of pre solar formation. This pebble-seized material, which known as "Hypatia stone", consists of visible diamond grains. Realization the extraterrestrial source of this diamondiferous material came accidently for its association the Libyan glass, which has been received considerable scientific interest. This may indicate the existence of other diamondiferous meteoritic materials that do not receive the required investigations to clarify their sources. This discovery calls attention to the possible occurrence of diamond meteorites [10], a topic, which is slowly rolling away from the realm of legends to science. We may find in the near future an additional class of meteorites, called "diamond meteorites", within the present day known classes. Who knows?

References:
[1] Beet, G; Terpend, T. L (1917): Romance and reality of the Vaal diamond diggings. Kimberley: *Diamond Fields Advertiser*.
[2] Farrington, O. C. (1915): Meteorites; their structure, composition, and terrestrial relations. *Chicago, U. S. A*.
[3] Meydenbauer, A. (1980): *Chemical News,* lxi, 209.
[4] Crookes, W. (1909) Diamonds. *Harper & Brothers*.
[5] Nikolaev, L. (1976) Space chemistry. *Mir Publishers, Moscow*.
[6] Kwok,S. (2013) Stardust: The Cosmic Seeds of Life. *Springer-Verlag Berlin Heidelberg*.
[7] Srinivasan, G. (2014) Life and Death of the Stars. *Springer-Verlag Berlin Heidelberg*.
[8] Barakat, A.A. (2012) The precious gift of meteorites and meteorite impact processes. *Nova Science Publishers, New-York, USA*.
[9] Barakat, A.A. (2018) Meteorite impact signs in the Libyan glass area, southwestern Egypt. *LAP LAMBERT Academic Publishing*.
[10] Belyanin, G.A., et al., (2018) *Geochim. Cosmo. Acta*. 223, 462–492.

BOSUMTWI IMPACT STRUCTURE: EVIDENCE FOR FLUIDIZED EMPLACEMENT OF THE EJECTA.

D. BARATOUX[1], Cheikh Ahmadou Bamba NIANG[2,3], Wolf Uwe REIMOLD[4], Marian Selorm SAPAH[5], Mark Walter JESSELL[1,6], Daniel BOAMAH[7], Gayane FAYE[8], Sylvain BOULEY[9], and Olivier VANDERHEAGHE[1] [1]Géosciences Environnement Toulouse, UMR5563, CNRS, Université de Toulouse & IRD, 14, Avenue Edouard Belin, 31400 Toulouse, France [2]Institut Fondamental d'Afrique Noire Cheikh Anta Diop, Dakar, Senegal, [3]Département de Géologie de l'Université Cheikh Anta Diop, Dakar, Senegal, [4]Institute of Geosciences, Laboratory of Geodynamics, Geochronology and Environmental Science, University of Brasília, Brasília, Brazil [5]Department of Earth Science, University of Ghana, Accra, Ghana [6]Centre for Exploration Targeting, School of Earth Sciences, The University of Western Australia, 35 Stirling Highway, Crawley, Western Australia 6009, Australia [7]Geological Survey Department, Accra, Ghana [8]Institut des Sciences de la Terre, Laboratoire de Télédétection Appliquée, Université Cheikh Anta Diop, Dakar, Senegal [9]GEOPS — Géosciences Paris Sud, Univ. Paris-Sud, CNRS, Université Paris-Saclay, Rue du Belvédère, Bât. 504-509, 91405 Orsay, France

Introduction: The about 10.5 km diameter Bosumtwi impact crater is one of the youngest large impact structures on Earth. The crater rim is readily noticed on topographic maps or in satellite imagery [1,2]. It defines a circular basin filled by water (Lake Bosumtwi) and lacustrine sediments. The morphology of this impact structure is also characterized by a circular plateau extending beyond the rim and up to 9–10 km from the center of the crater (about 2 crater radii). This feature comprises a shallow ring depression, also described as an annular moat, and a subdued circular ridge at its outer edge. The origin of this outermost feature has remained debated and could either correspond to the limit of an ejecta deposit, or to a ring fault [2].

Objective: In order to determine the origin of the topographic features observed outside of the rim, we combine the analysis of the topography and roughness at different scales using SRTM denoised data, with airborne radiometric data (Fig. 1) and field observations made in November 2017 [3].

Results: We report an association between rough topography, surface exposure of fresh rocks, and a K-rich annulus (see Fig. 1). These regions are currently being eroded and expose fresh outcrops of metasediments. In contrast, the K-poor areas within the moat are associated with smooth surfaces and a lateritic cover that likely developed since the time of impact. This provides evidence that the moat and outer ring are features inherited from the impact event and represent the partially eroded ejecta layer of the Bosumtwi impact structure. The presence of an outer ridge indicates that ejecta emplacement was not purely ballistic but, instead, requires ejecta fluidization and surface flow. The setting of Bosumtwi ejecta can therefore be considered as a terrestrial analog for rampart craters, which are common on Mars and Venus, and also found on icy bodies of the outer solar system. Future cosmonuclide studies at Bosumtwi will focus on the confirmation of the age of the lateritic cover observed on the ejecta layer.
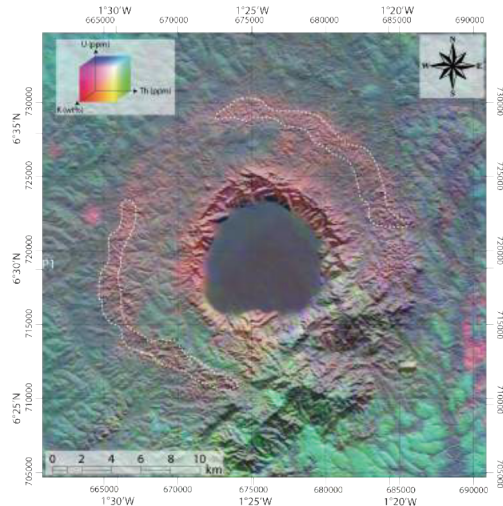

Fig. 1 – RGB map of K (0–2.5 wt%), Th (0–9 ppm), U (0–4 ppm) concentrations superposed onto a shaded relief image of the Bosumtwi impact crater. Dotted lines correspond to the rough areas associated with higher potassium concentrations (> 2wt%).

References: [1] Koeberl C. and Reimold W. U. 2005. Geological map of the Bosumtwi impact crater. Map Supplement to the Jahrbuch der Geologischen Bundesanstalt, Vienna, Yearbook of the Austrian Geological Survey, 145:31–70. [2] Wagner R., Reimold W. U., and Brandt D. 2002. Bosumtwi impact crater, Ghana: A remote sensing investigation. In Impacts in Precambrian Shields, edited by Plado J. and Pesonen L. J. Impact Studies, vol. 2. Heidelberg, Springer Publishers, pp. 189–210. [3] Baratoux et al. (2019) *Meteoritics & Planetary Science,* doi:10.1111/maps.13253.

FORMATION OF CHONDRULES AND MATRIX IN KAKANGARI CHONDRITES.

J. Barosch[1], D. S. Ebel[2], D. C. Hezel[1] and S. Alpert[2], [1]University of Cologne, Institute of Geology and Mineralogy, 50674 Köln, Germany, jbarosch@uni-koeln.de. [2]Dept. of Earth and Planetary Sci., American Museum of Natural History, New York, NY, 10024, USA.

Introduction: The K (Kakangari-like) chondrite grouplet is chemically and isotopically distinct from other chondrite classes. Nonetheless, similar to many primitive meteorites, the major components are chondrules and matrix. We present a comprehensive dataset, containing petrographic and chemical data to understand the origin and formation of chondrule textures, bulk chondrule compositions and chondrule-matrix complementarities in Kakangari chondrites. The chondrule-matrix complementarity in particular has been recognized as a key characteristic of carbonaceous and Rumuruti chondrites [1,2]. Various element and isotope ratios are different in chondrules than in matrix, while at the same time the bulk chondrite has close to CI chondritic ratios. As a consequence, chondrules and matrix must have formed from a single (solar) reservoir, which is a key constraint for all chondrule-forming models.

Methods: All samples were investigated with an electron microprobe by spot analyses and element mapping. Contiguous X-ray frames were stitched together, creating single element maps of the entire sample for image segmentation following the protocol of [1]. All sample objects were categorized, i.e. classified as chondrules, fragments, metal, matrix, etc. The components of each category were subsequently characterised for statistical evaluation (e.g. object abundances, sizes, compositions). Furthermore, we created phasemaps of all samples. A phasemap shows every mineral phase in false-colour. This is used to easily identify chondrule textures and mineral distributions throughout the samples. Bulk chondrule compositions were obtained from mineral spot analyses using modal recombination.

Results: We analysed four Kakangari sections and determined the bulk compositions of 60 chondrules. Matrix material is highly abundant (~70 vol%). Chondrules (~25 vol%) are mostly heavily fragmented. Only 7% of the chondrules are mineralogically zoned (e.g. ol cores with low-Ca px rims; Fig. 1). Chondrule bulk compositions vary strongly (e.g., Si: ~20–30 wt%, Mg: ~15–30 wt%). Average chondrule and matrix compositions agree with the few literature data available [3]. Preliminary results show that chondrule-matrix complementarities likely exist for Al/Ca, Al/Mg (Fig. 1), and possibly for Fe/Mg ratios.
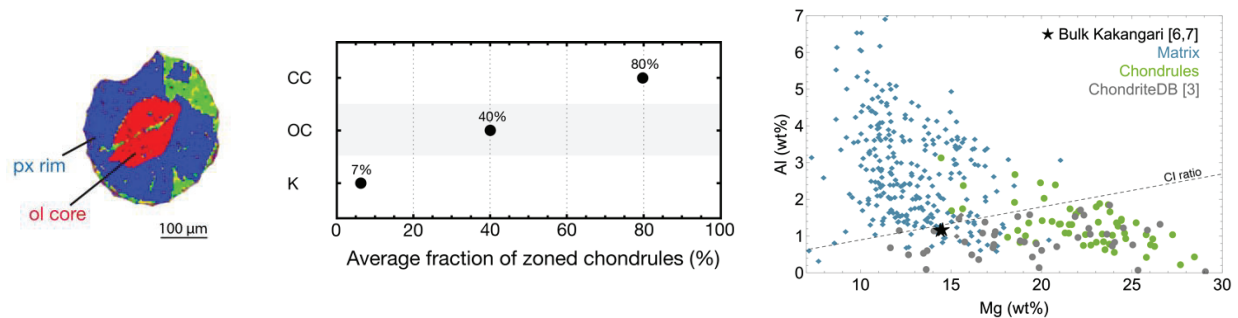

Fig. 1: Left: Phasemap of a mineralogically zoned chondrule (ol core, low-Ca px rim) in Kakangari. Center: Average fractions of mineralogically zoned chondrules in chondrites [4,5]. Right: Al/Mg chondrule-matrix complementarity in Kakangari. Bulk K composition was taken from [6,7].

Discussion: Our study emphasises and expands on the unique properties of Kakangari: (i) Mineralogically zoned chondrules are textural evidence for chondrule open system exchange, which also explain bulk compositional variations [4,5]. Zoned chondrules dominate all major chondrite groups, however, almost none were observed in Kakangari (Fig. 1). Thus, either Kakangari is the first meteorite without textural evidence for chondrule open system behaviour, or chondrules lost their initial zonation. The latter might be related to the widespread fragmentation most chondrules in Kakangari experienced, which is not seen in any other major chondrite group. (ii) We found chondrule-matrix complementarities for Al/Ca and Al/Mg. This suggests that chondrules and matrix likely formed from a single, common reservoir. Interestingly, no complementarity is observed for Mg/Si ratios, which is a prominent example for complementarity in carbonaceous chondrites [1,2], and although the Mg/Si ratio of Kakangari in average chondrules, matrix and bulk appears to be CI chondritic.

References: [1] Ebel et al. (2016) *Geochim. Cosmochim. Acta, 172,* 322–356. [2] Hezel et al. (2018) *Chondrules: Records of Protoplanetary Disk Processes,* 91–121. [3] Hezel et al. (2018) *Chemie der Erde 78*, 1–14. [4] Friend et al. (2016) *Geochim. Cosmochim. Acta, 173,* 198–209. [5] Barosch et al. (2019) *Geochim. Cosmochim. Acta, 249,* 1–16. [6] Mason & Wiik (1966*) American Museum novitates, 2272*. [7] Weisberg et al. (1996) *Geochim. Cosmochim. Acta, 60,* 4253–4263.

IMPACT CHRONOLOGY OF CHELYABISNK.

S. P. Beard[1], T. D. Swindle[2], D.A. Kring[3], T.J. Lapen[4]. [1]State Key Laboratory in Lunar and Planetary Science, M.U.S.T., Avenida Wai Long, Taipa, Macau. [2]Lunar and Planetary Laboratory, University of Arizona, Tucson AZ 85721 (tswindle@lpl.arizona.edu), [3]Lunar and Planetary Institute, Houston TX, [4]University of Houston, Houston TX.

Introduction: Chelyabinsk is a metal-rich LL5 chondrite [1] that has light clast-rich and dark melt-rich lithologies [2,3]. Geochronology studies of Chelyabinsk result in multiple ages that have been interpreted to represent at least eight impact events [5]. This work revisits Ar-Ar measurements of Chelyabinsk [6] for the purpose of comparison with other Ar-Ar studies (e.g. [7]) and multiple other ages from other systems to better understand Chelyabinsk's impact history.

Methods: Details of the Ar-Ar measurements for Chelyabinsk can be found in [6]. Literature geochronology results (U-Pb, Pb-Pb, Re-Os, Sm-Nd, Rb-Sr, K-Ar, Ar-Ar, and U-He; see references in [5]) of Chelyabinsk are evaluated for how well they agree with one another as well as the quality of the reported ages. Ages that are based on poor isochrons, determined by K-Ar, or on a mixture of lithologies in the Ar-Ar case, are not considered. If the ages of one method agree independently or are in agreement with multiple methods, this is considered a high probability to represent an impact event.

Results: Figure 1 shows the age distribution from multiple well-determined dating methods of Chelyabinsk, represented as summed Gaussians with a width proportional to the reported uncertainty. This refined impact distribution (compare to [5]) shows impact ages at **~4560 Ma** (Re-Os, Rb-Sr)**, ~4450 Ma** (Pb-Pb, U-Pb), **~2800 Ma** (Sm-Nd, Ar-Ar), and **~30 Ma** (Rb-Sr, U-He, U-Pb).

Discussion: Ar-Ar results from [6,7] agree that there is a young age 26 ± 11 Ma, the best defined age from the isotopic dating systems, meaning that many of the systems could have been disturbed by an event at ~30 Ma. They disagree on an older age (~1800 Ma compared to ~2800 Ma), but show very similar behavior. The reason for this discrepancy and how it affects the overall impact distribution is still being worked on, including modeling Ar diffusion [11]. Three studies of Sm-Nd yield four poorly-defined and very different ages; ~300, ~2900, ~3700, ~4452 Ma [2,5,9,5] respectively. The ~300 Ma isochron is consistent with 30 Ma. Two Rb-Sr isochrons yield ages of 150 ± 58 Ma and ~4567 Ma [10]. The ~150 Ma isochron could be representative of the ~30 Ma age found in argon, the difference being an artifact of different shock effects experienced by the different systems [8]. The Pb-Pb age of 4457 ± 35 Ma [12] agrees well with the U-Pb ages of apatite grains that have upper concordia ages of ~4450 Ma (4454 ± 67 Ma, 4452 ± 21 Ma, 4433 ± 110 Ma from [12,1,13] respectively), representing an early post-accretion impact [12]. Apatite has a less constrained lower concordia of 559 ± 180 Ma [12], which might indicate the most recent time lead was lost from the system, and is consistent with ~30 Ma.

Figure 1. Revised impact age distribution suggested by this work (compare to [5]) suggests a formation age ~ 4560 Ma, an early energetic impact ~ 4450 Ma, an energetic impact not seen in other LL chondrites at ~ 2800 Ma, followed by the most recent impact event ~30 Ma. See text for references.
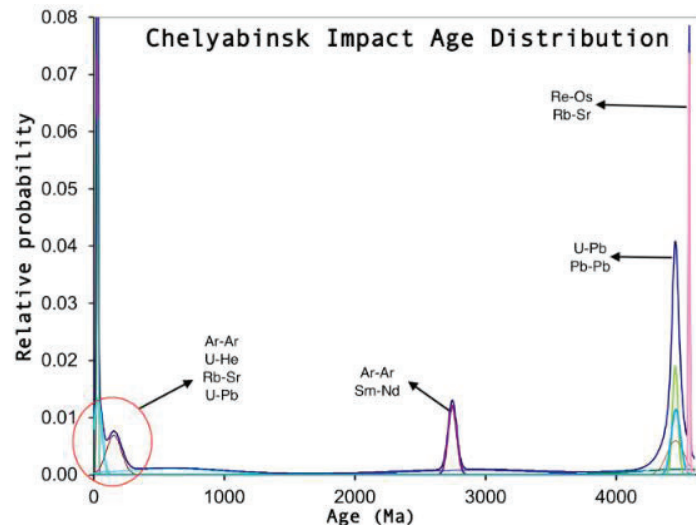
References: [1] Popova et al. (2013) *Science, 342,* 1069–1073. [2] Galimov et al. (2013) *Sol. Sys. Reas.* 47 255-259. [3] Badykov et al. (2015) *Petrology, 23, 103-115.* [4] Petrova et al. (2016) *MAPS, 51.* [5] Righter et al. (2015) *MAPS, 50, 1790-1819.* [6] Beard et al. (2014) *LPSC XXXXV,* #1807. [7] Trieloff et al. (2018) *MAPS, 53.* [8] Gaffney et al. (2011) *MAPS, 46, 35-52.* [9] Bogomolova et al. (2013) *Doklady Earth Sciences* 452. 1034-1038. [10] Nakamura et al. (2015) *LPSC XXXXV,* #1865. [11] Swindle and Weirich (2017) *LPSC XXXXVIII,* #1265. [12] Lapen et al. (2014) *LPSC XXXXV,* #2561 [13]. Kamioka et al. (2016) Mass Spec Conf., 62.

INFLUENCE OF METEORITE STRUCTURE ON NANOTUBES AND NANOCRYSTALS SYNTHESIS

A. S. Begunova, R. V. Kamalov, G. A. Yakovlev, and V. I. Grokhovsky, Ural Federal University, Ekaterinburg
(n.s.begun@gmail.com)

Introduction: In this work, the carbon nanotubes (CNTs) and oxide nanocrystals synthesis on ther metal part of Seymchan (PMG) as a substrate are presented. CNTs were grown using chemical vapor deposition (CVD) technique, which requires the substrate containing nuclei for the formation of carbon structures. Commonly usable metals for that purpose are Fe, Co, Ni [1]. The aim of our work was to reveal an influence of structural composition [2] (Fe-Ni alloys) and etching treatment of meteorite surface on CNTs growth and morphology. Additionally, there is a hypothesis that periodic structures could be the cause of the formation of orderliness in organic compounds [3].

Materials and Methods: Sample of Seymchan was prepared using standard metallographic procedures: grinding, polishing, and etching with nital. Etching for 15, 10, 5, and 0 minutes to rich different surface structure was carried out. Structural composition of the sample was investigated using optical microscopy with Zeiss Axiovert 40 MAT. Then areas of analysis were marked, and the sample was observed using scanning electron microscopy (SEM) with Zeiss Sigma VP.

CVD process was performed using "CVDomna" commercial equipment for carbon nanotube growth. A vapor-gas mixture of ethanol and air was passed in the reaction chamber. The ethanol pyrolysis was carried out at the temperature of 600°C and the pressure of 15 kPa for 10 minutes. After the growing process the sample was cooled under ambient air. The synthesized structures on Seymchan surface was investigated using SEM and Raman spectroscopy. Results of Raman spectroscopy were obtained in UB RAS Common use center "Geoanalyst" with LabRam HR Evolution, the lateral resolution was 1-2 μm. The purity of CNTs can be defined as a content ratio of CNTs to impurities and was evaluated using Raman spectroscopy. The evaluation based on the G/D bands intensity ratio. The G-band around 1600 cm^{-1} is the tangential mode of CNTs and the D-band around 1350 cm^{-1} is sensitive to defects [4, 5].

Results: The Raman study of the sample shown, that surface is covered with oxide crystals (Fe_2O_3, NiO) and CNTs. Furthermore, CNT purity is higher if the amount of NiO is higher. SEM investigation revealed that prism-shaped oxide crystals constitute the nearest to the sample layer, and CNTs are the upper layer.

There is an effect of phase composition on a synthesized nanostructure. Rhabdites are covered by ribbons with an average width of 60 nm and CNTs with a diameter of 20 nm. Low aspect ratio CNTs with an average diameter of 30 nm cover schreibersite. The 15 nm diameter nanotubes were synthesized on taenite, plessite, kamacite surface. The greatest purity of CNTs was obtained on a tetrataenite surface. External boundaries of taenite bands are covered with perpendicular to these boundaries arrays of CNTs. A fine-grained plessite is covered with curved CNTs. Quantity of CNTs on a kamacite surface is approximately 5 times less than on taenite surface. Detailed information is presented in table 1.

Table 1 – Characteristics of synthesized nanostructures

Mineral substrate	Synthesized structures on the surface
Schreibersite	110 nm oxide crystals, low aspect ratio (approximately 30) CNTs with average diameters of 30 nm
Rhabdites	60 nm oxide crystals, 60 nm width ribbons, CNTs with average diameters of 20 nm
Taenite	50 nm oxide crystals, vertical arrays of diameter CNTs with average diameters of 15 nm
Plessite	50 nm oxide crystals, curved CNTs with average diameters of 15 nm
Kamacite	50 nm oxide crystals, curved CNTs with average diameters of 15 nm, quantity of CNTs is 5 times less than on taenite and plessite

In addition, the influence of etching time treatment of substrate on CNT growth is also detected. Longer etching time leads to obtain more CNTs on the surface. The sizes of oxide crystals after the CVD process correlate with an initial surface grain structure formed due to etching treatment of the sample.

Discussion: We suppose that during the CVD, oxide crystals were formed first, and these crystals were the nuclei for the CNT formation. Etching treatment increases a surface area which may undergo oxidation, so we obtained more oxide crystals and then more CNTs. The nickel concentration in the initial sample affects on CNT quantity and purity, the greater amount of nickel gives purer CNTs. Initial sample structure has an influence on CNT shape. Arrays of vertical CNTs were synthesized on bands borders, and curved CNTs were obtained on kamacite and plessite surfaces.

References: [1] Ding F. et. al. (2008) *Nano letters* 8 (2):463-471. [2] Buchwald V.F. (1975) *The Regents of the University of California* 1:115–124. [3] Bernal J. D. *Proceedings of the Physical Society* (1949) A62:537-558 [4] López-Lorente A. I. et. al. (2014) *Analyst* 139:290-298. [5] Miyata Y. et. al. (2011) *Journal of Nanomaterials* 2011:786763–786770.

THE ANALYSIS OF THE METEOROID DANGER ON THE EARTH-MARS ROUTE

O. I. Belkovich[1], A. O. Andreev[1], Y. A. Nefedyev[1]
[1]Kazan Federal University, Russia, Kazan, Kremlyovskaya st., 18. E-mail: sky0606@mail.ru

Introduction: Currently, the exploration of Mars using unmanned spacecrafts is one of the most demanded by the International space agencies tasks. Now there are Mars Science Laboratory (MSL) and "Curiosity" rover [1] intensively working on the surface of the planet. This paper focuses on the determination of meteorite hazard on the Earth-Mars route and the development of the State Standard. This standard GOST is still the best compared to the American (by NASA) and European (by ESA) ones. There is also another standard "Meteor matter. Terms and definitions" [2] co-authored by the researchers of the meteor department of the Engelhardt astronomical observatory (EAO) [3]. Both standards are still binding documents when designing spacecrafts.

Methods: At EAO the works on the study of genetic connections between NEOs are being carried out [4]. The complexity of analyzing the meteor hazard is that observations of meteors taken on the Earth's surface could not provide the complete description of the meteorite environment at all parts of the Earth-Mars route: the closer to Mars, the less meteor orbits with the same elements cross the Earth's orbit and parts of spacecrafts' trajectory. The data on ground-based observations had therefore to be extrapolate [5]. Besides, the results of observations of meteors taken during the Mariner-2, Mariner-4, Pioneer-10, Pioneer-11, Mars Atmosphere and Volatile EvolutioN (MAVEN), Phoenix, Trace Gas Orbiter missions were used. The data on zodiacal light was involved as well. The derived formula for the transformation of sporadic meteor flow's density from one coordinate system to another allowed to reprocess the results of observations of meteors produced by the Mariner-4 and Pioneer-10 spacecrafts.

Results: According to the data provided by 3 sensors installed on the spacecraft travelling from the Earth's orbit to that of Mars, there is a twofold exponential increase in sporadic meteors flux density for bodies heavier than 10^{-6} g and sixfold increase for meteoroids in the mass range from 10^{-12} to 10^{-6} g. Beyond the orbit of Mars there is a sharp drop in flux density down to the normal level. This led to the conclusion that the surfaces of Mars and its 2 moons – Phobos and Deimos – are sources of secondary ejection of meteor bodies at their bombardment by meteorites from the main asteroid belt. This hypothesis was also confirmed by theoretical studies conducted at Saint Petersburg State University.

Discussion: At the analysis of geopotential height in the northern hemisphere the hypothesis of the existence of geostrophic winds was confirmed [6]. The circumterrestrial space including lower atmosphere, mesosphere, lower thermosphere, and ionosphere, was investigated using the radar methods; the parameters describing the influence of lower and middle atmosphere on wave propagation were determined [7].

Conclusions: It should be noted there was also another scientific program, in which the team of the EAO meteor department took part, called the Global Meteor Observations System (GLOBMET). The program was aimed at the analysis of radio and optical observations of meteor showers [8] and at the development of the physical principles of their interaction with the Earth's atmosphere. There are special methods of analyzing meteorological processes at the mesopause region of atmosphere [9]. It is well known that tidal temperatures strongly affect the predicted motion of geostrophic winds [10], and the determination of height characteristics is a complex problem [11]. The development of methods for accounting those processes is therefore a relevant task [12].

References: [1] Abbey W., et al. (2019) *Icarus* 319: 1-13. [2] Nefedjev J. and Rizvanov N. (2005) *Astronomy and Astrophysics* 444: 625 – 627. [3] Sokolova M.G., et al. (2018) *Advances in Space Research.* 62/8: 2355-2363. [4] Sokolova M., et al. (2016) *Advances in Space Research* 58/4: 541-544. [5] Roper R.G. (1990) *Advances in Space Research* 10/10: 189-192. [6] Sokolova M.G., et al. (2014) *Advances in Space Research* 54/ 11: 2415-2418. [7] Nefedyev Y.A. , et al. (2018) *Meteoritics & Planetary Science* 53/S1: 6192. [8] Usanin V. et al. (2016) *Advances in Space Research* 58/11: 2400–2406. [9] Sergienko M. V., et al. (2018) *Meteoritics & Planetary Science* 53/S1: 6165. [10] Andreev A.O. , et al. (2018) *Meteoritics & Planetary Science* 53/S1: 6157. [11] Usanin V., et al. (2017) *Advances in Space Research* 60/5: 1101–1107. [12] Sokolova M.G., et al. (2013) *Advances in Space Research* 52/7: 1217-1220.

THE NEW METHOD OF PROCESSING DATA ON METEOROIDS USING MODERN OBSERVATIONS

O. I. Belkovich[1], A. O. Andreev[1], Y. A. Nefedyev[1]
[1]Kazan Federal University, Russia, Kazan, Kremlyovskaya st., 18. E-mail: sky0606@mail.ru

Introduction: The work focuses on the reduction of modern observations of meteoroids from the databank formed both by professional researchers and by amateur astronomers. The new method of processing the modern observations of meteoroids, which provides comparable with the radar observations results, was developed at Engelhardt astronomical observatory (EAO) on the basis of modern physical theory of meteoroids. Due to the fact that the accuracy of the new method of modern observations processing has significantly increased, it is possible to process the modern observations of the Perseids and Leonids over a period of 120 years.

Methods: The physical theory of meteors was used in this study. Its application allowed to explain the observed at 2 MHz height distribution of meteor echoes, in which the upper part of the distribution relates to the heights of 140 km [1], for the first time. The instrumental methods of observing meteoroids were successfully developed in Kazan, and several interesting studies have been conducted. The orbit evolution of the two major meteor showers Geminids and Quadrantid, which were intensively observed at the EAO, was investigated and the possibility of the Quadrantid's genetic connections with comets 1860 I, Tuttle, Pons-Broocks, Stephan-Oterma, and Kosik-Peltier [2] was considered. The orbits of meteor showers that formed Bootid and Bielid streams [3] were studied as well.

Results: As a result, the Perseids meteor shower's orbit and its relationship to the matter ejection by the comet 1862 III Swift-Tuttle were investigated [4]. In this regard, the comet Grigg-Skjellerup was investigated as well. It is a periodic Jupiter-orbiting comet which at the same time passes near the Earth and is of great interest for researches dealing with comets. In 1967 the distance between it and Earth was estimated to be 0,003 AU. The meteor shower had therefore been expected and was actually observed [5]. However, the role of Jupiter extends beyond the comet. In this connection, close approaches with it will lead to a change in the radiant of the shower, and if the ejection from the nucleus continues, there will be almost simultaneously observed from 2 to 3 showers differing by 10° and 20° in declination. It is found that since 1874 the Perseids' activity has increased fourfold and solar longitude corresponding to the maximum of activity has not changed. The activity of the Leonids has not changed over this period, but solar longitude at maximum of activity has linearly increased, and this increase is 2,6° over 120 years. All of these discoveries for both showers relate to the stable periods only, but the parental comets of these streams –Swift, Tuttle, and Tempel-Tuttle – are far from the ecliptic plane. A method of determining the density of meteor shower on the basis of radio observations was developed [6].

Discussion: EAO scientific group developed a new "tomography" method of calculating the sporadic meteor density distribution on the celestial sphere using radar observations of the meteors at the same station with a goniometer. The method allows calculating the shower density on the celestial sphere with an angular resolution of 2°. Another major scientific achievement of the meteor studies conducted in Kazan is the proof that the distribution of the shower density of meteoroids on the celestial sphere has two planes of symmetry: the first one coincides with the plane of the ecliptic, the other one is perpendicular to the first one and passes through the apex and antiapex of the Earth [7]. This is explained by the fact that meteoroids moving on orbits with the same a, e, i have the even distribution of the argument perihelion ω.

Conclusions: Currently, Kazan specialists in the field of meteor astronomy continue their studies, advise on organizing and conducting the processing of observations of meteors provided by the International Meteor Organization (IMO), and arrange the school for young observers both at Kazan Observatory and abroad in Belgium and England [8, 9]. The research topics have also been expanded from simulating the formation of a shower to the study of gravitational and non-gravitational perturbations from a parental comet and meteoroids on the basis of comparison with a given shower's structure observed [10].

References: [1] Sokolova M., et al. (2016) *Advances in Space Research* 58/4: 541-544. [2] Sokolova M.G., et al. (2014) *Advances in Space Research* 54/ 11: 2415-2418. [3] Usanin V. et al. (2016) *Advances in Space Research* 58/11: 2400–2406. [4] Usanin V. (2017) *Advances in Space Research* 60/5: 1101–1107. [5] Sergienko M. V. et al. (2018) *Meteoritics & Planetary Science* 53/S1: 6162. [6] Sokolova M.G., et al. (2013) *Advances in Space Research* 52/7: 1217-1220. [7] Sokolova M.G., et al. (2018) *Advances in Space Research*. 62/8: 2355-2363. [8] Sergienko M. V., et al. (2018) *Meteoritics & Planetary Science* 53/S1: 6165. [9] Andreev A.O. , et al. (2018) *Meteoritics & Planetary Science* 53/S1: 6157. [10] Nefedyev Y.A. , et al. (2018) *Meteoritics & Planetary Science* 53/S1: 6192.

Tracing martian surface interactions with the triple O isotopic composition of meteoritic phosphates

J. J. Bellucci[1], M.J. Whitehouse[1], and A. A. Nemchin[2], [1]Swedish Museum of Natural History, Stockholm (Jeremy.Bellucci@nrm.se), [2]Curtin University, Perth Western Australia.

Introduction: There is ample evidence that Mars once had an ocean and thus, the possibility to sustain life. As such, it is critical to quantify the interactions between the lithosphere and hydrosphere on Mars. Martian meteorites are the only direct samples of Mars available for isotope analyses on Earth. While most of these rocks are igneous in origin and, thus, are expected to have stable isotope systematics in equilibrium with the martian mantle, some of these samples have minerals which have interacted with the surface and have recorded evidence of these interactions (e.g., [1]). Oxygen, in particular, is a useful isotopic tracer of interactions between some minerals, the atmosphere and the hydrosphere. Specifically, photochemical reactions in the atmosphere result in large, measurable mass independent oxygen isotope fractionations that are recorded in alteration products, reset minerals, or minerals that formed while interacting with surface water [2-3].

Phosphates in some martian meteorites are explicitly not in igneous equilibrium with their host rocks, having widely varying compositions on a sub-grain scale, complex inner structures, and zoning that strongly indicates interaction with the martian crust or a Cl-rich crustal fluid [4,5]. Some of these phosphates have halogen elemental ratios nearly identical to those in the alteration products measured in the nakhlites and those measured at Meridiani rocks by the Opportunity lander [4]. Samples that do not have zoned phosphate crystals or halogen enrichments, have a $\delta^{37}Cl$ within uncertainty of the Earth, the Moon, and chondritic materials [4]. Thus, the origin of the variable halogen ratios and $\delta^{37}Cl$ have been attributed to oxidized, halogen-rich species, specifically perchlorate, on the martian surface [4].

Perchlorate formation on Earth fractionates Cl isotopes both positively and negatively in $\delta^{37}Cl$ (resulting in values ranging from -14 to +5 ‰), and generates positive $\Delta^{17}O$ values of between +4 to +10 ‰ [6]. Natural perchlorate occurs on the Earth in arid deserts (e.g., the Atacama), similar to the martian surface, and forms through photochemical reactions in the upper atmosphere [6]. The formation processes of perchlorate are not well understood on Earth or on Mars. However, perchlorate has been measured at several landing sites on Mars. The ratio of ClO_4^-/Cl was measured as 4.4 in at least one surface location suggesting the oxidized Cl species is the most prevalent [7]. Further, the Cl isotope composition of the martian surface has been measured *in situ* in four locations and has a $\delta^{37}Cl$ value ranging from -51 to -1 ‰ [8]. On Earth, there are covariations in $\delta^{37}Cl$ and $\Delta^{17}O$ in perchlorate [6]. As some martian phosphates show textural and chemical evidence (including halogen ratios, and Cl isotope compositions) for exchange reactions with the martian hydrosphere while others are in equilibrium with the bulk sample, the goal for this study is to further investigate these phosphates via their triple O isotope compositions using Secondary Ion Mass Spectrometry (SIMS). Here we will present the triple isotope composition of phosphates from three enriched shergottites (Zagami, RBT 04262 and LAR 12011), one depleted shergottite (Tissint), an orthopyroxenite (ALH 84001), and a regolith breccia (NWA 7533). These compositions will be used to provide further constraints on the interactions with the martian surface recorded by these minerals and define the O-isotope composition of the oxidized surface of Mars (Figure 1).
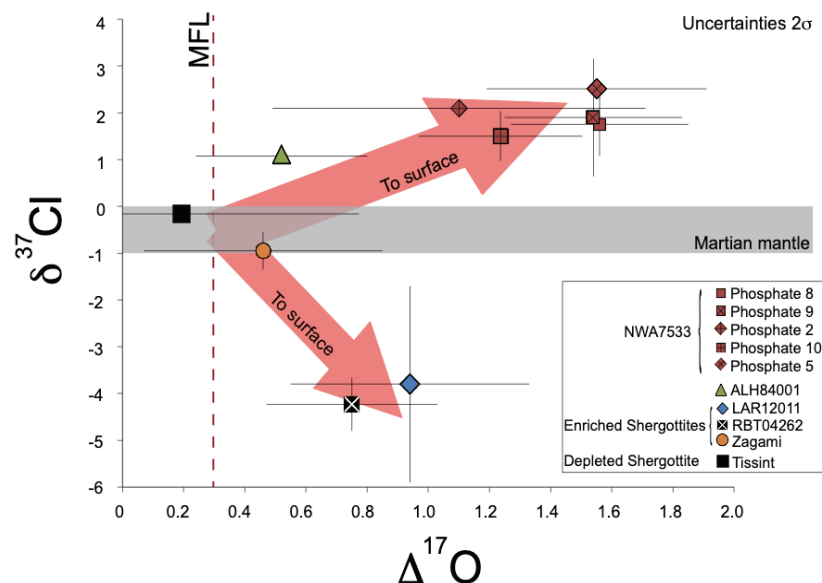
Figure 1. $\Delta^{17}O$ vs. $\delta^{37}Cl$ weighted averages for phosphates measured by SIMS in individual martian meteorites and individual phosphates from NWA 7533. $\delta^{37}Cl$ values for all meteorites presented here and the assumed martian mantle value for $\delta^{37}Cl$ are from [4].

References:

[1] Bridges et al., (2001) *Space Science Reviews.* 96, 365-392. [2] Farquhar et al., (1998) *Science* 280, 1580-1582. [3] Nemchin et al., (2014)*Nature Geoscience, 7*(9), 638-642. [4] Bellucci et al., (2017) *EPSL* 458, 192-202. [5] McCubbin et al., (2017) *MAPS* 51(11), 2036-2060. [6] Jackson et al., (2010) *Environ. Sci. Technol.* 44, 4869-4876. [7] Hecht et al., (2009) *Science* 325, 64–67. [8] Farley et al., (2016) EPSL 438, 14-24.

TELLURIC IRON FROM WABAR IMPACTITE.

Christian Bender Koch[1] and Takeshi Kasama[2], [1]Department of Chemistry, University of Copenhagen (cbk@chem.ku.dk), [2]DTU-Nanolab, Technical University of Denmark (takeshi.kasama@cen.dtu.dk).

Introduction: The Wabar craters were among the earliest rekocnized meteorite impact structures on Earth[1]. The craters formed as the result of the fall of an iron meteorite classified as Type IIIAB medium octahedrite and containing approximately 8 %wt of Ni. In the Wabar impactites the metallic phase dominantly is present as spherules between 5 and 100 µm in diameter. According to recent work [2] the nickel content of the spherules can be relative higher than for the average for the meteorite (up to 60 %wt) testifying to an all meteoritic origin. We report here on the finding of particles of pure iron in impactites from Wabar crater.

Results and Discussion: A small piece of a vesicular, white speckled, dark green impactite from Wabar was lightly crushed by hand, and subjected to magnetic separation using a ferrite hand magnet. Similarly, a magnetic fraction was prepared from the local, loose sand drift. Individual, sand sized, magnetic grains were mounted on a standard SEM holder using carbon tape and subjected to SEM observation and EDS analysis. Figure 1 shows the morphology of a particle of pure iron. In contrast to the solid, spherical morphology of FeNi spherules the iron particles show deep groves seemingly formed by folding of plates that locally exhibit different smoothness and cavities. Trace amounts of Ti and V can both be detected in the iron. These elements are also detected in analyses of magnetic titanomagnetite isolated from the local drift sand, suggesting that the telluric iron form by a series of processes overall leading to the reduction of oxide during the impact.
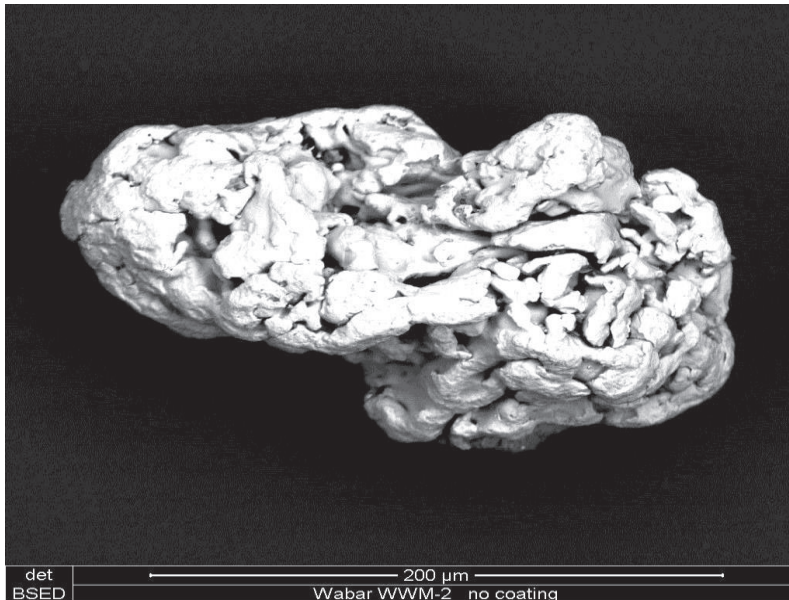

Figure 1. Telluric iron particle recovered from Wabar impactite.

References: [1] Spencer L.J. (1933) *Mineral Mag 23:387-404*. [2] Hamann C. et al (2013) *Geochemica et Cosmochemica Acta* 121:291-310.

TOWARDS A SURFACE AGE MAP OF MARS AT ULTIMATE RESOLUTION, AND THE SEARCH FOR SOURCE CRATERS OF THE MARTIAN METEORITES.

G.K. Benedix[1,5], A.L. Lagain[1], P.A. Bland[1,5,*], K. Chai[2], S. Meka[2], C. Norman[3], M.C. Towner[1], S. Anderson[1], J. Paxman[3], F. Cary[4] and J. Fairweather[4] [1]Space Science and Techonology Centre, School of Earth and Planetary Sciences, (g.benedix@curtin.edu.au); [2]Curtin Institution of Computation Curtin University; [3]School of Civil and Mechanical Engineering, Curtin University, GPO Box U1987, Perth, WA, 6845, Australia. [4]School of Earth Sciences, University of Western Australia, 35 Stirling Hwy, Perth, WA, 6009 Australia. [2]Western Australian Museum, Locked Bag 49, Welshpool, WA, 6986, Australia.

For planetary geologists who study the solar system, the baseline datasets are images of a surface and a geologic map with included age information. Ages for other worlds are determined by counting the number of craters of a given size over a given area on the surface. More craters equals an older surface. The technique was invented in the early-60s [e.g. 1]. On its own, crater counting provides a relative age, but if we can obtain a radioisotope age from a sample of a cratered surface, that relative age can be calibrated; it becomes an absolute chronometer. This was achieved with the return of Apollo samples. Since then, crater counting has been at the heart of virtually every major advance in planetary science, from deciphering the geological history of the Moon, to the concept of the late heavy bombardment, to the realisation that the icy satellites might have ocean mantles.

Advances in technology have increased spatial resolutions of orbit-derived imagery dramatically (from km/pixel to cm/pixel), allowing craters 10m in diameter to be resolved. However, there has been no change in how that data is processed to derive surface ages. The default method remains manual crater counts; effectively restricting us to craters >1km diameter. There are ~390,000 of these on Mars, which were counted and measured by hand [2]. When we get down to the smaller crater sizes, there are 10s millions of craters; a number that is intractable to count by hand. We have developed an advanced machine learning algorithm to do it automatically. We validated it against [2]. Our algorithm, summarised in [3], automatically counts craters of any size, but is especially helpful for small craters, on any number of high resolution images. Figure 1 illustrates our current capability. We are now applying our algorithm to the highest resolution global imagery dataset of Mars using High Performance Computing resources. It will allow us to develop surface age maps of Mars at ultimate resolution, and importantly, determine ages for all craters large enough to launch meteorites to Earth.

There is a unique repository of martian meteorites on Earth, but we don't know where they come from on Mars. Previous work has produced a number of potential source craters [4-7] for the martian meteorites, however the matches have been tentative or ambiguous. Recent work [8, 9] has focussed on limiting the number of potential source craters based on ages and crater properties. There are currently 8000 craters that could be sources. Using our algorithm will allow examination of all possible source craters of the meteorites to find the best matches.

References: [1] Hartmann, W.K., Comm. Lunar and Planet. Lab. (https://tinyurl.com/y4o3a3z3) (1964). [2] Robbins, S. J. & Hynek, B. M. *JGR Planets* **117,** E05004 (2012). [3] Benedix G.K., et al. *50th Lunar and Planet. Sci.*, #2140 (2019). [4] Mouginis-Mark, P., et al. *JGR Planets* **97,** 10213–10225 (1992). [5]. Hamilton, V., et al. *Meteoritics &Planetary Science* **38,** 871 (2003). [6] Werner, S. C., et al.. *Science* **343,** 1343–1346 (2014). [7] Tornabene, L. L. *et al*. *JGR Planets* **111,** (2006). [8] Herd, C.D.K., et al. *80th Meteoritical Soc. Meeting*, #6334 (2017). [9] .Herd, C.D.K., et al. *49th Lunar and Planet. Sci.*, #2266 (2018).
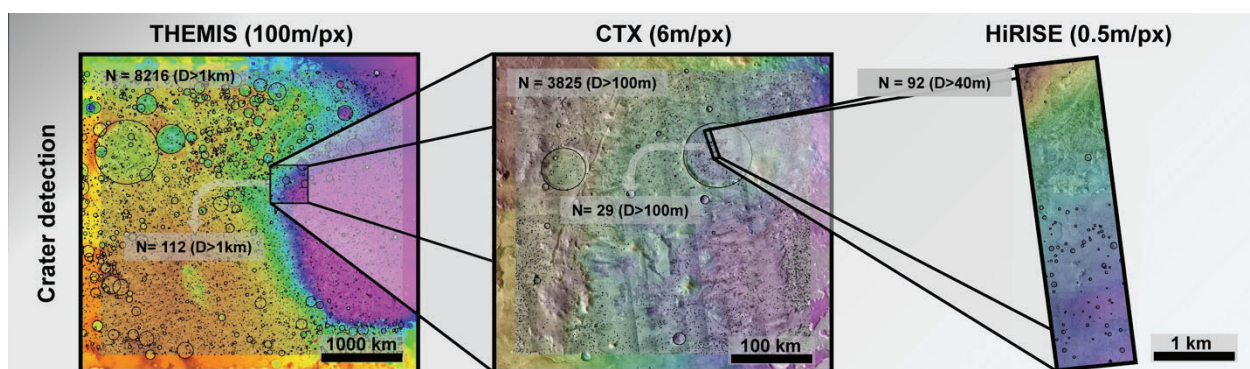

Figure 1. Results of crater counting algorithm for the Syrtis Major region of Mars. (left) at THEMIS Resolution, craters counted = 8216, outline is Jezero Crater region, which contains 112 craters >1km. (center) CTX resolution of outlined area– algorithm counts 3825 craters >100m. (right), highlighted area in CTX (29 craters) image at HiRISE resolution, 92 craters >40m.

COMPOSITIONAL CHARACTERIZATION OF THE HAYABUSA2 RETURNED SAMPLES WITH MICROMEGA, WITHIN THE CURATION FACILITY.

J-P. Bibring[1] (IAS, Bat 121, 91405 Orsay Campus, France, bibring@ias.u-psud.fr), R. Brunetto[1] , V. Hamm[1], M. Matsuoka[2], A. MoussiSoffys[3] (CNES, Toulouse, France, aurelie.moussisoffys@cnes.fr), T. Nakamura[4] (Tohoku University, Sendai, Japan, tomoki@m.tohoku.ac.jp), A. Nakato[2], T. Okada[2] (ISAS, Sagamihara, Japan, okada@planeta.sci.isas.jaxa.jp), C. Pilorget[1], L. Riu[2], T. Yada[2] and K. Yogata[2].

Introduction: The pioneering sample collection operation from a C-rich asteroid has been successfully performed by the ISAS/JAXA Hayabusa2 mission [1]. The samples are planned to depart from Ryugu late 2019, and arrive on Earth about a year later. Immediately after its recovery on Earth, the return capsule will be brought to ISAS, in Sagamihara (Japan), to enter a dedicated curation facility. It will be opened under vacuum, and samples will be extracted and transferred, through X-Y stages and gloveboxes, onto sample holders to be characterized, prior to be eventually distributed to selected initial analysis teams. The clean chamber in the curation facility is made of several contiguous compartments, in which either ultravacuum or ultrapure N_2 filling will be maintained. As a major feature of this global characterization, a purely non-destructive analysis of the composition of the samples, down their grain scale, will be performed, by means of near-infrared hyperspectral imagery, thanks to the MicrOmega instrument.

MicrOmega: It constitutes a fully integrated hyperspectral microscope, mounted on a flange equipped with a sapphire window so as to image samples maintained within the clean chamber in the curation facility, either under vacuum or with N_2 filling. The sample holders will be mounted an a X/Y/Z translation stage, so as to position the samples in focus within the 5x5 mm^2 large MicrOmega field of view (FOV). MicrOmega will then build 3D (x,y, λ) image-cubes, in 256x256 pixels, thus providing a spatial sampling of 20 µm. It will thus enable to image at once a number of grains, while acquiring for each of them its entire spectrum. The spectral dimension will be obtained by piling up monochromatic images of the entire FOV, covering the spectral range (0.99 to 3.6 µm) in ~350 contiguous spectral channels, 20 cm^{-1} large. This will be performed by illuminating sequentially the samples with a monochromatic beam, selected by an AOTF (Acousto-Optic Tunable Filter) tuned at a given RF frequency [2] : by scanning the RF frequency of the acoustic signal, the output wavelength covers the full spectral range 0.99 and 3.6 µm, chosen to contain diagnostic featres of most constituents of interest: minerals, both igneous and altered, as well as aqueous phases and organics. This AOTF dispersive system offers several advantages, with a high sensitivity and full flexibility to choose and possibly oversample (down 2 cm^{-1}) wavelengths of interest.

A fully resolved (spatial/spectral) image-cube will be acquired in typically 20 minutes, including the cooling of the MCT detector matrix, while providing a SNR > 100 over the entire spectrum.

Designed and developed at IAS, MicrOmega will constitute a facility instrument, integrated within the overall plan of activities performed under ISAS/JAXA lead to receive, handle, characterize, store and distribute the samples colleted at the surface of Ryugu, for a broad international community.

References:
[1] Watanabe S. et al. 2019, *Science*:eaav8032 DOI: 10.1126/science.aav8032. [2] Bibring et al. 2017, *Astrobiology*, 17, 6 and 7, DOI: 10.1089/ast.2016.1642

PLASTIC DEFORMATION OF CHONDRULES IN ORDINARY AND ENSTATITE CHONDRITES: EVIDENCE OF HOT ACCRETION OR IMPACT-RELATED REGOLITH PROCESSING?

J. N. Bigolski[1,2], M. K. Weisberg[1,2,3], and D. S. Ebel[2,3], [1]Dept. Phys. Sci., Kingsborough College CUNY, Brooklyn, NY 11235, USA (john.bigolski@kbcc.cuny.edu), [2]Dept. Earth and Planet. Sci., American Museum of Natural History, New York, NY 10024, USA, [3]Dept. Earth and Envi. Sci., CUNY Graduate Center, New York, NY 10016, USA.

Introduction: While chondrites and their constituent components are among the most primitive Solar System materials available for study, the period between the formation of chondrules and the accretion of the chondrite parent bodies remains poorly constrained. Unequilibrated ordinary chondrites (UOCs) are known to exhibit textures that apparently record post-accretionary brecciation and reconsolidation of clasts [1]. These clasts may represent several provenances of their components, thereby providing context for the period between chondrule formation and the final assemblage of chondritic components onto parent bodies. Although well established for UOCs, the history of brecciation and mixing of disrupted chondritic components in the enstatite chondrite (ECs) class of meteorites remains less well understood and constrained.

The hot accretion of chondritic components has been described throughout the literature [e.g. 2]. Recently, work on cluster chondrite clasts having highly compact structures with deformed and undeformed chondrules has strongly supported the hypothesis of rapid accretion of nascent chondrules [3]. Our goals are to expand upon our previous work [4, 5] on Watonga (LL3.1) in order to examine deformed and indented chondrule components, as well as examine from some of the least equilibrated ECs for evidence of deformation textures.

Results: Watonga contains a wide range of chondrule textural types, many of which are rimmed by fine-grained material, as well as chondrule fragments mixed with lithic and mineral fragments. In particular, fine-grained interchondrule matrix (<5 μm, [6]) represents a minor component (~3 vol%), whereas chondrules and chondrule fragments are the most abundant (~71 vol%). Coarse-grained matrix (5 – 100 μm) is composed of mineral fragments, which include olivine, pyroxene, metal and sulfide grains, and extends up to 15 vol%. The degree of deformation was determined in a total of 88 examined chondrules following procedures outlined in [3]. Of those chondrules examined, ~20% showed considerable degrees of deformation. Deformation extends over all chondrule textural types.

Petrologic Type 3 ECs examined for deformation include Elephant Moraine (EET) 90992, Queen Alexandra Range (QUE) 93351, both EL3s, and Pecora Escarpment (PCA) 91383, an EH3. The EL3s both have comparably less fine-grained interchondrule matrix (<3 vol%) than PCA 91383 (~5 – 10 vol%). Preliminary findings reveal that ~16 vol% and ~11 vol% of chondrules from EET 90992 and QUE 93351, respectively, show considerable degrees of deformation, with some that are indented around each other. PCA 91383 has far fewer examples (<10 vol%). The matrix from PCA 91383 is also coarser-grained than the predominantly fine-grained matrix in the EL3s, with the former composed mostly of enstatite fragments embedded in FeO-rich material. Indented chondrule clusters are numerous in the EL3s, yet are lacking in the PCA 91383 EH3.

Discussion: Previous work on Watonga has shown it to contain deformed and indented chondrules and chondrule/lithic fragments [5]. Cluster chondrite clasts have been previously found to occur as higher percentages in UOCs with minimal modal abundances of matrix (i.e. < 10 vol%) [3]. Like UOCs, the EL3 chondrites also show chondrule deformation and clustering and have low matrix. EET 90992 has also previously been shown to have a shock stage S3 [7], which we interpret to be a likely influence on deformation textures. PCA 91383, however, contains matrix that we interpret to be derived from cataclasis and the disruption of precursor material. Such mechanical processing evident in EH3s, coupled with the paucity of deformation textures, might instead record post-accretion comminution and fracturing in a regolith setting.

Implications: Two plausible models for the formation of deformation textures include deformation via hot accretion in the solar nebula, and impact-related deformation on the parent body regolith. For the hot accretion model, at least 2 distinct events are posited to have occurred prior to final lithification: 1) rapid assemblage of ephemeral planetesimals that accreted chondrules hot, and 2) subsequent disruption and brecciation to produce the clasts of cluster chondrites and the cataclastic portions common throughout Type 3 chondrites. Alternatively, compaction from impacts on the parent bodies could also have contributed to the deformation textures without the formation of cluster chondrites as demonstrated for friable ordinary chodnrites [8]. Further work is required to test the viability of each model for UOCs and Type 3 ECs.

References: [1] Bischoff A. et al. 1996. In: *Meteorites and the Early Solar System* II:679–712. [2] Zanda B. 2004. *Earth and Planetary Science Letters* 224:1–17. [3] Metzler K. 2012. *Meteoritics & Planetary Science* 47:2193–2217. [4] Bigolski J. N. and Weisberg M. K. 2017. *Meteoritics & Planetary Science* 52:A25. [5] Bigolski J. N. et al. 2019. *LPS L*, Abstract #2268. [6] Scott E. R. D. and Krot A. N. 2014. In: *Treatise on Geochemistry 2nd ed.*:65–137. [7] Rubin A. E. 2015. *Chemie der Erde* 75:1–28. [8] Friedrich J. M. et al. 2017. *Geochimica et Cosmochimica Acta* 203:157–174.

MINERALOGICAL CHARACTERISTICS OF 20 NEW SAMPLES FROM THE ALMAHATA SITTA STREWNFIELD.

A. Bischoff[1], S. Lentfort[1], K. Möhlmann[1], K. Klemm[1], and S. Haberer[2], [1]Institut fuer Planetologie, Wilhelm-Klemm-Str. 10, D-48149 Muenster, Germany (bischoa@uni-muenster.de). [2]Haberer-Meteorite, Eschenweg 1, D-79341 Nordweil, Germany (siegfried@haberer-meteorite.de).

Introduction: After asteroid 2008 TC_3 impacted Earth in 2008, many different meteorite types (achondritic and chondritic) were identified among the numerous meteorite fragments (e.g., [1-11]). The recognition of scientifically valuable samples is still ongoing [12,13]. Here, the mineralogical characteristics of 20 new samples are presented.

Results: All 20 new samples represent only one meteorite type (achondritic or chondritic) weighing between 1.7g (MS-227) and 18.0g (MS-207). The presence of a single meteorite type is the typical characteristic of the individual fragments, although a very interesting exception was recently described [13] showing that complex breccias also exist among the Almahata Sitta samples. Among the new samples are 15 ureilites (10 coarse-grained, 5 fine-grained) and 5 enstatite chondrites. Most of the samples were recovered in 2014.

E-chondrites: As in many cases the identified enstatite chondrite fragments are small: MS-211 (6.4g), MS 217 (13.2g), MS-221 (7.3g), MS-224 (7.8g), and MS-225 (6.8g). MS-221 (EL_b4; see [14] for the new classification system) and MS-224 (EH_a3) clearly show a perfect chondritic texture, wheres the others represent different EL_b6 chondrites. Olivine (Fa_{0-1}) was found in some chondrules from MS-224 (Fig. 1a). MS-225 contains some large, coarse-grained objects (perhaps chondrule relicts) having blue areas in transmitted light, which may be due to the occurrence of small $\ll 1$ µm Ti-rich grains (perhaps rutile) in plagioclase (Figs. 1b,c). Kamacite in MS-211, MS-217, MS-225, and MS-221 has mean concentrations of Si and Ni of ~1-1.5 and ~7-8 wt%, respectively (typical for EL_b-chondrites). The Cr-concentration in troilite in these samples is above 2.5 wt%. MS-224 (EH_a3) has kamacite with 3.2 wt% Si and 6.3 wt% Ni and troilite with 1.3 wt% Cr (see [14]).
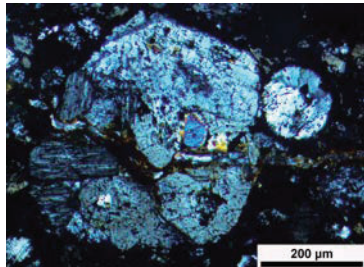

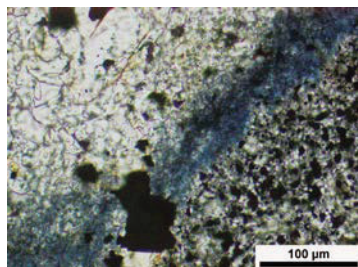
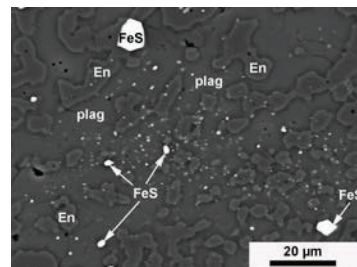Fig. 1a: Olivine (blue) in a chondrule   Fig. 1b: Blue area around a relict chondrule   Fig. 1c: Tiny white Ti-rich particles in plagioclase

Ureilites: 15 ureilites are among the new Amahata Sitta samples and can arbitrarily be subdivided into fine-grained ureilites, Ol-rich, coarse-grained, and Px-rich, coarse-grained ureilites. MS-207 (18.0g), MS-212 (1.8g), MS-213 (9.3g), MS-215 (7.2g), and MS-216 (3.8g) are heavily-shocked, fine-grained ureilites. MS-212 and MS-216 are completely fine-grained and olivine is ~Fa_{9-11}. Some have somewhat variable textures considering the sub-grain sizes of the mosaicized olivine (MS-207, MS-213, and MS-215). These olivines have cores with about 20-22 mol% Fa. MS-208 (9.7g; composition of olivine cores: Fa_{19-21}), MS-209 (7.6g; Fa_{18-20}), MS-214 (14.1g; Fa_{12-14}), MS-218 (6.1g; Fa_{19-21}), and MS-227 (1.7g; Fa_{8-9}) are coarse-grained ureilites with abundant olivine, whereas MS-210 (8.2g; Fa_{11-15}), MS-219 (2.5g; Fa_{10-11}), MS-220 (11.0g; Fa_{3-4}), and MS-222 (8.0g; Fa_{11-13}) have considerable abundances of pyroxenes. In MS-226 (2.8g; Fa_{11-12}) pyroxene is by far the most abundant silicate. MS-220 has Fe-poor silicates.

Conclusions: All samples from the Almahata Sitta strewn field are highly valuable samples. Every new sample confirms the importance and peculiarity of asteroid 2008 TC_3 and provides new information about the reaccretion of ureilitic fragments forming a second-generation parent body. The incorporation of xenolithic materials may have occurred in the same process of reaccretion or by later impacts.

References: [1] Jenniskens P. et al. (2009) *Nature* 458:485-488. [2] Bischoff A. et al. (2010) *Meteoritics & Planet. Sci.* 45:1638-1656. [3] Horstmann M. et al. (2010) *Meteoritics & Planet. Sci.* 45:1657-1667. [4] Horstmann M. and Bischoff A. (2014) *Chemie der Erde – Geochemistry* 74:149-184. [5] Goodrich C.A. et al. (2014) *Elements* 10:31-37. [6] Bischoff A. et al. (2012) *Meteoritics & Planet. Sci.* 47:A71. [7] Zolensky M.E. et al. (2010) *Meteoritics & Planet. Sci.* 45:1618-1637. [8] Horstmann M. et al. (2012) *Meteoritics & Planet. Sci.* 47:A193. [9] Bischoff A. et al. (2014) *Proceedings National Academy Sciences* 111:12689-12692. [10] Bischoff A. et al. (2015) *Meteoritics & Planet. Sci.* 50:#5092. [11] Bischoff A. et al. (2018) *Meteoritics & Planet. Sci.* 53:A25. [12] Fioretti A.M. et al. (2017) *Lunar Planet. Sci.* 48:#1846. [13] Goodrich C.A. et al. (2018) *Lunar Planet. Sci.* 49:#1321. [14] Weyrauch M. et al. (2018) *Meteoritics & Planet. Sci.* 53:394-415.

EVIDENCE FOR DELAYED CHONDRULE FORMATION IN THE OUTER SOLAR SYSTEM

M. Bizzarro[1], J. Bollard[2], J.N Connelly[1] and M. Schiller[1]
[1]Centre for Star and Planet Formation, University of Copenhagen, Copenhagen, Denmark (Bizzarro@snm.ku.dk)
[2]Center for Space and Habitability, University of Bern, Bern, Switzerland

Elucidating the timescales of solid formation in the early Solar System is critical for a better understanding of disk processes. Although short-lived radionuclides such as [26]Al can theoretically provide high resolution ages, such decay systems critically depend on the disputed assumption of homogeneous distribution of their parent nuclides [1,2]. A such, only the decay of U to Pb can provide assumption free ages with sufficiently high resolution to determine the timing of individual meteoritic components formed in the first few Myr of the Solar System's history. Using this approach, it has been established that the formation of chondrules, the most abundant chondritic component, started simultaneously with the condensation of the Solar system's first solids – calcium- aluminium-rich inclusions (CAIs) – and lasted ~4 Myr [3,4]. However, it is uncertain whether this distribution of chondrule ages is representative of the whole protoplanetary disk. Critically, better understanding the formation history of chondrule populations formed in distinct disk reservoirs may provide insights into the mechanism(s) responsible the thermal processing of disk solids.

To address this issue, we report on the U-corrected Pb-Pb ages of two populations of chondrules understood to have formed in spatially isolated disk reservoirs based on their nucleosynthetic [54]Cr compositions. Indeed, it is well established that the mass-independent $^{54}Cr/^{52}Cr$ composition (expressed as $\mu^{54}Cr$, i.e. the 10^6 deviations relative to the terrestrial value) of disk solids as well as asteroidal and planetary bodies can be used to track their accretion regions [5]. For example, inner Solar System material is typically characterized by deficits in $\mu^{54}Cr$ values whereas outer Solar System solids are characterized by excesses. The first chondrule population investigated consists of 15 individual objects from the NWA 5697 ordinary chondrite and Allende carbonaceous chondrite that are characterised by $\mu^{54}Cr$ values ranging from -87±12 to -24±12 ppm, i.e. typical of inner disk material [6], suggesting that these objects were formed in the accretion region(s) of the terrestrial planets. The second population comprises 17 individual objects from three CR chondrites (NWA 6043, NWA 7655 and NWA 7502) and have $\mu^{54}Cr$ values ranging from 44±6 to 137±4 ppm that suggest formation beyond the orbits of the gas giants [7,8]. The inner disk population displays U-corrected Pb-Pb dates ranging from 4567.61±0.54 Ma to 4564.71±0.30 Ma whereas the outer disk chondrules have ages that span from 4567.26±0.37 Ma to 4563.24±0.62 Ma. Although the age range recorded by the two populations are similar, their mean ages appear distinct. The inner disk population records a mean U-corrected Pb-Pb age of 1.00±0.62 Myr whereas the outer disk population displays a mean age of 2.38±0.53 Myr. To assess the statistical significance of this age offset, we performed a Mann-Whitney U test, which evaluates the null hypothesis that the medians of the two populations are identical. The results indicate that the null hypothesis can be rejected at the 3σ confidence level, establishing that the age difference of 1.4±0.8 Myr between the two populations is statistically meaningful.

It has been suggested that the preponderance of chondrules with ages that are within 1 Myr of Solar System formation reflects an early and efficient chondrule production mechanism. In this view, it is hypothesized that shock fronts associated with spiral arms generated in a gravitationally unstable early disk can provide an adequate energy to promote the melting of disk solids. Shocks generated in this regime are modelled to be highly efficient in the inner disk region thereby providing a possible mechanism for the thermal processing of disk solids at early times. However, because accretion to the disk decreases and the envelope dissipates, the resulting disk mass at later times is thought to be far too low to sustain gravitational instabilities. Thus, a distinct source of shock is required for the production of chondrules formed at a later time in the outer disk. A possibility is bow shocks associated with giant planet formation and migration during the disk lifetime [9]. Preliminary results indicate that nebular shocks caused by the presence of a large planet such as Jupiter can induce chondrule formation, in particular if Jupiter migrated inwards in the early times of the disk [10]. Collectively, our new age data support the view that multiple chondrule formation mechanisms existed in the early Solar System albeit perhaps with contrasting efficiencies. Finally, the mean outer Solar System chondrule age of 2.38±0.53 Myr reported here may record the migration of the gas giant planets.

References: [1] Larsen, K. et al. (2011) *ApJ* 735, L37. [2] Schiller, M. *et al.* (2015) *EPSL* 420, 45. [3] Connelly et al. (2012) *Science* 338, 651. [4] Bollard, J. *et al.* (2017) *Sc. Adv.* 3, e1700407. [5] Warren, P. (2011) *EPSL* 311, 93. [6] Trinquier, A. et al. (2007) *ApJ* 655, 1119 [7] van Kooten et al. (2016), *PNAS* 113, 211. [8] Olsen, M. *et al.* (2016) GCA 191, 118. [9] Ciesla et al. (2004) *MAPS* 39, 1809. [10] Bodénan, J.-D. et al. (2018) *81st Annual Meeting of The Meteoritical Society* (LPI Contrib. No. 2067).

SHOCKS PRODUCED BY JUPITER IN THE CONTEXT OF CHONDRULE FORMATION: EFFECTS OF COOLING AND DUST DENSITIES.

J.-D. Bodénan[1,2], C. Surville[2], L. Mayer[2], M. Schönbächler[1]. [1]ETH Zürich, Inst. für Geochemie und Petrologie, Claussisusstrasse 25, 8092 Zürich, Switzerland. (jean-david.bodenan@erdw.ethz.ch), [2]Institute for Computational Science, Winterthurerstrasse 190, 8057 Zürich, Switzerland.

Introduction: Shocks are one of the major mechanisms invoked to explain the formation of chondrules and their specific properties [e.g. 1]. They can induce fast heating to temperatures needed to melt chondrule precursors (> 1800 K) and allow for subsequent rapid cooling (0.5-3000 K/h). However, the origins of the shocks are still debated. Imaging of protoplanetary disks, for instance by the ALMA (Atacama Large Millimetre/submillimetre Array) telescope, identified large gaps in these disks potentially carved by massive planets [2]. Interactions between a massive planet and the disk create shocks travelling through the disk and large-scale vortices, in which dust can be concentrated, along with enhanced gas density and pressure [3]. These settings provide favourable conditions for chondrule formation, which requires such an environment to explain the retention of volatile species such as Na [4]. The largest regions of high vorticity are located on the outer edge of the gap formed by the planet and can cover areas of up to 1 AU in diameter. They are strongly affected by the shocks produced by shear forces resulting from the planet orbiting at less than Keplerian speeds, while the gas rotates around the sun at such velocities, causing strong friction. To be able to produce chondrules, these shocks must heat particles trapped in vortices to temperatures between 1800 and 2250 K and followed by rapid cooling. This work follows up on previous results [3], in which a Jupiter-mass planet generated temperatures sufficient to melt chondrule precursors. Here, we further explore the role of dust and cooling in the disk in this context.

Methods: The hydrodynamical code ROSSBI [5] was used to perform 2D simulations of the protoplanetary disk and explore the parameter space for shocks that originate from the presence of a massive planet (1 Jupiter mass (MJ)). Simulations include gas and dust, or gas only because the effect of gas drag is negligible over the duration of the runs for small grain sizes relevant to chondrule precursors (μm-sized). To study the influence of the shocks on the pressure and temperature regime of the disk, several parameters were tested and three cases for cooling were investigated: (i) Early simulations did not include a cooling mechanism (adiabatic case). (ii) Thermal relaxation, which applies a cooling function to the disk that depends on local orbit frequency and specifies a number of orbits (τ_c) for temperature variations to return to that of the background if no further disturbances occur. (iii) An approximation of radiation diffusion (κ-cooling) [6], which covers a range of cooling conditions with a smooth and continuous transition between extreme regimes. The cooling conditions depend on local temperature and the local optical depth.

Discussion: We previously showed that temperatures sufficient to melt chondrule precursors can be reached in a disk similar to the solar protoplanetary disk [3]. However, these simulations applied either adiabatic cooling or thermal relaxation with slow cooling rates ($\tau_c \geq 1000$ orbits). With lower values for thermal relaxation ($\tau_c < 1000$ orbits) or κ-cooling, it is difficult to reach temperatures exceeding 1800 K outside the planet's orbit, where vortices are located. When including this more intense, but more realistic, cooling regime, high enough temperatures are only achieved when the planet is very close to the star (~ 1.5 AU), even when considering a more massive planet (2MJ). However, when so close to the star, temperatures inside the orbit of the planet become too high (> 2500 K) to allow for chondrule formation under the effects of shocks propagating inwards and fast local cooling is prevented. Most simulations used the model of the minimum mass solar nebula (MMSN). In simulations adapting a more massive nebula (5MMSN), the planet migrates quickly towards the star (within 200 orbits). While conditions favourable for chondrule formation are achieved during this migration, the interior of the disk strongly heats and prevents the cooling of chondrules. Simulations including dust show that dust fractions (100 μm to 5 mm) will concentrate in vortices, although larger grains concentrate faster than finer ones. The finer grain fractions are also dragged more readily in the shocks, leading to size sorting in the regions affected by the shocks and vortices.

Conclusions: According to the current 2D simulations, chondrule formation in shocks created by Jupiter strongly depends on the cooling conditions considered for the disk. Under the investigated conditions, it seems unlikely that this process could explain chondrule formation in our solar system. The presence of a massive planet can, however, create concentrations of dust and gas in large regions that are favourable to chondrule formation, but this scenario would require an additional energy source to heat the chondrule precursors to adequate temperatures.

References: [1] Morris M. et al. (2010) *The Astrophysical Journal 722*:1474-1494. [2] Andrews S. et al. (2016) *The Astrophysical Journal Letters 820*:L40. [3] Bodénan J.-D. et al. (2018) *81st AMSM*, Abstract #6059. [4] Alexander C. M. O'D. et al. (2008) *Science 320*:1617-1619. [5] Surville C. et al. (2016) *The Astrophysical Journal 831:*82. [6] Stamatellos D. et al. (2007) *Astronomy & Astrophysics 475*:37-49.

ORGANIC COMPOUNDS IN EARLY SOLAR SYSTEM AQUEOUS FLUIDS.

R.J. Bodnar[1], A. Dolocan[2], M.E. Zolensky[3], H. Lamadrid[4], Y. Kebukawa[5], Q.H.-S. Chan[6], Z. Rahman[7]; [1]Dept. of Geosciences, Virginia Tech, Blacksburg VA 24061 USA; [2]Texas Materials Institute, Univ. of Texas, Austin, TX 78712 USA; [3]ARES, NASA JSC, Houston TX 77058, USA; [4]Dept. of Geological Sci., Univ. of Missouri Columbia, Columbia MO 75211, USA; [5]Faculty of Engineering, Yokohama National Univ., Yokohama 240-8501, Japan; [6]Dept. of Physical Sciences, The Open Univ., Milton Keynes, MK7 6AA, UK; [7]Jacobs JETS, Houston, TX 77058 USA.

Introduction: Two thermally-metamorphosed ordinary chondrite regolith breccias (Monahans 1998, hereafter simply "Monahans" (H5) and Zag (H3-6)) contain fluid inclusion-bearing halite (NaCl) crystals [1,2] dated to be ~4.5 billion years old [1,3,4]. Thus, compositional data on fluid inclusions in these halites will reveal unique information regarding the origin and activity of aqueous fluids in the early solar system, and especially their interactions with organic material. Our initial analyses of solid inclusions in Monahans halite has shown the presence of olivine, high- and low- Ca pyroxene, feldspars, magnetite, sulfides, phyllosilicates, zeolites, metal, phosphates and abundant organics [5,6]. We have reported a diverse assemblage of carbon, carbonates and organics in these residues [6], and low but significant amino acids concentrations in Monahans and Zag halite [7].

Techniques: Lamadrid et al. [8] recently succeeded in measuring compositions of solid daughter minerals and ice inside aqueous fluid inclusions using Time of Flight Secondary Ion Mass Spectrometry (TOF-SIMS) employing a freezing stage at the Texas Materials Institute of the University of Texas at Austin - we repeated this for our fluid inclusions. To reach the fluid inclusions located several microns below the sample surface, we performed TOF-SIMS depth profiling and attempted to determine the fluid composition of several Monahans halite fluid inclusions. We used a TOF-SIMS 5 instrument (ION-TOF GmbH) equipped with a pulsed Bi^+ analysis ion beam (30 keV ion energy) and a O_2^+ sputtering ion beam (1 kV ion energy). To access the inclusions in the halite crystals we sequentially sputtered areas of 500 x 500 μm^2 with the O_2 ion beam in steps of ~0.5 μm and analyzed the center of the sputtered area (200 x 200 μm^2) with the Bi ion beam. The analysis beam was set in either the high current (HC, ~1 μm lateral resolution, ~3.5 pA measured sample current, mass resolution m/dm >3000) or burst alignment (BA, ~200 nm lateral resolution, ~0.4 pA measured sample current, mass resolution ~100) modes, depending on whether the analysis required high mass resolution or high spatial resolution. Once the inclusion depth was reached, the location of interest was mapped in 100 x 100 μm^2 and 200 x 200 μm^2 areas in both positive and negative polarity and both HC and BA mode. This ensured that the inclusions were mapped with both high mass and lateral resolution. Samples were cooled to approximately -160º C to prevent immediate evaporation (sublimation) of the frozen aqueous fluids.

Results and Discussion: As we recently described in our preliminary report at LPSC [9] the best results were on a fluid inclusion measuring ~15 by 50 μm. The presence of water in the inclusion was confirmed by the detection two representative secondary ion species, $NaOH^-$ and H_2O^+, that map at the inclusion location. While the $NaOH^-$ fragment is mostly concentrated in the inclusion, the water content appears only slightly higher, a result of water being trapped throughout the halite (which we confirmed by FIBing a Zag halite crystal), which renders the H_2O^+ signal virtually uniform at any depth. One consequence of the high water content in the NaCl matrix is that the OH^- signal, a common marker for water, is simply saturated at the inclusion depth and thus does not show any enhancement at the inclusion location. A large number of organic species are identified: C^+, CH_3^+, $C_2H_3^+$ and $C_2H_2NO_2^+$, and C^-, C_2^-, CN^-, CNO^-, $CNCl^-$, $CHNCl^-$ and CNF^-/CHO_2^-. The detection of larger C-bearing fragments confirms the presence of larger organic molecules in the inclusion, such as amino acids and possibly nitroethylene ($C_2H_3NO_2$). A possible parent molecule in the inclusion is C2H2NO2, which could be a fragment of nitroethylene (C2H3NO2). We also detect expected inorganic species such as K^+, Si^+, $K_3(OH)_2^+$, K_3O^+, H_2O^+, NaOH-, NO- and Si-, and trace amounts of Fe+.

Conclusions and future work: The fluid inclusion in Monahans halite contained a high concentration of organic species. Our next step will be to use artificial halite crystals spiked with a known carbon content to permit quantification of the total carbon in the astromaterial halites. TOF-SIMS can be used successfully for astromaterial fluid inclusion composition measurements, provided sufficiently large inclusions are available. Inclusions we have located in carbonates, oxides and sulfides will be measured.

References: [1] Zolensky et al. (1999) Science 285, 1377-1379; [2] Rubin et al. (2002) *MAPS* **37**, 125-142; [3] Whitby et al. (2000) Science 288, 1819-1821; [4] Bogard et al. (2001) *MAPS* **36**, 107-122; [5] Zolensky et al. (2013) *Abstracts, 76th Annual Meeting of the Meteoritical Society*; [6] Kebukawa et al. (2016) *47th Lunar and Planetary Science Conference*. Abstract; [7] Chan et al. (2018) *Science Advances* 4, eaao3521; [8] Lamadrid et al. (2017) *Nature Communications* **8**, 16107 doi: 10.1038/ncomms16107; [9] Bodnar et al., *50th LPSC Conference*, abstract.

STUDY OF A SERIES OF FINE-GRAINED AMMs: MULTI-ANALYTICAL CHARACTERIZATION AND COMPARISON WITH CARBONACEOUS CHONDRITES

L. Bonal, M. Battandier, P. Beck, and E. Quirico - Institut de Planétologie et d'Astrophysique de Grenoble (IPAG) - Université Grenoble Alpes, CNRS (Grenoble, France) (lydie.bonal@univ-grenoble-alpes.fr)

Introduction: Micrometeorites are extraterrestrial micrometric particles that survived their atmospheric entry. Being the dominant contribution of extraterrestrial matter on Earth [1], they complete the sampling of small bodies of the Solar System represented by meteorites, Interplanetary Dust Particles and samples returned by space missions. Here, we report on the analysis of a series of Antarctic micrometeorites (AMMs) from the Concordia collection [2]. The present work is focused on the organic matter and hydration state of the AMMs in comparison to primitive chondrites. Our objective is to have a better appraisal of compositional variability across cosmomaterials.

Samples and methods: We considered a series of 58 AMMs from the Concordia 2006 and 2016 collections. This set of AMMs provides a large range of textural types reflecting different intensities of heating experienced during the atmospheric entry [3]: 40 unmelted fine-grained particles (Fgs), 12 particles intermediate partially melted (Fg-Scs), 1 partially melted scoriaceous particle (Sc) and 5 completely melted cosmic spherules (CSs). Each of these AMMs were characterized by Raman and IR spectroscopy [4]. Raman spectroscopy, sensitive to the structure of the polyaromatic carbonaceous matter, allows to constrain the thermal history of each sample and to distinct asteroidal thermal metamorphism from atmospheric flash heating. IR spectroscopy allows to characterize the aliphatic organic matter as well as the hydration state and the mineralogy of each sample. The bulk carbon and nitrogen isotopic composition of some Fg-AMMs were also determined (NanoSIMS). Systematic comparison with CM, CR and CI carbonaceous chondrites were led. We also performed some heating experiments of chondritic matrix grains, that we subsequently characterized through the same analytical sequence. Altogether these analytical and experimental results allow to disentangle modification induced by post-accretion processes and by atmospheric entry.

Results and discussion: The combination of Raman and IR techniques reveals differences among AMMs in terms of abundance, structure and chemical composition of the organic matter, mineralogy and hydration state. Heating laboratory experiments, on CM, CR and CI carbonaceous chondrite matrices, confirm that the atmospheric entry can induce : a dehydration of the samples, a decrease in the abundance of organic material and a structural modification of polyaromatic organic matter. The identification of Fgs-AMMs that are non-hydrated reveals that, in spite of their fine-grained texture, they may have experienced significant heating during the atmospheric entry. This study clearly shows that the hydration state and the organic matter are tracers of heating experienced by the micrometeorites during their atmospheric entry more sensitive than their texture [4]. We identified seven Fgs-AMMs that are hydrated and appear as the least affected by the atmospheric entry. Intrinsic differences, which cannot be explained by the atmospheric entry, are also revealed between those and CM, CR and CI chondrites. These differences are *(i)* a specific spectral signature of silicates in IR, *(ii)* enrichment in polyaromatic and aliphatic organic matter in comparison to chondrites and *(iii)* different characteristics of the aliphatic organic matter. Moreover, the analysis of the bulk isotopic composition of carbon and nitrogen shows large variabilities among AMMs, in contrast with observations among carbonaceous chondrites. All of these intrinsic differences are explained here as AMMs and carbonaceous chondrites having most likely sampled distinct parent bodies [4].

References: [1] Love S. G. and Brownlee D. E. (1993) *Science*, 262: 550. [2] Duprat J. et al. (2007) *Advances in Space Research*, 39: 605-611. [3] Genge M. J. et al. (2008) *Meteoritics and Planetary Science*, 43: 497-515. [4] Battandier M. et al. (2018) Icarus 306: 74-93.

A COMPLEX INTERPLAY OF HEAT AND AQUEOUS ALTERATION EXPERIENCED BY THE PARIS CM CHONDRITE

L. Bonal[1], P. Beck[1], T. Nakamura[2], Y. Enokido[2], J. Gattacceca[3], J. Eschrig[1] [1]Institut de Planétologie et d'Astrophysique de Grenoble – Université Grenoble Alpes, CNRS (Grenoble - France) (lydie.bonal@univ-grenoble-alpes.fr), [2]Laboratory for Early Solar System Evolution, Tohoku University (Japan), [3]CNRS, Aix Marseille Univ, IRD, Coll France, INRA, CEREGE (Aix-en-Provence, France).

Introduction: The Paris meteorite is a CM chondrite [1] that has been thoroughly studied to assess its parent body history. Paris was classified as type 2.7 [2] on the alteration scale defined by [3]. Paris is brecciated and petrographically heterogeneous, with distinct lithologies (typically metal-rich and metal-poor, [4]) having experienced various degrees of alteration [4, 5]. In particular, it is suggested that the least aqueously altered parts are type 2.9 [4, 5], resulting in Paris to be considered as among the most pristine meteorites. Paris being a CM chondrite, its aqueous alteration is the main secondary process that has been considered, while its thermal history has been mostly overlooked. In the present work, by combining several analytical techniques on sub-samples of Paris, our objectives are twofold: *(i)* assess, through independent tracers, aqueous and thermal alteration of the Paris meteorite at the millimeter scale; and *(ii)* further refine our understanding of reflectance spectra of such materials. Reflectance spectroscopy is one of the main tool to characterize asteroids and to establish genetic links with meteorites. However, the interpretation of some spectral bands in terms of composition is not necessarily straightforward. We are here particularly interested in the mineralogical control of the so-called 0.7-micron band used as a proxy for hydrated minerals on asteroids [e.g., 6] and that is sometimes observed and sometimes not on Ryugu [e.g., 7], the asteroidal target of Hayabusa-2.

Methods: Eleven raw sub-samples with mass in the 50-100 mg range were obtained from a slice of Paris. The magnetic properties of these sub-samples have been previously characterized [4]. Each of these sub-samples are several millimeter apart and were subsequently characterized through the following analytical sequence: *(i)* magnetic hysteresis measurements of bulk sub-samples to quantify the abundance of ferromagnetic minerals; *(ii)* Raman spectroscopy of matrix grains to characterized the structural order of the polyaromatic carbonaceous matter to assess their thermal history [e.g. 8]; *(iii)* IR measurements of matrix grains in transmission, under vacuum and a low temperature, to assess the extent of aqueous alteration [9]; *(iv)* reflectance spectroscopy in ambient conditions, and under vacuum with the SHADOWS instrument [10]; *(v)* synchrotron X-ray diffraction (Beam line 3A in KEK, Tsukuba, Japan) to identify and quantify the mineralogy.

Results and discussion: The combination of the above-mentioned analytical techniques reveals a high variability of hydration and thermal history among the considered sub-samples of Paris. In particular, some samples are characterized by *(i)* a variable hydration and absence of significant heating (group A, 7/11 samples), and *(ii)* a limited hydration, but clear evidence of heating (group B, 4/11 samples). Raman data will be further investigated to understand whether the thermal history is due to short-time heating related to e.g., shock, as commonly observed among CM chondrites [8, 11], or to radiogenic long-term thermal metamorphism. In comparison to non-heated samples, heated samples are characterized by higher abundances of magnetite, serpentine in decomposition, absence of tochilinite, very shallow 3-microns band, and reflectance spectra clearly distinct from typical CM chondrites and other heated CM chondrites [e.g., 12]. Hydrated and non-heated samples (group A) are characterized by a clear dominance of metal over magnetite, a variable 3 microns bands, presence of tochilinite and serpentine, and most likely presence of amorphous silicates. These sub-samples experienced aqueous alteration, but to an extent clearly lower than in most CM chondrites. They most likely correspond to the "pristine" lithology as described in the literature [4, 5]. The presence of a significant abundance of magnetite in the very poorly hydrated but heated samples (group B), and the presence of metal dominating over magnetite in poorly hydrated but non-heated samples of Paris could be explained by hydration (leading to the formation of magnetite) followed by dehydration (explaining serpentine decomposition) through the heating process. Interestingly, the reflectance spectra of the hydrated samples all exhibit the 3 micron band, but not systematically the 0.7 micron band, only visible on the most aqueously altered samples. We will further investigate its mineralogical carrier through comparison of spectral and diffraction data. The present study also clearly underlines the mm-scale variability of this meteorite. Such variability is often overlooked when tentatively establishing genetic link between meteorites and asteroids.

References: [1] Bourot-Denise M. et al (2010) *LPSC XLI* Abstract#1683. [2] Marrocchi Y. et al. (2014) *Meteoritics & Planetary Science* 49: 1232-1249. [3] Rubin et al. (2007) *Geochimica and Cosmochimica Acta* 71: 2361-2382. [4] Hewins R.H. et al. (2014) *Geochimica and Cosmochimica Acta* 124: 190-222. [5] Rubin (2015) *Meteoritics & Planetary Science* 50: 1595-1612. [6] Rivkin et al. (2002) in *Asteroids III:* 235-253. [7] Vilas (2008) *The Astrophysical Journal* 135: 1101-1105. [8] Quirico et al. (2018) *Geochimica and Cosmochimica Acta* 241:17-37. [9] Beck et al. (2010) *Geochimica and Cosmochimica Acta* 74: 4881-4892. [10] Potin et al. (2018) *Applied Optics* 57: 8279. [11] Nakamura (2005) *Journal of Mineralogical and Petrological Sciences* 100: 260. [12] Potin et al. (2019) this volume.

PROBING MAGMA OCEAN CRYSTALLIZATION IN ROCKY PLANETS USING ZIRCONIUM ISOTOPES – PRELIMINARY RESULTS FROM ANCIENT ZIRCONS FROM EARTH AND MARS

L.C. Bouvier[1], M. Schiller[1], M. Fehr[2], M. Costa[1], J.N. Connelly[1], A. Nemchin[3], M. Schönbächler[2] and M. Bizzarro[1]

[1]Centre for Star and Planet Formation, University of Copenhagen, Copenhagen, Denmark

[2] ETH Zürich, Inst. für Geochemie und Petrologie, Zürich, Switzerland

[3]Curtin Univertsity, Perth, Australia

Terrestrial planets are believed to have experienced episode(s) of large-scale melting early in their history resulting into the formation of deep magma oceans [1]. Magma ocean crystallisation can lead to the formation of an unstable, chemical stratification of the primitive mantle due to the progressive iron enrichment of the cumulate layers from the bottom upward, which may result in cumulate overturn, melting and extraction of a primordial crust [1]. Unravelling the timescales of these processes is key for a full understanding of planet formation processes. With a half-life of 36 Myr [2], the ^{92}Nb-to-^{92}Zr decay system is ideally suited to probe planetary differentiation processes, including magma ocean crystallisation. Indeed, Nb and Zr can be fractionated from each other by magma ocean crystallisation processes, which may lead to the establishment of mantle and/or crustal reservoirs with variable Nb/Zr ratios. However, given the relatively low initial Solar System abundance of the parent ^{92}Nb nuclide [3], fully utilising of the ^{92}Nb-^{92}Zr decay system to probe early planetary differentiation requires significant improvement in currently used methods for high-precision analyses of the zirconium isotope composition of silicate materials.

Zircon is a powerful tool for understanding early silicate differentiation processes in terrestrial planets, including the stabilization and reworking of primordial crustal reservoirs [4]. Indeed, zircon can be accurately dated using the U-to-Pb decay system and is resistant to secondary alteration processes. Moreover, this mineral is rich in Hf and Zr, making it ideally suited for concomitant studies of the ^{176}Lu-^{176}Hf and ^{92}Nb-^{92}Zr systematics of its source reservoir. Taking advantage of new protocols for high precision analysis of Zr isotopes by MC-ICPMS, we report on the ^{92}Nb-^{92}Zr systematics of ancient zircons from Earth and Mars to better understand the timing and style of differentiation of these bodies. Our sample suite includes 8 zircons from the Jack Hills metasedimentary belt that record concordant U-Pb dates defining ^{207}Pb/^{206}Pb ages ranging from 4260.3±0.9 Ma to 3953.8±0.7 Ma and initial Hf isotope composition at the time of crystallization (εHf$_T$) varying from –1.68±0.18 to –4.91±0.11. In addition, we have investigated 7 zircons from the NWA 7034 martian breccia with mostly concordant U-Pb dates that define ^{207}Pb/^{206}Pb ages ranging from 4476.3±0.9 Ma to 4429.7±1.0 Ma and εHf$_T$ varying from –0.71±0.32 to –2.06±0.26 [5]. In this contribution, we report the Zr isotope composition for the 8 Jack Hills zircons and for one of the NWA 7034 martian zircons – results for the remaining martian zircons will be presented at the meeting.

The Zr isotope data were obtained on the same sample digestions utilized for the U-Pb ages and Hf isotope measurements. In brief, following the U-Pb chemistry, a Zr cut was separated from the U-Pb washes using a single stage TEVA-spec ion exchange chemistry that provides >90% recovery of the Zr and ensures adequate separation from potentially interfering species. The accuracy and external reproducibility of our approach was assessed by repeated analyses of aliquots of the 91500 zircon standard processed through our entire chemical purification procedure. The Zr isotope composition of our samples was analysed using a Neptune Plus MC-ICPMS either at the Centre for Start and Planet Formation (Copenhagen) or Institute of Geochemistry and Petrology, ETH (Zurich). A total of 13 aliquots of the 91500 standard defines an external reproducibility estimate (2SD) of ± 7.1 ppm for μ^{91}Zr, ± 3.7 ppm for μ^{92}Zr and ± 24.5 ppm for μ^{96}Zr for quantities of Zr comparable to that present in our samples. Our preliminary data shows that 3 Jack Hills zircons have resolvable deficits of <10 ppm in μ^{92}Zr and normal compositions for the μ^{91}Zr and μ^{96}Zr. The anomalous Jack Hills zircons have the most ancient U-Pb ages in our suite, namely ranging from ~4.1 to 4.3 Ga and unradiogenic εHf$_T$ requiring formation of their source reservoir ≥4.4 Gyr ago. Similarly, a NWA 7034 zircon with ^{207}Pb/^{206}Pb age of 4429.7±1.0 Ma defines a resolvable deficit in μ^{92}Zr of 7.7±3.7 ppm, a normal μ^{91}Zr composition and an anomalous μ^{96}Zr value of 34.7±24.5 ppm, which is consistent that inferred for Mars based on ordinary chondrites [6]. For both Earth and Mars, our data suggest that the zircons with anomalous μ^{92}Zr were derived from a reservoir with a subchondritic Nb/Zr ratio extracted within the first ~100 Myrs of the Solar System. Although this timescale is consistent with a rapid formation of the primordial crust of Mars <20 Myr of Solar System formation, it is difficult to reconcile with a late Moon-forming event [7] and, hence, global remelting and homogenization of the early Earth at ~4.4 Ga. Alternatively, the anomalous μ^{92}Zr of some of the Jack Hills zircons may reflect the preservation of a signature associated with the initial differentiation of the proto-Earth prior to the Moon-forming impact.

References: [1] Elkins-Tanton, L.T. et al. (2003) *Meteorit. Planet. Sci.* 38, 1753. [2] Nethaway, D.R. et al. (1978) *Phys. Rev. C* 17, 1409. [3] Iizuka, T. et al. (2016) *EPSL* 439, 172. [4] Scherer, E.E. et al. (2007) *Elements* 3, 19. [5] Bouvier, L.C. et al. (2018) *Nature* 558, 586 [6] Akram, W. et al. (2015) *GCA* 165, 484. [7] Connelly, J., Bizzarro, M. (2016) *EPSL* 452, 36.

Dynamical Impact Bombardment Chronology Of The Terrestrial Planets From 4.5 Ga To 3.5 Ga.

R. BRASSER[1], S. C. WERNER[2] AND S. J. MOJZSIS[3]

[1]Earth Life Science Institute, Tokyo Institute of Technology, Tokyo, Japan; [2]Centre for Earth Evolution and Dynamics, Oslo, Norway; [3]University of Colorado at Boulder, Boulder, CO, USA

We report the intensity and effects of early impacts on the terrestrial planets by combining dynamical N-body and Monte Carlo simulations to determine impact probability, impact velocities, and expected mass augmentation onto the terrestrial planets from three sources after the formation of the Moon [1]. These sources are: planetesimals left over from primary accretion and the hypothetical E-belt, and comets arriving from the outer solar system. We present for the first time a robust estimate of the amount of cometary material striking the terrestrial planets during an episode of planetesimal-driven giant planet migration. The Moon and Mars suffer a proportionally much higher amount of cometary accretion than Venus and the Earth; for the Moon this contribution could be gleaned in its D/H ratio and Xe isotopes. The background mass augmentation from small leftover planetesimals to the Earth and Mars is far lower than the estimates based on the abundance of highly-siderophile elements in their mantles and terrestrial tungsten isotopes. This supports that both planets were struck well after their formation by single large bodies that delivered most of their late mass augmentation. We calculate the lunar, martian and mercurian chronologies using the impacts recorded onto the planets from dynamical simulations and present fits to the impact chronologies that are valid from 4.5 Ga to ca. 3.7 Ga (**Figure 1**). The dynamical lunar chronology thus obtained agrees reasonably well with the Werner [4] chronology, but not with that of Neukum [5]. For Mars the match

Figure 1. Lunar chronology (left) and martian chronology (right) from a combination of dynamical and Monte Carlo simulations. The three reservoirs are the comets from the outer solar system, leftover planetesimals and the E-belt with the best fits. The calibrated Werner and Neukum chronologies are shown separately as solid lines. The contribution from the main belt is included based on simulations from [2]. The filled circle data points are calibrations from [3]. The open circles are an attempt by us at a new, albeit somewhat provisional, calibration.

with the calibrated Werner chronology is also very good. For Mercury we present a theoretical chronology only. Neither of our dynamical chronologies match that of Neukum. The dynamical lunar and martian chronologies are also somewhat different from each other, so that the usual extrapolation from one body to the other does not apply. The dynamical chronology curves displayed here result in surface ages up to 150 Myr older on the Moon and on Mars at certain epochs compared to the Neukum chronology. This has implications for the interpretation of the geological evolution of these bodies.

Bibliography

[1]Brasser, R., Werner, S. C. and Mojzsis, S. J. (2019) *Icarus*, submitted

[2] Morbidelli A., Brasser R., Gomes R., Levison H. F., Tsiganis K., (2010) *Astronomical Journal* **140**, 1391-1401

[3] Neukum, G.:1983, Meteoritenbombardement und Datierung planetarer Oberflächen, Habilitation Dissertation for Faculty Membership, Ludwig-Maximilians Univ. München, Munich, Germany, 186 pp.

[4] Werner S. C., Ody A., and Poulet F., (2014), *Science* **343**, 1343-1346

[5] Neukum G., Ivanov B. A., and Hartmann W. K., (2001) *SSRv*, **96**, 55-86

VARIABLE METASOMATIC ALTERATION OF ALLENDE-LIKE OXIDIZED CV3 CHONDRITES: A COMPARISON OF ANTARCTIC AND NORTHWEST AFRICA CV3 CHONDRITES WITH ALLENDE

Adrian J. Brearley[1], Jessica M. Johnson[1], Brian Williams[1], and Jerome Gattacceca[2]. [1]Department of Earth and Planetary Sciences, MSC03-2040, 1University of New Mexico, Albuquerque, NM 87131, USA (brearley@unm.edu). [2]CNRS, Aix Marseille Univ, IRD, Coll France, INRA, CEREGE, Aix-en-Provence, France.

Introduction: The fall of the Allende meteorite in 1969 set in play a remarkable series of scientific investigations that have revolutionized our understanding of chondritic materials. Among the many discoveries has been the recognition of significant metasomatic alteration that affected all the primary chondritic components [1-4]. Efforts to understand the environment, timing, and mechanisms of these metasomatic processes has been a provocative scientific debate that has spanned several decades. Many questions still remain to be resolved, but there has been a significant shift in the interpretation of these secondary alteration effects from one that focused on a nebular environment involving interaction with a nebular gas to a parent body environment that involved fluid-rock interactions [4]. Allende is unquestionably the scientific reference for understanding these metasomatic effects. However, many new CV3 chondrites that have been recovered from Antarctica and Northwest African deserts are providing new insights into the diverse styles of alteration that have affected the CV3 chondrites. Here we report petrologic observations from two Northwest Africa and one Antarctic CV3 finds that are all classified as oxidized Allende-like CV3s, but diverge in important ways in their alteration effects from Allende itself.

Results: MET 00430 represents one of the least-altered oxidized CV3 chondrites, but nevertheless has a number of distinct alteration features. It is weakly metamorphosed, but most metal has been replaced by magnetite and sulfides. Pyroxenes show minimal evidence of replacement by ferroan olivine, nevertheless, large, euhedral fayalitic olivines are present in the matrix [5]. CAIs in MET 00430 show minimal replacement of melilite by nepheline, but no sodalite and other Ca-rich alteration phases are absent. Chondrule glass is preserved in many chondrules, but has been replaced by a sequence of Ca-Fe-rich phases including wollastonite, etc. in reaction zones on the periphery of chondrules.

NWA 2364 shows significantly more evidence of thermal metamorphism than MET 00430, comparable to that in Allende. Mg-Fe zoning is more pronounced in forsteritic chondrule olivine and enstatite has been extensively replaced by ferroan olivine around the periphery of type IA chondrules. Replacement of chondrule glass has resulted in significant interchondrule porosity. The abundance of sulfides is remarkably low throughout the meteorite and Na-rich mesostasis glass is absent. Fine-grained CAIs have been extensively replaced, but in coarse-grained compact type A CAIs only minimal patchy replacement has occurred. Melilite and anorthite have been altered to an Al-rich phase which may be kaolinite, but no Na-K-Cl-bearing alteration phases, such as nepheline or sodalite are present.

NWA 8331 has distinct features that set it apart from MET 00430, NWA 2364, and Allende, although its petrologic type is similar to the latter two meteorites. It shows extensive sulfidization of metal in type I chondrules, and enstatite and forsteritic olivine are replaced by massive, featureless ferroan olivine, rather than platy olivine that is typical in Allende. Mesostasis glass has also been replaced by ferroan olivine and relict glass is only present in the core of one large type IA chondrule. CAIs show only minor replacement of melilite by nepheline and minor sodalite and andradite, rather than grossular appears to be the garnet phase that is most common as a secondary alteration phase.

Discussion and conclusions: All three of these CV3 chondrites have been classified as oxidized Allende-like CV3 chondrites [5-7]. Primary metal has largely been replaced by magnetite in all of them. However, they exhibit a wide range of alteration features, which differ in significant ways from Allende. NWA 8331 and MET 00430 clearly show evidence of widespread sulfidization that also affected Allende. In contrast, NWA 2364 is remarkably depleted in sulfides suggest that it may have experienced loss, rather than gain of sulfur. Similarly, NWA 2364 contains no evidence of the pervasive alkali-halogen metasomatism that affected Allende and indeed appears to be highly depleted, rather than enriched in alkalis. The effects of Na-Cl metasomatism are also minimally developed in MET 00430 and NWA 8331. These observations demonstrate that the processes that affected Allende are not necessarily typical of oxidized CV3 chondrites in general and also show that the processes of oxidation, sulfidization, and alkali-halogen metasomatism that affected Allende and other CV3 chondrites are not necessarily coupled. On the contrary, they may represent distinct events and processes that affected different CV3 chondrites to different degrees, including both metasomatic addition and removal of fluid-mobile elements such as alkalis, Cl, S, and Fe.

References: [1] MacPherson, G.J. and Grossman, L. (1984) *Geochimica et Cosmochimica Acta* 48:29. [2] Hashimoto A. and Grossman, L. (1987) *Geochimica et Cosmochimica Acta* 51:1685. [3] Krot A.N. et al (1995) *Meteoritics* 30:748–775. [4] Brearley A.J. and Krot A.N. (2013) In '*Metasomatism and the Chemical Transformation of Rock: The Role of Fluids in Terrestrial and Extraterrestrial Processes.* pp. 653. [5] Krot, A.N. et al. (2006) In *Meteorites and the Early Solar System II*, pp 525. [6] Antarctic Meteorite Newsletter (2002) 25, No. 2. [6] Russell, S.S. et al. (2005) The Meteoritical Bulletin, no. 89, *Meteoritics and Planetary Science* 40, A201. [7] Ruzicka A. et al. (2017) The Meteoritical Bulletin no. 103 *Meteoritics & Planetary Science* 52.

FAST TRACE ELEMENT TOMOGRAPHY AND WDX REE PATTERN MEASUREMENT OF PRISTINE ASTEROIDAL SAMPLE MATERIAL

F. E. Brenker[1], L. Vincze[2], B. Vekemans[2], E. De Pauw[2], B. Tkalcec[1] and G. Falkenberg[3],
[1]Geoscience Institute / Mineralogy, Goethe University Frankfurt, Altenhoeferallee 1, 60438 Frankfurt am Main, Germany, f.brenker@em.uni-frankfurt.de, [2]Department of Chemistry, Ghent University, Krijgslaan 281, S12, B-9000 Ghent, Belgium, laszlo.vincze@ugent.be, [3]DESY – P06, Notkestr. 85, 22603 Hamburg, Germany

Introduction: The sample return mission to the pristine asteroids Ryugu (Hayabusa 2) [1,2] is almost completed and will return micron to mm-sized objects for study of modern instrumentation in laboratories on Earth soon.

Due to it´s immense importance these valuable samples should be treated with extreme care. Thus, any (more or less) non-destructive analytical approach should be the first choise. However, non-destructive measurement techniques, like low dose SEM, ESEM, synchrotron XRD and XRF, are scarce.

Synchrotron Techniques: Synchrotrons around the globe were used to study tiny particles of cometary [3,4] and interstellar sources [5,6,7] collected during NASAs Stardust mission. It was demonstrated that synchrotron sources are valuable tools to measure the main and trace element content of even the tiniest extraterrestrial particles. The development of new analytical approaches to measure REE-patterns in complex sub-micron inclusions applying confocal XRF set-ups and energy-dispersive X-ray imaging detectors [8] represent ongoing work in the framework of a long-term project of our group at the PETRA-III synchrotron facility (Hamburg, Germany) and is already applied to various sample types including asteroidal (e.g. UR-CAIs) as well as Martian sample material.

Rare Earth Elements: The non-destructive, quantitative measurements of REE patterns from mineral species in the collected rock fragments will allow to identify important processes associated with the formation of the first solids of our solar system as well as processing asteroidal material. The detailed study of samples returned from the surface of Ryugu will help to better understand the conditions and chemical variability on the surface of asteroids.

REE-patterns are especially useful as they may record changes in oxygen-fugacity, temperature, fluid content and chemical reservoirs, especially if combined with isotopic studies on the same samples. Important information on the rare earth element fractionation, especially at high temperature condensation and crystallization, as well aslow temperature surface alteration could be obtained from these samples. Also information about Eu-anomaly, the relative enrichment of light REE versus heavy REE and ultimately the overall pattern distribution could be retrieved with the high-energy XRF spectroscopy measurements.

New Analytical Approach: Detection of X-ray fluorescence is commonly performed by energy dispersive detectors, although this detection method is inferior when a high energy resolution is required. L-lines of rare earth elements (REEs) are often only separated by a few tens of eV and an energy dispersive setup results in overlapping signals especially in the presence of transition metal K lines. A novel wavelength-dispersive detection method for X-ray fluorescence spectroscopy is optimized specifically for the detection of REE L-lines. The characteristic X-rays emitted by the sample are dispersed by a fixed Ge(111) analyzer crystal over the active area of an energy dispersive pnCCD detector, enabling high energy resolution detection of X-rays differentiated by their corresponding diffraction angles in the energy range of 4-8 keV. An energy resolution of 12 eV for the Ti-Kα fluorescence line was achieved [9].

References: [1] Tachibana, S. et al. (2014) Geochemical Journal, Vol. 48, pp. 571 to 587. [2] Watanabe, S. et al. (2017) Space Sci. Rev. 208, 3-16. [3] Brownlee, D. et al. [2006] Science. [4] Flynn et al., (2006) Science. [5] Brenker et al. (2014) Meteoritics & Planet. Sci. 49, 1594–1611 [6] Westpfahl et al. (2014) Science, 345, 786-791. [7] Gainsforth, Z. et al. (2014) Meteoritics & Planet. Sci. 49, 1645-1665. [8] Garrevoet et al. (2014) Analytical Chemistry, 86, 11826–11832. [9] De Pauw, E. et al. (2019) Analytical Chemistry (in review).

FELDSPATHIC CUMULATE SAMPLES AND PLUTONIC ROCKS IN GALE CRATER: COMPARISONS TO MARTIAN METEORITES.

J. C. Bridges[1], A. Cousin[2], V. Sautter[3], W. Rapin[4], D. Bowden[1], L. Thompson[5], S.P. Schwenzer[6], C. Bedford[6], V. Payre[7], O. Gasnault[2], O. Forni[2], P. Pinet[2], R. Wiens[8], R A. Yingst[9] [1]University of Leicester, UK j.bridges@le.ac.uk [2]Institut de Recherches en Astrophysique et Planétologie, Toulouse, France, [3]Inst. de Minéralogie, de Physique des Matériaux et de Cosmochimie, Paris, France, [4]JPL/Caltech, Pasadena, USA, [5]University of New Brunswick, Canada,[6]Open University, UK, [7]EEPS, Rice University, Houston, USA, [8]LANL, Los Alamos, USA. [9]Planetary Science Institute, USA.

Introduction: The Curiosity Rover of Mars Science Laboratory has identified igneous float rocks in Gale Crater which offer new insights about the differentiation of the martian lithosphere. Here we describe likely origins for some unique Gale plutonic and cumulate rocks and compare to the martian meteorites. At the Ireson Hill locality around sol 1606 a group of float rocks with resistant, dreikanter morphologies were identified which include igneous textures, notably the 10 cm Pogy sample. On sol 2016 of the MSL mission, a group of float rocks were studied in detail, including Askival, which is a light toned rock igneous rock similar to Peacock_Hills (sol 19) and Bindi (sol 544).

Methods: ChemCam contains a NIR laser and telescope within MSL's mast and 3 spectrometers inside the body unit [1,2]. It remotely analyses targets by Laser Induced Breakdown Spectroscopy, with optimal performance at ≤4 m, and also has a Remote MicroImager. Typically, there are around 30-50 laser shots on a single observation point in a raster (e.g. two 10 x 1 rasters and one 3 x 1 raster on Askival). A combination of ICA and PLS are used to derive major oxide compositions [3]. H_2O is determined with a univariate method [4]. The Alpha Particle X-ray Spectrometer (APXS) provided 3 analyses on Askival [5]. This float rock was first identified during MSL operations using MastCam and MAHLI images.

Figure 1. Gale igneous and shergottite compositions. Dashed line shows silicification (with hydration) of Askival feldspathic cumulate. #1 is Askival LIBS is ferrohastingsite (with Fe oxide and sulfate). Jake_M [5], trachybasalt density contours [6].

Results: *Gale Feldspathic Cunulates.* Askival is a 10 cm long, partially buried, float rock. It contains light-toned subhedral mineral grains (up to ±10 mm long) as well as dark and grey-toned minerals and veins. The light-toned grains (phenocrysts) comprise 65/70 % of the rock, and are in places poikilitically enclosed by the dark-toned assemblage which comprises 30/35 % of the rock. Bindi has a cumulate texture defined by ~80% tabular feldspar grains. *Pogy and Related Samples at Ireson Hill Locality.* MAHLI images reveal that Pogy has a 1.5 mm equigranular, plutonic texture, which has not been identified before at Gale. A series of 4 other float rocks at this locality may be related. *Mineral Compositions.* All but one of the LIBS spots on Askival show non stoichiometric compositions. Figure 1 shows that the light toned Askival compositions are a mixture of a relict intermediate plagioclase phase with SiO_2 in a 70:30 ratio. Silica-rich point analyses range up to >80 wt%. Point Askival#1 has SiO_2 34 wt%, Al_2O_3 6.8 wt%, FeO 28.4 wt% CaO 14.4 wt% and $Na_2O + K_2O$ 2.1 wt% implying that it escaped the silica overprint. LIBS shot analyses indicate that this is a mixture of iron oxide, sulfate and ferrohastingsite. In Askival #1 fluorine is also detected. Pogy has a basaltic composition with SiO_2 (APXS) 42 wt% with $Na_2O + K_2O$ 2.5 wt%, MgO 7.8 wt%. *Hydration of Light Toned Phases.* LIBS of Askival suggest an equivalent H_2O content in the relict feldspar grains of ~9-13 wt% H_2O.

Discussion: Our compositional and textural data suggest that Askival was originally a plagioclase-mafic cumulate that has been silicified and hydrated. The other Gale feldspathic cumulate samples analysed e.g. Bindi did not experience this alteration.. These feldspathic cumulates are unique in the inventory of landing site igneous samples and martian meteorites. The cumulate melt is likely to be related to the trachybasalt/trachyandesites [6,7]. This in turn was formed through fractional crystallisation of an Adirondack-type melt [6]. In contrast, the Pogy textures and composition suggest a basaltic (Adirondack) plutonic origin. Gale Crater has preserved a record of igneous differentiation and plutonic activity with higher alkali contents than that recorded by the shergottites .

References: [1] Wiens R.C. et al. (2012) *Space Sci. Rev.* 170 [2] Maurice et al. (2012) *Space Sci. Rev.* 170 [3] Clegg S.M. et al. (2017) *Spectrochimica Acta Part B*: *Atomic Spectroscopy* 129. [4] Rapin W. et al. (2017) *Spectrochimica Acta Part B*: *Atomic Spectroscopy* 130. [5] Schmidt M.E. et al. (2014) *JGR*, 119. [6] Edwards et al. (2017) *MAPS* 52 [7] Cousin A. et al. (2017) *Icarus*, 288.
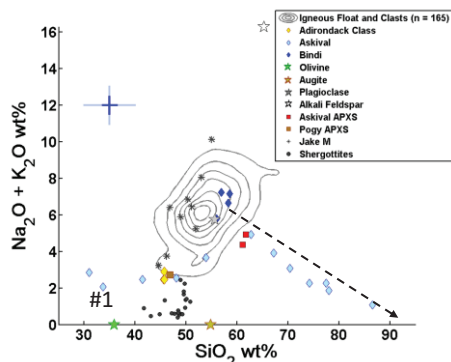
NOBLE GAS VARIATIONS IN UREILITES DEMONSTRATE HETEROGENOUS VOLATILE DISTRIBUTION IN THE EARLY SOLAR SYSTEM

M. W. Broadley[1], D. V. Bekaert[2], B. Marty[1], A. Yamaguchi[2], J-A, Barrat[3], [1] Centre de Recherches Pétrographiques et Géochimiques, 15 rue Notre Dame des Pauvres BP 20, 54500 Vandœuvre les Nancy, [2] National Institute of Polar Research, Tachikawa, Tokyo 190-8518, Japan, [3] Laboratoire Geoscience Océan, UMR 6538 CNRS—Université de Bretagne Occidentale et Institut Universitaire Européen de la Mer, Place Nicolas Copernic, 29280 Plouzané, France

Introduction:
Inner Solar System bodies are depleted in volatile elements relative to primitive chondritic meteorites. The origin of volatiles on inner solar system planetary bodies is therefore considered to be the result of late deliveries of volatile-rich material from the outer solar system [1]. However, Earth and Mars record evidence of solar volatiles within their mantles [2,3,4] indicating that these planets were able to accrete volatiles early [5] during the existence of the protosolar nebula (4 Myr after CAI) [6]. The timing and origin of volatile element accretion to terrestrial planets therefore remains enigmatic.

Ureilites are a group of achondrites, originating from a single, inner solar system body [7]. Ureilites are essentially the remnants of the mantle that has undergone extensive melt extraction [8]. The ureilite planetary body (UPB) is considered to have accreted ~1.6 Myr after CAI formation representing one of the oldest terrestrial planetary body in the solar system [9]. Ureilites therefore provide a unique opportunity to probe the composition of volatiles within the solar system and the mechanisms through which planetary bodies acquire and preserve volatiles throughout their accretion.

Samples and Methods: Six North West African ureilites (NWA 2236, NWA 7686, NWA 8049, NWA 8172, NWA 11368, NWA 11032) were chosen for heavy noble gas analysis. The details of the samples used in this study have been presented previously [10,11]. All samples analysed are unbrecciated main group ureilites, which are known to have extremely uniform and well-equilibrated olivine core compositions, with limited to no intergrain or intragrain variability [12]. Olivine cores within the samples analysed as part of this study have Mg# ranging from 76.9 to 96.9. Samples were specifically chosen to span the range of compositions previously measured within ureilites (Mg# = 74 - 97) [7]. Noble gases were extracted from bulk samples weighing between 6 and 32 mg. Noble gases were released at several temperatures using a tungsten filament furnace with Ar, Kr and Xe isotopes being measured.

Results and Discussion: Concentrations of ^{36}Ar, ^{84}Kr and ^{132}Xe are shown to be correlated with the Mg# of the olivine cores, with samples containing high Mg# olivines being enriched in noble gases relative to low Mg# number samples. The majority of ^{36}Ar/^{132}Xe and ^{84}Kr/^{132}Xe values fall intermediate between chondritic phase Q and solar. Krypton and xenon isotopes are similar to phase Q [13], however significant variations exist across the samples, with the Kr and Xe isotopic signatures lying along a mixing line between solar and the presolar HL component [14]. Interestingly, Xe isotopes also appear correlated with Mg#, with samples having the highest Mg# being more enriched in the heavy Xe-HL than low Mg# samples.

The correlation between noble gas elemental abundances and isotopic ratios suggests that that silicate fractions and noble gas bearing carbon phases may share a common origin. Previously, the similar highly-fractionated noble gas elemental and isotopic ratios in ureilites and phase Q, relative to solar, suggested they may have acquired noble gases through a similar nebular process [15]. However, it is not readily apparent why noble gas elemental abundances and isotopic ratios should be correlated with the Mg# of olivines. We therefore suggest that range of noble gas compositions in ureilites can be best accounted for by incomplete mixing between two distinct components, one being inherited directly from chondritic-like precursors (phase Q), and the other being derived from solar-like component potentially implanted from the solar wind.

References: [1] Rubie et al., (2015), Icarus, 248, pp.89-108. [2] Hallis et al., (2015) Science, 350, pp.795-797. [3] Mathew and Marti, (2001), Journal of Geophysical Research 106, pp.1401-1422. [4] William and Mukhopadhyay, (2019), Nature, 565, p.78. [5] Greenwood et al., (2017), Science Advances, 4(3), p.5928. [6] Wang et al., (2017), Science, 355, pp.623-627. [7] Downes, H., et al (2008). Geochimica et Cosmochimica Acta., 72(19), 4825-4844. [8] Goodrich et al., (2007), Geochimica et Cosmochimica Acta, 71, pp.2876-2895. [9] Budde et al., (2015), Earth and Planetart Science Letters 430, pp.316-325. [10] Barrat et al., (2016), Geochimica et Cosmochimica Acta, 194, pp.163-178. [11] Barrat et al., (2017), Earth and Planetary Science Letters 478, pp.143-149. [12] Goodrich et al., (1987), Geochimica et Cosmochimica Acta, 51), pp.2255-2273. [13] Busemann et al., (2000), Meteoritics and Planetary Science., 35(5), pp.949-973. [14] Huss and Lewis, (1994), Meteoritics, 29, pp.811-829. [15] Rai et al., (2003), Geochimica et Cosmochimica Acta, 67(22), pp.4435-4456

COMPARING THERMAL INFRARED SPECTRAL UNMIXING ALGORITHMS: APPLICATIONS TO BENNU AND OTHER AIRLESS BODIES.

E. C. Brown[1], K. L. Donaldson Hanna[1,2], N. E. Bowles[1], V. E. Hamilton[3], B. E. Clark[4], A. D. Rogers[5], D. S. Lauretta[6], and the OSIRIS-REx Team, [1]Atmospheric, Oceanic and Planetary Physics, University of Oxford, Clarendon Laboratory, Parks Road, Oxford OX1 3PU, UK (eloise.brown@physics.ox.ac.uk), [2]Department of Physics, University of Central Florida, FL, USA, [3]Department of Space Science, Southwest Research Institute, CO, USA, [4]Department of Physics & Astronomy, Ithaca College, NY, USA, [5]Department of Geosciences, Stony Brook, NY, USA, [6]Lunar and Planetary Laboratory, University of Arizona, Tucson, AZ, USA.

Introduction: The aim of this work is to examine a selection of fitting algorithms for determining composition when applied to the traditional linear unmixing model for thermal infrared (TIR; ~5− 50 μm or 2000 – 200 cm^{-1}) laboratory and remote sensing spectra. Here we outline the basic background knowledge required, discuss an alternative approach, and provide comparisons of these different algorithms using a subset of the Origins, Spectral Interpretation, Resource Identification, and Security – Regolith Explorer (OSIRIS-REx) TIR blind test spectra [1]. Current methods have produced geologically relevant mineralogies and abundances for situations with additional prior knowledge (e.g., Mars [2]), however it is uncertain if these methods work similarly in situations with limited prior information. It is therefore important to fully investigate whether such methods are appropriate for observational data that lack additional contextual information (e.g., spacecraft and telescopic data), and to see what new insights a Bayesian approach may bring.

Common approaches for unmixing TIR spectra: Several spectral unmixing algorithms have been developed with varying complexity, many of which have used the least squares technique to find end-members present in a mixture and their corresponding abundances (e.g., [2, 3]). Some of these methods have been adapted to ensure meaningful physical results (i.e., abundances must be non-negative). However, the degree of degeneracy in the retrieved compositional abundances is often unknown, especially in circumstances with relatively poor prior knowledge. When there is limited contextual information and/or noisy data (as is often the case for telescopic observations), the end-member minerals within the chosen spectral library could have multiple assemblages that each produce a statistically good fit to the data (e.g., as measured by the reduced χ^2), thus leading to degenerate results (including, possibly, geologically unlikely compositions). With traditional least squares algorithms, it can be difficult to account for these degenerate solutions, and alternative combinations of end-members may not be fully explored [4].

A Bayesian approach: In this work we adopt Bayesian inference techniques widely used to understand a variety of physical processes and phenomena (e.g., [5]). Such techniques include Markov Chain Monte Carlo (MCMC, [6]) which may be applied to the spectral unmixing problem by exploring the parameter space to determine the most probable end-member mineral abundances, each with an envelope of uncertainty. Sampling techniques such as MCMC are useful as they allow the exploration of a broad range of solutions, subject to the priors, and the analysis of the distribution of possible outcomes. Using a Bayesian perspective can be particularly insightful due to the quantitative inclusion of prior information. In the case of degenerate solutions being more likely (e.g., due to noisy spectra, low spectral contrast, or lack of wider geological context), quantitatively adding *a priori* information allows us to limit the parameter space explored whilst retaining knowledge of how this may affect the final (posterior) retrieved compositions. The input information for each parameter can be based on what is already known about the material (e.g., from the meteorite record) and can include uncertainties on this prior knowledge. Although it is still possible to retrieve unlikely compositions using MCMC, this technique will allow us to better explore possible degenerate solutions.

Data used: The OSIRIS-REx blind test study presented spectral measurements of materials thought to be compositionally analogous to target asteroid (101955) Bennu [1]. Here we use the TIR blind test physical mixtures of well-characterised mineral end-members as we have TIR spectra of both the mixtures and most of the mineral end-members, making it an ideal dataset to compare our Bayesian MCMC algorithm and more commonly used methods.

Future applications: With potential for Bayesian techniques to provide new insights into the quality of the linear fitting model, such alternative algorithms may be applied to additional laboratory data, and to data collected by missions including OSIRIS-REx [7] and the Spitzer Space Telescope [8].

References: [1] Donaldson Hanna K. L. et al. (2019) *Icarus* 319:701-723. [2] Rogers A. D. and Aharonson O. (2008) *JGR* 113:E06S14. [3] Ramsey M. S. and Christensen P. R. (1998) *JGR* 103:577-596. [4] Lapotre M. G. A et al. (2017) *JGR Planets* 122:983-1009. [5] von Toussaint U. (2011) *Reviews of Modern Physics* 83:943-999. [6] Metropolis N. et al. (1953) *J. of Chem. Phys.* 21:1087-1092. [7] Lauretta D. S. et al. (2017) *Space Sci. Rev.* 212:925-984. [8] Werner M. W. et al. (2004) *Asrtrophys. J. Supp. Series* 154:1-9.

LABORATORY ION IRRADIATION OF CARBONACEOUS CHONDRITES TO REPRODUCE SPACE WEATHERING OF DARK ASTEROIDS

R. Brunetto[1] and C. Lantz[1], [1]Institut d'Astrophysique Spatiale, UMR 8617, CNRS, Université Paris-Saclay, F-91405 Orsay, France (rosario.brunetto@ias.u-psud.fr).

Introduction: The unprotected surfaces of asteroids are continuously modified by space weathering processes such as micrometeorite bombardment or solar wind ion irradiation. These produce changes on the surface of airless bodies, impeding us to decipher their composition from their spectra. Surface space weathering has been widely studied in the case of the Moon and S-type asteroids, and it is now investigated for primitive asteroids [1]. By performing ion irradiation experiments on relevant asteroid analogues, we can simulate some of the energetic processes affecting asteroid surfaces.

Materials and methods: In order to understand the influence of space weathering on carbonaceous asteroids and to support current sample return missions (Hayabusa2/JAXA and OSIRIS-REx/NASA), we performed 40 keV He^+ and Ar^+ ion irradiation of carbonaceous chondrites (CCs) as a simulation of solar wind irradiation of C-complex asteroids. We used reflectance spectroscopy (0.4-16 μm) to probe our samples before, during and after irradiation. We studied several types of CCs [2] as they span a wide range of albedos (from 2-8% for CI/CM to 10-18% for CV/CO), initial composition (matrix- or chondrules-rich) and did not suffer the same thermal history (different aqueous alteration or metamorphism).

Results and discussion: In samples irradiated in the laboratory we observe spectral variations of organic and mineral components, as well as variations in albedo. These irradiation effects as a function of the dose are then compared on a micron-scale with the compositional heterogeneity of the original materials, to determine which spectral bands are more sensitive to the effects of space weathering. We will show measurements of FTIR spectral imaging on different irradiated CCs [3], obtained in collaboration with the SMIS beamline of the SOLEIL synchrotron (France). The results of these experiments will be used both to support the analysis of samples retrieved from space [4] and to formulate predictions about the weathering trends that should be measured on asteroid families by remote sensing spectroscopy [5].

References:
[1] Brunetto R. et al. (2015) in *Asteroids IV*, 597-616.
[2] Lantz C. et al. (2017) *Icarus* 285:43–57.
[3] Brunetto R. et al. (2018) *Planetary and Space Science* 158:38–45.
[4] Brunetto R. and Lantz C. (2019) *Nature Astronomy* 3:290–292.
[5] Lantz C. et al. (2018) *Icarus* 302:10-17.

FTIR MICRO-TOMOGRAPHY COUPLED TO X-CT ON EXTRATERRESTRIAL MATERIALS

R. Brunetto[1], Z. Dionnet[1,2], A. Aléon-Toppani[1], D. Baklouti[1], F. Borondics[3], Z. Djouadi[1], A. King[3], T. Nakamura[4], S. Rubino[1,3], C. Sandt[3], D. Troadec[5] and A. Tsuchiyama[6], [1]Institut d'Astrophysique Spatiale, CNRS, Université Paris-Saclay, Orsay, France (rosario.brunetto@ias.u-psud.fr), [2]DIST-Università Parthenope, Napoli, Italy, [3]SOLEIL synchrotron, Saint-Aubin, France, [4]Division of Earth and Planetary Materials Science, Graduate School of Science, Tohoku University, Japan, [5]Institut d'Electronique, de Microélectronique et de Nanotechnologie, Lille, France, [6]Research Organization of Science and Technology, Ritsumeikan University/Guangzhou Institute of Geochemistry

Introduction: Laboratory analyses of meteorites and interplanetary dust particles originating from asteroids and comets give us the opportunity to study directly the components that formed in the protoplanetary disk, but they also have intrinsic limits and biases, some of which are overcome by sample return space missions [1]. In the near future a new generation of sample return missions (Hayabusa2, OSIRIS-REx, MMX, etc.) will collect samples from small Solar System bodies. To maximize the scientific outcome of laboratory studies and minimize the loss of precious extraterrestrial samples, an analytical sequence from less destructive to more destructive techniques needs to be established. Among the possible techniques, infrared (IR) spectroscopy is important for being totally non-destructive and comparable to remote sensing observations of small bodies [2]. Thanks to IR imaging microspectroscopy, we are able to study the spatial distribution of molecular bonds associated to minerals, water and organics [3].

Materials and methods: In this work, we present the results of a Fourier-Transform infrared (FTIR) micro-tomography study of five particles from asteroid Itokawa collected during the Hayabusa mission (JAXA) and of several fragments of selected carbonaceous chondrites (CM Paris and Cold Bokkeveld, C2-ung Tagish Lake, CK NWA 5515). All samples size 20-50 μm and are mounted on needles. The FTIR measurements are performed at the SMIS beamline of synchrotron SOLEIL (France) with a spatial resolution that is diffraction-limited and a voxel size of about $0.66 \times 0.66 \times 0.66$ μm^3. Complementary X-ray micro-tomography analyses are performed at the PSICHE beamline of SOLEIL and at beamline BL47XU of the SPring-8 synchrotron (Japan) [4] with voxel sizes of about $0.127 \times 0.127 \times 0.127$ μm^3 and $0.084 \times 0.084 \times 0.084$ μm^3 respectively.

Results: Supported by X-ray micro-tomography analyses providing a shape model and 3D structures of the samples, the FTIR analyses allows the detection of mineral phases, water and organics, and their spatial co-localization in three dimensions. We show that a combined IR and X-ray micro-tomography analytical approach is able to provide a non-destructive 3D physical and chemical characterization of individual extraterrestrial particles. The two techniques together surmount the intrinsic limitations of each one, giving access to the identification and spatial distribution of individual components inside the analyzed particles, as well as their 3D structure and porosity. In addition, we show that it is possible to recover the samples after the analyses.

Discussion: We propose these techniques as an efficient first-step in a multi-technique analytical sequence on samples collected by space missions. In particular, we consider FTIR 3D micro-tomography an interesting starting point, as it will be able to provide a first quick look on the composition, abundance and 3D distribution of carbonaceous materials and water at the scale of few microns within individual grains sizing up to several tens of microns. Once the organics are revealed by IR measurements, thin sliced sections of the samples can be prepared to be analyzed by more destructive techniques, in order to retrieve the structure and elemental/isotopic composition of the carbonaceous component and its mineral host, down to nm scale. This top-down sequence applied to Ryugu samples collected by the Hayabusa2 mission (JAXA), may build a bridge between the observations at macroscopic scale [5] and the chemical and physical processes operating at the nano-scale.

References:
[1] Brunetto R and Lantz C. (2019) *Nature Astronomy* 3:290–292.
[2] Brunetto R. et al. (2011) *Icarus* 212:896–910.
[3] Dionnet Z. et al. (2018) *Meteoritics and Planetary Science* 53:2608–2623.
[4] Tsuchiyama A. et al. (2013) *Geochimica and Cosmochimica Acta* 116:5–16.
[5] Kitazato K. et al. (2019) *Science* DOI:10.1126/science.aav7432

THE STRUCTURE OF METAL PARTICLES IN THE LIGHT LITHOLOGY OF CHELYABINSK METEORITE

E. V. Brusnitsyna, V. I. Grokhovsky, G. A. Yakovlev and R. F. Muftakhetdinova, Institute of Physics and Technology, Ural Federal University, Ekaterinburg, 620002, Russian Federation, e-mail: jeka_bru@list.ru

Introduction: The Chelyabinsk meteorite is ordinary chondrites, type LL5 S4 W0 according to international classification. This meteorite substance consists of several visually distinguishable structural zones - lithologies [1]. Depending on the degree of metamorphism, lightly deformed light and shock-melted dark areas are distinguished. In the dark area, there are two zones - gray with melted silicates and black with melted sulfides [2]. The presence of such zones indicates that shock events occurred in the history of the parent body, which possibly causing a partial or complete remelting of the original structure. The fragments with light lithology are of particular interest since they more closely correspond to the original substance of the parent body.

Experimental: For the study, eight fragments of the Chelyabinsk meteorite with light lithology were selected from the collection of the Ural Federal University Meteorite Expedition. For convenience, the samples were divided into three groups (A, B, C). After cutting, the surface of the samples was prepared by grinding and polishing. A 2% solution of nitric acid in alcohol was used as an etchant. The meteoritic metal microstructure was examined using Zeiss Axiovert 40 MAT inverted microscope and FE-SEM ∑IGMA VP electron microscope with EBSD and EDS units.

Results and Discussion: Metal particles in the studied fragments have different phase and structural composition. There are α-Fe (Ni) kamacite and γ-Fe (Ni) taenite with a different structure. Therefore, we divided all the objects under study into three groups: 1) A1 fragment with unchanged chondrite metal structure, 2) fragments B1 and B2, which metal grains contain cloudy zone-like structure and 3) fragments C1, C2, C3, C4, and C5, which metal shows martensite-like structure.

The metal structure of the A1 fragment is characteristic of ordinary chondrites and has not undergone any changes. There are particles of zoned taenite with areas of tetrataenite and cloudy zones. In the same fragment, the mineral Haxonite and lenticular martensite were previously found in the particle of taenite [3, 4].

In the fragments of the second group, particles similar to zoned taenite with a highly etched fine-grained center and light polycrystalline rim are observed in the optical microscope. At a higher resolution, a plessite structure (α + γ) with an intergrowth size of the order of several hundred nanometers is revealed in the central part. However, cloudy zones and tetrataenite are absent. The Ni content at the edges varies in the range from 45 to 50 wt.%. In the central part, the value of Ni varies in the range from 30 to 40 wt.%. Linear mapping of the studied metal particles showed a small Ni gradient. Neumann lines were found in the kamacite particles of the B1 fragment of this group. There are particles of kamacite, in which the growth of new α-phase grains with an elongated columnar structure is observed.

Metallographic studies of the fragments of group 3 did not reveal the presence of zonal particles characteristic of ordinary chondrites. All fragments of this group contain martensite-like structures different in morphology, which can be divided into two types: 1) acicular, located along the grain edge around the plessite and 2) acicular in the central part of the grain and nucleated on troilite inclusions (FeS). Type 1 structures are found in fragments C2 and C3, type 2 in C1, C4, C5. Also for all fragments of this group, particles of recrystallized metal, with the structure of polycrystalline kamacite are characteristic. In addition, in the C5 fragment, there are several metal particles with growth twins in the γ-phase.

Conclusions: Summarizing the above and relying on the Fe-Ni phase diagram [5], we can suppose that the metal part of the parent substance of the parent body was cooled at a rate of about 5°C/Myr years below 400°C [3]. Then, as a result of a possible shock event, it underwent reheating to temperatures above 400° C, which led to the diffusion of Ni in the zonal metal particles of the taenite, disruption of their zonal structure, kamacite recrystallization, the formation of martensite-like structures and the growth twins in the taenite.

References: [1] Badyukov D. D. et al. (2015) *Petrology* 23:103–115. [2] Grokhovsky V. I. et al. (2014) *Meteoritics & Planetary Science* 49: A5364. [3] Grokhovsky V. I. et al. (2015) *Meteoritics & Planetary Science* 48: A5272. [4] Brusnitsyna E. V. et al. (2018) *Meteoritics & Planetary Science* 53: 6290. [5] Yang C.-W. et al. (1996) *Phase Equilibria 17*: 522–531.

THE OCTAHEDRITE AND PALLASITE PART METALLOGRAPHIC COMPARISON OF THE SEYMCHAN METEORITE

E. V. Brusnitsyna, R. F. Muftakhetdinova and G. A. Yakovlev, V. I. Grokhovsky, Institute of Physics and Technology, Ural Federal University, Ekaterinburg, 620002, Russian Federation, e-mail: jeka_bru@list.ru

Introduction: The Seymchan meteorite was found in 1967 near the village of the same name in the Magadan Region and was classified as an iron meteorite (octahedrite type). The participants of the following expeditions managed to find in the same area a more rare type of meteorites - pallasite, which in addition to metallic minerals contains a large number of silicates. The authors [1] found that octahedrite and pallasite are parts of the same meteorite. Thus, it was proved that the Seymchan meteorite is a pallasite with large areas of a metallic alloy. As is known, the more preferable places for the nucleation of a new phase are the grain boundaries. In the pallasite part quantity of such boundaries (olivine/metal) is higher than in octahedral and, therefore, the probability of segregate of the α-phase is higher. We assume that this could affect the mechanisms of metal growth and, consequently, the structure. In this work, various metallographic parameters of fragments from the pallasitic and octahedral parts were investigated.

Experimental: Fragments from octahedral and pallasite parts of Seymchan (PMG) have been chosen for the research. Samples were cutted, grinded, polished and etched in accordance with standard metallographic technique. The meteoritic metal microstructure was examined using Zeiss Axiovert 40 MAT inverted microscope and FE-SEM ∑IGMA VP.

Both in octahedral part and pallasite part, group of parameters were measured: average width of zoned taenite (from the kamacite/tetrataenite interface to martensite α_2), average width of cloudy zone, average width of tetrataenite rim and average size of high-nickel particles in cloudy zones. Sizes of these particles were determined in compliance with [2].

Results and Discussion: One can find kamacite α-Fe(Ni, Co), taenite γ-Fe(Ni, Co), zoned taenite and plessite (α + γ) in the metallic structure of both part of the Seymchan meteorite. The plessite has coarse structure and, consequently, was formed according to nucleation mechanism V γ → α2 + γ → α + γ [3] as in pallasite and in octahedrite.

Average values of metallic structure parameters have been measured. For pallasite: size high Ni particles in the cloudy zone – 118 nm, the width of cloudy zone – 7,8 μm, the width of tetrataenite rim – 2,3 μm, the width of zoned taenite – 54 μm. For octahedrite: size high Ni particles in the cloudy zone – 142 nm, the width of cloudy zone – 7,7 μm, width of tetrataenite rim – 2,2 μm, width of zoned taenite – 61 μm. The average width of the cloudy zone, the width of tetrataenite rim, the width of the zoned taenite are about the same. So, deviation in the sizes of high nickel particles can not be explained by stereological or orientation effects and hint to the difference in formation process of these zones in pallasite and octahedrite parts of Seymchan has been found.

References: [1] v. Niekerk D. et al. (2007) *Meteoritics & Planetary Science* 42:5196. [2] J. I. Goldstein et al. (2009) *Meteoritics & Planetary Science* 44:343–358. [3] Yang J. et al.(2010) *Geochimica et Cosmochimica Acta* 74:4471–4492.

SPACE WEATHERING OF ADJACENT PHASES IN SINGLE GRAINS FROM ITOKAWA.

K. D. Burgess[1] and R. M. Stroud[1], [1]U.S. Naval Research Laboratory, 4555 Overlook Ave. SW, Washington DC, 20375 (kate.burgess@nrl.navy.mil; rhonda.stroud@nrl.navy.mil).

Introduction: Analysis of space weathering features in returned samples from asteroid 25143 Itokawa generally show them to be immature compared to lunar samples, with thin amorphous or partially crystalline rims [1] and relatively low density of solar flare tracks in some grains [2]. Vesicular rims and "blisters" seen in SEM have been noted in a number of these grains [3,4], and these features are consistent with solar wind irradiation being the dominant driver of space weathering on Itokawa. Vesicles are most commonly seen in pyroxene rims while other phases show varying degrees of amorphization or changes in chemistry due to differential sputtering. Using scanning electron microscopy (SEM) and scanning transmission electron microscopy (STEM), we can relate surficial features on grains directly to those seen in cross-sections of space weathered rims.

Methods: Samples were prepared using focused ion beam (FIB) microscopy. The grains were coated with 30-60 nm of carbon followed by e-beam deposited C or Pt and a thicker protective strap of ion-beam deposited C or Pt before milling to prevent damage to the grain surface by the ion beam. The thinned sections were heated to 140°C for six hours to drive off adsorbed water before insertion in the UHV system.

Equipment. Electron energy loss spectroscopy (EELS) and energy dispersive x-ray spectroscopy (EDS) data were collected with PRISM, the NION UltraSTEM200-X at the U.S. Naval Research Laboratory, equipped with a Gatan Enfinium ER EEL spectrometer with and a Bruker SSD-EDS detector. The STEM was operated with at 200 kV, with a 0.1 nm probe. Spectra were collected as spectrum images (SI), with a spectrum collected for each pixel, allowing for mapping of variations in thickness, oxidation state, and composition.

Results: The samples are highly immature in terms of space weathering features, with thin to non-existent rims on some phases and very low density of solar flare tracks.

RB-QD04-0045. Phases present in FIB sections from this grain include plagioclase, pyrrhotite and olivine, with a merrillite grain that was not exposed to space weathering. The rim of the pyrrhotite grain is deficient in S compared to Fe to a depth of ~12 nm, indicating differential sputtering. The plagioclase has a slight depletion in O at the surface and a low density of <3 nm nanophase Fe^0 particles on the surface. Two pyrrhotite and chromite inclusions (200-300 nm) are present in the olivine, which shows very little evidence of alteration due to space weathering.

RA-QD02-0114. Phases in FIB sections include plagioclase, high-Ca pyroxene, olivine, and merrillite. Vesicles in the pyroxene were apparent in SEM images as blisters on the surface. Preliminary analysis of EELS data of these vesicles shows a broad feature from ~12-18 eV that is lacking in the material directly surrounding the vesicle (Figure), which is suggestive of volatiles being trapped in the vesicles [5]. As in the other grain, the plagioclase and olivine show very little evidence of alteration due to space weathering. Small nanophase Fe metal inclusions may be present along portions of the olivine rim, but the features are not well-developed.

Discussion: The Itokawa grains presented here are consistent with previous work showing immature space weathering features due primarily to solar wind irradiation. There are distinct differences in how different phases are altered, however, with plagioclase and olivine showing little alteration, pyrrhotite losing S to sputtering, and pyroxene forming a vesicular rim. The presence of volatiles in vesicles in the pyroxene, if confirmed, is also consistent with solar wind irradiation being the dominant driver of space weathering on Itokawa. However, a micron-scale impact crater is observed on one of the grains as well, indicating micrometeoroid bombardment is not completely absent.

References: [1] Harries, D., and Langenhorst, F. (2014) *Earth, Planets and Space*, *66*, 1-11. [2] Keller, L.P., and Berger, E.L. (2017) *Lunar and Planetary Science Conference*, 2353. [3] Matsumoto, T., et al. (2015) *Icarus*, *257*, 230-238. [4] Noguchi, T., et al. (2014) *Meteoritics & Planetary Science*, *49*, 188-214. [5] Bradley, J.P., et al. (2014) *Proceedings of the National Academy of Sciences of the United States of America*, *111*, 1732-1735.
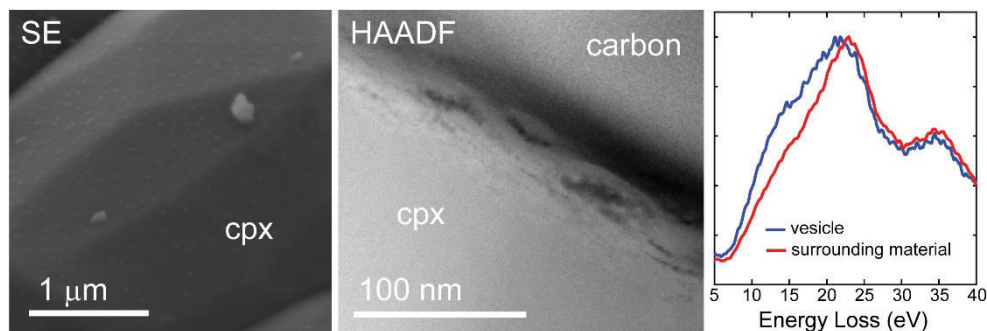
NOBLE GASES IN CARBONACEOUS CHONDRITES – THE EFFECTS OF AQUEOUS ALTERATION AS MONITORED BY CR AND OTHER CARBONACEOUS CHONDRITES.

H. Busemann[1], D. L. Schrader[2], C. M. O'D. Alexander[3], M. Kuga[1], and C. Maden[1], Institute of Geochemistry and Petrology, ETH Zürich, Switzerland (henner.busemann@erdw.ethz.ch), [2]Center for Meteorite Studies, Arizona State Univ., Tempe, AZ, USA, [3]Dept. of Terrestrial Magnetism, Carnegie Institution for Science, Washington, DC, USA.

Introduction: The volatile elements in early solar system materials are important tracers for understanding the formation of the terrestrial planets and their atmospheres. Noble gases complement the information that is carried, e.g., by the halogens, H, C, N and the rock-forming volatile elements [e.g., 1-3]. Carbonaceous chondrites (CC) represent, next to cometary matter, the least altered extraterrestrial materials available and are likely to have significantly contributed to the inner planet volatiles [3]. We have undertaken a comprehensive study aiming to (i) determine the noble gas content of the most primitive members of each CC group and (ii) understand the effects of parent body processing on their primordial volatile inventories. Here we present results of a large number of CR chondrites whose petrologic types have previously been determined, based on petrology, mineralogy and O isotopes as well as on H, C and N isotopic and elemental compositions [4,5]. We compare our CR chondrite results to those from other primitive CCs (CI, CO, CM, ungrouped) and describe an important Ar-rich component that is present in the most primitive chondrites whose abundance quickly diminishes with progressive aqueous alteration. It is essentially completely lost in type 1 CIs and CRs and may survive only in the least aqueously altered CM2s [6].

Experimental: We measured bulk samples (typically 5-30 mg) of more than 25 CR and other CCs in one total extraction step each at ~1700 °C [cf. 7]. Extractions at ~1750 °C proved the completeness of the main extractions. Blank corrections were for almost all samples and isotopes essentially negligible, or within a few % of the released amounts. More than 30 CMs have been studied separately [6].

Results and Discussion: All samples show the expected abundant primordially trapped noble gases. Only a few CR chondrites show solar wind (SW) Ne with $^{20}Ne/^{22}Ne$ near or >12. These samples originate from the CR chondrite parent body's regolith. More importantly, some samples including MIL 090657 and LAP 04720 have trapped $^{20}Ne/^{22}Ne$ of >9, significantly higher than the typically dominating Ne-HL ($^{20}Ne/^{22}Ne \approx 8.5$ in presolar diamonds [8]). This could possibly be due to a subtle SW-Ne contribution as found in CI Ivuna [9], which can be detected only by closed system step etching. The release of air Ne ($^{20}Ne/^{22}Ne$ ~9.8) is excluded based on the Ar isotopic composition. Ne-Q has similar $^{20}Ne/^{22}Ne$ ratios of 10.1-10.7, but Ne-Q is much less abundant than Ne-HL [10]. It is also possible that this a new Ne component. Indeed, an etch experiment on MIL 090657 identified two new, isotopically distinct trapped Ne components (one contains ~35% of the total ^{20}Ne) [11]. Other CR samples including GRA 06100 (heated [4]), Gao-Guenie (b) and, perhaps, Dhofar 1432 that are among the most aqueously altered CR2s [5], and GRO 95577 (the only CR1), do not show this new Ne component but are dominated by Ne-HL, with a small addition of Ne-E to GRO 95777 (from presolar SiC or graphite [8]). This is consistent with the carrier of this new Ne component being water-soluble [11]. Helium and Ne show variable additions of cosmogenic ^{3}He and ^{21}Ne. The $^{36}Ar/^{38}Ar$ ratios are typical for Q-Ar, and cosmogenic ^{38}Ar contributions are minimal. Xenon is dominated by Q-Xe [10].

Trapped ^{36}Ar is the most suitable noble gas component to indicate aqueous alteration. Most CR2s and CO3.0 DOM 08006 have much higher concentrations compared to CR1 GRO 95577, GRA 06100, the CIs, Sutter's Mill (C-ungrouped) and many CMs [6], where only the least aqueously altered CM2s, e.g., QUE 97990, NWA 10827 and LEW 85312 show similarly high trapped ^{36}Ar. DOM 08006 is the most primitive CO3. It contains the highest trapped ^{36}Ar concentration of all CO3s, which decreases with increasing metamorphic grade, showing that the carrier of the ^{36}Ar-rich component is also affected by metamorphism [12].

In summary, in addition to the well-known presolar and Q noble gas components, CCs carry primordially trapped components that are very susceptible to aqueous alteration. One Ne-rich component [11] is lost with progressing aqueous alteration of the CRs. An Ar-rich ("sub-solar") component (known to be carried in HF-soluble minerals, [e.g., 13]) is present in CR2s and CO3.0 but mostly lost in CR1, CIs and CMs.

References: [1] Clay P.L. et al. (2017) *Nature* 551:614-618. [2] Alexander C.M.O'D. et al. (2012) *Science* 337:721-723. [3] Schönbächler M. et al. (2010) *Science* 328:884-887. [4] Alexander C.M.O'D. et al. (2013) *Geochim. Cosmochim. Acta* 123:244-260. [5] Schrader D.L. et al. (2011) *Geochim. Cosmochim. Acta* 75:308-325. [6] Weimer D. et al. (2017) 80th Annual *Meeting of the Meteoritical Society*: Abstract 6300. [7] Riebe M.E.I. et al. (2017) *Meteoritics & Planetary Science* 52:2353-2374. [8] Ott U. (2014) *Chem. Erde* 74:519-544. [9] Riebe M. et al. (2017) *Geochim. Cosmochim. Acta* 205:65-83. [10] Busemann H. et al. (2000) *Meteorit. & Planet. Sci.* 35: 949-973. [11] Krietsch D. et al. (2019) 82nd Annual *Meeting of the Meteoritical Society*, *this volume:* Abstract 6296. [12] Davidson J. et al. (in prep.). [13] Alaerts L. et al. (1979) *Geochim. Cosmochim. Acta* 43:1421-1432.

MOLECULAR COMPOSITION OF A RECENT LUNAR METEORITE: NORTHWEST AFRICA 11474

O. Caliskan[1], M. Kaya[2], M. Yesiltas[3], [1]Department of Astronomy and Space Sciences, Istanbul University, Beyazıt, Istanbul, Turkey 34119 (caliskanozcan@hotmail.com),[2]Institute of Accelerator Technologies, Ankara University, Golbasi, Ankara, Turkey 06830, [3]Faculty of Aeronautics and Space Sciences, Kirklareli University, Kirklareli, Turkey, 39100

Introduction: Lunar meteorites provide information regarding the formation and evolution of the lunar surface. Examination of lunar meteorites contribute to our geochemical understanding of the lunar materials [1,2,3]. Lunar crust consists mostly of plagioclase feldspar, pyroxene, olivine and ilmenite while there is contribution, to a lesser extent, from potassium feldspar, oxide minerals, calcium phosphates, zircon, troilite or iron metal [4]. Northwest Africa 11474 (NWA 11474) was found in 2017, and it was subsequently classified as a Lunar Feldspathic breccia [5]. Initial analyses showed that it contains mainly olivine and pyroxene [5]. Fayalite, ferrosilite and wollastonite are identified in NWA 11474 as well [5]. To our knowledge, there is no spectral data available on this meteorite thus far. We acquired a slab of this meteorite from owner of the main mass and prepared a thin section at the Department of Geology Engineering of Istanbul University. Here, we present infared and Raman spectra of various phases and their diversity in NWA 11474.

Methods: We collected nano-scale Fourier Transform infrared (nano-FTIR) spectra of various phases present in NWA 11474 at Institute of Accelerator Technologies, Ankara University, using commercial microscopy system (Neaspec GmbH, Germany), which provides ~20 nm spatial resolution. Subsequently, the same sample was investigated using a micro-Raman microspectroscopy setup at Science And Technology Application and Research Center, Canakkale Onsekiz Mart University. Here, experimental setup consist of a commercial WiTec alpha300 R (WiTec GmbH) confocal microscopic imaging system, a 532-nm Nd:YAG laser, a spectrometer and a 50X objective. High spatial resolution chemical distribution maps (0.5 μm) of NWA 11474 were collected using a laser power of ~1-3 mW and integration time of 0.2 seconds.

Results: Micro-Raman spectra show that NWA 11474 contains abundant pyroxene, evident from the Raman bands observed near 1015 cm^{-1} and 675 cm^{-1}. The latter band is a singlet in some cases, and a doublet in others, indicating presence of different endmembers. A set of additional pyroxene bands appear between 443-302 cm^{-1}, which is a singlet, doublet, or triplet in different spectra collected from different points. This is indicative of a varying molecular composition depending on the endmember. A doublet centered near 840 cm^{-1} is due to olivine and is observed in the spectra of some of the phases. Although olivine is present in NWA 11474, its abundance is significantly less than that of pyroxene. We also observed a currently unidentified phase whose Raman bands appear around 495 cm^{-1} and 515 cm^{-1}. Using Raman positions of the observed bands, we generated chemical distribution maps of the phases to qualitatively investigate their spatial distributions and relations. Nano-FTIR spectra of NWA 11474 show silicate bands between 800-1200 cm^{-1} that are due to Si-O stretching vibrations, although variations in the peak positions exist and are indicative of difference in the molecular composition of the silicates. Some spectra present infrared peaks between 880-1080 cm^{-1}, while others present between 920-1240 cm^{-1}. Overall, our preliminary investigation shows that NWA 11474 contains various minerals with different chemical composition, and we are able to identify different endmembers through infrared and Raman spectroscopy. We have plans to do more detailed investigations to better understand its mineralogy.

References: [1] K. H. Joy et al. (2006) *Meteoritics & Planetary Science* 41, 7:1003–1025. [2] H. Nagaoka et al. (2013) *Polar Science* 7:241-259. [3] K. Koeberl (1996) *Meteoritics & Planetary Science* 31:897–908. [4] http://meteorites.wustl.edu/lunar/howdoweknow.htm [5]*Meteoritical Bulletin* 106.

EVIDENCE FOR SUBSOLIDUS QUARTZ-COESITE TRANSFORMATION IN IMPACT EJECTA FROM THE AUSTRALASIAN TEKTITE STREWN FIELD

F. Campanale[1,2], E. Mugnaioli[2], L. Folco[1], M. Gemmi[2], M. R. Lee[3], L. Daly[3], and B. P. Glass[4]
[1] Dipartimento di Scienze della Terra, Università di Pisa, V. S. Maria 53, 56126 Pisa, Italy (fabrizio.campanale@phd.unipi.it). [2] Center for Nanotechnology Innovation@NEST, Istituto Italiano di Tecnologia (IIT), Piazza San Silvestro 12, 56127 Pisa, Italy. [3] Department of Geographical and Earth Sciences, University of Glasgow, Glasgow G12 8QQ, UK. [4] Department of Geosciences, University of Delaware, Newark, DE, USA

Introduction: Coesite, a high-pressure silica polymorph, is a diagnostic indicator of impact cratering in quartz-bearing target rocks. The formation mechanism of coesite during hypervelocity impacts has been debated since its discovery (in impact rocks) in the 1960s. In impactites, coesite is preserved as a metastable phase in crystalline rocks that experienced peak shock pressures above ~30-40 GPa [1], and in porous sedimentary rocks shocked at pressures as low as ~10 GPa [2]. There is a general consensus that coesite within impactites originates by crystallization from a dense amorphous phase during shock unloading, when the pressure release path passes through the coesite stability field. The precursor amorphous phase may be a silica shock melt [1] or a densified diaplectic silica glass [3]. We present in turn evidence for direct solid-state quartz-to-coesite transformation in shocked coesite-bearing quartz ejecta from the Australasian tektite/microtektite strewn field, which is the largest and youngest (~0.8 Myr old) on Earth. These findings contradict conventional models for coesite formation, but appear consistent with recent observations from the Kamil crater, the smallest coesite-bearing impact crater reported so far [4].

Samples and methods: We used field emission gun - scanning electron microscopy (FEG-SEM) and μRaman spectroscopy to study four shocked silica ejecta particles associated with the Australasian microtektite (AAMT) layer, from two deep-sea sediment cores both located in the South China Sea: ODP-1144A and SO95-17957-2. We used focused-ion beam (FIB) instruments for the extraction of five electron-transparent lamellae from a particle with very prominent shock features. Lamellae were investigated by transmission electron microscopy (TEM), three-dimensional electron diffraction (3D ED) [5] and phase/orientation maps using the precession-assisted crystal orientation mapping technique (PACOM) [6] (similar to electron backscatter diffraction).

Results: All FIB lamellae consist of a mixture of coesite and quartz in variable proportions, the latter showing planar deformation features (PDFs) with typical {10-11} and {10-12} orientations. Quartz shows a common crystallographic orientation in the whole FIB cut, indicating each lamella and probably the whole particle was a single quartz crystal of the parent rock. Coesite crystals range in size from ~500 nm to few nanometres, with rounded or elongated habit. Twinning and planar disorder are rather evident along (010) planes. Where quartz and coesite are in contact, no appreciable amorphous or 'glassy' volume was detected. Instead, quartz boundaries are always lobate or sawtooth-like, with euhedral coesite crystals penetrating through the quartz boundaries. 3D ED and PACOM analysis show a recurrent pseudo iso-orientation between the (1-11) vector in quartz and the (010) vector of neighbouring coesite crystals. Moreover, PDFs in quartz clearly extend in the coesite domains, suggesting that the latter forms directly at the expence of the shocked quartz crystal.

Discussion: Our observations indicates that quartz transforms directly to coesite after PDF formation and through a solid-state process without enetering the silica liquid stability field. Mutual orientation and crystallographic similarities between quartz and coesite structures point to a martensitic-like transformation that involves a relative structural shift of {-1011} quartz planes, which would eventually turn into coesite (010) planes. This mechanism would explain the relation between the characteristic (010) twinning of impact coesite [7] and the common {10-11} PDF set in shocked quartz. Arguably, solid-state martensitic-like process could represent the dominant mechanism of coesite formation in a wide range of cratering events, at least for those with porous target rocks like at the Barringer [8] and Kamil craters [4]. This implies lower peak impact pressure and temparture conditions for the formation of impact coesite than previously thought.

References: [1] Stöffler D. and Langenhorst F. (1994) *Meteoritics* 29:155–181. [2] Kowitz A. et al. (2016) *Meteorit. Planet. Sci.* 51:1741–1761. [3] Stähle V. et al. (2008) *Contrib. to Mineral. Petrol.* 155:457–472. [4] Folco L. et al. (2018) *Geology* 46:739–742. [5] Mugnaioli E. and Gemmi M. (2018) *Zeitschrift für Krist. - Cryst. Mater.* 233:1–16. [6] Viladot D. et al. (2013) *J. Microsc.* 252:23–34. [7] Bourret A. et al. (1986) *Phys. Chem. Miner.* 13: 206–212. [8] Kieffer S. W. et al. (1976) *Contrib. Mineral. Petrol.* 59: 41–93.

MINERALOGY AND SHOCK EFFECTS IN MARTIAN REGOLITH BRECCIAS

F. Cao[1], R. L. Flemming[1], D. E. Moser[1], M. R. M. Izawa[1,2], [1]Department of Earth Sciences/ Centre for Planetary Science & Exploration, University of Western Ontario, London ON, Canada (fcao23@uwo.ca), [2]Institute for Planetary Materials, Okayama University, Misasa, Tottori, Japan.

Introduction: Nicknamed "Black Beauty", NWA 8171 and its pairings (e.g., NWA 7475 and NWA 11220) are pieces of a polymict regolith breccia with a basaltic composition [1,2] and represent the very ancient Martian crust [3,4]. Martian brecciated samples contain multiple lithologies in the fine-grained matrix, and chemically resembles outcrops sampled by Spirit and Curiosity rovers [1,5]. Moreover, these samples are relatively hydrous and contain secondary alteration components related to aqueous activities that may have occurred on the near-surface of Mars [1,6-8]. The brecciation is the consequence of bombardment of Mars' crust [3,9]; during which fragments with a range of shock histories were incorporated in lithic breccias [10,11]. Currently, there is some research about shock-metamorphic effects in the suite of "Black Beauty" meteorites using qualitative petrographic methods [8,12], and quantitative methods on accessory phases [13] which demonstrate that the Martian regolith breccia meteorites experienced low-level shock effects. *In situ* microXRD (μXRD) provides a quantitative approach to assessing shock metamorphism in the rock-forming minerals [14-16]. Many of the grains in NWA 8171 show shock-metamorphic features, such as line broadening, strain-related mosaicity (streaking), and asterism in their XRD patterns [17]. Our goal is to assess the degree of cumulative shock experienced by this ancient Martian crust, as preserved by rock-forming minerals. Cross-cutting relationships enable assessment of relative timing of shock events.

Samples and methods: Four slabs of Martian breccia, NWA 8171_medium, NWA 11220, NWA 7475, and NWA 8171_large, have been studied using μXRD, SEM and in most cases Raman spectroscopy. μXRD was performed using a Bruker-AXS D8 Discover diffractometer with a 300 μm nominal beam diameter, using CoKα radiation (λ=1.7889 Å) (operating at 35 kV and 45 mA) and a Vantec-500 Area Detector. 2D images were integrated to produce intensity vs. 2θ plots over 2θ range 25°-95°, with step size 0.04°, or intensity vs. χ plots, to measure strain-related mosaicity. Backscattered electron (BSE) images and distributions of Al, Mg, Ca were conducted at Zircon and Accessory Phase Laboratory (ZAPLab), Western University, using a Hitachi SU6600 FEG-SEM with a five-sector solid-state BSE detector at the accelerating voltage of 10 kV [18]. Raman spectra were collected in the range of 150-1200 cm^{-1} with a spectral resolution of 2 cm^{-1}. Spectra of various minerals with different shock effects were analyzed for comparison with μXRD data. Care was taken to analyze domains away from launch-related fractures/ strain effects.

Results: Combined mineralogical and chemical investigation by μXRD and SEM on various clasts yielded similar results for these samples. Lithic clasts in four slabs contain coarse- to fine-grained mixtures of primary orthopyroxene (opx), clinopyroxene (cpx), plagioclase, and magnetite, as well as occasional pyrite, hematite, and ilmenite in the matrix and opx, cpx, plagioclase as single crystal clasts. Cl-rich apatite is widely distributed in NWA 8171 and NWA 7475 and has some OH substitutions of Cl in the site, which means apatite should be a significant reservoir of both H and Cl in the Martian regolith. μXRD provides a quantitative measurement of shock metamorphism of single clasts through measuring strain-related mosaicity (SRM). Most medium-grained clasts in four slabs have shown streaking to varying degrees - presumably due to impact activities on Mars. The higher SRM of the crystal clasts in NWA 11220 compared to those in the other pairings suggests that it has probably experienced a relatively higher shock pressure.

Discussion and Conclusions: Preliminary μXRD, SEM and Raman results confirmed that four Martian breccias contain the same dominant mineralogy. Many lithic and crystal grains show streak characteristics in the 2D XRD images and the ones in NWA 11220 exhibit more extended streak lengths along χ. Future work will involve powder X-ray diffraction, and Rietveld refinement/modal analysis of NWA 11220, to quantitatively determine the major and minor phase abundances, especially the representative secondary phases (including hydrous phases) on the Martian surface. The study of the mineralogical composition, shock-induced deformation mechanisms, and spectral features of Martian breccia meteorites will contribute significantly to deciphering the evolution of regolith on Mars.

References: [1] Agee C. B. et al. 2013. *Science* 339: 780–785. [2] Humayun M. et al. 2013. *Nature* 503: 513–516. [3] Cassata W. S. et al. 2018. *Science Advances* 4: eaap8306. [4] Bellucci J. J. et al. 2015. *Earth and Planetary Science Letters* 410: 34–41. [5] McCubbin, F. M. et al. 2016. *Journal of Geophysical Research* 121. [6] Liu Y. et al. 2016. *Earth and Planetary Science Letters* 451:251–262. [7] Muttik N. et al. 2014. *Geophysical Research Letters* 41:8235–8244. [8] Wittmann A. et al. 2015. *Meteoritics & Planetary Science* 50:326–352. [9] Cannon K. M. et al. 2015. *Icarus* 252:150–153. [10] Hofmann B. A. et al. (2014) *77th Annual Meeting of the Meteoritical Society,* Abstract#5230. [11] Stöffler D. et al. 2018. *Meteoritics & Planetary Science* 53:5–49. [12] Leroux H. et al. 2016. *Meteoritics & Planetary Science* 51:932–945. [13] Moser, D.E. et al. (2017) *80th Annual Meeting of the Meteoritical Society*, Abstract#6301. [14] Flemming R. L. 2007. *Canadian Journal of Earth Sciences* 44:1333–1346. [15] Izawa M. R. M. 2011. *Meteoritics & Planetary Science* 46:638–651. [16] Jenkins et al. (2019) *Meteoritics & Planetary Science* 54: 902-918. [17] Cao F. et al. (2017) *LPSC XLVIII,* Abstract#2827. [18] Moser D. E. et al. 2013. *Nature* 499: 454–457.

METEORITES OF THE JURASSIC: POPULATIONS DETERMINED FROM REMNANT EXTRATERRESTRIAL CHROME-SPINELS IN SPANISH LIMESTONE

C. E. Caplan[1,2*], G. R. Huss[2], K. Nagashima[2], and B. Schmitz[3,2], [1]Department of Earth Sciences, University of Hawai'i at Mānoa, 1680 East-West Road, Honolulu, HI 96822, [2]Hawai'i Institute of Geophysics and Planetology, University of Hawai'i at Mānoa, 1680 East-West Road, Honolulu, HI 96822, [3]Department of Physics, University of Lund, P.O. Box 118, Lund SE-22100, Sweden. *caplance@hawaii.edu.

Introduction: The study of meteorites helps us understand solar system processes, but these samples only provide information about what has fallen in the past few thousands of years. Meteorite types have unique characteristics, but they can be altered once they reach Earth. Fortunately, remnant chrome-spinels are preserved throughout Earth's history, and they retain their original characteristics [1-2]. These grains originate from meteorites or micrometeorites and the host-meteorite type for each grain can be determined by measuring element abundances and oxygen isotopes. The overall goal of studying extraterrestrial chrome-spinels is to determine how meteorite populations have changed over time. This study focuses on samples from the Jurassic that were preserved in limestone from the Callovian-Oxfordian boundary (~160 Ma) in Southern Spain, near Carcabuey. Here we determined parent-meteorite types for large- (63-220 μm) and small- (32-63 μm) size fraction grains from Jurassic sediments.

Experimental: Chrome-spinel grains for this study were extracted from limestone at Lund University [e.g., 1]. The grains were mounted in quarter-inch-diameter stainless steel cylinders using epoxy at the University of Hawai'i (UH). The mounts were ground flat and polished using multiple grades of diamond lapping papers. The JEOL JXA-8500F field emission electron microprobe at UH was used to collect major- and minor-element abundances of each grain. Oxygen isotopes were measured using the Cameca ims 1280 ion microprobe (SIMS) at UH. Stillwater chromite was used as the standard for the SIMS and as an additional standard for the electron microprobe [e.g., 3].

Results and Discussion: Our data set consists of 62 large grains and 52 small grains. Multiple measurements were made for most grains and typically showed good reproducibility. Measurements from SIMS pits that intersected cracks or secondary alteration were not used. The two size fractions have similar compositional distributions (Fig. 1).

The grains in this study were classified by comparison with a database of chrome-spinel from modern meteorites. Element abundances provide much of the discriminating power, supplemented by oxygen isotopes. Jurassic grains generally occupy the same compositional space as database grains (Fig. 1). Gaps where the database and the Jurassic data do not overlap may indicate shifts in the population of infalling meteorites over time. Overall, ~30% of the grains were classified as ordinary-chondrite like, ~20% have ureilite, acapulcoite/ lodranite, or carbonaceous chondrite

Figure 1: Large (big squares) and small (little squares) chrome-spinels in TiO_2 vs. Al_2O_3 wt%. The $\Delta^{17}O$ (=$\delta^{17}O$-0.52x$\delta^{18}O$) color bar has an uncertainty of ±0.36‰ (2σ). Grey circles from chrome-spinel database of modern meteorites [e.g. 4-7].

origins, ~10% are possible terrestrial grains, and the remainder are extraterrestrial with unknown parentage (they did not have robust matches using our current chrome-spinel database).

Ordinary-chondrite-like grains (solid oval/reddish) form a well-defined cluster with all elements and oxygen isotopes (e.g. Fig. 1). The group of high-Al_2O_3 grains (dashed oval/lime) fall within limited fields based on a variety of elements and oxygen isotopes (e.g. Fig. 1). The database does not contain grains with these high-Al_2O_3 compositions, which suggests that they originated from meteorites not represented in modern meteorite collections. The region between these two groups (0-1 wt% TiO_2 and 5-20 wt% Al_2O_3) contains most of the remaining Jurassic grains (including the ~20% that are classified). This region also contains a majority of the meteorite types that are in the database. It is difficult to classify some grains in this region because of the extensive overlap of different meteorite types. Also, Jurassic grains with low TiO_2 concentrations have very few database counterparts for classification.

References: [1] Schmitz B. (2013) *Chemie der Erde-Geochemistry 73*, 117-145. [2] Schmitz B., et al. (2001) *Earth and Planetary Science Letters 194*, 1-15. [3] Caplan C. E., et al. (2017) *LPSC XLVIII*, Abstract #1690. [4] Wlotzka F. (2005) *Meteoritics & Planetary Science 40*(11), 1673-1702. [5] Goodrich, C. A., et al. (2014) *Geochimica et Cosmochimica Acta 135*, 126-169. [6] Mittlefehldt, D. W. (2015) *Chemie der Erde-Geochemistry 75*(2), 155-183. [7] Keil, K., & McCoy, T. J. (2018) *Chemie der Erde-Geochemistry 78*(2), 153-203.

Bulk Hydrogen Isotopes in Ordinary Chondrites

M. J. Cato[1] and Z. D. Sharp[1], [1]Department of Earth and Planetary Sciences, University of New Mexico, Albuquerque, NM 87131, United States

Introduction: Hydrogen isotope characterization of bulk samples from a wide range of bodies is a necessary step to better our understanding of the origins and proliferation of water in our solar system. Rough determinations of hydrogen isotope ratios in planetary atmospheres have been conducted through remote sensing (e.g. [1]), but high-quality measurements of hydrogen held within the rocks of a body requires physical samples to be measured on instruments we have on the Earth. Historically, there has been a particular focus on hydrated chondrites and meteorites from known bodies (e.g. [2], [3]). The extensive measurements of these specific meteorite groups can be attributed to the relative ease of measuring hydrogen in hydrated chondrites, CM chondrites' isotopic similarity to the Earth [4], and the inherent scientific benefit of fully characterizing a suite of meteorites attributed to a specific body. One class which has been largely ignored due to its nominally anhydrous nature is the ordinary chondrites.

Notably, there has been increased interest in hydrogen isotopes within ordinary chondrites over the past decade. However, the vast majority of studies have focused extensively on low petrologic types [5] and specific components of the sample, using techniques like Secondary Ion Mass Spectrometery (e.g. [6], [7]). Focused measurements within a sample are inherently flawed when considering the source of water to a body, as any water deposited will consist of the entire volume of the meteorite, not only that within specific minerals. Since the early 1980s [8], bulk hydrogen isotope measurements within ordinary chondrites have almost exclusively been conducted on Semarkona [5], one of the least thermally altered of the class with an anomalously high hydrogen isotope value compared to any other meteorite. Due to the recent measurements being the most significant studies of hydrogen isotopes in ordinary chondrites to date, the Semarkona hydrogen isotope value is often used as the average value for the class [9]. In this study, we are measuring a range of ordinary chondrite subclasses and petrologic types to create a more representative average hydrogen isotope value of ordinary chondrites.

Samples and Methods: Herein we intend to perform hydrogen isotope measurements from 25 ordinary chondrite falls from the collection of the Institute of Meteoritics at the University of New Mexico. Samples include at least one meteorite of each petrologic type, subgroups excluded, of H, L, and LL meteorites. Each sample, stored in a desiccator, is ground and placed into silver foil to be measured using continuous-flow gas-phase mass spectrometery. With our micro-extraction line, we step heat each sample at 150, 300, 500, 700, and 900°C followed by complete melting with an oxy-gas torch in a quartz glass tube. Each step is cryo-concentrated for at least an hour, allowing us to measure quantities of H_2 down to 0.13 micromols. Step-heating allows us to remove low-temperature terrestrial contamination that is inherent to meteorites and better understand how the hydrogen is incorporated into the material.

Initial Results & Discussion: Preliminary measurements were conducted on Chelyabinsk, Kheneg Ljouâd, Nuevo Mercurio and Dhajala. A consistently large release of hydrogen in all steps up to 500°C with a δD of -58 ± 25‰ across all meteorites has been observed. A significant drop in hydrogen release occurs past the 500°C step of up to an order of magnitude corresponding to higher measured δD values ranging from 19 ± 6‰ for Chelyabinsk to 202 ± 6‰ for Dhajala. More measurements still must be made to better understand trends within and between groups, but there appears to be a weak correlation between lower petrologic types and higher δD values.

Preliminary data shows that even for falls which are quickly collected, terrestrial contamination appears to be rampant in low temperature steps with hydrogen concentrations high enough to completely dominate the bulk hydrogen isotope value of the sample. Even for our Chelyabinsk sample, its tenure in the Russian snow and later rain appears to have been enough to contaminate even the higher temperature phases with both an increased concentration of hydrogen compared to any other meteorite measured so far and a lower δD value. The rampant contamination leads us to question earlier bulk ordinary chondrite data as it was previously impossible to step-heat the samples in order to remove the vast majority of terrestrial contamination while the low hydrogen isotope values compared to Semarkona highlight the necessity of more high-quality bulk measurements of this class.

References: [1] Trauger J. T. et al. 1973. *The Astrophysical Journal* 184:L137-L141. [2] Kerridge J. F. 1985. *Geochemica et Cosmochemicia Acta* 49:1707-1714. [3] Saal A. E. et al. 2013. *Science* 340:1317-1320. [4] Marty B. 2012. *Earth and Planetary Science Letters* 313-314:55-56 [5] Alexander C. M. O'D. 2012. *Science* 337:721-723. [6] Shimizu K. et al. 2019. *LPS L,* Abstract #6840. [7] Sanborn M. E. et al. 2019. *LPS L,* Abstract #6279. [8] McNaughton N. J. et al. 1981. *Nature* 294:639-641. [9] Lin, Y. and van Westrenen W. 2019. *National Science Review*.

REVISED TRAPPED MELT MODEL FOR IRON METEORITES.

Nancy L. Chabot[1], [1]Johns Hopkins University Applied Physics Laboratory, 11100 Johns Hopkins Rd, Laurel, MD, 20723, USA. Nancy.Chabot@jhuapl.edu

Introduction: The IIIAB group is the largest magmatic iron meteorite group, making it well-suited to investigate the process of core crystallization in the early Solar System. Previous studies have described strong evidence that the IIIAB core solidified by fractional crystallization but that the manner of crystallization also trapped pockets of metallic melt during that process [1–3]. This trapped melt model (Fig. 1a) resulted in the composition of IIIAB irons falling between the solid metal and liquid metal tracks from fractional crystallization of the core, due to different amounts of trapped melt during the formation of each individual iron meteorite specimen, providing an elegant conceptual model to explain the inherent spread in IIIAB irons about the fractional crystallization trend.

However, a major issue with the IIIAB trapped melt model calculations [1–3] is that the values of the solid metal/liquid metal partition coefficient (D) of Ir used in the models differ considerably from the experimental data [4] (Fig. 1b). In any model, the expression of D(Ir) is just a means to mathematically represent the partitioning behavior; however, having that expression be consistent with the experimental determinations of D(Ir) would be more physically plausible. Using a parameterization for D(Ir) derived from the latest experimental data [4], the IIIAB irons do not fall between the solid metal and liquid metal tracks (Fig. 1c).

Revised Trapped Melt Model: To date, trapped melt models have not included any effects on the element chemistry due to the formation of troilite and have mathematically just used mixtures between solid metal and liquid metal to model trapped melt. In the revised trapped melt model in this work, an effect on the element chemistry due to the formation of troilite from the trapped melt is included. In particular, the revised trapped melt model assumes a simple system where any trapped melt will solidify into troilite and solid metal. Given that S is nearly insoluble in Fe-Ni solid metal, the fraction of trapped liquid that solidifies to troilite rather than solid metal can be calculated by mass balance. Many siderophile elements are not expected to partition heavily into troilite in comparison to Fe-Ni metal, and thus, their concentrations in the troilite can be approximated as zero, resulting in a simplified equation:

$$C_{TrapSolidMetal} = C_{TrapLiq}/(1-x)$$

where $C_{TrapLiq}$ and $C_{TrapSolidMetal}$ are the concentrations of an element in the trapped liquid and resulting solid metal respectively, and x is the fraction of the trapped liquid that solidifies to troilite rather than solid metal. In this revised trapped melt model (Fig. 1c), the IIIAB irons largely fall between the tracks of solid metal formed from fractional crystallization and solid metal formed from trapped liquid. Conceptually, this is as envisioned by previous trapped melt models, but mathematically, this model is different in that 1) it uses parameterizations for D(Ir) and D(Au) derived from the experimental data and 2) it includes an effect on the element chemistry due to the formation of troilite from the trapped melt. This simple model shows great potential to resolve existing issues with previous models and to provide a consistent approach to model trapped melt in all magmatic iron meteorite groups.
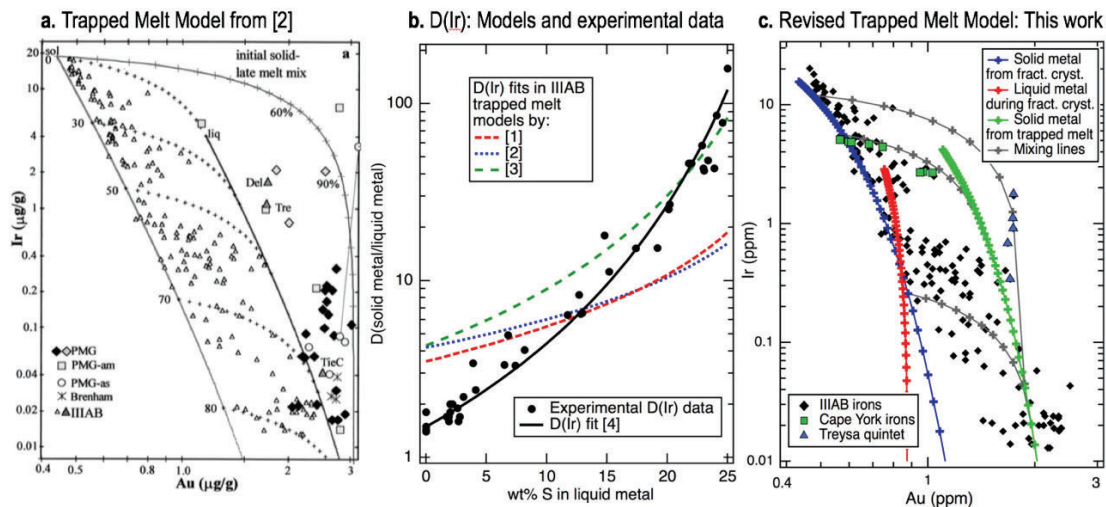

Fig. 1. Original (**a., b.**) and revised (**b., c.**) trapped melt models with D(Ir) fits applied to the IIIAB group.

References: [1] Wasson, J. T. (1999) *GCA* 63: 287–2889. [2] Wasson, J. T. & Choi, B.-G. (2003) *GCA* 67: 3079–3096. [3] Wasson, J. T. (2016) *MAPS* 51: 773–784. [4] Chabot, N. L. et al. (2017) *MAPS* 52: 1133–1145.

EFFECTS OF SHORT-TERM HEATING ON THE ORGANIC CONTENT OF THE EXPERIMENTALLY-HEATED TAGISH LAKE METEORITE

Q. H. S. Chan[1,2], A. Nakato[3], Y. Kebukawa[4], M. E. Zolensky[1], T. Nakamura[5], J. A. Maisano[6], M. W. Colbert[6], J. E. Martinez[7], A. L. D. Kilcoyne[8], H. Suga[9], Y. Takahashi[9], Y. Takeichi[10,11], K. Mase[10,11], and I. P. Wright[2] [1]ARES, NASA Johnson Space Center, USA (e-mail: queenie.chan@open.ac.uk), [2]Department of Physical Sciences, The Open University, UK, [3]Inst. Space Astronaut. Sci., Japan Aer-osp. Explor. Agency (JAXA), Japan, [4]Faculty of Engineering, Yokohama National University, Japan, [5]Graduate School of Science, Tohoku University, Japan, [6]Department of Geological Sciences, The University of Texas, USA, [7]Jacobs Engineering, USA, [8]Lawrence Berkeley National Laboratory, USA, [9]Department of Earth and Planetary Science, The University of Tokyo, Japan, [10]Institute of Materials Structure Science, High-Energy Accelerator Research Organization (KEK), Japan, [11]Department of Materials Structure Science, SOKENDAI (The Graduate University for Advanced Studies), Japan

Introduction: Carbonaceous chondrites exhibit a wide range of alteration characteristics, while some are known to demonstrate mineralogical and petrologic evidence of having been thermally metamorphosed after aqueous alteration. This group of dehydrated meteorites are commonly referred to as thermally metamorphosed carbonaceous chondrites (TMCCs), and their relatively flat visible near-infrared reflectance spectra resemble that of C-, G-, B-, and F-type asteroids that typically have low albedos [1, 2]. The Hayabusa2 (HYB2) mission is now under way with an aim to bring back samples from the near-Earth C-type asteroid 162173 Ryugu at the end of 2020 [3]. Visible and near infrared spectra of asteroid 162173 Ryugu obtained by the Near-InfraRed Spectrometer and Optical Navigation Camera onboard the HYB2 Spacecraft are relatively flat with no apparent absorption features but the presence of a small 2.72-μm absorption feature [4], which could be explained by short-duration local heating of hydrated carbonaceous like material [5]. In an attempt to understand the effects of short-term heating on chondritic organic matter (OM), we investigated the change in the OM contents of the experimentally heated Tagish Lake meteorite samples.

Samples and Analytical Techniques: The carbonate-poor lithology of the Tagish Lake meteorite was used in this study. This lithology was located by mineral identification via X-ray computed tomography (XRCT) at the High-Resolution XRCT Facility at The University of Texas, and scanning electron microscopy (SEM) and energy-dispersive spectrometry (EDS) at NASA JSC. Subsamples (~100 mg each) were subjected to heating experiments at 600 and 900 °C for 1 and 96 h at JAXA. The samples were then studied with Raman spectroscopy at NASA JSC using a Jobin-Yvon Horiba LabRam HR (800 mm) Raman microprobe with a 514 nm (green) laser. Focused ion beam (FIB) thin sections of the samples were prepared with a FIB (Hitachi, FB2200) at ISAS/JAXA for three STXM-XANES analyses using the compact-STXM installed at BL-13A beamline of the Photon Factory (PF), KEK, and the STXM installed at beamline 5.3.2.2 of the Advanced Light Source, Lawrence Berkeley National Laboratory.

Results and Discussion: Heating experiments have led to a notable reduction in the fluorescence background intensity of the Raman spectra of the heated Tagish Lake meteorite samples, the widening of the width of the Raman graphite (G) band at ~1580–1590 cm^{-1}, and the narrowing of the defect (D) band at ~1350–1380 cm^{-1}. The results indicate a development in the sizes of crystalline domains but significant graphitic ordering did not take place, which would otherwise have reduced the G band width [6]. A 1s–σ* exciton peak (~291.6 eV) in C-XANES spectrum that corresponds to a graphene structure is expected if highly conjugated sp^2 bonded C domains were present, as in the long-term thermally metamorphosed chondrites [7]. However, the peak at 291.6 eV is absent in the C-XANES spectra of all the experimentally heated Tagish Lake samples. Our experiment suggests that graphitization of OM did not take place in the Tagish Lake meteorite even though the samples were heated to 900°C for 96 h, as the OM maturity trend was influenced by the heating conditions, confining pressure, kinetics, and the nature of the OM precursor, e.g., heating of the Tagish Lake meteorite leads to the dehydration of phyllosilicates [8], which enhances the formation of OM with oxygenated moieties, inhibiting further transform into graphene-like material. In contrast, during prolonged parent body metamorphism, the loss of the aliphatic components and their conversion into aromatics far exceeds the formation of carbonyl [9]. This would have induced the ordering of the aromatic moieties, leading to the development of the 1s–σ* exciton peak. Our coordinated organic analyses account for the changes in the structure of TMCC organics in response to short-term heating, and offer insights for interpreting the nature of the OM of Ryugu – a hydrated carbonaceous chondrite-like material that experienced heating and partial dehydration [5].

References: [1] Hiroi T. *et al.* (1993) *Science, 261,* 1016-1018. [2] Hiroi T. *et al.* (1996) *Meteoritics & Planetary Science, 31,* 321-327. [3] Watanabe S.-i. *et al.* (2017) *Space Science Reviews, 208,* 3-16. [4] Kitazato K. *et al.* (2019) *Science, 364,* 272-275. [5] Nakamura T. *et al.* (2019) *Lunar and Planetary Science Conference, 50.* [6] Ferrari A.C. and Robertson J. (2000) *Physical Review B, 61,* 14095-14107. [7] Cody G.D. *et al.* (2008) *Earth and Planetary Science Letters, 272,* 446-455. [8] Amano K. *et al.* (2018) *LPI Contributions, 2067.* [9] Alexander C.M.O.D. *et al.* (2014) *Meteoritics & Planetary Science, 49,* 503-525.

COORDINATED ORGANIC ANALYSES OF HAYABUSA CATEGORY 3 CARBONACEOUS PARTICLES

Q. H. S. Chan[1,2], M. E. Zolensky[2], R. Brunetto[3], E. T. Parker[4], J. P. Dworkin[4], C. Sandt[5], I. P. Wright[1] and I. A. Franchi[1], [1]The Open University, Walton Hall, Milton Keynes MK7 6AA, UK (e-mail: queenie.chan@open.ac.uk), [2]NASA Johnson Space Center, Houston TX 77058, USA, [3]Institut d'Astrophysique Spatiale, CNRS/Université Paris-Saclay, Université Paris-Sud, Orsay, France, [4]NASA Goddard Space Flight Center, Greenbelt, MD 20771, USA, [5]Synchrotron Soleil, BP48, L'Orme des Merisiers, Gif sur Yvette Cédex, 91192, France.

Introduction: The first Hayabusa mission has returned to Earth samples from the near-Earth S-type asteroid 25143 Itokawa in 2010 [1]. 943 particles have been picked up and kept in a ISO 6 cleanroom at the Planetary Material Sample Curation Facility of JAXA. Despite a lithology related to ordinary chondrites that typically have low organic contents, 64 particles from the collection are composed predominantly of carbonaceous material [1, 2]. However, the small sizes (~20–200 μm) of the carbon rich 'category (cat.) 3' particles make the characterisation of their organic contents and determination of their origins (terrestrial vs extraterrestrial) challenging [2-5]. In this work, we explore the origins of five Itokawa cat. 3 carbonaceous particles via coordinated analyses of their soluble and insoluble organic contents.

Samples and Analytical Techniques: Five cat. 3 Itokawa particles (RA-QD02-0012, RA-QD02-0078, RB-CV-0029, RB-CV-0080 and RB-QD04-0052) were allocated for this study. Meteorite samples including CM2 Murchison, ordinary chondrites (falls) with similar lithology as Itokawa – LL3.6 Parnallee and LL5 Alta'ameem, and an insoluble organic residue of Murchison were analysed alongside the Hayabusa samples. The Itokawa particles and the meteorite samples of equivalent sizes were picked by a micromanipulator and pressed flat with a spectroscopic grade sapphire window into high-purity gold foils. The samples were analysed with Fourier-transform infrared (FTIR) microspectroscopy at the SMIS beamline of the synchrotron SOLEIL with Nicolet 5700, 8700 FTIR spectrometers coupled to Continuum microscopes and a iS50 with a Nic-Plan IR microscope, and a Cary 670 IR spectrometer coupled to a Cary 620 IR microscope, operating in reflectance mode. Spot and point-by-point mapping Raman spectroscopic analyses were conducted using a Jobin-Yvon Horiba LabRAM HR Raman microprobe at NASA JSC and the Open University using a 514 nm laser for which the power was maintained at ~60 μW. Finally, amino acids were extracted from the samples, derivatised, and analysed with a Waters nano-ACQUITY ultraperformance liquid chromatograph and a Thermo Scientific LTQ Orbitrap XL hybrid mass spectrometer (nLC-HRMS) at NASA Goddard [6]. All tools and materials that were in contact with the particles had been sterilised by baking at 500°C in air for >10h.

Results and Discussion: The five particles are ~86–100 μm in size exhibiting sheet- (#29,52,80), block- (#12) and rod-like (#78) morphologies. The sheet-like particles are flat and have sharp, rugged edges that appear to be produced by tearing. Their appearance is similar to the cat. 3 Itokawa grains described in [7], but their elemental compositions are similar to that reported for cat. 4 particles with a significant contribution of Al, Ti, which are potentially artificial material (e.g., alloy) [2]. Raman analysis shows that only 2 (#52,78) out of the 5 Itokawa grains exhibit the typical first-order defect (D) and graphite (G) band in the ~1350−1600 cm^{-1} region that correspond to the breathing mode of aromatic rings, and in-plane stretching mode of sp^2-bonded C atoms in both rings and chains [8]. The Raman spectral features are similar to that observed for cat. 3 Itokawa particles reported in [5]. It suggests that the organics had been subjected to minimal heating, which is incompatible to the LL4–6 lithology of Itokawa [9]. Yet, FTIR measurements in the mid-IR (650–4000 cm^{-1}) range show that their spectral features are atypical to that of extraterrestrial C. Rather, the main component of the grains are hydrous silicate (#78) and fluorinated-heterocycles (#52). The IR spectra of grains #12&80 are comparable to terrestrial protein dominated by the protein amide I and amide II bands 1500–1700 cm^{-1} corresponding to the C=O stretching and the NH bending of the peptide bond [10]. We are currently preparing the samples for amino acid analysis with nLC-HRMS. If these grains indeed contain terrestrial proteins, they should be easily discernable by the presence of exclusively the L-enantiomers of amino acids.

Implications: Despite the careful contamination control and curation efforts, some fractions of mission-returned samples are still reported to be contaminated by terrestrial material, e.g., Apollo [11], Stardust [12], and Hayabusa missions. The Hayabusa2 (HYB2) mission is now under way with an aim to bring back samples from the near-Earth C-type asteroid 162173 Ryugu at the end of 2020 [13]. Lessons learned from analysing Itokawa particles should be implemented in the analytical protocol of the HYB2 samples and their curatorial procedures.

References: [1] Yada T. *et al.* (2014) *Meteoritics & Planetary Science, 49,* 135-153. [2] Uesugi M. *et al.* (2014) *Earth, Planets and Space, 66,* 1-11. [3] Ito M. *et al.* (2014) *Earth, Planets and Space, 66,* 91. [4] Yabuta H. *et al.* (2014) *Earth, Planets and Space, 66,* 1-8. [5] Kitajima F. *et al.* (2015) *Earth, Planets and Space, 67,* 1-12. [6] Callahan M.P. *et al.* (2014) *Journal of Chromatography A, 1332,* 30-34. [7] Naraoka H. *et al.* (2015) *Earth, Planets and Space, 67,* 67. [8] Ferrari A.C. and Robertson J. (2000) *Physical Review B, 61,* 14095-14107. [9] Nakamura T. *et al.* (2011) *Science, 333,* 1113-1116. [10] Ami D. *et al.* (2016) *Scientific Reports, 6,* 29096. [11] Elsila J.E. *et al.* (2016) *ACS Central Science, 2,* 370-379. [12] Sandford S.A. *et al.* (2010) *Meteoritics & Planetary Science, 45,* 406-433. [13] Watanabe S.-i. *et al.* (2017) *Space Science Reviews, 208,* 3-16.

REDUCING INFORMATION LOSS FROM TRADITIONAL FOCUSSED ION BEAM THINNING OF CARBONACEOUS CHONDRITE MATRICES USING SLICE & VIEW METHODS: APPLICATION FOR CARBONACEOUS ASTEROID SAMPLE RETURN.

H. G. Changela[12], L. Yangting[1], L. Gu[1], X. Zhang[3] [1]Key Laboratory of Earth & Planetary Physics, Institute of Geology & Geophysics, Chinese Academy of Sciences. [2]Deptarment of Earth & Planetary Science, University of New Mexico. [3]China Academy of Space Technology. Email:changel@mail.iggcas.ac.cn; changela@unm.edu

Introduction: The characterisation of samples returned from carbonaceous asteroids will provide ground truths on the makeup of primitive bodies that seeded the Earth, examples being the *Hayabusa-2* and *OSIRIS-ReX* missions from Asteroids 162173Ryugu and 101955Bennu repsectively. Carbonaceous chondrites (CCs), providing potential C-type asteroid analogues, have matrices containing microscopic to nanoscopic phases and morphologies including porosity, minerals, amorphous grains and organic material (OM). This means that their accurate characterisation requires the ability to discriminate between different phases at the nano scale. Characterization of the morphology, functional chemistry and microscopic setting of OM by coordinating synchrotron X-ray and electron microscopy techniques will be paramount. Traditional FIB methods extract ~10 µm wide x 5 µm high x 2 µm thick sections that are subsequently thinned down to electron and soft X-ray transparency at ~100 nm thicknesses. In this current work we are preparing multiple times biggger FIB sections. In addition, rather than FIB polishing via destruction to the desired 100 nm thickness, we are applying slice and view methods whilst thinning down in order to reduce information losses. We are performing this on the unclassified anhydrous CC fall Ningqiang that uniquely has affinities with anhydrous CV and CKs but with organic abundances similar to the more hydrated CCs.

Figure 1. FIB thinning using slice and view methods. (a) An unconventional ~40 x 20 x 2.5 µm section was extracted from a fresh chip of Ningqiang thus eliminating EPOXY. The dark grey material is organic material. One half was thinned down to soft X-ray and electron transparency for STXM and TEM. The right hand side had slice and view after the initial identification of seemingly an organic 'inclusion' in a fayalite grain (red rectangle). (b)-(d) High magnification of red rectangle in (a). (b) First slice of right hand right of FIB section in (a) taking away ~ 200 nm. The 'organic inclusion' is circled in red. Note the smaller 'inclusion' circled in blue. (c) 2nd slice and (d) 3rd slice. Slicing away of the 3 layers and sequentially imaging shows the 'organic inclusion' to merge towards the edge of the grain and connect to the organic network surrounding finer fayalite grains. Based on this, the blue phase should also merge to the grain margin after further slicing along this profile. The similar composition between the finer fayalite grains and the larger one suggests that organic fluids disseminated the large grain into finer ones along its margins. Thus rather than an inclusion in fayalite, this phase is actually part of the organic groundmass/network surrounding the irregularly shaped large fayalite grain. If the sample was directly thinned using traditional methods, this information would have been lost. Due to the fine scale submicron heterogeneity of CC matrices, FIB methods for ultra thinning samples should employ slice and view techniques when thinning down to electron transparency, preventing information loss.
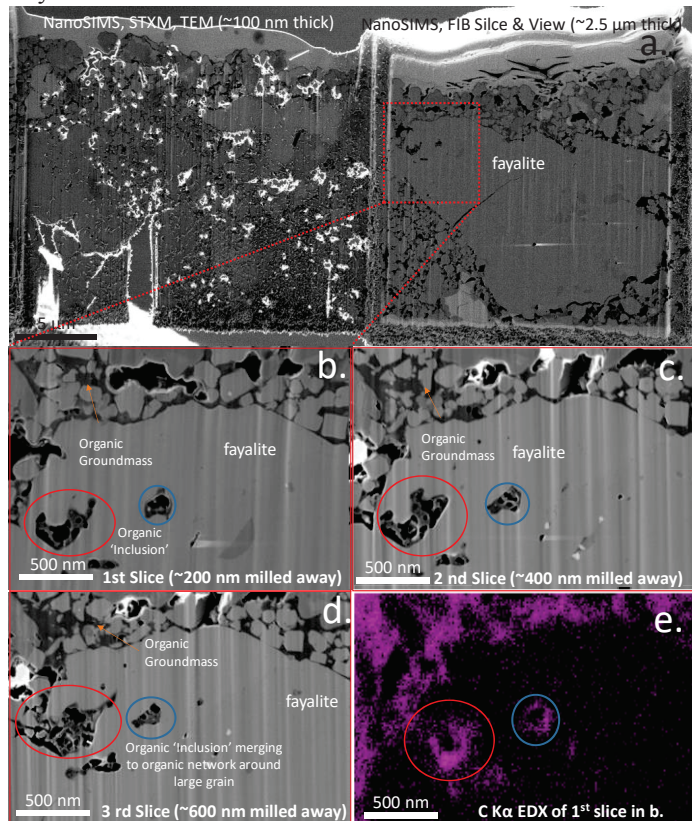
Implications for Sample Return from C-type Asteroids: Whilst traditional FIB techniques prove vital for analysing CC matrices *in situ*, the nanoscopic heterogeneity of CC matrices implies that important sample information is being lost. However, it could be retained if samples are imaged and elementally EDX mapped by simple FIB slice and view methods when thinning. Furthermore, FIB techniques can be applied to sample sections multiple times bigger than traditional samples (Fig. 1). By adopting his method on a chip of Ningqiang, important imformation on the organic groundmass/network in its matrix would have been lost if traditional FIB methods were employed.

UNDERSTANDING THE ROLE OF SULFIDES IN THE SPACE WEATHERING OF ASTEROIDAL REGOLITHS.

L. C. Chaves [1], M. S. Thompson[1], and M. J. Loeffler[2] [1]Department of Earth, Atmospheric, and Planetary Sciences, Purdue University, West Lafayette, IN, USA (lchavesm@purdue.edu) [2]Department of Physics and Astronomy, Northern Arizona University, Flagstaff, AZ, USA.

Introduction: Space weathering modifies the chemical, microstructural and spectral properties of grains on the surfaces of airless bodies and is driven by micrometeorite impacts and solar wind irradiation [1]. These processes cause the attenuation of characteristic absorption bands, and changes in spectral slope and reflectance. The chemical and microstructural characteristics of space weathering include vesiculated textures, amorphous rims on grain surfaces, and Fe-bearing nanoparticles [2]. Previous studies of returned samples have focused on the effect of space weathering on silicate minerals which dominate the collections from the Moon and asteroid Itokawa [3,4]. Similarly, laboratory simulations of these processes have also focused on silicate minerals, using ion irradiation to mimic solar wind exposure, and pulsed-laser irradiation to reproduce micrometeorite impact events [5]. However, the situation is less constrained for mineral phases such as Fe- and Fe-Ni sulfides which occur on more compositionally-complex planetary surfaces. These minerals have been identified in returned samples from S-type asteroid Itokawa [4,6,7] and are common in the carbonaceous chondrite meteorites that are thought to be compositional analogs of the target bodies of the Hayabusa2 and OSIRIS-REx missions [8]. Laboratory simulations of space weathering for sulfides have been shown to produce spectral changes, especially darkening [9]. In this study, we analyzed sulfide phases from the CM2 Murchison meteorite altered by pulsed-laser irradiation. These results will be compared to the chemical and physical features of five space-weathered particles from asteroid Itokawa allocated to us by the Japan Aerospace Exploration Agency.

Methodology: To understand the chemical and microstructural response of these phases to space weathering conditions, we simulated micrometeorite impacts by performing pulsed-lased irradiation of an unpolished, dry cut chip of the CM2 Murchison carbonaceous chondrite. The irradiation was performed under high vacuum (~10^{-8} Torr), using an Nd-YAG laser (1064 nm) with a pulse duration of 6-8 ns, and an energy of 48 mJ, similar to previous studies [10]. To identify the morphological features and chemical changes produced after the irradiation we used scanning electron microscopy (SEM) and energy dispersive X-ray spectroscopy (EDS) with a FEI Nova NanoSEM200. To determine changes in microstructures we will perform transmission electron microscopy (TEM) analyses of these samples. The results obtained through these experiments will be compared with future analyses of sulfide-bearing Itokawa particles.

Fig 1. BSE image showing vesicles and polygonal fracture pattern in a sulfide grain after pulsed-laser irradiation.

Results: Backscattered electron (BSE) images showed melt features, including melt droplets, on the surfaces of sulfide grains. We also identified abundant vesicles on the surfaces of the irradiated sulfides, similar in size and distribution to the vesicles observed in other laser-irradiated sulfide minerals [11]. BSE imaging of the sulfides also reveals a ubiquitous polygonal fracture pattern that suggests rapid cooling after laser irradiation (Fig. 1). EDS analyses indicate that Fe and S, Ni are the most significant elemental components of the sulfide surface melts, with stoichiometries similar to troilite and pentlandite. We will present results of transmission electron microscopy (TEM) analyses of focused ion beam (FIB) sections extracted from both troilite and pentlandite phases, and compare these results to the microstructural analyses of other experimentally space weathered sulfides.

References: [1] Hapke B. (2001) *Journal of Geophysical Research* 116:10039–10073. [2] Keller L. P. et al. (1997) *Geochimica et Cosmochimica Acta* 61: 2331-2341. [3] Noguchi T. et al. (2011) *Science* 333:1121-1124. [4] Thompson M. S. et al. (2014) *Earth, Planets and Space* 66:89. [5] Loeffler M. J. et al. 2016. *Meteoritics & Planetary Science* 51:261-275. [6] Nakamura T. et al. (2011) *Science* 333:1113-1115. [7] Noguchi T. et al. 2014. *Meteoritics & Planetary Science* 49: 188-214. [8] Bland P.A. et al. 2004. *Meteoritics & Planetary Science* 39:3-16. [9] Okazaki M. et al. (2014) ACM 415. [10] Matsuoka M. et al. (2015) *Icarus* 254: 230-238 [11] Thompson M. S. et al. (2019) *Icarus* 319: 499-511.
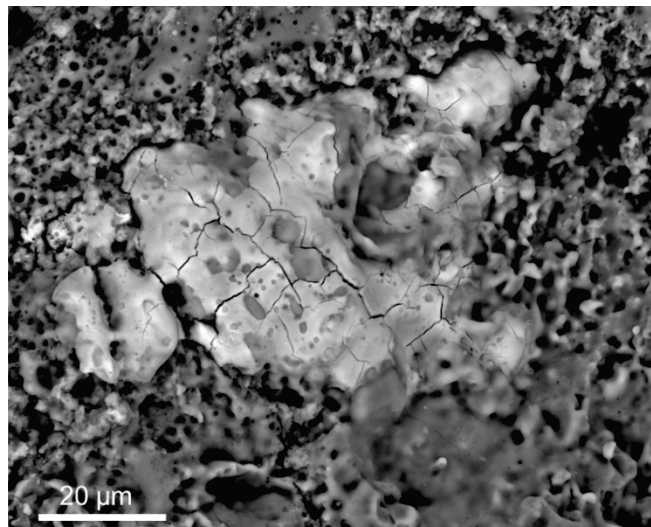
HIGH RESOLUTION SHRIMP PHOSPHATE U-PB AGES IN SAYH AL UHAYMIR 169: POSSIBLE AGE OF THE PRE-IMBRIUM IMPACT

X. C. Che[1,2], A. A. Nemchin[1,3,4], T. Long[1,2] and D. Y. Liu[1,2], [1]Beijing SHRIMP Center, Institute of Geology, Chinese Academy of Geological Sciences, Beijing, 102206, China (E-mail: cxc@bjshrimp.cn), [2]Shandong Institute of Geological Sciences, Jinan, 250013, China, [3]Department of Applied Geology, Curtin University, Perth, WA 6845, Australia, [4]Department of Geosciences, Swedish Museum of Natural History, Stockholm, SE-104 05, Sweden.

Introduction: Lunar meteorite **Sayh al Uhaymir 169** (SaU-169) was found in the Sayh al Uhaymir region of Oman in 2002. SaU-169 is an extremely KREEP (High K, P, REE)-rich polymict sample, which consists of crystalline impact-melt breccia and adherent regolith as described in Gnos et al [1]. The identical, within uncertainties, zircon ages of 3909 ± 13 [1], 3920 ± 13 Ma [2] and 3921 ± 3 Ma [3] in impact melt breccia of SaU-169 have been reported by several studies. Combined with results obtained for zircon from Apollo-12 samples [2], these ages were interpreted to represent the age of the Imbrium event. In this study, we have investigated phosphate grains from the impact melt breccia portion of SaU-169.

Meteorite Sample and Analytical Methods: Phosphate grains were identified in the mounted pieces of the sample by the energy-dispersive X-ray spectroscopy (OXFORD X-Max^{N}20) attached to ZEISS MERLIN Compact scanning electron microscope and U-Pb dating was performed on the SHRIMP IIe-Mc at the Beijing SHRIMP Center, Chinese Academy of Geological Sciences. Sample mounts for SHRIMP analysis were cleaned with ethanol and distilled water before gold coating. The analytical spot size was 10μm and the primary current was 2nA. The analytical conditions were identical to those described by [4, 5]. $^{206}Pb^+$, $^{238}U^+$, and $^{238}U^{16}O_2^+$ were measured sequentially in the single-collector electron multiplier (EM) positioned on the axis and the $^{206}Pb/^{238}U$ ratios calibrated using NW-1 apatite standard [6]. $^{204}Pb^+$, $^{206}Pb^+$, $^{207}Pb^+$ and $^{208}Pb^+$ isotopes were measured simultaneously in four EMs and the $^{204}Pb/^{206}Pb$, $^{207}Pb/^{206}Pb$ ratios were calibrated using BCR-2, BHVO-2 [7].
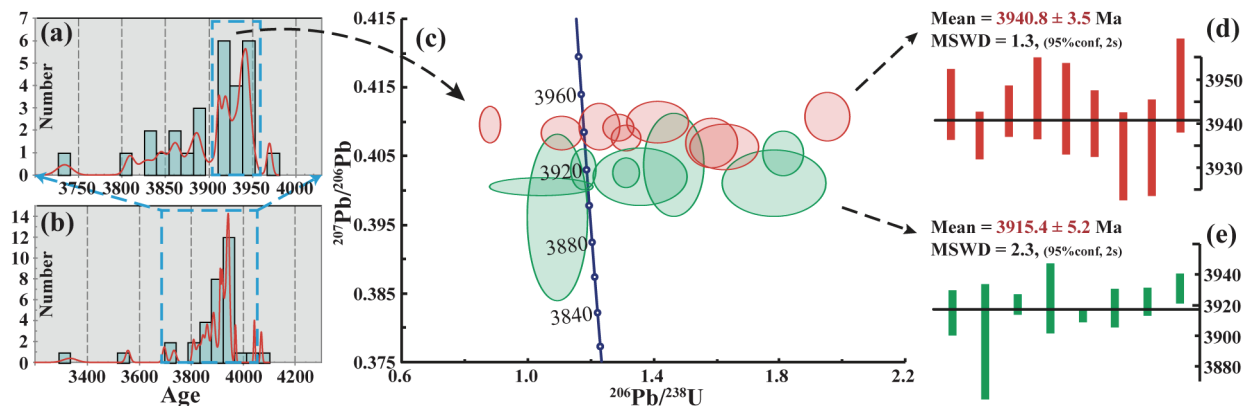
Fig. 1. (a, b) Histograms and relative probability curves for all of SaU-169 phosphates from this study; (c) Concordia plot of phosphate SHRIMP U–Pb analyses within dotted area of Fig. 1(b); (d, e) Weighted mean ages of two groups of phosphates analyzed in SaU-169.

Results and Discussion: Analysis of 33 spots on 33 different phosphate grains yielded $^{207}Pb/^{206}Pb$ ages between 3334-4068 Ma [Fig. 1(b)], which is broader than the range of zircon ages, probably because the U-Pb system in phosphates is easier to disturb under the high P-T conditions compared to that in zircon. Analyses with the younger $^{207}Pb/^{206}Pb$ ages are also significantly discordant. More concordant analyses show a narrower range of $^{207}Pb/^{206}Pb$ ages [Fig. 1(a, c)], and appear to form two groups. The weighted mean age for the first group is 3915.4 ± 5.2 Ma [Fig. 1(d)], which is consistent with the zircon results [1, 2, 3] and possibly represents Imbrium basin-forming event. An older age of 3940 ± 3.5 Ma is determined for the second group [Fig. 1(e)]. It is similar to ages obtained for apatites from different Apollo 14 impact melt breccias 3943 ± 5 Ma (14321,134), 3946 ± 15 Ma (14305,103), 3958 ± 19 Ma (14314,13), and might represent an impact event predating Imbrium basin formation [8, 9].

References: [1] Gnos E. et al. (2004). *Science* 305: 657–659. [2] Liu D. Y et al. (2012) *Earth and Planetary Science Letters* 319-320: 277–286. [3] Lin Y. T. (2012). *Geochimica et Cosmochimica Acta* 85: 19-40. [4] Williams I. S. (1998). *Rev Eco Geology* 7: 1–35. [5] Nemchin A. A. (2011). *Geochimica et Cosmochimica Acta* 75: 2940–2964. [6] Li Q. L. (2012). *Gondwana Research* 21: 745-756. [7] Woodhead J. D. and Hergt J. M. (2000). *Geostandards and Geoanalytical Research* 24: 33-38. [8] Merle R. E. (2014). *Meteoritics & Planetary Science* 49:Nr12 2241-2251. [9] Snape J. F. (2016). *Geochimica et Cosmochimica Acta* 174: 13-29.

PETROGENSIS OF HED METEORITES AND IMPLICATIONS
FOR MAGMATIC EVOLUTION OF PARENT BODY

H. Y. Chen[1,2] , B. K. Miao[1,2] and L.F.Xie[1,2] , [1]Guangxi Key Laboratory of Hidden Metallic Ore Deposits Exploration, Guilin; [2]College of Earth Sciences, Guilin University of Technology, Guilin, Guangxi, China, 541004. Email: chy@glut.edu.cn.

Introduction: The Howardite—Eucrite—Diogenite (HED) clan of meteorites are ultramafic and mafic igneous rocks, which is the largest quantity of magmatic meteorites available on the earth[1], providing an unmatched significance for studying the early magmatic evolution processes of the asteroids[2]. In this paper, nine different types of HED meteorites, including orthopyroxenite (NWA 7831 and Tatahouine), gabbro (NWA 11599 and NWA 11600), diabase (Tirhert), basalt (NWA 11602 and NWA 11603) and breccia (GRV 13001 and NWA 11598) were selected for systemic lithological observation and geochemistry analysis. Our studies are mainly concentrated on the structure and texture of rocks, major and trace elements geochemical characteristics in terms of whole rocks as well as minerals. Based on these new data, we have made some significant achievements regarding to the HED clan of meteorites petrogenesis, implication of magmatic evolution and thermal metamorphism.

Petrology and Mineralogical Chemistry: The HED meteorites are mainly composed by orthopyroxene, clinopyroxene, plagioclase, and minor quartz, spinel, iron, troilite, ilmenite and so on. These meteorites show a typical cumulated, gabbro, ophitic and basaltic texture from orthopyroxenite to basalt respectively. Generally, pyroxenes in orthopyroxenite are bronzite-hyersthene with generalized compositions of $Fs_{19.2\sim30.6}Wo_{1.43\sim5.00}$, while in cumulate gabbros mostly are hypersthenes with generalized compositions of $Fs_{34.1\sim37.9}Wo_{1.88\sim3.24}$ and minor augite—diopside exsolution lamella with generalized compositions of $Fs_{14.0\sim16.0}Wo_{41.3\sim46.5}$. The majority of pyroxenes in basalt are pigeonites with generalized compositions of $Fs_{44.1\sim65.3}Wo_{5.11\sim22.3}$, but slightly augite exsolution lamella with generalized compositions of $Fs_{26.1\sim47.7}Wo_{26.4\sim45.0}$ and ferro-hypersthenes with generalized compositions of $Fs_{57.8\sim62.9}Wo_{1.83\sim4.96}$. Mostly plagioclases found in the HED clan of meteorites are anorthites with generalized compositions of $An_{90.0\sim97.4}Ab_{2.20\sim9.73}$, and a small amount of bytownites and labradorites, with generalized composition of $An_{87.7\sim89.7}Ab_{10.0\sim11.3}$ and $_{An73.2\sim77.9}Ab_{20.8\sim24.4}$, respectively.

Result and Discuss: （1）The $Mg^{\#}$ value of pyroxene has been used extensively in identifying rock type and elucidating evolution process of magmas of HED family meteorites. Pyroxenes from orthopyroxenite, cumulate gabbro and basalts have distinctive $Mg^{\#}$ values. More specifically, the enstenite from the orthopyroxenite, cumulate gabbro and basalts have decreasing $Mg^{\#}$'s of 72.8, 63.5 and 36.6, respectively. Similarly, the clinopyroxene from these rocks yielded $Mg^{\#}$'s of 71.4, 73.9 and 44.7, respectively. （2）The whole—rock composition of the HED clan of meteorites indicates that the total amount of rare earth elements (REE), the ratio of LREE/HREE, the lithophile and incompatible trace elements are increasing from orthopyroxene through to cumulate gabbro and then to basalt. On the other hand, based on those pyroxene REE and incompatible trace elements results, we inferred that the accumulated pyroxenite and gabbro are the products of magma crystallization differentiation. In contrast, the fomation process of the basalt is much more complicated. Most of them are formed by the crystallization of residual magma[3], whilst a few of them derived from non-equilibrium crystallization of magma partial melting. （3）Crystallization sequence of the HED clan are accumulated pyroxenite, gabbro, diabase and basalt, which are characterized by homology and inheritance in magmatic evolution. These meteorites are formed from deep to shallow, corresponding to high temperature to low temperature as well as low thermal metamorphism to high thermal metamorphism. The thermal metamorphism of the superficial basalt can be caused by the heating of the multi-stage eruption of the basaltic magma[4].

References: [1] Chen H. Y. et al. (2016) Bulletin of Mineralogy, Petrology and Geochemistry 35:1037–1052. [2] Mittlefehldt D. W.(2015). Chemie der Erde Geochemistry, 75:155–183. [3]Warren P. H.(1997). Meteoritics & Planetary Science, 32: 945—963. [4]Yamaguchi, A. et al.(1996). Icarus, 124: 97–112.

KSAR EL GORAANE (H5): THE LATEST MOROCCAN METEORITE FALL ON 2018.

H. Chennaoui Aoudjehane[1], C. B. Agee[2], [1]GAIA Laboratory, Hassan II University of Casablanca, Faculty of Science Ain Chock, km 8 Route d'El Jadida 20150 Casablanca Morocco, (chennaoui.hasnaa@gmail.com), [2]Institute of Meteoritics, University of New Mexico, USA

Introduction: Morocco experienced since 2000 a large number of meteorite falls [1]. During 2018, at least two fireballs ending with a meteorite fall were reported. The first one was Gueltat Zemmour, which fell in the south of Morocco on August 21st[2, 3]. It is an L4 ordinary chondrite (presented at this meeting). The second one was witnessed on October 28th around 22:30 (GMT+1) in the east of Morocco very close to a small village called "Ksar El Goraane". Many people from this area and even from Erfoud (about 80 km in the South) saw the fireball. On the day after, the first pieces of the newly fallen meteorite were found by a Ksar El Goraane inhabitant. Many Moroccan meteorite hunters went to the site searching for more pieces. We received a 20 g piece from the "Moroccan Association of Meteorites" and 20 g from one of the finders of the meteorite for classification purposes.

Field mission report: On November 11th, we organized a field mission to the fall area to document it, by collecting the eyewitness testimonies, the coordinates of most found pieces, the direction of the fall, and the extent and orientation of the strewnfield. Many nomads living in this area (local nomadic tribe is called Ait Sgharouchent) and people from the southeast of Morocco reported a very bright light that was first yellow, then red, not very high in the sky. The light was comparable to brightness of sunlight entering nomad tents. The fall was coming from the east and headed west in the direction of Kaddoussa barrage. It was followed by 5 sonic booms, then a whistling sound that lasted 1 second, followed by a noise comparable to the unloading of a truck of rocks for about 5 seconds. The sound awakened sheep and scared people. On morning of October 29, the first piece weighting 185 g was found by a shepherd around 5 km east of Ksar El Goraane village, south of Jebel Tabouaroust lakbir and close to Jebel Tabouaroust Essghir, in Izanarzen plateau. Most middle size pieces were collected in this plateau, small ones were collected east of this area in Essnam plateau. A few days later, the largest piece collected so far (350 g) was found close to Kaddoussa barrage west of Ksar El Goraane village. This establishes the strewnfield as extending for about 15 km from ENE to WSW direction.

Physical description: We have seen complete pieces of 350 g, 32 g and 5 g totally covered by black matte to slightly shiny fusion crust; the 185 g piece was broken. Small pieces show primary and secondary fusion crust. Fusion crust is submillimeter in thickness. The interior of the meteorite is dark gray. Metal and sulfides are fine grained. Overall texture is fine-grained and homogeneous, no brecciation is visible. Small-sized (up to one mm) chondrules were visible. The rock is friable. Magnetic susceptibility measured in the field by SM30 was $\log\chi= 5.28$ to 5.42. Our estimation of the total known mass is around 2 kg.

Petrography and Geochemistry: Microprobe examination of a polished mount shows numerous porphyritic chondrules set in a recrystallized groundmass. Plagioclase grains are ubiquitous with sizes up to 25 microns in diameter. Abundant FeNi-metal and troilite observed throughout. Olivine composition is $Fa_{19.0\pm0.2}$ with a ratio Fe/Mn=38±2 ; low-Ca pyroxene composition is $Fs_{16.5\pm0.2}Wo_{1.4\pm0.3}$.

Classification and discussion: Based on the mineral compositions, chondrule forms and sizes, metal and sulfide size and distribution and magnetic susceptibility, the Ksar El Goraane meteorite is an ordinary chondrite of H5 class, with shock level S3, and no weathering present (W0). It is the 18th Moroccan official Moroccan meteorite fall and the 4th H5 fall occurring in Morocco after Tamdakht on 2008 [4], Izarzar on 2012 [3] and Tinejdad on 2014 [5]. In total, 175 H5 falls are known in all over the world.

References: [1] Chennaoui Aoudjehane H. (2016). *Meteoritics & Planetary Science* 51:S1 abstract 6119, [2] Chennaoui Aoudjehane H. et al. (2019). *Meteoritics & Planetary Science* 55, this meeting. [3] www.lpi.usra.edu/meteor/metbull.php. [4] Chennaoui Aoudjehane H. et al. (2009). *Meteoritics & Planetary Science* 44:S1 abstract 5038, [5] Chennaoui Aoudjehane H. et al. (2016). *Meteoritics & Planetary Science* 49:S1 abstract 5195.

GUELTAT ZEMMOUR: AN L4 ORDINARY CHONDRITE FALL IN MOROCCO ON AUGUST 2018.

H. Chennaoui Aoudjehane[1], M. D'Orazio[2], L. Folco[2], Å.V. Rosén[3], B. A. Hofmann[3] and V. Moggi Cecchi[4], [1]GAIA Laboratory, Hassan II University of Casablanca, Faculty of Science Ain Chock, km 8 Route d'El Jadida 20150 Casablanca Morocco, (chennaoui.hasnaa@gmail.com), [2]Scienze della Terra, Università di Pisa, Italy, [3] Natural History Museum Bern, Switzerland, [4]Museo di Storia Naturale – Sistema Museale di Ateneo, Università di Firenze, Italy

Introduction: On 21th of August 2018 around 14:20 (GMT+1), a fireball was seen by many people from the south of Moroccan Sahara. The fall occurred one day before the most important religious celebration for Muslim people "Aid Al Adha". The detection was immediately reported to Moroccan meteorite hunters. Because of the importance of this religious event, no one went to the fall area to search for a potential pieces of the meteorite on this time. A few days after the fall, the search began and first piece was found on the second week of September a few kilometers on the West of Gueltat Zemmour. It was the area where the report of the deflagration was the most important. We organized a field mission on 22th September to the fall site to document the fireball information, the fall coordinates and strewnfield and to collect samples. We got the support of the "Moroccan Association of Meteorites" on the field work as well as to get samples for the classification.

Field mission report: Gueltat Zemmour is a military campement, it is located in a desertic and extremely hot area. Close to this campement, many nomads are living. During summer time, mostly all nomads are moving to cooler places north of this area to feed their livestock. Only a few families were there around the time of the fall.

Eyewitnesses from different places, reported a fireball red then yellow-white colored and shining brighter than the sun during about three seconds. In the fall area, this fireball was very large comparable in size to a burning van. It was moving from the northeast to southwest during a few seconds. Nomads in the fall area heard a whistling sound almost identical to the ocean waves, then a strong sound similar to the explosion of a mine followed by a few (5) sonic booms that resonated in the entire Oueld Labiyad valley similar to the thunder and giving the feeling that the mountains will crumble. There was smoke in the sky directly above them.

A group of hunters found many small pieces (up to 15 g) in a valley between Wad Awzireft and Wad Labiyad and the North of Koudiat Rjilya. Larger pieces were found SW of this site. The direction of the fall was NNE-SSW and the strewnfield extends about 12 km in elongation.

Physical description: Very fresh and non weathered pieces where collected. In total, a few small pieces totalling around 500 g and 3 larger ones (5448 g, 1374 g and 426 g) have been reported so far. Large pieces are broken and show a grey coloured interior, they are partially covered by a fresh mat black fusion crust. Small pieces where complete and totally covered by a black matte fusion crust. The stones are very friable. Broken surfaces reveal a fine-grained texture with visible mm-sized chondrules.

Petrography and geochemistry: SEM observation of thick sections shows numerous well-defined chondrules (POP, PO, GPO, PP, RP and glassy chondrules) up to 3mm in diameter. Plagioclases are very small up to 2 μm in size. Mesostasis is microcrystalline. Most metal and sulphides are automorphous grains micron sized to large grains up to 500 microns, they occur inside chondrules as small grains, in the mesostasis as small and large grains and surrounding some chondrules. Magnetic susceptibility measured by SM30 give a $\log\chi$ of 4.95. EMPA analyses performed at the Firenze IGG-CNR laboratories allowed to determine this composition: olivine is $Fa_{25.95\pm0.69}$ with an Fe/Mn ratio of 51.23, orthopyroxene is $Fs_{20.69\pm0.81}Wo_{1.1\pm0.51}$ with an Fe/Mn ratio of 28.51and plagioclase is $An_{8.22\pm2.37}Or_{4.78\pm0.83}$. Taenite composition is $Ni_{50.27\pm2.73}$. Whole-rock trace-element concentrations by ICP-MS (μg/g): V 59, Cr 2799, Ni 10115, Co 399, La 0.329, Ce 0.879, Pr 0.138, Nd 0.645, Sm 0.211, Eu 0.088, Gd 0.284, Tb 0.054, Dy 0.364, Ho 0.081, Er 0.242, Tm 0.035, Yb 0.236, Lu 0.038.

Terrestrial age confirmation: cosmogenic radionuclides measurement by gamma-spectrometry at the GeMSE facility in October 2018 on a 21.74 g sample showed the presence of several short-lived cosmogenic radionuclides including ^{7}Be ($t_{1/2}$= 53 d) and ^{48}V ($t_{1/2}$= 16 d). Recalculated to August 21, 2018 the $^{22}Na/^{26}Al$ activity ratio is 1.7±0.1, which is consistent with a fresh fall. This measurement confirm the date of the fall reported by eyewitnesses.

Classification and discussion: According to its petrography, geochemistry, chondrules size and number and magnetic susceptibility, "Gueltat Zemmour" is an L4 ordinary chondrite, with a moderate shock intensity S2 and no weathering W0. The total known weight so far is about 8 kg. It is the second L4 fall in Morocco following "Sidi Ali Ou Azza" [1] and one of the 24 small group of L4 falls know in all over the word [2]. For its pristine state and relatively large mass Gueltat Zemmour provides an interesting material to work on this class of meteorites.

References: [1] Chennaoui Aoudjehane H. et al. (2016) *Meteoritics & Planetary Science* 51:S1 abstract 6120, [2] www.lpi.usra.edu/meteor/metbull.php

HETEROGENEOUS DISTRIBUTIONS OF SHOCK METAMORPHIC FEATURES IN EQUILIBRATED ORDINARY CHONDRITES

M. K. Cho and B.-G. Choi, Department of Science Education, Seoul National University, 08826, Korea. mkcho23@snu.ac.kr

Introduction: Chonrites experienced two different types of metamorphism since their formation into parent bodies; temperature-dominant thermal metamorphism [1] and pressure-dominant shock metamorphism [2, 3]. While thermal metamorphic features are more or less homogeneous (i.e., equilibrated) within a single chondrite, especially at that of high degree thermal metamorphism, shock features seem not. We have examined the distributions of shock features in (thermally) equilibrated ordinary chondrites.

Samples and Methods: We chose four H6 chondrites which experienced different degrees of shock metamorphism; Thiel Mountains 07004 (TIL 07004; H6, S2), Thiel Mountains 08008 (TIL 08008; H6, S3), Frontier Mountain 10018 (FRO 10018; H6, S4), Frontier Mountain 10035 (FRO 10035; H6, S5) (TIL 07004 and TIL 08008 are from SNU; FRO 10018 and FRO 10035 are from KOPRI). Shock effects in olivine, plagioclase and orthopyroxene were examined with polarizing microscopes. Scanning electron microscope equipped with energy dispersive X-ray spectroscopy was used for mineral identification, if necessary.

Results and Discussion: Since Stöffler et al. [2] and follow-up studies [3-7], degrees of shock metamorphism are divided into six shock stages, S1 (unshocked) to S6 (very strongly shocked) based on observations of shock effects in olivine, plagioclase and orthopyroxene produced by shock recovery experiments and also of those in natural meteoritic minerals. However, some of these schemes contain ambiguous expressions. For example, 'weak' and 'strong' mosaicism are used to distinguish S4 and S5 olivine grains [2] and 'occasionally', 'commonly' and 'typically' observed planar deformation features (PDFs) to distinguish S3, S4 and S5 olivine grains [4]. Thus, Schmitt & Stöffler [5] and Schmitt [6] suggest to use domain size to define weak mosaicism (~20μm) and strong mosaicism (~5μm). We suggest that degree of undulatory extinction can be used to distinguish olivine grains of S2 and S3 by measuring the range of extinction angle as method suggested by [8]. We found that the ranges of extinction angles are 2-30° at S2 and > 30° at S3. In previous studies, S2 and S3 of plagioclase and S3 and S4 of orthopyroxene were distinguished mostly using the presence or absence of irregular fractures [2, 3, 6]. However, since irregular fractures are found even plagioclase of S4 and orthopyroxene of S5, we do not recommend to use plagioclase to distinquish S2 and S3, similar pyroxene for S3 and S4.

Since shock features are heterogenous within chondrites, it was recommended to choose the highest shock stage shown by any significant fraction of grains (at least 25%) for shock level of a chondrite [2]. Using these slightly modified shock classification scheme, we examined 150-870 olivine grains, 50-90 plagioclase grains and 100-165 orthopyroxene grains from each thin section.

Our results of olivine agree with previous values in Meteoritcal Bulletin Database. All three minerals of TIL 07004 (S2) and FRO 10035 (S5) show the same results. However, minerals in FRO 1008 (S4) and TIL 08008 (S3) do not agree to each other in shock degree. For example, 55% of plagioclase in FRO 10018 indicate S5 (i.e., maskelynite). Orthopyroxene grains in TIL 08008 are mostly (82%) S2, and only 13% are S3 or higher. Our results quantitatively confirm the heterogenous distributions of shock features. We thus suggest that at least two minerals should be used for shock classification. In order to future examine the heterogeneous distribution of shock features, shock stages of adjacent mineral pair were compared. No obvious correlation was found indicating that even nearby minerals record different shock degree.

Conclusion: We reexamined shock criteria of olivine, plagioclase and orthopyroxene in four H6 chondrites. We found that the range of extinction angle can be used to distinguish olivine of S2 and S3. We suggest that irregular fracture can not be use to distinguish S2 and S3 of plagioclase and S3 and S4 of pyroxene. All four H6 chondrites we studied show highly heterogenous distributions of shock stages recorded in minerals. Shock metamorphic level need to be assigned by studying at least two kinds of minerals. The heterogeneity found even in nearby minerals.

References: [1] Huss et al. (2006) *Meteorites and the Early Solar System*, pp. 567-586 [2] Stöffler D. et al. (1991) *Geochim. Cosmochim. Acta* 55, 3845-3867. [3] Rubin A. E. et al. (1997) *Geochim. Cosmochim. Acta* 61, 847-858. [4] Stöffler D. et al. (1992) *Meteoritics* 27, 292-293 (abstr). [5] Schmitt R. T. and Stöffler D. (1995) *Meteoritics* 30, 574-575 (abstr). [6] Schmitt (2000) *Met. Planet. Sci.* 35, 545-560. [7] Fritz J. et al. (2017) *Met. Planet. Sci.* 52, 1216-1232. [8] DeHills S. M. and Corvalán J. (1964) *Geological Society of America Bulletin,* Vol. 75, 363-366.

# IN-SITU NOBLE GAS ANALYSIS OF MOUNT DEWITT 12007 LUNAR METEORITE.

J. Choi[1,2], K. Nagao[1], J. Park[3,4,5], J. M. Baek[1], J. I. Lee[1,2], D. S. Ebel[5,6], and M. K. Weisberg[3,5,6]. [1]Korea Polar Research Institute (KOPRI), Incheon 21990, Korea (jisu@kopri.re.kr), [2]University of Science and Technology (UST), Daejeon 34113, Korea, [3]Kingsborough Community College, Brooklyn, NY 11235, USA, [4]Deptment Chemistry and Chemical Biology, Rutgers University, Piscataway, NJ 08854, USA, [5]American Museum of Natural History (AMNH), New York, NY 10024, USA, [6]Deptment of Earth and Environmental Science, Graduate Center, City University New York, New York 10016, USA.

Introduction: Lunar meteorites were launched from the surface of the Moon, and provide information about formation of lunar crust. Mount DeWitt 12007 (DEW 12007) is a mingled regolithic breccia classified as a lunar meteorite [1,2]. DEW 12007 is composed of lunar crustal rocks of various origins, and it is suggested as a launch-paired meteorite with other mingled ones such as Yamato 793274 (Y 793274) and Queen Alexandra Range 94281 (QUE 94281) based on geochemical data [1]. It has complex cosmic-ray exposure history with a shielding depth of 340–360 g/cm^2 before its ejection from the Moon and the short transition time from the Moon to Earth [3]. As a result of short transition time, noble gases of DEW 12007 are largely related with its residence on surface of the Moon such as implantation of solar gases and cosmic-ray exposure. In this study, we report the results of noble gas analyses of various clasts and matrices observed on a thick section prepared from DEW 12007 by the laser heating method. The bulk sample was also measured by the furnace heating method.

Methods: Two kinds of samples were prepared for noble gas analyses; a bulk sample (0.213 mg in weight) without any distinguishable clasts, and a thick section. The thick section, 1mm thick, was prepared for in-situ noble gas analysis using a 1064 nm wavelength fiber laser. Both samples were preheated at 150 °C for 24 h to remove terrestrial gases in the noble gas extraction and purification line. Bulk sample was totally melted at 1800 °C for 30 min for noble gas extraction. On the other hand, 20 spots on either clasts or matrices of the thick section were melted by laser heating for gas extraction. In this laser analyses, the thick section of the sample was not penetrated by laser heating, due to the thickness of the sample. Weight of melted materials at the spots were calculated as ~6 μg based on observed dimensions of the laser-ablated area with assumed 200 μm depth of each laser pit and 3 g/cm^3 of density [1]. He, Ne, Ar, Kr, and Xe were measured with the modified-VG5400 noble gas mass spectrometer at KOPRI.

Results & Discussion: Bulk DEW 12007 contains high concentrations of solar gases, i.e., $^3He/^4He$ = (3.99 ± 0.07) × 10^{-4} with 1.6 × 10^{-4} ccSTP/g of ^4He, $^{20}Ne/^{22}Ne$ = 12.229 ± 0.016 with 1.8 × 10^{-4} ccSTP/g of ^{20}Ne, and $^{21}Ne/^{22}Ne$ = 0.0398 ± 0.0001. Results of Ne isotope ratios by laser analyses are distributed on mixing line between fractionated solar wind [4] and cosmogenic Ne as shown in the figure. High concentration of solar gases comparable with that of bulk sample was released only from the matrix part by the laser analyses. ($^{40}Ar/^{36}Ar_{trap}$) is calculated from bulk data and some laser data containing solar gases, and obtained value of 2.3 agrees well with 2.4 and 2.2 proposed for launch-paired meteorites, Y 793274 and QUE 94281, respectively [5,6]. Cosmogenic ^{21}Ne and ^{38}Ar concentrations are calculated by using bulk DEW 12007 data as end member of fractionated solar wind for trapped Ne and mixing lines from results of laser analyses with considering $(^{20}Ne/^{22}Ne)_c$ = 0.80, $(^{36}Ar/^{38}Ar)_c$ = 0.65, and $(^{36}Ar/^{38}Ar)_t$ = 5.32. $(^{21}Ne/^{22}Ne)_c$ = 0.85 was calculated from the mixing line. $(^{21}Ne/^{38}Ar)_c$ of plagioclase-rich clasts are lower than 1, while pyroxene-rich clasts have higher than 1, up to 24. In case of solar gas-poor and solar gas-rich matrices, the ratios are divided into two ranges of 0.1–0.4 and 1.2–3.5, respectively, while the bulk shows lower value of 0.6. The difference corresponds to different chemical composition of analysed phases, because main target elements to produce $^{21}Ne_c$ and $^{38}Ar_c$ are Mg and Ca, respectively. As the results obtained at present have large experimental uncertainties in determining melted mass by laser heating, we will present more quantitative studies of the complex exposure history of this meteorite on the lunar surface, at the meeting, by improving experimental settings.

References: [1] Collareta A. et al. (2016) *Meteoritics & Planetary Science* 51:351–371. [2] Ruzicka A. et al. (2017) *Meteoritics & Planetary Science* 52:1014. [3] Nishiizumi K. et al. (2016) *Annual Meteoritical Society Meeting* 79, Abstract #6514. [4] Grimberg A. et al. (2006) *Science* 314:1133–1135. [5] Eugster O. et al. (1992) *Proceedings of the NIPR Symposium on Antarctic Meteorites* 5:23–35. [6] Polnau E. and Eugster O. (1998) *Meteoritics & Planetary Science* 33:313–319.
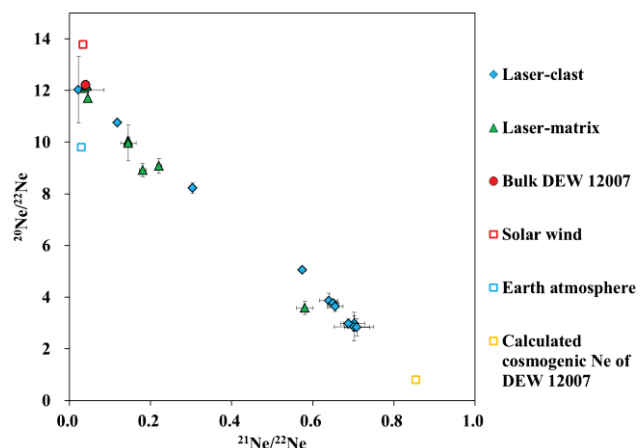
POST-IMPACT HABITABILITY AT THE CHICXULUB CRATER.

E.V. Christou[1,2*] and W. Bach[2], [1]University of Glasgow, School of Geographical and Earth Sciences, UK
[2]MARUM, Department of Geosciences, University of Bremen, Bremen, Germany
*(e.christou.1@research.gla.ac.uk)

Introduction: The origin of the primitive life in the Solar system is still unknown, but strong evidence points to a link with impact-induced hydrothermal environments [1]. This research assesses the habitability at the Chicxulub crater for the post-impact period of hydrothermal activity. Several results of numerical simulations and published research [2,3] record the evolution of the impact-induced hydrothermal system at Chicxulub for a period of more than 2Myr. This communication uses their thermodynamic constraints (temperature, pressure, water flux, enthalpy etc.) to construct geochemical reaction paths and to assess the catabolic energy availability for hydogenotrophy in the subsurface realm of the crater. Considering the upper temperature limit for life at 121°C [4], we investigate regions of the broader crater setting (radius=300 km) where habitable conditions could prevail (T < 121°C). [5] quantified the requirements for energetic habitability in various subsurface environments. [6] emphasized further in scenarios where H2 is the main energy source for supporting subterranean life. By comparing the hydrogen availability in Chicxulub with the energetic requirements of a putative hydrogenotrophic community, we finally assessed the post-impact habitability of the crater {Figure 1}.

Methodology - Modelling: [7] suggests that all ocean crust basement rocks release enough hydrogen to support hydrogenotrophic biomass, as the basaltic and ultramafic rocks interact with circulating seawater. Hydrogenotrophic communities have been inferred for oceanic basaltic and ultramafic crust [7,8,9], for granitic [10] and also for mixed mineralogy environments [11]. Hence, we adopted the same methodology and used the Geochemist's Workbench software [12] to simulate the geochemical reaction paths of the impactite dissolution and to compute the dihydrogen release after water-rock interactions in the crater. Finally, the correlation of the hydrogen availability with the energetic requirements of potential hydrogenotrophic communities at Chicxulub determines the habitability of the crater.

Results: The maximum release of H2 is observed at 30-38Kyr. As the hydrothermal cooling commences, only distant outer rim regions are within the habitable range. The hydrothermal system cools enough after 60 Kyr, so that it renders domains close to the peak ring and the central crater basin habitable. After 2 Myr, hydrogen availability in the setting fulfils, not only the survival and maintenance energetic requirements of the hydrogenotrophic biomass, but more significantly the microbial growth. Thus, we suggest the presented model to determine the catabolic energy availability and habitability of other terrestrial or extra-terrestrial impact-induced hydrothermal environments.
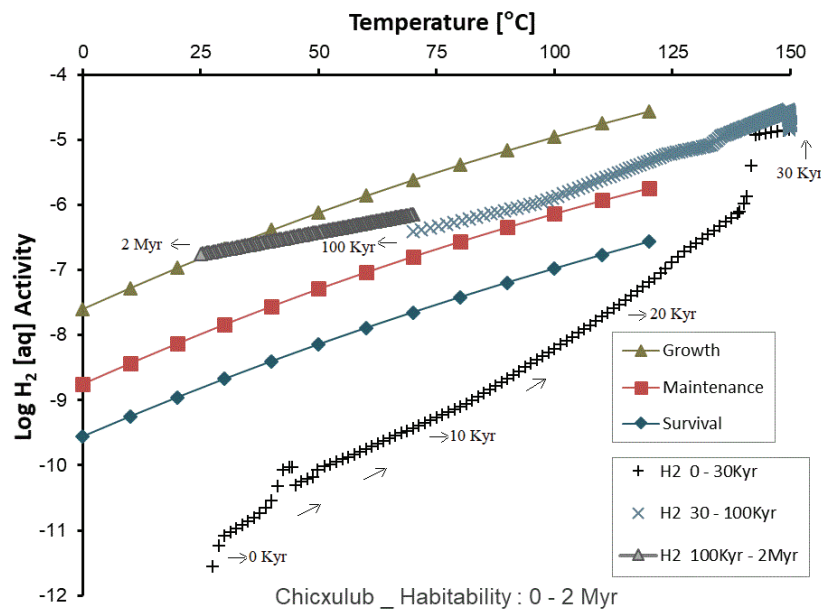
Figure 1. H2 release after impact-glass dissolution and thermal conditions at the Chicxulub Crater, plotted for comparison with the hydrogen demand (after [6]) of hydrogenotrophic microorganisms.

References: [1] Osinski G.R. et al. (2012) *Icarus* 224(2) pp. 347–363. [2] Abramov O. and Kring D.A. (2007) *Meteoritics & Planetary Science* 42: 93-112. [3] Christou E.V. (2018) *University of Bremen* MSc Thesis. [4] Kashefi K. and Lovley D.R. (2003) *Science* 301 (5635):934. [5] Hoehler T.M. et al. (2001) *FEMS Microbiology Ecology* 38(1) 33-41. [6] Hoehler T. M. (2004) *Geobiology* 2: 205-215. [7] Bach W. (2016) *Frontiers in Microbiology* 7:107. [8] Chapelle F.H. et al. (2002) *Nature* 415: 312–315. [9] Edwards K.J. et al. (2012) *Frontiers in Microbiology* 3(8):8. [10] Kotelnikova S. and Pedersen K. (1998) *FEMS Microbiology Ecology* 26: 121-134. [11] Lin L.H et al. (2005) *Geochemistry Geophysics Geosystems* 6(7). [12] Bethke C.M. (1996) *Oxford University Press New York* 397 pp.

UNUSUAL APATITE IN THE UNUSUAL MARTIAN METEORITE NORTHWEST AFRICA (NWA) 8159.

E.V. Christou[1*], L.J. Hallis[1], C.L. Hayward[2] and M.R. Lee[1]. [1]University of Glasgow, School of Geographical and Earth Sciences, Glasgow, UK [2]University of Edinburgh, School of Geosciences, Grant Institute, Edinburgh, UK *(e.christou.1@research.gla.ac.uk)

Introduction: The newly discovered martian meteorite Northwest Africa (NWA) 8159 is unique as it samples an era and lithology on Mars (early Amazonian) that is not represented elsewhere in meteorite collections [1-4]. We are investigating NWA 8159 apatite to define the parental melt and potential source region volatile composition, and compare this with those of other Martian meteorites.

Methodology: This study utilized one thin-section and one rock chip of NWA 8159. The mineralogy of these samples was characterized using the Carl Zeiss Sigma Variable Pressure Analytical SEM at the University of Glasgow. The University of Edinburgh Cameca SX100 electron microprobe, located at the Grant Institute (School of Geosciences), was subsequently used to determine the stoichiometric composition of NWA 8159 apatite grains.

Results: The NWA 8159 thin-section is cross-cut by calcite veins as a result of its terrestrial residence, and magnetite grains are at least partially altered to hematite and goethite [5,6]. Additional iddingsite-like alteration is present within the core of olivine grains, but this has been reported to be of potential martian origin [7]. Apatites are granular, anhedral and appear to contain a second Si-rich phase (darker in cathodoluminescence images: Figure A). The volatile content of NWA 8159 apatite is F-rich compared with apatite grains within other martian meteorites. The complicated history of this meteorite means that this unusual apatite texture and chemistry could be the result of sub-solidus reactions [8], martian aqueous alteration or terrestrial alteration.

Future Work: Detailed investigations of NWA 8159 apatite texture, chemistry and the nature of the Si-rich intergrown phase are planned, and will include transmission electron microscopy at the University of Glasgow, and atom probe tomography (Cameca Local Electrode Atom Probe (LEAP) 4000X) at the University of Sydney. As Martian mantle D/H ratios are lower than those of crustal fluids [9,10], SIMS D/H ratio analyses may also help us establish the nature of the event that formed the apatite.
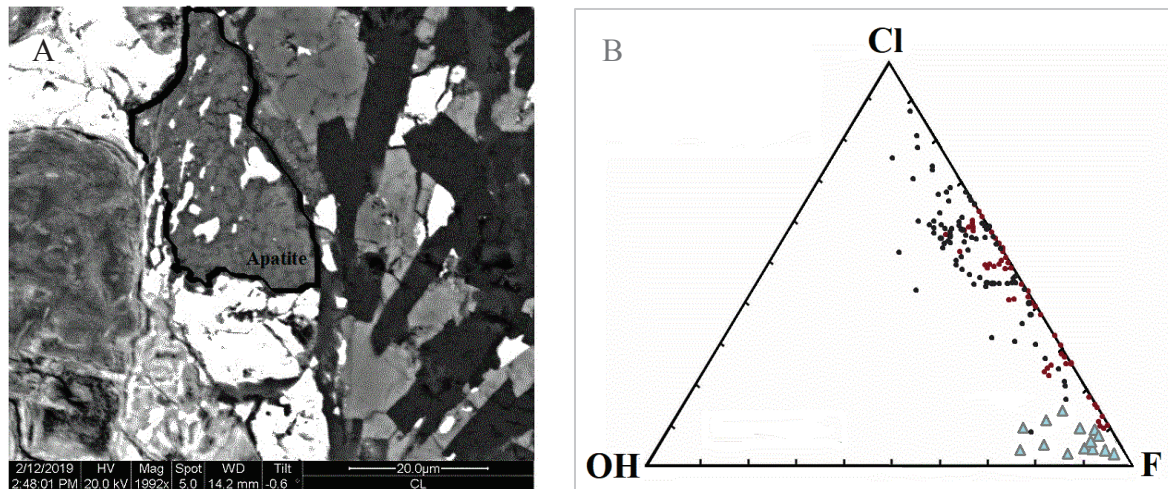
Figure: (A) Cathodoluminescence image for an apatite grain in NWA 8159; this grain has been selected for atom probe analysis. All apatites appear granular, anhedral and intergrown with a more Si-rich phase (darker grey). (B): Triplot diagram of Relative Volatile Abundance (RVA) for the apatites in NWA 8159 (light blue triangles) and comparison with plots (adapted from [11,12]) of apatite in chassignites (red dots) and nakhlites (dark grey dots).

References: [1] Herd C.D. et al. (2017) *Geochimica et Cosmochimica Acta* 218, 1–26. [2] Levy J. et al. (2010) *Icarus* 206, 229-252. [3] Ehlmann B.L. et al. (2011) *Nature* 479: 53-60. [4] Wray J.J. (2013) *International Journal of Astrobiology* 12, 25-38. [5] Lee M.R. et al. (2013) *Meteoritics and Planetary Science* 48(2):224. [6] Hallis L.J. et al. (2016) *79th Meteoritical Society meeting* Abstract #6442. [7] Vaci et al. (2016) *47th Lunar and Planetary Science Conference* Abstract #2538. [8] Shearer C.K. et al. (2015) *46th Lunar and Planetary Science Conference* Abstract #1483. [9] Usui T. et al. (2015) *Earth and Planetary Science Letters* 410, 140–151. [10] Hallis L.J. et al. (2012) *Geochimica et Cosmochimca Acta* 97, 105-119. [11] McCubbin F.M. et al. (2013) *Meteoritics & Planetary Science* 48(5):819–853. [12] Johnson M.C. et al. (1991) *Geochimica et Cosmochimica Acta* 55:349–366.

PHYSICAL PROPERTIES OF AN UNWEATHERED CO CHONDRITE FALL, MOSS.

F. Ciceri[1], L. Hanton[1], A. R. Hildebrand[1], [1]Department of Geoscience, University of Calgary, AB Canada T2N 1N4. fabio.ciceri@ucalgary.ca.

Introduction: Carbonaceous chondrite meteorites represent amongst the most primitive material of the Solar System. Understanding ther physical properties is needed to understand the evolution of the early Solar System and particularly the evolution of their parent bodies. For example, knowledge of physical and thermal properties of carbonaceous asteroids is required to quantify non-gravitational forces that perturb their orbits and rotation rates, and their response to impacts. Knowing the physical properties of carbonaceous meteorite lithologies is also helpful in designing spacecraft like OSIRIS-Rex, engineered to sample the surface of 101955 Bennu [e. g. 1].

Due to the rarity of samples of carbonaceous meteorites, just a few destructive measurements (such as strength) have been done compared to those for other types of meteorites. Our study consists of measuring physical properties of a CO meteorite, Moss, using both non-destructive and destructive methods. The Moss meteorite is a recent (and quickly recovered) fall (July 14, 2006) from Norway. Moss is a CO3.6 shock stage 2 that contains abundant small chondrules, olivine aggregates, troilite and kamacite in a gray matrix; it contains only 0.25% of carbon [2]. No previous destructive mechanical measurements have been done on a CO meteorite.

Methodology: Portions of an irregular interior Moss sample were cut into rectangular cuboid shapes using a diamond wire saw (Well, Model: 3032-4): to minimize sample contamination/modification all the cuts were done without the use of any fluid. A thin section billet was cut adjacent to the cuboids' volume. Cuboid dimensions were determined using a stainless steel digital micrometer. Porosity and grain density were measured using a gas (helium 99.9999%) pycnometer (Quantachrome Instruments, model: MVP-D160-E): The seismic waves velocity were measured using a pulse generator, oscilloscope (Tektronix Model DPO2014), two pairs of compressional and shear wave ultrasonic contact transducers (Olympus V133 and V156, respectively). Both the shear (Vs) and compressional wave velocities (Vp) were measured along three orthogonal directions. The compressive and shear strengths were measured with an electromechanical compression test machine (TestResource model 313 Q) using force transducer`s model SM-5000N-294 (TestResource).

Results: The mean bulk density and the grain density obtained for Moss are respectively 2.94 g/cm^3 and 3.71 g/cm^3. Moss has a porosity of 21.0 % ± 0.1 %. The Vp and Vs, mean values, are 2120 m/s and 1290 m/s respectvely: interestingly a seismic anisotropy exists in Moss that ranges, w.r.t. the average, from + 11.5% to – 9.8% in Vp, and from + 6.1 % to -5.8 % in Vs. This seismic anisotropy could be related to preferential orientation of some minerals or/and preferential orientation of the pores (still to be verified petrographically). We measured the compressive and shear strengths with the cuboids oriented along the fastest direction. The compressive strength ranged between 27.2 MPa and 27.8 MPa and the shear strength ranged between 8.3 MPa and 10.7MPa. The derived dynamic Young`s Modulus (E), Shear Modulus (μ), Bulk Modulus (K) and Poisson` ratio (υ) from the bulk density and the seismic velocities [3]; results are: υ = 0.21, E = 11.8 GPa, μ = 4.89 GPa and K = 6.72 GPa.

Discussion: The 31 MPa of tensile strength for Kainsaz (CO chondrite) reported by Svetsov et al. 1995, (only strength value ever reported for a CO chondrite) is significantly too high based upon our measurements of strengths: this likely reflects that the tensile strength for Kainsaz was derived from a theoretical model [4]. The porosity of the other CO falls range between 9.2 % (Lancé, fell 1872) and 34.2 % (Ornans, fell 1868) [5] with a mean of 19.6 %, very close to that observed for Moss. The Moss bulk density is within the range for the other CO falls, between 2.81 g/cm^3 (Felix, fell 1900) and 3.42 g/cm^3 (Ornans) [5] and Moss grain density is very close to the range of the other CO falls, from 3.50 g/cm^3 (Kainsaz, fell 1937) and 3.70 g/cm^3 (Warrenton, fell 1877) [5]. Moss`s bulk density excludes this CO lithology from composing asteroid Bennu since, as a macroporosity maximum limit (due to packing considerations) of ~50 % implies the lowest possible rubble-pile-asteroid density of ~ 1.46 g/cm^3 which is significantly higher than the Bennu density obtained by the OSIRIS-REx mission of 1.19 g/cm^3 ± 0.013 g/cm^3[1].

References: [1] Lauretta D. S. et al. (2019) *Nature 568,* 55-60. [2] Connolly H. C. et al. (2007) *Meteoritics & Planetary Science* 42, Nr 3, 413-466. [3] Ibrahim E.-M.I (2012) *M.Sc. Thesis, University of Calgary, Calgary, AB*. [4] Svetsov V. V. et al. (1995) *Icarus 116, 113-153*. [5] Macke R. J. (2010) *Ph D. Dissertation. Univeristy of Central Florida, Orlando, FL* (322 pp).

OSIRIS-REx SAMPLE SCIENCE AND THE GEOLOGY OF ACTIVE ASTEROID BENNU

H. C. Connolly Jr[1,2], E. R. Jawin[3], R. L. Ballouz[2], K. J. Walsh[4], T. J. McCoy[3], D. N. DellaGiustina[2], K. Burke[2], E. B. Biehaus[5], B. Rizk[2], C. d'Aubigny[2], V. E. Hamilton[4], W. F. Bottke[4], J. P. Dworkin[6], M. Delbo[7], S. Tachibana[8], H. Yurimoto[9], M. C. Nolan[2], D. S. Lauretta[2], and the OSIRIS-REx Team. [1]Dept. of Geology, Rowan University, Glassboro, NJ, USA (drhccjr@orex.lpl.arizona.edu), [2]Lunar and Planetary Laboratory, University of Arizona, Tucson, AZ, USA, [3]Smithsonian Institution National Museum of Natural History, Washington, DC, USA, [4]Southwest Research Institute, Boulder, CO, USA, [5]Lockheed Martin Space, Littleton, CO, USA, [6]NASA Goddard Space Flight Center, Greenbelt, MD, USA, [7]Observatoire de la Côte d'Azur, CNRS, Nice, France, [8]University of Tokyo, Tokyo, Japan, and [9]Hokkaido University, Sapporo, Japan.

Introduction: The OSIRIS-REx spacecraft went into orbit about (101955) Bennu on 31 December 2018 [1]. Data from the Approach, Orbital A, and Detailed Survey–Baseball Diamond mission phases have provided valuable insights into the geomorphological nature and the geological and dynamical processes that shaped the surface. Herein we report on the surface geology of Bennu with a goal of contextualizing the nature of the future returned sample.

The Surface Geology of Asteroid Bennu: Bennu has a top-like shape, i.e., spheroidal with an equatorial bulge [1-4]. The surface contains numerous candidate craters, many $\geq$ 50m in diameter. The larger craters are concentrated on or near the equator, suggesting that the ridge is an old feature of the asteroid, perhaps a relic of its original formation in the main belt due to catastrophic disruption [2,4].

The surface is littered with a diverse population of boulders [2,3] varying in normal albedo (suggestive of real compositional differences) and > 200 with an apparent diameter of over 10 m. Many boulders appear to be breccias, some of which may have or are being weathering *in situ* [2]. The boulders have interesting features: some have surface textures that are rough, similar to that of aa lava. Others appear to have textures with linear patterns that appear to be cleavage, perhaps thermally derived, and/or the product of an exfoliation process and many appear to be breccias [1-3]. Some areas on the surface have concentration of boulders, including several low-topography areas that are nearly completely covered. In a few regions, evidence of mass movement is observed, suggestive of a geologically active surface where boulder (and potentially finer regolith) movement is changing the site-specific surface expression. Fine-particulate regolith exists on Bennu [2,3], mostly between boulders or in small areas of ponding including small candidate impact craters ($\sim$ 5–20 m in diameter). However, the low abundance of regolith contrasts with the ground-based interpretation of the thermal inertia, which suggested a mean particle size of centimeters [3]. Albedo differences among boulders suggest compositional differences. Spectral data provide further insight into Bennu's composition: (1) a 2.74-μm absorption feature is suggestive of abundant hydrated phases; (2) $\sim$ 18- and 29.4-μm features indicate magnetite; and (3) the overall spectrum, visible through thermal infrared, is similar to that of CM chondrites [5].

Active Asteroid Bennu: After orbital insertion, visual observation using the OSIRIS-REx NavCam revealed that particles, centimeters to 10s of centimeters in diameter, were being ejected from Bennu [6]. To date, at least three major events and numerous minor events have been documented. These events appear to be restricted to particles, however, it may not be possible to detect of a major volatile component or very fine particles associated with the ejection events so caution is warranted on concluding cm-sized particles alone are being ejected. During the ejection events, some particles are completely lost from the Bennu environment, while others apparently re-impact, sometimes after a short-lived (few days) orbit around the asteroid. The exact cause of the particle ejection events is the focus of current research as is the exact geographical location of each event.

Implications for Sample Science: We do not yet know the discrete composition of boulders with different albedos, but, based on the current resolution of the observations, we suggest that the major component of Bennu is CM chondrite–like in bulk composition. Particle ejections events may be a newly recognized means of getting samples to Earth. Thus, we may have samples of Bennu in our collections and it is possible that they are, or are similar to, CM chondrites. Finally, the mission is in the process of selecting a primary and secondary site for sample collection wtih detailed geologic characterization of these sites starting in late summer 2019, details to be reported.

References: [1] Lauretta D. S. and DellaGiustina D. N. et al. (2019) *Nature* 568:55–60. [2] Walsh K. J. et al. (2019) *Nature Geoscience* 12:242–246. [3] DellaGiustina D. N. and Emery J. P. et al. (2019) *Nature Astronomy* 3:341–351. [4] Barnouin O. S. et al. (2019) *Nature Geoscience* 12:247–255. [5] Hamilton V. E. et al. (2019) *Nature Astronomy* 3:332–340. [6] Lauretta D. S. et al. (2019) *LPSC 50*, Abstract #2608.

EXOGENIC (?) CLASTS IN LL4 CHONDRITE MILLER RANGE (MIL) 15285.

C.M. Corrigan and T. J. McCoy, [1]Department of Mineral Sciences, National Musuem of Natural History, Smithsonian Institution, MRC-0119, 10th and Constitution NW, Washington, DC 20560-0119, USA. (corriganc@si.edu).

Introduction: While most chondrites contain one or more unusual chondrules or mineral fragments, these particles typically experienced a similar history of formation, accretion and metamorphism as other chondrules or fragments in the same meteorite.   An example of such a clast can be found in LL6 Miller Range (MIL) 07065, where a mm-sized, hemispheric barred spinel occurs in a chondrule which has experienced similar metamorphism and is of similar size as other chondrules in the same meteorite [1].   In contrast, a newly identified LL4 chondrite, MIL 15285, contains a number of chondrules and clasts that appear to have experienced a distinct history from the remainder of the meteorite, suggesting the possibility that these are exogenic in origin and that the meteorite may be a regolith breccia.

Host/Mineralogy: The LL4 chondrite host material is only modestly weathered and/or shocked. Two thin sections (,2 and ,3) were made of this meteorite and both were used in the classification. This meteorite contains a wide array of chondrule sizes, ranging from 0.2 to multiple mm in diameter. Chondrules are compound (with one unique barred olivine chondrule inside of a barred/porphyritic chondrule), barred olivine, porphyritic olivine, porphyritic olivine and pyroxene, and radial pyroxene. Matrix includes fragments/grains of olivine, pyroxene and feldspar. Some chondrules retain glassy mesostases. Generally, olivines range from Fa_{27-30} and pyroxenes are $Fs_{22-24}Wo_{0.5-2.0}$. Feldspars within the meteorite range from $An_{63-88}Or_{0.8-1.1}$ (see below).

Unique Clasts: Within this meteorite are found three notable particles.

Olivine Chondrule?: The first is a large (~3 mm diameter), polycrystalline olivine chondrule or grain, with a radiating texture that also includes embedded olivine grains. This olivine is generally the same composition as the rest of the host LL chondrite but with a slightly more variable composition (Fa_{25-30}).

Glassy Spherule: This 2 mm diameter glass sphere contains skeletal, cruciform dendrites of what appear to be chromite-rich spinel set in a microcrystalline mesostasis of Al-rich glass. The spinel only occupies a few percent of the entire spherule (Fig 1). The composition of this particle is not at all similar to the bulk chondrite. It may have been created through impact, but is an unusually high in CaO, TiO_2, Cr_2O_3, Al_2O_3, and Na_2O, and unusually low in FeO, SiO_2, and dramatically lower in MgO compared to bulk LL chondrites. Therefore, this clast is not likely a product of the bulk melting of the host chondrite.

Feldspar Grain: Most intriguing in the meteorite is what appears to be a single, large (2.4 x 3.5 mm) feldspar grain (Fig. 2) that is fractured and sheared, exhibiting multiple offsets. The composition of this grain is dominantly $An_{63}Or_{0.8}$ with two analyses at $An_{70}Or_{0.6}$. This composition is different than those seen in the chondrule feldspars ($An_{88-90}Or_{0.5-1.1}$). As with the glass spherule described above, the composition

of this clast is inconsistent with that of the host LL chondrite and is significantly more calcic. When compared to other types of meteorite feldspar, this grain is also more calcic than other equilibrated chondrites including ordinary and enstatite chondrites, but is within the broad range observed for equilibrated CK chondrites [2]. However, the large size of this grain is not generally observed in chondrites, suggesting a possible origin from a differentiated body. This grain is less calcic than lunar feldspars [3] or angrites [4]. The grain is less sodic than aubrites, brachinites and the GRA 06128/129 pair [4, 5]. The composition is similar to those observed in HED meteorites, although slightly more sodic [4], and is also within the range of Martian meteorites [6], although this grain is not maskelynitized, as is typically seen in Martian meteorites.
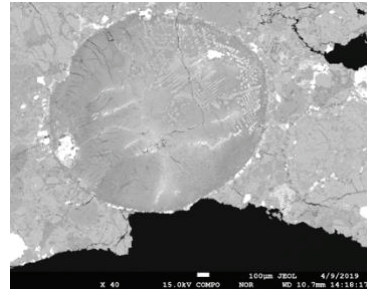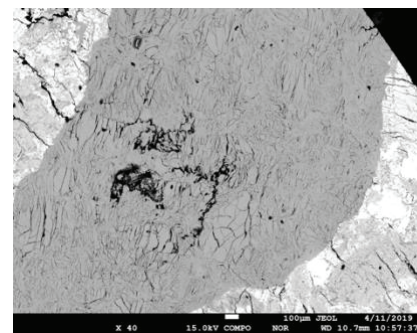
Future work: Additional studies of this meteorite could include measurement of solar wind implanted gases to test whether it is a regolith breccia, age dating of the feldspar grain, and oxygen isotopes of the grain to determine its parent body.

References: [1] Corrigan et al. (2016) *Meteoritics & Planetary Science* 51, #6479. [2] Brearley and Jones (1998) *Planetary Materials*, MSA 36, 3. [3] Papike et al. (1998) *Planetary Materials*, MSA 36, 5. [4] Mittlefehldt (1998) *Planetary Materials*, MSA 36, 4. [5] Day et al. (2012) *GCA* 81, 94-128. [6] McSween and Treiman (1998) *Planetary Materials*, MSA 36, 6.

MECA500 ROBOTIC ARM DEVELOPMENTS TOWARDS ASTROMATERIALS CURATION APPLICATIONS.

T. R. Cowden[1], C. J. Snead[1,2], J. H. Jang[2], Francis M. McCubbin[3] [1]JETS, NASA Johnson Space Center, Mailcode XI2, 2101 NASA Parkway, Houston TX 77058, [2]Texas State University, San Marcos, 601 University Dr, San Marcos, TX 78666, [3]NASA Johnson Space Center, Mailcode XI2, 2101 NASA Parkway, Houston, TX 77058, USA.

Introduction: As a part of the ongoing efforts to develop new curation tools and techniques for astromaterials [1] within the Astromaterials Acquisition and Curation office at NASA's Johnson Space Center, we are developing a variety of manually and electrically controlled micromanipulation systems. Most current techniques require manual manipulation, and in some cases the manipulation task is being done entirely freehand. The motorized systems available are restricted to three degrees of freedom and use proprietary control systems. For example, the MicroSupport AxisPro manipulation system currently used in microscale particle experiments is limited in its range of motion, as it can only move the manipulators in a three axis Cartesian range over a predetermined area above microscope slides. While having an efficient user interface, the control system is proprietary and prevents custom development and optimization to extend the viable applications of the system. In order to address some of these limitations, we have been testing robotic designs with multiple degrees of freedom and of a variety of designs. We are currently investigating the Meca500 robotic arm by Mecademic as a potential manipulation system to overcome some of these obstacles.

Meca500 Development: The Meca500 is a desktop-size industrial six-axis robotic arm with a range of motion reaching 260 mm, enabling it to reach further than currently implemented systems and making it suitable to a diversity of applications within micromanipulation and glovebox operations. Adding to the range of potential applications, the six-axes of motion allow for approaching points of interest from a variety of angles, which improves the effectiveness of tweezer operations. The manufacturer indicates that the system is capable of 5 μm of repeatability, but testing indicates it is capable of 1 μm increments of motion in the Cartesian motion format. While the Meca500 is proprietary, it connects using TCP/IP protocols and a standard Ethernet cable, and with the implementation of RoboDK, a software platform for controlling industrial robots, the control system can itself effectively be controlled through RoboDK, allowing for real time user operation of the arm. This opens up the Meca500 to external control and custom development, an avenue not currently available with the MicroSupport AxisPro. Using the Python programming language, several forms of control input (including a custom graphic user interface) are being developed. Currently an interface that allows click and drag commands from a mouse, as well as single Cartesian axis motion of user-determined size increments has been developed and is being investigated for use in curatorial facilities.

3D Printed Manipulators: Having demonstrated the accuracy of motion through real time control, a variety of end effectors for the robotic arm were developed. The first of these end effectors was a stylus mount, which allowed a pen to be held by the arm and controlled through our interface, allowing us to test the motion output of our controls as well as identify and correct a drift in the vertical axis when moving in the x-y plane. The next end effectors consisted of a few different sets of jaws that connected to a Schunk MEGP 25 miniature electrical parallel gripper. These sets of jaws allowed us to pick up 0.5-2 mm sized glass beads and, with some software modification, would allow us to determine and limit the force applied to gripping the object of interest. One of these jaws included a groove that could hold a pin vice. The pin vice held a glass rod that was then used to manipulate 10-30 um sized magnetite grains. As an intermediate component between the previous two designs, a set of mounts were designed to hold tweezers and operate them using the MEGP 25 gripper. However, the design of the MEGP 25 gripper does not allow for steps between entirely open and entirely closed, preventing efficient tweezer operation. Future developments on this approach will be continued, but with a different gripper design. The latest in manipulator prototypes is a mount to directly hold a pin vice allowing for more stability in manipulating small particles than the grooved jaw. All of these are first stage prototypes for designs that would be machined out of aluminum or steel to match materials requirements and limitations within curation laboratories.

Next Steps: While significant progress has been made towards a system that can be used for processing Astromaterials within curation laboratories, further development is necessary. For instance, not all of the materials used to construct the Meca500 are allowed in the labs; however, it should be possible to replace or isolate non-compliant components. In addition, we intend to refine and optimize end effector designs for the Meca500 using additive manufacturing techniques. Once a final design is determined, the parts can be machined or built using commercially available components or through machining in order to satisfy materials compliance requirements for curation labs.

References: [1] McCubbin F. M. and Zeigler R. A. (2017) *Hayabusa 2017 Symposium of the Solar System Materials*. [2] C. J. Snead et al. (2018) LPS XLVIII Abstract #2572

EVOLUTION OF PLATINUM-GROUP ELEMENT PHASES IN R CHONDRITES.

S. D. Crossley[1], R. D. Ash[1], J. M. Sunshine[1], C. M. Corrigan[2], T. J. McCoy[2], D. W. Mittlefehldt[3], [1]University of Maryland, Department of Geology, 8000 Regents Dr., College Park, MD 20740, USA (sdcross@umd.edu), [2]Smithsonian Institution, National Museum of Natural History, Department of Mineral Sciences, Washington, D.C., [3]NASA Johnson Space Center, Astromaterials Research Office, Houston, TX.

Introduction: Differentiation occurred on planetary bodies throughout the early Solar System. Most differentiated meteorites evolved from reducing geochemical environments [*e.g.*, 1], wherein the majority of Fe is held in FeNi metals. At the onset of differentiation, the first melts produced were dominated by the Fe-Ni system with a minor light element component that ultimately segregated from silicates to form metallic cores. The trace element abundances of these metallic melts and their residues have been used to interpret myriad processes involved in parent body petrogenesis [2]. However, processes of differentiation in more oxidized environments are not well-understood. Unusual highly siderophile element (HSE) distributions in sulfides of both brachinites and R chondrites may provide some insight into oxidized differentiation. Depletions in Ir and Pt relative to Os and Ru may be related to the presence of discrete platinum-group element (PGE) phases in R chondrites that fractionate from residual sulfides during partial melting [3], which may also apply to brachinite precursors. PGEs likely persist as discrete phases due to the lack of FeNi metal in primitive oxidized materials, but their evolution and behaviors during metamorphism prior to partial melting are not understood. To interpret the potential differentiation pathways of oxidized bodies and to model their formation, a basic understanding of HSE behavior at the onset of differentiation is required. We will present our preliminary findings on the evolution of PGE phases during thermal metamorphism of the R chondrite parent body.

Methods: PGE phases were identified via SEM/EDS. EDS element maps were constructed to determine modal mineralogy and mineral heterogeneity. Major element abundances of silicates, sulfides, and oxides were collected through EMPA for calculation of mineral closure temperatures. The petrologic grades of clasts in R chondrites were determined following methods in [4]. Trace element contents of R chondrite sulfides were measured via LA-ICP-MS.

Results: R chondrites in this study include a range of petrologic types. Northwest Africa (NWA) 11304 is a polymict breccia that includes petrologic types 3-4 (and possibly 5/6) based on heterogeneity of olivine and pyroxene FeO content. Higher petrologic grade clasts typically contain large (>100 µm) grains of pentlandite and pyrrhotite, while sulfides in unequilibrated clasts are typically smaller and more abundant in the matrix. NWA 753 is classified as R3.9 [5], consistent with our petrographic observations of chondrule textures and silicate heterogeneity.

In NWA 11304, PGE metals (*i.e.*, Os metal, Pt-Fe) populate type 3 clasts while discrete PGE phases in higher petrologic grades typically take the form of irarsite (IrAsS), platarsite (PtAsS), and semi-metal alloys such as niggliite (PtSn), which are usually adjacent to sulfides. PGE metals have been observed as inclusions within both silicates and sulfides, as well as within chondrules and matrix assemblages. A similar distribution of Pt metals and sulfarsenides was observed in NWA 753, but no Ir-bearing phases have been identified.

Discussion: The ubiquity of PGE phases throughout R chondrites is consistent with the conclusion that discrete PGE metals may have been the primary hosts of PGEs during high-T condensation from the nebula [6]. In reduced parent bodies, these elements presumably then diffused or reacted with FeNi metal in chondritic proportions during further nebular cooling. In oxidized R chondrites the majority of PGEs are held in sulfides. During formation of pentlandite and pyrrhotite, Pt likely experienced selective complexing with As and S, as observed in experimental work with As-bearing sulfide systems [7]. This likely accounts for ubiquitous Pt depletions in both pentlandite and pyrrhotite. Ir appears to have also formed similar complexes, but at higher temperatures, which is consistent with experimental results [7], and may account for irarsite observed within clasts of higher petrologic grade. This suggests that formation of discrete Ir-rich phases occurs during higher grade metamorphism than Pt-rich phases. Consequently, Ir and Pt depletions in brachinites may be explained by formation of sulfarsenides during metamorphism of precursors followed by removal of these phases with pentlandite from the residue during subsequent partial melting.

Future Work: We have collected major element data for olivine, pyroxene, oxides, and sulfides, and will determine mineral closure temperatures. These will be compared between clast types to assess the evolution of PGE phases in R chondrites through progressive metamorphism. Additional trace element data will also be collected for NWA 753 to assess the HSE content of pentlandite and pyrrhotite.

References: [1] Righter K. et al. 2016. *American Mineralogist* 101:1928-1942. [2] Day J.M. et al. 2016. *Reviews in Mineralogy and Geochemistry* 81:161-238. [3] Crossley S.D. et al. 2019. *LPS L*, Abstract #2018. [4] Dodd R.T. 1969. *Geochemica et Cosmochemica Acta* 33:161-205. [5] Grossman J.N. & Zipfel J. 2001. *Meteoritics and Planetary Science* 85:A293-A322. [6] Daly L. et al. 2017. *Geochemica et Cosmochemica Acta* 216:61-81. [7] Helmy H.M. & Bragagni A. 2017. *Geochemica et Cosmochemica Acta* 216:169-183.

OXYGEN ISOTOPIC COMPOSITIONS OF W-L RIM IN TWO CAIS FROM KAINSAZ CO3 CARBONACEOUS CHONDRITES

D. DAI[1], S. LIU[1,2] and H. BAO[1,2], [1]Institute of Geology, Hunan University of Science and Technology, ddqygf@163.com, [2]Institute of Geochemistry, Chinese Academy of Sciences, 1696012756@qq.com, 2430514218@qq.com.

Introduction: Ca-, Al-rich inclusions (CAIs) are the oldest known Solar System objects (4567.2 ± 0.6 Myr; 4567.30 ± 0.16 Myr)[1,2] that were formed in a short time interval. They are often surrounded by thin mono- or bimineralic rims known as Wark–Lovering (W-L) rims [3]. Unaltered W-L rims are composed of the same primary high temperature minerals as CAIs, such as melilite, spinel, pyroxene, hibonite, perovskite, anorthite and olivine. CAIs and their W-L rims offer a record of conditions during the earliest stages of Solar System formation in the inner regions of the solar accretion disk [4,5]. Therefore, textual, chemical and isotopic compositions of W-L rims can be used to probe nebular or parent body conditions at the time of their formation. CAIs are known to have large O isotopic anomalies with $\delta^{17,18}$O down to ~-50 permil relative to the SMOW value [6]. Previous oxygen isotope analyses revealed that rims also formed in an environment similar to that for the CAI main body. We report here the results of O isotopes in W-L rims of two CAIs from the Kainsaz (CO3) carbonaceous meteorites.

Samples and Experiments: Analyses were performed for an altered FTA (K2-9, 180 μm x 160 μm in size) and a CTA (K2-10, 300 μm x 250 μm in size) from the Kainsaz meteorites. The Cameca NanoSIMS 50L ion microprobe at the Key Laboratory of Earth and Planetary Physics, Institute of Geology and Geophysics, Chinese Academy of Sciences was used to measure the oxygen isotope ratios in the two CAIs. A focused Cs$^+$ primary beam of 16 keV, ~100 pA was defocused to produce a spot of about 1.5×2 μm. ^{16}O and ^{18}O were measured simultaneously using multi-collection Faraday Cup (FC) and ^{17}O was measured simultaneously using mono-collection electron multiplier (EM), respectively. The instrument was set to give a mass resolving power (MRP) ~6000 (Cameca NanoSIMS definition, based on the measured peak width containing 80% of the ion beam; see [7]) on the ^{17}O detector, sucient to resolve the ^{16}OH peak from that of ^{17}O (contribution of ^{16}OH typically ≤25 ppm). Oxygen isotope compositions are reported as per mil deviations from standard mean ocean water (SMOW) and as ^{16}O excesses relative to terrestrial samples(Δ^{17}O = δ^{17}O - 0.52 δ^{18}O). Under the analytical conditions employed, the internal (1σ) precision of individual oxygen isotope analyses is typically better than 0.5 ‰ for 0.5 ‰ for δ^{18}O and <1 ‰ for δ^{17}O.

Results and discussion: Inclusion K2-9 contains 15 vol% spinel, 10 vol% melilite, 4 vol% olivine, 5 vol% Ca–rich pyroxene, 1 vol% perovskite, and 65 vol% altered minerals in the core. K2-10 contains 15 vol% spinel, 60 vol% melilite, 2 vol% olivine + perovskite, 5 vol% Ca–rich pyroxene, and 18 vol% altered minerals. The W-L rims are ~30 μm (K2-9) and 20 μm (K2-10) thick, respectively, and composed of, from innermost to outermost, spinel, melilite + perovskite , Ca–rich pyroxene and olivine layer. The oxygen isotope measurements for the W-L rims of K2-9 and K2-10 CAIs plot within error of the Carbonaceous Chondrite Anhydrous Minerals (CCAM). This indicates that the inclusion has not been significantly affected by mass-dependent fractionation processes. The O isotopic compositions of minerals in W-L rim from K2-9 mostly fall into ^{16}O-rich cluster (δ^{18}O: -28.8~-41.7 ‰, δ^{17}O:-32.4~-41.7 ‰, Δ^{17}O: -19.6~-23.3 ‰), however, the O isotopic compositions of minerals in core from K2-9 are more ^{16}O-poor compositions (Δ^{17}O: -6.6~10.1 ‰). The O isotopic compositions of K2-10 are similar with K2-9, and the O isotopic compositions of W-L are richer than the core of that. High-precision O isotopic spot analyses in W-L rims of K2-9 and K2-10 CAIs show that the two CAIs and their W-L rims formed in an ^{16}O-rich gaseous reservoir, like the majority of CAIs in other chondrite groups. As described above, the two CAIs contain feldspathoids in the cores, which are typical alteration products and are common in CO carbonaceous chondrites [8,9]. The isotopically heterogeneous CAIs subsequently experienced oxygen-isotope exchange in an ^{16}O-poor nebular gas when CAIs altered.

References: [1] Amelin, Y. et al. 2002. *Science* 297: 1678-1683. [2] Connelly, J.N. et al. 2012. *Science* 338: 651-655. [3] Wark, D.A. and Lovering, J.F. 1977. *Proc. Lunar Sci. Conf.* 8: 95-112. [4] Bodénan, J.D. 2014. *Earth Planet. Sci. Lett.* 401: 327-336. [5] Dai D. et al., 2016. *Acta Petrologica Sinica* 32: 64-70. [6] Clayton R. N. et al. 1977. *Earth Planet. Sci. Lett.* 34: 209-224. [7] Hoppe, P. et al. 2013. *Geostand. Geoanal. Res.*37: 111-154. [8] Lin Y. et al. 2006. *Meteorit. Planet. Sci.* 41: 67-81. [9] Dai et al., 2015. *Earth, Moon and Planets* 115: 101-114.

ATOM PROBE TOMOGRAPHY IN PLANETARY SCIENCE.

L. Daly[1*], [1]School of Geographical and Earth Sciences, University of Glasgow, Glasgow, G12 8QQ, UK
(luke.daly@glasgow.ac.uk).

Introduction: Atom probe tomography (APT) is an atomic-scale technique that is capable of measuring the composition (major, minor, trace and isotopes) as well as nano-scale chemical variations and the position of atoms within a sample in 3 dimensions within small volumes (100x100x1000 nm) [1]. As such APT has the potential to be a powerful tool in geology and planetary science [2]. APT has been used in material science for over 52 years, however, the first application on an extraterrestrial sample wasn't until 1992 and even then, focused on the conductive FeNi metal [3]. It was not until the development of the laser assisted atom probe, where the ionization energy is provided by an ultraviolet laser [4] that non-conductive materials in meteorites such as silicates, oxides, sulphides and carbonates could be analysed. Here I will provide an overview of the APT technique, how it works, what type of information can be obtained, how samples are prepared and summarise the current planetary science applications.

Sample preparation: APT samples are extracted from meteorites using a focused ion beam (FIB) where a 10-20 μm long and 2 μm wide triangular prism is cut out of the sample using FIB [5]. After this lift out, 1 μm sections of the prism are then welded to a pre-prepared post using a gas injection system coupled with the ion beam. The sections are then further milled using an annular milling pattern to generate the needle shape until the apex of the tip is <100 nm in diameter with a half shank angle generally <10 ° [5]. Recently FIB lift out procedures have been developed to target interfaces and submicrometre particles such as the 'button method' [6], as well as new approaches to prepare the sample in situ to avoid extraction such as the Satellite dish method [7].

Current APT applications in planetary science: APT is being applied to a rapidly broadening number of extraterrestrial materials. Particular attention has been afforded to pre-solar grains, especially nanodiamonds in carbonaceous chondrites in the search for the carrier phase of the Xe-HL pre-solar signal [8-10]. APT is the only technique with the sensitivity to measure the carbon isotopic ratios of these nanodiamonds and if analytical instrument biases such as CH formation can be overcome could be used to measure the isotopic ratios of pre-solar grains *in situ* [11]. The capability of APT to measure isotope abundances is also important from a geochronological perspective. The U-Pb decay system has been successfully applied to nanostructures in zircon, baddeleyite and lunar meteorites to unpick their impact and metamorphic history [12-14]. In addition, a recent, robust approach has been developed to extract Re-Os isotope systematics by APT [15] and is being applied to calculate the formation age of refractory metal nuggets (RMN) in carbonaceous chondrites to determine whether some may have a pre-solar origin [16]. The ability of APT to measure trace elements has been used to detect Sulphur in RMN that suggest some were originally 'free-floating' in the disk and migrated large distances early in the solar systems history [17], as well as element redistribution in apatite in Lunar KREEP basalts caused by shock metamorphism [18]. This capability has also been used to measure Fe-nanoparticles and vesicles [18] and directly detect water [20] in space weathered surfaces throughout the Solar System. The 3D tomography of APT datasets has been used to reveal nanoscale phase separations on Mars [21, 22], Itokawa [23] and in chondritic carbonates [24] generated by shock and thermal metamorphism, as well as in iron meteorites to better constrain their magnetic properties [25]. Targeted lift outs have revealed cation migration in water-rock reaction surfaces in Martian meteorites with implications for how these reactions progress [26].

Summary: APT can provide a vast array of nanoscale information from spatial to isotope abundances at an atomic level. However, the true interpretive power of APT is revealed at the end of a correlative set of analyses across several length scales [e.g. 6, 25] from remote sensing, to hand sample, to thin section, to electron microscopy, to transmission electron microscopy, culminating in atom probe tomography.

References: [1] Kelly T.F., and Larson D.J., (2012) *Annual Review of Materials Research,* 42, 1-31. [2] Saxey D. W. (2018) *Scripta Materialia*, 148, 115-121 [3] Miller M.K., & Russel K.F. (1992) *Surface Science*, 266, 411-445. [4] Larson D. J., (2013) *Local Electrode atom probe tomography*. [5] Thompson K., et al., (2007) *Ultramicroscopy*, 107(2)131-139. [6] Rickard W., et al., (in review) *Ultramicroscopy*. [7] Halpin J.E., et al., (2019) *Ultramicroscopy*. [8] Isheim D., et al., (2013) *Microscopy and Microanalysis*, 19(S2), 974-975. [9] Heck P.R., et al., (2014) *Meteoritics & Planetary Science*, 49, 453-467. [10] Lewis J.B., et al., (2015) *Ultramicroscopy*, 159, 248-254. [11] Lewis J.B., et al., (2018) *Metsoc*, 6269. [12] Montalvo S. D., et al., (2019) *Chemical Geology*, 507, 58-95. [13] White L. D. et al., (2017) *Nature Communications*, 8, 15597. [14] White L. F., et al., (2019) *Geoscience Frontiers*. [15] Daly L., et al., (2018) *Geostandards and Geolanalytical Research*, 42(3) 279-299. [16] Daly L., et al., (2019) *LPSCL*, 1514. [17] Daly L., et al., (2017) *Geology*, 45(9), 847-850. [18] Černock, A., et al., (2019) *LPSCL*, 2228. [19] Greer J., et al., (2017) *Metsoc*, 6137. [20] Daly L., et al., (this meeting) *Metsoc*. [21] Daly L. et al., (2018) *Metsoc*, 6237. [22] White L. F., et al., (2018) *Contributions to Mineralogy and Petrology,* 173(10), 87. [23] Timms N. E., et al., (2018) *6th Symposium of Solar System Materials*. [24] Daly L., et al., (2018) *Metsoc,* 6239. [25] Einsle J. F. et al., (2018) *Proceedings of the National academy of Sciences*, 115(49), E11436-E11445. [26] Daly L., et al., (2019) *LPSCL*, 1521.

SOLAR WIND HYDRATION OF ITOKAWA OLIVINE

L. Daly[1,2,*], M. R. Lee[1], L. J. Hallis[1], D. W. Saxey[2], D. Fougerouse[2], W. D. A. Rickard[2], N. E. Timms[2], F. Jourdan[2], S. M. Reddy[2], T. Salge[3], H. A. Ishii[4], J. P. Bradley[4], M. Z. Quadir[2], M. A. Cox[2], P. A. Bland[2], J. Aguiar[5], K. Hattar[6], A. Monterrosa[6], L. P. Keller[7], R. Christoffersen[7] and M. S. Thompson[8]. [1]School of Geographical and Earth Sciences, University of Glasgow, Glasgow, G12 8QQ, UK (luke.daly@glasgow.ac.uk), [2]Space Science and Technology Centre, School of Earth and Planetary Sciences, Curtin University, GPO Box U1987, Perth, WA 6845, Australia, [3]Imaging and Analysis Centre, Natural History Museum, London, SW7 5BD, UK. [4]Hawaii Institute of Geophysics and Planetology, University of Hawai'i at Mānoa, Honolulu, HI, 96822. [5]Idaho National Lab, Idaho Falls, ID, 83402 USA. [6]Sandia National Laboratories, PO Box 5800, Albuquerque, NM, 87185, USA, [7]Astromaterials Research and Exploration Science, NASA Johnson Space Centre, Houston, TX 77058, USA, [8]Department of Earth, Atmospheric, and Planetary Sciences, Purdue University, West Lafayette, IN 47907, USA.

Introduction: Space weathering affects surfaces exposed to the vacuum of space and results from the combination of solar wind irradiation, ultraviolet radiation, micrometeorite impacts and galactic cosmic rays [1]. Spectrometry shows that irradiation of silicate minerals by H ions from the solar wind can produce water [2], and Fe nanoparticles in 20-40 nm amorphous, vesiculated rims [1, 3]. However, direct mass-charge measurement of the concentration and distribution of OH or H_2O has not been undertaken. We present the first detection of OH and H_2O ions in space-weathered particles by atom probe tomography (APT) analysis of Itokawa grains from *JAXA's* Hayabusa mission [3].

Methods: Itokawa particle RA-QD02_0279 was mounted on a rod. The grain's surface was characterised by scanning electron microscopy (SEM) imaging, then sputter coated with a 200 nm thick layer of Cr for protection. An electron transparent lamella was extracted for transmission electron microscopy (TEM) imaging using a focused ion beam (FIB)-SEM instrument at Curtin University (CU). Two areas of the grain's surface were characterized with a FIB-time of flight secondary ion mass spectrometer (FIB-TOF-SIMS) at CU collecting positive and negative ions datasets. Finally, two sets needle-like specimens with 100 nm diameter tips were extracted for APT from the 'front' and 'back' sides of the grain at CU. To calibrate the Itokawa asteroid results, we also measured a San Carlos olivine (SCO) (n-SCO), a He^+ irradiated SCO (He-SCO) and a D^+ irradiated SCO (D-SCO) using the same approach.

Results and discussion: SEM imaging of Itokawa particle RA-QD02_0279 showed it is free of micrometeorite impact craters, suggesting that it has experienced a minimal duration of space weathering. This conclusion is corroborated by TEM results showing that it has a 40 nm thick space weathered rim characterized by slight density variations; Fe nanoparticles are absent (Fig. 1B). The beam sensitivity of the space weathered rim suggests it may be volatile rich. FIB-TOF-SIMS data from this grain indicate that the rim is rich in ^{16}O (Fig. 1A), ^{14}N and ^{12}C which is consistent with the isotopic composition of the solar wind e.g. [4]. APT results revealed density variations consistent with the TEM observations as well enrichment of H within the outermost 40 nm of the rim. This H enrichment is predominantly detected as OH^+ and H_2O^+ ions 1-3 at. % above normal background (Fig. 1C). APT analysis of the n-SCO and He-SCO reference materials indicate that H enrichment is not a property of olivine grain surfaces or the irradiation process, as they did not have a comparable profile of enrichment in OH or H_2O. The outermost part of the D-SCO sample was enriched in D_2, DO, and D_2O; importantly, no comparable enrichment in OH or H_2O was observed. These results demonstrate that solar wind hydrogen irradiation of olivine grain surfaces does indeed produce water, and space weathered rims retain at least part of their volatile abundances and isotopic signature over curatorial timescales.

The amount of water that can be implanted into mineral surfaces by solar wind irradiation is significant, particularly for grain sizes <10 μm where solar wind derived water could represent between 0.1-4 at. %. As such, fine-grained space weathered particles could represent a significant reservoir of isotopically light water in the Solar System.
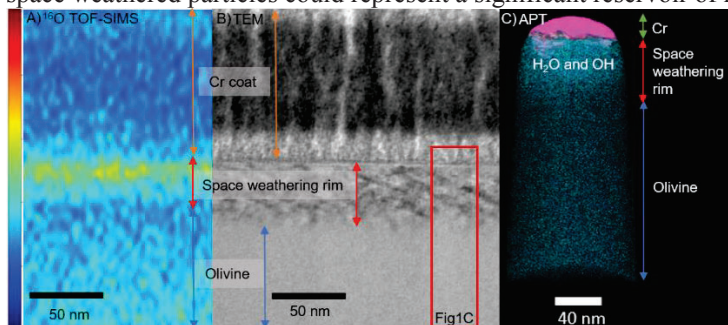
Figure 1: Space-weathering analysis of Itokawa particle RA-QD02_0279 A) TOF-SIMS depth profile data showing ^{16}O enrichment (yellows and reds) of the space weathering rim. B) TEM image of the space-weathering induced damage layer. C) APT dataset showing a direct detection of water enrichment in the space-weathered rim. Pink dots are Cr atoms and blue dots are H_2O and OH atoms.

References: [1] Chapman C.R., (2004) *Annual Review of Earth & Planetary Science*, 32, 539-567. [2] Bradley J.P., et al., (2014), *Proceedings of the National Academy of Science*, 111, 5, 1732-1735. [3] Noguchi T., et al., (2011) *Science*, 333, 6046, 1121-1125. [4] Marty B., et al., (2016) *Earth & Planetary Science Letters*, 441, 91-102.

COMBINING FOCUSED ION BEAM AND SYNCHROTRON TOMOGRAPHY TO IDENTIFY FLUID PATHWAYS IN HEATED CM CHONDRITES WITH IMPLICATIONS FOR RYUGU AND BENNU

L. Daly[1], M. R. Lee[1], A. Macente[1,2], J. Halpin[3], S. McFadzean[3], W. Smith[3], J. E. Einsle[4,5], M. R. Ball[5], A. Miyake[6], J. Matsuno[6], M. Matsumoto[6], A. Tsuchiyama[6]. [1]School of Geographical and Earth Sciences, University of Glasgow, G12 8QQ, UK (luke.daly@glasgow.ac.uk), [2]Civil and Environmental Engineering, University of Strathclyde, Glasgow, G1 1ZQ, UK, [3]Materials and Condensed Matter Physics, School of Physics and Astronomy, University of Glasgow, Glasgow, G12 8QQ, UK, [4]Royal School of Mines, Imperial College London, London, SW7 2AZ, UK, [5]Department of Earth Sciences, Cambridge University, Cambridge, UK, [6]Division of Earth and Planetary Sciences, Graduate School of Science, Kyoto University, Kyoto, 606-8501 Japan.

Introduction: CM chondrites are among the most chemically primitive meteorites in our collections and also the most aqueously altered [1, 2]. Analysis of CM chondrite porosity and permeability using transmission electron microscopy (TEM) indicates that the permeability of these meteorites is very low and would only permit fluid flow across length scales of <100 μm over the duration of aqueous alteration [3]. However, a subset of CM chondrites have been thermally metamorphosed [e.g. 4] and they are currently some of the best analogues for material on the surfaces of the asteroids Bennu and Ryugu, which are currently being sampled by OSIRIS-Rex and Hayabusa2 respectively [5, 6]. The driver of this metamorphism is unknown, but solar radiation, impact and radiogenic heating have all been suggested [7]. During heating CMs have lost a proportion of their volatiles, including water, and this process requires transport over the order of meters to kilometers, at odds with the low permeability calculated by TEM [4]. However, TEM samples are generally limited to $20\times10\times0.1$ μm volumes and as such larger scale features may be missed. The development of plasma focused ion beam (P-FIB) technology now enables extraction of much larger sample volumes (e.g. $100\times100\times100$ μm) in reasonable time frames (2-3 hours). These large samples can then be characterized in 3D, either using FIB tomography combined with 3D energy dispersive X-ray spectroscopy (EDS) and/or synchrotron tomography, to identify features that may not be present in a typical TEM sample.

Method: We extracted two quadrilateral shaped $60\times60\times40$ μm samples of the heated CM Elephant Moraine (EET) 96029 across the boundary between a fine-grained rim (FGR) and the matrix using the P-FIB at the University of Glasgow. The internal structures of these samples were studied by X-ray tomography at the Spring8 synchrotron in Japan, and by FIB tomography. EDS maps were collected at the middle and end of the FIB-tomography analysis. The 3D porosity was calculated from both datasets using Avizo®.

Results: Both P-FIB and synchrotron tomography results show that the matrix and FGR porosity is similar to previous published values [3]. However, the FGR-matrix interface is characterized by 5-33 μm wide fractures (Fig. 1). The high permeability of these fractures would permit fluid flow over the order of meters [8]. The synchrotron data reveal that some of these fractures have been infilled (Fig. 1A; yellow), while EDS data collected during the P-FIB tomography indicate that the fractures are decorated with soluble elements such as S, and Ca (Fig. 1C). These observations suggest that fluids once flowed along these fracture surfaces and as such could facilitate volatile loss.

Implications for Bennu and Ryugu: Our data indicate that volatile loss from CM chondrites is possible through a network of fractures at the matrix-FGR interface. In addition, complete 3D characterization of large sample volumes can be undertaken through a work flow of P-FIB extraction followed by synchrotron and FIB tomography.
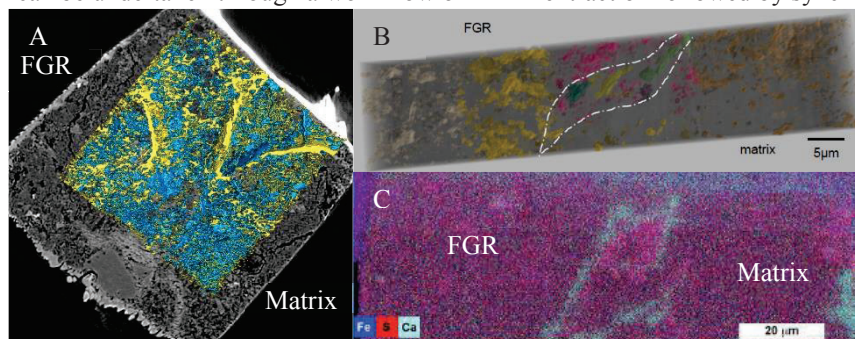
Figure 1. Porosity analysis data from the Sprin8 beamline (A) and FIB tomography (B) revealing large interconnected fractures across the interface between the matrix and FGR of EET 96029. (C) EDS imaging half way through the FIB tomography analysis revealing that the FGR-matrix interface is decorated with Ca and S.

References: [1] Brearley A.J., (2003) *Treatise in Geochemistry* 1, Ed: Davies A.M. [2] Maiorca E., et al., 2014) *Astrophysical Journal,* 788, 149. [3] Bland P.A., et al., (2009) *Earth and Planetary Science Letters*, 287, 3-4, 559-568. [4] Lee M.R., et al., (2016) *Geochimica et Cosmochimica Acta,* 187, 237-259. [5] Perna D., et al., (2017), *Astronomy and Astrophysics,* 599, L1. [6] Clark B.E., (2011) *Icarus,* 216(2), 462-475. [7] Akai J., (1988) *Gechimica et Cosmochimica Acta,* 74, 1593-1599. [8] Nelson R.A., (2001) *Geologic analysis of naturally fractured reservoirs,* Elsevier.

EXPERIMENTAL MODELLING OF THE THERMAL EFFECT ON CHELYABINSK METEORITE.

I. A. Danilenko[1,2], E. V. Petrova[1], G. A. Yakovlev[1], and V. I. Grokhovsky[1], [1]Ural Fededral University (620002 Mira str., 19/5, Ekaterinburg, Russia, e-mail: evgeniya.petrova@urfu.ru), [2] Institute of Geology and Geochemistry, Ural Branch of RAS (620016 Vontsovskogo str., 15, Ekaterinburg, Russia)

Introduction: Ordinary chondrites material was affected by various pressures and temperatures during the formation and evolution. Their texture was formed at several processes: accretion from the nebula, thermal metamorphism at the meteorite parent body and, in most cases, shock events. Thermal influence made a significant contribution to the metamorphism of a primitive substance. In the present study, the heating experiments were performed to reproduce the thermal metamorphism. The Chelyabinsk LL5 meteorite material of the light-colored lithology was chosen for the study because it was carefully studied previously [1-3] and Chelyabinsk has the dark-colored lithology, which could be compared with experimental results. Here the thermal effect on the meteoritic texture and composition was analyzed in comparison to the known impact applied.

Samples and Methods: Chelyabinsk LL5 ordinary chondrite samples were cut from the one fragment of the light-colored lithology as the cubes ~1x1x1 cm using water-cooled Buehler IsoMet saw with subsequent drying. Polished sections were prepared using Buehler Beta Grinder-Polisher. The identification of the structural features of the studied fragments was performed using the Carl Zeiss Axiovert 40 MAT optical inverted microscope with AxioVision image recording, as well as an FE-SEM ∑IGMA VP electronic microscope. Heating experiments were carried out using a vacuum electric furnace SNVE-9/18 at a pressure of 10^{-2} Pa. Samples of the bright lithology of the Chelyabinsk LL5 meteorite were subjected to thermal effects up to temperatures of 700, 900, 1100, 1300 and 1500°C.

Results and Discussion: The initial structure of the Chelyabinsk LL5 meteorite samples with light lithology is represented by the chondrite structure, which is composed of groups of silicate minerals of olivine (Fe, Mg) $_2SiO_4$, pyroxene (Fe, Mg) SiO_3, and plagioclase. The silicate matrix contains mainly individual grains of the metal Fe (Ni, Co), troilite FeS and their intergrowing. After the heating up to the 700°C the shape of the metal and troilite grains was sharp, it has not changed, while the metal grains became polycrystalline. The troilite grains and intergrowing of metal and troilite were changed at the samples heated to the 900°C. Moreover, the traces of the grain boundaries migration was observed at the metal structure. Micrograins of troilite at the impact veins were transformed into the small veins and caused spot silicates darkening.

The fragment of the meteorite Chelyabinsk LL5, which was initially of light-colored lithology, got an external similarity with the dark-colored lithology after the heat exposure up to the 1100°C. From the visual inspection of a sample heated to a temperature of 1300°C shows that this sample has acquired an external similarity with the impact melt lithology of the Chelyabinsk LL5 meteorite.

The study of the microstructure of the sample of light lithology after thermal exposure (1100°C, 1300°C) revealed the melting of the metal Fe (Ni, Co) and troilite FeS phases, followed by crystallization upon the surface of the sample. It was noted at the plane of the polished section. For the sample heated up to the 1300°C, a partial changing of the sample shape was observed. While heating to a temperature of 1500°C caused massive melting of the sample, even the fragment completely lost its shape. The study of the sample topology using secondary electron imaging revealed the melt flow and its slow crystallization with the large fragile parallel crystals growth. It should be noted, that the texture of the sample transformed from temperature experiments is different in comparison with the texture of the lithology of the impact melt. It concerns both its external characteristics (color) and the shape and the size of the crystals in the structure.

Conclusions: As a result of the heating experiments with the substance of light-colored lithology of ordinary chondrite Chelyabinsk LL5, it is shown that the structure of the substance was transformed differently depending on the temperatures experienced. The experimentally heated fragments of light-colored lithology have both similarities and differences with the samples of dark-colored lithology and the impact melt of the Chelyabinsk LL5 meteorite, which have been heated under natural conditions during a shock event in space. It was shown that the formation of lithologies was influenced not only by the temperature effect but also by the impact transformation, as it was studied in [Petrova et al., 2018]. The structures obtained after the heating experiments have not found yet among the studied samples of the Chelyabinsk meteoritic shower.

References: [1] Galimov E.M. et al. (2013) *Geochemistry International* 51:522-539. [2] Kohout T. et al. (2014) *Icarus* 228:78-85. [3] Badyukov D.D. et al. (2015) *Petrology* 23(2):103-115. [4] Petrova et al. (2018) *Meteorit. & Planet. Sci.* 53:A245.

WHY IS THE MOON DEPLETED IN MODERATELY VOLATILE ELEMENTS?

N. Dauphas[1] and N. X. Nie[2],
[1]Origins Laboratory, Department of the Geophysical Sciences and Enrico Fermi Institute, The University of Chicago, Chicago IL 60637 (dauphas@uchicago.edu).

Compared to chondrites, which all have somewhat similar K/U ratios (between ~0.3×CI in CV and 1.4×CI in EH), planets and differentiated meteorites are variably depleted in K, reaching a factor of ~500 lower than CI in the angrite parent-body [1-3]. Closer to us, lunar rocks are depleted in K and Rb by a factor of ~6 relative to terrestrial rocks [3]. The origin for this depletion is poorly constrained. It is unlikely to have been inherited from a volatile element depleted impactor. The reason is that it would require Theia to have contributed at least ~83% of the mass of the Moon if Theia was as potassium-depleted as the angrite parent-body but even then, it would fall short of explaining the greater depletion measured for Zn [4]. Most likely, this depletion reflects processes that occurred during or after the Moon-forming giant impact. Wang and Jacobsen [5] showed that the Moon was enriched in the heavy isotopes of K by ~+0.4 ‰ compared to Earth. Pringle and Moynier [6] also found hints of a heavy Rb isotope enrichment in lunar rocks relative to terrestrial rocks but the extent of this enrichment was uncertain. Recently, we have revisited this question by measuring the Rb isotopic composition of several lunar rocks to more precisely define the Rb isotopic composition of the Moon [7]. Wang and Jacobsen [5] interpreted the heavy K isotopic composition of the Moon to reflect evaporative loss of K under equilibrium conditions. *Ab initio* studies have shown, however, that the equilibrium K isotopic fractionation between monoatomic K vapor and condensate (K-feldspar, taken as a proxy for liquid) under temperature conditions relevant to lunar formation would be too small to account for the heavy K isotopic composition of the Moon [8,9].

We have re-evaluated the extent to which K and Rb are depleted in the Moon. While it is commonly assumed that K/U and K/Rb ratios are relatively unfractionated during magmatic differentiation, we have found that mare basalts and KREEP-rich samples display variations in those ratios that correlate with ratios of incompatible non-volatile elements. These variations must therefore reflect processes of magmatic differentiation most likely associated with crystallization of the lunar magma ocean [3]. Our reassessment of the degree of K and Rb depletions in the Moon [3], together with our determination of the Rb isotopic composition of the Moon [7] allow us to reassess the cause of depletion in moderately volatile elements of lunar rocks relative to Earth. The models put forward to explain those depletions involve (1) transport in the protolunar disk of condensed material across the Roche limit when most volatile elements remain behind in the inner disk [10], (2) partial condensation in a Synestia structure produced by a high-energy impact between the protoEarth and Theia [11], (3) drainage of vapor onto the Earth when the liquid remains in a disk orbiting the Earth [12], and (4) loss by evaporation from the lunar magma ocean. The scenarios that involve partial condensation cannot explain the heavy isotope enrichments because equilibrium isotopic fractionation is too small and kinetic isotope effects would produce condensates enriched in the light isotopes, which is opposite to what is observed [9]. It is also not clear whether a magma ocean could have led to sufficient loss of K and Rb, at least not if volatile escape operated under Jeans' regime [13].

At the meeting, we will evaluate these scenarios and show that the heavy K and Rb isotopic compositions of lunar rocks can provide new and critical constraints on the setting of lunar formation, specifically with regard to evaporative loss in the aftermath of the Moon-forming impact. We will show that the heavy isotope enrichments of K, Rb, and possibly Zn can all be quantitatively explained in the context of a single scenario.

References: [1] Halliday A. and Porcelli D. J. (2001) *EPSL* 192:545-559. [2] Davis A. M. 2006. In Meteorites and the early solar system II, 295-307. [3] Dauphas N. (2019) *LPSC* 50, #1466. [4] Albarède F. et al. (2015) *Icarus* 50: 568-577. [5] Wang K. and Jacobsen S. B. (2016) *Nature* 538: 487-490. [6] Pringle E. A. and Moynier F. (2017) *EPSL* 473: 62-70. [7] Nie N. X. and Dauphas N. (2019) *LPSC* 50, #2098. [8] Li Y. et al. (2019) *GCA* 245: 374-384. [9] Dauphas N. et al. (2018) *LPSC* 49, #2481. [10] Canup R. M. *et al.* (2015) *Nature Geoscience* 8, 918-921. [11] Lock S. J. et al. (2018). *Journal of Geophysical Research Planets* 123: 910-951. [12] Charnoz S. and Michaut C. J. (2015) *Icarus* 260: 440-463. [13] Saxena P. *et al.* (2017) *EPSL* 474, 198-205.

WATER ON MARS: INSIGHTS FROM NOMINALLY ANHYDROUS PYROXENE IN NAKHLA AND NORTHWEST AFRICA 7034.

J. Davidson[1,2*], M. Wadhwa[1,2], and R. L. Hervig[2], [1]Center for Meteorite Studies, [2]School of Earth and Space Exploration, ASU, 781 E. Terrace Rd, Tempe AZ 85287-6004, USA. *Email: jdavidson@asu.edu

Introduction: Determining the source of planetary water from the hydrogen isotopic compositions of martian meteorites is complicated by overprinting of geologic and atmospheric processes on Mars, shock metamorphism during ejection, and terrestrial weathering on Earth. As the only known samples with compositions representative of the average martian crust [1], the regolith breccia Northwest Africa (NWA) 7034 and its paired samples provide an important opportunity to investigate the water content and hydrogen isotopic composition of the martian crust. Moreover, the clinopyroxenite Nakhla provides the opportunity to investigate the H systematics of a martian sample whose igneous minerals are thought to contain magmatic water [2]. Nakhla and NWA 7034 are the least-shocked martian samples available for study (<20 GPa [3] and 5 to 15 GPa [4], respectively).

While other studies of the martian meteorites have largely concentrated on determining D/H ratios (expressed as δD) and H_2O contents of the hydrated mineral apatite [e.g., 2,5], earlier-formed primary igneous minerals, such as pyroxene, may be more reliable for determining the δD-H_2O systematics of their parent magmas. This is because later-formed apatite crystallizes from highly fractionated melt that may additionally have undergone other processes such as degassing. As such, we target nominally anhydrous pyroxene in this study. Pyroxene is abundant in the clinopyroxenite Nakhla [2] and occurs in the groundmass and a variety of clastic igneous lithologies in NWA 7034 including Fe-, Ti-, and P-rich (FTP) clasts and basaltic clasts [1,6], providing the opportunity to compare the H isotopic compositions and H_2O contents of different lithologies within the breccia and between different geologic settings on Mars.

Analytical Methods: Interior, fusion-crust free samples of Nakhla (one chip) and NWA 7034 (two chips) were co-mounted with terrestrial standards in indium metal in three aluminum discs; no water was used in any of the sample preparation techniques utilized here. Quantitative compositional analyses of pyroxene were obtained with a Cameca SX-100 electron probe microanalyzer (EPMA) at University of Arizona while high-resolution secondary and backscattered electron imaging was undertaken on a JEOL JXA-8530F EPMA at Arizona State University (ASU) before and after isotopic analysis. Secondary ion mass spectrometry (SIMS) measurements of H isotopic compositions and H_2O contents of pyroxenes were performed on the Cameca IMS-6f at ASU using analytical protocols similar to those described in [5]. The H_2O concentrations were estimated using a $H^-/^{16}O^-$ vs. H_2O calibration curve on terrestrial standards. Background H_2O concentrations (18 ppm for Nakhla; 9 and 19 ppm for NWA 7034), determined by analyses of nominally anhydrous San Carlos olivine, were corrected via the method of [7]. Instrumental mass fractionation was monitored throughout analytical sessions on terrestrial pyroxene and basaltic glass standards.

Results: Pyroxenes in Nakhla, which occur as minimally fractured, large crystals (up to ~900 μm diameter), have heavy H isotopic compositions ($\delta D = 310 \pm 170$ ‰ to 1300 ± 155 ‰), and low H_2O contents (12 ± 2 ppm to 70 ± 15 ppm). Most pyroxenes in NWA 7034 occur as large orthopyroxene phenocrysts in the groundmass (up to 700 μm diameter), and have light H isotopic compositions ($\delta D = -162 \pm 12$ ‰ to 280 ± 220 ‰), and high H_2O contents (40 ± 8 ppm to ~2240 ± 500 ppm) compared to Nakhla pyroxenes. Pyroxenes were also analyzed in a basaltic clast (<60 μm diameter; $\delta D = 260 \pm 70$ ‰ to 290 ± 60 ‰; ~330 ± 65 ppm to 570 ± 115 ppm H_2O) and an FTP clast (~300 μm diameter; $\delta D = 130 \pm 110$ ‰ to 330 ± 110 ‰; ~100 ± 20 ppm to 900 ± 180 ppm) in NWA 7034.

Discussion: Pyroxenes in Nakhla and NWA 7034 exhibit an inverse relationship between H_2O contents and H isotopic compositions. Degassing via dehydrogenation (i.e., H_2 loss) typically leads to isotopically heavier δD and an inverse relationship between δD and H_2O concentrations (e.g., [8]), such as seen here for Nakhla and NWA 7034 pyroxenes and previously in NWA 7034 apatites [5]. Data for Nakhla pyroxenes agree with a previous study [9].

The H_2O contents in some NWA 7034 pyroxenes are slightly higher than those reported for clinopyroxene in the shergottite Tissint (1300 ± 200 ppm H_2O) [10]. It is unlikely that the highest H_2O contents in NWA 7034 pyroxenes were incorporated during crystallization; they may, however, be explained by post-eruption addition of water. Since both Nakhla and NWA 7034 were prepared via the same anhydrous method, it seems unlikely that this water was introduced during sample preparation.

References: [1] Agee C. B. et al. (2013) *Science* 339:780–785. [2] Hallis L. J. et al. (2012) *Earth & Planetary Science Letters* 359–360:84–92. [3] Greshake A. (1998) *Meteoritics & Planetary Science* 33:A63. [4] Wittman A. et al. (2015) *Meteoritics & Planetary Science* 50:326–352. [5] Davidson J. et al. (2019) *LPS L,* Abstract #1596. [6] Santos A. R. et al. (2015) *Geochimica et Cosmochimica Acta* 157:56–85. [7] Mosenfelder J. L. et al. (2011) *American Mineralogist* 96:1725–1741. [8] Demény A. et al. (2006) *Rapid Communications in Mass Spectrometry* 20:919–925. [9] Peslier A. H. et al. (2018) *LPS XLIX*, Abstract #1246. [10] Hallis L. J. et al. (2017) *Geochimica et Cosmochimica Acta* 200:280–294.

COMPARING NEODYMIUM NUCLEOSYNTHETIC ANOMALIES IN ORDINARY AND ENSTATITE CHONDRITES

V. Debaille[1], R. M. G. Armytage[2], A. N. Wainwright[3], H. Pourkhorsandi[1], G. Hublet[1], [1]Laboratoire G-Time, Université Libre de Bruxelles, Brussels, Belgium (vdebaill@ulb.ac.be), [2]Jacobs/JETS, NASA JSC, 2101 NASA Parkway, Mailcode XI3, Houston, TX, 77058, USA, [3]School of Earth, Atmosphere and Environment, Monash University, Clayton, Australia.

Introduction: While the discrepancy between the Earth and chondrites for ^{142}Nd systematics has been well documented since 2005 [1], understanding its origin has proven to be more complicated. The identification of small variations in nucleosynthetic processes (rapid or slow) within Nd isotopes has been advocated for this difference [2,3], and after correction of those nucleosynthetic excess or deficit, the Earth has a chondritic composition in ^{142}Nd. Amongst chondrites, enstatite chondrites (EC) are particularly interesting as they share many isotope characteristics with Earth, even though their composition in major elements cannot be reconciled with the bulk composition of the Earth.

Results and discussion : Here we combine forty (mainly) Antarctic enstatite and ordinary chondrites for high-precision multi-static Nd measurements to further investigate this issue. No systematic variation has been observed between groups or petrological types. As previously observed, ordinary chondrites (OC) are statistically different from Earth in μ^{145}Nd and μ^{148}Nd, while EC are indistinguishable from terrestrial values for those isotopes. Analytical error on μ^{150}Nd precludes firm interpretation. On the other hand, both EC and OC share a similar μ^{142}Nd value of -15 ± 5 and -15 ± 12 respectively. Reconciling a discrepancy in ^{145}Nd and ^{148}Nd between OC and Earth-EC on one side, with a discrepancy in ^{142}Nd between EC-OC and Earth on the other side, cannot solely be related to s-process nucleosynthetic anomaly. Preliminary Lu-Hf data on the same samples indicate a petrological type effect on the Lu/Hf ratio, not entirely correlated to ^{176}Hf/^{177}Hf, possibly related to metamorphism [4]. On the other hand, μ^{178}Hf and μ^{180}Hf, mainly related to s-process, do not show any deviation compared to terrestrial values. A careful use of ^{148}Nd and ^{150}Nd values is advocated here, especially in traditional analytical schemes.

References: [1] Boyet and Carlson (2005) *Science* 309, 576-581; [2] Bouvier and Boyet (2016) *Nature* 357, 399-402; [3] Burkhardt et al., (2016) *Nature* 537, 394-398; [4] Debaille et al. (2017) *EPSL* 473, 52-61.

COMPUTER-ASSISTED DETECTION OF INTERSTELLAR DUST IMPACTS IN STARDUST FOILS.

B. T. De Gregorio[1], J. Opsahl-Ong[2], L. Chizmadia[3], T. D. Brintlinger[1], and R. M. Stroud[1] [1]U.S. Naval Research Laboratory (4555 Overlook Ave. SW, Washington, DC 20375 USA; bradley.degregorio@nrl.navy.mil), [2]Science and Engineering Apprenticeship Program, [3]Nova Research, Inc.

Introduction: Observational spectroscopy of contemporary dust in the interstellar medium indicates that it is dominated by ~200 nm amorphous silicate particles [1,2], but the exact particle size distribution, shape, and grain compositions are highly model dependent [3]. The NASA Stardust spacecraft included an extra array of aerogel cells for collecting contemporary interstellar dust for laboratory study [4]. Al foils lining the collector tray also captured interstellar dust as impact residues inside craters, but fewer than 40 particles across all of the foils are expected, in addition to a known background of on average 1 to 3 secondary impact craters per foil from spacecraft debris. [5]. We have developed a fast computer algorithm for detecting foil craters based on their morphological characteristics, which significantly reduces the time and mental fatigue of manually reviewing tens of thousands of images of the foil surfaces.

Sample and Methods: Twelve Stardust interstellar foils were imaged using either a FEI Nova Nanolab 600 or a FEI Helios G3 focused ion beam scanning electron microscope (FIB-SEM). Between 7,000 and 22,000 images were acquired from each foil strip, depending on its length, at spatial resolutions between 30 and 40.5 nm/pixel, sufficient to observe craters as small as 250 nm. Automated mapping software or scripting was used to acquire the images overnight. The same FIB-SEM systems were used for re-imaging at higher resolution following candidate detection, energy-dispersive X-ray spectroscopy (EDS) of crater residues, and FIB extraction of likely interstellar residues for transmission electron microscopy (TEM).

We developed a Python-based algorithm which detects circular features with a dark center and bright rim, the same morphological characteristics that a human expert uses to recognize an impact crater. The core of the algorithm uses Canny edge detection, followed by a circular Hough transform, to detect the inner and outer edges of the crater rim, followed by a number of conditional tests for roughness, center brightness, and rim brightness. The code also includes multi-core processing to significantly decrease the time required to process an entire foil dataset.

Results: The crater searching code detects a crater candidate in approximately 1-5% of the images, requiring manual review of > 600 candidate features. Of these, only ~20 candidates from each foil were considered likely craters and reimaged. In total, 28 impact craters were located on ten of the foils (analysis of the last two foils are in progress), in keeping with previous estimates of crater abundance [5]. The algorithm was successful in identifying craters that were also previously identified by citizen scientists using the Foils@Home website, an extension of the Stardust@Home effort [6].

Two foils, I1009N,1 and I1020W,1, contained 13 and 6 craters, respectively, while the remaining foils contained 0-4 craters each. All of the crater residues on these two foils were consistent with secondary impacts from the spacecraft solar cells [7], suggesting that dust impacts onto the solar cells can create ricochet ejecta sprays and multiple craters on a single foil. These two foils are also adjacent to each other on the collector tray, and it is likely that all secondary impacts on these foils were caused by a single large dust impact onto the solar cells. FIB lift out and TEM analysis of the remaining crater residues is ongoing.

Discussion: The new crater searching code significantly speeds up evaluation of SEM imaging datasets of Stardust interstellar foils for locating dust impact craters, and was validated against known craters in datasets from the Interstellar Preliminary Examination (ISPE). The reliability of the core algorithm for crater detection stems from its procedural similarity to the way a human expert would recognize an impact crater, and is an improvement from the image cross-correlation approach used during the ISPE period [8]. The algorithm was also able to successfully detect craters in image datasets acquired under non-optimal imaging conditions (e.g., defocus and/or astigmatism), but suffered when processing high noise datasets.

References: [1] Draine B. T. (2003) *Annual Review of Astronomy and Astrophysics* 41:241-289. [2] Frisch P. C. and Slavin J. D. (2013) *Earth Planets and Space* 65:175-182. [3] Westphal A. J. et al. (2014) *Science* 345:786-791. [4] Stroud R. M. et al. (2014) *Meteoritics & Planetary Science* 49:1698-1719. [6] Westphal A. J. et al. (2016) *LPSC XLVII*, Abstract #2275. [7] Stroud R. M. et al. (2016) *LPSC XLVII*, Abstract #2989. [8] Ogliore R. C. et al. (2012) *Meteoritics & Planetary Science* 47:729-736.

Origin and timing of volatile (N, H) delivery to the angrite parent body

C. Deligny[1], E. Füri[1], and E. Deloule[1]. [1]Centre de Recherches Pétrographiques et Géochimiques, CNRS-UL, 54501 Vandoeuvre-les-Nancy, France. E-mail: cecile.deligny@univ-lorraine.fr.

Introduction: The volcanic angrites D'Orbigny and Sahara 99555 are two of the oldest meteorites known, with ages of 4563.51 ± 0.8 and 4564.07 ± 0.43 Ma, respectively [1]. They are derived from the differentiated angrite parent body (APB), which was accreted ~1.5 Myrs after CAIs [2] inside Jupiter's orbit, as indicated by the isotopic signatures of ^{50}Ti and ^{54}Cr [3]. Previous studies have revealed a non-neglibible amount of H, C, and N in D'Orbigny [4, 5]. The goal of this study was to determine the content and isotopic signature of N and H in the primitive and more evolved melt from which the two angrites were formed. To this end, we measured, for the first time, the N content and isotopic ratio (^{15}N/^{14}N) of glass inclusions (in anorthite, pyroxene, and olivines), interstitial glasses, and silicate minerals – in four polished sections of D'Orbigny and one polished section of Sahara 99555 – by *in-situ* high-resolution secondary ionization mass spectrometry [6]. The new data allow us to better constrain the source(s) and timing of volatile delivery to planetary bodies in the inner Solar System.

Results: Glass in D'Orbigny contains 15.4 ± 2.1 to 655.3 ± 189.1 ppm N with isotopic ratios (δ^{15}N corrected for cosmogenic ^{15}N) from 0.6 ± 29.7 to 1068.2 ± 174.2 ‰. The nitrogen content of all minerals is below 1 ppm. Sahara 99555 contains very little N (≤ 23 ± 1 ppm), precluding δ^{15}N measurements. The water content in D'Orbigny glass ranges from 81.1 ± 2 ppm to 5.49 ± 0.44 wt.% and H isotope ratios (δD corrected for cosmogenic D) from -346.7 ± 19.1 to +146.7 ± 69.7 ‰. For Sahara 99555, the water concentration ranges from 475 ± 60 ppm to 1.25 ± 0.06 wt.% and the δD value varies from -178.1 ± 79.5 to +254.7 ± 62.9 ‰. Compared to D'Orbigny, Sahara 99555 is enriched in deuterium and contains less water and nitrogen, indicating that it samples a more degassed melt.

Discussion: The most primitive melt, trapped in Mg-rich olivines, is characterized by a δ^{15}N value between 0.2 ± 25 and 82.2 ± 54.9 ‰. This value is similar to that of the terrestrial mantle or CM chondrites [7]. Similarly, the H isotope signature of inclusions in Mg-rich olivines is comparable to that of OIBs [8]. During its evolution, the melt is expected to experience degassing and/or mixing. However, open-system degassing of N_2 or NH_3 cannot explain the highest δ^{15}N values observed in D'Orbigny. Instead, mixing between two components with distinct ^{15}N/^{14}N ratios has to be considered. According to this scenario, the δ^{15}N signature of the more evolved melt, trapped in inclusions with low a Mg-number, is consistent with a cometary contribution (δ^{15}N ≈ +1000 ‰; [7]). Therefore, given the very old age of the two angrites, volatile-rich CM-like and cometary materials must have been delivered from the outer Solar System to the terrestrial planet-forming region within the first ~4 Myrs after CAI formation. Jupiter is thought to have prevented the influx of volatile-rich material to the inner Solar System for at least 3 to 4 Myrs [9]. Once the nebular gas started to disperse, CM-like and cometary objects could have been scattered inward, due to the growth/migration of Jupiter [10]. Thus, angrites may record the earliest delivery of outer Solar System volatiles. These results imply that a cometary volatile contribution to the building blocks of the terrestrial planets cannot be ruled out.

[1] Tissot, F.L. et al. (2017) *GCA*, 213, 593-617. [2] Kleine, T. et al. (2012) *GCA*, 84,186-203. [3] Warren, P.H. (2011) *EPSL*, 311(1-2), 93-100. [4] Sarafian, A.R et al. (2017) *Phil. Trans. R. Soc. A* 375: 20160209. [5] Varela, M.E. et al. (2003) *GCA* **67**(24), 5027-5046. [6] Füri, E. et al. (2018) *Chem. Geol.*, 493, 327-337. [7] Alexander, C.M.O.D. (2017) *Phil. Trans. R. Soc. A375*: 20150384. [8] Deloule, E. et al. (1991) *EPSL 105*(4), 543-553. [9] Kruijer, T.S. et al., (2017) *Proceedings of the National Academy of Sciences*, *114*(26), 6712-6716. [10] Raymond, S.N. and Izidoro, A. (2017) *Icarus*, *297*, 134-148.

OLIVINE INCLUSIONS IN THE FUKANG PALLASITE AND IMPLICATIONS FOR THE MAIN-GROUP PARENT BODY

D. N. DellaGiustina[1], K. Domanik [1] D. H. Hill[1], N. Habib[1,2], and D. S. Lauretta[1]
[1] Lunar Planetary Lab, University of Arizona, 1415 N 6th Ave, Tucson, AZ 85705 (danidg@lpl.arizona.edu),
[2]Institute of Astronomy, University of Cambridge, Madingley Road, Cambridge CB3 0HA

Introduction: Fukang is a Main-group pallasite that consists of semi-angular olivine grains (Fo 86.3) embedded in an Fe-Ni matrix with 9-10 wt. % Ni and low-Ir (45 ppb). Olivine grains sometimes occur in large clusters up to 11 cm across. The Fe-Ni phase is primarily kamacite with accessory taenite and plessite. Minor phases include schreibersite, chromite, merrillite, troilite, and low-Ca pyroxene.

We report the results of a study of the Fukang pallasite that includes measurements of bulk composition, mineral chemistry, mineral structure, and petrology. In particular, we focus on a variety of silicate inclusions enclosed in olivine that contain phases rarely or not previously reported in Main-group pallasites, including clinopyroxene (augite), tridymite, K-rich felsic glass, and an unknown Ca Cr-silicate.

Olivine Inclusions: Inclusions found in Fukang's olivine exhibit features that are rare in Main-group pallasites and preserve important information from the parent body. They include measurable amounts of clinopyroxene (augite), the presence of the silica phase tridymite, K-rich felsic glasses, and an unidentified Ca-Cr silicate. Below we highlight the implications from the presence of each of these inclusion phases:

1) Clinopyroxene (augite) in Main Group pallasites has not previously been observed. However, augite in the "pyroxene" pallasites has been analyzed by Boesenberg et al. (2000) and appears to be similar in composition to the augite in Fukang. Extremely uniform composition of both low-Ca pyroxene and augite in Fukang olivine inclusions suggests that the pyroxenes have equilibrated with each other, either during their formation or at a later time, and has enabled us to perform two-pyroxene thermobarometry.

2) Tridymite is an SiO_2 polymorph that crystalizes within a narrow range of low-pressure, high-temperature conditions. It can stably form at vacuum pressures and temperatures between 867 and 1470°C. Fukang was the first pallasite in which the presence of tridymite was reported (DellaGiustina 2011). It has also been reported in the Omolon pallasite by Lavrentjeva et al. (2012). Although tridymite can persist metastably at temperatures below its stability field, it cannot withstand pressures >0.4 GPa at any temperature, even for short durations. It is therefore widely recognized as a pressure indicator in terrestrial and planetary materials (Black 1954) and can be used to infer the range of pressures (shock or otherwise) experienced by Fukang.

3) K-rich felsic material is unusual in meteorites and has not been previously observed in other Main-group pallasites. The observation that K-rich felsic material co-exists with tridymite in many instances suggests that these assemblages are a trapped melt from a more evolved silicic magma and may reveal information about upper mantle regions in the pallasite parent body. These inclusions could have been overlooked in other pallasites, were rare and heterogeneously distributed, or in some cases were not trapped by them at all.

4) A Ca Cr-silicate phase that could not be identified as any known mineral phase, and may have also been observed in the Pavlodar pallasite Steele (1994).

Parent Body Size: Evidence indicates that Fukang originated deep in the interior of a differentiated parent body. Slow cooling rates inferred from the Widmanstätten pattern in the metal phase, and the lack of elemental zoning in olivine further support this conclusion. The morphology of olivine indicates that many grains formed in direct contact with one another to form nodules, most likely at the base of a magma chamber. This evidence supports formation at the core-mantle boundary of the Main-Group parent body.

Pressure constraints determined from two-pyroxene barometry of ortho- and clinpyroxene (0.39 ± 0.07 GPa), tridymite (< 0.4 GPa), and geophysical calculations that assume pallasite formation at the core-mantle boundary, provide an upper estimate on the size of the Main-group parent body from which Fukang originated. Using these constraints, we conclude that Fukang formed at the core-mantle boundary of a large differentiated planetesimal, up to 400-680 km in radius.

References: [1] Boesenberg J. S., Davis A. M., Prinz M., Weisberg M. K., Clayton R. N., and Mayeda T. K. 2000. The pyroxene pallasites, Vermillion and Yamato 8451: Not quite a couple. Meteoritics and Planetary Science 35:757-769. [2] DellaGiustina D. N., Lauretta D. S., Hill D. H., Killgore M., Yang H., Downs R. T. 2011. Implications of the Presence of Tridymite in the Fukang Pallasite. (abstract #1915) 42nd Lunar and Planetary Science Conference [3] Lavrentjeva Z. A., Lyul Yu., and Kolesov G. M. 2012. The Omolon pallasite: Chemical composition, mineralogy, and genetic implications. Geochemistry International 50:34-43. [4] Black G.P. 1954. The significance of tridymite in igneous and metamorphic petrogenesis. Mineralogical Magazine 30:518-524.

UREILITES: MIXES OF A VESTA-LIKE PARENT BODY AND AN IMPACTOR FROM PROTO-MARS.

S. J. Desch[1], J. G. O'Rourke[1], L. K. Schaefer[2], T. G. Sharp[1], and D. L. Schrader[1,3]. [1]School of Earth and Space Exploration, Arizona State University, Tempe AZ 85287 USA. [2]School of Earth, Energy and Environmental Sciences, Stanford University, Stanford CA 94035. [3]Center for Meteorite Studies, Arizona State University, Tempe AZ 85287. Corresponding author: steve.desch@asu.edu

Ureilites: Ureilites are unusual and enigmatic meteorites. They are as carbon-rich (~3 wt% C [1]) as carbonaceous chondrites, but compositionally resemble ordinary chondrites [2]. Their ^{50}Ti and ^{54}Cr abundances place them in the inner solar system [3], near 2.7 AU [4]. They are achondrites but saw only partial (~15%) extraction of melt [2]. Most (95%) ureilites are monomict with olivines of uniform Mg# varying from 74 to 96, strongly peaked at 80. Several properties (e.g., Δ^{17}O and δ^{18}O, Fe/Mn ratios), correlate with Mg# [5]. The range of Mg# has been attributed to "smelting": $(Mg,Fe)_2SiO_4 + CaO$ (melt) $+ SiO_2$ (melt) $+ C \rightarrow (Mg,Ca)SiO_3 + Fe + CO$ (gas). The equilibrium Mg# depends on pressure and depth in the ureilite parent body (UPB) [6,7], but why ureilites would so preferentially sample Mg# of 80 is a mystery [8]. C content does not correlate with Mg# [9]. Pyroxene thermometers suggest the UPB last equilibrated at about 1050-1100°C [10], after peak temperatures ≈1200-1300°C [2,11,12]. Thermal models including melt migration reproduce these temperatures if the UPB had radius ≈ 100-250 km and formed at t=0.6 Myr (relative to CAIs) [13]. Soon after t=5 Myr [14], the UPB was catastrophically disrupted by impact at ~5 km/s (consistent with typical S4 shock stages; [15]), as inferred from reduction rims around olivines attributed to "smelting" initiated by release of pressure by an unroofing event, followed by a quench in temperatures. The UPB must have broken into chunks < 10 m in size [16] that reassembled into ureilite daughter bodies (UDBs) [2,17], from which ureilites derive. Impact shock would have produced the copious nanodiamonds in ureilites [18], but this does not explain the large (100 μm) sngle-crystal diamonds with δ^{15}N zoning observed in the polymict ureilite Almhata Sitta MS-170, which formed in metallic melt in a planetary mantle at pressures ≈ 4 GPa [19,20].

Model for Ureilite Origins: We hypothesize the following. The UPB formed at 2.7 AU at t=0.6 Myr. Disk models predict it was 1.3wt% CAIs [21]. Its initial composition was like 0.63 H+0.33 CV+0.04 CI chondrites, similar to the 0.75 H+0.25 CV mix inferred for Vesta [22]. This composition yields Mg# 80 olivines and ~1wt% C. Some silicates at low pressures underwent equilibrium smelting, forming high-Mg# olivines. The smelted fraction constrains the peak pressure; we infer the UPB radius was 173 km. We interpret the ≈25% of olivines with Mg# < 80 to be from the impactor, mixed in during the impact. Its composition corresponds to end-member "A" of [5]. The impactor had 30% the mass of the UPB, consistent with [8], and had radius ≈115 km. It delivered metal and abundant C, including large diamonds. During reassembly into UDBs, temperatures were ≈1100°C, so that silicates did not melt, but metallic melts from both bodies mixed, explaining HSE abundance trends [23]. Carbon was redistributed by the melt.

Largest Daughter Body: We further hypothesize that 15 Eunomia at 2.64 AU is the largest UDB. Based on the radii above and the 5 km/s impact speed, using [24] we estimate a radius of the largest UDB ≈139 km; Eunomia's radius is 132 km. Although the polymict ureilite Almahata Sitta derived from the F-type asteroid 2008 TC$_3$ [25], most ureilites are spectrally associated with S-type asteroids [26]; Eunomia is the largest S-type asteroid. 15 Eunomia has an extensive and ancient collisional family with a dynamical pathway to deliver fragments to 2.55 AU [27]. We suggest the F-type asteroid 438 Zeuxo at 2.55 AU is from the Eunomian family, and 2008 TC$_3$ derived from it and underwent drifted to the 3:1 resonance at 2.5 AU to reach Earth, consistent with its inferred dynamics [25].

Impactor Origin: Finally, we suggest the impactor derived from the proto-Martian surface at t~5 Myr, after magma ocean crystallization but before mantle overturn [28]. It would be Fe-rich bulk Mars, plus late-accreted carbonaceous chondrite material, with Mg# ≈74-80. We find in oxygen isotopes, Mg#, and Fe/Mn it would match end-member "A" of [5]. The compositional similarity between the UPB (Mg# = 80) and the impactor is somewhat coincidental, but they did derive from similar starting materials. Ejection by the Borealis basin impactor would have generated > 100 fragments larger than 100 km in radius that would have impacted objects out to 2.9 AU at 5 km/s [29]. The impactor could have delivered diamonds, formed in Mars's mantle at P > 4 GPa, to the UPB and UDBs.

References: [1] Hudon, P et al. (2004) *LPSC* 35, 2075. [2] Goodrich, C et al. (2015) *MAPS* 50, 782. [3] Warren, P (2011) *GCA* 75, 6912. [4] Yamakawa, A et al. (2010) *ApJ* 720, 150. [5] Barrat, J et al. (2017) *EPSL* 478, 143. [6] Walker, D & Grove, T (1993) *Metics*. 28, 629. [7] Singletary, S & Grove, T (2003) *MAPS* 38, 95. [8] Michel, P et al. (2015) *P&SS* 107, 24. [9] Goodrich et al. 1992. [10] reference. [11] Goodrich, C (2004) *ChEG* 64, 283 . [12] Goodrich et al. 2007. [13] Wilson, L et al. (2008) GCA 72, 6154. [14] Goodrich, C et al. (2010) *EPSL* 295, 531. [15] Stoeffler et al. (1991) *GCA* 55, 3845. [16] Herrin, J et al. (2010) *MAPS* 45, 1789. [17] Downes, H et al. (2008) *GCA* 72, 4825. [18] Lipschutz, M (1964) *Science* 143, 1431. [19] Miyahara, M et al. (2015) *GCA* 163, 14. [20] Nabiei, F et al. (2018) *Nat Comm* 9, 1327. [21] Desch, S et al. (2018) *ApJS* 238, 11. [22] Righter, K & Drake, M (1997) *MAPS* 32, 929. [23] Goodrich, C & Desch, S (2019) this conference. [24] Leinhardt, Z & Stewart, S (2012) *ApJ* 745, 79 [25] Jenniskens, P et al. (2010) *MAPS* 45, 1590. [26] Gaffey, M et al. (1993) *Icarus* 106, 573. [27] Carruba, V et al. (2007) *A&A* 473, 967. [28] Elkins-Tanton, L et al. (2003) *MAPS* 38, 1753. [29] Hyodo, R & Genda, H (2018) *ApJ* 856, L36.

VARIABLE COSMOGENIC ARGON IN L/LL5 CHONDRITE KNYAHINYA.

M. Di Gregorio, H. Busemann, A. C. Hunt, D. Krietsch, M. Schönbächler, and C. Maden, Institute of Geochemistry and Petrology, ETH Zurich, Switzerland (henner.busemann@erdw.ethz.ch).

Introduction: The study of stable and radiogenic cosmogenic nuclides, as the duration a rock was exposed to cosmic rays, is an important tool in meteoritics. It helps to determine impact events on meteorite parent bodies, typically in the asteroid belt, but also on the Moon or Mars [e.g., 1-3]. Such events also directly affect the Earth, as documented by the discovery of fossil remains of the catastrophic impact that disrupted the L chondrite parent body ~480 Ma ago [4]. In addition, cosmogenic nuclides help to confirm or exclude pairing of meteorites of the same chemical class, or –if differently determined cosmic ray exposure (CRE) ages disagree– can give hints at (i) complex exposure histories such as the exposure of a meteorite in two periods, e.g. on a parent body and later in space, (ii) the residence time on Earth or (iii) heating experienced on the surface of a parent body, during transfer to Earth or atmospheric entry.

Cosmogenic (cosm) noble gases such as ^{3}He, ^{21}Ne and ^{38}Ar are often used because their measurement requires little sample mass and preparation, and per experiment several cosmogenic nuclide concentrations can be determined, leading to a set of CRE ages that can be compared. However, discrepancies are frequently observed, and their origin is often unknown. Here we study the effect of chemical, i.e. target mineral heterogeneity on cosmogenic noble gas concentrations in the well-studied [5,6] LL/L5 chondrite Knyahinya.

We will show that in ~20 mg aliquots of ordinary chondrites, typical for our noble gas examinations, the chemical composition of the major target elements varies significantly from sample to sample. Particularly the concentrations of Ca, K and Fe, essential for the production of ^{38}Ar$_{cosm}$, should be determined in the same split aliquots. Otherwise, errors in the ^{38}Ar CRE age of up to almost a factor of two can occur.

Experimental: 15 samples of ~20-40 mg were taken from a single 0.55 g fusion crust-free fragment of Knyahinya (ETH collection) and powdered. The 15 powders were each split for the determination of noble gas (8-24 mg) and major element (2-17 mg) concentrations. Noble gases were measured with the "Albatros" mass spectrometer at ETH [see 3 for details]. We used 45 eV electron acceleration and ^{84}Kr and ^{129,132}Xe were measured together with Ar. Blank corrections were significant ($\leq$1% for ^{4}He, 19-79% for ^{36}Ar, 5-21% for ^{40}Ar) but much smaller for cosmogenic ^{3}He (<0.02%), ^{21}Ne (<0.2%) and ^{38}Ar (6-21%). The elements Na, Mg, Al, P, K, Ca, Sc, Ti, V, Cr, Mn, Fe, Ni, and Co were determined by ICP mass spectrometry using a Thermo Scientific Element XR. Reproducibility was assessed by repeated analysis (4-6 times) of a representative sample aliquot, and was 3-8% (2 RSD; relative standard deviation) for the various elements.

Results and Discussion: All results are broadly consistent with each other and literature data [5,6]. ^{3}He, ^{21}Ne and ^{38}Ar are entirely cosmogenic. However, ^{38}Ar$_{cosm}$ concentrations vary by 66%, while ^{21}Ne$_{cosm}$ and ^{3}He$_{cosm}$ vary by only 37% and 25%, respectively. In contrast, the essential ratio $(^{22}$Ne/^{21}Ne$)_{cosm}$, which constrains the shielding conditions of the sample against cosmic rays varies by only <2%. ^{38}Ar$_{cosm}$ correlates with Ca, its major target element (r^2 ~0.87), which shows a spread of more than a factor of two. All major target elements show significant scatter, well beyond analytical uncertainty, suggesting that Knyahinya's minerals are relatively coarse-grained and heterogeneously distributed at the 10-20 mg scale. The three important target elements for ^{38}Ar$_{cosm}$, Ca, Fe and K (together producing ~93% [7,8]) show the largest scatter: RSD for Ca and Fe concentrations in the aliquots are 25% and 18%, respectively, whereas the major targets for the production of ^{21}Ne$_{cosm}$, Mg, Al and Na, only show 9-12% each. ^{3}He is produced by a larger number of target elements (O, Mg, Al, Si, Fe, Ni) and in similar rates and is, hence, more robust against element variations. We also note here that the purely physical model that we commonly use to predict cosmogenic nuclide production rates for ordinary chondrites, depending on the shielding and chemical composition [9], does not include K. Hence, based on formulas for ^{38}Ar$_{cosm}$ [7,8] and the chemistry of our Knyahinya samples, we may underestimate the ^{38}Ar$_{cosm}$ production by ~15%.

In summary, the determination of CRE ages with ^{38}Ar$_{cosm}$ in a 10-20 mg sample of ordinary chondrite requires caution, and preferably the determination of the target element concentrations of Ca, Fe (and K) in an aliquot of the same sample. In unfavourable cases, the age can otherwise be wrong by up to a factor of two, due to heterogeneously distributed main carrier minerals. The production of ^{21}Ne$_{cosm}$ from Mg, Al and Na shows much less variation (~10%), well within the assumed uncertainty for *ab initio* modelled production rates of perhaps 20%.

References: [1] Herzog G.F. and Caffee M. (2014) in *Treatise on Geochemistry 2nd ed. - Vol. 2*:419-453. [2] Weimer D. et al. (2018) 81st Annual *Meteoritical Society Meeting*: abstract #6300. [3] Riebe M.E.I. et al. (2017) *Meteoritics & Planet. Sci.* 52:2353-2374. [4] Heck P.R. et al. (2004) *Nature* 430:323-325. [5] Graf T. et al. (1990) *Geochim. Cosmochim. Acta* 54:2511-2520. [6] Lavielle B. et al. (1997) *Meteoritics & Planet. Sci.* 32:97-107. [7] Cressy Jr. P.J. and Bogard D.D. (1976) *Geochim. Cosmochim. Acta* 40:749-762. [8] Freundel M. et al. (1986) *Geochim. Cosmochim. Acta* 50:2663-2673. [9] Leya I. and Masarik J. (2009) *Meteoritics & Planet. Sci.* 44:1061-1086.

WEATHERING OF ORDINARY CHONDRITES FROM ATACAMA DESERT – A NEW DATASET.

E. Dos Santos[1], R. B. Scorzelli[2], J. Gattacceca[3], P. Rochette[3], M. Valenzuela[4], S. Letichevsky[5], R.R. de Avillez[5]
[1]Instituto de Ciência e Tecnologia – ICT/UFVJM, Minas Gerais, Brazil. E-mail: edivaldo.santos@ict.ufvjm.edu.br. [2]Centro Brasileiro de Pesquisas Físicas – CBPF, Rio de Janeiro, Brazil. [3] Aix Marseille Univ, CNRS, IRD, Coll France, INRA, CEREGE, Aix-en-Provence, France. [4]Servicio Nacional de Geología y Minería - SERNAGEOMIN, Santiago, Chile. [5]Dep. de Engenharia Química e de Materiais – DEQM/PUC, Rio de Janeiro, Brazil.

The Atacama Desert is located between the western central Andes and the Pacific coast and extends from southern border of Peru (18 °S) to Copiapó, Chile (30 °S). It is the oldest desert on Earth, comprising areas with semiarid, arid, and hyper-arid conditions [1]. These climatic and geomorphological features are extremely favorable for preservation and accumulation of meteorites. Meteorite densities are up to above 100 meteorites per km^2, [2], in accordance with an average terrestrial age of ~700 ka [3]. A large number of meteorites, mostly ordinary chondrites, have been collected in the Atacama desert. Their old terrestrial ages and statistical significance make them a choice material to study the effects of terrestrial weathering [3-8]. Here we present a new dataset about weathering of ordinary chondrites from the Atacama Desert, in order to better understand how weathering processes occur in different areas of the desert.

We studied about seventy ordinary chondrites recovered in San Juan, El Médano and Caleta el Cobre dense collection areas of the Atacama Desert. These meteorites have been characterized using ^{57}Fe Mössbauer spectroscopy. Following [9], transmission ^{57}Fe Mössbauer measurements using a 25 mCi 57Co/Rh radioactive source in sinusoidal mode were performed at room temperature (RT) and at liquid helium temperature (4.2 K). Mössbauer powder absorbers were prepared with nearly 100 mg/cm^2 of the bulk meteorite sample.

Combining the RT and 4.2 K Mössbauer measurements, the following iron-bearing primary phases were detected in all samples: olivine, pyroxene, troilite and Fe,Ni metal (kamacite, taenite). The following oxides/oxyhydroxides weathering products were found: goethite, akaganeite, maghemite. As described in [9], the abundance of oxidized iron in ordinary chondrites, as measured by Mössbauer spectroscopy, defines the weathering degree. The Mössbauer data reveals that for San Juan, El Médano and Caleta el Cobre samples the average weathering degree are 31%, 53% and 47%, respectively. Therefore, the lowest weathering degree was found for San Juan area. The Mössbauer data will be combined with ^{14}C terrestrial age as well as results from other techniques, in order to establish not only a broad picture of weathering processes (kinetics and mineralogy of weathering products) but also a possible proxy for paleoclimatic changes in Atacama Desert [6].

References: [1] Dunai T.J. et al (2005) *Geology* 33:321-324. [2] Hutzler A. et al. (2016) *Meteoritics & Planetary Science* 51:468-482. [3] Drouard A. et al. (*in press*) *Geology*. [4] Munayco J. et al. (2010) *Meteoritics & Planetary Science* 45:A143. [5] Munayco P. et al. (2011) *Meteoritics & Planetary Science* 46:A169. [6] Valenzuela E. M. et al. (2013) *Meteoritics & Planetary Science* 48:A354. [7] Munayco J. et al. (2013) *Meteoritics & Planetary Science* 48:A255. [8] Valenzuela E. M. et al. (2014) *Meteoritics & Planetary Science* 49:A414. [9] Munayco P. et al. (2013) *Meteoritics & Planetary Science* 48:457-473.

Melting of Sahara 97072 Meteorite at High Pressure and High Temperatures

Wei Du[1, 2*], Hiroaki Ohfuji[3], and Tetsuo Irifune[3, 4], [1]Institute of Geochemistry, Chinese Academy of Sciences, Guiyang, Guizhou 550081, China; [2]CAS Center for Excellence in Comparative Planetology, Hefei, Anhui 230026, China; [3]Geodynamic Research Center, Ehime University, Matsuyama 790-8577, Japan; [4]Earth-Life Science Institute, Tokyo Institute of Technology, Tokyo 152-8550, Japan

Introduction: The large range of oxygen fugacity values measured from meteoritic materials indicates the diversity of materials found in the solar nebula[1]. The oxidation state of the materials from solar nebula is a critical parameter in determining the planetary formation and differentiation in the early solar system. Based on partial melting experiments on Allende CV3 carbonaceous chondrite, Agee (1990) proposed an early stage differentiation model of the Earth with a FeO-rich magnesiowüstite layer in the deepest levels of the Earth's interior and a proto-core rich in sulfur (13 wt%) and oxygen (12 wt%). As Agee suggested, the maximum content of sulfur and oxygen in the proto-core could be balanced if the model was modified with some enstatite chondrites[2]. This is because enstatite chondrites are undifferentiated meteorites and among the most reduced material with an average total iron content of 29 wt% [3]. In addition, because their isotopic composition is identical to the Earth, enstatite chondrite was also proposed as primary materials for the Earth formation[4]. And the enstatite chondrite model fit with one of the proposed formation mechanisms of the Earth: the original subjects (building block) of the Earth were highly reduced, Fe-metal and ferrous iron were extracted from silicate crystalline after partial melting at subsolidus temperatures, and the metallic liquid segregated to the core by percolation through a solid silicate matrix. There are obstacles to an enstatite chondrite model of the Earth's bulk composition. For example, enstatite chondrites are depleted in refractory elements comparing with the Earth's primitive upper mantle[5], and the proto-core forming mechanism that the metal iron and ferrous iron segregating from silicate cannot operate in the system which has same oxygen fugacity as today's Earth mantle.

In order to derive constraints on the formation of terrestrial planets from enstatite chondrites and to test the possible effect of volatile element on melting interval of sulfide and silicate, we have conducted a series of melting experiments on the Sahara 97072 (EH3) meteorite at 5 GPa and 1000-1700°C by using multi-anvil apparatus. Starting material of natural Sahara 97072 meteorite was used for all the experiments. The bulk composition of Sahara 97072 used in this study is similar but not identical to the composition reported by Lehner et al. (2014)[6]. For each experiment, machined double graphite capsules were chose as sample container because graphite has high melting temperature and allows an effective control of the oxygen fugacity, which make them good container to keep the reduce condition during heating. This study reports the melting relations at 5 GPa and variable temperatures: (1) (Fe, Ni)-sulfide melt completely at 1200°C; (2) silicate partial melting begins at 1400°C, and quenched sample shows immiscibility between (Fe, Ni)-sulfide melt and FeO-rich silicate melt. and (3) the Sahara 97072 meteorite is completely melted when temperature is reaching 1600°C. At 5 GPa, both pyroxene and olivine appear to be stable near the liquidus, indicating that 1600°C and 5 GPa is very close to the pyroxene-olivine cotectic.

By overheating the Sahara 97072 meteorite sample to 1650 and 1700°C, (Fe, Ni)-alloy saturated from (Fe, Ni)-sulfide. The spherical shape of the (Fe, Ni)-alloy indicates that the lost of sulfur to the silicate melt happened during melting rather than quenching. The silicate liquid at overheating conditions show less FeO content than the completely melt condition, indicating that FeO was partially reduced back as Fe-alloy. EPMA measurement results show that about 3 wt% C was dissolved in (Fe, Ni)-alloy, which caused the sample reached the metallic liquid immiscibility gap between Fe-C and Fe-S phases as showed by previous study[7].The overheating experiments on Sahara 97072 suggest that the relatively small planetary bodies with elevated sulfur and carbon content would have likely experienced sizable core stratification during early melting event.

References: [1] Righter K. et al. (2006) *In Meteorites and the Early Solar System II, vol. 2 (eds. D.S. Lauretta and, Jr. H.Y. McSween). The University of Arizona Press*, 803-828. [2] Agee C. B. (1990) *Nature,* 346, 834-837. [3] Wasson J. T. and Kallemeyn G. W. (1988) *Philosophical Transactions of the Royal Society, A* 325, 535-544. [4] Javoy M. et al. (2010) *Earth and Planetary Science Letters,* 293, 259-268. [5] Palme H. and O'Neill H.S.C. (2003) *In Treatise on Geochemistry, vol. 2 (ed. R. W. Carlson). Elsevier Science,* 1-38. [6] Lehner S.W. et al. (2014) *Meteoritics and Planetary Science, 49: 2219–2240.* [6] Corgne et al. (2008) *Geochim Cosmochim Acta,* 72:2409–2416.

CO3 AND CH/CB CAIs SUGGEST [10]Be WAS DISTRIBUTED UNIFORMLY IN THE SOLAR NEBULA.

E. T. Dunham[1], M.-C. Liu[2], A. T. Hertwig[2], S. J. Desch[1] and M. Wadhwa[1], [1]Arizona State University, Center for Meteorite Studies, Tempe AZ 85287 (email: etdunham@asu.edu) , [2]Dept. of Earth, Planetary, and Space Sciences, University of California, Los Angeles, CA 90095.

Introduction: Studies of ^{10}Be-^{10}B isotope systematics in the first-formed Solar System solids (calcium-aluminum-rich inclusions, or CAIs) can provide insights into the astrophysical environment of the early Solar System. The short-lived radionuclide ^{10}Be decays to ^{10}B ($t_{1/2}$= 1.4 Ma) and is produced almost exclusively by energetic particle irradiation [1]. The most likely astrophysical sites for ^{10}Be production are: (1) in the molecular cloud, as galactic cosmic rays (GCRs) spalled heavier nuclei, followed by ^{10}Be homogenization as the cloud collapsed to form the solar nebula [2,3]; or (2) in the nebular disk, as solar flare high-energy particles interacted with nebular gas and solids, producing ^{10}Be heterogeneously in space and time [4-7]. Most normal CAIs studied thus far have been from CV3 chondrites; these have initial ^{10}Be/^{9}Be ~(6-9)×10^{-4} [5-11], although a few with higher ^{10}Be/^{9}Be have been reported [12,13]. The few CH/CB CAIs studied so far have ^{10}Be/^{9}Be like those in normal CV3 CAIs, but one CAI has a significantly higher ^{10}Be/^{9}Be ~10^{-2} [14]. CAIs with Fractionation and Unknown Nuclear effects (FUN CAIs) and hibonites have lower ^{10}Be/^{9}Be~(3-5)×10^{-4} [7,9,15,16]. Here we report ^{10}Be-^{10}B systematics in normal, pristine CAIs from CO3 and CH/CB chondrites, to better constrain how and where ^{10}Be was produced.

Methods: Epoxy-mounted polished thick sections of CO3 chondrites Dar al Gani (DaG) 005 and DaG 027 contained six coarse-grained CAIs, and two polished mounts of the CH/CB chondrite Isheyevo contained five coarse-grained CAIs. We characterized the CAIs with the JEOL JXA-8530F electron microprobe at Arizona State University, then determined the ^{10}Be−^{10}B isotope systematics in these 11 CAIs using the IMS-1290 secondary ion mass spectrometer (SIMS) at UCLA. Using a 1-2 nA ^{16}O$_2^-$ primary beam (generated by a *Hyperion-II* source [17]), we pre-sputtered a 10×10 μm rastered square, then decreased the rastered area to 5×5 μm for the analysis. Secondary ion intensities were measured with multiple electron multipliers (EMs) with a mass resolving power of ~2,500 in dynamic multi-collection mode. A NIST 614 glass was used as a standard to determine the ^{9}Be/^{11}B relative sensitivity factor (RSF) and the ^{10}B/^{11}B instrumental mass fractionation (IMF).

Results: *CO3 CAIs.* The six CO3 CAIs range in their size, mineralogy, texture, and shape: 300-830 μm in size; coarse-grained texture with melilite ±spinel, hibonite, perovskite; rounded to irregularly fragmented in shape. The ^{10}Be-^{10}B data for each of these CAIs define isochrons that yield a weighted average initial ^{10}Be/^{9}Be = (8.4±1.6)×10^{-4} (2SE weighted, MSWD=0.3).

CH/CB (Isheyevo) CAIs. The five Isheyevo CAIs range in their size, mineralogy, and texture: 120-290 μm in size; fine- to coarse-grained texture with melilite ±hibonite, spine, grossite, and perovskite, all are rounded in shape. Taken together, the ^{10}Be-^{10}B data for all five CAIs yields an initial ^{10}Be/^{9}Be = (10.5±2.8)×10^{-4} (MSWD=1.2).

Discussion/Conclusions: The six CO3 CAIs and five CH/CB CAIs measured in this study record initial ^{10}Be/^{9}Be ratios similar to those in most normal CV3 CAIs, and all have the same ^{10}B/^{11}B initial value within error. If well-behaved ^{10}Be-^{10}B isochrons (i.e., with MSWDs close to ~1) of all previously studied normal CAIs from CV3 [5-12], CR2 [18], CH/CB [14], and CO3 chondrites are considered, they yield a weighted mean initial ^{10}Be/^{9}Be = (7.0±0.3)×10^{-4} (2SE weighted). This suggests that ^{10}Be was distributed homogeneously in at least those regions of the solar nebula where normal CAIs formed; in this scenario, FUN CAIs (with lower ^{10}Be/^{9}Be) either formed in an isotopically distinct region or formed later than normal CAIs. This further indicates that ^{10}Be was likely produced in the molecular cloud, and was mostly homogenized during its collapse and formation of the solar nebula. If we consider this initial ^{10}Be/^{9}Be value as the steady-state level generated in the molecular cloud by interactions with GCRs, the GCR ion flux ~4.6 billion years ago in the region where our molecular cloud core was forming was about 8 times higher than present-day GCR ion flux in the solar neighborhood [3].

References: [1] Davis A.M. & McKeegan K.D. (2014), *Treatise on Geochemistry (2nd Ed.),* 361. [2] Desch S.J. et al. (2004) *ApJ 602*, 528. [3] Tatischeff V. et al. (2014) *ApJ 796*, 124. [4] Jacquet E. (2019) *A&A accepted* [5] McKeegan K.D. et al. (2000) *Science 289,* 1334. [6] Sugiura N. et al. (2001) *MAPS 36,* 1397. [7] MacPherson G.J. et al. (2003) *GCA 67,* 3165. [8] Chaussidon M. et al. (2006) *GCA 70,* 224. [9] Wielandt D. et al. (2012) *ApJ 748,* 25. [10] Srinivasan G. et al. (2013) *EPSL 374*, 11. [11] Mishra R.K. & Marhas K.K. (2019) *Nature Astronomy* s41550-019-0716-0 [12] Sossi P.A. et al. (2017) *Nature Astronomy 1*, 0055. [13] Dunham E.T. et al. (2017) *Meteoritics & Planetary Science* 80:A6381 [14] Gounelle M. et al. (2013) *ApJ 763,* 33. [15] Liu M.-C. et al. (2009) *GCA 73,* 5051. [16] Fukuda K. et al. (2018) *Geochem J. 52*, 3. [17] Liu M.-C. et al. (2018) *IJMS 1*, 9 [18] Dunham E.T. et al. (2019) LPS *L*, Abstract #1928.

IN-SITU TRACE ELEMENTS & REE GEOCHEMISTRY OF CHONDRITES (H & L) : INSIGHTS INTO COSMOCHEMICAL PROCESSES.

Dutta, A[1]*, Raychaudhuri, D[2], Raghuram[3], Mishra, M[3], Bhattacharya, A[2] And Chakraborti, R[4]. [1]Geological Survey of India (GSI), 29, J.L.N Road, Kolkata – 700016, India. [2]Geological Survey of India (GSI), 15, A and B Kyd Street, Kolkata – 700016, India. [3]Geological Survey of India, LA-ICP-MS Laboratory, NH 5P NIT, Faridabad – 121001, Haryana, India. [4]CEaS, IISc Bangalore, Bangalore-560012, India. Email:arindamdutta2000@gmail.com[1]*; chotorc@gmail.com[2]; raghu8185@gmail.com[3]; monica.88610@gmail.com[3]; baparajitagsi@gmail.com[2]; ramananda@ceas.iisc.ernet.in[4].

Introduction: Two unequilibrated ordinary chondrites e.g. Dhajala (H3.8) and Khohar (L3.6) have been analyzed by LA-ICPMS (Quadrapole) to decipher in-situ trace elements (TEs) and REEs distribution among different types of chondrules/clasts and mesostasis (composed of feldspathic glass ± Cpx). Selective fractionations of TEs and REEs among these H and L-type of chondrites may involve stellar cosmo chemical process(es). The partitioning of different trace elements and REEs among the various silicate phases, in particular olivine, enstatite chondrules and mesostasis, is very sensitive to its nebular formation conditions [1, 2].

Analytical Setup: Trace elements were analysed using the 213 nm, Teledyne Cetac Technologies, LSX G2 laser ablation unit installed at GSI, Faridabad and coupled with a Agilent Technologies 7700x mass spectrometer. The ICP-MS was operated at 1350 W plasma power. Ablations were performed in pure He-atmosphere (550ml min^{-1}) mixed before entering the Plasma torch with a flow of Ar (830 ml min^{-1}). Laser ablation conditions are: Laser power ~ 55% (2.5mJ) with pulse frequencies varying between 5 and 10 Hz and spot sizes of 50 - 30 μm, carrier gas flow (He + Ar) is 1.38 L min^{-1} in ICP unit. With such pulse frequencies, depth speed for silicates analysis is about 1 μm s^{-1}. Each analysis consists of 60 s of background analyses and 30 s of ablation or sample run time. Data reduction was carried out using the GeoPro software. Calibration for the analysis was carried out using NIST 612 and NIST 614 glasses as external standards [3].

Results and Interpretation: Detailed petrography, mineral phase chemistry, and P-T calibrations of solid-state thermal metamorphism have been attempted so far (Table-1). In-situ laser ablation was performed on olivine and enstatite chondrules (e.g. BO, PO, GO, POP, PP and GP) and mesostases. Our studies help to constrain trace elements and REEs budget among different genetic types of chondrites (H and L) highlighting elemental fractionation involving cosmo chemical process(es). Being of varied chemical and petrologic types, these two ordinary chondrites show microdomains of chemical and textural inhomogenity ([Ol]X_{Mg} = 0.73 – 0.86 and 0.68 - 1.00 varied in Dhajala and Khohar respectively), thermally equilibrated at ~ 850°C (± 50°), and having comparable HREE and LREE distribution pattern. Both the chondrites show characteristic (+ve) anomaly observed in U, Zr and strong (-ve) anomaly in Sr, Ti and Th, except for Khohar in which Th shows (+ve) anomaly (Figure 1a & b). Fractionation of these selective elements in various textural phases can be correlated either to their inherent chemical heterogeneity or other cosmochemical exogenic process (es) like solid to melt fractional crystallization due to collisions and/or cosmic nebular condensation.

a. Dhajala (H3.8)

b. Khohar (L3.6)
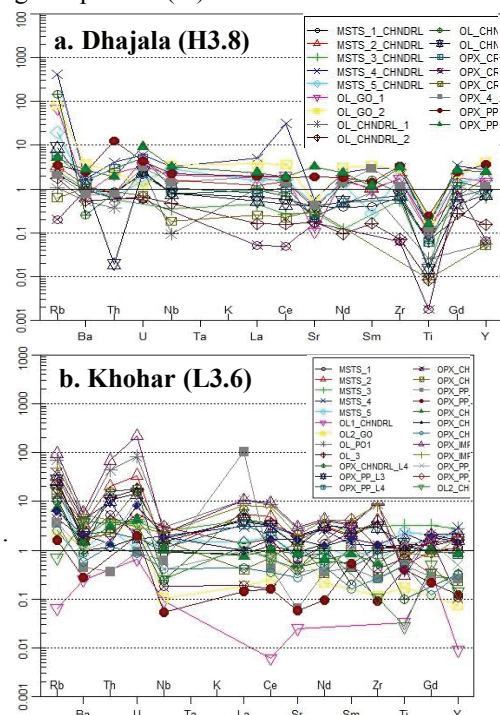
Table 1: Comparative data table of Dhajala (H3.8) and Khohar (L3.6) chondrites			
Meteorite Name & Type	Chondrule Texture / Type	Mineral Phase Chemistry	Equilibration Temperatures in °C
Dhajala (H3.8)	BO, POP, PP, PO, GO	[Ol]X_{Mg} = 0.73 – 0.86 and [Opx]X_{Mg} = 0.608 to 0.890.	850 (± 52)
Khohar (L3.6)	POP, BO, PO, PP, GP	[Ol]X_{Mg} = 0.68 – 0.88 & 0.92-1.00. [Opx]X_{Mg} = 0.70 to 0.86 and 0.91-0.98.	780 – 880 (± 50)

Figure 1a & b: Chondrite normalised REEs and trace elements spidergram [4] of Dhajala (H3.8) and Khohar (L3.6) chondrites obtained from olivine & Opx chondrules / clasts and mesostasis, analyzed by LA-ICPMS (Quadrapole).

References: [1] Jacquet E. et al. (2012) *Meteoritics & Planetary Science* 47:1695–1714. [2] Jacquet E. et al. (2015) *Geochimica et Cosmochimica Acta* 155:47–67. [3] Pearce N. J. G. et al. (1997) *Geostandard News Letters* 21: 115–144. [4] Sun S. S. (1982) *Cosmochim. Acta*, 46: 179-192.

Accounting for SLRs in the Early Solar System with a Triggered Star Formation Model for the Solar System

V. V. Dwarkadas[1], N. Dauphas[2], and B. Meyer[3], [1]Department of Astronomy and Astrophysics, University of Chicago (vikram@astro.uchicago.edu), [2]University of Chicago, [3]Clemson University.

Introduction: The early Solar System (ESS) was characterized by a value of ^{26}Al that exceeded the Galactic average [1,2,3,4], while ^{60}Fe in the ESS was about an order of magnitude less than the Galactic value [4,5]. These results disputed the existence of a supernova near the solar system at the time of formation. An alternative source of ^{26}Al is Wolf-Rayet (W-R) stars [5,6,7,8,9,10,11]. Aluminium-26 is carried out in the winds of these stars. No ^{60}Fe is ejected in the wind. [12] showed that a single W-R star above about 50 M$_\odot$ could be sufficient to provide the measured amount of ^{26}Al in the ESS. W-R stars have strong winds that sweep up the surrounding medium to form wind bubbles bordered by a dense shell. The ^{26}Al is carried out by dust grains in the wind from the star to the dense shell, where it is released. The solar system could be formed by triggered star formation in the dense shell.

Besides ^{26}Al and ^{60}Fe, many other short-lived radionuclides (SLRs) were present in the ESS [13,14]. We investigate whether the triggered star-formation model can account for the abundance of these SLRs, which could be (1) emitted by the star, carried out in the wind (via dust grains in this model) and injected into the dense shell, (2) be already prevalent in the local interstellar medium that was swept-up to form the dense shell or (3) be due to irradiation, from the SN following the W-R star if a SN explosion occurs, or from the early Sun.

Short-lived radionuclides: *^{10}Be* The abundance of this SLR is found to have a large range of values in meteorites. It does not correlate with ^{26}Al, which suggests a different source. It is most likely due to cosmic ray irradiation.

^{26}Al As was shown in [12], most stars above 50 M$_\odot$ can provide the level of ^{26}Al seen in the ESS, even accounting for the fact that only 10% of the ^{26}Al may eventually reach the dense shell.

^{36}Cl has a half-life of 0.3 Myr. The ESS ratio of ^{36}Cl/^{35}Cl was $1.7–3 \times 10^{-5}$ [15]. A single W-R star above 50 M$_\odot$ can account for the initial ESS ratio, according to stellar models [16]. Given the short half-life, this depends on when the ^{36}Cl is emitted. Being volatile, it is unlikely to be transported by dust grains, which makes a stellar origin difficult in this model. It can be formed by irradiation, which could be sufficient to explain its ESS abundance.

^{41}Ca has a half-life of 100,000 yr. [17] determined the value of ^{41}Ca/^{40}Ca in the ESS to be 4.2×10^{-9}. In principle the models of [16] suggest that W-R stars above 50 M$_\odot$ could easily provide the requisite amount of ^{41}Ca in the ESS. Due to the short half-life, one must account for exactly when in the evolution of the star the ^{41}Ca is emitted.

^{53}Mn has a large half-life whose exact value is still debated. It may be overproduced in massive stars that collapse to a supernova [18]. However a negligible amount is emitted in the winds of massive stars [16]. In our model we expect that the observed ^{53}Mn in the ESS would arise from the Galactic background, and be in the swept-up dense shell, part of which collapses to form the solar system. It could also be due to irradiation, as shown by [19].

^{60}Fe The ^{60}Fe in this model arises primarily from the Galactic background, similar to ^{53}Mn, and is present in the swept-up dense shell. With a half-life of 2.6 Myr, the ^{60}Fe will have time to decay, since the shell is swept up mainly in the main-sequence phase, and will therefore have a value equal to or less than the Galactic value.

^{107}Pd is produced by neutron capture on to ^{106}Pd. It can have contributions from both the *s* and *r* processes [14]. A recent investigation of the Muonionalusta meteorite quoted a value of ^{107}Pd/^{108}Pd in the ESS of $3.5–6.6 \times 10^{-5}$ [20]. [7] have shown that this required amount of ^{107}Pd can be produced in W-R stars.

^{129}I is exclusively produced by the *r*-process [22], but could include contributions from shell nucleosynthesis in massive stars [21]. Irrespective, ^{129}I in this model already existed in the Galaxy and was swept-up in the dense shell.

^{182}Hf This radionuclide can have both *r* and *s* process contributions, the latter primarily from AGB stars [22]. It is swept-up by the wind and is a part of the dense shell that ultimately collapses to form the solar system.

Summary: Triggered star formation in the shell of a W-R star can explain abundances of most SLRs. ^{41}Ca and ^{107}Pd, being refractory elements, would condense into dust grains and be transported similarly to ^{26}Al in our model.

References: [1] Lee T. et al (1976), *Geo. Res. Let., 3*, 109-112. [2] Jacobsen et al. (2008) *EPSL, 272*, 353-364. [3] McPherson et al. (1995) *Meteoritics, 30*, 365-386. [4] Tang H. & Dauphas N. (2012) *EPSL, 359*, 248. [5] Tang H. & Dauphas N. (2015) *ApJ, 802*, 22. [6] Arnould M. et al. (1997), *A&A, 321*, 452-464. [7] Arnould M. et al. (2006), *A&A, 453, 653-659*. [8] Gaidos E. et al. (2009) *ApJ, 696*, 1854. [9] Gounelle M. & Meynet G. (2012) *A&A, 545*, A4. [10] Young, E. D. (2014) E&PSL, 392, 16. [11] Young, E. D. (2016) ApJ, 826, 129. [12] Dwarkadas, V. V., Dauphas, N., Meyer, B., Boyajian, P., and Bojazi, M., (2017), ApJ, 851, 147. [13] Dauphas, N, & Chaussidon, M., (2011), *AREPS*, 39, 351. [14]Lugaro, M. et al (2018), *PrPNP*, 102, 1. [15] Tang, H. et al (2017), *GCA*, 2017, 1-18. [16] Sukhbold, T. et al (2016), *ApJ*, 832, 73. [17] Liu, M.-C. et al (2012), *ApJ*, 761, 137. [18] Vescovi, D., et al (2018), *ApJ*, 863, 115. [19] Leya, I., et al. (2003), *ApJ*, 594, 605-616 [20] Matthes, M. et al. (2018), *GeoCosmoActa*, 220, 82-95. [21] Bojazi, M., and Meyer, B., (2018), LPSC 49, 2083. [22] Lugaro, M. et al. (2014), *Sci*, 345, 650.

MURCHISON AND ALLENDE: CONTRASTS AND PERSISTENT PUZZLES.

D. S. Ebel[1,2,3] and K. V. Fendrich[1]. [1]Dept. of Earth and Planetary Sci., American Museum of Natural History, New York, NY, 10024, USA (debel@amnh.org), [2]Dept. Earth and Environmental Sci., Columbia U., New York, NY, USA, [3]Earth and Environmental Sci., CUNY Graduate Center, New York, NY, 10016, USA.

Introduction: Murchison (CM2) and Allende (CV3ox) falls are 2/3 of the 1969 "annus mirabilis" for sample-based planetary science. Murchison, a least-altered CM2 [1], is a breccia with planetary noble gas-rich accretionary dust rimming coarse components in primary accretionary rock, and solar noble gas and solar wind tracks in regolith-sourced clastic matrix portions [2,3]. Allende is a primitive accretionary rock affected by aqueous alteration [3, 4].

Methods: In [5] we describe methods of image analysis used to query every pixel in high resolution x-ray maps, such that the abundances of elements per pixel may be obtained for every inclusion, all matrix pixels, and for the entire mapped area (bulk). Samples of Murchison (6.56 mm^2, 3µm/pxl, 15ms, 40nA, primary accretionary portion [3]) and Allende (422.97 mm^2, 4-5µm/pxl, 20ms, 20nA) were mapped and analyzed. The figure shows outlined (in white) portions of each at the same scale, in Mg-Ca-Fe composite X-ray mosaics.
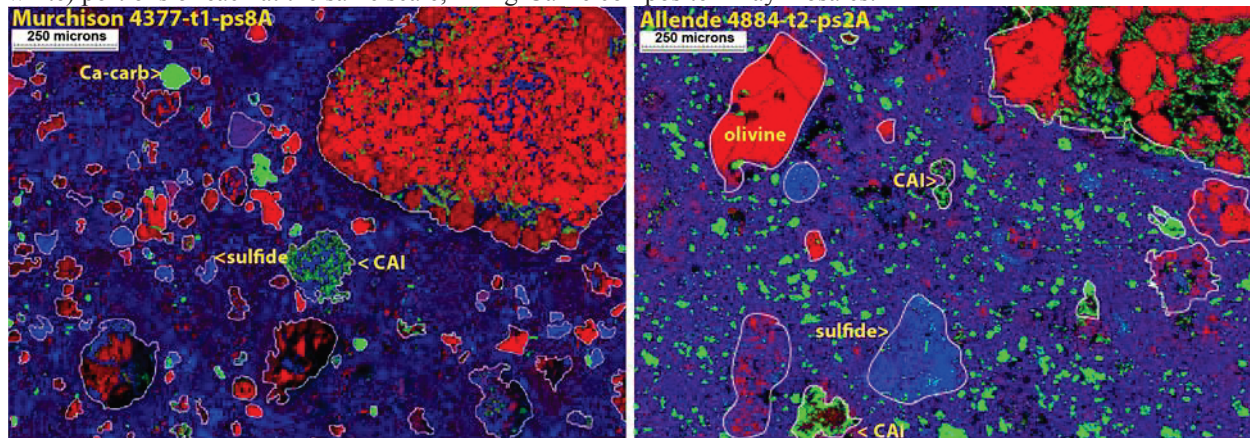
Fig. 1: Left: Murchison (partial), 3µm/pxl.   Mg-Ca-Fe = Red-Green-Blue   **Right:** Allende (partial), 4µm/pxl.

Results: Fig. 1 contrasts map portions at the same scale. Murchison has 23.3 vol% chondrules, 0.2 AOAs, 1.5 CAIs, 1.7 opaque phases, 2.1 isolated silicates and 71.3% matrix, compared to 35.5, 3.5, 4.3, 0.1 and 55.2% in Allende, respectively, based on our preliminary work. Murchison inclusions (Fig. 2) average 20% the size of Allende's.
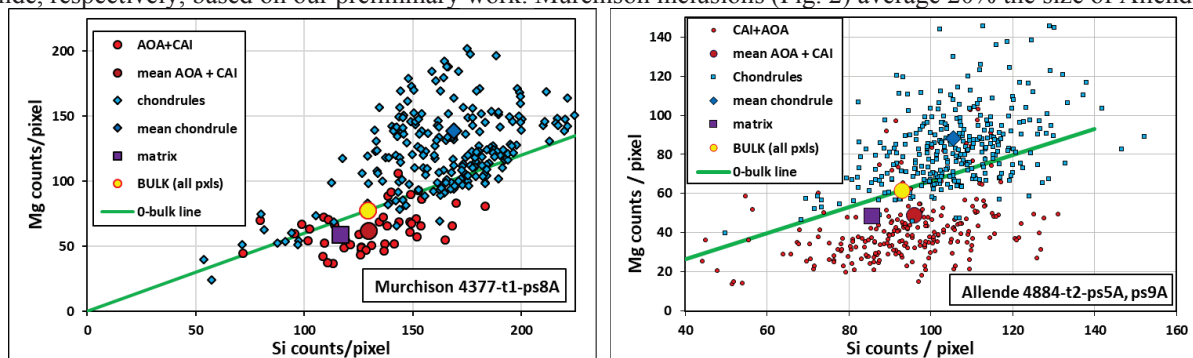
Fig 2: Mg-Si relationships as in [5]. Scales reflect different dwell time (ms) and current (nA). Matrix sums carbonate, opaques and isolated silicate. Both whole rock (bulk) Mg/Si are within a few % of the CI (solar) value.

Conclusion: Despite well-documented alteration, Murchison and Allende retain signals of chondrule and matrix origins in single reservoirs of precursors with ~solar Mg/Si. The role of CAIs and AOAs in Allende's 2.02 (±0.11) and Murchison's 0.89 (±0.03) mean (both flat) REE compositions (relative to Orgueil) remains mysterious [6].

References: [1] Browning et al. (1996) *Geochim. Cosmochim. Acta* **60**: 2621–2633. [2] Nakamura T. et al. (1999) *GCA* **63**: 241–255. [3] Bischoff et al. (2006) In *Meteorites and the Early Solar System II*, pp. 679-712. [4] Brearley A. J. (2006) In *MESS II*, pp. 567-586. [5] Ebel D. S. et al. (2016) *GCA* **172**: 322-356. [6] Dauphas & Pourmand (2015) *GCA* **163**: 234–261.

LABORATORY CT: A REVOLUTION IN PLANETARY SAMPLE PETROLOGY.

D. S. Ebel[1,2,3] and J. M. Friedrich[4,1]. [1]Dept. of Earth and Planetary Sciences, American Museum of Natural History, New York, NY, 10024, USA (debel@amnh.org), [2]Dept. Earth and Environmental Sci., Columbia U., New York, NY, USA, [3]Earth and Environmental Sci., CUNY Graduate Center, New York, NY, 10016, USA. [4]Department of Chemistry, Fordham University, Bronx, NY 10458 USA (friedrich@fordham.edu)

Introduction: High-resolution, non-synchrotron computed tomography or "laboratory CT" has rapidly become a standard method of sample characterization since being described as "a breakthrough technology for earth scientists" [1]. Most such systems are "cone beam" with helical instruments as a variant. In the USA, lab CT was pioneered in 1999 at U. Texas, Austin as an NSF-supported national shared multi-user facility [2, note web resources]. Tomography has become a topic with its own workshops (e.g., [3], with 8 instrument and 2 software vendors]. Tomography for Scientific Advancement (ToScA) is in its 7th year and will soon become a stand-alone society [4].

It is a good rule never to apply a single technique like CT to *all* of a sample. [8] reviews best practices for CT on natural history specimens, with lists of hardware and software vendors. Recent investigations have established that while x-ray CT induces thermoluminescence [5], it does not have measurable effects on amino acid chemistry [6,7].

While some vendors have a historical focus on research (e.g., XRE, spun off U. Ghent 2017, purchased by TESCAN 2018; SkyScan founded 1996 in Belgium, acquired by Bruker 2012), others (e.g., NSI) began focused on industrial metrology. The penetrating power (kV), resolution (nm, μm, mm per voxel edge) and specimen size accommodation within the shielded instrument volume are all critical in deciding on the best instrument for specific applications. Scan resolution depends on sample size; however, the unique optics of the ZEISS Xradia allow higher resolution scanning of subvolumes (UTCT has had one since 2008). The Johnson Space Center (Houston, USA) Curation Facility recently purchased a Nikon XT H 320 micro focus instrument with interchangeable 180, 225 and 320 tubes to characterize meteorites, clasts in lunar breccias, etc. Their policy is never to scan > 70% of any lunar rocks without very careful review, and to only scan smaller fractions of other samples (e.g., chondrites).

CT at AMNH: The AMNH purchased a GE/Phoenix VtomX S dual tube scanner in 2010 with NSF support. The instrument has interchangeable 35-180 kV and 40-250 kV tubes capable of imaging a wide range of materials. In a typical year with 260 days of operation, 5% were used by Earth and Planetary Science, 63% by Paleontology, 30% by zoology and 2% by Anthropology. Curators travel or send specimens to other locations for specialized imaging. Advantages of an "in house" CT facility include 1) proximity - travel is unnecessary, 2) no need to apply for synchrotron time, 3) lower risk to rare, sensitive samples. Disadvantages include competition for instrument time.

The technique: Interpretable data shows x-ray attenuation per volume element (voxel) [9]. Useful quantitative information from CT scans depends on segmentation. While determining porosity [10], object (chondrule) sizes [11], metal grain [12,13] and chondrule [14-17] orientations, and rim thicknesses [18] currently requires significant manual labor, CT represents a fundamental shift from the previous 150 years of understanding based on 2D slices of rocks as thin sections. We can now cut surfaces for 2D chemical analysis with precise 3D prior knowledge [19].

Challenges: Among the most pressing challenges are improving the ability to integrate (match) 3D data with electron beam, ion beam and other data on 2D surfaces. Composition based only on x-ray attenuation places inherent limits requiring 2D information. Visualization challenges depend on 3D segmentation quality, where automated neural networks (machine learning) are now being applied (e.g., by Marsh of ORS in [3]). Data size is also a growing barrier, particularly for the most cutting-edge applications (e.g., De Carlo in [3], 20 TB in 9 hours).

Outlook: Many laboratory CT vendor choices exist, each with a range of instruments. Improvements in workflow and machine learning will improve data extraction. Software packages [8, app. 8.3] allow for very hands-on data segmentation. The future of both synchrotron and laboratory CT looks bright [20]!

 References: [1] Rowe T. et al. (1997) Geotimes **42**:23-27. [2] UTCT lab, Texas: http://www.ctlab.geo.utexas.edu/ [3] ToScA N.A.: https://www.rms.org.uk/discover-engage/event-calendar/tosca-north-america-2019.html [4] ToScA international: https://www.toscainternational.org/ [5] Sears D. et al. (2018) *Meteor. Planet. Sci.* **53**:2624-2631. [6] Friedrich J. M. et al. (2016) *Meteor. Planet. Sci.* **51**: 429-437. [7] Friedrich J. M. et al., this workshop. [8] Keklikoglou K. et al. (c. 2017) http://synthesys3.myspecies.info/node/696 [9] Ebel D.S. & Rivers M.L. (2007) *Meteor. Planet. Sci.* **42**:1627–1646. [10] Friedrich J.M. et al. (2008) *Planet. Space Sci.* **56**:895–900. [11] Friedrich J.M. et al. (2015) *Lunar Planet. Sci.***46**, abs. 1937. [12] Friedrich J.M. et al. (2008) *Earth Planet. Sci. Lett.* **275**:172-180. [13] Friedrich J.M. et al. (2013) *Geochim. Cosmochim. Acta* **116**:71–83. [14] Friedrich J. M. et al. (2014) *Earth Planet. Sci. Lett.* **394**:13-19. [15] Ruzicka A.M. et al. (2017) *Meteor. Planet. Sci.* **52**:1963-1990. [16] Hanna R.D. et al. (2015) *Geochim. Cosmochim. Acta* **171**:256-282. [17] Lindgren et al. (2015) *Geochim. Cosmochim. Acta* **148**:159-178. [18] Hanna R.D. & Ketcham R.A. (2018) *Earth Planet. Sci. Lett.* **481**:201-211. [19] Ebel D.S. et al. (2008) *Meteor. Planet. Sci.* **43**:1725-1740. [20] Hanna R.D. and Ketcham R.A. (2017) *Chemie der Erde* **77**:547-572.

(Na-)Al-RICH CHONDRULES AND Ca,Al-RICH INCLUSIONS FROM UNEQUILIBRATED ORDINARY CHONDRITES

S. Ebert[1,2], A. Bischoff[1], and A. N. Krot[2]. [1]Universität Münster, Institut für Planetologie, Wilhelm-Klemm-Str. 10, 48149 Münster, [2]Hawai'i Institute of Geophysics and Planetology, School of Ocean and Earth Science and Technology, University of Hawaii at Manoa, 2525 Correa Road, Honolulu, HI 96822, USA; samuel.ebert@uni-muenster.de

Introduction: Meteorites carry the cosmological information and history of the first particles formed, evolved, and accreted into planetesimals. Ca,Al-rich inclusions (CAIs) are considered to be the oldest solids formed in the solar system [1] and are embedded together with chondrules, metals, and sulfides within matrix material of chondrites. Variations in mineralogy, petrology, and isotopic compositions of CAIs in different chondrite groups suggest that there are multiple generations of refractory inclusions. A connection between the generations of CAIs and chondrules has been insufficiantly clarified until today. Ebert and Bischoff [2] showed that Na-Al-rich chondrules, a variety of Al-rich chondrules [3,4], in ordinary and CO chondrites have volatility fractionated bulk rare earth element (REE) patterns similar to CAIs [5], and suggested that refractory materials, like CAIs, were a main part of the precursor material for these chondrules. However, Na-Al-rich chondrules in ordinary chondrites (OCs) have no enrichment in ^{50}Ti, which is in contrast to CAIs from carbonaceous chondrites (CCs) and Na-Al-rich chondrules in CO chondrites [6]. They concluded that refractory precursors – similar in mineralogy and chemistry to CAIs in CCs, but different in their ^{50}Ti – was part of the precursors of the Na-Al-rich chondrules in OCs. If this is the case, differences in isotopic compositions of CAIs in OCs and CCs may be expected. To gain more information about the origin of the Na-Al-rich chondrules and their precursors, additional (Na-)Al-rich chondrules and CAIs from ordinary chondrites were studied by SEM and EDX. Oxygen and Al-Mg studies of the (Na-)Al-rich chondrules and the refractory inclusions are in progress.

Results: 50 Al-rich chondrules (20 are Na-rich), 14 CAIs, and 2 AOAs from the unequilibrated ordinary chondrites NWA 3358 (H3.1), Adrar 003 (L/LL 3.1), Krymka (LL3.2), and Vicência (LL3.2) were identified. The Na-Al-rich chondrules are enriched in sodium (Na_2O >5 wt%) and aluminum (Al_2O_3 >10 wt%) and typically composed of magnesian olivine (Fa_{0-7}) and high-Ca pyroxene ($Fs_{0-9}Wo_{20-50}$) embedded in a glassy mesostasis (Figs. 1 and 2). The CAIs consist mainly of melilite, spinel, perovskite, and Al±Ti-diopside; secondary alteration minerals are minor (for example Fig. 3).
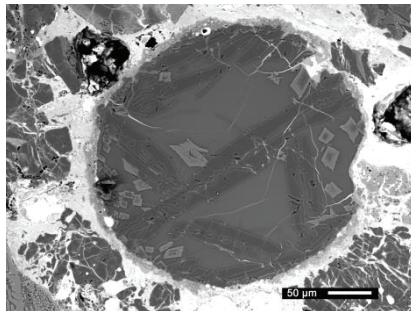
Figure 1: Na-Al-rich chondrule from NWA 3358 (H3.1) composed of magnesian olivine and high-Ca pyroxene phenocrysts embedded in a Na-rich glassy mesostasis.
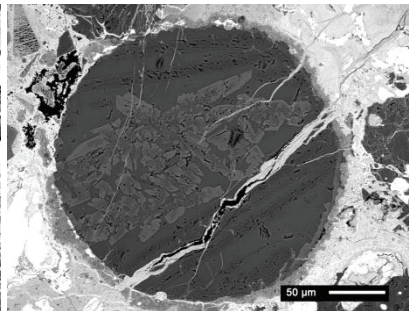
Figure 2: Na-Al-rich chondrule from NWA 3358 (H3.1) composed of magnesian olivine and high-Ca pyroxene phenocrysts embedded in a Na-rich glassy mesostasis.
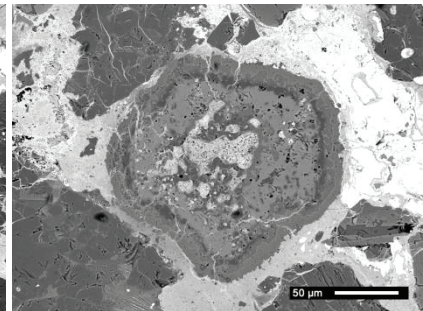
Figure 3: CAI from NWA 3358 (H3.1) consists of nepheline and anorthite (partly altered), melilite, spinel, and perovskite; it is rimmed by Al-diopside.

Discussion and Conclusions: (Na-)Al-rich chondrules and refractory inclusions are rare in ordinary chondrites [e.g., 2–4]. Therefore, a large number of these objects identified in UOCs provides an important dataset for investigating a genetic relationship between the Al-rich chondrules and refractory inclusions in these meteorites. The mineralogy and petrology of these objects combined with O- and Al-Mg-isotope measurements will help to reveal more information about their refractory precursors, which differ in their ^{50}Ti compared to those of known CAIs and Na-Al-rich chondrules in CCs [6].

References: [1] MacPherson G. J. (2014) *Treatise on Geochemistry* 1:139-179 [2] Ebert S. and Bischoff A. (2016) *Geochimica et Cosmochimica Acta* 177:182–204. [3] Bischoff A. and Keil K. (1983) *Nature* 303:588–592. [4] Bischoff A. and Keil K. (1984) *Geochimica et Cosmochimica Acta* 48:693-709 [5] Mason B. and Martin P. M. (1977) *Smithsonian Contribution to the Earth Sciences* 19:84-95 [6] Ebert S. et al. (2018) *Earth and Planetary Science Letter* 498:257–265.

RARE EARTH ELEMENTS AND O-Al-Mg ISOTOPE SYSTEMATICS FROM A >200 μm CORUNDUM GRAIN IN A CAI OF THE CK3 CHONDRITE NORTHWEST AFRICA 4964.

S. Ebert[1], M. Patzek[1], Q. R. Shollenberger[1], A. Bischoff[1], and G. A. Brennecka[1]. [1]Institut für Planetologie, Universität Münster, Wilhelm-Klemm-Str. 10, 48149 Münster; samuel.ebert@uni-muenster.de

Introduction: Corundum (Al_2O_3) is one of the first minerals predicted to condense from a gas of solar composition at pressures $<10^{-3}$ atm [1,2]. However, because it reacts with the cooling solar gas to form hibonite—and later grossite and melilite—corundum is rarely found in meteorites. Since corundum represents such an early formed phase, it is critical for our understanding of possible ^{26}Al heterogeneity in the protoplanetary disk and the evolution of its O-isotopic reservoir(s) (e.g., [3]). In this work, we present a very large (>200 μm) corundum grain from the CAI "Homer" [4] of the CK chondrite Northwest Africa 4964 which was investigated by measuring its chemical compositions, including rare earth elements (REE) contents, and the O and Al-Mg isotope systematics.

Results: Next to many small corundum grains (Fig. 1a, figure from [4]), the CAI "Homer" contains a very large single corundum grain of >200 μm length and 50 μm width (Fig. 1b). REE concentrations of the sample were measured by LA-ICP-MS (spotsize: 10μm and 40μm). Multiple elements were below detection limit in the corundum, and the combined results are shown Fig. 2. The light REEs are mostly depleted compared to those of the bulk CAI measurement and the surrounding material (mixture of plagioclase (An_{32-95}), Fe-rich spinel, and ilmenite). However, the heavy REEs exhibit a group II pattern similar to that of the bulk CAI "Homer" with the exception of a notable difference in Yb. This condensation pattern is well known from CAIs [5] and also from Na-Al-rich chondrules [6]. The O-isotopes of the grain plot with $\delta^{17}O$ = -3.93 ‰ and $\delta^{18}O$ = -0.69 ‰ directly in the field of CK chondrites next to the CO-CK-CM-Line. The Al-Mg isotopic data create a well-defined line with a slope of 3.15×10^{-6} which is significantly shallower than the canonical value of 5.23×10^{-5} [8].
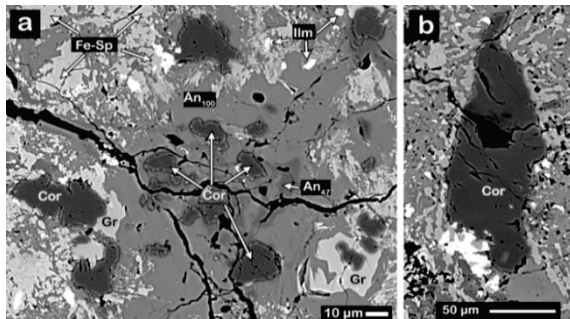
Figure 1: a) small corundum (Cor) grains intergrown with grossular (Gr) and Fe-rich spinel (Fe-Sp) and enclosed by anorthitic plagioclase (An). b) The large corundum grain with the surrounding material consisting of plagiclase, Fe-Sp, and ilmenite.
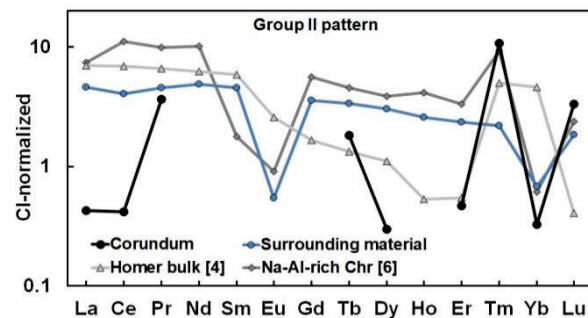
Figure 2: REEs of the corundum normalized to CI [7] indicating a group II pattern and similar to "Homer" bulk from [4]. Also sown are REE pattens of the surrounding material and a Na-Al-rich chondrule from [6]

Discussion and Conclusion: The group II REE pattern reveals a condensation origin of the corundum grain, showing that it was not formed during a later melting process. As corundum is one of the first oxides formed in a cooling gas of solar composition, it is of special interest when establishing relationships between O and Al-Mg isotopic systematics. However, Al-Mg work on the corundum grain indicates a significantly lower $^{26}Al/^{27}Al_{initial}$ than the canonical CAI value. Whereas a non-canonical value in a CAI could be caused by initial ^{26}Al heterogeneity in the CAI forming region, it could also be caused by secondary alteration processes. First, O isotopes of the corundum are indistinguishable from that of bulk CK chondrites, possibly pointing to alteration resetting the O-isotope composition on the parent body. Secondly, as the calculated initial $^{26}Al/^{27}Al$ of 3.15×10^{-6} (~3 Ma after CAIs) fits within the formation age of chondrules [e.g. 9 and references therein], it is likely that the Al-Mg and O isotopic systems are indicative of a heating event during chondrule formation and/or by thermal metamorphism on the CK parent body. Regardless of the origin of the disturbance, it does not appear that the O and Al-Mg isotopes in this very large corundum grain are useable for determining any potential links between the two isotopic systems.

References: [1] Grossman L. (1972) *Geochimica et Cosmochimica Acta* 36:597-619. [2] Yoneda S. and Grossman L. (1995) *Geochimica et Cosmochimica Acta* 59:3413-3444. [3] Makide K. et al. (2011). The Astrophysical Journal Letters 733:L31. [4] Shollenberger Q. et al. (2018) *Geochimica et Cosmochimica Acta* 228:62-80. [5] Mason B. and Martin P. M. (1977) *Smithsonian Contribution to the Earth Sciences* 19, 84-95. [6] Ebert S. and Bischoff A. (2016) *Geochimica et Cosmochimica Acta* 177:182-204. [7] Barrat J.-A. et al. (2012) *Geochimica et Cosmochimica Acta* 83:79-92. [8] Jacobsen B. et al. (2008) *Earth and Planetary Science Letters* 272:353-364. [9] Pape J. et al. (2019) *Geochimica et Cosmochimica Acta* 244:416-436.

VISUAL SPECTRUM OF CHONDRITE L6 METEORITE OZERKI

A.V. Efimov[1], A.P. Kartashova[2], A. K. Murtazov[1], [1]Ryazan State University, 390000, 46 Svobody St., Ryazan, Russia; (a.efimov@365.rsu.edu.ru, akmurtazov@gmail.com), [2]Institut of astronomy of The Russian academy of sciences, 119017, 48 Pyatnitskaya St., Moscow, Russia (akartashova@inasan.ru)

The task of measuring terrestrial rock reflectance spectra and their comparison with the spectra of meteoroids and asteroids is extremely important. It is related both to the Solar system body origin and evolution problem, and the problem of detecting space bodies dangerous for the Earth.

One of our coauthors was lucky to find a small fragment of the Ozerki meteorite.

The Ozerki meteorite fall occurred June 21, 2018 near the city of Lipetsk, Russia. It is classified as an Ordinary chondrite L6S4-5W0 (Шарыгин). The meteorite is covered with the crust resulting from its burnout while passing through the atmosphere (Figure 1). The inside part with the basic substance looks typical of chondrites.

We measured the scattering spectrum of this part of the Ozerki meteorite.

We conducted the measuring of the reflectance spectra, based on the methods previously used for the experiments on physical simulation of photometric and spectral characteristics of satellite and asteroid surfaces.

We used a small-size monochromator with a 3-4 nm/mm dispersion concave diffraction grating. As a receiving instrument, we used a photoconductor which is sensitive within the range of 400-900 nm. The incident and scattering light beams formed the angles of 0 and 45 degrees, respectively, to the sample surface normal. For the standard, the flat surface of MgO was used. The relative error of the measurements was 3-4% in the middle of the spectral range and grew up to 10-12% at the range's limits.

Figure 2 shows the averaged Ozerki meteorite spectrum as compared to the basalt lava from Tenerife.

The simplest comparative analysis of the Ozerki meteorite spectrum and volcanic basalt lava with the spectra of stony meteorites and asteroids shows, that visibly they are sufficiently close.

Figure 1. Fragment of Ozerki meteorite L6 (Lipetsk, 2018)
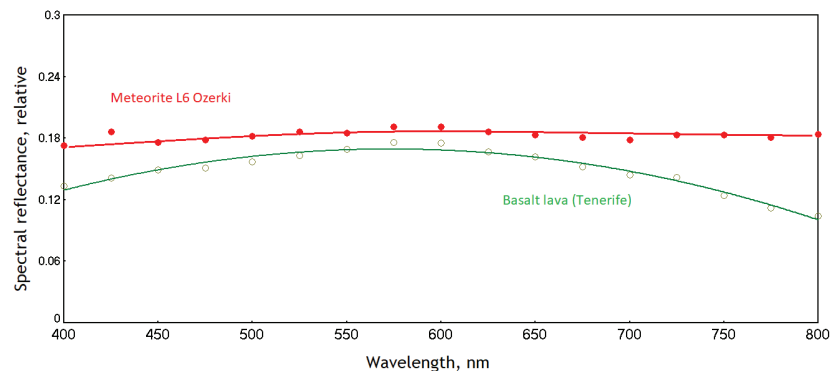
Figure 2. Ozerki meteorite and basalt lava spectra

References

[1] Busarev V.V. (2016) *Solar system research* 50:13-23. [2] Chapman D., Morrison B., Zellner B. (1975) *Icarus* 25:104-–130. [3] Cloutis E.A., Gaffey M.J., Moslow T.F. (1994) *Icarus* 107:276-287. [4] Cloutis E.A., et al. (2011) *Icarus* 212:180–209. [5] Hiroi T., et al. (1993) *Icarus* 102:107-116. [6] Johnson T. V., Fanale F. P. (1973) *Journal of Geophysical research* 78:8507-8518. [7] McFadden L.A. et al. (2015) *Icarus* 259:150-161. [8] Moroz L.V., et al. (1996). *Icarus* 122:366–382. [9] Murtazov A.K. (2016) *Astronomical and Astrophysical Transactions* 29:519-528. [10] Murtazov A. K., Efimov A. V. (2017) *Ecological Bulletin of Research Centers of the Black Sea Economic Cooperation* 4:117-123. [11] Murtazov A. (2018) *Meteoritics&Planetary Science*. 53: A 218. [12] Sharygin V.V. (2018) 18th Russian conference on fluid inclusions at Moscow, September. [13] Trigo-Rodriguez J.M., et al. (2013) *MNRAS* 437:227-240. [15] Vernazza P., et al. (2008) *Nature* 454:858-860.

THE ORIGIN OF THE MISSING NUCLEOSYNTHETIC ISOTOPE VARIATIONS IN HEAVY REFRACTORY ELEMENTS.

M. Ek[1], A. C. Hunt[1], M. Lugaro[2,3] and M. Schönbächler[1], [1]Institute for Geochemistry and Petrology, ETH Zürich, 8092 Zürich, Switzerland. [2]Konkoly Observatory, Hungarian Academy of Sciences, H-1121 Budapest, Hungary. [3]Monash Centre for Astrophysics, Monash University, VIC 3800, Australia.

Introduction: Terrestrial planets and asteroids are characterized by distinct nucleosynthetic compositions. These stem from the heterogeneous distribution of presolar grains from different stellar sources in the solar protoplanetary disk. Four first order characteristics of theses variations are: (i) Enrichments in neutron-rich isotopes of lighter elements (e.g., ^{48}Ca, ^{50}Ti and ^{54}Cr) relative to the Earth are well established for carbonaceous chondrites. These data point towards an enrichment of supernova material in the outer solar system. (ii) Correlated variations of Zr, Mo, Ru and Pd isotopes in different planetary bodies reflect the heterogeneous distribution of *s*-process material, with the Earth displaying the strongest *s*-process enrichment [1]. (iii) Such *s*-process excesses are also identified for the heavier elements Nd and W e.g., [2]. However, these elements show variations that are consistently smaller (few parts per million) than those of lighter isotopes (e.g. Zr and Mo; 10 - 200 ppm). Overall, nucleosynthetic variations of heavier elements (Hf, W, Os, Pt, Hg) at bulk rock scale are very small or not resolvable. (iv) Non-refractory elements (Pd, Cd, Sn) display subdued or no nucleosynthetic variations [1,3].

Discussion: In previous work, we attributed the subdued nucleosynthetic variations in Pd isotopes relative to the neighboring refractory elements (Zr, Mo, Ru) to incomplete condensation around asymptotic giant branch (AGB) stars, the site of *s*-process nucleosynthesis [1]. It mirrors the fact that Pd is less refractory than Zr, Mo and Ru. This conclusion is also supported by new high precision data of moderately volatile elements (Cd, Sn), which generally show isotopic homogeneity in the solar system [3]. In agreement with this idea, a limited fraction of the synthesized mass in AGB stars condenses in the envelope of the star itself, while the rest enters the interstellar medium (ISM) as a gas [4]. The more volatile elements returned in the gas phase to the ISM become well mixed with those from other nucleosynthetic sources and are incorporated into ISM solids without preserving a distinct *s*-process signature [5]. In line with this, most presolar grains in primitive meteorites originate from AGB stars with only small contributions from supernovae environments.

While the volatility dependence readily explains the general nucleosynthetic homogeneity in volatile elements, it cannot account for the subdued or missing effects in heavy refractory elements. Missing nucleosynthetic offsets in neutron-rich Hf isotopes compared to the geochemically similar, lighter Zr isotopes were attributed to the decoupling of nucleosynthetic production sites [6]. Akram and co-worker [6] proposed that the light neutron-capture isotopes (e.g., ^{96}Zr) were mainly produced in Type II supernovae (SN) with higher mass progenitors than the SN that synthesized the heavy *r*-process isotopes. Since recent advances indicate that neutron star mergers may be the source of the main *r*-process, this could also indicate a decoupling of SN versus neutron star merger material. In the context of the Akram et al. model [6], the light isotopes (e.g. ^{96}Zr or ^{50}Ti) were mainly formed via charged-particle reactions in a high entropy wind environment, in which Hf isotopes are not produced, thereby explaining the missing Hf isotope variations. Hence, this scenario can account for the missing *r*-process/supernova anomalies in heavier elements (Z > 55). It cannot, however, explain the subdued or missing anomalies in *s*-process isotopes. Here, we propose that the *s*-process trend was set by the initial metallicity of the AGB stars that contributed most presolar grains to the solar system. Based on SiC grains, most *s*-process presolar grains in the solar protoplanetary disk likely originated from AGB stars with high metallicities [7]. Elements heavier than Cs (Z > 55) are less readily produced in AGB stars as metallicity increases, relative to Zr, Mo, Ru and Pd. This is because Fe seeds are more abundant in higher metallicity stars and thus capture more neutrons [8]. This impedes the production of heavier *s*-process elements. At the same time, the production of SiC and silicate dust increases with metallicity [4]. The reduced production of heavy nuclei combined with increased dust production leads to a presolar grain population depleted in heavy isotopes. As a result, the concentrations of heavier elements (Z > 55), relative to Zr, Mo and Ru, are lower than in the bulk solar system *s*-process component inherited from ISM dust. The heavier elements are primarily carried by ISM dust, which acquired homogenized material from AGB stars with a variety of metallicities. This led to the smaller or non-detectable *s*-process effects of heavier refractory elements in planets and asteroids.

References: [1] Ek M. et al. (2018) *LPS 49,* Abstract #1973. [2] Burkhardt C. et al. (2016) *Nature* 537:394-398. [3] Toth E. R. et al. (2017) *80th Annual Meeting of the Meteoritical Society,* Abstract #6122. [4] Ferrarotti, A.S. and Gail, H.-P. (2006) *Astronomy & Astrophysics* 447:553-576. [5] Zhukovska, S. et al. (2008) *Astronomy & Astrophysics* 479: 453-480. [6] Akram, W. et al. (2015) *The Astrophysical Journal Letters* 777:169-181. [7] Lugaro M. et al. (2018) *Geochimica et Cosmochimica Acta* 221: 6-20. [8] Cseh, B. et al. (2018). *Astronomy & Astrophysics* 620:A146.

INNER SOLAR SYSTEM IRRADIATION HISTORY OF MINERALS IN AN ULTRACARBONACEOUS ANTARCTIC MICROMETEORITE (UCAMM).

C. Engrand[1], E. Charon[2], H. Leroux[3], C. Le Guillou[3], J. Duprat[1], E. Dartois[4], S. Bernard[5], B. Guérin[1], L. Delauche[1], M. Godard[1]. [1]CSNSM CNRS/Univ. Paris Sud, Univ. Paris-Saclay, 91405 Orsay Campus, France (cecile.engrand@csnsm.in2p3.fr), [2]NIMBE, CEA, CNRS, Univ. Paris-Saclay, CEA Saclay 91191 Gif-sur-Yvette France. [3]UMET Univ. Lille 1, 59650 Villeneuve d'Ascq, France. [4]ISMO CNRS/Univ. Paris Sud, Univ. Paris-Saclay, 91400 Orsay, France. [5]IMPMC, CNRS, Sorbonne Université, MNHN, 4 place Jussieu, 75005 Paris, France.

Introduction: Ultracarbonaceous Antarctic Micrometeorites (UCAMMs) are interplanetary dust particles containing large amounts of N-rich polyaromatic organic matter exhibiting large D enrichments, with heterogeneous distributions of both D/H and ^{15}N/^{14}N isotopic ratios [1-8]. UCAMMs most probably originate from the outer regions of the protoplanetary disk, i.e. the cometary reservoir [2, 4, 5]. At least three kinds of organic matter have been identified in UCAMMs, with different nitrogen abundances and highly variable concentrations of small (typically 30-500 nanometer) minerals embedded in the organic matter [8-11]. The formation process(es) of the different kinds of organic matter found in UCAMMs and the origin of their mixing with minerals are still a matter of debate. We focus here on a mineral assemblage embedded in one UCAMM (DC06-04-43) in which we have found evidence of irradiation.

Results and discussion: A 100 nm-thick FIB section was made at IEMN Lille from a fragment of UCAMM DC06-04-43. This section was examined by STXM-XANES followed by transmission electron microscopy (TEM) [11]. The mineralogy of this UCAMM is dominated by a crystalline assemblage consisting of µm-sized Mg-rich pyroxenes, Fe sulfides, Mg-rich olivines, and Fe-Ni metal. GEMS are embedded in the organic matter, close to the crystalline assemblage. We identified irradiation features (rims and tracks) in some crystalline pyroxenes. The rims' thicknesses range from 20 to 100 nm (average 60 ± 20 nm, 1σ) and irradiation track lengths from 15 nm to ~ 1 µm (average 175 ± 110 nm, 1σ). The average track density is 1.72×10^{10} cm^{-2} (772 tracks over 4.2×10^6 nm^2).
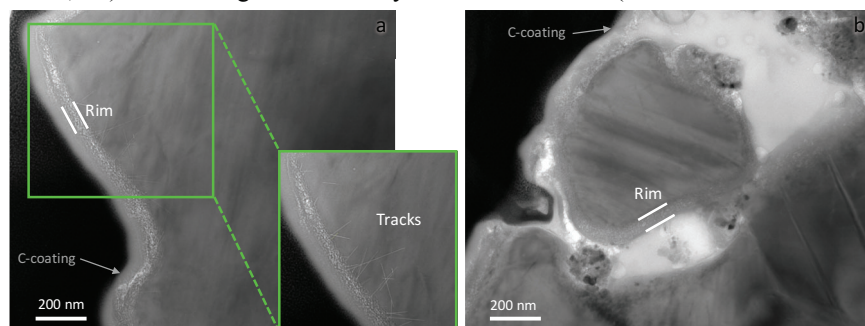
Figure: a) TEM micrograph of a pyroxene showing both irradiation rim and tracks. The tracks are highlighted in the bottom-right inset. b) irradiation rim observed around another pyroxene mineral, including on the side in contact with the organic matter. a & b: the smooth grey layer in contact with the platinum (in black) is a carbon coating applied to the sample for initial investigation by scanning electron microscopy before FIB-sectioning.

SRIM calculations [12] indicate that the observed average rim thickness corresponds to irradiation of the pyroxene by ions with energies ranging from 1 to 10 keV/nucleon, whereas the track lengths are compatible with an irradiation by Solar energetic particles (SEP). The irradiation damages of these minerals are compatible with irradiation in the inner solar system (solar wind and SEP). The average track density corresponds to a few hundred thousand years exposure in space, using the current track production rate at 1 AU determined by Berger & Keller [13]. This exposure time may have been shorter considering early irradiation by the more active young Sun. The observation of irradiation rims in minerals embedded in the organic matter implies an irradiation of these minerals before transport to the outer regions of the protoplanetary disk and later incorporation in the UCAMM parent body. In the scenario where the N-rich organic matter is formed by irradiation of ices by Galactic cosmic rays [4, 14], these minerals would be shielded from irradiation (e.g. buried in ice) in the parent body. The fact that crystalline minerals are usually found in association with low-N organic matter suggests that the low-N and N-rich organic matters in UCAMMs formed in different locations, and/or over different timescales.

References: [1] Nakamura T., et al. (2005). *MAPS* 40S: #5046. [2] Duprat J., et al. (2010). *Science* 328: 742-745. [3] Dobrică E., et al. (2011). *MAPS.* 46: 1363-1375. [4] Dartois E., et al. (2013). *Icarus* 224: 243-252. [5] Dartois E., et al. (2018). *A&A* 609: A65. [6] Duprat J., et al. (2014). *MAPS.* 49S #5341. [7] Bardin N., et al. (2015). *MAPS* 50S #5275. [8] Yabuta H., et al. (2017). *GCA* 214: 172-190. [9] Dobrică E., et al. (2012). *GCA* 76: 68-82. [10] Engrand C., et al. (2015) *LPSC* 46: #1902. [11] Charon E., et al. (2017). *LPSC* 48: #2085. [12] Ziegler J.F. (2013) SRIM - http://srim.org/. [13] Berger E.L. and Keller L.P. (2015) *LPSC* 46: 1543. [14] Augé B., et al. (2016). *A&A.* 592: A99.

SYNTHESIS OF GEMS IN THE SYSTEM Fe-Mg-Si-O-S WITH CHANGE IN REDOX CONDITION

Satomi Enju[1], Hayate Kawano[2], Akira Tsuchiyama[1,3], Tae-Hee Kim[4], Aki Takigawa[2,5], Jyunya Matsuno[2] and Hisashi Komaki[6] [1]Research Organization of Science and Technology, Ritsumeikan University. [2]Department of Earth and Planetary Sciences, Graduate School of Science, Kyoto University. [3]Guangzhou Institute of Geochemistry. [4]Institute for Nuclear Science and Technology, Department of Nuclear and Energy Engineering, Jeju National University. [5]The Hakubi Center for Advanced Research, Kyoto University. [6]JEOL Ltd.

Introduction: Glass with embedded metal and sulfides (GEMS) is a major component of chondritic-porous interplanetary dust particles (CP-IDPs) [1] and also found in micrometeorites [2], which are thought to be one of the most primitive materials in the solar system. Materials similar to GEMS are also observed in the matrices of primitive carbonaceous chondrite meteorites [3,4,5]. Several formation models based on observation of GEMS are proposed, but they are still under debate [6,7]. Synthetic experiments are performed to form GEMS analog particles [8,9]. These experiments, however, did not examine the effect of sulfur, which is one of the major elements in GEMS. In this study, synthetic experiments are performed in the system Fe-Mg-Si-O-S, with the systematic change in redox condition, to understand the GEMS forming condition.

Methods: Induction thermal plasma (ITP) system was used for the condensation experiment. This system creates a high-temperature plasma (around 10^4K) which evaporates injected starting materials. Fine particles then condense in rapid cooling environments. Plasma gas is Ar and He, with a chamber pressure of 70 kPa. The starting material is a mixture of powder regents (SiO_2, Si, MgO, Fe, FeS_2) with the GEMS mean composition [7]. Redox condition was controlled by changing the SiO_2/Si ratio and feeding rate of the starting material. Products were analyzed using X-ray diffraction, scanning electron microscope, and transmission electron microscope.

Result and Discussion: The condensed products were amorphous silicates with Fe-bearing nano-inclusions with various textures and chemical compositions depending on the experimental conditions. The condensed grains were categorized into five types based on the Fe content and the existence of liquid immiscibility of the amorphous silicate and the phase of the nano-particles, which showed correlation with the redox conditions. In oxidizing conditions, Fe is mostly included in amorphous silicate as FeO, with FeS nano-particles. In intermediate redox conditions, the FeO content in amorphous silicate decreases and Fe metal and FeS nano-particles are present. In reducing conditions, amorphous silicate contains little FeO and Fe_3Si, FeS and MgS nano-particles appears. FeO-poor amorphous silicates showed texture indicating two-liquid immiscibility, which strongly suggests that the amorphous silicate particles condensed as melt phase and was transferred to the amorphous state by rapid cooling. The shape and peak position of the IR spectrum of the condensate in the present experiments is similar to those of GEMS [10]. Spectral feature showing the two-liquid immiscibility can be recognized in GEMS but not clearly seen in interstellar dusts. This suggests that GEMS formed by condensation in the early solar nebula.

The formation model on each type of the condensed grains was proposed by considering the timing of the nucleation of Fe metal nano-particle and glass transition of from the silicate melt, transportation of the Fe particles into silicate melt, and reaction of the Fe nanoparticles with S-rich gas. The condensation condition of typical GEMS may have occurred in intermediate or slightly reducing condition of the present experiments, with more Fe-rich and/or Si-poor condition than the present experiments.

Condensates of Fe-rich amorphous silicates with FeS nano-particles in oxidizing runs have similar textures to GEMS-like materials in the matrices of primitive carbonaceous chondrites [3,5]. This indicates the possibility of the formation of the GEMS-like material by direct condensation from nebula gas. FeO-rich features of amorphous silicates in the GEMS-like materials is not only the result of aqueous alteration causing Fe-enrichment of amorphous silicates by oxidation of Fe metal nanoparticles but also the result of direct condensation of oxidative grains [11].

References: [1] Bradley J. P. (1994) *Geochim. Cosmochim. Acta,* 58, 9, 2123-2134. [2] Noguchi T. et al. (2015) *Earth and Planetary Science Letters,* 410, 1–11. [3] Leroux H. et al. (2015) *Geochim. Cosmochim. Acta,* 170, 247-265. [4] Nittler L.R. et al. (2019) *Nature astronomy*, published on April 15. [5] Matsumoto M. et al., *Meteoritics & Planetary Sciences* 53, Issue S1. 6100. [6] Bradley J.P. and Dai Z.R. (2004) *The Astrophysical Journal*. J. 617, 650–655. [7] Keller L.P. and Messenger S. (2011) *Geochim. Cosmochim. Acta*, 75, 5336-5365. [8] Matsuno J. (2015) *Ph.D. thesis*. [9] Kim T. et al. (2017) *ISPC*, Abstract, 23, P2-33-7. [10] Bradley J. P., et al. (1999) *Science*, 285, 1716–1718. [11] Tsuchiyama A. et al. (2019) *This meeting*.

FORMATION PROCESSES OF SECONDARY DMISTEINBERGITE AND ANORTHITE IN ALLENDE CAI.

Y. Enokido[1], T. Nakamura[1], M. Matsumoto[1], A. Miyake[2], [1]Division of Earth and Planetary Sciences, Graduate School of Science,Tohoku University, Japan (yuma.enokido.r8@dc.tohoku.ac.jp), [2]Division of Earth and Planetary Sciences, Graduate School of Science, Kyoto University.

Introduction: Polymorph of anorthite, "dmisteinbergite" ($CaAl_2Si_2O_8$) has been reported only in some CV_{oxA} CAIs [1-5]. Previous studies have shown that there are two types of dmisteinbergite which have different origins; one crystallized from melts [6] (we call this type "primary dmisteinbergite") and one by aqueous alteration of primary minerals [7] (secondary dmisteinbergite). In CV_{oxA} chondrites, the secondary dmisteinbergite often co-occurs with secondary anorthite in the same CAI [2]. Formation condition of these secondary phases and relationships between them still remain unknown. To uncover these problems, we performed mineralogical and petrological observation of one large CAI in Allende meteorite.

Methods: We studied one coarse-grained CAI (~1 mm in diameter) in a polished thin section of Allende chondrite. The mineralogy and petrology of the sample were examined using scanning electron microscopy (FE-SEM/EDS: JEOL JSM-7001F/Oxford INCA), and electron probe microprobe analyzer (FE-EPMA/WDS: JEOL JXA-8530F). Mineral identification was based on micro-laser Raman spectroscopy (NRS-5100 532nm). We extracted two ultra-thin sections using a focused ion beam (FIB: Thermo Fisher Scientific Quanta 200 3DS) and investigated them using a transmission electron microscopy (TEM: JEOL JEM-2100F).

Results and Discussion: In the CAI, secondary dmisteinbergite and anorthite mostly occur in different areas. Only in limited areas, they intergrow in μm-scales. Dmisteinbergite crystal shows platy morphology and coexists with grossular and gehlenite-rich melilite (Geh_{80-85}). Melilite is one of the major primary minerals in CAI. We found that dmisteinbergite only formed in outer margin of coarser melilite grains by partial alteration and that grossular occurs between dmiteinbergite and melilite. Therefore, it is suggested that melilite is the precursor of dmisteinbergite (i.e. dmisteinbergite is pseudomporph of melilite). Sequential alteration seems to occur from melilite to grossular and then grossular to dmisteinbergite. These formation orders are consistent with previous experimental studies [7, 8]. These studies have shown that the alterations could have occurred at moderate temperature (200–250 °C) and high-pH fluids environment. Therefore, moderate temperature and high-pH had been kept during the sequence alteration to form dmisteinbergite.

Secondary anorthite is more abundant than dmisteinbergite and coexists with grossular and melilite. What is the formation process of secondary anorthite? What caused the difference between formation of secondary anorthite and dmisteinbergite? To uncover this problem, we performed TEM observations of the area where dmisteinbergite and anorthite intergrow in μm-scale. TEM observation shows that coarse-grained dmisteinbergite is dominant and partially replaced by fine-grained anorthite. This texture indicates that secondary anorthite was formed through phase transition from secondary dmisteinbergite. There are two possible mechanisms for the phase transition: further water-rock interactions and shock induced transformation. The occurrence of both dmisteinbergite and anorthite mean that distribution of aqueous solution and/or shock induced pressure were heterogeneous at a few hundrends of μm scale inside the CAI. What caused this heterogeneity? We found that many dmisteinbergite grains are enclosed by other primary minerals such as Ca, Ti-rich pyroxene, which limits the exposure to solution or shock deformation. In either case, the position and distribution of dmisteinbergite is important for phase transition to occur.

Chemical composition of the secondary anorthite is close to the stoichiometry. On the other hands, composition of dmisteinbergite shows some variation of Si, Al-contents. This variation is resulted from (1) the presence of co-existing micron-size mineral grains and/or (2) just the chemical variation of dmisteinbergite itself. Especially, the vatiation caused by (2) is important because, during phase transition from dmisteinbergite to anorthite, chemical composition must have changed. We found that some anorthites coexist with Al-rich unknown phase. This phase may have been formed during the phase transition.

Conclusion: Our observation strongly supports the idea that, in CV_{oxA} CAI, secondary dmisteinbergite was formed from melilite via grossular in presence of liquid water of high pH at moderate temperature (200–250 °C). And we suggested the new idea that secondary anorthite formed from secondary dmisteinbergite probably caused by continuous water-rock reaction or shock induced transformation.

References: [1] Ma C. et al. 2013. *American Mineralogist*, **98**: 1368–1371. [2] Fintor K. et al. 2014. *Meteoritics & Planetary Science* **49**, 812–823. [3] Park. C. et al. 2013. 76th *Meteoritical Scoiety Meeting #5048.* [4] Enokido Y. et al., 2014. 5th *Symposium on Polar Science* [5] Krot A. N. et al. 2019. *GCA* **246**: 419–435. [6] Abe T. and Sunagawa I. 1995. *Mineralogical Journal,* **17**: 257–281. [7] Borglum B. P. et al. 1993. *J. Am. Ceram. Soc.* **76**: 1354–1356. [8] Nomura K. and Miyamoto M. 1998. *GCA* **62**: 3575–3588.

INVESTIGATING THE LINK BETWEEN CARBONACEOUS AND ORDINARY CHONDRITES AND THEIR ASTEROIDAL PARENT BODIES.

J. Eschrig, L. Bonal, P. Beck, T. J. Prestgard - Institut de Planétologie et d'Astrophysique de Grenoble – Université Grenoble Alpes, CNRS (Grenoble - France) (jolantha.eschrig@univ-grenoble-alpes.fr)

Introduction: Reflectance spectroscopy is currently the only measuring method for the remote characterization of asteroidal bodies besides the characterization in laboratory of asteroidal samples collected through space missions. It is thus important to improve the understanding we have of the different spectral features observed in the asteroidal reflectance spectra. As these features are generally very faint [e.g., 1] in the 0.45 - 2.45 μm spectral region, this task becomes increasingly difficult. Analyzing the reflectance spectra acquired for different carbonaceous and ordinary chondrite types in the laboratory allows to further interpret the asteroidal spectra and establish some genetic links between meteorites and asteroids. This has been the subject of several papers in the past [e.g., 2]. Here we are taking advantage of a new spectro-radio goniometer available at IPAG [3] to measure a large set of samples with a well-constrained post-accretion history. Measurements under vacuum and at 80°C significantly improve the quality of the spectra. Our objectives are to *(i)* further our understanding of spectral features, *(ii)* understand if some are controlled by secondary processes such as thermal metamorphism, and *(iii)* establish some genetic link between asteroids and carbonaceous chondrites, that are in some cases only very faint.

Samples and Methods: In this work a total of 21 CV chondrites, 16 CO chondrites, 4 CR chondrites and 15 ordinary chondrites are measured with the SHADOWS instrument [3]. The measurements were done on powdered bulk material in the 0.4 – 4.2 μm spectral region, at 80°C and under vacuum (P < 10^{-4} mbar). The selected samples feature a wide range of metamorphic grades, that were previously determined through Raman spectroscopy [4]. A set of well-defined spectral properties, including absorption band depths, positions and spectral slopes, are considered following previous works [e.g., 2] to describe the individual whole-rock reflectance spectra. Additionally, 12 mean reflectance spectra from the asteroidal belt [1] of the types A, K, L, O, Q, R, S, Sa, Sq, Sr, Sv, and V, 24 EOS family member spectra [5] and 8 CK chondrites (RELAB database (http://www.planetary.brown.edu/relab/)) were treated in the same way as the other chondrites and added for comparison purposes.

Results and Discussion: Generally, a large variability in the reflectance spectra of samples of the same chondrite group is observed. Nevertheless, there are clear differences in the reflectance spectra of different chondrite groups. Ordinary chondrites systematically exhibit deeper absorption features which are located at lower wavelengths in comparison to carbonaceous chondrites. Type 2 CR chondrites exhibit 1000 nm absorption features at even lower wavelengths than ordinary chondrites, thus clearly separating them from type 3 chondrites. On the other hand, independent of the spectral features, CO and CV chondrites do not plot appart which is not that surprising due to their comparable mineralogical composition [6]. Several spectral features appear to be controlled by the metamorphic grade of the samples. The depth of the 1000 nm absorption band becomes deeper with increasing metamorphic grade for CV chondrites. This was not previously observed [2] which might be related to the much higher number of CV chondrites considered here. To be noted, this correlation is not observed for the other chondrite groups. For CO chondrites the visual slope defined in the 340 to 520 nm wavelength range becomes steeper with bluer overall spectral slopes. Moreover, the visual slope seems to be linked to the peak reflectance value in the visible wavelength range located at approximately 700 nm and the 2000 nm absorption band feature. With increasing visual slope, the peak reflectance in the visible becomes higher and the 2000 nm absorption feature becomes deeper. Moreover, for CO chondrites, the 2000 nm absorption feature becomes deeper with increasing metamorphic grade of the samples. For ordinary chondrites, the visual slope becomes less steep with increasing metamorphic grade. Interestingly, two specific trends are observed for ordinary chondrites. The cause of this dichotomy is not understood yet, however, it does not seem to be related to the metal content in the sample or the weathering degree.

The comparison of spectral features of asteroids and chondrites led to a good match for a few of them. S-type asteroids have similar 1000 nm and 2000 nm absorption band depths as ordinary chondrite samples. This is expected [7], and validates our approach. The parent bodies of CK and CV/CO chondrites have previously been suspected to be K-type asteroids, particularly EOS family members [e.g. 8]. This genetic affiliation is confirmed here by our data for CK chondrites which exhibit similar 1000 nm and 2000 nm absorption features as K-type asteroids. For CO/CV chondrites the absorption band depths and 1000nm absorption band position match those of the EOS family but also those of L-type asteroids.

References: [1] DeMeo F. E. et al. (2009) *Icarus* 202: 160-180. [2] Cloutis E. A. et al. (2012) *Icarus* 221: 328 – 358. [3] Potin et al. (2018) *Applied Optics* 57 : 8279-8296. [4] Bonal L. et al. (2016) *Geochimica et Cosmochimica Acta* 189: 312–337. [5] Monthé-Diniz T. et al. (2008) *Icarus* 195 : 277-294. [6] Krot A. N. et al. (2014) *Classification of Meteorites and Their Genetic Relationships*, pages 1–63. [7] Nakamura T. et al. (2011) *Science* 333: 1113–1116. [8] Clark B. E. et al. (2009) *Icarus* 202 : 119-133.

CHONDRULE SHAPES IN 3-D: PANCAKES VS. BASEBALLS INDICATE PREFERENTIAL COMPRESSION OF REDUCED VS. OXIDIZED CV CHONDRITES

T.J. Fagan[1*], R. Aoki[1], M. Uesugi[2] and A. Tsuchiyama[3,4], [1]Dept. Earth Sci., Waseda University, Tokyo, Japan. [2]Japan Synchrotron Radiation Research Institute (JASRI, SPring-8), Hyogo, Japan. [3]Division Earth Planet. Sci., Kyoto Univ., Kyoto, Japan. [4]Research Org. Sci. Tech., Ritsumeikan Univ., Shiga, Japan ([*]fagan@waseda.jp).

Introduction: The distribution of Fe and Ni into metals, sulfides and silicates was used to divide CV3 chondrites into oxidized and reduced ($CV3_{red}$) groups [1], and the oxidized CV3s were subsequently divided into Allende-like ($CV3_{oxA}$) and Bali-like ($CV3_{oxB}$) groups [2]. The $CV3_{oxA}$ group has undergone higher temperatures of metamorphism than the $CV3_{red}$ group based on infrared spectra of organic matter [3] and recrystallization of olivine in amoeboid olivine aggregates (AOAs, [4]). It has been argued that at least one early impact event on the CV parent body closed pores and expelled ices from the part of the body where $CV3_{red}$ chondrites originated, limiting fluid-rock interaction during metamorphism [5,6]. In this project, we test the early shock hypothesis by characterizing deformation textures in a set of $CV3_{oxA}$ and $CV3_{red}$ chondrites using 2-D and 3-D techniques.

Analytical Methods: *Polished thin section observations.* Chondrule shapes and modes of chondrite components (mostly matrix, chondrules, Ca-Al-rich inclusions [CAIs], and AOAs) were determined in polished thin sections (pts) of the $CV3_{red}$ chondrites Efremovka (2 pts), Leoville (1 pts) and Vigarano (3 pts), and the $CV3_{oxA}$ chondrites Allende (2 pts) and Axtell (1 pts). Elemental X-ray maps of the pts were collected by electron probe microanalysis (EPMA) using a JEOL JXA-8900 microprobe at Waseda University. Plane-polarized light (PPL) mosaics were also collected from each pts. The elemental maps and PPL images were input as layers into Adobe Illustrator. Long and short axes of chondrules were drawn and modes of chondrite components were determined on a grid in overlying layers in the Illustrator file for each pts.

X-ray computer tomography. X-ray computer tomography was conducted using an ELE SCAN instrument at Kyoto University for one sample each of Efremovka, Vigarano and Allende. Materials with contrasting linear attenuation coefficient (LAC) were imaged and output as stacked two-dimensional tiff files. Boundaries of chondrule-like objects with low LAC values in each tiff file were traced using Adobe Photoshop. The traced files were re-assembled using SLICE software [7], which was also used to fit ellipsoids to the traced objects, with a = minor, b = intermediate and c = major axes.

Results: Matrix abundances can be represented by modal ratios of matrix/inclusions (m/i), where "inclusions" = objects such as chondrules, CAIs and AOAs [8]. Matrix abundances of the CV3 chondrites in this study fall into three groups: (1) $CV3_{red}$ Leoville and Efremovka (m/i = 0.3–0.4); (2) $CV3_{red}$ Vigarano (m/i = 0.7–0.8); (3) $CV3_{oxA}$ Allende and Axtell (m/i = 0.9–1.4). Similar values were determined by [8] for Leoville (m/i = 0.42), Vigarano (m/i = 0.63) and Allende (m/i = 1.31). The three groups defined by matrix/inclusions correlate with porosities determined by [9]: Efremovka and Leoville, 0.6–2.1% porosity; Vigarano, 8.3% porosity; Allende and Axtell, 22–23% porosity. Two-dimensional chondrule shapes determined from pts are somewhat ambiguous, but can be divided into the same three groups, with chondrules of Leoville and Efrmovka having the highest aspect ratios, those of Vigarano appearing less elongate in thin section, and more equant chondrules in Axtell and Allende.

Distinct clastic domains with abundant broken chondrule fragments were identified in two of the Vigarano pts. One of these clastic domains is bounded by a micro-fault that off-sets a CAI and a chondrule.

The X-ray tomographic data show that Efremovka and Vigarano chondrules vary from somewhat equant to oblate (pancake-shaped), with most axial ratios b/c > 0.6 and a/b < 0.8, whereas Allende chondrules are more equant (baseball-shaped) with most axial ratios b/c > 0.7 and a/b > 0.8). Furthermore, short axes of the Efremovka and Vigarano chondrules are clustered, whereas short axes of the Allende chondrules are scattered.

Implications for Deformation: The relatively low matrix/inclusions ratios and pancake-shaped chondrules are consistent with the interpretation that $CV3_{red}$ chondrites come from a part of the CV parent body that was deformed during an impact event that closed pores in matrix domains [5,6]. Vigarano was not as pervasively compressed as Leoville and Efremovka, but underwent cataclastic deformation along micro-faults. Though Allende and Axtell have undergone some shock deformation [10], compression was relatively weak, leaving matrix pores open for fluid flow and fluid-rock interaction during metamorphism of the $CV3_{oxA}$ chondrites.

References: [1] McSween H.Y.,Jr. (1977) *GCA* 41: 1777–1790. [2] Weisberg M.K. et al (2006) in Lauretta D.S. and McSween H.S.,Jr. (editors) *MESS II*, p. 19-52. [3] Bonal L. et al (2006) *GCA* 70: 1849-1863. [4] Komatsu M. (2015) *MaPS* 50: 1271-1294. [5] Rubin A.E. (2012) *GCA* 90: 181-194. [6] MacPherson G.J. and Krot A.N. (2014) *MaPS* 49: 1250-1270. [7] Nakano T. et al (2006) *Japan Synchrotron Radiation Institute*, http://www-bl20.spring8.or.jp/slice. [8] Ebel D.S. et al (2016) *GCA* 172: 322-356. [9] Macke R.J. et al (2011) *MaPS* 46: 1842-1862. [10] Forman L.V. et al (2016) *EPSL* 452: 133-145.

CAMPO DEL CIELO: IDENTIFICATION OF A FRAGMENT FROM THE LONG-LOST "MESÓN DE FIERRO" AT NATURHISTORISCHES MUSEUM WIEN

G. Faivovich & N. Goldberg, Dorrego 1940 5.A/T-D, C1414CLO Buenos Aires, Argentina. (guidetocdc@gmail.com).

Introduction: "Mesón de Fierro", a mass of Campo del Cielo, is the first recorded meteorite of the Americas, as early as 1576. In 1774, begun a sequence of four expeditions that measured the massive iron, estimated its weight between 14 and 23 metric tons (300 to 500 quintals), and extracted a considerable number of samples. During the last expedition, in 1783, on-site procedures were conducted which resulted in the meteorite being dumped into an excavated hole and abandoned. This was the last time it was ever seen.

Historical aspects: In 1786, Don Miguel Rubin de Celis, who led the last expedition, submitted a detailed report to the Royal Society of London, attaching some specimens chiseled off from the mass [1]. At the dawn of meteoritics science, his report contributed to convince Chladni that "Mesón de Fierro" was an iron fallen from the sky. In 1799, Prof. Proust, from Madrid, made the earliest detection of nickel in a meteorite, and in 1802, Howard used a Campo del Cielo specimen for his famous experiment on native irons. Both samples came from "Mesón de Fierro" [2]. The missing "Mesón de Fierro" became a legend, and was searched for with no success for more than 200 years.

Proposing a new approach: In 2008, we travelled to London in search of the samples submitted by Don Miguel Rubin de Celis. However, at the Royal Society, we came across unpublished pages from de Celis' original manscript and found out that the specimens had been given to the British Museum. After a thorough search in the collections and archives at the Natural History Museum of London, it was determined that these samples, inventoried as "König 9" and "König 10", had vanished by 1904. It is important to note that by 1826 this institution received as a gift from Argentina a 1400 lb. specimen from the Campo del Cielo fall. This specimen was named "Otumpa", and became the main source of Campo del Cielo material for research and exchange for at least a century. Most probably, all of the available Campo del Cielo samples before that year were obtained from "Mesón de Fierro".

In 2017, at the meteorite collection of the Natural History Museum, in Vienna, we found a fragment that, we think could have been extracted from "Mesón de Fierro". It is a well-documented specimen of 19.37 g. acquired in 1807 from Leopold Von Fichtel, a mineral trader from Madrid. It was originally labeled as "Tucuman" (synonym for Campo del Cielo), and later inventoried as "A.18". The sample is morphologically different from any of the hundreds Campo del Cielo specimens we have seen before, as it does not have the appearance of a rock, crust, or a slab. It looks like a curl made of iron, with a shape that clearly conveys the force involved in a mechanical procedure. This shape is consistent with de Celis' report of how samples had been chiseled off from "Mesón de Fierro" and also matches Prousts' descriptions about the specimens he analyzed in 1799 "...according to every appearance (my pieces) were taken off from a greater mass… where the chisel has passed" [3].

Conclusion: Based on the historical records of the different expeditions that reported "Mesón de Fierro", we could sum 40 lb. of fragments extracted from the main mass. It is well documented how they were distributed and extensively analyzed, both in South America and Europe [4]. Most of those pieces were probably exhausted or ended up either being lost or mixed-up with the numerous samples of Campo del Cielo that became increasingly available from 1826 onwards. Our research suggests that "A.18" is likely to be a fragment of "Mesón de Fierro", and that there might be more samples that could surface in other collections.

References: [1] De Celis M. Rubin (1788) *Philosophical Transactions of the Royal Society, London* 78:37-42 (in Spanish); 183-189 (in English). [2] Marvin U. (1994). *Geological Sciences in Latin America. Scientific Relations and Exchanges* 155-174. [3] Proust J. (1800) *Journal of Natural Philosophy, Chemistry and the Arts* 3:374-375. [4] Alvarez A. (1926) *El meteorito del Chaco*. 222p.

BENCUBBINITE FORMATION: THE TURBULENT LIFE OF METAL AS INFERRED FROM GERMANIUM ISOTOPES

G. Florin[1,2], B. Luais[1], T. Rushmer[2] and O. Alard[2], [1]CRPG-CNRS UMR7358, University of Lorraine, 54501 Vandoeuvre-les Nancy, France (gflorin@crpg.cnrs-nancy.fr, luais@crpg.cnrs-nancy.fr), [2]Macquarie University Sydney, Australia (tracy.rushmer@mq.edu.au, olivier.alard@mq.edu.au)

Introduction: Bencubbinites (CB) are carbonaceous chondrites that show an unusual enrichment in metal, up to 80% in the form of FeNi metal rounded grains. Their siderophile element composition is volatility-controlled, with a strong depletion in moderately siderophile and volatile elements (e.g. germanium) relative to CI abundances [1]. CB chondrites are subdivided in two subgroups, CBa and CBb, on the basis of their differences of texture and composition, including the presence of elemental and isotopic zonations in CBb (e.g. Fe, Ni, refractory and transitional elements), which are rare in CBa [2]. These zonations have been first described to result of condensation under canonical nebula conditions [3]. However, inconsistencies between PGEs zoning patterns in metal grains and equilibrium condensation from a solar gas at $P^{tot}=10^{-4}$bar [1] have led researchers to debate in favor of non-equilibrium condensation under metal-rich supersaturated gas [1]. Condensation modeling based on elemental, isotopic data in silicate and metal [4] and Fe, Ni isotope data in zoned metal grains [5] have described a zoned impact plume model through equilibrium/kinetic condensation for CBas and CBbs, respectively. As Fe and Ni variations record high temperature condensation ($T_{50\%} \approx 1300$ K at 10^{-4}atm), here we propose a complementary isotopic investigation of germanium (Ge) ($T_{50\%} = 883$ K at 10^{-4} atm) in CB bulk metal and metal grains in order to identify lower temperature condensation.

Samples and Methods: Two CBa (Gujba, Benccubin) and one CBb (HaH 237) have been chosen to study equilibrium and kinetic condensation processes. As CBs metal have very low Ge contents (0.1-1.5 ppm [1]), 300mg of metal bulk of each meteorite, and two large metal grains separates from Gujba have been processed for Ge elemental and isotopic measurements. Bulk metal has been digested using HNO_3, while separate metal grains have been sequentially digested into three fractions of ≈33% each, from the edge, the middle and the core of the grains to assess isotopic zonation, called hereafter *"in situ"* fractions. Germanium purification from Fe-Ni matrix has been adapted from Luais protocols [6, 7] to allow the chemistry of large sample amount, by using 10ml of cationic (AG 50W-X8, H+ form) resin. Germanium isotopic measurements have been performed at the CRPG-Nancy (France) [6, 7] using the Neptune*Plus* MC-ICP-MS coupled to a hydride generator system. Ge isotopic compositions are reported as ‰ $\delta^{74/70}$Ge ratios relative to NIST 3120a Ge standard solution, and with a long-term reproducibility of 2SD ≈ 0.1‰.
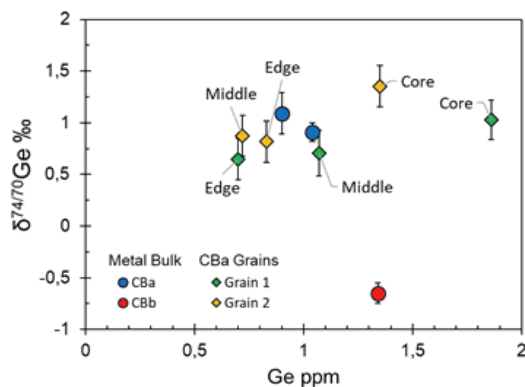
Figure 1: $\delta^{74/70}$Ge vs Ge in CB chondrites

Results and Discussion: We report the first Ge isotopic analyses on bulk metal of CB chondrites and "*in situ*" individual metal grain fractions. The two CB groups are easily resolvable for their bulk metal isotopic compositions, with $\delta^{74/70}$Ge= +0.97±0.16‰ and $\delta^{74/70}$Ge= -0.65±0.1‰ for CBa and CBb, respectively. The sequentially digested metal grains from Gujba (CBa) show a zonation in $\delta^{74/70}$Ge that decreases from the core to the edge (*Figure 1*).

During kinetic condensation, light isotopes are preferentially incorporated in the condensed phase. Our data indicate two cooling modes for CBa and CBb that reflect the thermal zoning of an impact plume [4]. Lower [Ge] and higher $\delta^{74/70}$Ge of CBa suggest condensation at equilibrium in an environment with low cooling and condensation rates such as the interior of the plume. CBb with higher [Ge] and lower $\delta^{74/70}$Ge would experience high cooling rates and kinetic condensation as expected for the external part of the plume. As most of Gujba (CBa) metal grains are known to be isotopically homogeneous in Fe and Ni [4], the $\delta^{74/70}$Ge zonations in the two analyzed grains are unexpected. We propose a two-step condensation at equilibrium. As the plume is cooling from the edge to the core, the centre of the plume would be to hot for metal to condense, thus CBa core had been firstly formed in a colder intermediate part. Then, due to turbulence, grains are carried in a warmer region (i.e. the centre) where Ge and its light isotopes evaporate, causing the metal of the core to be enriched in heavy isotopes. Finally, as temperature slowly drops, vapor re-condensation on the surface of previous metal grains leads to the light external Ge isotopic composition of new metal condensates.

References: [1] Campbell A. J., et al. (2002) *Geochimica et Cosmochimica Acta* 66: 647–660. [2] Weisberg M. K., et al. (2001) *Meteoritics and Planetary Science* 36, 401-418. [3] Newsom H. E. and Drake M. J. (1979) *Geochimica et Cosmochimica Acta* 43: 689–707. [4] Fedkin A. V. et al. (2015) *Geochimica et Cosmochimica Acta* 164: 236–261. [5] Weyrauch M. et al. (2019) *Geochimica et Cosmochimica Acta* 246 :123-137 [6] Luais B. (2007) *Earth and Planetary Science Letters* 262: 21-36. [7] Luais B. (2012) *Chemical Geology* 334: 295-311.

PARENT BODY/TERRESTRIAL ALTERATION OF FE,NI METAL IN CARBONACEOUS AND ORDINARY CHONDRITES: IMPLICATIONS FOR SAMPLE RETURN.

C. Floyd[1] and M. R. Lee[1]
[1]School of Geographical and Earth Sciences, University of Glasgow, Glasgow, G12 8QQ, U.K.
(2118495F@student.gla.ac.uk)

Introduction: Fe,Ni metal is one of the most reactive constituents of carbonaceous chondrites when exposed to low temperature oxidizing aqueous solutions. It can be altered pre-terrestrially in a parent body environment [1] and after the meteorite's fall to Earth (i.e., terrestrial weathering) [2]. Discriminating between these two environments is crucial for understanding parent body evolution but can be particularly challenging, as discussed for altered metal grains in the Antarctic CM chondrite Yamato 791198 [3]. Even meteorite falls are not free from these uncertainties as their metal can undergo significant terrestrial weathering during museum curation [4]. Here we have sought to establish criteria to help differentiate between parent body and terrestrial alteration of Fe,Ni metal by comparing Antarctic equilibrated ordinary chondrites (whose alteration should be solely terrestrial) with Antarctic carbonaceous chondrites (potentially altered in both parent body and terrestrial environments).

Samples and methods: Fe,Ni metal grains and their alteration rims were studied in thin sections of two Antarctic ordinary chondrites (OCs) and two CM carbonaceous chondrites: Dominion Range (DOM) 14010 (L5), Allan Hills (ALH) 77180 (L6), Lewis Cliff (LEW) 85311 (CM), LaPaz Icefield (LAP) 02239 (CM). These samples were imaged and chemically analysed using SEM and energy-dispersive X-ray spectroscopy (EDS). Their alteration rims were further analysed by Raman spectroscopy using a 514 nm laser source and 2400 mm grating.

Results: Fe,Ni metal within the OCs is characterized by Fe-oxide alteration rims that range in thickness from 5 µm to 100+ µm. Imaging shows two distinct textures within the rims; an ordered texture with fine laminations that is heavily fractured, and a disorderd texture with coarser and more chaotic laminations. Any one alteration rim may display one or both textures. Where they occur together, the ordered texture is closest to the remaining Fe,Ni metal with fractures trending perpendicular to the metal. The disordered texture is present on the periphery of the rim and cross-cuts the fractures. Raman spectroscopy indicates that the ordered material is dominantly akaganeite whilst the disordered material returns spectra for both akaganeite and goethite. EDS analysis of these rims reveals differences in Cl concentrations, with the ordered material containing ~1.2 wt% Cl and the disordered material ~0.4 wt.% Cl.

Most alteration products of Fe,Ni metal in the CM samples are dominated by S-rich material (tochilinite) of a parent body origin. However, some metal grains have thick 'halos' of Fe-oxide, probably a terrestrial weathering product. SEM imaging shows these 'halos' can have ordered and disordered textures. In LAP 02239 Raman and EDS analysis revealed that the ordered texture comprises akaganeite with ~1.9 wt% Cl and disordered texture goethite with ~0.7 wt% Cl. By contrast, both textures in LEW 85311 are composed of akaganeite, but blocks of tochilinite occur around the edge of the disordered texture and are broken up by veins of goethite.

Discussion: The presence of two textures within the alteration rims of OC metal demonstrates the evolution of terrestrial alteration from Cl bearing akaganeite to goethite. Akaganeite forms during the initial stages of alteration when Cl is freely available. As alteration progresses and sample porosity begins to decrease (a result of weathering) [5] an outer layer starts to develop and thicken (the disordered texture). This outer layer limits the ability of Cl ions to reach the metal [6]. With Cl now limited the remainder is concentrated in the ordered material closest to the metal grain and is consumed in final phases akaganeite production [7] facilitating the gradual transition to goethite [6]. Similar textures observed within the CM's suggests that they too have experienced significant terrestrial alteration. The fragments of tochilinite detected show that prior to terrestrial weathering the Fe,Ni metal grains had undergone parent body aqueous alteration, but that this material has subsequently been almost entirely destroyed. Nonetheless, the presence of these relict fragments of tochilinite allows a complete evolutionary history of the Fe,Ni metal alteration to be inferred, from initial parent body alteration (tochilinite) to advanced terrestrial weathering (goethite). Our results highlight the need for thorough analysis of Fe,Ni metal grains within CMs to accurately determine the extent to which pre- and post-terrestrial processes may have affected these meteorites. Samples soon to be returned from Bennu and Ryugu will help greatly in unambiguously identifying pre-terrestrial alteration products of Fe,Ni metal.

References: [1] Palmer E. and Lauretta D. S. (2011) *Meteoritics & Planetary Science* 46:1587–1607. [2] Buchwald V. F. and Clarke R. S., Jr. (1995) *American Mineralogist* 74:656–667. [3] Chizmadia L. J. et al. (2008) *Meteoritics & Planetary Science* 43:1419–1438. [4] Lee M. R. and Bland P. A. (2004) *Geochimica et Cosmochimica Acta* 68: 893–916. [5] Bland P. et al. (1996) *Geochimica et Cosmochimica* Acta 60: 2053–2059. [6] Xiao H. et al. (2017) *Materials* 10:1262. [7] Rémazeilles C. and Refait P. (2007) *Corrosion Science* 49: 844–857.

HYPERVELOCITY IMPACT OF CI1 AND CM1 METEORITE ANALOGS:
IMPLICATIONS FOR THE SURVIVAL OF ORGUEIL-LIKE BODIES IN SPACE.

G. J. Flynn[1], D. D. Durda[2], M. J. Molesky[3], B. A. May[3], S. N. Congram[3], C. L. Loftus[3], J. R. Reagan[3], M. M. Strait[3], and R. J. Macke[4], [1]SUNY-Plattsburgh, 101 Broad St., Plattsburgh, NY 12901 (george.flynn@plattsburgh.edu), [2]Southwest Research Institute, 1050 Walnut Street, Suite 300, Boulder, CO 80302, [3]Alma College, Alma, MI 48801, [4]Vatican Observatory, V-00120 Vatican City.

Introduction: Most CI and CM meteorites have cosmic ray exposure ages (CREs) shorter than 2 m.y., while the ordinary chondrite meteorites have much longer CREs, some more than 60 m.y. [1]. Scherer and Schultz [2] suggest three possible reasons: 1) the CI/CM parent bodies were close to a resonance, 2) the parent bodies were in an Earth crossing orbit when a collision ejected the meteorites, or, 3) the fragile nature of these bodies lowers their survival time in space. To test the third idea we conducted a series of hypervelocity impact experiments comparing the survival of targets of CI1/CM1 analog material to targets of Northwest Africa 869 (NWA 869) ordinary chondrite.

Samples and Experimental Procedure: NWA 869 was available in sufficient quantity to allow disruption of 10 targets, ranging from 32 g to 324 g, of this meteorite. However CI1 and CM1 meteorites are rare and generally small, so samples of these meteorites were not available for destructive testing. We prepared hydrous meteorite analog targets by crushing NWA 869 and CV3, Northwest Africa 4502 (NWA 4502), carbonaceous chondrite material after we completed disruption measurements on these meteorites. This powder was laboratory hydrated in a solution of slightly alkaline water at high temperature in a pressure bomb for several months, using a procedure developed by Jones and Brearly [3] intended to mimic, on a shorter time scale, the hydration process that occurred on asteroidal parent bodies. The resulting hydrous material was dried to produce cylindrical targets that ranged in bulk density from ~1.7 to 1.8 g/cm^3, only slightly higher than the 1.61 g/cm^3 of the CI1 meteorite Orgueil. Infrared spectroscopy confirmed a high degree of conversion of anhydrous silicates to clays, as is the case for Orgueil.

The minimum impactor kinetic energy per unit target mass ($Q*_D$) that results in a catastrophic disruption of the target, ie., produces a largest fragment (M_L) that is one-half the mass of the target (M_T), is found by disrupting a series of targets using impactors spanning a range of kinetic energies, fitting the disruption data, and finding the value of impactor kinetic energy per unit target mass that would produce an $M_L/M_T = 0.5$. The meteorite targets were suspended at the end of a 2 m long fishing line from the ceiling of the chamber of the NASA Ames Vertical Gun Range (AVGR) and impacted by 1/16", 1/8" or 1/4" diameter Al-projectiles moving at ~5 km/s, the mean collision speed in the main-belt [4]. However, these CI1/CM1 analog materials, like Orgueil, were too weak and friable to attach to this line, so they were suspended in a light, hair net sling. This sling did not interfere with the disruption and retained the disruption fragments, eliminating further fragmentation from the pieces hitting the floor.

Results: Figure 1 shows M_L/M_T vs the impact specific kinetic energy for NWA 869 and CI1/CM1 analog targets. Both types of material plot along clear trend lines. The ten disruptions of NWA 869 targets give $Q*_D = 1795$ J/kg [5]. Earlier disruptions of nine H, L, and LL ordinary chondrites gave $Q*_D$ of 1419 J/kg [6], indicating that the $Q*_D$ value of NWA 869 is generally characteristic of ordinary chondrite material. Our new data gives a much lower value of $Q*_D$, only ~280 J/kg, for this CI1/CM1 analog material, demonstrating that it is much easier to disrupt.

Conclusions: The minimum energy for catastrophic disruption of the NWA 869 ordinary chondrite is over six times the value we obtained for catastrophic disruption of the six laboratory hydrated CI1/CM1 analog targets. Even accounting for the smaller size of an ordinary chondrite target of the same mass as an analog target, *in the same impactor environment this CI1/CM1 analog material is far more susceptible to disruption than ordinary chondrites.* This indicates the absence of CI/ CM meteorites with long CREs is significantly influenced by the lifetimes against catastrophic disruption of this weak, highly friable material.

References: [1] Eugster, O. et al. (2006). in *Meteorites and the Early Solar System II,* U. of Ariz. Press, 829-851. [2] Scherer, P and L. Schultz (2000), *Meteoritics & Planet. Sci*., 35, 145-153. [3] Jones, C., and A. Brearley (2006) *Geochim. Cosmochim. Acta*, 70, 1040-1058. [4] Bottke, W.F. et al. (1994) *Icarus*, 107, 255–268. [5] Flynn, G. J. et al. (2018) *Planet. Space Sci.*, 164, 91-105. [6] Flynn, G. J. and D. D. Durda (2004) *Planet. Space Sci.,* 52, 1129-1140.

Figure 1: Plot of M_L/M_T vs impact specific kinetic energy for ten NWA 869 ordinary chondrite and six CI1/CM1 analog material targets.
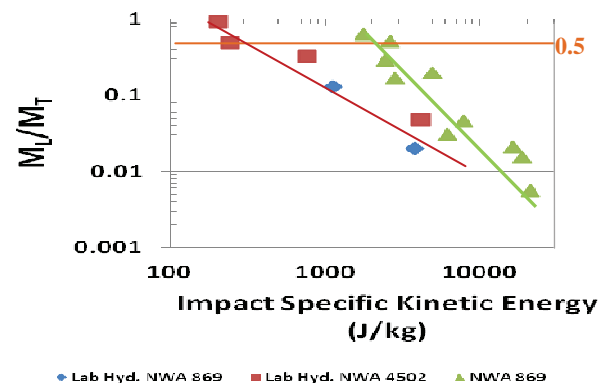
PHOSPHOROUS SPECIATION IN PRIMITIVE INTERPLANETARY DUST: CLUES TO GRAIN FORMATION IN THE SOLAR PROTOPLANETARY DISK.

G. J. Flynn[1], S. Wirick[2], and P. Northrup[3], [1]Physics,, SUNY-Plattsburgh,., Plattsburgh, NY, 12901 [george.flynn@plattsburgh.edu], [2]Focused Beam Enterprises, Westhampton, NY 11977, [3]Stony Brook University, Stony Brook NY 11794.

Introduction: Anhydrous chondritic porous interplanetary dust particles (CP IDPs) are believed to be the best preserved samples of the original condensates of the Solar Protoplanetary Disk [1]. Thus, the mineralogy of CP IDPs tests predictions of condensation models. Most equilibrium condenstion models starting with a gas of Solar composition predict P condenses as schreibersite [2]. A ~1 µm grain of schreibersite was identified in an unusual, hydrous, CM-like IDP [3]. But there has been no comprehensive measurement of P speciation in the anhydrous, primitive CP IDPs that best preserve the original minerals that formed from the Solar Protoplanetary Disk.

Procedure and Samples: The Tender Energy Spectroscopy (TES) instrument (Beamline 8BM, National Synchrotron Light Source II, Brookhaven National Laboratory) can map elements by x-ray fluorescence (XRF), and provide speciation by K-edge X-ray Absorption Near-Edge Structure (XANES) spectroscopy of the elements from P to Ca. We mapped the spatial distribution of elements from Mg to Ca in 9 large, cluster IDPs, most of which were of the anhydrous CP-type, and determined the P speciation by XANES spectroscopy. These IDPs were analyzed while still in the silicone oil in which they were collected to minimize interaction with the atmosphere since collection.

Results: Reduced P (e.g., schreibersite) is easily distinguished from oxidized P (e.g., apatite) by P-XANES since there is a large difference in their peak energies (Figure 1). The P XRF mapping produced numerous P hot-spots, but only 17 of them were intense enough to produce useful P-XANES spectra. Based on the P count rates in XRF these spots contain a large majority of the total P in these IDPs. We obtained spectra of: 0 P hot-spots in L2005 AS9, 1 in L2005 AS10, 3 in L2005 AS11, 0 in L2008 Z1, 1 in L2008 Z2, 6 in L2009 R1, 1 in L2009 R2, 0 in L2021 S1, and 5 in L2036 AL14. In all 17 spots that we analyzed P was present in oxidized rather than reduced form. However, not all spots in these cluster IDPs exhibit the same P-XANES spectra. The majority of the P-XANES spectra of these cluster IDPs show no shoulder on the high energy side of the major absorption peak. However, a few spots, for example Spot 2 in L2005AS11 (Figure 1), exhibit a shoulder on the high energy side of the major absorption peak. Ingall et al. [4] performed P K-edge XANES spectroscopy of 12 apatite-group minerals and found that each exhibited "a distinct shoulder or widening on the main absorption peak, [with this shoulder] centered at approximately 2155.6 eV," consistent with some of our P-XANES spectra. The second, more common, P phase in the IDPs we analyzed has no shoulder. This phase has not yet been identified. We found no evidence of reduced P, e.g. schreibersite, in any P hot-spot intense enough to produce a useful P-XANES spectrum,

Conclusions: The absence of schreibersite indicates that either P did not condense from the disk as schreibersite or that schreibersite was subsequently altered to oxidized P in these primitive nebular dust samples. Alternatively, P condensation may have occurred under different conditions than were assumed in most of the equilibrium nebular condensation models. For example, equilibrium calculations from cosmic gases made by total vaporization of dust-enriched systems by Ebel and Grossman [5] found the condensation of whitlockite at 1350 K from a gas of 10^{-3} bar with an enrichment of 1000 times the dust of CI composition relative to a system of Solar composition. The P-XANES spectrum of whitlockite reported by Kar et al. [6] has a shoulder on the high energy side of the absorption peak, but one reported in Ingall et al. [4] does not show a pronounced shoulder. Measurements are in progress to compare the shape and peak energy of our IDP spectra with a whitlockite standard under our analysis conditions. The presence of oxidized P in these primitive IDPs may indicate that the P minerals in the primitive CP IDPs formed under atypical conditions compared to what is assumed in the equilibrium condensation models for assumed Solar conditions.

References: [1] Ishii et al. (2008) *Science*, 319, 447-450. [2] Lodders, K. (2003) *Astrophysical J.*, 591:1220–1247. [3] Bradley and Brownlee (1991) *Science*, 251, 549552. [4] Ingall et al. (2011) *J. Synch. Rad.*,18, 189-197. [5] Ebel, D. S. and L. Grossman (2000) *Geochimica et Cosmochimica Acta*, 64, 339–366. [6] Kar, G. et al. (2017) *Canadian Journal of Soil Science*, 97, 626-636.

Figure 1: P-XANES spectra of schreibersite, apatite and three P hot-spots in IDP L2005 AS11.
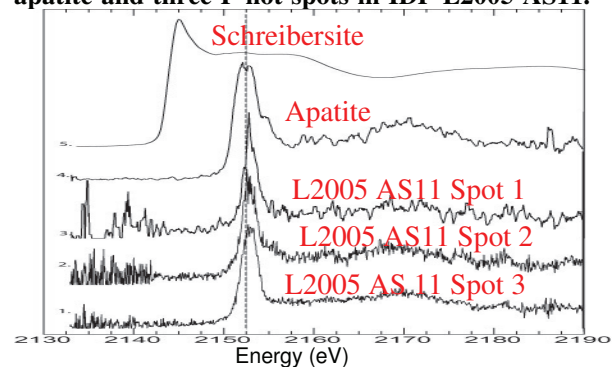
PARTICLE STATISTICS FROM THE TAM MICROMETEORITE COLLECTION – INVESTIGATING THE RELATIONSHIP BETWEEN COSMIC SPHERULE TEXTURE AND PARTICLE SIZE

Folco, L. and Suttle, M.D., Dipartimento di Scienze della Terra, Università di Pisa, 56126 Pisa, Italy (martindavid.suttle@dst.unipi.it, luigi.folco@unipi.it).

Introduction: We provide a comprehensive overview of micrometeorite statistics from a single sediment trap within the TAM (Transantarctic Mountain) micrometeorite collection[1]. Trap No.65 was recovered from the glacially eroded, flat-toped nunatak: Mille Bute, within Victoria Land, Antarctica. The analysis of large numbers of micrometeorites is essential for the accurate characterization of the cosmic dust flux arriving on Earth. Here we provide the first data on micrometeorite size distribution by textural subtype, as well as unmelted micrometeorite abundance data.

Methods: Following an exhaustive search effort, potential micrometeorites were imaged optically and under BSE (back-scattered electron imaging), collecting both external and internal cross-section images. Micrometeorite classification follows an updated version of the conventional system, previously outlined by Genge et al., (2008)[2].

In total we picked ~1784 micrometeorites, ranging in size between 100-1500μm. Currently, we have complete data for all particles >200μm, while the remaining 100-200μm size fraction (~616 particles) will be characterized in full prior to the conference. Particles were retrieved from ~2542g of sediment, however, because we performed partial searches of the smaller (<400μm) size fractions the total expected micrometeorite population accounting for the un-picked micrometeorites lies at ~2,271 particles (>200μm) among the entire 2542g sediment aliquot.

Results: From the 200-1500μm size fraction we identified 1168 micrometeorites as well as 69 microtektites and 1 meteorite fragment (a chip of ordinary chondrite, containing fusion crust). This includes 53 unmelted/scoriaceous particles, representing 4.54% of the total collection at a ratio of 1:22 unmelted:cosmic spherules. Of these fine-grained precursors are overwhelmingly dominant (~75% of unmelted particles).

Among the cosmic spherule population, both I and G types occur in equal proportions (1.6%), while S-types represent 96.7%. S-types can be subdivided based upon quench textures into porphyritic (PO - 13.3%), barred olivine (BO – 19.2%), cryptocrystalline (CC – 48.7%) and vitreous (V – 15.5%) subtypes. Splitting further, the PO group is composed of "*normal*" PO spherules (10.1%) containing "*large*" (>10μm) euhedral olivine crystals and μPO (3.2%) – as defined by van Ginneken et al., 2017[3], dominated by many smaller equant olivine crystals (<10μm) as well as containing abundant vesicles. Collectively, among the PO group 25.3% are relict grain bearing, containing crystals which survived atmospheric entry unmelted. We also elected to further subdivide the CC class into "microcrystalline" (MC – 26.8%) – containing localized regions with a barred texture as well as regions lacking bars and dominated by randomly oriented olivine and magnetite crystallites, CC-*normal* (12.0%) – containing submicron olivine and magnetite dendrites with no evidence of barred textures and CC-*turtleback* (7.7%) composed of multiple crystalline domains whose boundaries present a "*stitched*" texture generated by crystal growth from the surface inward[4]. These subdivisions better reflect the transitional nature between BO-CC-V subtypes and address somewhat the subjective problems of micrometeorite classification by texture.

Morphological features: S-type spherules with elongate *tailed* morphologies or *arrow*-shaped forms[5] occur at a frequency of 3.7%, while those with hollow centers occupied by a single large vesicle represent <1.5% – they may reflect particles which entered the atmosphere with extremely high rotation rates (>1000 radians s^{-1}) potentially indicating immature dust recently released from their parent bodies[6]. Particles with evidence of metal bead formation during atmospheric entry represent (as a conservative estimate) 17.4% of S-type spherules.

Size distribution: The particle size distribution is accurately described (R^2=0.97) by a power law matched against the size range 200-700μm (96% of the population by number) and produces a slope exponent of -3.8. Neither the slope function nor fitting statistics change appreciably if cosmic spherules from only a single subtype are considered – Slope values varying between -3.4 (PO spherules) to -4.2 (V-types) and fitting statistics between R^2=0.96 and 0.99. Likewise, median spherule size by subtype varies within a narrow range: 239μm (I-types) and 325μm (V-types). There does not appear to be a strong relationship between cosmic spherule texture and particle size – although a subtle statistical trend may be present, and this will be the focus of further research once the 100-200μm fractions are considered.

Conclusions: Population statistics from the TAM65 sediment trap are similar to data previously reported from other Antarctic micrometeorite collections. Further data is required before a statistically rigorous assessment of the relationship between cosmic spherule textural subtypes and particle size can be determined. At present the null hypothesis that "*these variables are independent*" appears to be valid.

References: [1] Rochette et al., 2008. PNAS, doi:10.1073/pnas.0806049105. [2] Genge et al., 2008, MAPS, doi: 10.1111/j.1945-5100.2008.tb00668.x. [3] van Ginneken et al., 2017, GCA, doi:10.1016/j.gca.2017.05.008. [4] Sedaghatpour et al., 2009, MAPS, doi:10.1111/j.1945-5100.2009.tb00761.x. [5] Suttle et al., 2018 Space dust and debris in the vicinity of the Earth - Royal Astronomical Society Nov 2018. [6] Genge, 2016, MAPS, doi:10.1111/maps.12805.

MACROSCALE AND MICROSCALE FABRIC ANALYSIS OF ALLENDE.

L. V. Forman[1*], L. Daly[1,2], P. A. Bland[1], C. M. Corrigan[3], T. J. McCoy[3], J. Hoskin[3], C. Anders[3] G. Polley[3], P. W. Trimby[4], S. Piazolo[5], S. Griffin[2], A. E. Pickersgill[2], A. C. O'Brien[2], [1]Space Science and Technology Centre, School of Earth and Planetary Science, Curtin University, GPO Box U1987, Perth, WA, Australia (lucy.forman@curtin.edu.au) [2]School of Geographical and Earth Sciences, University of Glasgow, Glasgow, G12 8QQ, UK [3]Smithsonian Institution, National Museum of Natural History, Washington DC, USA. [4]Oxford Instruments Nanoanalysis, High Wycombe, HP12 5SE, UK. [5]School of Earth and Environment, University of Leeds, Leeds, LS2 9JT, UK.

Introduction: The Allende CV3 meteorite is arguably the most well studied meteorite. However, even 50 years after its discovery with the advancement of modern analytical techniques we are still learning new information about how our solar system formed from this meteorite. For example, recent electron backscatter diffraction (EBSD) analysis of fine grained rims [1], chondrules [2] and matrix [3] within Allende have revealed textures consistent with impact induced compaction of meteorites from initially highly porous 'candy floss' like bodies [4]. Additionally the contrasting heterogeneous Fe contents of chondrule olivine and homogenous Fe content of matrix olivine are consistent with the action of metasomatic fluids on the Allende parent body [5]. Here we examine a 25 cm slab of Allende (USNM-3529), and new EBSD analyses of matrix and chondrule olivine to investigate macro-scale effects of impact induced compaction and microscale effects of fluid rock reactions during parent body metasomatism.

Methods: The 25 cm slab of Allende was imaged on both sides using a high resolution digital camera. High resolution EBSD maps (120 nm step size) of chondrules and matrix olivine in Allende were obtained using an Hitachi SU70 scanning electron microscope equipped with an Oxford Instruments, Symmetry CMOS EBSD detector.

Macro: Visual investigations of the slab reveal a clear and pervasive shape preferred alignment of the Ca-Al-rich Inclusions (CAIs) (Fig. 1). It is unclear whether this fabric is a foliation of lineation due to the 2D nature of the slice surface. This texture is interpreted as further evidence of compaction of asteroids during low velocity collisions [4] supporting previous EBSD studies [1-3 & 6]. Quantitative fabric analyses will be presented at the meeting.

Micro: EBSD of Allende matrix and chondrule olivine grains reveal that some are twinned (60° rotation about <100>) (Fig. 2). However, olivine typically does not form twins. These twins propagate from neighboring twinned pyroxene crystals consistent with replacement of pyroxene with olivine, supporting previous inferences that pyroxene replacement may be a source of fayalitic olivine during metasomatism [7]. This observation suggests that the original mineralogy of Allende was substantially changed. Through further crystallographic investigations the primary mineralogy of the CV parent body may be revealed.
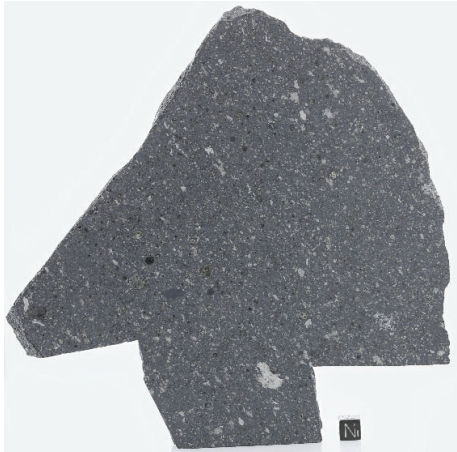
Figure 1: A slab of the Allende meteorite. CAIs (white objects) form a distinct shape preferred orientation aligned from the top left to the bottom right of the image.
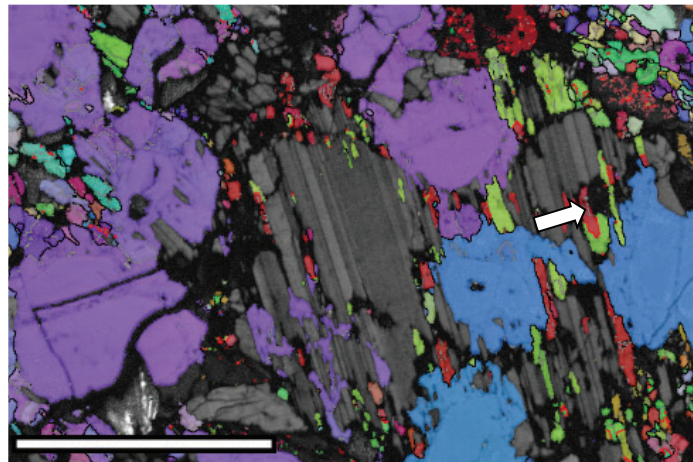
Figure 2: An Inverse pole figure EBSD map of a chondrule in Allende. Olivine is in colour and pyroxene is in greyscale. Twins in pyroxene propagate into the olivine in a replacement texture highlighted by the white arrow. Scale bar 50 μm.

References: [1] Watt L., et al., (2006) *Meteoritics and Planetary Science,* 41, 989-1001. [2] Forman L.V., et al., (2016) *Earth and Planetary Science Letters*, 452, 133-145 [3] Forman L.V., et al., (2017), *Geology*, 45, 559-562. [4] Bland P.A., et al., (2014) *Nature Communications*, 5, 5451. [5] Krot A.N., et al., (1998) *Meteoritics and Planetary Science*, 33, 1065-1085. [6] Watt L., (2006), *PhD Thesis,* Imperial College London, pp.297 [7] Housley R.M. & Cirlin E.H., (1983) In: *Chondrules and their origins.*

OXYGEN ISOTOPE VARIATION OF CM AND RELATED CHONDRITES: MULTIPLE PARENT BODIES OR A SINGLE HETEROGENEOUS SOURCE?

I. A. Franchi[1], R. C. Greenwood[1], K. T. Howard[2], A. J. King[3], M. R. Lee[4], M. Anand[1], & R. Findlay[1] [1]Planetary & Space Sciences, Open University, Milton Keynes MK7 6AA, UK. (ian.franchi@open.ac.uk). [2]Physical Sciences Department, Kingsborough Community College, NY 11235, USA. [3]Department of Earth Science, Natural History Museum, London SW7 5BD, UK. [4]School of Geographical & Earth Sciences, University of Glasgow G12 8QQ, UK.

Introduction: CMs are the largest group of carbonaceous chondrites (CC), comprising ~35% of observed CC falls [1]. The CMs display evidence for significant aqueous alteration, with considerable variation in the nature and amount of secondary minerals reported across the group. Indeed, many CMs are complex breccias containing a range of different lithologies, often showing significant mineralogical variation [e.g. 2, 3]. Here we present the results of an extensive oxygen isotope study of a wide range of CMs and related meteorites. Our aim is to explore the diversity and linkages within and between samples in order to understand the nature of the CM parent body(s). The results of this work will have important implications for the forthcoming detailed investigation of samples returned by Hayabusa2 and OSIRIS-REx from their respective C-type target asteroids.

Materials and Methods: O-isotope data were obtained at the Open University using laser-assisted fluorination [10]. Some results have been previously published, or samples were provided from other investigations, including CM1 and CM1/2 chondrites [5], CM2s [6,7,8,9] and CO3s [10]. The mineralogy of typical CMs pose particular problems for laser fluorination analyses due to pre-reaction with BrF_5 at room temperature and therefore most analyses were obtained with a modified technique where just one sample and one standard are loaded into the system [9].

Results and Discussion: The CM2s analysed by the new method reveal a range of O-isotope compositions along a mixing line with slope ~0.7 (Fig 1), which is almost identical to that observed previously using a reaction bomb method [11]. With the exception of MCY 05231, the CM1s and CM1/2s (not shown) plot along a separate mixing line, with slope ~0.48, that appears to represent the effects of interaction with ^{18}O-depleted Antarctic water [12]. While the CM2s display a broad overall pattern of increasing $\delta^{18}O$ with increasing alteration, the pre-terrestrial composition of the CM1s and CM1/2s appears to be rather restricted and within, but not beyond the range of the less altered CM2s, indicating that these meteorites likely suffered different alteration conditions rather than just an increase in severity/duration of that experienced by the CM2s.

A link between the CO3s and CM2s was suggested by [11], despite a large gap between the two groups. However, there is a population of C2 ungrouped meteorites that have O-isotope whole-rock compositions that fall in this gap. It is also apparent that some of the mineralogical variation observed within individual samples is reflected in O-isotopic variation between different sub-samples (Fig 1). Sub-samples of some individual meteorites extend across the entire range of CO and CMs. This suggests that CMs, COs and C2 ungrouped meteorites experienced similar alteration processes and raises the possibity that they are derived from a common parent body. These results also highlight the need for careful characterization of CM-like samples prior to O-isotope anal-

Fig 1: O-isotope plot of C2 ungrouped [also 1,11, 13], CM and CO meteorites. Analyses of different clasts of LEW 85311 [also 1] and NWA 5958 [also 1,13] show large variation.

yses in order to properly relate mineralogy and bulk isotopic information. Small clasts present in some samples [e.g. 2] pose additional challenges. However, new analytical protocols permit high precision O-isotope measurements on such samples (<100 µg). Samples returned from Ryugu and Bennu will provide constraints on the variation in CM/CI-like bodies and help define the number of parent bodies that contributed to the CO-C2 ungrouped-CM association.

References: [1] Meteoritical Bulletin Database. [2] Lindgren P. et al. (2013) *MAPS* 48, 1074-1090. [3] Howard K. T. et al. (2015) *GCA* 149, 206-222. [4] Greenwood et al. (2017) *Chemie der Erde – Geochem.* 77, 1-43. [5] King A. J. et al. (2018) *LPSC* 49, Abs #2201. [6] Howard K. T. et al. (2010) *LPSC* 41, Abs#1595. [7] Howard K. T. et al. (2011) *LPSC* 42, Abs #2429. [8] Howard K. T. et al. (2013) *LPSC* 44, Abs #2520. [9] Greenwood R. C. et al. (2014) *LPSC* 45, Abs #2610. [10] Alexander C. M. O'D et al. (2018) *GCA* 221, 406-420. [11] Clayton R. N. & Mayeda T. K. (1999) *GCA* 63, 2089-2104. [12] Greenwood R. C. et al. (2019) *LPSC* Abs #3191. [13] Jacquet E. et al. (2016) *MAPS* 51, 851-869.
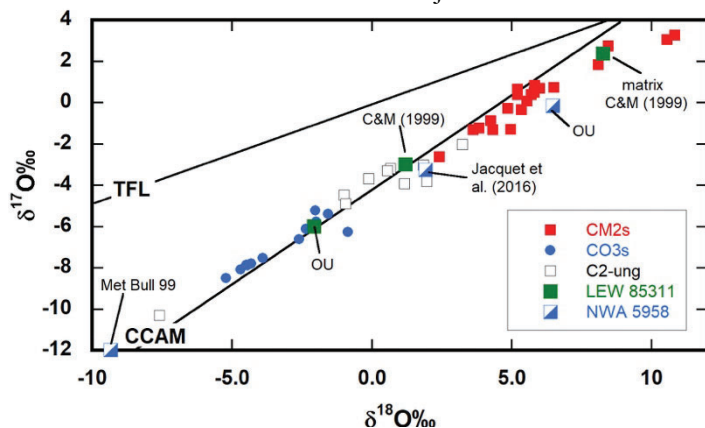
RELATIONSHIPS AMONG PHYSICAL PROPERTIES INDICATE THE IMPACT ORIGINS OF FRIABLE ORDINARY CHONDRITES.

J. M. Friedrich[1,2] M. L. Rivers[3], A. Ruzicka[4], [1]Department of Chemistry, Fordham University, 441 East Fordham Road, Bronx, New York 10458, USA e-mail: friedrich@fordham.edu, [2]Department of Earth and Planetary Sciences, American Museum of Natural History, 79th Street at Central Park West, New York City, New York 10024, USA, [3]Consortium for Advanced Radiation Sources, University of Chicago, Argonne, Illinois 60439, USA, [4]Cascadia Meteorite Laboratory, Portland State University, Department of Geology, Portland, OR 97207 USA.

Introduction: Collisions were important for the compaction of asteroidal-sized bodies, including those from which ordinary chondrites were derived. After primary accretion, parent bodies would have retained significant amounts of ancient porosity, owing to their small diameters. High velocity impact deformation alters the physical properties of materials in two ways: by reducing porosity, and by introducing foliation, both as a result of compaction [1-8]. During a high-energy collision on a high porosity (e.g. >20-25%) body, porosity is reduced, but in low (≤2-3%) porosity bodies, the shock cracks the brittle silicates which actually reintroduce porosity to a rock. Approximately 5-7% porosity can be reintroduced by such micro-cracking [9, 10]. Metal foliation, or planar grain shape preferred orientation of metal in ordinary chondrites has been observed and the strength of foliation correlates with increasing shock intensity recorded in a rock [4,5,8]. All of this leads to a simple model [see 11] in which metal foliation is inversely related to porosity. Previously, Friedrich et al. [11] examined a suite of ordinary chondrites that deviated from the simple model. They concluded that low-porosity, weakly foliated, and apparently weakly-shocked chondrites experienced either post-shock annealing or experienced impacts occurred under warm conditions which allowed more reduction of porosity. In this work, we place a suite of high porosity and friable ordinary chondrite chondrites into the context of the porosity and foliation scheme from [11].

Samples and Methods: For this study, we imaged four ordinary chondrites with the 3D technique x-ray computed microtomography (μCT). Samples of Bjurböle (L/LL4, S1), Quenggouk (H4), Saratov (L4, S2), and Tennasilm (L4, S3) from the AMNH collection were studied. Each of these have been noted for their friability or lack of cohesion in hand sample [12-15]. We collected μCT data at the GeoSoilEnviro Center for Advanced Radiation Sources (GSE-CARS) beamline 13-BMD at the Advanced Photon Source at Argonne National Laboratory. Typical data collection parameters and procedures can be found in [5]. μCT data were collected at resolutions ranging from 2.8 to 15.9 μm/voxel edge. Lower resolutions were used for qualitative inspection and quantitative foliation investigation [5,11]. Higher resolutions are sufficient to see all of the porosity in a chondrite [10] and the images can be used to investigate the small-scale porosity or "microcracks"[9], in the samples. For our investigations, total porosity data [11,16] and quantitative foliation data [5,11] were taken from the cited works.

Results: Total porosity in the four friable chondrites range from 10.7% (Tennasilm) to 19.8% (Bjurböle). Foliation in the friable ordinary chondrites is moderate: higher than that seen in high porosity uncompacted chondrites such as Baszkówka [6] or Miller (AR) [17], but clearly less than the most compacted ordinary chondrites.

Discussion and Conclusions: Our μCT results show that the four friable ordinary chondrites have high porosity, but also some degree of metal grain foliation evident. We postulate that prior to a gentle crushing impact, the friable equilibrated ordinary chondrites such as Bjurböle, Quenggouk, Saratov, and Tennasilm were composed of high-porosity (~20%) uncompacted material. The mild impact occurred post metamorphism when the chondrites were cool. The impact was intense enough to slightly deform the metal grains and cause breakage of the brittle silicates. Some primordial porosity, like that found in the high porosity uncompacted chondrites, was removed but an equal amount was created during the impact due to crushing of silicate mineral grains.

References: [1] Hirata N. et al. 2008. *Physics of the Earth and Planetary Interiors* 174:227–241. [2] Nakamura T. et al. 1995. *Meteoritics* 30:344–347. [3] Nakamura T. et al. 2000. *Icarus* 146:289–300. [4] Gattacceca J. et al. 2005. *Earth and Planetary Science Letters* 234:351–368. [5] Friedrich J. M. et al. 2008. *Earth and Planetary Science Letters* 275:172–180. [6] Friedrich J. M. et al. 2008. *Planetary and Space Science* 56:895–900. [7] Friedrich J. M., et al. 2013. *Geochimica et Cosmochimica Acta* 116:71–83. [8] Friedrich J. M. et al. 2014. *Earth and Planetary Science Letters* 394:13–19. [9] Consolmagno G. J. et al. 2008. *Chemie der Erde* 68:1–29. [10] Friedrich J. M. and Rivers M. L. 2013. *Geochimica et Cosmochimica Acta* 116:63-70. [11] Friedrich J. M. 2017. *Geochimica et Cosmochimica Acta* 203:157–174. [12] Lewis J. A. et al. 2018. *Geochimica et Cosmochimica Acta* 240: 293-313. [13] Wilkison S. L. et al. 2003. *Meteoritics & Planetary Science* 38:1533-1546. [14] Ashworth J. R. 1981. *Proc. R. Soc. Lond. A* 374:179-194. [15] Merrill G. P. 1919. *Mem. Nat. Acad. Sci.* XIV:1-15. [16] Macke R. J. 2010. *Ph. D. thesis*, Univ. Central Florida. [17] Sasso M. R. et al. 2009. *Meteoritics & Planetary Science* 44:1743-1753.

THE EFFECT OF X-RAY MICROTOMOGRAPHY IMAGING ON AMINO ACIDS AND THERMOLUMINESCENCE IN CHONDRITES.

J. M. Friedrich[1,2], D. W. G. Sears[3], D. P. Glavin[4], D. S. Ebel[2], M. L. Rivers[5], H. L. McLain[4,6], A. Sehlke[7], J. P. Dworkin[4], H. Sears[3]. [1]Department of Chemistry, Fordham University, 441 East Fordham Road, Bronx, New York 10458, USA e-mail: friedrich@fordham.edu, [2]Department of Earth and Planetary Sciences, American Museum of Natural History, 79th Street at Central Park West, New York City, New York 10024, USA, [3]NASA Ames Research Center/BAER Institute, Mountain View, California 95035, USA, [4]Solar System Exploration Division, NASA Goddard Space Flight Center, Greenbelt, Maryland 20771, USA,   [5]Center for Advanced Radiation Sources, University of Chicago, Argonne, Illinois 60439, USA, [6]Catholic University of America, Washington, District of Columbia 20064, USA, [7]NASA Ames Research Center/USRA, Mountain View, California 95035, USA.

Introduction: X-ray computed microtomography (μCT) and synchrotron μCT are a useful means of characterizing cosmochemical samples such as meteorites or robotically returned samples. Interesting mineralogies, lithologies, or petrographic structures can be identified in 3D prior to cutting the sample, resulting in critical material conservation and preservation [1]. Petrography and physical properties can be investigated without the making of traditional petrographic thin sections, whose study can complicate interpretation of complex 3D structures [e.g. 2-4]. With respect to chondrites, μCT is generally considered a nondestructive technique since the chemical structures of silicate and metallic minerals are generally unaffected by x-ray exposure at the intensities and wavelengths used for μCT imaging. However, there are concerns that the use of μCT may be detrimental to other components or aspects of chondritic samples. In a series of experiments described and reported in [5,6], we examined if exposure to μCT causes detectable changes in the soluble organic compound (amino acid) content of a carbonaceous chondrite. We have also reported [7,8] on the effects of exposure to x-rays during μCT imaging on the natural radiation record of chondrites, in the form of thermoluminescence (TL).

Samples and Methods: For experiments examining amino acids in chondrites, we used powdered aliquots of the Murchison CM chondrite, a sample for which the natural abundances of amino acids has been established [9,5,6]. For TL experiments we used powdered aliquots of the Bruderheim (L6) chondrite heated to 500°C to remove the natural TL before imaging experiments were carried out [7,8]. Synchrotron μCT imaging was done at the 13-BM-D bending magnet beamline at the of the GeoSoilEnviroCARS (GSECARS) facility at the Advanced Photon Source (APS), Argonne National Laboratory. The synchrotron beamline setup exposed the samples to monochromatic x-rays at energies between 25 and 47 keV [5,8]. "Benchtop" or laboratory μCT imaging [10] was performed with a GE phoenix v|tome|x s240 μCT system of the AMNH, which generates characteristic and bremsstrahlung X-rays from an inclined tungsten target [6,7]. In each experiment, we irradiated our samples (imaged using common to harsher than typical duration and intensity) but also kept appropriate unexposed control samples. Most x-ray exposed samples experienced between ~300 to 1500 Gy [see 5-8 for details]. Amino acid abundance and enantiomeric ratio quantification [9,5,6] and TL analysis [7,8] were done with established methods.

Results and Discussion:

Amino acids. We found that the abundances and enantiomeric ratios of amino acids extracted from the irradiated Murchison samples were within analytical errors of the measurements made on the control Murchison sample [1,2].

Thermoluminescence. Samples of the Bruderheim chondrite imaged by μCT were shown to absorb a radiation dose comparable to that observed by meteorites from cosmic rays, during their 10 to 100 million year exposure, and from internal radioactivities during their lifetime.

Conclusions: We conclude that a synchrotron μCT and polychromatic μCT experiments do not alter the abundances of amino acids or their enantiomeric ratios to a degree greater than how well those abundances or ratios are measured with our techniques and therefore any damage to amino acids is minimal. However, more detailed experiments on organic compound exposure should be considered before concluding absolutely no damage is done to small organic compounds. We also conclude that typical x-ray radiation dosages imparted into a chondrite with μCT eradicates the natural radiation history of the sample, as measured by TL.

References: [1] Ebel D.S. and Rivers M.L. 2007. *Meteoritics & Planetary Science* 42:1627–1646. [2] Friedrich J. M. et al. 2008. *Planetary and Space Science* 56:895–900. [3] Friedrich J. M., et al. 2013. *Geochimica et Cosmochimica Acta* 116:71–83. [4] Friedrich J. M. et al. 2014. *Earth and Planetary Science Letters* 394:13–19. [5] Friedrich J. M. et al. 2016. *Meteoritics & Planetary Science* 51:429-437. [6] Friedrich J. M. et al. 2019. *Meteoritics & Planetary Science* 54:220-228. [7] Sears D. W. G. 2016. *Meteoritics & Planetary Science* 51:833-838. [8] Sears D. W. G. 2018. *Meteoritics & Planetary Science* 53:2624-2631. [9] Glavin D. P. et al. 2010. *Meteoritics & Planetary Science* 45:1948-1972. [10] Ebel D. S. and Friedrich J. M. this workshop.

SIMULATION OF A COLD CURATION PRELIMINARY EXAMINATION USING A HAMBURG METEORITE

M. Fries[1], F. McCubbin[1], R. A. Zeigler[1], A. Burton[1], A. Harrington[1], R. Landis[1], J. Mitchell[1], P. Niles[1], K. Righter[1], A.B. Regberg[1], M. Zolensky[1], T. Slisher[2], C.D.K. Herd[3], R. Harrington[6], N. Haney[4], D. Archer[4], J. Hogencamp[4], Z. Wilbur[4], J. Barnes[4] L. Welzenbach[5], A. Steele[6]
[1]Astromaterials Research and Exploration Science (ARES), NASA Johnson Space Center, [2]Sloan*Longway Museum, Flint, MI, [3]University of Alberta, Canada, [4]Jacobs, Houston TX, [5]Open University, UK, [6]Carnegie Institution for Science, Washington DC. Contact: marc.d.fries@nasa.gov

Introduction: The Hamburg, Michigan (H4 chondrite) meteorite fall occurred at 01:08:33 UTC on 17 Jan 2018 (8:08:33 PM local time, 16 Jan). The fireball traveled west of Detroit, MI along an azimuth of approximately 288° according to 674 eyewitness accounts compiled by the American Meteor Society (AMS), which records the event as #168 for the year 2018. Shortly after the fall, meteorites were recovered from the frozen surface of small lakes near Hamburg. One ~5g stone was collected in a clean fashion, kept frozen, and delivered to the Astromaterials Acquisition and Curation Office at NASA Johnson Space Center without allowing it to thaw. This meteorite provides a unique opportunity to study a meteorite that has not thawed since its recovery. A plan to study this frozen sample of Hamburg meteorite is being executed as if it were a returned sample from a cold sample return mission. The purposes are to perform an end-to-end trial of a conceptual Curatorial Preliminary Examination process for a cold sample, and to identify procedural, technological, and analytical strengths and shortcomings in the PE process for cold astromaterials. Lessons learned will feed forward to actual cold sample return missions.

Description: Curatorial Preliminary Examination (PE) is the process whereby astromaterials from a sample return mission are first described and analyzed for the purpose of documenting their as-received condition. PE is the first step before addressing the science goals of a sample return mission. The PE Team (PET) performs a broad suite of analyses to characterize mineralogical, organic, isotopic, and other aspects of the material in accordance with the defined mission goals. This characterization is used to guide future analyses. To date, NASA has not performed a cold sample return spaceflight mission, but upcoming potential missions will do so (e.g. comet, lunar volatiles, and/or icy world sample return). The primary purpose of the Hamburg meteorite study is to test established PE procedures adapted for a cold sample, and to identify strengths and weaknesses in the protocol. The principal science product will be a thorough lessons-learned description and recommendations for cold curation of actual sample return materials which will feed forward to cold curation processing capabilities at NASA JSC.

The Hamburg meteorite was generously loaned for this purpose by the Sloan Museum and Longway Planetarium (Sloan*Longway) in Flint, MI. The meteorite was delivered cold (-20°C) to NASA Curation and is maintained at -20°C. A metal-free, cold container was fashioned and used for XCT imaging as a first step in the analytical sequence. To characterize the background contamination environment, microbial swab samples were collected before and after XCT and the Opera (v.1) [1] instrument followed the meteorite through the XCT process, monitoring the particulate and organic contaminant background. XCT imagery was performed without removing Hamburg from its packaging, and it was returned to the freezer afterwards. The meteorite will be transported to the Subzero Facility for Curation of Astromaterials at the University of Alberta [2] for sub-sampling, using clean NASA Curation hardware in a cold (-20°C) glovebox environment. Next steps in the analytical sequence include thermal analysis to measure volatile content of the frozen meteorite, FT-IR before and after thaw to assess chemical changes incurred during thaw, pyrolysis-GC-MS to obtain bulk organic content, extraction-based GC analysis of the interior and exterior of the stone, C-XANES of minor carbon phases, petrography/mineralogy examination and description, and imaging Raman spectroscopy to provide spatial context for the mineralogical and carbonaceous components. Microbial swab and Opera measurements will be performed during transport and handling of the meteorite. Finally, the remaining meteorite mass will be cut and polished for public display at the Longway Planetarium. 3-D printed models of the meteorite will be produced from XCT data and referenced throughout the processing steps, and will be provided to Sloan*Longway along with XCT imagery for science outreach purposes.

Summary: Cold sample return is a component of future NASA mission planning. Cold Curation is a significant but achievable technical challenge, and the Hamburg exercise provides NASA Curation with unique experience needed to prepare for upcoming missions.

References: [1] Fries, M.D., Fries, W.D., McCubbin, F.M. and Zeigler, R.A., 2018. 49th LPSC, Abstract #2276. [2] Herd C.D.K. et al. (2016) *MAPS*, 51, 499-519.

RECOVERING THE 07 MAR 2018 METEORITE FALL INTO THE OLYMPIC COAST NATIONAL MARINE SANCTUARY

M. Fries[1], J. Waddell[2], OET and crew of E/V *Nautilus*[3], SOI and crew of R/V *Falkor*[4], B. Pugel[5], R. Zeigler[1], R. Harvey[6], L. Welzenbach[7], F. McCubbin[1], and P. Abell[1]
[1]NASA JSC, [2]NOAA Olympic Coast NMS, [3]Ocean Exploration Trust, [4]Schmidt Ocean Institute, [5]NASA GSFC, [6]Case Western Reserve U., [7]Rice U. Email: marc.d.fries@nasa.gov

On 07 March 2018 at 20:05 local time (08 March 03:05 UTC), a dramatic meteor occurred over the Olympic Coast Marine Sanctuary off of the Washington state coast. Eyewitnesses reported the sky brightening significantly and those near the coast reported sonic booms loud enough to shake homes and cars, although the number of witnesses to the actual fireball was limited by cloud cover. Data from seismometers (including several mounted on the seafloor), weather radars, and even a moored weather buoy indicate that a massive meteorite fall resulted from this event, with many kilograms of meteorites deposited into the ocean around 47.441713° N 124.661732° W. Dominant winds were out of the WSW, and so the largest meteorites landed at the western end of a strewn field approximately 11 km long, with progressively smaller meteorites trending towards the east. Weather radar data indicate that this was the largest meteorite fall to occur within the range of the NOAA NEXRAD nationwide radar network since the system went online in the mid-1990s, during which time over two dozen meteorite falls have been recorded by the network (*Fig.1*). The falling meteorites included individual rocks large enough to create splashes recorded by the KLGX radar (Langley Hill, WA) in multiple lowest-elevation sweeps.

Figure 1: Composite image of NEXRAD signatures of falling meteorites. Credit: Google Earth

The size distribution of meteorites observed on radar indicate a scientifically important feature - this meteorite fall was mechanically much tougher than all meteorite falls observed in NEXRAD data to date. Total mass estimates are provided by the Niðhöggr radar-based mass estimate model in terms relative to the Park Forest, IL meteorite fall (27 Mar 2003)[2]. From the 1-10g meteorite range, the Washington coast fall is 4.9x the mass of Park Forest, and for the 10-1,000g mass interval it is 9.5x the mass of the same interval of the Park Forest fall. This fall has favored the survival of large meteorites, suggesting that the meteorite is significantly tougher than the Park Forest L5 chondrite, or other meteorites (almost all OCs) analyzed using Niðhöggr to date. This makes recovery of meteorite(s) scientifically important for two reasons. One, whatever type of meteorite this is more capable of causing more damage on the ground than the average meteorite fall. Second, knowing the meteorite type will allow identification of future falls through weather radar alone.

Figure 2: SEM image of melt spherule recovered in the R/V Nautilus expedition. This 2mm-diameter sphere features magnetite dendrites throughout, minor carbonaceous inclusions, and a thin vesicular silicate rim. These features are consistent with a recently fallen meteorite melt spherule [1].

In June 2018, the Ocean Exploration Trust and the crew of the E/V *Nautilus* attempted recovery of meteorites at the fall site. During an eight-hour ROV dive, *Nautilus* recovered seven samples of seafloor sediment but did not locate large stones. Analyses produced a single 2mm-diameter sphere of unweathered, melted meteorite material (*Fig.2*). Raman spectroscopy and SEM/EDS reveal the spherule is predominantly silicate glass with abundant magnetite dendrites, minor carbonaceous inclusions, and minor sulfides consistent with mildly distorted pentlandite. However, unmelted material is needed to address the primary science questions of the full identity of the meteorite and its mechanical strength.

The Schmidt Ocean Institute (R/V *Falkor*) will attempt a second recovery effort in early June 2019. The primary goal is to recover at least one meteorite fragment containing unmelted meteorite material, preferably >5g in mass. This effort will draw upon lessons learned from the *Nautilus* expedition, focusing on small material in the "small end" of the meteorite strewn field, with secondary search targets drawn from splashes seen in KLGX data and calculated landing sites of the largest meteorites seen on radar.

References: [1] Harvey, R.P. et al, 1998. Geology, 26(7), pp.607-610. [2] Fries, M., et al 80th MetSoc (2017) Abstract #6251.
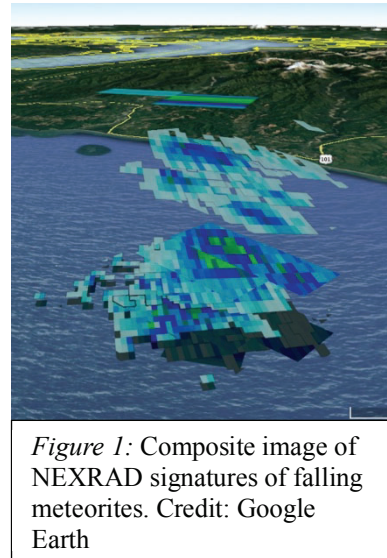
Short-lived radioisotopes in meteorites from Galactic-scale correlated star formation

Y. Fujimoto[1], M. R. Krumholz[2], and S. Tachibana[3], [1]Research School of Astronomy & Astrophysics, Australian National University, Canberra, Australian Capital Territory 2611, Australia (yusuke.fujimoto@anu.edu.au), [2]Research School of Astronomy & Astrophysics, Australian National University, Canberra, Australian Capital Territory 2611, Australia (mark.krumholz@anu.edu.au), [3]UTokyo Organization for Planetary and Space Science (UTOPS), The University of Tokyo, 7-3-1 Hongo, Tokyo 113-0033, Japan (tachi@eps.s.u-tokyo.ac.jp)

Introduction: Short-lived radioisotopes (SLRs) are radioactive elements with half-lives ranging from 0.1 Myr to more than 15 Myr that existed in the early Solar system. They were incorporated into meteorites' primitive components when the oldest solids formed in the Solar protoplanetary disc. Most SLRs form in the late stages of massive stellar evolution, followed by injection into the interstellar medium (ISM) by stellar winds and supernovae (SNe) [e.g., 1]. Explaining how they travelled from these origin sites to the primitive Solar system before decaying is an outstanding problem [e.g., 2]. Proposed mechanisms fall into three broad scenarios. The first scenario is a SN-triggered collapse: a nearby Type II SN injects SLRs and triggers the collapse of the early Solar nebula [e.g., 3, 4, 5]. The second scenario is direct pollution: the Solar system's SLRs were injected directly into an already-formed protoplanetary disc by SN ejecta within the same star-forming region [e.g., 6, 7]. The third scenario is sequential star formation events and self enrichment in a giant molecular cloud (GMC) [e.g., 8, 9, 10]. Consensus has not reached yet, and no one has yet investigated galactic-scale SLR distributions. However, one should take account of Galactic-scale chemodynamics for chemical enrichment due to massive stars.

Method: We study the abundances of ^{60}Fe and ^{26}Al in newly-formed stars by performing a high-resolution chemo-hydrodynamical simulation of the ISM of a Milky-Way like galaxy. The simulation includes hydrodynamics, self-gravity, radiative cooling, photoelectric heating, stellar feedback in the form of photoionisation, stellar winds and supernovae to represent dynamical evolution of the turbulent multi-phase ISM. Further details on our numerical method are given in Fujimoto et al. (2018) [11].

Results: The distributions of ^{60}Fe and ^{26}Al are strongly correlated with the star-forming regions (see Fig. 3 of [11]). This is as expected, since these isotopes are produced by massive stars, which, due to their short lives, do not have time to wander far from their birth sites. However, there are important morphological differences between the distributions of ^{60}Fe, ^{26}Al, and star-forming regions. The ^{60}Fe distribution is the most extended, with the typical region of ^{60}Fe enrichment exceeding 1 kpc in size, compared to 100 pc or less for the ISM density peaks that represent star-forming regions. The ^{26}Al distribution is intermediate, with enriched regions typically hundreds of pc in scale. The larger extent of ^{60}Fe compared to ^{26}Al is due to its larger lifetime (2.62 Myr versus 0.72 Myr for ^{26}Al) and its origin solely in fast-moving SN ejecta (as opposed to pre-SN winds, which contribute significantly to ^{26}Al).

To investigate abundance ratios of isotopes in newborn stars, whenever a star particle forms in our simulations, we record the abundances of ^{60}Fe and ^{26}Al in the gas from which it forms, since these should be inherited by the resulting stars (see Fig. 5 of [11]). The probability distribution function (PDF) of ^{60}Fe peaks near ^{60}Fe/^{56}Fe $\sim$ 3e−7, but is $\sim$ 2 orders of magnitude wide, placing all the meteoritic estimates well within the ranges covered by the simulated PDF. The ^{26}Al abundance distribution is similarly broad, but the measured meteoritic value sits very close to its peak, as ^{26}Al/^{27}Al $\sim$ 5e−5. Clearly, the abundance ratios measured in meteorites are fairly typical of what one would expect for stars born near the Solar Circle, and thus the Sun is not atypical.

Conclusion: The SLRs are not confined to the molecular clouds in which they are born. However, SLRs are nonetheless abundant in newborn stars because star formation is correlated on Galactic scales. Thus, although SLRs are not confined, they are in effect pre-enriching a halo of the atomic gas around existing GMCs that is very likely to be subsequently accreted or to form another GMC, so that new generations of stars preferentially form in patches of the Galaxy contaminated by previous generations of stellar winds and supernovae.

Reference: [1] Huss, G. R. et al. (2009) *Geochimica et Cosmochimica Acta* 73, 4922-4945. [2] Adams, F. C. (2010) *Annual Review of Astronomy and Astrophysics* 48, 47-85. [3] Cameron, A. G. W. and Truran, J. W. (1977) *Icarus* 30, 447-461. [4] Boss et al. (2010) *The Astrophysical Journal* 708, 1268-1280. [5] Gritschneder et al. (2012) *The Astrophysical Journal* 745, 22. [6] Chevalier, R. A. (2000) *The Astrophysical Journal* 538, L151-L154. [7] Ouellette et al. (2010) *The Astrophysical Journal* 711, 597-612. [8] Gounelle, M. and Meynet, G. (2012) *Astronomy & Astrophysics* 545, A4. [9] Young, E. D. (2014) *Earth and Planetary Science Letters* 392, 16-27. [10] Kuffmeier et al. (2016) *The Astrophysical Journal* 826, 22. [11] Fujimoto et al. (2018) *Monthly Notices of the Royal Astronomical Society* 480, 4025-4039.

ANHYDRITE IN THE JBILET WINSELWAN CM CHONDRITE: IMPLICATIONS FOR THE HEAT SOURCE OF POST-ALTERATION THERMAL METAMORPHISM

W. Fujiya[1], H. Higashi[1], A. Yamaguchi[2], M. Kimura[2], and K. Hashizume[1], [1]Faculty of Science, Ibaraki University, 2-1-1 Bunkyo, Mito 310-8512, Japan (wataru.fujiya.sci@vc.ibaraki.ac.jp), [2]National Institute of Polar Research, Midoricho10-3, Tachikawa, Tokyo 190-8518, Japan.

Introduction: CM chondrites are aqueously altered in their parent body [e.g., 1]. Some of them apparently underwent post-alteration thermal metamorphism associated with changes in their mineralogy and chemical composition [2,3]. However, the heat source for this thermal metamorphism has remained poorly understood. Here we report petrology and mineralogy of the Jbilet Winselwan (JW) CM chondrite, especially focusing on the evidence for post-alteration heating. We note that this meteorite contains Ca-sulfate, a rare mineral in CM chondrites [4]. The presence of Ca-sulfate in JW suggests a unique physicochemical condition of aqueous alteration not common for typical CM chondrites.

Experimental: A polished thin section of JW was observed with a Scanning Electron Microscope (SEM) at NIPR (JEOL JSM-7100F). The chemical compositions of tochilinite/cronstedtite intergrowths (TCIs), a unique material which can be found only in CM chondrites, were determined with an Electron Probe Micro Analyzer (EPMA) at NIPR (JEOL JXA-8200). Polymorphs of Ca-sulfate were identified with Raman spectroscopy at NIPR (JASCO NRS-1000).

Results and discussion: The chondrules in the JW thin section have an average diameter of ~0.29 mm. The chondrule phenocrysts are mildly altered, while the chondrule mesostases are completely replaced by phyllosilicate. Carbonate minerals in JW are predominantly calcite. Fe-Ni metal grains account for ~0.26 vol.%, which are present mainly in the chondrule interior. These features are consistent with those of CM chondrites with a petrologic subtype of 2.3 [5].

Sulfide minerals in JW are pyrrhotite with abundant pentlandite blebs, indicating mild heating as category B defined by Kimura et al. [3]. Large TCI clumps, which are commonly found in CM chondrites, are rare in JW. TCIs in JW have lower S/SiO_2 and higher FeO/SiO_2 ratios (~0.16 and ~3.2, respectively) than expected from the correlation between TCI compositions and degrees of alteration [5]. These observations suggest that TCIs in JW were, at least partially, decomposed by heating because tochilinite is unstable at high temperatures of >170 ^{o}C [6]. The decomposition of TCIs has also been confirmed for other thermally metamorphosed CM chondrites and an experimentally heated Murchison sample [7].

In many cases, Ca-sulfate grains are surrounding calcite grains, indicating that Ca-sulfate subsequently precipitated after calcite at the same alteration event. The Ca-sulfate is identified as orthorhombic or cubic anhydrite ($CaSO_4$), although possible presence of metastable bassanite ($CaSO_4 \cdot 0.5H_2O$) cannot be ruled out because of their similar Raman bands (anhydrite at 1017 cm^{-1} and bassanite at 1015 cm^{-1} [8]). Gypsum ($CaSO_4 \cdot 2H_2O$), which is stable at low temperatures of <110 ^{o}C [8], is absent. The absence of gypsum also indicates that JW underwent heating.

In summary, JW was heated after aqueous alteration. Because we found substantial amounts of Ca-sulfate, Ca-sulfate is one of the main carriers of sulfur. We propose that sulfur in Ca-sulfate was supplied from TCIs decomposed by heating, and that the compositions of aqueous solutions changed to be favorable for precipitation of sulfate over carbonate. If correct, then Ca-sulfate may have precipitated as anhydrite (or bassanite) at high temperatures of >170 ^{o}C, not as gypsum at low temperatures which was subsequently dehydrated and transformed to anhydrite by heating. The intimate association of calcite and anhydrite may be inconsistent with later impact heating. Thus, the energy for the heating of JW was most likely provided from ^{26}Al decay. We will conduct Mn-Cr dating of calcite to determine the timing of calcite/anhydrite precipitation, and to see whether the formation age of calcite/anhydrite in JW is similar to the ages of typical CM carbonates, namely, ~4563 Ma [9].

References: [1] Brearley A. J. (2006) in *Meteorites and the Early Solar System II*, D. S. Lauretta & H. Y. McSween Jr., Eds. (The Univ. of Arizona Press, Tucson), pp. 587-624. [2] Nakamura T. (2005) *J. Mineral. Petrol. Sci.* 100, 260–272. [3] Kimura M. et al. (2011) *Meteorit. Planet. Sci.* 46, 431-442. [4] Lee M. R. (1993) *Meteoritics* 28, 53-62. [5] Rubin A. E. et al. (2007) *Geochim. Cosmochim. Acta* 71, 2361-2382. [6] Zolensky M. E. (1984) *Meteoritics* 19, 346–347. [7] Nakato A. et al. (2008) *Earth, Planets and Space* 60, 855–864. [8] Prieto-Taboada N. et al. (2014) *Anal. Chem.* 86, 10131–10137. [9] Fujiya W. et al. (2012) *Nat. Commun.* 3, 627.

MAGNESIUM ISOTOPE ANALYSIS OF OLIVINE BY SIMS: CALIBRATION OF MATRIX EFFECTS.

K. Fukuda[1], B. L. Beard[1,2], M. J. Spicuzza[1], and N. T. Kita[1]. [1]Department of Geoscience, University of Wisconsin-Madison, Madison, WI 53706, USA (kfukuda2@wisc.edu), [2]NASA Astrobiology Institute, USA.

Introduction: Magnesium has three naturally occurring stable isotopes (^{24}Mg, ^{25}Mg, and ^{26}Mg) allowing one to study mass-dependent and mass-independent isotope fractionation induced by natural processes. While Secondary Ion Mass Spectrometry (SIMS) can potentially provide high precision (sub per mil) Mg isotope data with ~3-40 µm spatial resolution [e.g., 1-6], SIMS instrumental mass fractionation (IMF) of Mg isotope analysis tend to be much larger than that of multi-collector inductively coupled plasma mass spectrometry (MC-ICP-MS) [7 and references therein]. The magnitude of IMF is a function of the chemical composition of the sample [e.g., 8], and this is referred to as a 'matrix effect'. Thus, matrix-matched standards are required and IMF must be evaluated for accurate measurements by SIMS.

Recently, we investigated SIMS matrix effects on Mg isotope analysis of olivine and observed a complex IMF for $\delta^{25}Mg$ as a function of Mg#60-100 [9]. In this study, we conducted additional SIMS Mg isotope and minor element concentration analyses of 17 terrestrial and meteoritic olivines for further evaluation of SIMS matrix effects. Mg isotope ratios of 7 out of 17 olivines have been determined by solution MC-ICP-MS [10, 11], and the rest of the olivines have been measured by laser ablation MC-ICP-MS [9]. Our goal is to develop a protocol of high accuracy and high spatial resolution Mg isotope analysis and to apply this for meteoritic olivine (e.g., in chondrules and amoeboid olivine aggregates) as well as small and precious particles obtained by sample return missions (e.g., *Stardust*, *Hayabusa2*, and *OSIRIS-REX*).

Multi-FC Mg isotope analysis: Magnesium three-isotope analyses of 17 olivine samples were performed with the Cameca IMS 1280 at the University of Wisconsin-Madison (WiscSIMS) equipped with a radio-frequency plasma ion source. The analytical conditions are generally similar to those described in [6]. A 7 µm diameter (1 nA) primary O_2^- beam was used for analyses. The secondary ion intensity of $^{24}Mg^+$ on San Carlos olivine (Fo$_{88.8}$) was typically ~2 $\times$ 10^8 cps. The external reproducibilities (2SD) of raw $\delta^{25}Mg$, $\delta^{26}Mg$, and $\delta^{26}Mg^*$ of San Carlos olivine were 0.09‰, 0.16‰, and 0.07‰, respectively.

Single-EM minor element concentration analysis: Minor element concentration analyses of 17 olivine samples were performed with the Cameca IMS 1280. A ~1.3 µm diameter (6 pA) primary O_2^- beam was used for analyses. Secondary $^{23}Na^+$, $^{24}Mg^+$, $^{27}Al^+$, $^{28}Si^+$, $^{40}Ca^+$, $^{52}Cr^+$, $^{55}Mn^+$, $^{56}Fe^+$, and $^{60}Ni^+$ ions were detected by an axial EM that operated by peak jumping.

Results and Discussion: Olivine IMF ranges over ~3‰ in $\delta^{25}Mg$ as a function of Mg#60-100. The IMF is not a smooth function of Mg# but rather the IMF jumps by 1.2 and 1.5‰ between Mg#86 and 88, and 97.5 and 100, respectively. We also observed systematic differences in magnitudes of IMF by 0.3‰ between two olivine samples with similar Mg#s (94.7 and 94.9, respectively), suggesting that the IMF is not solely controlled by Mg (and Fe) contents. In order to examine the additional factor(s) that effect the IMF, we compared the magnitude of IMF, minor element abundances, and ionization efficiencies of each element. Large and non-linear variabilities in ionization efficiencies of Mg and Si were observed against Mg#s. The relationship between $^{24}Mg^+/^{28}Si^+$ ratios and Mg#s are similar to the complex IMF as a function of Mg#s, suggesting that the part of IMF results from differences in the ionization efficiencies of Mg and Si. The observed relationships imply that the IMF correction for $\delta^{25}Mg$ in olivine can be constrained by using a combination of Mg contents and $^{24}Mg^+/^{28}Si^+$ ratios. It is unclear why ionization efficiencies of Mg and Si vary between different olivines but one possibility is differences in minor element abundances. For instance, olivine samples with higher Mg contents (Mg#>90) and Cr-bearing (CrO ~0.40 wt%) olivine samples show higher magnitudes of IMF and also higher $^{24}Mg^+/^{28}Si^+$ ratios than those of the other olivine samples. The results suggest that minor element abundances create a secondary, but important effect on the IMF.

References: [1] Kita N. T. et al. (2012) *Geochimica et Cosmochimica Acta* 86, 37-51. [2] Bullock E. S. et al. (2013) *Meteoritics & Planetary Science* 48, 1440-1458. [3] Luu T.-H. et al. (2013) *Journal of Analytical Atomic Spectrometry* 28, 67-76. [4] Ushikubo T. et al. (2013) *Geochimica et Cosmochimica Acta* 109, 280-295. [5] Ushikubo T. et al. (2017) *Geochimica et Cosmochimica Acta* 201, 103-122. [6] Hertwig A. T. et al. (2019) *Geochimica et Cosmochimica Acta* 253, 111-126. [7] Chaussidon M. et al. (2017) *Reviews in Mineralogy & Geochemistry* 82, 127-163. [8] Valley J. W. and Kita N. T. (2009) *Mineralogical Association of Canada Short Course* 41, 19-63. [9] Fukuda K. et al. (2019) *LPS L*, Abstract #1989. [10] Xiao Y. et al. (2013) *Geochimica et Cosmochimica Acta* 115, 241-261. [11] Kita N. T. et al. (2016) *Goldschmidt,* Abstract #1538.

MG ISOTOPE RATIOS AND MINOR ELEMENT ABUNDANCES OF AOAS:
INSIGHTS INTO THEIR ORIGINS.

K. Fukuda[1], N. T. Kita[1], T. J. Tenner[2], and M. Kimura[3].
[1]Department of Geoscience, University of Wisconsin-Madison, Madison, WI 53706, USA (kfukuda2@wisc.edu),
[2]Chemistry Division, Nuclear and Radiochemistry, Los Alamos National Laboratory, MSJ514 Los Alamos, NM 87545, USA. [3]National Institute of Polar Research, Tachikawa, 190-8518 Tokyo, Japan.

Introduction: Amoeboid olivine aggregates (AOAs) are irregularly shaped objects composed of olivine, Ca, Al-rich minerals, and FeNi metal. AOAs show variations in terms of their textures and minor element abundances, which are in some cases correlated with each other and suggest that they formed under various physicochemical conditions in the solar nebula [1]. Another important thing is that some AOAs have negative δ^{25}Mg values [2-5] relative to the Earth and bulk chondrites (δ^{25}Mg = –0.13‰ in DSM3 scale [6]). The light isotope enrichments imply that some AOAs condensed from the nebular gas [7]. Because AOAs appear to have escaped extensive melting after their genesis [e.g., 8 and reference therein], their formation processes would reflect specific physicochemical conditions in the solar nebula that AOAs had experienced. However, relationships between chemical, textural, and isotopic signatures of AOAs have not been systematically investigated extensively. In this study, we conducted SIMS minor element concentration analyses of AOAs with known O and Mg isotope ratios from our previous study [5], and discuss their origins.

Sample and methods: Eight AOAs, one from the Kaba (CV3.1) and seven from the DOM 08006 (CO3.01 [9]) chondrites, were analyzed. Olivines in these AOAs have no any ferroan rims. Oxygen and Mg isotope ratios of olivines in these AOAs have been determined by [5]. Eight AOAs studied here have variations in porosity and compactness. Three out of eight AOAs appear to be dense objects with little porosity (referred to as "compact" texture by [1]). The rest of the five AOAs have more irregular shapes and abundant porosity ("porous" texture by [1]). Minor element concentration analyses were performed with the Cameca IMS 1280 (WiscSIMS). Because of limited analysis areas on samples, we focused a primary O_2^- beam down to 1.3 µm in diameter (6 pA) that were placed inside the previous SIMS pits (5 µm in diameter) from Mg isotope analyses [5]. Secondary $^{23}Na^+$, $^{24}Mg^+$, $^{27}Al^+$, $^{28}Si^+$, $^{40}Ca^+$, $^{52}Cr^+$, $^{55}Mn^+$, $^{56}Fe^+$, and $^{60}Ni^+$ ions were detected by an axial EM with magnetic peak jumping mode. We re-evaluated previous Mg isotope analyses of the same AOAs [5] by applying a new SIMS bias correction method using Mg/Si ionization yields [10].

Results and Discussion: AOA olivines studied here show negative correlations between Ca and Cr, Mn abundances, such as Ca-rich olivines tend to show Cr, Mn-poor signatures. The trend is qualitatively explained by condensation and/or evaporation processes due to differences in their volatility [1]. In particular, porous AOAs are volatile rich and refractory poor (i.e., Ca-poor and Cr-rich) relative to compact AOAs. Similar textures and minor element systematics in AOA olivines have been indicated from a previous electron microprobe study [1], which were confirmed by the present SIMS analyses.

With the new bias correction method [10], Mg isotope ratios of the AOAs all show negative δ^{25}Mg values (–3.9 to –0.4‰ in DSM3 scale) that are systematically offset from those reported in [5]. Mg isotope ratios of porous AOAs show a larger variability and are positively correlated with Cr abundances. These results may be explained by slightly non-equilibrium condensation from the solar nebula at different temperatures (e.g., P = 10^{-3} bars at T = ~1100-1400 K [7]). Mg isotope ratios of compact AOAs are near-chondritic and do not show a significant variation. Considering their textures, compact AOAs likely experienced reheating processes in the nebula. If so, less refractory Cr might be lost by volatilization during reheating, while Ca abundances in olivine might increase by diffusion from adjacent Ca, Al-rich halos and/or minerals [1].

Conclusions: The present results demonstrate that porous AOAs formed by non-equilibrium condensation from the nebula, but compact AOAs experienced reheating processes after their formation.

References: [1] Sugiura N. et al. (2009) *Meteoritics & Planetary Science* 44, 559-572. [2] Larsen K. K. et al. (2011) *The Astrophysical Journal* 735, L37 (7pp). [3] Olsen M. B. et al. (2011) *Meteoritics & Planetary Science* 46, 1688-1702. [4] MacPherson G. J. et al. (2012) *Earth and Planetary Science letters* 331-332, 43-54. [5] Fukuda K. et al. (2019) *LPS L*, Abstract #1989. [6] Teng F.-Z. et al. (2010) *Geochimica et Cosmochimica Acta* 74, 4150-4166. [7] Richter F. M. et al. (2004) *Geochimica et Cosmochimica Acta* 68, 4971-4992. [8] Krot A. N. et al. (2004) *Chemie der Erde* 64 185-239. [9] Tenner T. J. et al. (2018) *LPS XLIX*, Abstract #1510. [10] Fukuda K. et al. (2019) this meeting.

SAVIOUR OF PRESOLAR GRAINS – ICE MANTLE : MYTH OR TRUTH.

A. Garg[1,2], V. Goyal[1] and K. K. Marhas[1], [1]Planetary Science Division, Physical Research Laboratory,Ahmedabad, Gujarat, 380009, India Email: kkmarhas@prl.res.in, [2]Dept. of Earth Sciences, Indian Institute of Technology Roorkee, Roorkee, Uttrakhand 247667, India Email: agarg@es.iitr.ac.in

Introduction: Presolar grains travelling in interstellar medium(ISM) at low density and temperature region allow molecules to be adsorbed on the grain, forming an ice mantle on the grain. The composition of ice in a molecular cloud varies with the local conditions depending on various factors like shock waves, the collision of grains, absorption of photons etc.Model calculations have been carried out to show the destructive nature of the ice mantle when exposed to the high energy galactic cosmic rays (GCR). Preliminary results indicate that ice mantle increases the effect of GCR on the Presolar core of the grain. Also, the ice mantle absorbs the energy of the ejected atoms from the core. According to observations on the lifetime estimates of large grains analyzed by Hirashita [1], SiC grains with radius $\geq$ 1µm seems to survive for more than 1 Gyr in the interstellar medium. For ice composition, we use the data obtained in [2] for Elias 16, a quiescent region, and compared it with a hypothetical case of a grain having no ice thickness. For ice thickness, we used extrapolated the data provided by [3].

Approach: We report calculations using recoil and energy data obtained from SDTrimSP (Version 5.07) for a given set of inputs over Vikram 100 (HPC Supercomputing Facility at PRL, Ahmedabad). Data obtained by [4] for the composition of galactic cosmic rays at several points has been considered in this work.

Results: We compared the data for recoils generated due to collision of grain core with GCRs for two types of SiC grains having diameter 1µm and same temperature conditions, one with no ice mantle and another for an ice mantle 0.02µm thick, for GCRs having energy between 10MeV – 1GeV and incidence angle between 0-89.9°. The difference in the number of recoils due to GCRs incident at an angle between 0-40° ranges between 27 - 0. The results for angles greater than 40° are highly ambiguous mainly because the GCR, when it enters the ice mantle at large incident angles, experiences a strong deflection and the angle becomes less or more than the incident angle. Following graph shows the plot between the Average difference in the number of Recoils per GCR(n) and the incident energy of the GCR.
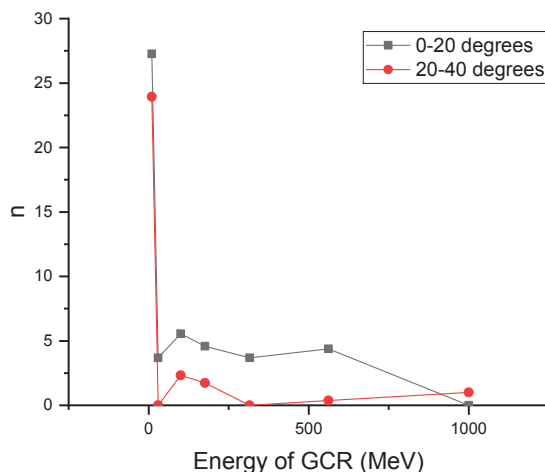
According to preliminary data, the possible explanation for the difference in the number of recoils is that the sputtering yield and the energy transferred by GCRs to the target atoms decreases with increase in energy for GCR having energy in range 10MeV to 1GeV, at which the abundance of GCR is maximum. Therefore, as the GCRs pass through the ice mantle, they loose a significant amount of energy in transit. Thus, in the grain with ice mantle, the GCR enters the core part with lower energy and therefor experience more recoil and sputtering.

Upon further analysis, it is established that the ice mantle retains most of the Si and C atoms which are ejected from the core of the grain and their Kinetic Energy (KE) which increases the temperature of the mantle. The energy lost, for instance, due a GCRs travelling at 100MeV which entered a grain at angles between 40°-60° was calculated to be 166KeV. This represents a small fraction of total number of GCRs entering the grain and therefore the total K.E lost to ice mantle is enough to partially destroy it due to thermal energy.

References: [1] Hirashita (2016) PSS 133 (2016) 17–22. [2] Gibb et al. 2004 ApJS, 151:35–73. [3] Pauly & Garrod 2016, 817:146. [4]Webber and Higbie (2008) JGR, volume. 113, A11106.

Meteorite Heating During Atmospheric Entry

J. Gattacceca[1], L. Bonal[2], G. Montagnac[3]. [1]CNRS, Aix Marseille Univ, IRD, Coll France, INRA, CEREGE, Aix-en-Provence, France (gattacceca@cerege.fr), [2]Institut de Planétologie et d'Astrophysique de Grenoble – Université Grenoble Alpes, CNRS, Grenoble, France. [3]LGLTPE ENS Lyon, CNRS, Lyon, France

Introduction: The extent of meteorite heating during atmospheric entry has to be considered when studying properties that are highly temperature sensitive. This is the case for instance of paleomagnetic studies: even mild heating ($\geq$150°C) can impart a partial thermoremanent magnetization to the meteorite (because cooling occurs in the geomagnetic field), interfering and potentially obliterating the original paleomagnetic signal. Another example is the study of incipient parent body thermal metamorphism in primitive chondrites. Modeling and thermoluminescence data show that strong heating ($\geq$400°C) is restricted to only about 1 mm below the fusion crust [1]. However, it is not well known how deeper mild heating (200-400°C) can affect the meteorite. In view of the recent renewal of meteorite paleomagnetism and the never-ending quest for the most pristine chondritic materials, we address here the question of how much the heat wave can penetrate a meteorite during atmospheric entry.

Results: We studied two meteorites that have suffered no or very weak thermal metamorphism on their parent body (Murchison CM2, and EET 90628 LL3.0). These two meteorite groups were chosen to span a wide range of porosity (17.1% in Murchison, 6.0% in EET 90628 [2]). Porosity is indeed a parameter that may strongly affect the penetration of the heat wave. We studied two fusion crusted sample of these meteorites. A sample of Murchison bearing a fusion crust created artificially in a wind tunnel experiment [3] was also studied. The penetration of the heat wave below the fusion crust was evaluated using two properties that are highly sensitive even to mild temperatures: remanent magnetization and degree of maturity of the polyaromatic organic matter.

We acquired Raman spectra in matrix-rich areas at increasing distances from the fusion crust (in both punctual and mapping modes) and monitored the evolution of the spectral parameters of interest compared to the same parameters measured away from the fusion crust [e.g., 4].

Paleomagnetism will be used as an independent proxy for the heat wave penetration in Murchison. Indeed, when heated during atmospheric entry, Murchison will have acquired a partial thermal remanent magnetization (pTRM) in the geomagnetic field (about 57 µT at the location of Murchison fall). This pTRM can easily be distinguished from the original extraterrestrial magnetization of Murchison that was acquired in much weaker field of about 1 µT [5]. Using progressive thermal demagnetization, we can estimate the maximum unblocking temperature of this pTRM, which corresponds to the peak temperature during atmospheric entry. Based on the Raman spectroscopy results, we prepared samples at different distances from the fusion crust and estimate the peak temperature they have reached. The spatial resolution is lower than for Raman spectroscopy, but this technique can provide quantitative temperature estimates whereas the Raman technique provides only relative temperatures.

Discussion and conclusions: The Raman maps reveal a clear effect of the heat wave over several hundreds of micrometers below the fusion crust in both meteorites. The paleomagnetic results will constrain deeper and milder heat wave penetration. These results will allow evaluating the "safe zone" where highly temperature sensitive properties can be studied. This is especially relevant when studying small meteorites with a small volume to surface ratio.

References: [1] Sears D.W. (1975) *Modern Geology* 5: 155-164. [2] Britt D.T. and Consolmagno G.J. (2003) *Meteoritics and Planetary Science* 38:1161-1180. [3] Drouard A. et al. (2018) *Astronomy and Astrophysics* 613:A54. [4] Bonal L. et al. (2016) *Geochimica and Cosmochimica Acta* 189 : 312-337 [5] Cournède C. et al (2015) *Earth and Planetary Science Letters* 410:62-74.

CV Chondrites: More than One Parent Body

J. Gattacceca[1], L. Bonal[2], C. Sonzogni[1], J. Longerey[1]. [1]CNRS, Aix Marseille Univ, IRD, Coll France, INRA, CEREGE, Aix-en-Provence, France (gattacceca@cerege.fr), [2]Institut de Planétologie et d'Astrophysique de Grenoble – Université Grenoble Alpes, CNRS, Grenoble, France.

Introduction: CV chondrites have been classically divided into reduced (CV_{Red}) and oxidized (CV_{Ox}) sub-groups, based on a number of mineralogical features, the Ni content of sulfides and the abundance of Fe,Ni metal [1]. The oxidized sub-group has been further divided into Allende- (CV_{OxA}) and Bali- (CV_{OxB}) type, based on a combination of chemical and petrographic criteria [e.g., 2, 3]. These three sub-groups are interpreted as coming from a single parent body, with a common protolith affected by significant parent body fluid-assisted metasomatism occurring at different temperature and/or redox conditions [2,4]. CK chondrites have been interpreted as coming from a more thermally metamorphosed (deeper) part of the same CV parent body [e.g., 5,6], but this interpretation has been recently challenged [7]. In this work we will argue that although CV_{OxA} and CV_{OxB} are likely to originate from a single parent body, CV_{Ox} and CV_{Red} originate from two different parent bodies.

Results: We investigated a suite of 50 CV chondrites. The main dataset, composed of the 30 meteorites (7 falls and 23 finds, mostly from Antarctica) whose thermal metamorphism and aqueous alteration have been characterized in details [8], is completed by 20 NWA meteorites. For all these meteorites, we determined the sub-group (Ox_A, Ox_B or Red) by combining three proxies (the average Ni content of sulfides, the Fe,Ni metal abundance, and magnetic parameters) which allow for a clear separation of the three sub-groups. We then estimated their matrix abundance (by image analyses and point counting), and measured their chondrule apparent diameters (by optical microscopy, over 2000 chondrules measured). For a subset of samples, we measured the bulk oxygen isotopes composition by laser fluorination coupled with mass spectrometry.

Discussion and conclusions: Matrix abundances and the distribution of chondrule apparent diameters are identical for CV_{OxA} and CV_{OxB} chondrites but significantly different between CV_{Ox} and CV_{Red} chondrites. These robust and simple petrographic indicators can be interpreted in two different ways: a different stratigraphic position of CV_{Ox} and CV_{Red} within a single parent body, or provenance from two distinct parent bodies. A different stratigraphic position would imply contrasted metamorphic temperatures with the deeper group being metamorphosed to higher temperatures. This is not observed, as both CV_{Ox} and CV_{Red} meteorites span the whole range of type 3 metamorphic subtypes [6]. Therefore, we conclude that CV_{Ox} and CV_{Red} meteorites originate from two different parent bodies. This claim is also supported by slightly overlapping but distinct oxygen isotopes compositions. The existence of CV_{Ox} clasts in Vigarano CV_{Red} regolith breccia [9], often used as an evidence for a single parent body is not a decisive argument as xenolithic clasts from different meteorite groups are found in a number of meteorites. For instance, several ordinary chondrites contain cm-size clasts from another ordinary chondrite group [e.g., 10], and because ordinary chondrites are usually studied in much less details than CV chondrites more such examples have been probably overlooked.

References: [1] McSween H.Y. (1977) *Geochimica and Cosmochimica Acta* 41:1777-1790. [2] Krot A.N. et al. (1995) *Meteoritics* 30:748–775. [3] Krot A.N. et al. (1998) *Meteoritics and Planetary Science* 33:1065-1085. [4] Ganino C. and Libourel G. (2017) *Nature Communications* 8. [5] Wasson J.T et al. (2013) *Geochimica and Cosmochimica Acta* 108:45-62. [6] Greenwood et al. (2010) *Geochimica and Cosmochimica Acta* 74:1684-1705. [7] Yin Q.-Z. and Sanborn M.E. (2019) *50th LPSC*, abstract #3023. [8] Bonal et al., submitted to *Geochimica and Cosmochimica Acta*. [9] Krot A.N. et al. (2000) *Meteoritics and Planetary Science* 35:817-825. [10] Gattacceca J. et al. (2017) *Meteoritics and Planetary Science* 52:2289-2304.

OVERVIEW OF THE COMET ASTROBIOLOGY EXPLORATION SAMPLE RETURN (CAESAR) NEW FRONTIERS MISSION

D. P. Glavin[1], S. W. Squyres[2], K. Nakamura-Messenger[3], A. G. Hayes[2], D. F. Mitchell[1], V. E. Moran[1], M. B. Houghton[1], D. Douglas-Bradshaw[1], D. S. Lauretta[4], S. Messenger[3], K. Yamada[5], S. Okazaki[5], Y. Satoh[5], Y. Maru[5], T. Nakao[5], A. Kukita[5], T. Shimoda[5], T. Yamawaki[5], T. Nakamura[6], J. E. Parker[1], D. C. Wegel[1], H. L. Peabody[1], J. P. Dworkin[1], A. N. Nguyen (Jacobs)[3], S. Clemett (Jacobs)[3], T. J. Zega[4], E. Mazarico[1], D. Rowlands[1], S. A. Aslam[1], N. Gorius (CUA)[1], G. Quilligan[1], Y. Furukawa[6], Y. Kimura[7], A. Takigawa[8], G. Blake[9], M. J. Mumma[1], S. N. Milam[1], P. A. Gerakines[1], J. I. Lunine[2], J. L. Mitchell[3], L. F. Pace[3], C. D. K. Herd[10], S. Gorevan[11], J. Spring[11], K. Zacny[11], P. C. Chu[11], M. M. Hasegawa[1], C. Güttler[12], H. Sierks[12], J.-B. Vincent[13], N. Oklay[13], H. Campins[14], Y. Fernandez[14], J. Makowski[15], D. Oberg[15], E. L. Morse[15], J. M. Soderblom[16], D. Bodewits[17], M. Kelley[17], B. Davidsson[18], J. Johnson[19], A. Kulchitsky[19], R. Kirk[20], L. Leshin[21], K. Öberg[22], M. Ravine[23], and the CAESAR Project Team. [1]NASA Goddard Space Flight Center, Greenbelt, MD, USA, [2]Cornell University, Ithaca NY, USA (E-mail: squyres@astro.cornell.edu), [3]NASA Johnson Space Center, Houston TX, USA, [4]University of Arizona, Tucson AZ, USA. [5]JAXA/ISAS, Yoshinodai, Chuo, Sagamihara, Kanagawa, Japan. [6]Tohoku University, Sendai, Miyagi Prefecture, Japan. [7]Hokkaido University, Sapporo, Hokkaido, Japan. [8]Kyoto University, Kyoto, Kyoto Prefecture, Japan. [9]California Institute of Technology, Pasadena, CA, USA. [10]University of Alberta, Edmonton, AB, Canada. [11]Honeybee Robotics, Pasadena, CA, USA. [12]Max Planck Institute, Göttingen, Germany. [13]DLR Institute of Planetary Research, Berlin, Germany. [14]University of Central Florida, Orlando, FL, USA. [15]Northrop Grumman Information Systems, McLean, VA, USA. [16]Massachusetts Institute of Technology, Cambridge, MA, USA. [17]University of Maryland, College Park, MD, USA. [18]Jet Propulsion Laboratory, Pasadena, CA, USA. [19]Coupi, Inc., University of Alaska, Fairbanks AK, USA. [20]US Geological Survey, Flagstaff, AZ, USA. [21]Worcester Polytechnic Institute, Worcester, MA, USA. [22]Harvard University, Cambridge, MA, USA. [23]Malin Space Science Systems, San Diego, CA, USA.

Introduction: The Comet Astrobiology Exploration Sample Return (CAESAR) mission was selected by the NASA New Frontiers Program for Phase A study in December 2017. CAESAR will acquire and return to Earth for laboratory analysis a minimum of 80 grams of surface material from the nucleus of comet 67P/Churyumov-Gerasimenko (67P). CAESAR will characterize the surface region sampled, preserve the collected sample in a pristine state, and return evolved volatiles by capturing them in a separate gas reservoir. NASA Goddard Space Flight Center provides project management, systems engineering, safety and mission assurance, contamination control, mission operations, and many other important functions. Northrop Grumman Information Systems (formerly Orbital ATK) will build the spacecraft, based on Dawn mission heritage, which like CAESAR, uses solar electric propulsion.

Collection of a sample from the surface of comet 67P is facilitated by a set of cameras that together provide images to support sample site selection, perform optical navigation, and document the sample before, during, and after collection. The sample is collected at the end of an arm during a 5-second touch-and-go (TAG) maneuver with the Sample Acquisition System (SAS) designed by Honeybee Robotics for the surface properties of comet 67P observed by the Rosetta mission. After sample collection, and while the sample is still cold (< -80°C), the TAG Arm inserts the sample container into the Sample Containment System (SCS) mounted inside the Sample Return Capsule (SRC). The SCS is sealed, preventing the sample from escaping into space. The sample is slowly warmed inside the SCS to enable sublimation of volatiles, which are collected in the Gas Containment System (GCS), a passively cooled gas reservoir. Separating the volatiles from the solid sample protects the solid sample from alteration. Once all sublimated H_2O is transferred to the GCS, the GCS is sealed to capture the volatiles it contains, and the SCS is vented to space to maintain the solid sample under vacuum. The SCS vent is closed before Earth entry to prevent atmospheric contamination.

The CAESAR SRC is provided by the Japanese Aerospace Exploration Agency (JAXA). Its design is based on the SRC flown on the Hayabusa and Hayabusa2 missions. The SRC lands at the Utah Test and Training Range (UTTR) in November 2038 and is immediately placed in cold storage for transportation to the NASA Johnson Space Center, where the solid and gas samples are removed and delivered to a dedicated CAESAR curation facility.

Detailed laboratory analyses of the sample from 67P will trace the history of volatile reservoirs, delineate the chemical pathways that led from simple interstellar species to complex molecules, constrain the evolution of the comet, and evaluate the role of comets in delivering water and prebiotic organics to the early Earth. CAESAR will achieve these goals by carrying out coordinated sample analyses that will link macroscopic properties of the comet with microscale mineralogy, chemistry, and isotopic studies of volatiles and solids. Most of the sample ($\geq$75%) will be set aside for analyses by generations of scientists using continually advancing tools and methods, yielding an enduring scientific treasure that only sample return can provide.

COSMIC DUST IN PERMIAN EVAPORITES

M.S. Glukhov[1], R.Kh. Sungatullin[1], R.I. Kadyrov[1], B.M. Galiullin[1], E.O. Statsenko[1]
[1]Kazan Federal University, Institute of Geology and Petroleum Technologies, Russia, Kazan, Kremlyevskaya st., 18. E-mail: gluhov.mixail2015@yandex.ru

Introduction: Saliferous basins are good objects for the accumulation of cosmic dust [4]. Among the microparticles of cosmic dust there are microspheres with magnetic properties. However, their origin is controversial. The hypotheses of natural (terrestrial), cosmic and technogenic origin are considered [1-5]. Therefore, the study of magnetic microspheres can help to understand information about mineral formation .

Our research is devoted to the study of magnetic microspheres from the Permian evaporites of the East European Platform and the Urals foredeep. We studied structure, chemical and mineral composition of 30 microspheres from the gypsum of the Kamsko-Ustinskoe deposit (~ 265 million years, Guadalupian epoch of the Permian system) and 13 microspheres from the potassium-magnesium salts of the Verkhnekamskoe deposit (~ 280 million years, Cisuralian epoch of the Permian system).

Methods: Before crushing the gypsum samples (1.5 x 2 x 2.5 cm), we studied them using an X-ray microtomography (Phoenix V | tome | XS 240) with a nanofocus X-ray tube with a maximum accelerating voltage of 180 kV and a power of 15 W. Measurements were conducted for detection objects with high density in the rocks (iron oxide magnetic microspheres). After rocks were crushed and carried out magnetic separation with a neodymium magnet; then microspheres were taken from magnetic separat. Microspheres were studied using a Phillips XL-30 electron microscope equipped with an energy dispersive spectrometer with an accelerating voltage of 20 kV and a working interval of 8.9–15 mm. The probing depth was 1.0–1.5 μm, the measurement accuracy was 0.1–1%.

Results: On the microtomographic images of gypsum there are inclusions of X-ray dense minerals (Fig. 1a), which allows us to disprove their technogenic origin. All microspheres have a diameter of 5-150 μm, ideal spherical shape (Fig. 1b, c) and a strong metallic luster. Microspheres have a diverse texture surface with a predominance of dendritic. The main elements of the microspheres are Fe and O, according to the ratio of which the surface of most microspheres consists of wustite and, more rarely, native iron (Fig. 1b-c).

Fig. 1. Cosmic dust in Permian evaporites (a – tomographic image of the gypsum sample from Kamsko-Ustinskoe deposit (yellow - X-ray dense minerals, b – microsphere from the potassium-magnesium salts of the Verkhnekamskoe deposit, c, d - microspheres from the gypsum of the Kamsko-Ustinskoe deposit.
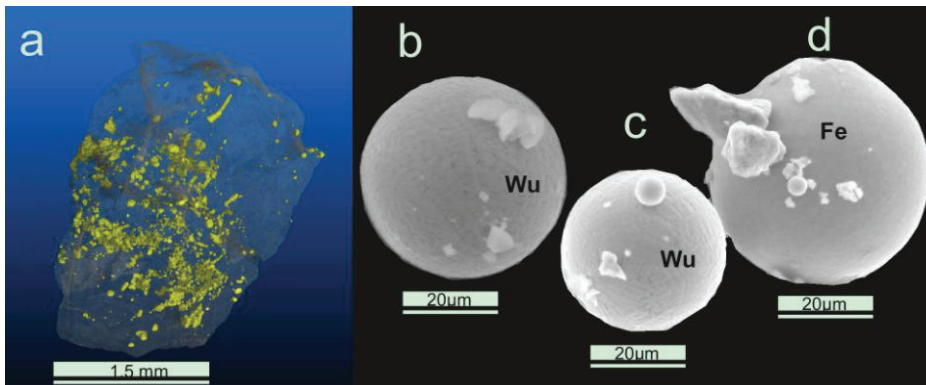
Discussion: In terms of chemical composition, the objects we investigated are close to microspheres that arose during the ablation of meteorites and falling out of cosmic dust [3]. The texture of pattern of the surface of microspheres depends on the amount of iron: with increasing of iron, the surface of the microsphere becomes smoother with the complete disappearance of the texture, which is typical for the surface of native iron microspheres.

Conclusions: Microspheres from different evaporites (gypsum, potassium-magnesium salts) have a great similarity, which may testify in favor of a single (cosmic) process of their formation. Findings of microspheres in evaporites can be additional tool for stratigraphic correlation of terrestrial rocks.

References: [1] Glukhov M.S. et al. 2018. Meteoritics & Planetary Science 53: A6202. [2] Karpov G.A., Mokhov A.V. 2010. Journal of Volcanology and Seismology, 3: 19-35. [3] Korchagin O.A. 2010. Doklady Earth Sciences, 431, 6: 783-787. [4] Sungatullin R.Kh. et al. 2018. Meteoritics & Planetary Science 53: A6291. [5] Sungatullin R. et al. 2018. Proceedings Kazan Golovkinsky Stratigraphic Meeting «Advances in Devonian, Carboniferous and Permian Research: Stratigraphy, Environments, Climate and Resources»: 431-439.

TEXTURES AND COMPOSITIONS OF OPAQUE PHASES OF JINJU H5 CHONDRITE

S. Goh[1], B.-G. Choi[1], M. Byeon[2] and T.E. Hong[2]. [1]Earth Science Education, Seoul National University, 08826, Korea. likeio02@snu.ac.kr. [2]Busan Center, Korea Basic Science Institute, 46742, Korea.

Introduction: Along with silicates, opaque phases including metal and sulfide are major components of ordinary chondrites; kamacite, taenite and troilite are three most common opaque minerals [e.g., 1, 2]. In addition to these major opaque minerals, chromite, merrilite, tetrataenite, near Ni-free kamacite and metallic Cu are minor or rare but often found in ordindary chondrites [2-6]. Jinju, the most recent meteorite fall in Korea (May 2014), is a H5 chondrite with unusually high porosity and numerous subhedral or euhedral vug-filling minerals [7]. Since Fe-Ni metal is one of the vug-filling minerals, we have studied petrographic characteristics and chemical compositions of the opaque minerals in Jinju in order to understand the process that formed the high-porosity.

Analytical Methods: Polished thin sections of Jinju were metallographically studied by optical microscope and JEOL JSM-6380A scanning electron microscope. Chemical compositions of metals and triolites are analized by JEOL JXA-8530F field emission electron microprobe under analytical condition of 15kV, 20nA and spot size of ~3 μm at Korea Polar Research Institute. Siderophile elemental images of selected opaque assemblages were obtained using resistive anode encoder (RAE) detector of Cameca IMS 7f Auto at KBSI.

Results and Discussion: Majority of Fe-Ni metal and troilite in Jinju are those of typical equilibrated ordinary chondrites reported in various previous studies. Rare occurences are taenite grains containing fine mixture of kamacite + tetrataenite + troilite ± metallic Cu.

Opaque minerals make up ~11 vol.% of Jinju with Fe-Ni metals (~7.6 vol.%), troilite (~3.5 vol.%) and minor chromite, merrilite and scarce metallic Cu. Most of them, especially large grains or assemblages, are placed outside of the relic chondrules. Fe-Ni metals occurr as kamacite, taenite and taetrataenite phases. The most dominant opaque phase is kamacite having irregular margins with grain size up to ~1.5 mm. Taenite and tetrataenite are smaller in size (typically ~100 μm). Taenite is often observed in void space as subhedral or euhedral crystals. Tetrataenite is rare but occured at the grain boundary of associated kamacite or troilite. Troilite is common with irregular shape of ~300 μm.

Majority of taenite grains are inclusion-free, while some contain irregular-shaped and fine-grained (> 20 μm) kamacite, tetrataenite and troilite with or without metallic Cu. The assemblage is similar to that of Cu bearing assemblage 2 (adjacent to small triolite grains inside Ni-rich metal) of [5]. From two thin sections studied, we found 32 taenite grains containing such inclusions; 8 of them have metallic Cu. Since typical size of metallic Cu is < 10 μm, the occurrence of Cu may simply depends on the cutting direction of taenite. Note that metallic Cu is very scarce (~ 0.0001 vol.%) in Jinju and only situated in this assemblage. Many of these taenite grains have zoned textures where low-Ni taenite surrounded by high-Ni one. In low-Ni taenite core, fine and irregular shaped kamacite, tetrateanite and troilite are found with or without metallic Cu. Electron microprobe data show that in this assemblage kamacite grains are low in Ni (2.28-3.36 wt.%), while troilite rather high in Ni (0.28-0.72 wt.%). The low Ni contents in kamacite and high Ni troilite may indicate high temperature assemblage [8]. Shape of troilite-metal interface is similar to eutectic texture. Thus the assemblage may have formed by localized metal-troilite melting possibly by shock, as inferred by [5]. Five of Cu-bearing ordinary chondrites in [5] have porosity data by [9]. When we plot Cu abundance against porosity of these chondrites with Jinju, there is a week but noticeable positive correlation. Thus formations of both Cu-bearing assemblage and high porosity may have related with shock event.

We have obtained isotope images of some siderophiles (Fe, Ni, Co, Cu, Ge, Ga) from these opaque assemblages using resistive anode encoder (RAE) detector of Cameca IMS 7f. Preliminary results show the distributions of these elements as expected from previously known partition coefficients [e.g., 10]. We plan to do additional work to obtain better resolution images.

References: [1] Kort A. N. and Scott, E. R. D. (2014) *Treatise on Geochemistry*. pp. 65-137 [2] Brearley A. J. and Jones, R. H. (1998) *Planetary materials*. pp. 3-001 - 3-398. [3] Rambaldi, E. R. and Wasson J. T. (1982) *Geochimica et Cosmochimica Acta* 46, 929-939. [4] Holland-Duffield C. E. et al. (1991) *Meteoritics* 26, 97-103. [5] Rubin A. E. (1994) *Meteoritics* 29, 93-98. [6] Leedahl B. el al. (2016) *RSC Advances* 6, 85844-85851. [7] Choi B.-G. et al. (2016) 78th Annual Meeting of the Meteoritical Society. No. 5091. [8] Ma L. et al. (1998) *J. of phase Equilibria* 19, 299-309. [9] Consolmagno et al. (2006) *Meteoritics & Planetary Science* 41, 331-342. [10] Rasmussen et al. (1988) *Meteoritics* 23, 107-112.
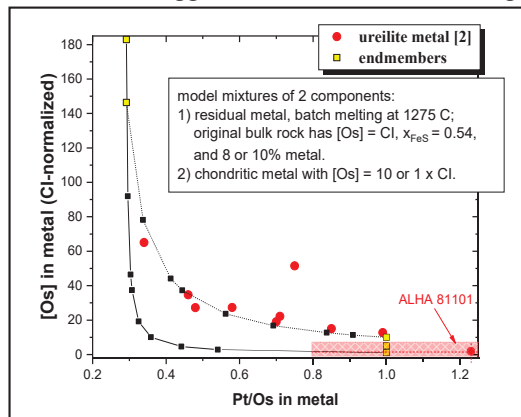
EXOGENOUS METAL IN UREILITES.

C. A. Goodrich[1] and S. J. Desch[2], [1]Lunar and Planetary Institute, USRA, Houston, TX 77058 USA, goodrich@lpi.usra.edu; [2]School of Earth and Space Exploration, Arizona State University, Tempe AZ 85287 USA

Introduction: Main group ureilites, which are ultramafic achondrites interpreted to represent the mantle of a differentiated asteroid, typically contain a few % metal (kamacite) as strips along silicate grain boundaries [1,2]. Siderophile elements in bulk ureilites suggest mixing between two distinct metallic components, but hypotheses for the origins of these components vary [3-9]. [7-10] argued that extraction of S-enriched metallic liquid played a major role, and [7] argued for mixing between an FeS-depleted metallic residue and a broadly chondritic 2nd component.

More stringent constraints are provided by in situ analyses of siderophile elements in ureilite metal [2], which allow the use of absolute abundances in addition to ratios (bulk rock absolute abundances are not reliable due to terrestrial weathering). HSE in ureilite metal show a correlation between degree of fractionation (e.g., Pt/Os) and absolute abundance (e.g., [Os]), which suggests mixing between an indigenous highly-fractionated residue and an unfractionated component [2]. Modeling in the Fe-FeS system showed that if the most fractionated ureilite metal represents the indigenous endmember, then very high degrees of batch Fe-S melt extraction (≥98%) are required, implying temperatures of 1250-1275°C and high x_{FeS} (= wt. FeS/[Fe+FeS]) of ~0.5 in the precursors. These temperatures are consistent with peak temperatures inferred from ureilite silicates [1], and x_{FeS} = ~0.5 is consistent with values in ordinary chondrites. However, to match abundances of HSE in this metal ([Os] ~65×CI), initial metal abundances of ≥20 wt.% are required. Such metal + sulfide contents (~40 wt.% Fe+FeS) are not observed in any chondrite, and seem implausible [2]. In addition, because the mixing is seen in the metal itself, it must have occurred when the metal was liquid [2]. Thus, addition of exogenous metal in a "late-veneer" scenario [3-9] seems implausible.

Catastrophic Disruption of the Ureilite Parent Body (UPB): Various lines of evidence suggest that the UPB was catastrophically disrupted by a major impact after differentiation but while still hot (~1050-1100°C), with subsets of its fragments reassembling into daughter bodies (UDB) from which ureilites are derived [11-15]. Recently, [16] proposed that metal (and other components) from the impactor was added to the UDB, mixing with indignous metal to became the metal now present in ureilites. A mass ratio of 0.3:1 between the impactor and the UPB is typically assumed [15]. If the UDBs contained the same proportion of hot UPB and cold (~0°C) impactor materials, the UDBs would form with temperatures of 800±50°C, plus the increase generated by the impact, which for 5 km s^{-1} relative velocity might be 300±50 °C [17], yielding UDB assembly temperatures of 1100±100 °C. This is hot enough that metal would have been molten (but not most silicates) and flowed along silicate grain boundaries [16]. This scenario suggests a re-evaluation of mixing models for siderophile elements in ureilite metal.

Model mixtures of 2 components:
1) residual metal, batch melting at 1275 C; original bulk rock has [Os] = CI, x_{FeS} = 0.54, and 8 or 10% metal.
2) chondritic metal with [Os] = 10 or 1 x CI.

Mixing Calculations: We carried out two-component mixing calculations. One endmember (indigenous) was the residue from batch partial melting in the Fe-FeS system at 1275°C, for 8-10% initial metal and x_{FeS} = 0.54 [2]. The other endmember was unfractionated chondritic metal (exogenous) with [Os]=10×CI (consistent with several types of CC). Results (Fig. 1) show that ~50:50 to 1:99 (indigenous:exogenous) mixtures provide a good match to the ureilite metal, except ALHA 81101 whose metal has ~1×CI HSE abundances [2]. ALHA 81101 is highly shocked and its metal may have been diluted by pure Fe from shock-smelting.

Discussion: This model can explain the correlation of siderophile element fractionation and HSE abundances for ureilite metal [2] with plausible starting material for the UPB (OC-like in metal-sulfide content, consistent with [18,19]), solving several of the problems discussed in [2]. Mixing of indigenous and exogeneous metal in the liquid state (while silicates are solid) during assembly of UDB explains the location of ureilite metal along silicate grain boundaries and the lack of correlation of siderophile elements with mg# of silicates. It is also consistent with the argument that ureilite metal is exogenous based on Ni and Co disequilibrium between metal and silicates [20,21].

References: [1] Mittlefehldt D.W. et al. (1998) In *RIM* 36. [2] Goodrich C.A. et al. (2013) *GCA* 112, 340-373. [3] Wänke H. et al. (1972) *Meteoritics* 7, 579-590. [4] Wasson J. et al. (1976) *GCA* 40, 1449-1458. [5] Higuchi H. et al. (1976) *GCA* 40, 1563-1571. [6] Boynton W.V. et al. (1976) *GCA* 40, 4139-1447. [7] Rankenburg K. et al. (2008) *GCA* 72, 4642-4659. [8] Janssens M.-J. et al. (1987) *GCA* 51, 2275-2283. [9] Goodrich C.A. et al. (1987) *GCA* 51, 2255-2274. [10] Warren P.H. et al. (2006) *GCA* 70, 2104-2126. [11] Goodrich C.A. et al. (2004) *Chemie der Erde* 64, 283-327. [12] Downes H. et al. (2008) *GCA* 72, 4825–4844. [13] Herrin J.S. et al. (2010) *MAPS* 45, 1789–1803. [14] Goodrich C.A. et al. (2015) *MAPS* 50, 782-809. [15] Michel P. et al. (2015) *Planet. Space. Sci.* 107, 24-28. [16] Desch S.J. et al. (2019) *LPSC* 50, #1646. [17] Stöffler D. et al. (1991) *GCA* 55, 3845-3867. [18] Goodrich C.A. (1999) *MAPS* 34, 109-119. [19] Warren P.H. (2011) *GCA* 75, 6912-6926. [20] Gabriel A.D. and Pack A. (2008) *LPSC* 39, #2195. [21] Gabriel A.D. and Pack A. (2009) *LPSC* 40, #2462.

RELATIONS BETWEEN ACCRETIONAL DEFORMATION AND TEMPERATURE IN CLUSTER CHONDRITE CHONDRULES.

S. P. Goudy[1] and A. M. Ruzicka[2], [1]Portland State University (goudy@pdx.edu), [2]Portland State University (ruzick-aa@pdx.edu).

Introduction: Cluster chondrites are ordinary chondrites that consist of 88-92 vol% of chondrules [1]. Chondrules in these rocks are highly shape-deformed compared to non-cluster chondrites, which has been interpreted to be a result of plastic deformation at elevated temperatures [1]. We used electron backscatter diffraction (EBSD) methods [2] to analyze chondrule deformation, crystalline deformation, and deformational temperatures of cluster chondrite chondrules to test for relations between deformation and temperature within cluster chondrites.

Methods and Samples: Samples used are cluster chondrite clasts in NWA 5205, NWA 5421, NWA 5781, and Tieschitz. All are type 3 and shock classified in this study as S1, suggesting they were little-affected by post-accretion thermal or shock metamorphism. Whole chondrule deformation was determined using the chondrule shape deformation parameter of Metzler [1]. Grain orientation spread (GOS) and temperature parameter metrics, measuring olivine intracrystalline deformation and codeformational temperature respectively, were measured as per the methods of Ruzicka and Hugo [2]. Two EBSD maps were made of each sample, and from each 10 chondrules representing a full spread of deformation extents were selected for measurement of deformation parameters, mean GOS, and temperature paramters. For each meteorite, each metric was compared to each of the others and trendlines were fitted to the resulting datasets. Correlations between the metrics were tested using ANOVA so as to determine if the metrics are related.

Results: Probabilities of there being no correlation between measured metrics in each meteorite are listed in the table below.

Table 1. ANOVA Statistics of Temperature and Deformation Metrics in Sample Meteorites. Probabilities displayed represent the probability of there being no relationship between the two given metrics within a sample.

Meteorite	Deformation Parameter vs. Temperature Parameter	Mean GOS vs. Temperature Parameter	Deformation Parameter vs. Mean GOS
NWA 5205	40.47%	64.58%	6.81%
NWA 5421	0.25%	73.38%	8.22%
NWA 5781	13.97%	12.39%	1.23%
Tieschitz	68.76%	66.24%	0.94%

Conclusions: The calculated statistics indicate that there is no strong relation between codeformational temperature and either chondrule deformation or crystal deformation within the studied samples. However, the consistently low probabilities of a lack of relation between the metrics representing chondrule and intracrystalline deformation suggest that these two scales of deformation are linked – indicating that observations derived from the deformations of chondrule olivine grains can be interpreted to represent the deformation of the chondrule as a whole. This allows temperatures interpreted from olivine deformation, such as those from Ruzicka and Hugo's temperature parameters [2], to represent chondrule deformational temperatures.

References: [1] Metzler K. (2012) *Meteoritics & Planetary Science* 47:2193–2217. [2] Ruzicka A. M. and Hugo R. C. (2018) *Geochimica et Cosmochimica Acta* 234:115-147.

CO-ORDINATED UV REFLECTANCE AND RAMAN SPECTROSCOPY OF MARTIAN METEORITES AND TERRESTRIAL ANALOGUE SAMPLES

Monica M. Grady[1,2], F. A. J. Abernethy, T. J. Barrett, C. Batty[1], C. Bedford[1] and P. Rowden[1]
[1]School of Physical Sciences, Open University, Milton Keynes MK76AA, UK (monica.grady@open.ac.uk)

Introduction: Reflectance spectroscopy acquired by orbiting spacecraft over a range of wavelengths is a common tool used to determine the mineralogy of planetary surfaces. Hydrous and anhydrous silicate minerals, sulphides, sulphates and carbonates have prominent features in the Vis-NIR ($\lambda \sim 300 - 2100$ nm). Organic species are detectable at lower wavelengths, $\lambda \sim 180 - 300$ nm. Raman spectroscopy is a method employed to identify minerals and organic species *in situ* and will be part of the instrument suites carried by the Mars 2020 and ExoMars 2020 rovers for analysis of surface materials.

Aim: to investigate mineral-organic relationships in martian meteorites by UV-Vis microspectrophotometry (MSP) and Raman spectroscopy. Our intention is to produce spatial distributions of organic species on broken surfaces of martian meteorites and terrestrial analogues, providing a series of measurements to assist in interpretation of data acquired on Mars. That would then help in identifying suitable (potentially organic-rich) rocks for acquisition and caching. The project has synergies with the investigations that the Sherloc instrument will carry out on the surface of Mars

Method: Diffuse reflectance spectra of a series of minerals, powdered organic compounds and martian meteorites were obtained using a CRAIC UV-Vis MSP fitted with 3 Cassegrain objective lenses. The system has two lamps, deuterium and xenon, that operate in parallel, resulting in a useful spectral range of 200 – 900 nm. The lamp output is delivered to the microscope by fibre-optic, resulting in a focusable area of 2 x 2 µm to 10 x 10 µm, depending on the combination of mirrors selected. Incidence and exit angles are perpendicular to sample. Raman spectra were obtained using a Jobin Yvon Labram HR laser Raman microprobe equipped with 3 lasers (514 nm Ar ion, 632 nm HeNe and a 785 nm diode); separate spectra were taken using each of the three lasers. Material (usually < 5 mg) broken from chips of martian meteorites and terrestrial basalts from Iceland, Norway and Canada were coarsely crushed (grain-size < 200 µm) and placed on quartz-glass slides for UV-Vis then Raman analysis.

Results: UV-Vis spectra (240 – 400 nm) from broken surfaces of inorganic minerals relevant to the composition of Mars' surface and from the Chassigny, Nakhla, Shergotty and Zagami martian meteorites are shown in the figures below. The marked weak features at 257 nm and 280 nm are possibly from electronic transitions, whilst the stronger features in the meteorites at 320 nm and 345 nm may be from organic functional groups. Raman analysis will assist in absolute identification of these features. The next stage of the project is to re-analyse the specimens after they have been mixed with (a) individual organic molecules and (b) combinations of molecules, with the aim of determining the minimum concentration of organics detectable, both in UV-Vis and Raman spectra.

Summary: UV-Vis microspectrophotometry complemented by Raman spectroscopy is a potential tool for rapid, non-invasive and non-destructive laboratory analysis of planetary samples. Comparison with spectra from organic and inorganic species should allow elucidation of interactions between organics and mineral matrices, and assist in interpretation of data from the surface of Mars.
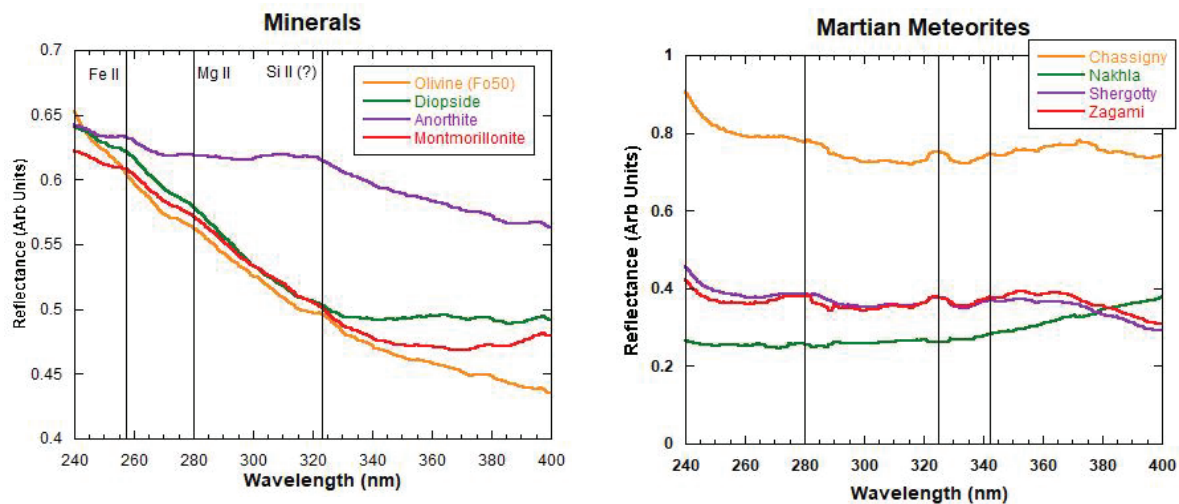
LAYING THE GROUNDWORK: ADVANCE PLANNING IN PREPARATION FOR SCIENTIFIC ANALYSIS OF SAMPLES RETURNED FROM MARS.

MSR Science Planning Group (MSPG): Monica. M. Grady[1], M. A. Meyer, E. Sefton-Nash, D. W. Beaty, B. L. Carrier, D. Bass, F. Gaubert, T. Haltigin, A. D. Harrington, Y. Liu, B. Marty, R. Mattingly, S. Siljeström, E. Stansbery, K. Tait, M. Wadhwa, L. White. [1]School of Physical Sciences, The Open University, Milton Keynes MK7 6AA, UK (monica.grady@open.ac.uk),

Introduction: The Mars Sample Return Science Planning Group (MSPG) was instituted by ESA and NASA in November 2018. It is an international team with a brief to ensure that planning activities undertaken by the two space agencies in support of Mars Sample Return (MSR) are co-ordinated and consistent. MSPG is using several approaches during 2019 to identify issues and concerns for different potential international partners, and to formulate and propose mechanisms through which the international scientific community can achieve the shared scientific objectives of MSR. A series of workshops has been scheduled to establish and document positions amongst a diverse set of sample scientists related to planning assumptions and/or potential requirements involving the handling and analyses of returned samples.

The first workshop was held in Columbia, Maryland between 14th – 16th January 2019. Its theme was 'Science in Containment', and its scope covered the initial examination of samples and formulation of strategies for how much sample science should or must be planned for within containment. The report from the workshop can be found at https://mspg.jpl.nasa.gov. The second workshop will be held in Leicester, UK between 1st-3rd May 2019. Its theme is 'Contamination Control', and its scope will cover high-level strategies related to future preparation of science-driven contamination control requirements associated with sample handling and analisys. The third workshop, focused on reconciling science and Sample Safety Assessment Protocol (SSAP) recommendations, will tentatively be held in summer 2019.

Workshop 1: A key planning question related to a potential future Mars Sample Return Campaign is "To what extent does MSR science need to be done in containment?" The answer will determine the character of the science-sourced requirements of the Sample Receiving Facility (SRF), including the number and definition of additional supporting science-related facilities (both within and outside containment). The first workshop focused on investigations that need to be performed while under biological quarantine, which is how we define here as being "in containment". The workshop concluded with 11 findings, two of which were assigned of higher import than the others:

> **Major Finding #1**: It appears that a large majority (> 90%) of the MSR-related science investigations, as identified by iMOST, can be performed acceptably on sterilized samples, thus potentially enabling the analysis of MSR samples in uncontained laboratories without a dependency on the results from SSAP testing.
>
> **Major Finding #2**:The scientific community, for reasons of scientific quality, cost, timeliness, and other reasons, strongly prefers that as many sample-related investigations as possible be performed in PI-led laboratories outside containment.

Workshop 2: The overarching topic of MSPG Workshop #2 (May 1-3, 2019 in Leicester, UK) is the potential impact of science-driven contamination control requirements, derived from the requirements on the sample caching system on Mars 2020, and their implications for the possible future Sample Receiving Facility. The challenge considered is what is practical in terms of managing potential contamination during sample transportation, characterization, manipulation, processing and analysis.

Other Processes: A set of Town Hall meetings and MSPG related presentations have been scheduled for several major 2019 planetary science conferences in both the United States and Europe (and Japan?). The same kinds of topics have been, and will be, discussed, and community feedback will be compiled. Finally, certain kinds of issues, particularly related to the overall scientific governance of MSR, are being studied by the MSPG committee itself, using large analogous science operations here on Earth.

The Findings from Workshops 1 and 2 will be presented and discussed at the Annual Meeting, alongside preparatory material for Workshop 3. Input from the sample science community is especially welcomed and encouraged in response to this presentation and the MSPG findings in general.

A RADIATIVE HEATING MODEL FOR THE FORMATION OF CHONDRITES AND THE LAST MELTING EVENT OF CHONDRULES.

J. P. Greenwood[1], W. Herbst[2], and K. Abe[1], [1]Dept. of Earth and Environmental Sciences, Wesleyan University, Middletown, CT 06459 USA, [2]Dept. of Astronomy, Wesleyan University, Middletown, CT 06459 USA.

Introduction: We have recently proposed a chondrite formation model that accounts for most properties of chondrules and chondrites [1]. This radiative heating model builds upon our earlier work on forming chondrules during short flyby's of molten planetesimals in the early solar system (< 5 Ma) [2]. To form chondrites, we envision that small porous planetesimals (m-to-km scale) are heated during close encounters with large (~100 km scale) differentiated planetesimals via radiative heating by exposed magma oceans or lava on their surfaces. Chondrite lithification occurs by hot isotatic pressing simultaneously with chondrule melting and crystallization. Thermal models of large differentiated planetesimals predict a narrow time window in the planet-forming disk when the crusts of these bodies are thin enough to be ruptured frequently by impact and magmatism [3], coincident with the ages of chondrules [4]. We have modeled the heating and cooling of the small porous planetesimals as they are accreted to these large differentiated planetesimals. This leads to symmetrical heating and cooling curves above 1000K on the order of several 10's of minutes for the objects. The heating of the small porous planetesimal leads to excess pressure of Na, Si, and O (over the solar nebula) in the last chondrule forming event, thus accounting for properties of chondrules not expected in typical nebular environments. This type of heating environment would naturally lead to nucleosynthetic isotopic complementarity [4] as well as the phenomena of cluster chondrites [5].

Experimental: Laboratory experiments demonstrate that FeO-poor porphyritic olivine chondrules can be synthesized with the predicted thermal histories of this model. We have undertaken 1 atm experiments at IW-1 with chondrule analog materials that possess a range of chemistry and mineralogy. Porphyritic olivine chondrules are a dominant textural product, with barred and skeletal olivines much lower abundance, using symmetrical heating and cooling curves from [1]. Experimental olivine Mg# and glass compositions are excellent chemical matches to Semarkona Type I PO chondrules [6]. Experiments using a Type IAB composition show olivine and pyroxene chondrules with textures expected from equilibrium crystallization. These textures are not similar to pyroxene-rimmed Type IAB chondrules [7], demonstrating that Type IAB chondrule textures support open-system behavior with a Si-enhanced gas [7]. Further work on the similarity of our experiments with chondrules in primitive meteorites will be presented by [8]. For the meeting, we will present work on Type II porphyritic olivine chondrule synthesis. We are also working on the replication of chondrule olivine minor element zoning [9], and will report on this progress as well.

Implications of this model for the abundance of chondrites in primitive asteroids: One of the interesting predictions of this model is that the majority of material in the asteroid belt cannot be similar to the chondritic meteorites, as the mass of material heated in this fashion cannot be similar to the mass of the asteroid belt. This would predict that the material of primitive asteroids would be mostly chondritic in composition, but not in texture, porosity, and density. We would predict that asteroids such as Ryugu and Bennu will be composed mostly of much lower density material, material that has been less thermally processed in comparison to the chondritic meteorites in our collections. The asteroidal material is likely more representative of the material hitting the upper atmosphere of Earth. The chondritic meteorites are the objects from those asteroids able to survive passage through our atmosphere, rather than the main type of material from these bodies.

References:
[1] Herbst W. and Greenwood J. P. (2019) *Icarus* Accepted, in press. [2] Herbst W. and Greenwood J. P. (2016) *Icarus* 267:364. [3] Hevey P. J. and Sanders I. S. (2006) *Meteor. & Planet. Sci.* 41:95. [4] Budde G. et al. (2016) *Proc. Natl. Acad. Sci.* 113:286. [5] Metzler K. (2012) *Meteor. & Planet. Sci.* 47:2193. [6] Jones R. H. and Scott E. R. D. (1989) Proc. 19th Lunar Planet. Sci. Conf. 19:523. [7] Friend P. et al. (2016) *Geochim. Cosmochim. Acta* 173:198. [8] Abe K., Greenwood J. P. and Herbst W. (2019) this meeting. [9] Marrocchi Y. et al. (2018) *Earth Planet Sci. Lett.* 496:132.

NANOSCALE HETEROGENEITIES IN SILICATES FROM SUTTER'S MILL

J. Greer[1,2,*], D. Isheim[3], D. N. Seidman[3], and P. R. Heck[1,2], [1]Chicago Center for Cosmochemistry, Dept. of the Geophysical Sciences, Univ. of Chicago, Chicago IL, USA (*E-mail: jennika@uchicago.edu). [2]Robert A. Pritzker Center for Meteoritics and Polar Studies, The Field Museum of Natural History, Chicago, IL, USA. [3]Northwestern Univ. Center for Atom-Probe Tomography, Dept. of Materials Science & Engineering, Northwestern Univ., Evanston, IL, USA.
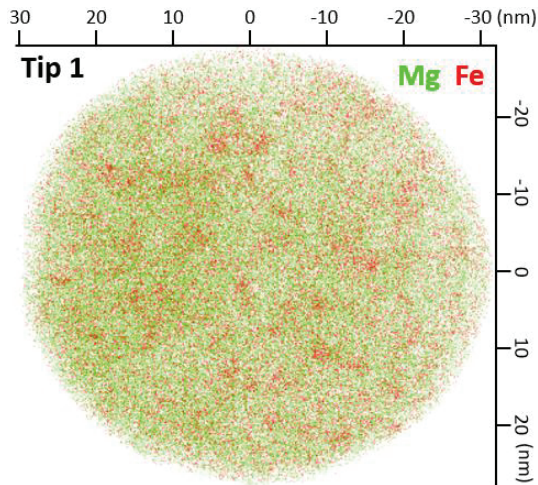

Fig 1. Atom-probe tomographic (APT) reconstruction of matrix minerals in Sutter's Mill, with individual atoms shown as dots (Mg in green, Fe in red). Fe shows clustering, Mg is relatively homogenous.

Introduction: Sutter's Mill is a CM chondrite regolith breccia (fall; April 22, 2012), with lithologies ranging from CM 2.0 to 2.1 [1]. The meteorite has experienced varying degrees of aqueous and thermal alteration, and contains clasts of non-CM material, making this meteorite complex on the macroscale [2]. On a microscale, understanding the fine-grained mixture of hydrated and thermally altered components requires characterization techniques with high-spatial analytical resolution. Here, we use atom-probe tomography (APT) to analyze the matrix minerals in Sutter's Mill at near-atomic resolution in 3D in order to enhance our understanding of this unique meteorite with minimal sample consumption.

Samples and Methods: We studied a polished section of the SM47 specimen (FMNH Me 5799.4). The section contains abundant grains of olivine, pyroxene, troilite, pentlandite, sulfide and calcite. Some of the olivines were strongly zoned (Fa_{14-36}), others, occurring as individual grains in the matrix are almost pure forsterite [1].

We prepared two microtips from the matrix using the Tescan Lyra3 FIB-SEM microscope at the University of Chicago. The area of interest was coated with Pt to protect the mineral surface from Ga ion implantation. Several spokes were prepared with our method developed for APT of lunar ilmenite [4]. Total sample consumption in the production of one tip was ~20 μm^3. A sample of the San Carlos olivine (FMNH Me 7688.2) served as a reference material.

The tips were analyzed with a LEAP 5000X Si atom probe tomograph at the NUCAPT facility of Northwestern University. In APT, atoms of the sample surface are field field-evaporated, assisted by UV laser pulses, and field-ionized, ifrom the sample surface in a high electric field using UV laser pulses. The ions' times-of-flight and positions are detected with a multimicro-channel plate detector. APT records elemental and isotopic compositions and the 3D distribution of atoms in the sample. The current detection efficiency is ~80% which makes it ideal to study small volumes [3]. We used CAMECA's IVAS software to reconstruct the tomographic dataset for each sample.

Results and Discussion: We obtained 5.5 million atoms for Tip 1 and 1 million for Tip 2. Both samples were forsteritic olivine that exhibited compositional variations on the nanoscale. The composition of a ~5 x 5 x 15 nm representative volume within Tip 1 ($Fa_{0.13-0.18}$) is similar to olivine of Type I chondrules. In a volume with the same size, Tip 2 has a higher compositional variability ($Fa_{0.03-0.70}$). This intrachondrule variability is smaller than the inter-chondrule variability ($Fa_{0.5-2}$), reported in [5].

In Tip 1 we observed nanoclusters with $[Fe]^{++}$ and $[FeO]^{+}$ enhanced by up to 2× (~4 wt%) compared to the surrounding volume. The clusters measured 1.5 to 8 nm (average ~3 nm, Fig. 1) on the long axis. Mg and O were homogeneously distributed. Similar nanoclusters were observed in Tip 2. None of this nanoscale variability was observed in our San Carlos olivine reference material that we analyzed with similar analytical conditions. We therefore conclude that this compositional nanoscale variability is intrinsic to the Sutter's Mill olivines. These clusters are similar in size to the nanophase Fe particles observed in the surfaces of lunar ilmenite [4], but likely have a different origin. Characterization of this fine-grained material is important for better understanding C-chondrites, including materials expected from the Hayabusa 2 and OSIRIS-Rex sample-return missions.

References: [1] Jenniskens, P. et al. (2012) *Science,* 338:1583-1587. [2] Zolensky, M. et al. (2014) *Meteoritics & Planetary Science,* 49:1997-2016. [3] Kelly, T. F. and Lawson, D. J. (2012) *Annual Review of Materials Research,* 42:1-31. [4] Greer, J. et al. (2017) *80th Annual Meeting of the Meteoritical Society,* Abstract #1987. [5] Nagashima, K. et al. (2012) *75th Annual Meeting of the Meteoritical Society,* Abstract #5160. [6] Schrader, D. L. and Davidson, J. (2017) *Geochimica et Cosmochimica Acta,* 214:157-171.

THE YAMATO NAKHLITES: A CASE STUDY FOR THREE DIMENSIONAL ANALYSIS

S. Griffin[1], L. Daly[1], M. R. Lee[1] and B. E. Cohen[1], [1]School of Geographical and Earth Sciences, University of Glasgow, Glasgow, G12 8QQ, UK (s.griffin.3@research.gla.ac.uk).

Introduction: The Yamato nakhlites are basaltic igneous rocks that were impact-ejected from Mars. They comprise three separate stones, Y-000593, Y-000749, and Y-000802, that were recovered from the Yamato Mountains, Antarctica by the 41st Japanese Antarctic Reseach Expedition (JARE) in 2000 [1,2]. Previous petrographic studies of thin sections (which provide 2-D views of rock structure), and geochemical analyses, have suggested that the three Yamato nakhlites are paired. However, $^{40}Ar/^{39}Ar$ geochronology of Y-000593 and Y-000749 [3] have indicated a crystallisation age discrepancy of 69 ± 15 Ma (2σ), which is inconsistent with pairing. There is currently no published age for Y-000802. Here we have used electron backscatter diffraction (EBSD) to obtain new 3-D information on igneous and impact-generated fabrics of the Yamato nakhlites, and to identify and characterise similarities and differences between the three stones that may in turn elucidate their original petrologic relationships.

Methods: We studied three thin sections (Y-000593,127-A, Y-000749,64-A, Y-000802,36-A) that were cut without considering the orientation of any petrofabric that may or may not have been present. These samples were mechanically and chemically polished using standard EBSD preparation methods then carbon coated for analysis [4]. EBSD data were collected at the University of Glasgow using a Zeiss Sigma variable pressure field emission gun scanning electron microscope (VP-FEGSEM) equipped with a NordlysMax² EBSD detector. Kikuchi patterns were indexed using the AZtec v3.3 software package from Oxford instruments following the settings and processing described in [5].

Results: Augite crystals in all three stones are aligned with their [001] axes roughly parallel [6]. Such alignment is commonplace in pyroxene-rich terrestrial lava flows [7]. Deformation observed within the Yamato stones is linked to weak amounts of shock. This shock deformation is represented by different combinations of slip systems within constituent olivine and clinopyroxene crystals (Figure 1). Of the three stones, Y-000802 differs the most in its type of shock deformation microstructures. The significance of these slip system differences was tested by analysing multiple thin sections of two other nakhlites: Northwest Africa (NWA) 998 and Governador Valadares. Results show that slip systems remain the same between different thin sections of each nakhlite [5].

Implications: In providing 3-D information on mineral microstructures from 2-D thin sections, our EBSD results have revealed important new differences between the Yamato nakhlites. The differences observed between the three sections in olivine and clinopyroxene slip systems indicates that they were deformed at contrasting pressures and temperatures [5]. Such heterogeneity in intensity and style of shock deformation is typical of terrestrial impact structures [8] and so should also be expected for the nakhlite source crater.

Conclusion: 3D analysis by EBSD has revealed new petrofabric and textural features within the Yamato nakhlites. We are able to discern petrofabric orientation regardless of the sample's cut orientation and observe features that would otherwise be unobservable using standard 2D analysis .

Figure 1: slip systems, olivine (left) and augite (right), of the Yamato nakhlite stones. CS crystal co-ordinate roatation axis, upper hemisphere equal area projection, cluster size 0°, half width 10°.

References: [1] Imae N. et al. (2005). *Meteoritics and Planetary Science* 40:1581–1598. [2] Misawa K. et al. (2003). *Antarctic Meteorite Research* 16:1–12. [3] Cohen B. E et al.. (2017) *Nature Communications* 640:1–9. [4] Lee, M. R. et al. (2018) *Meteoritics and Planetary Science* 53:2395-2412. [5] Griffin S. et al. (2019). In *50th Lunar and Planetary Science Conference A#1845*. [6] Griffin S. et al. (2019). In *50th Lunar and Planetary Science Conference A#1842*. [7] Mauler, A. et al. (2000) *Journal of Structural Geology* 22:1633-1648. [8] Grieve, R. A. F. & Robertson, P. B. (1976) *Contributions to Mineralogy and Petrology* 58 (1):37-49.

CRYSTALLISATION AND ALTERATION OF THE YAMATO NAKHLITES

S. Griffin[1], M. R. Lee[1], B. E. Cohen[1] and, L. Daly[1], [1]School of Geographical and Earth Sciences, University of Glasgow, Glasgow, G12 8QQ, UK (s.griffin.3@research.gla.ac.uk).

Introduction: Published geochemical and petrographic studies of the three Yamato nakhlites, Y-000593, Y-000749, and Y-000802, have lead to the interpretation that they are paired, consistent with their recovery from the same ice sheet [1,2]. However, $^{40}Ar/^{39}Ar$ geochronology of the Y-000593 and Y-000749 stones has indicated a crystallisation age discrepancy of 69 ± 15 Ma (2σ) [3] (there are currently no published crystallisation age data for Y-000802). Here we combine new large area mapping electron dispersive X-ray spectroscopy (LAM-EDS) by scanning electron microscopy (SEM) with wavelength dispersive X-ray spectroscopy (WDS) and published geochemical data to investigate the geological histories and genetic relationships of the Yamato nakhlite stones. We assess how Y-00802 relates to the other Yamato nakhlites and how each stone relates to the nakhlite source volcano on Mars.

Methods: Geochemical data for all three Yamato nakhlites were compiled and interrogated from the published literature e.g. [4,5]. LAM-EDS, LAM-electron backscatter diffraction (EBSD), and LAM-SEM images were collected at the University of Glasgow using a Zeiss Sigma variable pressure field emission gun SEM (VP-FEGSEM) equipped with a NordlysMax[2] EBSD detector; Kikuchi patterns were indexed using Oxford Instruments AZtec analysis software. Quantitative chemical analyses of the alteration assemblages in these meteorites is being collected using WDS on the same Zeiss Sigma VP-FEGSEM.

Results: Here we consider rare earth element (REE) data for Y-000593 and Y-000749 only as no REE data have been published for Y-000802. The geochemical data from the Yamato stones sit within the overall pattern of the nakhlite group. However, geochemical differences between Y-000593 and Y-000749 exceed analytical uncertainties; for example, there is a 25% difference in La/Yb between the stones, and there are also differences in Zr/Nb, La/Ba and La/Nb values. LAM-EBSD mapping reveals differences in mineral distribution and grain size (Y-000593: 52.6% augite, 12.3% olivine, 33.4% mesostasis; Y-000749: 44.7% augite, 3.54% olivine, 51.2% mesostasis; Y-000802: 61.3% augite, 6.8% olivine, 30.7% mesostasis; Figure 1).

Implications: Y-000593 and Y-000749 show similar petrology and major element geochemistry [1, 2, 5]. Modelling suggests two different scenarios for the Yamato stones; either that the geochemical differences can be explained by subtle difference in soure melting, or that the differences are caused by fractional crystalisation. Using La/Yb REE ratio we see a fractional crystallisation difference that is substantially greater than what would be expected from the modal mineralogy of the two stones. Other REE geochemical modelling related to the mantle source of the Yamato stones reveals that the samples likely derived from a similar - and related - but not identical mantle source. Studies of multiple flows from the same terrestrial volcano show similar geochemical characteristics to those observed in Y-000593 and Y-000749 [6].

Conclusions: Our modelling of published Yamato nakhlite geochemical data show the two stones to have similar geochemistry, but with subtle variations in REE and some other trace elements. These geochemical differences between Y-000593 and Y-000749 can be explained by minor differences in source melting or crystal fractionation, which is consistent with these stones representing different eruptions from the same source volcano.

References: [1] Imae N. et al. (2005) *Meteoritics and Planetary Science* 40:1581–1598. [2] Misawa K. et al. (2003) *Antarctic Meteorite Research* 16:1–12. [3] Cohen B. E et al.. (2017) *Nature Communications* 640:1–9. [4] Bridges, J. C. and Warren C. D. (2006) *Journal of the Geological Society* 163:229-251. [5] Udry, A. and Day, J. M. D. (2018) *Geochimica et Comochimica Acta* 238:292-315. [6] Fenton et al. (2004) *The Journal of Geology* 112:91-110.
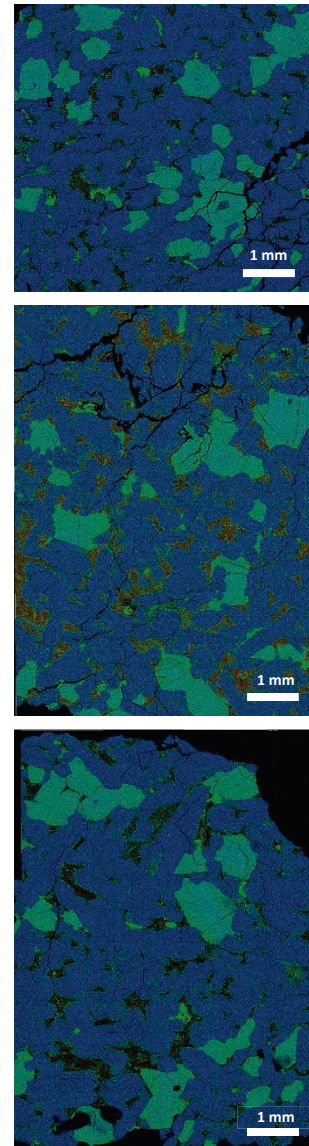
Figure 1: The Yamato nakhlites: Y-000579 (top), Y-000749 (middle), Y-000802 (bottom). False coloured EDS maps Al (orange), Mg (blue), Fe (green). Note the differences in grain size and mineral abundances..

BRITTLE FRACTURE RESISTANCE OF CHINGA AND SEYMCHAN METEORITES UNDER STATIC AND IMPACT LOADING

V.I. Grokhovsky[1] and S.V. Gladkovsky[1,2]. [1]Ural Federal University, Ekaterinburg, 620002, Russian Federation, E-mail: grokh47@mail.ru. [2]Institute of Engineering Sciences of UB RAS, Ekaterinburg, 620219, Russian Federation

Introduction: Most scientific researches of meteorites are concerning their chemical and mineralogical aspects, but mechanical behavior of such kind of materials is not clear enough [1, 2]. Most of the iron and stony meteorites mechanical properties were obtained from compressive or tensile tests and very seldom from impact and fracture toughness tests [3-5]. Thus, in this study, a comparative evaluation of Chinga and Seymchan iron meteorites brittle fracture resistance by means of static fracture toughness and impact strength tests is presented.

Experimental: Tested samples were prepared from Chinga ataxite and the metal part of Seymchan PMG. Static fracture toughness tests of meteoritic materials were performed at room temperature on standard pre-cracked specimens with a thickness of 10 mm according to 3-point bend scheme using the universal testing machine INSTRON8801 and following the regulations of GOST 25.506-85. The initiation of fatigue crack as a stress concentrator was carried out on high-frequency resonant MIKROTRON (RUMUL) machine at a loading frequency of $\approx$ 100 Hz. Impact strength KCU values of meteoritic materials were performed according to the requirements of GOST9454 with use of instrumented Tinius Olsen IT542 impact test machine at temperatures of 190 and 300 K. The sizes of impact samples with an U-notch of 2 mm in depth were 10 x 10 x 55 mm. Scanning electron microscopes JEOL JSM-66490LV and TESCAN VEGA were used for fractographical analyses of studied materials.

Results and Discussion A subject of the real researches were substances of Chinga and Seymchan meteorites. According to experimental results presented in Table 1 static fracture toughness Kc value at room temperature of Chinga meteorite is in 1.5 times higher as compared with Seymchan meteorite. Because of rather a high ductility of both materials thickness of tested specimens does not correspond to Braun-Srawley plain-strain criteria. So the experimental K_c values are related to the plain-stress condition. It means that for gaining correct K_{1c} values (plain-strain fracture toughness) specimens of higher thickness are needed.

Table 1 - The values of impact strength (KCU) and static fracture toughness (Kc) of Chinga and Seymchan meteoritic materials impact strength. *Test temperature 300/190 K

Type of meteorite	KCU*, MJ/m^2	K$_c$, MPa·m$^{1/2}$
Chinga ataxite	1.55/1.10	81.1
Seymchan octahedrite	0.67/0.19	55.5

Impact strength KCU values of Chinga ataxite are in 2.3 and 5.8 times higher in comparison with Seymchan meteorite at 300 and 190 K correspondingly. Fractographical observations of meteorites specimens surface have shown that higher values of impact strength and fracture toughness of Chinga meteorite are associated with mainly viscous dimples fracture mechanism of this material in comparison with Seymchan meteorite. The fracture relief of Seymchan meteorite impact and static specimens has more non-uniform structure and contains some pores alongside with the sites of brittle fracture relief elements.

References: [1] Lauretta D.S., McSween H.Y. 2006 Meteorites and the Early Solar System II. The University of Arizona Press, Tucson, Arizona. 943 p. [2] Ostrowski D., Bryson K. 2019. *Planetary and Space Science*. **165.** 148-178. [3] Petrovic J.J. 2001. *J. Materials Sci.* **36**. 1579-1583. [4] Sluta E.N. 2017 *Solar System Research*. **51**, 64–85. [5] Remo J. L., Johnson A. 1975 *Journal of Geophysical research*. **80**. 3744–3748.

SM-ND, LU-HF AND MN-CR COMPOSITIONS OF EUCRITE, DIOGENITE AND UNGROUPED ACHONDRITES: IMPLICATIONS FOR THE FORMATION AND SOURCES OF DIFFERENTIATED PLANETESIMALS

Z. Guo[1], J. Liu[2], L. Qin[2], M. Gannoun[3], M. Boyet[3], Z. Zajacz[3], A. Bouvier[1,4], [1]The University of Western Ontario, Department of Earth Sciences & Centre for Planetary Science and Exploration, Canada (zguo226@uwo.ca), [2]University of Science and Technology of China, Hefei, China, [3]Université Clermont Auvergne, Laboratoire Magmas et Volcans, France, [3]University of Toronto, Department of Earth Sciences, Canada, [4]Universität Bayreuth, Bayerisches Geoinstitut, Germany

Introduction: Achondrites are formed by igneous melting and single or multi-stage crystallization within planetary crusts. While the Howardite-Eucrite-Diogenite (HED) meteorites are the most abundant achondrites and are proposed to originate from the asteroid 4-Vesta [1], more than 80 ungrouped achondrites highlight the diversity of meteorite parent bodies. As chondrites, achondrites have a dichotomy in their O-Cr-Ti isotopic compositions [2] which can be used to establish genetical links between planetary objects, and compared with the timing of their formation. The HED belong to the non-carbonaceous (NC) clan, while the ungrouped achondrites NWA 2976, NWA 6704 and Tafassasset are affiliated with the carbonaceous (CC) clan, and linked to the CR chondrites [2]. To gain further constraints on planetary formation and differentiation and their reservoirs, we carried out geochemical analyses and isotopic analyses for short-lived and long-lived radiogenic systems ^{53}Mn-^{53}Cr, ^{147,146}Sm-^{143,142}Nd and ^{176}Lu-^{176}Hf (including their stable isotopes) in selected achondrites from both clans.

Samples: Bilanga and NWA 7977 are diogenites, while NWA 11001 and Tirhert are both unbrecciated gabbroic eucrites. NWA 12338 is an ungrouped achondrite with eucrite-like elemental composition but distinct isotopic and petrological features [3]. Literature ages of Bilanga [4], NWA 6704 [2], NWA 2976 [5] or Tafassasset [6] indicate that their crystallization occurred contemporaneously within 5 Ma after Solar System formation, while eucrites may have formed over a more protacted history [7]. Whole-rock powders for each meteorite ranging from 1.1g to 2.8g were prepared from individual interior chips or fragments without fusion crust. Plagioclase-rich and pyroxene-rich fractions were separated for NWA 11001, NWA 12338 and Tirhert.

Methods: LA-ICPMS analyses of minor and trace elements for minerals of NWA 6704, NWA 11001, NWA 12338 and Tirhert were obtained using a NWR193UC laser coupled with an Agilent 7900 qICP-MS at the University of Toronto. For Sm-Nd and Lu-Hf analyses, all samples including whole-rock and mineral separates were processed for analyses as described in [8]. Whole-rock compositions for minor and trace elements were obtained using a qICPMS iCAP at Western. Sm-Nd and Lu-Hf spiked isotopic dilutions, and unspiked Hf isotopic compositions were carried out using a Thermo Neptune Plus MC-ICPMS at UCA. Unspiked isotopic analyses of Sm and Nd by Thermo Triton Plus TIMS are ongoing at UCA. Cr isotopic data were obtained by Triton TIMS at Carnegie IW.

Results and Discussion: *LA-ICPMS* data shows Eu/Eu* anomalies of plagioclase are variable (17.0-32.7) for NWA 11001, NWA 12338 and Tirhert, while as low as 2.5 for NWA 6704; while for pyroxene, Eu/Eu* anomalies are absent. The whole rock have Eu/Eu* of 0.2-0.4 for diogenites, 1.3-1.8 for NC achondrites, and 0.6 to 2.4 for CC achondrites. Their compositions indicate various degrees of silicate partial melting and crystallization processes, and thus differentiation histories.

Mn-Cr systematics: NWA 6704 has a WR ε^{54}Cr of 1.63±0.10 similar to the report in [2]. NWA 11001 has a WR ε^{54}Cr of -0.26±0.08 which is on a lower end of the range reported for eucrites and suggests a formation towards a more inner region of the disk (e.g. [2]). The ε^{53}Cr of mineral fractions do not have a strong correlation with Mn/Cr ratios, which indicates that NWA11001 formed relatively late at 4543.9±12.3 Ma (when anchored to LEW 86010).

Whole-rock isochrons: When regressed with literature data on eucrites and angrites [7,9-11], we obtain a ^{176}Lu-^{176}Hf age of 4614±53 Ma for achondrites and ^{147}Sm-^{143}Nd age of 4538±58 Ma for eucrites consistent with their early formation (e.g. [4]). We do not find an anomalous λ^{176}Lu for Lu-Hf WR isochron. A deficit in μ^{178}Hf = -43±5 ppm in Bilanga, while other achondrites are similar to our standard. The stable Sm and Nd isotopic compositions are ongoing and will be presented at the meeting.

 References: [1] McSween H. Y. et al. (2013) *Meteoritics & Planet. Sci.* 48: 2090–2104. [2] Sanborn M. E. at al. (2019). *Geochim. Cosmochim. Acta*, 245, 577-596. [3] Guo Z. et al. (2019) 50th *LPSC*, Abstract #1583. [4] Hublet G. et al. (2017) *Geochim. Cosmochim. Acta* 218: 73–97. [5] Bouvier A. et al. (2011). *Geochim. Cosmochim. Acta* 75: 5310-5323. [6] Göpel C. et al. (2015). *Geochim. Cosmochim. Acta* 156: 1-24. [7] Bouvier A. et al. 2015. *Meteoritics & Planet. Sci.* 50: 1896-1911. [8] Bouvier A. and Boyet M. (2016) *Nature* 537: 399-402. [9] Bast R. et al. (2017) *Geochim. Cosmochim. Acta* 212: 303–323. [10] Blichert-Toft J. et al. (2002) *Earth & Planet. Sci. Lett.* 204: 167-181. [11] Sanborn M. E. at al. (2015). *Geochim. Cosmochim. Acta* 171: 80-99.

CHRONOLOGICAL EVIDENCE FOR MESOSIDERITE FORMATION ON VESTA BY A HIT-AND-RUN COLLISION.

M. K. Haba[1,2*], J. F. Wotzlaw[1], Y.-J. Lai[1], A. Yamaguchi[3] and M. Schönbächler[1]. [1]Institute of Geochemistry and Petrology, ETH Zürich, 8092 Zürich, Switzerland, [2]Department of Earth and Planetary Sciences, Tokyo Institute of Technology, Tokyo 152-8551, Japan (haba.m.aa@m.titech.ac.jp), [3]National Institute of Polar Research, Tachikawa, Tokyo 190-8518, Japan.

Introduction: Mesosiderites are a type of stony-iron meteorites that formed by mixing of differentiated crust and molten core materials [1]. These meteorites provide insights into the catastrophic break-up of differentiated asteroids. The petrology and chemical compositions of mesosiderite silicates are similar to howardite-eucrite-diogenite (HED) meteorites [2], which are believed to originate from the asteroid Vesta based on the agreement of their laboratory and astronomically observed infra-red spectra [3]. In addition, the O, Cr, and Ti isotope compositions of mesosiderite silicates are excellently consistent with those of HED meteorites [4–6], indicating that mesosiderites also came from Vesta or that their parent bodies formed in the neighbouring region in the solar nebula. If the parent body of mesosiderite silicates is Vesta, the large-scale disruption that formed mesosiderites should have left a chronological mark on both mesosiderites and HED meteorites. In this study, we focus on the zircons in mesosiderites and report the first comprehensive high-precision U-Pb dataset to determine the precise timing of the metal-silicate mixing event and propose a formation model.

Samples and Methods: Zircons were hand-picked from five mesosiderite samples (Vaca Muerta, NWA 1242, NWA 8402, Estherville, NWA 8741) after dissolving the metal parts in concentrated HCl and the silicate parts in concentrated HNO_3-HF mixtures. Samples for U-Pb dating were spiked with 3–5 mg of EARTHTIME ^{202}Pb-^{205}Pb-^{233}U-^{235}U tracer solution and dissolved in concentrated HF using Parr® bombs. Uranium and Pb isotopes were separated using a HCl-based column chemistry and were then measured using a TRITON Plus TIMS at ETH Zurich [7].

Results and Discussion: The ^{207}Pb-^{206}Pb dates of analyzed zircons show two distinct populations with a weighted mean of $4,525.39 \pm 0.85$ Myr and $4,558.5 \pm 2.1$ Myr (2σ). The older zircons are likely magmatic relict zircons that formed before the metal-silicate mixing event. Intriguingly, the younger zircons are characterized by unusually low U and Th concentrations (<1 ppm), which are best explained by growth after secondary phosphate minerals during the metal-silicate mixing [8]. Therefore, the younger zircon dates correspond to the timing of the metal-silicate mixing. The ages of the two populations are in good agreement with the timing of crustal formation (4,550–4,560 Myr [9]) and large-scale reheating (~4,530 Myr) on the eucrite parent body, i.e. Vesta. This chronological coincidence corroborates that Vesta is the parent body of mesosiderite silicates.

Since the mesosiderite metal was molten at the time of mixing [1], the parent body size can roughly be estimated to ≥530 km in diameter based on comparison to numerical calculations of Vesta's thermo-chemical evolution [10]. If the mesosiderite metal was derived from the core of another different asteroid [1], the direct collision between such large protoplanets likely would have led to a wholescale disruption of Vesta. As an alternative, a hit-and-run collision with a smaller planetesimal (mass ratio 0.1) only disrupts one hemisphere of Vesta. It produces significant ejecta consisting mainly of crust and mantle materials, but also small amounts of core [11]. In such a case, the collisional debris re-accretes opposite of the collision site and mixes with the underlying crust in the early stage, whereas subsequently pure ejecta debris accumulates in the upper layer. Considering the extremely slow cooling rate of mesosiderites at temperature below 500°C (~0.4°C/Myr) [12] and their low olivine contents, they presumably formed in the lower part consisting of a mixture of collisional debris and underlying crust. Long after the hit-and-run collision, mesosiderites and possibly HED meteorites were ejected from the south pole basin, Rheasilvia, whose initial depth corresponds to 20–80 km [14]. If correct, the hit-and-run collision must have occurred in the northern hemisphere of Vesta, thickening the original crust in the southern hemisphere, which resulted in the two different estimates for crustal thickness reported from HED meteorites (30–60 km) [15,16] and the Dawn mission (>80 km) [14].

References: [1] Hassanzadeh J. et al. (1990) *Geochimica et Cosmochimica Acta* 54:3197–3208. [2] Mittlefehldt D. W. et al. (1979) *Geochimica et Cosmochimica Acta* 43:673–688. [3] McCord T. B. et al. (1970) *Science* 168:1445–1447. [4] Greenwood R. C. et al. (2006) *Science* 313:1763–1765. [5] Trinquier A. et al. (2007) *The Astrophysical Journal* 655:1179–1185. [6] Rüfenacht M. et al. (2018) *Annual Meeting of the Meteoritical Society* Abst. #6264. [7] Wotzlaw J. F. et al. (2017) *Journal of Analytical Atomic Spectrometry* 32:579–586. [8] Haba M. K. et al. (2017) *Geochimica et Cosmochimica Acta* 215:76–91. [9] Misawa K. et al. *Geochimica et Cosmochimica Acta* 69:5847–5861 (2005). [10] Neumann W. et al. (2014) *Earth and Planetary Science Letters* 395:267–280. [11] Asphaug E. (2010) *Chemie Der Erde-Geochemistry* 70:199–219. [12] Hopfe W. D. and Goldstein J. I. (2001) *Meteoritics & Planetary Science* 36:135–154. [13] Schenk P. et al. (2012) Science 336:694–697. [14] Clenet H. et al. (2014) *Nature* 511:303–306. [15] Mandler B. E. and Elkins-Tanton L. T. (2013) *Meteoritics & Planetary Science* 48:1–17. [16] Barrat J.-A. (2010) *Geochimica et Cosmochimica Acta* 74:6218–6231.

THE USE OF GEORADAR TO EXPLORE THE IMPACT EJECTA LAYER AROUND THE MAÂDNA STRUCTURE (TALEMZANE, ALGERIA).

L. Hamai[1, 2], A. Lamali[1, 2], A. Yelles-Chaouch[1], A. Abtout[1], A. Nadjemi[2], N. Merabet[1], S. Bentridi[2], Leila Djadia1 and S. A. Mokhtar[3], [1]Centre de Recherche en Astronomie Astrophysique et Géophysique, Route de l'Observatoire, BP 63, Algiers, Algeria (lamine.hamai@yahoo.fr), [2]Laboratoire de l'Énergie et des Systèmes Intelligents (LESI), Université Djillali Bounaâma Khemis Miliana, Faculté des Sciences, et de la Technologie, Route de Théniat El Had, 44225 Khemis Miliana, Ain Defla, Algeria, [3]Centre de recherche nucléaire de DRARIA, BP 43, Sebala, Draria, Algiers, Algeria.

Introduction: Nowadays a large number of confirmed impact structures on Earth were first identified as geophysical anomalies, whereas their impact origin only established later through detailed petrophysical investigations. Although the complexities of geophysical characters and the lack of unique signatures for terrestrial impact craters, geophysics continue to play a critical role in the future discovery of these structures, even when they are deeply eroded or are completely buried under ground. In the case of Maâdna crater (33°19' N, 4°19' E), the previous works [1, 2, 3] was based on a more limited data set to ascertain the formation process and its origin. More recently, a geological and geophysical study conducted by Lamali et al (2016) [4] on this structure do not confirm an impact origin for this structure and suggested a dissolved diapir with inverted relief as an alternative to the impact hypothesis.

Results and discussion: In contrast to previous investigations, the crater was investigated again using several other geophysical surveys including Ground Pentrating Radar (GPR) technique. Though the limited use of this method in the case of the impact structures, it has been mostly used to detect the ejecta-bedrock contact, as well as subsurface lithological contacts and faults. According to our obtained results in the case of the Maâdna crater, its efficiency was tested to discriminate the electromagnetic signature of supposed ejectas that widely supported at Maâdna. However, GPR allowed the confirmation of nonexistence of such as signature at Maâdna crater. Moreover, our different scans were interpretative against the structural context of the Maâdna structure. Therefore, most of the analyzed profiles allowed us recognizing the typical deformation effects at Maâdna structure, which should be related to a diapiric system rather than to the meteoritic impactism as supported in Lamali et al (2016) [4].

References:
[1] Lambert P. et al. 1980. *Meteoritics* 15:157–179. [2] Karpoff R. 1953. *Meteoritics* 1:31–38. [3] McHone J. F. Jr. and Greeley R. 1987. *Meteoritics* 22:253–264. [4] Lamali A. et al. 2016. *Meteoritics & Planetary Science* 12:2249–2273.

SPECTRAL CHARACTERISTICS OF (101955) BENNU FROM OSIRIS-REx OBSERVATIONS.

V. E. Hamilton[1], A. A. Simon[2], P. R. Christensen[3], D. C. Reuter[2], J. P. Emery[4], H. H. Kaplan[1], B. E. Clark[5], D. S. Lauretta[6], and the OSIRIS-REx Team; [1]Southwest Research Institute (hamilton@boulder.swri.edu), [2]Goddard Space Flight Center, [3]Arizona State University, [4]University of Tennessee, [5]Ithaca College, [6]University of Arizona.

Introduction: Visible to near infrared (VNIR) and thermal infrared (TIR) spectral data collected by the Origins, Spectral Interpretation, Resource Identification, Security–Regolith Explorer (OSIRIS-REx) mission have revealed evidence of widespread, hydrated materials across the surface of asteroid (101955) Bennu [1]. Here we describe spectral features identified in data collected through the Detailed Survey phase of the mission.

OSIRIS-REx Spectrometers: The OSIRIS-REx Visible and InfraRed Spectrometer (OVIRS) is a point spectrometer covering the range from 0.4 to 4.3 µm with a 4-mrad field of view (FOV) and a spectral sampling of 2 nm from 0.392 to 2.4 µm, and 5 nm from 2.4 to 4.3 µm [2, 3]. The OSIRIS-REx Thermal Emission Spectrometer (OTES) is a point spectrometer that measures from ~100 to 1650 cm^{-1} (~5.5 to 100 µm), with an 8-mrad FOV and a spectral sampling of 8.66 cm^{-1} [4]. The OVIRS FOV is within that of OTES but the two boresights are not precisely co-aligned.

OVIRS Results: OVIRS disk-integrated Approach data revealed a VNIR spectrum that is consistent with the ground-based data of [5], having a blue (negative) slope and no visible features above the level of the noise. Because space weathering can cause both blueing and reddening of the spectral slope [e.g., 6], we have not arrived at any definitive conclusions about this process at Bennu. There is no apparent rotational variation in the OVIRS whole-disk spectra. A 0.55-µm feature observed in OCAMS data [7] is not present in the OVIRS data acquired to-date [1, 8]. At longer wavelengths, an unambiguous "3-µm" band is present, consistent with the presence of hydrated silicates, including those contained in low petrologic type CI and CM chondrites. The specific position of this band in OVIRS spectra is 2.74 ± 0.01 µm, most consistent with the positions observed in low petrologic subtype CM2 meteorites [9]. To date, no additional features have been identified with confidence in post-Approach data, but small variations in albedo and spectral slope are apparent; we cannot say if these differences arise from composition, particle size, space weathering, or some combination of these. The optimal equatorial mapping station for OVIRS observations (in terms of signal-to-noise ratio and spatial coverage) is planned to occur on 16 May 2019 and will be used to confirm results to date and look for additional spectral features.

OTES Results: Spatially resolved spectra at ~80 m/spot that were acquired during one of the Preliminary Survey equatorial passes revealed a spectrum with low contrast (~2%) and a spectral shape that is broadly consistent with carbonaceous chondrites in the CI/CM groups and does not vary with rotation [1]. The silicate bending feature in the spectra has a minimum at 440 cm^{-1} (~22.7 µm) and is indicative of a volumetrically dominant phyllosilicate component (i.e., >55%) based on comparison to laboratory meteorite spectra of analogue CM carbonaceous chondrites [1, 10, 11] and laboratory measurements of the meteorites' modal mineralogy [12]. Features at 555 and 346 cm^{-1} in the OTES spectra are attributable to magnetite [1]. At the improved spatial resolutions (~40 m/spot) of more recent Detailed Survey measurements, there is spectral variability, primarily in the shape of the silicate stretching feature and the depth of the silicate bending feature. We also observe variability in the emissivity at low wavenumbers (>1100 cm^{-1}; <8 µm) that may indicate previously unresolved spatial variations in the dominant particle size on the surface. The optimal equatorial mapping station for OTES observations is planned to occur on 9 May 2019.

Summary: The surface of Bennu not only exhibits evidence of hydrated silicates but appears to be dominated volumetrically by such minerals and is consistent spectrally with CI and CM carbonaceous chondrites. Analysis of Bennu's surface geological characteristics indicates that it is a rubble pile that has experienced recent geological processes despite also retaining much older surface features [13]. Small-scale (centimeter to meter) variability in albedo and geologic features suggest that multiple lithologies are present [14], and we will continue to search for spectral signatures of differing compositions in our equatorial mapping data.

References: [1] Hamilton V. E. et al. (2019) *Nature Astronomy 3*:332–340. [2] Reuter D. C. et al. (2018) *Space Science Reviews 214:*54. [3] Simon A. A. et al. (2018) *Remote Sensing 10:*1486. [4] Christensen P. R. et al. (2018) *Space Science Reviews 214:*87. [5] Clark B. E. et al. (2011) *Icarus 216*:462-475. [6] Lantz C. et al. (2018) *Icarus 302*:10–17. [7] Lauretta D. S. et al. (2019) *Nature 568*:55–60. [8] Clark B. E. et al. (2019) *LPS L*, Abstract #2132. [9] Takir D. et al. (2013) *Meteoritics & Planetary Science 48*:1618–1637. [10] Hamilton V. E. et al. (2018) *LPS XLIX*, Abstract #1753. [11] Donaldson Hanna K. L. et al. (2019) *Icarus 319*:701–723. [12] Howard K. T. et al. (2019) *Geochimica et Cosmochimica Acta 73*:4576-4589. [13] Walsh K. J. et al. (2019) *Nature Geoscience 12*:242–246. [14] DellaGiustina D. N. et al. (2019) *Nature Astronomy 3:*341–351.

COMPLEX INTERGROWTHS OF NON-STOICHIOMETRIC DEFECT-STRUCTURED HIBONITE AND Al-RICH SPINEL IN AN ALLENDE Ca-Al-RICH INCLUSION.

J. Han[1,2], I. Ohnishi[3], and L. P. Keller[2]. [1]Lunar and Planetary Institute, USRA, 3600 Bay Area Boulevard, Houston, TX 77058, USA (han@lpi.usra.edu), [2]ARES, NASA Johnson Space Center, 2101 NASA Parkway 1, Houston, TX 77058, USA,[3]JEOL Ltd., 3-1-2 Musashino, Akishima, Tokyo, 196-8558, Japan.

Introduction: Hibonite is a primary ultra-refractory mineral occurring in many Ca-Al-rich inclusions (CAIs) [1] and is predicted to condense as the second major phase from a cooling gas of solar composition [2]. Our previous microstructural studies of hibonite in carbonaceous chondrites revealed its unique microstructures consisting of numerous defects that contain Mg-enriched, wider spinel blocks in stoichiometric hibonite [e.g., 3-5]. [6,7] demonstrated experimentally that defect-structured hibonites can grow easily in the presence of minor Mg and are kinetically more stable than equilibrium assemblages predicted by thermodynamic calculations [2]. However, a thermodynamic vs. structural stability of defect-structured hibonite relative to other early-condensed Al-rich phases such as corundum, grossite, and spinel remains poorly constrained. Here, we present the results of atomic resolution TEM imaging of hibonite in a compact Type A CAI in the Allende CV3 chondrite in order to better understand the crystal structure and chemistry of defect-structured hibonite and its associated Al-rich phases, especially non-stoichiometric, Al-rich spinel, in the context of the formation of first refractory solids in the early solar nebula.

Sample & Methods: In the Allende CAI, elongated hibonite crystals up to ~60 μm long are intergrown with spinel and minor perovskite as inclusions in a ground mass of coarse-grained melilite. The hibonite crystal show oscillatory zoning, readily shown by SEM BSE imaging and EDS mapping, with MgO and TiO_2 contents up to 3.2 wt% and 7.2 wt%, respectively. We prepared a FIB section from hibonite using a FEI Quanta 3D SEM/FIB at NASA JSC. The section was analyzed using a JEOL 2500SE scanning TEM at NASA JSC and a JEOL JEM-ARM300F Grand ARM TEM at JEOL.

Results & Discussion: Based on our initial analyses using the 2500SE STEM, the FIB section consists of two hibonite subgrains surrounded by spinel and melilite. The first hibonite crystal contains an Al-rich spinel inclusion (160 nm long and 20 nm wide), which shares the crystallographic orientation relationship with the host hibonite such that $[110]_{hib}//[011]_{sp}$ and $(001)_{hib}//(111)_{sp}$. The hibonite crystal is nearly defect-free, but the spinel inclusion is associated with a few defects along the (001) plane of the host hibonite that are extended up to ~1.5 μm from its top and bottom tips. In contrast, the second hibonite crystal contains a higher number of defects that show a range of (001) spacings. Most defects are developed across the entire crystal, but a few are terminated within the crystal.

Atomic resolution high angle annular dark-field images provide direct information about the spatial distribution of heavy atoms in hibonite, which allows us to determine the structure and chemistry of layers having a range of (001) spacings in comparison with stoichiometric hibonite and spinel. In the first hibonite crystal dominated by 1.1 nm wide (001) layers, the spinel inclusion is decorated by a single layer of 1.6 nm (001) spacing along its top, as well as stepwise layers of 2.0 nm (001) spacing extended from its bottom end. In the second hibonite crystal, isolated layers of 1.6 nm and rarely 2.5 nm (001) spacings are randomly intergrown within the prominent hibonite layers of 1.1 nm (001) spacing. The 1.6 nm wide (001) layers are commonly observed in hibonite from many CAIs [e.g., 3-5], but wider layers of 2.0 nm and 2.5 nm (001) spacings appear extremely rare.

Stoichiometric hibonite contains five Al sites (three octahedral M1, M4, and M5 sites, a trigonal bipyramidal M2 site, and a tetragonal M3 site) that are distributed within basic Ca-containing and spinel blocks [8]. The common 1.6 nm wide (001) layers are interpreted as forming wider spinel blocks in non-stoichiometric, Mg-enriched hibonite that contain twice as many M1 and M3 sites and 50% more M5 sites compared to stoichiometric hibonite having 1.1 nm (001) spacing [5,9]. The 2.0 nm and 2.5 nm wide (001) layers lack Ca-containing blocks and are therefore interpreted as distinct lamellae of Al-rich spinel up to 6 unit cells that formed contemporaneously and are intergrown with hibonite.

The defect-structured hibonite and Al-rich spinel intergrowths observed in this study imply that both of these phases were kinetically stable at high-temperatures, which conflicts with thermodynamic calculations showing essentially no stability of Al-rich spinel even in dust-enriched systems [10]. The metastability of such non-stoichiometric assemblages in which kinetics were important may have suppressed grossite and krotite formation, but enhanced the abundance of spinel in CAIs.

References: [1] MacPherson G. J. (2014) Treatise on Geochemistry II vol.1 pp.139-179. [2] Yoneda S. & Grossman L. (1995) *GCA* 59:3413-3444. [3] Han J. et al. (2015) *MAPS* 50:2121-2136. [4] Han J. et al. (2017) 80th MetSoc, abstract #6380. [5] Keller L. P. et al. (2018) 49th LPSC, abstract #2392. [6] Han J. et al. (2016) 79th MetSoc, abstract #6534 [7] Han J. et al. (2017) 48th LPSC, abstract #2895. [8] Nagashima M. et al. (2010) *Mineral Mag* 74:871-885. [9] Schmid H. & De Jonghe L. C. (1983) *Philos Mag A* 48:287-297. [10] Ebel D. S. et al. 77th MetSoc, abstract #5268.

MICROSTRUCTURAL RECORD OF EVOLVING CONDENSATION PROCESSES IN FINE-GRAINED Ca-Al-RICH INCLUSIONS FROM THE REDUCED CV3 CHONDRITES.

J. Han[1,2], C. Park[3], and L. P. Keller[2]. [1]Lunar and Planetary Institute, USRA, 3600 Bay Area Boulevard, Houston, TX 77058, USA (han@lpi.usra.edu), [2]ARES, NASA Johnson Space Center, 2101 NASA Parkway 1, Houston, TX 77058, USA,[3]Division of Earth-System Sciences, Korea Polar Research Institute, 26 Songdomirae-ro, Yeonsu-gu, Incheon 21990, South Korea.

Introduction: Fine-grained, spinel-rich Ca-Al-rich inclusions (FGIs) in carbonaceous chondrites consist of numerous layered nodules having cores of spinel, hibonite, and/or perovskite surrounded by multiple thin layers of melilite, anorthite, diopside, and/or olivine [e.g., 1,2]. They are interpreted as aggregates of direct high-temperature condensates from an ^{16}O-rich nebular gas that escaped significant melting [e.g., 3,4]. However, FGIs are very complex objects composed of intimate intergrowths of fine-grained refractory phases and show extremely large variations in mineralogy, modal abundance, and textures. Thus, detailed FIB/TEM analyses of FGIs are required to fully characterize their micro-to-nanometer scale textures, mineralogy, and chemical compositions and hence elucidate their formation processes and conditions in the early solar nebula. Here, we present our on-going study of pristine FGIs from the reduced CV3 chondrites Efremovka and Thiel Mountains (TIL) 07003 and 07007 that have minimal evidence for secondary parent body alteration [5].

Methods: We identified six FGIs from Efremovka using a JEOL 7600F SEM at NASA JSC [6]. We used a FEI Quanta 3D SEM/FIB in order to document the detailed petrologic and mineralogical characteristics of FGIs from Efremovka and to prepare TEM sections from them. The sections were examined in detail using a JEOL 2500SE field emission scanning TEM equipped with a Thermo-Noran thin window energy dispersive X-ray spectrometer. In addition, eleven FGIs from TIL 07003 and twelve FGIs from TIL 07007 were identified and studied their petrology and mineralogy using a JEOL JXA-8530F EPMA at KOPRI.

Results & Discussion: The FGIs from Efremovka and TIL 07003 and 07007 are irregularly-shaped, often elongated inclusions (up to ~4 mm in size) that share the basic internal structure consisting of numerous nodules of a core of spinel ± hibonite ± perovskite, each nodule is surrounded by thin sequential layers of ±melilite, ±anorthite, and pyroxene. None of the FGIs are porous. Significant variations in mineralogy, modal abundance, and nodule size and shape among the inclusions are observed. Five inclusions from TIL 07003 and six inclusions from TIL 07007 show a mineral zoning with a distinct core-mantle structure. Only seven inclusions (one from TIL 07003 and six from TIL 07007) are surrounded by an olivine-rich accretionary rim.

Our preliminary SEM and TEM analyses of FGIs from Efremovka and TIL 07003 and 07007 are consistent with their condensation origin. We infer the evolving sequence of high-temperature condensation and gas-solid reactions that grew single grains into layered nodules: perovskite condensation > hibonite condensation > spinel formation by reaction of hibonite + $Mg_{(g)}$ > Al,Ti-pyroxene formation by reaction of spinel + perovskite + $Si_{(g)}$ > zoned melilite formation by reaction of spinel + $Si_{(g)}$ + $Ca_{(g)}$ > zoned pyroxene formation by reaction of melilite + spinel + $Si_{(g)}$ + $Mg_{(g)}$ ± $Ti_{(g)}$ ± perovskite > forsteritic olivine condensation > anorthite replacing melilite + Al-diopside. All the reactions did not go to completion, protecting underlying grains from further back reactions [7]. This inferred mineral formation sequence differs from that predicted by thermodynamic calculations, suggestive of disequilibrium conditions during CAI formation. The first inconsistency between the observed vs. predicted mineral condensation sequence is the complete absence of corundum as the first phase to form in FGIs, suggesting that minor corundum condensed first and reacted completely with $Ca_{(g)}$ to form hibonite [8]. However, corundum as the first condensate must form by homogenous nucleation, which requires a nebular gas at temperatures higher than hibonite condensation for a long time [9]. Thus, rapid cooling of a nebular gas may have suppressed homogenous nucleation of corundum, instead allowed the gas to cool into the temperature ranges of perovskite and hibonite condensation [10]. The second inconsistency addresses a long-standing question regarding spinel formation before melilite. The presence of stacking defects in hibonite and its crystallographic orientation relationships with adjacent spinel suggest that spinel formation after hibonite and before melilite was kinetically controlled process due to their structural similarity [10].

Detailed FIB/TEM analyses, as well as coordinated O and Mg isotopic study using SIMS and NanoSIMS, of FGIs in Efremovka and TIL 07003 and 07007 are under way, in particular to better understand the origin and nature of the observed mineral zoning in some FGIs.

References: [1] Holmberg B. B. & Hashimoto A. (1992) *Meteoritics* 27:149-153. [2] Krot A. N. et al. (2004) *MAPS* 39:1517-1553. [3] Aléon J. et al. (2005) *MAPS* 40:1043-1058. [4] Bodénan J.-D. et al. (2014) *EPSL* 401:327-336. [5] Brearley A. J. & Krot A. N. (2013) In: Metasomatism and the Chemical Transformation of Rock. pp.659-789. [6] Han J. & Keller L. P. (2019) 50th LPSC, abstract #2902. [7] Petaev M. I. & Wood J. A. (2005) In Chondrites and Protoplanetary Disk vol.341 pp.373-406. [8] Yoneda S. & Grossman L. (1995) *GCA* 59:3413-3444. [9] Nakamura T. M. et al. (2007) *MAPS* 42:1249-1265. [10] Han J. et al. (2015) *MAPS* 50:2121-2136.

BENNU: AN AQUEOUSLY ALTERED AND MILDLY HEATED CM CARBONACEOUS ASTEROID.

R.D. Hanna[1], C.W. Haberle[2], V.E. Hamilton[3], M.R. Lee[4], A.J. King[5], P. Lindgren[6], E.S. Howell[7], J.L. Molaro[8], H.H. Kaplan[3], N. Abreu[9], J.M. Friedrich[10], D.S. Lauretta[7], and the OSIRIS-REx team. [1]Jackson School of Geosciences, University of Texas at Austin, TX, (romy@jsg.utexas.edu), [2]School of Earth and Space Explor., Arizona State University, Tempe, AZ, [3]Southwest Research Institute, Boulder, CO, [4]School of Geographical and Earth Sci., University of Glasgow, [5]Dept. of Earth Sci., Natural History Museum, London, [6]Dept. of Geology, Lund University, Sweden, [7]University of Arizona, Lunar and Planetary Laboratory, Tucson, AZ [8]Planetary Science Institute, Tucson, AZ, [9]Pennsylvania State University, DuBois, PA, [10]Fordham University, Bronx, NY

Introduction: The OSIRIS-REx mission is currently observing asteroid (101955) Bennu to prepare for sampling in 2020. Spectra acquired with the OSIRIS-REx Visible and InfraRed Spectrometer (OVIRS) and Thermal Emission Spectrometer (OTES) during the Approach and Preliminary Survey mission phases indicate that hydrated materials, similar to aqueously altered CM chondrites, dominate Bennu's surface [1]. Here we present the results of a laboratory spectral study of a suite of CMs with variable degrees of aqueous alteration and heating to correlate and characterize spectral changes associated with petrologic subtype. This will aid in the interpretation of OVIRS and OTES spectral data and help assess the degree of alteration and heating across Bennu's surface and at the sampling site.

Methods: We analyzed a group of 13 CMs representing a range of aqueous alteration (2.0–2.7; [2]) and degree of natural heating (stages II–III/IV; [3]) as well as one CI (Alais). In addition, we experimentally heated chips of CM 2.1 ALH 83100 to observe the mineralogical and spectral modification resulting from the heating of a highly aqueously altered CM. For the initial experimental heating, small chips of ALH 83100 were placed in platinum crucibles and heated in a tube furnace under vacuum for 24 hours at 400°C. We collected mid-infrared (4,000–400 cm^{-1}; 2.5–25 μm) reflectance spectra of all samples in thin section with a Thermo Scientific iN10 FTIR microscope (μFTIR) at a spectral resolution of 4 cm^{-1}[4]. We performed complementary mineralogical and textural analysis of the sample sections using backscattered electron (BSE) imagery and energy-dispersive (EDS) x-ray analysis.

Results and Discussion: We observe several spectral trends correlated to both the degree of aqueous alteration and heating among the CMs. With increased aqueous alteration, the Christiansen feature (CF) moves to smaller wavenumbers, the SiO stretching (~950 cm^{-1}) and SiO bending (~440 cm^{-1}) bands move to larger wavenumbers, and the depth of the MgOH deformation band (~625 cm^{-1}) increases. With increased degree of natural heating, the SiO stretching band first broadens and then, with higher heating (stage III+), becomes sharp with bands that can be attributed to secondary olivine formation [3]. The SiO bending minimum also moves to smaller wavenumbers with heating, forming strong olivine bands as well at higher stages (III+). The MgOH deformation band is absent from all naturally heated samples. The main spectral modifications of the experimentally heated ALH 83100 are lowered emissivity due to formation of sulfides [5], a broadening of the SiO stretching band, and decreased depth of the MgOH band.

Analysis of a globally averaged OTES spectrum acquired during a Preliminary Survey equatorial pass confirms the initial interpretation that Bennu resembles a highly aqueously altered CM [1]. The positions of its CF (1117 cm^{-1}), SiO stretching minimum (950 ± 8 cm^{-1}), and SiO bending minimum (442 ± 9 cm^{-1}) are most consistent with a CM of subtype 2.5 or below. However, Bennu's spectrum lacks a detectable MgOH band, which is prominent among all aqueously altered CMs, and its SiO stretching band has a long wavelength broadening that is markedly different from that of unheated CMs. While the latter could be caused by the presence of fine particles, an MgOH band should still be observable (e.g., Fig. 4 in [1]). Both of these features could be attributed to heating of CM material however, as evidenced by both our naturally and experimentally heated CMs. Because the heating did not lead to the formation of secondary olivine typical of stage III+ CMs, we conclude that temperatures remained below 500°C [3]. Other evidence for heating of Bennu's surface include the presence of magnetite [1], which is found in mildly heated (stage II–III) CMs [6], in-situ breakdown of boulders that may be thermally induced [7], and particle ejection that may be related to volatile release, perhaps from the breakdown of hydrous minerals [8]. Despite this evidence for mild heating, we cannot rule out the presence of unheated materials on Bennu, especially in forthcoming higher-spatial-resolution data.

Conclusions and Ongoing Work: Our analysis of the globally averaged OTES spectrum suggests that the best spectral match to Bennu may be an aqueously altered (subtype ≤ 2.5) CM that has been mildly heated (< 500°C). We are currently heating chips of ALH 83100 for longer durations at lower temperatures to further constrain the nature of heating on Bennu's surface. We are also analyzing the 2.74-μm feature in OVIRS data to search for evidence of heating in the 3-μm region, which should be sensitive to heating as has been found for asteroid Ryugu [9].

References: [1] Hamilton V.E. et al. (2019) *Nat. Astron.* 3:332–340 [2] Rubin A. et al. (2007) *GCA* 71: 2361–2382 [3] Nakamura T (2005) *J. Mineral. Petrol. Sci.* 100:260–272 [4] Hamilton V.E. et al (2018) *LPS IL* abst. 1753 [5] Lindgren P. et al. (2019) *MetSoc 82 abst.6682* [6] Tonui E. et al. (2014) *GCA* 126:284–306 [7] Walsh K. et al. (2019) *Nat. Geosci.* 12:242-246 [8] Lauretta D. et al. (2019) *LPS L* abst. #2608 [9] Kitazato K. et al. (2019) *Science*, eaav7432.

3D CRYSTALLOGRAPHIC ORIENTATION OF OLIVINE IN BJURBÖLE CHONDRULES.

R.D. Hanna[1], R.A. Ketcham[1], M. Zolensky[2], H. Bale[3], J. Sun[4]. [1]Jackson School of Geosciences, University of Texas at Austin, TX, (romy@jsg.utexas.edu),[2]ARES, NASA JSC, Houston, TX, USA , [3]Carl Zeiss X-ray Microscopy, Pleasanton, CA, USA, [4]Xnovo Technology ApS, Køge, Denmark

Introduction: The crystallographic orientations of chondrule minerals can provide important insights into their formation and deformational history. For example, the orientations of the olivine bars and surrounding rim in barred olivine chondrules provide information on the conditions of crystallization [e.g., 1-2] and the orientations and shapes of olivines within porphritic chondrules can record the reactions with the surrounding nebular gas during chondrule formation [3]. Later deformation on the parent body can cause crystal-plastic deformation of chondrule minerals that is evident through their intracrystalline lattice misorientations [4]. Typically these crystal orientations and lattice misorientations are determined using electron backscatter diffraction (EBSD) on thin sections but this gives only a 2D picture for what is actually a 3D texture. While it is possible to combine EBSD with serial sectioning to build a 3D dataset of texture, this is a destructive, time-intensive process.

X-ray diffraction contrast tomography (DCT) is a recent technological development that enables non-destructive, 3D crystallographic orientation measurement using the X-ray diffraction of the crystal lattice to determine orientation. Originally only possible using monochromatic X-ray beams at 3rd generation synchrotron light sources [5], DCT has been recently adapted to polychromatic sources of laboratory X-ray microscopes (referred to as LabDCT) [6]. Up to this point LabDCT has only been applied to large, well-formed crystals of high symmetry (i.e., metals) [6], but we recently acquired DCT datasets for a pair of Bjurböle chondrules to determine the applicability of the technique to natural, mutlimineralic samples composed predominately of olivine (i.e., chondrules).

Methods: We first extracted a set (~10) of chondrules from the Bjurböle chondrite by manually segregating them from the highly friable matrix using hand crushing, tweezers, and a binocular microscope. Adhering matrix was removed as much as possible by rolling the chondrules between fingers, scraping with tweezers, and/or dusting with a brush. The cleaned chondrules were imaged with X-ray computed tomography (XCT) using an Xradia MicroXCT scanner (80 kV, 10W, ~5 µm voxels) at the University of Texas High Resolution XCT Facility in order to select two candidates for DCT - a porphyritic olivine chondrule and a barred olivine chondrule. The chondrules were then imaged in LabDCT mode on a Zeiss Xradia 520 Versa system. Individual diffraction contrast projections were collected with 160kV-10W source setup and 600s exposure time, 1.6 µm/pixel resolution. The data was then imported into Grain-Mapper3D[TM] for reconstruction of 3D grain map.

Results: LabDCT was successful in mapping the 3D orientation of olivine within the interior of both chondrules. Due to the large size of the barred olivine chondrule (~1.85 mm) relative to the field of view of the DCT system (~ 750 µm), only the interior portion of the chondrule was mapped (Fig. 1A). However, two sets of bars with distinct crystallographic orientations are clearly visible. The porphyritic chondrule shows a variety of olivine orientations as well as a radial distribution in crystal quality (Fig. 1B). Olivine grains in the interior are relatively large and well-defined while the those on the rim are significantly smaller with highly irregular boundaries. The majority of these rim grains share an orientation with the closest large interior olivine. We hypothesize that these peripheral grains record reactions with the surrounding nebular gas during chondrule formation [3,7]. We are continuing to analyze both datasets to extract additional information on the relative orientation of the bars and the 3D spatial distribution of the porphyritic olivine orientations.

References: [1] Miura et al. (2011) *Earth, Planets and Space* 63:1087-1096. [2] Tsuchiyama et al. (2004) *GCA* 86, 3:653-672. [3] Libourel G. and Portail M. (2018) *Science Advances* 4:eaar3321. [4] Forman et al. (2016) *Earth and Planetary Science Letters* 452:133-145. [5] Ludwig W. et al. (2009) *Review of Sci. Instr.* 89:033905 [6] McDonald S.A. et al. (2015) *Nature Sci. Reports* 5:14665. [7] Friend et. al (2016) *GCA* 173: 198-209.
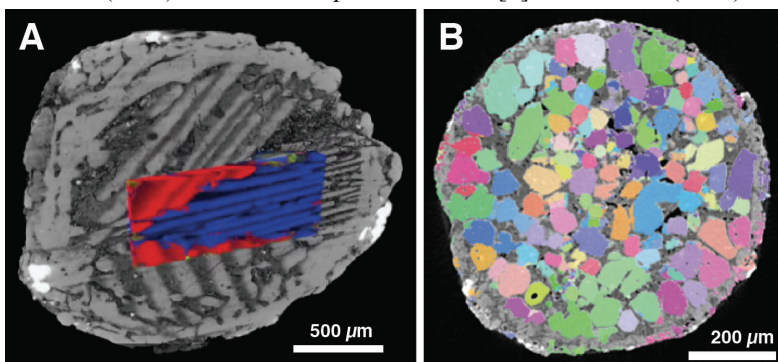
Figure 1. DCT orientation data (color) of olivine overlain on absorption tomography data (grayscale) of the Bjurböle chondrules. A) Barred olivine showing two different crystallographic orientations. B) Porphyritic olivine chondrule showing varied olivine orientations and thin rim of small, irregular olivines, most of which share an orientation with the closest large interior olivine.

THERMAL RELEASE OF WATER FROM CM2 CHONDRITES: INSIGHT FROM MASS SPECTROMETRIC EVOLVED GAS ANALYSIS (DEGAS)

D. Harries, R. Fürst, and F. Langenhorst, Friedrich Schiller University Jena, Institut für Geowissenschaften, Carl-Zeiss-Promenade 10, 07745 Jena, Germany (dennis.harries@uni-jena.de).

Introduction: The hydrous minerals serpentine and tochilinite are important constituents in primitive meteorites, such as CI1, CM2, and CR2 chondrites, and hydrous interplanetary dust particles (IDPs). Meteoritic evidence indicates that some CM- and CI-like chondrites have experienced heating and water loss. Compared to typical CM2 and CI1 chondrites, the mineralogical and geochemical characteristics of these rocks range from subtle dehydration effects (e.g., Yamato 793321, Sutter's Mill, Jbilet Winselwan; [1-3]) to petrologically distinct lithologies (e.g., Yamato 86720, Belgica 7904, Yamato 980115; Belgica grouplet or 'CY chondrites' [4,5]). The mechanism of heating is currently unknown but of interest to the ongoing Hayabusa2 and OSIRIS-REx space mission to C-group asteroids. Radiogenic heat production, impact-induced heating or solar irradiation are possible processes that could have contributed to water loss within parent bodies or in their surface regolith. In order to better understand the thermal decomposition of hydrous minerals in CM2 chondrites we have conducted heating experiments in a high vacuum furnace equipped with a mass spectrometer to analyze the evolved gases.

Samples and Methods: The samples investigated in this study are Mg-rich serpentine (lizardite/polygonal serpentine [6]) from Totalp (Davos, Switzerland), cronstedtite from Hohe Warte mine (Gernrode, Germany), tochilinite from Otamo quarry (Siikainen, Finland), and the CM2 chondrites Murchison (MUR) and Jbilet Winselwan (JW).

The experimental technique uses a directly coupled evolved gas analysis system (DEGAS) custom-build at FSU Jena [7]. The samples (2-50 mg) are heated in Al_2O_3 crucibles in high vacuum ($<10^{-6}$ mbar based pressure) generated by two turbomolecular pumps (255 and 230 l/sec). The crucibles are placed on a sensitive thermogravimetric balance (Netzsch STA 429) and can be heated to 1450 °C at controlled rates. The evolved gases are analyzed by a quadrupole mass spectrometer (Balzers QMA-125), which is directly coupled to the furnace chamber without differential pressure apertures. This increases sensitivity and largely avoids re-equilibration of evolved gases compared to techniques working in inert atmospheres. Experimental runs were conducted at heating rates of 5 and 10 K/min.

Results: The pure minerals show distinct dehydroxylation peaks at m/z = 18 for H_2O^+. The Mg-rich serpentine shows an onset of H_2O release at 400–500 °C with a peak at 620–630 °C. In cronstedtite H_2O release starts at ~200 °C and peaks at 310–320 °C. Tochilinite shows an onset of H_2O release at ~100 °C and a first peak at ~210 °C. The main H_2O release occurs at 350–360 °C. Evaluation of the mass spectra recorded during heating of the CM2 chondrites indicates significant differences among MUR and JW (Fig. 1). MUR shows incipient H_2O release immediately after the start of heating. The release peaks at about 200 °C and then grades into a second, dominant release peak at 320–350 °C. Also JW starts to release H_2O immediately after the start of heating, but shows two well separated release peaks at 170–210 °C and at 430–480 °C, separated by a release minimum at 350–380 °C.

Discussion: The release at ~200 °C most likely results from terrestrial weathering products [3], but higher temperatures release indigenous water from phyllosilicates and tochilinite. The contrasting release minima and maxima at 320–380 °C in JW and MUR, respectively, suggest that JW was naturally heated to a maximum temperature of about 400 °C consistent with XRD results [8,9]. The release profile indicates that JW lost most of its indigenous water during this process, despite little textual effects and subtle mineralogical changes limited to the formation of amorphous or poorly crystalline silicates. This suggests a brief heating event with incomplete phase equilibration. The release of carbon-bearing species is currently being

Fig. 1: DEGAS release profiles of H_2O from Murchison and Jbilet Winselwan (heating at 10 K/min, 2 replicates each).

analyzed to better understand the fate of organic materials and carbonates during the transient heating event(s).

References: [1] Nakamura T. (2006) *Earth and Planetary Science Letters* 242:26–38. [2] Zolensky M. E. et al. (2014) *Meteoritics & Planetary Science* 49:1997–2016. [3] King A. J. et al. (2019) *Meteoritics & Planetary Science* 54:521–543. [4] Ikeda Y. et al. (1992) *NIPR Symposium on Antarctic Meteorites* 5:49–73. [5] King A. J. and Russell S. S. (2019) *50th LPSC*, abstract #1386. [6] Harries D. et al. (2019), this meeting. [7] Heide K. et al. (2000) *Thermochimica Acta* 354:165–172. [8] Nakamura T. (2005) *Journal of Mineralogical and Petrological Sciences* 6:260–272. [9] Mogi K. et al. (2017) *80th Meteoritical Society Meeting*, abstract #6225.

DYNAMICAL COMPRESSION OF SERPENTINE IN MEMBRANE-DRIVEN DIAMOND ANVIL CELLS: INSIGHTS INTO AMORPHIZATION BY SYNCHROTRON XRD.

D. Harries[1], D. Schmidt[1], A. Fazio[1], H.-P. Liermann[2], and F. Langenhorst[1], [1]Friedrich Schiller University Jena, Institut für Geowissenschaften, Carl-Zeiss-Promenade 10, 07745 Jena, Germany (dennis.harries@uni-jena.de), [2]Deutsches Elektronen-Synchrotron (DESY), FS-PE, P02, Notkestraße 85, 22607 Hamburg, Germany.

Introduction: Minerals of the serpentine-subgroup are important water-bearing phyllosilicates in primitive meteorites, and hydrous interplanetary dust particles (IDPs). They form through the reaction of ferromagnesian silicates with aqueous fluids at low to moderate temperatures. Samples to be returned by Hayabusa2 and OSIRIS-REx from the C-group near-Earth asteroids 162173 Ryugu and 101955 Bennu will shed light on the behavior of these minerals during space weathering due to solar radiation and meteoroid impacts. This understanding is crucial for assessing the spectroscopic properties of asteroid regoliths with remote techniques. The physical state of dust within planetary debris disks around stars other than the Sun provides additional, important insights into planetary evolution. Its understanding relies on computational simulations, which require reliable material models.

Because serpentine minerals can be altered by a variety of physicochemical processes, such as thermal metamorphism, particle irradiation, and impact-generated shock loading, it is important to understand how their structural and spectroscopic properties change in response. Here, we focus on the pressure-induced changes by applying rapid compression in membrane-driven diamond anvil cells (mDACs) to tens of GPa within <150 sec (e.g., [1-4]).

Methods: Starting material was natural serpentine of the composition $(Mg_{2.70},Fe_{0.16},Al_{0.12})(Si_{1.89},Al_{0.12})O_5(OH)_4$, collected from the Totalp serpentinite (Davos, Switzerland). It was gently powdered in ethanol and dynamically compressed under non-hydrostatic conditions in mDACs at beamline P02.2 of PETRAIII at DESY Hamburg. During compression XRD patterns were recorded at 25.6 keV using a Perkin-Elmer XRD 1621 fast flat panel detector. Powdered gold served as an internal pressure standard. The starting materials and recovered samples were analyzed using a Witec alpha300M+ Raman microspectrometer equipped wih a 532 nm laser operated at <10 to 40 mW.

Results: The Raman spectrum of the starting material shows OH stretching vibrations at 3589, 3682, and 3705 cm^{-1} as expected for lizardite and/or polygonal serpentine [5]. Synchrotron XRD patterns acquired during rapid compression in the mDACs show that changes in structure and/or grain size occur at pressures as low as 4 GPa at a compression rate of ~0.1 GPa/s (Fig. 1). Complete amorphization is attained at about 25 to 30 GPa at a compression rate of ~0.3 GPa/s. After recovery of the gasket, the amorphized samples do not show discernable Raman bands but display continuous scattering spectra with intensity maxima between 1000 and 3000 cm^{-1}.

The results are somewhat in contrast to shock experiments using gun-driven shock wave generators [6], from which it was inferred that shock does not produce significant structural damage in serpentines at pressures below 32 GPa. However, lizardite samples subjected to peak pressures of 16.1 GPa and 26.3 GPa by the gun method showed evidence for partial, heterogeneous amorphization, suggesting that mDAC experiments with small, homogeneously compressed sample volumes are well-capable of monitoring the amorphization process despite of the difference in compression rates. Further characterization of the structural states by TEM is ongoing and additional synchrotron mDAC+XRD experiments and structural and spectroscopic studies of partially amorphized samples will be conducted, including Fe-rich cronstedtite as a starting material.

Fig. 1: (a) Single synchrotron XRD pattern of lizardite/polygonal serpentine in the mDAC. (b) Shift of Bragg peaks and eventual loss of diffraction intensity during compression of lizardite/polygonal serpentine in the mDAC.

References: [1] Konôpková Z. et al. (2015) *Physical Review B* 91:144101. [2] Carl E.-R. et al. (2017) *Meteoritics & Planetary Science* 52:1465-1474. [3] Sims M. et al. (2019) *Earth and Planetary Science Letters* 507:166-174. [4] Langenhorst F. et al. (2017) *80th Annual Meeting Meteoritical Society*, abstract #6275. [5] Tarling M. S. et al. (2018) *Journal of Raman Spectroscopy* 49:1978-1984. [6] Akai J. and Sekine T. (1994) *Proceedings of the NIPR Symposium on Antarctic Meteorites* 7, 101-109.

IN-SITU ANALYSIS OF SOLUBLE ORGANIC COMPOUNDS FOR HAYABUSA CATEGORY 3 PARTICLES.

M. Hashiguchi[1], H. Naraoka[1, 2], M. Uesugi[3], T. Yada[4], and M. Abe[4].
[1] Research Center for Planetary Trace Organic Compounds (PTOC) and [2]Department of Earth and Planetary Sciences, Kyushu University. 744 Motooka, Nishi-ku, Fukuoka, 819-0395 Japan. [3]Japan Synchrotron Radiation Research Institute (JASRI), 1-1-1 Koto, Sayo, Hyogo 679-5198, Japan. [4]Space Exploration Innovation Hub Center, Japan Aerospace Exploration Agency (JAXA), 3-1-1 Yoshinodai, Sagamihara 252-5210, Japan.

Introduction: More than 700 Hayabusa-returned particles have been identified by Extraterrestrial Sample Curation Center (ESCuC) of Japan Aerospace Exploration Agency (JAXA) [1]. In preliminary examination on organic materials in silicate particles, no clear evidence was obtained for extraterrestrial organic materials [2]. Some carbonaceous particles composed mainly of C, N, and O were found and categorized as "category 3" based on initial description using FE-SEM-EDS by ESCuC. Previous studies suggested that the category 3 particles were likely contaminants [e.g. 3-6], however, their origin(s) has not been clear yet. In this study, we investigated the category 3 particles by in-situ analysis using desorption electrospray ionization coupled with high-mass resolution mass spectrometry (DESI-HRMS) [7] to characterize the soluble organic compounds in these particles to discuss their origins.

Samples and Methods: Two Hayabusa category 3 particles, RB-CV-0008 and RB-CV-0031 were used in this study. Initial description on by ESCuC showed that C, N, and O were dominant in both particles. The size of both particles is approximately 50 μm. These particles were pressed into an Au plate with a diameter of 3 mm and thickness of 300 μm in a clean booth at ESCuC. They were stored under N_2 or Ar atmosphere and transported to PTOC at Kyushu University for DESI/HRMS analysis. The DESI/HRMS analysis was performed using a 2D DESI ion source (Omni Spray Source 2D, Prosolia) equipped with a hybrid quadrupole-Orbitrap mass spectrometer (Q-Exactive Plus, Thermo Scientific) under the ambient environment in a clean room (Class 1000). Electrospray voltage was set at 3 kV for positive mode, and 4 kV for negative mode. A spray solvent was methanol of Q-ToF-MS grade (100%) with the flow rate of 2.5 μL/min. The positive and negative ions were collected in a full scan mode (m/z=70-1,000) with mass resolution of ~140,000 ($m/\Delta m$ at m/z 200) on the surface of the sample (~3.2×3.2 mm^2). After the analysis, a small piece of VITON gloves (~ 2 mm) used in clean chambers was also analyzed using same analytical condition as a possible contaminant for comparison.

Results and Discussion: Numerous peaks as background peaks from a spray solvent and air in the clean room were detected in a range of m/z 70-1000. About 200 positive ions and 30 negative ions, which are concentrated around particle-embedded region, were detected from RB-CV-0008. These ions were identified among the range of m/z 100-990 for positive ions, and m/z 160-680 for negative ions. The spatial distributions (concentrated region) of these positive ions and negative ions was partially matched but different from each other. Particularly, the positive ions were detected from the surface that is slightly (~ 200 μm) shifted from the particle, whereas the negative ions were almost detected from nearly the surface of the particle. These positive ions were possibly be desorbed from the surface of Au disk, however, further investigation is needed to discuss the location difference. For both positive and negative ions, most of them were not identified from a blank Au disk and VITON, which suggests that these compounds were derived from the particle. The RB-CV-0008 particle is not likely a contaminant from VITON glove.

By using their exact masses (< 3 ppm of mass precision) and Kendrick mass defect, an CH_2 homologue (every m/z 14. 0156) with high ion intensity and several different families containing units of m/z 58.042 were identified in the positive ions. A possible candidate for this units is C_3H_6O. Some negative ions could be assigned as CHO and CHNO compounds, however, any homologous families could not be identified due to the small number of identified ions. Presence of other elements (e.g. Mg, Si, and S) in the particle reported by previous studies on category 3 particles [e.g. 4, 6] were not clear because that their isotopomers could not be identified in DESI-HRMS images.

We also analyzed RB-CV-0031, however, the particle was lost during the analysis unfortunately by N_2 nebulizing gas and solvent spray of DESI, probably due to high porosity of the particle. Although some compounds were detected from the Au disk and showed concentrated spatial distribution, the position is clearly shifted from the surface of particle and we could not determine whether they were particle origin. Other possible contaminant materials will be analyzed for comparison to discuss the origin and nature of the category 3 particle.

References: [1] Yada T. et al. (2017) *80th Annual Meetings of the Meteoritical Society*, #6204, [2] Naraoka H. et al. (2012) *Geochemical Journal* 46: 61-72. [3] Ito M. et al. (2014) *Earth, Planets and Space*, 66: 102-110. [4] Kitajima F. et al. (2015) *Earth, Planets and Space* 67:20-32. [5] Naraoka H. et al. (2015) *Earth, Planets and Space* 67:67-76. [6] Uesugi M. et al. (2019) *Meteoritics & Planetary Science*, 54: 638-666. [7] Hashiguchi M. and Naraoka H. (2019) *Meteoritics & Planetary Science*, 54: 452-468.

MULTI-LAYER FINE-GRAINED RIM AROUND CHONDRULE IN THE YAMATO 75273 LL3 CHONDRITE: NEBULAR AND PARENT-BODY PROCESSES.

Yukina Hashimoto[1], Tomoki Nakamura[1], and Megumi Matsumoto[1], [1]Division of Earth and Planetary Materials Science, Graduate School of Science, Tohoku University, Aoba, Sendai, Miyagi 980-8578, Japan (email:yukina.hashimoto.p2@dc.tohoku.ac.jp)

Introduction: Chondrules in primitive chondrites are commonly surrounded by fine-grained rims. The origin and formation process of the rims is controversial [e. g., 1–4]. Many studies have proposed that fine-grained rims were formed by accretion of pristine dust particles in the solar nebula [1]. However, recent studies showed that some fine-grained rims were formed by parent-body processes [2, 3]. Chondrule rim formation by the parent-body process requires desruption and reacceretion of an earlier-formed regolith material. To uncover the origin of fine-grained rims, we performed FE-SEM and FE-EPMA analyses of a primitive LL3 ordinary chondrite Y 75273.

Results : Most chondrules in Y 75273 are surrounded by fine-grained rims. Among them, we found one chondrule surrounded by a multi-layered fine-grained rim. The rim consists of five layers from innermost 1st to outermost 5th layer. Mineral combination is similar, but relative mineral abundance, grain size, and chemical composition of the minerals differ among the rims. The 1st layer contains abundant euhedral olivine (typically <5 μm but occasionally up to 10 μm in size), Al–Na rich mesostasis glass, and minor amounts of high–Ca pyroxene (typically <5 μm), Fe sulfide (typically <3 μm), and Fe–Ni metal (typically <3 μm). The 2nd layer is similar in mineral composition with 1st layer, but the abundance of the glass is much lower than the 1st layer. The 3rd layer is rich in sulfide and consists mainly of olivine and Fe sulfide (typically <15 μm) with minor amounts of high–Ca and low–Ca pyroxene (typically <15 μm), Fe–Ni metal (typically <15 μm), and mesostasis glass. The 4th layer is similar in mineral composition with 3rd layer, but the abundance of Fe–Ni metal and Fe–Ni–Si bearing minerals is much higher than the 3rd layer and that of glass is relatively low. Grain size of the 5th layer is much smaller (typically ~a few hundreds of nm in scale) than the other four layers. In the 1st–4th layer, Fe sulfide and Fe–Ni metal seem to have melted, but silicates are not melted completely. Metal and silicates in the 5th layer are not melted and the same feature is also observed in single rims around other chondurules. The boundaries between the central chondrule and the 1st layer, between the 1st and 2nd layer, between the 2nd and 3rd layer are not easily discernible, while the boundaries between the 3rd and 4th layer, between the 4th and 5th layer are distinct and smooth (no topographic depressions).

The chemical composition differs between the layers. Defocused (10μm diameter) electron beam analysis of each layer shows compositional variation in individual rims: in the Si–Mg–Fe ternary diagram, the 2nd- layer data distribute close to the solar abundance and the 1st- and 2nd- layer data make a trend from solar toward the Si-apex suggestive of addition of Si-rich material such as glass, while the 3rd- and 4th- layer data distribute from solar to the Fe-apex indicative of addition of Fe-rich material such as Fe Sulfide and Fe–Ni metal. On the other hand, the 5th- layer data fall on the different compositional field in Mg-poor areas relative to solar. The compositional field of the 5th layer overlaps those of the single rims on the other chondrules.

Discussion: Clear boundaries between the layers can not be explained by simple monotonous dust accretion. Rather, we suggest the following nebula and parent-body processes for the formation of the multi-layered rim: The 1st and 2nd layer was formed by accretion of fine dust with solar elemental abundance. The 3rd and 4th layer formed by accretion of Fe Sulfide-rich and Fe–Ni metal-rich fine-grained dust relative to solar abundance, respectively, in the solar nebula. After accretion of the 1st to 3rd layers, some heating process occurred and caused partial melting of the 1st to 3rd layers. The 1st and 2nd layer formed from the same dust reservoir, but melted mesostasis glass was supplied to only 1st layer from the center chondrule because the 1st layer is closer to the chondrule, which is verified by the enrichment of Si and Na in the 1st layer. Dust accretion on the surface of solidified 3rd layer resulted in the formation of the 4th layer. Probably, similar heating process could have occurred after the formation of the 4th layer. Similarities in the bulk chemical composition and texture between the 5th layer and single rims suggest that they have the same origin. Chondrules, including that with the 1st to 4th layers, in an earlier-formed parent body might have been excavated by an impact and re-accumlated to the present location with irregular-shaped fine-grained rims once constitutes matrix material between chondrules. Our observation indicates that the multi-layer fine-grained rim was formed by both nebular and parent-body processes.

References:[1] Metzler K., Bischoff A., and Stöffler D. (1992) *Geochimica Cosmochimica. Acta*, 56, 2873–2897. [2] Tomeoka K. and Ohnishi I. (2015) *Geochimica Cosmochimica. Acta*, 164, 543–555. [3] Tomeoka K. and Tanimura I. (2000) *Geochimica Cosmochimica. Acta*, 64, 1971–1988. [4] Krot A. N. and Wasson J. T. (1995) *Geochimica Cosmochimica. Acta*, 59, 4951–4966.

CRYSTALLIZATION HISTORY OF THE NORTHWEST AFRICA 7203 ANGRITE.

H. Hayashi[1], T. Mikouchi[2] and M. Bizzarro[3], [1]Dept. of Earth & Planet. Sci., University of Tokyo, Hongo, Tokyo 113-0033, Japan (E-mail: h.hayashi@eps.s.u-tokyo.ac.jp),[2]University Museum, University of Tokyo, Hongo, Tokyo 113-0033, Japan,[3]Center for Star &Planet Formation, University of Copenhagen, Copenhagen, Denmark.

Introduction: Angrite constitutes one of the oldest basaltic achondrite groups and shows ususual mineral assemblages due to depletion in alkaline elements and enrichment in refractory elements [1]. Angrites lack shock metamorphism except for NWA 1670 and NWA 7203, and are therefore widely employed as useful time anchors [2]. In our previous study we reported shock metamorphism in NWA 7203 and suggested the importance of this sample to understand the evolution of the angrite parent body [3]. NWA 7203 shows a quenched texture and its grain size exhibits large variations, but the formation process of this texture is unclear [4]. In this study, we performed detailed mineralogy of NWA 7203 in order to clarify the crystallization history of this interesting angrite.

Results: NWA 7203 is mainly composed of dendrites consisting of intergrowth of olivine and anorthite, and pyroxene fills in between the dendrites. Grain size varies from fine grains (~1 μm) to coarse grains (>100 μm) (Fig. 1). The fine-grained areas show radial textures that grew into coarse-grained areas. We estimated bulk compositions of both fine-grained and coarse-grained areas by EPMA grid analyses of each area. The bulk composition of the fine-grained area is slightly more Fe-rich (SiO_2=41, Al_2O_3=14, FeO=23, MgO=7, and CaO=15) than that of the coarse-grained area (SiO_2=41, Al_2O_3=15, FeO=21, MgO=7, and CaO=15) (all in wt%). Olivines (except xenocrysts) in the fine-grained area are Fo_{54-4}, while those in the coarse-grained areas are Fo_{59-0}, which is consistent with more magnesian bulk composition of the coarse-grained area. On the other hand, pyroxenes in the fine-grained area are Mg#=0.50-0.22, while those in the coarse-grained area are Mg#=0.44-0, which is different from the olivine result. We found rare Mg-rich olivine grains (Fo_{64}, size: ~0.1 mm) in the fine-grained area. One such a grain shows a blade shape (~1 mm long, ~20 μm wide) intergrown with anorthite with the core of Mg-rich olivine (Fo_{64}) (Fig. 1).

Discussion and Conclusion: The texture of NWA 7203 (e.g., large variation of grain sizes) is unusual and could not be formed by simple fractional crystallization because coarse-grained areas are more Mg-rich than fine-grained areas. It is texturally evident that fine-rained areas first crystallized and coarse-grained areas subsequently formed as shown by the radial texture in the fine-grained areas. This is contrary to what is observed for olivine compositions since olivine is more Mg-rich in coarse-grained areas than fine-grained areas. Another important observation is the presence of Mg-rich olivine grains in the fine-grained areas. We interpret that they are xenocrysts as found in other quenched angrites. However, the texture of NWA 7203 olivine xenocrysts are different from other samples and Cr_2O_3 is not so high (up to 0.1 wt%) unlike other angrites' xenocrysts (e.g., Asuka 881371: mm-sized large grains and >0.3 wt% Cr_2O_3) [5]. We consider the crystallization history of NWA 7203 as follows (Fig. 2). First, fine-grained areas rapidly crystallized with Mg-rich olivine xenocrysts as crystallization seeds, and then coarse-grained areas were subsequently formed. However, it is required to consider some process to change the melt composition of the coarse-grained areas into more Mg-rich than that of the fine-grained areas. One explanation is the incorporation of Mg-rich melt (e.g., magma mixing) because coarse-grained areas have more Mg-rich bulk composition.
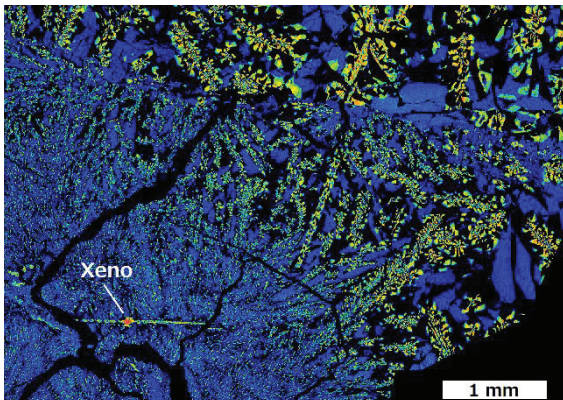
Fig. 1. Mg X-ray map of NWA 7203. Mg-rich olivine xenocryst is present ("Xeno") at the lower left.
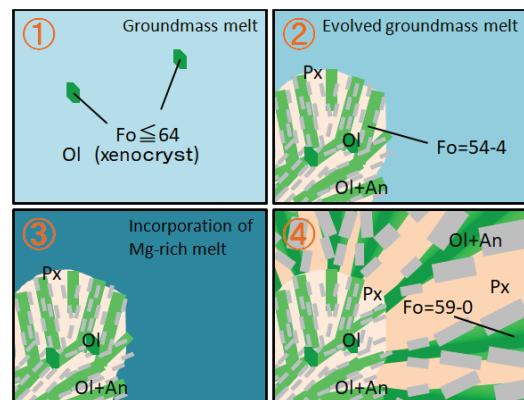
Fig. 2. Crystallization history of NWA 7203.

References: [1] Keil K. (2012) *Chemie der Erde-Geochemistry* 72:191-218. [2] Amelin Y. (2007) *Geochimica et Cosmochimica Acta* 72:221-232. [3] Hayashi H. et al. (2018) *LPS XLIX,* Abstract #1932. [4] Mikouchi T. and Bizzarro M. (2012) *Meteoritics and Planetary Science* 39: Suppl., id.5120. [5] Mikouchi T. et al. (1996) *Proceedings of NIPR Symposium on Antarctic Meteorites* 9:174-188.

EVIDENCE FOR PRESOLAR GRAIN SIC AGGREGATES FROM COSMOGENIC NUCLIDES

P. R. Heck[1,2], J. Greer[1,2], L. Kööp[1,2], R. Trappitsch[3], F. Gyngard[4], H. Busemann[5], C. Maden[5], J. N. Ávila[6], A. M. Davis[1,2], R. Wieler[5]. [1]Robert A. Pritzker Center for Meteoritics and Polar Studies, The Field Museum of Natural History, 1400 S Lake Shore Dr, Chicago, IL 60605, USA, [2]Chicago Center for Cosmochemistry and Department of the Geophysical Sciences, The University of Chicago, Chicago, IL 60637, USA, [3]Nuclear and Chemical Sciences Division, Lawrence Livermore National Laboratory, Livermore, CA, USA, [4]Center for NanoImaging, Harvard Medical School, Cambridge, MA, [5]Institute of Geochemistry and Petrology, ETH Zurich, Zurich, Switzerland, [6]Research School of Earth Sciences, The Australian National University, Canberra, ACT 2601, Australia.

Introduction: Presolar grains are the oldest solid samples accessible to laboratory-based analysis. They are identified by their large isotopic anomalies that match the isotopic compositions of their stellar sources [1]. Presolar grains are preserved in minimally altered solar system materials and have been found in unequilibrated meteorites and micrometeorites, interplanetary dust particles (IDPs) and comet dust [1]. Presolar grain compositions contain valuable information on their stellar sources but also preserve a record of their exposure to galactic cosmic rays (GCR) in the interstellar medium (ISM) [2,3]. Cosmogenic nuclide concentrations in single grains can be determined with mass spectrometric methods [2,3]. Together with the knowledge of cosmogenic nuclide production rates and a correction for nuclear recoil loss [4], a presolar cosmic-ray exposure (CRE) age can be determined [2,3]. Our most recent work on cosmogenic He and Ne in large presolar SiC grains extracted from the Murchison CM2 chondrite revealed ^{3}He and ^{21}Ne ages (T_3, T_{21}) ranging from 3.9±1.6 Ma to 3±2 Ga before the grains were shielded from GCR in the forming solar system [5]. The majority of the grains have presolar CRE ages <300 Ma while a minority has CRE ages >1 Ga. Nuclear recoil loss varies with grain size, primary cosmic ray nuclide and target cross sections, among other parameters [4]. Here, we utilize the large difference in nuclear recoil loss of cosmogenic ^{3}He and ^{21}Ne to estimate the original size of the irradiated presolar objects in the ISM.

Samples & Methods: We analyzed 27 presolar SiC grains from the "LS+LU" extraction from Murchison [6]. In addition to the new grain data we also include data from 22 grains from our previous work [3]. Grains were imaged with SEM/EDS (geometric mean diameters: 2 µm to 34 µm; average: 8.2 µm), classified with NanoSIMS (44 mainstream SiC; 3 AB type SiC) and analyzed for He and Ne isotopes with ultra-high sensitivity noble gas mass spectrometry [3,5]. For the purposes of this study we assume that no significant amount of He and Ne was lost from the grains prior to mass spectrometry. If there was gas loss, the determined exposure ages would be lower limits, and the T_3 would be more affected and lower than the T_{21}. We identified three major Ne components with distinct isotopic compositions: cosmogenic Ne, nucleosynthetic Ne, and terrestrial Ne (air). Nucleosynthetic and atmospheric ^{3}He are negligible and the cosmogenic ^{3}He component dominates the measured amounts in presolar SiC [3]. Cosmogenic ^{3}He and ^{21}Ne from the combined data set were processed with improved recoil corrections and interstellar production rates from [4].

Results & Discussion: Our combined dataset of 27 newly analyzed grains and 22 previously published grains [3] yielded 18 grains which showed clearly resolvable presolar cosmogenic ^{3}He *and* ^{21}Ne from the same grain. 16 of these grains had nominal recoil-corrected $T_3 > T_{21}$. We explain this as an overcorrection of the recoil loss that occurred because the sizes of the analyzed grains were smaller than the sizes of the irradiated objects in the ISM. This indicates that these 16 grains were either larger, or parts of larger grain aggregates in the ISM. We determined cosmogenic ^{3}He and ^{21}Ne recoil corrections by increasing the nominal grain diameters in the model until the recoil-corrected T_3 and T_{21} matched. These grain diameters correspond to the estimated original sizes of the irradiated objects in the ISM. Our estimated original object sizes in the ISM are between 15 µm and 200 µm, factors of ~3× up to ~30× higher than the sizes of the analyzed grains. 75% of these 16 grains had euhedral shapes, which indicates they were not fragments of larger grains but rather aggregated to form larger objects. Aggregates of suspected presolar minerals in an organic material matrix were recently observed in IDPs [7]. Organic coatings were observed on ~60% of presolar SiC that were physically separated from their host meteorite without the use of chemical reagents [8]. Our grains did not show or retain any coatings as the outermost surface layers were removed during the chemical separation procedure. The finding of this study, that grains were likely large aggregates in the ISM, will help to improve models of dust condensation in outflows of the parent stars of the presolar SiC grains.

References: [1] Nittler L. R. and Ciesla F. (2016) *Annual Review of Astronomy and Astrophysics* 54:53–93. [2] Gyngard F. et al. (2009) *The Astrophysical Journal* 700:359–366. [3] Heck P. R. et al. (2009) *The Astrophysical Journal* 698:1158–1164. [4] Trappitsch R. and Leya I. (2016) *The Astrophys Journal* 823:#12 (11 pp). [5] Heck P. R. et al. (2019) *in review.* [6] Amari S. et al. (1994) *Geochimica et Cosmochimica Acta* 58:459–470. [7] Ishii H. A. et al. (2018) *Proceedings of the National Acadamey of Sciences* 115:6608–6613. [8] Bernatowicz T. J. et al. (2003) *Geochimica et Cosmochimica Acta* 67:4679–4691.

ADVANCES IN COLD CURATION: DEALING WITH DUST.

C. D. K. Herd,[1] L. Tunney,[1] and R. W. Hilts[2], [1]Department of Earth and Atmospheric Sciences, 1-26 Earth Sciences Building, Edmonton, Alberta, Canada, T6G 2E3, herd@ualberta.ca, [2]Department of Physical Sciences, MacEwan University, Edmonton, Alberta T5J 4S2, Canada.

Introduction: Modern astromaterials curation routinely involves the use of controlled environment and glove box technology in order to isolate samples from the conditions at the Earth's surface. The advantages of curation of astromaterials under cold conditions are increasingly being realized: curation and handling at temperatures well below standard room temperature, but warm enough to ensure user comfort and safety (i.e., -10 to -20 °C) enables – among other things – the retention of intrinsic volatiles, the inhibition of microbial activity, and the reduction in reaction rates of oxidation and hydrolysis of intrinsic organic compounds and minerals [1]. The Subzero Facility for the Curation of Astromaterials [1] provides a facility in which to develop and test cold curation methods that are potentially applicable to a wide range of astromaterials, such as freshly fallen meteorites (including the Hamburg meteorite, [2]), and those from sample return missions. Here we report on a study of best methods for mitigation of dust during processing of the Tagish Lake meteorite within the Subzero Facility.

The Tagish Lake Dust Problem: The Tagish Lake C2 ungrouped chondrite is exceptionally friable and porous; subsampling has routinely been carried out within the Ar glove box at -10 °C using sterile scalpels rinsed in ultrapure water prior to use [e.g., 3]. Processing of larger specimens in recent years has been accomplished using a guillotine cutter (HSE Harvard Apparatus). The friable nature of the meteorite results in a significant amount of dust and small fragments generated during subsampling, especially using the guillotine. This material represents a loss of sample, either because it cannot be readily recovered, or because what is recovered has come into contact with the interior of the glove box and is therefore contaminated. Furthermore, the dust represents a potential source of cross-contamination between Tagish Lake lithologies [4] or between different samples processed within the glove box.

Methods: All materials used in this study were carefully cleaned with ultrapure water and/or dichloromethane (DCM) prior to use within the glove box. HPLC-grade DCM was used as a solvent for potential organic contaminants, via soaking of cotton-tipped swabs, for most materials; ultrapure methanol was used for testing of the keyboard vacuum due to the solubility of the plastic in DCM. Two mL of either DCM or methanol were added to the swab tips and analyzed by GC-MS at MacEwan University following the methods of [3].

Guillotine Enclosure. In order to mitigate the spreading of dust and small fragments during guillotine cutting, we constructed an enclosure for the guillotine cutter using 0.8 mm thick Teflon sheets mounted using zip ties to an aluminum wire frame (Figure 1a). The enclosure is just large enough to enable the use of the guillotine, which was tested on a specimen of the Tagish Lake meteorite (Fig. 1b) inside the glove box under Ar at -10 °C. A Teflon sheet was used as a base beneath the guillotine and enclosure in order to facilitate collection of material.

Mini Portable Vacuum Cleaner. We used a handheld (e.g., keyboard) vacuum cleaner to test the collection of dust generated by cutting of the same Tagish Lake specimen (Fig. 1c). The advantage of the vacuum is that has a relatively simple design, and is powered by a Li-ion battery. The cloth dust filter was replaced by Kimwipe cut to fit.
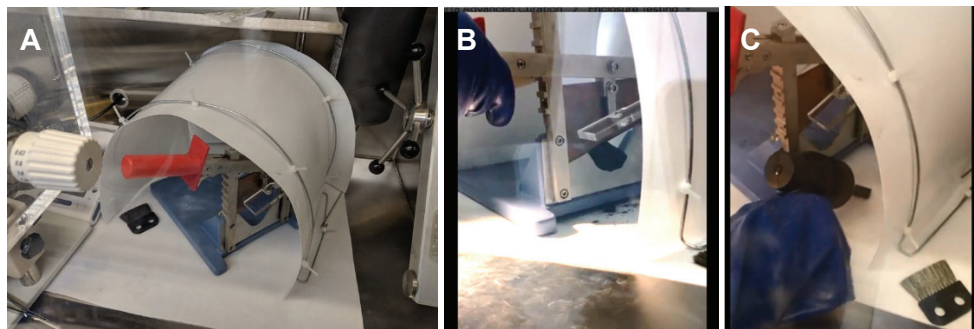
Figure 1. Photos of the guillotine enclosure and vacuum in use with Tagish Lake (UAb specimen MET11611/P-10a)

Results and Conclusions: The combination of guillotine enclosure and handheld vacuum enabled the collection of most of the dust and small fragments generated during cutting of the Tagish Lake specimen (a total of 0.17 g) with the exception of a small amount of dust adhered to the Teflon base which could not be recovered, and dust trapped within the filter of the vacuum. None of the materials were found to have detectable organic contaminants.

References:: [1] Herd C.D.K. et al. (2016) *Meteoritics & Planetary Science* 51:499-519. [2] Fries M.D. et al. (2019) *This Meeting*. [3] Hilts R.W. et al. (2014) *Meteoritics & Planetary Science* 49:526-549. [4] Herd C.D.K. et al. (2011) *Science* 332:1304-1307.

NORTHWEST AFRICA 12563 CM2-AN, AND THE DIFFERENT ALTERATION STYLES IN C2 CHONDRITES.

R. H. Hewins[1,2], P.-M. Zanetta[3], B. Zanda[1], C. Le Guillou[3], J. Gattacceca[4], C. Sognzoni[4], S. Pont[1], L. Piani[5], T. Rigaudier[5], H. Leroux[3], S. Bernard[1], D. Deldicque[6], Y. Marrocchi[5].

[1]IMPMC, Sorbonne Univ., MNHN, UPMC Paris 06, UMR CNRS 7590, 75005 Paris, France. [2]EPS, Rutgers Univ., Piscataway, NJ 08854, USA. [3]Univ. Lille, CNRS, UMR 8207 - UMET, 59000 Lille, France. [4]CNRS/Aix-Marseille Univ., IRD, Coll France, INRA, CEREGE, Aix-en-Provence, France. [5]Univ. Lorraine and CNRS, CRPG, UMR 7358, Vandoeuvre les Nancy, 54501, France. [6]Labo. de Géologie, Ecole Normale Supérieure, 75231 Paris, France.

Characteristics of chondrite: Northwest Africa 12563 (NWA 12563) contains 14% chondrules and 86% matrix, consistent with a CM2 chondrite, but has abundant magnetite framboids and lacks TCI in the matrix. The magnetic susceptibility ($\log\chi = 4.67$) and oxygen isotope data ($\delta^{18}O=12.61‰$ and $\delta^{17}O=5.26‰$) are close to the values for Bells and Essebi C2-ung, and higher than those of most CM2 chondrites [1,2]. The magnetite content of 6.8 wt% is high, as in Bells and Essebi, while the average CM chondrite contains ~1 wt%. It contains 0.72 wt.% H (i.e. 6.5 wt.% H_2O) with $\delta D = -57.5$ ‰, resembling heated CM chondrites [3]; 2.13 wt.% C with a normal CM ‰ $\delta^{13}C$ of -12.2 [4]; and 0.095 wt.% N. The C/H ratio is very high and also resembles that of heated CMs, though we have no evidence of dehydration in NWA 12563. We consider it to be an anomalous CM2 chondrite.

Chondrules: There are Type IA, IABm, and IIA chondrules. Olivine is unaltered but pyroxene shows incipient alteration on cleavage planes. Mesostases are replaced by fibrous to lathy Mg-rich serpentine-saponite and more ferroan chlorite. Chondrule metal ovoids are largely pseudomorphed by serpentine, as in WIS 91600 [5], sometimes with Ni-Cr-bearing P-rich sulfide speckles, and resemble serpentine micro-spherules in CR chondrule rims [6].

Matrix mapping and mineralogy: We quantified the modal abundance and bulk matrix composition using the ACADEMY method [7] (250 nm-sized pixels). The matrix groundmass consists of amorphous silicates and phyllosilicates with embedded sulfides, oxides, anhydrous silicates, carbonates and organic compounds, with ~77% amorphous/phyllosilicate material, and ~23% other discrete phases. TEM shows that abundant amorphous silicate regions with nanosulfides and organics are juxtaposed with well-ordered phyllosilicate areas. Amorphous silicates contain much less Fe than in other chondrites [8,9], and slightly lower Mg than adjacent phyllosilicates, due to the higher magnetite content. In particular areas, well-ordered phyllosilicates of intermediate composition are embedded within amorphous silicates, from which they must be derived. STXM-XANES at the Fe-L edge indicates that the amorphous silicate and phyllosilicate have a high $Fe^{3+}/\sum Fe$ ratio (~70%). Raman spectroscopy and STXM-XANES at the carbon C-edge show that the organic matter resembles that in CM chondrites.

Comparison to other chondrites: NWA 12563 is an unusual meteorite with a high abundance of magnetite. The main matrix alteration assemblage is Mg-rich phyllosilicates and magnetite, which is different from the typical CM association of serpentine, cronstedtite and tochilinite, and suggests different alteration conditions than for other CM chondrites. Though magnetite is associated with heavy alteration, it occurs here with olivine and amorphous silicate in the matrix. Both magnetite and Mg-rich phyllosillicates are stable over wide temperature ranges, and have been suggested to replace cronstedtite and tochilinite at higher temperatures [6,11,12]. Nonetheless, Raman and XANES results indicate that the temperature remained relatively low and comparable to other CM chondrites. A slightly higher alteration temperature for NWA 12563 than for CM2 chondrites would suggest formation in a large asteroid or by impact heating.

[1] proposed a new magnetite-rich chondrite group including Tagish Lake, Adelaide, Bells, Essebi, and Niger (C2). On the other hand, [10] considered Bells and Essebi to be CM/CI transitional types and indeed magnetite abundance and oxygen isotope composition for these three meteorites are intermediate between those of CI and CM chondrites. However, the D/H and C/H ratios of NWA 12563 resemble those heated CM chondrites, although the mineralogy is different. The metal alteration is like that in the TCI-free, magnetite-rich WIS 91600 chondrite [5], while mesostasis alteration is like that of CR chondrules. There seem to be different types of anomalous or ungrouped C2, consistent with the large number of C-complex asteroids [13].

References: [1] Rochette P. et al. (2008) *Meteoritics & Planetary Science* 43:959-980. [2] Rowe M.W. et al. (1994) *Geochimica et Cosmochimica Acta 58:*5341-5347. [3] Alexander C.M.D. et al. (2013) *Geochimica et Cosmochimica Acta 123*:244-260. [4] Pearson V.K. et al. (2006) *Meteoritics & Planetary Science* 41:1899-1918. [5] Brearley A.J., (2004) *LPS XXXV*, Abstract #1358. [6] Weisberg M.K. et al. (1993) *Geochimica et Cosmochimica Acta* 57:1567–1586. [7] Zanetta P.-M. et al. (2019) *Chemical Geology* 514:27–41. [8] Le Guillou C. et al. (2015) *Earth and Planetary Science Letters* 420:162-173. [9] Leroux H. 2015. *Geochimica et Cosmochimica Acta* 170:247-265. [10] Harries D. and Langenhorst F. (2013) *Meteoritics & Planetary Science* 48: 879– 903. [11] Zolotov M. Y. (2014) *Icarus* 228:13–26. [12] Hyman M. et al. (1985) *Journal of Geophysical Research: Solid Earth* 90(S02):C710-C714. [13] Vernazza P. et al. (2017) *The Astronomical Journal* 153:72.

Using the ChondriteDB database to study chondrule – matrix complementarities

D. C. Hezel and M. Harak

University of Cologne, Department of Geology and Mineralogy, Zülpicher Str. 49b, 50674 Köln, Germany,
dominik.hezel@uni-koeln.de

Introduction: Chondrules and matrix are the major components in chondrites (~95 vol%). Their relationship is much debated, with some favouring an origin from a single, common reservoir [e.g., 1-7], while others argue for different reservoirs with subsequent mixing [e.g., 8-10]. A major argument to decide this question are complemenatry element [1-7] or isotope ratios [11,12] between chondrules and matrix, while the bulk chondrite has solar ratios. Here we expand this argument and show that element ratios are not only complementary between chondrules and matrix in various chondrite classes, but that these complementaries are even variable among individual chondrites of the same class. This further supports the complementary argument that chondrules and matrix likely formed from a single, common reservoir.

Method: The ChondriteDB database contains more than 3500 chondrule and matrix data from >160 meteorites and >80 literature sources [13]. We developed an algorithm to automatically search the database for complementary element relationships.

Results: We found a large number of known, but also new complementarities. The know complementarities confirm the reliability of our algorithm. So far unknown compmelentarities were e.g., found for Al/Ti ratios in CM, CR, CV and CO chondrites. Complementaritis in immobile, refractory elements are in particular strong arguments for the formation of chondrules and matrix from the same reservoir.

Discussion: A new, and particularly interesting aspect was found when studying the complementary element ratios of various chondrites of the same chondrite class. This was, however, only possible for very few chondrites and element ratios. Figure 1 displays the Mg/Si ratios of average chondrules (panel a), and average matrix (panel b) in various CV chondrites. Average chondrules in all chondrites have super-chondritic Mg/Si ratios, while average matrices always have sub-chondritic Mg/Si ratios. The Mg/Si ratios of average chondrules and matrix, however, vary across a significant range of ~1.02 to 1.4 for chondrules, and ~0.69 to 0.97 for matrices. There is no correlation between Mg/Si and reduced/oxidised CV type or the petrologic type. Therefore, the various Mg/Si ratios likely represent pre-accretionary nebula signatures. For example, formation conditions of chondrules and matrix might have varied slightly for the various CV chondrites, thereby producing the variable average chondrule and matrix Mg/Si ratios. Regarding complementarity, it is highly implausible that for each CV chondrite chondrules and matrix were always mixed in the required proportions to result in the CI chondritic bulk compositions. The variations of Mg/Si ratios in chondrules and matrix, together with their always complementary relationships therefore support the formation of chondrules and matrix not only in single, but also highly local environments. Mixing chondrules and matrix cannot explain this.
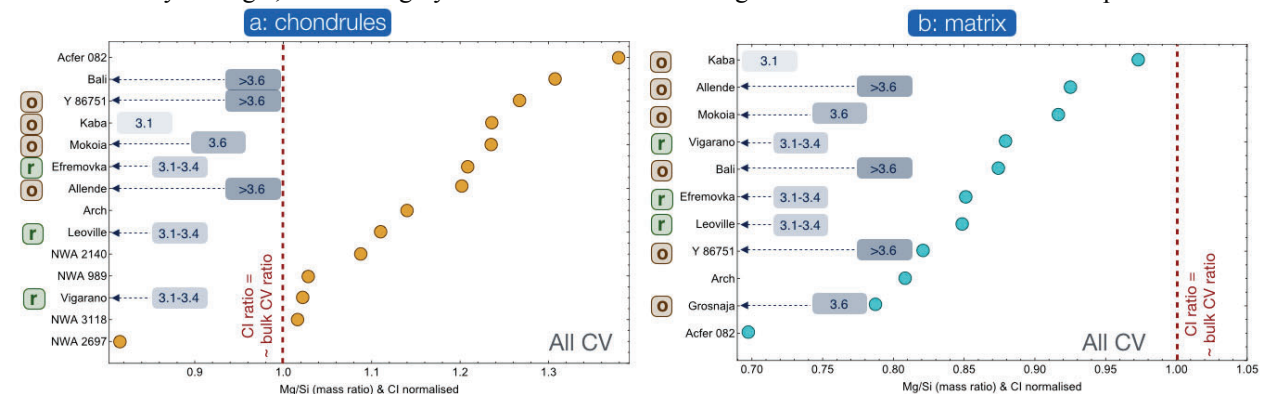
Fig. 1: Mg/Si ratios in average chondrules (a) and matrices (b) from various CV chondrites. o: oxidised; r: reduced; numbers designate the petrologic type of the chondrite (if known).

References: [1] Bland et al. 2005. *PNAS* 102:13755 [2] Hezel and Palme 2010. *EPSL* 294:85 [3] Palme et al., 2014. *CdE* 74:507 [4] Ebel et al. 2016. *GCA* 172:322 [5] Friend et al. 2018. *EPSL* 480:87 [6] Hezel et al., 2018. In: *Chondrules: Records of Protoplanetary Disk Processes*. CUP, pp. 457 [7] Braukmüller et al., 2018. *GCA* 239:17 [8] Zanda et al., 2018. In: *Chondrules: Records of Protoplanetary Disk Processes*. CUP, pp. 457 [9] Olsen et al., 2016. *GCA* 191:118 [10] Alexander 2019 *GCA* in press [11] Becker et al. 2015. *EPSL* 432:472. [12] Budde et al., 2016. *PNAS* 113:2886. [13] Hezel et al., 2018. *CdE* 78:1.

The initial abundance of niobium-92 in the outer solar system.

Y. Hibiya[1,2], T. Iizuka[2] and H. Enomoto[2], [1]JAMSTEC, Japan (hibiyuki@jamstec.go.jp), [2]University of Tokyo.

Introduction: The *p*-process radionuclide niobium-92 (^{92}Nb) decays to zirconium-92 (^{92}Zr) by electron capture with a half-life of 37 Myr. The system is a promising chronometer for addressing the early solar system evolution and planetary differentiation [1, 2]. The initial abundance of ^{92}Nb and its distribution in the early solar system provide valuable constraints on the time-scale of our solar system evolution, and on the origin of *p*-process nuclides. Previously, the initial ^{92}Nb abundance at the solar system formation was determined to be $(^{92}\text{Nb}/^{93}\text{Nb})_0 = (1.7 \pm 0.6) \times 10^{-5}$ by applying the internal isochron approach to the NWA 4590 angrite (U–Pb age: 4557.93 ± 0.36 Ma) [2]. This value is consistent with those obtained from internal Nb-Zr isochrons of eucrites, ordinary chondrites, and mesosiderites [1, 3], indicating that ^{92}Nb was homogeneously distributed among their source regions. Yet, all samples previously studied for ^{92}Nb are thought to have originated from the inner solar system. Here we report internal Nb-Zr isochron dating of the NWA 6704 achondrite that is considered to have originated from the outer solar system.

Sample and Methods: NWA 6704 is a primitive achondrite having a fresh igneous texture [4] with a U–Pb age of 4562.76 ± 0.30 Ma [5]. The mineralogy and petrography indicate that this meteorite underwent melting above liquidus temperature and subsequent rapid cooling ($> 10^{-1}$ °C/yr; [4]), making the effect of differing closure temperatures between the U-Pb and Nb-Zr systems insignificant. Furthermore, this meteorite has Δ^{17}O, ε^{50}Ti, ε^{54}Cr and ε^{84}Sr values similar to those of carbonaceous chondrites [4-6], indicating that it samples the same reservoirs in the solar nebula as the carbonaceous chondrite parent bodies (i.e., the outer solar system). Thus, NWA 6704 enables us to evaluate the distribution of ^{92}Nb between the inner and outer solar system for the first time.

We prepared mineral and whole rock fractions from five fragments of NWA 6704. The Nb/Zr ratios were obtained using a *Thermo Fisher Scientific*$^{\text{TM}}$ *iCAP Q*$^{\text{TM}}$ ICP–MS at the University of Tokyo without chemical separation. Zr was separated and purified from samples using a protocol modified from [2]. The Zr isotopic compositions were measured using a *Thermo Fisher Scientific Neptune Plus* MC-ICP-MS interfaced to a *Cetac Aridus II* desolvating nebulizer at the University of Tokyo.

Results & Discussion: The isochron defines an initial ^{92}Nb/^{93}Nb of $(2.8 \pm 0.3) \times 10^{-5}$ at the time of NWA 6704 formation. By combining this value with the U–Pb age of NWA 6704, an initial ^{92}Nb/^{93}Nb of $(3.0 \pm 0.3) \times 10^{-5}$ at the time of solar system formation is derived. The obtained value is distinctly higher than the initial value in the inner solar system of $(1.7 \pm 0.6) \times 10^{-5}$ [2]. This indicates that ^{92}Nb was heterogeneously distributed in the protoplanetary disk before the formation of NWA 6704, and was relatively enriched in the outer solar system. The difference between these two initial values causes the apparent Nb-Zr age difference of ~30 Myr, demonstrating that the current canonical value of $(^{92}\text{Nb}/^{93}\text{Nb})_0 = (1.7 \pm 0.6) \times 10^{-5}$ should not be used for the Nb–Zr dating of planetary materials from the outer solar system. The newly obtained initial ^{92}Nb/^{93}Nb value is clearly higher than the expected value in the model of ^{92}Nb synthesis by Type Ia supernova (SNIa) [7]. Thus, our results require another production site to be invoked for selectively producing ^{92}Nb. At the moment, only the *v*-process in Type II supernova (SNII) [8] satisfies such requirement. If so, our finding suggests that the time-interval from the last SNII explosion to the formation of our solar system needs be <100 My and that nuclides synthesized by the last SNII were preferentially implanted or preserved in the outer solar system. Such enrichment of the last SNII components in the outer solar system may account for the isotopic dichotomy between carbonaceous and non-carbonaceous meteorites [e.g., 9].
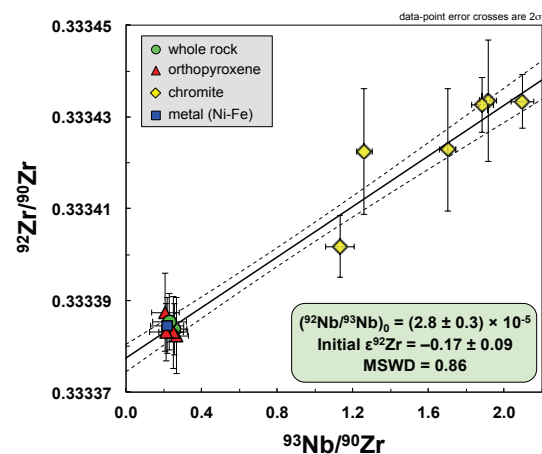
Figure 1. Nb-Zr isochron diagram for NWA 6704.

References: [1] Schönbächler et al. (2002) *Science*, 295: 1705–1708., [2] Iizuka et al. (2016) *Earth and Planetary Science Letters*, 439: 172–181., [3] Haba et al. (2017) *LPS XLVIII*, Abstract #1739. [4] Hibiya et al. (2019) *Geochimica et Cosmochimica Acta*, 245: 597–627., [5] Amelin et al. (2019) *Geochimica et Cosmochimica Acta*, 245: 628–642., [6] Hibiya et al. (2019) *Geostandards and Geoanalytical Research*, 43: 133–145., [7] Lugaro M. et al. (2016) *Proceedings of the National Academy of Sciences*, 113: 907–912., [8] Hayakawa et al. (2013) *The Astrophysical Journal*, 779: 9–13., [9] Warren (2011) *Earth and Planetary Science Letters*, 311: 93–100.

ANALYSIS OF SPACE WEATHERED ITOKAWA GRAINS USING FE-K XANES AND TEM

L. J. Hicks[1], J. C. Bridges[1], T. Noguchi[2], A. Miyake[4], J. D. Piercy[1], and A. Hogan[1], [1]Space Research Centre, University of Leicester, LE1 7RH, UK (ljh47@leicester.ac.uk), [2]Kyushu University, Japan, [4]Kyoto University, Japan.

Introduction: Space weathering is largely the result of the bombardment by electrons and protons from the solar wind upon the exposed surface. Asteroids like S-type 25143 Itokawa show these effects as an apparent darkening and reddening of the affected surfaces [1].

Samples returned by the JAXA Hayabusa mission from the Itokawa asteroid have featured space weathered rims to depths of >100 nm, consisting of a partially amorphised composite rim of the substrate grain mineralogy with nanophase Fe^0 (npFe) particles, and an outer rim of amorphous redeposited vapor material from dust impacts of neighboring minerals [2].

Samples and Methods: Five Itokawa grains from the first touchdown site have been allocated to this study: RB-QD04-0063; RB-QD04-0080; RB-CV-0089; RB-CV-0011; and RB-CV-0148. Each were embedded in epoxy resin and ~100 nm thick FIB-SEM sections were obtained for TEM analyses and X-ray synchrotron nanoprobe analyses. Four of the five Itokawa grains are olivines, one of which (#0063) also features plagioclase inclusions, and the fifth grain is pyroxene (#0089). All of the FIB sections have amorphous space weathering rims measuring up to 100 nm thick, and feature npFe particles (e.g. Figure 1 shows space weathering in #0063).

Figure 1: Bright-Field image of amorphised space weathered rim on RB-QD04-0063, imaged using a JEOL JEM-ARM200F at ePSIC.

Three of the Itokawa grains (#0063, #0080, and #0089) have been analysed using the I-14 X-ray Nanoprobe Beamline at the Diamond Light Source synchrotron. In order to analyse any Fe-redox changes in the space weathered rim from substrate mineralogy, Fe-K XAS spectra are obtained from a series of XRF maps typically measuring between 7000 and 7300 eV, with a higher resolution range of energy increments over the XANES features (~7100-7150 eV).

Results: The Fe-K absorption spectra between the space weathered rim and the substrate mineralogy are compared in Figure 2. The olivine grains #0063 and #0080 typically show a trend of positive shifts of up to ~0.5 eV (±0.25 eV) in the Fe-K absorption edge positions, whereas the pyroxene grain #0089 shows very little to no variation in the weathered rim. The shift is minor, but such positive shifts in the Fe-K absorption edge can be deduced semi-quantitatively as an increase in the oxidation state from ferrous (Fe^{2+}) to ferric (Fe^{3+}), as previously observed in other Itokawa grains, Comet Wild 2 samples, and martian meteorites [2-5]. A positive shift of ~0.5 eV (±0.25 eV) in our results suggests an increased oxidation state ($Fe^{3+}/\Sigma Fe$ >0.11 ±0.05) on the surface rims of the Itokawa olivine grains.

Discussion: Studies of Apollo lunar soils have observed metallic npFe particles [8,9], possibly related to radiation induced segregation of the Fe from the silicates by solar wind and ion implantation. This is also seen in other Itokawa samples [10]. The lunar npFe particles were shown to contain oxidised Fe as Fe^{2+} and even components of Fe^{3+}, with increasing ferrous and ferric contents correlating with increased soil maturity [8].

The increased oxidation state shown by our results is small, but reveals the possible breakdown of the olivine into its amorphous state and the oxidation of the material, including npFe particles. The oxidation may be due to interaction with trace amounts of H_2O molecules by solar wind irradiation. However, the olivine-composed amorphised rim remains the dominant phase shown in our Fe-K XAS measurements.

Further similar studies are being considered for more Itokawa grains and lunar samples to be analysed using the I-14 nanoprobe to directly compare and reveal insights into the redox changes associated with space weathering.

References: [1] Hiroi T. et al. (2006) *Nature*, 443:56-58. [2] Noguchi T. et al. (2014) *Earth, Planets and Space*, 66:124. [3] Hicks L.J. et al. (2017) *Meteorit. Planet. Sci.*, 52:2075-2096. [4] Changela H.G. (2012) *GCA*, 98:282-294. [5] Hicks L.J. et al. (2014) *GCA*, 136:194-210. [8] Thompson M.S. et al. (2016) *Meteorit. Planet. Sci.*, 51:1082-1095. [9] Burgess K.D. and Stroud R.M. (2018) *GCA*, 224:64-79. [10] Noguchi T. et al. (2011) *Science*, 333:1121-1125.
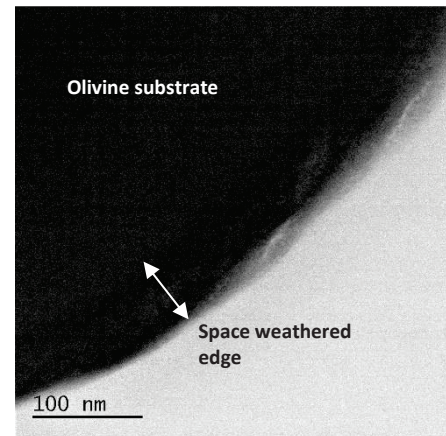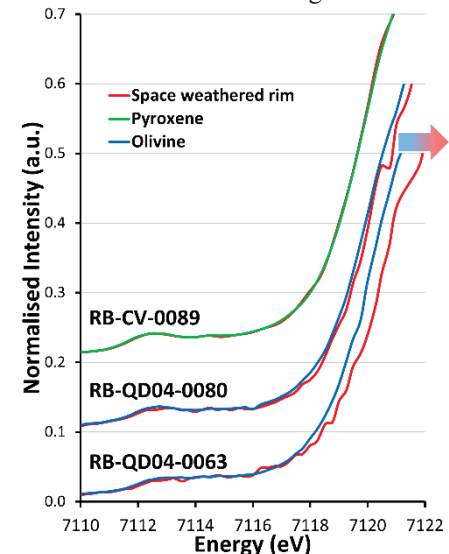

Figure 2: Fe-K XAS spectra of three Itokawa grains, including the substrate minerals olivine and pyroxene and their space weathered rims. RB-QD04-0063 shows a positive shift of ~0.5 eV in the Fe-K absorption edge.

SAMARIUM ISOTOPIC COMPOSITIONS OF LUNAR METEORITES

H. Hidaka[1] , K. Nishiizumi[2], M. Caffee[3], and S. Yoneda[4], [1]Department of Earth and Planetary Sciences, Nagoya University (Furo-cho, Chikusa-ku, Nagoya 464-8601, Japan. E-mail: hidaka@eps.nagoya-u.ac.jp), [2]Space Science Laboratory, University of California, Berkeley (7 Gauss Way, Berkeley, CA 94720-7450, USA. E-mail: kuni@ssl.berkeley.edu), 3Department of Physics and Astronomy, Purdue University (525 Northwestern Ave. West Lafayette, IN 47907-2036, USA. E-mail: mcaffee@purdue.edu), [4]Department of Science and Engineering, National Museum of Nature and Science (Amakubo 4-1-1, Tsukuba 305-0005, Japan. E-mail: s-yoneda@kahaku.go.jp)

Introduction: It is known from the analytical data of long-lived cosmogenic nuclides like ^{10}Be, ^{26}Al, ^{36}Cl, and ^{41}Ca that most lunar meteorites have complicated cosmic-ray exposure (CRE) histories with relatively longer CRE ages than the other stony meteorites, and that their transfer durations from Moon to Earth are quite short [1]. This suggests that most lunar meteorites have long CRE ages in the lunar surface by 2π irradiation and short CRE ages in space by 4π irradiation for the transit from the Moon to the Earth. Besides the cosmogenic nuclides, neutron-captured isotopes like ^{150}Sm and ^{158}Gd produced by cosmic-ray irradiation also provide useful information to discuss the CRE records of extraterrestrial materials [2]. There are many reports on long-lived cosmogenic nuclides of lunar meteorites [e.g., 1,3,4], while there are few on their neutron-captured isotopes [2,5]. In this study, CRE records for seven lunar meteorites were characterized from the systematic data set given by cosmogenic nuclides and neutron-captured isotopic shifts of ^{149}Sm-^{150}Sm.

Samples and Experiments: Seven lunar meteorites, NWA 2996, NWA 3163, NWA 4734, NWA 4932, Dhofar 081, Dhofar 910, and Dhofar 911, whose abundances of several cosmogenic nuclides were already reported [e.g., 3,4], were used to obtain additionally new information on the CRE records from their Sm isotopic data. 30-50 mg of each powdered sample was completely decomposed by mixed acid of HF - HClO$_4$. After then, the residue was redissolved in 1 mL of 1.7 M HCl. The sample solution was divided into two portions: Approximately 90% of the solution was used for conventional two-step of resin chemistry to separate Sm and some other rare earth elements (REE), Gd, Dy, and Er, for their isotopic analyses by a thermal ionization mass spectrometer [6], and the other 10% of the solution was used for the determination of the elemental abundances of REE by an ICP-MS.

Results and Discussion: The burial depths on the Moon, CRE duration, and neutron fluences for the seven samples were estimated from the combination of the data given by cosmogenic nuclides and neutron-captured Sm isotopes. All seven samples show significant ^{149}Sm-^{150}Sm isotopic shifts in the range from ε_{150Sm}=+123.4 for Dhofar 910 to +6.2 for Dhofar 911, which correspond to the neutron fluences from 11.6×10^{16} to 0.6×10^{16} ncm^{-2}. The systematic data set suggest that five of seven samples, NWA 2996, NWA 3163, NWA 4734, Dhofar 081, and Dhofar 910, had resided for 160-740 Ma at the depth levels between 200 and 330 g cm^{-2} in the Moon. On the other hand, the burial depths of NWA 4932 and Dhofar 911 in the Moon estimated from the abundances of the cosmogenic nuclides are more than 1000 g cm^{-2}, which is apparently inconsistent with their Sm isotopic shifts. It is unlikely to produce the significant degree of Sm isotopic shits by neutron capture at the deeper level over 1000 g cm^{-2} in the Moon, considering the depth-dependence of Sm isotopic shifts observed in the lunar regolith drill core [7,8]. It is reasonable to consider the two-stage irradiation model in the Moon to explain the systematic data of NWA 4932 and Dhofar 911. We propose the model that these two meteorites had once resided at shallower depth, preserved the Sm isotopic shifts, and then migrated at the deeper level over 1000 g cm^{-2} before the ejection from the Moon.

References: [1] Nishiizumi K. et al. (1996) *Meteoritics & Planetary Science* 31: 893-896. [2] Hidaka H. et al. (2017) *The Astronomical Journal* 153: 274 (7pp). [3] Nishiizumi K. and Caffee M. (2001) *LPS XXXII*, Abstract #2101. [4] Nishiizumi et al. (2004) *LPS XXXV*, Abstract #1130. [5] Welten et al. (2013) *LPS XXXXIV*, Abstract #2933. [6] Hidaka H. and Yoneda S. (2007) *Geochim. Cosmochim. Acta* 71: 1074-1086. [7] Russ et al. (1972) *Earth Planet. Sci. Lett.* 15: 172-186. [8] Hidaka et al. (2000) *Meteoritics & Planetary Science* 35: 581-589.

IN-SITU CHEMICAL ANALYSES OF WINONAITE METALS: IMPLICATIONS FOR THE ORIGIN OF IAB NON-MAGMATIC IRON METEORITES.

Y. Hidaka[1, 2], M. K. Haba[3, 4], N. Shirai[5], A. Yamaguchi[3] and V. Debaille[1] [1]Laboratoire G-Time, Department of Geoscience, Environment and Society, Université libre de Bruxelles, Bruxelles 1050, Belgium, [2]Department of Earth Sciences, Waseda University, Tokyo, 169-8050 Japan, [3]National Institute of Polar Research, Tokyo, 190-8518 Japan, [4]Department of Earth and Planetary Sciences, Tokyo Institute of Technology, Tokyo, 152-8551 Japan, [5]Department of Chemistry, Tokyo Metropolitan University, Tokyo, 192-0397 Japan.
E-mail: yhidaka@aoni.waseda.jp,

Introduction: Winonaites are primitive achondrites that are defined as the partial melting residues of asteroids and might share the same parent body with IAB irons [1]. IAB irons have several subgroups according to its Au and Ni abundances [2]. However, the relationship among each subgroup and their evolution processes are not well understood [2, 3]. Recently, it was suggested that there were at least 3 or 4 parent bodies for IAB irons on the basis of their Mo isotopic abundances [4]. Since the chemical diversity among winonaite metals is supposed to be the result of early stages of metal partial melting, we will try to understand the chemical evolution of metals in the IAB-winonaite parent body by model calculation of metal partial melting. In this study, we performed *in-situ* chemical analyses of metal grains in winonaites and found genetic relationships between winonaites and IAB irons, and among IAB iron subgroups.

Results & Discussion: We have analysed thick sections of winonaites Y-8005,51-4 and A 10077,51-1 by an laser ablation inductively coupled mass spectrometry (LA-ICP-MS) at National Institute of Polar Research, Tokyo (NIPR). The Ni- and CI-normalized chemical compositions are shown in Fig. 1. Y-8005 metals have nearly chondritic composition. On the other hand, highly siderophile elements, W, Ge and Ga abundances of A 10077 metals are severely depleted ($\sim$0.1 in $(X/Ni)_{CI}$). These results indicate that Y-8005 metals retain chemical compositions of their precursor materials and A 10077 metals are originated from metallic melt. Based on a Ge/Ni-Au/Ni diagram, Y-8005 metal compositions are consistent with those of IAB-sLL (subgroup low-Au, low-Ni) [2], while A 10077 metal compositions are similar to those of IAB-sLM (subgroup low-Au, medium-Ni) [2]. When Y-8005 metals and IAB-sLL metals are considered to be the starting material, the chemical compositional difference between Y-8005 metal (IAB-sLL) and A 10077 metal (IAB-sLM) could be explained by metallic partial melting model calculation [5-7]. In this calculation, A 10077 metal and IAB-sLM are indicated as partial melt liquid, and IAB-MG (main group) is indicated as partial melt residue. However, volatile siderophile element (like Ge and Ga) compositions of A 10077 and IAB-sLM show severe depletion relative to model calculated partial melt liquid. We thus suggest that there was evaporative loss of these volatile siderophile elements at the timing of melting or during cooling of parent metallic liquid. The presence of evaporative loss strongly suggests that a shallow metallic melt pool was the origin of IAB-sLM.
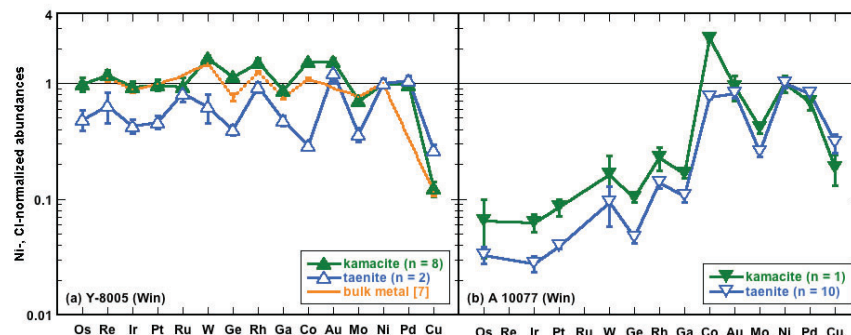
Fig. 1. Ni- and CI-normalized chemical compositions of winonaite metals. Bulk metal data of Y-8005 are from [7]. CI chondrite data used for normalization is from [8]. The order of elements is according to solid-metal/liquid-metal partition coefficients in Fe-Ni-S eutectic composition.

References: [1] Clayton R. N. and Mayeda T. K. (1996) *Geochimica et Cosmochimica Acta* 60:1999-2017. [2] Wasson J. T. and Kallemeyn G. W. (2002) *Geochimica et Cosmochimica Acta* 66:2445-2473. [3] Goldstein J. I. et al. (2009) *Chemie der Erde* 69:293-325. [4] Worsham E. A. et al. (2017) *Earth and Planetary Science Letters* 467:157-166. [5] Chabot N. L. and Jones J. H. (2003) *Meteoritics & Planetary Science* 38:1425-1436. [6] Chabot N. L. et al. (2017) *Meteoritics & Planetary Science* 52:1133-1145. [7] Hidaka Y. et al. (2019) *Meteoritics & Planetary Science* 54:1153-1166. [8] Anders E. and Grevesse N. (1989) *Geochimica et Cosmochimica Acta* 53:197-214.

Heterogeneity of Cometary Dust Particles in the Coma of Comet 67P.

M. Hilchenbach[1], J. Paquette[1], H. Fischer[1], O. Stenzel[1] and S.Merouane[1], [1]Max Planck Institute for Solar System Research, Justus-von-Liebig-Weg 3, 37077 Göttingen, Germany, email: hilchenbach@mps.mpg.de

Introduction: The COmetary Secondary Ion Mass Analyser (COSIMA) instrument on board ESA's Rosetta mission to comet 67P/Churyumov–Gerasimenko has collected and analysed dust particles in the inner coma from August 2014 to September 2016. The instrument has applied the laboratory techniques of optical microscopy and secondary ion mass spectrometry (SIMS) to in-situ measurements of cometary particles collected between 1.25 and 3.8 AU solar distance and 4 to 1000 km off the comet nucleus. The dust particles have been collected at low impact speeds on metal targets and constitute a sample of the dust particles in the inner coma collected during the whole mission. After impact, the larger particles tend to stick together, spread out or consist of single or a group of clumps, and the flocculent morphology of the fragmented particles have been revealed. The elemental composition and the optical reflectance of the dust particles is heterogeneous [1-9]

Methods: Captured dust particles were identified with an optical microscope with 14 um resolution. The footprint of the primary ion beam of the SIMS mass spectrometer was 35x50 μm^2 FWHM , thus much larger than in laboratory SIMS instruments. The instrument temperature is about 10°C, therefore dust particles are analysed without any ices [10]. The advantage is a large integration area and therefore achieving reasonable averaging for the composition measurements. The mass spectra of the time-of-flight reflectron mass spectrometer were calibrated and either summed up for elemental ratios or analysed by statistical methods [11]. The optical images were re-calibrated and the reflectance of the collected dust particles analysed for the illumination by red LED diodes at 645 nm. The fragmentation of the particles on impact as well as due to charging by the primary ion beam was quantified by modeling as well as laboratory experiments with terrestrial analog material [12-14]. Fragments of different meteorites have been analysed with the COSIMA laboratory reference model [15].

Discussion: The elemental composition of the dust particles collected and analysed with SIMS is heterogeneous. and no statistical significant differences beyond the one sigma confidence limit have been identified for the mineral forming elements Mg, Si, Ca and Fe. The composition is close to unequilibrated meteorites such as Tieschitz except for the high carbon content of up to 45% by weight. The fragmentation, either by low speed impact or by the Lorentz forces due to charging shows clumps or elements in the 10 to 40 μm size range which do not seem to break further up unlike laboratory analog material such as SiO_2 beads. Meteorite fragments from Renazzo, Murchison, Allende, Tieschitz, Ochansk do not break up on charging in the COSIMA reference instrument. The reflectance of the dust particles at 645 nm covers a wide range from 3 to 23%. No relation between reflectance and dust particle composition has been identified yet.

References: [1] M. G. G. T.Taylor et al. (2017). *Phil. Trans. R. Soc. A* 375, 20160262. [2] R. Schulz et al. (2015) *Nature* 518, 216. [3] S. Merouane et al. (2016) *Astron. Astrophys.* 596, A87. [4] S. Merouane et al. (2017) *Mon. Not. R. Astron. Soc.* 469, S459. [5] Y. Langevin et al. (2016) *Icarus* 271, 76. [6] Y. Langevin et al. (2017) *Mon. Not. R. Astron. Soc*. 469, S535. [7] N. Fray et al. (2016) *Nature* 538, 72. [8] A. Bardyn et al. (2017) *Mon. Not. R. Astron. Soc.* 469, S712. [9] J. A. Paquette et al. (2016) *Meteorit. Planet. Sci.* 51, 1340. [10] J. Kissel et al., *Space Sci. Rev.* (2007) 128, 823. [11] M. Hilchenbach et al. (2016) Astrophys. J. 816, L32. [12] K. Hornung et al. (2016) *Planet. Space Sci.* (2016) 133, 63 [13] L. E. Ellerbroek et al. (2017) *Mon. Not. R. Astron. Soc.* 469, S204. [14] M. Hilchenbach et al. (2017) *Phil. Trans. R. Soc. A* 375, 20160255. [15] O. J. Stenzel et al. (2017) *Mon. Not. R. Astron. Soc.* 469, S492.

THE AUSTRALASIAN TEKTITE STREWN FIELD (HIGHLY OBLIQUE) SOURCE IMPACT IS IN CHAMPASAK PROVINCE, LAOS.

A. R. Hildebrand[1], [1]Terrext Research Ltd., 3248 Boulton Rd NW, Calgary, AB, Canada T2L 1M3
(abrazosriver@gmail.com).

Introduction: The ~790,000 year-old Australasian tektite strewn field is the largest known on Earth extending across southeastern Asia and Australia to Antarctica (and adjacent ocean basins). The asymmetric strewn field has "butterfly wings" and a downrange lobe (and rays) extending southeastwards suggesting that it formed as a result of a highly oblique impact [1, 2]. Variations in tektite size, form, mineralogy, isotopes, and volatile and major element compositions indicate a source in central Indochina, but no expected large crater (≥30 km diameter) has been found [e.g. 3, 4]. A highly oblique impact (e.g., ~5°) also explains why no large crater has been found as impact energy is strongly partitioned into jetting rather than excavation, yielding a >10 times smaller volume crater [5].

Source Impact Location Constraints: The distribution of the most proximal ejecta type is the best clue to locating a source crater and the Muong Nong (MN) tektites are the most proximal [e.g., 3]. Schnetzler [3] proposed that the MN size distribution and elemental abundance gradients indicated that the source impact was located near the southern Laos-Thailand border area; Hildebrand [2] partly filled in MN collection gaps and the augmented elemental gradient data shows that the source crater occurs in southwestern Laos near the Cambodian and Thai borders.

The Champasak Craters: Two elliptical craters occur just north of the Laos-Cambodian border in the southwestern Annamite Mountains (~600 m relief) of Champasak province: Champasak A (~ 3 by 1.6 km; 14.5094° N; 105.9681° E) and B (~ 1.1 by 0.7 km; 14.4076° N; 105.9923° E). Both craters are breached to the east and particularly Champasak A has been somewhat enlarged by erosion. The two craters cut the regional structural lineaments and exhibit some of the steepest slopes in the area, indicating their relatively young age.

The impacted protolith. The craters formed within a Lower Middle Triassic rhyolitic to dacitic extrusive succession with minor clastic sediments up to 1 km thick [6]; fieldwork broadly confirms the succession mapping. The geographic MN elemental variations [3, 4] likely reflect rhyolitic to dacitic succession variation plus a quartoze sediment component for the northwestern sector of Champasak A. The clast-rich melt rock in Champasak A [2] forms a now-dissected melt sheet with thickness of >50 m remaining near its centre; southwards >100 m of melt remains; the melt rock contains rare clasts of clastic sediments indicating a quartoze sedimentary layer in the protolith. The mean elemental composition of the remaining melt sheet is plotted vs. average australite composition in Fig. 1; the agreement is generally good with deviations reflecting volatile loss, projectile contamination and local variation in protolith composition. For example, while the remaining melt sheet is relatively homogenous for most elements, Ca abundance variation is large N to S reflecting variations in the impacted protolith based upon adjacent wall rock.
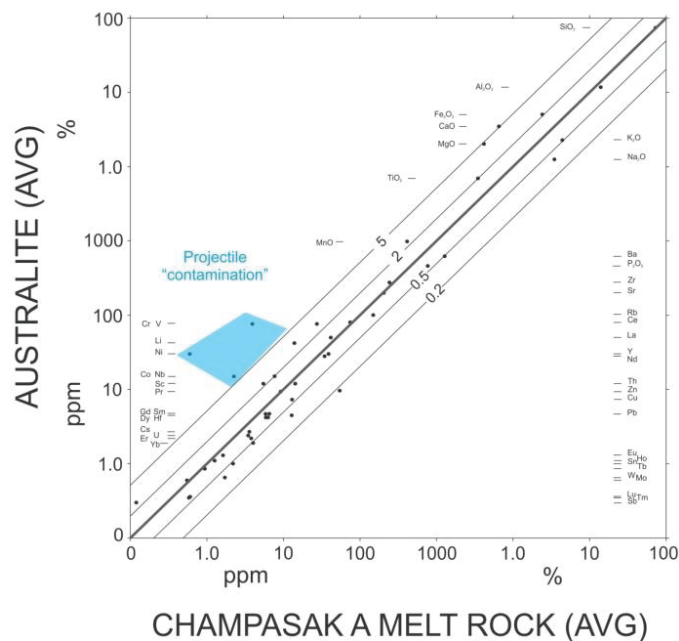
Figure 1: Comparison of average australite composition to average Champasak A melt sheet composition for 46 major, minor and trace elements.

References: [1] Hildebrand, A.R. (1988) *LPS XIX*, 493-494. [2] Hildebrand, A.R. (2019) *LPS V* Abstract #3116. [3] Schnetzler, C.C. (1992) *Meteoritics, 27*, 154-165. [4] Folco, L., et al. (2010) *Earth and Planetary Science Letters 293*, 135-139. [5] Gault, D.E. and Wedekind, J.A. (1978) *Proeedings Lunar Planeary Science Conference 9*, 3843-75. [6] Ha Xuan Binh, et al. (2009) Map of geology and mineral resources south region of Laos. Ministry of Energy and Mines - Geological Department, The PDR of Laos.

INTERACTION BETWEEN ORGANIC MATTER AND MINERALS IN METEORITE PARENT BODIES DURING THERMAL PROCESSES

N. Hirakawa[1*], Y. Kebukawa[1], K. Kobayashi[1] and H. Nakano[2], [1]Graduate School of Engineering Science, Yokohama National University, 79-5 Tokiwadai, Hodogaya-ku, Yokohama 240-8501, Japan. [2]Faculty of Culture and Sport Policy, Toin University of Yokohama, 1614 Kurogane-cho, Aoba-ku, Yokohama 225-8503, Japan. *Email: hirakawa-naoki-bg@ynu.jp

Introduction: Carbonaceous chondrites and some primitive ordinary chondrites contain up to a few wt.% of organic matter. The chemical structures and compositions of organic matter reflect the physical and chemical environments in meteorite parent bodies [1,2]. Minerals could have some effects on molecular structural changes of organic matter during parent body processes. Although the possibility of organic reactions on the surface of some minerals was pointed out [3], experimental studies evaluating effects of minerals were limited [4,5]. In this study, heating experiments of organic matter with/without minerals were conducted. Kebukawa et al. [2] showed that carbonyl groups (C=O) were a good tracer to understand both the degrees of thermal metamorphism and chemical environments in parent bodies. The changes in C=O groups were thus particularly focused on in this study to investigate the effects of minerals on changes in organic matter during thermal processes.

Experiments: Molecular cloud organic material analog (hereinafter referred to as MC), which is a mixture of various organic compounds prepared by the method of Kouchi et al. [6], was heated in an autoclave with/without minerals (olivine and montmorillonite powders). The starting materials were (1) MC 5 g, (2) MC 0.25 g + olivine 0.25 g and (3) MC 0.25 g + montmorillonite 0.25 g. Each sample was put in a Pyrex glass tube without sealing and the tube was placed in the autoclave. The autoclave was purged with $N_2 + H_2$ gas (99 : 1, v/v) for three times at 60 atm to eliminate air. The samples were heated at 200°C, 300°C, or 400°C in the autoclave for 5 hours. The pressures were initially set at the normal pressure and room temperature. The gas pressures were approximately 1-8 atm during heating.

Experimental products were analyzed by using X-ray diffraction (XRD), Fourier transform infrared spectroscopy (FTIR), gas chromatography mass spectrometry (GC/MS) and scanning electron microscope equipped with energy dispersive X-ray spectroscopy (SEM-EDS).

Results and Discussion: The IR absorption spectra of C=O changed significantly, particularly with montmorillonite, with increasing heating temperature. The increases in the intensity ratios of C=O/aromatic C=C of MC + montmorillonite products at 200°C was smaller than that of MC heated products and MC + olivine products (Fig. 1). The intensity ratios of MC + montmorillonite products at 300°C and 400°C were much lower than those of MC heated products and MC + olivine products. The GC/MS results of MC heated products showed the changes of C=O were relevant to long-chain carboxylic acids. The XRD showed that MC was intercalated into the interlayer of montmorillonite. These results indicate that decarboxylation and/or cracking of long-chain carboxylic acids could be promoted by Lewis and Brönsted acid sites of montmorillonite. Al^{3+} and/or Fe^{3+} ions in octahedral sheets of montmorillonite are known to contribute to producing CO_2 [7]. Cracking is known to be catalyzed by Brönsted acid sites [8]. On the other hand, olivine did not show significant effects on decomposition of MC compared with montmorillonite.

Figure 1. Changes in C=O/aromatic C=C peak height ratios with temperature.

Decreases of C=O would result in the decreases of O/C ratios of organic matter in meteorites. Our results further imply that the smaller O/C ratios of insoluble organic matter in heated CM chondrites than those in ordinary chondrites, CO and CV chondrites with similar H/C ratios [1] might be due to co-existing phyllosilicates during the thermal processes.

SEM-EDS analyses indicated the possibility of alteration of the olivine surface to hydrated phase during the heating experiments. The hydration could be triggered by the dehydration of MC. These results suggest that organic matter could have contributed to hydration of minerals in meteorite parent bodies, particularly in dry environments.

References: [1] Alexander C. M. O'D. et al. (2007) *Geochimica et Chosmochimica Acta* 71:4380-4403. [2] Kebukawa Y. et al. (2011) *Geochimica et Chosmochimica Acta* 75:3530-3541. [3] Sephton M. A. (2002) *Natural Product Report* 19:292-311. [4] Kebukawa Y. et al. (2010) *Meteoritics & Planetary Science* 45:99-113. [5] Vinogradoff V. et al. (2017) *LPS, XLVIII*. Abstract #2681. [6] Kouchi A. et al. (2002) *The Astrophysical journal* 566:121-124. [7] Almon W. and Johns W. (1975) In: *Advance of organic geochemistry, 7th International Meeting; 1975*. 157–171. [8] Liu H. et al. (2013) *Applied Clay Science* 80:398-406.
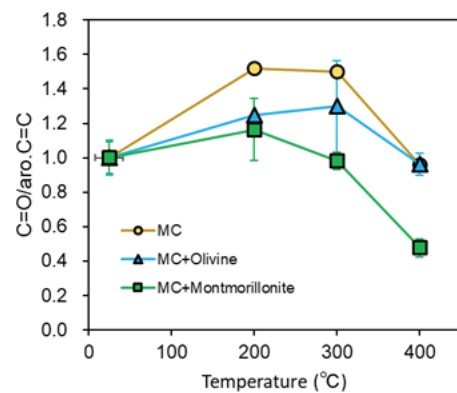
EXCESS BORON 10 OBSERVED IN CHONDRULES FROM Y82094 (C3.2) CHONDRITE.

H. Hiyagon[1], K. Fukuda[2], Y. Tanimura[1], W. Fujiya[3], N. Sugiura[1], T. Kagoshima[4], N. Takahata[4], and Y. Sano[4]. [1]Department of Earth and Planetary Science, The University of Tokyo (7-3-1 Hongo, Bunkyo-ku, Tokyo 113-0033, Japan: hiyagon@eps.s.u-tokyo.ac.jp for HH), [2]WiscSIMS, Department of Geoscience, University of Wisconsin-Madison (Madison, Wisconsin 53706-1692, USA), [3]Faculty of Science, Ibaraki University (2-1-1 Bunkyo, Mito, Ibaraki 310-8512, Japan), [4]Atmosphere and Ocean Research Institute, The University of Tokyo (5-1-5 Kashiwa-noha, Kashiwa-shi, Chiba 277-8564, Japan).

Introduction: Beryllium-10 (^{10}Be), which decays to ^{10}B with a half-life of 1.4 Myr [1], is considered as a key indicator of irradiation processes by solar or galactic cosmic rays (SCR or GCR) in the early solar system (ESS). A number of Be-B isotopic studies have been conducted on coarse-grained CAIs mostly from CV chondrites [2-6], which suggest the presence of live ^{10}Be at the time of CAI formation. The inferred initial ^{10}Be/^{9}Be ratios are mostly in the range of $(0.5-1) \times 10^{-3}$. Recent studies including small CAIs from CH/CB chondrites [7-9] have revealed that the initial ^{10}Be/^{9}Be ratios in CAIs may be much more variable (from ~10^{-4} to ~10^{-2}), strongly suggesting the SCR origin of ^{10}Be in CAIs [9].

Chondrules are thought to be originated from isotopically and spatially different regions from CAI formation regions, because of their ^{16}O-poor *vs* ^{16}O-rich compositions, high *vs* low ambient temperatures, etc. (e.g., [10, 11]). Hence, ^{10}Be in chondrules, if present, would give important constraints for the origin and distribution of ^{10}Be in ESS. Sugiura [12] analyzed anorthite in chondrules from Y82094 (ungrouped C3.2) chondrite [13] and found a possible correlation between ^{10}B excesses and Be/B ratios, but the results were not conclusive due to large errors. In order to better understand the distribution of ^{10}Be in chondrules, we conducted Be-B isotope analyses for chondrules in Y82094 chondrite using NanoSIMS 50 at Atmosphere and Ocean Research Institute, the University of Tokyo.

Samples and Analytical Conditions: Y82094 was originally classified as CO, but now classified as an ungrouped C3.2 chondrite because of its high abundances of chondrules, CAIs and AOAs than other CO chondrites [13]. We so far conducted Be-B isotope analyses for four POP chondrules, Y94-42C2, Y94-42C14, Y94-73A3 and Y94-73A5. We analyzed fine-grained mesostasis and euhedral high-Ca pyroxene grown in mesostasis in these chondrules. Be-B isotopic measurements were performed with NanoSIMS 50. Analytical conditions were essentially the same as those described in [9, 14]. The ^{9}Be/^{11}B relative sensitivity factor was determined from measurements of NIST 610 and 612 glasses [14].

Results and Discussion: In the ^{10}B/^{11}B *vs* ^{9}Be/^{11}B diagrams, the two chondrules, Y94-42C2 and -42C14, show almost equilibrated B isotopic compositions with the slopes (i.e., the inferred initial (^{10}Be/^{9}Be)$_0$ ratios) of ~zero, $(0.6 \pm 1.2) \times 10^{-3}$ and $(0.1 \pm 0.8) \times 10^{-3}$ (2σ errors), respectively, and the elevated initial ^{10}B/^{11}B ratios of 0.257 ± 0.007 and 0.260 ± 0.005 (2σ errors), respectively, compared with the chondritic value (^{10}B/^{11}B = 0.248 [15]). In chondrule Y94-73A5, the data show a clear positive correlation with the inferred (^{10}Be/^{9}Be)$_0$ = $(6.3 \pm 1.7) \times 10^{-3}$ (10 times higher than those for the typical CV CAIs!) and a normal (^{10}B/^{11}B)$_0$ = 0.2459 ± 0.0051. However, the data show a better correlation if plotted in the ^{10}B/^{11}B *vs* $1/^{11}$B diagram, so that the data may be better understood as a mixing line, instead of an isochron: one component is B-rich with a normal B isotopic composition (possibly a surface contamination) and another is B-poor with excess ^{10}B. In chondrule Y94-73A3, only one analysis spot shows a very high ^{10}B/^{11}B ratio of 0.298 ± 0.019, but the other four spots show normal ^{10}B/^{11}B ratios within uncertainties. The results show that B isotope heterogeneity has been well preserved in this chondrule (i.e., little secondary alteration effect on the parent body) and localized existence of excess ^{10}B-carrier within the precursor materials of this chondrule. At least four chondrules so far analyzed in Y82094 show clear excess in ^{10}B. However, there is no clear evidence of live ^{10}Be at the time of the chondrule formation, but it is more likely that excess ^{10}B was introduced into these chondrules by excess ^{10}B-bearing precursor materials (CAI-like materials?). Further Be-B isotope studies for chondrules, esp. those in other types of chondrites, are required to better understand the distribution of ^{10}Be or excess ^{10}B-bearing materials in ESS.

References: [1] Korschinek G. et al. (2010) *Nuclear Instruments & Methods in Physics Research* B268:187-191. [2] McKeegan K. D. et al. (2000) *Science* 289:1334-1337. [3] Sugiura N. et al. (2001) *Meteoritics & Planetary Science* 36, 1397-1408. [4] MacPherson G. J. et al. (2003) *Geochimica et Cosmochimica Acta* 67:3165-3179. [5] Wielandt D. et al. (2012) *The Astrophysical Journal Letters* 748:L25 (7pp). [6] Srinivasan G. and Chaussidon M. (2013) *Earth & Planetary Science Letters* 374, 11-23. [7] Gounelle M. et al. (2013) *The Astrophysical Journal Letters* 763:L33 (5pp). [8] Fukuda K. et al. (2017) *Meteoritics & Planetary Science Suppl.* 52 #6210. [9] Fukuda K. et al. (2019) *The Astrophysical Journal* (revision). [10] Krot A. N. et al. (2009) *Geochimica et Cosmochimica Acta* 73 4963–4997. [11] Alexander C. M. O'D. and Ebel D. S. (2012) *Meteoritics & Planetary Science* 47, 1157–1175. [12] Sugiura N. et al. (2001) *Lunar & Planetary Science* XXXII, Abstract #1277. [13] Kimura M. et al. (2014) *Meteoritics & Planetary Science* 49, 346–357. [14] Fukuda K. et al. (2018) *Geochemical Journal* 52, 255-262. [15] Zhai M. et al. (1996) *Geochimica et Cosmochimica Acta* 60 4877–4881.

MAGNETIC CLASSIFICATION AND SHOCK STAGE (OF PLAGIOCLASE BY RAMAN SPECTROSCOPY) OF THE SARIÇIÇEK METEORITE (HOWARDITE)

V.H. Hoffmann[1,2], K. Wimmer[3], R. Hochleitner[4], M. Kaliwoda[4], I. Uysal[5]. [1]Faculty Geosciences, Dep. Geo- and Environmental Sciences, Univ. Munich, [2]Dep. Geosciences, Univ. Tübingen, Germany; [3]Nördlingen, Germany; [4]Mineralogical State Collection, Munich, Germany; [5]Karadeniz Technical University, Trabzon, Turkey.

Introduction

At September 2, 2015, a large meteorite fall was observed and documented near Sariçiçek in Turkey. Detailed results on the meteorite fall, find and laboratory investigations have been published from a large consortium study [Unsalan et al., MAPS 2019, 1]. The meteorite was shown to be a howardite, a complex breccia which belongs to the HED clan. HED meteorites are believed to originate from the asteroid Vesta, see [1] for all further details.

In extention of our consortium study [1] we have investigated the magnetic signature, focusing on magnetic susceptibility (MagSus) as a fast stony meteorite classification tool. Magnetic susceptibilities were measured on two stones at the Universities of Tuebingen and Munich (#22 and #182). The investigations were done using both SM 30 and SM 100 Magnetic Susceptibility Meters manufactured by ZH Instruments, Czech Republic. The measurements were done at a frequency of 9 kHz. In some cases, two or more fragments of the same stone were measured, in which case the magnetic susceptibility values for the same stone were averaged.

The following magnetic susceptibility values have been found (log X [10^{-9} m^3/kg]):

# 22	3.08
#182	3.36
Mean	3.22

The MagSus values are within the range of 3.06–3.60 for howardites reported by [2] and of 3.11–3.62 reported by [3]. The relatively large range in values may arise from heterogeneity in the parent body of the Sariçiçek meteorite. On the other hand, there is a suggestion that the lower magnetic susceptibility values are associated with samples that are more fully covered with fusion crust. A possible interpretation of this result is that the conversion of iron into iron-oxides in the fusion crust is accompanied by a decrease in magnetic susceptibility.

The shock stage of the Sariçiçek meteorite was investigated by LASER Raman spectroscopy on selected plagioclase grains. Polished thick sections of #182 have been prepared and first observed by optical microscope. LASER Micro Raman Spectroscopy was applied in order to study mineral phase composition and shock stage of the Sariçiçek stones. A Horiba Xplora Integrated confocal LASER micro Raman system was used with a Nd-YAG Laser (532nm) and a low laser power of less than 6mW. Magnifications were between 100 and 1000x (LD) with acquisition times of 5 to 10 sec and accumulation numbers of 2–5. An additional series of Raman experiments were performed on non-prepared specimen, pristine material that excludes any effects of sample preparation/polishing or sputtering (coating). High resolution mappings were performed in order to really detect and identify all present, including accessory, phases and also exolution- /zonation-effects. Varying the LASER energy allows to investigate sub-surface mineral phases.

Shock classification was performed by Raman Spectroscopy on plagioclase grains. The shock distribution was found to be quite inhomogeneous which should be expected in a regolith breccia. Most plagioclase Raman spectra point to quite low shock stages, S 1–2, but also severely shocked feldspar grains have been detected, revealing maskelynite or even recrystallization effects (S 4-5). We also have some indication for the presence of ringwoodite, which would point to a minimum shock of at least 22 GPa.

References:

[1] Unsalan O. and the Sariçiçek consortium, 2019. The Sariçiçek howardite fall in Turkey: Source crater of HED meteorites on Vesta and impact risk of Vestoids. Meteor. Planet. Science, doi: 10.1111/maps.13258.
[2] Macke R. J. et al., 2011. Density, porosity, and magnetic susceptibility of achondritic meteorites. Meteor. Planet. Science 46, 311 – 326.
[3] Gattacceca J. et al. 2008. Magnetic anisotropy of HED and Martian meteorites and implications for the crust of Vesta and Mars. Earth Planet. Sci. Lett. 270, 280 – 289.

WHY IS THE DEGREE OF AQUEOUS ALTERATION VARIABLE?

K. T. Howard[123] and B. Zanda[4] [1]Kingsborough Community College, City University of New York (CUNY). [2]CUNY Graduate Center. [3]American Museum of Natural History. [4]Muséum National d'Histoire Naturelle, Paris, France.

Introduction: Minerals containing water form inside of asteroids during aqueous alteration. We have quantified the range in degrees of aqueous alteration for carbonaceous chondrites from all groups [1]. Here we focus on the CM chondrite Paris and selected CM falls. We aim to answer the question: *why did aqueous alteration inside of the CM parent body asteroid(s) vary?*

Our approach: The fraction of hydrated silicates to anhydrous silicates (PSF) measures the degree of aqueous alteration [1]. The key parameter controlling hydration reactions is water/rock ratio. Water/rock ratios have only been inferred to date, e.g., from O-isotope compositions [2] and O-stoichiometry [1]. Paris preserves large volumes of primary matrix in the form of amorphous Fe-(Mg)-silicate [3], quantifying its abundance allows us to place an upper limit on the fraction of ice accreted in CM matrix. From bulk modal mineralogy and component (chondrule vs. matrix) abundances, we reconstruct the initial H_2O contents of CMs to reveal the cause of variable hydration.

Samples and methods: Using Position Sensitive Detector X-ray Diffraction (PSD-XRD) and pattern fitting [1], we determine the first bulk modal data for Paris. Here we report on the abundances of crystalline anhydrous silicates (olivine+pyroxene), phyllosilicates (cronstedtite+MgFe-serpentine) and X-ray amorphous Fe-(Mg)-silicate. The petrography of Paris has been described and the proportions of chondrules and matrix in the sample are known [3]. Results for Paris are compared to CM fall samples with constrained chondrule/matrix proportions [4]: Murchison, Murray, Mighei, Nogoya and Cold Bokkeveld. Modal data are for 100-200 mg aliquots and are reported in vol.%.

Results: For two aliquots of Paris the silicate mineralogy is comprised of olivine (19-26%), pyroxene (16-19%), phyllosilicate (38-40%) and X-ray amorphous Fe-(Mg)-silicate (9-12%). Paris is the first CM in which PSD-XRD has detected large volumes of amorphous Fe-(Mg)-silicate. Phyllosilicate in Paris is well-crystalline (cronstedtite) and yields sharp peaks in diffraction patterns. Diffuse *hkl* reflections from disordered/extremely fine grained material (MgFe-serpentine), which dominate PSD-XRD patterns of more altered CMs, are largely absent in diffraction patterns for Paris. The PSF for Paris is 0.54-0.56 and ranges from 0.76-0.82 for the other CMs reported here. On 1.0-3.0 classification schemes [1,5], Paris is a petrographic sub-type 2.0 - the least altered CM chondrite so far (on the 2-3 classification scheme of [6], Paris is a 2.9/3.0; despite being ≈ 50% hydrous).

Discussion: Amorphous Fe-(Mg)-silicates are rapidly hydrated and converted to phyllosilicates in reactions with H_2O. Therefore, the determined abundances of amorphous Fe-(Mg)-silicates in Paris should be considered a minimum estimate of the initial abundance. Petrographic studies of Paris indicate that amorphous Fe-(Mg)-silicate is located in matrix and that 47% of the meteorite is matrix [3]. A bulk abundance of 12% amorphous silicate, located entirely in matrix, corresponds to a 25% matrix proportion of amorphous Fe-(Mg)-silicate. This constrains the maximum initial ice/H_2O content in the matrix of Paris to 75%, corresponding to an initial maximum bulk H_2O fraction of 0.35. Using this estimate of the matrix ice fraction in Paris as proxy for matrix in the other studied CMs, we can can reconstruct maximum initial bulk H_2O contents in these samples from their matrix/chondrule proportions [4]. For all samples, calculated maximum bulk initial mass fractions of H_2O range from 0.35 to 0.63 and correlate with the PSF/degree of aqueous alteration [1] and measured H/OH abundances [5]. This indicates that the chondrule/matrix ratio is primary and that the proportion of matrix controls the water/rock ratio and the degree of alteration - the inverse of the original suggestion [7] that matrix abundance is a product of the degree of alteration.

Greater volumes of phyllosilicate formed in samples with greater initial H_2O contents. Extended duration of fluid supply drove recrystallization of phyllosilicates in the most hydrated samples, increasing Mg/Si ratios [7,8] as Fe from phyllosilicate was lost to fluid, forming Fe,Ni-sulfides+FeOH [1]. S (bulk and matrix) and Na/Si (bulk) abundances [9] decrease as the PSF increases, otherwise aqueous alteration appears to have been isochemical. The abundance of cronstedtite in Paris is ~15% lower than a typical CM2 (e.g., Murchison) ≈ the volume of amorphous Fe-(Mg)-silicate that the sample preserves. With an initial bulk mass H_2O fraction of 0.35, fluid in Paris was likely exhausted hydrating amorphous Fe-(Mg)-silicate to form cronstedtite. For CMs with larger initial fractions of H_2O (0.43-0.63), hydration reactions progressed further. As H_2O was consumed, the rock fraction came to dominate reactions, this yielded excess nucleation sites, inhibiting crystal growth (even with higher effective water/rock ratios in matrix, cronstedtite formation is inhibited at H_2O fractions <0.5 [10]). Subsequently, disordered/extremely fine grained phyllosilicates (MgFe-serpentine±saponite) became the dominant late-stage alteration products.

Conclusion: The accreted fraction of matrix can explain variations in the degree of aqueous alteration. Prolonged, large-scale, fluid flow or dynamic transport of chondrules and matrix inside asteroids are not required.

References: [1] Howard K. T. et al. (2015) *GCA* 149: 206-222. [2] Clayton R. N. & Mayeda T. K. (1999) *GCA* 63: 2089-2104. [3] Hewins R. H. et al. (2014). *GCA* 124: 190-222. [4] McSween H. Y. (1979) *GCA* 43: 1761-1770. [5] Alexander C. M. O'D et al. (2013) *GCA* 123: 244-260. [6] Rubin A. E. et al. (2007) *GCA* 71: 2361-2382. [7] McSween H. Y. (1987) *LPS 18*: 631. [8] Browning L. et al. (1996) *GCA* 60: 2621-2633. [9] Zolensky M. E. et al. (1993) *GCA* 57: 3123-3148. [10] Dyl K. et al. (2006) *LPS 37,* Abstract #2060.

U-PB DATING, HYDROGEN AND CHLORINE ISOTOPIC SYSTEMATICS OF THE WHITLOCKITE AND APATITE FROM THE UNGROUPED ACHONDRITE NORTHWEST AFRICA 11119.

S. Hu[1,2], M. Anand[2], I. Franchi[2], X. Zhao[2], Q. H. S. Chan[2], B. Zhang[3], A. Bouvier[4], Y. T. Lin[1], J. C. Zhang[1], J. L. Hao[1], W. Yang[1], Y. Liu[5], G. Q. Tang[5], Q. L. Li[5] and C. Agee[6,7]. [1]Key Laboratory of Earth and Planetary Physics, Institute of Geology and Geophysics, Chinese Academy of Sciences (19 Beituchengxi Road Chaoyang District, Beijing, China, 100029, husen@mail.iggcas.ac.cn), [2]School of Physics Sciences, The Open University, [3]Department of Earth Sciences, University of Western Ontario, [4]Bayerisches Geoinstitut, Universität Bayreuth, [5]State Key Laboratory of Lithospheric Evolution, Institute of Geology and Geophysics, Chinese Academy of Sciences, [6]Institute of Meteoritics, University of New Mexico,[7]Department of Earth and Planetary Sciences, University of New Mexico.

Introduction: Apatite $Ca_5(PO_4)_3(F,Cl,OH)$ and merrillite $Ca_{18}Na_2Mg_2(PO_4)_{14}$ are the two most common phosphates occurring in meteorites [1-3]. Apatite, a hydrous mineral, has been intensively studied in lunar, martian, and HED meteorites to constrain the volatile concentrations of their parent bodies [4-7]. Here we report a potential natural occurrence of whitlockite $Ca_9(Mg,Fe^{2+})(PO_4)_6[PO_3(OH)]$, another hydroxyl bearing phosphate, in the ungrouped achondrite meteorite NWA 11119. In this study, the water content, hydrogen and chlorine isotopic compositions, and U-Pb date of apatite and whitlockite in NWA 11119 were measured to shed light on the nature of the most evolved volcanism in the early Solar System [8].

Sample and Methods: The polished section of NWA 11119 studied by [8] was used for this work. Petrography and mineral compositions were determined using FE-SEM and EPMA, respectively, at the Institute of Geology and Geophysics, Chinese Academy of Sciences (IGGCAS). Raman spectra of apatite, whitlockite, and plagioclase were obtained by Raman spectrometry at the Open University (OU). The water content and hydrogen isotopic compositions of apatite were measured using the NanoSIMS 50L at IGGCAS [9, 10] and that of whitlockite will be measured at OU [11]. Chlorine isotopes of whitlockite and apatite were measured using the NanoSIMS 50L at OU [12, 13]. U-Pb dating of whitlockite and apatite was carried out using IMS 1280 at IGGCAS [14].

Results and Discussions: Two types of phosphate minerals with grain sizes up to ~60 μm were found in NWA 11119. They are usually enclosed by plagioclase or coexisting with ilmenite that is interstitial to pyroxene and plagioclase. EPMA analysis shows that one phosphate in NWA 11119 is pure fluorapatite with very low Cl contents (<150 ppm). The other phosphate has varied Cl contents, ranging up to 0.21 wt. %, significantly higher than that of apatite. This Cl-bearing phosphate appears to be consistent with whitlockite supported by the Raman spectra having one major characteristic peak at 970 cm^{-1} as well as a broad peak in the range of 2000-4000 cm^{-1} and minor peaks at 154, 406, 436, 547, 605 and 742 cm^{-1}. U-Pb dating of phosphates defines an upper intercept date of 4516 ± 7 Ma, much younger than the Al-Mg date of 4564.8 ± 0.3 Ma [8]. The U-Pb age of the phosphates from NWA 11119 suggest a slow cooling or late thermal event, possibly caused by impact. This age is remarkably similar to the proposed timing for the Moon-forming giant impact [15]. The Cl, F, and $\delta^{37}Cl$ of whitlockite are 287 to 3100 ppm, 39 to 880 ppm, and -1.0 to 16.8 ‰, respectively. Apatite in NWA 11119 has 3.9 wt% F, 122 ppm Cl, and $\delta^{37}Cl=11.1\pm1.8$ (2σ) ‰. The water content of apatite from NWA 11119 is comparable to the H background of the instrument, and has a terrestrial-like hydrogen isotopic composition. Analyses of water content and hydrogen isotopes of whitlockite are planned. The presence of both fluorapatite and whitlockite as observed here in NWA 11119 has not been reported previously in other groups of meteorites. The presence of whitlockite component in merrillite has been used as an indication of a low-T hydrothermal activity [3]. However, apatite and whitlockite from NWA 11119 have igneous textures without any obvious evidence for shock metamorphism (supported by the absence of maskelynite), aqueous alteration, and terrestrial alteration. Furthermore, the large Cl isotopic variation recorded in whitlockite and apatite from NWA 11119 is significantly larger than that of GRA achondrite [7], but comparable to that of lunar and HED meteorites [4, 16], probably induced by metal chloride degassing [16] or mixing between different reservoirs.

References:[1] Hughes J.M. et al. (2008) *American Mineralogist* 93:1300-1305. [2] Jolliff B.L. et al. (2006) *American Mineralogist* 91:1583-1595. [3] McCubbin F.M. et al. (2014) *American Mineralogist* 99:1347-1354. [4] Sarafian A.R. et al. (2017) *Earth and Planetary Science Letters* 459:311-319. [5] McCubbin F.M. et al. (2012) *Geology* 40:683-686. [6] Boyce J.W. (2010) *Nature* 466:466-469. [7] Tartèse R. et al. (2019) *Geochimica Et Cosmochimica Acta*. [8] Srinivasan P. et al. (2018) *Nat Commun* 9:3036. [9] Hu S. et al. (2014) *Geochimica Et Cosmochimica Acta* 140:321-333. [10] Hu S. et al. (2015) *J. Anal. At. Spectrom.* 30:967-978. [11] Barnes J.J. et al. (2014) *Earth and Planetary Science Letters* 390:244-252. [12] Tartèse R. et al. (2014) *Meteoritics & Planetary Science* 49:2266-2289. [13] Barnes J.J. et al. (2016) *Earth and Planetary Science Letters* 447:84-94. [14] Li Q.-L. et al. (2012) *Gondwana Research* 21:745-756. [15] Barboni M. et al. (2017) *Science Advances* 3:e1602365. [16] Sharp Z.D. et al. (2010) *Science* 329:1050-1053.

GEOCHEMICAL STUDY OF TYPE 3 ORDINARY CHONDRITES.

G. Hublet[1,2], A. Yamaguchi[2], V. Debaille[1], N. Shirai[3], M. Kimura[2], [1]Laboratoire G-Time, Université Libre de Bruxelles, Brussels, Belgium, [2]Antarctic Meteorite Research Center, National Institute of Polar Research, Tokyo, Japan,

[3]Department of Chemistry, Tokyo Metropolitan University, Tokyo, Japan.
E-mail: ghublet@ulb.ac.be

Introduction: Chondrites are the most primitive objects in the Solar System. The study of those meteorites gives information to constrain the initial compositions, formation and evolution of the earliest objects and planetesimals in the Solar System. One of the most powerful methods used to study chondrites and achondrites is geochronological methods using long and short-lived isotopic systems. A major issue for using the information obtained with these methods is that samples must have remained undisturbed after their initial formation (i.e., in a closed-system). However, in most meteorites, secondary processes like metamorphism disturbed these isotopic systems. To evaluate the impact of such secondary processes on elemental composition, we have conducted a systematic bulk and mineral analyses of minor and trace elements in type 3 to 6 ordinary chondrites (OC). Major element will be also analyzed to obtain at the same time a large and complete elemental composition database for this type of chondrites.

For the first part of this study, we particularly focused on unequilibrated type 3 OC. Seventeen samples in the NIPR Antarctic meteorite collection were selected: seven of them are LL3 (Asuka (A) 9046; Allan Hills (ALH-) 77304; Yamato (Y-) 74660; Y-790448; Y-791558; Y-791835 and A-87319), five L3 (A-881244; A-881683; A-882102; ALH-77260 and Y-793375) and five H3 (A-882073; ALH78084; Y-980053; Y-980135 and Y-983276). The Smithsonian Institute Allende meteorite powder was also analyzed as a control sample.
In this study, we present the results obtained for the bulk composition of REE, Th, U and some trace and minor elements.

Analytical method: REE, minor and trace element measurement were performed on an ICP-MS Element XR at NIPR. An enriched isotope [149]Sm was added before the dissolution of samples to control the sample loss during the chemical preparation. The value of Sm was determined by both isotope dilution and external calibration method. Major element measurement will be also performed on ICP-AES at ULB on a different aliquot.

Results and discussion:

REE, Th and U: all the samples present a flat pattern higher than CI chondrite. The range of this enrichment is larger for the LL3 sample (1.1 to 1.8x to CI). Both L3 and H3 are within the range of LL3 (L3: 1.3 to 1.7x CI; H3 1.2 to 1.6x CI). These results are consistent with the values of OC from the previous studies [1,2].

Minor and trace element: all OC analyzed in this study presented an enrichment in minor and trace element compared to CI. These samples have higher Nb/Ta and Zr/Hf ratios compared to those of CI chondrite. These two positive anomalies are more important for the LL3 compared to L3 and H3. Lead is depleted in these types of OC.

Volatile element: We also analyzed some volatile elements (Zn, Cu, Ga, Cs and Pb). Most of them are largely depleted compared to CI. This depletion has almost the same amplitude in the three types of UOC. Among the five elements, Zn and Pb are highly depleted. There are large variation of Cs contents, especially for the LL3 and L3 compared to H3. These results are consistent with previous studies [3-5].

These preliminary results obtained on OC samples from LL3, L3 and H3 show no significant variation for bulk minor and trace elemental composition.

References:
[1] Nakamura N. (1974), *Geochim. Cosmochim. Acta* 38: 757-775, [2] Evensen N. M. et al., (1978) *Geochim. Cosmochim. Acta* 42:1199-1212, [3] Kallemeyn G.W. et al. (1989) *Geochim. Cosmochim. Acta* 53: 2747-2767, [4] Binz C. M. et al. (1976) *Geochim. Cosmochim. Acta* 40: 59-71, [5] Kong P. and Ebihara M. (1996) *Geochim. Cosmochim. Acta* 60: 2667-2680.

<div align="center">

SULFIDE ASSIMILATION AND MINERALIZATION IN ANCIENT (2.4 Ga) SHERGOTTITES.

</div>

M. Humayun[1], S. Yang[1], A. J. Irving[2] and K. Righter[3], [1]Florida State University, Tallahassee, FL 32310, USA (humayun@magnet.fsu.edu); [2]University of Washington, Seattle, WA 98195, USA; [3]NASA Johnson Space Center, Mailcode XI2, 2101 NASA Parkway, Houston, TX 77058, USA.

Introduction: Due to economic importance, and the ease of sampling, orthomagmatic mineralization in terrestrial igneous rocks has been well studied. Baumgartner et al. [1] argued that martian igneous rocks could generate orthomagmatic Ni-Cu ore deposits in similar ways to terrestrial komatiites. For this to occur, a shergottite magma would need to flow over a pre-existing (possibly sedimentary) sulfide-rich formation. The assimilation of sulfur by the magma would result in formation of immiscible Ni-Cu sulfide droplets, and loss of Ni-Cu and platinum group elements to a basal ore deposit. Here, we report the first evidence of potential orthomagmatic mineralization in two ancient, 2.4 Ga, shergottites [2-3] involving a two-step process: formation of sulfide-rich Fe-Zn deposits assimilated by shergottite magmas leading to formation of orthomagmatic Ni-S deposits. These deposits may remain on Mars, but the telltale signs of Fe-Zn enrichment and Ni-Co depletion in the two shergottites speak to their formation conditions. In a related study, Yang et al. [4] reported on unusual Zn enrichments in olivine from NWA 8159 and pyroxenes from both NWA 7635 and NWA 8159. We further argue that the "evolved" character of these shergottites is due to Fe-assimilation rather than from intense fractional crystallization.

Samples and Analytical Metholoy: The ancient shergottites NWA 7635 [2] and NWA 8159 [3] were analyzed for elemental abundances in their plagioclase, pyroxene and olivine mineral grains by laser ablation ICP-MS [4-5]. Plagioclase and pyroxene from QUE 94201 were analyzed to establish magmatic fractionation trends for depleted shergottites.

Results: In this study, we report that Ni and Co abundances in olivines and/or pyroxenes from NWA 8159, NWA 7635 and QUE 94201, three depleted shergottites that share a large range in Mg#, are exceptionally low. For example, in NWA 7635 olivine Ni ranges from 6-12 ppm at an Mg# of ~40, and in NWA 8159 olivine Ni ranges from 12-15 ppm at Mg# ~ 37; pyroxene from NWA 8159 and NWA 7635 has <5 ppm Ni. Both olivine and pyroxene in NWA 7635 and NWA 8159 have Co a factor of two lower than for other shergottites. There are striking enrichments in Zn in olivine (400-700 ppm Zn vs. 200 ppm Zn in depleted shergottites) and pyroxene from NWA 7635 relative to the trends defined by other shergottites [4]. Higher Zn and Pb are also evident in plagioclase grains from NWA 7635 and NWA 8159, but not in plagioclases from other depleted shergottites.

Discussion: The low Mg# of the three depleted shergottites has been previously considered to be the result of intense fractional crystallization of the parental magmas for these shergottites [2-3]. We propose that an encounter of the parental magma(s) of these two shergottites with an Fe-Zn-S ore would result in Fe-contamination driving down the Mg# more than by fractional crystallization alone. Assimilation of S-rich material by the magmas would result in sulfide saturation, followed by extreme Ni, Co and possibly Cu loss to an immiscible sulfide liquid resulting in the extreme depletions of Ni and Co observed.

One key piece of evidence for the lack of extreme fractional crystallization in the ancient shergottites comes from incompatible element abundances plotted vs. Mg#. Fractional crystallization defines a trend of Th, Nb, La, etc., vs. Mg# for depleted shergottites. The abundances of highly incompatible elements in the two ancient shergottites would be expected to plot on the high end of the abundance range as these rocks have the lowest Mg#s, as seen for QUE 94201. Instead, incompatible element abundances are lower in the two ancient shergottites than in any of the other depleted shergottites, except those with Mg# ~65-70. To assess whether this was the result of partial melting of an ultra-depleted source, the incompatible element abundances of the depleted shergottites were compared. The two ancient shergottites exhibit systematically lower incompatible element abundances while having exactly the same relative depletion pattern in all incompatible elements as other depleted shergottites, e.g. QUE 94201. Based on the low incompatible element abundances, the high Zn, low Mg# and low Ni and Co abundances, we conclude that the two ancient shergottites represent residual magma(s) after assimilation of sulfide followed by loss of an immiscible sulfide liquid. As anticipated by [1], these two shergottites provide the first evidence of sulfide mineralization of potentially economic interest on ancient Mars. This evidence implies the existence of Fe-Zn-S ores formed prior to 2.4 Ga, followed by Ni(±Cu)-S ores formed coevally with the emplacement of the magmas of NWA 8159 and NWA 7635. Further, this finding indicates that at a minimum S, Fe, Zn and Pb isotopic compositions within these meteorites provide clues to surface processes on ancient Mars.

References: [1] Baumgartner R. J. et al. (2015) *Ore Geology Reviews* 65: 400-412. [2] T. Lapen et al. (2017) *Sci. Adv. 3,* e1600922. [3] C. Herd et al. (2017) *GCA 218:* 1-26. [4] S. Yang et al. (2019) *LPSC* 50, abstract # 1908. [5] Yang S. et al. (2018) *Geochem. Geophys. Geosyst.* 19, (https://doi.org/10.1029/2018GC007593).

INTERPRETING THE ISOTOPIC DICHOTOMY AMONG SOLAR SYSTEM MATERIALS.

G. R. Huss[1], [1]Hawaiʻi Institute of Geophysics and Planetology, University of Hawaiʻi at Mānoa, 1680 East-West Road, Honolulu, HI 96822. ghuss@higp.hawaii.edu.

Introduction: In recent years, an extensive database has been produced that separates meteorites into two groups based on their isotopic systematics [e.g., 1-5; Fig. 1]. Various models have been proposed to explain this dichotomy [e.g., 2-6]. A dominant theme in these models is the need for rapid Jupiter formation, separating the region where carbonaceous chondrites and associated iron meteorites formed from that where other chondrites and iron meteorites and the terrestrial planets formed. This separation is often accompanied by a postulated evolution of the dust accreting to the solar nebula as the chondrites are forming, generating different reservoirs. The data set that drives these models is robust and requires explanation. But models involving Jupiter and time-dependent isotopic nebular evolution have serious problems and are distracting from approaches that are more likely to explain the dichotomy.
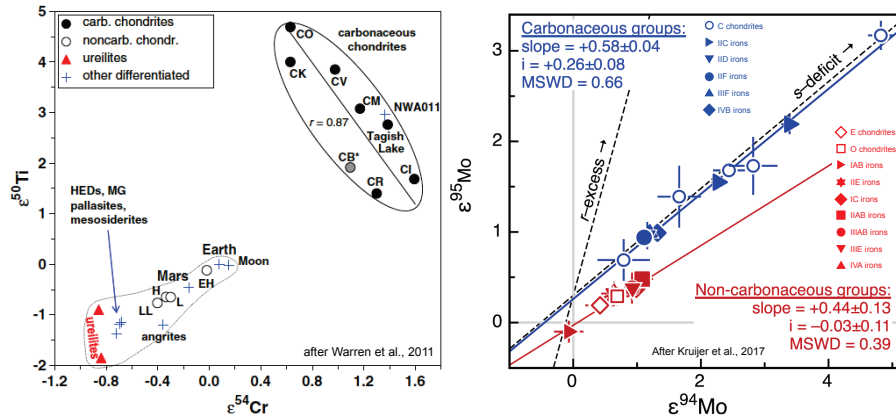

Figure 1: Some of the data that drives the inference that there are two different groups of chondritic and associated differentiated meteorites. The same groupings appear in O, Ca, Ni, and W data.

Problems with current models: The idea that carbonaceous chondrites accreted in the outer solar system has several serious problems. For example, carbonaceous chondrites include meteorites that are chemically unfractionated (CI), and meteorites that have experienced the most extreme thermal processing among chondrites (CV, CO). CV, CO, and CM chondrites, contain the highest abundances of CAIs, materials that reflect the highest-temperature processing of chondritic materials. Why should the most extreme thermal processing have been in the outer solar system, and where is the environment outside of Jupiter that can drive such variable and extreme thermal processing? Second, the formation times of most chondrite classes are both early and overlapping, starting as early as 1 my after CAIs and ending at the latest by 3-4 my after CAIs. Some iron meteorite parent bodies apparently accreted before that. Early accretion within distinct isotopic reservoirs would, in this model, require Jupiter to have open a gap in the disk very early (<<1 my after CAIs). Time-dependent isotopic variation of accreting material is also problematic. The processes that generate molecular clouds work to mix and spatially homogenize the raw materials for the solar system, and the presolar grains complexes that were accreted by ordinary and carbonaceous chondrites appear to have been the same [7,8]. Other major problems can also be enumerated.

A better interpretive framework: There is no requirement that the isotopic dichotomy reflect accretion in widely separated regions of the disk. What is necessary is that each package of material underwent a specific set of processes and then accreted to form an asteroid. The dust that made up the Sun's parent molecular cloud consisted of stellar condensates from a wide variety of stars and dust that formed in the interstellar medium after their precursors were evaporated by supernova shocks. The behavior of an element during solar system processing depends of the mineralogy of the carriers, and only very generally on its equilibrium condensation temperature. There is no reason to expect that any single source will dominate the budget of an element, or that any mineral phase will be dominated by a single nucleosynthetic source. It is not valid to infer that because a refractory element and a volatile element show the isotopic dichotomy, nebular processing could not have generated the two components. A first-order observation is that carbonaceous chondrites experienced primarily volatility-based fractionation in the nebula, while ordinary and enstatite chondrites and related objects experienced volatility-based fractionation, variable oxygen fugacity, and metal-silicate fractionation. Why should these processing histories not produce different outcomes?

References: [1] Warren P.H. (2011) *Earth and Planetary Science Letters* 311, 93-100. [2] Kruijer T.S. et al. (2017) *Proceeding of the National Academy of Sciences of the United States of America* 114, 6712-6716. [3] Nanne J.A.M. et al. (2019) *Earth and Planetary Science Letters* 511, 44-54. [4] Scott E.R.D. et al. (2018) *Astrophysical Journal* 854, 164. [5] Budde G. et al. (2016) *Earth and Planetary Science Letters* 454, 293-303. [6] Schiller M. et al. (2018) *Nature* 555, 507-510. [7] Huss G.R. and Lewis R.S. (1995) *Geochimica et Cosmochimica Acta* 59, 115-160. [8] Huss G.R. et al. (2003) *Geochimica et Cosmochimica Acta* 67, 4823-4848. Supported by NASA 80NSSC18K0586.

INVESTIGATING DUST SIZE AND PRESOLAR GRAIN DISTRIBUTION IN THE PROTOPLANETARY DISKS USING SPH SIMULATIONS.

M. Hutchison[1,2], J.-D. Bodénan[2,3], L. Mayer[2], M. Schönbächler[3]. [1]Center for Space and Habitability, Gesellschaftstrasse 6, 3012 Bern, Switzerland, [2]Institute for Computational Science, Winterthurerstrasse 190, 8057 Zürich, Switzerland, [3]ETH Zürich, Inst. für Geochemie und Petrologie, Claussisusstrasse 25, 8092 Zürich, Switzerland. (jean-david.bodenan@erdw.ethz.ch).

Introduction: Various isotopic systems studied in meteorites exhibit nucleosynthetic heterogeneity in solar system material. Some of them display a dichotomy between objects formed in the inner solar system (ordinary (OC) and enstatite (EC) chondrite signatures) and those formed further out (carbonaceous chondrites (CC)) [e.g., 1,2]. These heterogeneities stem from presolar grains generated in different stellar environments before they were delivered to our solar system. However, how these presolar grains were originally distributed in the solar system, and how they were subsequently transported or concentrated, and processed in different locations, remains unclear. It has been suggested that the formation of Jupiter's core may explain the observed separation of the two reservoirs defined by the OC+EC and CC chondrites – being located inside and outside of Jupiter's orbit, respectively [e.g., 2]. Large planets carve a gap in the disc, depleting the surrounding orbital region of both gas and dust. The resulting pressure maxima that form on either side of the gap act like dust traps and prevent most of the solid material from being transported between the inner and outer disc. While it is difficult to trace the isotopic abundances themselves, hydrodynamical simulations can track the dynamical evolution of the presolar grains in which they are incapsulated. We use smoothed particle hydrodynamics (SPH) simulations to assess, whether we can replicate the isotopic anomalies observed in the solar system via the interaction between the dust grains and the background gas disk alone when they are (initially) distributed homogeneously through the disk relative to the silicate grains.

Methods: We use the SPH code PHANTOM [4] to perform 3D gas and dust simulations of protoplanetary discs to study how the back-reaction of pebble-sized grains (~mm) affects the (sub-)micron grain population when a Jupiter-mass planet carves a gap in the disc at different radii. We use the MULTIGRAIN algorithm [5] to simultaneously simulate a total of 17 dust phases comprised of ten `silicate' phases (size: 0.1 microns -- 1 cm; density: 3 g/cm^3), four `silicon-carbide' phases (size: 0.25 -- 4.225 microns; density: 3.16 g/cm^3), and three `oxide' phases (size: 0.1 -- 0.6 microns; density: 3.93 g/cm^3). We determine the abundances of the silicate grains with a standard power-law grain-size distribution of slope -3.5 (e.g. [6]). The abundances for the silicate-carbide and oxide phases come from generalised extreme value distributions that fit the catalogued abundances from meteoritic studies [7]. Finally, we attribute different anomalous isotopic tracers to the oxides (r-process elements, e.g., ^{54}Cr) and silicon-carbide (s-process elements, e.g., Zr, Mo, Ru, Pd) populations to assess whether variations in intrinsic grain density, grain-size distribution, and/or back-reaction from larger grains in the disc can drive differences in the local concentration of presolar grains and their tracers.

Discussions: Preliminary analysis of single-grain and multi-grain simulations show some visible differences between a few of the larger silicate phases (particularly near the disc/gap edges), but little changes in our presolar grain populations. This suggests that back-reaction and/or variations in the grain-size distribution and intrinsic grain density cannot be the main driver for the sorting of presolar grains in the protoplanetary disk. The pressure maximum just outside of the planet's orbit trap dust grains of all sizes, but with varying levels of concentration. Large grains migrate efficiently towards the middle of the pressure bump, while small grains, more affected by the motions of the gas, show a much looser clustering near the maximum. A similar phenomenon occurs for the pressure maximum interior to the planet's orbit. However, in contrast to the continual accumulation of migrating dust at the inner edge of the outer disc, the combination of viscous accretion onto the star and limited transport of material across the gap leads to a general attenuation of all grain sizes in the inner disc. Consequences for this observed behaviour are twofold. First, the enhanced density in the pressure bumps outside the planets orbit would make them an ideal formation region for CCs, which display much higher matrix contents and thus presolar grain abundances than their EC and OC counterparts. They would also be advantageous regions to concentrate the larger Calcium, Aluminium-rich Inclusions (CAIs) and chondrules found in CCs, in CV especially. Secondly, the strong density variations in the largest dust grains compared to the finer fractions can create regions with increased presolar grains abundances favourable to create CC with particularly enhanced presolar grain abundances such as CR chondrites [8].

References: [1] Leya I. et al. (2008) *Earth and Planetary Science Letters 266*:233-244 [2] Alibert Y. et al. (2018) *Nature Astronomy 2*:873-877. [3] Price D. J. et al. (2018) *Publications of the Astronomical Society of Australia 35*:82. [4] Hutchison M. A. et al. (2018) *Monthly Notices of the Royal Astronomical Society 476*:2186-2198. [5] Mathis J. S. et al. (1977) *The Astrophysical Journal 217*:425-433. [6] Hynes K. M. and Gyngrad F. (2009) LPSC XL, Abstract #1198. [7] Davidson et al. (2014) *Geochimica et Cosmochimica Acta 139*: 248-266.

ELASTIC PROPERTIES OF THE TAGISH LAKE FALL (C2, UNGROUPED)

M. I. Ibrahim[1], F. Ciceri[1], and A. R. Hildebrand[1], [1]Department of Geoscience, University of Calgary (2500 University Dr NW, Calgary, Alberta, T2L 1N4, Canada)

Introduction: Carbonaceous chondrites (CCs) represent ~ 4% of the total meteorite falls; however, their reputed parent bodies – dark asteroids – represent at least half the Earth-crossing asteroid population [1]. CCs have become increasingly important as the only physical samples that provide some constraints on dark asteroid lithologies; constraints that are needed now to better develop sample return missions from asteroids, such as Bennu and Ryugu [e.g. 2; 3]. Measurements of CCs physical (microporosity) and elastic properties provide the only approximation of how a dark asteroid surface responds to impact processes. Micro- and macroporosities and the elastic properties of asteroids play a major control on energy transfer (and attenuation) during collisions [4]. In this study, we present preliminary measurements of elastic wave velocity of the Tagish Lake meteorite; Ungrouped C2 with affinities to CM-chondrites [5]. The samples studied represent the high inclusion phase of Tagish Lake. These data complement a previous survey that included 49 carbonaceous chondrite falls, of which 12 samples were CM-chondrite falls [6]. Tagish Lake represents the highest measured microporosity and lowest elastic wave velocities among CM-chondrites (see Figure 1).

Methodology: Measurements of the elastic wave velocity were carried out using a manually controlled electric pulse generator/receiver (Olympus Model 5077 PR) with a 35 MHz ultrasonic bandwidth, a 100-MHz-bandwidth Oscilloscope (Tektronix Model DPO2014), a pair of 13-mm-diameter P-wave ultrasonic contact transducers (Olympus V153), and a digital micrometer. Slabs of Tagish Lake were prepared – using a wire saw to minimize material consumption and contamination – for better coupling with the transducers. A vise was used to produce pressure on the transducers, which improved coupling with samples surfaces (and the quality of the signals). The bulk volume necessary for bulk density measurement was measured using a desktop laser scanner (NextEngine Desktop 3D Scanner Model 2020i) [7]. A helium pycnometer (Quantachrome Instruments, Model MVP-D160-E) was used to measure porosity and grain density.

Results and Discussion: Preparing slabs of Tagish Lake reveals a brecciated texture, which will be further examined petrographically. Comparison of the elastic properties of Tagish Lake with a suite CM-chondrite falls suggests that Tagish Lake has the lowest values of bulk density (1.54 ± 0.03 gm/cm^3), porosity (0.45 ± 0.001) and p-wave velocities (1240 ± 10 m/sec). The measured bulk density and porosity values are consistent (within uncertainty) with previous measurements of other samples measured approximately 18 years ago indicating adequate isolation from the terrestrial atmosphere in curation [8]. The low elastic wave velocities measured for Tagish Lake were expected based on bulk density–elastic wave velocity relationships observed in terrestrial rocks and in ordinary and carbonaceous chondrites. The low P-wave velocities for Tagish Lake are also consistent with the high microporosity. Tagish Lake provides the observed lower limits of density and seismic velocities of CM-chondrite-like lithologies, and, by proxy, their parent bodies.
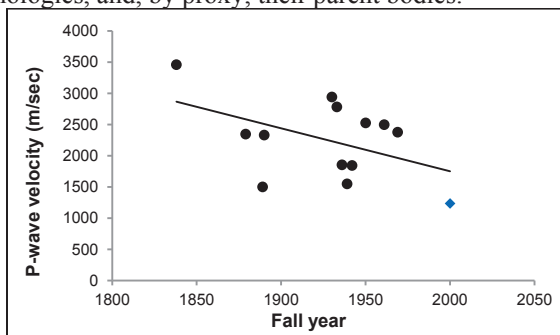

Figure (1): P-wave velocity of CM-chondrites versus Fall Date. Tagish Lake is represented by blue (grey) diamond data point. Note that the downward trend vs. fall date is mostly resulting from the fastest (Cold Bokkeveld, Vp = 3460 m/sec) and the slowest meteorite (Tagish Lake, Vp = 1240 m/sec). Most CM-chondrites range from 1500 to 3000 m/sec.

Implications: Tagish Lake shows the lowest values of seismic wave velocities and elastic moduli among CM-chondrites. Such low velocities result in anomalously low values of bulk (volumetric elasticity) and Young moduli (tensile elasticity). Bulk modulus denotes the tendency of bodies to deform in all directions under uniformly applied pressure, an extension of Young's modulus to three dimensions. In the case of analogous parent bodies, these low values of the elastic moduli may suggest a strong collapse response (along the axis of applied stress) to collisions.

References: [1] Mainzer A. et al. (2011) *ApJ* 731: 53. [2] Lauretta D. S et al. (2019) *Nature 568*: 55–60. [3] Kitazato, K et al. 2019 *Science* 364: 6437: 272–275. [4] Flynn G. J. et al. (2017) *Chem. der Erd.*78- 3: 269-298. [5] Zolensky, M. E, et al (2002) *MAPS* 37:737 – 761. [6] Ibrahim, M. (2012) Unpublished M.Sc. Thesis, University of Calgary. [7] Ghanizadeh A. et al. (2018) BCPG 66; 2: 1–27. [8] Hildebrand A.R. et al. (2006) *MAPS* 41, 3: 407–431.

Mineralogical study of TCIs in CM carbonaceous chondrites and implications to the formation processes.

A.Iemoto[1] , Y.Seto[1] , A. Miyake[2].
[1]Department of Planetology, Kobe University, Rokkodaicho 1-1, Nada, Kobe 657-8501, Japan (e-mail: a.iemoto@stu.kobe-u.ac.jp) [2]Division of Earth and Planetary Sciences, Kyoto University, Japan.

Introduction: TCIs, fine intergrowths of tochilinite ($6(Fe_{0.9}S) \cdot 5[(Mg,Fe)(OH)_2]$) and cronstedtite (Fe-bearing serpentine), are characteristic objects within CM chondrites. TCIs are considered to be aqueous alteration products on the parent bodies, and divided into two types based on the textural feature. Type I TCI is generally found in the chondrules and believed to be altered from iron metal because they often contain kamacite inside [e.g., 1]. On the other hand, type-II exhibit fibrous, fluffy textures found within the matrices. Although several formation processes of type-II have been proposed [e.g., 2,3], the argument has not yet been settled. TCIs potentially provide important information regarding aqueous environments on chondrite parent bodies. Here, we report microtextures of type-II TCIs in five CM chondrites and discuss the formation processes.

Materials and methods: We observed the following five CM chondrites; QUE 97990 (2.6), Murchison (2.5), Murray (2.4-2.5) , Cold Bokkeveld (2.2), Nogoya (2.2). The numbers in parenthesis are the alteration index for CM chondrites proposed by Rubin et al. (2007) [4], in which the index is defined ranging from 2.6 (less altered) to 2.0 (highly altered). Textural observation and chemical analyses were performed using an SEM-EDS (JEOL, JSM-6480LAII), and nanometer-scale observations using an STEM-EDS (JEOL, JEM-2100F) after processing into thin films using an FIB (FEI, Quanta 3DS).

Results and discussion: In the less altered CM chondrites (QUE 97990 and Murchison), the type-II TCIs showed a similar texture. Both are widely distributed in the matrices as aggregates of a few hundred nm-sized tochilinite and cronstedtite (Fig. 1a). From the TEM observations, thin veins of tochilinite were developed inside cracks or cleavages of cronstedtite (Fig. 1b), suggesting that tochilinite had been crystallized after the formation of cronstedtite. In contrast, the TCIs in Cold Bokkeveld (highly altered) showed core-rim structure (Fig. 1c). The core region (upper-left in Fig. 1d) is often rich in mixed layer phase (MLP; alternately stacked phase of tochilinite/cronstedtite layer in nanometer scale), and the rim (lower-right in Fig. 1d) mainly consists of coarse-grained tochilinite and cronstedtite, which resembles those of the less altered meteorites. Another highly altered me-teorite Nogoya (2.2) also has TCIs with zonal texture where very fine (several tens of nm) serpentine rich material is located around core, and toward rim, gradually changed to fibrous cronstedtite and MLP. Murray, intemidiately al-tered CM, has both type of TCIs seen in less and highly altered ones as noted above, indicating Murray was at an intermediate stage during the course of TCIs formation.

All observed type-II TCIs in the present study do not include any precursor minerals such as anhydrous silicates or iron metal. TCIs of the two highly altered CM chondrites (Cold Bokkeveld and Nogoya) showed fluffy texture at their core region. These results probably suggest that (at least fluffy) type-II TCIs were not formed directly from solid material (like type-I), but crystallized under mobile environments such as water solution. In the case, changes of the fluid condition during the TCI formation resulted in the zonal texture as seen in the highly altered meteorites (Fig. 1c). The fact that the TCIs in QUE 97990 and Murchison resembles the coarse-grained rim of those in Cold Bokkeveld indicates the two less altered meteorites had experienced aqueous alteration similar to the last stage of aqueous alteration that Cold Bokkeveld had experienced.
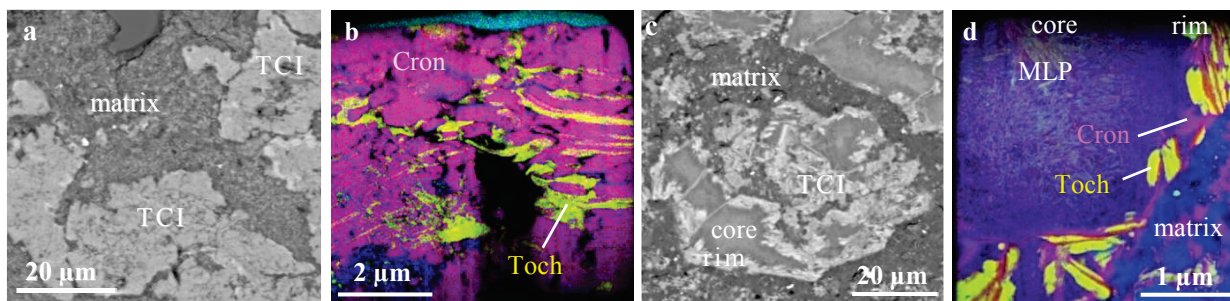
Figure 1: SEM-BEIs and STEM-EDS elemental maps (red:Fe, green:S, blue:Si) of TCIs (tochilinite-crondstedite intergrowths) in Murchison (a, b) and Cold Bokkeveld (c, d). Toch: tochilinite, Cron: cronstedtite, MLP: mixed layer phase.

References: [1] Tomeoka K. and Buseck P. R. (1985) *Geochimica et Cosmochimica Acta* 49:2149–2163. [2] Pignatelli I. et al. (2016) *Meteoritics & Planetary Science* 51:785-805. [3] Lee M. R. et al. (2013) *Geochimica et Cosmochimica Acta* 121:452-466. [4] Rubin A. E. et al. (2007) *Geochimica et Cosmochimica Acta* 71:2361-2382.

X-RAY DIFFRACTIONS OF STONY METEORITES USING THE GANDOLFI ATTACHMENT.

N. IMAE[1,2] and M. KIMURA[1], [1]National Institute of Polar Research, 10-3 Midori-cho, Tachikawa-shi, Tokyo 190-8518, Japan (imae@nipr.ac.jp), [2]SOKENDAI, 10-3 Midori-cho, Tachikawa-shi, Tokyo 190-8518, Japan.

Introduction: The X-ray diffraction (XRD) techniques have been applied to various extraterrestrial materials from macroscopic [e.g., 1-3] to microscopic [e.g., 4-6] approaches. Macro XRD has been developed mainly in laboratories [1-3]. While micro XRD has been developed normally in synchrotron radiation facilities [4, 5] but recently also in laboratories [e.g., 6]. We applied the apparatus (SmartLab, RIGAKU) at NIPR, which have been used mainly for macro XRD, to micro XRD, combining with the polycapillary unit and the Gandolfi attachment in the present study. We show that the technique in air is convenient for the rapid characterization of tiny stony meteorites.

Experiments: Cu Kα X-ray from sealed X-ray tube was generated on the condition of 40 kV and 30 mA for glass tube and 40 kV and 40 mA for ceramic tube. Goniometer radius was 30 cm. Only the strip detector was scanned mainly on the range of 2θ = 28-50º (5-33º only for the Jbilet Winselwan CM2 chondrite), where θ is Bragg angle, while the incident X-ray position was not scanned but fixed. Sample diameter was in the range of 0.2-0.8 mm. Fragment or powder sample was used. The sample was adhered normally on the tip of the glass fiber of 13 μm in diameter and 1 cm in length using cyanobond. Various samples of the San Carlos olivines and NWA 4719 L6 chondrites were measured and used for the calibration focused on the olivine 130 index. The measured samples were ordinary chondrites (OCs) of 14 H, 8 L, and 5 LL, five various carbonaceous chondrites (CCs), and four others.

Results: *Characteristics of the Ol 130 position.* The 2θ positions of the San Carlos olivine and NWA 4719 for powder aggregates are consistent with expected positions by [7], respectively. However, those of grains for both are commonly slightly (< 0.1º) higher than the expected values by [7], and the intensities of the NWA 4719 L6 chondrite grain are heterogeneous among each grains depending on the modal abundance of olivine.

OCs. The 2θ positions (2θ = ~32º) of Ol 130 for grains show the slightly positive correlation with the grain diameter but not for powders. The Oen 511 peak (2θ = ~31.5º) is the useful indicator to distinguish the unequilibrated ordinary chondrites (UOCs) and equilibrated ordinary chondrites (EOCs) [1,2]. Oen 511 peak usually appears for EOCs, but are not clear for some EOCs, which is due to the low intensity of the peak and possibly low abundance of Oen.

CCs. The powders were only measured. The Ol 130 peak is common, and the peak positions for three (A-882094 CO3.5, Y-86751 CV3, and Allende CV3) are smaller than the others. That for Jbilet Winselwan is higher than EOCs and that for Y-86720 CY2 is within the range of EOCs. Oen is commonly lacking, but Cen occurs except Y-86720.

The other stony meteorites. Their diffraction patterns are different from ordinary and carbonaceous chondrites: Oen is dominant for the NWA 7401 EL6 chondrite and the Bilanga diogenite, Cen is dominant for the Pena Blanca Spring aubrite, and the pigeonite (ferroan) and anorthite is mixed for the Cachari eucrite.

Discussion: Powder sample may nearly represent mean bulk compositions, since olivine and pyroxenes commonly coexist for chondrites. However, it may be suggested that grains are heterogeneous for the stony meteorites since the relative peak intensities of the phases are highly changeable. The least square fitting for the peak position of Ol 130 of grains of EOCs was carried out against grain diameter, D (mm). Then the dependence of $\Delta 2\theta$ against D is given by D (mm) = $11.28 \times \Delta 2\theta$ (º) with one σ of 0.055º. When the 2θ is corrected from the equation, the chemical group of H, L, and LL for EOCs may be distinguished. The matrices of the Jbilet Winselwan CM2 chondrite are altered, since the serpentine 001 peak is detected at 2θ = ~12º, and only forsteritic olivines in chondrules is detected. The olivines with the intermediate compositions (which is consistent position of Ol 130 with EOCs) for Y-86720 may be originated from the dehydration from the precursor phyllosilicates, since they are commonly fine-grained [8,9]. The lower peak positions of the other three CCs correspond to the ferroan olivine in matrices.

Summary: We successfully explored the convenient technique for characterizing the tiny extraterrestrial materials.

References: [1] Imae N. and Nakamuta Y. (2018) *Meteoritics & Planetary Science* 53:232-248. [2] Imae N. et al. (2019) *Meteoritics & Planetary Science* 54:919-937. [3] Howard K. T. et al. (2009) *Geochimica et Cosmochimica Acta* 73:4576-4589. [4] Nakamura T. (2005) *Journal of Mineralogical and Petrological Sciences* 100:260-272. [5] Mikouchi T. et al. (2014) *Earth, Planets and Space* 66:82. [6] Flemming R. L. et al. *Canadian Journal of Earth Sciences* 44:1333-1346. [7] Yoder H. S. Jr. and Sahama T. G. (1957) *American Mineralogist* 42:475-491. [8] Ikeda Y. (1992) *Proceedings of the NIPR Symposium on Antarctic Meteorites* 5:136-154. [9] Tomeoka K. et al. (1989) *Proceedings of the NIPR Symposium on Antarctic Meteorites* 2:55-74.

ACCUMULATION OF PLANETESIMALS BY FORMING TERRESTRIAL PLANETS FROM DIFFERENT REGIONS OF THEIR FEEDING ZONE

S. I. Ipatov, Vernadsky Institute of Geochemistry and Analytical Chemistry (Kosygina st., 19, Moscow 119991, Russia, siipatov@hotmail.com).

The model of calculations: Earlier (e.g. [1]) computer simulations of the evolution of disks of bodies coagulated at collisions were made. It was obtained in [1] that, due to the mutual gravitational influence of bodies, the mean eccentricity of orbits of bodies in the feeding zone of the terrestrial planets could exceed 0.2 during evolution. Below in the series *MeN* of runs, the migration of bodies, originally located in a relatively narrow ring, was studied under the gravitational influence of all planets (from Mercury to Neptune). In the series *MeN₀₃* of calculations, the masses of the embryos of the terrestrial planets were equal to 0.3 of the present masses of the planets. In the series *MeS₀₁* of calculations, I considered the embryos of the terrestrial planets with masses equal to 0.1 of the present masses moving in present orbits of the planets, and also Jupiter and Saturn with their present masses and their present orbits (Uranus and Neptune were excluded). The symplectic integrator from the Swift integration package [2] was used.

In each variant of calculations, 250 initial bodies were considered. The initial values a_o of the semimajor axes of orbits of the bodies varied from a_{omin} to $a_{omin}+d_a$, and the number of bodies with a_o was proportional to $a_o^{1/2}$. The values of a_{omin} varied with a step of 0.2 AU from 0.3 to 1.5 AU. d_a=0.5 AU for a_{omin}=1.5 AU. For other runs d_a=0.2 AU. In some variants of the *MeN* calculations, initial eccentricities e_o of orbits equaled to 0.05, and in other runs they were 0.3. For *MeS₀₁* and *MeN₀₃* calculations, I considered only e_o=0.05. The initial inclinations i_o were equal to $e_o/2$ rad. In each run only one value of a_{omin} was considered. As the mutual gravitational influence of bodies was not considered, the considered model of calculations shows minimum estimates of mixing of bodies. Collisions of bodies with planets were not simulated. The orbital elements of the migrated bodies were recorded in computer memory with a step of 500 years. Based on these arrays, similar to the calculations [3-7] of migration of bodies from outside the Mars's orbit, for the considered time interval, I calculated the probabilities of collisions of bodies with forming planets and the Moon. Compared with computer simulations of the evolution of disks of bodies coagulated at collisions, this approach allows one to obtain large statistics of the probabilities of collisions of bodies with planets or their embryos.

The total masses of planetesimals delivered to forming terrestrial planets from different distances from the Sun: Based on the calculated probabilities of collisions of migrating bodies (planetesimals) with forming terrestrial planets [8], I made conclusions on the process of formation of the planets. The embryos of the terrestrial planets with masses about 0.1 of masses of the present planets accumulated mainly planetesimals from the neighbourhoods of their orbits. Probabilities of collisions of planetesimals, originally located at distances from 0.7 to 0.9 AU from the Sun, with embryos of the Earth and Venus with masses equal to 0.3 of masses of present planets, differed for these embryos by no more than twice. The total mass of planetesimals, originally located in each of the regions of the zone located at a distance from 0.7 to 1.5 AU from the Sun, and colliding with the almost formed Earth and Venus, differed for these planets, probably by not more than a factor of two. The inner layers of each terrestrial planet were formed mainly of planetesimals from the vicinity of the orbit of this planet. The outer layers of the Earth and Venus could accumulate the same material for these two planets from different parts of the feeding zone of the terrestrial planets.

In the considered model, the Earth and Venus could acquire more than a half of their masses in 5 million years. The times could be greater for the model for which not all collisions result in coagulation. The assumption of the formation of the Mars embryo with a mass that was several times smaller than that of Mars, as a result of compression of a rarefied condensation, can explain a relatively fast growth (in not more than 10 Myr) of the main mass of Mars. With the ratio of the masses of embryos of the Earth and the Moon equal to 81, the ratio of probabilities of collisions of planetesimals with the embryos of the Earth and the Moon did not exceed 54. The formation of the terrestrial planets can be explained even with a relatively smooth decrease of the semimajor axis of Jupiter due to its ejection of planetesimals into hyperbolic orbits, without the Grand Tack model or the Nice model.

References: [1] Ipatov S. I. (1993) *Solar System Research* 27: 83-101. [2] Levison H. F., Duncan M. J. (1994) *Icarus* 108: 18-36. [3] Ipatov S.I., Mather J.C. (2003) *Earth, Moon, and Planets* 92: 89-98, http://arXiv.org/format/astro-ph/0305519. [4] Ipatov S.I., Mather J.C. (2004) *Annals of the New York Academy of Sciences* 1017: 46-65, http://arXiv.org/format/astro-ph/0308448. [5] Ipatov S.I., Mather J.C. (2004) *Advances in Space Research* 33: 1524-1533, http://arXiv.org/format/astro-ph/0212177. [6] Ipatov S.I., Mather J.C. (2006) *Advances in Space Research* 37: 126-137, http://arXiv.org/format/astro-ph/0411004. [7] Marov M. Ya., Ipatov S. I. (2018) *Solar System Research* 52: 392-400. [8] Ipatov S. I. (2019) *Solar System Research* 53, N 5, in press.

PROBABILITIES OF COLLISIONS WITH THE EARTH AND THE MOON OF PLANETESIMALS MIGRATED FROM OUTSIDE THE ORBIT OF MARS

S. I. Ipatov, Vernadsky Institute of Geochemistry and Analytical Chemistry (Kosygina st., 19, Moscow 119991, Russia, siipatov@hotmail.com).

The model and initial data used for calculations: Below I study the migration of planetesimals from different distances from the Sun to the Earth and the Moon. Such studies allow one to understand better the delivery of water and volatiles to the Earth and the Moon. Earlier we studied migration of bodies with initial orbits close to known Jupiter-family comets [1-5] and migration of planetesimals from the zone with initial semi-major axes from 4.5 to 12 AU [6]. In most new calculations, initial semi-major axes a_o of planetesimals varied from a_m to a_m+2.5 AU with a number of initial planetesimals proportional to $a_o^{1/2}$. In other runs, initial semi-major axes of all initial planetesimals equaled to r_f. For different runs, a_m and r_f varied from 2.5 to 40 AU with a step equaled to 2.5 AU. Initial eccentricities e_o of planetesimals equaled to 0.05 or 0.3. Initial inclinations i_o equaled to e_o/2 rad. The mean eccentricities equaled to 0.3 could be reached due to mutual gravitational influence of planetesimals during evolution of a disk of planetesimals in the feeding zone of the giant planets [7-8]. The gravitational influence of 7 planets (from Venus to Neptune) or of 5 planets (from Venus to Saturn) was taken into account. The symplectic code from the Swift integration package [9] was used. The orbital elements of the migrated planetesimals were recorded in computer memory with a step of 500 years. Based on these arrays of the orbital elements, similar to the calculations presented in [1-6], I calculated the probabilities p_E and p_M of collisions of planetesimals with the Earth and the Moon.

Results of calculations: The probabilities of collisions of planetesimals initially located beyond Jupiter's orbit with the Earth and the Moon calculated for 250 planetesimals can differ by more than a factor of several tens for different runs with similar orbits. While considering thousands of planetesimals with $5 \leq a_m \leq 10$ AU, the mean value of p_E could be larger than 2×10^{-6} by at least a factor of several. It means that if most of the mass of planetesimals in the feeding zone of Jupiter and Saturn was in a large number of relatively small planetesimals, then for estimates of the delivery of material from this zone to the Earth one may use the values of p_E about 10^{-5}. On average, for initial planetesimals in the region at 20 - 40 AU from the Sun, the value of p_E could be about 10^{-6}. This region also could play a valuable role in migration of icy bodies to the Earth. For planetesimals initially located in the asteroid belt, the probabilities of their collisions with the Earth were about 10^{-4}-10^{-2}, i.e., were much greater than for planetesimals initially located beyond Jupiter's orbit. The ratio of the probabilities of collisions of considered planetesimals with the Earth to those with the Moon was mainly in the range from 16 to 17. At e_o=0.3 probabilities p_{Sun} of collisions of planetesimals with the Sun were 0.17 for a_m=2 AU, 0.04 for a_m=2.5 AU, and 0.76 for r_f=2.5 AU. For all other runs, p_{Sun}<0.01, and p_{Sun}=0 for most runs for a_m or r_f not less than 5 AU.

Most of the planetesimals from the Jupiter's feeding zone were ejected into hyperbolic orbits in a few Myr under the gravitational influence of Jupiter and Saturn. Most of collisions with the Earth of bodies initially located in the zone at 5-30 AU from the Sun took place in less than 20 Myr. This testifies in favor of that the planetesimals from beyond Jupiter's orbit could fall onto the Earth and the Moon in the process of their growth, and the matter, including water and volatiles, delivered from beyond the orbit of Jupiter was incorporated into the internal layers of the Earth and the Moon. The delivery of matter to the Earth and the Moon from the zone of Uranus and Neptune depended on when these giant planets acquired large masses and began to move in orbits close to their present orbits. After the planetesimals from this zone began to experience a significant influence of these giant planets, the typical time until the fall of the planetesimals onto the Earth and the Moon often did not exceed 20 Myr, but a small fraction of the planetesimals could fall onto the Earth during hundreds of Myr.

References: [1] Ipatov S.I., Mather J.C. (2003) *Earth, Moon, and Planets* 92: 89-98, http://arXiv.org/format/astro-ph/0305519. [2] Ipatov S.I., Mather J.C. (2004) *Annals of the New York Academy of Sciences* 1017: 46-65, http://arXiv.org/format/astro-ph/0308448. [3] Ipatov S.I., Mather J.C. (2004) *Advances in Space Research* 33: 1524-1533, http://arXiv.org/format/astro-ph/0212177. [4] Ipatov S.I., Mather J.C. (2006) *Advances in Space Research* 37: 126-137, http://arXiv.org/format/astro-ph/0411004. [5] Ipatov S.I., Mather J.C. (2007) Proc. of IAU Symp. No. 236 "*Near-Earth Objects, Our Celestial Neighbors: Opportunity and Risk*". Cambridge: Cambridge Univ. Press, 55-64,. http://arXiv.org/format/astro-ph/0609721 [6] Marov M.Ya., Ipatov S.I. (2018) *Solar System Research* 52: 392-400. [7] Ipatov S.I. (1987) *Earth, Moon, and Planets* 39: 101-128. [8] Ipatov S.I. (1993) *Solar System Research* 27: 65-79. [9] Levison H.F., Duncan M.J. (1994) *Icarus* 108: 18-36.

DEEP THERMAL METAMORPHISM (NOT MELTING) OF ORDINARY AND CARBONACEOUS CHONDRITE PRECURSORS PRODUCED TYPE 7 AND PROPOSED TYPE 8 CHONDRITES

A. J. Irving[1, 5], S. M. Kuehner[1], P. K. Carpenter[2], K. Ziegler[3] and P. P. Sipiera[4] [1]Dept. of Earth & Space Sciences, University of Washington, Seattle, WA, USA, irvingaj@uw.edu; [2]Dept. of Earth & Planet. Sciences, Washington University, St. Louis, MO, USA; [3]Institute of Meteoritics, University of New Mexico, Albuquerque, NM, USA; [4]Planetary Studies Foundation, Galena, IL, USA

Progressive thermal metamorphism (driven mainly by ^{26}Al heating) of ordinary and carbonaceous chondrites should be expected to have occurred on their parent bodies as a function of increasing depth. The bodies that are the ultimate sources for the well-known H, L and LL chondrites of Types 3-6 and also many carbonaceous chondrites (mostly Types 2 and 3) were probably disaggregated long ago by major collisions. Any deeper, more thermally metamorphosed specimens, as well as samples of related mantles and cores (pallasites and irons), would be expected to be less voluminous and hence rarer as recovered meteorites. Over the past 15 years there has been a steady increase in the number of chondrule-free specimens possessing bulk elemental and isotopic (O, Cr, W) compositional affinities to the much more common chondrule-bearing specimens. The term *metachondrite* was proposed for these specimens [1], but adopting the suggestion by [2] a consensus developed that the proper terminology should be Type 7 chondrite.

Yet all "Type 7" chondrites are not texturally identical, and here we propose that an additional Type 8 category should be established to reflect those differences. Among specimens currently grouped as Type 7, there is a textural distinction between those that contain poikiloblastic aggregates of orthopyroxene oikocrysts enclosing olivine chadacrysts (logically representing recrystallized former chondrules) and others (here designated as Type 8) that possess a completely recrystallized, triple grain junction texture with no hint of either chondrules or oikocrysts. This textural evolution has parallels to the well-established sequence observed for terrestrial hornfelses in thermal metamorphic aureoles adjacent to intrusive plutons. Apart from Types 7 and 8 with affinities to H, L and LL chondrites, we recognize the following categories based on analogous textures: CR7 chondrites (Tafassasset, NWA 11561), CR8 chondrites (NWA 12455), CV8 chondrites (NWA 2653/3133 [3]), CK8 chondrites (NWA 8186 [4]), and Types 7 and 8 among acapulcoites and winonaites (which also evidently are related to chondrule-bearing precursors).

LL7 (NWA 8417)   15 mm   **LL7/8** (NWA 6260)   15 mm   **H8** (NWA 4226)   15 mm

CV8 (NWA 3133)   15 mm   **CR7** (NWA 11431)   15 mm   **CR8** (NWA 12455)   15 mm
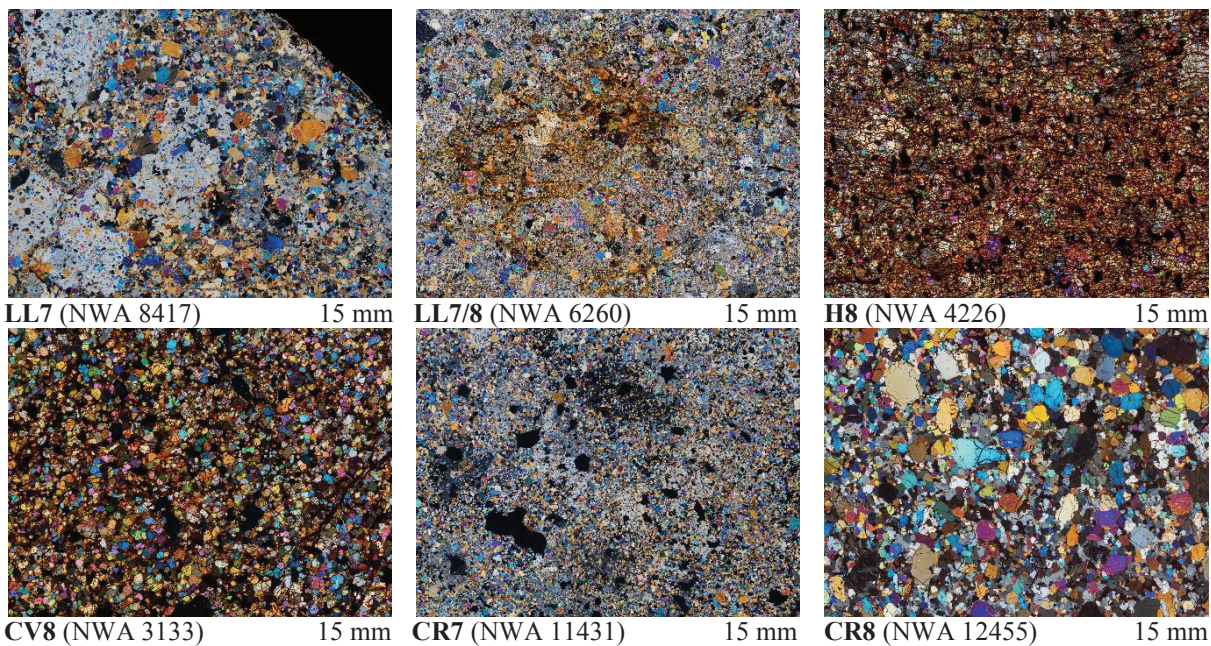
Figure 1. Textures (in cross-polarized light) of proposed Type 7 and Type 8 chondrites. Photos © Neil Buckland.

References: [1] Irving A. *et al.* (2005) *68th Meteorit. Sci. Mtg.*, #5218. [2] Dodd R. *et al.* (1975) *GCA* **39**, 1585-1594. [3] Irving A. *et al.* (2004) *EOS, Trans. AGU*, #P31C-02. [4] Srinivasan P. *et al.* (2017) *LPS* **XLVIII**, #1995.

PETROLOGIC-ISOTOPIC CHARACTERIZATION OF NAKHLITE NORTHWEST AFRICA 12542

A. J. Irving[1], S. M. Kuehner[1], M. Righter[2], T. J. Lapen[2], H. Busemann[3], K. Ziegler[4] and B. Hoefnagels, [1]Dept. of Earth & Space Sciences, University of Washington, Seattle, WA, USA, irvingaj@uw.edu; [2]Dept. of Earth & Environmental Sciences, University of Houston, TX, USA; [3]Institut für Geochemie und Petrologie, ETH Zürich, Switzerland; [4]Institute of Meteoritics, University of New Mexico, Albuquerque, NM, USA

Nakhlites are Martian augite-olivine-rich rocks which have been interpreted as a probably launch-paired group of igneous cumulates from one or more layered lava flows or intrusive sills which crystallized at ~1.3 Ga on Mars [1, 2, 3]. They have isotopic and chronologic affinities with the three known chassignites, which may represent samples from the basal zone(s) of the same target region(s) that yielded nakhlites.

Northwest Africa 12542, the 11th known nakhlite recovered in Mauritania in late 2018, is a 1082 gram oriented black stone partly coated by remnant fusion crust exhibiting flow lines (see Figure 1). The specimen has a cumulate texture, with larger grains of minimally zoned olivine (up to 2 mm, $Fa_{65.7-70.2}$, FeO/MnO = 50-55) and chromian titanomagnetite (up to 1 mm, Al_2O_3 = 3.2 wt.%, Cr_2O_3 = 4.5 wt.%) together with twinned, prismatic grains of augite (up to 2 mm long, $Fs_{22.8-28.9}Wo_{39.2-38.2}$, FeO/MnO = 34-37) with thin rims of ferroan augite ($Fs_{45.6}Wo_{40.2}$, FeO/MnO = 41). Intercumulus regions contain pyrrhotite, K-feldspar ($Or_{75.2}Ab_{23.6}An_{1.1}$), intermediate plagioclase, ferrosilite ($Fs_{54.9}Wo_{3.1}$, FeO/MnO = 36), ferroan pigeonite ($Fs_{65.2-66.1}Wo_{6.6-5.8}$, FeO/MnO = 23-28), cruciform grains of titanomagnetite and very rare chlorapatite together with K-bearing glass. Secondary chlorophaeite-like material (orange in thin section) is present in some intercumulus regions and also filling fractures in olivine phenocrysts (see Figures 2, 3). The most similar nakhlite specimen would be NWA 817, but we do not consider these two stones to be paired.

Figure 1: Whole NWA 12542 stone showing flow striations in remnant fusion crust and pits from desert wind ablation. Long dimension = 10 cm. Photo © Neil Buckland.

Figure 2: Partially cross-polarized thin section image showing dominant twinned augite, subordinate olivine, opaque Fe-Ti oxides, and orange "chlorophaeite" in the groundmass and within olivine grains.
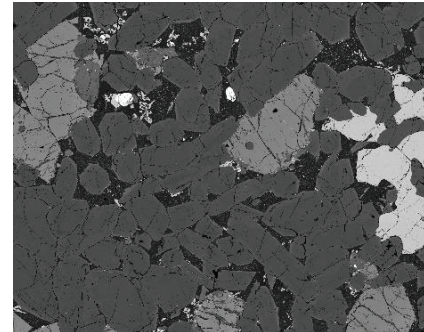
Figure 3: BSE image showing augite (gray), olivine (light gray, with veinlets of "chlorophaeite"), Fe-Ti oxide (lightest gray) and intercumulus material (dark) + cruciform oxides and pyrrhotite (bright).

Elemental and isotopic compositions: Analyses of a small subsample gave Mg/(Mg+Fe) = 0.505 and FeO/MnO = 41. The chondrite-normalized REE pattern (Figure 4) is light-REE enriched and resembles that for the Yamato 00 specimens [4]. Hf and Nd isotopic analyses are in progress to assess whether the crystallization age is similar to those for other nakhlites [5, 6]. Cosmic ray exposure ages based on analyses of ^{21}Ne, ^{3}He and ^{38}Ar are 10-12 Myr, in agreement with such ages for most other nakhlites [7].

References: [1] Treiman A. (2005) *Chemie Erde* **65**, 203-270. [2] Treiman A. and Irving A. (2008) *MaPS* **43**, 829-854. [3] Irving A. *et al.* (2015) *78th Meteorit. Sci. Mtg.*, #5251. [4] Dreibus G. et al. (2003) *LPS* **XXXIV**, #1586. [5] Righter M. *et al.* (2016) *LPS* **XLVII**, #2780. [6] Cohen B. *et al.* (2017) *Nature Commun.* **8**. [7] Wieler R. *et al.* (2016) *MaPS* **51**, 407-428.
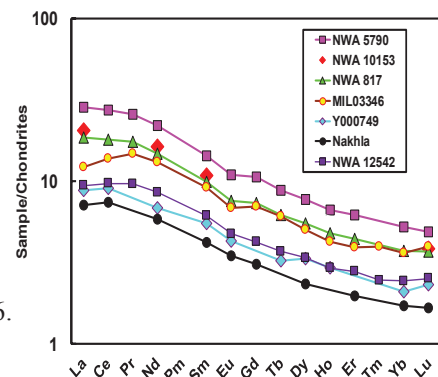
NON-TARGETTED ANALYSES ON SOLUBLE ORGANIC COMPOUNDS IN CHONDRITES.

J.Isa[1]and F.-R. Orthous-Daunay[1] and H.Naraoka[2]
[1]Univ. Grenoble Alpes, CNRS, IPAG (CS 40700 38058 Grenoble Cedex 9, France. isaj@univ-grenoble-alpes.fr)
[2]Kyushu University, (744 Motooka, Nishi-ku, Fukuoka 819-0395 Japan)

Introduction: The solar system origin and subsequent evolution of organic matter are still not well understood. Inorganic chondritic components, bulk elemental compositions, and the petrography of chondrites group reflect different accretionary components. Also, the petrological observations of alterations/metamorphism in the chondrites shows evidence of the geological evolution since accretion and of the parent body processes that result in the variety of rock types we see today across chondrite groups. The fact that the vast majority of organic compounds are subject to reactions that lead to synthesis, degradation, and alteration during geological processes helps to explain why the overall picture of organic compound distribution is still unclear. Although the majority of organics in chondrites are large, insoluble organic compounds and soluble organic compounds (SOCs) such as the ones that are essential for life have been identified in meteorites and are of great interest to the origin of life in the universe. Targeted analyses have successfully identified a wide variety of pre-biotic organic compounds in meteorites [1]. Non-targeted analyses have started revealing the complexity of SOCs including the discovery of a new type of metalorganic [2,3]. In order to comprehensively study SOCs in meteorites including carbonaceous and non-carbonaceous chondrites, we have applied non-targeted analyses on the solvent extracts from chondrites and measured them by using the nano-ESI direct-infusion with a high-resolution Orbitrap mass spectrometer.

Measurements an data processing: We have studied CR, CM, LL, and R chondrites from Antarctic meteorites, (MIL 090657, EET 96029, Y-793596, and PRE 95404). Each meteorite was subsequently extracted by solvent (hexane, dichloromethane, methanol, and 100 °C water). The methanol extracted organics were analyzed using the high-resolution Orbitrap mass spectrometer at Kyushu University. After we acquired the spectra, we utilized post processing data analysis tools developed in-house (R programming language and Igor) to study the Orbitrap data. The analysis used the mzR package in the Bioconductor tool kit and Proteowizard software to convert the data format from vendor raw data to mzML mass spectrometer data [4]. The Igor-based software was also used for the data analyses. The post-processing includes mass-drift correction, peak detection, blank subtractions, and noise rejection.

Results: Chemical formulae were heuristically assigned for individual peaks in the Orbitrap data and we have been able to identify the major compounds found in the CM chondrite extract by using the positive ion modes. The CM extract contains N-bearing organic compounds that are similar to and consistent with the organic compounds found in a methanol extract from the Murchison meteorite. In our CM chondrite analysis, we were able to assign approximately 60% of major peaks that were detected as singly plus charged $CnHnNnOn$ compounds to within 5 ppm of mass precision between *m/z* 300 and 750. For this data reduction, we used the following assumptions: 1) ion intensity consistent with the ^{12}C /^{13}C isotope pattern; 2) select singly charged state compounds or *m/z* of doubly charged state compounds are multiplied by two; and 3) reasonable H/C, N/C, and O/C ratios that are 0.1-6, 0-4, and 0-3 (by atomic weight), respectively. Among the assigned $CnHnNnOn$ compounds, approximately 20% of compounds were assigned as $CnHnNn$. In contrast to CM analyses, very few peaks were detected from LL extract. The LL data set is not large enough to demonstrate the characteristics of chemical formulae. In contrast, a significantly complex spectrum was obtained from the R chondrite extract. In order to decode the complex spectra, we performed some filtering: 1) subtracted peaks that appeared in the CM and LL analyses; 2) made subsets for peaks of singly charged ions and doubly charged ions; and 3) selected the data which only have ion intensities consistent with the ^{12}C /^{13}C isotope pattern. After the subtraction of CM and LL spectra, nearly 5000 unique peaks were detected in the R chondrite spectra in the m/z range of 50 to 750. However, only about 50 peaks remained after selection steps 2) and 3) were applied. One of the remaining peaks can be assigned with the elemental pattern of $CnHnNnSn$. The results suggest that this complex spectrum includes compounds consisting of multiple hetero-elements possibly besides N, O, and S. We will develop new tools to identify such elements. We are in the process of performing CR chondrite data analysis and data reduction for the negative mode analyses. We will present results outlining major differences in organic compound distributions amongst the different chondrite groups.

References: [1] Naraoka H, et al., ACS Earth Space Chem. 2017;1:540-550 [2] Schmitt-Kopplin, P., Proceedings of the National Academy of Sciences, 107(7), 2763-2768. [3] Ruf, A. et al., (2017) Proceedings of the National Academy of Sciences, 114(11), 2819-2824. [4] Chambers, M. C. et al., (2012) Nature biotechnology, 30(10), 918.

GEMS-LIKE MATERIAL IN PARIS MATRIX AND GEMS IN INTERPLANETARY DUST PARTICLES: AN EDX AND EELS COMPARISON

H. A. Ishii[1†], K. K. Ohtaki[1†], J. P. Bradley[1], K. C. Bustillo[2], K. L. Villalon[3], A. M. Davis[3], T. Stephan[3], and P. Longo[4], [1]Hawaiʻi Institute of Geophysics and Planetology, University of Hawaiʻi at Mānoa, Honolulu, HI, USA, [2]National Center for Electron Microscopy, Molecular Foundry, Lawrence Berkeley National Laboratory, Berkeley, CA, USA, [3]Department of Geophysical Sciences, The University of Chicago, Chicago, IL, USA, [4]Gatan Inc., Pleasanton, CA, USA. Email: hope.ishii@hawaii.edu or kohtaki@hawaii.edu.

Introduction: The Paris meteorite is the least altered CM chondrite yet identified [1]. It is a breccia of lithologies that have undergone a range of aqueous alteration, sometimes with poorly defined boundaries. In the least altered regions, the Paris matrix contains amorphous silicate material (ASM) that is approximately chondritic in bulk composition and contains Fe-sulfide nanograins [2]. Because of these similarities to GEMS (glass with embedded metal and sulfides) in chondritic-porous interplanetary dust particles (CP IDPs), it has been suggested that GEMS grains may have been the building blocks of the CM matrices [2]. The amorphous silicate GEMS grains in CP IDPs are of considerable interest, because some are demonstrably presolar and thus remnants of the original interstellar amorphous silicate dust that dominated the rock-forming dust in the presolar molecular cloud [3]. Recent studies of the organic distribution in GEMS further support their formation in cold presolar environments [4]. Here, we apply our newly developed method of TEM sample preparation [5] to prepare sections sufficiently thin to enable comparison of the glassy matrix of the AMS in Paris and the glassy matrix of GEMS in CP IDPs, excluding inclusions. (See Villalon et al., this volume, for discussion of inclusions in Paris ASM.) We carried out a side-by-side comparison of GEMS in CP IDPs with the GEMS-like ASM in Paris using spectral imaging by two methods, energy dispersive X-ray spectroscopy (EDX) and electron energy loss spectroscopy (EELS), and we describe the differences observed.

Materials and Methods: A petrographic section of Paris, 2010-7, provided by the Muséum National d'Histoire Naturelle (Paris, France), was first mapped by back-scattered electron (BSE) imaging and EDX in the FEI Helios 660 dual beam focused ion beam instrument (FIB-SEM) at the University of Hawaiʻi to identify regions that retain Fe as metal. Electron transparent TEM sections were (and are being) prepared from matrix material and fine-grained chondrule rim material from a total of 5 locations in minimally-altered regions of Paris matrix. CP IDPs were prepared by ultramicrotomy. The FEI Titan (scanning) transmission electron microscope (S/TEM) at the University of Hawaiʻi is used for conventional and STEM imaging, nanodiffraction, and individual EDX and EELS analyses. Another Titan S/TEM at the Molecular Foundry, with a quadruple Bruker silicon drift detector EDX system is used for high spatial resolution elemental mapping by EDX. Finally, a JEOL F200 S/TEM with a Gatan Continuum GIF spectrometer is used for high spatial resolution EELS spectral imaging (mapping).

Results and Discussion: Initial analyses from one location in the ASM in Paris show the ASM regions have little void space and some surrounding organic carbon. ASM material has poorly defined boundaries, but regions bounded by carbon appear comparable in size to GEMS in CP IDPs. Sulfide inclusions are generally larger (~20-200 nm) than most metal and sulfide inclusions in CP IDP GEMS (~1-30 nm). Within the Paris ASM, the Fe content in the glassy matrix is higher than that of GEMS, likely the result of some aqueous processing in even the minimally-altered lithologies. Fe is fairly uniformly distributed in the glassy phase and concentrated in sulfide inclusions, similar to the amorphous silicate material reported in Acfer 094 [6]. EELS confirms the very low Fe content in GEMS glassy matrix versus higher, oxidized Fe content in the Paris ASM glassy matrix. Our initial results indicate significant differences between the glassy matrices of GEMS and of GEMS-like material in the Paris meteorite matrix, but it remains unclear if, or how, they may be related. It is possible that the first location in Paris ASM that we have analyzed, although from a region containing Fe metal, is more altered than the subsequent locations that have been extracted, and we will report on additional locations analyzed.
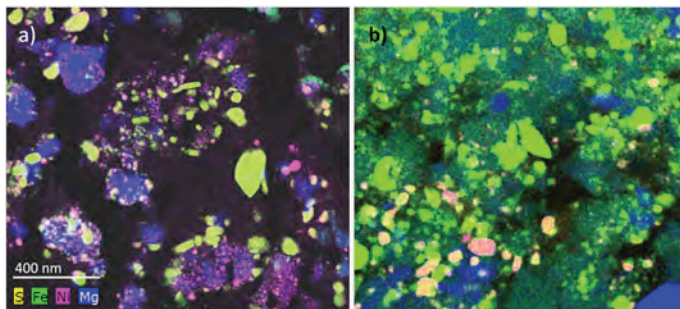
← Figure 1: Element maps extracted from EDX spectral imaging on (a) LT 29, a fragment of CP IDP U220GCA and (b) Paris meteorite matrix. Scale bar and color legend apply to both images.

References: [1] Hewins R. H. et al. (2014) *Geochimica et Cosmochimica Acta* 124:190–222. [2] Leroux H. et al. (2015) *Geochimica et Cosmochimica Acta* 170:247–265. [3] Messenger S. et al. (2003) *Science* 300:105–108. [4] Ishii H. A. et al. (2018) *Proceedings of the National Academy of Sciences* 115:6608–6613. [5] K. K. Ohtaki et al. (2019) in preparation. [6] Hopp T. and Vollmer C. (2018) *Meteoritics & Planetary Science* 53:153–166.

EFFECT OF WATER FUGACITY FOR OXYGEN SELF DIFFUSION IN GEHLENITE

S. Ishikubo[1], S. Tachibana[2,3], N. Kawasaki[1], D. Yamamoto[1], M. Kuroda[1], and H. Yurimoto[1,3], [1]Natural History Sciences, Hokkaido University, Sapporo 060-0810, Japan (shogo@ep.sci.hokudai.ac.jp) [2]UTokyo Organization for Planetary Space Science, The University of Tokyo, Hongo, Tokyo 113-0033, Japan. [3]ISAS/JAXA, Sagamihara, Kanagawa 252-210, Japan.

Introduction: Calcium-aluminium-rich refractory inclusions (CAIs) are the oldest objects in the Solar System, and exhibit oxygen isotopic variations among different minerals [1]. A mechanism to produce mineralogical-controlled oxygen isotopic variations is the diffusive oxygen isotope exchange between CAI-constituting minerals and oxygen bearing gas species (e.g., H_2O) in the protosolar disk or on parent bodies after the CAI formation. The oxygen self-diffusion coefficients in melilite have been experimentally determined using isotopically labelled CO_2 and/or CO [2, 3], but the combination of oxygen diffusivity in melilite and those in other CAI constituting minerals cannot explain the mineralogical-controlled oxygen isotope distributions observed in CAIs. However, oxygen self-diffusion in CAI-constituting minerals could be variable under hydrous conditions as in the case of some silicate minerals [4]. Especially, melilite may be highly enhanced with increasing water fugacity compared with other CAI minerals to form the oxygen isotope distribution in CAIs. In order to examine the effect of water fugacity on oxygen self-diffusion in melilite, we conducted oxygen diffusion experiments in gehlenite ($Ca_2Al_2SiO_7$) in the presence of water vapor.

Experiments: Oxygen self-diffusion experiments in a single crystal of gehlenite, synthesized by the Czochralski pulling method by M. Morioka, U. Tokyo, were conducted at 800, 850, and 900°C and water vapor pressure (P_{H2O}) of 0.3 and 0.01 Pa for 24 and 120 hr. A gold-mirror vacuum furnace equipped with a gas flow system for water vapor (Thermo- Riko GFA 430VN) [5, 6] was used for the experiments under the low P_{H2O} conditions, inferred in protoplanetary disks. ^{18}O enriched water (97-atom% ^{18}O) was used as a source of water vapor. The P_{H2O} in the furnace (0.3 and 0.01 Pa) was controlled by adjusting a flow rate of $H_2^{18}O$ vapor and a gas evacuation rate. The melilite crystals showing smooth cleavage surfaces ((001) plane; 2 mm × 10 mm) were used for the experiments. The observations of crystal surfaces were made with a field-emission scanning electron microscope with EDS (energy dispersive X-ray spectroscopy) and EBSD (electron backscatter diffraction) (FE-SEM-EDS-EBSD; JEOL JSM-7000F) and depth profiles of $^{16}O^-$, $^{18}O^-$ and $^{28}Si^-$ along the [001] axis were obtained by secondary ion mass spectrometry (Cameca ims-1280HR) at Hokkaido University.

Results & Discussion: No reaction products were observed on the surface of run products, and the surface remained gehlenite. The depth profiles of oxygen isotopes show that the sample surface is enriched in ^{18}O due to oxygen isotope exchange with $H_2^{18}O$ vapor. The ^{18}O fraction decreases with depth from the surface, and it drops down to that of the terrestrial value at the depths of ~100 nm and ~150 nm at 800 and 900°C, respectively. No significant P_{H2O} dependences of the depth profiles of oxygen isotopes were observed. The observed ^{18}O profiles were fitted with a one-dimensional diffusion equation in a semi-infinite medium with a constant surface concentration [7]. The obtained self-diffusion coefficient of oxygen along the [001] axis is about one order of magnitude smaller than that in [2] at 800–900°C with a similar activation energy (~200 kJ/mol). The smaller oxygen self-diffusion coefficient in the present study could be due to the difference in the point defect concentration within the crystals. Present results show that oxygen self-diffusion in melilite is not enhanced in the presence of water vapor, at least at the disk-like P_{H2O} of 0.01-1 Pa, and that the diffusion coefficient of oxygen self-diffusion in melilite obtained under dry conditions are applicable for discussion on oxygen isotope evolution for CAI constituting minerals in the protosolar disk.

References: [1] Clayton R. N. (1993) *Annual Review of Earth Planetary Sciences* 21:115-149. [2] Yurimoto H. et al. (1989) *Geochimica et Cosmochimica Acta* 53:2387-2394. [3] Ryerson F. J. and McKeegan D. K. (1994) *Geochimica et Cosmochimica Acta* 58:3713–3734. [4] Stephen C. E. et al. (1988) *Contributions to Mineralogy and Petrology* 100:490–495. [5] Yamamoto D. and Tachibana S. (2018) *ACS Earth and Space Chemistry* 2:778-786. [6] Yamamoto D. et al. (2018) *The Astrophysical journal* 865:98 (14pp). [7] Crank J. (1956) *The Mathematics of diffusion*. 2nd edition Oxford:Oxford University Press.

DEHYDRATION AND RECRYSTALLIZATION EXPERIMENTS OF SERPENTINE FOR UNDERSTANDING THERMAL HISTORY OF HYDRATED ASTEROIDS.

K. Ishimaru[1], S. Tachibana[2,3], and D. Yamamoto[3], [1]Department of Earth and Planetary Science, Faculty of Science, The University of Tokyo, 7-3-1 Hongo, Tokyo 113-0033, Japan (kanaishimaru@eps.s.u-tokyo.ac.jp), [2]UTokyo Organization for Planetary and Space Science, The University of Tokyo, [3]Institute of Space and Astronautical Science, Japan Aerospace Exploration Agency.

Introduction: JAXA's Hayabusa2 and NASA's OSIRIS-REx spacecrafts have been exploring asteroids (162173) Ryugu and (101955) Bennu, respectively [1, 2]. Spectroscopic observations revealed that Ryugu shows a weak absorption feature of hydrous minerals at 2.7 μm [3], while Bennu shows a clear 2.7 μm absorption feature of hydrous minerals [4]. This indicates that two asteroids experienced different thermal histories, and dehydration of hydrous phases could have occurred more effectively on Ryugu [5], similarly to parent bodies of heated CM chondrites [6]. If this is the case, it is important to understand thermal transformation processes of hydrous minerals to constrain the thermal histories of the asteroids. With the aim of understanding thermal processes on Ryugu and Bennu, we conducted dehydration and recrystallization experiments of serpentine in vacuum to obtain kinetic data for dehydration and recrystallization processes.

Methods: Natural serpentine (lizardite, occurrence), ground into 1- μm sized powder, was used as a starting material. Samples were heated at 500–800°C for durations of 2–88 hours in a vacuum furnace. The furnace consists of a tubular electric heating system with a silica glass tube connected to a pumping system. The pressure inside the silica glass tube during experiments was 10^{-4}–10^{-5} Pa. The starting material and heated samples were examined with XRD (PANalytical X'Pert Pro MPD) and FTIR (JASCO FT-IR4200). The weight losses of the samples were obtained by weighing them before and after the experiments using an electric balance.

Results: The serpentine samples heated at 500°C were dehydrated with heating, but crystalline serpentine was still present in the sample heated for 36 hours. The samples heated at 600°C were decomposed into amorphous with a small amount of recrystallized olivine after heating for 8-48 hours. The XRD patterns of the samples heated at 650°C clearly show the presence of olivine that recrystallized from the dehydrated amorphous with a weak halo representing the presence of dehydrated amorphous phase. The samples heated at 700°C for 2-84 hours also show the evidence of recrystallization of olivine from the dehydrated amorphous phase. There seems no evident amorphous halo in their XRD patterns. The XRD spectra of the samples heated at 800°C for 8-66 hours show the strongest peak of enstatite in addition to the peaks of olivine, suggesting that crystallization of enstatite occurred at 800°C. The dehydration and crystallization behavior of the sample at different tempeartures are roughly consistent with [7], where dehydration and recrystallization of serpentine were examined with TEM. FTIR analysis of the samples also confirmed the recrystallization of olivine from the dehydrated amorphous phase.

Discussion: The 10-μm features of FTIR spectra of the samples heated at 650 and 700°C were analyzed further to obtain the kinetics of recrystallization of olivine from dehydrated serpentine. We focused on the absorbance ratio of the peaks of olivine at 10.4 and 11.4 μm because the absorbance of olivine at 10.4 μm is affected by a broad 10 μm peak of amorphous silicate and its relative strength to the 11.4-μm strong feature could be a measure of the crystallization degree of olivine. We used the absorbance data of 10.4 and 11.4 μm of a mixture of crystalline and amorphous forsterite [8] to produce a calibration curve for the abundance ratio of olivine and amorphous silicate. Temporal changes of olivine abundance in heated samples, evaluated from the absorbance ratio of 10.4- and 11.4-μm peaks, at 650 and 700°C were fitted by the Johnson-Mehl-Avrami-Kolmogorov equation with the Avrami exponent of 1.5 [8] to obtain a crystallization rate constant. Our preliminary data give the rate constant [$h^{-1.5}$] of ~0.03 and 0.34 at 650 and 700°C, respectively. The activation energy for the olivine recrystallization is estimated to be ~360 kJ mol^{-1}. Assuming that the present data can be extrapolated to lower temperatures, combined with the dehydration kinetics of serpentine [9], dehydration of serpentine and recrystallization of olivine from dehydrated serpentine could occur at ~350 and ~550 K for a million years.

References: [1] Watanabe S. et al. (2019) *Science* 364, 268. [2] Lauretta D. et al. (2019) *Nature* [3] Kitazato, K. et al. (2019) *Science* 364, 272. [4] Hamilton V. E. et al. (2019) *Nature Astronomy* 3, 332-340. [5] Sugita S. et al. (2019) *Science* 364, 252. [6] Nakamura T. (2005) [7] Akai J. (1992) *Proceedings of the NIPR Symposium, Sixteenth Symposium on Antarctic Meteorites* 5, 120-135. [8] Yamamoto D. and Tachibana S. (2018) *ACS Earth Space Chem.* 10:1021. [9] Yamamoto D. (2016) Master thesis, Hokkaido University.

DEVELOPMENT OF SAMPLE PREPARATION TECHNIQUE FOR ISOTOPE ANALYSIS OF FLUID INCLUSIONS BY SIMS

Y. Isono[1], N. Sakamoto[2], A. Ishibashi[1], J. Song[1] and H. Yurimoto[1,3], [1]Department of Natural History Sciences, Hokkaido University, Sapporo 060-0810, Japan (isono@ep.sci.hokudai.ac.jp), [2]Isotope Imaging Laboratory, Creative Research Institution, Hokkaido University, Sapporo, Japan, [3]Institute of Space and Astronautical Science, Japan Aerospace Exploration Agency, Sagamihara, Japan

Introduction: Fluid inclusions in halite crystals from meteorites provide direct information of extraterrestrial liquid water [1]. In-situ isotope analysis of the fluid inclusions was realized by SIMS equipped with a cold-stage [2]. However, the analytical precision is limited to ±14 ‰ (1σ) and ±7 ‰ for $\delta^{18}O$ and $\delta^{17}O$, respectively, due to electrostatic charge up by deep sputter crater to excavate fluid inclusions. One of the methods to improve the analytical precision would be to expose fluid inclusions on the sample surface before sputtering. In order to realize the condition, we developed cryogenic sample preparation techniques including cryo-polishing, cryo-coating and cryo-transfer system for SIMS instruments.

Cryogenic Sample Preparation for SIMS: We froze the fluid inclusions and polished under cryogenic condition using a cryo-polishing system consists of a customized polisher (JEOL, HLA-2) in a glove box filled with nitrogen gas. The temperature of the polisher was controlled by liquid nitrogen flow through internal trench to –35 °C when the dew point in the glove box was about –45 °C. The sample surface was observed by an optical microscope (KEYENCE, VHX) integrated into the polisher to check whether the fluid inclusion is exposed or not in between polishing. The exposed fluid inclusion on the sample surface was coated with conductive Au thin film using a cryo-coating system consists of an Au ion-coater (SANYU DENSHI, SC-701AT) in a glove box. The polished sample was settled on the bottom of deep well of a cryo-coating stage for the coater. The sample and the cryo-coating stage were cooled by liquid nitrogen before coating to prevent sublimation of the frozen fluid in the vacuum coating chamber. The temperature of the sample maintained under –120 °C after the coating process. The Au coated sample was set into a sample holder of Cameca ims-1270/1280 milled from a stainless-steel block. The machined sample holder is useful to suppress deformation with temperature change until liquid nitrogen temperature. The sample holder was put into a cryo-transfer vessel filled with liquid nitrogen and carried to the Cameca ims-1270/1280. The vessel has a connection port compatible to the loadlock chamber of the Cameca ims-1270/1280 for sample introduction. We attached a valve to the loadlock chamber in order to keep the frozen sample in nitrogen gas atmosphere. The sample holder was picked up from the vessel to the loadlock chamber and transferred to the cryo-stage of SIMS instrument cooled to –190 °C with liquid nitrogen. The liquid nitrogen cooled the cryo-stage supplied by a roots pump which was adopted to reduce the sample stage vibration.

Isotope Analysis: Oxygen isotopic compositions of synthesized fluid inclusions in halite crystal were measured with the Camaca ims-1280 SIMS in Hokkaido University using the cryogenic sample preparation techniques developed in this study. A Cs^+ primary ion beam was focused on the frozen fluid inclusion. A normal incidence electron flood gun was applied to compensate positive charging. Entrance slit and exit slit was 60 μm and 180 μm, respectively. We obtained mass spectrum of oxygen isotopes from the H_2O-ice. Intensity of $^{16}O^-$ peak was about 2.8×10^5 cps and a tale was observed symmetrically at both side of the peak below 3 cps. Three oxygen isotopes were collected using peak jumping mode: $^{16}O^-$ was measured on a Faraday cup, $^{17}O^-$ and $^{18}O^-$ were measured with an axial electron multiplier. Total count rate of $^{16}O^-$ was ~5–6 × 10^6 cps. We obtained the reproducibility of ±2.8 ‰ and ±5.2 ‰ for $\delta^{18}O$ and $\delta^{17}O$ when the calculated statistical errors were ±1.8 ‰ and ±3.8 ‰, respectively. The $\delta^{18}O$ deviation was suppressed successfully in this study. The interference of tail from $^{16}OH^-$ to $^{17}O^-$ was estimated to be about 10 ‰ because the intensity of $^{16}OH^-$ was comparable to $^{16}O^-$ peak. Oxygen isotope analysis using $^{16}OH^-$ and $^{17,18}OH^-$ signal would be effective for further high precision oxygen isotope analysis for H_2O ice as well as the tail correction method used in [2].

References: [1] Zolensky M. et al. (1999) *Science*, 285:1377–1379. [2] Yurimoto H. et al. (2014) *Geochemical Journal*, 48:549–56.

THE RYUGU GRAIN ANALYSIS: APPROACH BY THE PHASE 2 CURATION "TEAM KOCHI".

M. Ito[1], N. Tomioka[1], M. Uesugi[2], K. Uesugi[2], T. Ohigashi[3], A. Yamaguchi[4], N. Imae[4],
Y. Karouji[5], N. Shirai[6], T. Yada[7] and M. Abe[7].

[1]Kochi Institute for Core Sample Research, JAMSTEC (motoo@jamstec.go.jp), [2]JASRI/SPring-8,
[3]UVSOR Synchrotron Facility, Institute for Molecular Science, [4]National Institute Polar Research,
[5]JSEC/JAXA, [6]Tokyo Metropolitan University, [7]ISAS/JAXA.

Hayabusa2 space craft successfully conducted a touchdown onto the surface of the asteroid Ryugu on Feb. 2019. According to the camera monitoring during the touchdown, the sample catcher most likely contains the asteroid surface regolith. Reports by the Near-IR Spectrometer (NIRS3) on Hayabusa2 spacecraft presented that the asteroid Ryugu may consist of either CM chondritic materials or shocked/heated carbonacesous chondrites [1–3]. Matsuoka et al. pointed out that the low albedo of the asteroid Ryugu could be explained by a combination of C-rich material, grains size, porosity and space weathering effects on the asteroid surface materials [3]. Unique Ryugu materials require to take extra care of vulnerability and terrestrial contamination (i.e., atmospheric water/air, organics) during sample curation, sample transportation and analysis.

Phase 2 curation team "Kochi" was authorized by the steering committee of the the Astromaterial Science Research Group of JAXA in 2017. The team "Kochi" consist of members from the Kochi Institute for Core Sample Research, JAMSTEC (KOCHI), JASRI/SPring-8, UVSOR Synchrotron/National Institutes of Natural Sciences, Institute for Molecular Science, National Institute of Polar Research (NIPR) and Tokyo Metropolitan University. We will conduct an *in-depth* analysis of a few grains by the *state-of-the-art* instruments/techniques, and in parallel with the initial analysis team led by the Hayabusa2 project.

Returned samples from Ryugu will provide an opptunity to investigate the origin and nature of the Solar System as well as the asteroid-meteorite connections, space weathering processes, water-rock interaction, evolution of organics and small asteroidal body formation in the Solar System. For the systematic analysis of the Ryugu grains consisting of hydrous/unhydrous minerals and organics, we have developed universal sample holders (the Okazaki cell, the Kochi grid and the Kochi clamp) for a linkage analysis utilizing FIB, TEM, STXM-NEXAF and NanoSIMS for minimizing terrestrial contaminations and sample lost or breakage [4, 5]. A sample transport vessel (FFTC: facility to facility transfer container) under vacuum or inert gas was also established [5, 6].

We will conduct a coordinated synchrotron based-CT (SPring-8) – 3D-XRD (SPring-8) – FIB (JAMSTEC KOCHI) – STXM (UVSOR Synchrotron) – NanoSIMS (JAMSTEC KOCHI) – TEM (JAMSTEC KOCHI) analysis to obtain complex structure inside of the sample, light element/isotope images to obtain their spatial distributions, speciation of elements: type of bonding, chemical species, redox state and ultra-fine textural observation: mineralogy and crystallography in fine-grained mineral and organic assemblages in few tens to hundreds of the micrometer-scale Ryugu samples. In addition, we recently have installed glove boxes in three institutes of SPring-8, UVSOR Synchrotron and JAMSTEC KOCHI. Most of our experiments including sample preparation, mounting and analysis can be done under the N_2 conditon. Okazaki et al. [7] pointed out that most outer layer materials (amorphous phases, space wethering layer materials) of the Itokawa particles are susceptible to the chemical reaction and decomposition with oxygen and water in the atmosphere. We are expecting that there may be small amount of extraterrestrial water (as hydrous mineral phases) and organics in 100 mg of the Ryugu samples. To prevent these materials from reactions with a terrestrial atmosphere (atmospheric water, oxygen and organics) the anti-terrestrial atmosphere exposure system may help to obtain original characteistics of the Ryugu grains.

We will apply the coordinate analyses to the Antarctic micrometeorites, CM and CI chondrites (the NIPR meteorite collections) as analogues of the Ryugu sample [e.g., 5, 8].

References: [1] Kitazato K. et al. (2019) *Science* 364:272–275. [2] Hiroi T. et al. (2019) *50th LPSC* (LPI Contrib. No. 2132), abstract#1129. [3] Matsuoka et al. (2019) *50th LPSC* (LPI Contrib. No. 2132), abstract#1534. [4] Ohigashi T. (2019) in preparation. [5] Uesugi K. (2019) in preparation. [6] Uesugi M. et al. (2019) this meeting. [7] Okazaki R. et al. (2017) *Space Sci. Rev.* 208:107–124. [8] Ito M. et al. (2018) *Hayabusa symposium 2018*, abstract#30.

POST HYDROTHERMAL ALTERATION PROCESS BEFORE ACCRETION PROCESS: TRACE ELEMENT DISTRIBUTION IN MATRIX FROM A REDUCED CV CHONDRITE

S. Itoh[1] [1]Dept. Earth and Planetary Sciences, Kyoto University (sitoh@kueps.kyoto-u.ac.jp)

Introduction: Carbonaceous chondrites are composed of chondrules, refractory inclusions (Ca-Al-rich inclusions (CAIs), amoeboid olivine aggregates (AOAs)) and matrix. These constituents are believed to preserve information at the time of formation without melting even once after accumulation of the parent body. However, various kinds of carbonaceous chondrites have experienced various hydrothermal alteration effects, although there is a difference in degree before and after accumulation of parent body, and the information at the time of formation has been lost (e.g., [1]). Among them, the matrix, which is one of the major constituents of chondrites, consists of a mixture of fine-grained silicates, metals and oxides filling in between chondrules and CAIs. These matrix particles are small in size and highly porous and highly permeable, so that they are susceptible to alteration process such as water. However, there is no indicator for evaluating the presence or absence of alteration before and after accumulation of the parent body in the whole chondrites. In general, it has been believed that chonderites are brecciated rock but there are no way to estimate the clear boundary for the unit of brecciated crusts. In addition, it is unclear whether the constituent unit of the crust before accumulation is independent of chondrule and CAIs, or composed of chondrules, CAIs and a matrix including matrices. Therefore, in order to estimate the presence or absence of alteration and the constituent size of crust in the matrix of reduced NWA 7865 CV3 chondrite, which is hardly affected by hydrothermal alteration, petrographic studies including major element distribution and trace element distribution were applied.

Experimental procedure: The petrological features were evaluated by combining the main element map by SEM-EDS and trace element maps of LA-ICPMS of ^{25}Mg, ^{27}Al, ^{44}Ca, ^{51}V, ^{52}Cr, ^{57}Fe, ^{60}Ni, ^{88}Sr, ^{140}Ce, ^{208}Pb and ^{238}U.

Results and discussion: We focused on two regions with different Mg-Fe contents in olivine in the matrix. From the comparison of trace element maps, ^{238}U was distributed over a wide range in the Fe-poor region. Phosphate and sulfide were distributed in the Fe-poor matrix. Particularly in the concentrated part of ^{238}U, there were submicron phosphate and ring-shaped hedenbergite of tens of microns. On the other hand, these minerals were absent in the ^{238}U depleted area.

Sulfide and phosphate are distributed in Fe-poor matrix where Uranium is widely distributed, suggesting that the matrix has been experienced aqueous alteration process accompanied by fluid (e.g., [2]). In addition, since the boundary among these two matrices containing uranium and no uranium is clear, it was suggested that the aqueous alteration process accompanying this fluid is before the accumulation of the parent body. Furthermore, the constituent unit of the crust containing the matrix in which Uranium is widely distributed contains chondrules and CAIs, suggesting that it was a few mm crust before accumulation of the parent body. Such post hydrothermal alteration process in chondrites has been also suggested by previous studies (e.g., [3]).

References: [1] Scott E. R. D. and Krot A. N. (2014) Chondrites and their components. In Meteorites and Cosmochemical Processes (ed. A. M. Davis) Vol. 1, Treatise on Geochemistry Second edition, pp. 65-137. Elsevier, Oxford. [2] Brearley A. J. and Krot A. N. (2013) Metasomatism in the early solar system: the record from chondritic meteorites, in Metasomatism and the Chemical Transformation of Rock, Springer, 659-789. [3] Tomeoka K. and Ohnishi I. (2015) Redistribution of chondrules in a carbonaceous chondrite parent body: A model, Geochimica et Cosmochimica Acta, 164, 543-555.

PROPERTIES OF A NEW GROUPLET OF G METAL-RICH CHONDRITES

M. A. Ivanova[1], C. A. Lorenz[1], M. Humayun[3], K. Richter[5], C. M. Corrigan[2], I. A. Franchi[4], A. B. Verchovsky[4], E. V. Korochantseva[1], V. V. Kozlov[6], S. N. Teplyakova[1], Kononkova N. N.[1], and A. V. Korochantsev[1], Vernadsky Institute of Geochemistry and Analytical Chemistry, Moscow 119991, Russia; meteorite2000@mail.ru, [2]National Museum of Natural History, Smithsonian Institution, USA; [3]National High Magnetic Field Laboratory and Department of Earth, Florida State University, USA; [4]Planetary and Space Sciences Research Institute, Open University, UK, [5]Mailcode XI2, NASA - JSC, USA [6]Oxford Instruments OM & Gatan Inc., Moscow, Russia .

Introduction: The metal-rich (MR) chondrites (>20 vol% of Fe,Ni-metal) have attracted a lot of attention recently. MR chondrites include Carbonaceous (C) chondrites (CHs, CBs [e.g., 1-4], CH/CBb chondrite Isheyevo [5], G chondrites (GC), Northwest Africa (NWA) 5492, and Grosvenor Mountains (GRO) 95551 [6] and new ungrouped chondrites, Northwest Africa (NWA) 12379/12273 [7,8]. Here we discuss the main properties of a new grouplet of MR GCs and discuss possible origin of their components based on our comprehensive study of the Sierra Gorda (SG) 009 ungrouped MR chondrite.

Results and Discussion: SG 009 (S1, W2), a new MR chondrite, consists of FeNi-metal (22 -25 vol%), chondrules and their fragments; matrix is absent. Chondrules, up to 2 mm, are PP (predominant), BO, POP, SiO_2-bearing and Al-rich with clear boundaries. The meteorite also contains large (up to 1 cm) chondrule-like clasts. The main minerals of SG 009 are pyroxene, Fe,Ni-metal, and olivine. Accessories are sulfides (troilite and daubreelite), schreibersite, silica, Mg-chromite, anorthite, spinel, and PGE-metal nuggets. Olivine is Fa0.47±0.10, pyroxene is represented by Opx (Fs1.42, Wo0.88, Fe/Mn -2.83), and diopside (Fs1.34, Wo47.32). FeO-rich Opx occurs in some chondrules (Fs9.33-32.48, Wo0.23-4.74). Plagioclase varies in composition: An32.28-95.04. Mesostasis in chondrules is enriched in K_2O (up to 9.18 wt%) and TiO_2 (up to 6.53 wt%); kamacite contains 5.07 wt% of Ni, 0.43 wt% of Co, Co/Ni - 0.09, Si and Cr are below detection limit (<0.03 wt%); taenite has Ni - 32.3 wt%, Co - 0.25 wt%; troilite is enriched in Cr (up to 2.4 wt%); MgO-chromite is almost pure MgO-end member. The average metal composition of SG 009 is a good match to that of the metal in NWA 5492 [6]. However, there are important differences – SG 009 metal shows a wide range of compatible element abundances (Re,Os, Ir, Pt, Ru) which implies that the metal underwent some igneous fractionation . Volatile elements that are not fractionated by igneous processes, Ga and Ge, completely overlap between these two chondrites. The Cu abundances slightly differ, but the average Sn abundances and Ni/Co ratio are identical between the two chondrites. REEs in chondrules show positive anomalies in Ce and Yb which might be cosmochemical in origin and recorded volatilization in a gas rapidly changing its fO_2. Other evidence for a highly reducing environment is provided by subchondritic Nb/Ta ratios in the silicates. We analyzed 6 sulfide grains and found strong enrichment of V, Cr and Nb, confirming that Nb has acted like a chalcophile element and corroborating the evidence of Nb depletion in the silicates due to reduction. We also observed fractionation of the Th/Sc ratio possibly indicating igneous processing in the chondrule precursors [9]. Using the metal, olivine, and orthopyroxene compositions, and assuming a temperature of 1273 K, we calculated $logfO_2 = -18.2$, which relative to the IW buffer is -3.29, indicating highly reduced formation conditions of this material [10]. Oxygen isotopic compositions of SG 009 silicates are between OCs and ECs ($\delta^{17}O$ 3.763, 3.736; $\delta^{18}O$ 6.263, 6.169; $\Delta^{17}O$ 0.506, 0.528 ‰,) similar to other G-chondrites [7]. Average $\delta^{13}C$ (+1.6 ‰) and $\delta^{15}N$ (+14.4 ‰) are in the range of ECs and OCs, respectively [11]; ^{20}Ne and ^{36}Ar contents are 53.6 and 18.2 ($\times 10^{-7}$ cm^3 STP/g), respectively.

Conclusions: The MR-chondrites are a unique phenomenon among chondrites. SG 009 has affinity to two GCs described by [6]. The GC grouplet is characterized by abundant metal, very reduced silicates (like ECs), absence of matrix (like CH-CBs), lack of Si in the metal, and oxygen isotopic compositions between OCs and ECs. However, the metal geochemistry of SG 009 [9] demonstrates igneous origin, and various silicate chondrules and fragments might have igneous precursors unlike for other GCs, but similar to the CBb chondrite Gujba [10]. GCs differ from NWA 12379 and 12273 [7,8], possessing OCs (L/LL) affinities and geochemically and isotopically different from CB and GCs. However, it is still unclear whether the major components of GCs grouplet originate from the same cosmochemical reservoir in the early solar system or formed separately and were mixed together afterwards.

References: [1] Weisberg M. et al., (2001) *Meteoritics & Planetary Science* 36:401-418. [2] Krot A. et al., (2002) *Meteoritics & Planetary Science* 37:1451-1490. [3] Campbell A. et al., (2001) *Geochimica et Cosmochimica Acta* 65:163-180. [4] Ivanova M. and Petaev M. (2015) *Petrology* 23:150–167. [5] Ivanova M. et al. (2008) *Meteoritics and Planetary Science* 43:915-940. [6] Weisberg M. et al. (2015) *Geochimica et Cosmochimica Acta* 167:269-285. [7] Jansen C. et al. (2019) *LPS L*, Abstract #2741. [8] Agee C. et al. (2019) *LPS L*, Abstract #1176. [9] Oulton J. et al. (2016) *Geochimica et Cosmochimica Acta* 177:254-274. [10] Righter K. and Drake, M. (1996). *Icarus*, *124*:513-529. [11] Grady M. M. and Wright I. P. (2003) *Space Sci. Rev*. 106:231-248.

A NEW UNUSUAL BENCUBBINITE (CBa), SIERRA GORDA 013 WITH UNIQUE V-RICH SULFIDES.

M. A. Ivanova[1], C. Ma[2], C. A. Lorenz[1], I. A. Franchi[3], and N. N. Kononkova[1]. [1]Vernadsky Institute of Geochemistry and Analytical Chemistry, Moscow 119991, Russia; meteorite2000@mail.ru, [2]Division of Geological and Planetary Sciences, California Institute of Technology, Pasadena, CA 91125, USA; chi@gps.caltech.edu; [3]Planetary and Space Sciences Research Institute, Open University, Milton Keynes, MK7 6AA, UK; ian.franchi@open.ac.uk.

Introduction: The metal-rich (>20 vol% Fe,Ni-metal) carbonaceous chondrites include CH chondrites, CB chondrites [1] and the Isheyevo CH/CBb chondrite [2]. The CB chondrites are rare and divided into two subgroups based on their petrologic characteristics: CBa (e.g., Bencubbin, Weatherford, Gujba) and CBb (e.g., Hammadah al Hamra (HH) 237 and Queen Alexandra Range (QUE) 94411/94627) [1]. A recently described chondrite, Quebrada Chimborazo (QC) 001 is similar to CBa but unusual in containing shock melt and high pressure mineral phases [3]. Here we present preliminary results of study of unusual CB chondrite from Chile, Sierra Gorda (SG) 013, and describe V-rich sulfides which have not previously been found in the meteorite material.

Results and Discussion: SG 013 was found 300 km from QC 001. It contains two lithologies presented by separated samples of the meteorite. The first lithology is typical for CBs and consists of Fe,Ni-metal nodules (~80 vol%), up to 0.5 cm, BO, CC and POP chondrules, and their fragments up to 0.4 cm, matrix is absent; minerals are olivine, pyroxene, anorthite, Fe,Ni-metal (kamacite only), daubreelite, V-rich sulfides, schreibersite and magnesiochromite. Glassy mesostasis in chondrules is represented by nonstoicheometric anorthite and clynopyroxene. Many chondrule-like objects contain tiny simplectites consisting of chromite enriched in Al and Mg, clinopyroxene and olivine. There is assemblage of daubréelite with chromite. Shock stage of most chondrules is S2, but several fragments have stage S3-4, abundant melt pockets enclosing tiny blebs of Fe,Ni-metal occur.

The second lithology consists of less abundant Fe,Ni-metal (~50 %) and unevenly grained silicates (~50%, olivine, pyroxene, anorthite and chromite) and very rare unclear relic chondrules. Many fractures filled by Fe,Ni-metal and products of Fe,Ni-metal oxidation crosscut the lithology. in the second lithology any sulfides and schreibersite were absent. Unlike the first lithology, in the second lithology Fe,Ni-metal is represented by kamacite and taenite (23 wt% of Ni).

Olivine (Fa2.23), orthopyroxene (Fs3.37), clinopyroxene representing by diopside (Fs1.91, Wo45.74), plagioclase (An 95.78, Ab4.04) in both lithology are typical for CBs. Fe,Ni-metal is not zoned, kamacite contains 6.90 wt% of Ni, 0.39 wt% of Co, 0.16-0.39 wt% of P, magnesiochromite contains up to 15.0 wt% of Al_2O_3, 18.0 wt% of MgO and 7.5 wt% of FeO, having an empirical formula of $(Mg_{0.81}Fe_{0.19})(Cr_{1.38}Al_{0.62})O_4$. Oxygen isotopic compositions of the first lithology are in the range of CBs (‰) ($\delta^{17}O$ -1.889, -1.9; $\delta^{18}O$ 0.65, 0.59; $\Delta^{17}O$ -2.226, -2.206).

The sulfide assemblage in the first lithology is represented by daubréelite $FeCr_2S_4$, V-rich daubréelite enriched in V (up to 2.0 wt%, $Fe(Cr,V)_2S_4$), V-rich brezinaite $(Cr_{2.05}V_{0.62}Fe_{0.33})S_4$ and probably an unknown V,Fe,Cr-rich sulfide presented as tiny mineral phases (< 1 μm) in the V-rich daubrelite (Table 1). All minerals were confirmed by crystal structure using EBSD investigations. Based on the EPMA and EBSD analyses, chemical composition of the unknown V,Fe.Cr-sulfide corresponds to mineral formula (based on 5 S): $(V_{1.55}Fe_{1.52}Cr_{0.92})S_5$, e.g., $(V,Fe,Cr)_4S_5$.

Table 1. Chemical composition (wt%) and formulae units of sulfids from a new bencubbinite (CBa), SG 013.

	S	V	Cr	Fe	Total	S	V	Cr	Fe	Sum
daubreelite	44.65	0.01	35.43	19.92	100.01	4.00	0.00	1.96	1.02	6.98
V-daubreelite	44.09	6.22	29.74	18.54	98.6	4.00	0.36	1.66	0.97	6.98
V-brezinaite	44.14	10.64	36.90	6.27	98.26	4.00	0.62	2.05	0.33	7.00
unknown V-sulfide	43.56	21.61	13.05	21.49	99.71	5.00	1.55	0.92	1.52	8.99

Conclusions: SG 013 is an unusual bencubbinite with affinity to the CBa subtype. Unlike most known CBs it contains two texturally and mineralogically different lithologies and doesn't contain in Fe,Ni-metal any troilite blebs typical for CBs. Similar to QC 001 [3] it records impact event. Probably the second lithology represents slowly crystallized melt. Simlectites from the first lithology may be also a result of melting event. V-rich brezinaite and unknown V,Fe,Cr-sulfide, simplectites and magnesiochromite-daubreelite assemblage have never been described in the CBs chondrite material. V-rich brezinaite and unknown V,Fe,Cr-sulfide were not observed in the meteorite material.

References: [1] Weisberg M. K. et al. (2001) *Meteoritics & Planet. Sci.*, 36, 401–418. [2] Ivanova M. et al. (2008) *Meteoritics and Planetary Science* 43:915-940. [3] Koch T. E. et al. (2016) *LPS XLVII*, Abstract #1968.

SHOCK METAMORPHISM OF THE NEW FALL ORDINARY CHONDRITE MANGUI IN CHINA

J. L. Ji[1], S. Hu[1], Y. T. Lin[1], Q. Zhou[2], Y. Xiao[2], N. Imae[3] and M. Kimura[3]

[1]Institute of Geology and Geophysics, Chinese Academy of Sciences, Beijing 100029, China. E-mail: ji-jianglong@mail.iggcas.ac.cn. [2]National Astronomical Observatories, Chinese Academy of Sciences, Beijing 100101, China. [3]National Institute of Polar Research, Tokyo 190-8518, Japan.

Introduction: The Mangui meteorite is the newest meteorite fall in Yunnan, China on June 1, 2018. More than 500 fragments have been collected in a total mass of ~50 kg along the projectile area of about 20 km^2 [1]. Mangui is classified as a L6 chondrite and its shock stage is S5 [1]. Here we report the progress on the high-pressure polymorphs from Mangui to constrain the P-T-t history of the shock processes for the parent body.

Experimental Methods: Four polished sections were studied in this work. The petrography was observed by Zeiss-Supra55 SEM at the National Astronomical Observatories of the Chinese Academy of Sciences (NAOC). The mineral chemistry was determined by JEOL JXA-8230 EPMA at NAOC and the Institute of Geology and Geophysics, Chinese Academy of Sciences (IGGCAS). Raman spectra was acquired by Renishaw inVia-Reflex Micro-Raman Spectrometer at the Technical Institute of Physics and Chemistry, Chinese Academy of Sciences. The X-ray diffraction data was obtained by using the X-ray diffractometer (XRD, SmartLab, RIGAKU) at the National Institute of Polar Research. The preparation of TEM samples by Zeiss Auriga Compact focused ion beam (FIB) system at IGGCAS. The structural characterization of minerals was analyzed by JEM-ARM200F TEM at the Institute of Physics Chinese Academy of Sciences.

Results and Discussions: Mangui has a black fusion crust and was highly shocked as the presence of shock melt veins and pockets in the specimen. Mangui is mainly composed of olivine, pyroxene, plagioclase, Fe-Ni metal and troilite, with minor phosphates and chromite. The chemical compositions of olivine ($Fa_{25.1\pm0.3}$, n=71), low-Ca pyroxene ($Fs_{21.1\pm0.3}Wo_{1.5\pm0.2}$, n=58) and plagioclase ($Ab_{84.1\pm0.7}Or_{7.3\pm0.4}$, n=49) are homogeneous in the host rock [1]. The peak of olivine 130 gives 2 theta = 32.1116º and the FWHM = 0.1639 by the measurement of XRD.

Two high pressure polymorphs, jadeite and majorite, have been found in the shock melt veins (SMV) and pockets. Jadeite is the major high-pressure polymorph in the SMV and pockets with granular morphology similar to the texture of Chelyabinsk [2], coexisting with maskelynite. Jadeite varies from 2 to 20 µm in grain sizes, and has strong Raman peaks at 698 and 1035 cm^{-1} as well as some minor peaks at 205, 376 and 990 cm^{-1}. The analysis of TEM shows that the subhedral jadeite grains coexisted with maskelynite with hundreds of nanometre. In one location, needle-shaped grains, probably stishovite or silica glass, were found in maskelynite that is coexisting with jadeite. The needle-shaped silica phases have similar texture to stishovite observed in some martian meteorites [3-4], indicating that they recrystallized from melt rather than dissociated from plagioclase. However, we did not detect any Raman peaks of coesite, stishovite, and higher pressure silica polymorph from these needle-shaped grains, suggesting that early formed high-pressure silica polymorphs might have been inverted to glass during decompression.

Majorite coexisted with a jadeite assemblage, occurring as inclusions enclosed by jadeite and an overgrowth layer of the jadeite assemblage. Micrometer-sized polycrystals of majorite enclosed by jadeite has subhedral textures and mainly located around the border of the inclusion in where the central area is componented of olivine, pyroxene, and Fe-Ni metal. The layered mjaorite has similar textures to that enclosed by jadeite. Both types of occurrences of majorite have a strong Raman peak at 930 cm^{-1}. Moreover, micrometer-sized recrystallized pyroxene in the matrix surrounding to the jadeite assemblage has typical Raman peaks of pyroxene as well as a minor peak at ~930 cm^{-1}, indicating the presence of majorite. The morphology and textures of majortie are consistent with the scenario that majorite crystallized from the melt instead of solid-solid transformation.

The presence of jadeite and majorite in Mangui indicate that the parent body experienced strong shock metamorphism in good consistent with the XRD measurement [6]. The shock pressure and temperature should be 17–20 GPa and 1900-2000 °C respectively in terms of the coexistence of jadeite and majorite [2,5]. However, no ringwoodite and other high-pressure polymorphs were detected in the SMV, probably indicating that they were converted to room pressure phase during decompression or did not formed in the shock processes.

References: [1] J. L. Ji. et al. (2019) *Chinese Science Bulletin* 64:579–587. [2] Ozawa S. et al. (2014) *Scientific Reports* 4: 5033. [3] Chennaoui Aoudjehane H. et al. (2005) *Meteoritics & Planetary Science* 40:967–979. [4] El Goresy A. et al. (2013) *Geochimica et Cosmochimica Acta* 101:233-262. [5] Tomioka N. et al. (2016) *Advanced Science* 2: 1–5. [6] Imae N. et al. (2019) *Meteoritics & Planetary Science* 54:919–937.

RECENT DEVELOPMENTS IN ELECTRON TOMOGRAPHY AND FIB/SEM SERIAL SECTIONING for 3D MORPHOLOGICAL ANALYSIS IN POLYMER COMPOSITES.

H. Jinnai[1]
[1] Institute of Multidisciplinary Research for Advanced Materials (IMRAM), Tohoku University, 2-1-1, Katahira, Aoba-ku, Sendai, Miyagi 980-8577, JAPAN. email: hiroshi.jinnai.d4@tohoku.ac.jp

Introduction: In order to satisfy the increasing demands for high-performance polymeric materials, polymers are often mixed with inorganic or metal components. In such composite materials, often called polymer composites, the polymers usually constitute the matrix whereas the metal or inorganic compounds are mixed to achieve certain additional properties, such as mechanical, electrical, or optical properties. Three-dimensional (3D) structures of such composite materials are essential to understand their properties.

Electron tomography [1], alternatively called 3D TEM, has been used not only to visualize the morphologies but also to predict properties together with computer simulation techniques [2]. A forcused ion beam (FIB) equipped with scanning electron microscopy (SEM) has also been used to investigate 3D morphologies of polymer composites. While electron tomography has higher resolution than FIB/SEM serial sectioning, FIB/SEM for short, observable volume is much larger for FIB/SEM compared with electron tomography.

3D morphological observations under stretching in nanometer scale resolution: Recent main interest in electron microscopy is to go beyond the 3D imaging, adding one more dimension. In polymer composites, deformation can be a key "dimension". Namely, it is particularly important to observe *in-situ* morphologies under (uniaxial) stretching. Recently, we have developed a 3D tomography holder for in-situ tensile deformation for polymeric materials in transmission electron microscope (TEM) [3]. Unlike the existing stretching holders, the newly-developed holder has some unique futures: the drifting of field of view for TEM observations becomes minimum because both ends of (microtomed) thin sections are stretched simultaneously at the same stretching rate. Another essential feature of the newly-developed holder is that we can achieve much larger strain can be applied to the specimen than the predecessor holder does: the largest strain achievable with this tensile deformation holder is, in principle, about 50 (when the initial specimen length is 20 μm). Moreover, the tensile holder allows us to tilt the specimen up to 60 ～ 75°for tomographic reconstruction.

The tensile deformation tomographic holder was used to observe deformation processes of rubber composite, in which nano-scale fillers dispersed in polymeric matrix. The morphological changes of rubber composites as well as the fracture processes under stretching were directly observed at nanometer scale. It was successfully observed that the aggregates were deformed under extension, and then the nano-voids formed around the aggregates.

Super-resolution for asymmetric resolution of FIB-SEM using AI with deep learning: In FIB-SEM, the specimen surface is stripped by an ion beam and imaged by an SEM installed orthogonally to the FIB. The lateral resolution is governed by the SEM, while the depth resolution, i.e., the FIB milling direction, is determined by the thickness of the stripped thin layer. Thus, in most cases, the lateral resolution is superior to the depth resolution. In polymeric systems, the depth resolution is typically on the order of 10 nm (most likely 20 nm), so the application of FIB/SEM is limited to morphologies with rather large characteristic length. [4].

Here, a new approach based on an image-processing or deep-learning-based method for super-resolution of 3D images with such *asymmetric resolution* is proposed [5]. In this way, it became possible to restore the depth resolution to achieve symmetric resolution. It was found that this this new methodology was effective not only to restore the depth resolution but also to considerably reduce the observation time of polymer composite materials. Details will be given at the conference time.

References:
[1] Jinnai H., Spontak R. J. and T. Nishi (2010) *Macromolecules*, 43(4): 1675-1688.
[2] Akutagawa K., Yamaguchi K., Yamamoto A., Heguri H., Jinnai H. and Shinbori Y. (2008) *Rubber Chem. Technol.*, 81(2), 182-189.
[3] Higuchi T., Gondo T., Miyazaki H., Kumagai A., Akutagawa K. and Jinnai H., *Microscopy*, 67(5), 296-300.
[4] Kato M., Ito T., Aoyama Y., Sawa K., Kaneko T., Kawase N. and Jinnai H. (2007) *J. Polym. Sci. Part B: Polym. Phys.,* 45(6), 677-683.
[5] Hagita K., Higuchi T. and Jinnai H. (2018) *Sci. Rep.*, 8, 5877.

14C STUDIES OF SHADOWED LUNAR SOIL AT APOLLO 17.

A. J. T. Jull[1,2], L. Cheng[1], and G. S. Burr[3], [1]Department of Geosciences, University of Arizona, Tucson, AZ 85721 (jull@email.arizona.edu), [2]Institute for Nuclear Research, Hungarian Academy of Sciences, 4026 Debrecen, Hungary. [3]National Taiwan University, Taipei, Taiwan.

Introduction: During the Apollo 17 mission, astronauts sampled a series of soil samples adjacent to a large boulder (5x4x3m, boulder no.4). One soil sample (76240) was sampled as it was thought to be permanently shadowed location, so the sample should be shielded from direct solar radiation [1,2]. Two samples from soils outside the permanently-shaded area were also collected (76260 and 76280). These were skim samples from a depth of up to ~2cm. A further soil 76320 was collected from the top of an adjacent boulder. These samples have recently become of renewed interest since they are in the suite of samples, indeed some small portions of 76240 were stored frozen by NASA. Our measurements were made some considerable time ago, but this is our first report of these results. We also review some related ^{14}C results from other Apollo 17 samples.

Permanently-shadowed soil: Keith et al. [3] and Yokoyama et al. [4] measured ^{22}Na in sample 76240 and found it to be apparently low in ^{22}Na (41±3 dpm/kg) suggesting shielding by the adjacent boulder and similarly, and ^{26}Al at 156±14 dpm/kg was less than full exposure to solar (SCR) and galactic cosmic rays (GCR). Similarly, Rancitelli et al. [5] measured a similar level of ^{26}Al (151±6 dpm/kg), but below the expected value for a 2π exposure on the Moon if there was no shielding. However, sample 76261, which is outside the shaded area showed higher levels of ^{22}Na but similar levels of ^{26}Al, still below expected levels for a 2π flat surface [5]. This is due to partial shielding of the sky to GCR as well as SCR. Rancitelli et al. [5] estimated the exposure age of soil 76240 as ~0.5Ma, although measurements of the cosmogenic and track exposure ages of sample (76315) removed the boulder gave ages of ~22Ma [6,7,8].

^{14}C Measurements: We extracted the samples for cosmogenic ^{14}C at the University of Arizona using previously reported procedures [9,10]. Briefly, samples were preheated to 500°C in air for one hour (to remove any terrestrial sources) and then placed in an alumina crucible with Fe chips as a combustion accelerant. The sample is heated in a RF furnace to melting in a flow of oxygen. The CO_2 is collected from the gas stream, measured volumetrically and reduced to graphite for ^{14}C measurement by accelerator mass spectrometry (AMS). Results obtained were 14.7±0.5 dpmkg (76241,6), 22.8±0.9 dpm/kg (76261,1) and 17.4±0.5 dpmkg (76281,1). Soil 76321,105 which was taken from the top of an adjacent boulder gave 26.0±0.5 dpm/kg and soil 10084,60 for comparison was 30.1±0.7 dpm/kg.

Discussion: We can compare the results to the expected GCR and SCR concentrations in lunar rocks and soils [9]. An average value of about 32-33 dpm/kg ^{14}C is expected for a soil averaging over 0-2cm (the depth of collection of these samples) and ~29 dpm/kg from GCR alone, based on scaling from levels in lunar cores, meteorites and soil 10084 [9,10]. We conclude from our results that all the three samples at station 6 are undersaturated for ^{14}C. A simple geometric model suggests that these samples should be exposed to about 1.55 steradians (78%) of the sky. If we take a baseline of 30 dpm/kg, this would be ~49%, 76% and 58% for samples, 76241, 76261 and 76281 respectively. Our estimate for 76241 may underestimate the amount of shielding.

Is the shaded area stable? We also undertook a simple geometric calculation of the stability of the "shaded area". We determined that the shadowed area should not move by than about 17cm over the time of precession of the lunar orbit, so the shaded area shouldn't reach 76261 (see picture in [1]). Hence, the area should be extremely stable as a recorder of lunar shaded temperatures as proposed by Durrani et al. [2]. Further studies on other cosmogenic nuclides will be useful to better understand the exposure history of these and other similar samples.

References: [1] Meyer C. (2009) 76240 Shadowed Soil. Lunar Sample Compendium. http://curator.jsc.nasa.gov/lunar/lsc/76240.pdf. [2] Durrani S. A. et al. (1976) Proc. Lunar Sci. Conf. 7th. 1157-1172. [3] Keith J.E. et al. (1974) Proc. Lunar Sci. Conf. 5th p.2121-2138. [4] Yokyoyama Y. et al. (1974) Proc. Lunar Planet. Sci. Conf 4th. p. 2209-2227. [5] Rancitelli L. A. et al. (1974) Proc. Lunar Sci. Conf. 5th. p. 2185-2203. [6] Meyer C. (2008) Impact Melt Breccia 76315. Lunar Sample Compendium. http://curator.jsc.nasa.gov/lunar/lsc/76315.pdf. [7] Crozaz G. et al. 1974. Proc. Lunar Sci. Conf. 5th. p. 2475-2499. [8] Arvidson R. et al. (1975) The Moon 13: 259-276. [9] Jull A. J. T. et al. (1998) Geochim. Cosmochim. Acta 62, 3025-3036. [10] Jull A. J. T. et al. (2010) Meteorit. Planet. Sci. 45, 1271-1283.

CHANGES IN REFLECTANCE SPECTRA OF A CM2 CARBONACEOUS CHONDRITE: SIMULATION OF SPACE WEATHERING BY ULTRAVIOLET IRRADIATION.

H. Kaiden[1,2], T. Hiroi[3], K. Misawa[1,2], H. Tanaka[4], S. Sasaki[4], K. M. Robertson[3], R. E. Milliken[3], H. Masai[5], J. Terao[5], [1]Geoscience Group, National Institute of Polar Research, Tokyo 190-8518, Japan (kaiden@nipr.ac.jp), [2]Department of Polar Science, SOKENDAI (The Graduate University for Advanced Studies), Tokyo 190-8518, Japan, [3]Department of Earth, Environmental and Planetary Sciences, Brown University, Providence, RI 02912, USA, [4]Department of Earth and Space Science, Osaka University, Osaka 560-0043, Japan, [5]Department of Basic Science, The University of Tokyo, Tokyo 153-8902, Japan.

Introduction: Space weathering is the alteration of the regolith of airless bodies and causes chemical, physical, and optical changes of the regolith. Solar wind bombardment and micrometeorite impacts are considered major causes of space weathering, and thus various laboratory experiments have been conducted to simulate such causes [e.g., 1]. For example, ion beam [2] and pulse-laser [3] irradiation experiments were carried out to simulate solar wind bombardment and micrometeorite impacts, respectively. It is important, however, to consider other causes of space weathering to fully understand its processes and effects on materials on asteroid surfaces. In our previous study [4], we obtained spectral changes of ultraviolet (UV)-irradiated olivine and the Murchison CM2 carbonaceous chondrite, which suggests that space weathering could occur by UV light from the Sun. In this study, UV irradiation experiments on another CM2 carbonaceous chondrite were performed to further investigate possible mechanisms of space weathering on asteroid surfaces.

Material and Methods: A chip of Meteorite Hills (MET) 00630 was used for this experiments. MET 00630 is classified as a CM2 carbonaceous chondrite [5], which is one of the proposed compositional analogs to asteroids 162173 Ryugu [6] and 101955 Bennu [7]. Experimental procedures were the same as our previous study [4] except for the form of the sample. The chip of MET 00630 was placed in a vacuum chamber ($\sim 10^{-4}$ Pa) and irradiated with focused (5.0 mm in diameter) UV light in the wavelength range of 250–385 nm emitted from a 300 W xenon arc lamp housed in the Asahi Spectra MAX-303 at the University of Tokyo. The duration of UV irradiation was 312 and 624 hours. The duration of UV irradiation for 312 hours with the xenon light source is estimated to be equivalent to that for 2–3 years with the Sun at a distance of 1 AU. Bidirectional UV–visible–near-infrared (VNIR) diffuse reflectance spectra of the unirradiated and the irradiated samples were obtained using a Bunko Keiki DRS-25 UV-VNIR spectrometer at Osaka University.

Results and Discussion: Reflectance spectra of the MET 00630 chip sample before and after UV irradiation were compared. The spectra became brighter with increasing the duration of UV irradiation. The spectral changes were inconsistent with those of UV-irradiated olivine and Murchison pellet samples obtained by our previous study [4], in which the spectra became darker with increasing the duration of UV irradiation. The timescale for the spectral changes corresponds to the order of years of UV irradiation by the Sun at 1 AU. Although we still need to investigate and explain the mechanisms of the spectral changes by UV irradiation, our results that space weathering by UV light could occur in the order of years would be applicable to interpreting the spectroscopic data obtained by Hayabusa2 for Ryugu and by OSIRIS-REx for Bennu.

References: [1] Bennett C. J. et al. (2013) *Chemical Reviews* 113: 9086–9150. [2] Loeffler M. J. et al. (2009) *Journal of Geophysical Research* 114: E03003. [3] Sasaki S. et al. (2001) *Nature* 410: 555–557. [4] Kaiden et al. (2019) *LPS L*, Abstract #2630. [5] Connolly, Jr. H. C. et al. (2007) *Meteoritics & Planetary Science* 43: 571–632. [6] Kitazato K. et al. (2019) *Science* 364: 272–275. [7] Hamilton V. E. et al. (2019) *Nature Astronomy* 3: 332–340.

CRYSTALLIZATION OF TYPE B CAI MELT IN LOW-PRESSURE HYDROGEN GAS AND IMPLICATIONS FOR FORMATION CONDITIONS OF IGNEOUS CAIs.

M. Kamibayashi[1], D. Yamamoto[2], S. Tachibana[1,2], and H. Yurimoto[2,3]
[1]Department of Earth and Planetary Science, The University of Tokyo (michiru@eps.s.u-tokyo.ac.jp),
[2]Institute of Space and Astronautical Science, JAXA, [3]Department of Natural History Sciences, Hokkaido University.

Introduction: CAIs are the oldest objects formed in the early Solar System. Chemical and petrological characteristics observed in some CAIs show that they formed through high-temperature processes such as melting and evaporation, followed by crystallization. Many laboratory and theoretical studies have discussed evaporation and crystallization of CAI melts (e.g., [1-4]), but crystallization of CAIs in the presence of nebula-like low pressure hydrogen gas, where evaporation and crystallization take place simultaneously, has not yet been fully understood. In this study, crystallization experiments of type B CAI-composition melts at low hydrogen pressures were conducted to investigate the effect of evaporation during crystallization of type B CAIs and to constrain the formation conditions of type B CAIs.

Experiments: The starting material was prepared by mixing SiO_2, TiO_2, Al_2O_3, MgO, and $CaCO_3$ powders to make a composition named CAIχ. This is a composition on the condensation trajectory of [4] and a possible precursor for type B1 CAIs. Premelted glassy spherical samples on Ir wire loop (2.5 mm in diameter) were used as starting materials. The experiments were conducted at Hokkaido University using a vacuum furnace equipped with a hydrogen gas flow system. Cooling experiments were conducted from 1420°C to 1120–1277°C at controlled cooling rates of 5–50°C/hr and under 3 different pressures (P_{H2}=10, 1, 0.1 Pa) to examine the pressure dependence of compositional and textural change. All the samples were quenched after each run. Run products were weighed and mounted into epoxy resin and then polished to expose the cross section of the samples. Textural observation and quantitative analysis were conducted by FE-SEM (JEOL JSM-7000F) with EDS at Hokkaido University.

Results and discussions: All the run products showed the compositional change due to evaporation of mainly MgO and SiO_2 components, and their measured bulk compositions were within the compositional field of type B CAIs. Weight losses of the samples indicated that the degree of evaporation increases at a higher P_{H2} or with a slower cooling rate. However, the evaporative loss at higher P_{H2} is less than expected from the lower P_{H2} experiment considering that the evaporation rate is proportional to the square root of P_{H2} [5]. In the samples evaporated at $P_{H2} = 10$ Pa, their outer regions are relatively enriched in melilite, as observed in natural type B1 CAIs, compared to the samples heated at P_{H2} of 1 and 0.1 Pa. The compositional zoning of the melilite near the sample rim (melt droplet surface) shows that it becomes Mg-rich toward the inside, suggesting that these melilites crystallized inward from the melt droplet surface. This could be attributed to the difference in P_{H2} dependence of evaporation rate and elemental diffusion rate in the melt; evaporation is enhanced by hydrogen, while diffusion is not. At higher P_{H2} (i.e., 10 Pa), evaporation could occur faster than diffusive homogenization of the melt, resulting in effective crystallization of melilite near the melt droplet surface enriched in Ca and Al. The crystallization of melilite at the droplet surface prevents further evaporation of the melt, which explains the lower degree of evaporation at 10 Pa than expected. The present experiments suggest that type B1 CAIs with melilite rim formed at P_{H2} of ~10 Pa or higher, while type B2 CAIs without melilite mantle formed at <10 Pa, which is consistent with the prediction by [3]. The fluctuation of disk gas pressure may have been responsible for the formation of type B1 and B2 CAIs.

References: [1] Stolper, E. and Paque, J. M. (1986) *Geochimica et Cosmochimica Acta* 50: 1785–1806. [2] Richter, F. M. et al. (2002) *Geochimica et Cosmochimica Acta* 66: 521–540. [3] Mendybaev, R. A. et al. (2006) *Geochimica et Cosmochimica Acta* 70: 2622–2642. [4] Grossman, L. et al. (2002) *Geochimica et Cosmochimica Acta* 66: 145–161. [5] Kamibayashi, M. et al. (2018). *Lunar and Planetary Science Conference*. Vol. 49 #2432.

SHOCK METAMORPHIC DEGREE OF EURITES BASED ON THE TEXTUAL AND XRD ANALYSES.

R. Kanemaru[1], N. Imae[1, 2], A. Yamaguchi[1, 2] and H. Nishido[3], [1]Department of Polar Science, School of Multidisciplinary Science, The Graduate University for Advanced Studies (SOKENDAI), Tokyo 190- 8518, Japan (kanemaru.rei@nipr.ac.jp), [2]National Institute of Polar Research, Tokyo 190-8518, Japan, [3]Okayama University of Science, Okayama 700-005, Japan.

Introduction: Most of the eucrites are considered to have experienced shock metamorphism after their solidification. The evidence of the shock metamorphism in eucrites is recognized from the petrographic textures. However, the systematical classification of shock degrees for eucrites has not been established. Recently, Imae et al. [1] used X-ray diffraction (XRD) technique to the semi-quantitative determination of the shock stage of ordinary chondrites. We applied this method for 13 basaltic and 3 cumulate eucrites. We recently defined the shock degrees of studied eucrites from A to D by the petrographic and mineralogical features of thin sections [2]. The criterion is similar to the shock stages of enstatite chondrites [3] and other achondrites [4]. The comparative study of the petrographic and XRD data can provides better interpretations for shock metamorphism on the eucrite parent body (probably asteroid 4 Vesta). We thus further examined the features more quantitatively in the present study.

Measurement methods and samples: We performed the X-ray measurements by an X-ray difractometer, SmartLab (RIGAKU) at the National Institute of Polar Research (NIPR), on the condition of Cu Kα with 40 kV and 40 mA through the slit of 10 x 5 mm in size with the divergence angle of $(1/6)°$. The measured 2θ range was 8-75°. We performed petrological and mineralogical studies using an optical microscope, a field emission scanning electron microscope (FE-SEM: JEOL JSM-7100) with an energy dispersive spectrometer (EDS) (Oxford AZtec Energy) and cathodoluminescence system (GATAN Chroma CL), an electron probe microanalyzer (EPMA: JEOL JXA-8200), and a micro-Raman spectroscopy (JASCO NRS-1000), at NIPR. For identification of maskelynite or plagioclase, we also used a luminoscope (ELM-3) at the Okayama University of Science.

Results: Agoult, EET 90020 and Moama, are unbrecciated eucrite, showing sharp optical extinction of plagioclase and pyroxenes. These eucrites do not have any shock textures (which is defined shock degree A). Juvinas and Y-791195 are recrystallized breccias showing a mosaic texture (shock degree B). Pyroxene and plagioclase in Camel Donga, Millbillillie, Stannern, NWA 5356, Y-792510 and Y 983366 show weak undulatory extinction and mosaic texture (shock degree B). A-881747, Cachari, Y-790266, Y 980433 have maskelynite with various modal abundance (< 40vol%) (shock degree C). Most plagioclase (>70-80 vol.%) in A-87272 is converted to maskelynite (shock degree D).

XRD patterns mainly consist of diffractions of plagioclase, pigeonite, and augite. The macro XRD data has several correlations for shock degrees. The full width at half maximum (FWHM) values (for both average and total) shows a positive correlation for the shock degrees. The XRD peaks become weaker and broader by increasing the shock degrees. On the other hand, the number of peak in the XRD pattern shows a negative correlation for the increase of shock degrees. Unshocked eucrites, Agoult, EET 90020, and Moama, show the total number of the peak as 163, 159, 148, respectively. Shocked eucrites, A-87272, Cachari, and Y 980433, show the total number of the peak at 35, 70, 64, respectively. The decrease of the diffraction peak is remarkable for plagioclase rather than pyroxene. Based on the Williamson–Hall plot [5] of pigeonite, the lattice strain value positively correlate with the shock degrees. The specific peaks of plagioclase (especially -202) show the decreasing peak intensity and increasing FWHM values for the increase shock degree. The pyroxene peaks (pigeonite 310 and augite -311) show a positive correlation between the FWHM values and shock degrees, whereas there is no correlation between the peak intensities and shock degrees.

Discussion: The shock degrees from A to D in the eucrites studied here are cleary distinguished from the averaged FWHM value (total FWHM value / the total number of peak). The averaged FWHM value is composed of two correlations, 1) a positive correlation between the FWHM values (of specific peaks) and shock degrees and 2) a negative correlation between the total number of the peaks in diffraction patterns and shock degrees. The broadening of diffraction peak is observed in plagioclase and pyroxene. A positive correlation between the lattice strain values and shock degrees indicates that the increase of FWHM value is due to the increase of disturbed crystal lattice. The decrease of the total peak number is mainly due to the maskelynization of plagioclase. In particular, most of the plagioclase peaks in A-87272, the strongest shocked sample (D) studied here, have disappeared. Instead, the shock metamorphism produces the strain in pyroxenes. We plan to examine the shock pressure from the lattice strain value.

References: [1] Imae N. et al. (2019) *Meteoritics & Planetary Science* 54:919-937. [2] Kanemaru R. et al. (2019) *50th LPSC*, abstract # 2321. [3] Rubin A. et al. (1997) *Geochimica et Cosmochimica Acta*, 61, 847-858. [4] Bischoff A. and Stöffler D. (1992) *European Journal of Mineralogy*, 4, 707-755. [5] Williamson G. K. and Hall W. H. (1953) A*cta Metallurgica* 1:22–31.

TIN BIDER IMPACT STRUCTURE (ALGERIA): SHOCK METAMORPHISM IN ALBIAN SANDSTONES.

F. Kassab[1], L. Ferrière[2], and D. Belhai[1], [1]University of Sciences and Technologies Houari Boumediene, Algeria (kassabfazia@gmail.com), [2]Natural History Museum, Burgring 7, A-1010 Vienna, Austria.

Introduction: The Tin Bider impact structure, centered at 27°36' N and 05°07' E, is 6 km in diameter, and is the largest complex impact crater known in Algeria. It excavates sedimentary rocks, mainly Albian sandstones and Upper Senonian limestones. The age of the impact event is constrained to <65 Ma by stratigraphy, the youngest formation affected by the impact being ~65 Myr old limestones. The complex structure of Tin Bider is characterized by a central uplift where sandstones are exposed [1]. A few shocked quartz grains (i.e., with "planar elements") were described by Lambert et al. [1] but no detailed information on their nature (i.e., it is not clear if they are planar fractures (PFs) or planar deformation features (PDFs)) and orientations is presented (i.e., a few orientations are reported in a table in [1] but it is not clear if they were properly indexed or if only the angular relation to the c-axis was used), and the microphotographs are also not very convincing.

We report here on petrographic investigations of a few sandstone samples from the central uplift in which we were able to characterize shock metamorphic features in quartz grains.

Methods: A total of 11 polished thin sections were prepared and carefully searched for shock metamorphic features in quartz grains, such as PDFs, using an optical microscope. Considering the rarity of the grains showing PDFs, they were systematically marked (using a marker pen directly on the section) to be able to easily find them again under the Universal stage (U-stage). The crystallographic orientations of PDFs in quartz grains [e.g., 2, 3] were measured using a four-axis U-stage [e.g., 4, 5] at the Department of Lithospheric Research, University of Vienna. PDFs were indexed by hand using the new version of the stereographic projection template (NSPT) by Ferrière et al. [6].

Results and Discussion: Optical microscope investigations show that most quartz grains do not exhibit obvious shock features even most of the grains show undulose extinction. Rare grains with PDFs were detected during our survey, with only 1 or 2 sets (as seen under the U-stage). PDFs are mostly decorated with fluid inclusions indicating that the originally amorphous material in PDFs was recrystallized and that this recrystallization was water-assisted [2, 3, 7]. The investigated PDFs are mainly oriented parallel to $\pi\{10\bar{1}2\}$ and $\omega\{10\bar{1}3\}$, but also to $\xi\{11\bar{2}2\}$ and $x\{5\bar{1}\bar{6}1\}$, all typical PDFs orientations [e.g., 2, 6]. Planes parallel to the $r\{10\bar{1}1\}$, $m\{10\bar{1}0\}$, $s\{11\bar{2}1\}$, and $a\{10\bar{1}4\}$ orientations also occur but in lower proportions. A few quartz grains with one set of PDFs are oriented parallel to $c(0001)$, corresponding to mechanical Brazil twins [8]. No PFs, neither feather features, were detected in the investigated thin sections. Also, no diaplectic glass or melted grains were detected during our investigations.

Conclusion: We report here for the first time on the occurrence of PDFs oriented parallel to $c(0001)$, corresponding to Brazil twins, in samples from Tin Bider. The extremely low abundance of PDFs in quartz in the investigated samples is possibly due to the erosion of the structure. Additional samples will be collected and investigated to confirm the preliminary observations presented here and to constrain shock pressures recorded by samples outcropping at the central uplift of the Tin Bider structure.

References: [1] Lambert Ph. et al. (1981) *Meteoritics* 16:203–227. [2] Stöffler D. and Langenhorst F. (1994) *Meteoritics & Planetary Science* 29:155–181. [3] Grieve R. A. F et al. (1996) *Meteoritics & Planetary Science* 31:6–35. [4] Emmons R. C. (1943) *Geological Society of America Memoir* 8, 205 p. [5] Engelhardt W. V. and Bertsch W. (1969) *Contributions to Mineralogy and Petrology* 20:203–234. [6] Ferrière L. et al. (2009) *Meteoritics & Planetary Science* 44:925–940. [7] Leroux H. (2005) *Meteoritics & Planetary Science* 40:1347–1352. [8] Goltrant O. (1991) *Earth and Planetary Science Letters* 106:103–115.

Polycyclic aromatic hydrocarbons and aliphatic hydrocarbons in Jbilet Winselwan carbonaceous CM chondrite, a possible analog of asteroid Ryugu's surface.

H. Kato[1] and H. Yabuta[1], [1]Department of Earth and Planetary Systems Science, Hiroshima University (Kagamiyama 1-3-1, Higashi-Hiroshima 739-8526, Japan. E-mail: m180489@hiroshima-u.ac.jp).

Introduction: On June 27, 2018, Hayabusa2 spacecraft arrived at the C-type asteroid Ryugu [1]. The surface of Ryugu is thought to have experienced thermal metamorphism, according to the remote sensing observations [2, 3]. Therefore, it is important to investigate the chemical compositions of thermally metamorphosed CM chondrites for understanding the surface process of asteroid Ryugu. Although the extents of thermal metamorphism of CM chondrites have been evaluated by mineralogical compositions [4] and elemental and molecular compositions of insoluble organic matter (IOM) [5, 6], the estimated temperature varies widely. On the other hand, soluble organic molecules from the thermally metamorphosed CM chondrites have not been quantified or below detection [7], and there has been no study which evaluated thermal metamorphism based on the compositions of soluble organic molecules. Therefore, in this study, we analyzed polycyclic aromatic hydrocarbons (PAHs) and aliphatic hydrocarbons in Jbilet Winselwan CM chondrite, which is a thermally metamorphosed CM chondrite with highly brecciated and partially shocked lithologies [8] and show similar reflectance spectrum to that of asteroid Ryugu [2], for precise evaluation of parent body thermal metamorphism. The relative abundances of the hydrocarbons were compared with those of Murray CM chondrite.

Samples and Methods: Powdered samples of Jbilet Winselwan meteorite and Murray meteorite (0.2-0.4g) were extracted with dichloromethane/methanol (9:1) by sonication. The extracts were applied to a silica gel column. From the column, aliphatic hydrocarbons were eluated with hexane and then PAHs were eluated with dichloromethane. The hexane and dichloromethane eluates were concentrated to 100 μl individually under a nitrogen flow for analysis by a gas chromatography coupled with mass spectrometry (GC-MS). Identification and quantification of compounds were made by comparison of peak retention times on mass chromatograms and mass spectra, and peak areas, respectively, with those of standard compounds. For compounds without standard compounds, identification was made by comparison of mass spectra with library data.

Results and discussion: Total concentration of PAHs from Jbilet Winselwan meteorite (0.05 μg/g meteorite) was 1000 times lower than those from Murray meteorite (62.0 μg/g meteorite). Di- and trimethylnaphthalenes, fluorene, phenanthrene (PHE), pyrene (PYR), fluoranthene (FLR), methylbiphenyl (0.003-0.039 μg/g meteorite) were identified from Jbilet Winselwan, while low molecular weight PAHs, such as naphthalene, methylnaphthalene, and acenaphthene, were not detected. PAHs with high volatility in Jbilet Winselwan meteorite were probably lost or involved in further aromatization during thermal metamorphism. On the other hand, the ratios of dimethylnaphthalene (DMN) isomers ([2.6-DMN + 2.7-DMN]/1,5-DMN) and FLR to PYR were similar between Jbilet Winselwan and Murray meteorites, indicating that Jbilet Winselwan meteorite experienced a mild degree of thermal metamorphism. According to the shock experiments of PAHs, relative amounts of PHE, FLR, and PYR are significantly reduced to one hundredth under the pressure of 25 GPa [9], while the ratio of FLR to PYR is not changed by impact [10]. The molecular and isomer compositions of PAHs in Jbilet Winselwan meteorite may have resulted by impact pressure higher than 25 GPa.

Total concentration of *n*-alkanes from Jbilet Winselwan meteorite (1.97 μg/g meteorite) was 40 times lower than those from Murray meteorite (80.7 μg/g meteorite). Relative abundances of short-chain *n*-alkanes (C_{14} - C_{18}) were dominant in Jbilet Winselwan meteorite, while those of long-chain *n*-alkanes ($C_{19} – C_{24}$) were dominant in Murray meteorite. Assuming that these *n*-alkanes are indigenous in the meteorites, this difference implies that short-chain *n*-alkanes were resulted from cracking of long-chain *n*-alkanes and/or IOM during thermal metamorphism of the parent body of Jbilet Winselwan meteorite. Alternatively, the different distributions of *n*-alkanes may be reflected by different sources, as whether the meteoritic *n*-alkanes are indigenous or terrestrial contamination is still under debate.

In this study, we were able to quantify very small abundances of hydrocarbons in a thermally metamorphosed CM chondrite by GCMS, and thus it is expected that soluble organic molecules are detectable from the surface materials of asteroid Ryugu by higher resolution MS, even if they are heated. In order to apply the organic chemistry of Jbilet Winselwan meteorite to understanding of the parent body condition of Ryugu, further investigation of other aliphatic hydrocarbons (that are likely indigenous) and soluble organic molecules, and insoluble organic solids from this meteorite will be necessary.

References: [1] Watanabe S. et al. (2019) *Science* 364: 268-272. [2] Sugita S. et al. (2019) *Science* 364: eaaw0422. [3] Kitazato K. et al. (2019) *Science* 364: 272-275. [4] Nakamura T. (2006) *EPSL* 242: 26-38. [5] Naraoka H. et al. (2004) *MAPS* 39: 401–406. [6] Yabuta H. et al. (2005) *MAPS* 40: 779–787. [7] Shimoyama A. et al. (1989) *Geochemical J.* 23:181-193. [8] Zolensky M. et al. (2016) 47th *LPSC* abstract #2148. [9] Mimura K. and Toyama S. (2004) *GCA* 69: 201-209. [10] Mimura et al. (1994) *Geophys. Res. Lett* . 21: 2071-2074.

GLOBAL IMCOMPLETE FORMATION OF LUNAR MINERALS WITHOUT SUCCESSIVE FLUID SYSTEM.

T. Kato and Y. Miura. Yamaguchi University, Yamaguchi, 753-8512, Japan. yasmiura50 @ gmail.com.

Introduction: Analysis of lunar samples including the Apollo samples have been applied by analytical method and terminology based on terrestrial samples [1]. This is mainly because typical extraterrestrial samples of meteorites found and collected on the terrestrial surfaces show primordial formation of chondrules and shocked textures [2-9]. However, lunar samples of the Apollo and lunar meteorites contains larger rock-forming minerals of feldspar, olivine and pyroxene, which have been considered to be formed by some interior process of igneous rocks (without Earth-type sediment process of global fluids and related plate-movement). Therefore probable formation of lunar rock-forming minerals should be investigated comparatively. Main differences with formed processes of Earth's minerals compared with the extraterrestrial lunar minerals (including feldspar minerals) are less answered clearly by many investigators. In this paper, one of many evidences of the lunar rock formation (with limited data) is considered to be compositional data by "impact growth" of impact-heating and shocked cooling processes (with volatiles of carbon elements)[1-9]. Main purpose of the paper is to elucidate comparative differences with formed processes (including volatile components) of lunar rock-forming minerals (including plagioclases) compared with terrestrial rock-forming minerals.

Rock-forming minerals analyzed by Electron probe microanalyzer (EPMA): Large grains of lunar rock-forming minerals (olivine, pyroxene, feldspar and silica) can be analyzed with normal electron microanalyzer (EPMA) used for all Earth-type rock-forming minerals to obtain these compositional ranges [1, 4-9]. This is mainly because later stage minerals of lunar feldspar and silica minerals indicate lower temperature formation (formed as crust-minerals) from higher-temperature formation of olivine and pyroxene (formed as mantle minerals based on Earth-type database). Analytical EPMA data suggest limited compositional range of plagioclases (and less silica quartz) which is considered to be "local heating process" of impact melting produced by many impact craters on the lunar surface, though we cannot observe globally active volcanic activity on the Moon to form Earth-type feldspar and quartz minerals clearly [1, 4-9].

Plagioclase feldspar minerals analyzed by FE-electron probe microanalyzer (FE-EPMA): Large grains of lunar feldspar minerals can be analyzed with Field Emission electron probe microanalyzer (FE-EPMA) used for micro-grains with carbon volatiles to obtain quenched and solidified grains [1, 5-9]. This is mainly because later stage minerals of plagioclase feldspars indicate rapid cooled formation (from high-temperature vapor state including carbon volatiles), where lager plagioclase grains on the Moon (with less carbon) have been formed by prolonged heating process of larger impact process on the Moon. However short impact heating samples of lunar breccias contained higher carbon contents because of its rapid-cooled process. The FE-EPMA data suggest carbon-bearing plagioclases which is considered to be "local and quenched mixed process between vapor and solid states" of impact melting produced by many impact craters on the global lunar surface, though we cannot observe other quenched process of global fluids-water on the lunar surface [7-9].

Difficult remained process to form fluid water on the Moon: The impact process is largely difficult to form and kept fluid water during impact process, because it cannot be passed through liquid-state of intermediate phase-range between vapor and solid states by rapid decrease of temperature or pressure on airless surface of the Moon. Therefore, lunar underground caves might be relics of vapor room during larger shocked processes remained at the interior followed evaporation from vapor or some fluids locally, which would be checked at the present quenched indicator of carbon-bearing solids remained on the rocks with the FE-EPMA method [7-9].

Old lunar rocks remained on the Moon without Earth-type successive process: Main difference with rock-forming minerals between young-aged Earth and old-aged Moon is macroscopic observation of *global fluids water* on active Earth [2-3]. Complicated Earth's activity of interior magmatic formation with Earth's shock-wave events of volcano, earthquake and asteroid impact has been produced continuously younger-aged rocks with larger crystals with clear composition through global Earth's systems separated to the ocean water and atmospheric systems above the rock system continuously [2, 3]. If there is no global water and active air-water system on the Moon and Exo-Earth, rock-forming minerals and surface outcrops show waterless-formation of primordial Earth planet [1, 4-5].

Summary: The present study is summarized as follows

1) Analytical evidences of the lunar rock formation (including plagioclases) can be discussed by two types of mineral analysis with macro- and micro-grains (with carbon elements) by the EPMA and FE-EPMA methods, where comparative compositional data formed by impact growth compared with terrestrial rock-forming minerals.

2) Impact process which is difficult to form and kept fluid water from phase changes can be explained lunar interior caves as probable relics of vapor room during larger shocked processes locally, which can be checked clearly by present quenched indicator of carbon-bearing solids with the FE-EPMA method.

3) Young-aged Earth planet shows macroscopic existence of global fluids water, however the Moon without any global fluids can be explained as waterless-formation of primordial Earth planet, because of its definition of macroscopic existence generally.

References: [1] Miura Y. (1983) *Lunar and Planetary Sci. XIV, Abstract* paper #1255. [2] Wilson J.T. (1965) *Nature*, 207 (4995), 343-347. [3] Grove T.L. (2012) *An. Rev. Earth & Planetary Sci.* 40 (1), 413-439. [4] French B. (1998): *Traces of Catastrophe* (LPI), 120 pp. [5] Miura Y. *et al.* (1997) *Shock Waves* (World Scientific), 20. 1473-1478. [6] Miura Y. *et al.* (1999) *J. Materials Proc. Tech.,* 85, 192-193. [7] Miura Y. *et al.* (2010) *LEAG2010,* Abstract #3005. [8] Miura Y. *et al.* (2017) *Planet. Science Vision 2050 Workshop 2017*, Abstract #8101. [9] Miura Y. (2018) International Mineralogical Association 2018 (Melbourne, Australia), Abstract #1189.

VARIATIONS IN INITIAL ^{26}AL ABUNDANCES AMONG FINE-GRAINED CA-AL-RICH INCLUSIONS IN THE REDUCED CV CHONDRITES.

N. Kawasaki[1], C. Park[2], N. Sakamoto[3], and H. Yurimoto[1,3,4]
[1]Natural History Sciences, Hokkaido University (kawasaki@ep.sci.hokudai.ac.jp), [2]Division of Earth-System Sciences, KOPRI, [3]Isotope Imaging Laboratory, Hokkaido University, [4]ISAS/JAXA.

Introduction: Ca-Al-rich inclusions (CAIs) are composed of high-temperature condensates from a solar-composition gas [1] and the oldest objects formed in our Solar System, as determined by U-corrected Pb−Pb chronology [2]. Most of CAIs are thought to have contained detectable amounts of live ^{26}Al, a short-lived radionuclide with a half-life of ~0.7 Myr, at their formation [3]. Recent high-precision ^{26}Al–^{26}Mg mineral isochron studies using secondary ion mass spectrometry (SIMS) revealed detailed distributions of initial ^{26}Al/^{27}Al values, $(^{26}$Al/^{27}Al$)_0$, for individual CAIs in the CV chondrites [4−10]. The data show that coarse-grained, igneous CAIs and fluffy Type A CAIs show similar variations in $(^{26}$Al/^{27}Al$)_0$, which range from ~5.2 to ~4.2 × 10^{-5} [10]. However, few studies have obtained such high-precision ^{26}Al–^{26}Mg mineral isochrons of fine-grained inclusions (FGIs); only two FGIs have been examined [4, 10]. Volatility-fractionated trace-element patterns [11, 12] and complex multi-layered structures [13, 14] of FGIs in CV chondrites are indicative of condensates formed directly from the solar nebular gas. In this study, we obtained new ^{26}Al–^{26}Mg mineral isochrons of five FGIs from the reduced CV chondrites, Efremovka, Vigarano and Thiel Mountains 07007 (TIL 07007), by *in situ* measurements using SIMS. Since FGIs are likely to be condensates from a solar nebular gas, ^{26}Al–^{26}Mg mineral isochrons of them enable a more systematic comparison of $(^{26}$Al/^{27}Al$)_0$ between CAIs formed by condensation and by melt crystallization than has previously been achieved.

Experimental: Al−Mg isotopic compositions of minerals in FGIs were measured using a Cameca ims-1280HR SIMS instrument at Hokkaido University. An ^{16}O$^-$ primary beam accelerated to 23 keV was employed in the experiment. We used both the peak-jumping mode and the multicollection mode, depending on the secondary ion intensities of Mg-isotopes from the minerals. The full analytical procedures are reported in [8, 10].

Results and Discussion: FGIs *HKE02* and *HKE03* from Efremovka, *HKV03* from Vigarano, and *TIL01* from TIL 07007 are fine-grained, spinel-rich inclusions. They have irregular shapes and complex multi-layered textures composed mainly of spinel, melilite, and diopside. The CAI *TIL02* from TIL 07007 is a compound object consisting of fine-grained, anorthite-pyroxene-rich core enclosed by fluffy Type A CAI-like melilite-rich mantle. The entire inclusion of *TIL02* is surrounded by Wark-Lovering rim [13]. We measured Al−Mg isotopic compositions of melilite and spinel in each FGI and defined ^{26}Al–^{26}Mg mineral isochrons. The obtained ^{26}Al–^{26}Mg mineral isochrons give $(^{26}$Al/^{27}Al$)_0$ of (5.19 ± 0.17) × 10^{-5} for *HKE02*, (5.00 ± 0.17) × 10^{-5} for *HKV03*, (4.53 ± 0.18) × 10^{-5} for *TIL02*, (4.43 ± 0.31) × 10^{-5} for *TIL01*, and (3.35 ± 0.21) × 10^{-5} for *HKE03*. The $(^{26}$Al/^{27}Al$)_0$ values for the FGIs *HKE02* and *HKV03* are essentially identical to the whole-rock CAI value of $(^{26}$Al/^{27}Al$)_0$ ~ 5.2 × 10^{-5} [15, 16], while those for the other three FGIs are clearly lower than the whole-rock CAI value. The observed significant variation in $(^{26}$Al/^{27}Al$)_0$ for the FGIs, from (5.19 ± 0.17) to (3.35 ± 0.21) × 10^{-5}, corresponds to a formation age spread of 0.44 ± 0.07 Myr. These variations are similar to, but slightly larger than those for igneous CAIs ranging from ~5.2 to ~4.2 × 10^{-5} [5, 7]. Our data imply that CAI condensation events continued for, at least, ~0.4 Myr at the very beginning of our Solar System, if ^{26}Al was distributed homogeneously in the forming region. Alternatively, the observed variation in $(^{26}$Al/^{27}Al$)_0$ would also raise a possibility of heterogeneous distributions of ^{26}Al in the forming region, corresponding to a range over, at least, 3.4 × 10^{-5} < $(^{26}$Al/^{27}Al$)_0$ < 5.2 × 10^{-5}.

References: [1] Grossman (1972) *GCA* 36, 597–619. [2] Connelly et al. (2012) *Science* 338, 651–655. [3] MacPherson et al. (1995) *Meteoritics* 30, 365–386. [4] MacPherson et al. *ApJL* 711, L117–L121. (2010) [5] MacPherson et al. (2012) *EPSL* 331−332, 43−54. [6] Kita et al. (2012) *GCA* 86, 37–51. [7] MacPherson et al. (2017) *GCA* 201, 65−82. [8] Kawasaki et al. (2017) *GCA* 201, 83−102. [9] Kawasaki et al. (2018) *GCA* 221, 318–341. [10] Kawasaki et al. (2019) *EPSL* 511, 25–35. [11] Boynton (1975) *GCA* 39, 569–584. [12] Davis and Grossman (1979) *GCA* 43, 1611–1632. [13] Wark and Lovering (1977) In: Proc. of the 8th LPSC, pp 95–112. [14] Krot et al. (2004) *MaPS* 39, 1517–1553. [15] Jacobsen et al. (2008) *EPSL* 272, 353−364. [16] Larsen et al. (2011) *ApJL* 735, L37−L43.

SPACE EXPOSURE EXPERIMENTS OF CARBONACEOUS CHONDRITES, CHONDRITIC ORGANIC MATTER AND ITS ANALOGUES IN TANPOPO2, ASTROBIOLOGY SPACE MISSION ON ISS.

Y. Kebukawa[1*], M. Koga[1], I. Sakon[2], I. Endo[2], K. Kobayashi[1], M. Matsuoka[3], M. Ito[4], M. E. Zolensky[5], C. M. O'D. Alexander[6], H. Mita[7], and H. Yano[3], [1]Yokohama National University, 79-5 Tokiwadai, Hodogaya-ku, Yokohama 240-8501, Japan, [2]The University of Tokyo, 7-3-1 Hongo, Bunkyo-ku, Tokyo 113-8654 Japan, [3]ISAS, JAXA, 3-1-1 Yoshinodai, Chuo-ku, Sagamihara, Japan, [4]Kochi Institute for Core Sample Research, JAMSTEC, B200 Monobe, Nankoku, Kochi 783-8502, Japan, [5]ARES, NASA Johnson Space Center, 2101 NASA Parkway, Houston, TX 77058, USA, [6]DTM, Carnegie Institution of Washington, 5241 Broad Branch Rd NW, Washington DC 20015, USA [7]Fukuoka Institute of Technology, 3-30-1 Wajiro-higashi, Higashi-ku, Fukuoka, 811-0295 Japan.
*Email: kebukawa@ynu.ac.jp

Organic matter (OM) is susceptible to environmental conditions and changes its structures relatively easy. UV irradiation and high-energy particle bombardment in space environments are likely to alter OM. Therefore, it is important to evaluate modifications of OM in space environments to understand dust surface processes and asteroidal surface processes. Many laboratory experiments have been performed simulating space environments to evaluate the effects of high-energy particles and UV irradiations [e.g., 1], as well as space exposure experiments [e.g., 2]. However, the experiments focusing on chondritic organic matter are limited.

The Tanpopo mission is an astrobiology space experiment using the ExHAM facility of the Japanese Experiment Module (JEM) 'Kibo' on the International Space Station (ISS) to understand the delivery of extraterrestrial organic compounds to the Earth and potential interplanetary transfer of life [3]. The Tanpopo2 is the successor of the Tanpopo mission, and will be launched in the summer of 2019. One of the Tanpopo2 exposure panels, the Tanpopo2-QCC exposure panel (TNP2QCC, Fig. 1) [4] features the direct exposure to solar radiation without MgF_2 or SiO_2 windows that were used in the exposure experiments of Tanpopo. The TNP2QCC is dedicated for exposure experiments to understand the organic evolution from circumstellar medium, molecular clouds and the Solar System small bodies, including the exposure of quenched carbonaceous composite (QCC) [5], nitrogen-included QCC [6] and simulated interstellar organics [7]. The exposure experiments of carbonaceous chondrites, chondritic IOM, and analog material of chondritic organic matter are one of subthemes of the TNP2QCC.

We prepared the Murchison meteorite powder, the Tagish Lake meteorite powder, insoluble organic matter (IOM) from Murchison, Leonardite humic acid standard (obtained from International Humic Substances Society), organic solid prepared by the method described in Kebukawa et al. [8] (250ºC, 72h). The powdered samples are pressed on gold substrates and indium substrates (10 mm diameter, Fig. 2A), with and without MgF_2 windows. These samples will be analyzed with attenuated total reflection Fourier-transform infrared spectroscopy (ATR-FTIR) and nanoscale secondary ion mass spectrometry (NanoSIMS). 100-nm thick sections were prepared with focused ion beam (FIB), and covered with MgF_2 windows to avoid destruction by reactive oxygen species at lower Earth orbit. The FIBed sections will be analyzed with scanning transmission X-ray microscopy (STXM) and NanoSIMS. In addition, special holders (Fig. 2B) were made for visible-infrared (VIR) diffuse reflectance spectroscopy for selected samples (Murchison and humic acid).

We will present the current status of the exposure experiments, as well as ongoing laboratory UV irradiation experiments using the equivalent flight samples.
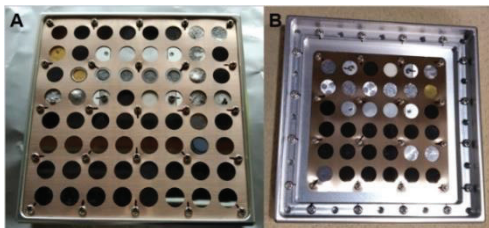

Fig. 1: The sample exposure pael equivalent to the flight model (99.5 mm × 19 mm). (A) Exposure surface and (B) back side for dark controls.
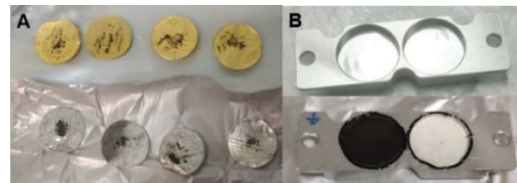

Fig. 2: (A) the Murchison mteorite powderes pressed onto Au (upper) and In (lower) substrates (the flight samples). (B) The sample holders for VIR diffuse reflectance spectroscopy equivalent to the flight model without samples (upper) and with dummy powderes (lower). The inner diameter is 10 mm.

References: [1] Bennett C. J. et al. (2013) *Chemical Reviews* 113:9086–9150. [2] Cottin H. et al. (2017) *Space Science Reviews* 209:83–181. [3] Yamagishi A. et al. (2009) *Transactions of the Japan Society for Aeronautical and Space Sciences* 7:Tk_49-Tk_55 [4] http://exoplanets.astron.s.u-tokyo.ac.jp/QCC/index_tanpopo2_qcc-type.html [5] Sakata A. et al. (1983) *Nature* 301:493–494 [6] Sakon I. et al. (2015) *Asian Journal of Physics* 24:1143–1150. [7] Kobayashi K. et al. (1995) *Advances in Space Research* 16:21–26. [8] Kebukawa Y. et al. (2013) *The Astrophysical Journal* 771:19.

COORDINATED EELS, EDX, AND FTIR ANALYSES OF ORGANIC MATTER IN A HYDRATED IDP.

L. P. Keller[1], I. Ohnishi[2]. G. J. Flynn[3], and S. Wirick[4]
[1]ARES, Code XI3, NASA-JSC, 2101 NASA Parkway, Houston, TX 77058, USA (Lindsay.P.Keller@nasa.gov),
[2]JEOL Ltd., 3-1-2 Musashino, Akishima, Tokyo 196-8558, JAPAN, [3]SUNY-Plattsburgh, 101 Broad St., Platts-burgh, NY, 12901, and [4]Focused Beam Enterprises, 79 Baycrest Ave, Westhampton, NY 11977

Introduction: Hydrated interplanetary dust particles (IDPs) are widely believed to be derived from main belt asteroids that have undergone aqueous alteration. However, recent work on solar flare track densities in IDPs have identified a group of hydrated IDPs with high track densities that suggest an outer solar system source body (e.g. Edgeworth-Kuiper belt objects) [1]. Here we report our coordinated analyses of organic-rich materials in a hydrated IDP using a next-generation scanning and transmission electron microscope (STEM).

Methods: IDP U2153M1 was embedded in elemental sulfur and ultramicrotome thin sections ~50 nm thick were placed on amorphous carbon substrates for analyses by synchrotron FTIR, STEM EELS and EDX, and NanoSIMS. Synchrotron FTIR data were collected on Beamline 1.4 at the Advanced Light Source (Lawrence Berkeley National Laboratory). We used an aberration corrected JEOL JEM-ARM300F scanning and transmission electron microscope (STEM) equipped with a cold field emission gun operated at 200 and 60 kV and a Gatan Continuum GIF for electron energy-loss spectroscopy (EELS). The STEM is equipped with a newly developed ultrahigh sensitivity energy-dispersive X-ray (EDX) system composed of a wide gap objective lens pole-piece and two windowless silicon drift detectors whose individual active area is 158 mm^2 (each) for a total collection solid angle of ~2.2 sr [2]. The high collection efficiency of the EDX system enabled the simultaneous acquisition of EDX and EELS spectrum images. To minimize possible artifacts from beam damage, we collected both the EDX and EELS data at 60kV using a ~0.4 nm ~1 nA probe, with a dwell time of 0.1 s/pixel, with a zero loss FWHM of 0.3 eV.

Results and Discussion: The IDP U2153M1 contains abundant fine-grained Mg-rich saponite, FeNi sulfides, a large forsterite grain, and abundant carbonaceous material dispersed throughout matrix and as discrete nanoglobules (individuals and clusters as noted previously [3,4]). The presence of solar flare tracks in forsterite (~3×10^{10}/cm^2) and lack of magnetite on outer surfaces suggest that U2153M1 was not significantly heated during atmospheric entry. FTIR spectra from microtome thin sections show a strong 10 μm silicate complex, hydration features at 3 and 6 μm, a strong aliphatic C-H feature at 3.4 μm (Fig. 1d) and a broad carbonyl feature centered at ~5.8 μm.

We obtained preliminary EDX and EELS data from a cluster of nanoglobules and associated matrix in U2153M1. The EDX data show that the globule cluster contains major C, minor O and trace S, but N was not detected. The O is not homgeneously distributed but is concentrated in the outer margins of the cluster. The EELS data from the cluster show three distinct π* peaks (Fig 1a) that we assign to C=C and C=O (both carboxyl and ketone) functionality similar to previous work [e.g. 4]. The EELS data from nanoglobule cluster shows higher C=O in the rim where the highest O concentrations are observed by EDX. We hypothesize that the oxidized rim on the nanoglobule cluster resulted from parent body aqueous processing. We did not detect a N k-edge above background levels consistent with a lack of N detection by EDX. EELS data from the matrix immediately surrounding the nanoglobule cluster are distinct (Fig 1b). Compared to the nanoglobule cluster, the C-C π* peak in the matrix region is broad with a distinct shoulder at 286 eV, and another broad peak occurs between 287-288.5 eV. These broad features may result from greater aromatic and especially aliphatic diversity in matrix regions. The isotopic characteristics of the organic matter will be investigated by NanoSIMS to determine if they are isotopically anomalous in H and N.

References: [1] Keller, L. P. and Flynn, G. J. (2019) *LPSC 50,* #2002. [2] Ohnishi I. et al. (2016) *Microscopy & Microanalysis* 22:218. [3] Nakamura-Messenger, K. et al. (2006) *Science* 314, 1439. [4] DeGregorio, B. T. et al. (2013) *MAPS* 48, 904.
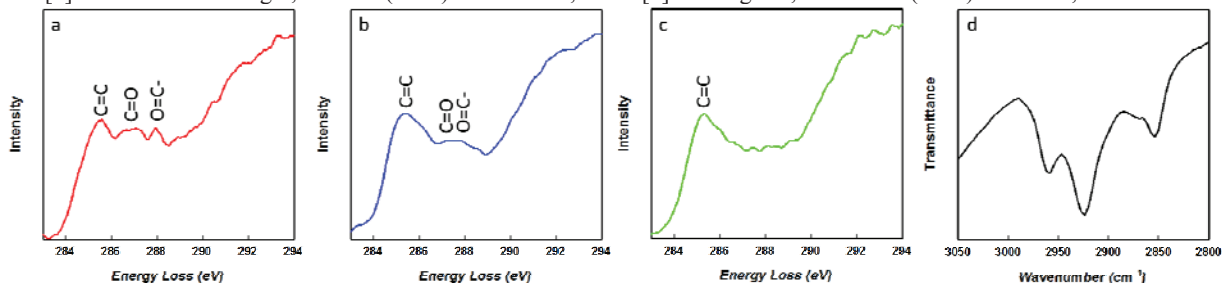

Figure 1. EELS spectra from the oxidized rim of the nanoglobule cluster (a) an area of adjacent matrix (b), and the carbon support substrate (c). Multiple π* peaks provide clues to the organic functionality in these regions. (d) FTIR spectrum from a microtome thin section of U2153M1 showing the C-H stretching region with well-resolved aliphatic CH_3 and CH_2 features.

PLANETARY DEFENSE EXERCISES WITH REAL ASTEROIDS: 2012 TC4 AND 1999 KW4.

M. S. Kelley[1] and R. R. Landis[2], V. Reddy[3], [1]NASA Headquarters, Mail Stop 3E46, 300 E St. SW, Washington, DC 20546 (michael.s.kelley@nasa.gov), [2]NASA Johnson Space Center, 2101 NASA Parkway, Houston, TX 77058 (rob.r.landis@nasa.gov), [3] Lunar and Planetary Laboratory, University of Arizona, 1629 E University Blvd, Tucson AZ 85721, USA. 808-342-8932, (reddy@lpl.arizona.edu).

We conducted the first planetary defense exercise using a real asteroid with coordination support from the NASA Planetary Defense Coordination Office [1]. The target of this global, community-led exercise was 2012 TC4, an ~10 m diameter asteroid that made a close pass by the Earth on 2017 October 12 at a distance of about 50,000 km. The goal of the TC4 observing campaign was to recover, track, and characterize 2012 TC4 as a hypothetical impactor in order to exercise the global planetary defense system involving observations, modeling, prediction, and communication. Here we summarize some lessons learned during the campaign that would be helpful for improving global preparedness for future impact scenarios. For astrometric observations, we noted along-track residuals when we remeasured observations from 2012 opposition to support the recovery attempts and refine the ephemeris. We identify the cause of this error to timing information when the data were collected (1-3 seconds error) and the rate of motion of the object. Providing GPS-based time signals for observers, especially citizen scientists, would be one way to overcome this issue in the future. Characterization studies were affected by technical issues at the NASA Infrared Telescope Facility (IRTF) that prevented spectral observations during the closest flyby although data collected under suboptimal weather days prior was adequate for basic taxonomic classification. NASA IRTF remains a single point of failure in the NASA Planetary Defense capabilities and deploying instruments similar to SpeX on IRTF on other 6-8 meter class facilities would mitigate this risk. In addition, interpretation of the spectral data were limited by the lack of adequate laboratory spectra of meteorites slabs. 2012 TC4 has a diameter of ~10 meters suggesting a surface devoid of regolith. Existing laboratory spectral databases are based on meteorite powders that mimic surfaces of larger NEOs (>1 km). Laboratory spectral studies of meteorites would help better interpret spectra of small NEOs in the future. We also performed probabilistic impact risk assessments for hypothetical impactors based on the 2012 TC4 observing campaign. Risk assessments were calculated at several epochs before and during the close approach; incorporating new information about 2012 TC4 as it became available. Across the epochs, we found that only irons caused significant damage for smaller sizes similar to the actual size of 2012 TC4 ($H = 26.7$). For larger sizes ($H = 21.9$), however, hydrous stones caused the greatest damage, anhydrous stones caused the least damage, and irons caused moderate damage. We note that the extent of damage depends on composition in different size regimes and, after astrometry; size is the most important physical property to determine for an incoming object.

Building on the experience of the 2012 TC4 obsering campaign, we recently conducted a second exercise targeting near-Earth asteroid 1999 KW4, which made a close pass by the Earth in May and June of this year. The TC4 campaign was an end-to-end test of the NASA's planetary defense system, whereas the KW4 campaign was focused almost entirely on characterization of the target. Although, the KW4 exercise did include probabilistic impact risk assessments using real measurements from the target asteroid. Experience with and results from the characterization and modeling campaign for 1999 KW4, a non-contact binary, may yield benefits in the preparation for the DART mission to the Didymos binary. Participation in this second global exercise was coordinated primarily, though not exclusively, through the International Asteroid Warning Network (IAWN). Observations included photometry, spectroscopy, and radar. We will summarize here early results of the 1999 KW4 characterization campaign.

References: [1] Reddy V. et al. 2019. *Icarus* 326:133-150.

A CHONDRITIC XENOLITH IN THE MURCHISON (CM2) CHONDRITE FORMED BY FLUID-ASSISTED PERCOLATION DURING METASOMATISM

I. Kerraouch[1], A. Bischoff[2], M. E. Zolensky[3], S. Ebert[2], M. Patzek[2], A. Pack[4], P. Schmitt-Kopplin[5,6], D. Belhai[1], A. Bendaoud[1] and L. Le[7]. [1]LGGIP, FSTGAT, Université des Sciences et de la Technologie Houari Boumediene, Alger, Algeria (kerrimene@gmail.com), [2]Institut für Planetologie, Westfälische Wilhelms-Universität Münster, Wilhelm-Klemm Str. 10, D-48149 Münster, Germany, [3]ARES, NASA Johnson Space Center, Houston TX, USA, [4]Universität Göttingen, Geowissenschaftliches Zentrum, Goldschmidtstr. 1, D-37077 Göttingen, Germany, [5]Helmholtz-Zentrum, München, German Research Center for Environmental Health, Analytical BioGeoChemistry, Ingolstädter Landstraße 1, D-85764 Neuherberg, Germany, [6]Chair of Analytical Food Chemistry, Technische Universität München, D-85354 Freising-Weihenstephan, Germany, [7]Jacobs ESCG, Houston, TX 77058 USA.

Introduction: The CM chondrites are generally complex impact breccias, in which lithic clasts and mineral fragments showing various degrees of aqueous alteration and possibbly originating from different parent bodies are mixed together (e.g., [1-9]). The occurrence of CM-like clasts in other chondritic and achondritic meteorite breccias is also well-documented (e.g., [4,10-12]), however, reports on the occurrence of foreign clasts in CM chondrites are rare [6-9].

In this study, we reinvestigated the white clast in the Murchison CM chondrite [6,8] and demonstrate that the clast is not related to R chondrites as earlier suggested [7]. In addition to the classification we discuss the origin and the history of its formation by studying several aspects like mineralogy, bulk chemistry, Rare Earth Elements (REE), oxygen isotopes, and the soluble organic compounds.

Results: The petrographic study shows that the white clast consists of two areas with different granoblastic texture: (1) a coarse-grained (average grain size: ~200 μm) and (2) a fine-grained lithology (average grain-size: ~20 μm). The Fa-content of olivine in the clast is the same as Fa within olivine from Rumuruti (R) chondrites (Fa: ~38 mol%); however, the concentrations of the elements Ni and Ca in olivine are significantly different. The fragment also contains Ca-rich pyroxene, $\sim An_{30-38}$-plagioclase/maskelynite, Cr-rich spinel, several sulfide phases, a nepheline-normative glass, and traces of merrillite and metal. The O-isotope composition of the clast falls below the terrestrial fractionation line (TFL) in the field of CM chondrites and is significantly different to data for bulk R chondrites. Considering the soluble organic matter a highly-oxidized carbon chemistry and organomagnesium compounds were found reflecting high temperature and pressure processes.

Discussion and Conclusions: O-isotope composition of the clast falls in the field of CM chondrites ($\Delta^{17}O = -3.16$ ‰) compared to [13] a relationship to R-chondrites ($\Delta^{17}O = +2.72$ ‰) [14] can be ruled out. The occurrence of nepheline-normative glass and maskelynite in a rock with a well-recrystallized texture is very surprising. Their present in restricted areas of the well-recrystallized rock may indicate remarkable P-T-excursions during shock metamorphism The white clast may have formed in the interior of the (or a CM-like) CM parent body by fluid-assisted percolation during metasomatism triggered by shock-induced annealing.

References: [1] Metzler K. et al. (1992) *Geochim. Cosmochim. Acta* 56:2873-2897. [2] Bischoff A. (1998) *Meteoritics & Planet. Sci.* 33:1113-1122. [3] Bischoff A. and Schultz L. (2004) *Meteoritics & Planet. Sci.* 39:A15. [4] Bischoff A. et al. (2006) *Meteorites and the Early Solar System II*, University of Arizona Press:679-712. [5] Bischoff A. et al. (2017) *Meteoritics & Planet. Sci.* 52:A26. [6] Bischoff A. et al. (2018) *Meteoritics & Planet. Sci.* 53:6217. [7] Isa J. et al. (2014) *Geochim. Cosmochim. Acta* 124:131–151. [8] Kerraouch I. et al. (2018) *Meteoritics & Planet. Sci.* 53:6363. [9] Ebert S. et al. (2018) *Meteoritics & Planet. Sci.* 53:6246. [10] Zolensky M. E. et al. (1992) *Meteoritics* 27:596-604. [11] Zolensky M. E. et al. (1996) *Meteoritics & Planet. Sci.* 31:518-537. [12] Patzek M. et al. (2018) *Meteoritics & Planet. Sci.* 53:2519-2540. [13] Clayton R. N. and Mayeda T. K. (1999) Geochimica et Cosmochimica Acta 63:2089-2104. [14] Bischoff A. et al. (2011) Chemie der Erde - Geochemistry 71, 101-134.
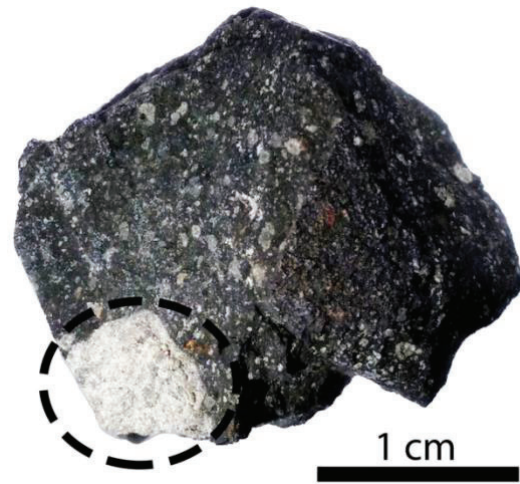
A RE-INVESTIGATION OF [41]K-K COSMIC RAY EXPOSURE AGES FOR IRON METEORITES

H. Khan[1] and I. Leya[2], [1]University of Bern, Physics Institute, Space Research and Planetary Sciences, Sidlerstrasse 5, 3012 Bern, Switzerland, [2]University of Bern, Physics Institute, Space Research and Planetary Sciences, Sidlerstrasse 5, 3012 Bern, Switzerland.

Introduction: In studies of constancy of galactic cosmic rays the cosmic ray exposure (CRE) ages calculated via [10]Be-[21]Ne, [26]Al-[21]Ne, and/or [36]Cl-[36]Ar have often been compared to so-called [41]K-K cosmic ray exposure ages that have been measured earlier by H. Voshage [1,2]. Such comparisons often indicate that the [36]Cl-36Ar CRE ages are on average 30% lower than [41]K-K CRE ages. Such a massive change could have some consequences not only for meteorite CRE ages, but they would also impact studies of the dynamics of small bodies in the solar system; it even might also influence Earth climate [1]. While the [40]K-K ages are often used for such studies, they come with their own complications. For example, the production of [39]K, [40]K, and [41]K in iron meteorites is far from understood and is expected to depend on radius and shielding. In the original study this size and shielding dependence has been empirically corrected using relationships between [39]K/[41]Kr and [4]He/[21]Ne [2]. However, the established relationship is most likely compromised by too high and extremely variable cosmogenic [21]Ne concentrations caused by contributions from the common trace elements sulphur and phosphorous [3]. This effect has never been fully considered for the calculations of [41]K-K CRE ages. Moreover it is also important to state that not only the database for these CRE ages only cover meteorites before 1984, but also there has been no new data produced for more than 30 years; whereas there are hundreds of meteorites waiting to be dated.

We have started re-studying [41]K-K CRE ages for iron meteorites. For the extraction of extremely low amounts of potassium, which is in the range of 10-13 ng/g, we plan two different, but complementary extraction procedures. First, we developed a system for in vacuum melting and electric extraction of potassium from the iron meteorite. Thus, the system is very similar to the extraction device originally used by H. Voshage. Briefly the iron meteorite samples are molten in a hot crucible and the potassium is electrically extracted with a strong electric field and is collected onto a filament. Second, we plan for chemical extraction if the blanks can be kept low enough. Considering the isotope ratio measurements, we also plan two different approaches; first measurements on a thermal ionization mass spectrometer (TIMS). First test were very successful and we managed to measure [40]K/[41]K ratios in 100 ng of potassium with a precision of 6 ng/ml. Current tests with even lower potassium amounts down to 1 ng are underway. Secondly, we plan to measure potassium isotopes using the ionprobe 1280HR.This data is not only vital to answer whether or not the fluence of galactic cosmic rays (GCR) was constant over long time periods, but also is needed by both the planetary sciences and astrophysics community.

References

[1] Th. Smith, S. Merchel, S. Pavetich, G. Rugel, A. Scharf, I. Leya. The constancy of galactic cosmic rays as recorded by cosmogenic nuclides in iron meteorites. Submitted to Meteoritics & Planetary Science (2019).
[2] H. Voshage, H. Hintenberger. Massenspektrometrische Isotopenhäufigkeitsmessungen an Kalium aus Eisenmeteoriten und das Problem der Bestimmung der [41]K-[40]K-Strahlungsalter. Zeitschrift für Naturforschg. A 1961 16(10).
[3] H. Voshage. Investigations of cosmic-ray-produced nuclides in iron meteorites, 6. The Signer-Nier model and the history of the cosmic radiation. Earth Planet Sci Lett. 1984;71(1):181–94.
[4] K. Ammon, J. Masarik, I. Leya Noble gases in Grant and Carbo and the influence of S- and P-rich mineral inclusions on the [41] K- [40] K dating system. Meteoritics & Planetary Science 2008.43:685–99.

High precision analysis of three oxygen isotopes in silicates using an automated laser fluorination

N. K. Kim[1], M. Kusakabe[2], C. Park[3], J. I. Lee[1], and K. Nagao[3], [1]Unit of Antarctic K-route Expedition, Korea Polar Research Institute, Incheon 21990, Republic of Korea (kimnk@kopri.re.kr, jilee@kopri.re.kr), [2]Department of Environmental Biology and Chemistry, University of Toyama, Toyama 930-8555, Japan (mkh2314@gmail.com), [3]Division of Earth-System Sciences, Korea Polar Research Institute, Incheon 21990, Republic of Korea (changkun@kopri.re.kr, nagao@kopri.re.kr).

Introduction: The precise determination of the oxygen three isotope compositions in terrestrial/extraterrestrial materials is important to understand the geochemical/cosmochemical processes related to their origin and secondary effects. High precision oxygen isotope analysis can provide understanding for isotopic heterogeneity of early solar system and origin of undifferentiated and differentiated meteorites [1]. Furthermore, it also can reveal an isotopic variation of terrestrial silicates caused by mass dependent fractionation (e.g., rock-water interaction) [2, 3].

An infrared laser fluorination method coupled with dual-inlet isotope ratio mass spectrometer is widely used as a fundamental system for oxygen extraction from silicate samples and can perform most precise oxygen three isotope analysis. A CO_2 laser-BrF_5 fluorination system for oxygen three isotope measurement at the Korea Polar Research Institute (KOPRI) was refurbished a new vacuum line made of stainless steel [4]. O_2 liberated from silicate sample (~2 mg) by laser fluorination is purified using cryogenic technique in vacuum line. The $^{17}O/^{16}O$ and $^{18}O/^{16}O$ ratios of the extracted O_2 are measured with the mass spectrometer (MAT 253 Plus, Thermo Fisher Scientific). Recently, we have adopted an automated lasing method that provides a constant increase rate of laser power output with defocused laser beam at a fixed position. To confirm the reproducibility of the laser fluorination system, we have analyzed well-known international standard (UWG2 garnet, San Carlos olivine and NBS28 quartz) and in-house standard samples (mid-ocean ridge basalt glass and obsidian). The analytical precisions (1σ) for $\delta^{18}O$ and $\Delta^{17}O$ values of each standard samples are ±0.04‰ and ±11 ppm for UWG2 garnet (n = 24), ±0.07‰ and ±9 ppm for NBS28 quartz (n = 10), ±0.08‰ and ±11 ppm for San Carlos olivine (n = 9), ±0.09‰ and ±10 ppm for MORB glass (n = 45) and ±0.07‰ and ±11 ppm for obsidian (n = 42). The results showed that the overall external reproducibilities are better than 0.1‰ (1σ) for $\delta^{18}O$ and 11 ppm (1σ) for $\Delta^{17}O$. Now we can provide the oxygen isotope data more precise than those obtained from previously used laser fluorination system [5].

Analysis of the VSMOW (Vienna Standard Mean Ocean Water) and SLAP (Standard Light Antarctic Precipitation) reference water is underway to achieve high accuracy. Precise calibration of working standard oxygen gas relative to the VSMOW is necessary for intercomparison of isotope data between different laboratories [6, 7, 8]. The two-point normalization using these reference waters is expected to provide us with an improved determination of oxygen isotope ratio in silicates. Analysis of meteoritic samples is also under way to validate that our system is available for extraterrestrial silicate samples.

References: [1] Clayton R. (1993) *Annual Review of Earth and Planetary Sciences* 21:115-149. [2] Pack A. and Herwartz D. (2014) *Earth and Planetary Science Letters* 390:138-145. [3] Sharp Z.D. et al. (2016) *Geochimica et Cosmochimica Acta* 186:105-119. [4] Kim N. K. et al. (2019) *Rapid Communications in Mass Spectrometry* 33:614-649. [5] Ahn I et al. (2012) *Geosciences Journal* 16:7-16. [6] Gonfiantini R. (1978) *Nature* 271:534-536. [7] Kusakabe M. and Matsuhisa Y. (2008) *Geochemical Journal* 42:309-317. [8] Schoenemann S. W. et al. (2013) *Rapid Communications in Mass Spectrometry* 27:582-590.

PRIMITIVE CM-RELATED CHONDRITES: THEIR CHARACTERISTIC FEATURES AND CLASSIFICATION.

M. Kimura[1], N. Imae[1], A. Yamaguchi[1], R. C. Greenwood[2], M. Komatsu[3], and T. Noguchi[4], [1]National Institute of Polar Research, Tokyo 190-8518, Japan (kimura.makoto@nipr.ac.jp), [2]The Open University, Milton Keynes MK7 6AA, United Kingdom, [3]SOKENDAI, Kanagawa 240-0193, Japan, [4]Kyushu University, Fukuoka 819-0395, Japan

Introduction: CM chondrites are the most abundant group of carbonaceous chondrites (CC) (37 % of CC falls according to the Met. Bull. Database) and appear to be widely distributed within the inner Solar System, occurring as brecciated fragments and clasts in a wide range of meteorite types [1]. In addition, CM chondrites are likely to be related to samples returned by the Hayabusa2 and OSIRIS-REx missions. CMs experienced varying degrees of aqueous alteration and thermal metamorphism [2,3]. Their primitive features are not well understood, although some weakly altered CM and related chondrites have been identified [4]. Recently, Yamaguchi et al. [5] reported three CM chondrites, Asuka (A) 12085, A 12169, and A 12236, that experienced very low degrees of thermal metamorphism and aqueous alteration. Here we present our preliminary results on these samples and discuss their classification and primary features.

Results: A 12085, A 12169, and A 12236 show typical carbonaceous chondritic textures and mineral assemblages, including refractory inclusions (CAIs and AOAs) (4.2, 4.3, and 3.8 vol.%, respectively), abundant chondrules (36.0, 38.6, and 28.9 %), and matrices (57.7, 53.4, and 64.8 %). Melilite commonly occurs in CAIs. Secondary phases, such as nepheline and phyllosilicates, in these CAIs and AOAs are extremely rare. FeO-rich rims on magnesian olivines in AOAs, which are often present in more metamorphosed COs [6], are absent in these meteorites. The average chondrule diameters in A 12085, A 12169, and A 12236 are 0.31, 0.26, and 0.29 mm, respectively. Glass and unaltered anorthite commonly occur in A 12169 chondrules and were also identified by Raman spectroscopy. These phases are also present in some chondrules from A 12236, but occur only rarely in A 12085. The distribution of olivine compositions in Type II chondrules in these chondrites are similar to those in primitive COs [7] and some CM chondrites [8]. The abundances of Fe-Ni metal are 1.2, 2.3, and 1.5 vol.% in A 12085, A 12169, and A 12236, respectively. Metal in chondrules is usually homogeneous. Positive Ni-Co relationships were detected in metal grains present within the matrices of these meteorites. The mean totals of the matrices by electron microprobe measurement are 91.3, 95.9, and 90.1 wt. % in A 12085, A 12169, and A 12236, respectively. No typical tochilinite-cronstedtite intergrowth (TCI) was observed and carbonate minerals are very rare in these chondrites. The X-ray diffraction patterns, measured by the method of [9], show no detectable phyllosilicates or tochilinite in A 12169 and A 12236. Cronstedtite was detected only in A 12085. Troilite was identified in A 12085, A 12169, and A 12236 by the X-ray diffraction and is often accompanied by pentlandite.

Discussion: The modal abundance and chondrule size distribution of A 12085, A 12169, and A 12236 are typical of CM chondrites. However, the common occurrence of melilite in CAIs and glass in chondrules, abundant Fe-Ni metal, no TCI, almost no phyllosilicate, and high total weight % of the matrix in A 12169, suggest that this chondrite experienced only minimal aqueous alteration. Based on petrographic evidence, the degree of the alteration increases from A 12169, through A 12236, to A 12085. The texture and compositional distribution of Fe-Ni metal in these chondrites is closely similar to that of the ungrouped, primitive chondrite Acfer 094 [10]. Sulfide features are typical of CM chondrites that did not experience dehydration [11]. Therefore, petrographic and compositional evidence indicates that these chondrites did not experience either significant thermal metamorphism or dehydration. The occurrence of glass, lack ferroan rims on AOA olivines and compositional distribution of olivine in Type II chondrules, also support this conclusion. From these features, we suggest that these chondrites, especially A 12169, are the most primitive CM or CM-related chondrites so far reported. Therefore, these new primitive CMs and in particular A 12169, provide a unique opportunity to investigate the primary features of CM chondrites, as well as the genetic relationships of CM-CO clan chondrites. These chondrites are of particular significance in view of the imminent return of sample material from CM-related asteroids Ryugu and Bennu.

References: [1] Zolensky M. E. et al. 1996. *Meteoritics & Planetary Science* 31:518-537. [2] Rubin A. E. et al. 2007. *Geochim. Cosmochim. Acta* 71:2361-2382. [3] Nakamura T. 2005. Journal of Mineralogical and Petrological Science 100:260-272. [4] Ebert S. et al. 2019. *Meteoritics & Planetary Science* 54: 328-356. [5] Yamaguchi A. et al. 2018. *Meteorite Newsletter* 26. [6] Chizmadia L. J. et al. 2002. *Meteoritics & Planetary Science* 37:1781-1796. [7] Grossman J. N. and Brearley A. J. 2005. *Meteoritics & Planetary Science* 40:87-122. [8] Schrader D. L. and Davidson J. 2017. *Geochim. Cosmochim. Acta* 214:157-171. [9] Imae N. et al. 2019. *Meteoritics & Planetary Science* 54:919-937. [10] Kimura M. et al. 2008. *Meteoritics & Planetary Science* 43:1161-1177. [11] Kimura M. et al. 2011. *Meteoritics & Planetary Science* 46:431-442.

A NEW CARBONACEOUS CHONDRITE GROUPLET, CA.

M. Kimura[1], A. Yamaguchi[1], R. C. Greenwood[2], N. Imae[1], and M. Komatsu[3], [1]National Institute of Polar Research, Tokyo 190-8518, Japan (kimura.makoto@nipr.ac.jp), [2]The Open University, Milton Keynes MK7 6AA, United Kingdom, [3]SOKENDAI, Hayama, 240-0193 Kanagawa, Japan.

Introduction: While the majority of carbonaceous (C) chondrites can be assigned to one of eight major groups, some meteorites are less easy to categorize and hence are designated as "ungrouped" [1]. Yamato (Y)-82094 is one such example, having a number of characteristics which distinguish it from other C chondrites: 1) chondrules are highly abundant, 2) chondrule size is intermediate between CV and CO, and 3) the matrix abundance is low, being similar to that of ordinary (O) chondrites. However, the abundance of refractory inclusions, and oxygen isotopic and chemical compositions are typical of C chondrites. Therefore, Y-82094 is an ungrouped C chondrite [2]. Recently, two further unusual carbonaceous chondrites, Asuka 09003 and A 09535 have been reported [3, 4]. Here we present our results for these new chondrites, compare them to Y-82094 and discuss their classification.

Petrography: Y-82094, Asuka 09003, and A 09535 show typical carbonaceous chondritic textures, including abun-dant refractory inclusions (CAI and AOA) (8.2, 4.2, and 6.3 vol.%, respectively). However, chondrules are the most abundant component (78.1, 80.1, and 78.5 %, respectively), with matrix present in low abundance (11.1, 13.0, and 12.6 %, respectively). CAIs mainly consist of melilite, spinel, Ca-rich pyroxene and anorthite with perovskite. Sec-ondary phases in CAIs and AOAs, such as nepheline, are not common in these chondrites. FeO-rich rims to magne-sian olivines in AOAs are usually less than 3μm in width. Average chondrule diameters in Y-82094, Asuka 09003, and A 09535 are 0.33, 0.29, and 0.30 mm, respectively. Type I chondrules comprise olivine, clinoenstatite, and anorthite or weakly devitrified mesostasis. Anorthite often contains thin lamellae of nepheline in Asuka 09003 and A 09535. A silica phase is present in the mesostasis of some Type I chondrules. Fe-Ni metal in chondrules consists predominantly of kamacite, containing fine-grained Ni-rich metal. Type II chondrules in Y-82094, Asuka 09003, and A 09535 are relatively uncommon (0.9, 7.5, and 11.3 % among all chondrules, respectively). The matrix is predominantly FeO-rich, submi-cron-sized, olivine. X-ray diffraction patterns, measured using the method of [5], reflect the major minerals men-tioned above. Phyllosilicates were not identified in these chondrites. Fe-Ni metal is highly abundant in chondrule and the matrix, especially 7.9 vol.% in unweathered Y-82094.

Discussion: Y-82094, Asuka 09003, and A 09535 show similar features to one another and partly resemble type 3 O chondrites. However, the abundant occurrence of CAIs and AOAs is more typical of C chondrites and this affinity is confirmed by their oxygen isotopic and chemical compositions. The petrologic subtypes of Y-82094, Asuka 09003, and A 09535 are low based on the width of the FeO-rich rims to AOA olivines and the abundance of melilite-bearing CAIs. The metal features mentioned above indicate that the subtypes of these chondrites are 3.2 [6]. However, they display a number of individual distinguishing features. Nepheline lamellae in anorthite are common in chondrules from both Asuka 09003 and A 09535, but are not observed in Y-82094, which suggests that the degree of secondary alteration is higher in Asuka 09003 and A 09535 compared to Y-82094. Type II chondrule abundance is different between the three chondrites. In spite of such differences, these chondrites display similar features and are distinguishable from other carbonaceous chondrites based on their high chondrule and low matrix abundances. On the basis of their sampling locations they are not paired. Therefore, these three chondrites may belong to a new carbonaceous chondrite grouplet, which we propose to call "CA", where A refers to Asuka. In the Meteoritical Bulletin database, no similar chondrites appear to have been reported, especially among ungrouped chondrites. However, on the basis of their abundant, small chondrules and low matrix content, it is possible that some potential members of the CA grouplet have been misclassified as type 3 ordinary chondrites, in particular H chondrites.

References: [1] Weisberg M.K. et al. 2006. *Meteorites and the Early Solar System II*, 19-52. [2] Kimura M. et al. 2014. *Meteoritics & Planetary Science* 49:346-357. [3] Yamaguchi A. et al. 2018. *Meteorite Newsletter* 26. [4] Ki-mura M. et al. 2018. *Antarctic Meteorite Symposium 41st*, Abstract # OAp4. [5] Imae N. et al. 2019. *Meteoritics & Planetary Science* 54:919-937. [6] Kimura M. et al. 2008. *Meteoritics & Planetary Science* 43: 1161-1177.

KINETIC ESTIMATION OF THE THERMAL HISTORY OF ORGANIC MATTER IN CHONDRITES USING RAMAN SPECTROSCOPY.

K. Kiryu[1], Y. Kebukawa[1], M. Igisu[2], T. Shibuya[2] and K. Kobayashi[1]
[1]Graduate School of Engineering Science, Yokohama National University, 79-5 Tokiwadai, Hodogaya-ku, Yokohama 240-8501, Japan
[2]Japan Agency for Marine-Earth Science and Technology, 2-15 Natsushima-cho, Yokosuka 237-0061, Japan

One of the characteristics represent CI, CM, and CR chondrites is to contain organic carbon up to a few wt%. Organic matter (OM) in chondrites above 70 wt% exists in the form of insoluble organic matter (IOM), which is complex and macromolecular compounds [e.g., 1]. IOM consists of carbon skeletons as polycyclic aromatic hydrocarbons (PAHs) with aliphatic side chains, carboxyl, hydroxyl, and carbonyl groups [2]. OM is a good index of the parent body processes because the final molecular structures of OM in chondrites depend on the degrees of the parent body processes. OM changes its structure reflecting aqueous alteration and/or thermal metamorphism. In this study, we utilized the property of OM which is susceptible to heating in order to estimate the thermal history of chondrites.

Kinetic approaches are an effective way to predict the thermal history of OM in chondrites and its parent bodies [3,4]. Kebukawa et al. [4] obtained the kinetics of degradation of aliphatic C-H through in-situ heating experiments of bulk of the Murchison meteorite and IOM using the Fourier transform infrared micro-spectroscopy (microFTIR). According to them, low-temperature and/or short-duration heating in chondrites' parent bodies can be traced by the peak intensity of aliphatic C-H. However, this method is insufficient under high-temperature and/or long-duration heating, since IR signals of aliphatic C-H are unlikely to be detected.

To overcome the problem, we applied Raman spectroscopy, which is a complementary tool to IR spectroscopy. Raman spectral features of OM in the chondrites reflect thermal changes not in aliphatic C-H but in aromatic structure in the complex OM ([5-8]). While heating, chondritic OM changes into more ordered graphitic structure. The irreversible process appears as the alteration in disordered (D_1: ~1350 cm^{-1}) and graphite (G: ~1590 cm^{-1}) bands of Raman spectra. That is, Raman spectroscopy is a promising tool for assessing thermal processes of OM in the chondrites under high-temperature and/or long-duration heating. Although D_1- and G-bands could be used as indicators of degree of thermal metamorphism, researches in kinetics using the two Raman spectral parameters are relatively limited. We performed a series of heating experiments of the Murchison meteorite powders with relatively higher temperature and longer duration compared to Kebukawa et al. [4], to analyze Raman spectral parameters for kinetic estimation of the thermal history of OM in chondrites.

We heated the Murchison meteorite powders under low-oxygen condition for 3-48 h at 600-900°C in a vacuum gas replacement furnace. The low-oxygen condition was certainly sustained by purging a gas mixture of N_2 and H_2 (99:1, v/v). After heating, the samples were analyzed using a Raman spectrometer with a 532 nm laser (RAMANtouch; Nanophoton). D_1- and G-bands were obtained in the Raman spectra of all the samples, and we determined 5 Raman spectral parameters: the full width at half maximum (FWHM) and the peak positions of D_1- and G-bands, and the ratio of the peak intensities of D_1- to G-band. These Raman spectral parameters variously changed with time at each temperature. We will fit these data with algebraic kinetic equations deduced by possible physical mechanisms, and estimate reaction rate constants. Then, based on the Arrhenius equation, the apparent activation energies and frequency factors will be calculated by the reaction rates. In the end, we will be able to use the Raman spectral parameters as functions of heating temperature and time. Combining kinetics of aliphatic C-H previously reported in Kebukawa et al. [3], it may enable us to calculate time and temperature of thermal processes in chondrites' parent bodies.

References: [1] Pizzarello S. et al. (2006) In *Meteorites and the early solar system II* edited by Lauretta D. S., Leshin L. A., and Mcsween H. Y. Jr. Tucson, AZ: The university of Arizona Press. pp. 625–651. [2] Hayatsu R. et al. (1977) *Geochimica et Cosmochimica Acta* 41:1325–1339. [3] Cody G. D. et al. (2008) *Earth and Planetary Science Letters* 272: 446-455. [4] Kebukawa Y. et al. (2010) *Meteoritics and Planetary Science* 45:99–113. [4] Quirico E. (2003) *Meteoritics and Planetary Science* 38:795–811. [5] Bonal L. et al. (2006) *Geochimica et Cosmochimica Acta* 70:1849–1863. [6] Bonal L. et al. (2007) *Geochimica et Cosmochimica Acta* 71:1605–1623. [7] Busemann H. et al. (2007) *Meteoritics and Planetary Science* 42:1387–1416.

PETROGRAPHIC EXAMINATION OF UNEQUILIBRATED ORDINARY CHONDRITES WITH LOW PETROLOGIC SUBTYPES.

N. T. Kita[1] G. Siron[1], and M. Kimura[2], [1]Department of Geosciene, University of Wisconsin-Madison, Madison, WI 53706, USA (noriko@geology.wisc.edu), [2]National Institute of Polar Research, Tachikawa, 190-8518 Tokyo, Japan.

Introduction: Chondrules acquired chemical and isotope signatures that reflect their formation environments and processes, which help us to understand the evolution of solids in the protoplanetary disk. However, most chondrites experienced parent body thermal metamorphism and/or aqueous alteration processes at various degrees [1,2]. Therefore, it is important to identify pristine chondrites that experience minimal parent body processes in order to investigate early Solar Systen evolution through the studying of chondrules. In particular, Al-Mg chronology requires chondrule samples from pristine chondrites with the lowest petrologic subtypes <3.1, because Mg self-disffusion in Al-rich minerals and glass is relatively fast [3, 4]. For the purpose of finding chondrules that are suitable for Al-Mg chronology, we selected six unequilibrated ordinary chondrites that have been classified as 3.00-3.05 based mainly from Cr_2O_3 contents in olivine [1]. Here we report results of our petrologic examination of metal phases in these meteorites that are sensitive to mild thermal metamorphism [2]. In addition, we compare petrography and mineral analyses of individual chondrules in these meteorites along with those of Semarkona (LL3.01).

Samples and Methods: Three North West Africa (NWA) meteorites were allocated from Institute of Meteorites, University of New Mexico; NWA 7731 (L3.00 [5]), NWA 8276 (L3.00; possibly paired with NWA 7731 [6]), and NWA 8649 (LL3.05 [6]). Three Antarctic meteorites were allocated from NASA-JSC; QUE 97008 (L3.05 [1]), MET 00526 (L/LL3.05 [1]) and MET 00452 (L/LL3.05; paired with MET 00526). We used scanning electron microscope (SEM) at NIPR for the observations of metal phases in chondrules in these six UOCs according to the method described in [2]. Chondrules from these meteorites and Semarkona (USNM 1805-9) were examined for their petrography and mineral compositions using Hitachi S-3400N SEM equipped with EDS spectrometer at UW-Madison.

Results and Discussion: The results of metal phase observations are shown in Fig. 1. All data fall in the range of 3.05-3.10 UOCs, which are consistent with their Cr abndance in olivine. However, NWA 7731 and NWA 8276 are more metamorphosed than Semarkona (L3.01), suggesting they are not as pristine as 3.00 subtype.

We examined olivine and pyroxene compositions for 80-165 chondrules from NWA 7731, NWA 8649, QUE 97008, and Semarkona (other meteorites are in progress). Although pyroxene compositions often show igneous zoning, the ranges of olivine and pyroxene Mg# (=[MgO]/[FeO+MgO] molar %) are consistent within each chondrule excluding obvious relict olivine grains. Secondary zoning in olivine is visible mainly toward the rim of large crystals (2-5 μm) and small crystals in mesostasis usually show lower Mg#. While a part of these zoning could be caused by the diffusional Fe-Mg exchange in olivine during parent body metamorphism, most of these olivine zoning would be igneous origins during chondrule formation. Chondrule mesostasis are generally unaltered, very similar to those in Semarkona. However, preliminary examination of chondrules in NWA 8276 show more extensive zonation in olivine and slightly altered mesostasis, suggesting that the meteorite would have experienced higher degree of thermal metamorphism and/or alteration.

The total range of olivine Fo contents among chondrules seem to be systematically different between L (NWA 7731 and QUE 97008) and LL (NWA 8649 and Semarkona). Olivine compositions in LL chondrites show a narrower peak at ~90, while L chondrite contains more type II (Mg#<90) chondrules with a broader range of Fo compositions between 75 and 90. The difference may be related to bulk Fe contents (21.6% and 18.5% in L and LL, respectively [7]) and may suggest that Fe-Ni metal would have been depleted in formation regions of LL chondrites prior to the time of chondrule formation.
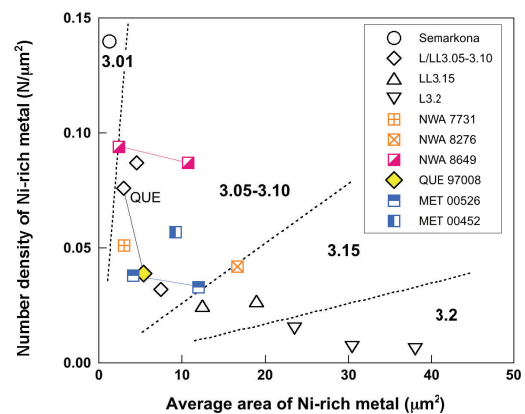

Fig. 1. Average areas versus number density of Ni-rich metal grains in metal spherules in chondrules from six UOCs. Some samples were analyzed from two sections and data are shown individually. Open symbols are those of L/LL3.01-3.2 from [2], which include data from a separate section of QUE 97008.

References: [1] Grossman J. N. and Brearley A. J. (2005) *Meteoritics & Planetary Science* 40:87-122. [2] Kimura M. et al. (2008) *Meteoritics & Planetary Science* 43:1161-1177. [3] Kita N. T. and Ushikubo T. (2012) *Meteoritics & Planetary Science* 43:1108-1119. [4] Van Orman J. A. et al. (2014) *EPSL* 38:79-88. [5] Agee C. B. et al. (2013) *Meteoritics & Planetary Science Suppl.* 48 #5130. [6] Ruzicka A. et al. (2014) *The Meteoritical Bulletine* 103. [7] Kallemeyn G. W. et al. (1989) *GCA* 53:2747-2767.

New implications for Tunguska explosion based on magnetic, dendrological, and lacustrine records

G. Kletetschka[1,2,3], R. Kavková[2], T. Navrátil[1], M. Takáč[2], J. Prach[2], D. Vondrák[2], E. Stuchlík[4], R. Štorc[2], E. Švecová[2], Z. Hořická[4], J. Klokočník[5], J. Kostelecký[6,7], A. Bezděk[7,8], D.Y. Rogozin[9], A. Meydus[10], L. Krivobokov[11], L. Mukhortova[11], A.V. Darin[12], R. Serra[13], C. Stanghellini[14], and O.G. Gladysheva[15], [1]Institute of Geology, Czech Academy of Sciences, [2]Faculty of Science, Charles University, Czechia, [3]Department of Geology and Geophysics, University of Alaska Fairbanks, USA, (Kletetschka@gmail.com),[4]Institute of Hydrobiology, Biology Centre, Czech Academy of Sciences, Na Sádkách 7, České Budějovice, Czechia, [5]Astronomical Institute, Czech Academy of Sciences, Fričova 298, Ondřejov, Czechia, [6]Research Institute of Geodesy, Topography and Cartography, Zdiby 98, Czechia, [7]Faculty of Mining and Geology, VSB-TU, Ostrava, Czechia, [8]Faculty of Civil Engineering, Czech Technical Univeristy in Prague, Prague, Czechia,[9]Russian Acad Sci, Inst Biophys, Siberian Branch, Krasnoyarsk 660036, Russia, [10]Krasnoyarsk State Pedag Univ, Krasnoyarsk, Russia,[11]Russian Acad Sci, VN Sukachev Inst Forest, Siberian Branch, Krasnoyarsk, Russia, [12]Russian Acad Sci, Sobolev Inst Geol & Mineral, Siberian Branch, Novosibirsk 630090, Russia, [13]Univ Bologna, Dipartimento Fis & Astron, I-40126 Bologna, BO, [14]Italy, INAF, Ist Radioastron, Bologna, Italy, [15]Russian Acad Sci, AF Ioffe Phys Tech Inst, St Petersburg 196140, Russia.

Introduction: Evenkia is a district in Krasnoyarsk Krai, Russia, characteristic of preserved areas of East Siberian continental taiga. In 1908, this region experienced catastrophe (Tunguska event = TE). Over 2,000 km^2 of boreal forest were felled and burned [1,2]. The exact cause of this event is not known but this event has often been associated with either an asteroid or comet encounter [3,4,5].

Material and Methods: We collected tree samples that survived the explosion within the tree collapse area. Most of the tree is Siberian larix. Samples were analyzed for elemental composition (XRF and similar). We collected sediment from three lakes, Zapoviednoe, Cheko, and Gin. Lake Zapoviednoe and Cheko varved sediment came from similar depth of about 35-40 m with conical bottom bachymetry. Lake Gin was shallow (50-60 cm) and had no varves. Chronology of the sediment was already established in Cheko lake using ^{210}Pb, ^{137}Cs, and ^{226}Ra radioactive isotopes analysis [6]. An increase in ^{137}Cs corresponded to 1961 [6]. We ran similar analysis for the two new lakes, Gin and Zapoviednoe and established the sediment chronology. Zapoviednoe lake sediment was exposed to 0-50 keV X-Ray Fluorescence and major element data, including magnetic susceptibility, were obtained across the TE containing sediment. We plotted aeromagnetic data from the world magnetic map flown at ~4 km [7,8] over the tree fall area. Magnetic paleointensity was obtained from the samples collected from Mount Stoikovich and Farrington near epicentre.

Results: Tree samples provided an evidence that the ovepressure wave compressed the floem fluid rich in Ca, Sr, Mn into the xylem at the time of TE. This compression had strong anisotropy with maximum compression directed towards the epicenter. We detected that after TE, during the past 40 years the Larix trees in Tunguska have anomalous increase in Hg concentration. Lake sediment revealed 2-4 mm thick clay layer deposited at the time of TE. The layer has anomalous decrease in Fe, while magnetic susceptibility increased. In addition the TE layer has significant increase in Pa, Mo, Th, Cd, Nb, Y, Cu, Cr, Sr, Ti, and V. Aeromagnetic data showed negative magnetic anomaly covering the toppled forest area around the epicenter. Samples from Mount Farrington indicated magnetic paleofields exceeding 1 mT. Four samples from Mount Stoikovitch detected paleofields consistent with geomagnetic field intensity while two samples indicated magnetic paleofield exceeding 0.1 mT.

Discussion and Conclusion: TE was shown to leave a biochemical signature in the wood of Larix Sibirica sensitive to explosion direction. TE area was subjected to large energy pulse that may have compromised the permafrost in the area. This was indicated here by an excess of Hg detected in the last 40 years of tree ring material. Tunguska layer in the Zapoviednoe lake is of very fine nature, resembling the clay. While the content of Fe dropped from 160 ppm to 19 ppm the magnetic susceptibility increased two fold. This is an evidence of quick and intense burst of energy, melting vapourizing the dust, causing agglutination of the dust material. This resulted in a ubiquitous presence of nanophase iron with large magnetic susceptibility that became part of molten dust particulates and deposited in the lake sediment. Anomalous elemental increase in lake suggested possible allochtonous material. Paleomagnetic data revealed presence of plasma during the TE near rock surfaces.

References: [1] Kulik L. (1928) *Petermanns Mitteilungen* 74: 338–341. [2] Kletetschka G. et al. (2017) *Tree-Ring Res*. 73(2): 75-90. [3] Boslough M.B.E. and Crawford D.E. (2008) *Int. J. Impact Eng*. 35(12): 1441-1448. [4] Bunch T. et al. (2012) *PNAS* 109(28): E1903–E1912. [5] Wittke et al. (2013) *PNAS* 110(23): E2088–E2097. [6] Rogozin D.Y. et al. (2017) *Dokl. Akad. Nauk* 476(2): 1226-1228. [7] Bankey V. A. et al. (2002) Digital data grids for the magnetic anomaly map of North America *Rep.*, Denver, Colorado, USA. [8] Ravat et al. (2002) *Geophysics*, 67(2), 546-554.

INTEGRATING CRYSTAL CHEMISTRY WITH LABORATORY ANALYSIS TO MODEL BOUND AND ADSORBED OH AND H2O

R. L. Klima[1], B. Young[1,2], and A. S. Rivkin[1], [1]Johns Hopkins University Applied Physics Laboratory, Laurel, MD 20723, USA (Rachel.Klima@jhuapl.edu), [2]Portland State University, Portland, OR.

Introduction: Investigating the specific characteristics of the H_2O/OH absorption bands near 3 microns is critical for understanding how these molecules are adhered to a remotely observed surface and for assessing their abundance. Current methods for analyzing the form and amount of water in or on rocks range from precise laboratory measurements of oriented single crystals and glasses in transmission, where individual absorptions can be modeled and examined, through more generalized band-depth analysis where a 3-micron band, observed in reflectance spectra of powdered samples in the lab or remote measurements, is treated as a single integrated absorption and compared to empirically calibrated water abundances. Understanding the relationship between the component band strengths and shapes and the bonding to the mineral also has the potential to provide a method to mathematically model terrestrial adsorbed water out of spectral measurements that were not obtained under vacuum conditions, increasing the number of laboratory spectra available for spectral analysis dramatically.

Distinguishing internal and bound water/hydroxyl: Water and/or hydroxyl detected remotely on the lunar surface may originate from several sources: 1) comets and other exogenous debris; 2) solar-wind implantation; 3) the lunar interior. While each of these sources are interesting in their own right, distinguishing among them is critical for testing hypotheses for the origin and evolution of the Moon and our solar system. Existing spacecraft observations provide limited spatial and/or spectral resolution, depending on the instrument used, to uniquely characterize the bonding energies of the hydroxyl molecules that have been detected. Because remote observations likely combine water and hydroxyl from various sources, it is important to understand whether they can be clearly distinguished from one another first in a highly controlled laboratory environment.

As part of the VORTICES SSERVI team, we are working to spectrally and mathematically characterize the distribution of energies for absorption bands caused by bound and adsorbed hydroxyl and water. To increase the amount of information that can be derived from spectra of hydrated terrains throughout the solar system, we are working to combine both transmission and reflectance spectra of a series of samples to develop a methodology for reliably separating out the specific component absorptions in the 3 micron region of reflectance spectra. For a suite of nominally anhydrous minerals, we are currently obtaining combined transmission measurements of thin sections and powdered rock measurements in ambient air and in ultra-high vacuum. Samples are dehydrated in vacuum, resulting in a suite of spectra with a decreasing amount of adsorbed water. Transmission measurements, which are dominated by internal water/hydroxyl absorptions, are used to characterize absorption bands of any internal water present. The thin sections are then also dehydrated enabling the baseline absorption to be characterized. We will present new modeling results for analog and meteorite materials.

Sample Characterization: For our preliminary analysis, we have selected two ordinary chondrites (H and LL) as well as 8 Stillwater complex samples as analogs of lunar material. Stillwater samples include harzburgite, norite, anorthite, gabbro and orthopyroxenite. Each sample is being prepared as a double polished thin section for transmission analysis of internal water, powdered for UHV measurements, and characterized in a Hitachi Desktop SEM with a Bruker EDS attachment. Terrestrial samples have been prepared first to test our methods and to ensure that the chondrites can be handled in a way that uses the minimum amount of sample.

Spectral Measurements: Spectra of each sample are being measured in transmission to characterize the shapes and relative strengths of internal water bands. Powdered samples, with water adsorbed from the atmosphere at ambient temperature and pressure, are then measured, taken to UHV and measured again before being heated to drive the adsorbed water off. Samples are measured at progressively warmer temperatures to monitor the shapes and strengths of the absorption bands at each step. Spectra are then modeled using Gaussian curves in energy space. The current objective is not to explicitly quantify the amount of water through modeling, but to determine whether the positions and shapes of bands resulting from adsorbed water are distinct enough from the water and/or hydroxyl bands in each mineral or rock type to be spectrally distinguished.

STRUCTURE AND CRYSTALLIZATION OF AMORPHOUS ENSTATITE SYNTHESIZED BY INDUCED THERMAL PLASMA AND SOL-GEL METHOD

K. Kobayashi[1], D. Yamamoto[2] and S. Tachibana[2,3], [1]Department of Natural History Sciences, Hokkaido University (kodai@ep.sci.hokudai.ac.jp), [2]Institution of Space and Astronautical Science, Japan Aerospace Exploration Agency, [3]UTokyo Organization for Planetary and Space Science (UTOPS), University of Tokyo

Introduction: Infrared spectroscopic observations of astronomical environments show that silicate dust is almost amorphous in the interstellar medium, while both crystalline and amorphous silicate dust are present in protoplanetary disks [1, 2]. This indicates that amorphous silicate dust, a precursor of dust in protoplanetary disks, transforms into crystalline dust due to thermal processes in protoplanetary disks. Amorphous silicate dust is mainly formed by non-equilibrium condensation from oxygen-rich gas in the winds of evolved stars and by destruction of crystalline dust in the interstellar medium [3, 4]. The structural property of amorphous silicate could vary with its formation process, and could affect its thermal evolution in protoplanetary disks. In this study, we investigate the structures and crystallization behaviors of amorphous enstatite synthesized by induced thermal plasma (ITP) and sol-gel methods to study the effect of amorphous structure on thermal evolution on amorphous enstatite dust in protoplanetary disks.

Experiments: Amorphous enstatite was synthesized by a sol-gel method following the procedure of [5] to compare the structure and crystallization behavior with ITP-synthesized amorphous enstatite [6]. Solid state ^{29}Si-NMR (JEOL RESONANCE ECA600II) and Raman spectroscopy (Acton SP-2750) were applied to investigate the amorphous structure, and TG-DTA (Thermo plus EVO TG 8120) was used to estimate the amount of water in the sol-gel amorphous enstatite. Crystallization experiments of amorphous enstatite were conducted at 780, 800 and 850°C in air and at $P_{H2O} \sim 10^{-4}$ Pa using a muffle furnace (Thermolyne FB1314M) and a gold-image vacuum furnace (Thermo-Riko GFA430VN), respectively. Starting materials and the heated samples were examined with FE-SEM (JEOL JSM-7000F), XRD (Rigaku SmartLab), and FT-IR (JASCO FT-IR).

Results and Discussion: The XRD profile showed that ITP amorphous enstatite has a typical halo of amorphous silicate at 2θ of 26°, while the sol-gel amorphous enstatite has broad peaks at 2θ of ~23, 35 and 60°, suggesting its close relation to magnesium silicate hydrate [7]. The TG curve of sol-gel amorphous showed a 10.6 wt% weight loss at 50−800°C most likely due to dehydration. The sol-gel amorphous enstatite in this study is hydrated and has a structure similar to magnesium silicate hydrate. The solid state ^{29}Si-NMR and Raman spectroscopy showed that the sol-gel amorphous enstatite has a larger number of bridging oxygen than the ITP amorphous enstatite, suggesting that the sol-gel amorphous enstatite has a more polymerized network structure of SiO_4 tetrahedra and could be chemically heterogeneous with SiO_2-rich and SiO_2-poor regions.

The XRD spectra of the heated samples showed that the sol-gel amorphous enstatite transforms into forsterite at 500−600°C and into enstatite and forsterite at ~800°C, while ITP amorphous enstatite transforms into enstatite with a small amount of forsterite in the entire temperature range. The 10-µm infrared feature of the heated sol-gel amorphous enstatite has a shoulder at 8 µm as SiO_2 glass, and its 20-µm infrared feature is similar to that of SiO_2 glass. This suggests that the sol-gel amorphous enstatite crystallizes into primarily forsterite leaving silica-rich amorphous.

The time evolution of infrared spectra of samples heated at 780°C and $P_{H2O} \sim 10^{-4}$ Pa showed that crystallization of the sol-gel amorphous enstatite occurred faster than the ITP amorphous enstatite. This could be because the sol-gel amorphous enstatite crystallizes into forsterite, which has a lower energetic barrier for crystallization [8], within the SiO_2-poor region. Alternatively, crystallization of forsterite may be enhanced by the presence of OH in the amorphous structure [9]. The crystallization experiments of dry amorphous enstatite synthesized by the sol-gel method [10] also showed that the amorphous enstatite crystallizes into forsterite at temperatures below the glass transition temperature, which indicates that the structure of amorphous enstatite affect its crystallization behavior.

[1] Waters, L. B. F. M. et al. (1996) *Astronomy and Astrophysics* 315:361−364. [2] Kemper, F. et al. (2005) *The Astrophysical Journal* 633, 534. [3] Gail H. P. et al. (2009) *The Astrophysical Journal* 698:1136–1154. [4] Brucato, J. R. & Nuth, J. A., III (2010) *Protoplanetary Dust* 128-160. [5] Murata, K. (2009) *Ph.D. thesis*. [6] Imai, Y. (2012) *Ph.D. thesis*. [7] Dominik, N. (2016) *Cement and Concrete Research* 79:323–332. [8] Yamamoto, D. & Tachibana, S. (2018). *American Chemical Society Earth and Space Chemistry* 2:778–786. [9] Jäger, C. et al. (2003) *Astronomy and Astrophysics*, 408:193−204. [10] Roskosz, M. (2011) *Astronomy and Astrophysics* 529, A111.

EXPERIMENTAL HEATING OF A HYDRATED CARBONACEOUS CHONDRITE TO SIMULATE SOLAR RADIATION HEATING OF 3200 PHAETHON.

Shiho Kobayashi[1*], Tomoki Nakamura[1], Kana Amano[1], Megumi Matsumoto[1], Gregor Golabek[2], Katsuhito Ohtsuka[3]. [1]Graduate School of Science, Tohoku University, Sendai, Miyagi 980-8578, Japan; [2]Bayerisches Geoinstitut, University of Bayreuth, 95440 Bayreuth, Germany; [3]National Astronomical Observatory of Japan, Osawa 2-21-1, Mitaka, Tokyo 181-8588, Japan; [*]Email: shiho.kobayashi.p7@dc.tohoku.ac.jp.

Introduction: 3200 Phaethon is a 6-km size, near-Earth B-type asteroid with an orbital period of 1.43 yr. and a rotation period of 3.6 hours [1]. It is a target asteroid of the Japanese DESTINY[+] mission. It is also a near-Sun asteroid whose perihelion distance from the Sun is 0.14 au and therefore the surface material is heated intensively up to 700 °C by solar radiation [2] and the surface properties and the spectrum would have changed during heating. Phaethon shows blue to flat spectra and the spectral shape is similar to those of CI/CM chondrites that experienced aqueous alteration and subsequent heating [2]. Phaethon is also known as the parent body of the Geminid meteor shower, which can be observed every mid-December, but it remains unknown how the Geminid meteoroid-size aggregates (mm-size aggregates) were formed on the surface of Phaethon. Spectroscopic observation shows that some Geminid meteors have already depleted their sodium abundances before entering the Earth's atmospheric [4]. CI/CM chondrites contain abundant phyllosilicates. Various experimental studies investigated heating and dehydration of CI/CM chondrites [e. g., 3], however, in those experiments, a meteorite powder sample was transferred to another container after heating for spectral measurements and during the transfer the sample surface was disrupted. Therefore, the reflectance spectra of the heated sample surface could not be measured. Therefore, in order to study spectral changes by the solar radiation heating of primitive asteroids such as Phaethon, the sample surface should remain undisturbed during heating and subsequent spectral measurements. We have carried out such heating experiments of a carbonaceous chondrite.

Experimental methods: A powder sample (particle size < 77 µm) of the Murchison CM chondrite was heated to 400, 700, 900 and 990 °C in vacuum for the duration of 50 hours at IW oxygen fugacity. After heating at each temperature, without explosure to the atmosphere, reflectance spectra of the same surface area of the Murchison sample was measured for wavelength range from 0.4 to 15 µm . This enabled us to study the precise changes of the reflectance spectra caused by radiation heating. In addition to spectral changes, we observed the sample surface with an optical microscope, examined mineralogical changes by synchrotron X-ray diffraction (S-XRD), and measured elemental composition by FE-EPMA.

Results and Discussion: Many aggregates larger than original particle size (< 77 µm) start to form at 400°C, grow to several-hundred µm in size at 700°C, and finally up to 1mm at 900°C. S-XRD of an aggregate indicates that phyllosilicate serpentine starts to decompose at 400 °C, serpentine decomposition is complete and secondary olivine form (thus dehydration is complete) at 700 °C, and metallic iron crystallizes at 900 °C. Polished sections of 1-mm size aggregates from the 990 °C-heated sample was analyzed to study the internal texture and chemical composition by FE-EPMA. The observations showed that the 1-mm size aggregate consists of loosely-packed smaller particles with approximately < 50 µm in size. The small particles are probably original powder particles that were rich in Fe-rich serpentine, but now consisting of anhydrous Mg-rich olivine, low-Ca pyroxene, and spherical metallic irons of typically <1 µm in size. As for the elemental composition, sodium and sulfur, which were present at ~0.5 wt % and ~6 wt%, respectively, in the matrix of unheated Murchison, are lost from the 990 °C-heated sample due to evaporation.

Spectral analysis indicates that the heating causes flattening and bluing of the spectra. 3 µm absorption feature of serpentine becomes smaller at 400 °C and disappeared by dehydration at 700 °C, which is consistent with the mineralogical analysis. The reflectance at 0.55 µm decreases from 4.5% to 2.6% by heating at 400 °C, but turns to increase to 8.3% at 990 °C. Spectral comparison indicates that Phaethon is still bluer than the experimentally heated Murchison samples. This suggests that Phaethon surface material would be larger grain size and suffered significant space weathering, both of which tend to change the spectra towards a blue colour [e. g., 5].

These observation clearly indicates that solar radiation heating induces dehydration of phyllosilicates and evaporation of Na and S as well as formation of mm-size aggregates by shrinkage and sintering of pre-existing small phyllosilicate particles on the surface of asteroids. Along with mineralogical and grain-size changes of the surface material, overall reflectance spectra become much bluer and 3 µm absorption feature disappears. We suggest that the mm-size aggregates would be released from Phaethon surface thus becoming Geminid meteoroid material when Phaethon passes its perihelion.

References: [1] S.F. Green et al. (1985) *Monthly Notices of the Royal Astronomical Society* 214:29–36. [2] K. Ohtsuka et al. (2009) *Publications of the Astronomical Society of Japan* 61:1375–1387. [3] T. Hiroi et al. (1996) *Meteorics & Planetary Science* 31:321-327 [4] J. Borovicka et al. (2005) *IAU symp.* [5] C. Lantz et al. (2017) *Icarus* 285:43-53.

SHOCK HISTORY OF THE METAL-RICH CB CHONDRITE QUEBRADA CHIMBORAZO (QC) 001.

T.E. Koch[1]*, F.E. Brenker[1,2], D.J. Prior[3], K. Lilly[3], A.N. Krot[2], M. Bizzarro[4]
[1]Insitut for Geoscience, Goethe University Frankfurt, Germany, [2]Hawai'i Institute of Geophysics and Planetology, School of Ocean and Earth Science and Technology, University of Hawai'i at Mānoa, USA. [3]University of Otago, Department of Geology, New Zealand. [4]Centre for Star and Planet Formation, Natural History Museum of Denmark, Denmark. *t.koch@em.uni-frankfurt.de.

Introduction: The Quebrada Chimborazo (QC) 001 meteorite belongs to the rare group of CB chondrites. These metal-rich carbonaceous chondrites show characteristics that sharply distinguish them from other chondrites [1]. Furthermore, they reached higher shock stages (S3–S4) than most other carbonaceous chondrite groups [1–5]. The high-pressure shock history of CB chondrites is of great interest as they seem to resemble the *P-T* conditions of the Earth transition zone, which might help to understand deep Earth processes as well.

The high density contrast between its two main components, metal and silicate, might lead to a heterogeneous *P-T* distribution during shock [6]. Previous studies of shock metamorphism in CB chondrites reveal several high-pressure phases such as wadsleyite, ringwoodite, majorite, majorite-pyrope solid solution, and coesite [1–5], which indicate *P-T* shock conditions of ≥ 19 GPa and ~ 2100 K. Up to now, the QC 001 meteorite is one of only two geological samples which contain asimowite, the Fe-analog of wadsleyite [7]. It is likely that asimowite crystallized from a Fe-enriched melt produced by a mixture of partially molten Fe,Ni-metal and silicate at very high temperature > 2000 K and pressure ≥ 15 GPa [7]. The purpose of this study is to expand the previous knowledge about the *P-T* conditions and their variation during and after the shock event.

Methods: Transmission electron microscopy on focused ion beam (FIB) sections was performed to obtain detailed high-resolution images, element maps and detailed chemical analysis. Furthermore, we use electron structure refinement techniques (ADT [8]) to better characterize the crystal structure of some high-pressure phases.

Results: Several FIB sections from shock melted areas were studied using TEM. One of the studied FIB sections was cut from an 10×10 µm-sized silicate melt droplet within the metal matrix. This melt droplet consists mostly of wadsleyite grains with unusual high Fe-contents ranging from Fa_{30} to Fa_{40} together with ringwoodite (Fa_{50}) and olivine (Fa_{35-42}, one grain with Fa_{10}) and a few pyroxenes.

Another FIB section was cut from a 68×110 µm-sized chondrule fragment. It consists of an assemblage of olivine ($Fa_{1.4}$) and low-Ca pyroxene with interstitial garnets. Two compositional trends were observed in the garnets: they either have composition of majorite-pyrope solid solution or a composition similar to the Al-rich diopsides of this meteorite.

Discussion: The dominant phase found in silicate melt droplets is Fe-rich wadsleyite which supports the theory of crystallization during post shock *P-T* release when the pressure and temperature were still high, close to peak conditions. The two types of garnet solid solutions, the Ca,Al-rich and the Mg,Al-rich have been found in the CB chondrite Gujba as well [2]. The chemistry of the pyrope-grossular solid solution is close to the chemistry of the Al-enriched diopsides in QC 001 which are also found in other CB chondrites [9]. Deduced from the chemical composition of the garnets and the resemblance between the Ca,Al-rich garnet and the Al-rich diopsides it is very probable that these garnets represent high-pressure polymorphs. Ca-rich (tetragonal) high-pressure garnets in a meteorite formed by solid state transformation has been described by [10] and the importance of majorite to draw conclusions regarding the *P-T* conditions and cooling rate has been shown by [11]. The results from this study propose peak shock condition of $\sim 15 \pm 2$ GPa and $\sim 2100 \pm 200$ K for QC 001.

References: [1] Weisberg M. K. et al. 2006. *Meteoritics & Planetary Science* 36:401–418. [2] Weisberg M. K. et al. 2010. *Meteoritics & Planetary Science* 45:873–884. [3] Koch T. K. et al. 2016. *Annual Meeting of the Meteoritical Society LXXIX*, Abstract #6287. [4] Brenker F. E. et al. 2017. *LPSC XLVIII*, Abstract #1967. [5] Koch T. E. et al. 2017. *LPSC XLVIII*, Abstract #1303. [6] Stöffler D. et al. 1991. *Cosmochimica et Cosmochimica Acta* 55:3845–3867. [7] Bindi L. et al. 2019. *American Mineralogist* in press. [8] Kolb U. 2012. *Uniting Electron Crystallography and Powder Diffraction* 337–347. [9] Krot A. N. et al. 2006. *Meteoritics & Planetary Science* 36:1189–1216. [10] Xie Z. and Sharp T. G.. 2007. *Earth & Planetary Science Letters* 254:433–445. [11] Tomioka N. et al.. 2016. *Science Advances* 2:1–5.

EXCISS, A CHONDRULE FORMATION EXPERIMENT ABOARD THE ISS - FIRST RESULTS.

T. E. Koch[1*], D. Spahr[1], D. Merges[1], A. A. Beck[1], O. Christ[1], S. Fujita[1], P.-T. Genzel[1], J. Kerscher[1], M. Lindner[1], D. Mederos Leber[1], F. Wilde[2], W. Morgenroth[1], B. Winkler[1], F. E. Brenker[1]. [1]Goethe University Frankfurt, Institute of Geoscience, Germany. [2]Helmholtz-Zentrum Geesthacht, HZG Outstation at DESY, Hamburg, Germany.
*t.koch@em.uni-frankfurt.de

Introduction: The EXCISS (Experimental Chondrule Formation aboard the International Space Station ISS) experiment was developed to acquire new insights into one of the most enigmatic processes in planetary science — the formation of chondrules. The purpose of the experiment is to investigate if chondrule formation caused by "nebular lightning" [1–5] is a viable process. Synthetic forsterite (Mg_2SiO_4) dust particles are exposed to electrical discharges at conditions of long-term micro gravity with the aim to observe if particles fuse and/or form chondrule-like objects under this conditions. The experiment is carried out inside a 1.5 U NanoRacks NanoLab aboard the ISS. The experiment was launched with NG-10 on November 17, 2018. After return of the chamber to Earth, we will analyze the experimental products in great detail. In order to adjust the experimental parameters and to compare the results, we performed fusion experiments in our lab on Earth.

Here we present details of the experimental setup as well as the first preliminary results based on data downloaded from the International Space Station ISS together with results from our Earth-based experiments.

Experimental Details: In the experiment aboard the ISS, well characterized olivine dust particles with grain sizes between 80–120 μm were levitating between two W-electrodes in an optically transparent glass sample chamber, filled with Ar at 100 mbar pressure, where they could be subjected to electric arcs. The limitation of the available space made the implementation of this experiment challenging, especially with respect to the generation of high energetic lightning and the integration of an optical recording system. An appropriate circuit was designed in which a DC-DC converter is used to charge three 150 uF capacitors up to 550 V. After being triggered by a high voltage peak generated from an ignition coil causing an ignition spark, the stored energy was released into an arc discharge.

In the first stage of the experiment aboard the ISS we observed the behavior of the dust particles while moderate electrical voltages below those required for discharges were applied. We also induced ignition sparks in order to define the experimental conditions for the fusion experiment. The second stage of the experiment included high energy arc discharges.

On Earth, we used a similar experimental setup to fuse dust particles at the same pressure conditions. We characterized the starting material and the products of the Earth-based experiments by X-ray diffraction, scanning electron microscopy, Raman spectroscopy and synchrotron micro-tomography.

Results: The video material received from the ISS showed that some dust particles initially stuck on the walls and the electrodes. More interesting, most of the particles formed an irregular shaped agglomerate levitating in the sample chamber. This agglomerate was attracted by the charged electrodes. The agglomerate disintegrated when an ignition spark was generated, but shortly afterwards the dust particles agglomerated again. High energy arc discharge experiments led to changes in the particles.

Discussion: The overall structure and the high amount of pores of the agglomerates resemble that of amoeboid olivine aggregates (AOA) present in many primitive meteorites [6], although the mean agglomerate sizes is about 10 times higher. The video material also revealed that the dust particles favor being connected to other dust particles rather than to the electrodes. A quantitative analysis of this behavior and its origin is currently being carried out as well as an analysis of the particle changes.

Outlook: The capsule return is planned with SpaceX flight CRS17 scheduled for end of May 2019.

References: [1] Whipple F. L. (1966) Science 153:54–56. [2] Horányi, M. et al. (1995) Icarus 114:174–185. [3] Desch S. J. and Cuzzi, J. N. (2000) Icarus 143:87–105. [4] Johansen A. and Okuzumi A. (2018) Astronomy & Astrophysics A31:1–22. [5] Güttler C. et al. (2008) Icarus, 195:504–510. [6] Krot A. N. et al. (2004) Geochemistry 64: 185–239.

ASTEROID RYUGU: A "DIAMOND" IN THE SKY LIKE MANY OTHER SMALL CELESTIAL BODIES

G.G. Kochemasov, IGEM of the Russian Academy of Sciences, 35 Staromonetny, 119017 Moscow, RF,(kochem.36@mail.ru).

A first hint on " diamond" shape in cosmos was presented by images of Amalthea –a small Jupiter satellite - acquired by Galileo mission. This hint was not adequately appreciated and did not evoke any discussion. Later on some features of polyhedron shapes were observed in some other asteroids (Mathilde, Ida, Eros, Dactyl, Steins)[1] but were noticed and commented only by a few observers [1, 2]. Now, wealth of small icy bodies are imaged by Cassini cameras and their sometimes almost artificial appearance (like the Plato's polyhedrons and "flying saucers") is commented [3-6]. Such a massive evidence of polyhedron shapes in cosmos claims for an explanation different from seldom impacts usually presumed.

The wave planetology [7-12 & others] main assertion is: "Orbits make structures". As all celestial bodies move in non-round (elliptical, parabolic) orbits with periodically changing accelerations they all are subjected to an action of inertia-gravity forces. These forces arouse in them warping waves that in rotating bodies (but they all rotate!) acquire a stationary character and 4 directions of propagation (ortho- and diagonal). Interferences of these waves produce three kinds of tectonic blocks: uplifting (+), subsiding (-) and neutral (0). Their size depends on warping wavelengths. The longest fundamental wave 1 produces ubiquitous tectonic dichotomy – an opposition of two segments: uplifted and subsided, expanded and contracted ($2\pi R$-structure). The first overtone wave 2 superposes on this segmentation smaller features - sectors (πR-structure, Figs. 1-4). Next overtones give smaller features-granulations.

An essence of tectonic dichotomy is in tendency of 4 interfering waves 1 to make from a body a tetrahedron – the simplest Plato' figure [3, 4]. A dichotomous nature of this figure is revealed in opposition of a vertex and a face (cutting any of its 4 axes one always gets from one side a vertex, from another a face). In one direction three faces narrow towards a vertex (contraction), in opposite direction they expand towards a fourth face (expansion). Most often in small bodies (not only in satellites but also in asteroids and comets) one observes an oblong convexo-concave shape [12 & others] but sometimes at certain points of view a flatten concave side and a sharpened convex side are presented by such a way that a tetrahedron develops. Interfering waves 2 produce an octahedron . At the first time it was observed in a shape of Amalthea (see Kolva's drawing of this satellite after Galileo mission), and name "diamond" was pronounced but no explanation followed. Now some octahedron faces one can observe at a number of small bodies, just to mention Yanus Steins, Ryugu, Bennu (Fig. 1-4). Interfering waves 4 produce a cube. Shorter wavelengths – more vertices in a polyhedron: tetrahedron 4, octahedron 6, cube 8 and so on. Various polyhedrons are present in a body simultaneously because the wave warping occurs in various wavelengths at the same time but particular viewpoints present better view of one of them (for examples, Yanus, Amalthea, Hyperion, Helene, Steins, Ryugu, Bennu).

So, produced by warping waves polyhedron shapes, often detected in small bodies due to their weak gravity, present a real fundamental property of these cosmic bodies. In larger bodies this forms are smoothed by gravity making bodies globular, but still some vertices and edges can be distinguished with help of analyses of geology, geomorphology and geophysics. For an example, "famous" hexagon feature in the northern hemisphere of Saturn presents a face of structural tetrahedron, whereas the southern hemisphere "hurricane" is its opposite vertex. Thus looks the structural dichotomy of this giant gas planet. A hidden octahedron is in Earth (antipodal vertices: 1. New Guinea, 2. Equatorial Atlantic, 3. Easter Isl. 4. Pamirs-Hindukush, 5. Bering Strait, 6. Bouvet Island).

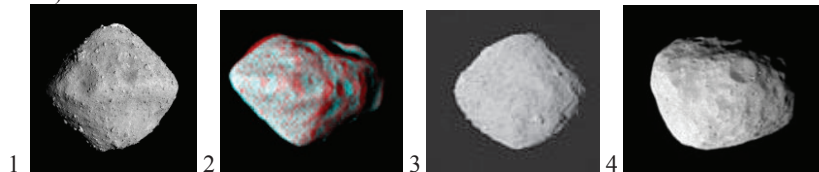1   2   3   4

Fig. 1 Asteroid Ryugu – size 0.92 km   Fig. 2. Asteroid Steins – size 4.6 km. Fig. 3 Asteroid Bennu – 0.56 km. Fig. 4. Yanus PIA06613, radii 110x95x80 km.   The asteroids (Figs. 1-3) demonstrate geometric forms nearing octahedrons and fine intercrossing lineations reflecting stresses due to wave formation of the bodies shape and tectonics.   **References:**

[1] ESA News. Steins: a diamond in the sky, 6 September, 2008 (http://www.esa.int/rosetta); **[2]** Kochemasov G.G. (1999) "Diamond" and "dumb-bells"-like shapes of celestial bodies induced by inertia-gravity waves // 30th Vernadsky-Brown microsymposium on comparative planetology, Abstracts, Moscow, Vernadsky Inst.., 49-50; **[3]** Kochemasov G.G. (2006) The wave planetology illustrated – I: dichotomy, sectoring // 44th Vernadsky-Brown microsymposium "Topics in Comparative Planetology", Oct. 9-11, 2006, Moscow, Vernadsky Inst., Abstr. m44_39, CD-ROM; **[4]** Kochemasov G.G. (2008) Plato' polyhedra as shapes of small icy satellites // Geophys. Res. Abstracts, Vol. 10, EGU2008-A-01271, CD-ROM; **[5]** Porco C.C., Weiss J.W., Thomas P.C. et al (2006) LPSXXXVII, Abstract 2289.pdf; **[6]** NASA News releases-2007-142 Images of Saturn's small moons tell the story of their origin, December 6, 2007**; [7]** Kochemasov G.G. (1992) Concerted wave supergranulation of the solar system bodies // 16th Russian-American microsymposium on planetology, Abstracts, Moscow, Vernadsky Inst. (GEOKHI), 36-37; **[8]** Kochemasov G. G. (1994) 20th Russian-American microsymposium on planetology. Abstr., Moscow, Vernadsky Inst., 46-47; **[9]** Kochemasov G. G. (1998) Proceedings of international symposium on new concepts in global tectonics ('98 TSUKUBA), Tsukuba, Japan, Nov. 1998, 144-147; **[10]** Kochemasov G.G. (1999) Theorems of wave planetary tectonics // Geophys. Res. Abstr., , V.1, №3, p.700; **[11]** Kochemasov G.G. (2004) Mars and Earth: two dichotomies – one cause // In Workshop on "Hemispheres apart: the origin and modification of the martian crustal dichotomy", LPI Contribution # 1203, Lunar and Planetary Institute, Houston, p. 37; **[12]** Kochemasov G.G. (1999) On convexo-concave shape of small celestial bodies // Asteroids, Comets, Meteors. Cornell Univ., July 26-30, 1999, Abstr. # 24.22.

CENTIMETER SIZE CROSSING RIPPLES BOTH ON THE NEAR AND FAR SIDES OF THE MOON (CHANG'E 3 & 4): MODULATION OF THE MOON'S ORBIT BY THE GALACTIC ROTATION.

G. G. Kochemasov, IGEM of the Russian Academy of Sciences, Moscow, RF, 109017, Staromonetny 35,
kochem.36@mail.ru

Intersecting ripples of certain wavelengths and produced them tectonic granules are inversely proportional to the satellite main orbital frequencies (1/1 month – πR/4 and 1/1 year- πR/60 for the Moon) and calculated side frequencies (division and multiplication of the higher frequency by the lower one- πR/15 and πR/240).   Rare chances present the landings of the Chinese probes Chang'e 3 & 4 on the Mare Imbrium and the SPA Basin areas. Landing surfaces possibly cleaned by thruster jets of landing device revealed clear crossing lineation of a few centimeters spacing and produced them granules. This very fine granulation fortunately can be calculated comparing it with a track of the Yutu' rovers weels. (about 10 cm wide). An explanation of the granule size should be done with the above modulation procedure using two frequencies as was done for some celestial bodies earlier [1] . The Moon main frequencies are 1/1 year and 1/1 month, the modulating Galaxy frequency is about 1/200 000 000 years. A scale is the Earth's orbiting period 1 year with the corresponding tectonic granule size πR/4.

Calculations for the Moon:

(1y. : 200 000 000y)πR = (1 : 200 000 000) 3.14 x 1738 km = 5.46 cm wave length for the circumsolar orbiting (or 0.46 cm wavelength for the around Earth orbiting). By the same galactic frequency modulation one obtains enigmatic metric radio waves for the Sun and decametric waves for Jupiter. Radio emission of the Moon at 2.5 cm wavelength was described in Berezhnoi et al., 2001. It is worth to note that well known radio wave and gamma-ray background observations are added by soft X-rays emitting from various celestial bodies – from cold comets to the hot Sun and measured by the Chandra X-ray Observatory.

The Chinese Chang'E-1 orbiter was equipped with a passive microwave radiometer (MRM) to measure the natural microwave emission from the lunar surface. The microwave emission, characterized by a frequency-dependent brightness temperature, is related to the physical temperature and dielectric properties of the lunar surface. By measuring the brightness temperatures at different frequencies, detailed thermal behavior and properties of the lunar surface can be retrieved. The resulting maps show fine structures unseen in previous microwave maps that disregarded the local time effect. The new features revealed and their possible connections with the lunar geology were discussed. Daytime brightness temperatures are found to correlate well with TiO_2 abundance by numerical analysis.

Thus, some relationship between lunar microwave emission and the geological background was discussed earlier. In the present work we show existence of the fine crossing rippling of the lunar surface at the microwave lengths and its origin indicating at galactic structuring trace [1] . Both the far and near sides, south and north of the Moon - thus, the whole body - are affected.
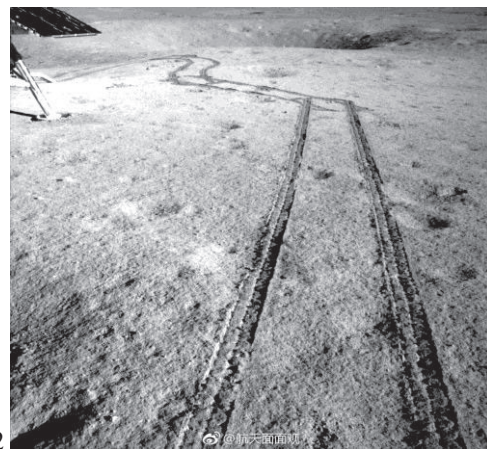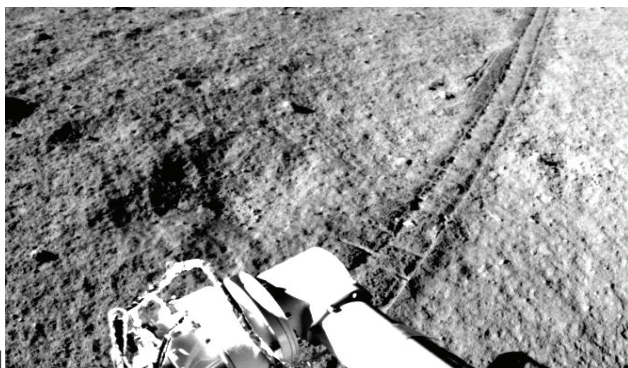

Fig. 1. Yutu's rover weel track on Mare Imbrium surface clearly showing fine intercrossing lineation (centimeters spacing). A portion of Chang'E 3 image 00

Fig. 2. Image Chang'E 4 DwEFLIgUwAEMYFq-1(Credit: CNSA/CLEP) in the SPA Basin. Crossing centimeter spacing rippling.

[1] Kochemasov G.G. Modulated wave frequencies in the Solar system and Universe // Universal Journal of Physics and Application 12(4): 68-75, 2018. Doi: 10.13189/ujpa.2018.120402.

A FRESH IN SITU SEARCH FOR SIGNS OF ^{60}FE IN PRIMITIVE CHONDRITES.

J. Kodolányi[1], P. Hoppe[1], C. Vollmer[2], [1]Max Planck Institute for Chemistry (Hahn-Meitner-Weg 1, 55128 Mainz, Germany; j.kodolanyi@mpic.de), [2]University of Münster, Institute for Mineralogy (Corrensstrasse 24, 48149 Münster, Germany)

Introduction: The presence of the short-lived radioactive isotope ^{60}Fe (t½ ~ 2.60×10^6 years) at the birth of our solar system has been debated, and so has its importance as a heat source for the differentiation of early solar system bodies. In particular, there is a discrepancy between the initial ^{60}Fe/^{56}Fe ratios inferred from bulk rock and in situ mineral data (e.g., [1,2]), with some in situ measurements yielding 1–2 orders of magnitude higher inferred initial ^{60}Fe/^{56}Fe ratios than bulk rock and other in situ data. In order to unequivocally answer the question, whether there was any time or place in the early solar system with ^{60}Fe present at significantly higher levels than the Galactic background (^{60}Fe/^{56}Fe $\leq$ ~3×10^{-7} [3,4]), or the level suggested for the source region(s) of angrite and HED parent body matter (^{60}Fe/^{56}Fe ~1×10^{-8}, [2]), we are measuring the ^{60}Ni/^{62}Ni and Fe/Ni ratios of high Fe/Ni phases (troilite, chondrule silicates, and CAI minerals with sufficiently high Fe/Ni ratios) from primitive L/LL, CO, and CR chondrites in situ, using the NanoSIMS. The new Hyperion primary ion source of this instrument allows Fe-Ni isotope analysis with a better spatial resolution than before (2–3 vs. ~10 μm spot diameter) at the same primary ion intensity.This helps to avoid cracks and grain boundaries for improved in situ analyses at the same precision, following the protocol of [1].

Results and Discussion: Detailed petrography and electron microprobe measurements of thin sections of Semarkona (LL3.0), North West Africa 8276 (L3.0), and Dominion Range 08006 (CO3.0) have been completed, and we performed our first isotope measurements on Semarkona troilite grains. Prior NanoSIMS test measurements on troilite from the Mundrabilla meteorite and on artificial iron-sulphide minerals, as well as Monte Carlo simulations suggest that statistical effects resulting from the low nickel count rates during NanoSIMS analyses do not cause a significant positive bias in the measured ^{60}Ni/^{62}Ni as a function of Fe/Ni ratios. Our preliminary isotope measurements do not indicate the former presence of ^{60}Fe in Semarkona troilite grains, as all of them yielded identical ^{60}Ni/^{62}Ni ratios within two times analytical uncertainty (Figure 1). This is in contrast to the results of [1], who observed a positive correlation between ^{60}Ni/^{62}Ni and ^{56}Fe/^{58}Ni ratios in Semarkona troilites, which they interpreted to be the result of in situ ^{60}Fe decay. Note however, that we have not yet analysed troilite with the highest Fe/Ni ratios found by [1] (Figure 1).
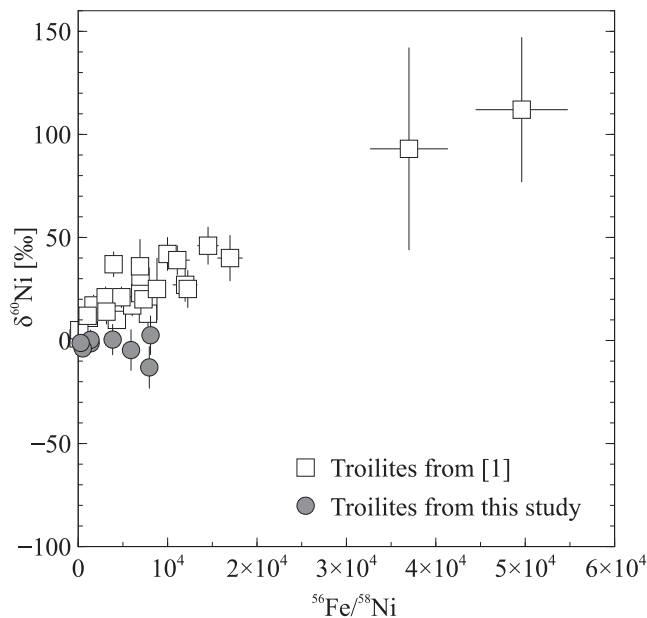

***Figure 1.** 60-Nickel isotope anomalies as a function of ^{56}Fe/^{58}Ni ratios in Semarkona troilites. $\delta^{60}Ni = 1000 \times [(^{60}Ni/^{62}Ni)_{Troilite}/(^{60}Ni/^{62}Ni)_{Terrestrial}-1]$. ^{56}Fe/^{58}Ni ratios were calculated from measured ^{54}Fe/^{62}Ni ratios, assuming that the troilite grains have terrestrial ^{54}Fe/^{56}Fe and ^{62}Ni/^{58}Ni ratios. Errors are 1σ.*

Outlook: We plan to re-analyse minerals with high inferred initial ^{60}Fe/^{56}Fe ratios with the Chicago Instrument for Laser Ionization [5]. Being able to measure all nickel isotopes simultaneously, the latter instrument can reveal isotope fractionation effects that cannot be detected by (Nano)SIMS [6] and avoids isobaric interferences on ^{60}Ni and ^{62}Ni. The Al-Mg isotopes of high Al/Mg phases associated with the targets of our Fe-Ni isotope measurements will be also analysed (NanoSIMS) to constrain the objects' age relative to canonical CAIs. Transmission electron microscopy is also planned, to track possible disturbance of the iron-nickel system in minerals with or without apparent initial excess of ^{60}Fe.

References: [1] Mostefaoui S. et al. (2005) *The Astrophysical Journal* 625:271–277. [2] Tang H. and Dauphas N. (2012) *Earth & Planetary Science Letters* 359–360:248–263. [3] Wang W. et al. (2007) *Astronomy & Astrophysics* 469:1005–1012. [4] Vescovi D. et al. (2018) *The Astrophysical Journal* 863:115. [5] Stephan T. et al. (2016) *International Journal of Mass Spectrometry* 407:1–15. [6] Boehnke P. et al. (2017) *80th Meeting of the Meteoritical Society*, Abstr. #6243.

HYDROXY AMINO ACIDS IN CARBONACEOUS CHONDRITES.

Toshiki Koga[1,2,3*], Hannah L. McLain[2,4], José C. Aponte[2,4], Eric T. Parker[2], Jamie E. Elsila[2], Jason P. Dworkin[2], Daniel P. Glavin[2], Hiroshi Naraoka[1]
[1]Kyushu University, Nishi-ku, Fukuoka, Japan. [2]NASA Goddard Space Flight Center, Greenbelt, MD, USA. [3]University of Maryland, Baltimore County, Baltimore, MD, USA. [4]Catholic University of America, Washington, DC, USA. (*Email: koga.toshiki.590@s.kyushu-u.ac.jp)

Introduction: Carbonaceous chondrites contain a variety of organics of potential importance for life. Of these, amino acids have been extensively studied since they: 1) plausibly contributed to the origin of life on Earth, 2) provide insight into parent body chemistry, 3) serve as a vehicle to examine the origin of homochirality, and 4) analytical methods are mature ([1] and references therein).

While aliphatic amino acids have been well studied in meteorites, until recently, -OH bearing amino acids, or hydroxy amino acids (HAAs) have been neglected, except for serine. Nine C3 and C4 HAAs were detected in both the acid hydrolyzed hot water extract of the Murchison (CM2) meteorite and in the acid hydrolyzed post-extraction residue [2]. Interestingly, aliphatic amino acids, such as isovaline, were detected at lower abundances in the post-extraction residue than in the hot water extract, while the reverse is true for some HAAs. Perhaps HAAs have a stronger affinity to minerals than aliphatic amino acids. It is possible that such an affinity could manifest in strong correlations between HAA chemistry and meteorite petrology. Since the isomeric and enantiomeric compositions of meteoritic amino acids have provided implications for parent body processes [1], similar analyses of HAAs should provide additional insight into the early Solar System, and perhaps contributed to the origin of life on Earth.

To this end, we describe here the development of a new gas chromatography–mass spectrometry (GC-MS) method to detect and quantify structural isomers and enantiomers of C3 and C4 HAAs (**Figure 1; Table 1**). Target analytes underwent pre-column derivatization by heptafluorobutyric anhydride and isopropanol (HFBA-IPA derivatization). Subsequently, we are applying this new method in parallel with established liquid chromatography–mass spectrometry methods [3] to analyze the following meteorites, which have differing petrology and mineralogy, for HAAs in the water extracts and the extracted residues of these meteorites: Yamato 791198 (CM2), Asuka 881458 (CM2), LEW 90500 (CM2), LON 94101 (CM2), ALH 83100 (CM1/2), MET 00426 (CR3), MIL 07525 (CR2), GRO 95577 (CR2), and LAP 02342 (CR1). This paper will detail results from our analyses of these meteorites for HAAs using our newly developed method.
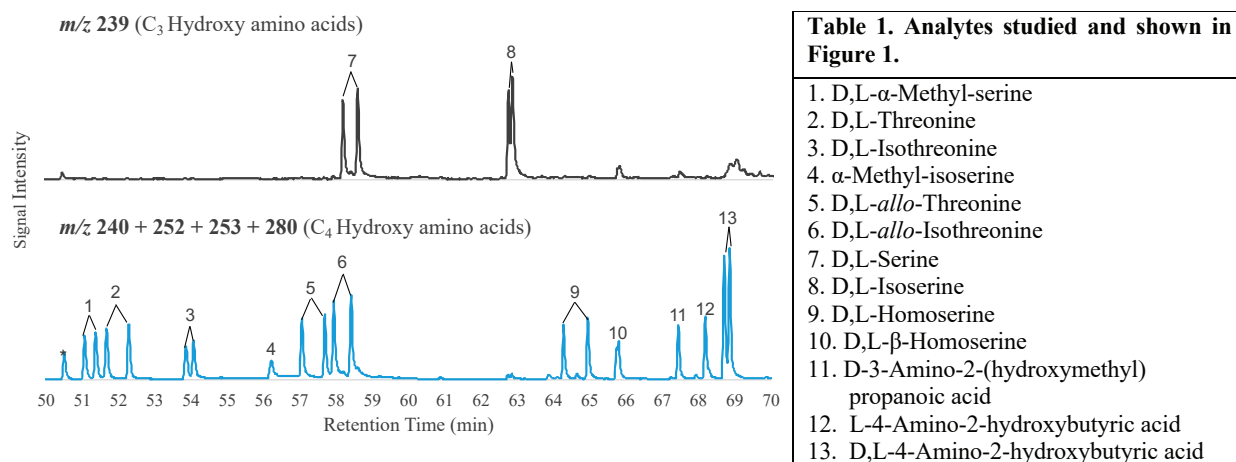

Table 1. Analytes studied and shown in Figure 1.

1. D,L-α-Methyl-serine
2. D,L-Threonine
3. D,L-Isothreonine
4. α-Methyl-isoserine
5. D,L-*allo*-Threonine
6. D,L-*allo*-Isothreonine
7. D,L-Serine
8. D,L-Isoserine
9. D,L-Homoserine
10. D,L-β-Homoserine
11. D-3-Amino-2-(hydroxymethyl) propanoic acid
12. L-4-Amino-2-hydroxybutyric acid
13. D,L-4-Amino-2-hydroxybutyric acid

Figure 1. The 50.8–69.4 min regions of the GC-MS extracted ion chromatograms of HFBA-IPA HAA derivatives (C3 HAA: m/z = 239; C4 HAA: m/z = 240 + 252 + 253 + 280). Peak identities are in Table 1.

References:
[1] Elsila J. E. et al. (2016) *ACS Central Science*, 2:370-379. [2] Koga, T. and Naraoka, H. (2017) *Scientific Reports*, 1–8. [3] Glavin, D. P. et al. (2010) *Meteoritics & Planetary Sci*ence 45: 1948-1972.

ULTRA-REFRACTORY CAI IN A LOW-CA PYROXENE- AND SILICA-BEARING AMOEBOID OLIVINE AGGREGATE IN A CR CHONDRITE: FORMATION BY GAS-SOLID CONDENSATION OVER A WIDE TEMPERATURE RANGE.

M. Komatsu[1,2], T. J. Fagan[2], A. N. Krot[3], K. Nagashima[3], M. I. Petaev[4], M. Kimura[5], and A. Yamaguchi[5], [1]SOKENDAI (The Graduate University for Advanced Studies), Hayama, Kanagawa 240-0193, Japan (komatsu_mutsumi@soken.ac.jp), [2]Dept. Earth Sci., Waseda Univ., Japan, [3]HIGP, Univ. Hawai'i at Mānoa, USA, [4]Dept. Earth Planet. Sci., Harvard Univ., USA, [5]National Institute for Polar Research (NIPR), Japan.

Introduction: Calcium-aluminum-rich inclusions (CAIs) and amoeboid olivine aggregates (AOAs) are thought to have formed in a high-temperature region of the protoplanetary disk, most likely near the proto-Sun, characterized by approximately solar chemical and oxygen isotopic compositions [e.g., 1]. The AOAs are enriched in equant grains of forsterite with variable proportions of embedded CAIs; AOAs have avoided significant melting after the aggregation. Therefore, AOAs from the weakly-metamorphosed chondrites may retain records of nebular gas-solid interactions. Here we describe an AOA from the CR chondrite Y-793261 providing an evidence for gas-solid condensation over a wide temperature range.

Analytical methods: A polished thin section of Y-793261 was studied using SEM, EPMA, Raman spectroscopy at NIPR, and SIMS oxygen isotopic analyses with the University of Hawai'i Cameca ims-1280. Condensation temperatures and cooling rates were modeled using the GRAINS thermodynamic/kinetic code [2].

Results and Discussion: *Mineralogy and Petrography.* Y-793261 consists of chondrules, refractory inclusions, mineral fragments, and a fine-grained matrix. It experienced a minor degree of aqueous alteration, including partial replacement of chondrule glass and matrix by phyllosilicate and of Fe,Ni-metal by magnetite and Fe,Ni-sulfides; olivine and pyroxene phenocrysts in chondrules are largely unaltered. These alteration features and Raman characteristics of matrix areas suggest that the petrologic type of Y-793261 is ~ 2.5–2.6 [3].

One of the Ca-Al-rich domains of AOA #4 in Y-793261 is mineralogically distinct: it consists of Zr,Sc,Al,Ti-rich pyroxenes, compositionally similar to davisite [4], enclosing submicron grains of Zr-rich oxides and spinel, all surrounded by Al,Ti-diopside. The Zr,Sc-rich pyroxene and oxides are characteristic minerals of ultrarefractory (UR) CAIs, and in light of the high condensation temperatures of Zr and Sc, are indicators of crystallization at UR conditions [e.g., 5]. A detailed description of AOA #4 is reported in [6].

A peculiar characteristic of AOA #4 is the presence of silica at a few localities in the AOA interior, where it occurs as anhedral, ~5 µm-sized grains associated with low-Ca pyroxene. Raman spectra of the silica grains show a sharp peak at 464 cm^{-1} diagnostic of quartz.

Oxygen-Isotope Compositions. Forsterite, Al-diopside, low-Ca pyroxene, quartz, and Zr,Sc-rich pyroxenes in AOA #4 have similar ^{16}O-rich compositions (Δ^{17}O ~ −22±2‰) typical of CAIs and AOAs from unmetamorphosed chondrites (Δ^{17}O ~ −24‰; e.g., 7). The uniformly ^{16}O-rich composition of the AOA is distinct from the ^{16}O-poor compositions of whole rock samples of CR chondrites [e.g., 8], olivine and pyroxene phenocrysts in CR chondrules (Δ^{17}O ~ −6 to 0‰) [9], and secondary carbonates and magnetite that precipitated from aqueous solutions in CR matrices (Δ^{17}O ~ −3 to +2‰) [10]. These observations indicate that the minerals in AOA #4 originated in an ^{16}O-rich gaseous setting of approximately solar composition, and subsequently avoided oxygen isotopic exchange with ^{16}O-poor reservoirs, such as a nebular gas associated with chondrule formation and an aqueous fluid associated with alteration of CR chondrites.

Origin and Astrophysical Implications. The presence of an UR CAI, forsterite, low-Ca pyroxene and silica in the Y-793261 AOA#4 records its formation by gas-solid reactions over a wide temperature range from ~1800 to ~1150 K. Based on the condensation calculations, we find that the observed forsterite grain size (~5 µm) and chemical composition of low-Ca pyroxene are reasonably matched by condensation of a nebular gas depleted in H$_2$ and He by ~10× that has cooled at a constant rate of 50K/h at a total pressure of 10^{-4} bar. The presence of both UR minerals and silica in the same AOA implies an effective isolation of condensates during formation of the Y-793261 refractory object [10]. Our observation provides the first direct evidence for gas-solid condensation of ^{16}O-rich silica coincident with formation of refractory inclusions in the solar nebula.

References: [1] Scott E. R. D. and Krot A. N. (2014) *Treatise on Geochemistry* 1:65–137. [2] Petaev M.I. (2009) *Calphad* 33:317–327. [3] Harju E. R. et al. (2014) *GCA* 139:267–292. [4] Ma C. (2009) *Am. Mineral.* 94:845–848. [5] Ivanova M. A. et al. (2012) *MaPS* 47:2107–2127. [6] Komatsu et al. (2018) *PNAS* 115:7497–7502. [7] Yurimoto H. et al. (2008) *Reviews in Mineralogy and Geochemistry* 68:141–186. [8] Schrader D. L. et al. (2011) *GCA* 75:308–325. [9] Tenner T. J. et al. (2015) *GCA* 148:228–250. [10] Jilly-Rehak C. E. et al. (2018) *GCA* 222:230–252. [11] Petaev M. I. and Wood J. (1998) *MaPS* 33:1123–1137.

RYUSEITO: THE JAPANESE SWORDS MADE FROM SHIRAHAGI IRON METEORITE.

M. Komatsu[1], A. Yamaguchi[2], M. Ito[3], S. Yoneda[4], T. Saito[5], T. Ohgane[6], T. Hayashi[7], M. Sakamoto[5], T. Mikouchi[8], M. Kimura[2]. [1]SOKENDAI (The Graduate University for Advanced Studies), Hayama, Kanagawa 240-0193, Japan (komatsu_mutsumi@soken.ac.jp), [2]National Institute for Polar Research, [3]Kochi Institute for Core Sample Research, JASMTEC, [4]National Museum of Nature and Science, [5]National Museum of Japanese History, [6]Otaru Museum, [7]Toyama Science Museum, [8]University Museum, The University of Tokyo.

Introduction: Meteorites are not only scientifically important, but they also give us information about the history of interaction of people with extraterrestrial objects. Many cultures have considered the arrival of meteorites as celestial omens: meteorites were, and occasionally still are considered to be intricately linked to gods, and treated as objects of religious devotion. In addition, recent studies of meteorite artifacts revealed the use of meteor metal such as beads and knife [1,2], and the ancient trade network in North America [3].

Ryuseito, the Meteor Swords, are the Japanese swords made from iron meteorite in 1898. They were manufactured by Japanese notable swordsmith Okayoshi Kunimune by the order of Viscount Enomoto Takeaki in Meiji period. Enomoto stayed in Russia as a special envoy to conduct negotiation with Russia, where he was fascinated by the Russian meteor sword *Sowerby's Sword* for the Czar Alexander I [4, 5].

Ryuseito are made from Shirahagi iron meteorite (IVA). Shirahagi meteorite, weighing 22.7 kg, was reported in 1890 to have been found in the bed of the Kamiichigawa river, Toyama prefecture, Japan, and then was purchased by Enomoto in 1895. Enomoto reported the chemical analysis of the Shirahagi iron meteorite, and described the processes of producing meteor swords in *Ryuseito Kiji* (The Meteor Swords Report)[6], which is one of the first science paper about the iron meteorite in Japan. According to his report, about 4 kg of Shirahagi iron meteorite was consumed to produce the total of five swords including two long swords and three short swords. One of the long sword was donated to the crown prince who later became the Taisho Emperor. In this study, we have investigated the historical background of making the meteor swords and non-destructive observation of the *Ryuseito* itself.

Methods: We have investigated the short sword which is the one of the five *Ryuseito* swords, the one now owned by Toyama Science Museum. We performed a research on historical background of making *Ruyseito*, and non-destructive surface observation on *Ryuseito* itself.

Results and Discussion: The short sword investigated in this study is ~30 cm long in size, and the blade length is ~21 cm. The words "Sei Tetsu (Star Iron)" and "Meiji 31 nen 3 gatsu jitsu (March 1898)" are carved on the front and the back side of the tang of the sword, respectively. The blade of the sword shows a tree ring-like pattern on their surface (Fig.1). It is likely the pattern is the same one that *Ryuseito Kiji* described, in which it is explained that the pattern is the characteristics of the meteor swords, and the long sword showing a fine tree ring-like pattern was donated to the crown prince [6].

One of the most characteristics of manufacturing Japanese sword is the forging process, where the swords are made by repeatedly heating, hammering and holding the iron sand metal. Enomoto described that the swordsmith had a difficulty in making swords from meteorite, but finally found a reasonable forging conditions to produce meteor swords [6]. Later study on the examination of manufacturing meteorite sword concluded that impurities play an important affect for forging process -- the amount of impurities such as S and P increases the difficulty in heat-forging [7]. These impurities are attributed to FeS and schreibersite, and the cracks during heat-forging are caused by these crystals. We find the surface of the studied sword is quite homogeneous, showing no evidence of these crystals or cracks.

In conclusion, *Ryuseito* are the meteorite artifacts with the full record of the identification as a meteorite, chemical analysis, and the manufacturing process of meteor sword [4-6], which holds both scientifically and historically valuable information.

References: [1] Rehren T. et al. (2013) *Jour. of Archaeological Sci.* 40:4785-4792. [2] Comelli D. et al. (2016) *MaPS* 51:1301-1309. [3] McCoy T. J. et al. (2017) *Jour. of Archaeological Sci.* 81:13-22. [4] Enomoto T. (2003) *Jour. of Geography* 112:453-457. [5] Murayama S. (1953) *Meteoritics* 1:99-102. [6]Enomoto T. (1898, abr in 1902) *Jour. of Geography,*14:33-35. [7] Taguchi I. (1991) *Bull. of the National Museum of Japanese History* 35:355-372.
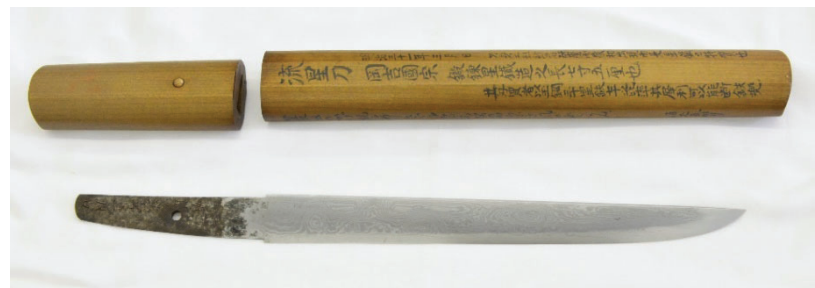
Fig.1. Photograph of *Ryuseito*. A tree-like pattern is observed on the surface of the blade. The full length of the sword is ~30cm.

THE OZERKI METEORITE: PETROLOGY AND THE FIRST DATA ON NOBLE GASES AND NITROGEN RELEASED BY STEPWISE COMBUSTION AND CRUSHING METHODS.

E. V. Korochantseva[1], A. B. Verchovsky[2], C. A. Lorenz[1], A. I. Buikin[1], A. V. Korochantsev[1], [1]Vernadsky Institute of Geochemistry and Analytical Chemistry RAS, Kosygin St. 19, 119991 Moscow, Russia, [2]School of Physical Sciences, The Open University, Milton Keynes, MK7 6AA, UK (sasha.verchovsky@open.ac.uk).

Introduction: The Ozerki meteorite shower fell on June 21, 2018 in Russia. More than 100 individual stones were found. The total recovered mass of the meteorite rain is >10 kg. Ozerki is classified as ordinary chondrite (L6, W0, S5) [1]. Preliminary study of the chondrite indicates absence of heavy particle tracks in olivine (Ol) grains presumably due to the low cosmic-ray exposure (CRE) age of this meteorite and the deep location of the studied sample ($\geq$ 30 cm) in the pre-atmospheric body with radius $\geq$ 50 cm [2]. We report petrological information on this meteorite and preliminary data on noble gases and nitrogen extracted by stepped combustion and crushing methods.

Results and discussion: Ozerki has a brecciated texture. Some individual samples are completely chondritic, while others represent fragments of melt matrix breccia. These two lithologies have different degrees of shock metamorphism. In thin sections the completely chondritic species of the meteorite show recrystallized texture with rare relics of large (up to 1.5 mm) chondrules. Ol is only weakly and irregularly fractured and has mostly sharp optical extinction corresponding to shock stage S1 by [3]. The melt matrix of the breccia consists of rounded chondritic fragments from tens of µm to several cm in size joined together by shock melt (matrix). The fragments demonstrate different degrees of shock darkening. Ol in the fragments has weak wavy extinction and some planar fractures. Feldspar has also wavy extinction. These impact features correspond to shock stage S3 [3]. Large troilite (Tr) inclusions are polycrystalline. The veins of Tr and FeNi metal (Met) are abundant in the chondritic fragments. The melt matrix varies in texture from emulsion aggregate of submicron-sized Met, Tr and silicate phases to devitrified crypto- to microcrystalline (1-2 µm) silicate melt with Met-Tr globules of 5-200 µm in size. Some Met-Tr veins cross both chondritic fragments and melt matrix of the breccia and are associated with the fragmentation zones composed of chondritic and shock melt fragments cemented by troilite. Obviously these objects were formed after the impact breccia formation during a subsequent shock event on the L-chondrite parent body.

The samples of chondritic material (5.059 mg) and fine-grained melt matrix breccia (3.006 mg) have been studied by stepped combustion method. The specimens were stepwise heated in oxygen from 200 °C to 1500 °C (12-14 temperature steps). Chondritic material contains ^{4}He = 191, ^{20}Ne = 5.71, ^{36}Ar = 1.07 and ^{40}Ar = 1171 ($\times 10^{-7}$ cm^3 STP/g). The contents of these isotopes in melt matrix breccia are 104, 1.21, 1.28 and 649 ($\times 10^{-7}$ cm^3 STP/g), respectively. ^{20}Ne/^{22}Ne ratios in the samples are < 10. Ozerki experienced a significant shock event, and ^{36}Ar amounts in both samples are comparable to these in highly shocked meteorites that trapped gases during impact events: e.g., dark chondritic lithology of Chelyabinsk (LL5) contains ^{36}Ar$_{trapped}$ = 1.86 $\times$ 10^{-8} cm^3 STP/g accounting for ~95 % of the total ^{36}Ar release [4]; (7-33) and (15-43) $\times$ 10^{-8} cm^3 STP/g were released from the Gubara chondrite (L5) during stepwise combustion and crushing, respectively [5]. Hence, it could be expected that Ozerki also contains gases redistributed and trapped during a shock event. We conducted noble gas and nitrogen stepwise crushing of the sample of chondritic material (86 mg) with cumulative number of strokes of 6000. The data of the first two factions were lost due to technical problems. In the next four crushing steps 9.06 $\times$ 10^{-9} of ^{36}Ar and 1.68 $\times$ 10^{-5} of ^{40}Ar (in cm^3 of STP/g) were extracted. ^{40}Ar/^{36}Ar ratios in all extraction steps are ~2000 (varying from 1831 to 2120). A similar isotopic composition of trapped argon was previously determined in the high temperature steps of the dark chondritic lithology of Chelyabinsk: (^{40}Ar/^{36}Ar)$_{trapped}$ = 1869 $\pm$ 214 [4]. N abundance released by crushing is only12 ng/g (a significant part of nitrogen could be released in the first two lost steps). It is not possible to calculate correctly nitrogen isotopic composition because of its very low content in steps. We intend to repeat crushing experiment on a sample of chondritic material of Ozerki, significantly increasing the sample weight as well as to perform crushing analyses on a sample of the fine-grained melt matrix breccia of this meteorite.

The amount of ^{21}Ne$_{cos}$ in the sample of chondritic material studied by stepped combustion is 0.47$\times 10^{-8}$ cm^3 STP/g calculated using the endmember compositions of Ne$_{SW}$ with ^{20}Ne/^{22}Ne=13.78 and ^{21}Ne/^{22}Ne=0.0329 [6] and Ne$_{cos}$ with ^{20}Ne/^{22}Ne=0.8 [7] and ^{21}Ne/^{22}Ne = 0.86 (the average value for the (^{21}Ne/^{22}Ne)$_{cos}$ range, see [5]). The CRE age is ~1.3-1.5 Ma calculated using the model by [8] and the assumption of the pre-atmospheric meteoroid radius of Ozerki to be 65-85 cm (taking into account radius evaluation by [2]).

References: [1] Meteoritical Bulletin, no. 107 (2018) https://www.lpi.usra.edu/meteor/ . [2] Alexeev V. A. et al. (2019) *Proceed. Rus. An. Sem. on Exp. Mineral., Petrol. and Geochem.,* in press *(in Russian)*. [3] Stöffler D. et al. (1991) *GCA* 55:3845-3867. [4] Trieloff M. et al. (2018) *MAPS* 53:343-358. [5] Korochantseva E.V. et al. (2018) *Geochemistry International* 56:1384-1397. [6] Heber V. S. et al. (2009) *GCA* 73:7414-7432. [7] Eugster O. and Michel Th. (1995). *GCA* 59:177-199. [8] Leya I. and Masarik J. (2009) *MAPS* 44:1061-1086.

HF-W AND U-PB DATING AND REE AND TI ANAYLYSIS OF ZIRCONS EXTRACTED FROM MESOSIDERITES.

Y. Koyama[1], Y. Sano[1], N. Takahata[1], M. Koike[2] and M. K. Haba[3], [1]Atmosphere and Ocean Research Institute, The University of Tokyo, (5-1-5 Kashiwanoha, Kashiwa, Chiba 277-8564, Japan e-mail: koyama@aori.u-tokyo.ac.jp), [2]Department of Solar System Sciences, Institute of Space and Astronautical Science, Japan Aerospace Exploration Agency, [3]Department of Earth and Planetary Sciences, Tokyo Institute of Technology (Tokyo 152-8551, Japan).

Introduction: Mesosiderites are a group of stony-iron meteorites, consisting of about equal parts of metallic iron-nickel and silicates. Their silicates are similar to howardite-eucrite-diogenite (HED) meteorites in mineralogy, chemistry and oxygen isotopes [1]. One of the models for mesosiderite parent body is proposed by [2]. In this model, the earlier stratified parent body was possibly destroyed by a catastrophic impact and reaccreted with a core, mantle, crust materials mixture [2]. To study the history of mesosiderite parent body, we have conducted Hf-W and U-Pb dating, rare earth elements and titanium concentration analyses of zircons. Their crystallization temperatures were estimated according to Ti-thermometer [3]. The accurate Hf-W dating of zircons in a mesosiderite was firstly reported by an ion microprobe study [4]. However, there is no natural zircon standard with abundant tungsten because of its incompatibility in zircon crystal. To overcome this difficulty, we created the new standard zircons with known amount of Hf and W, and applied them to Hf-W dating of three mesosiderites [5]. We also report the U-Pb ages, REE and Ti concentrations of the same mesosiderites zircons in order to discuss their origins and evolutions.

Experiment: Fourteen zircon grains in total were extracted from 3 mesosiderites (Asuka 882023, Northwest Africa 1242, Vaca Muerta) [6] and embedded on epoxy resin disk. They are all anhedral with grain sizes of 40–60 μm. No growth bands or heterogeneous bright pattern was observed by a cathodoluminescence. All isotopic and leelmental analyses were conducted using NanoSIMS 50 at AORI, UTokyo. A 2 nA O- primary beam was used to sputter a 7–8 μm diameter crater on the zircon surface. A high mass resolving power of 9,400 at 10 % peak height was attained to separate the heavy REEs from the oxide of light REEs with adequate flat top. A multi-collector system combined with peak-jumping by magnetic field was adjusted to detect REEs and matrix ions (^{30}Si). All REEs and Ti intensities relative to ^{30}Si (i.e. REE/^{30}Si and ^{49}Ti/^{30}Si ratios) were calibrated against those of NIST SRM610 glass standard, under the assumption that the matrix effects are insignificant at the high mass resolving power mode [7]. Titanium concentration analysis and Pb-Pb dating of the zircons were conducted separately, where the latter experiment followed the previous study [8].

Results & Discussion: The concentrations of REEs and Ti of the zircons were calculated to acquire their crystallization temperature. Lead-Pb ages of the individual zircon grains were calculated under the assumption that the isotopic compositions of initial Pb are identical to those of Canyon Diablo Troilite [9]. NanoSIMS relative sensitivity factor of Hf/W ratio was determined with our new standard zircons [5]. Absolute ages of individual zircon grains were calculated with their ^{182}Hf/^{180}Hf values and the anchor age of 4565.3 Ma for Ste. Marguerite [10]. Hf-W ages vary from 4532 Ma to 4548 Ma with the average of 4540 Ma, younger than 4563 Ma of smaller and euhedral zircon in Vaca Muerta measured by SHRIMP [11]. The titanium thermometer suggests the formation temperature of zircon between 791 °C and 952 °C. It may be possible to calculate the cooling rate by the combination of Hf-W age and the temperature. Enrichment of heavy REE with increasing mass number, positive Ce anomaly and negative Eu anomaly in normalized patterns are common features of terrestrial zircon samples [12]. REE contents of mesosiderite zircons are generally lower than terrestrial ones similar to the previous report [13], while the graph rising to the right in REE patterns is similar to that of terrestrial ones. In some samples, the enrichment from La to Gd is smaller than that from Tb to Lu, suggesting metamorphic signature [14].

References: [1] Greenwood R. C. et al. (2006) *Science* 313:1763–1765. [2] Scott E. R. D. et al. (2001) *Meteoritics & Planetary Science* 36:8569–881. [3] Watson E. B. et al. (2006) *Contributions to Mineralogy and Petrology* 151:413–433 [4] Koike M. et al. (2017) *Geophysical Research Letters* 44:1251–1259. [5] Koyama Y. et al. (2019) *JpGU 2019,* abstract SGL27-08. [6] Haba M. K. et al. (2019) *Annual Meeting of the Meteoritical Society Abst.* (submitted) [7] Sano Y. et al. (2002) *Chemical Geology* 184:217–230. [8] Takahata N. et al. (2008) *Gondwana Research* 14:587–596. [9] Stacey J. S. and Kramers J. D. (1975) *Earth and Planetary Science Letters* 26:207–221. [10] Kleine T. et al. (2004) *Geochimica et Cosmochimica Acta* 68:2935–2946. [11] Ireland T. R. and Wlotzka F. (1992) *Earth and Planetary Science Letters* 109:1–10. [12] Hinton R. W. and Upton B. G. J. (1991) *Geochimica et Cosmochimica Acta* 55:3287–3302. [13] Haba M. K. et al. (2017) *Geochimica et Cosmochimica Acta* 215:76–91. [14] Takehara M. et al. (2018) *Chemical Geology* 484:168–178.

CALETA EL COBRE 022: AN UNUSUAL NAKHLITE WITH ABUNDANT AQUEOUS ALTERATION

L. Krämer Ruggiu[1], J. Gattacceca[1], B. Devouard[1], A. Udry[2], V. Debaille[3], P. Rochette[1], J.-P. Lorand[4], L. Bonal[5], P. Beck[5], V. Sautter[6], M. M. M. Meier[7], M. Gounelle[6], Y. Marrocchi[8], C. Maden[7], and H. Busemann[7].

[1]Aix Marseille Univ, CNRS, Coll France, IRD, INRA, Aix-en-Provence, France (kramer@cerege.fr), [2]Department of Geoscience, University of Nevada Las Vegas, Las Vegas, NV 89154, USA, [3]Laboratoire G-Time, Université Libre de Bruxelles, Belgium, [4]LPG, CNRS UMR 6112, Nantes Univ., France, [5]Univ. Grenoble Alpes, CNRS, IPAG, Grenoble, France, [6]IMPMC, MNHN, Paris, France, [7]ETH Zurich, Inst. Geochem. Petrol., Zurich, Switzerland,[8]CRPG, CNRS, Université de Lorraine, UMR 7358, Vandoeuvre-les-Nancy, France.

Introduction: Nakhlites are Martian clinopyroxene-rich cumulates [1] showing variable amounts of aqueous alteration [2]. They are keys to better understand the martian crust. Caleta el Cobre 022 (CeC 022) is one of only 11 nakhlites (after pairing) discovered to date.

Results: CeC 022 is a clinopyroxenite that crystallized at 1224±69 Ma (Sm-Nd age) and with a cosmic ray exposure age of about 11 Ma (for ^{3}He, ^{21}Ne and ^{38}Ar), similar to other nakhlites. Augite is the major mineral (~58 vol%). It displays rounded cores with iregular sector zoning (ca. $En_{34}Fs_{27}Wo_{39}$) (*Fig. 1*) and Fe-richer overgrowth ($En_{31}Fs_{29}Wo_{40}$). Fe-richer sharp rims ($En_{27}Fs_{35}Wo_{38}$, 10-15 μm wide) are observed only when augite is in contact with the mesostasis. Low-Ca pyroxene ($En_{35}Fs_{61}Wo_4$) is found replacing augite overgrowth near olivine phenocrysts (*Fig. 1*). Olivine crystals ($Fa_{69.7}±_{1.5}$) represent ~3 vol%, and are not zoned (*Fig. 1*). CeC 022 contains large plagioclase laths (up to 1 mm) for ~19 vol%, with homogenous $An_{29.7}±_{4.3}Ab_{67.2}±_{4.0}Or_{3.1}±_{0.5}$ composition, that differs from K-rich feldspar in the mesostasis (up to $An_{4.5}Ab_{60.4}Or_{35.1}$). Intergranular Fe-Ti oxides are abundant (~3 vol%), up to 1 mm size, and present fine-scale ilmenite exsolutions in magnetite. The mesostasis (~16 vol%) contains alkali feldspar, low-Ca pyroxene ($En_{31}Fs_{65}Wo_4$), dendritic apatite, quenched dendritic iron oxides and silica. Olivine presents abundant aqueous alteration as iddingsite, with at least two phases differing in their Fe and Si contents. Both phases are hydrated. Their crystallinity is also different with the Fe richer phase being more crystallized. This material is found mainly in the olivine phenocrysts (*Fig. 1*), with oxides and sulfides often present in the center of the veins. Iddingsite is also found in patches in mesostasis pockets replacing relict olivine crystals. In addition, some mesostasis pockets show iddingsite at a microscale, evidencing pervasive aqueous alteration.

Discussion: All petrographic, chemical, noble gas and isotopic analyses confirm that CeC 022 is a nakhlite. It shows similarities with the subgroup formed by Nakhla, Lafayette, Goverador Valadares, and NWA 998 [3], slow-cooled nakhlites. It has similar bulk composition, pyroxene and olivine (unzoned Fe-rich olivine) composition, crystal size distribution analysis, and large plagioclase phenocrysts. Also, CeC 022 displays new unique features with the Fe-richest augite cores measured to date (higher than NWA 5790 [4]). This points to a relatively slow cooling history similar to the Nakhla subgroup [3]. Nonetheless, the plagioclase and the REE compositions are closer to faster-cooling nakhlites NWA 817, NWA 5790 or NWA 10153 [3]. The sharp fine Fe-rich augite rim in contact with mesostasis, the quenched oxides, and the high glassy proportion in the abundant mesostasis pockets also point to a fast crystallization. The abundant aqueous alteration and large amount of mesostasis possibly place CeC 022 close to the surface. These overall characteristics set CeC 022 apart from other nakhlites and suggest it might originate from a different lava flow or sill from the same volcanic system.

Conclusion: In comparison with other nakhlites, CeC 022 is unusual in terms of petrography, mineral composition, and extent of aqueous alteration. This brings a new complexity in the nakhlite formation with possibly several lava flows, and/or magma mixing prior to eruption and/or complex post-eruption aqueous alteration.

References: [1] Treiman, A.H. (2005). *Chemie der Erdre-Geochemistry,* 65(3), 203-270, [2] Hicks, L.J., et al. (2014) *Geochim. Cosmochim. Acta* 136:194-210, [3] Udry and Day (2018) *Geochil. Comm. Acta* 208, 292-315, [4] Jambon A. et al. (2016) *Geochim. Cosmochim. Acta* 190:191-212.

Fig. 1 : Olivine crystals in CeC 022. A : Olivine, B : Iddingsite veins in olivine, C: (Titano)magnetite, D : Pyroxene with irregular cores, E : Low-Ca pyroxene overgrowth.
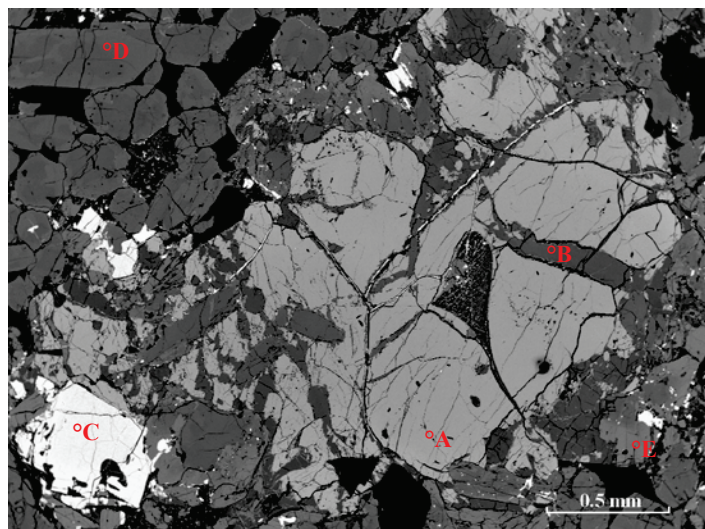
COMPLETE CHARACTERIZATION OF THE NOBLE GAS INVENTORY IN CR CHONDRITE MILLER RANGE 090657 BY DIRECT ETCH RELEASE.

D. Krietsch[1], H. Busemann[1], M. E. I. Riebe[1], A. J. King[2], and C. Maden[1], [1]Institute of Geochemistry and Petrology, ETH Zurich, Switzerland (daniela.weimer@erdw.ethz.ch), [2]Dept. of Earth Science, The Natural History Museum, London, U.K.

Introduction: Most carriers of primordial noble gas components in primitive carbonaceous chondrites (CCs) identified to date are acid-resistant. Their study, thus, mainly occurred on meteoritic "acid-resistant residues" [1]. Nevertheless, there is also evidence for primordial noble gases residing in acid-soluble phases (e.g., [2]). In this work, we investigate a very primitive CC using the "closed system step etching" (CSSE) technique, which allows a direct stepwise measurement of noble gases in these "solubles" in vacuum. For the first time, we used a series of five different etching agents targeting various mineral groups, in order to selectively release and detect all primordial components contained in a primitive meteorite. We aim to further constrain the initial composition of the primordial noble gases within the parent body before any secondary processing, and look for the Ar-rich component susceptible to aqueous alteration [3,4], as well as the respective (maybe unknown) carriers. Furthermore, we aim to detect potential nucleosynthetic isotope anomalies and test if they correlate with those discovered in other elements, e.g., by inductively coupled plasma mass spectrometry in leaching experiments using the same acids (e.g., [5]).

Experimental procedure: The very pristine CR chondrite Miller Range (MIL) 090657 [6] is an ideal sample for this experiment: it contains large amounts of primordial noble gases, shows no obvious evidence for solar wind, and has a short cosmic ray exposure age [4]. [7] classified this CR as a petrologic type 2.7. XRD analysis (at NHM London) confirmed a relatively low phyllosilicate fraction and, hence, a high petrologic type. CSSE was performed using our unique, all Au and Pt extraction line in five separate etch runs (for method details, see [2,8,9]). Water (cf. [3,4]) and acetic acid (HAc) were used for the first time as "etching" agents for noble gas extraction. Subsequent etching was done with HNO_3, HF, and finally HCl.

Results and discussion: The treatment of MIL 090657 with H_2O released surprisingly large amounts of light noble gases: ~35% of ^{20}Ne (percentages always refer to the expected bulk concentration in MIL 090657 measured by [4]), ~25% of ^{22}Ne, and ~25% of the ^4He content. In a Ne-three-isotope plot, the data of the H_2O etch run plot close to the trapped components and are clearly different from air composition, showing that large amounts of primordially trapped noble gases are indeed released by H_2O treatment alone. An extrapolation of the error weighted linear regression through the data results in a $(^{20}Ne/^{22}Ne)_{tr}$ ratio of ~10.3 (assuming $(^{21}Ne/^{22}Ne)_{tr} = 0.0294$). This implies a release of a component with a composition in the range of Ne released from phase Q. However, almost no release of $^{(36,38)}Ar$ was induced by H_2O treatment (< 2%). Hence, intense parent body aqueous alteration processes were not reproduced in this experiment on this already mildly aqueously altered CR2 chondrite. In contrast, most of the $^{(36,38)}Ar$ was released by etching with HAc: ~60% of the total expected amount (for comparison: all other four etch runs together delivered only ~10% of the total $^{(36,38)}Ar$). Thus, with HAc, we likely dissolved the sought after Ar-rich carrier, which is lost upon moderate parent body aqueous alteration (cf. [3,4]). Smaller, but still high fractions of the expected totals of heavy noble gases were also released by HAc etching (~45% of ^{84}Kr and ~35% of ^{132}Xe). The Ne isotope ratios as well as the elemental ratios differ from the composition of known noble gas components [1]. Hence, we likely found a new noble gas component in a yet unknown, HAc-soluble carrier. As expected, etching with HNO_3 mainly resulted in the detection of heavy noble gases: ~30% ^{132}Xe and ~20% ^{84}Kr of Q composition, but also significant amounts of, mainly cosmogenic, ^3He and ^{21}Ne (both ~20%). The release of cosmogenic noble gases continues in the HF and HCl etch runs. Etching with HF further reveals lower cosmogenic endmember $^{21}Ne/^{22}Ne$ ratios compared to all other etch runs. This points to a different chemical composition and possibly the dissolution of a Na-rich or Mg-poor carrier by HF. The last etch steps from HCl treatment under harsh etching conditions plot close to Ne-HL composition indicating the release of HL-gases, which are usually carried by predominantly acid-resistant presolar nanodiamonds [1].

Offline etching of MIL 090657 aliquots, using the same acids under similar conditions, and subsequent analysis for their mineralogy by XRD is currently performed in order to better constrain potential noble gas carrier phase(s).

References: [1] Ott U. 2014. *Chemie der Erde* 74:519-544. [2] Riebe M. E. I. et al. 2017. *Geochimica et Cosmochimica Acta* 205:65-83. [3] Weimer D. et al. (2017) *80th Meteoritical Society Meeting*, Abstract #6300. [4] Busemann H. et al. (2019) *82nd Meteoritical Society Meeting,* this volume. [5] Schönbächler M. et al. 2005. *Geochimica et Cosmochimica Acta* 69:5113-5122. [6] Davidson J. et al. (2015) *LPS XLVI*, Abstract #1603. [7] Alexander C. M. O'D. et al. 2013. *Geochimica et Cosmochimica Acta* 123:244-260. [8] Wieler R. et al. 1986. *Geochimica et Cosmochimica Acta* 50:1997-2017. [9] Busemann H. et al. 2000. *Meteoritics & Planetary Science* 35:949-973.

EXPERIMENTAL INSTALLATION FOR INVESTIGATION OF MECHANICAL PROPERTIES OF METEORITES.

Krivenko A.P.[1], Martynov L.Yu.[1], Voropaev S.A.[1]
[1]V.I. Vernadsky Institute of Geochemistry and Analytical Chemistry RAS, Moscow; E-mail: voropaev@geokhi.ru

Introduction: Usually, meteorites are fragments of theirs parent bodies surface. So, their properties provide important information about the composition and evolution of asteroids and small bodies of the Solar system [1]. But frequently the body of the fallen meteorite is broken with the cracks and splits, like Chelyabinsk. In order to identify the different failure mechanisms, we have to experimentally investigate the strength properties of the small part of meteorite. Most industrial facilities for researching mechanical properties of materials don`t allow provide the estimation of such meteorites, because it need dimensions of sample at least 25 mm diameter and 50 mm length [2]. To avoid these constraints, we have designed special installation for evaluation such elastic mechanical values as Poisson`s ratio, Young`s modulus, and ultimate tensile and compression strengths.

Methods: Design of the developed installation for estimation of mechanical properties comprises sensors, electronic unit, personal computer. The cylindrical samples with dimensions starting from 5 mm in diameter and 10 mm length can be studied on it. The only limited factor is size of chondra, main components of chondrites. The study of so small samples can be performed by tiny foil strength sensors with nominal impedance from 300 Ohms to 1000 Ohms, whith different base size. Electronic unit has 4 channels. 2 channels intended for signals from sensors of relative longitudinal and transverse deformation. The third channel used for force sensor, which measure the force applying to sample. The fourth channel can be used for external temperature sensor in case when sample is only one. Usage sensors of relative longitudinal and transverse deformation in pair increase accuracy by 2 times per channel. Each pair of sensors connects to 32-bit analog to digital converter. All analog to digital convertors send digital data to controller, which proceed it and send on personal computer. The electronic unit has power station unit to stabilize supply current. The schematics of electronic unit optimize out signal and increase accuracy of evaluation. Installation can compensate the fluctuation of signal from temperature and added impedance of wires.
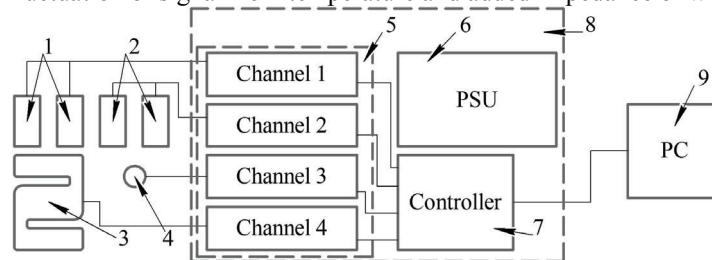

Figure 1. Block-scheme of installation. 1,2 – foil sensors, 3 – force sensor, 4 – temperatures sensor, 5 – ADC group, 6 – power station unit, 7 – controller, 8 – electronic unit, 9 – personal computer

Results and Discussion: Developed facilitie allowed us to perform measurement of mechanical properties of small samples of meteorites in according to GOST 28985-91 Rocks. Method for determination of deformation characteristics is uniaxial compression. The calculation of the charactrestics can be carry out according to the following formulas: Young`s modulus:

$$E_y = \frac{\sigma_\text{к} - \sigma_\text{н}}{\varepsilon'_{1\text{к}} - \varepsilon'_{1\text{н}}} \tag{1}$$

Poisson`s ratio:

$$\mu = \frac{\varepsilon'_{2\text{к}} - \varepsilon'_{2\text{н}}}{\varepsilon'_{1\text{к}} - \varepsilon'_{1\text{н}}} \tag{2}$$

where $\sigma_\text{к}$, $\sigma_\text{н}$ – tension at finish and at start of loading and unloading range of sample, $\varepsilon_{1\text{к}}$, $\varepsilon_{1\text{н}}$ – relative longitudinal deformation of sample at finish and at start of range on loading, $\varepsilon_{2\text{к}}$, $\varepsilon_{2\text{н}}$ – relative transverse deformation of sample at finish and at start of range on loading, $\varepsilon'_{1\text{к}}$, $\varepsilon'_{1\text{н}}$ – relative longitudinal deformation of sample at finish and at start of range on unloading, $\varepsilon'_{2\text{к}}$, $\varepsilon'_{2\text{н}}$ – relative transverse deformation of sample at finish and at start of range on un-loading.

Further, we will modify this installation to perform the Brazilian test. The great advntage of the Brazilian test is determination of the elastic modulus, tensile strength and fracture toughness of rock materials in one test. [3].

References: [1] Petrovic J.J. 2001.Journal of Materials Science, 36: 1579-1583. [2] Voropaev S. et al. 2017. Doklady Physics, 62(10), 486-487. [3] Wung Q.Z. et.al. 2004. International Journal of Rock Mechanics and Mining Sciences 41: 245-253.

MINERALOGY, PETROGRAPHY, AND OXYGEN ISOTOPIC COMPOSITIONS OF ULTRAREFRACTORY INCLUSIONS FROM CARBONACEOUS CHONDRITES.

A. N. Krot[1,2*], C. Ma[3], K. Nagashima[1], A. M. Davis[4,5,6], J. R. Beckett[3], S. B. Simon[7], M. Komatsu[8], T. J. Fagan[9], P. T. Genzel[2], F. Brenker[2], M. A. Ivanova[10], and A. Bischoff[11]

[1]University of Hawai'i at Mānoa, USA, *sasha@higp.hawaii.edu; [2]Goethe University, Germany; [3]California Institute of Technology, USA; [4]Department of the Geophysical Sciences, [5]Enrico Fermi Institute, [6]Chicago Center for Cosmochemistry, The University of Chicago, USA; [7]University of New Mexico, USA; [8]The Graduate University for Advanced Studies, Japan; [9]Waseda University, Japan; [10]Vernadsky Institute of Geochemistry of Russian Academy of Sciences, Russia; [11]Institut für Planetologie, Germany

Introduction: Fine-grained CAIs with Group II rare earth element (REE) patterns condensed from a gaseous reservoir from which the ultrarefractory (UR) REEs had been removed. The carriers of UR REEs are poorly known. Here we report on the mineralogy, petrography and O-isotope compositions of 25 CAIs, presumably UR (REEs have not yet measured), from CR2, CM2, C3.0, CO3.0–3.6, CV3.1–3.6, and CH3.0 carbonaceous chondrites (CCs).

Mineralogy and Petrography: The UR CAIs studied are dominated by Zr, Sc, Ti, and Y-rich oxides (allendeite, kangite, lakargite, panguite, Y-perovskite, tazheranite, warkite, zirconolite) and silicates (davisite, eringaite, thortveitite) and often contain refractory metal alloy nuggets; most are surrounded by rims of Sc-pyroxene, ±eringaite, Al,Ti-diopside, and ±forsterite. These CAIs occur as (*i*) individual objects, (*ii*) constituents of amoeboid olivine aggregates and Fluffy Type A CAIs, and (*iii*) relict objects in forsterite-bearing Type B CAIs and chondrules.

Oxygen-isotope compositions: Nearly all UR CAIs from the least metamorphosed CCs [Murchison (CM2), Y-793261 (CR2), Acfer 182 (CH3.0), and DOM 08006 (CO3.0)] have uniform O-isotope compositions ($\Delta^{17}O \sim -24\pm2‰$ and $\sim -6\pm2‰$) (Fig. 1a,b). In contrast, most UR CAIs from CCs of petrologic type $\geq$3.1 (CVs: Kaba, Vigarano, Efremovka, and NWA 3118, and COs: DOM 08004, Moss, and Ornans) are isotopically heterogeneous: spinel, hibonite and forsterite are ^{16}O-rich ($\Delta^{17}O \sim -24‰$), but warkite, eringaite, kangite, Y-perovskite, and davisite are ^{16}O-depleted to various degrees (Fig. 1b,c).
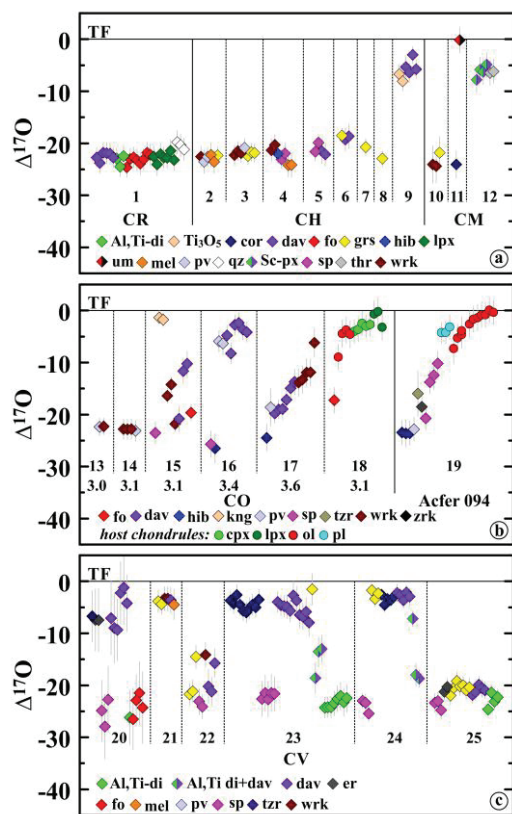

Figure 1. $\Delta^{17}O$ ($=\delta^{17}O-0.52\times\delta^{18}O$) of UR CAIs from (a) CM2, CR2, and CH3.0 chondrites; (b) CO3.0–3.6 chondrites and Acfer 094 (C3.0 ungrouped); (c) CV3 chondrites. 1 = *4* from Y-793261; 2 = *5-2* from NWA 470; 3 = *418/P* from Acfer 182; 4 = *1573-1* from Acfer 214; 5 = *35* from ALH 85085; 6 = *6* from PCA 91326; 7 = *3* from PCA 91452; 8 = *MB 111-1* from Acfer 214; 9 = *A0031* from SaU 290; 10 = *M11*; 11 = *M80-1*; 12 = *M10* from Murchison; 13 = *100-1* from DOM 08006 (CO3.0); 14 = *22-4* and 15 = *YY* from DOM 08004 (CO3.1); 16 = *Oscar* from Ornans (CO3.4); 17 = *1* from Moss (CO3.6); 18 = *50-1* from MAC 88107; 19 = *17* from Acfer 094; 20 = *V3*, 21 = *V7*, and 22 = *V13* from Vigarano; 23 = *3N* from NWA 3118; 24 = *33E* from Efremovka; 25 = *Al-2* from Allende. Abbreviations: Al,Ti-di = Al,Ti-diopside; cor = corundum; cpx = Sc-bearing high-Ca pyroxene; dav = davisite; er = eringaite; fo = forsterite; grs = grossite; hib = hibonite; kng = kangite; lpx = Sc-bearing low-Ca pyroxene; um = unidentified Sc-, Zr-, and Y-rich oxide; mel = melilite; ol = Fe-Mg olivine; pl = plagioclase; pv = perovskite; qz = quartz; Sc-px = Sc-bearing Al,Ti-diopside; sp = spinel; TF = terrestrial fractionation line; thr = thortveitite; Ti_3O_5 = Sc-rich Ti_3O_5; tzr = tazheranite; wrk = warkite; zrk = zirkelite. Diamonds and circles indicate minerals in CAIs and host chondrules, respectively.

Discussion: Most UR CAIs formed in a ^{16}O-rich gaseous reservoir; some subsequently experienced incomplete melting and O-isotope exchange in the CAI- and chondrule-forming regions. UR CAIs from CCs of petrologic type 2−3.0 largely retained their original O-isotope compositions, whereas those from CV and CO chondrites of higher petrologic type that experienced fluid-assisted thermal metamorphism, recorded mineralogically-controlled O-isotope exchange mostly with a ^{16}O-depleted aqueous fluid on the host chondrite parent asteroids. UR CAIs melted during chondrule formation (CAIs 18 and 19 in Fig. 1b) and possibly a relict UR CAI in a FoB CAI (CAI 23 in Fig. 1c) appear to have experienced O-isotope exchange with a ^{16}O-depleted nebular gas during melting.

HYPERSPECTRAL IMAGING OF METEORITES

N. A. Kruglikov[1,2,3], R.F. Muftakhetdinova[1], and V. I. Grokhovsky[1], [1]Ural Federal University, [2]Institute of Metal Physics of Ural Branch of RAS,[3]Ural State University of Economics, Ekaterinburg, Russian Federation, e-mail: nick@imp.uran.ru

Hyperspectral imaging is a very new area that can be useful for meteorites investigations. Using the hyperspectral camera you could obtain information about the spectrum of the object in every pixel of the image. We have used the Specim IQ push broom scanner [1] for a different kind of meteorites imaging. Specim IQ has 512x512 resolution, 10-bit line CMOS sensor, 42 µm slit and manual focusing. This is a mobile device that can be used both in laboratories and in expeditions. Previously, for the majority of the objects under study, spectra were obtained on stationary equipment.

Using this equipment has some features. Quality of hyperspectral images strongly depends on used light sources and imaging conditions. We have used two halogen and two infrared lamps to take images. Specim IQ spectra (Fig.1) resemble usual spectrometer spectra in the interval from 450 to 900 nm. Peaks near 880 nm most likely produced by the camera itself. All spectra with artificial light sources were obtained in a special darkened chamber for polished samples in diffuse scattering conditions. Wavelengths positions were checked with standard narrow band filters for 460, 677 and 780 nm. Spectra value was averaged over for least 100 pixels. The Specim IQ could not be used as usual spectrometer because of not fixed distances between object, camera and light sources. So it should be calibrated for each configuration.
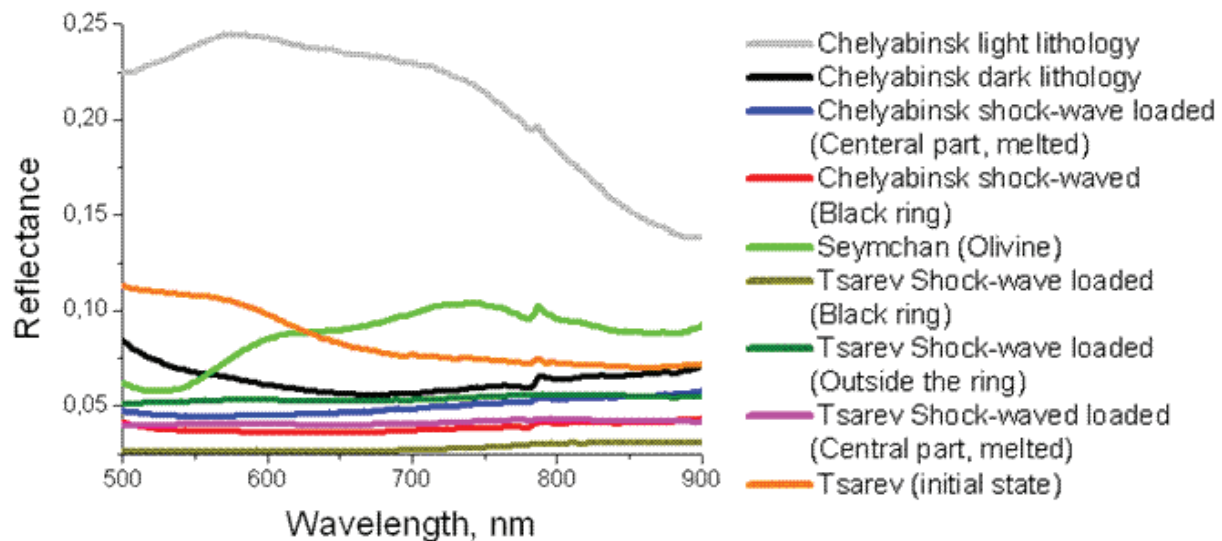

Fig.1. Reflection spectra of silicates phases of some meteorites.

The possibility of using Specim IQ to study such complex objects as meteorites is shown. For spectra obtaining it should be stationary placed to the special darkened chamber and fixed with regarding object and light sources. Spectrum should be corrected by camera function. In field condition, it is necessary to have white reference and tripod. The camera could be used for emission, reflection and absorption spectra.

References: [1] http://www.specim.fi/iq/ [2] Kruglikov N.A., Grokhovsky V.I. (2017) *Meteoritics & Planetary Science* 52: 6350. [3] Kruglikov N.A., Grokhovsky V.I. (2018) *Meteoritics & Planetary Science* 53: 6356.

VISIBLE RANGE SPECTROSCOPY OF SHOCK-WAVE LOADED CHELYABINSK LL5

N.A. Kruglikov[1,2,3], R.F. Muftakhetdinova[1], and V.I. Grokhovsky[1], [1]Ural Federal University, [2]Institute of Metal Physics of Ural Branch of RAS,[3]Ural State University of Economics, Ekaterinburg, Russian Federation, e-mail: nick@imp.uran.ru

Reflectance spectra of atmosphereless bodies are changing due to space weathering caused by damaging of their surfaces. Chelyabinsk meteorite matter is quite convenient for modeling experiments because of enough amount of the matter and complex history [1]. So, shock-wave loading experiments were produced [2]. The microstructure was studied [3] and different kind of structures was distinguished [4]. Previous spectroscopic studies of the Chelyabinsk have focused on the different wavelength ranges commonly used for asteroid remote sensing [5]. Some of FTIR microspectroscopic investigations for comparison between different minerals and lithologies and shock-waved light lithology were made earlier [6,7]. As aresult, we fixed substantial shifts of some olivine peaks in infrared range [7].

Our new experiments were made on bulk samples obtained from the Chelyabinsk meteorite fragments with different lithologies. We used Lambda 35 spectrometer for spectra obtaining. One light lithology sample was shock-wave loaded, cut and polished [2]. Additionally, we annealed one of light lithology samples up to 1100°C for 15 minutes. It is clearly seen that the slope of the spectrum strongly depends on the structure and the treatment (Fig. 1).
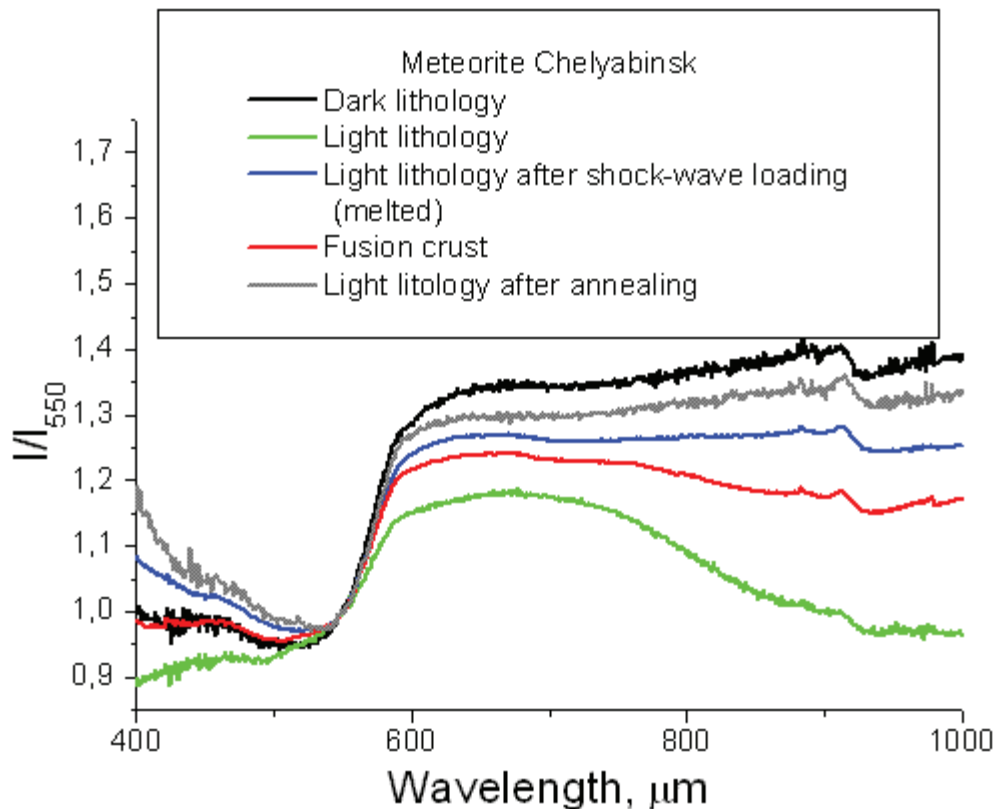

Fig.1. Visible spectra of different structures of the Chelyabinsk meteorite.

References:[1] Morlok A. et al. (2017) *Icarus* 284: 431–442. [2] Grokhovsky V.I. et al. (2018) *Meteoritics & Planetary Science* 53: 6347 [3] Petrova E.V. et al. (2018) *Meteoritics & Planetary Science* 53: 6335. [4] Kohout T. et al. (2018) *Meteoritics & Planetary Science* 53: 6327. [5] Kohout T. et al. (2014) *Icarus* 228:78-85. [6] Kruglikov N.A., Grokhovsky V.I. (2017) *Meteoritics & Planetary Science* 52: 6350. [7] Kruglikov N.A., Grokhovsky V.I. (2018) *Meteoritics & Planetary Science* 53: 6356.

Enhancement of the degree of impact heating in pressure-strengthened rocks

K. Kurosawa[1], H. Genda[2], T. Niihara[3], M. Kayama[4], M. Koike[5], T. Mikouchi[6], Y. Sano[7], and T. Matsui[1], [1]Planetary Exploration Research Center, Chiba Tech. (2-17-1, Tsudanuma, Narashino, Chiba 275-0016, Japan, E-mail: kosuke.kurosawa@perc.it-chiba.ac.jp), [2]Earth-Life Science Institute, Tokyo Tech., [3]Department of Systems Innovation, The Univ. of Tokyo, [4]Dpt. of General Sys. Studies, The Univ. of Tokyo, [5]ISAS, JAXA, [6]The University Museum, The Univ. of Tokyo, [7]Atmos. and Ocean Res. Inst., The Univ. of Tokyo.

Introduction: Hypervelocity mutual collisions between small bodies occur throughout the solar-system hostory. A strong compression and thermal pulse caused by an impact can produce various unique features, such as a change in spectral properties, mosaicism, planer deformation features, high-pressure minerals, atomic diffusion, volatile loss, shock veins, impact melt, and so on. We can obtain these features in meteorites [e.g., 1–3]. Given that we have a reliable model connecting the degree of shock metamorphism with the impactor/target conditions, the impact histories of the parent bodies of meteorites is reproduced more correctly. Frequently, the table from Stöffler et al. [1, 2] is used to deduce the shock stage of meteorites using observed shock features, which are subsequently used to infer impact velocities on target bodies. Recently, [4] reported that the degree of heating in low-velocity impacts (<10 km/s) is expected to be much higher than previously expected. In this abstract, we introduce the significance of the strength effects on the degree of impact heating based on the results by [4].

Numerical model: We used the two-dimensional model of the iSALE shock physics code [5-9], combined with a simple well-established constitutive model. The strength model for rocks [8, 10] and ANEOS [11] for dunite [12] were applied for both projectile and target. The detail of the numerical simulation is described in [4]

Results: We confirmed that the results in the case without strength, i.e., purely hydrodynamic, are consistent with the thermodynamic prediction (Fig.1ac). In contrast, we found that the post-shock temperature in strength-supported media could be much higher than previously expected. For example, if we consider a spherical impactor colliding onto a flat target at 3 km/s, the post-shock temperature of the target materials experiencing 10 GPa-compression exceeds 1,000 K (Fig.1bd). Low-velocity impacts do not produce large-scale impact melting, but trigger a comminution of both impactor and target materials. Although the materials experiencing compression do not have a tensile strength, they still have a compressive one. Plastic deformation of the pressure-strengthend comminuted rocks dissipates the energy, and converts from the kinetic energy of the flow field to the internal energy. Thus, the required impact velocities for producing the unique features produced mainly by the rise in temperature is greatly lowered.

Discussion and Conclusions: Our results imply that the experienced peak temperatures in shocked meteorites would be much higher than the prediction by the Stöffler's table at a given shock stage. We are planning to revisit the accuracy of the Stöffler's table by using both labolatory and numerical approaches.

References: [1] Stöffler D. (1971) *Journal of Geophysical Research* 51:1-11. [2] Stöffler D. et al. (2018) *Meteoritics & Planetary Science* 53:5-49. [3] Scott E. R. D. et al. (1992) *Geochimica et Cosmochimica Acta* 56:4281-4293. [4] Kurosawa K. and Genda H. (2018) *Geophysical Research Letters* 45:620-626. [5] Amsden A. A., et al. (1980) *LANL Report* LA-8095. 101 p. [6] Ivanov B. A., et al. (1997), *International Journal of Impact Engineering* 20: 411-430. [7] Wünnemann, K., et al. (2006), *Icarus* 180: 514-527. [8] Collins G. S. et al. (2004), *Meteoritics & Planetary Science*, 39, 217-231. [9] Collins G. S. et al. (2016) *Figshare* https://doi.org/ 10.6084/m9.figshare.3473690.v2 [10] Lundborg, N. (1968), *Int. J. Rock Mech. Min. Sci.*, **5**, 427-454. [11] Thompson S. L. and Lauson H. S. (1972) (SC-RR-71 0714, 119 pp.). Albuquerque, NM: Sandia Laboratories. [12] Benz W. et al. (1989) *Icarus* 81:113-131.
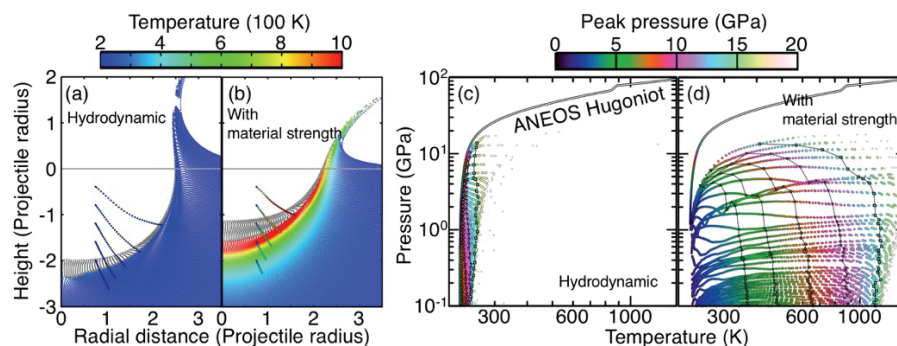

Figure 1. Snapshots of the simulation (a and b). The pressure -temperature pathes of the selected tracers (c and d). The results in the pure hydrodynamic case are shown in Panels a and c. The roles of material strength on impact heating are shown in Panels b and d.

EXTRATERRESTRIAL MATTER FROM LAKE BOLSHOE MIASSOVO, SOUTH URAL, RUSSIA

D. M. Kuzina[1], A. R. Iusupova[1], D. K. Nurgaliev[1], V. V. Vorob'ev [2], Yu. N. Osin[2].
[1]Kazan Federal University, Institute of Geology and Petroleum Technologies, Russia, Kazan, Kremlyevskaya st., 18.
[3]Kazan Federal University, Interdisciplinary Center for Analytical Microscopy, Russia, Kazan, Paris Commune st. 9.
E-mail: di.kuzina@gmail.com

Introduction: Previous studies [1, 2] shows that micrometeorites and cosmic dust can be found in different types of sediments and rocks. In this paper we describe scanning electron microscopy results of magnetic fraction of Lake Bolshoe Miassovo (Chelyabinsk region, Russia). It is shown that lake sediments are good archives for extraterrestrial matter.

Methods: Magnetic fraction from lake sediments were removed by using permanent magnet. The morphology and elemental composition of magnetic separates studied using scanning electron microscopy "Merlin" Carl Zeiss equipped with an energy-dispersive spectrometer "Aztec X-Max" Oxford Instruments. Surface morphology was investigated at an accelerating voltage of 5 keV on SE mode (secondary electrons). Elemental analysis and surface mapping was carried out at an accelerating voltage of 20 keV with AsB mode. Microscopy investigation was performed in Interdisciplinary Center for Analytical Microscopy of Kazan Federal University.

Results: Microscopic investigations showed wide spread of micrometeorites in all studied samples. Shape of particles usually round. Size of particles varies from 5 to 30 microns. Almost all microparticles have specific wavy surface. More interesting samples are found at the depth 4 meters which corresponds to the age ~ 10 Ka. Several particles of iron composition with minor oxygen content were found. Some of them contain areas with high nickel content, up to 82% (Pic. 1). There are some small particles sized not exceed 20 μm, with nickel content up to 85%.
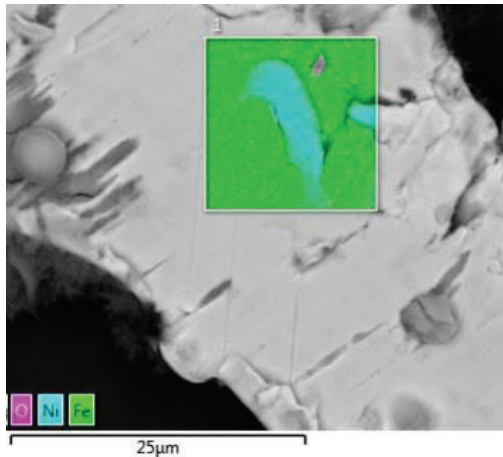
Picture 1. Results of surface mapping. Green – Fe, blue – Ni.

Conclusions: The presence of almost pure particles of iron with zones rich in nickel probably indicates a process of differentiation of a substance during entry and reheating in the atmosphere. Layers with increased quantity of extraterrestrial matter with ages ~ 10 Ka were found also in other lakes of Ural. This indicates an increased flow of cosmic matter during this period.

References: [1] Kuzina D.M. et al. 2018. *Meteoritics & Planetary Science* 53 (SI): P. 6306. [2] Murdmaa I.O. et.al., 2015. *Lithology and Mineral Resourses*, 50(2): 117-133.

ESTIMATION OF FE-NI MATTER FLUX TO THE EARTH BASED ON MAGNETIC INVESTIGATION

D. M. Kuzina[1], D. K. Nurgaliev[1], D. M. Pechersky[2]
[1]Kazan Federal University, Institute of Geology and Petroleum Technologies, Russia, Kazan, Kremlyevskaya st., 18.
[2]IPE RAS, Russia, Moscow, Bolshaya Gruzinskaya str., 10-1.
E-mail: di.kuzina@gmail.com

Introduction: The amount of cosmic matter entering Earth is estimated by the intensity of the zodiacal light, the number of meteorites dropped, meteor tracks, registration of particles of various sizes by satellites, and finally the content of Ni, Co, Ir, Os and cosmogenic radionuclides 10Be, 3He, 14C, 26Al in glaciers, deep-sea sediments, etc [1]. Magnetic characteristics measure only in meteorites. The paper shows the possibility of using magnetic methods to estimate the amount of incoming cosmic matter on example of studying samples from Atlantic Ocean and Lake Baikal.

Methods: Differential thermomagnetic analysis was carried out for tracing magnetic minerals according their Curie temperature for samples of Atlantic Ocean and Lake Baikal. Measurements of the samples' induced magnetization as a function of temperature were made in a heating rate of 100°C/min up to 800 °C. The measurements made in a constant magnetic field - 400 mT. Concentration of Fe-Ni alloys in sample were calculated based on signal obtained from indused magnetization curve of first heating. Ammount of Ni in Fe-Ni alloys were calculated using next equation [2]:

Ni (%) = 0.243 * (770 – T_c),

770 - Curie point of pure iron;

T_c - Curie point of the alloy of iron and nickel in the sample, detected during experiment

Results: From thermomagnetic analysis data we calculate the average flux of Fe-Ni composition extraterrestrial matter onto the surface of the planet Earth over a fairly long period of time ~ 150 million years, for the Atlantic Ocean is 3924.7 + 3452.6 tons/year, Baikal Lake - 14209 + 9958 tons/year. On average, the nickel content in iron-nickel alloys is 8%.

Conclusions:

The obtained values of the flux of iron-nickel particles onto the surface of the Earth are in complete agreement with the data presented by other authors, where estimations for total flux of extraterrestrial matter varias between 1.8 to 150 thousand tons / year [3, 4].

References: [1] Plane J.M.C. 2012. *Chem. Soc. Rev.* Vol. 41: 6507–6518. [2] Pechersky D.M. et.al. 2013. *Russian Geology and Geophysics*, 54 (12): 1045-1055. [3] Mathews et al. 2001. *Geophysical Research Letters*, 28(10): 1929–1932. [4] Barker, Anders, 1968. *Geochimica et Cosmochimica Acta*. 32(6): 627–645.

Estimation of Fe-Ni matter flux to the Earth on basis of magnetic investigation

ON NEW MEMBERS OF ASTEROID CLUSTERS SIMILAR TO ASTEROID PAIRS.

E. D. Kuznetsov, M. A. Vasileva, Ural Federal University, Lenina Avenue, 51, Yekaterinburg, 620000, Russia, eduard.kuznetsov@urfu.ru, maxa1907@icloud.com.

Introduction: Here we report about results of search for new members of young asteroid families. We have found six possible new members of Rampo asteroid family and one possible new member of Hobson asteroid family. We also have discovered new asteroid cluster, which includes three asteroids.

Methods: The search of new candidate asteroids within families has been carried out by means of the computation of the values of the natural metrics ϱ_2 and ϱ_5 [1]. The metric ϱ_2 is the distance between two orbits in the five-dimensional space of Keplerian orbits. The metric ϱ_5 is a distance in three-dimensional factor-space of positional orbital elements. Osculating elements of orbits were used to calculate the metric ϱ_2 and proper elements of orbits were used to calculate the metric ϱ_5. Orbital elements of asteroids have been taken from Asteroids Dynamic Site – AstDyS. Criterias for finding the new asteroids within clusters were value of metrics for all pairs in cluster $\varrho_2 <$ 0.004 au$^{1/2}$ and $\varrho_5 < 0.001$ au$^{1/2}$.

We will perform numerical integrations of the orbits of all pairs of asteroids within clusters backward in time with the code known as Orbit9. It is necessary to take into account the Yarkovsky effect accurately to carry out precise simulations of the dynamical evolution of asteroid pairs. We estimated the Yarkovsky semimajor axis drift for all asteroids in this three clusters according to [2].

Results and discussions: In our results, six new members of Rampo family (2009 SR371, 2013 RL101, 2013 VC30, 2015 TA367, 2015 TM372, 2017 UH21), not listed in [3], were detected (table 1). One new member of Hobson family (2017 SQ83), not listed in [4], was detected (table 2). The new cluster comprising three asteroids ((381362) 2008 EP15, (405843) 2006 BT227, 2012 XC32), not listed anywhere, was discovered.

Table 1. Keplerian elements of Rampo and six new family members at epoch 58400.0 MJD

Asteroid	H [mag]	a [au]	e	i [deg]	Ω [deg]	ω [deg]	$\lvert\dot{a}\rvert \cdot 10^4$ [au/Myr]
(10321) Rampo	14.2	2.32902	0.094412	6.059	53.930	278.874	0.79
2009 SR371	18.7	2.32898	0.094711	6.070	56.788	274.624	5.01
2013 RL101	18.4	2.32765	0.094099	6.091	61.665	267.151	4.30
2013 VC30	18.4	2.32800	0.094574	6.081	59.355	270.502	4.32
2015 TA367	18.8	2.32921	0.094422	6.056	53.308	279.728	5.12
2015 TM372	18.5	2.32876	0.093933	6.073	57.712	273.399	4.63
2017 UH21	18.4	2.32849	0.093907	6.090	60.373	269.12	4.40

Table 2. Keplerian elements of Hobson and one new family member at epoch 58400.0 MJD

Asteroid	H [mag]	a [au]	e	i [deg]	Ω [deg]	ω [deg]	$\lvert\dot{a}\rvert \cdot 10^4$ [au/Myr]
(18777) Hobson	14.9	2.56213	0.184068	4.323	105.45	180.896	0.94
2017 SQ83	18.4	2.56524	0.179669	4.315	105.60	180.833	3.89

Table 3. Keplerian elements of asteroids from new discovered cluster at epoch 58400.0 MJD

Asteroid	H [mag]	a [au]	e	i [deg]	Ω [deg]	ω [deg]	$\lvert\dot{a}\rvert \cdot 10^4$ [au/Myr]
(381362) 2008 EP15	18.6	2.2386	0.103787	2.048	147.705	309.138	29.04
(405843) 2006 BT227	17.9	2.2381	0.103974	2.059	146.866	310.418	21.04
2012 XC32	18.9	2.2378	0.104567	2.056	147.448	309.818	35.41

References: [1] Kholshevnikov K. V. et al. (2016) *Monthly Notices of the Royal Astronomical Society* 462:2275–2283 [2] Del Vigna A. et al. (2018) *Astronomy & Astrophysics* 617:A61. [3] Pravec P., Vokrouhlicky D. (2009) *Icarus* 204:580 [4] Rosaev A., Plavalova E. (2017) *Icarus* 282:326.

THE YARKOVSKY EFFECT ESTIMATION FOR SOME ASTEROID PAIRS WITH CLOSE ORBITS.

E. D. Kuznetsov[1], A. E. Rosaev[2] and E. Plavalova[3], [1]Ural Federal University, Lenina Avenue, 51, Yekaterinburg, 620000, Russia, eduard.kuznetsov@urfu.ru, [2]Yaroslavl State University, Sovetskaya Street,14, Yaroslavl, 150000 Russia, hegem@mail.ru , [3]Mathematical Institute of the Slovak Academy of Sciences, Stefanikova 848/49, 81473, Bratislava, Slovakia plavalova@komplet.sk.

Introduction: The mutual asteroid collisions and disruptions may be an important source of meteoritic flux on the Earth. In this aspect, studying very young asteroid families and pairs, which are originated in such events has a great interest. It is known, that non-gravity thermal effects play an important role in small bodies dynamics. The fundament of the Yarkovsky effect theory was established in Vokrouhlicky papers [1] and [2]. The Yarkovsky effect has still not been measured in the main belt. Thus Spoto et al. [3] used a calibration based on asteroid (101955) Bennu to compute the ages of more than 50 families in the main belt. In the present paper, we have calculated the values of maximal Yarkovsky acceleration for some pairs of asteroids with very close orbits and (potentially) very small ages.

Methods: According to Vokrouhlicky [1], it is possible to obtain:

$$\frac{da}{dt} = -\frac{8}{9}\frac{(1-A)}{n}\Phi W(K,R)\cos\phi \approx \frac{8}{45}\frac{(1-A)\Phi}{n}\cos\phi.$$

Here n is the mean motion; Φ is the standard radiation force factor, which is inversely proportional to the bulk density ρ, the diameter of asteroid D, and the square of the orbital distance r. The bond albedo A expressed through geometric albedo p_v as $A = 1/3\,p_v$. Function $W(K,R)$ is determined by the thermal parameters of the body and a frequency. Simple account of the Yarkovsky effect in the semimajor axis may be obtained by normalization using (101955) Bennu parameters, because it is known with the smallest errors [3]:

$$\dot{a} = \frac{da}{dt} = \left(\frac{da}{dt}\right)_B \frac{\sqrt{a_B}(1-e_B^2)D_B}{\sqrt{a}(1-e^2)D}\frac{\rho_B\cos\phi}{\rho\cos\phi_B}\frac{1-A}{1-A_B}.$$

The symbols with a "B" refer to asteroid (101955) Bennu. The value of $\dot{a}_B = (19 \pm 0.1)\cdot 10^{-4}$ au/Myr [4]. After the substitution of (101955) Bennu physical parameters [5], we obtain for the Yarkovsky semimajor axis drift (in au/Myr):

$$\dot{a} = \frac{da}{dt} = 12.09\cdot 10^{-4}\frac{\cos\phi}{\sqrt{a}(1-e^2)D}\frac{1-A}{\rho}.$$

Here diameter of asteroids is estimated by absolute magnitude H (in the assumption of equal albedo). The coefficient $(1-A)$ usually is very close to the unit. By acception for density value $\rho = 1.1$ g/cm^3 and for obliquity $\cos\phi = \pm 1$ we obtain the maximal value of modulus of semimajor axis drift for any studied asteroid. This value is slightly overestimated due to the underestimated value of density.

Results and discussions: As a result, we can estimate the most probable value of $|\dot{a}|$. As an example, we give results of our calculations for some famous asteroid pairs with a common origin (table 1). However, for more exact estimation, we must take into account the spectral type of studied asteroids.

Table 1. The estimations of the semimajor drift $|\dot{a}|$ due to the Yarkovsky effect for the asteroid pairs with a common origin

# pair	Asteroid	H [mag]	$D/2$ [km]	a [au]	$|\dot{a}|\cdot 10^{-4}$ [au/Myr]
1	(87887) 2000 SS$_{286}$	15.2	1.129	2.755	1.48
	(415992) 2002 AT$_{49}$	16.5	0.621	2.755	2.70
2	(6070) Rheinland	13.8	2.152	2.388	0.86
	(54827) Kurpfalz	15.4	1.043	2.388	1.78
3	(356713) 2011 UK$_{160}$	16.5	0.620	2.289	3.06
	2014 QX$_{220}$	18.7	0.225	2.289	8.44
4	(1741) Giclas	11.4	6.50	2.883	0.50
	(258640) 2002 ER$_{36}$	15.8	0.86	2.883	3.80
5	(2110) Moore-Sitterly	13.4	2.59	2.199	1.48
	(44612) 1999 RP$_{27}$	15.5	0.98	2.199	3.91
6	(5026) Martes	13.9	2.05	2.378	1.84
	2005 WW$_{113}$	17.8	0.34	2.378	11.10

References: [1] Vokrouhlicky D. (1998) *Astronomy & Astrophysics* 335:1093–1100. [2] Vokrouhlicky D. (1999) *Astronomy & Astrophysics* 344:362–366. [3] Spoto F. et al. (2015) *Icarus* 257:275–289. [4] Farnocchia D. S. et al. (2013) *Icarus* 224:1–13. [5] Del Vigna A. et al. (2018) *Astronomy & Astrophysics* 617:A61.

COORDINATED ANALYSIS OF AN ION IRRADIATED CARBONACEOUS CHONDRITE

D. L. Laczniak[1], M. S. Thompson[1], C. A. Dukes[2], R. V. Morris[3], S. J. Clemett[4], L. P. Keller[3], and R. Christoffersen[4]. Earth, Atmospheric, and Planetary Sciences Department, Purdue University, West Lafayette, IN, 47907 (dlacznia@purdue.edu), [2]Laboratory for Atomic and Surface Physics, University of Virginia, Charlottesville, VA, 22904, [3]ARES, NASA Johnson Space Center, Houston, TX 77058, [4]Jacobs, NASA Johnson Space Center, Mail Code XI3, Houston, TX 77058.

Introduction and Methods: Space weathering processes such as micrometeorite bombardment and solar wind irradiation alter the microstructural, compositional, and optical properties of airless body regoliths over time. Space weathering complicates the interpretation of remote sensing data, posing a problem for JAXA Hayabusa2 and NASA OSIRIS-REx data analysis—missions which are returning samples from C-type asteroids Ryugu and Bennu, respectively [1,2,3]. To promote our understanding of the effects of space weathering on hydrated, organic-rich materials, maximize scientific return from remote sensing data, and prepare for the analysis of returned samples from these missions, we simulate solar wind exposure through ion irradiation of CM2 Murchison—a suitable analog for C-complex asteroids [4]. Here, we present coordinated analysis of a dry-cut slice of Murchison before and after 2 keV H_2^+ and 4 keV He^+ ion irradiation up to total fluences of 8.1×10^{17} ions/cm^2 and 1.1×10^{18} ions/cm^2, respectively. Analytical techniques include X-ray photoelectron spectroscopy (XPS), visible to near infrared (VNIR; 0.35 – 2.50 μm) reflectance spectroscopy, and two-step laser-desorption mass spectrometry (μL^{2}MS).

Surface Chemistry: XPS spectra before and after H_2^+ and He^+ irradiation show similar effects on the matrix's surface chemistry. Carbon peaks are significantly lowered after irradiation, suggesting that both ion types cause net removal of carbon-bearing species on the monolayer depth scale (or possibly their re-distribution in the sample by ion mixing). This effect exceeds what would be expected for simple removal of "adventitious" carbon. All other elements—except F, S, and Ni in the H_2^+-irradiated region—exhibit an increase in peak intensity. Preliminary peak-fitting data indicates reduction of iron from Fe^{2+} to Fe^0 and alteration of sulfate to sulfides from both ion irradiations.

Reflectance Spectroscopy: He^+ ion irradiation yields darkening shortwards and brightening longwards of the 0.7 μm wavelength. Spectral reddening (i.e., increasing reflectance with increasing wavelength) also occurs in the He^+-irradiated sample. In contrast, the H_2^+-irradiated sample is similar in brightness to the unweathered surface. Both irradiated spectra show weakened ~1.0 μm (olivine or Fe^{2+} phyllosilicates), ~0.7 μm (Fe^{2+}-Fe^{3+} phyllosilicates), and ~1.94 μm (water) absorption bands, with He^+ inducing a more significant change [5]. He^+ irradiation also slightly strengthens absorptions at ~0.44, 0.47, and 0.50 μm bands, of which the latter two correspond to Fe-oxides.

Organics Analysis: Consistent with the XPS carbon results, μL^{2}MS mapping at the 118 nm photoionization wavelength shows a ~30-40% reduction in overall organic abundance after irradiation. Concentrations of aromatic species remain relatively unchanged post-irradiation, suggesting aromatics may be more resistant to irradiation-driven chemical and structural modifications compared to other organics. Subsequent mapping with 266 nm photoionization will highlight the chemistry and evolution of these aromatics.

Discussion: Ion irradiation of carbonaceous material yields complex spectral results. XPS and μL^{2}MS mapping show a net decrease of carbon associated with alteration and removal of orgainics. XPS also shows the reduction of iron and creation of sulfides, which may potentially indicate irradiation-induced nanophase Fe^0 and Fe-sulfide production. Reflectance data exhibits attenuation of the 0.7 and 1.0 μm bands after irradiation, reflecting the breakdown of matrix phyllosilicates and possibly olivine, the partial reduction of iron, and/or minor production of nanophase particles [6]. In contrast to XPS, the strengthening of bands near 0.47 and 0.50 μm may reflect the presence of Fe^{3+} bearing oxides (e.g., magnetite) in the form of nanophase particles which can be produced in reducing environments containing free OH^-. Such a process may be further supported by the weakening OH/H_2O band at 1.94 μm which would provide volatile phases necessary for oxide formation via loss of OH^- from phyllosilicates during irradiation. Similar trends were observed in Murchison pulsed-laser irradiation experiments conducted by [7]. Minor slope reddening of both irradiated surfaces compared to the unweathered Murchison surface could further suggests the formation of nanophase Fe^0 or sulfides in addition to nanophase oxides e.g., [1]. In contrast, the mechanism behind spectral brightening is uncertain. The decrease in nearly all organic species (except aromatics) suggests volatilization by He^+ irradiation. Compared to organic analyses of pulsed-laser irradiation experiments in [8], He^+ irradiation appears to destroy a variety of organic species while pulsed-laser irradiation breaks down complex refractory hydrocarbons, thus leading to an increased abundance of organic free species. Future chemical and microstructural TEM analyses will help us correlate nanoscale features to the complicated spectral effects mentioned here.

References: [1] Pieters, C. & S. Noble (2016) *JGR*, *121*(10), 1865-1884. [2] Lauretta, D. *et al.* (2015) *Met. Planet. Sci.*, *50*, 834-849. [3] Yoshikawa, M. *et al.* (2015) IAU Gen. Assem. 22, 54481. [4] Clark, B. *et al.* (2011) *Icarus*, *216*, 462 – 475. [5] Cloutis E. A. *et al.* (2012) *Icarus*, *220*, 586-617. [6] Keller, L. P. et al. (2015) LPSC XLVI, Abs. 1913. [7] Thompson, M. S., *et al.* (2018) *LPSC XLIX*, Abs 2408. [8] Matsuoka M. *et al.* (2017), *Icarus*, *254*, 135-143.

A CONTRIBUTION OF GAMMA RAY SPECTROMETRIC DATA IN UNDERSTANDING THE STRUCTURE OF THE MAÂDNA CRATER (TALEMZANE, ALGERIA).

A. Lamali[1, 2], L. Hamai[1, 2], S. A. Mokhtar[3], A. Yelles-Chaouch[1], A. Abtout[1], N. Merabet[1], S. Bentridi[2], L. Djadia[1] and A. Nadjemi[2], [1]Centre de Recherche en Astronomie Astrophysique et Géophysique, Route de l'Observatoire, BP 63, Algiers, Algeria (lamali_atmane@yahoo.fr), [2]Laboratoire de l'Énergie et des Systèmes Intelligents (LESI), Université Djillali Bounaâma Khemis Miliana, Faculté des Sciences, et de la Technologie, Route de Théniat El Had, 44225 Khemis Miliana, Ain Defla, Algeria, [3]Centre de recherche nucléaire de DRARIA, BP 43, Sebala, Draria, Algiers, Algeria.

Introduction: The Most of the used geophysical methods on terrestrial impacts craters often focus on exploration of anomalies caused by changes in physical properties or by structures associated with the formation of the crater. Among these geophysical methods, gamma-ray spectrometry is not wildly used in the context of impact cratering, despite its efficiency to evidence the physical/chemical changes in the country rocks, thus including the impacted rocks. The Maâdna crater in southern Algeria [1, 2, 3], at which the meteoritic impact origin has not yet been completely established, we have used this method as a marker of any modification in the composition of target rocks that may be related to the impact cratering process in this structure.

Results and discussions: Numerous in situ measurements were carried out using a field portable gamma-ray spectrometer (PGS-2-21). These data revealed that most of surface lithologies which are predominantly calcareous, outcropping on the rim and flanks of the crater, give a very low radiometric response in all three channels (K, Th and U). The recorded total numbers of counts did not exceed 90 Cps inside and outside the crater. This rate is expected to slow significantly in these types of sedimentary rocks with low clay content that generally appear to have very much lower radioelement concentrations. In contrast, the constructed radioelement concentration maps showed an anomalously high gamma response with Potassium-dominated peaks in the central part of the crater and in its surrounding wadis. However, a good correlation is observed between this central part Potassium anomaly and the magnetic one that has been described in earlier studied [4]. This anomalously high radioactivity levels in this zone may be associated with post-emplacement accumulation weathered deposits, since there is no objective criterion allowing us to link these results to an impact event at Maâdna structure.

References:
[1] Lambert P. et al. 1980. *Meteoritics* 15:157–179. [2] Karpoff R. 1953. *Meteoritics* 1:31–38. [3] McHone J. F. Jr. and Greeley R. 1987. *Meteoritics* 22:253–264. [4] Lamali A. et al. 2016. *Meteoritics & Planetary Science* 12:2249–2273.

"MISSION TO ROCHECHOUART" PROJECT: A REVIEW.

P. Lambert[1] and CIRIR Consortium[2], [1]CIRIR-Center for International Research and Restitution on Impacts and on Rochechouart-87600 Rochechouart-France, lambertbdx@gmail.com,
[2] https://drive.google.com/open?id=1uy5BUqBIl6qPhrzYTb_eEcqsI3h0OUj_

Introduction: In 2019 the Rochechouart structure celebrates the 50th anniversary of its recognition as a meteoritic impact by François Kraut [1]. It is also the 5th anniversary of its "revival" with the launch of the project "Mission to Rochechouart" presented at the Meteoritical Society Meeting in Casablanca [2]. We focuss on what has been achieved since its announcement, and what will be achieved in the future.

Objective and means: The general objective of the project was announced in 2008 at the LMI-IV Conference and published in [3]. The aim is valorizing the Rochechouart impact structure as an international natural laboratory for ground truth data mining of impact cratering and its collateral effects on planetary surfaces. Inspired by Apollo, the means proposed in Casablanca for mobilizing the community worldwide on Rochechouart was realizing the first drilling campaign within the geosite and making the targeted 300 m of cumulated cores available to the world community via a dedicated storage facility on site and an organisation to facilitate interactions and coordination [2].

Results: Thanks to the support of the local territories, the State and a number of scientists who endorsed these two complementary projects, the CIRIR (Center for International Research and Restitution on Impacts and on Rochechouart) was created in 2016 and the drilling program was undertaken in 2017-2018. A total of 8 sites in the "Reserve Naturelle Nationale de l'Astroblème de Rochechouart-Chassenon" were drilled delivering over 540 m of core [4]. In parallel, the CIRIR has grown by associating individuals and organisations (currently over 60 scientists from a dozen countries) taking advantage of the geosite, the geomaterials, the facilities on site, and the group itself for carrying out projects of their own. They all contribute to the valorization of the impact geoheritage to the mutual benefit of the scientific community, the geoheritage, the Reserve, and the public at large. The combined effort forms the CIRIR program currently counting 60 research projects covering essentially all impact-related topics (details at https://drive.google.com/open?id=1uy5BUqBIl6qPhrzYTb_eEcqsI3h0OUj_). Projects unrelated to the cores and/or not requiring core samples have started (age, alteration, paleoenvironment, stratigraphic relationship between the diverse impactites, size and shape of the initial crater, etc...) and already resulted in a significant increase in the bibliographic record on Rochechouart within the last 5 years [4,6-12]. In parallel, the CIRIR facility has been installed at Rochechouart It is composed of two units. One is designed for accommodating and managing the cores and the surface samples collected by scientists and by the public (participative science). It builds up a unique "dynamic" impact sample library made available to the community ("impact on shelf") [5]. Beyond storage, it includes a laboratory for sample preparation and for optical studies. The second unit provides housing and office facilities (to be completed in late 2019) for up to 10 visiting scientists, students and professionals coming to take advantage of the sample library and/or the field itself and/or the presence of CIRIR members for their research and/or training. A linked lodge unit located 12 km from Rochechouart can accommodate up to 50 people in 16 chalets. These facilities are maintained by public money and are available at no charge as part of a "world public service" for promoting the Rochechouart geosite and impact science in general.

Curent developments and perspectives: Most of the outcomes of the drilling campaign are still to come. The first series of samples requested by CIRIR PI's will be delivered in the fall. The next call for samples is open and will close in Spring 2020. Until then the curent CIRIR members have a priority for requesting samples. Yet new incomers and new projects are most welcome and encouraged. The site and the facilities are open to the community at large. Beyond research, the CIRIR program and teams expand into education and outreach including geoconservation and geotourism, for empowering the science achieved on Rochechouart and on impact cratering in general and the human adventure that goes with it, and make it profitable to the public at large. Projects in these fields are most welcome too.

References: [1] Kraut F. (1969) *Geologica Bavarica*. 61, 428–450. 77 [2] Lambert et al.(2014) *MAPS* 49 s1 Abstract #5171. [3] Lambert P. and Trumel H. (2010), in *Materials under extreme loadings: Application to penetration and impact, John Wiley* 1-44 [4] Lambert P. and al. (2019) *LPS 50th*, Abstract #2005 [5] Lambert P. et al.(2017) *in LPS 48th*, abstract #1936.pdf. [6] Sapers H.M et al. (2014), *Meteoritics & Planetary Science* 49, Nr 12, 2152–2168 [7] Horne A. (2016), *ASU Master Thesis*. [8] Simpson et al. (2017) *Earth and Planetary Science Letters* 460, 192–200. [9] Cohen, B. E. et al. (2017) *Meteoritics and Planetary Science*, 52(8), 1600-1611. [10] Rasmussen R. and Stockli D. F. (2019), *LPS 50th*, Abstract#2820. [11] Plan A et al. (2019) *MAPS*, abstract this conference. [12] Ormö et al. (2019) *LPS50th,* abstract #1785.

DYNAMIC COMPRESSION AND PHASE TRANSFORMATIONS OF BADDELEYITE IN SYNCHROTON-BASED DIAMOND ANVIL CELL EXPERIMENTS.

F. Langenhorst[1], E. Adelhardt[1], U. Mansfeld[1], and H.P. Liermann[2], [1]Institute of Geoscience, Friedrich Schiller University Jena, Germany (Falko.Langenhorst@uni-jena.de), [2]Deutsches Elektronen-Synchrotron (DESY), FS-PE, P02, Notkestraße 85, 22607 Hamburg, Germany.

Introduction: Recently, fast membrane-driven diamond anvil experiments (mDAC) were tested for their suitability to simulate the effects of shock compression in rock-forming minerals [1-3]. A major advantage of such experiments is the ability to obtain time-resolved *in-situ* X-ray diffractice data of rapidly compressed crystalline solids and thus to detect their structural changes directly during the compression and decompression paths. Despite the absence of shock waves in DAC experiments and their distinctly slower compression rates compared to shock experiments, the mDAC technique yielded known shock effects such as the amorphization of quartz and feldspars [1,3] and [001] dislocation glide in olivine [2].

In this study, we performed dynamic mDAC experiments on baddeleyite (monoclinic form of ZrO_2), a reliable geochronometer and accessory mineral in planetary basaltic rocks. The ZrO_2 phase diagram displays several phase transformations along the temperature and pressure axes. Phase transitions along the pressure axis involve the formation of various orthorhombic structures at 6 GPa (ort-I), 22 (ort-II), and 40 GPa (ort-III) [4,5]. Further orthorhombic polymorphs and cotunnite-structured ZrO_2 are predicted to occur at even higher pressures [6]. Here, we focus on the nature and kinetics of these pressure-induced phase transformations, which are much less constrained than the temperature-induced martensitic and displacive transitions.

Methods: Polycrstalline, 1 µm sized ZrO_2 powder served as starting material in two mDAC experiments run up to 37 GPa and 64 GPa. The ZrO_2 powder was loaded into a Re gasket and then dynamically compressed under non-hydrostatic conditions at a rate of 1 GPa/s. X-ray diffraction patterns were acquired at beamline P02.2 of PETRAIII, DESY Hamburg at 25.6 keV using a Perkin-Elmer XRD 1621 fast flat panel detector. Powdered gold was used as an internal pressure standard. Recovered samples were investigated by transmission electron microscopy (TEM) to detect persistent structural modifications in baddeleyite.

Results and Discussion: In line with previous slow compression experiments [4,5], our synchroton X-ray diffraction experiments reveal the immediate transformation of monoclinic baddeleyite to the orthorhombic phases I, II, and III at 6, 22, and 40 GPa, respectively. On unloading these phases even persist without reversion to the baddeleyite structure. The lattice constants *a*, *b*, and *c* of the orthorhombic phases abruptly change at the transformation pressures (Fig. 1), while the overall cell volume almost linearly increases with increasing pressure.

TEM inspection of recovered samples confirms the persistence of orthorhombic phases at ambient pressure and shows the conversion of the material into nanocrystalline aggregates. Individual nanocrystals are strongly strained but otherwise defect-free. These observations indicate the displacive nature of the pressure-induced phase transformations. The persistence of the orthorhombic phases at ambient pressure is attributed to internal strain in nanocrystalline aggregates.

References: [1] Carl E.-R. et al. (2017) Meteoritics & Planetary Science 52:1465-1474. [2] Langenhorst F. et al. (2017) 80th Annual Meeting of MetSoc: #1987. [3] Sims M. et al. (2019) Earth and Planetary Science Letters 507:166-174. [4] Leger J.M. et al. (1993) Phys. Rev. B 47:14075. [5] Bouvier et al. P. (2000) Phys. Rev. B 62: 8731. [6] Nishio-Harmane D. et al. (2015) Phys. Chem. Minerals 42:385-392.
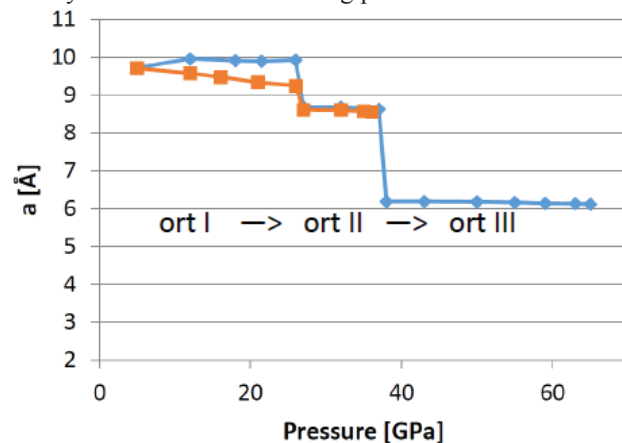
Fig. 1: Lattice constant a of the orthorhombic phases I, II, and III in two mDAC experiments as a function of pressure.

ALKALI-HALOGEN METASOMATISM OF METEORITE HILLS 01075 (CM2) DRIVEN BY SHOCK HEATING: AN ANALOGUE FOR RYUGU.

M. R. Lee[1], B. E. Cohen[1] and A. J. King[2]
[1]School of Geographical and Earth Sciences, University of Glasgow, Gregory Building, Lilybank Gardens, Glasgow G12 8QQ, UK (Martin.Lee@glasgow.ac.uk) [2]Department of Earth Science, Natural History Museum (London), Cromwell Road, London SW7 5BD, UK.

Introduction: Reflectance spectra of the asteroid 162173 Ryugu that have been recently obtained by the Haya-busa2 spacecraft are similar to those of thermally/shock metamorphosed carbonaceous chondrites, with the CM meteorite Hills (MET) 01072 being highlighted as a good analogue [1]. MET 01072 has a strong petrofabric show-ing that it has undergone impact deformation, but was not heated sufficiently to dehydrate its phyllosilicates [2]. This apparent contradiction could be reconciled if MET 01072 had been deformed by multiple low intensity impacts that generated little heat [2]. Here we describe evidence from MET 01075 (a pair of MET 01072) for an alternative explanation, namely that heating produced by early shock deformation initiated alkali-halogen metasomatism, most of the evidence for which was later overprinted by lower temperature aqueous alteration.

Samples and methods: MET 01075 was collected by ANSMET in 2001. This study used a chip (MET 01075,8) that was divided into two parts. One was impregnated in epoxy resin, made into a polished block, and studied by scanning electron microscopy (SEM) at the University of Glasgow. The other part was used to determine modal mineralogy by X-ray diffraction (XRD) at the Natural History Museum.

Results: MET 01075 is composed of rimmed chondrules/chondrule fragments and refractory inclusions set in a fine-grained matrix that is dominated by tochilinite-cronstedtite clumps. This lithology is therefore comparable to the 'primary accretionary rock' of [3]. MET 01075 has a modal mineralogy of (vol. %): Mg-serpentine (63.9), Fe-cronstedtite (18.7), olivine (9.7), enstatite (2.8), magnetite (1.4), Fe-sulphide (2.7), calcite (0.6) and gypsum (0.2). Tochilinite was identified but its abundance was not quantified owing to the lack a pure standard for profile strip-ping. MET 01075 has a phyllosilicate fraction of 0.87, corresponding to a petrologic subtype of 1.3 on the scale of [4], and so has been highly aqueously altered. Its chondrules and refractory inclusions have been flattened (mean aspect ratio = 1.72) and together define a strong foliation petrofabric. One of the refractory inclusions is 0.6 mm in size and contains spinel, perovskite, diopside, calcite, phyllosilicate and ~20-40 μm grains of sodalite. This feldspa-thoid mineral occurs nowhere else in the sample.

Discussion: In common with its pair MET 01072 and several other CMs, MET 01075 has undergone both aqueous alteration and impact deformation. MET 01075 is however unique among the CMs in containing sodalite. The origin of this mineral may be understood by analogy with the CV carbonaceous chondrites. Feldspathoids are widespread in the CVs where they have commonly formed by the replacement of Ca-aluminosilicates (e.g., melilite) in refractory inclusions during parent body alkali-halogen metasomatism [5]. As the MET 01075 sodalite occurs only in a refractory inclusion, it is interpreted to have formed in the same way (i.e., by relatively high-temperature metasomatic replacement of melilite). Metasomatism must have predated aqueous alteration because melilte is high-ly reactive in the presence of low temperature aqueous solutions (i.e., it occurs only in the least altered CMs such as EET 96029 [6]) and so would not have survived the intensity of aqueous alteration that MET 01075 has expe-rienced. The preservation of serpentine and tochilinite in the matrix of MET 01075 also argues against significant post-hydration heating that would have been needed for late-stage metasomatism.

We conclude that MET 01075 evolved as follows: (i) accretion of rimmed chondrules, refractory inclusions, fine-grained matrix and water ice; (ii) impact deformation and heating through pore collapse [7]; (iii) alkali-halogen metasomatism leading to the replacement of melilite by sodalite; (iv) lower temperature aqueous alteration, either during post-impact cooling of the parent body or accompanying later radiogenic heating. Further details are pro-vided in [8]. The scarcity of feldspathoids in the other CMs may be because such early shock heating was a rare event, or because the products of alkali-halogen metasomatism have typically been destroyed by later aqueous alte-ration. The samples that will be returned from Ryugu may help to answer these questions.

References: [1] Kitazato K. et al. (2019) *Science* 364:272–275. [2] Lindgren P. et al. (2015) *Geochimica et Cosmochimica Acta* 148:159–178. [3] Metzler K. et al. (1992) *Geochimica et Cosmochimica Acta* 56:2873–2897. [4] Howard K. T. et al. (2015) *Geochimica et Cosmochimica Acta* 149:206–222. [5] Krot A. N. et al. (1995) *Meteo-ritics* 30:748–776. [6] Lee M. R. et al. (2016) *Geochimica et Cosmochimica Acta* 92:148–169. [7] Bland P. A. et al. (2014) *Nature Communications* 5:5451. [8] Lee M. R. et al. (2019) *Meteoritics and Planetary Science* (in review).

AMORPHOUS SILICATES IN CARBONACEOUS AND ORDINARY CHONDRITES

C. Le Guillou[1], P.-M. Zanetta[1,2], H. Leroux[1], A. Brearley[3], B. Zanda[2], R. Hewins[2],[4].
[1]Univ. Lille, CNRS, UMR 8207 - UMET - Unité Matériaux et Transformations, F-59000 Lille, France, corentin.san@gmail.com [2]IMPMC, Sorbonne Univ., MNHN, UPMC Paris 06, UMR CNRS 7590, 75005 Paris, France. [3]Dept. of Earth and Planetary Sc., Univ. of New Mexico, Albuquerque, NM 87131. [4]EPS, Rutgers Univ., Piscataway, NJ 08854, USA.

Introduction: Amorphous silicate (AmS) is the major matrix constituent of pristine carbonaceous and ordinary chondrites [1,2]. Its origin and evolution is however difficult to assess, in part because of its nanometer size and the presence of embedded nano-sulfides that make it challenging to analyze. It has been proposed that AmS could originate directly from the "primordial" dust inherited from the molecular cloud. It shares similarities with GEMS (Glass Embedded with Metal and Sulfides) found in IDPs and UCAMMs. It could also have formed by metastable condensation from an unknown gas reservoir, which could be – but is not necessarily – related to chondrule formation. Alternatively, it has been suggested that AmS could be the parent body secondary alteration product of an unknown precursor. Here, we analyzed and compared the compositions of amorphous silicate in the most pristine chondrites of different petrologic groups in order to limit the effects of differential aqueous alteration and be able to test the different formation models.

Method: About 20 FIB sections from CR (QUE 99177 and Renazzo), CM (Paris, Y-791198 and QUE 97990), CO (DOM 08006 and ALH 77307), ordinary (Semarkona and QUE 97008) and Acfer 094 were extracted from either the rims or the matrix and analyzed by quantitative analytical TEM. In particular, we developed a method to measure and map the water content of amorphous silicate *in situ*. Using dedicated calibrations and home-made absorption correction routines, we reached an absolute precision of about ± 1.5 H_2O wt. %.

Results and discussion: AmS are found in all chondrite groups, but their association with other phases and their composition depend on the chondrite group. A major difference is observed between ordinary and carbonaceous chondrites. Compositions averaged per FIB section (see Figs.) indicate that the former are much richer in silicon ((Si+Al)/(Fe+Mg) ~ 1.18 vs. 0.8). Their Na/Si ratios are elevated and higher than in CC (~ 0.15 vs 0.03 at. %), in agreement with their bulk values. The Al/Si ratio is similar between OC and CC, ranging from 0.08 up to 0.22. The water content appears to be highly variable, and is not correlated with any of the major elements. However, we do observe a correlation with the S/Si ratio. Even at the FIB section scale, hyperspectral mapping reveals that AmS has a variable Fe/Mg ratio (50% variation, pixel size of ~ 100 nm), but has a more homogeneous (Si+Al)/(Fe+Mg) ratio (10% variation). The Mg/Si ratio is lower than the solar composition (in CC: 0.55 vs. 1.02 (bulk and CI)).

The AmS is by far the main matrix carrier of Mg and Si and it had been suggested that the matrix Mg/Si ratio could be complementary to that of chondrules [3]. However, no clear correlation between the AmS Mg/Si ratio and the chondrule content (of each meteorite group) is observed, which would have been expected if chemical fractionation had occurred. On the other hand, it has also been proposed that matrix could have a CI-like composition [4], but it does not seem to be the case either, as the matrix olivine (Mg/Si ratio of ~ 2) abundance is not high enough to compensate for the low Mg/Si ratio of the AmS. All chondrite groups share an AmS that was formed by a common process. However, AmS in OC is different from that in CC, which might exclude the idea of a disk-wide homogeneous dust of CI/interstellar origin. Using these constraints, we should be able to constrain if and how secondary processes have affected the AmS and evaluate the formation scenarios. So far, it might be that none of the "usual" models fully explains the data.
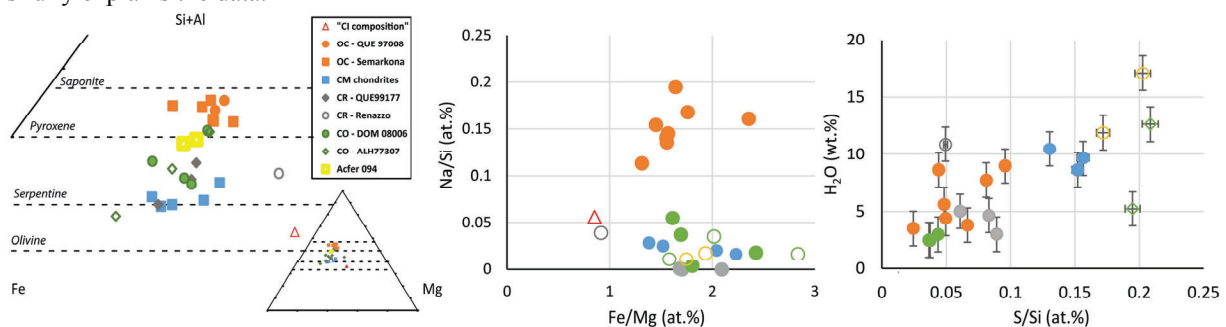
References: [1] Brearley. (1993) Geochimica Cosmochimica acta 57(7), 1521-1550. [2] Le Guillou et al., (2015). Earth and Planetary Science Letters 420, 162-173. [3] Hezel, D. C., & Palme, H. (2010). Earth and Planetary Science Letters, *294*(1-2), 85-93. [4] Zanda, et al. (2018), in Chondrules, Records of Protoplanatary Disk Processes, 122-150.

PRESOLAR GRAINS FROM HIGHER-MASS AGB STARS?

J. Leitner[1], P. Hoppe[1], and J. Kodolányi[1], [1]Max-Planck-Institut für Chemie, Hahn-Meitner-Weg 1, 55128 Mainz, Germany, jan.leitner@mpic.de

Introduction: Isotopically anomalous dust that formed in the outflows of evolved stars or in the ejecta of stellar explosions [1] is a minor, but important component of primitive solar system materials. Silicates are the most abundant type of "presolar" dust available for single grain analyses [2], with characteristic sizes of ~150 nm [3]. Based on their O isotopes, most (>99%) presolar silicates and oxides are divided into four distinct groups [4]. Group 1 grains (~70%) are believed to come from low-mass (1.2–2.2$M_\odot$) asymptotic giant branch (AGB) stars of ~solar metallicity, with higher than solar $^{17}O/^{16}O$ ratios and $^{18}O/^{16}O$ ratios ranging from about solar down to ~1×10^{-3}. However, recent studies of Mg-isotopes in Group 1 silicates showed that not all of these grains come from low-mass AGB stars; instead, a fraction of them displays large ^{25}Mg-excesses incompatible with a low-mass AGB origin, indicating stellar explosions as their sources [5]. Group 2 grains also have enhanced $^{17}O/^{16}O$ ratios, but significantly lower $^{18}O/^{16}O$ (<1×10^{-3}). Likely sources are red giant/AGB stars of M <1.5 $M_\odot$ and Z <$Z_\odot$ experiencing additional mixing processes like cool bottom processing [e.g., 6]. Alternatively, some of the grains could stem from higher-mass (4–8 $M_\odot$) AGB stars undergoing hot bottom burning (HBB) [7]; and finally, a few of the Group 2 grains might have formed in the winds of post-AGB stars [e.g., 8]. Here, we report on two Group 2 silicates with Mg-isotopic compositions indicative of an origin in ~6 $M_\odot$ AGB stars, and on several Group 1 silicates possibly coming from ~4-5 $M_\odot$ AGB stars with higher-than-solar metallicities.

Methods: Mg isotope studies were conducted with the new Hyperion RF plasma O primary ion source installed on the MPIC Cameca NanoSIMS 50 on presolar silicates previously identified during standard O-isotopic mapping of Meteorite Hills 00426, Elephant Moraine 92161, and Acfer 094. A focused O$^-$ beam (<100 nm, ~0.5 pA) was rastered over 2×2 μm^2-sized areas around the presolar silicate grains, and secondary ion images of $^{24,25,26}Mg^+$, $^{27}Al^+$, and $^{28}Si^+$ were acquired simultaneously. Subsequently, $^{24,25}Mg^+$ and $^{28,29,30}Si^+$ were measured for selected grains.

Results and Discussion: The two Group 2 silicates display ^{25}Mg-enrichments of 165 ‰ and 1050 ‰, respectively, and $\delta^{26}Mg$-values of 200–300 ‰; five Group 1 silicates have ^{25}Mg-enrichments of 104 ‰–280 ‰, with $\delta^{26}Mg$ between 18 and 65 ‰ (all errors ≤13 ‰). For low-mass AGB stars, no major modifications of the Mg isotopes are expected, and their compositions mainly reflect Galactic chemical evolution (GCE) [e.g., 9]. HBB, however, can strongly affect the $^{25,26}Mg/^{24}Mg$ ratios, resulting in larger excesses for the Group 2 grains [7,10]. Comparison of these models with the grain data indicates an origin from 6–7 $M_\odot$ AGB stars of ~solar metallicity for the two Group 2 silicates, as similarly inferred previously for two Group 2 spinel grains [7]. The ^{25}Mg-enrichments of the five Group 1 silicates are not accompanied by similarly high ^{26}Mg-excesses; thus, a GCE-related origin can be excluded. One possible explanation for their isotopic signatures is the occurrence of explosive H-burning in supernova explosions [5], but given the only moderate ^{25}Mg enrichments another potential source are intermediate-mass AGB stars of supersolar metallicity [10]. In the latter case, we find a good match between the 3.75–4.75 $M_\odot$-models with Z = 0.03 and the grain data, especially when adopting a less effective ^{26}Mg-production via $^{22}Ne(\alpha,\gamma)^{26}Mg$ than typically assumed [11]. The Group 2 silicate grain with the largest ^{25}Mg-excess also shows small enrichments in ^{29}Si and ^{30}Si, while the three Group 1 grains measured so far show no significant deviations from the Solar System Si-isotopic composition. In summary, we find that, by taking the latest AGB star models and reaction rate updates into account [7,10], the two Group 2 silicates discussed here originate from higher-mass AGB stars (M~6 $M_\odot$). Several Group 1 silicates with moderate ^{25}Mg-enrichments could have formed around AGB stars with masses of 3.75–4.75 $M_\odot$ and Z>$Z_\odot$, although an alternative source of this sub-population could be core-collapse supernovae with H-ingestion [5]. AGB stars with M>4 $M_\odot$ are expected to have contributed a significant fraction of silicate and oxide dust to the presolar grain inventory of the nascent Solar System [12]; however, evidence for such grains has been exceptionally rare so far [7], and was restricted to presolar grains of Group 2. Our results show that high-resolution Mg isotope studies are a suitable tool for the identification of HBB signatures, and that the Group 1 grains might contain a sub-population of dust from intermediate-mass AGB stars with supersolar metallicity.

References: [1] Zinner E. (2014) In *Meteorites and Cosmochemical Processes* (ed. Davis A. M.). Elsevier, Amsterdam, pp. 181–213. [2] Floss C. & Haenecour P. (2016) Geochem. J., 50, 3–25. [3] Hoppe P. et al. (2017) Nat. Astron., 1:617–620. [4] Nittler L. R. et al. (1997) Astrophys. J., 483:475–495. [5] Leitner J. & Hoppe P. (2019) Nat Astron., in press. [6] Palmerini S. et al. (2011) Astrophys. J., 728:3–23. [7] Lugaro M. et al. (2017) Nat. Astron., 1:0027. [8] Buntain J. et al. (2012) In *Proceedings of the International Astronomical Union*, IAU Symposium, Vol. 283, pp. 322–323. [9] Hoppe P. et al. (2018) Astrophys. J. 869:47–59. [10] Karakas A. I. & Lugaro M. (2016) Astrophys. J., 825:26–47 [11] Iliadis C. et al. (2010) Nucl. Phys. A, 841:31–250. [12] Zhukovska S. et al. (2015) Astrophys. J., 810:128–141.

IN SITU ISOTOPIC STUDY OF NITROGEN CARRIERS IN UNEQUILIBRATED ORDINARY CHONDRITES.

J. Leitner[1], C. Vollmer[2], and P. Hoppe[1], [1]Max-Planck-Institut für Chemie, Hahn-Meitner-Weg 1, 55128 Mainz, Germany, jan.leitner@mpic.de, [2]Universität Münster, Inst. f. Mineralogie, Corrensstr. 24, 48149 Münster, Germany.

Introduction: Nitrogen, the most abundant component in the terrestrial atmosphere, has been one of the key elements for the evolution of Earth's biosphere. The N-isotopic ratios of the terrestrial planets differ significantly from those of the Sun and the protosolar nebula [e.g.,1–3]. Thus, other nebular components must have contributed significantly to terrestrial N. Besides enstatite chondrites, ordinary chondrites (OCs) have been identified as suitable analogue material for the terrestrial building blocks [e.g., 4,5]. Whole-rock N-abundances between 1 and 160 ppm have been found [e.g., 6–8], and bulk δ^{15}N-values (relative to terrestrial air) range from –230 ‰ to +760 ‰ [8]. Organic material (OM) in OCs has bulk N-isotopic compositions between –50 ‰ and +60 % [9], i.e., less variability than on the whole-rock scale, indicating the presence of further N-carriers in the OCs with more extreme isotopic compositions. Previous studies reported graphitic carbon in a set of OCs of low petrologic type with N-isotopic anomalies corresponding to the heavy bulk-N-compositions [10,11]. Furthermore, small amounts (12 to 148 ppb) of Si_3N_4 were identified in three ordinary chondrites [12], but no comprehensive investigation of the inventory of N-carriers in OCs has been conducted to date. Here, we present first results of an ongoing isotopic and mineralogical study of organic and inorganic nitrogen-bearing phases in ordinary chondrites.

Methods: Polished sections of Semarkona (LL3.00) and Mezö-Madaras (L3.7) were characterized by BSE imaging and EDS mapping with a LEO 1530 FE-SEM at the Max Planck Institute for Chemistry (MPIC), equipped with an Oxford X-Max 80 SDD detector to identify potential N-carriers. The C- and N-isotopic compositions of suitable N-bearing phases were then measured by NanoSIMS at the MPIC by rastering a ~100 nm Cs^+ primary ion beam (~1 pA) over selected sample areas. Secondary ion images of $^{12,13}C^-$, $^{12}C^{14}N^-$, $^{12}C^{15}N^-$, and $^{28}Si^-$ were recorded in multi-collection mode.

Results and Discussion: Twenty-nine Si_3N_4 grains were identified by SEM-EDS investigation in a metal-sulfide-inclusion in Mezö-Madaras. The largest grain measures 830×360 nm, while 21 of the 29 nitrides are smaller than 300 nm in diameter. Twenty-eight grains were quantitatively investigated with SEM-EDS, and all grains contained Cr above detection limit, with Cr/Si atomic ratios ranging from 0.05 to 1.3. However, the Cr abundances especially for the smaller grains are clearly affected by Cr from the surrounding host metal, thus, further work is required for a proper characterization. Several of the larger nitrides contain resolvable subgrains in both BSE and EDS maps, suggesting they are rather Si_3N_4-CrN-intergrowths than Cr-bearing silicon nitrides. Six grains were subsequently measured by NanoSIMS. The δ^{15}N-values range from –236±147 ‰ to 10±25 ‰, with a weighted average of –27±14 ‰. The abundance of Si_3N_4 in the host grain is ~14 ppm, well below the values reported for individual metal-sulfide host grains in enstatite chondrites [13].

While organic matter in carbonaceous chondrites has been extensively studied with a variety of techniques, far less work has been conducted on OM in ordinary chondrites [e.g., 14,15]. Previous isotopic investigations of extracted insoluble OM showed large D-enhancements compared to the terrestrial value, while ^{15}N-enrichments appear to be much rarer than in the carbonaceous chondrite (CC) OM [14,15]. So far, ~1500 µm² of matrix material in Semarkona have been investigated, revealing six hotspots with δ^{15}N ranging from 350 ‰ to 1060 ‰ (4σ significance level), as well as one "cold spot" with a ^{15}N-depletion of –238±48 ‰. Further isotopic and structural analysis will be performed to allow a more thorough comparison between OC and CC organics. Extending this study to OM from other OCs, together with further investigation of inorganic N-carriers like Si_3N_4 and graphite will enable us to obtain a more comprehensive picture of the inventory of nitrogen carriers of these meteorites, which represent a good analogue material for a significant fraction of the terrestrial building blocks.

References: [1] Marty B. et al. (2011) *Science* 332:1533–1536. [2] Pollack J. B and Black D. C. (1979) *Science* 205:56–59. [3] Mathew K. J. and Marti K. (2001) *J. Geophys. Res.* 106:1401–1422. [4] Warren P. H. (2011) *Earth Planet. Sci. Lett.* 311:93–100. [5] Dauphas N. (2017) *Nature* 541:521–524. [6] Kung C.-C. and Clayton R. N. (1978) *Earth Planet. Sci. Lett.* 38:421–435. [7] Hashizume K. and Sugiura N. (1995) *Geochim. Cosmochim. Acta* 59:4057–4069. [8] Sugiura N. et al. (1998) *Meteorit. Planet. Sci.* 33:463–482. [9] Alexander C. M. O'D. et al. (1998) *Meteorit. Planet. Sci.* 33:603–622. [10] Mostefaoui S. et al. (2000) *Geochim. Cosmochim. Acta* 64:1945–1964. [11] Mostefaoui S. et al. (2005) *Meteorit. Planet. Sci.* 40:721–743. [12] Russell S. S. et al. (1995) *Meteoritics* 30:399–404. [13] Leitner J. et al. (2018) *Geochim. Cosmochim. Acta* 235:153–172. [14] Alexander C. M. O'D. et al. (2010) *Geochim. Cosmochim. Acta* 74:4417–4437. [15] Remusat L. et al. (2016) *Earth Planet. Sci. Lett.* 435:36-44.

CLASSIFICATION OF 13 CM CHONDRITE BRECCIAS AND CM CLASTS IN TWO ACHONDRITES

S. Lentfort[1], A. Bischoff[1], and S. Ebert[1]. [1]Institut für Planetologie, Wilhelm-Klemm-Str. 10, 48149 Münster, Germany (s_lent03@uni-muenster.de).

Introduction: CM chondrites are complex impact (mostly regolith) breccias, in which lithic clasts and mineral fragments show various degrees of aqueous alteration. These fragments are mixed together and lithified in a fine-grained clastic matrix; however, the conditions of aqueous alteration are still controversial (e.g., [1-8]). This is in particular the case considering the chronological relationship between aqueous alteration and brecciation. Different classification schemes have been proposed to quantify the degree of alteration (e.g., [7-8]). Unfortunately, brecciated CM-chondrites are forced into an alteration sequence. Rubin et al. [8] mentioned the brecciated nature of CMs, but used only one alteration index for these complex rocks. Earlier, we noticed [9] that our thin section of the CM-breccia of Nogoya (classified as a CM2.2 [8]) contains most fragments that are significantly less altered than CM2.2 and was therefore classified as a CM2.2-2.6 [9] in the same way as ordinary chondrite breccias (e.g., [10,11]).

Results: Here, we have studied individual fragments of 13 CM chondrite breccias and CM clasts in two achondrites (Tab. 1). The alteration index of 97 fragments was determined based on the optical appearance and chemistry of their PCPs using the procedure suggested by [8].

Tab. 1: Subtype classification of CM chondrite breccias and CM clasts in two achondrites. * contains also C1-clasts

Sample	Subtypes	Sample	Lit. [8]	Subtypes	Sample	Subtypes
LON 94101	CM2.0*-2.8	Maribo		CM2.4-2.6	Santa Cruz	CM2.4-2.8
ALH 85013	CM2.0-2.8	Jbilet Winselwan		CM2.3-2.9		
ALHA 77306	CM2.0-2.6	Cold Bokkeveld	CM2.2	CM2.0-2.8	Fragments in:	HEDs
Banten	CM2.4-2.9	Nogoya	CM2.2	CM2.0-2.6	EET 87513	CM2.4-2.6
NWA 10907	CM2.3-2.4	Murchison	CM2.5	CM2.4-2.9	NWA 7542	CM2.2-2.8
NWA 10908	CM2.3-2.4	Y-791198	CM2.4	CM2.4-2.8		

Optically, strongly-altered fragments (2.0-2.2) and moderately-altered fragments (2.4/2.5-2.6 [8] or >2.6 [this study]) can be distinguished. However, an accurate subclassification can only be performed by obtaining the chemical composition of the PCPs considering the S/SiO_2- and "FeO"/SiO_2-ratios and the SiO_2, FeO, and MgO contents. For certain clasts in the brecciated CM chondrites "FeO"/SiO_2-ratios were obtained that were significantly above the values of 2.9 ± 0.6 being the hightest ratios and indicating the lowest degree of alteration (e.g., 2.6 by [8]). This leads to the definition of new subtypes for less-altered samples in this study (CM2.7-2.9). Although PCPs within a distinct subtype have similar "FeO"/SiO_2-ratios, the S/SiO_2-ratio can vary significantly. However, not all investigated samples contain clearly-defined fragments. It is important to mention that samples free of well-defined clasts were also classified by the analyses of different PCP objects randomly distributed throughout the sample. Examples are NWA 10907, NWA 10908, and Maribo (Tab. 1).

Discussion and Conclusions: The new data set of this study allows a more precise classification and expands the actual scheme by the definition of the new subtypes of 2.7-2.8 and 2.9. Furthermore, the study clearly shows that the degree of aqueous alteration can strongly vary from clast to clast within a single thin section and between thin sections. In this respect LON 94101 is an exceptional example; most studied thin sections contain fragments with a wide range of subtypes from 2.0 to 2.8, whereas one thin section contains only clasts with subtypes between 2.0-2.3. Thus, the CM subtype classification based on the most abundant fragment-type as used by Rubin et al. [8] is not appropriate for the classification of complex CM chondrite breccias. Therefore, an extended classification scheme from 2.0-2.9 that takes into account the brecciation and includes the minimum to maximum degree of alteration is more precise and preferable.

References: [1] Fuchs L.H. et al. (1973) *Smiths. Contrib. Earth Sci*. 10:1-39. [2] Metzler K. et al. (1992) *Geochim. Cosmochim. Acta* 56:2873-2897. [3] Metzler K. (1995) *Lunar Planet Sci*. 26:961-962. [4] Bischoff A. (1998) *Meteoritics & Planet. Sci*. 33:1113-1122. [5] Bischoff A. and Schultz L. (2004) *Meteoritics & Planet. Sci*. 39:A15. [6] Metzler K. (2004) *Meteoritics & Planet. Sci*. 39:1307-1319. [7] Browning L. et al. (1996) *Geochim. Cosmochim. Acta* 60:2621-2633. [8] Rubin A.E. et al. (2007) *Geochim. Cosmochim. Acta* 71:2361-2382. [9] Bischoff A. et al. (2017) *Meteoritics & Planet. Sci*. 52:A26. [10] Bischoff A. et al. (2006) *Meteorites and the Early Solar System II*, University of Arizona Press:679-712. [11] Bischoff A. et al. (2018) *Geochim. Cosmochim. Acta* 238, 516-541.

A DFT STUDY OF THE STRUCTURE AND PROPERTIES OF NITROGEN DOPING SPINEL $MgAl_2O_{3.5}N_{0.5}$

P. K. Leong1, C. P. Tang1, S. I. Tam1 and T. Sekine2, 1State Key Laboratory of Lunar and Planetary Sciences, Macau University of Science and Technology, Macau. E-mail: cptang@must.edu.mo, 2Center for High Pressure Science and Technology Advanced Research (HPSTAR) Shanghai Laboratory of HPSTAR, Shanghai, P.R. China. E-mail: toshimori.sekine@hpstar.ac.cn

Introduction: Since spinel has an important role of planetary composition, doped spinels are also studied for their properties[1-3] (electronic, optical, magnetic, etc.) in astronomical implications.[4] In this work, we report a possible nitrogen-doped oxygen structure of spinel with density functional theory (DFT). The studies of the structural and electronic properties (band structure, density of states and phonon) of the spinel ($MgAl_2O_4$) and the N doping spinel ($MgAl_2O_{3.5}N_{0.5}$) compounds are performed using the generalized gradient approximation and the Perdew-Burke-Ernzerh of (GGA/PBE) functional. The density and space group (in brackets) of the two crystal cells are 3.47 g/cm^3 (Fd3m) for $MgAl_2O_4$ and 3.38 g/cm^3 (R3m) for $MgAl_2O_{3.5}N_{0.5}$, respectively. The calculated direct band gaps at the Γ-point are approximately 5.13 eV for $MgAl_2O_4$ and 4.24 eV for $MgAl_2O_{3.5}N_{0.5}$. The density of states analysis shows that the tops of the valence bands are constituted ~93% of the p(O) states and ~60% of p(N) + ~32% of p(O) states (for $MgAl_2O_4$ and $MgAl_2O_{3.5}N_{0.5}$, respectively). In the phonon analysis, the lowest frequency of $MgAl_2O_{3.5}N_{0.5}$ is redshifted to 36.6 cm^{-1} (MgAl2O4 is 39.8 cm^{-1}) caused by the N-doped. Finally, we calculated the cohesive energy dependence for the pressure of the two spinels. We found that the cohesive energy of $MgAl_2O_{3.5}N_{0.5}$ is lower than $MgAl_2O_4$ when the pressure is higher than ~115 GPa. It implies that $MgAl_2O_{3.5}N_{0.5}$ is more stability than $MgAl_2O_4$ at high pressure. Base on these results, we suggest that nitrogen atom would replace the oxygen of spinel in the depths of the earth or other planets.

References: [1]Park M. S. et al. (1999) *Physical Review B* 59:10018–10024. [2] Wang H. et al. (2010) *Journal of Alloys and Compounds* 491:550–559. [3] Kahn M. L. and Zhang Z. J. (2001) *American Institute of Physics* 78:3651–3653. [4] Richter H. et al. (2005) *Mineralogy and Petrology* 85:53–65.

SPECTRAL AND MICROSTRUCTURAL MODIFICATIONS OF OLIVINE UNDER ION IRRADIATION.

H. Leroux[1], F. de la Peña[1], C. Le Guillou[1], C. Lantz[2], R. Brunetto[2]
[1]Unité Matériaux et Transformations, University of Lille, France (hugues.leroux@univ-lille.fr), [2]Institut d'Astrophysique Spatiale, UMR 8617, CNRS, Université Paris-Saclay, F-91405 Orsay, France.

Introduction: Atmosphere-less bodies of the Solar System are submitted to surface alteration processes (solar wind irradiation and micrometeorites impacts) collectively known as space weathering. Space weathering strongly modifies the spectral properties of their surfaces, usually darkening and reddening the VIS-NIR region of the spectrum and attenuating their characteristic absorption bands [e.g., 1-3]. The study of lunar and Itokawa samples by transmission electron microscopy (TEM) revealed that those changes are due to chemical and structural changes of the surface materials at the nanoscale, such as the formation of an amorphous rim typically 50-100 nm thick [e.g., 4-5]. Here we report on the spectral properties in the VIS-NIR and in the MIR and nanostructure studied by TEM of experimentally weathered Fe-rich olivine ($\approx Fa_{30}$) by ion irradiation.

Methods: Olivine samples were irradiated with 20-40 keV He and Ar ions with fluences ranging from 1 to $6x10^{16}$ ions/cm^2. The irradiated samples were studied spectroscopically in the VIS-NIR and in the MIR (part of the spectral properties are published in [6]). The microstructural characteristics of the modified surfaces were studied by transmission electron microscopy after FIB extraction, using conventional bright field imaging, HAADF imaging, EDXS and EELS spectroscopies.

Results: In the MIR range, we observed a shift of the silicate bands toward longer wavelengths that increases with ion fluence. In the visible-NIR range, the irradiated olivines show darkening and reddening. At the TEM scale, the sample irradiated with He at low fluence (10^{16} ions/cm^2) shows localized and partial amorphization at the predicted maximum implantation depth. In this area, the olivine lattice displays evidence of strong elastic deformation, as revealed by Bragg contrast perturbation on bright field images. At high fluences ($6x10^{16}$ ions/cm^2) the samples are almost fully amorphized and contain nanometer-sized vesicles due to the implantation and precipitation of He or Ar. The amorphous layers do not contain any Fe nanoparticules (npFe). Slight chemical evolution occurred with a preferential loss of Mg and O close to the surface. With a combined set of data obtained with HAADF imaging and EELS and EDS spectroscopies, we show that the density of the material strongly decreases. This is caused by a double contribution, on the one hand by the phase transformation (crystalline state to the amorphous state) and on the other hand by the implantation of incident ions and the formation of small vesicles.

Discussion: The absence of npFe in the irradiated layer suggests that they do not form by irradiation only. NpFe have frequently been observed in both lunar and Itokawa samples [e.g., 4-5]. However, they could be formed by a secondary process such as a precipitation induced by a thermally activated process. Experimental studies have shown, for instance, that nanoparticles can form by a vapor deposition process simulating micrometeorite impacts [e.g., 7]. Despite the absence of npFe, the spectral properties are strongly modified by irradiation. In addition to the amorphization process, the remaining olivine lattice is highly strained due to the implantation of the incident ions. We suggest that the progressive shift of the MIR characteristics bands of olivine is due to lattice swelling related to the high concentration of interstitials species mostly coming from the implanted ions. Swelling in irradiated materials, including silicates, is a well-known process [e.g., 8-9]. The formation of gas nano-vesicles and the drastic change of density are likely the main cause of the modification of optical properties of the irradiated olivine.

References: [1] Hapke B. (2001) (1997) *Journal of Geophysical Research* 106:10,039-10,073. [2] Clark B.E. et al. (2002) *In* Asteroids III, pp. 585–599. [3] Pieters C. M. and Noble S. K. (2016) *Journal of Geophysical Research* 121:1865-1884. [4] Keller L. P. and McKay D. S. (1997) *Geochimica et Cosmochimica Acta* 61:2331–2341. [5] Noguchi T. et al. (2014) *Meteoritics & Planetary Science* 49:188–214. [6] Lantz et al. (2017) Icarus 285:43-57. [7] Sasaki et al. (2001) *Nature* 410:555-557. [8] Zhang and Salje (2001) *Journal of Physics Condensed Matter* 13:3057-3071. [9] Nasdala et al. (2018) *Physics and Chemistry of Minerals* 45:855–871.

ALTERATION PHASES IN THE E101.1 COMPOUND CAI: EVIDENCE OF NEBULAR PROCESSES?

D. Levy[1,2], J. Aléon[1], A. Aléon-Toppani[2], R. Brunetto[2]. [1] IMPMC, Sorbonne Université, MNHN, UPMC, IRD, CNRS, UMR 7590, 61 rue Buffon, 75005 Paris, France; [2] IAS, Université Paris Saclay, CNRS, UMR 8617, 91405 Orsay. Mail: dan.levy@mnhn.fr

Introduction: Ca-Al-rich inclusions (CAIs) found in chondrites, are the oldest rocks of the solar system. They formed at high temperature at the inner edge of the solar system in reducing conditions [1]. However, many CAIs contain secondary phases formed at relatively low temperature and high oxygen fugacity. After proposing that these phases formed in the nebula [e.g. 2], it has been admitted that the majority of these phases formed by fluid circulations on the parent-body [3,4]. However, the distribution of FeO-rich minerals of some CAIs, such as E101.1 [5,6], still suggests a possible nebular origin, which would imply oxidizing conditions not expected by thermodynamics in a gas of solar composition. E101.1 is a compound CAI from the reduced CV3 chondrite Efremovka. The host is a compact type A CAI cristallized from a melt and mainly composed of melilite ($\sim$Åk$_{25}$), associated with spinel, perovskite, fassaite and FeNi metal [5]. Xenoliths are sinuous fragments dominated by diopside having isotopic signatures consistent with condensation [6] and containing anorthite. The FeO-rich minerals are systematically enclosed inside these fragments. In order to determine if the FeO-rich minerals could have formed before accretion on the parent asteroid, we performed a detailed mineralogical study.

Methods: Secondary phases were characterized by electron microprobe (EPMA) whenever possible. Fine grained minerals and complex assemblages were studied by transmission electron microscopy (TEM) using nine focused ion beam sections. Mid-infrared (MIR) spectroscopy was used to locate amorphous melt pockets previously noticed in the sample [5,6].

Results: Secondary phases are predominantly kirschsteinite (61-79 mol%) and Mg-rich melilite enriched in ferro-åkermanite (13-28 mol%, hereafter Fe-åkermanite) associated with wollastonite. Anorthite is locally enriched in Na and replaced by nepheline. Local variations in this unusual mineral assemblage are observed. Notably, Fe-åkermanite is only present when the secondary assemblage is in contact with the host. By contrast, it is absent and kirschsteinite is the dominant mineral when enclosed completely in primary xenolith diopside. At the submicron scale, the contact between kirschsteinite and diopside is not sharp. The kirschsteinite-diopside interface often consists of Fe-enriched diopside, kirschsteinite enriched in Mg, monticellite and minute Fe metal, all smaller than 50 nm in size, which replace coarser-grained and sometimes euhedral kirschsteinite. Anorthite and Fe-åkermanite are sometimes locally amorphous. Numerous veins of amorphous Si-rich materials are observed. MIR spectroscopy confirms the presence of 1 to 100 µm amorphous melt pockets spatially associated with the xenoliths, chemically consistent with a mixture between the host and the xenoliths including secondary minerals.

Discussion: The interfaces between minerals indicating notably reduction of kirschsteinite into monticellite and metal, the amorphous phases and the amorphous melt pockets show that E101.1 underwent several high temperature events. An impact on the Efremovka parent body and the incorporation of the xenoliths into the host type A CAI are the two major high temperature events [6]. Fe-åkermanite and anorthite were most likely amorphized by a late impact. Distribution of Fe and Na in the amorphous melt pockets indicates that they formed after the formation of FeO and Na$_2$O-rich minerals but predate amorphization of Fe-åkermanite and anorthite. It is not clear whether they consist of residual glass resulting from the incorporation of the xenoliths into the host or of impact melts. Fe-åkermanite probably formed during the incorporation, as supported by its systematic location at the contact with the host CAI. All interface reactions indicate that coarse grained kirschsteinite and wollastonite are early phases, initially associated with condensate diopside. This strongly suggests that they were present before incorporation of the xenoliths and formed in the solar nebula. If correct, this implies that refractory xenoliths witnessed fO$_2$ conditions inconsistent with the canonical astrophysical context of formation of CAIs.

References: [1] Grossman et al. (2008) *Reviews in Mineralogy* 68:83-140. [2] Keller and Buseck (1991) *Science* 252:946-949. [3] Krot et al. (1998b) *Meteoritics & Planetary Science* 33:1065-1085. [4] Krot et al. (2000) *Geochemistry International* 38:S351-S368. [5] El Goresy et al. (2002) *GCA* 66:1459-1491. [6] Aléon et al. (2018) *GCA* 232:48-81.

ASTEROID COOLING RATES FROM FELDSPAR EXSOLUTION TEXTURES IN THE H4 CHONDRITE AVANHANDAVA

J. A. Lewis[1] and R. H. Jones[2,3], [1]ARES, NASA JSC, Houston, TX 77058 (jonathan.lewis@nasa.gov), [2]School of Earth and Environmental Sciences, University of Manchester, Manchester, M13 9PL, UK, [3]Department of Earth and Planetary Sciences, University of New Mexico, Albuquerque, NM 87131.

Introduction: Thermal metamorphism in ordinary chondrites (OCs) is thought to occur through the radioactive decay of ^{26}Al in an onion-shell-like structure [e.g. 1]. However, cooling rates determined by pyroxene diffusion and metallographic methods are inconsistent with onion-shell-like cooling [2-3]. These inconsistencies have led to models of asteroid disruption and reaccretion into a rubble pile, after peak metamorphism [2-4]. To further examine these models, we can obtain cooling rates from observations of feldspar microstructures in OCs. In OCs, potassium-feldspar exsolution occurs in albite, in a perthite texture [5-6]. Here, we report cooling rates determined from feldspar exsolution textures in the H4 chondrite Avanhandava and compare these to cooling rates determined by other methods.

Methods: We examined a thin section of Avanhandava (UNM 88). BSE images were taken on an FEI Quanta FEG-SEM/FIB. Quantitative X-ray chemical analysis was performed using a JEOL 8200 EPMA. A TEM section was prepared using the focused ion beam on the FEG-SEM/FIB and imaged using a JEOL 2010F STEM using a HAADF detector for dark field images. Analytical work was carried out at UNM.

Results: Perthite was investigated in chondrule 6 (Fig. 1a). Broad-beam EPMA analysis of the perthite texture (Fig. 1b) yielded an average composition of $An_{2.5}Ab_{64.8}Or_{32.7}$ from which we estimate the solvus temperature to be 700-765 °C [7-8]. Assuming that exsolution occurred around this temperature, and given a measured exsolution wavelength of 650 nm (Fig. 1c), we determined a cooling rate of 1 °C per 1-4 months over a temperature interval of 765-670 °C. Peristerite is also present in the Na-rich lamellae (Fig. 1c) for which we estimate a cooling rate of 1 °C in 10^3-10^4 years from 570-540 °C.

Discussion: Feldspar cooling rates are plotted in Fig. 1d along with cooling rates determined by pyroxene diffusion and metallographic methods. In general, the relatively fast cooling rate determined by perthite is consistent with cooling rates determined by pyroxene diffusion at a similar high temperature [2]. The peristerite cooling rate is closer to the slow, lower temperature metallographic cooling rates [3]. These observations support a breakup and reassembly model [4] in which erosional bombardment causes fast cooling at high temperatures. Residual heat from breakup and reassembly results in the observed slow cooling rates at low temperatures.

References: [1] Pellas P. and Storzer D. (1981) *Proc. Roy. Soc. London. A.* 374, 253–270. [2] Ganguly J. et al. (2013) *GCA* 105, 206–220. [3] Scott E. R. D. et al. (2014) *GCA* 136, 13–37. [4] Blackburn T. et al. (2017) *GCA* 200, 201–217. [5] Jones R. H. and Brearley A. J. (2011) *74th MetSoc*, Abstract #5475. [6] Lewis J. A., Jones R. H., and Brearley A. J. (2016) *47th LPSC*, Abstract #2559. [7] Parsons I. and Lee M. R. (2009) *Contrib. Min. Pet.* 157, 641–661. [8] Elkins L. T. and Grove T. L. (1990) *Am. Min.* 75, 544–559.

Figure 1: Feldspar exsolution and cooling rates. (a) BSE image of chondrule 6 in which perthite (b) is present. Line in (b) indicates region from which TEM section was extracted: darker grey is albite and lighter grey is K-feldspar. (c) HAADF image of perthite with an average 650 nm wavelength and peristerite in the Na-rich lamellae. (d) Plot of cooling rates from feldspar, pyroxene diffusion [2], and metallographic methods [3].
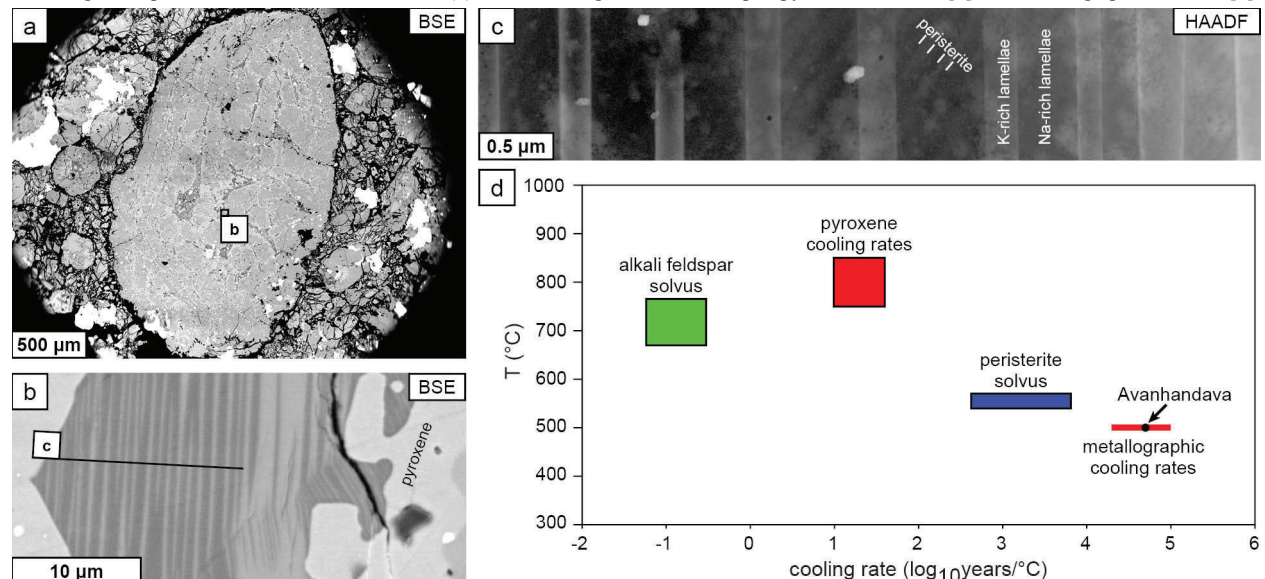
COSMIC-RAY EXPOSURE AGES OF SOME PRIMITIVE ACHONDRITES

S. Li[1], I. Leya[2], T. M. Smith[3], and H. He[3], [1]Center for Lunar and Planetary Sciences, Institute of Geochemistry, Chinese Academy of Sciences, Guiyang 550081, China, [2]Physikalisches Institut, Universität Bern, Switzerland, [3]State Key Laboratory of Lithospheric Evolution, Institute of Geology and Geophysics, Chinese Academy of Sciences, Beijing 100029, China.

Introduction: Acapulcoites and lodranites are two groups of primitive achondrites which are considered to originate from a common parent body [1,2]. The detailed mineralogical, chemical, and isotopic studies have revealed that the parent asteroid of acapulcoite-lodranite clan has a multilayered structure [3,4]. Up to now, only about 20 acapulcoite-lodranite clan members have been studied for cosmic-ray exposure (CRE) history investigations [3 and the references therein]. Previous studies indicated the CRE ages of acapulcoite-lodranite clan vary over a narrow range of ages from ~4 Ma to ~15 Ma and most of the reported ages fall between ~4 Ma to ~10 Ma [3, 5]. In order to further understand the parent body breakup history of the acapulcoite-lodranite clan, seven acapulcoite-lodranite meteorites (NWA 2871, NWA 4478, NWA 6484, NWA 6685, NWA 7474, NWA 8118, and NWA 11901) have been selected for CRE age measurement.

Experimental methods: The light noble gases (He, Ne, and Ar) were measured on two fragments with masses of 99.64 and 47.29 mg, respectivly. The isotopic concentrations of light noble gases have been measured by noble gas mass spectrometry at the University of Bern following standard procedures described in e.g. [6, 7]. The noble gases were extracted in one single temperature step at ~1700°C for 45 minutes. The extracted gases were further cleaned via various getters (SAES[®]) working in the temperature range between room temperature and 280°C. After cleaning, Ar was trapped on an activated charcoal held at the temperature of liquid N_2 and the remaining He and Ne fraction was further purified and inlet into a 90° sector field mass spectrometer. Smilarly, the Ar fraction was expanded into a self-made tandem mass spectrometer.

Results: Here we only report the CRE age of the lodranite NWA 8118. The CRE ages of other selected acapulcoite-lodranite clan meteorites will be reported during the conference. We calculated the production rates of ^{3}He and ^{21}Ne using the same formulas for L ordinary chondrites, which was reported in [8] and [9], respectively. In this study, we did not measure the bulk chemistry of NWA 8118;note that the concentration of target elements producing cosmogenic ^{38}Ar (i.e. Fe, Ca, K) in lodranites are much variable [3], therefore we decided to not calculate the ^{38}Ar CRE age (T_{38}) of NWA 8118. Regarding the 99.64 mg fragment of NWA 8118, the calculated ^{3}He CRE age (T_3) and ^{21}Ne CRE age (T_{21}) are 37.7±11.3 Ma and 39.4±11.8 Ma, respectively. For the 47.29 mg fragment, the calculated T_3 and T_{21} are 40.9±12.5 Ma and 39.6±12.2 Ma, respectively. The ages are in good agreement; the adopted CRE age of NWA 8118 is 39.4±11.9 Ma. The calculated CRE age is much longer than any reported CRE ages of acapulcoite-lodranite clan members [3 and the references therein].

Conclusions: The reported CRE age of NWA 8118 is a clear indication of a breakup event which happened on the acapulcoite-lodranite parent asteroid ~40 Ma ago. Based on the so far measured acapulcoites and lodranites, we can conclude that their members derived at least from three different breakup events (e.g., at 4-10, ~15, and ~40 Ma ago) on their parent body.

References: [1] Patzer, A. et al. (2004). *Meteoritics & Planetary Science* 39, 61-85. [2] Rubin, A. (2007). *Geochimica et Cosmochimia Acta* 71, 2383-2401. [3] Eugster, O. and Lorenzetti, S. (2005). *Geochimica et Cosmochimia Acta* 69:2675-2685. [4] Li, S. et al. (2018). *Geochimica et Cosmochimia Acta* 242:82-101. [5] Herzog, G. F. and Caffee, M. W. (2014) Cosmic-ray exposure ages of meteorites. In: Treatise on Geochemistry, Second Edition, Vol. 1 (Eds.: Holland H.D. and Turekian K.K.) Oxford: Elsevier. [6] Leya, I. (2013).*Meteoritics & Planetary Science* 48:1401-1414. [7] Li, S. et al. (2017). *Meteoritics & Planetary Science* 52:937-948. [8] Dalcher, N. et al. (2013). *Meteoritics & Planetary Science* 48:1841-1862. [9] Eugster, O. (1988). *Geochimica et Cosmochimia Acta* 52:1649-1662.

MINERALOGY AND IN SITU PB–PB DATING OF SILICATE INCLUSIONS IN MILES (IIE)

S.-L. Li[1,2] and W.-B. Hsu[2,3], [1]School of Astronomy and Space Sciences, Nanjing University, Nanjing, China. [2]CAS Center for Excellence in Comparative Planetology, Purple Mountain Observatory, Nanjing, China. Email: slli@pmo.ac.cn. [3]The State Key Laboratory of Lunar and Planetary Science, Macau University of Science and Technology, Taipa, Macau. Email: wbxu@pmo.ac.cn.

Introduction: IIE irons contain silicate inclusions that are chemically and isotopically related to H chondrites [1, 2]. These inclusions display an array of compositional and textural diversity, from "ultra-metamorphosed chondritic" to basaltic or more evolved andesitic to rhyolitic lithic fragments [1]. The Miles IIE iron contains a few U-bearing phases (armalcolite and phosphates) with different occurrences, providing opportunities to date the timing of igneous fractionation of silicates and dynamic mixing with metal. We conducted a thorough analysis of the mineralogy and in-situ Pb–Pb dating of silicate inclusions in Miles with the aim of better understanding of the complex thermal history experienced by the IIE parent body.

Results and Discussions: Silicate inclusions in Miles are mostly <1 cm and have irregular margins. Most of them contain pyroxene and plagioclase but their proportions vary considerably. Subhedral clinopyroxene commonly has a lamellar exsolution texture and usually shows intergrowths with orthopyroxene. The matrix consists of intergrowths of alkali feldspar (mainly antiperthite) and tridymite. Petrographic and mineralogical evidence indicates that Miles experienced a slow–rapid–slow cooling history. The first stage is indicated by the coarse-grained phenocrysts and lamellar textures in clinopyroxene. It was followed by a rapid cooling at temperature around silicate solidus, as indicated by the formation of thin-sliced antiperthite and the existence of glass in the gabbroic inclusions. The rapid cooling is also required for preventing the gravitational separation of metal and silicate [1, 2]. The last stage of slow cooling is implied by the coarse Widmanstätten pattern of host metal [2].

Euhedral or acicular apatite (< 150 μm) occurs in the silicate matrix whereas large irregular grains (up to 1.5 mm) are present at the boundary of host metal and inclusions (Fe–SI boundary). The euhedral apatite in the matrix is likely to have crystalized from a fractionated melt, which may be related to the impact that mixed the metal and silicates in Miles [3, 4]. The large irregular apatite grains, on the other hand, may have formed by subsolidus reduction processes during the mixing. Cr–Zr–Ca armalcolite also have two occurrences. One is commonly (partly) included in Pl and Py phenocrysts (< 150 μm), indicating crystallization as a liquidus phase. The other occurs at the Fe–SI boundary (> 200 μm), and these armalcolite may also be formed by subsolidus processes.

Armalcolite has a relatively high closure temperature (similar to baddeleyite) for the U–Pb system, which is estimated from its ionic porosity [5]. Therefore, the Pb–Pb age of armalcolite enclosed by Opx phenocryst could record the primary crystallization timing in the silicate protolith. In this study, only two sets of data were obtained, defining a range of 4564–4592 Ma. The euhedral apatites could have recorded the timing of the impact mixing that generated the IIEs, but their U–Pb system could have been reset during the subsequent subsolidus slow cooling due to their low closure temperature. The euhedral apatites yield a Pb–Pb "age" (4578 ± 24 Ma) indistinguishable from that of large irregular apatites (4561 ± 19 Ma) at the Fe–SI boundary. This indicates that the igneous fractionation of silicates and their dynamic mixing with metal were invoked very early, concurring with the solar system formation. These processes occurred contemporarily that could not be resolved by the current SIMS technique.

References: [1] Ruzicka A. (2014) *Chemie der Erde* 74: 3–48. [2] Wasson J. T. (2017) *Geochimica et Cosmochimica Acta* 197: 396–416. [3] Hsu W. (2003) *Geochimica et Cosmochimica Acta* 67: 4807–4821. [4] Takeda H. et al. (2003) *Geochimica et Cosmochimica Acta* 67: 2269–2287. [5] Dahl P. S. (1997) *Earth and Planetary Science Letters* 150: 277–290.

THE RELATIONSHIP BETWEEN SHOCK-INDUCED PHASE TRANSFORMATION AND ISOTOPIC RESETTING: INSIGHTS FROM PB ISOTOPIC SYSTEMATICS OF PHOSPHATES IN L CHONDRITES

S.-L. Li[1,2] and W.-B. Hsu[2,3], [1] School of Astronomy and Space Sciences, Nanjing University, Nanjing, China. [2]CAS Center for Excellence in Comparative Planetology, Purple Mountain Observatory, Nanjing, China. Email: slli@pmo.ac.cn. [3]The State Key Laboratory of Lunar and Planetary Science, Macau University of Science and Technology, Taipa, Macau. Email: wbxu@pmo.ac.cn.

Introduction: Isotope geochronology has become a preponderant tool for dating impact events and provides one of the most robust constraints on the impact history of solar system. However, the interpretation of isotopic data are not always straightforward, which was largely hampered by the lack of knowledge about how shock metamorphism affects isotopic systematics in individual minerals and in whole rocks. This is best illustrated by the considerable investigations and debates on the age of shergottite (>4.0 Ga versus <0.6 Ga) [e.g. 1–4], shocked lunar and terrestrial samples [e.g. 5–6]. The controversies for many meteorites in general, and for shergottites in particular, mainly resulted from the blurred relationship between isotopic disturbance and pervasive shock-induced melting as well as phase transformation [7]. In this study, the shock-induced phase transformation and Pb isotopic compositions of phosphates in two strongly shocked L6 chondrites (Suizhou and Sixiangkou) were investigated in order to clarify their relationships.

Results and Discussions: Merrillite grains in the host of Suizhou and Sixiangkou well preserved their crystal structure along with other silicate minerals. Raman spectra indicate that merrillite in the SMV of Suizhou has transformed to its high-pressure polymorph tuite, consistent with the P–T conditions (20–22 GPa and 1800–2000 °C) constrained by the high-pressure assemblage in the SMV [8]. The merrillite in the SMV of Sixiangkou, though experienced peak shock conditions of 20–24 GPa and 2000–2300 °C [9], have a low-pressure crystal structure. Because merrillite can be transformed to tuite at pressure as low as 2 GPa under 1000 °C [10], it is possible that merrillite in the SMV of Sixiangkou had been transformed to tuite during the peak shock but reverted to its original structure due to post-shock relatively "slow cooling". This is similar to the transformation scenario experienced by baddeleyite in shergottite, as suggested by El Goresy et al., (2013). They further suggested that phase transformations would result in a polycrystalline aggregate, which prompts resetting of radiogenic Pb via rapid grain boundary diffusion within this phase [4].

Pb compositions of phosphates experienced different extent of transformation in Suizhou show a considerable overlap. The merrillite in the host yields a Pb–Pb age of ~4550 Ma, consistent with our previous results on the undisturbed apatite [11]. The Pb–Pb "ages" of tuite in the SMV show a variation of 4560–4460 Ma. The upper limit is similar to the age of undisturbed phosphates in the host and the the lower limit is close to the "age" of the partially transformed apatite (4480 Ma) [11]. The merrillite in the host of Sixiangkou yields Pb–Pb "ages" similar to that of Suizhou, and those in the SMV of Sixiangkou show a wide variation (4560–4090 Ma). These "ages" are generally related to the position of analysis relative to the SMV, and are significantly older than the impact age of Sixiangkou (480 Ma) [12]. Therefore, the merrillite in the SMV of Sixiangkou seems to have largely retained original Pb compositions during the impact, although the merrillite was subjected to shock-induced phase transformation in the compression and back inversion in the decompression stage. The wide "age" ranges observed in phosphates from the SMV of both meteorites indicate that Pb isotopic resetting is far from achieved, and it is local thermal conditions rather than phase transformation that result in the isotopic disturbance.

Based on these observations, it can be concluded that phase transformation of merrillite during impacts does not necessarily result in Pb isotope resetting. Because the Pb diffusion in zircon and baddeleyite is much sluggish than that of merrillite, we suggest that these U-bearing phases could retain their original Pb compositions during the peak-shock P–T conditions experienced by the host meteorites, if only diffusion are considered.

References: [1] Borg et al. (2005) *Geochimica et Cosmochimica Acta* 69:5819–5830. [2] Bouvier et al. (2005) *Earth and Planetary Science Letters* 240: 221–233. [3] Bouvier et al. (2009) *Earth and Planetary Science Letters* 280: 285–295. [4] El Goresy et al. (2013) *Geochimica et Cosmochimica Acta* 101: 233–262. [5] Grange et al. (2013) *Geochimica et Cosmochimica Acta* 101: 112–132. [6] Moser et al. (2011) *Canadian Journal of Earth Sciences* 48: 117–139. [7] Bloch and Ganguly (2014) *Earth and Planetary Science Letters* 395: 173–183. [8] Xie et al. (2001) *European Journal of Mineralogy* 13: 1177–1190. [9] Chen et al. (1996) *Science* 271: 1570–1573. [10] Zhai et al. (2014) *Physics of the Earth and Planetary Interiors* 228: 144–149. [11] Li and Hsu (2018) *American Mineralogist* 103: 1789–1799. [12] Li and Hsu (2018) *Meteoritics & Planetary Science* 53: 2107–2122.

CALCIUM ISOTOPIC COMPOSITION OF SEVERAL CHONDRITES

X. Li[1], F. Liu[1], Y. L. Xue[1.2], J. T. Kang[3], Y. J. An[1] and Z. F. Zhang[1], [1]State Key Laboratory of Isotope Geochemistry, Guangzhou Institute of Geochemistry, Chinese Academy of Sciences, Guangzhou 510640, China, [2]School of Earth and Planetary Science, University of Chinese Academy of Sciences, Beijing 100049, China, [3]CAS Key Laboratory of Crust-Mantle Materials and Environments, School of Earth and Space Sciences, University of Science and Technology of China, Hefei 230026, China.

Introduction: Calcium is a typical refractory incompatible alkaline element, with a 50% condensation temperature at 1517°K[1]. Calcium isotopic compositions of chondrites could be very helpful to understand the earlier evolution processes of the Earth, the origin and evolution of solar system materials, the building blocks of planets and the heterogeneity of the proto-planetary disk (e.g. [2], [3], [4]). Chondrites investigated in previous studies include CM, CR, CI, CO, CV, H, L, LL, EH, EL etc. Generally, carbonaceous-chondrite groups displayed a relatively wider range than other groups (e.g. [3], [4], [5], [6], [7]), and variations in a single chrondrite could be bigger (e.g. Allende CV3). Obviously, this kind of variation directly reflected the heterogeneity in chondrite samples, and trigged debates in understanding the real isotopic signatures of calcium in chondrites. In this study, Murchison (CM2), Kainsaz (CO3.2), Allende (CV3), Vigarano (CV3), Leoville (CV3), LaPaz Icefield 03601 (H4) and Indarch (EH4) were selected to analyse their calcium isotopic compostions. Different from literature, we used a relatively bigger amount of samples (~0.5-2grams) and no pre-treatments were done after those samples were grounded. Note that the calcium isotopic compositions of Kainsaz, Leoville and LaPaz Icefield 03601 were probably not investigated and reported before.

Experiments: All the analyses were done in the State Key Laboratory of Isotope Geochemistry, Guangzhou Institute of Geochemistry, Chinese Academy of Sciences (GIG, CAS). Samples were grounded to 200 mesh and mixed well first. About 20–30 mg of the well-mixed powders were dissolved using a $HF-HNO_3$ (3:1) mixed acids following the procedure described in Zhu et al. (2016)[8]. The calcium concentrations were measured on an ICP-OES instrument. Calcium isotopes were measured on a Triton TIMS instrument, each sample was measured at least 3 times and precisions were given based on these repeated measurements. The long term precision of NIST 915a and seawater measured during the sample running period are all at ±0.12‰ leval.

Conclusions: Our data are consistent with or falls into the range of the previous published data. All 3 CV3 chondrites displayed a limited range of calcium isotopic compositions, maybe indicate that analyses based on bigger sample amounts might be more representative because sample heterogeneity in small scales could be weighted and erased. If this is true, the variations of calcium isotopic compositions in carbonaceous chondrite groups could be smaller than the observed values. However, the difference between carbonaceous and non-carbonaceous is still there due to their different origins. Compared with the data reported in documents, our data for Indarch didn't show a higher $\delta^{44/40}Ca$ value, maybe because the sample was not rinsed with water and solute (e.g. oldhamite CaS) which might have a lower $\delta^{44/40}Ca$ value were retained.

References: [1] Lodder K. (2003) *Astrophysical Journal* 591:1220-1247. [2] Huang et al., (2012) *Geochim. Cosmochim. Acta* 77: 252-265. [3] Simon J. L. and DePaolo D. J. *Earth Planet. Sci. Lett.* 289:457-466. [4] Valdes M.C. et al. (2014) *Earth Planet. Sci. Lett.* 394:135-145. [5] Huang S. and Jacobsen S.B. (2017) *Geochim. Cosmochim. Acta* 201:364-376. [6] Simon J. I. et al. (2017) *Earth Planet. Sci. Lett.* 472:277–288. [7] Amsellem M. et al. (2017) *Earth Planet. Sci. Lett.* 469:75–83. [8] Zhu et al. (2016) *Geostandards and Geoanalytical Research* 40:185-194.

U-PB ZIRCON AND APATITE CHRONOLOGY OF A QUARTZ-RICH BASALTIC EUCRITE AND CONSTRAINT ON THERMAL HISTORY OF THE VESTAN CRUST

S. Y. Liao[1] and W. B. Hsu[1,2,]
[1]CAS Center for Excellence in Comparative Planetology, Purple Mountain Observatory, Nanjing, China.E-mail: syliao@pmo.ac.cn, wbxu@pmo.ac.cn,[2]State key laboratory for lunar and planetary sciences, Macau University of Science and Technology, Macau.

Introduction: The ubiquitous thermal metamorphic features of HEDs have been studied for decades. The timing of thermal metamorphism could provide key informations for understanding the thermal history of eucrite and the mechanism of thermal metamorphism. However, it is difficult to discriminate the ages that record the primary metamorphism from those of secondary heating, because most of the ages determined on eucrites were made either on whole rocks or mineral separates and have no clear petrological contexts [1-5]. Isotopic and genetic studies of zircon provided constraint on the peak thermal metamorphic age [6-7], whereas the closure temperature of zircon U–Pb system (usually>900 °C) is generally beyond the thermal metamorphic temperatures of eucrites (700 to 1000°C). Evidence from isotopic systems with relatively low temperatures (i.e., apatite U–Pb, in situ Ar–Ar) are essential to cover the full range of metamorphic history of eucrites.

Results and Discussion: Northwest Africa (NWA) 6594 is an unbrecciated basaltic eucrite comprised of about 46 % pyroxene, 47% plagioclase, 6% silica, 1% opaque phases. Silica phases are mainly tridymite (~5%) and subordinate quartz (~1%). Such high abundance of quartz in HEDs has not been observed before. Silica phases in NWA 6594 are usually coexisting with apatite in mesostasis areas. The crystal structure of silica is very sensitive to both pressure and temperature [8-9]. Therefore it is useful to reconstruct the thermal history of apatite grains and to set crucial thermal constraints on the U–Pb system of apatites.

After detailed petrographic and mineralogical studies, we found that silica phases in NWA 6594 have two generations, corresponding to two major thermal pulses. The first generation includes primary quartz that crystallized slowly below 870°C during thermal metamorphism. The second generation is composed dominantly of monoclinic tridymite, which was formed by partial melting of quartz and minor other minerals induced by a later reheating event followed by a rapid cooling. This genetic sequence of quartz and tridymite in NWA 6594 is different from those proposed by previous authors, who suggested a crystallization of tridymite prior to quartz [10-11].

In situ U–Pb analyses were carried out on zircon and apatite. Twenty-four spots from seven zircons are concordant to nearly-concordant on the normal concordia diagram and yield almost identical $^{207}Pb/^{206}Pb$ ages, which have a weighted average of $^{207}Pb/^{206}Pb$ age of 4547±11 Ma (95% confidence, MSWD=1.3). This age could be interpreted as the crystallization age. As zircons in eucrite may have formed during global metamorphism [6-7], instead of solely crystallized during magmatism [12-14], the igneous age of the rock would thus not be latter than 4547±11 Ma.

Most Pb–Pb ages of apatite grains in NWA 6594 are identical within error. Eleven spots from seven apatites define a weighted mean $^{207}Pb/^{206}Pb$ age of 4523±2 Ma (95% confidence, MSWD=0.76), which is distinctly younger than the age of zircon (4547±11 Ma) beyond 2σ analytical uncertainties. Integrated petrographic and isotopic studies indicate that the younger Pb-Pb age of apatite could not be simply attributed to slow cooling after formation of NWA 6594. It is most likely due to an independent thermal event related to formation of quartz. The protracted time lag (~24±13Myr) between the two ages indicate that the later thermal metamorphism cannot be related to burial of successive lava, but is most likely induced by a reheating event of the Vestan crust that had a steep thermal gradient.

References: [1] Nyquist et al. 1986. *Journal of Geophysical Research: Solid Earth* 91: 8137–8150. [2] Tera et al. 1997. *Geochimica et Cosmochimica Acta* 61: 1713–1731. [3] Kleine et al. 2005. *Earth and Planetary Science Letters* 231: 41–52. [4] Bogardand Garrison, 2003. *Meteoritics & Planetary Science* 38: 669–710. [5] Kennedy et al. 2013. *Geochimica et Cosmochimica Acta* 115: 162–182. [6] Iizuka et al. 2015. *Earth and Planetary Science Letters* 409: 182–192. [7] Liao and Hsu, 2017. *Geochimica et Cosmochimica Acta* 204: 159–178. [8] Fenner, 1913. *American Journal of Science* 36: 331–384. [9] Heaney, 1994. *Reviews in Mineralogy and Geochemistry* 29: 1–40. [10] Hervig et al. 1986.*Meteoritics* 21: 395–396.[11] Yamaguchi et al. 2009. *Geochimica et Cosmochimica Acta* 73: 7162–7182. [12] Misawa et al., 2005. *Geochimica et Cosmochimica Acta* 69: 5847–5861. [13] Zhou et al. 2013. *Geochimica et Cosmochimica Acta* 110: 152–175. [14] Roszjar et al., 2014. *Earth and Planetary Science Letters* 452: 216–226.

GLOBAL PRESENCE OF SUBSURFACE GLACIER ON MARS EVIDENCED BY THE CORRELATION BETWEEN WATER CONTENTS AND HYDROGEN ISOTOPIC RATIOS OF MARTIAN METEORITES.

Yangting Lin[1*], Sen Hu[1], A. Yamaguchi[2], J. C. Zhang[1], J. L. Hao[1], and W. Yang[1]. [1]Key Laboratory of Earth and Planetary Physics, Institute of Geology and Geophysics, Chinese Academy of Sciences, 19 Beituchengxi rd., Beijing 100029, China. *LinYT@mail.iggcas.ac.cn. [2]National Institute of Polar Research, Tokyo 190-8518, Japan

Introduction: At present Mars is prevailed by frigid and dry climate. It is widely accepted that there was flowing water on the surface of Mar probably 3.7 Ga ago [1], based on the topography and the presence of phyllosilicates, sulfates and carbonates. The vanishing of surface water was partly attributed to sputtering escape of H_2O by the solar wind due to cessation of the internal dynamo action of Mars 4 Ga ago [2]. The escaping of water from Mars resulted in enhancing of D/H ratios in the remained water, which could be recorded in Martian meteorites [3]. Another fraction of water could be preserved as subsurface glacier [4] and mixed with carbon dioxide ice in the polar ice sheets. The subsurface glacier would be melted when basalt erupted, and the event could be recorded in the basalt via rock-water reaction. This scenario was revealed by high resolution topography [5] and evidenced by our previous study of the lherzolitic basalt GRV 020090 [6], which recorded the highest D-enrichment of Martian meteorites with $\delta D = 6034 \pm 72$ ‰ (2σ). We extended the measurements to more Martian meteorites, and the results argue for the global presence of subsurface glacier on Mars.

Sample and Experiments: Beside GRV 020090, other 5 shergottites NWA 8657, NWA 6162, Y 002192, Y 980459 and Tissint, have been studied in this work. The petrography and mineral chemistry of these Martian basalts were studied with an FE-SEM, an EPMA and laser Raman spectroscopy. Silicate melt inclusions in olivine, pyroxene and a few in chromite, apatite, maskelynite and shock melt glass were selected for analysis of water contents and H isotopes, which were carried out with NanoSIMS 50L. The NanoSIMS analyses were calibrated for the matrix effects, using the standards of apatite and basaltic glass.

Results and Discussions: The analyses of melt inclusions in all 6 Martian basalts GRV 020090, Tissint, NWA 6162, NWA 8657, Y 002192 and Y 980459 plot on the same two-endmember mixing line, with one reservoir representative of the δD-normal Martian mantle and the other for Martian underground water that was produced by melting of subsurface glacier due to eruption of basalt magma. The Martian underground water reservoir shows a rather narrow range of δD values (5200-6000 ‰). These observations argue for the global presence of subsurface glacier, and suggest that the transformation from flowing water on the surface to the subsurface glacier took place very fast. The δD values of the Martian subsurface glacier should have been fixed since the red planet became frigid. Beside those plotted on the two-endmember mixing line, some analyses of the melt inclusions in Y 002192 contain lower water contents with higher δD values, probably due to moderately degassing loss of water accompanying isotope exchange with the D-enriched molten subsurface glacier. The global presence of the D-enriched molten subsurface glacier was confirmed by the measurements on shock-induced melt veins and pockets in these meteorites, which plots on the same mixing line defined by the melt inclusions. In Y 980459, it was also noticed that the shock-induced glasses contain more water with higher δD values than the melt inclusions in the same meteorite, suggestive of addition of water mainly by impact. During impact events, water vapor could be released and mixed with the silicate melt.

References: [1] Ehlmann B. L., et al. 2011. *Nature* 479: 53-60. [2] Acuña M. H., et al. 1999. *Science* 284: 790. [3] Watson L. L., et al. 1994. *Science* 265: 86-90. [4] Holt J. W., et al. 2008. *Science* 322: 1235-1238. [5] Neukum G., et al. 2004. *Nature* 432: 971-979. [6] Hu S., et al. 2014. *Geochimica et Cosmochimica Acta* 140: 321-333.

MINERAL FINGERPRINTS OF THE POST-HYDRATION HEATING OF CM CARBONACEOUS CHONDRITES: IMPLICATIONS FOR UNDERSTANDING RYUGU AND BENNU.

P. Lindgren[1], L. J. Hallis[2], B. E. Cohen[2], R. D. Hanna[3] and A. J. King[4] and M. R. Lee[2], [1]Department of Geology, Lund University, Sölvegatan 12, 223 62 Lund, Sweden (paula.lindgren@geol.lu.se), [2]School of Geographical and Earth Sciences, University of Glasgow, Glasgow G12 8QQ, U.K., [3]University of Texas at Austin, TX, USA, [4]Department of Earth Sciences, Natural History Museum, Cromwell Road, London SW7 5BD, U.K.

Introduction: Recent results from Hayabusa2 and OSIRIS-Rex have shown that the surfaces of Ryugu and Bennu are spectroscopically analogous to carbonaceous chondrites that have undergone both aqueous alteration and heating [1,2]. In preparation for studying the returned samples it is therefore very important to understand the processes and products of heating of carbonaceous chondrites - either by characterising meteorites that have been naturally (i.e., pre-terrestrially) heated [e.g., 3] or by simulating heating in the laboratory [e.g., 4]. Here we have taken the latter approach because it enables pre- and post-heating samples to be compared so that the thermal evolution of various constituents can be tracked. We are especially interested in the behaviour of carbon-containing phases, namely organic matter and carbonates.

Meteorites and methods: We used the CM carbonaceous chondrite Allan Hills (ALH) 83100. It has been highly aqueously altered (classified as CM2.1 [5]) yet has escaped natural post-hydration heating [6]. Chips and powders were heated to 400 °C and 800 °C in a tube furnace under vacuum for 24 hours. The powder and chip both lost 9% of their original mass in the 400 °C experiment whereas heating to 800 °C resulted in mass losses of 18.4% and 19.0 % from the powder and chip, respectively. Polished thin sections were made from the unheated and heated chips for SEM work at the University of Glasgow, and the mineralogy of the unheated and heated powders was determined by X-ray diffraction (XRD) at the Natural History Museum.

Results and discussion: Here we focus on changes to the mineralogy of bulk samples, as determined by XRD, and on thermal alteration to carbonate mineral grains, as revealed by SEM. XRD patterns of the unheated sample are consistent with results from previous studies of highly altered CM chondrites [7, 8]. They contain sharp peaks from well ordered Fe-rich serpentines (e.g., cronstedtite) and broad reflections from finer grained, poorly crystalline intergrown Mg-serpentines. Olivine, enstatite, tochilinite, magnetite, calcite and pyrrhotite were also detected (Table 1). Patterns from the 400 °C sample are subtly different. Fe-rich serpentines produce only a single peak rather than the double feature often observed in the highly altered CM chondrites [8]. The Mg-serpentine reflection is smaller but there is no evidence of 'amorphous scattering' that would be consistent with the presence of a highly disordered, dehydrated phyllosilicate. Tochilinite is absent, while pentlandite and oldhamite occur, and the pyrrhotite peak is broader (Table 1). The 800 °C samples yield quite different XRD patterns, with peaks from olivine, enstatite, Fe-sulphides and metal (Table 1). The olivine and Fe-sulphide peaks are more intense and broader than the unheated and 400 °C sample, suggesting that these phases are fine-grained and/or poorly crystalline. There is also no "amorphous scattering", which would be expected from a highly disordered, dehydrated phyllosilicate phase.

Table 1. Modal mineralogy of the ALH 83100 samples determined by XRD (vol. %)

	Phyllosilicate	Olivine	Pyroxene	Magnetite	Fe-sulphide	Carbonate	Metal	Total
Unheated	82.8	5.8	3.3	4.1	2.1	2.0	----	100.1
400 °C	80.3	4.4	3.8	4.9	4.5	2.2	----	100.1
800 °C	----	88.1	4.2	----	7.6	----	0.1	100.0

SEM imaging shows that unheated ALH 83100 contains tens of micrometer size grains of calcite and dolomite. Both minerals appear to be unaltered in the 400 °C sample but are destroyed by 800 °C. In the place of calcite are ~1-3 μm size grains of a material containing S (~19 wt. %), Ca (~24 wt. %) and Fe (~42 wt. %). There is no mineral with this composition, but it is consistent with an intergrowth of oldhamite (CaS) with magnetite (Fe_3O_4). Although further work is needed for a definitive identification, the presence of oldhamite would agree with its occurence in the naturally heated Tagish Lake carbonaceous chondrite [9], and in samples of Murray (CM2) that have been experimentally heated to 800 °C [10].

References: [1] Kitazato K. et al. (2019) *Science* 364:272−275. [2] Hanna et al. (2019) *MetSoc 82*, Abstract. [3] Nakamura T. (2005) *J. Miner. Petrol. Sci.* 100:260–272 [4] Nakato A. et al. (2008) *Earth Planets. Space* 60:855−864. [5] de Leuw S. et al. (2010) *Meteoritics & Planetary Science* 45:513−530. [6] Alexander C. M. O'D. et al. (2013) *Geochmica et Cosmochimica Acta* 123:244−260. [7] Howard K. T. et al. (2015) *Geochmica et Cosmochimica Acta* 149:206−222. [8] King A. J. et al. (2017) *Meteoritics & Planetary Science* 52:1197−1215. [9] Haberle C. W. and Garvie L. (2017) *Am. Min.* 102:2415−2421. [10] Lee M. R. et al. (2019) *LPSC 50*, Abstract #1540.

U-Pb and Pb-Pb DATING OF THE APATITE FROM IAB IRON METEORITES.

K. D. Litasov[1], Y. Sano[2], N. Takahata[2], T. Miki[2], S. N. Teplyakova[3] and A. Y. Skripnik[3], [1]Sobolev Institute of Geology and Mineralogy SB RAS, 3 Koptyuga Ave, Novosibirsk, 630090, Russia (klitasov@igm.nsc.ru); [2]Atmosphere and Ocean Research Institute, University of Tokyo, Chiba, 277-8564, Japan; [3]Vernadsky Institute of Geochemistry and Analytical Chemistry RAS, 19 Kosygina St, Moscow, 119334, Russia.

Introduction: The IAB is a non-magmatic group of iron meteorites that has been classified into several sub-groups based on the trace element chemistry of metal. They include the main group (MG), multiple 'low-Au low-Ni' (sLL), 'low-Au medium Ni' (sLM), 'low-Au high-Ni' (sLH), sHL and SHH, and several grouplets and ungrouped samples [1]. The isotopic study indicates that high-Au sub-groups (sHL and sHH) may derive from a distinct parent body [2]. This is consistent with the appearance of silicate inclusions, which are mostly related to low-Au subgroups. The metal-silicate separation age was estimated at 6.0±0.8 Ma according to $\varepsilon^{182}W$ data [5], whereas catastrophic impact and re-assembly of parent body [3-4] appeared at 10-14 Ma after the formation of CAI [5]. Here we provide additional evidence for early formation of silicate-bearing IAB irons based on U-Pb dating of apatite from silicate-bearing inclusions.

Samples and Methods: The isotope ratios were measured in Copiapo (IAB-MG), NWA 6369 (sLL), Udei Station, Woodbine, Maslyanino (intermediate between sLL and sLM) and the anomalous meteorite Sombrerete. For all meteorites, from 3 to 10 grains of apatite or crystallized phosphate melt (Sombrerete) were studied. All samples were mounted into epoxy, polished, baked at ~100°C for 1-2 days and kept in the SIMS vessel at <5E-9 Torr for another 2-3 days before analyses. ^{238}U-^{206}Pb and ^{207}Pb-^{206}Pb datings were obtained on a NanoSIMS 50 instrument at the AORI, University of Tokyo. Apatite from the alkaline rocks (Ontario, Canada) aged 1155 ± 5 Ma was used as a standard. Other analytical methods were explained in the previous works [6].

Fig.1. Correlations between Pb/Pb ratios for apatites from IAB iron meteorites and Sombrerete. Solid lines are regressions constrained using IsoplotR [7]. Red – for all samples. Blue – without crossed samples.

Results and Discussion: All studied apatites have rather low concentrations of U = 0.5-2.0 ppm. This made it difficult to obtain data with minimal measurement error. The obtained data for all meteorites quite densely fall on the isochronous age 4563 ± 29 Ma. However, without taking into account several points that deviate from the narrow trend, the age is 4532 ± 24 Ma (Fig.1). The data for anomalous meteorite Sombrerete are consistent with the IAB isochron.

Comparison with the Hf-W data for iron metal meteorites of the IAB group [2] shows that the formation of silicates probably was not much broken in time with the formation of metal. Most of the data for metal intersect in the region of 3-6 million years [2,5] after the formation of CAI (4568 Ma).

The obtained data are consistent with estimations of the early event during the formation of IAB parent body (e.g., based on I-Xe chronology 4558-4563 Ma [8]) and is older than some Ar-Ar ages (~4320 Ma) [8], which may correspond to later metamorphism, when Pb-Pb system was not reset.

References: [1] Wasson J. and Kallemeyn G. (2002) *Geochim. Cosmochim. Acta* 66: 2445-2473. [2] Worsham E. A. et al. (2017) *Earth Planet. Sci. Lett.* 467: 157-166. [3] Benedix G. et al. (2000) *Met. Planet. Sci.* 35: 1127-1141. [4] Ruzicka A. (2014) *Chem. der Erde Geochem.* 74: 3-48. [5] Hunt A. C. et al. (2018) Earth Planet. Sci. Lett. 482: 490-500. [6] Koike M. et al. (2014) *Geochemical Journal* 48:423-431. [7] Vermeesch P. (2018) *Geosci. Front.* 9: 1479-1493. [8] Bogard D. D. et al. (2005) *Met. Planet. Sci.* 40: 207-224.
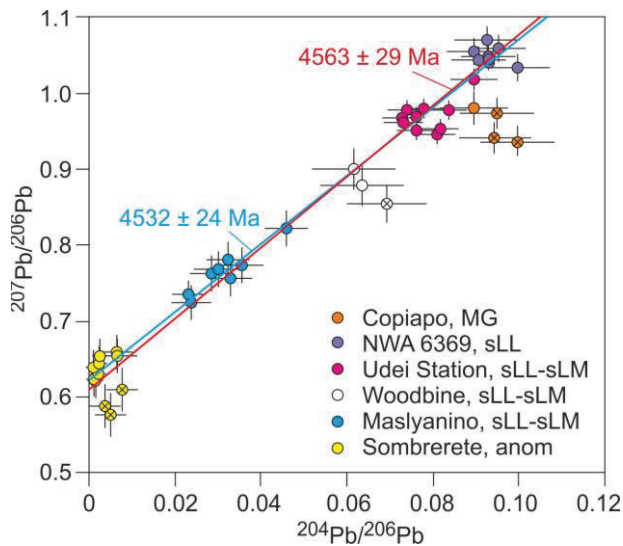
FE-NI-P-S MELT POCKETS IN ELGA IIE IRON METEORITE: EVIDENCE FOR THE ORIGIN AT HIGH PRESSURES UP TO 20 GPA.

K. D. Litasov[1,2] , S. N. Teplyakova[3], A. Shatskiy[1,2] and K. E. Kuper[4], [1]Sobolev Institute of Geology and Mineralogy SB RAS, 3 Koptyuga Ave, Novosibirsk, 630090, Russia (klitasov@igm.nsc.ru); [2]Novosibirsk State University, 2 Pirogova st, Novosibirsk 630090, Russia; [3]Vernadsky Institute of Geochemistry and Analytical Chemistry RAS, 19 Kosygina St, Moscow, 119334, Russia; [4]Budker Institute of Nuclear Physics SB RAS, 16 Lavrentieva Ave., Novosibirsk, 630090, Russia

Introduction: The shock-melt veins and high-pressure minerals are common in chondritic and rare in other types of meteorites including martian and lunar samples. Shock-induced deformations, melt pockets, and other microstructural features are also common for iron meteorites. However, there were only few finding of high-pressure minerals, including stishovite in IVA iron meteorite Muonionalusta [1], $(Fe,Ni)_2P$-allabogdanite in anomalous Ni-rich ataxites Onello, Santa Catharina and Barbianello [2-3] and tuite in IIE iron Elga [4]. Here we report new evidence for high-pressure microstructures in IIE iron Elga, made of Fe-Ni-P-S aggregates, which could be formed only at high pressures and temperatures according to the experimental phase diagrams. Elga represents IIE iron meteorite group, which contain 5-20% of silicate inclusions in the metallic matrix [4-5]. The metal part includes kamacite with rare taenite inclusions and abundant zones with plessite textures. Large rounded troilite and irregular schreibersite $(Fe,Ni)_3P$ inclusions are abundant. Rounded or irregular shape silicate inclusions can be divided into three major types: 1) silicate glass with abundant large Cr-diopside and minor small enstatite crystals; 2) silicate glass with tiny quenched crystals of enstatite, plagioclase and silica phases; 3) silicate/phosphate inclusions with liquid immiscibility. Major phases of silicate inclusions are Cr-diopside and enstatite, accessory minerals are represented by chromite, ilmenite, rutile, armalcolite, aenigmatite, and phosphate minerals. Solidified shock melt is represented by an immiscible fine-grained mixture of silicate-phosphate and metallic parts. The metal captured to shocked zone appears as Fe-Ni-P or Fe-Ni-P-S-bearing symplectite-like or cryptocrystalline melt pockets. Tuite was identified by Raman spectroscopy in shock-melted zones at the boundary of silicate inclusions [4].

Results: Various Fe-Ni-P-S melt pockets can be subdivided into the following types according to the bulk composition: (a) FN3 – corresponding to stoichiometric $(Fe,Ni)_3(P,S)$; (b) FN2 – corresponding to stoichiometric $(Fe,Ni)_2(P,S)$; (c) FN3-Ox – partially oxidized $(Fe,Ni)_3(P,S)$; (d) FN2-Ox – partially oxidized $(Fe,Ni)_2(P,S)$; (e) FNX – other compositions with the P and S contents deviating from stoichiometric proportions; and (f) FNX-Ox – partially oxidized $(Fe,Ni)_n(P,S)$. FN3 appears as micro- or nanocrystalline mixture of two or three phases at the boundary between schreibersite and troilite, where melt pockets can form zoned patterns with FN2 near troilite and intermediate compositions between FN2 and FN3. They can also form crystal-like aggregates surrounded by a partially oxidized quenched zone with the same composition. The composition of FN3 varies from $(Fe,Ni)_3P_{0.8}S_{0.2}$ to $(Fe,Ni)_3P_{0.4}S_{0.6}$. The EBSD data on nanocrystalline aggregates of FN3 and on single crystal-like areas of FN3 indicate the presence of a phase with $I\bar{4}$ space group. No troilite can be identified in such aggregates strongly indicating the presence of crystalline FN3 or nanocrystalline mixture with the FN3 composition. FN2 form micro- and nanocrystalline mixtures of dendritic crystals and appears near the boundary with troilite along with FN3 aggregates or as interstitial pockets in the non-stoichiometric FNX zones. Its composition varies from $(Fe,Ni)_2P_{0.5}S_{0.5}$ to $(Fe,Ni)_2P_{0.2}S_{0.8}$ and it is easy to identify troilite microcrystals by EBSD measurements.

Discussion: Fe_3P and Fe_3S are isostructural at high pressure and form a complete solid solution at P>20 GPa. This may indicate partial solubility of S in Fe_3P at lower pressures. Recently Gu et al. [6] calibrated the pressure dependence of S solubility in tetragonal Fe_3P and argued that it can be used as a pressure marker for natural Fe-Ni alloys containing P and S. We applied calibration of Gu et al. [6] to Elga aggregates and argued that most FN3 crystals and nanocrystalline aggregates correspond to the pressures of 10-20 GPa. The origin of FN2 is not clear at present. Gu et al. [6] reported that Fe_2P dissolves S at high pressures. However, quantitative data on the S solubility in Fe_2P as a function of pressure are not yet available. The close textural relations between FN3 and FN2 in Elga meteorite and the lack of stable sulfides with the Fe_2S stoichiometry in the studied pressure range indicate the possibility of the high-pressure origin of FN2. In this regards, the stoichiometric composition of these aggregates may not be accidental.

References: [1] Holtstam D. et al. (2003) *Met. Planet. Sci.* 38: 1579-1583. [2] Britvin S. N. et al. (2002) *Amer. Mineral.* 87: 1245-1249. [3] Britvin S. N. et al. (2019) *Sci. Rep.* 9: 1047. [4] Litasov K. D. and Podgornykh N. M. (2017) *J. Raman Spectr.* 48: 1518-1527. [5] Teplyakova S. N. et al. (2018) *Geochem. Int.* 56: 1-23. [6] Gu T. et al. (2016) *Amer. Mineral.* 101: 205-210.

ALUMINUM-26 CHRONOLOGY OF DUST COAGULATION AND EARLY SOLAR SYSTEM EVOLUTION.

M.-C. Liu[1], J. Han[2,3], A. J. Brearley[4] and A. T. Hertwig[1], [1]Department of Earth, Planetary and Space Sciences, UCLA (mcliu@ucla.edu), [2]Lunar and Planetary Institute, [3]NASA JSC, [4]Department of Earth and Planetary Sciences, University of New Mexico.

Introduction: The formation timescale of the first solids in the Sun's protoplanetary disk has been of major interest because it is the first step towards the formation of terrestrial planets. Our current understanding of the chronology of the formation of the first solids in the Solar System is largely based on the short-lived ^{26}Al–^{26}Mg systematics ($t_{1/2}$ = 0.72 Myr) in Ca-Al-rich Inclusions (CAIs) found in chondritic meteorites. It has been established by numerous high precision in-situ and bulk-inclusion studies that pristine, large (>5 mm) CAIs in CV3 chondrite are characterized by ^{26}Al/^{27}Al of 5.2 ($\pm$0.1)$\times 10^{-5}$, and the initial (pre-^{26}Al-decay) ^{26}Mg/^{24}Mg ratio ($\equiv \Delta^{26}$Mg$_0^*$) ranging from −0.13‰ to −0.014‰ relative to the chondritic value [REFs], implying a <30,000-year timescale for the formation of large CAIs in a reservoir with uniformly distributed ^{26}Al, but slightly heterogeneous initial ^{26}Mg/^{24}Mg [e.g., 1−5]. However, these cm-sized CAIs in CV3 chondrites are thought to have formed by melting and agglomeration of smaller particles (<10 μm) that condensed directly from the nebular gas. This fact calls into question how representative ^{26}Al/^{27}Al = 5.2 ($\pm$0.1)$\times 10^{-5}$ recorded by these large CAIs is of the true initial ^{26}Al abundance and distribution in the protoplanetary disk. Here we focus on the ^{26}Al–^{26}Mg isotopes of small refractory inclusions (mostly 30-50 μm in size) in the ALHA77307 CO3.0 chondrite, which are best understood as products of initial coagulation of high-temperature dust condensates, in the hopes of evaluating the ^{26}Al/^{27}Al distribution during the condensation period and then inferring the chronologies of these small inclusions relative to those of the large CAIs in CV3 chondrites that have been the focus of many studies.

Experimental: The 22 CAIs studied here were discovered in situ on a polished thin section of ALHA77307 (CO3.0) by using a FEI field-emission scanning electron microscope. In-situ ^{26}Al–^{26}Mg isotope analyses were performed on the CAMECA ims-1290 ion microprobe at UCLA by following a method described in [6]. The target inclusions on the polished meteorite thin section were bombarded with a 1−8 nA ^{16}O$^-$ primary ion beam (φ ~ 1.5−4 μm) generated by a Hyperion-II oxygen ion source, yielding Mg and Al secondary ion signals intense enough to be simultaneously measured with multiple Faraday cups (FCs).

Results and discussion: Of 22 CAIs studied, 18 were found to have fossil records of ^{26}Al decay. The inferred ^{26}Al/^{27}Al ratios span a range from 8 ($\pm$16.5)$\times 10^{-6}$ to 5.73 ($\pm$1.20)$\times 10^{-5}$ (2σ errors). Five CAIs are characterized by ^{26}Al/^{27}Al = 5.2$\times 10^{-5}$ within errors (reduced χ^2 < 2), and together yield a multi-CAI isochron with a slope corresponding to ^{26}Al/^{27}Al = 5.40($\pm$0.13)$\times 10^{-5}$ and an intercept of (−0.14$\pm$0.03)‰ as the initial Δ^{26}Mg$_0^*$ (reduced χ^2 = 1.1). Another 6 samples also form a well-defined multi-CAI isochron (reduced χ^2 = 4.3), from which ^{26}Al/^{27}Al = 4.89($\pm$0.10)$\times 10^{-5}$ and Δ^{26}Mg$_0^*$ = (−0.04$\pm$0.03)‰ can be inferred. The rest of the ^{26}Al-bearing inclusions are found to have lower, yet nonzero, ^{26}Al/^{27}Al ratios and more positive Δ^{26}Mg$_0^*$ compared to those in the aforementioned two main populations. Such an ^{26}Al/^{27}Al−Δ^{26}Mg$_0^*$ relationship can be best understood in the context of post-formation thermal processing, similar to that suggested to account for the ^{26}Al/^{27}Al differences between pristine (unmelted) and thermally reprocessed (igneous) CV3 CAIs [e.g., 5]. In this context, inclusions having ^{26}Al/^{27}Al = 5.4$\times 10^{-5}$ and Δ^{26}Mg$_0^*$ = −0.14‰ could be considered the most pristine among those analyzed here and should most faithfully record the isotopic signatures of their formation region. A major thermal event appears to have occurred to reset the majority of inclusions when ^{26}Al/^{27}Al = 4.9$\times 10^{-5}$, i.e., ~10^5 years after initial formation. It is worth noting that ^{26}Al/^{27}Al = 4.9$\times 10^{-5}$ has been registered not only by the CO3 inclusions, but also by many CM2 and CV3 CAIs [2,5,7–8], implying that such thermal processing was widespread in the regions where refractory inclusions resided or formed.

The ^{26}Al/^{27}Al = 5.40 ($\pm$0.13)$\times 10^{-5}$ ratio inferred from multiple small CAIs also suggests <50,000 years (deduced from the error of ^{26}Al/^{27}Al, which corresponds to ±25,000 years) for the formation of refractory inclusions several tens of μm in size by accretion of μm-sized dust. Centimeter-sized CAIs would have started to emerge during the late period of this coagulation stage and formed in abundance ~40,000 years after the majority of 30−100 μm-sized inclusions appeared in the nebula. This timescale is consistent with that predicted by a recent astrophysical model, which couples CAI formation to the physics of material infall and disk building [9].

References: [1] Jacobsen B. et al. (2008) *Earth Planetary Sciences Letters* 272:353–364. [2] MacPherson G. J. et al. 2010. *The Astrophysical Journal* 711:L117–L121. [3] Larsen K. K. (2011) *The Astrophysical Journal*, 735:L37–L43. [4] Wasserburg G. J. et al. (2012) *Meteoritics and Planetary Sciences*, 47:1980–1997. [5] MacPherson G. J. et al. 2017. *Geochimica et Cosmochimica Acta* 201:65–82. [6] Liu M.-C. et al. (2018) *International Journal Mass Spectrometry* 424: 1–9. [7] Liu M.-C. et al. (2012) *Earth Planetary Sciences Letters* 327: 75–83. [8] Kööp et al. (2016) *Geochimica et Cosmochimica Acta* 184:151–172. [9] Pignatale F. C. et al. (2018) *The Astrophysical Journal Letters* 867:L23.

NanoSIMS Isotopic Imaging of Volatile-rich Clasts from Achondritic Kapoeta Meteorite.

N. Liu[1], R. C. Ogliore[1], [1]Washington University in St. Louis, St. Louis, MO, 63130, USA (nliu@physics.wustl.edu).

Introduction: Volatile-rich carbonaceous chondrite xenoliths (C-rich clasts), mainly composed of fine-grained material, have been commonly found in various groups of meteorites, reflecting vigorous collisional and mixing processes occurring in the early solar system [1]. It is, however, still unclear whether these C-rich clasts share the same parent bodies with carbonaceous chondrites and how and when they were added into the parent bodies of their current hosts. To better understand the origin of C-rich clasts and their linkage to carbonaceous chondrites, we identified 13 C-rich clasts (50−100 μm in size) in the howardite Kapoeta meteorite and acquired C, N, O, and H isotope images with NanoSIMS (reported previously [2,3]). Our NanoSIMS scanning ion images revealed the existence of presolar grains and isotopically anomalous organic matter (OM) in the these carbonaceous xenoliths. The abundances and isotopic compositions of the identified presolar grains and OM further confirm their linkage to CI- and CM-like materials as suggested by previous petrologic studies [1].
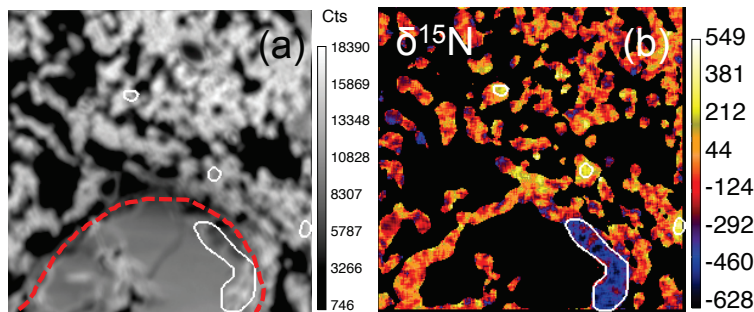

Fig. 1. SE (left) and NanoSIMS N isotope (right) images of one 10×10 μm area in clast 024-011.

Results: We identified two C-poor, N-rich particles with $^{14}N/^{15}N$ ratios (439 ± 8 and 424 ± 19, 1σ error) similar to the Sun's N isotopic composition (440 ± 5) [4]. While one of the ^{15}N-poor particles sits along the rim of an iron sulfide grain, the other particle sits along a ~5 μm magnetite grain (highlighted by the red dashed line in Fig. 1). In comparison to the surrounding micron-sized OM particles with normal and ^{15}N-rich compositions (highlighted by white circles in Fig. 1), the ^{15}N-poor region in Fig. 1 shows much lowered C contents. The enhanced $^{14}N/^{15}N$ isotope and lowered C/N elemental ratios are statistically significant according to the corresponding absolute σ plots. Both particles had normal C isotope ratios. To our knowledge, such association of isotopically anomalous N-rich phases with host minerals has never been found in any of the primitive carbonaceous chondrites, which could hint at the different formation environments of C-rich clasts with respect to carbonaceous chondrites.

Discussion & Conclusions: Previous studies showed that insoluble OM particles in primitive meteorites exhibit a wide range of N isotope ratios varying from the Sun's composition to large ^{15}N enrichments, e.g., [5,6]. In addition, it has been proposed that meteoritic insoluble OM could have been formed in the early solar system by Fischer–Tropsch reaction, during which Fe-rich minerals can act as catalysts [7]. Thus, if the two particles are organic, the Fischer-Tropsch reaction could provide an explanation to the association of these two particles with Fe-rich minerals and their N isotope ratios. Both particles, however, show C/CN ratios an order of magnitude lower than those of the surrounding OM particles. Because the formation of CN molecules requires the presence of both C and N, the inferred C/N ratios for these two particles based on C/CN are likely upper limits because of their low C contents. Therefore, it seems very unlikely that these two particles are organic. On the other hand, if they are inorganic, their ^{15}N-poor isotopic signatures seem to be quite puzzling. This is because in primitive meteorites such ^{15}N-poor isotopic signatures have only been observed in osbornite (TiN) in CAIs [9] other than insoluble OMs. In contrast, meteoritic magnetite and some of the iron sulfides are known to have formed by aqueous alteration on meteorite parent bodies [8]. Therefore, if the association of the two particles with their host minerals is not a coincidence, they are likely to have formed as a result of aqueous processing of the host minerals. Thus, it remains a puzzle how these particles preserved the protosolar N isotopic signature while forming on the rim of aqueously formed mineral phases. We will carry out Auger nanoprobe and TEM analyses to characterize the compositions of the two particles to better understand their correlated morphological and isotopic signatures, which could yield important information on the evolution of N isotope ratios in the early Solar System.

References: [1] Gounelle M. et al. (2003) *Geochimica et Cosmochimica Acta* 67:507–527. [2] Liu N. and Ogliore R.C. (2018) *MAPS 81*, Abstract #6151. [3] Liu N. and Ogliore R.C. (2019) *LPS L*, Abstract #2778. [4] Marty B. et al. (2011) *Science* 332, 1533– 1536. [5] Busemann H. et al. (2019) *Science*, 312:727–730. [6] Nittler L.R. et al. (2018) *Geochimica et Cosmochimica Acta* 226: 107−131. [7] Hill H.G.M. and Nuth J.A. (2003) *Astrobiology*, 3:291−304. [8] Kerridge J.F. et al. (1979) *Science*, 205: 395−397. [9] Meibom A. et al. (2007) *Astrophysical Journal Letters*, 656: L33−L36.

Isotopic and Elemental Analyses of Meteorites and Mars Analogues by Hyperion-NanoSIMS.

N. Liu[1], R. C. Ogliore[1], L. R. Nittler[2], N. X. Nie[3], N. Dauphas[3], [1]Washington University in St. Louis, St. Louis, MO, USA (nliu@physics.wustl.edu), [2]DTM, Carnegie Institution of Washington, Washington, DC, USA, [3]The University of Chicago, Chicago, IL, USA.

Introduction: NanoSIMS isotope imaging has been demonstrated to be especially powerful in characterizing meteoritic components, interplanetary dust particles, and cometary particles with high sensitivity and high spatial resolution. While NanoSIMS can achieve a primary beam spot size of ~50−100 nm with the primary Cs^+ ion source, the spatial resolution is compromised in the negative mode (by a factor of several) when using the Duoplasmatron (DP) ion source, which limits our ability to investigate certain isotope systems requiring positive secondary ions at very high spatial resolution. This problem has been recently addressed by the development of a new radio-frequency plasma oxygen ion source (Hyperion-II), which produces a much higher primary beam current (~150 nA) with <~1% variation over the course of one day and with reduced spot size. Here we present some recent studies on presolar grains, meteoritic carbonates, and Mars analogues with the Hyperion-II source on the NanoSIMS.
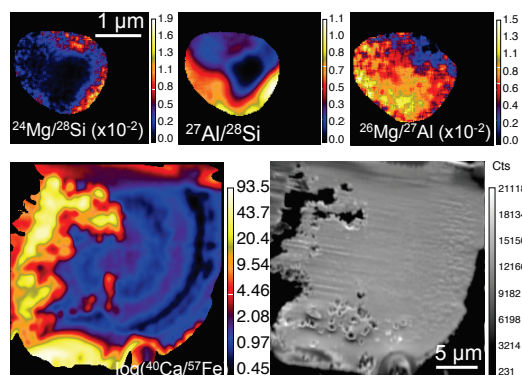

Fig. 1. *Upper panel*: Ratio images of a presolar mainstream SiC grain 1.5 μm in size. *Lower panel*: $\log_{10}(Ca/Fe)$ atomic ratio (left) and SE (right) images of a hematite spherule of 25 μm in size from Mauna Kea volcano, Hawaii (RSF is not corrected).

Presolar SiC: Mainstream (MS) SiC grains originated from low-mass asymptotic giant branch (AGB) stars. AGB stars produce ^{26}Al ($t_{1/2}$=0.72 Myr) during shell H- and He-burning and by neutron capture, and determining $^{26}Al/^{27}Al$ ratios in MS grains can thus yield valuable information on nucleosynthesis in AGB stars. However, the literature $^{26}Al/^{27}Al$ data might have suffered from Al contamination due to the poor spatial resolution of the DP source and mainly represent lower limits [1]. We reinvestigated the Mg-Al isotope ratios of 30 MS grains with the Hyperion-NanoSIMS 50L at Carnegie. The improved spatial resolution reveals heterogeneous distributions of ^{24}Mg, ^{26}Mg, and ^{27}Al within a single SiC grain. Figure 1 shows that the upper right part of this grain has lowered $^{26}Mg/^{27}Al$ ratios that are accompanied by increased Mg contents, likely pointing to Mg, Al-contamination. We reduced the data by carefully examining the isotope images, and the inferred initial $^{26}Mg/^{27}Al$ ratios range from 5×10^{-4} to 2×10^{-3} with a mean of 9×10^{-4}, which are higher than the literature data [2] by about a factor of two on average and are more consistent with recent AGB models [3].

Meteoritic Carbonates: ^{53}Mn-^{53}Cr ($t_{1/2}$=3.7 Myr) radiometric dating has been widely applied to constraining the timing of aqueous processes in the early solar system, e.g., [4, 5]. Most of previous analyses were carried out on Cameca IMS ion probes with a primary beam size of ~5 μm in spot-analysis mode, which limited our capability of studying smaller samples or sampling variable Mn/Cr ratios. We recently developed an analytical protocol to measure Mn-Cr isotopes with the Hyperion-NanoSIMS 50 instrument at WashU with a primary beam of ~150 nm in size (10 pA). Our first results for carbonates from Renazzo CR2 meteorite were reported in [6]. We found large variations in the Mn/Cr ratio within single carbonate grains of 10−100 μm in size. We collected isotope data in imaging mode in order to better sample the large variations in Mn/Cr seen across a single grain. As a result, we were able to reproduce the isochron slope and uncertainty for Renazzo reported in [4] by analyzing only one of their seven dolomites. This greatly reduces the required amount of samples for ^{53}Mn-^{53}Cr dating and is essential for analyzing micrometeorites and mission-returned samples in the future.

Mars Analogue: Hematite spherules from Mauna Kea volcano, Hawaii, which are formed by aqueous precipitation under acid-sulfate conditions, show mineralogical and morphological similarities with hematite spherules (blueberries) observed in sulfate-rich outcrops at Meridiani Planum on Mars [7]. To understand the formation process of hematite spherules, we imaged three MK spherules of 10−30 μm in size for their C, Mg, Al, S, Cl, K, Ca, V, Mn, Ni elemental abundances with the NanoSIMS 50 at WashU. We, for the first time, observed oscillatory zonings in many of the elements within each spherule, likely reflecting cyclic variations in the fluid composition during the growth of the spherules. These measurements have important implications to the formation of Martian blueberries.

References: [1] Groopman E. et al. (2015) *The Astrophysical Journal* 90:1151–1154. [2] Zinner E. (2014) *Presolar Grains in Treatise on Geochemistry* 1:181–210. [3] Liu N. et al. (2018) *The Astrophysical Journal* 865: 112 (14pp). [4] Jilly-Rehak C.E. (2018) *Geochimica et Cosmochimica Acta* 222, 230– 252. [5] Matzel J.E.P. *LPS XLV*, Abstract #1645. [6] Ogliore R C. et al. (2019) *LPS L*, Abstract #2778. [7] Morris R. V. et al. (2005) *Earth and Planetary Science Letters* 240: 168−178.

The Tl content and Tl isotope composition constraints on the magnitude of late-accretion of Earth and meteorite type

Y. Liu[1] and T. Fang[1], [1]Institute of Geochemistry, Chinese Academy of Sciences, Guiyang, 550081, China
(Liuyun@vip.gyig.ac.cn)

Introduction: The contents of highly siderophile elements (HSEs) of mantle were used to estimate how much materials were delivered during the late accretion period (Day et al. 2007; Walker 2014). By using the average Tl concentration of 500 ng/g for the continental crust, 200 ng/g for the oceanic crust and 0.7 ng/g for the mantle, the content of Tl in bulk silicate Earth (BSE) has been estimated to be about 3.03 ng/g (Shaw 1952; McDonough and Sun 1995; Salters and Stracke 2004; Nielsen et al. 2006c; Nielsen et al. 2014). Because Tl is a highly volatile element and its abundance is extememly low (less than 0.02 ng/g) in magmatic iron meteorites (Andreasen 2012), we can assume that most of the Tl would be volatilized and lost during the accretion of proto-Earth. The low Tl concentration of current BSE can be assumed that it was almost entirely delrivered by the late veneer.

There are very similar Tl isotopic compositions between BSE and chondrites (Baker et al. 2010; Palk et al. 2018) (see Fig. 1). We also checked the possible Tl isotope fractionations, especially with the inclusion of the nuclear volume effect, during core-mantle differentiation and vaporization. We find that vaporization can significantly change the Tl isotope composition of BSE, but no observed signal of it at all. The core segregation, however, may slightly lower the Tl isotope composition of BSE.

If BSE's Tl was delivered by the late-accretion, considering the similar contents of the Tl of enstatite chondrites (EC) and carbonaceous chondrites (CC) (Baker et al. 2010; Palk et al. 2011; Palk et al. 2018) (Fig. 1), we use the an average value (50 ng/g) of to represent EC and CC with 60 ng/g. Meanwhile, the average concentration of Tl in ordinary chondrites (OC) is 6 ng/g (Andreasen et al. 2009). We can set x as the fraction of material from CC and EC added delivered in the early mantlelate veneer stage relative to the total mass of the Earth, and the fraction of OC is y. If we assume that the material of late-stage accretion had constituted the entire Tl concentration of BSE, which was defined as nBSE (ng/g), then $60x + 6y = nBSE$ and $nBSE = 3.03 \times 67.4\% = 2.04$ (ng/g). It turns out that needs more chondritic materials, especially CC and EC to satisfied the above equation. Therefore, the amount of 0.5 wt.% late veneer estimated by HSEs is not enough to explain the Tl content in BSE. It needs at least 5 more times of materials.
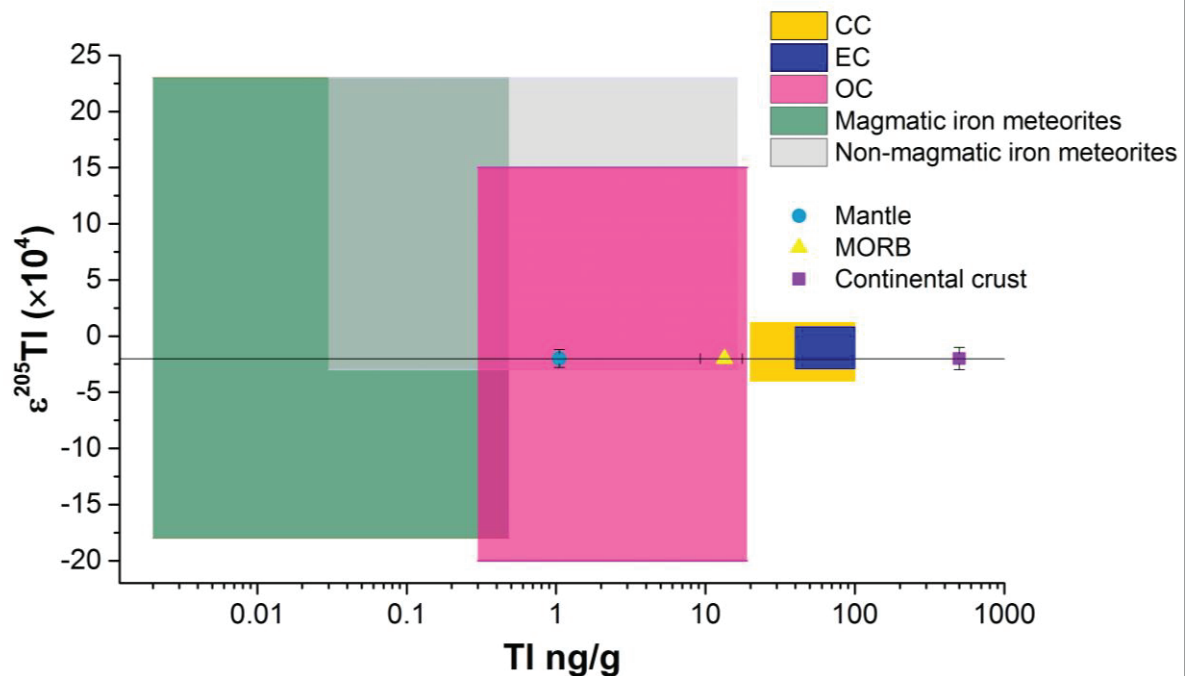

Figure 1

MOST SHERGOTTITES WERE ONCE VESICULAR: EVIDENCE FROM 3D COMPUTED X-RAY TOMOGRAPHY

Y. Liu[1], S. A. Eckley[2], and E. H. Blumenfeld[3,4], [1]Jet Propulsion Laboratory, California Institute of Technology, Pasadena, CA 91109, USA (yang.liu@jpl.nasa.gov). [2]Jackson School of Geosciences, University of Texas at Austin, Austin, TX 78712 (seckley@utexas.edu). [3]Transdiscplinary Artist (www.erikablumenfeld.com) 4LZ Technology-JETS contract, NASA JSC, Houston, TX 77058 (erika.h.blumenfeld@nasa.gov).

Introduction: Shergottites are commonly regarded to be dense rocks without vesicles. However, this view is changing for shergottites containing abundant impact melt pocekts [1-2]. Impact melt pockets are rounded to irregular regions of shock-generated melts that are common in shergottites (e.g., [3-6]). Shock experiments and modeling demonstrated that impact melts form readily under moderate shock conditions in powder or vesicle-bearing rocks, easier than those in relatively denser rocks under the same shock conditions (e.g., [7-10]). Most previous observations were confined to 2D observations, but the unique 3D perspectives gained by using X-ray computed tomography reveal the relationship between residual vesicles, fractures and host rocks [2]. Built upon previous reports of 3D tomography of Tissint, here we present the reconstructed 3D texture of Tissint and additional 3D CT results of other shergottites.

Results: Several interesting features were reported in [2] for Tissint, which are also present in at least two other shergottites. Melt pockets with a diameter >140 μm are randomly distributed and rounded without connecting melt veins inbetween. All impact melt pockets contain irregular shaped voids in the middle of the glass regions. All pockets are associated with clusters of fractures. Moreover, larger pockets are associated with ring fractures in the rock matrix, which follow the contour of the pockets. For the largest pocket, there are two layers of ring fractures. Additionally, minerals inside the ring fractures are stretched with a preferred orientation converging to the melt pockets.

We used a semi-automated segmentation method to emphasize the fractures and vesicles, and generated the 3D internal view between these two features.

Discussion: Similar to previous report in [2], the irregular voids in the interior of every pocket are likely residual pore space from incomplete collapse of pre-impact vesicles. They differ from spherical ones that are typical from volatile outgassing. Moreover, profile analysis of volatiles near these voids was inconsistent with outgassing [6]. Residual vesicles are also reported in other shergottites in 2D observations (e.g., [3,4]). Thus, impact melt pockets of >140 μm diameters in shergottites represent locations of pre-impact vesicles. A further *implication is that pre-impact rocks for the impact-melt-pocket-bearing shergottites were likely crystallized from volatile-rich melts.*

It has been demonstrated that impact melt pockets are enriched in volatiles compared to the surrounding rocks (e.g., [1, 6, 11-12]). The volatile source for enriched H, F, and Cl is most likely related to subsurface fluids (alteration or vaporied subsurface ice or salts carried by subsurface source). Considering shergottites were delivered from >1 m depth, *impact melt pockets in shergottites provide the best, if not only, means to study the surface or subsurface fluids at different times and locations, before we can collect, analyze, or return subsurface samples from Mars.*

References: [1] Liu, Y. et al. (2018) *EPSL.*, *490*, 206-215. [2] Liu, Y. (2019) 50th LPSC, #1767, [3] Walton, E. L. & Spray, J. G. (2003) *MAPS, 38*, 1865-1875. [4] Walton, E. L. & Shaw, C. S. J. (2009) *MAPS*, *44*, 55-76. [5] Shaw, C. S. J. & Walton, E. (2013) *MAPS*, *48*, 758-770. [6] Chen, Y. et al. (2015) *EPSL, 425*, 55-63. [7] Schaal, R. B. et al. (1979) *LPSC X*, 2547-2571. [8] Hörz, F. & Cintala, M. (1997) *MAPS*, *32*, 179-209. [9] Beck, P. et al. (2007) *GRK.*, *3*. [10] Chen, Y. et al. (2016). *LPSC* 47th, #1777. [11] Bogard, D. D. & Johnson, P. (1983) *Science*, *221*, 651-654. [12] Rao, M. N. et al. (2018) *MAPS*.

TEXTURALLY ZONED SILICON-BEARING IRON-NICKEL METAL INCLUSIONS IN THE LUNAR FELDSPATHIC REGOLITH BRECCIA NORTHWEST AFRICA 11303.

N. G. Lunning and J. Gross, The State University of New Jersey, Department of Earth and Planetary Sciences, 610 Taylor Road, Piscataway, NJ 08854-8066 USA

Introduction: Metal grains in lunar regolith provide records of space weathering and meteoroid bombardment, which contribute to our understanding of the evolution of the Moon's surface. Most of the mass of metal in lunar regolith formed by deposition of Fe-metal from micrometeorite impact induced vaporization of lunar target materials and subsequent reduction [e.g., 1]. The Fe-metal formed by space weathering associated with micrometeorite bombardment are commonly very small Fe^0 (most < 10 nm), referred to as $npFe^0$ [e.g., 1]. In rare instances, larger metal grains formed by this space weathering process have been found, such as the discovery of a ~35 μm metal grain of hapkeite (FeSi with 3.1 wt.% Ni) and associated other Fe-silicides in Dhofar 280 by [2].

Lunar regolith also commonly includes FeNi-metal that was added to the lunar surface by chondrite, pallasite and/or iron meteoroids [e.g., 3-4]. These exogenic additions are distinguished by Co and Ni concentrations consistent with metal in most asteroidal meteorites. The exogenic metals previously described in lunar regolith are silicon-poor (< 0.05 wt.% Si), if Si was included in the metal analyses [4]. In this work, we investigate metals in Northwest Africa (NWA) 11303, and particularly focus on two metal inclusions that are chemically distinct from previously described metals in lunar regolith.

Materials and Methods: We have investigated three polished thick sections of NWA 11303 that are part of the research collection of JG at Rutgers University (RU). NWA 11303 is part of the a pairing group of at least 19 lunar feldspathetic breccias with 12.9 kg cumulate mass, which NWA 8046 was the first classified member [5-6]. We have obtained quantitative and qualitative geochemical data on a selection of metal grains (> 5 μm) in NWA 11303 with the JEOL JXA-8200 Superprobe (EMP) at RU.

Results: Two round metal inclusions in NWA 11303 are concentrically zoned with smooth central interiors and polygonally-fractured exterior zones. These inclusions do not appear to be inside of larger clasts or melt units; they respectively have diameters of ~500 μm and ~30 μm. Both grains are dominated by FeNi metal with compositions consistent with an exogenic provenance [e.g., 3-4] based on averages of 5.9 and 9.0 wt. % Ni and 0.29 and 0.34 wt. % Co. There are no zoning trends with respect to Ni, Co, or P in either of these inclusions. This FeNi metal in both zoned inclusions is Si-bearing metal, with averages of 1.3 and 1.2 wt. % Si. In contrast, all other (non-concentrically zoned) metal grains in NWA 11303 analyzed by EMP in this study are effectively Si-free, but also have Ni and Co have concentrations consistent with exogenic provenances. The larger of these concentrically zoned metal inclusions contains sulfide grains that vary between the two zones: the smooth central interior has Cr-bearing sulfides (1.3-15.0 wt.% Cr), whereas in contrast, the polygonally-fractured exterior zoned has typical troilite (0.23-0.35 wt. % Cr).

Discussion: These are the first reported Si-bearing metals with Ni and Co concentrations consistent with exogenic provances found in a lunar sample. There are two potential mechanisms for the formation of these inclusions: (1) These Si-bearing metals formed by space weathering of exogenic material on the lunar surface. The Ni concentrations in the hapkeite-bearing inclusion previously found in Dhofar 280 are not high enough to be considered exogenic, but the Ni concentrations was high enough that [2] proposed there was some exogenic contribution in their precursor regolith. However, lunar space weathering has not been recognized to form sulfides akin to widely occurring $npFe^0$ [e.g., 1,7], with the caveat that np(Fe,Mg)S have been recognized in Itokawa regolith [e.g., 8]. (2) These Si-bearing metals originated from a highly reduced meteoroid and thus their Si concentrations directly reflect their provenance. Specifically, Si-bearing metal is found in aubrites, enstatite chondrites, and several ungrouped iron meteorites [9-10]. Cr-bearing sulfides (e.g., daubréelite) can be found in aubrites, enstatite chondrites, and many iron meteorites [9-10].

The combination of Si-bearing metal and Cr-bearing sulfides is more consistent with these texturally zoned metal inclusions inheriting their reduced geochemical features from their source meteoroid. Thus, these two Si-bearing metal inclusions along with the non-Si-bearing exogenic metals provide evidence that regolith that NWA 11303 formed from incorporated material from multiple geochemical distinct impactors. Direct evidence for two separate impactors have not previously been recognized in a lunar regolith sample. As exemplified by the Si- and non-Si-bearing exogenic metals in NWA 11303, recognizing inputs from multiple impactors is feasible and may be a powerful tool for connecting unpaired lunar meteorites from similar regions of the Moon and for investigating the history of impacts on the Moon.

References: [1] Keller & McKay (1993) *Science* 261:1305. [2] Anand et al. (2004) *PNAS* 101:6847. [3] Goldstein & Yakowitz (1971) *Proc. of 2nd Lunar. Sci. Conf.* 1:177. [4] Goldstein et al. (1972) *Proc. of 3rd Lunar. Sci. Conf.* 1: 1037. [5] Meteoritical Bulletin Database www.lpi.usra.edu/meteor/ [6] Korotev R. Website meteorites.wustl.edu/lunar/stones/nwa 8046.htm. [7] Domingue et al. (2014) *Space Sci Rev* 181:121. [8] Noguchi et al. (2011) *Science* 333:1121. [9] Brearley and Jones (1998) *Rev. Mineral.* 36:4-01. [10] Mittlefehldt et al. (1998) *Rev. Mineral.* 36:4-01.

BULK CHONDRITE VARIABILITY IN MASS-INDEPENDENT MAGNESIUM ISOTOPE COMPOSITION – IMPLICATIONS FOR INITIAL SOLAR SYSTEM ^{26}AL/^{27}AL.

T.-H. Luu, R. C. Hin, C. D. Coath and T. Elliott,
Bristol Isotope Group, School of Earth Sciences, University of Bristol, Bristol BS8 1RJ, UK (tutu.luu@bristol.ac.uk)

Introduction: The ^{26}Al-^{26}Mg short-lived chronometer (half life of 0.72 Myr) has been extensively used to date objects formed in the solar protoplanetary disk, SPD (e.g. [1-2]). However, the use of the Al-Mg systematics as a chronometer relies on the assumption that $(^{26}Al/^{27}Al)_0$ was initially homogeneously distributed in the different formation regions of the objects being dated. Improvements in bulk analytical techniques over the past decades now allows differences of a few parts per million (ppm) in mass-independent Mg isotopic compositions, $\Delta'^{26}Mg_{DSM-3}$, to be distinguished. This capability provides a valuable perspective on possible $(^{26}Al/^{27}Al)_0$ heterogeneity in solar system bodies.

So far, variability in $\Delta'^{26}Mg_{DSM-3}$ among solar system objects has been interpretated as reflecting either (i) variability in Al/Mg, based on the observation that the $\Delta'^{26}Mg_{DSM-3}$ of bulk chondrites correlate with their Al/Mg, suggesting a common, canonical $(^{26}Al/^{27}Al)_0$ in the parent bodies of these samples [3-4], or (ii) variability linked to a heterogeneous initial distribution of $(^{26}Al/^{27}Al)_0$ within the SPD, based on the covariation of $\Delta'^{26}Mg_{DSM-3}$ and $\varepsilon^{54}Cr$ between bulk chondrites [5-6], or (iii) nucleosynthetic Mg-isotope heterogeneity across the SPD, as is evident on a small scale by the different intercepts of Al-Mg isochrons of some unusual CAIs [7]. Thus, to date, the bulk chondrite $\Delta'^{26}Mg_{DSM-3}$ data have not clearly resolved the question of whether or not $(^{26}Al/^{27}Al)_0$ in the SPD was homogenous.

Here we consider new data of our own together with the most recent data of the literature [8-9] to reassess the problem. We have also focused on better characterizing the composition of enstatite chondrites, in order to expand the existing dataset of single values reported by [3] and [5]. As well as their bearing on the cause of bulk chondrite $\Delta'^{26}Mg_{DSM-3}$ variability, enstatite chondrites provide a likely protolith composition for the Earth [e.g., 10].

Results and Discussion: Bulk carbonaceous (CV, CI, CM, CO, CK) and ordinary (H, LL) chondrites define a primordial Al-Mg isochron whose slope and intercept yield $(^{26}Al/^{27}Al)_0 \sim (4.7\pm0.8)\times10^{-5}$ and $(\Delta'^{26}Mg_{DSM-3})_0 = -31.6 \pm 5.7$ ppm, within uncertainty of the canonical value of $(^{26}Al/^{27}Al)_0 \approx 5.2\times10^{-5}$ and $(\Delta'^{26}Mg_{DSM-3})_0 \approx -34$ ppm previously defined by the oldest, dated solar system objects, namely calcium-, aluminium-rich inlusions (CAIs) from CV chondrites [e.g., 11]. This is indicative of a near homogenous initial $(^{26}Al/^{27}Al)_0$ during formation of normal CAIs and precursor grains of most bulk chondrite groups, and strongly supports the use of the Al-Mg systematics as a short-lived chronometer.

The $\Delta'^{26}Mg_{DSM-3}$ of enstatite chondrites are slightly more radiogenic (~ 3 ppm) at similar Al/Mg to the ordinary chondrites. This is an entirely new observation. We speculate that the higher $\Delta'^{26}Mg_{DSM-3}$ of enstatite chondrites is explained by ~ 0.5 Ma delay in condensation and removal of a refractory component from the source reservoirs of EH and EL enstatite chondrites.

References: [1] Schiller M. et al. (2015). *Earth and Planetary Science Letters* 420:45-54. [2] Luu T.-H. et al. (2015). *Proceedings of the National Academy of Sciences* 112:1298-1303. [3] Schiller M. et al. (2010). *Earth and Planetary Science Letters* 297:165-173. [4] Kita N.T. et al. (2013). *Meteoritics & Planetary Science* 48:1383-1400. [5] Larsen K.K. et al. (2011). *Astrophysical Journal* 735:L37-L43. [6] Van Kooten E.M.M.E. et al. (2016). *Proceedings of the National Academy of Sciences* 113:2011-2016. [7]Wasserburg G.J. et al. (2012). *Meteoritics & Planetary Science* 47:1980-1997. [8] Olsen M.B. et al. (2016). *Geochimica et Cosmochimica Acta* 191:118-138. [9] Larsen K.K. et al. (2016). *Geochimica et Cosmochimica Acta* 176:295-315. [10] Javoy M. et al. (1986). *Chemical Geology* 57:41-62. [11] Jacobsen B. et al. (2008). *Earth and Planetary Science Letters* 272:353-364.

HIGH SPATIAL RESOLUTION ISOTOPE ANALYSES OF PRESOLAR SIC GRAINS FROM THE COLD BOKKEVELD (CM2) CARBONACEOUS CHONDRITE.

I.C.Lyon[1]

[1]School of Earth and Environmental Sciences, The University of Manchester, M13 9PL UK.
Ian.Lyon@manchester.ac.uk

Introduction: Measurements of ^{12}C/^{13}C, ^{14}N/^{15}N and $\delta^{29,30}$Si as well as the isotope systems of other elements have been obtained from ~17,000 presolar SiC grains cumulatively from many laboratories over a period of >25 years [1]. 14,731 (~85%) of these reported analyses are of SiC grains extracted from the Murchison (CM2) meteorite. The wide spread of ^{12}C/^{13}C, ^{14}N/^{15}N and $\delta^{29,30}$Si values measured from these grains [2] lead to models of diverse astrophysical environments where the grains formed. There are however instrumental artefacts associated with high spatial resolution SIMS analyses that can potentially distort measured isotope ratios of grains [3-5] and this work continues the effort to quantify and understand these effects in order that more accurate analyses may be obtained.

In this study, SiC grains separated from the CM2 carbonaceous chondrite Cold Bokkeveld were analyzed by NanoSIMS for ^{12}C/^{13}C, ^{14}N/^{15}N, δ^{26}Mg and $\delta^{29,30}$Si. An aim was to test whether the grain types and distribution of isotope ratios found from the Murchison meteorite were matched by another CM2 meteorite. A further aim was to obtain high spatial resolution (~100nm) analyses with depth profiling through grains to build up 3 dimensional reconstructions of the distribution of ^{12}C/^{13}C, ^{14}N/^{15}N and $\delta^{29,30}$Si in the grains to test for isotopic heterogeneity in the grains Systematic high spatial resolution (< 100nm) analyses of SiC grains have, in general, not previously been obtained. A particular target of study was to obtain ^{14}N/^{15}N distributions with high spatial resolution. The determined ^{14}N/^{15}N range of 8000 to 290 (the terrestrial value) for mainstream grains and 8000 to 50 for A+B SiC grains is difficult to understand from nucleosynthetic models [6] and detailed modelling of molecular ion transmission artefacts in the NanoSIMS suggest that some isotopic fractionation may be related to instrumental fractionation processes [3]. An aim of this study was to establish to what degree this range would be reproduced when cognizant of instrumental fractionation effects.

Experimental Methods: SiC grains isolated from the Cold Bokkeveld meteorite were produced by J. Arden nearly 30 years ago using the methods of [7]. A NanoSIMS 50L installed at the University of Manchester was used for analyses, simultaneously detecting ^{12,13}C$^-$, ^{12}C^{14}N$^-$, ^{12}C^{15}N$^-$ and ^{28,29,30}Si$^-$ on 7 multiplier detectors. A primary Cs$^+$ current of ~0.5pA (D1-5 aperture setting) and spatial resolution ~100nm was used. A Hyperion source for high spatial resolution O$^-$ analysis of the grains was subsequently used to acquire ~100spatial resolution analyses of δ^{26}Mg, Al/Mg and $\delta^{29,30}$Si using positive secondary ions. The residue containing presolar SiC was spread over gold foil and imaged using secondary ions, in particular C and Si to establish the presence of SiC grains.

Experimental Results: As in Murchison, the average size of SiC grains was found to be >1 µm and A+B grains (^{12}C/^{13}C<10) were found to be more prevalent (~17%) than in Murchison (4-5%). The CN$^-$ distribution could be complex within and around the grains and δ^{13}C and δ^{15}N was measured to be heterogeneous within some grains. Detailed analytical data for analyses of 93 SiC grains from Cold Bokkeveld will be presented and implications discussed.

References:
[1] Hynes K. M. and Gyngard F., (2009), *LPS XL*, Abstract #1198
[2] Davis A., (2011) *Proceedings National Academy Sciences, 48, 19142-19146*
[3] Lyon I.C., Clarke A., Henkel T., Moore K.L., McMahon G., (2016) *Meteoritical Society abstract #6464*
[4] Yang W. et al., (2015) *Science China Earth Sciences, 58, 1758-1767*
[5] Tang G-Q. et al., (2015) *Journal Analytical Atomic Spectroscopy 30, 950-956*
[6] Hedrosa et al., *arXiv:1303.6418v1*.
[7] Amari et al., (1989) *Geochimica et Cosmochimica Acta, **58**, 459-470*.

DISCOVERY OF KAITIANITE, $Ti^{3+}_2Ti^{4+}O_5$, IN ALLENDE: A NEW REFRACTORY MINERAL FROM THE SOLAR NEBULA.

Chi Ma
Division of Geological and Planetary Sciences, California Institute of Technology,
Pasadena, CA 91125, USA; Email: chi@gps.caltech.edu.

Introduction: The Allende meteorite, fell in Mexico on February 8, 1969, is a CV3 carbonaceous chondrite. It is often called the best-studied meteorite in history. Fifty years after it fell, this meteorite continues to be source of new discoveries. Allende has yielded 19 new minerals since 2007 [e.g., 1-4], including 11 ultrarefractory or refractory phases. Each new mineral adds a new puzzle piece toward our understanding of nebular or parent body processes in the early solar system. Reported here is the discovery of kaitianite, $Ti^{3+}_2Ti^{4+}O_5$, a refractory titanium oxide from the solar nebula – the latest new mineral in Allende.

During an ongoing nanomineralogy investigation of the Allende CV3 carbonaceous chondrite, new mineral kaitianite, $Ti^{3+}_2Ti^{4+}O_5$ with a $C2/c$ V_3O_5-type structure, was identified in section USNM 3510-5. Field-emission scanning electron microscope (SEM), energy-dispersive X-ray spectroscopy (EDS), electron back-scatter diffraction (EBSD) and electron probe microanalyzer (EPMA) were used to characterize kaitianite and associated phases. Fine-grained Ti_3O_5 phase was observed in a chondrite matrix clast in the Nilpena polymict ureilite [5]. Synthetic Ti_3O_5 with the $C2/c$ V_3O_5 structure is reported as γ-Ti_3O_5 [6,7]. Kaitianite, the natural occurrence of $Ti^{3+}_2Ti^{4+}O_5$ with the $C2/c$ V_3O_5 structure as a new mineral in Allende, has been approved by the IMA-CNMNC (IMA 2017-078a) [8]. The name is after two Chinese words "Kai Tian", meaning *creating the heaven / the sky*, from the story of "Pan Gu Kai Tian" in the ancient Chinese mythology. Pan Gu, the giant, created the world by separating the heaven and earth from an egg-shaped chaos in the beginning. Panguite ((Ti^{4+},Sc,Al,Mg,Zr,Ca)$_{1.8}O_3$; IMA 2010-057 [1]) was named after "Pan Gu" in allusion to the mineral with an ultrarefractory origin being among the first solid materials in the solar system. Kaitianite ($Ti^{3+}_2Ti^{4+}O_5$) is also a refractory phase formed in the solar nebula.

Occurrence, Chemistry, and Crystallography: Kaitianite occurs as two crystals, 0.3~0.6 μm × 3.6 μm and 0.2 μm × 1.1 μm, within one irregular grain in contact with tistarite and rutile, along with Ti^{3+}-bearing corundum, Ti^{3+},Al,Zr-oxide, and Ti-bearing xifengite grains in a crack in the Allende matrix. These grains are likely from the cluster of refractory phases identified in a chondule in USNM 3510-6, where Ti^{3+}-bearing corundum grains, mullite, khamrabaevite (TiC) and the type tistarite (Ti_2O_3; IMA 2008-016) were first identified [9,10]. USNM 3510-5 and USNM 3510-6 are series cut thin sections. The O-isotope analyses of two corundum grains in the cluster in USNM 3510-6 reveal that the grains have compositions well above the terrestrial fractionation line but on the CCAM line [10], which is consistent with formation or alteration in an O^{16}-depleted reservoir.

The chemical composition of type kaitianite by low-voltage EPMA (WDS) is (wt%) Ti_2O_3 56.55, TiO_2 39.29, Al_2O_3 1.18, MgO 1.39, FeO 0.59, V_2O_3 0.08, sum 99.07, showing an empirical formula (based on 5 O atoms *pfu*) of $(Ti^{3+}_{1.75}Al_{0.05}Ti^{4+}_{0.10}Mg_{0.08}Fe_{0.02})(Ti^{4+}_{1.00})O_5$, with Ti^{3+} and Ti^{4+} partitioned, based on stoichiometry. The end-member formula is $Ti^{3+}_2Ti^{4+}O_5$. The EBSD patterns of kaitianite can be indexed only by the $C2/c$ V_3O_5-type structure and give a perfect fit by the synthetic γ-Ti_3O_5 cells from [6,7], with a mean angular deviation of 0.33º, revealing a = 10.115 Å, b = 5.074 Å, c = 7.182 Å, β = 112º, V = 341.77 Å^3, and Z = 4.

Associated Ti^{3+},Al,Zr-oxide is a new Zr-rich ultrarefractory phase from Allende. It has an empirical formula (based on 3 O atoms *pfu*) of $(Ti^{3+}_{1.16}Al_{0.57}Zr_{0.11}Si_{0.07}Mg_{0.03})_{\sum1.95}O_3$ and a general formula of $(Ti^{3+},Al,Zr,Si,Mg)_{1.95}O_3$. Its crystal structure is related to panguite-kangite-type but highly-ordered, as revealed by EBSD.

Origin and Significance: Kaitianite ($Ti^{3+}_2Ti^{4+}O_5$) is γ-Ti_3O_5, the Ti-analog of oxyvanite (V_3O_5), a new member of the oxyvanite group. Kaitianite is a refractory titanium oxide, joining other Ti-rich refractory minerals from carbonaceous chondrites including perovskite, Al,Ti-diopside, tistarite, rutile, grossmanite, davisite, panguite, kangite, anosovite, paqueite, zirkelite, tazheranite, rubinite, and Ti^{3+},Al,Zr-oxide.

Multiple refractory phases (tistarite, corundum, kaitianite, Ti^{3+},Al,Zr-oxide, khamrabaevite) are potentially useful as probes of their formation environments. These grains either indicate or are consistent with extremely reducing conditions. Kaitianite is a first solar titanium oxide with structurally essential Ti^{3+} and Ti^{4+}, probably crystallized from a refractory melt or condensed from a gaseous reservoir under highly-reduced conditions.

References: [1] Ma C. et al. 2012. *American Mineralogist* 97:1219–1225. [2] Ma C. et al. (2014) *American Mineralogist* 99:654–666. [3] Ma C. and Krot A.N. (2018) *American Mineralogist* 103:1329–1334. [4] Ma C. and Beckett J.R. 2018. *American Mineralogist* 103:1918–1924. [5] Brearley A.J. 1993. *Meteoritics* 28:590–595. [6] Hong S.H. and Asbrink S. 1982. *Acta Crystallographica B* 38:2570–2576. [7] Tanaka K. et al. 2015. *Crystal Growth & Design* 15:653–657. [8] Ma C. 2018. *Mineralogical Magazine* 82:450. [9] Ma C. and Rossman G.R. 2009. *American Mineralogist* 94:841–844. [10] Ma et al. 2009. *LPSC* 40:A2138.

EDSCOTTITE, Fe_5C_2, A NEW IRON CARBIDE MINERAL
FROM THE WEDDERBURN IRON METEORITE.

Chi Ma[1] and Alan Rubin[2]. [1]Division of Geological and Planetary Sciences, California Institute of Technology, Pasadena, CA 91125, USA; [2]Department of Earth, Planetary, and Space Sciences, University of California, Los Angeles, CA 90095-1567, USA; Email: chi@gps.caltech.edu.

Introduction: The Wedderburn iron meteorite, found as a single 210-g mass in Victoria, Australia in 1951, is a Ni-rich ataxite belonging to subgroup sLH of the IAB complex (Low-Au, High-Ni subgroup). It is one of the most Ni-rich irons known (23.4 wt.% Ni [1]), initially classified as group IIID. During a re-investigation of a polished thick section of Wedderburn, we identified a new iron-carbide mineral, Fe_5C_2 with the $C2/c$ Pd_5B_2-type structure, named "edscottite" (Fig. 1). Field-emission scanning electron microscopy, energy-dispersive X-ray spectroscopy, electron back-scatter diffraction (EBSD) and electron probe microanalysis (EPMA) were used to characterize edscottite and associated phases. This mineral was first identified in Wedderburn [2,3]; synthetic Fe_5C_2 was previously known (e.g., [4-6]). We report here the first natural occurrence of Fe_5C_2 in an iron meteorite as a new carbide mineral. Edscottite (IMA 2018-086a) was approved by the IMA-CNMNC [7]. The mineral name is in honor of Edward (Ed) R. D. Scott, University of Hawai'i, USA, for his seminal contributions to meteorite research. He discovered haxonite, $(Fe,Ni)_{23}C_6$ [8] as well as this new iron carbide [2,3].

Occurrence, Chemistry, and Crystallography: Edscottite occurs as subhedral, lath-shaped or platy single crystals, ~0.8 μm × 15 μm to 1.2 μm × 40 μm in size, which is the holotype material, in an assemblage with low-Ni iron (kamacite), taenite, nickelphosphide (Ni-rich schreibersite), and small amounts of cohenite in a matrix of fine-grained iron (plessite) (Fig. 1).

The mean chemical composition of type edscottite, determined by EPMA, is (in wt%) Fe 87.01, Ni 4.37, Co 1.04, C 7.90, total 100.31, yielding an empirical formula of $(Fe_{4.73}Ni_{0.23}Co_{0.05})C_{1.99}$. The end-formula is Fe_5C_2. The EBSD patterns are indexed only by the $C2/c$ Pd_5B_2-type structure and give a best fit by the synthetic χ-Fe_5C_2 cell from [5], with a mean angular deviation of 0.45º - 0.48º, revealing $a = 11.57$ Å, $b = 4.57$ Å, $c = 5.06$ Å, $\beta = 97.7°$, $V = 265.1$ Å^3, and Z = 4. The calculated density is 7.63 g/cm^3 using the empirical formula.

Origin and Significance: Edscottite is Hägg-carbide, χ-Fe_5C_2, a new iron-carbide mineral, joining cohenite (Fe_3C) and haxonite ($(Fe,Ni)_{23}C_6$) as a naturally occurring phase. During cooling from high temperature, edscottite (like cohenite and haxonite) forms metastably in iron meteorites in kamacite, but unlike the other two carbides it forms laths, possibly due to very rapid growth after supersaturation of carbon.

Computational studies of Earth's inner core shows that the most stable Fe carbides are Fe_3C, Fe_7C_3 and Fe_2C; edscottite (along with Fe_4C) is close to stability at these high pressures (~350 GPa, [9]) and might be present.

References: [1] Wasson J.T. and Kallemeyn G.W. 2002. *Geochimica et Cosmochimica Acta* 66:2445–2473. [2] Scott E.R.D. and Agrell S.O. 1971. *Meteoritics* 6:312–313. [3] Scott E.R.D. 1972. University of Cambridge, Ph.D. thesis. [4] Hägg G. 1934. *Zeitschrift für Kristallographie - Crystalline Materials* 89:92–94. [5] Jack K.H. and Wild S. 1966. *Nature* 212:248–250. [6] Leinweber et al. 2012. *Zeitschrift für Kristallographie - Crystalline Materials* 227:207–220. [7] Ma C. and Rubin A. 2019. *European Journal of Mineralogy* 31:204. [8] Scott E.R.D. 1971. *Nature* 229:61–62. [9] Weerasinghe et al. 2011. *Physical Review B* 84:174110.
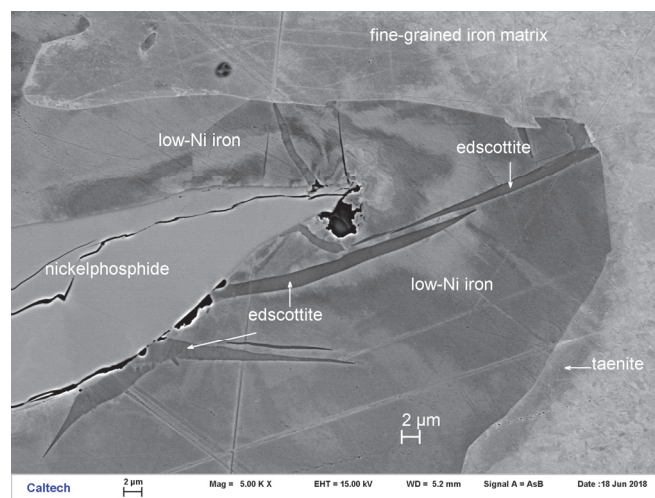

Fig. 1. Back-scatter electron image revealing edscottite in the Wedderburn iron meteorite.

RARE EARTH ELEMENT DISTRIBUTION AND LU-HF AND SM-ND ISOTOPE SYSTEMATICS OF ANTARCTIC H CHONDRITES

R. Maeda[1*], S. Goderis[1], V. Debaille[2], G. Hublet[2], H. Pourkhorsandi[2] and P. Claeys[1],
[1]Analytical, Environmental and Geo-Chemistry (AMGC), Vrije Universiteit Brussel, Pleinlaan 2, 1050 Brussels, Belgium (*Ryoga.Maeda@vub.ac.be),
[2]Laboratoire G-Time, Université Libre de Bruxelles, Avenue Franklin Roosevelt 50, 1050 Bruxelles, Belgium

Introduction: Long-lived radioactive isotopes such as ^{176}Lu and ^{147}Sm, which decay to ^{176}Hf (half-life ~37.1 Gyr) and ^{143}Nd (half-life ~10.6 Gyr), respectively, are known to be important chronometers and tracers for chemical differentiation processes. The redistribution of rare earth elements (REEs) and other large ion lithophile elements during planetary processes have strong effects on the Lu-Hf and Sm-Nd isotope systems, as observed in a wide range of chondritic and achondritic materials [*e.g.,* 1]. However, the relative mobility of these elements during aqueous alteration or thermal metamorphism on their parent bodies, as well as during weathering in hot and cold desert remain poorly understood, even in the case of common chondrites [*e.g.,* 2]. Although the Lu-Hf system has been applied to H chondrites due to their large abundance (~30% of all meteorites), previous studies have mostly focused on falls [*e.g.,* 3]. Based on published isotopic data [3, 4], there is a small but significant difference in ^{176}Hf/^{177}Hf between unequilibrated and equilibrated L chondrites. However, we cannot conclude whether the isotopic shift reflects a primary characteristic or results from the applied experimental procedures as no systematic study has been done on H chondrites. In addition, almost no data has been collected for Antarctic meteorites. In this study, therefore, the results of Lu-Hf and Sm-Nd isotope systematics in Antarctic H chondrites are examined in a methodical manner.

Samples and Methods: Ten Antarctic H chondrites from H3.0 to H7 are studied for their REE distribution and subsequently analyzed in bulk, for a determination of the Sm, Nd, Lu and Hf isotopic compositions and major and selected trace elemental abundances, including REEs. Three H chondrites (H3-H5) obtained from hot deserts are also considered to quantitatively constrain any effects related to weathering. The corresponding powdered samples were digested using acids, and the solutions were divided into two aliquots for elemental abundance and isotope ratio analysis. The abundances of major and trace elements were determined using ICP-OES and Q-ICP-MS at the Université Libre de Bruxelles (ULB). Once isolated from the aliquots for isotope analysis using ion exchange chromatography, the isotopic compositions of Nd and Hf were determined using the Nu II MC-ICP-MS at ULB. At the same time, the corresponding polished thick sections were investigated for their major and trace element distribution. After elemental maps for each sample were produced using micro-XRF, constituent mineral phases in the samples were identified that were subsequently confirmed using an SEM-EDS. Major components in constituent minerals of each sample, which are used as an internal standard element for LA-ICP-MS, will be determined by using EPMA at the National Institute of Polar Science in Japan, and then the REE distribution between minerals will be investigated using LA-ICP-MS/TOF based on single point drilling and mapping at Ghent University.

Results and Discussion: According to the first micro-XRF results, the average modal abundance of Ca-phosphates in equilibrated H chondrites is 0.83±0.11 vol. % (equivalent to 0.71±0.10 wt. %, n=6), which is good agreement with literature values [5, 6]. Surprisingly, however, the average modal abundance in unequilibrated H chondrites is 0.47±0.13 vol. % (equivalent to 0.40±0.11 wt. %, n=7), which is a significantly lower abundance relative to equilibrated H chondrites. In addition, there is no resolvable difference in the bulk P and REE abundances between unequilibrated and equilibrated H chondrites based on our primary results for the determination of elemental abundances (n=2 for unequilibrated H chondrite and n=4 for equilibrated H chondrite), which is consistent with published bulk analyses [7, 8]. Therefore, the difference in the modal abundances of Ca-phosphates can only be explained by the generation of Ca-phosphates during thermal metamorphism in H chondrites. Because Ca-phosphates in H chondrites must have formed or grown larger during thermal metamorphism, REEs may have been re-distributed to Ca-phosphates during that time [9]. The isotopic shifts of the Lu-Hf and Sm-Nd systems between unequilibrated and equilibrated H chondrites may thus be linked to the Ca-phosphates that are known to be important host phases of REEs in equilibrated ordinary chondrites [*e.g.,* 10]. Systematic bulk and phosphate analyses will indicate whether the observed isotopic differences result from different time scales or efficiencies for the re-distribution of REE during thermal metamorphism between unequilibrated and equilibrated H chondrites.

References: [1] Patchett P.J. and Tatsumoto M. (1980), *Nature* **288**, 571–574. [2] Tatsumoto M. *et al.* (1981), *Memoirs of NIPR. Special issue* **20**, 237-249. [3] Bouvier A. *et al.* (2008), *EPSL* **273**, 48-57. [4] Patchett P.J. *et al.* (2004), *EPSL* **222**, 29-41. [5] McSween Jr. H.Y. *et al.* (1991), *Icarus* **90**, 107-116. [6] Van Schmus W.R. (1969), *Earth-Sci. Rev.* **5**, 145-184. [7] Jarosewich E. (1990), *Meteoritics* **25**, 323-337. [8] Kallemeyn G.W. *et al.* (1989) *GCA* **53**, 2747-2767. [9] Shinotsuka K. and Ebihara M. (1995), *LPS* **XXVI**, 1293-1294. [10] Debaille V. *et al.* (2017) *EPSL* **473**, 52-61.

VARIABILITY IN THE PHASE COMPOSITION IN CHELYABINSK LL5 FRAGMENTS WITH DIFFERENT LITHOLOGIES: STUDY USING X-RAY DIFFRACTION AND MÖSSBAUER SPECTROSCOPY.

A. A. Maksimova[1], A. V. Chukin[1], E. V. Petrova[1] and M. I. Oshtrakh[1], [1] Institute of Physics and Technology, Ural Federal University, Ekaterinburg, 620002, Russian Federation (oshtrakh@gmail.com).

Introduction: Five fragments of Chelyabinsk LL5 ordinary chondrite (meteorite fall was on February 15, 2013) collected by the Meteoritical Expedition of the Ural Federal University on the next day after fall were chosen for comparative study by means of optical microscopy, scanning electron microscopy (SEM) with energy dispersive spectroscopy (EDS), X-ray diffraction (XRD) and Mössbauer spectroscopy. These samples demonstrate different lithologies such as: light lithology (two samples marked No 1 and No 1a), mixed light and dark lithologies (two samples marked No 2 and No 2a) and black lithology (one sample marked No 3). The dark lithology of samples No 2 and No 2a was different from the black lithology of No 3. The latter lithology was similar to the dark lithology mentioned in [1].

Materials and Methods: The polished thin sections of Chelyabinsk LL5 fragments were prepared by the standard methods for optical microscopy and SEM with EDS characterization. Then powdered matter was prepared from the slice surface for XRD and Mössbauer spectroscopy. Optical microscopy was done using an Axiovert 40 MAT microscope (Carl Zeiss) and SEM analysis was carried out using a ΣIGMA VP electron microscope (Carl Zeiss) with an X-max (Oxford Instruments) EDS device. Similar measurements were performed using an AMRAY 1830 scanning electron microscope equipped with EDAX PV9800 energy dispersive spectrometer. The XRD study was carried out using the XRD–7000 powder diffractometer (Shimadzu) while the ^{57}Fe Mössbauer spectra were measured at 295 K using SM-2201 spectrometer with a high velocity resolution. Detailes were described in [2].

Results and Discussion: Characterization of Chelyabinsk LL5 fragments by means of optical microscopy and SEM with EDS showed the presence of silicate matrix with Fe-Ni-Co alloy grains and inclusions of troilite FeS, chromite $FeCr_2O_4$ with hercynite $FeAl_2O_4$ and ilmenite $FeTiO_3$ which was found in fragment No 2a only. The results of the full profile Rietveld analysis of the XRD patterns and the best fits of the Mössbauer spectra of the studied Chelyabinsk LL5 fragments are collected in Table 1. The data from XRD were obtained in wt.%. Mössbauer spectroscopy permits to estimate the subspectra relative areas of the iron-bearing phases only which can be roughly considered as the relative Fe content in these phases. The results obtained for Chelyabinsk LL5 meteorite fragments demonstrated some variations in the phase composition for all fragments with the same and different lithologies studied by two techniques.

Table 1. Comparison of various phases obtained using XRD and corresponding relative areas revealed from the Mössbauer spectra (MS) in different fragments of Chelyabinsk LL5 ordinary chondrite.

Phase	No 1		No 1a		No 2		No 2a		No 3	
	XRD (wt.%)	MS (%)	XRD (wt.%)	MS (%)	XRD (wt.%)	MS (%)	XRD (wt.%)	MS (%)	XRD (wt.%)	MS (%)
Olivine	56.0	59.97	50.6	51.56	48.6	46.32	55.8	58.64	52.0	54.45
Orthopyroxene	25.9	22.48	24.8	13.70	25.2	12.34	25.8	15.09	21.2	11.89
Clinopyroxene	3.9	–	5.5	4.62	6.9	6.98	5.9	5.17	6.2	5.49
Anorthite	9.0	–	8.2	–	8.2	–	6.1	–	10.7	–
Troilite[a]	4.1	13.25	6.7	20.53	6.2	19.77	3.7	11.44	6.3	18.47
Chromite	0.5	0.83	1.5	1.63	1.5	2.69	0.6	1.18	1.8	2.51
Kamacite[b]	0.4	1.98	1.4	5.05	1.8	7.26	1.0	4.53	0.6	2.56
Taenite	0.2	1.50	0.9	2.19	0.8	2.90	0.7	2.44	0.7	3.86
Hercynite	–	–	0.4	0.72	0.8	1.73	0.3	0.69	0.5	0.78
Ilmenite	–	–	–	–	–	–	0.1	0.82	–	–
Total	100.0	100.01	100.0	100	100.0	99.99	100.0	100.00	100.0	100.01

[a]For fragments No 1a and No 3 the total relative area for FeS and $Fe_{1-x}S$ is shown.
[b]For fragments No 1a, No 2 and No 3 the total relative area for the α_2-Fe(Ni, Co) and α-Fe(Ni, Co) phases is shown.

References:

[1] Kohout T. et al. (2014) *Icarus*, 228:78–85. [2] Oshtrakh M. I. et al. (2019) *Spectrochimica Acta, Part A: Molecular and Biomolecular Spectroscopy*, in press (DOI: 10.1016/j.saa.2019.03.036).

Fe^{2+} OCCUPANCIES IN THE M1 AND M2 SITES IN SILICATE CRYSTALS IN CHELYABINSK LL5 FRAGMENTS WITH DIFFERENT LITHOLOGIES ANALYZED USING X-RAY DIFFRACTION AND MÖSSBAUER SPECTROSCOPY.

A. A. Maksimova[1], E. V. Petrova[1], A. V. Chukin[1] and M. I. Oshtrakh[1], [1] Institute of Physics and Technology, Ural Federal University, Ekaterinburg, 620002, Russian Federation (oshtrakh@gmail.com).

Introduction: The distribution of Fe^{2+} and Mg^{2+} cations between crystallographically nonequivalent M1 and M2 sites in silicates crystals is related to the thermal history of silicates and meteorites containing these phases. Recently, we demonstrated that the data obtained from the study of Annama H5 and Northwest Africa 6286 and 7857 LL6 ordinary chondrites by means of two independent techniques, X-ray diffraction (XRD) and Mössbauer spectroscopy, can be used for calculation of the Fe^{2+} occupancies of the M1 and M2 sites in olivine, orthopyroxene and clinopyroxene which results were in a good consistency [1, 2]. Therefore, we applied this approach for the study of Chelyabinsk LL5 fragments with different lithologies.

Materials and Methods: The samples of the powdered internal matter from five fragments of Chelyabinsk LL5 meteorite with different lithologies such as light lithology (two fragments marked No 1 and No 1a), mixed light and dark lithologies (two fragments marked No 2 and No 2a) and black lithology (one fragment marked No 3) were prepared for XRD and Mössbauer studies. The XRD–7000 powder diffractometer (Shimadzu) was used for XRD measurements while the SM-2201 spectrometer with a high velocity resolution was used for the ^{57}Fe Mössbauer spectra measurements at 295 K. Detailed description can be found elsewhere [3].

Results and Discussion: Using the Rietveld full profile analysis of the XRD patterns the values of the Fe^{2+} occupancies in the M1 and M2 sites (X_{Fe}^{M1} and X_{Fe}^{M2}) in silicate crystals were determined (see Table 1). The best fits of the Mössbauer spectra of the studied fragments revealed spectral components assigned to the ^{57}Fe in the M1 and M2 sites in silicates (A^{M1} and A^{M2}). The ratio A_{Fe}^{M1}/A_{Fe}^{M2} corresponds roughly to the ratio of the Fe^{2+} occupancies of the M1 and M2 sites. The results are presented in Table 1 for selected fragments. These results demonstrate a good consistency for two techniques and some variations in the Fe^{2+} occupancies for the same silicate crystals in different fragments.

Table 1. The ratios of Fe^{2+} occupancies in the M1 and M2 sites in olivine, orthopyroxene and clinopyroxene in selected Chelyabinsk LL5 fragments calculated using XRD and Mössbauer spectroscopy data.

Silicates in different fragments	XRD			Mössbauer spectroscopy
	X_{Fe}^{M1}	X_{Fe}^{M2}	X_{Fe}^{M1}/X_{Fe}^{M2}	A^{M1}/A^{M2}
Olivine				
No 1a (light lithology)	0.29	0.24	1.21	1.21
No 2 (mixed light and dark lithologies)	0.27	0.23	1.17	1.18
No 2a (mixed light and dark lithologies)	0.33	0.25	1.32	1.37
No 3 (black lithology)	0.30	0.25	1.20	1.17
Orthopyroxene				
No 1a (light lithology)	0.09	0.41	0.18	0.33
No 2 (mixed light and dark lithologies)	0.08	0.40	0.20	0.25
No 2a (mixed light and dark lithologies)	0.10	0.38	0.26	0.40
No 3 (black lithology)	0.11	0.38	0.29	0.30
Clinopyroxene				
No 1a (light lithology)	0.34	0.09	3.78	4.78
No 2 (mixed light and dark lithologies)	0.32	0.18	1.78	1.90
No 2a (mixed light and dark lithologies)	0.33	0.13	2.54	2.31
No 3 (black lithology)	0.34	0.14	2.43	2.33

References:
[1] Kohout T. et al. (2017) *Meteoritical & Planetary Science* 52:1525–1541. [2] Maksimova A. A. et al. (2018) *Spectrochimica Acta, Part A: Molecular and Biomolecular Spectroscopy* 192:275–284. [3] Oshtrakh M. I. et al. (2019) *Spectrochimica Acta, Part A: Molecular and Biomolecular Spectroscopy*, in press (DOI: 10.1016/j.saa.2019.03.036).

OXYGEN ISOTOPIC IMAGING OF A HIBONITE-GROSSITE-RICH INCLUSION FROM THE MILLER RANGE (MIL) 090019 CO3 CHONDRITE.

P. Mane[1,2] , A. N. Nguyen[2,3], J. J. Barnes[2], A. W. Needham[2,3], S. Messenger[2], D. K. Ross[2,3] and J. I. Simon[2], [1]Lunar and Planetary Institute, USRA, 3600 Bay Area Boulevard, Houston, TX 77058 USA (pmane@lpi.usra.edu), [2]Robert M Walker Laboratory for Space Science, EISD/Astromaterials Research Exploration Sciences, NASA Johnson Space Center, 2101, NASA Parkway, Houston, TX 77058 USA, [3]Jacobs, Houston, TX, 77058, USA.

Introduction: Calcium-Aluminum-rich Inclusions (CAIs) in primitive meteorites are the first solids to condense in the Solar System [e.g., 1, 2]. The oxygen isotopic compositions recorded in various mineral components of CAIs provide clues about their origin and post-formation history [e.g., 3], including processes such as condensation, melting, nebular alteration, and fluid-rock reactions on the parent body. Among primitive meteorites, CO3 carbonaceous chondrites are one of the minimally altered and the CAIs within them retain records of their earliest histories. Here we report results from oxygen isotopic imaging of a grossite-hibonite bearing CAI (CAI 44) from the Miller Range (MIL) 090019 CO3 chondrite, using NanoSIMS. The goal of this study is to search for evidence of nebular processes in phases that are most susceptible to parent body alteration.

Methods: The mineralogical and petrological characterization of CAI 44 was performed using the JOEL Hyperprobe 8530 electron microprobe at NASA JSC. Oxygen isotopic imaging of the CAI was done using the Cameca NanoSIMS 50L ion microprobe at NASA JSC. We followed the analytical protocol described in [4]. O-isotopic maps of the CAI were acquired by rastering a ~3 pA primary Cs^+ beam at 16 keV over an area of 20×20 μm over a period of ~7 hours. Negative secondary ions of $^{16}O^-$, $^{17}O^-$, $^{18}O^-$, $^{28}Si^-$, $^{24}Mg^{16}O^-$, $^{27}Al^{16}O^-$, and $^{40}Ca^{16}O^-$ were simultaneously acquired using electron multiplier detectors at a mass resolving power of >10,000, sufficient to resolve the $^{16}OH^-$ interference from the $^{17}O^-$ peak. An electron flood gun was used to mitigate sample charging during the analyses. We used San Carlos olivine and Madagascar hibonite as isotopic standards to correct for the instrumental mass fractionation. The O-isotopic ratios were corrected for the quasi simultaneous arrival (QSA) effect and the detector dead time.

Results and Discussion: CAI 44 contains a grossite and hibonite-rich core with spinel and perovskite grains. This core is surrounded by a melilite layer followed by a thin diopside layer. This CAI has some alteration products including sodalite and Fe-, Zn-rich spinel (hercynite). The O-isotopic compositions of the refractory phases grossite, hibonite, spinel, melilite, as well as the alteration phase Fe-, Zn-rich spinel, and the meteorite matrix are shown in Figure 1. The spinel and hibonite have ^{16}O-rich compositions as expected [5]. The melilite layer surrounding the CAI interior has an intermediate O-isotopic composition. The core grossite exhibits a ^{16}O-poor composition, plotting at the intersection of the terrestrial fractionation (TF) line and the carbonaceous chondrite anhydrous minerals (CCAM) line. The Fe-rich spinel grains derived from grossite [6] exhibit O-isotopic compositions close to the meteoritic matrix. This suggests that the formation of grossite and its alteration phases involved a more complex scenario than simply a fluid-rock interaction on the meteorite parent body. These observations suggest that the O-isotopic variation seen in the different CAI minerals likely recorded distinct nebular reservoirs as the CAI formed, consistent with the O isotope analysis of a spinel-rich CAI from the same meteorite [7].

Figure 1: Oxygen isotopic composition of various mineral phases in CAI 44. Errors shown here are 1σ.

References: [1] Amelin Y. et al. (2010) *EPSL*, 300; 343-350, [2] Connelly J. N. et al. (2012) *Science*, 338: 651-655.[3] Yurimoto H. et al., (1998) Science 282 (5395), 1874-1877. [4] Ito M. & Messenger S. (2008) *Appl. Surf. Sci.* 255: 1446-1450. [5] Simon S. B. et al., (2019) *MAPS* https://doi.org/10.1111/maps.13282 [6] Maruyama S. & Tomioka N. (2011) *MAPS*, 46: 690-700. [7] Simon J. I. et al., (2017) *MAPS* 52: A325.

THERMODYNAMIC MODELING OF PYROXENE SOLID SOLUTIONS: REVISITING THE CONDENSATION SEQUENCE OF REFRACTORY MINERALS IN CALCIUM- AND ALUMINIUM-RICH INCLUSIONS

Venkateswara Rao Manga, Thomas J. Zega, Krishna Muralidharan
Department of materials science and engineering, University of Arizona, Tucson, AZ 85721, Lunar and planetary laboratory, University of Arizona, Tucson, AZ 85721

Introduction: Calcium-aluminum-rich inclusions (CAIs) have radiometric age dates in excess of 4.5 billion years [1,2] and are believed to be the first solids formed in the solar system. CAIs formed via condensation of the nebular gas within the high temperature region of the protoplanetary disk [3]. Stored in the crystal chemistry and structure of their constituent mineral phases is information on their high-temperature origins.

Pyroxene is among the primary phases in CAIs [4]. It can occur in meteorites in both orthorhombic and monoclinic structures, the latter of which exhibits a huge range in composition space involving three different sublattices for cation-mixing, i.e., $(Ca^{2+},Mg^{2+},..)^{M2}(Ti^{3+},Mg^{2+},Ti^{4+},..)^{M1}(Al^{3+},Ti^{4+},Si^{4+},..)^{T}_2O_6$, within its crystal structure. Thermodynamic data for the full range of compositions within this family are not known and experimental determination of them would be exceedingly challenging. As a result, condensation of many Al-Ti-rich pyroxene compostions within that family cannot be predicted using existing models in literature.

First-principles quantum-mechanics methods offer an attractive alternative approach toward determining the thermodynamic parameters of a wide range of materials and solid solutions [5]. Here we employ density functional theory (DFT), in conjunction with the available experimental data, to fill in the thermodynamic knowledge gaps of the pyroxene solid-solution family. The incorporated solid solutions in this work have a direct influence on the condensation sequence and stability of various refractory minerals under nebular conditions.

Methods: We employ thermodynamic modeling within the CALPHAD framework [6] to model condensation of mineral solid solutions by combining DFT calculations and available experimental thermochemical data with accurate crystal structure-based models. The pyroxene solid solutions of compositions, $(Ca^{2+},Mg^{2+},..)(Ti^{3+},Mg^{2+},Ti^{4+},..)(Al^{3+},Ti^{4+},Si^{4+},...)_2O_6$ in addition to the other relevant solid-solution phases such as V-alloyed $CaTiO_3$ and $MgAl_2O_4$, are modeled by employing compound-energy formalism. For the gas phase, we consider all the elements/species pertinent to the solar nebula [e.g., 7-9]. DFT calculations employing Vienna *Ab initio* Simulation Package (VASP) [10] are performed to calculate thermochemical data of the solid solutions. Special quasirandom structures (SQS) predict enthalpies of mixing in solid solutions as a function of composition with respect to their end-members. The entropic contributions to the free energy are obtained from phonons and/or a Debye-Gruneisen approach [11].

Results and Disucssion: We find that cubic perovskite is the first phase to condense with a condensation temperature between 1682 K and 1637 K in the pressure range of 10^{-3} to 3×10^{-5} bar. This result is in stark contrast to previous calculations [5-7] which invariably predict Al_2O_3 corundum as the first phase to condense from a gas of solar composition. The reason for the difference is that our calculations take into account all three polymorphs of perovskite for which we calculated the thermochemical data employing DFT. Similarly, in contrast to the previous calculations, Al-Ti-rich pyroxene with an endmember composition of $CaTiAl_2O_6$, condenses at temperatures as high as 1670 K at a total gas pressure of 10^{-4} bar. The pyroxene phase exhibits a miscibility gap with Al-Ti-rich and Mg-Si-rich phases that are stable at high- and low-temperature regions, respectively.

The revised condensation calculations have important implications for the identification of equilibirum versus non-equilibirum nature of condensation based on the reported microstructures and phase relationships within CAI mineral assemblages. Further, as revealed in this work, the incorporation of solid-solution phases that are relevant to CAI assemblages and other planetary materials, are crucial to predicting the sequence of solids that condensed and deducing thermal processes in the high-temperature region of the protoplanetary disk.

References: [1] Amelin Y. et al. (2002) *Science* 297:1678-1683. [2] Connelly J. N. et al. (2012) *Science* 338:651-655 [3] MacPherson G. J. (2005) *ASP Conference Series* 341:225-250 [4] Grossman L. and Larimer J. W. (1974) *Review of Geophysics and Space Physics* 12:71-101. [5] Turchi P.E.A et al. (2007) *CALPHAD* 31:4-27 [6] Saunders N. and Miodownik A.P. (1998) *CALPHAD (Calculation of Phase Diagrams): A comprehensive guide. Pergamon.* [7] Lodders K. (2003) *The Astrophysical Journal* l591:1220-1247. [8] Ebel D.S. and Grossman L. (2000) *Geochimica et Cosmochimica Acta* 64:339-366. [9] Yoneda S. and Grossman L. (1995) *Geochimica et Cosmochimica Acta* 59:3413-3444. [10] Perdew J.P. et al. (1996) *Physical Review Letters* 33:75-87. [11] Anderson O.L. (1995) *Equations of state of solids for geophysics and ceramic science. New York: Oxford university press.*

ASTEROID TERRESTRIAL-IMPACT LAST ALERT SYSTEM (ATLAS).

A. A. Mardon[1] and G. Zhou[2], [1]University of Alberta (aamardon@yahoo.ca), [2]George Washington University (gzhou@gwu.edu).

Introduction: The Asteroid Terrestrial-Impact Last Alert System (ATLAS) is a NASA-funded robotic survey and acts as an early warning system for asteroid impacts to Earth [1]. The current two 0.5-meter telescope system is developed and ran out of the University of Hawaii's Institute of Astronomy at two separate locations on the Hawaiian Islands. Although the ATLAS system is also used to identify drawf planets, supernova explosions and life exposure remanence from a star being absorb by a supermassive black hole in a distant galaxy, the main purpose of this project is to search for large "killer asteroids" that may have a tremendous impact on life on earth.

Summary: The Chicxulub Crater created from an asteroid impact located in the Yucatan Peninsula (Mexico) estimated to be 65 million years ago, is hypothesized to be the major contributor to the extinction of the Dinosaurs [2]. More recently, the Chelyabinsk meteor which was a near Earth asteroid entered the earth's atmosphere over Russia on February 15, 2013 exploded in the air burst generating a total kinetic energy of over 400 tons. The visible phenomenon created by the bright burning object included hot light flashes, trailing smoke and a power blast wave that shocked residents in Chelyabinsk, Kurgan, Sverdlovsk, Tyumen, and Orenburg Oblasts, the Republic of Bashkortostan, and in neighboring regions in Kazakhstan [3]. Over the lifetime of this planet, asteroids have been entering earth's atmosphere and becoming meteors with some impacting the earth with life-rocking consequences.

Although the solar system has now stabilized over the last tens of millions of years, there remains asteroids that pose a real danger to life on Earth. The system is supposed to offer one-week warning for a 50-year diameter asteroid and three weeks' notice for larger diameter, "country destroyer" asteroids [4].

Next Steps: There is now additional funding in place from NASA for two additional telescopes to be tentatively located in the Southern Hemisphere. Combined with the current two located in Hawaii, this will give NASA a fuller coverage of the entire observable sky once it is operational. Cooperation between international countries should be encouraged.

References:

[1] Wikipedia. (2019). *Asteroid Terrestrial-impact Last Alert System*. Retrieved from April 24, 2019 from https://en.wikipedia.org/wiki/Asteroid_Terrestrial-impact_Last_Alert_System

[2] National Geographic. (2013). Asteroid Impacts: 10 Biggest Known Hits. Retrieved from April 24, 2019 from https://news.nationalgeographic.com/news/2013/13/130214-biggest-asteroid-impacts-meteorites-space-2012da14/

[3] Wikipedia. (2019). *Chelyabinsk meteor*. Retrieved on April 24, 2019 from https://en.wikipedia.org/wiki/Chelyabinsk_meteor

[4] Institute of Astronomy – University of Hawaii. (2018). ATLAS: The Asteroid Terrestrial-Impact Alert System. Retrieved on April 24, 2019 from http://www.ifa.hawaii.edu/info/press-releases/ATLAS/

ASTEROID MINING AND IN-SITU RESOURCE UTILIZATION

A. A. Mardon[1] and G. Zhou[2], [1]University of Alberta, [2]George Washington University.

Introduction: Like many space exploration missions, cost is a determining factor. Transportation alone imposes a cost of $10,000 per kilogram for the entire mission making it simply not profitable or attractive to potential investors. A potential near-instantaneous solution would be to develop an asteroid mining economy developing of a human-commercial market. It is suggested that this scenario will create the economic and technological opportunities not available today. Future manned missions would require the use of native material and energy on celestial objects to support future human and robotic explorations. The process of collecting and processing usable native material is known as in-situ resource utilization (ISRU). Currently, space travelling requires missions to carry life necessities such as air, food, water and habitable volume and shielding needed to sustain crew trips from Earth to interplanetary destinations. [1] The possibility of a mission depends on the deduced market value from commercial sale of the product. Engineering choices are identified; a matrix of mineralogy, product and process choices can be developed. [2] One major consideration in the process of obtaining energy and life supporting materials from the lunar surface is the identification and excavation of raw material. [3] Lunar soil is produced primarily by meteorite impacts on the surface. This process caused for mineral fragmentation with composition consisting of miscellaneous glasses, agglutinates and basaltic and brecciated lithic fragments. The natural specific gravity of lunar soil is said to be between the values of 2.90 and 3.24. [4] Professor Xiangwu Zeng and his team at the NASA Glenn Research Center have developed a design calculation model to determine the excavation force based on basic principles of soil mechanics. Simulants with the properties of Apollo Regolith were used: the JSC1a fines, JSC1a very fines and the JSC1a. A hydrometer test was used to determine particle size. This test is based on Stoke's Equation. Unlike traditional models, the Zeng model takes into account the ability to handle acceleration of the tool blade while other models assume constant velocity. It is also able to calculate passive earth pressure. [6] The model is based on the principles of basic soil mechanics and the parameters can be determined by soil tests. These include horizontal and vertical acceleration, soil blade friction angel and external friction angel. A relationship between the total excavation force, the passive earth pressure components and the side friction and the above variables are drawn.

These principles are likely to be applied to a broad parameter aside from lunar conditions including asteroid environments. These failed planetesimals have varying composition including volatile-rich elements to metallic bodies with high concentrations of rare elements such as iron, nickel, platinum, gold, silver and other useful rare metals for human use and consumption. Due to the inherent difficulty of asteroid mining given the current level of technologies, governments and companies has not been considering asteroid mining as a feasible solution to depleting natural research on Earth. Cost analysis have shown that a cost for a future mission to return 500-ton asteroid to low earth orbit would be in the range of $2.6 billion USD which does not include the initial capital costs for infrastructure and technological development and testing [7]. Challenges include difficulty in categorization and identification of mineral deposits, infrastructure development to develop, refine and transport processed materials back to earth [7] as examples. Significant advances in robotic technology will be part of the equation to overcoming such challenges.

Conclusion: The results find the Zeng model have high dependence on soil cohesion and therefore forms a linear relationship with the amount of excavation force needed for ISRU. The results will deviate from the actual lunar specimen as simulants were used for the experiments. The use of real samples may give a more accurate understanding of soil properties and experimental results. Although this investigatory tool can be used on a broad basis including under asteroid conditions, current technology is still being developed to bring down the massive initial capital costs down for asteroid mining to becoming a reality. There are many challenges as outlined above that needs to be considered and resolved to making asteroid mining a feasible solution.

References:

[1]. National Aeronautics and Space Administration. (2005). In-Situ Resource Utilization (ISRU) Capability Roadmap Final Report. Retrieved from http://www.lpi.usra.edu/lunar_resources/docments/ISRUFinalReportRev15_19_05%20_2_.pdf
[2]. Sonter, M. J. (1998). The Technical and Economic Feasibility of Mining the Near-Earth Asteroids. Retrieved from http://www.spacefuture.com/archive/the_techncal_and_economic_feasibility_of_mining_the_near_earth_asteriods.shtml.
[3]. [4]. Carrier, W.D., Costes, N.C., Houston W.N., & Mitchell, J.K. (1974). Apollo Soil Mechanics ExperimentS-200. Space Sciences Laboratory, 7, 1-135.
[5]. [6]. Agui, J.H., Burnoski, L. Wilkinson A., & X. Zeng. (2007). Calculation of Excavation Force for ISRU on Lunar Surface. Cleveland, OH: NASA Glenn Research Center.
[7] Massachusetts Institute of Technology (2016). Asteroid Mining. Retrieved from http://web.mit.edu/12.000/www/m2016/finalwebsite/solutions/asteroids.html

PREHISTORICAL MARTIAN PERMAFROST FROM METEORITICAL EVIDENCE

A. A. Mardon[1] and G. Zhou[2], [1]University of Alberta, [2]George Washington University.

Introduction: Terrestrial permafrost is sustained on Earth in vast expansive regions with surface temperatures below the water freezing point. Specifically, in Antarctica where the average surface temperature does not exceed the freezing point, specific surface change processes are not present. This includes frost heaving, patterned ground formation, soifluction, gelifluction, cryoplanation, thermokarst, etc.[1] This is because a water-containing active layer does not form at the top layer. These features characteristic of active layer processes are apparent on Martian surface, especially, at the northern and southern polar caps. Using high resolution surface images provided by MOC camera, several types of permafrost-related features are witnessed but we will focus on Martian polygons. Martian polygons share similarities to terrestrial ice wedges which is the result of surface modifications due to activities of the active layer of permafrost. Terrestrial polygon-shaped areas are also common in regions with fine grained sediments such as in the North and Norwegian Sea. [2] This suggests that, where surface temperature routinely exceeds the water freezing point such as around the equatorial zone, there may have existed seasonal temperature fluxations. This condition may have created an ideal environment for the thawing and sublimation of ice in Martian permafrost. However, the current data that has been collected in this region, suggests that there is currently no water available for the creating of an active zone. Since there is currently no permafrost present, it is assumed that if Martian polygons were to have formed due to permafrost-related processes that it needed to have been from a different climatic regime. The probable explanations for the formation of an active layer in prehistoric times are many. Astronomical forcing which describes the planetary spin and orbit parameters may have greatly influenced the creation of an active layer. The eccentricity of Mars and the characteristics of its spin axis may cause regular patterned fluctuations that can influence surface temperature. The obliquity of the planet's axial tilt is also thought to be a strong driver for planetary climate change that may have given rise to an active layer in pre-historical Martian permafrost. [3] If Martian permafrost exists today, there should be substantial differences in characteristics between terrestrial and Martian permafrost. Assuming the atmospheric properties were relatively similar in the past as it is in the present, the thin atmosphere, as well as, the non-existence of greenhouse gases, suggests that the planet has an annual average surface temperature below the water freezing point. Cold permafrost would form in this condition; however, no active layer would be present due to lack of temperature fluctuations. Should there be fluxations above the water-freezing point such as in the summer around the equatorial zone, the thickness of an active layer is likely to be similar between that of Mars and Earth. The reasoning behind this is because although there may be a thinner active layer due to lower cold season temperatures slowing the propagation of the thawing wave, this is off balanced by the warmer season due to longer summer days at high obliquity. [4] Based on historical data relating to the changes of Martian obliquity, the angle of twist is likely to remain the same. With the understanding that the obliquity of the planet to be a major driver of climate change, it is not likely that temperature conditions will change substantially from what exists today and therefore permafrost and the formation of an active layer is unlikely.

Usui et. al. found that through their investigations and research that the evolution of surface water and ice formation on the Martian surface and its interaction with the atmosphere can be measured using hydrogen isotopes found in meteorites. The hypothesis that deeply buried permafrost layer has potentially survived under Martian hydraulic and thermal condition is supported and needs further investigations [5].

References:

[1], [3], [4] Kreslavsky, M. A., Head, J.W. ,and Marchant D.R. (2007). Periods of active permafrost layer formation during the geological history of Mars: Implications for circumpolar and midlatitude surface processes. *Planetary and Space Science*: 56, 289–302.

[2] Moscardelli, L., Dooley, T., Dunlap, D., Jackson, M., and Wood L. (2012). Deepwater polygonal fault systems as terrestrial analogs for large-scale Martian polygonal terrains. *The Geological Society of America Today*, 22, 4-9.

[5] Usui, J.H., Jones, J.I., Simon, C.M. Alexander, & J. Wang. (2014). Evidence from Hydrogen Isotopes in Meteorties from a Martian Permafrost. 45th Lunar and Planetary Science Conference.

CHLORINE ABUNDANCE IN THE SHERGOTTITE PARENTAL MELT AMPHIBOLE AND APATITE IN TISSINT AND ZAGAMI

N. Mari[1], L. J. Hallis[1], and M. R. Lee[1]
[1]School of Geographical and Earth Sciences, University of Glasgow, Glasgow, UK. Email: n.mari.1@research.gla.ac.uk.

Introduction: Volatile abundances in amphibole and apatite can be used to estimate the volatile content of their parental melts and mantle source regions in Martian meteorites. It has been suggested that the Martian parental melts which produce the shergottites had water/chlorine and water/fluorine ratios of ~0.4–18, similar to terrestrial MORB ratios [1]. Amphibole differs in composition among Martian meteorites. Shergottite amphibole is generally Cl-poor [2], whereas nakhlite and chassignite amphibole is Cl-rich – reportedly due to the interaction of the nakhlite parental melt with surficial/subsurface fluids [3]. This study investigates the composition of amphibole in two shergottites - Tissint and Zagami. In addition, previously unreported apatite was analysed in Tissint. Using the Cl content of amphibole and apatite, along with previously published Cl partition coefficients for these minerals [4, 5], the abundance of Cl in the parental melts of these meteorites can be calculated.

Methods: Tissint and Zagami were selected for this study as both meteroites had been previously reported to contain amphibole within their pyroxene-hosted melt inclusions [2,6]. Major element chemical data and X-ray elemental maps were obtained from thin sections of both meteorites at the Imaging Spectroscopy and Analysis Centre of the University of Glasgow (UoG) using a Zeiss-Sigma variable pressure field emission gun scanning electron microscope (VP-FEG-SEM), equipped with backscattered electron and EDS detectors. Amphibole-rich areas of interest were then extracted from thin-sections using a dual column FIB-SEM at UoG. These FIB-sections were subsequently chemically and crystallographically analysed using the UoG JEOL ARM200cF MagTEM (with EDS capabilities) and FEI Tecnai T20, respectively.

Results: All amphibole and apatite in Tissint and Zagami are present within pigeonite-hosted melt inclusions. Amphibole grains were found with up to 8 µm diameter in Tissint, and 10 µm diameter in Zagami. Apatite in Tissint has similar Cl content to Zagami apatite (from 0.02 to 0.26 wt.%). In both meteorites amphibole contains low Cl abundances (< 2 wt.%). These Cl abundances suggest the abundance of Cl in the shergottite parental melt is between 1789 ppm (calculated from apatite) and 1560 ppm (calculated from the amphibole). These low shergottite Cl values contrast with the Cl-rich chassignite and nakhlite parental melt values (0.3 and 16 wt.%, respectively) [1, 4].
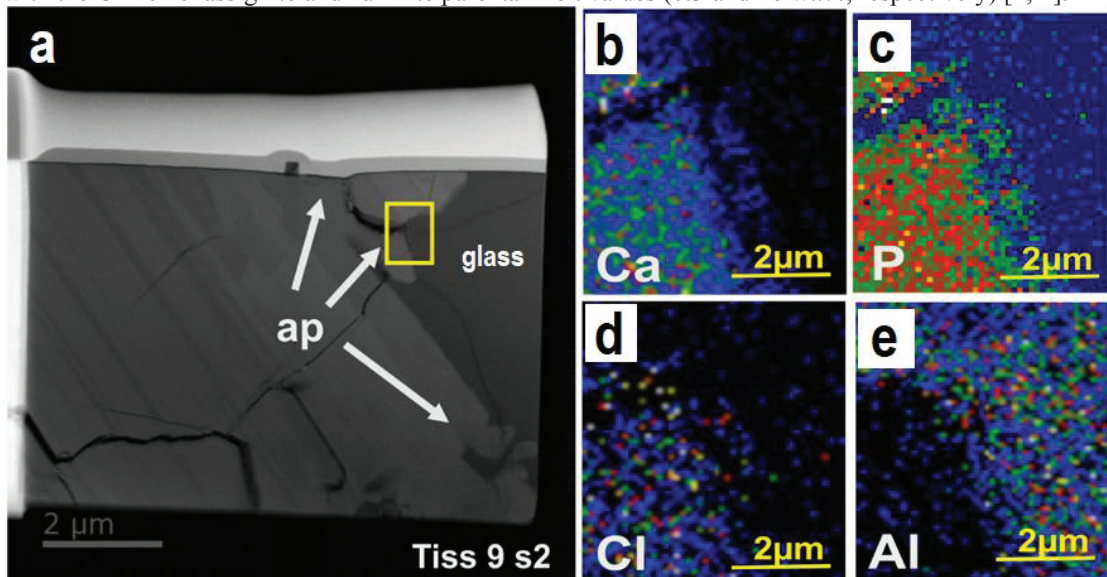

Fig. 1 – TEM images of a Tissint FIB-section containing the largest apatite (~8 µm diameter) detected in this study. (a) Dark-field image of the FIB-section containing the apatite, white arrows indicate the apatite grains; (b, c, d, e) Ca, P, Cl, and Al elemental maps of the area highlighted in yellow in (a).

References: [1] Filiberto J., Gross J., and McCubbin F. M., 2016. *Meteoritics & planetary Science* 51:2023–2035. [2] Williams K. B., Sonzogni Y., and Treiman A. H., 2014. *LPS XXXXV,* Abstract #1435. [3] McCubbin F. M., Elardo S. M., Shearer C. K., Smirnov A., Hauri E. H. and Draper D. S., 2013. *Meteoritics & Planetary Science* 48:819-853. [4] Filiberto J. and Treiman A. H., 2009. *Geology* 37:1087-1090. [5] Li H. and Hermann J., 2017. *American Mineralogist* 102:580-594. [6] Treiman A. H., 1985. *Meteoritics* 20:229-243.

THERMAL CONDITIONS OF FLUID CIRCULATION IN HYDRATED ASTEROIDS

Y. Marrocchi[1], L.G. Vacher[1,2] and M. Piralla[1]
[1]CRPG, CNRS, Université de Lorraine, UMR 7358, Vandoeuvre-lès-Nancy, 54501, France (yvesm@crpg.cnrs-nancy.fr), [2]Department of Physics, Washington University in St. Louis, St. Louis, MO, USA,

Introduction: Asteroids are super-kilometer-sized bodies formed by gravitational instability in turbulent regions of the protoplanetary disk. Hydrated C-type asteroids −the most common bodies in the main asteroid belt experienced subsequent heating due to heat released by the decay of ^{26}Al. However, quantitative estimation of their thermal histories has not yet been possible, leading to considerable uncertainty on the physical characteristics of early-formed primitive rocky bodies. Aqueously-formed carbonaceous chondritic minerals such as carbonates represent direct snapshots of the asteroidal fluids and can in theory be used to decipher their thermal evolution. However, determining carbonate precipitation temperatures requires knowing the O-isotopic compositions of their parent fluids, which itself requires to know the carbonate precipitation temperatures, leading to a seemingly endless problem. Here we report *in situ* O-isotopic analyses of Ca-carbonates and propose a new isotopic alteration model that reconciles petrographic observations and formation temperatures of CM carbonates.

Methods: Detailed observations of calcite grains in polished sections of the CM2 Murchison and Mukundpura were made using a scanning electron microscope (SEM) JEOL JSM-6510 equipped with an Energy Dispersive X-ray (EDX) Genesis detector. Their oxygen isotopic compositions were determined using a CAMECA ims 1280 HR2 ion microprobe at CRPG (Nancy, France).

Results: Only calcite grains surrounded by serpentine (hereafter T1 calcite) were found in the two polished sections of Murchison. O-isotopic measurements show that Murchison's T1 calcites have δ^{18}O values between 25.5 and 41.5‰, δ^{17}O values between 14.5 and 23.5‰ and Δ^{17}O values between -1.1 and 1.8‰ (n = 24). In contrary, two types of carbonates were found in the polished section of Mukundpura: (i) T1 calcite grains and (ii) polycrystalline grains of calcite containing Fe-Ni sulfide inclusions (hereafter T2 calcite). O-isotopic analyses on Mukundpura's Ca-carbonates reveal that (i) T1 calcites have δ^{18}O values between 27.4 and 38.2‰, δ^{17}O values between 13.3 and 18.5‰ and Δ^{17}O values between -1.4 and -0.2‰ (n = 8), whereas (ii) T2 calcites have δ^{18}O values between 12.4 and 18.6‰, δ^{17}O values between 4.2 and 7.3‰ and Δ^{17}O values between -4 and -0.9‰ (n = 13).

Discussion: Our data define a mass-independent trend that is similar, within errors, from those commonly reported in different CM chondrites [1-3]. In first approximation, this trend suggest that the O-isotopic compositions of CM carbonates is essentially controlled by variable degrees of isotopic exchanges between ^{16}O-rich anhydrous silicates and a $^{17-18}$O-rich fluid [4]. However, when considering only T1 calcites, their O-isotopic compositions define a distinct trend that is indistinguishable, within errors, from the TFL (i.e., average Δ^{17}O = - 0.4 ± 1.0). Conversely, T2 calcites exhibit clustered δ^{17}O- δ^{18}O values with average Δ^{17}O of -2.6 ± 1.0, which artificially generate the aforementioned mass-independent trend. This demonstrates that petrographic observations of carbonates are essential for understanding the O-isotopic evolution of asteroidal fluids and the constraints they bear.

Direct estimations of the O-isotopic composition of asteroidal alteration fluids was possible thanks to CO_2 clumped-isotope thermometry (Δ^{47}, [5]). Based on measurements performed on the T1 calcite-dominated CM chondrites Murchison and Murray, this led to alteration fluids ranging from δ^{18}O = 2 ‰ and Δ^{17}O = - 0.55 ‰ to δ^{18}O = 6.8 ‰ and Δ^{17}O = - 0.49 ‰. As these fluids experienced oxygen isotopic exchanges with the anhydrous CM chondrite protolith (δ^{18}O = -3.8 ‰, δ^{17}O = -6.5 ‰; [6]), they define two trends that delimit the possible O-isotopic compositions of the alteration fluids. Considering these extreme trends, the precipitation temperatures of each calcite and serpentine can be calculated according their respective isotopic fractionation factor α. Our isotopic approach allows a formation sequence of CM secondary phases to be proposed, characterized by a temperature increase from T1 calcites < serpentines < T2 calcites. This implies that fluid circulation in CM parent body-(ies) occurs during a prograde evolution of the temperature, where T1 calcites formed first at T = 0-30 °C, followed by the precipitation of (Fe,S)-rich serpentine and tochilinite at T = 30-100°C and then T2 calcites at T = 110-140°C.

References:
[1] Vacher L. G. et al. (2016) *The Astrophysical Journal Letters* 827:1–6. [2] Marrocchi Y. et al. (2018) *Earth and Planetary Science Letters* 482:23-32. [3] Vacher L. G. et al. (2017) *Geochimica et Cosmochimica Acta* 213:271–290. [4] Verdier-Paoletti M. J. et al. (2017) *Earth and Planetary Science Letters* 458:273–281. [5] Guo W. and Eiler J. M. (2007) *Geochimica et Cosmochimica Acta* 71:5565–5575. [6] Clayton R. N. and Mayeda T. K. (1984) *Earth and Planetary Science Letters* 67, 151–161.

SMOOTH RIMS IN QUEEN ALEXANDRA RANGE (QUE) 99177: THE EARLIEST STAGES OF FLUID-ROCK INTERACTIONS IN THE MOST PRISTINE CR CHONDRITE

M. Martínez[1] and A. J. Brearley[1], [1]Department of Earth & Planetary Sciences, The University of New Mexico, Albuquerque, New Mexico 87131, USA (mmartinezjimenez@unm.edu).

Introduction: The CR carbonaceous chondrites are highly primitive meteorites that escaped thermal metamorphism and exhibit a complete aqueous alteration progression, from nearly intact nebular materials to full replacement by secondary alteration products [1-3]. The least-altered CR chondrite, Queen Alexandra Range (QUE) 99177 [3-5], is an excellent sample to study the earliest stages of aqueous alteration that affected pristine solar system materials. In this work, we focus on the characterization of smooth rims around the periphery of chondrules in QUE 99177, because they can provide information on the chemical and isotopic evolution of the altering fluid(s) that were present in the matrix and modified the anhydrous phases in chondrules. Previous studies on smooth rims [2,6,7] suggested that they are the result of interaction of fluids present in the matrix with chondrules, but the precursor of the rims and the mechanisms of their formation remain unconstrained. Here, we aim to characterize the phases that constitute smooth rims in QUE 99177, unravel their formation mechanisms, and constrain the precursor materials of the rims.

Experimental procedure: Representative smooth rims around seven chondrules and corresponding adjacent matrices from two thin sections of QUE 99177 were studied using Scanning Electron Microscopy (SEM), Transmission Electron Microscopy (TEM), and Electron Probe Micro-Analysis (EPMA). TEM work was performed on FIB sections obtained using a FEI Quanta 3D Dualbeam® FEG-SEM/FIB instrument.

Results: Smooth rims represent about ~70% of the total rims in QUE 99177 and they are texturally very distinct from fine-grained and coarse-grained rims, because individual grains cannot be resolved even by FEG-SEM. Smooth rims have thicknesses up to 30 µm and exhibit two distinct Z-contrasts in backscattered imaging: darker patches are irregular in shape (~5-30 µm) and randomly distributed in a lighter groundmass. Smooth rims are also texturally very distinct from the matrix and the interface is very sharp, sometimes decorated with micron-sized sulfur grains. Smooth rims are typically found on the edges of chondrules with silica-rich igneous rims (SIRs) [8], characterized by the presence of silica grains, which appear to have been partially replaced.

Chemical Composition. EPMA data show that the smooth rim compositions are dominated by SiO_2 and FeO (37.4 and 37.0 wt%, respectively, averaged data of 111 analyses in seven chondrules) with minor other elements that constitute <10 wt%. The average EPMA total for smooth rims measured using a 3-5 micron beam size is ~83.5 wt%, lower than the adjacent matrices, which is ~88.4 wt%, indicating an elevated degree of hydration. In comparison with adjacent matrix materials, the smooth rims are generally S- and Ni-free, and enriched in Fe, Mn, Al, and Ca, although there is some overlap between the two datasets. Alkalis are variable and do not show any systematic relationship.

TEM results. Smooth rims are mainly (~70%) composed of an Fe- and Si-rich phase that electron diffraction shows is amorphous. Anhedral, equant crystals of pyroxene (~1 µm-size) occur isolated or as elongated arrays embedded within the amorphous silicates. These pyroxenes are Mn-rich (~7.5 MnO wt%), with two distinct compositions; Ca-rich from diopside to augite, and Ca-poor from pigeonite to ferrosilite. Crystalline, anhedral to euhedral albite and alkali-bearing silica-rich glass (0.5-1 µm-size) also occur interstitially to the regions of the amorphous silicates.

Discussion and conclusions: There is very little information on the effects of aqueous alteration on chondrules in the least-altered CR chondrites such as QUE 99177. Previous studies, focused on alteration of chondrule glass in type IIA chondrules, have shown that glass exhibits limited evidence of interaction with an aqueous fluid [9]. Our new data show that smooth rims in QUE 99177 formed by aqueous alteration of an igneous precursor that is extremely susceptible to alteration. Several lines of evidence suggest that this precursor is silica in SIRs. This is consistent with (i) the presence of silica relicts in the smooth rims, (ii) the outlines of the amorphous silicate regions, which are often straight or curved, indicating that they represent the replacement of primary crystals, and (iii) the compositional similarity of the amorphous material to silica replacement products [6]. The remarkable occurrence of the hydrated amorphous alteration products of silica in direct contact with very fine-grained regions of unaltered alkali-bearing glass and albite demonstrates that silica is extremely susceptible to aqueous alteration. These new discoveries thus show that silica is a highly sensitive monitor of the earliest stages of fluid-rock interaction and additionally, the presence of smooth rims is not necessarily indicative of higher degrees of alteration for QUE 99177, as previously suggested [2].

References: [1] Howard K. T. et al. (2015) *Geochimica et Cosmochimica Acta* 149:206–222. [2] Harju E. R. et al. (2014) *Geochimica et Cosmochimica Acta* 139:267–292. [3] Abreu N. M. and Brearley A. J. (2010) *Geochimica et Cosmochimica Acta* 74:1146–1171. [4] Floss C. and Stadermann F. (2009) *Geochimica et Cosmochimica Acta* 73:2415–2440. [5] Schrader D. L. et al. (2011) *Geochimica et Cosmochimica Acta* 75:308–325. [6] Jones R. H. et al. (2015) *Met. Soc. Meeting LXXVIII*, Abstract #5190. [7] Abreu N. M. (2016) *Geochimica et Cosmochimica Acta* 194:19–122. [8] Krot A. N. et al. (2004) *Meteoritics & Planetary Science* 39:1931–1955. [9] Martínez-Jiménez M. and Brearley A. J. (2018) *LPS XLIX*, Abstract #2274.

X-RAY MICROTOMOGRAPHY SHOWS ELLIPSOIDAL INCLUSION-FREE HALO AROUND CUBIC PHASE IN BRAZILIAN CARBONADO: FIRST STRAIN ANALYSIS OF PRE-SOLAR MATERIAL?

S. Master[1], L. Bam[2], J. Karfunkel[3], [1]EGRI, School of Geosciences, University of the Witwatersrand, Johannesburg, South Africa, sharad.master@wits.ac.za; [2]Radiation Science, Nuclear Energy Corporation of South Africa, Pretoria, South Africa, [3]Universidade Federale de Minas Gerais, Belo Horizonte, Minas Gerais, Brazil.

Introduction: Carbonado is a microcrystalline form of diamond, with a porous structure, found in diamondiferous gravels in Brazil and Central African Republic (CAR). It contains inclusions of highly reduced phases and native metals, such as SiC, FeC, Si, Ti, TiN, Fe-Cr, Ni and Ag, and secondary REE-phosphates like florencite, and is not found in kimberlites where gem macro-crystalline diamonds originate [1]. The origin of carbonados is still a very contentious issue, with the latest ideas arguing against a terrestrial origin, but there is no consensus about which extra-terrestrial environment carbonados formed in [1].

Carbonado from Brazil: A carbonado from CAR was examined using X-ray microtomography by [2], who found pseudomorphs, up to 0.3mm across, after what they interpreted as a primary dodecahedral phase. In this study we examine a Brazilian carbonado from the <1.16 Ga Macaubas Group, Minas Gerais [3], also using microfocus X-ray tomographic techniques. We used lower energies and long scans to enhance the contrast between phases of differing densities and X-ray attenuation, with a resolution of 5.2 μm. In common with observations on other carbonados, we have found evidence for a fabric in the Brazilian carbonado, showing up as a preferred planar alignment of inclusions. We also find a thin surficial zone free of inclusions next to surfaces showing a high patina. In addition, we have discovered novel macrostructures, in the form of large inclusion-free haloes (≤ 2.4 mm diameter) surrounding extra-large crystal inclusions (≤1 mm across and 1 mm^3 in volume), which seem to have a cubic morphology.

Strain Analysis: The depleted halo would originally have been spherical in an isotropic medium. Our measurements show it has the shape of a triaxial oblate ellipsoid slightly flattened parallel to the plane of preferred orientation of inclusions (XY) with dimensions a:b:c= 320μm:302μm:237μm (where a>b>c). Using the strain ellipsoid, the following parameters were calculated: R_{XY} = 1.06; R_{YZ} = 1.27; k = $(R_{XY}-1)/(R_{YZ}-1)$ = 0.22; d = $[(R_{XY}-1)^2+(R_{YZ}-1)^2]^{0.5}$ = 0.27; % shortening = 100(1- [1/R_{XZ}]) = 25.8%. On a Flinn Diagram (R_{XY} vs R_{YZ}), the ellipsoid plots in the field of flattening strain, where 1>k ≥0. This may be the first measured strain ellipsoid in presolar material, and alludes to regions of high stress, possibly in the pre-solar nebula, following the crystallization of carbonados and their primary inclusions. The resultant strain may have been aided by high temperatures produced by radioactive decay of large amounts (more than a few weight %) of U and Th in the primary inclusions in the carbonados. The nature of the original mineral making up the large primary crystals in the centre of the inclusion-free ellipsoids is still unknown, and further studies are needed. Apparent interfacial angles of close to 90° have been measured in a large crystal inclusion within the carbonado, surrounded by a large inclusion-free halo. The crystal was replaced by a secondary phase (which appears medium grey in grey-scale rendering) which was partly removed by dissolution, and then a dense phase (appearing white; probably florencite) was deposited in the cavity.

References: [1] Haggerty, S., 2014. Earth-Science Reviews, 130, 49-72. [2] Ketcham, R., Koeberl, C., 2013. Geosphere, 9(5), 1336-1347. [3] Martins, M., et al., 2008. Revista Brasileiras do Geociências, 38(4), 761-772.
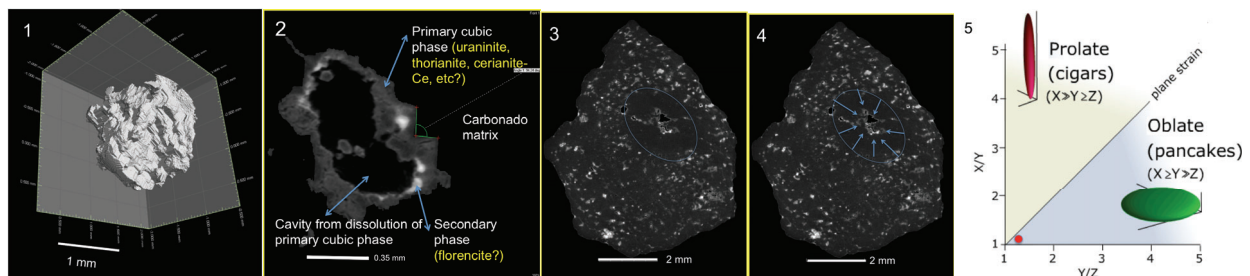
Figures. 1. A 1 mm^3 cubic crystal in centre of the carbonado. 2. Large cubic crystal in carbonado matrix, partly dissolved away, and replaced by a dense secondary phase, possibly florencite. 3. Cross sectional view through carbonado with numerous dense mineral inclusions, showing large cubic crystal surrounded by inclusion-free elliptical halo. 4. Possible growth mechanism of large cubic crystal from concentration of components in surrounding carbonado matrix, resulting in inclusion-free halo. 5. Flinn diagram showing the oblate nature of the inclusion-free halo surrounding the large cubic crystal in the carbonado (red dot).

FIRST EVIDENCE FOR AN IMPACT ORIGIN OF THE >45 km DIAMETER SIMLIPAL RING STRUCTURE, SINGHBHUM CRATON, ODISHA, INDIA

S. Master[1,2], G.R.J. Cooper[2], T.M. Chakraborti[3], T. Mukherjee[4]. [1]EGRI, [2]School of Geosciences, University of the Witwatersrand, Johannesburg, South Africa, sharad.master@wits.ac.za, [3]Department of Geology, Presidency University, Kolkata, West Bengal, India, [4]Geological Survey of India, Kolkata, West Bengal, India.

Introduction: The Simlipal Basin consists of a 2-3 km-thick sequence of supracrustal rocks deposited on 3.44 Ga TTG gneisses, and 3.3 to 3.12 Ga granites and greenstone belts of the Archean Singhbhum Craton, in NE Odisha, Eastern India [1,2]. Lithologically, the Simlipal Basin is made up mainly of basaltic lavas and pyroclastics interbedded with three quartzite units, the lowest of which also contains conglomerates [1,2]. The basin outcrops in the form of a concentric ring structure (centered on 21°52'07.66" N; 86°20'08.75" E), with a diameter of c. 45 km, situated within a NNE-SSW trending plateau with a long axis of about 70 km (Fig. 1A). The beds within the ring structure dip inwards at angles varying from 18 to 76° towards the centre. Three topographic rings are defined by the resistant quartzites (Fig. 1B). The centre of the Simlipal Structure is occupied by an 800m-thick differentiated ultramafic-mafic intrusion, the Amjori Sill, covering an area of 130 km^2. The layers consist, from bottom to top, of dunite, peridotite, picrite, gabbro, and quartz norite [1,3]. The basalts of the Simlipal ring structure are intruded by the Mayurbhanj suite of gabbros, granophyres, and pyroxene granites, dated at 3.09 Ga [2], thus the age of the structure is constrained between 3.12 and 3.09 Ga. There is a gravity high in the centre of the structure, with a bouguer anomaly rising steadily from -25 mgal at the edge of the structure, to about -10 mgal at 5km from the centre [4]. Then there is a change in slope, with the central part of the structure having a sharper increase in the gravity anomaly, to -2 mgal at the centre, modeled as being due to a thick mafic volcanic unit [4].

Evidence for Impact Origin- shatter cones: Few processes on earth, aside from impact cratering, can form a large circular structure with inward dipping beds, in a cratonic setting, such as the Simlipal Structure. The first evidence for an impact origin of the Simlipal Structure has been found at a locality called Uski Falls, ~6 km NW from the geometric center of the ring structure. Outcrops here consist of massive basalts, some containing large unfilled vesicles and lithophysae. Numerous examples of partial shatter cones, and clusters of amalgamated shatter-cone-type striated and curved, corrugated surfaces are present on the loose basalt boulders at the foot of the Uski Falls. In some boulders, there are multiple examples of shatter cones, in different orientations. The partial shatter cones consist of conical striated surfaces, with striations radiating out from the cone apex. Some shatter cones have the appearance of being twisted or almost braided. The largest shatter cone measured 14 cm in length (Fig. 1C). The apical angle is typically 35 degrees or less. In the NW, outer parts of the structure, centripetally-dipping crossbedded quartzites young normally, and are not overturned, and *in situ* brecciated basalt has been observed.

We consider the presence of shattercones as the best macroscopic evidence for shock metamorphism in the Simlipal Structure, which we regard as being of impact origin. The gravity profile [4] indicates a 3 km-thick central intrusion, which we regard as an undeformed, horizontally bedded differentiated impact melt sheet occupying the inner part of a central peak ring within a large complex impact structure, similar to the differentiated melt sheet in the Sudbury structure. *In situ* brecciated and slickensided felsites are present in the older basement rocks on the outside of structure, to the north. At a radius of 84 km from the center, there is an outer arc of greenstone belt rocks, but they are not concentric with, and are probably unrelated to, the Simlipal Structure. Further field, petrographic, geochemical and remote sensing studies are planned on the Simlipal Structure and surrounding areas. The location of the Simlipal Tiger Reserve (and future National Park) wholly within the Simlipal Structure will ensure that these rocks will be conserved and protected in the future, and they may also serve as a drawcard for scientific studies, geotourism, ecotourism, and earth and planetary science education.

References: [1] Iyengar, S.V.P., et al., 1981. Indian Journal of Earth Sciences, 8, 61–65. [2] Mishra, S., et al., 1999. Precambrian Research, 93, 139-151. [3] Chennakesavulu, N., Sahu, K.C., 1985. The Indian Mineralogist, 22(2), 231. [4] Verma, R.K., et al., 1984. Tectonophysics, 106, 87-107.
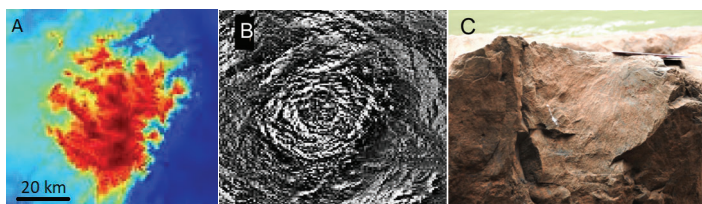

Figure 1. (A) Digital Elevation Model of Simlipal Structure, derived from SRTM data (B) Centrally-illuminated sunshaded DEM of (A), showing concentric topographic rings (C) Large (14 cm radius) partial shattercone in basalt, Uski Falls

HEATING HISTORY OF IGNEOUS RIM FORMATION DEDUCED FROM MICRO-SCALE MIGRATION OF OXYGEN ISOTOPES

N. Matsuda[1], N. Sakamoto[2], S. Tachibana[1,3] and H. Yurimoto[1,4], [1]Department of Natural History Sciences, Hokkaido University, Sapporo 060-0810, Japan (e-mail address: nozomi@ep.sci.hokudai.ac.jp), [2]Isotope Imaging Laboratory, Creative Research Institution, Hokkaido University, Sapporo 001-0021, Japan, [3]UTokyo Organization for Planetary and Space Science (UTOPS), University of Tokyo, Tokyo 113-0033, Japan. [4]Institute of Space and Astronautical Science, Japan Aerospace Exploration Agency, Sagamihara, Kanagawa, 252-210, Japan.

Introduction: The ubiquitous occurrence of igneous rims across the chondrite groups suggests that igneous rim formation commonly occurred in the solar nebula and is related to chondrule formation [e.g., 1-3]. The rim formation process is not well understood compared with chondrule formation, especially the heating duration to form the igneous rim. Olivine grains within igneous rims sometimes contain extreme ^{16}O-rich areas in their interiors [3]. Such extreme ^{16}O-rich olivines cannot form during chondrule formation because the oxygen isotopic compositions of the minerals crystallized from the melted chondrules are typically close to those of the rocky planets [4]. Therefore, the extreme ^{16}O-rich olivines are the igneous rim feedstocks and heating process survivors from the igneous rim formation. The rim formation process could be traced from the extreme ^{16}O-rich olivine. In this study, we focus on two-dimensional chemical and oxygen isotopic distributions in an igneous rim of a chondrule within CV_{oxA} chondrite with sub-micrometer resolution in order to constrain the rim formation process.

Sample and Analytical methods: A porphyritic FeO-poor olivine chondrule with an igneous rim in a polished thin section of Northwest Africa 3118 CVoxA chondrite was used in this study. The petrographic observation and chemical analysis were performed by FE-SEM (JEOL JSM-7000F) equipped with an EDS (Oxford X-Max 150). Crystal orientation analysis was conducted by an EBSD (Oxford HKL) on the FE-SEM. Point analyses of oxygen isotopes of individual rim grains were performed using a secondary ion mass spectrometer (Cameca ims-1280HR). Quantitative oxygen isotope distribution within the rim was obtained by the Hokudai isotope microscope system (Cameca ims-1270 + SCAPS).

Results and discussion: The chondrule with type I porphyritic texture is completely surrounded by a coarse-grained igneous rim. The coarse-grained rim is mostly dominated by olivine. The olivine grains are rich in FeO compared with those within the host chondrule (Fa_{2-5}). The FeO contents show a bimodal distribution with peaks at MgO-rich (Fa_{11-22}) and FeO-rich (Fa_{40-49}) compositions. The oxygen isotopic composition ($\delta^{17}O = 2.0 \pm 1.8$ (2σ) ‰, $\delta^{18}O = 8.1 \pm 3.6$ ‰), the mass-dependent isotope fractionation, and the porous texture filling between the MgO-rich olivine grains indicate that the FeO-rich olivine precipitated from an aqueous fluid with ^{16}O-poor composition on the parent body. The MgO-rich olivine shows Fe-Mg chemical zoning at the interface to the FeO-rich olivine (Fa_{40-49}), indicating that Fe-Mg inter-diffusion occurred during the aqueous alteration on the parent body. The disturbance of Fe-Mg distribution in the MgO-rich olivine (Fa_{11-22}) due to the aqueous alteration is only limited to a 1 µm scale. Under the parent body alteration condition, no oxygen isotopic disturbances can be achieved at a scale greater than 0.1 µm using any oxygen self-diffusion coefficients. The oxygen diffusion scale across the FeO-rich and MgO-rich olivine is smaller than the spatial resolution of the oxygen isotopography (0.8 µm). The MgO-rich olivine, a primary phase of igneous rim formation, has oxygen isotopic compositions of $\delta^{17}O = -5.6 \pm 3.2$ ‰, $\delta^{18}O = -0.7 \pm 3.6$ ‰, and sometimes contains extreme ^{16}O-rich areas ($\delta^{17, 18}O = \sim-30$ ‰) nearly <10 µm across. We detected an oxygen isotopic migration of about 1 µm at the boundaries of the extreme ^{16}O-rich areas, which should reflect oxygen diffusion during the rim formation. Considering oxygen self-diffusivity, the igneous rim formation could have continued from several hours to several days at near liquidus temperatures (~2000 K) in the solar nebula. The calculated heating duration was similar to those for a chondrule formation event that was molten for up to several tens of hours [e.g., 5, 6], suggesting that the igneous rim was also formed during transient heating events.

References: [1] Rubin A. E. (1984) *Geochimica et Cosmochimica Acta* 48:1779–1789. [2] Krot A. N. and Wasson J. T. (1995) *Geochimica et Cosmochimica Act* 59:4951–4966. [3] Nagashima K. et al. (2015) *Geochimica et Cosmochimica Act* 151:49–67. [4] Yurimoto H. et al. (2008) *Reviews in Mineralogy and Geochemistry* vol68:141–186. [5] Hewins R. H. (1996) *In Chondrules and the Protoplanetary Disk*:3–9. [6] Hewins R. H. et al. (2005) *In Chondrites and the Protoplanetary Disk*:286–316.

ULTRA POROUS LITHOLOGY, A FOSSIL ASTEROIDAL ICE, IN CARBONACEOUS CHONDRITE ACFER 094: IMPLICATIONS FOR PARENT BODY FORMATION BY ICY DUST AGGLOMERATION.

M. Matsumoto[1,2], A. Tsuchiyama[2,3,4], A. Nakato[2,5], J. Matsuno[2], A. Miyake[2], A. Kataoka[6], M. Ito[7], N. Tomioka[7], Y. Kodama[8], K. Uesugi[9], A. Takeuchi[9], T. Nakano[10], E. Vaccaro[11].
[1]Departmet of Earth and Planetary Materials Science, Tohoku University, Miyagi, Japan. [2]Division of Earth and Planetary Sciences, Kyoto University. [3]Research organization of Science and Technology, Ritsumeikan University. [4]Guangzhou Institute of Geochemistry. [5]Institute of Space and Astronautial Sceince, Japan Aerospace Exploration Agency. [6]National Astronomical Observatory of Japan. [7]Kochi institute for Core Sample Research, Japan Agency for Marine-Earth Science and Technology. [8]Marine Works Japan Ltd. [9]Japan Synchrotron Radiation Research Institute. [10]Geological Survey of Japan, National Institute of Advanced Industrial Science and Technology. [11]Department of Earth Sciences, The Natural History Museum, London, U.K. (e-mail: m_matsumoto@tohoku.ac.jp)

Introduction: It has been believed that dust grains, including ice, accreted to form planetesimals in the solar nebula, and subsequent collisions and coalescing of planetesimals resulted in the formation of large planets. The pristine dust no longer exist in its original form in the present Solar System, but its derivatives are found in primitive extraterrestrial materials. For the last few dicades, a few primitive carbonaceous chondrites have been recognized to have escaped significant aqueous alteration and thermal metamorphism [e.g., 1,2]. In order to uncover evidence of primordial ice and pristine planetary materials, we examined one of these meteorites, Acfer 094 [e.g., 1], in detail using a novel analysis protocol systematically combining various nanoanalytical techniques: FE-SEM, FIB micro-sampling, synchrotron-radiation-based X-ray computed nanotomography (SR-XCT), STEM-EDS, and NanoSIMS.

Results and Discussions: We examined two polished Acfer 094 sections containing abundant fine-grained matrix (~ 60 vol.%). In FE-SEM observations, we found a lot of small regions (~11 μm in diameter), which show ultraporous textures, distributed throughout the matrix. Hereafter we call the regions as ultra-porous lithologies (UPLs). In SR-XCT, we found some UPLs located below the polished sample surfaces ensuring that they were originally present in the Acfer 094 meteorite. TEM observations revealed that UPLs consist mainly of fine-grained Fe–Mg-rich amorphous silicates, forsterite, enstatite, Fe–Ni sulfides, organics and contain abundant pores among the constituents (porosity ~40 %). The amorphous silicates occur at scales of several hundreds of nm to 1 μm and contain variable quantities of Fe–Ni sulfide microcrystals as inclusions. These characteristics and their O-isotopic compositions are similar to those of pristine amorphous silicates, known as glass with embedded metals and sulfides (GEMS) [e.g., 3], in cometary dust, but without the Fe–Ni metal inclusions common in GEMS. The surrounding matrix consists of essentially the same materials as UPLs. We found enstatite wiskers with a-axis elongation, which are thought to be primitive condensates from nebula gass [e.g., 4], both in UPLs and the matrix. All these suggest that UPLs and the matrix are highly pristine lithology preserving pristine dust materials.

UPLs with abundant pores are flagile, nevertheless, they show no evidence of pore compaction, which could have occurred during accretion. This strongly suggests that the pores in UPLs are used to be filled with some solid material(s). Ice is one of the major components of cometary nuceli and should be present in the pores of cometary dust. Therefore, it is reasonable that some ice was the original solid material, subsequently lost by evaporation and/or melting. In this study, we found that the amorphous silicates in UPLs and the matrix have been hydrated (H_2O contents: 3–18 wt.%). We infer that the hydration may have been caused by the ice melting. However, the volume of UPLs (i.e. ice) (~0.2 vol.%) is not sufficient to justify the water contens in the amorphous silicates, suggesting that the distribution of ice in Acfer 094 parent body was heterogeneous and that ice was much more abundant elsewhere in the parent body.

Based on recent astrophysical models [e.g., 5–7], we assume Acfer 094 parent body formation by fluffy dust agglomeration during its radial migration from the outer to inner regions of the solar nebula. As the source dust, we assume fluffy silicates dust with and without ice, which originally present in the outer and inner regions of the H_2O snow line, respectively. Recent simulations have shown that the fluffy icy-dust suffered sintering around the H_2O snow line and formed solid aggregates of silicate grains embedded in ice [e.g., 8]. The aggregates may correspond to ice-bearing UPLs. We infer that Acfer 094 parent body growth during the radial migration across the H_2O snow line would produce a radial variation of ice abundance in the parent body and be consistent with the presence of UPLs. The meteorite's major source of water was the ice-rich core of the parent body. This is the first practical model to provide new insight to asteroid formation by dust agglomeration, combining both analytical results and theoretical studies.

References: [1] Greshake A. (1997) *Geochimca Cosmochimica Acta* **61**, 437–452. [2] H. Leroux et al. (2015) *Geochimica Cosmochimica Acta* **170**, 247–265. [3] L. P. Keller and S. Messenger (2011) *Geochimica Cosmochimica Acta* **75**, 5336–5365. [4] J. P. Bradley et al. (1983) *Nature* **301**, 473–477. [5] S. Okuzumi et al. (2012) *The Astrophysical Journal* **752**, 106, 1–18. [6] K. Tsiganis et al. (2005) *Nature* **435**, 459–461. [7] K. J. Walsh et al. (2012) *Meteoritics and Planetary Sciences* **47**, 1941–1947. [8] S. Sirono (2011) *The Astrophysical Journal Letters* **733**, L41, 1–4.

SHOCK MELTING FEATURES IN REGOLITH PARTICLES OF S-TYPE ASTEROID ITOKAWA.

T. Matsumoto[1], A. Miyake[2], D. Harries[3], T. Noguchi[1], and F. Langenhorst[3]. [1] Faculty of Arts and Science, Kyushu University, 744 Motooka Nisi-ku Fukuoka 819-0395 (matsumoto.toru.502@m.kyushu-u.ac.jp), [2] Division of Earth and Planetary Sciences, Kyoto University, [3] Institut für Geowissenschaften, Friedrich Schiller University Jena.

Introduction: Impact-induced modification is a fundamental process that can alter mineralogical and petrographic features of asteroidal materials. The Hayabusa spacecraft recovered regolith samples from a S-type asteroid Itokawa. Itokawa is a ruble-pile asteroid that was formed by gravitational re-accumulation after a catastrophic impact event of its parent body [1]. The regolith particles from Itokawa are considered to be impact fragments formed on Itokawa [2]. The Itokawa regolith samples record a moderate shock history of Itokawa's materials [3-5]. In addition, Itokawa samples might have important information about impact events related to regolith alternation such as space weathering, lithification, and volatile loss from asteroids. Although shock features of crystalline minerals in Itokawa particles have been reported by many authors [3-5], there are few studies about melting textures of Itokawa samples [6]. In this study, we investigated shock veins and a large impact splash melt found among Itokawa particles.

Methods: Itokawa particles examined in the present study are RA-QD02-0275 and RA-QD02-0292. We observed the Itokawa particles by a scanning electron microscope (SEM: Hitachi SU6600). After SEM observation, the Itokawa samples were coated by carbon. Then, the particles were coated with platinum using a focused ion beam (FIB) system (FEI Helios G3, Quanta 3D FEG, Quanta 200 3DS). We extracted electron-transparent sections from regions of interest by milling with a Ga^+ beam. The electron transparent sections were analyzed by transmission electron microscopes (TEM: JEOL JEM-3200, FEI Tecnai G^2 FEG, JEOL JEM-2100F) equipped with EDX.

Results: RA-QD02-0275 consists of an olivine fragment of approximately 46 μm × 86 μm ×120 μm in size. A largest splash melt covers approximately 6.8×10^2 μm^2 of the olivine surface. The outline of the splash melt is irregular and wavy. A vertical section of the splash melt showed that multiple layers of Mg-rich silicate melt and iron sulfide alternate in the splash melt. The Mg-rich silicate melt layer is composed of amorphous silicate glass that contains numerous nanophase FeS particles of several nm to 150 nm in size. The composition of the silicate melt ($Wo_{0.9-2.8}En_{72-76}Fs_{20-26}$) is similar to low Ca pyroxene in LL chondrites. A single orthopyroxene grain ($Wo_2En_{77}Fs_{21}$) was found in the silicate melt, which is presumably a remnant that has not been melted. The pyroxene grain has parallel stacking faults and solar flare tracks. The density of the tracks is up to 4×10^{-9} cm^{-2}, which is higher than the track density of the substrate olivine, where tracks are rarely observed. The distinct track densities suggest their different irradiation histories prior to the melt formation. The iron sulfide layers are polycrystalline and have high Fe/S ratio up to 2.3 compared to troilite (Fe:S = 1:1) that is a major sulfide phase in Itokawa samples. Many bright spots (< 20 nm) in the Fe-S layer in z-contrast images. They are possibly Fe metals and may increase the average Fe/S ratio of the sulfide layer.

RA-QD02-0292 is a olivine grain of approximately 70 μm in size. Numerous mineral fragments up to 5 μm in size are aggregated on the host olivine. The fragments consist of olivine, pyroxene, plagioclase, and iron sulfide. TEM observation of thin sections including the fine fragments revealed that silicate melt veins are distributed across the fine fragments. The silicate melt vein contains abundant nanophase FeS. The width and length of the silicate veins are approximately 700 nm and 10 μm, respectively. In addition, there is a sulfide vein filling cracks of silicate fragments.

Discussion: Local silicate melt-glass with submicron-sized particles of FeS and Fe metal have been observed in powders of a L6 ordinary chondrite recovered from shock experiments, when the shock pressure is higher than 38 GPa [7]. Besides this, silicate melt veins containing FeS particles have been found in ordinary chondrites [e.g., 8]. Melting textures in Itokawa grains seems consistent with the shock melting features in ordinary chondrite materials. The high Fe/S ratio of iron sulfide layers in the melt splash indicates sulfur loss during melting and metal formation. Nanophase FeS particles are expected to alter reflectance spectra in the same manner as npFe^0 in lunar regolith [9]; nanophase FeS up to 150 nm in size in melts could cause spectral reddening and darkening. Impact melts could contribute to spectral change of larger S-type asteroids, where more extensive impact melting might occur compared to the surface of Itokawa.

References: [1] Fujiwara A. et al. (2006) *Science* 312.1330. [2] Tsuchiyama A. et al. (2011) *Science* 333. 1125. [3] Nakamura T. et al. (2011) *Science* 333. 1113. [4] Langenhorst F. et al. (2014) *Earth, Planets and Space* 66:118. [5] Mikouchi T. (2014) *Earth, Planets and Space* 66:82 [6] Dobrica and Ogliore. (2014) *Earth, Planets and Space* 66:21. [7] Hörz F. et al. (2005) *Meteoritics & Planetary Science*, 40, 1329. [8] Righter K. et al. (2015) *Meteoritics & Planetary Science*. 50, 1790-1819. [9] Britt D. T. and Pieters M. (1994) *Geochimica et Cosmochimica Acta*, 58, 3905-3919.

VIS-NIR REFLECTANCE MICRO-SPECTROSCOPY OF IDPs

R. Maupin, Z. Djouadi, R. Brunetto, C. Lantz and O. Mivumbi, IAS, CNRS, UMR- 8617, Université Paris Sud, Bât. 121, F-91405 Orsay Cedex, France. E-mail: romain.maupin@ias.u-psud.fr

Introduction: Some classes of asteroids (B-, C-, Cb-, Cg-, P- and D-types, representing not less than 66% of the mass of the main belt) have no analogues clearly identified in the meteorite collections [1]. However, meteorites are not the only cosmomaterials found on Earth since no less than 30 000 tons of interplanetary dust particles (IDPs) enter the Earth's atmosphere each year [2]. IDPs originate from different parent bodies throughout the solar system [3, 4, 5]. Two IDP classes are identified, the Chondritic Smooth (CS-) IDPs that have platy and/or fibrous texture with mineralogy dominated by hydrous silicates and Chondritic Porous (CP-) IDPs that have a very porous texture with mineralogical component dominated by anhydrous silicates [6]. The reflectance measurements in the visible range (0.4 – 0.8 μm) performed on CP- and CS-IDPs in the 90s [7] and the simulated visible near infrared (Vis-NIR) spectra of IDPs with comparison of mid infrared (Mid-IR) spectra [1] have shown that IDPs may be good analogues to some asteroids and in particular to the classes not sampled by meteorites. These results are supported by the fact that some asteroids eject dust [8], as recently observed by OSIRIS-REx around Bennu asteroid (B-type) [9].

We report here the recent developments of a reflectance measurement device and the results obtained on the IDPs in the Vis-NIR range (0.45 – 1.0 μm). Mid-IR measurements (2.5 – 15 μm) are also performed at the French synchrotron SOLEIL (*https://www.synchrotron-soleil.fr/fr*) to better constrain the composition.

Experiments: Our setup, installed in a clean room, consists of a Vis-NIR spectrometer (Maya2000 Pro from Ocean Optics) coupled to a macroscope (Leica Z16 APO). A Vis-NIR optical fiber (100 or 50 μm in diameter) is used to collect the light diffused by the sample which is unilaterally illuminated by a halogen source through a 1000 μm diameter fiber (phase angle of ~ 45°). By changing the magnification and/or the diameter of the collection fiber it is possible to adapt the collection spot to the grain size down to 7 μm size. To obtain the reflectance spectrum of a micrometric grain with this setup, it is necessary to rotate the particle several times in the observation plane with respect to the incident light [10]. For the Mid-IR measurements the grains are transferred and crushed in a diamond compression cell [5, 11]. Transmission infrared spectroscopy (spectral resolution of 4 cm^{-1}) is performed on the SMIS beamline of SOLEIL thanks to a microscope coupled to a Fourier transform infrared spectrometer with its Mercury–Cadmium–Tellurium detector cooled with liquid nitrogen.

Results and discussion: We obtained spectra of 10 IDPs with reflectance levels covering a wide range (~ 1 to 11 % at 0.55 μm). The very low reflectance levels of some IDPs indicate that they could represent very dark asteroids like Ryugu, whose visible reflectance at 0.55 μm is 1.88 ± 0.17 % [12, 13]. The Vis-NIR spectra of IDPs show some absorption bands which are discussed using the Mid-IR measurements. IDPs exhibit also different spectral slopes. Some of IDPs have a red slope on the entire wavelength range, that will be compared with spectral slope of some asteroids. Other IDPs show a fall of the reflectance beyond 0.8 μm that can be produced by magnetite and/or by the absorption of minerals such as olivine and pyroxene.

We propose our analytical technique as a useful non-destructive tool to be applied on samples which will be collected by Hayabusa2 and OSIRIS-REx on asteroids Ryugu and Bennu. The laboratory spectra acquired on these precious grains will be compared to those obtained in-situ in space as well as by remote-sensing observations. Coupling other analytical techniques (FTIR and Raman) will be helpful to link the Vis-NIR spectra of grains (and thus their parent bodies surfaces) to their composition.

References: [1] P. Vernazza et al. (2015) *The Astrophysical Journal 806 :204*. [2] Love and Brownlee. (1993) *Science, 262, 550-553*. [3] Dermott et al. (1994) *Nature, 369, 719-723*. [4] Liou et al. (1996) *Icarus, 124, 429-440*. [5] Brunetto et al. (2011) *Icarus, 212, 896-910*. [6] Bradley, J. P. (2003) *Treatise on Geochemistry, 1, 689*. [7] Bradley, et al. (1996) *Meteoritics & Planetary Science, 31, 394-402*. [8] Jewitt, D. (2012) *The Astronomical Journal, 143:66*. [9] Hergenrother et al. (2019) *Nature communications 10*, Article #1291. [10] Maupin et al., (2019) *50th Lunar and Planetary Science Conference (2019),* Abstract #1775. [11] Merouane et al. (2014) *The Astrophysical Journal 780 :174*. [12] S. Watanabe et al., (2019) *Science 10.1126/science.aav8032*. [13] S. Sugita et al. (2019) *Science 10.1126/science.aaw0422*.

REEVALUATING THE UNBRECCIATED EUCRITES FOR EVIDENCE OF METASOMATISM.

R. G. Mayne[1], R. L. Funderburg[1] and N. G. Lunning[2], [1]Monnig Meteorite Collection, 2950 West Bowie Street, SWR 244, Texas Christian University, Fort Worth, TX 76109 (r.g.mayne@tcu.edu), [2]Rutgers, State University of New Jersey, Department of Earth and Planetary Sciences, Piscataway, NJ 08854

Introduction: Duke and Silver [1] were the first to observe the breakdown of pyroxene to silica and troilite within eucrites. This reaction was not attributed to metasomatism until many decades later; however, now, metasomatism in eucrites has been identified by many authors [e.g. 2,3,4,5,6,7,8,9]. Barrat et al. [4] created a three-stage classification scheme that describes progressive metasomatism within the eucrites: Stage 1 results in Fe-enrichment along fractures in pyroxene; in Stage 2, fayalitic olivine veinlets form; Stage 3 sees the development of Fe-rich, but Al-depleted pyroxenes and the formation of secondary Ca-rich plagioclase. Both fluid-driven [4,8,9] and vapor-driven alteration [10] have been suggested as mechanisms for the metasomatic alteration.

Old Data, New Age: The eucrite collection is dominated by equilibrated samples, as the Eucrite Parent Body (EPB; Vesta), is widely believed to have undergone a late-stage, widespread, perhaps even global, metamorphic event [11,12]. However, metasomatism is found primarily in unequilibrated eucrites [4,7,13]. Almost ten years ago, Mayne et al. [14], surveyed the unbrecciated eucrite population and presented data on 31 different eucrites, but metasomatism was not considered in their description of these samples. In this study, we reevaluate the data from [14] to examine the evidence for metasomatism in the unbrecciated eucrites.

In the first round of analysis, all unequilibrated or partially-unequilibrated eucrites were identified using the criteria outlined in [14]. 12 eucrites were selected for review: Queen Alexandra Range (QUE) 99033, Graves Nunataks (GRA) 98098, Grosvenor Mountains (GR0) 95533, Queen Alexandra Range (QUE) 94484, Elephant Moraine (EET) 92004, Pescora Escaprment (PCA) 91078, Elephant Moraine (EET) 90029, Lewis Cliff (LEW) 88010, Lewis Cliff (LEW) 88009, Pescora Escaprment (PCA 82501), Allan Hills (ALH) 81001, and MacAlpine Hills (MAC) 02522. The data was reevaluated using the following procedure: (1) SEM mineral maps of each sample were examined for textural evidence of metasomatism, such as the breakdown of pyroxene to silica and troilite. (2) Electron microprobe analyses (EMPA) of pyroxene were mapped to their recorded locations in each sample. Analyses close to fractures were compared to those in pyroxene cores to identify if they were Fe-rich (Stage 1 metasomatism). (3) All EMPA analyses were plotted to identify any Fe-rich, Al-poor pyroxenes (Stage 3 metasomatism). Textural and mineralogical evidence of metasomatic features (breakdown of pyroxene) was identified in GRO 95533, QUE 94484, EET 90029, and PCA 82501 (Figure 1); however, none of the unbreccaited eucrites examined showed Stage 1-3 metasomatism.

Comparison: All samples in the eucrite literature that have Stage 1 and 2 metasomatism are brecciated eucrites (monomict or polymict). The effects of early-stage metasomatism in terrestrial systems is strongly controlled by the ability of fluids to permeate the rock; it is possible this also holds true for Vesta, where the fractures from impacts make it easier for the metasomatizing fluid to travel. The breakdown of pyroxene to silica and troilite, which is likely vapor-controlled [10], is observed in the unbrecciated unequilibrated eucrites. This suggests that there may be several controls on the metasomatism of eucrites and that both fluid- and vapor-driven alteration occur in different populations of eucrites.
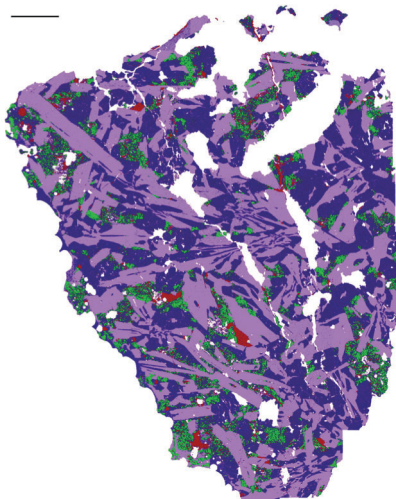

Figure 1: SEM mineral map of QUE 94484. Pink=plagioclase, purple=pyroxne, green=silica, red=oxides/sulfides. Areas rich in silica and sulfides are formed from the breakdown of pyroxene during metasomatism. Scale bar is 1mm.

References: [1] Duke M. B. and Silver L. T. (1967) *Geochimica et Cosmochimica Acta* 31:1637-1665 [2] Mittle fehldt D. W. and Lindstrom M. M. (1997) *Geochimica et Cosmochimica Acta* 61:453-462 [3] Schwartz J. M. and McCallum S. I. (2005) *American Mineralogist* 90:1871-1886 [4] Barrat J. A et al. (2011) *Geochimica et Cosmochimica Acta* 75:3839-3852 [5] Mittle fehldt D. W. et al. (2011) *Meteoritics & Planetary Science* 46:1133-1151 [6] Roszjar J. et al. (2011) *Meteoritics & Planetary Science* 46:1754-1773 [7] Warren P. H. et al. (2014) *Geochimica et Cosmochimica Acta* 141:199-227 [8] Chen H. Y. et al (2015) *Meteoritics & Planetary Science* 50 [9] Warren P. H. et al. (1997) *Meteoritics & Planetary Science* 52:737-761 [10] Zhang A. C. et al. (2013) *Geochimica et Cosmochimica Acta* 109:1-13 [11] Yamaguchi A. et al. (1996) *Icarus* 124:97-112 [12] Takeda H. and Graham A. L. (1991) *Meteoritics & Planetary Science* 26:129-134 [13] Mayne R.G. et al. (2016) *Meteoritics & Planetary Science* 51:2387-2402 [14] Mayne R. G. et al. (2009) *Geochimica et Cosmochimica Acta* 73:794-819.

MEASUREMENTS OF CARBON AND OXYGEN ISOTOPES IN ALLAN HILLS 84034 CARBONATES

K. A. McCain[1], K. D. McKeegan[1], M.-C. Liu[1], and A. J. Brearley[2], [1]Dept. of Earth, Planetary, and Space Sciences, UCLA, Los Angeles, CA. (kamccain@ucla.edu), [2]The University of New Mexico, Albuquerque, NM.

Introduction: The CM chondrites represent a wide range of fluid-rock alteration products spanning weakly to highly altered samples. Stable isotope measurements of carbonate minerals which precipitated from aqueous solution can be used to constrain the temperatures, fluid sources, and chemical reactions proceeding in these varied samples. Lightly altered samples contain carbonate populations consisting mostly of calcite, and more extensively altered samples contain complex assemblages of dolomite in addition to calcite. The complex petrology and small size of carbonate grains require in-situ study. While in-situ stable isotope measurements by ion probe of calcites are reliable, dolomite grains in highly-altered CM chondrites contain 3-12 mol% Fe, presenting an analytical challenge to accurately quantify the matrix effect during the analysis. Here we present C and O stable isotopic measurements of calcites and dolomites in the highly altered CM chondrite Allan Hills 84034, performed with matrix-matched standards.

Methods: $\delta^{18}O$ and $\Delta^{17}O$. We used a 700 pA Cs+ beam in the UCLA ims 1290 ion microprobe to analyze $\delta^{18}O$ and $\Delta^{17}O$ in ~6 μm diameter spots at mass resolution of 7000.

$\delta^{13}C$. Analyses of $\delta^{13}C$ were also performed with the UCLA ims 1290 with a 1 nA Cs+ beam, corresponding to a spot size of ~10 μm, at mass resolution of 5500.

Correction for the matrix effect. EPMA data collected at UNM and SEM/EDS data collected at UCLA, as well as previously-described matrix-matched dolomite standards [1] were used to correct for the matrix effect caused by variations in Fe content in the target carbonates. Measurements of $\delta^{13}C$, $\delta^{17}O$, and $\delta^{18}O$ were all corrected using methods outlined in [2,3].

Results: Calcite in ALH 84034 is similar in oxygen isotopic composition to Murchison calcites (black 'x' symbols in Figure 1), a more weakly altered meteorite. The dolomites fall along an approximately mass-dependent line which passes slightly below the bulk O isotopic value for the paired sample Allan Hills 83100. The calcite and dolomite are not in isotopic equilibrium, as the calcite grains have higher $\Delta^{17}O$ values and appear to define a mixing line of significantly steeper slope than do the dolomites. The correction for the matrix effect is critical to the interpretation of these carbonate data; reducing the data using only a calcite or a single dolomite standard would cause dolomite analyses to appear collinear with the calcite which could create a misleading steep slope for the calcite-dolomite assemblage. Values of $\delta^{18}O$ and $\delta^{13}C$ both decrease as the iron content of the dolomite increases, suggesting the coevolution of water chemistry and carbon isotopic composition. The $\delta^{13}C$ of the carbonates ranges from +20 to +80 ‰.

Figure 1. Oxygen isotope compositions of ALH 84034 carbonates. Filled and open circles represent analyses of calcite and dolomite, respectively. Error bars represent 2σ. Small x symbols represent Murchison calcites [4,5]. The star symbol represents the bulk O isotopic value of ALH 83100 [6] which is paired with ALH 84034. The CCAM (Carbonaceous Chondrite Anhydrous Mineral) and Y&R (Young and Russell 99) 'slope-1' lines are plotted in black as a reference. Blue dashed line represents mass-dependent fractionation from the bulk meteorite oxygen isotopic composition.
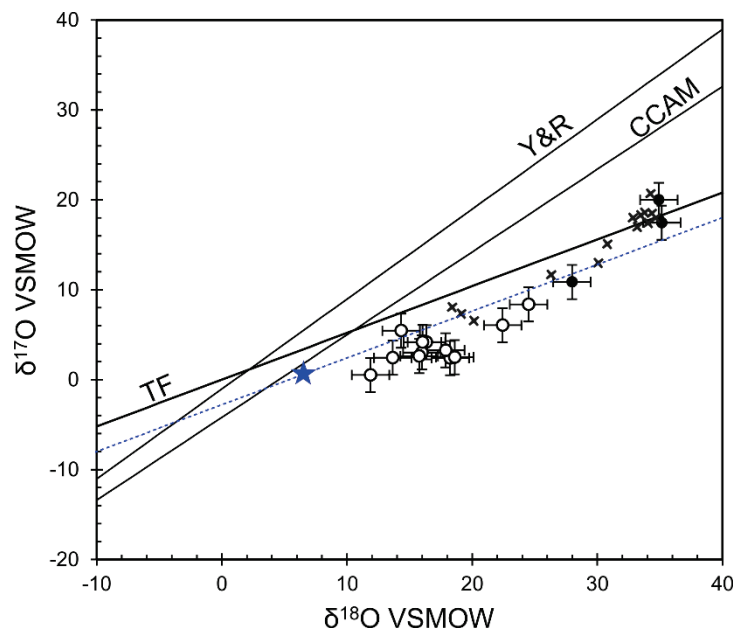
References: [1] McCain K. A., McKeegan K. D., Young E. D., Brearley A. J. and Alexander C. M. O. (2018) *LPI Contrib.* 2067, 6172. [2] Śliwiński M. G et al. (2016) *Geostand. Geoanalytical Res.* 40, 157–172. [3] Śliwiński M. G et al. (2016) *Geostand. Geoanalytical Res.* 40, 173–184. [4]Fujiya W. et al. (2015) *Geochim. Cosmochim. Acta* 161, 101–117. [5] Lindgren P. et al. (2017) *Geochim. Cosmochim. Acta* 204, 240–251.[6] Clayton R. N. and Mayeda T. K. (1999) *Geochim. Cosmochim. Acta* 63, 2089-2104.

BRECCIATED BOULDERS: EVIDENCE FOR IMPACT MIXING ON BENNU'S PARENT BODY

T.J. McCoy[1] , H.C. Connolly Jr.[2,3], C.M. Corrigan[1], E.R. Jawin[1], S. Sandford[4], J. Molaro[5], D. N. DellaGiustina[3], B. Rizk[3], M. C. Nolan[3], D. S. Lauretta[3], and the OSIRIS-REx Team, [1]Dept. of Mineral Sciences, National Museum of Natural History, Smithsonian Institution, Washington, DC, USA (mccoyt@si.edu), [2]Dept. of Geology, Rowan University, Glassboro, NJ, USA, [3]Lunar and Planetary Laboratory, University of Arizona, Tucson, AZ, USA, [4]NASA Ames Research Center, Mountain View, CA, USA, [5]Planetary Science Institute, Tucson, AZ, USA
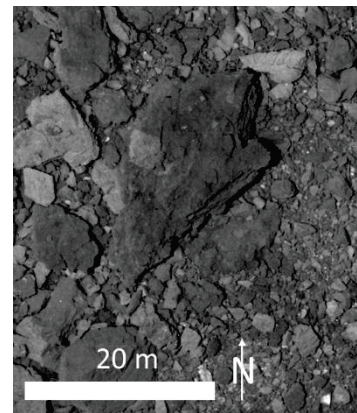
Introduction.   OSIRIS-REx has revealed an abundance of meter-scale brecciated boulders on the surface of asteroid Bennu. On its own, this result is not surprising. Impact bombardment has dominated most of the history of the parent asteroids of hydrated carbonaceous chondrites similar to Bennu. Impacts produced shock effects within individual components [1], shock melting [2], and brecciation [3]. These effects are well-documented in meteorites. Of 30 hydrated carbonaceous chondrites (CI, CM, CR) surveyed, all of them contain solar wind–implanted gases and are regolith breccias [3], suggesting that the surfaces of asteroids are dynamic environments for mixing. The revelation that brecciation is widespread at the meter scale on the surface of Bennu allows us to examine the extent and timing of brecciation.

Brecciation in meteorites: Petrographic study of CI, CM, and CR chondrites reveals widespread evidence of brecciation at the thin section scale [3 and references therein]. In all cases, these are genomict breccias composed of material of the same chemical group with different states of aqueous alteration. CI chondrites exhibit prominent sub-centimeter clasts that differ in texture and mineralogy, including abundance of carbonates. Clasts are angular, and boundaries between clast and host are distinct, suggestive of impact mixing after aqueous alteration. Brecciation in CM chondrites ranges from areas of more extensive aqueous alteration adjacent to areas in which chondrules are only modestly aqueously altered, to CM chondrites (e.g., Nogoya) in which clasts are visible in hand sample. CR2 chondrites exhibit the lowest degree of aqueous alteration, but contain clasts that appear to have experienced more extensive aqueous alteration akin to a CR1. Although brecciation is common at the millimeter to centimeter scale, masses of Murchison—the only >100-kg hydrated carbonaceous chondrite shower—do not exhibit substantial stone-to-stone variations suggestive of brecciation at the decimeter scale.

Brecciated boulders on Bennu: Boulders of the scale of tens of meters on the surface of Bennu exhibit differences in albedo and texture suggestive of brecciation [4,5]. Although many breccias appear monomict, albedo variations in some suggest differences (e.g., extent of aqueous alteration, mineralogy) indicative of genomict breccias with clasts derived from distinct portions of the asteroid. The differences between these clasts will require additional data to discern. Meter-scale genomict breccias suggests a dynamic environment of fragmentation, mixing, and reconsolidation. Impact and thermal cycling may have played a role in fragmentation, with millimeter- to centimeter-scale fragments expected to far outnumber meter-scale fragments. Whether movement of particles occurs via impact mixing, or via migration on the surface or in the interior of asteroids, smaller particles may be easier to move and mix than meter-sized blocks. Processes that reconsolidate breccias, particularly grain boundary melting that is commonly invoked for ordinary chondrites [3], may be more effective at the millimeter to centimeter scale. Although exceptionally rare, impact and shock melts of hydrated carbonaceous chondrites are known both in situ [3] and as clastic material in howardites [6]. To invoke such a process at the meter scale would require shock melt veining of a scale not previously observed in meteorites but known from terrestrial impact breccias. Alternatively, such breccias could form prior to the cessation of aqueous alteration and be cemented by subsequent alteration. In either case,

Meter-scale breccia on Bennu. PolyCam low-altitude flyby image of boulder at 247°E, 6° S

whether by impact melting or aqueous alteration, those processes likely occurred prior to the formation of Bennu as a rubble pile, suggesting that the meter-scale breccia on Bennu predates the formation of the current asteroid and may provide clues to a previous generation of Bennu's parent body(ies) in the asteroid belt.

References: [1] Scott E.R.D. et al. (1992) *GCA* 56:4281–4293. [2] Zolensky M. et al. (2015) *LPS XLVI*, Abstract #2261. [3] Bischoff A. et al. (2006) *MESS II*, 679–712. [4] Walsh K. et al. (2019) *Nature Geoscience* 12**:**242-246. [5] Lauretta D.S. et al. (2019) *Nature* 568;55-60. [6] Lunning N.G. et al. (2016) *GCA* 189:338–358.

ORIGINS OF REFRACTORY INCLUSIONS IN CM AND CV CHONDRITES: CONTINUITY OR DICHOTOMY?

K. D. McKeegan and M.-C. Liu, Department of Earth, Planetary, and Space Sciences, UCLA, Los Angeles, CA. (mckeegan@epss.ucla.edu)

Introduction: The early recognition of the large, white inclusions of the Allende CV meteorite as compositionally similar to the first mineral phases expected to condense from a cooling solar nebula [1] and the subsequent discovery that they are enriched in ^{16}O relative to terrestrial materials along a non-mass dependent trajectory [2], opened Pandora's box. Intensive study by an evolving suite of mass spectrometric techniques has revealed anomalies in both stable and short-lived radioactive isotopes that clearly demonstrate that the inner solar nebula was, in fact, not fully homogenized by passage of all incoming presolar materials through processes of evaporation, mixing, and recondensation (neglecting possible subsequent melting and alteration in asteroids). Some individual (micron-sized) grains somehow escaped thermal processing and mixing, and these are clearly recognized as original stellar condensates by virtue of their extreme isotopic compositions [3]. The isotopic anomaly signatures, reflecting distinct admixtures of nucleosyntheitic components, also persist at spatial scales of individual CAIs (sub-mm to cm) up to planetesimal (10's of km), with generally decreasing magnitude. By virtue of their very heterogeneous distributions among different classes of primitive meteorites [4], and their isotopic differences from chondrules and other chondritic components, CAIs are generally thought to be xenoliths, perhaps formed near the Sun and then later introduced into the accretion regions of chondrites [5]. Among issues that are not clear is the relationship(s) between these small scale anomalies and large, nebula-scale, distributions of isotopic signatures, some of which (e.g., Mo, Ti) have been interpreted as reflecting a fundamental dichotomy in accretion regions and/or timing in the nebula [6].

Seven months after the fall of Allende, an even more exotic gift arrived above the skies of south-eastern Australia in the form of the Murchison CM chondrite. CM chondrites contain refractory inclusions that, while distinctive in petrology, mineral chemistry, and some isotopic compositions from CV CAIs, are likewise generally thought to have formed in the solar nebula [6]. These inclusions are also presumably xenoliths that, for unknown reasons, are very rare in other classes of chondrites, including in particular, the CV chondrites. Fifty years of study of the Murchison and Allende meteorites presents an opportunity to reconsider the relationships of the refractory phases present as xenoliths in different class of chondrites in light of new perspectives gained regarding the nature and distributions of isotopically anomalous material in the solar nebula, including oxygen isotopes, short-lived radioactivity, and distinctive nucleosynthetic components.

CM hibonite grains: The remarkable isotopic anomalies in major elements (e.g., Ca, Ti) of CM hibonite grains are only exceeded by (some) anomalies in stellar condensate grains. Importantly, nucleosynthetic anomalies are highly distinctive compared to those exhibited by CAIs in CV chondrites in at least two ways: they can be larger by more than a factor of 100 and they can be both "positive" and "negative", i.e., exhibiting either excesses or deficits of the most neutron rich isotopes relative to chondritic and planetary values [7]. Ireland [8] identified a petrologic class of such inclusions consisting of single platy hibonite crystals ("PLACS") that exhibit the largest ^{48}Ca and ^{50}Ti anomalises but generally lack ^{26}Al. PLACS have been shown to contain ^{10}Be and non-radiogenic Mg isotope anomalies [9], ^{244}Pu, and a wide variety of trace element patterns. They have solar-like oxygen isotopes but their heavy stable isotope compositions (e.g., Mo) and formation ages are presently unknown. This contribution will explore the relationships between these different refractory components of two of the most important meteorites in our collections.

References: [1] Grossman, L. et al. Geophy. Res. Lett., 2, 37, 1975; [2] Clayton et al., Science 182, 485, 1973; [3] Zinner, E., et al. Nature, 330, 730, 1987; [4] MacPherson, G. J., Treatise on Geochemistry, 2nd edition, 139, 2014; [5] McKeegan et al., Science 281, 414, 1998. [6] Burkhardt, C., et al. Earth Planet. Sci. Lett., 391, 201, 2014; [7] [Fahey et al Ap. J. 323, L91, 1987; [8] Ireland, T. R. Geochimica et Cosmochimica Acta, 52, 2827, 1988. [9] Liu et al. Geochimica et Cosmochimica Acta, 73, 5051-5079, 2009.

ASTEROID TO AIRBURST; COMPARING SEMI-ANALYTICAL AIRBURST MODELS TO HYDROCODES

S. McMullan[1], G. S. Collins[1], and T. M. Davison[1], [1]Impact and Astromaterials Research Centre, Dept. Earth Science and Eng., Imperial College London, SW7 2AZ, UK, email: s.mcmullan16@imperial.ac.uk

Introduction: The 2013 Chelyabinsk event in Russia brought to light the potential hazard a Near-Earth Object (NEO), ~20 m in diameter can have on the Earth's surface [1]. NEOs 1-100m in size are abundant, difficult to observe astronomically, and strike the Earth with little to no warning [2]. There is likely to be at least one significant event in a human lifespan (e.g. Chelyabinsk, Tunguska), so being able to model their potential energy deposition and damage on the ground accurately is imperative. Semi-analytical models are fast predictors of energy deposition but make many assumptions and have several free parameters that are poorly defined [3-5]. These parameters are usually tuned to reproduce a particular event, such as Chelyabinsk [4]. In previous work, we showed that it is possible to tune multiple semi-analytical models to match the Chelyabinsk energy deposition [1], however, when these same models are then applied to a different event, such as Tunguska, the results diverge [6]. Previous studies have shown that shock physics codes are capable of reproducing the fragmentation of meteoroids in the atmosphere and their energy deposition rates [7-9]. They make fewer assumptions than semi-analytical models, so have fewer independent model parameters, but have a higher computational cost. Here we use the iSALE shock physics code [10-12] to simulate the atmospheric entry of meteoroids. From our simulation results, we can produce synthetic energy deposition curves with known initial entry conditions. This provides an additional data set with which to calibrate existing semi-analytical models and develop new approaches for the fast prediction of airburst outcomes.

Modelling Airbursts with iSALE: We have adapted the iSALE shock physics code [10-12] for the purpose of simulating atmospheric fragmentation of a meteoroid. We implemented a dynamic air-inflow bottom boundary condition that allows the atmospheric traverse to be simulated in the reference frame of the meteoroid. This avoids undesirable regridding or advection of the meteoroid through the Eulerian mesh. An example simulation is shown in Figure 1, with initial conditions similar to the Chelyabinsk event (diameter = 20 m, velocity = 19 km/s, density = 3300 kg/m^3). From these simulations, we produce synthetic data sets, including energy deposition curves for comparison with the energy deposition curve inferred from light-curve observations.

Discussion: Comparisons of our preliminary iSALE results with predictions of semi-analytical models show that while the timing and altitude of principal energy deposition are similar, the details of meteoroid spreading and ablation are different. iSALE predicts spreading rates of 2.5 times the initial radius, far lower than those of semi-analytical models which are calculated at 6-9 times the initial radius. This is consistent with previous hydrocode simulations of meteoroid entry [13]. Further simulations will investigate the effect of asteroid strength and porosity on the rate of deceleration and spreading.

Figure 1: iSALE atmospheric fragmentation simulation, showing the velocity and density profiles at 0.39, 1.1, 1.65 and 2.0 secs.

References: [1] Brown P. G. et al. (2013) *Nature* 503:238-241, [2] Harris A. et al. (2015) *In Asteroids IV, Univ. of Arizona, Texas,* 835-854, [3] Chyba C. F. et al. (1993) *Nature* 361:40-44, [4] Hills J. G. and Goda M. P. (1993) *The Astronomical Journal* 105:1114-1144, [5] Avramenko M. I. et al. (2014) *Journal of Geophysical Research: Atmospheres* 119:7035-7050, [6] McMullan S. and Collins G. S. (2019) *Icarus* 327:19-35, [7] Crawford D.A et al. (1994) *Shock Waves* 4:47-50, [8] Shuvalov and Artemieva (2002) *Planetary and Space Science* 50:181-192. [9] Robertson D. and Mathias D. (2017) *Journal of Geophysical Research: Planets* 122:599-613, [10] Amsden A. et al. (1980) *Los Alamos National Laboratories Report* LA-8095:101p, [11] Collins G. S. et al. (2004) *Meteoritics and Planetary Science* 39:217-231, [12] Wünnemann K. (2006) *Icarus* 180:514-527, [13] Artemieva N. and Pierazzo E. (2009) *Meteoritics & Planetary Science* 44:25-42.
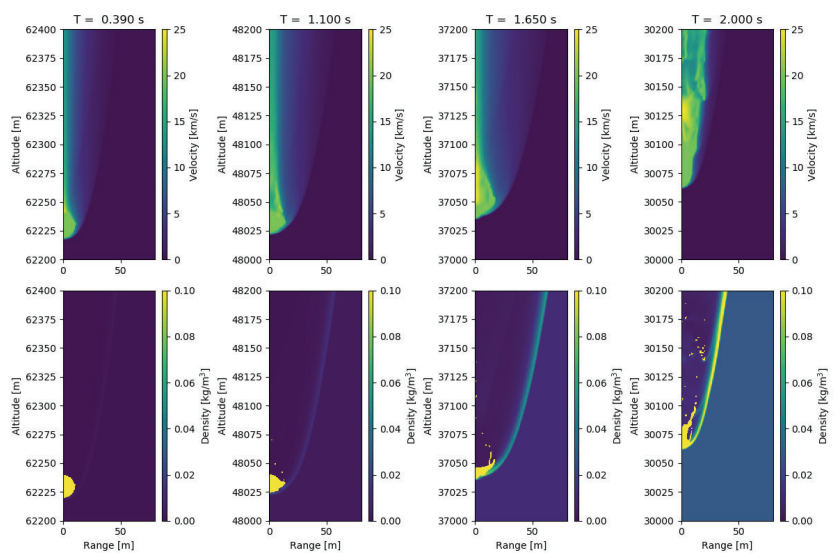
THE UK FIREBALL NETWORK: STAGE TWO OF THE GLOBAL FIREBALL OBSERVATORY.

S. McMullan[1], L. Daly[2,3], G. S. Collins[1], P. Bland[3], and the Desert Fireball Network Team[3]. [1]Impact and Astro-materials Research Centre, Department of Earth Science and Engineering, Imperial College London, SW7 2AZ, UK, (email: s.mcmullan16@imperial.ac.uk), [2]School of Geographical and Earth Sciences, University of Glasgow, Glasgow, G12 8QQ, UK, (email: luke.daly@glasgow.ac.uk), [3]Space Science and Technology Centre, School of Earth and Planetary Science, Curtin University, GPO Box U1987, Perth, WA, 6845, Australia.

Introduction: The UK-Fireball Network (UKFN) is part of a larger effort by the Desert Fireball Network (DFN) to install autonomous cameras that continually monitor the night sky to capture fireball events as they enter Earth's atmosphere [1], ultimately creating the first Global Fireball Observatory (GFO) [2]. The primary aim is to provide accurate fall locations of any surviving meteorites, allowing for rapid recovery, and to calculate their orbit, and hence, origin in the solar system.

The UK Fireball Network: As part of a collaboration between Imperial College London, the University of Glasgow, and Curtin University, four cameras have been installed so far, with a further seven cameras planned (Fig. 1). This should provide nearly complete double-station coverage of the skies over the UK, with each camera having a field of view with a radius of 150 km. We anticipate that this network will observe 1-2 meteorites of searchable size per year [3]. UKFN have teamed up with several other UK-based networks, such as UKMON and SCAMP, collectively known as the UK Fireball Alliance (UKFAll), to put in place protocol for when such an event occurs. We have already had several joint fireball observations. A meteorite fall has not been recovered in the UK for nearly 30 years and it is the aim of the UKFN, with the GFO and UKFAll, to rectify this. The DFN have developed a free app with Thoughtworks, called Fireballs in the Sky, to allow for members of the public to report a sighting using their smartphones and increase the data set available [4].

Each camera has an 8-mm stereographic fisheye lens and takes one long exposure image every 30 seconds. The onboard computer performs an automated event detection search of each image, and if an event is detected, neighbouring cameras are autonomously checked to see if they also observed the event. Fireball velocities and trajectories are calculated using a de Bruijin sequence embedded in the long exposure images, which provides absolute timing data with temporal precision better than one millisecond after triangulation [5].

The installation of these cameras in the UK faces different challenges to those of DFN in Australia, including light pollution, higher rainfall, and cloud cover. However, so far, these factors seem to have had minimal impact on the operation of the installed cameras.

Figure 1: Zenith light pollution map of the UK with the blue dots marking the installed cameras to date, and the white dots showing planned installation locations. Anywhere 20.6 or higher (yellow-black) are considered optimum installation locations.

References: [1] P.A. Bland et al. (2012) *Australian Journal of Earth Sciences* 59:2:177-187. [2] R.M. Howie et al. *Experimental Astronomy* 43:3:237-266. [3] M. Zolensky et al. (2006) *Meteorites and the Early Solar System II* 869-888. [4] P.A. Bland, et al., (2014) *Elements*, 160-161. [5] R.M. Howie et al. (2017) *Meteoritics and Planetary Science* 52:8:1669-1682.
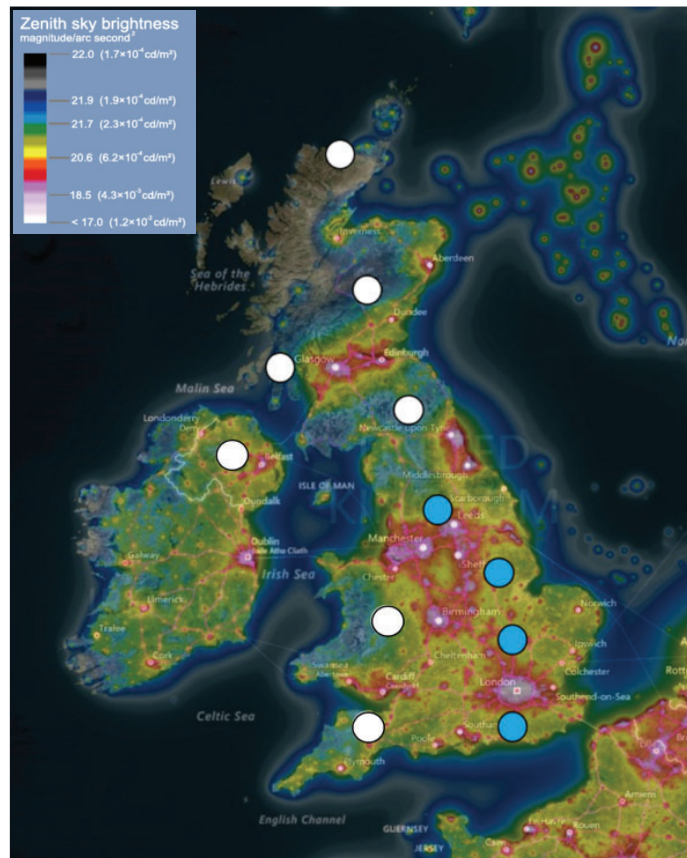
SILICON ISOTOPIC FRACTIONATION DURING EVAPORATION OF CAI-LIKE MELTS IN LOW-PRESSURE CONDITIONS.

R. A. Mendybaev[1], P. S. Savage[2], M. Kamibayashi[3,4], R. B. Georg[5], and S. Tachibana[3,4]　[1]Department of the Geophysical Sciences, University of Chicago, Chicago, IL 60637, USA (ramendyb@uchicago.edu); [2]School of Earth and Environmental Sciences, University of St. Andrews, KY16 9AL, Scotland; [3]Department of Natural History Sciences, Hokkaido University, Sapporo 060-0810, Japan; [4]Department of Earth and Planetary Science, University of Tokyo, Tokyo 113-0033, Japan; [5]Agilent Technologies, Mississauga, ON L5N 5M4, Canada.

Introduction: The coarse-grained igneous texture of CAIs suggests that their precursors underwent melting followed by slow cooling. If such melting occurred under low-pressure conditions, evaporation of chemical elements and their mass-dependent isotopic fractionation would be expected. Isotopic fractionations observed in CAIs have been successfully reproduced by vacuum evaporation experiments using CAI-like melts; until recently, however, it was unclear if vacuum experiments adequately describe evaporation under the low P_{H2} conditions of the solar nebula. Recent experiments showed that at 1600°C and 2×10^{-4} bar H_2 Mg and Si evaporate from FoB CAI-like melt ~40 times faster than in vacuum, but chemical evaporation trajectories and Mg isotopic fractionation remains the same [1, 2]. Here we present results on Si isotopic fractionation in samples evaporated in low P_{H2} and in vacuum.

Experimental: In addition to the initial experiments at 2×10^{-4} bar H_2 and in vacuum using 2.5 mm samples [1, 2], new sets of low P_{H2} evaporation experiments at 1600°C with the same starting material were conducted at Hokkaido University: at 2×10^{-4} bar H_2 using 1.5 mm sized samples and at 2×10^{-5} bar H_2 using 1.5 and 2.5 mm samples. The Si isotopic compositions of evaporation residues were measured using established solution techniques [3, 4] on a NuPlasma HR MC-ICP-MS at Trent University and a Neptune Plus MC-ICP-MS at University of St. Andrews. Chemical composition of run products was determined using a TESCAN LYRA3 FIB/FESEM equipped with an Oxford AZtec X-ray microanalysis system.

Results and Discussion: New experiments showed that evaporation trajectories of all run products follow the same trend established earlier [1, 2]. This further confirms the conclusion that presence of H_2 increases evaporation kinetics of Mg and Si (relative to vacuum), but relative evaporation rates of Mg and Si, and thus chemical evaporation trajectories, remain the same.

The Si isotopic composition measurements of evaporation residues from the first set of experiments at 2×10^{-4} bar H_2 give a fractionation factor of $\alpha_{29,28}$=0.9927±0.0004 which is significantly different from $\alpha_{29,28}$=0.9901±0.0004 obtained from previous vacuum evaporation experiments using different composition CAI-like melts [5, 6]. To check if smaller Si isotopic fractionation (larger $\alpha_{29,28}$) is due to Si recondensation (back reaction), we measured Si isotopes in evaporation run products from the new low P_{H2} experiments. By lowering P_{H2} and sample size we also lowered the amount of Si evaporating and thus limited possible Si recondensation. We also measured Si isotopes in evaporation residues from vacuum experiments.

Our new Si isotopic composition measurements of evaporation residues, including those from vacuum runs, resulted in $\alpha_{29,28}$=0.9917± 0.0004. The independence of $\alpha_{29,28}$ on run conditions (vacuum, 2×10^{-4} and 2×10^{-5} bars H_2) and sample size (2.5 and 1.5 mm) indicates that there is no detectable recondensation of Si in the experiments. This is in accord with the conclusion made based on Mg isotopic measurements [2].

It remains unclear why $\alpha_{29,28}$=0.9917±0.0004 is different from $\alpha_{29,28}$=0.9901±0.0004 reported for different composition melts [5, 6]. We should note that most previous experiments were conducted at 1900°C and thus we cannot exclude the temperature effect, as was observed for Mg isotopes [7]. However, no temperature effect on Si isotopic fractionation was reported from SIMS measurements of the same evaporation residues, but instead dependence of $\alpha_{29,28}$ on melt composition was observed [8]. However, it should be noted that this last conclusion was based on ion-probe measurements of Si isotopic composition, and no compositional effect on $\alpha_{29,28}$ (and $\alpha_{25,24}$ for Mg) was observed when solution ICP-MS data were interrogated [5].

Conclusions: The experiments show that, although evaporation of CAI-like melts in low-pressure H_2 is faster than in a vacuum, the chemical and isotopic fractionation of both Mg and Si remains the same. Therefore, the extensive experimental database on chemical and isotopic fractionation in vacuum can be safely used to model evaporation of CAI precursors in solar nebula, and previous interpretations of the isotopic fractionations of natural CAIs based on vacuum experiments do not require revision.

References: [1] Kamibayashi M. et al. (2018) *49th LPSC*, Abst. #2432. [2] Mendybaev R. A. et al. (2018) *49th LPSC*, Abst. #2580. [3] Georg R. B. et al. (2006) *Chem. Geol.* 235:95–104. [4] Savage P.S. and Moynier F. (2013) *EPSL* 361:487–496. [5] Mendybaev R. A. et al. (2013) *GCA* 123:368–384. [6] Mendybaev R. A. et al. (2017) *GCA* 201:49–64. [7] Richter F. M. et al. (2007) *GCA* 71:5544–5564. [8] Knight K. B. et al. (2009) *GCA* 73:6390–6401.

XENON ISOTOPES IN THE SCANDINAVIAN ALUM SHALE: A CLUE FOR THE ORIGIN OF P1(Q) AND P3 XENON COMPONENTS IN NANODIAMOND-RICH RESIDUES FROM PRIMITIVE METEORITES.

Alex Meshik[1], Niels H. Schovsbo[2], Olga Pravdivtseva[1], [1]Physics Department and McDonnell Center for Space Sciences, Washington University, St. Louis, MO 63117, USA (ameshik@physics.wustl.edu), [2]Geological Survey of Denmark and Greenland (GEUS), Øster Voldgade 5-7, Dk-1350 Copenhagen K, Denmark.

We have analyzed isotopic composition of Xe released from the sample of Alum Shale and found that isotopic structure and Xe release pattern from this sample are remarkably similar to Xe released at temperatures below 1300°C from nanodiamond residues remaining after dissolution of main mass of primitive meteorites. This similarity provides a clue for origin of P3 and P1(Q) components in meteoritic nanodiamonds.

The Scandinavian Alum Shale Formation was deposited in a large, shallow epicontinental sea that covered substantial parts of paleocontinent Baltica. The shale is rich in amorphous organic matter (up to 25 wt. % C) and in syngeneic trace elements, including uranium [1]. Generally, shales are known to carry large quantities of heavy noble gases, to the extend to be considered as a potential sink for "missing" terrestrial Xe [2]. In this work we have analyzed isotopic composition of heavy noble gases released from a particularly uranium rich part of the Alum Shale known as Kolm which have uranium content exceeding 1% [1].

Nanodiamond-rich residues (~ 0.15 wt. %) remaining after chemical dissolution of primitive meteorites contain four distinct xenon components: P3, P1(Q), HL and P6 sequentially releasing from the residue with increase of extraction temperature [3, 4]. The first two components, P3-Xe and P1-Xe, are nearly "normal", seem to be closer to mass-fractionated solar Xe than the HL-Xe and P6-Xe which are considered to be "exotic" [5]. P3-Xe, released below 800°C, exhibits 1.5 – 3% excesses in A = 129, 131, 132 and 134 relative to more retentive P1-Xe, typically releasing at 1100-1200°C (Fig.1, top panel). All other Xe isotopes are indistinguishable within uncertainties.

The Kolm shale exhibits two peaks of fission Xe release: minor 450-850°C and major 1000-1300°C. The isotopic composition of the major Xe release corresponds to fission spectrum of ^{238}U, while the composition of the minor, low temperature Xe release is clearly anomalous (Fig. 1, bottom panel) and is evidently produced by the CFF (Chemically Fractionation Fission) process caused by migration of radioactive Xe precursors in fission chains [6].

It seems highly unlikely that the evident similarities of isotopic differences between P3-Xe and P1-Xe in nanodiamond residue and those between low and high temperature fission Xe in shales are accidental. Rather, they suggest that isotopic excesses in P3-Xe relative to P1-Xe are due to CFF-modified ^{244}Pu which was a dominating source of fission Xe 4.5 Ga ago.

If our interpretation is correct, there is little hope to trace galactic evolution using the low-temperature Xe components (P3 and P1) in nanodiamond-rich residue [7]. The origins of these Xe components are likely to be "local" rather than "presolar". An apparent excess of ^{129}Xe in P3-Xe may not be entirely from decay of primordial ^{129}I.
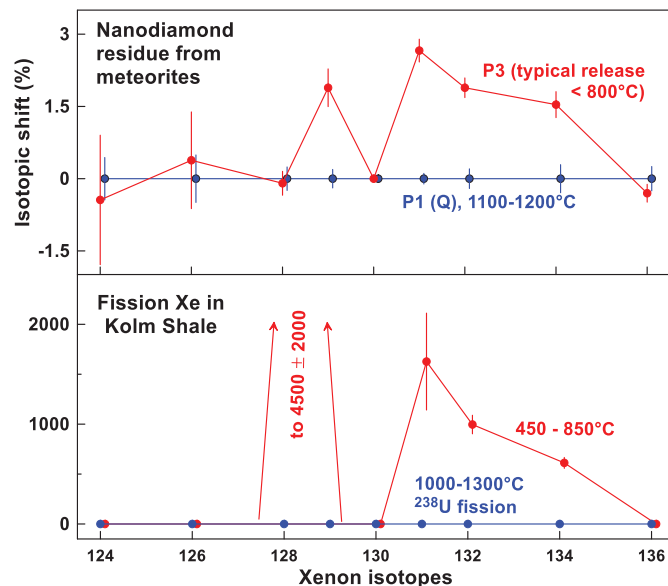
Fig. 1. Isotopic shifts in P3-Xe relative to P1(Q)-Xe in nanodiamond residue (top panel) are nearly identical to those in low temperature release of fission Xe in the sample from Kolm shale (bottom panel). Similar isotopic structure is observed in acid-resistant residue from U-bearing samples [7]. Chemically Fractionated Fission (CFF) is the only known process which can produce the isotopic shifts observed in these diverse samples.

[1] Schovsbo N. H. (2002) *GFF (Journal of the Geological Society of Sweden)* 124: 107–116. [2] Podosek F.A. et al, *Geochimica et Cosmochimica Acta* 45: 2401–2415. [3] Huss G. R. and Lewis R. S. (1994) *Meteoritics & Planetary Science* 29: 701–810. [4] Huss G. R. and Lewis R. S. (1994) *Meteoritics & Planetary Science* 29: 811–829. [5] Ott U. (2014) *Chemie der Erde* 74: 519–544. [6] Meshik A. P. et al. (2016) *Physical Review* C 93: 44614-1–9. [7] Gilmour J. D. (2010) *Geochimica et Cosmochimica Acta* 74: 380–393.

Zinc-bearing iron-dominant member of (Fe,Zn,Mn)S solid solution from Eagle enstatite chondrite

N. Mészárosová[1,2] and R. Skála[1,2], [1]Institute of Geochemistry, Mineralogy and Mineral Resources, Faculty of Science, Charles University in Prague, Albertov 6, 128 43 Prague 2, Czech Republic; meszarosova@gli.cas.cz [2]Institute of Geology of the Czech Academy of Sciences, Rozvojová 269, 165 00 Prague 6, Czech Republic

Introduction: Enstatite chondrites are divided into two groups based on their bulk composition: EH (high bulk iron) and EL (low bulk iron) [1 and references therein]. They formed under highly reducing conditions which are also reflected in their mineralogy [2]. Eagle meteorite belongs among enstatite chondrite of the EL group and petrologic type 6 [3]. Zinc bulk concentration in enstatite chondrites has been shown to be extremely variable among EH and EL groups and also among distinct petrologic types across the groups and simultaneously it has been observed that overall content of sphalerite as a potential main Zn carrier in these meteorites is low [4,5 and references therein]. It should be noted, however, that not only sphalerite represents zinc carrying mineral in enstatite chondrites; other Zn-bearing minerals reported from enstatite chondrites include Zn-bearing daubréelite and Fe-dominant members of (Fe,Zn,Mn)S solid solution: buseckite and rudashevskyite. Last two minerals differ mutually in their crystal structures [6; 7 and references therein]. Rudashevskyite crystalizes in sphalerite structure type (space group $F\bar{4}3m$) whereas buseckite crystalizes in würtzite structure type (space group $P6_3mc$). Here, (Fe,Zn,Mn)S phase from Eagle enstatite chondrite is presented. This mineral has not been reported from Eagle chondrite before.

Preliminary results and discussion: Next to vastly dominant almost iron-free enstatite, the studied sample of Eagle meteorite contains plagioclase, Si-bearing Fe-Ni metal and sulfides (Cr-Ti-bearing troilite, daubréelite and alabandite). Minor phases as tridymite, quartz, graphite, schreibersite and sinoite are also present. No chondrules were observed. During the detailed mineralogical investigation, few grains of (Fe,Zn,Mn)S mineral were found in a single area (approx. 400 x 400 μm^2) of Eagle sample. The mineral occurs associated with troilite grains that contain daubréelite exsolution lamellae. Chemical composition determined by electron microprobe (average of 10 analyses) of the (Fe,Zn,Mn)S mineral is (in wt%) Fe 29.97, Zn 22.98, Mn 10.31, Mg 0.42, S 35.24. Corresponding empirical formula (calculated on the basis of 2 atoms per formula unit) is $(Fe_{0.49}Zn_{0.32}Mn_{0.17}Mg_{0.02})_{\Sigma1.00}S_{1.00}$. The presented chemical composition is very close to the composition of buseckite from Zakłodzie meteorite [7]. Consequently, it is feasible to assume that the reported (Fe,Zn,Mn)S phase corresponds to buseckite. Other features also favor the identification of the mineral as buseckite rather than rudashevskyite. In general, the würtzite-type structure is stable at higher temperatures than the sphalerite-type structure. In addition, iron and also Mn (+Mg) contents significantly lower the inversion temperature of buseckite (würtzite-type) to rudashevkyite (sphalerite-type) from approx. 1020-800°C (depending on Fe content) down to ~ 350°C (depending on Mn content) [6;7]. Published data on EL4-6 enstatite chondrites report more (Fe,Zn,Mn+Mg)S phases with relatively high Mn (+Mg) content. Taking into account relatively high formation temperatures, fast cooling rates, high Mn content and low oxygen fugacities, they probably correspond to buseckite as well [7]. However, no indication of crystal structure type is available for these minerals so far preventing their unequivocal identification.

Further mineralogical research is planned to reveal the trace element composition and more importantly the crystal structure to distinguish whether the minerals represent rudashevskyite or buseckite (EBSD and Raman microspectroscopy and if possible also the single-crystal X-ray diffraction). Note, that no complete crystal structure determination was performed for buseckite; instead only its EBSD pattern was matched to that of würtzite-structured analog.

References: [1] Weyrauch M. et al. (2018) *Meteoritics & Planetary Science* 53:394–415. [2] Keil K. (1989) *Meteoritics* 24:195–208. [3] Meteoritical Bulletin, no. 67. (1989) *Meteoritics* 24:57–60. [4] Buseck P. R. and Holdsworth E. F. (1972) *Meteoritics* 7:429–447. [5] Moynier F. et al. (2011) *Geochimica et Cosmochimica Acta* 75:297–307. [6] Britvin S. N. et al. (2008) *American Mineralogist* 93:902–909. [7] Ma C., Beckett J. R., & Rossman G. R. (2012) *American Mineralogist* 97:1226–1233.

MODELS OF THE CHEMICAL EVOLUTION OF CALCIUM, TITANIUM, AND CHROMIUM ISO-TOPES AND THEIR PRESOLAR CARRIERS

Bradley S. Meyer, Dept. of Physics and Astronomy, Clemson University, Clemson, SC 29634-0978 USA (mbradle@clemson.edu).

Introduction: The isotopes of the light iron-group elements calcium, titanium, and chromium have long played an important role in cosmochemistry. Primitive samples such as hibonite grains and FUN CAIs show roughly correlated anomalies in the neutron-rich isotopes of these elements (e.g. [1-8]). Bulk meteorites also show anomalies in the isotopes of these elements (e.g., [9]). These anomalies have long indicated the incomplete homogenization of carrier components in the early Solar System.

Because of the significance of isotopic anomalies in calcium, titanium, and chromium for understanding processes in the early proto-planetary disk [9,10,11], it is useful to consider the Galactic chemical evolution of these elements, their isotopes, and their possible carriers into the Solar cloud. In this work I present some models of such evolution.

Methods: To follow the chemical evolution of calcium, titanium, and chromium, I use the open-source code toolset ICE (inhomogeneous chemical evolution) developed over the last several years [12]. The code models multiple zones of the interstellar medium and attaches a full nuclear reaction network to each zone. I evolve the Solar annulus over the lifetime of the Galaxy from initial infall of metal-poor gas to the time of the Sun's birth. I divide up the annulus into multiple zones and allow mass to mix between those zones on a timescale of 10^7 years. I use a density-dependent star-formation rate and a Kroupa initial mass function to distribute new stars in zones throughout the Solar annulus [13]. I use yields from massive stars [14], thermonuclear supernovae [15], and low-mass stars to account for the enrichment of the interstellar medium by stellar debris. I use schematic yields for the low-mass stars derived from a combination of stellar models and expected s-process production from AGB phases. I include yields from rare stellar explosions that are responsible for the most neutron-rich stable isotopes of each element. These events are not fully identified, but are likely electron-capture supernovae [16] or complete thermonuclear explosions of dense C/O white dwarf stars [17] or partial thermonuclear explosions of O/Ne white dwarf stars [18]. For simplicity, I treat these events as single-degenerate thermonuclear explosions of C/O white dwarf stars but explore possible variations due to other scenarios.

To follow the evolution of the isotope carriers, I allow the stars to eject their isotopes into distinct dust reservoirs representing the interstellar dust. Dust cycles into and out of molecular clouds on a timescale of 100 million years, and dust is destroyed in the hot phases of the interstellar medium by sputtering and shattering on a timescale of 200 million years. Free atoms can re-condense onto "old dust" in molecular clouds. Dust is also incorporated into forming stars.

Results: At the time of the Sun's birth, I record the masses of the various isotopes in each dust reservoir. Each reservoir contributes to multiple isotopes, which indicates that several isotopes can be carried by multiple carriers. Nevertheless, for some isotopes, particularly the most neutron-rich species, a single dust reservoir is the dominant carrier. A database of stellar yields used in the model along with the results of the present calculations is available at https://sourceforge.net/u/mbradle/wiki/Research/. From the results of the calculation, interested users may estimate isotopic anomalies that would result from varying mixtures of the dust reservoirs.

References: [1] Lee T. et al.(1978) *Astrophys. J. Lett.* 220:L21-L25. [2] Niederer F. R. et al. (1980) *Astrophys. J. Lett.* 240:L73-77. [3] Birck J. L. and Allegre, C. J. (1984) *Geophys. Res. Lett.* 11:943-546. [4] Papanastassiou D. A. (1986) *Astrophys. J.,* 308:L27-L30. [5] Fahey A. et al. (1987) *Astrophys. J. Lett.* 323:L91-L95. [6] Papanastassiou D. A. and Brigham C. A. (1989) *Astrophys. J. Lett.* 338:L37-L40. [7] Ireland T. (1990) *GCA* 54:3219-3237. [8] Sahijpal S. et al. (1990) *GCA* 64:1989-2005. [9] Trinquier A. et al. (2009) *Science* 324:374-376. [10] Warren P. H. (2011) *EPSL* 311:93-100. [11] Kruijer T. S. et al. (2017) *PNAS* 114:6712:6716. [12] Bojazi M. J. and Meyer B. S. (2018) *LPS XLIX*, Abstract #2890. [13] Kroupa P. (2002) *Science* 295:82-91. [14] Woosley S. E. and Weaver T. A. (1995) *Astrophys. J. Suppl.* 101:181-235. [15] Nomoto K., Thielemann F.-K., and Yokoi K. (1984) *Astrophys. J.* 286:644-658. [16] Wanajo S. et al. (2013) *Astrophys. J.* 767:L26. [17] Woosley S. E. (1997) *Astrophys. J.* 476:801-810. [18] Jones S. et al. (2019) *Astron. Astrophys.* 622:A74.

THE SHOCK EEFECTS OF GRANITIC IMPACTITE FROM ALETAI IRON METEORITE, XINJIANG, CHINA.

B. Miao (miaobk@glut.edu.cn) and Y. Wang, [1]Institution of Meteorites and Planetary Materials Research, [2]Key Laboratory of Planetary Geological Evolution, [3]Guangxi academician workstation for astrochemistry and planetary science, Guilin University of Technology, Guilin 541004, China.

Introduction: The longest meteorite strewn field was identified as Aletai iron meteorite in 2016 by Wang and Xu [1]. Akebulake, a member of Aletai iron meteorite rain with a mass of 18 t, was found in N48°6.25', E88°16.57' in 2011, which classification information is issued in Meteoritical Bulletin 105. During the recovery of Akebulake, some glassic rock fragments were found. These glassy rock samples have been confirmed as the impactite from Akebulake iron meteorite. Here we represent some preliminary work on shock effects of the impactite of Akebulake.

Geological Setting: The Akebulake iron meteorite locates on the top of a mountain in Kelan Canyon in Aletai Mountains, Xinjiang. It was surrounded by huge rocks and half buried. The site is in the granite region. The granite is mainly a kind of medium grain sized biotite granite. When we went and worked in the field, a piece of half-melted biotite granite is found only about 2 m away from the original location of Akebulake. Due to the close distribution of huge granite boulders, no outcrop of granite base rock could be found. However, based on the geological information and field survey, the imactite should be the product when Akebulake iron impacted directly on the granite base rock.

Petrographic Texture and Shock Effects: The impactite has a kind of vitriphyric texture consisting mainly of quartz phenocrysts among a large number of glass matrix. There are a lot of bubbles in glass. The other shock effects mainly include: (1) Except the relics of quartz, other major minerals are shocked into glassy melt, the glass has two kinds of white and brown bands which probably originated from plagioclase and biotite; (2) the quartz grains have mosaic fractures, generally with wavy extinction, some with mosaic extinction, and some boundary has converted into diaplectic glass; (3) some zircon grains were decomposed to ZrO_2 and SiO_2 to form symplectite rims; (4) no high-pressure polymorphs was not found yet.

Mineral Chemistry: Based on EPMA analyses, the glass show varying features: (1) the white band glass has relative high SiO_2 (63.4 wt%), Al_2O_3 (21.6 wt%), Na_2O (4.76 wt%) and K_2O (5.96 wt%) contents while the brown band has high FeO (6.04 wt%), MgO (3.47 wt%) and CaO (6.77 wt%) contents; (2) the quartz relict grain has the SiO_2 of 98.9 wt% and less other elements (e.g. FeO (0.15 wt%), Al_2O_3 (0.06 wt%), TiO_2 (0.06 wt%), K_2O (0.05 wt%)); (3) the diaplectic glass of quartz is nearly pure of SiO_2 only with less of FeO (0.10 wt%).

Discussion: The impactite should originate from target granite, hence, it is of great significance of gaining insight into the conditions of the impact of the iron meteorite. Based on the shock effects, especially the diaplectic glass convertion of quartz, the peak shock pressure is estimated as 50-60 GPa, the peak temperature should be probably about 1800 ℃. In addition, the compositions of the white and brown glass bands, coupled with geological setting and a half-melted granite fragment, suggest that the target rock of Akebulake iron meteorite should be a biotite granite or monzonitic granite.

References: [1] Wang K. and Shu W. (2016) *Chinese Science Bulletin* 61: 2834-2842 (in Chinese with English abstract). [2]Stöffler D. and Langenhorst F. (1994) *Meteoritics* 29:155-181.

NAGARA: A NEW JAPANESE IAB IRON METEORITE FIND.

T. Mikouchi[1], A. Yamaguchi[2], N. Shirai[3], J. Isa[4], M. Komatsu[5], S. Kawakami[6], N. Katsuta[7], T. Kawamata[8], K. Sugiyama[8], [1]University Museum, University of Tokyo, Hongo, Bunkyo-ku, Tokyo 113-0033, Japan (E-mail: mikouchi@um.u-tokyo.ac.jp), [2]National Inst. Polar Res. (NIPR), Midori-cho, Tachikawa, Tokyo 190-8518, Japan, [3]Dept. of Chemistry, Tokyo Metropolitan University, Minami-Osawa, Hachioji, Tokyo 192-0397, Japan, [4] University of Grenoble Alpes, CNRS, IPAG, 38000 Grenoble, France, [5]The Graduate University for Advanced Studies (SOKENDAI), Hayama, Kanagawa 240-0193, Japan, [6]Faculty of Education, Gifu Shotoku Gakuen University, Gifu, Gifu 501-6194, Japan, [7]Faculty of Education, Gifu University, Gifu, Gifu 501-1193, Japan, [8]Inst. Materials Res., Tohoku University, Katahira, Sendai, Miyagi 980-8577, Japan.

Introduction: Nagara is the newest Japanese iron meteorite found in Nagara, Gifu, Japan. A 6.5 kg piece was first found in 2012 and classified as a IAB iron meteorite in 2018 [1]. Then, the second piece (9.7 kg) was recognized to have been found ~300 m from the discovery site of the first sample and considered to be paired. In this abstract we report mineralogy and geochemistry of this IAB iron meteorite and compare this iron with other known IABs.

Macroscopic Description: Both samples show exterior with rounded ridges and the dark brownish surface is mostly coated by rust. Rare black fusion crust is preserved. The cut surfaces after etching exhibit a granular texture (~1 cm in grain size) and no typical Widmanstätten patterns are observed (Fig. 1). Small patches of silicate inclusions are present in the first sample (Fig. 1), but such inclusions were absent in the second one (~10 x 10 cm etched surface), probably due to sample heterogeneity (~tens of cm scale).

Mineralogy and Petrology: >95% of the polished sections (both samples) consist of kamacite with veins of terrestrial weathering products (~0.5 mm wide). Therefore, the granular texture of the etched surface is due to different orientations of kamacite grains (Fig. 1). The kamacite composition determined by electron microprobe (JEOL JXA-8530F @Univ. of Tokyo) shows a small variation (Fe=92.0-94.5, Ni=5.5-6.5 and Co=0.55-0.65, all in wt%) mainly due to atomic diffusion towards the interface to the schreibersite grains (Fe=45-54, Ni=30-38 and P=15, all in wt%) that are present at the center of weathered veins. Taenite is present as small elongated grains (~0.1 mm wide and ~0.5 mm long) with less than 0.1% abundance (Fe=61-65, Ni=34-39 and Co=0.1-0.2, all in wt%).

Silicate inclusions are up to 1 mm in size and consist of olivine (Fo$_{95}$, Molar Fe/Mn=12), orthopyroxene (En$_{93-91}$Wo$_{1-2}$, Al$_2$O$_3$=0.3, TiO$_2$=0.2, Cr$_2$O$_3$=0.3, all in wt%), augite (En$_{53-54}$Wo$_{44}$, Al$_2$O$_3$=0.8, TiO$_2$=0.7, Cr$_2$O$_3$=1.1, all in wt%) and plagioclase (An$_{16}$Or$_3$). These mineral compositions are close to those in other silicate-bearing IAB irons [2]. Two pyroxene thermometers gave 940-960 °C for equilibration temperature.

Trace Element Abundance: LA-ICP-MS analysis (average of 4 traverses (~5 mm long) on the section of the first sample by Thermo Element XR + CETAC LSX-213 @NIPR using Hoba and North Chile as standards) gave 6.10 wt% Ni, consistent with the electron microprobe analysis. The obtained trace element contents are Ge=402, Ga=91.4, As=11.2, Cr=4.53, Ir=4.24, Au=1.58, and W=1.43 (all μg/g), classifying Nagara as a IAB main group (MG) iron meteorite [3]. Although no LA-ICP-MS analysis has been done for the second piece, its high Ge content (~400 ppm) detected by electron microprobe analysis and their identical mineralogy suggest that they are likely paired.

Comparison with Other IABs: Among known IAB-MG samples, the trace element contents of Nagara are most similar to those of Yardea, Soledade, Duel Hill (1873) and Campo del Cielo [3] except for lower Cr content of Nagara. The ~1 cm granular texture of Nagara is especially similar to some samples of Campo del Cielo [2] although textures of Yardea, Soledade, and Duel Hill (1873) are not known in the literatures. These textural and geochemical similarities may suggest that Nagara and Campo del Cielo originated from the same region in the IAB-MG parent body [4,5].

Nagara
(IAB-MG)

1 cm
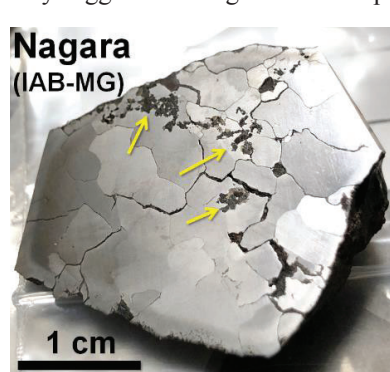
Pairing with Sakauchi?: In Gifu prefecture, there is one iron meteorite known (Sakauchi: 4.18 kg) whose recovery site is *ca*. 40 km from Nagara [6]. However, there is no detailed description of Sakauchi since it was found more than 100 years ago and the sample has been later lost. Because Sakauchi is reported to be hexahedrite, we cannot rule out their pairing.

References: [1] https://www.lpi.usra.edu/meteor/metbull.php?code=66476. [2] Ruzicka A. (2014) *Chemie der Erde* 74:3-48. [3] Wasson J. T. and Kallemeyn G. W. (2002) *Geochimica et Cosmochimica Acta* 66:2445-2473. [4] Worsham E. A. et al. (2017) *Earth and Planetary Science Letters* 467:157-166. [5] Hunt A. C. et al. (2018) *Earth and Planetary Science Letters* 482:490-500. [6] https://www.lpi.usra.edu/meteor/metbull.php?code=23103.

Fig. 1. The etched surface of Nagara (first sample), showing a ~1cm granular texture. Silicate inclusions are scattered on the surface (indicated by yellow arrows).

THERMAL INERTIA OF FINE-GRAINED POWDER OF THE MURCHISON CM CHONDRITE DETERMINED BY EXPERIMENTAL HEATING.

Hikari Mita[1], Kana Amano[1], Shiho Kobayashi[1], Yuma Enokido[1], Naoya Sakatani[2], Takehiko Arai[3], Tomoki Nakamura[1]: [1]Division of Earth and Planetary Materials Science, Graduate School of Science, Tohoku University, Aoba, Sendai, Miyagi 980-8578, Japan, [2]Institute of Space and Astronautical Science (ISAS), Japan Aerospace Exploration Agency (JAXA), Sagamihara, Kanagawa 252-5210, Japan, [3]Ashikaga University, Tochigi 326-0845, Japan. (e-mail: hikari.mita.q3@dc.tohoku.ac.jp)

Introduction: Thermal inertia, the degree of thermal resistance, strongly depends on grain size and porosity of material. Using this parameter, we can estimate what types of materials are on the surface of asteroids. There are several studies measuring the thermal diffusivity of meteorite bulk samples [1] including carbonaceous chondrites [2]. However, no previous studies have obtained the thermal inertia of powders of carbonaceous chondrite with different grain size. In this study, we conducted heating experiments using a powder of carbonaceous chondrite to determine the thermal inertia. The results will contribute to interpret the thermal inertia distribution of C-type asteroid 162173 *Ryugu* observed with NIRS3 and TIR onboard Hayabusa2 [3] [4].

Experimental methods: We prepared a chip of Murchison CM chondrite and crushed into particle sizes less than 2000μm, and measured its thermal inertia. Then the sample was further crushed into finer grains (<512μm, <155μm and the final size <77μm). A part of the powder was separated from each grain-size fraction and measured for the grain-size distribution and the mean-particle diameter, d (μm). For each sample, and we carried out the thermal inertia measurements by applying the following procedures. We packed the meteorite powder into a sample holder (φ10mm x 5mm: Fig. 1). The bulk-porosity of the powder was controlled from 32% to 59% by the number of tapping. In the sample container, 4 thermocouples were inserted horizontally every 1mm depth (Fig. 1). We used CO_2 laser to heat the surface of the sample up to about 450K in a vacuum chamber ($\sim 10^{-6}$ torr) for 5 minutes and cooled it rapidly for 30 minutes by turning off the laser. For each experimental condition (grain size and bulk-porosity), we repeated this heating/cooling cycle more than 5 times to improve precision and reliability. During the experiment, we measured temporal variation of the temperatures for each thermocouple inside of the sample powder.

Results and discussion: The obtained temperature profiles were used to calculate thermal diffusivity K, thermal conductivity k, and thermal inertia Γ. We first determined Δt, a time difference (sec.) of peak temperature between the two neighboring thermocouples, and then, assuming a semi-infinite medium, we simply calculated K, k, and Γ as follows:

$$K = \frac{\Delta z^2}{2\omega \, \Delta t^2}, \qquad k = K\rho' c, \qquad \Gamma = \sqrt{\rho' c k}$$

Here Δz is the depth difference of the thermocouples (m), ω is circular frequency (rad/s), c is specific heat [6], and ρ' is apparent density of the sample. Bulk porosity is calculated from $\phi = 1 - \rho'/\rho$ (from 32% to 59%), where ρ is the true density of Murchison (2.27 g/cc, determined in this study using a specific gravity bottle). Since our experimental system did not have ideal geometry (finite size of the sample container and spot heating), we carried out 2-dimensional numerical calculation simulating the geometry of our experiment, and introduced a coefficient in the thermal diffusivity K to compensate the difference in geometry between analytical solution and our experiment.

For fine-grained Murchison powder with the grain size less than 155μm ($d = 73 \pm 8$μm) and the porosity of 49%, we obtained a good reproducibility in temperature profiles among 5-time heating/cooling circles and the results show that $K = 1.0 \times 10^{-9}$ m^{2}s^{-1}, $k = 1.0 \times 10^{-3}$ Wm^{-1}K^{-1} and $\Gamma = 30$ Jm^{-2}K^{-1}s$^{-1/2}$. These values are similar to those of silicate powder [5], but much lower than those of a chip of CM carbonaceous chondrite (e. g., $K = 6.02 \times 10^{-7}$ m^{2}s^{-1} in [2]).

References: [1] Yomogida and Matsui (1983) *Journal of geophysical research*, 88, 9513-9533. [2] Opeil et al. (2010) *Icarus*, 208, 449-454. [3] Sugita et al. (2019) *Science*, 364, 10.1126/science.aaw0422. [4] K. Kitazato et al. (2019) *Science*, 364, 10.1126/science.aav7432. [5] S. Henke et al. (2012) *Astronomy & Astrophysics*, 537, A45. [6] Wada et al. (2018) *Progress in Earth and Planetary Science*, 5:82.
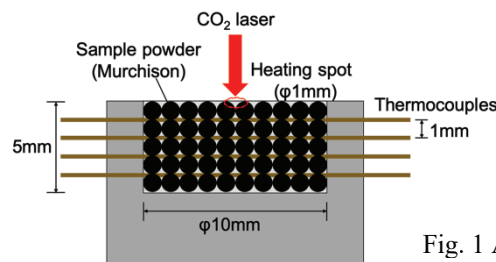

Fig. 1 A cross section of the sample holder

RECENT DEVELOPMENTS IN THE CURATION OF COLD, VOLATILE-RICH EXTRATERRESTRIAL SAMPLES.

J. L. Mitchell[1], E. K. Lewis[2], R. A. Zeigler[1], F. M. McCubbin[1], K. R. Fisher[1], and M. D. Fries[1], [1]NASA Johnson Space Center, 2101 NASA Pkwy, Houston, TX (Julie.L.Mitchell@nasa.gov) [2]Texas State U/Jacobs Engineering.

Introduction: In recent years, the study of samples from cold, potentially volatile-rich Solar System bodies has increased dramatically. Returned samples from low- or cryogenic-temperature regions are highly sensitive to ambient temperatures, pressures, and materials. In order to maximize the scientific utility of such samples, they must be returned, handled, and stored under conditions that minimize sample alteration and contamination. The Johnson Space Center (JSC) Astromaterials Acquisition and Curation Office (hereafter called the Curation Office) is currently developing the ability to curate cold, volatile-rich samples [1]; this abstract summarizes these efforts for Apollo lunar samples, organic-rich meteorites, comet samples, and lunar polar samples.

New Initiatives: *Apollo Lunar Samples and Organic-Rich Meteorites.* The Apollo Next-Generation Sample Analysis (ANGSA) program has provided a mechanism for studying specially curated lunar samples, including several that have been in cold (-20°C) storage since their initial processing. Recent selections for the ANGSA program include samples of shadowed soils and vacuum-sealed samples collected during Apollo 17. In addition, recent meteorite falls into frozen terrain provide opportunities for studying organic-rich chondrites and other meteoritic materials. Both sample types require a cold (≤ 20°C), clean (ISO 6 or better) environment in which to perform curatorial preliminary examination (PE) activities. The Curation Office has recently undertaken the retrofit of a walk-in freezer and glovebox specifically for processing ANGSA and meteorite samples. When complete, this facility will allow for N_2, Ar, or He processing using specially selected materials that are both particulate clean and cold-tolerant.

Comet Samples. The 2013-2022 Planetary Decadal Survey [2] lists comet nucleus sample return as one of the top-priority missions for the coming decade. Recent studies of comet nuclei (e.g., by the Rosetta mission) have discovered a suite of volatile and organic compounds, all of which would require special curation conditions for preservation and study [e.g., 3]. To enable the study of cometary volatiles, the Curation Office is enhancing its organic-clean and sterile sample storage processes. In addition, the capabilities for gas sampling and non-destructive PE are being added to the existing (and extensive) solid sample PE repertoire. In particular, techniques such as cavity ring-down and near-infrared reflectance spectroscopy will be included to allow the identification of temperature-sensitive or reactive gases and the subsequent tailoring of storage conditions for compounds of interest.

Lunar Polar Samples. JSC recently awarded an Internal Research and Development (IRAD) award for the development of lunar polar sample simulants for both curation and ISRU studies. While initially for conceptual lunar operations, the recent announcement of the U.S. plan to send humans to the lunar south pole in 2024 focuses this work for specific mission goals. First, a high-fidelity volatile-rich simulant is being developed that includes compounds detected by the LCROSS mission [4] and other compounds not detected by LCROSS that may be stable within lunar permanently shadowed regions (PSRs) [5]; highlands [6] or mare-type [7] particles are the solid component. Storage testing under a range of temperatures/pressures will constrain alteration under non-cryogenic conditions, in addition to assessing the storage efficacy of a lunar-like (10^{-8}-10^{-9} torr, liquid-He-cooled/cryogenic) environment.

In addition to curatorial requirements, we will also outline the first sample collection and spacecraft requirements (temperatures, pressures, and materials) for sample return from the lunar poles. Several new capabilities have been or are being developed in FY19 to that end. First, a thermal vacuum chamber has been constructed and is being outfitted for liquid-He operations. This chamber will also include: 1) a cooled stage specifically designed for lunar materials, 2) a sealed sample handling system to mitigate atmospheric contamination, and 3) an in-line, gas-phase mass spectrometer for real-time compositional monitoring. In addition, a corrosion-resistant, negative-pressure glovebox will be used for safe and clean volatile-rich simulant preparation. This glovebox will also be used for materials storage testing to better constrain the design of tools and sample storage containers that will keep the sample sealed and will not chemically react with the various highly reactive compounds in the sample.

Conclusions: In recent years, the demand for a cold curation capability has increased dramatically. In particular, existing lunar samples and meteorites, along with the possibility of comet nucleus and lunar polar sample return, provide a rich catalog of materials for which targeted studies will be conducted. The Curation Office is actively preparing for these samples, facilitating both robotic and human sample return missions that will provide a wealth of scientific insights for decades to come.

References: [1] McCubbin, F. M., et al. (2016) *LPSC* XLVII, Abst. #2668; [2] Veverka, J., et al. (2010) *Planetary Science Decadal Survey - Mission Concept Study*, App. G.; [3] Le Roy et al. (2015) *A&A, 583*, A1; [4] Colaprete, A. et al. (2010) *Sci., 330, 463*; [5] Paige, D. A., et al. (2010) *Science, 330, 6003*; [6] Battler, M. M. and Spray, J. G. (2009) *PSS* 57, 2128-2131; [7] McKay, D., et al. (1994) *Eng, Const, & Ops in Space IV*, ASCE, 857-866.

COMPOSITIONAL DIVERSITY OF ORTHOPYROXENITIC DIOGENITES & OLIVINE-BEARING DIOGENITES LINKED TO VARIABLE fO_2 & POST-EUCRITIC MAGMATISM

J.T. Mitchell[1] and A.G. Tomkins, School of Earth, Atmosphere & Environment, Monash University, Clayton, VIC Australia. [1]Corresponding author: Jennifer.Mitchell@monash.edu

Introduction: Diogenites are thought to represent either a) magma ocean cumulates [1,2] or b) late-stage crustal intrusions [3,4]. pMELTS [5] modelling of the melt and evolution of bulk silicate Vesta compositions [1,2,5,6,7] in a magma ocean scenario was carried out to determine whether or not diogenites can be formed in such a manner.

Results: Orthopyroxene compositions in diogenites range from En_{85-60}, with those in olivine-bearing diogenites being restricted to En_{71-76}. As such, olivine-bearing diogenites are not the most magnesian, contrary to what is expected from magma ocean mineral settling and accumulation. pMELTS modelling of orthopyroxene evolution found that equilibrium crystallization does not reproduce the observed range in orthopyroxene compositions, and that the intial degree of partial melting has no impact on compositions generated. The effects of varying oxygen fugacity were then investigated over the range ΔIW -2.5 to -1.0. As conditions become more oxidizing, orthopyroxene compositions become less magnesian, with fO_2 ΔIW -1.6 to -1.2 providing the best fit in terms of En-Fs for orthopyroxenitic and olivine-bearing diogenites. It was noted that the transition from dunitic to orthopyroxenitic diogenites occurs over approximately 20 °C of cooling. More advanced modelling used starting compositions with 5-20 % eucrite [8] removal at fO_2 ΔIW -1.6 and -1.2. Models with 10-15 % eucrite removal most accurately match the observed orthopyroxene compositions.

Discussion: Across all models, olivine-bearing diogenites are not commonly produced in comparison to orthopyroxenitic diogenites. This accurately reflects the global diogenite collection, in which less than 3% are classified as olivine-bearing diogenites. Small variations in oxygen fugacity were found to cause large changes in orthopyroxene composition. To account for this heterogeneous fO_2, we propose that the following sulfidation reaction: S_2 + $MgFeSiO_4$ = FeS + $MgFeSiO_3$ + O_2 variably affected the diogenite source region. It was observed that in all initial models pyroxene compositions were too Wo-rich, meaning that the modelled source was too rich in calcium to accurately reproduce the orthopyroxene compositions found in diogenites. Eucrites are high in Ca, and low in Mg, thus the removal of a eucrite component from the source composition would reduce the Ca available for diogenitic orthopyroxenes without greatly effecting the Mg content. Models with 10-15 % eucrite component removed satisfactorily reduced the Ca content of the generated orthopyroxenes to provide a more accurate match to the observed diogenite collection (Wo_{0-6}).

Our findings support the view that diogenites represent late-stage intrusions, and that a magma ocean scenario is an inappropriate model for their formation. Source heterogeneity in $fO2$ and an initial stage of eucrite removal are required to accurately reproduce diognenite orthopyroxene compositions. This is further supported by geochemical evidence that suggests diogenites interacted with a feldspar-rich lithology [9], and observations from the Dawn mission, which found no large mantle exposure in the southern impact basins, but instead detected olivine in the northern hemisphere [10,11].

References: [1] Righter, K. and Drake, M.J. (1997) *Meteoritics & Planetary Science* 32:929-944. [2] Ruzicka, A. et al. (1997), *Meteoritics & Planetary Science* 32:825-840. [3] Mittlefehldt, D.W. (1994), *Geochimica et Cosmochimica Acta* 58:1537-1552. [4] Barrat, J.A. (2004), *Meteoritics & Planetary Science* 39:1767-1779. [5] Ghiorso, M.S. et al. (2002), *Geochemistry, Geophysics, Geosystems* 3:1-35. [5] Bosenberg, J.S. and Delaney, J.S., (1997), *Geochimica et Cosmochmica Acta* 61:3205-3225. [6] Dreibus, G. and Wänke, H., (1980), *Zeitschrift für Naturforschung* 35a:204-216. [7] Toplis, M.J. et al. (2013), *Meteoritics & Planetary Science* 48:2300-2315. [8] Mittelfehldt, D.W., (1994) *Geochimica et Cosmochimica Acta* 58:1537-1552. [9] Barrat, JA. et al. (2010), *Geochimica et Cosmochimica Acta* 74:6218-6231. [10] Ammannito, E. et al. (2013), *Nature*, 504:122-125. [11] Thangjam, G. et al. (2014), *Meteoritics & Planetary Science* 49:1831-1850.

THE VESTAN REGOLITH: PETROLOGIC-CHEMICAL STUDY OF HED POLYMICT BRECCIAS.

D. W. Mittlefehldt[1] and W. P. Buckley[2], [1]Astromaterials Research Office, NASA Johnson Space Center (david.w.mittlefehldt@nasa.gov), [2]Jacobs JETS-NASA Johnson Space Center, Houston, TX 77058, USA.

Introduction: The howardite, eucrite and diogenite (HED) clan of meteorites consists of igneous rocks and derived impact breccias of an asteroid, quite likely (4) Vesta, that differentiated within the first few million years of formation of the first solids in the Solar System [1]. The HED clan includes a suite of polymict breccias that are the products of impact fragmentation, mixing and gardening of crustal igneous rocks; lower crustal diogenites, and upper crustal eucrites. In order of increasing fraction of eucritic material, these breccias are polymict diogenites, howardites and polymict eucrites. There are two types of howardites: regolithic and fragmental [2]. The former are samples of the true regolith whilst the latter are intermediate members of the polymict diogenite/polymict eucrite series [1-5]. Lithophile-element compositions of HED polymict breccias are consistent with simple mixing of main-group basaltic eucrite with diogenite; other crustal components – e. g., cumulate gabbro and evolved basalt – are subordinate [3]. However, petrologic studies show that the mixtures are much more complex [3, 6-10]. We are continuing the study of HED polymict breccias using the methodologies of [3] to further understand regolith mixing processes on Vesta.

Petrology: Petrologic studies are defining textural components and determining mafic mineral compositions of polymict diogenites, polymict eucrites and howardites. We include here the meteorites discussed in [3], and two diogenites that are paired with the PCA 02 howardite group [6]. Considering possible pairings, the number of falls being investigated amongst the 60 named meteorites might be as low as 7 polymict eucrites and 24 howardites.

We have found pyroxenes with compositions like those of cumulate eucrites – with low-Ca and high-Ca pyroxenes between the fields for diogenites and basaltic eucrites (see [1]) – in 5 howardite and 2 polymict eucrite falls. We have yet to positively identify cumulate eucrite pyroxenes in members of the GRO 95534 pairing group. This is in contrast to [7], but in that study, compositions of low-Ca pyroxenes only were used to identify a cumulate eucrite component, a potential shortcoming noted by those authors. Our analyses of the GRO pairs include numerous low-Ca pyroxene analyses within the field of cumulate eucrites, fully consistent with [7]. Three polymict eucrite and 7 howardite falls contain pyroxenes that are more ferroan than those found in Nuevo-Laredo-group eucrites, and an additional polymict eucrite and 4 howardite falls contain pyroxenes compositionally similar to those of Nuevo-Laredo-group eucrites. Thus, evolved basaltic components are commonly present in the breccias.

Composition: Whole-rock analyses are underway. Multiple splits and paired samples are being studied to evaluate cm- to decimeter-scale heterogeneity (cf., [3]). Our previous study noted that the major and trace element contents of HED polymict breccias are consistent with mixtures of average diogenite and main-group basaltic eucrite [3], but we did not attempt quantitative mixing-model calculations. Exceptions noted were: (i) polymict eucrite LEW 86001 that is dominated by Stannern-group eucrite material; (ii) howardite LAP 04838 that contains a significant component of evolved basaltic material; and (iii) howardite PRA 04401 that contains ~55 wt% CM chondrite material. These compositional exceptions are consistent with petrologic observations [3, 10, 11].

Discussion: One conclusion of [3] is that because many howardites contain >30% of a lower-crustal diogenite component, the lack of a cumulate-eucrite compositional signature in the breccias is unlikely to have been caused by under sampling deep-seated intrusions. Whilst [3] did conclude that main-group eucrites are the dominant upper-crustal component in the breccias, they also noted that the result could be explained by thorough blending of all mafic components in the breccias. This latter possibility was not explored. Petrogenetic models for vestan differentiation indicate that the upper crust ought to be basically main-group eucrite in bulk composition (e.g., [12]). Thus, regolithic howardites, posited to represent ancient, well-mixed regolith [2], ought to contain a mafic component that averages to main-group eucrite in composition regardless of what other components are petrologically identifiable: cumulate gabbro + evolved basalt ≈ main-group eucrite. Fragmental polymict breccias with higher percentages of mafic component, would be more likely to deviate from simple diogenite-main-group-eucrite mixing lines. This is the case for LEW 86001 and LAP 04838, but not for three other howardites/polymict eucrite falls with >80% mafic component [3]. Continuing work will focus on comparing mixing signatures in different types of vestan polymict breccias.

References: [1] Mittlefehldt D. W. (2015) *Chemie der Erde-Geochemistry* 75:155–183. [2] Warren P. H. et al. (2009) *Geochimica et Cosmochimica Acta* 73:5918-5943. [3] Mittlefehldt D. W. et al. (2013) *Meteoritics & Planetary Science* 48:2105-2134. [4] Cartwright J. A. et al. (2013) *Geochimica et Cosmochimica Acta* 105:395-421. [5] Cartwright J. A. et al. (2013) *Geochimica et Cosmochimica Acta* 140:488-508. [6] Beck A. W. et al. (2012) *Meteoritics & Planetary Science* 47:947-969. [7] Lunning N. G. et al. (2015) *Earth and Planetary Science Letters* 418:126-135. [8] Lunning N. G. et al. (2016) *Meteoritics & Planetary Science* 51:167-194. [9] Hahn T. M. et al. (2018) *Meteoritics & Planetary Science* 53:514-546. [10] Patzer A. & McSween H. Y. Jr. (2012) *Meteoritics & Planetary Science* 47:1475-1490. [11] Herrin J. S. et al. (2011) *LPS XLII, Abstract #2806*. [12] Mandler B. E. & Elkins-Tanton L. T. (2013) *Meteoritics & Planetary Science* 48:2333-2349.

QUENCHED INDICATOR OF CARBON-BEARING SOLIDS FOUND IN THE NIO METEORITE.

Y. Miura[1] and T. Kato[2], [1]Yamaguchi University (Chuou 4-1-23, Yamaguchi, Japan, 753-0074), [2]Yamaguchi University (Yoshida 1677-1, Yamaguchi, Japan, 753-8512).

Introduction: Mineral solids of meteorites formed by any collision process are generally discussed of crystalline minerals and chemical composition [1]. Quenched process of collisions in meteorites are mainly found by round shapes of many chondrules[2-4]. The present paper is discussed on quenched formations of carbon-bearing solids formed at fusion crust and chondrules of the Nio chondrite shower, which can be applied as quenched indicator of many meteorite collisions and formation in the Solar System.

Significance of cooling process of dynamic meteorite activity: Cooling process is previously found by textures of grains and glassy solids. Carbon-bearing grains are considered to be significant indicator of rapid cooling process, because volatile element and stable phases of mineral, vapor and liquid states are principal states of high-temperature and pressure reactions of shocked collisions and evaporated impact ejection [1-4].

Carbon-bearing solids formed by rapid reaction: Macroscopic evidences of quenched indicator of meteorite are proved by formation of glassy solids and shocked textures previously, where it shows mainly descriptive expression of glass and shocked lamellae. Present paper indicates that submicroscopic and dynamic signature of shocked evidence is related with state changes among solid-liquid-vapor (SLV) states during quenched process with carbon-bearing element considered as stable vapor element in the SLV states [1-4].

Carbon-bearing solids of natural and artificial products: Hot jet-stream of carbon dioxide air has been experimentally putted on rock to observe carbon-bearing grains with the analytical FE-SEM machine. Many fine grains with various compositions have been obtained as solidified grains on the surface. Natural volcanic and meteoritic impact rocks shows carbon-bearing grains formed by fired and/or shocked reaction with dynamic carbon streams, where submicroscopic carbon-bearing grains have been observed with the FE-SEM instrument [1-4].

Historical meteoritic shower of the Nio chondrite: The Nio meteorite shower (observed on 1897AD, Meiji 30) has been recorded 2 pieces (Niho site) and 3 pieces (Miyano site) by the Yamaguchi Prefectural Office and Police Station (at the Tokyo Nichi-Nichi News Paper), where 2 more pieces missing (at Niho site) and one piece (at Miyano site) are remained now. Our research group has been investigated huge meteoritic fragments at two impact sites (at Niho and Miyano). The FESEM investigation of the collected fragments (by magnetic separation method in the rice-paddy solids) have been obtained by characteristic iron and carbon-rich spherules (quenched by meteoritic shower process in air) [2] .

Evidence of quenched process of Nio chondritic meteorite: Characteristic evidence of quenched process at meteorite formation in the Solar System have been obtained by characteristic magnesium and carbon-rich chondrule from present study of the Nio chondritic meteorite. The same method of quenched process can be applied to other meteorites (the Chelyabinsk Meteorite fallen in 2013 and the Hayabusa samples etc.).

Figure 1. Electron-micrograph of FeC-bearing spherule formed by quenched process from the Nio meteorite shower in air , which has been collected by magnetic separation method at impact site of the Nio rice-paddy soils.

Summary: The present study can be summarized as follows. 1) Quenched formations of carbon-bearing solids are discussed on any FeC-bearing fusion crust and MgC-bearing chondrules of the Nio chondrite shower. 2) Quenched indicator of carbon-bearing grains can be applied to many meteorite collisions and formation in the Solar System.

References: [1] Miura Y. (1986) *LPSC XVII*, Abstract #1258. [2] Miura Y. (2001) *Meteoritics & Planetary Science* 36:A136. [3] Miura Y. (2017): *LPSC2017,* Abstract #3028. [4] Miura Y. (2017): *JpGU-AGU 2017 (Makuhari, Japan)*, Abstracts #C5357, #C2249, # C2158

NOBLE GASES IN A PRIMITIVE ACHONDRITE NORTHWEST AFRICA 3250.

Y. N. Miura[1] and R. Okazaki[2], [1]Earthquake Research Institute, University of Tokyo, Yayoi, Bunkyo-ku, Tokyo 113-0032, Japan (email address: yayoi@eri.u-tokyo.ac.jp), [2]Department of Earth and Planetary Sciences, Faculty of Sciences, Kyushu University, 744 Motooka, Nishi-ku, Fukuoka 819-0395, Japan.

Introduction: NWA 3250 is a primitive achondrite that consists of olivine (58 %), low-Ca pyroxene (38 %), and accessory plagioclase, taenite, troilite and chromite [1]. The previous studies indicated that the oxygen isotope composition plots on the bulk CR chondrite field and is close to those of some other primitive achondrites (e.g., NWA 011 and 6901) and equilibrated CR chondrites (e.g. [2]). From mineralogical and petrological investigations, a close affinity among NWA 3250, 2994, 3100, 6901, 6921, 7317 and 8548 has been suggested [3-6]. NWA 2994 and 3100, in which relict chondrule signatures were found, have been identified to be highly equilibrated and metasomatized CR6 chondrites, and Tafassasset to be CR7 chondrite [7]. These results imply that the large scale thermal heating has occurred at the CR chondrite parent body. However, current observations for these meteorites are not straightforward and detailed scenario about the parent body(ies) is still unclear. In this study, we conducted noble gas analyses for two small fragments separated from a specimen of NWA 3250 in order to obtain additional information for chronology such as cosmic-ray exposure ages and gas retention ages as well as primordial noble gas indication.

Noble gas measurement: Noble gases were measured with a MM5400 sector-type mass spectrometer at Kyushu University. The first sample #1 (3.7 mg) was heated at 700 and 1750 °C and the second sample #2 (3.7 mg) at 900 and 1750 °C, respectively, for gas extractions. Extracted gases were purified by Ti-Zr getters, and then noble gases were separated in He-Ne, Ar and Kr-Xe fractions, each of which was introduced into the mass spectrometer.

Result and discussion: The results of noble gases in the two samples are mostly consistent with each other with some exception. Remarkable differences are observed in concentrations of ^{3}He, ^{4}He and nucleogenic Xe isotopes. Helium and Ne are dominated by cosmogenic component plus radiogenic ^{4}He. The concentrations of cosmogenic ^{3}He are 0.57 and 1.0×10^{-6} cm^{3}STP/g, those of ^{21}Ne are 1.2 and 1.0×10^{-7} cm^{3}STP/g, and the measured ^{22}Ne/^{21}Ne ratios are 1.174 ± 0.107 and 1.068 ± 0.062 for #1 and #2, respectively. The low ^{22}Ne/^{21}Ne ratio of #2 implies heavier shielding, though unfortunately the uncertainty of #1 is large to discuss. Assuming the average bulk chemical compositions of the probably paired meteorites (NWA 2994 and 3100) and a temporal shielding condition (somewhat heavier shielding; at 40 - 50 cm depth in a meteoroid with 50 cm in radius), the production rates of ^{3}He and ^{21}Ne are calculated using elemental production rates given in [8], from which we obtained cosmic-ray exposure ages of 31 and 56 Ma for T_3, and 31 and 37 Ma for T_{21}, respectively. Preliminary the average of T_{21}, 34 Ma, is considered as the cosmic-ray exposure age of NWA 3250. In previous works for CR chondrites and a possibly related primitive achondrite group (brachinites/-like), the cosmic-ray exposure ages range in <1 - 12 Ma with a cluster of 5 - 7 Ma for CR2 [9] and 3 - 50 Ma for brachinites/-like [10], respectively. The exposure age of Tafassasset (proposed as CR7) is 76.1 ± 15.2 Ma [10]. Equilibrated meteorites tend to have longer cosmic-cray exposure ages, however, numbers of measured samples belonging to these classes are still limited.

The sample #1 contains large amounts of radiogenic ^{4}He and ^{129}Xe, and fission $^{129-136}$Xe; but #2 does not (the concentration of ^{4}He is about one sixth and fission Xe has not been detected). The isotopic compositions of Xe also show more abundant cosmogenic Xe in #1 than #2. This is likely because the former sample included phosphate mineral. Trace amounts of merrillites were reported for NWA 2994 and 3100, though it is unknown for NWA 3250, presence of such mineral can simply explain observed cosmogenic and fission Xe. The excess ^{134}Xe/^{136}Xe ratio is preliminary calculated to be 0.96 ± 0.28 after the correction of cosmogenic and trapped Xe components, which agrees with the ratio of 0.939 from ^{244}Pu-derived fission (c.f., 0.818 from ^{238}U-derived fission). There may be small contribution from ^{238}U fission as well. Many of CR chondrite-related equilibrated meteorites (including CR6, 7 and primitive achondrites) show old formation ages by short lived nuclides such as Mn-Cr, Al-Mg and Hf-W systems (e.g., [11] and references therein). Our result on NWA 3250 also suggests that extinct nuclides ^{129}I ($T_{1/2} = 15.7$ Ma) and ^{244}Pu ($T_{1/2} = 80$ Ma) must have been alive at the time of Xe closure and that the ^{244}Pu-Xe age is obtained as 107 ± 24 Ma before Angra dos Reis based on the calculation we applied to eucrites [12], where the target element ratio for cosmogenic and the trapped Xe composition is customized to chondritic; the age is slightly changed but not sensitive to them.

References: [1] Meteoritical Bulletin No. 97 (2010). [2] Greenwood et al. (2017) *Chemie der Erde* 77:1-43. [3] Zipfel (2014) *Meteoritics & Planetary Science* 39, Abstract #5346. [4] Irving et al. (2014) *LPS XXXXV*, Abstract #2465. [5] Bunch et al. (2008) *LPS XXXIV*, Abstract #1991. [6] Meteoritical Bulletin No. 97 (2010); Meteoritical Bulletin No. 102 (2015). [7] Sanborn et al. (2014) *LPS XXXXV*, Abstract #2032. [8] Leya et al. (2000) *Meteoritics & Planetary Science* 35:259-286. [9] Busemann et al. (2016) *Developments in noble gas understanding and expertise IV (Nancy, France)*, Abstract. [10] Patzer et al. (2003) *Meteoritics & Planetary Science* 38:1485-1497. [11] Huyskens et al. (2019) *LPS XXXXX*, Abstract #2736. [12] Miura et al. (1998) *Geochimica et Cosmochimica Acta* 62:2369–2387.

SHOCK-INDUCED MELTING AND HIGH-PRESSURE POLYMORPHS IN LUNAR BASALTIC METEORITES

M. Miyahara[1], K. Kozuma[1], E. Ohtani[2], A. Yamaguchi[3], T. Sakai[4], H. Ohfuji[4], N. Tomioka[5], Y. Kodama[6]. [1]Department of Earth and Planetary Systems Science, Graduate School of Science, Hiroshima Univ., Higashi-Hiroshima, Japan, E-mail: miyahara@hiroshima-u.ac.jp, [2]Department of Earth Sciences, Graduate School of Science, Tohoku Univ., Japan, [3]National Institute of Polar Research, Tokyo, Japan, [4]Geodynamics Research Center, Ehime Univ., Japan, [5]Kochi Institute for Core Sample Research, Japan Agency for Marine-Earth Science and Technology (JAMSTEC), Kochi, Japan, [6]Marine Works Japan, Nankoku Kochi, Japan.

Introduction: Since the Moon was born, countless meteoroids have collided on the moon. Lunar meteorites and lunar return samples record the meteoroid impacts occurred on the moon. The high-pressure polymorphs occurring in these samples are the intriguing clues for clarifying the impact events on the lunar surface, because we can constrain several physical parameters (e.g., shock pressure, duration of shock pulse) for the meteoroid impacts using the kinetics of high-pressure polymorphs [e.g., 1, 2, 3]. We have investigated only a few lunar meteorites and return samples about the high-pressure polymorphs so far. Hence, we initiated to conduct systematic investigation about the shock-induced melting and high-pressure polymorphs in the lunar mare basaltic samples NWA 032, NWA 479, NWA 2727, NWA 2977, and NWA 4898 using FE-SEM, micro-Raman spectroscopy, EMPA, and FIB-TEM techniques to obtain the clues for clarifying the impact events occurred on the moon.

Results and Discussion: NWA 032 and NWA 479 had a basaltic lithology. Olivine, Ca-pyroxene, and low-Ca pyroxene occurred as phenocrysts. The matrix was filled with spherulitic textures consisting of plagioclase and Ca-pyroxene. Several shock-melt veins and melt-pockets occurred both in NWA 032 and NWA 479. Olivine grains next to the shock-met veins have transformed into ringwoodite in NWA 032. Olivine grains entrained in the shock-melt veins of NWA 479 have dissociated into bridgmanite (vitrified) + (Mg,Fe)O. The estimated shock pressures for NWA 032 and NWA 479 are ~13 GPa and ~23 GPa at least, respectively.

NWA 4898 also had a basaltic lithology. Olivine occurred as phenocrysts, and the matrix consisted mainly of Ca-pyroxene and plagioclase. Shock-melt veins cut the basaltic lithology. The shock-melt veins entrained a trace amount of silica minerals. The silica minerals in the shock-melt veins were stishovite and silica-glass. Ca-pyroxene next to the shock-melt veins has dissociated into ahrensite, pyroxene-glass, and (probably) silicate titanite. The estimated shock pressure for NWA 4898 is ~9 GPa at least.

NWA 2977 showed a gabbroic lithology and consisted mainly of olivine, low-Ca pyroxene, Ca-pyroxene, and plagioclase. Olivine grains entrained in the shock-melt veins have transformed into ringwoodite. The estimated shock pressure for NWA 2977 is ~16 GPa at least.

Two third of NWA 2727 had a breccia lithology and the other had a gabbroic lithology. The gabbroic lithology consisted mainly of olivine, low-Ca pyroxene, Ca-pyroxene, and plagioclase. Shock-melt veins and melt-pockets occurred both in the breccia and gabbroic lithologies. The breccia lithology included silica minerals besides the fragments of the gabbroic lithology. Silica minerals entrained in the shock-melt veins or melt-pockets have transformed into coesite. The estimated shock pressure for NWA 2727 is ~3 GPa at least.

We found shock-induced melting (shock-melt veins and melt-pockets) and high-pressure polymorphs therein in all investigated lunar samples. Most lunar return samples are brecciated, which is suggestive of heavy meteoroid impacts. Our present systematic investigations revealed that most lunar mare basalts also have experienced a heavy meteoroids impact. We plan to estimate the duration of shock pulse using the kinetics of high-pressure polymorphs identified in the present study. We also found minerals suitable for the radio-isotope dating in the shock-induced melting textures and host rocks. As a next step, we will conduct the radio-isotope dating using the same samples studied here in feature to evaluate the relevance between the radio-isotope ages and shock features (shock pressure, temperature, duration of shock pulse, etc.).

References: [1] Ohtani E., Ozawa S., Miyahara M., Ito Y., Mikouchi T., Kimura M., Arai T., Sato K., Hiraga K., 2011. Coesite and Stishovite in a shocked lunar meteorite, Asuka-881757, and impact events in lunar surface. *Proc. Nat. Acad. Sci. U.S.A*. 108, 463–466. [2] Kaneko S., Miyahara M., Ohtani E., Arai T., Hirao N., Sato K., 2015. Discovery of stishovite in Apollo 15299 sample. *Amer. Mineral*. 100, 1308–1311. [3] Miyahara M., Kaneko S., Ohtani E., Sakai T., Nagase T., Kayama M., Nishido H., Hirao N., 2013. Discovery of seifertite in a shocked lunar meteorite. *Nature Communications*, doi: 10.1038/ncomms2733.

Structure analysis of the hyper velocity impact tracks of the particles captured by silica aerogels on the International Space Station

Nishi Mizuho[1], Akira Tsuchiyama[2], Hajime Yano[3], Hikaru Yabuta[4], Kyoko Okudaira[5], Junya Matsuno[2], Masayuki Uesugi[6], Kentaro Uesugi[6], Tukasa Nakano[7], Takaaki Noguchi[8], Hajime Mita[9], and Akihiko Yamagishi[10], [1]Kyoto University, Kyoto, 606-850 (nishi.mizuho.82e@st.kyoto-u.ac.jp), [2]Ritsumeikan University, Kusatsu, 525-8577 (atsuchi@fc.ritsumei.ac.jp), [3]Institute of Space and Astronautical Science, Japan Aerospace Exploration Agency, [4]Hiroshima University, [5]The University of Aizu, [6]JASRI/SPring-8, [7]National Institute of Advanced Industrial Science and Technology, [8]Kyusyu University, [9]Fukuoka Institute of Technology, [10]Tokyo University of Pharmacy and Life Science.

Introduction: In Japan's first astrobiology experiment "Tanpopo", we have attempted to capture cosmic dust intact by utilizing ultra-low-density amorphous silica aerogel of 10 mg/cc onboard the exposed platform of the International Space Station (ISS) - Japanese Experiment Module "Kibo"[1]. This mission aims to test a hypothesis that life precursors are delivered from the extraterrestrial origin[2]. Similar but denser silica aerogels had been used for NASA's cometary dust sample return mission "Stardust"[3]. Among the Stardust samples, impact tracks were formed on the aerogels by hypervelocity impacts of cometary dust at 6.1 km/s and they were classified into 3 types (types A, B, and C), based on their morphologies[4]. The track morphologies keep useful information for estimating size and density of impacting dust particles[5]. Thus the purposes of this research are as follows: (1) to search for impact tracks formed by cosmic dust onto the Tanpopo aerogels and (2) to describe three-dimensional morphologies of the impact tracks with different origins not only of cosmic dust but also of orbital debris, and finally (3) to clarify the relationship between the track shapes and their origins.

Methods: At the beamline 47XU in SPring-8, we obtained three-dimensional morphologies for eight impact tracks (D1-231, D1-298, D1-362, E1-200, E1-304, F1-328, F1-389, and F1-623) on the Tanpopo aerogels located at o the space pointing face of ISS, by using absorption tomography. The imaging experiments were conducted at 7, 8, and 9 keV, with the voxel size of $0.24 \times 0.24 \times 0.24$ or $0.47 \times 0.47 \times 0.47$ μm^3. The CT images at 8 keV were used to extract the track morphologies to obtain track length (L_t), the maximum track diameter (D_m), aspect ratio, and other shape properties. In order to evaluate the degree of track shape symmetry, we need to determine the deviation of the center of gravity from the averaged center in a cross section of a track normal to its elongation, as a function of the distance from the track entrance. These values were compared with those of the Stardust tracks. Dual-energy tomography (DET)[6], where we can obtain information on the distributions of Fe and Ni by using the K-adsorption edges of Fe and Ni between 7 and 8 keV (7.11 keV) and 8 and 9 keV (8.33 keV), respectively, was applied to estimate the materials of particles captured in the tracks. Another track (E2-000) was observed only with an optical microscope. For D1-231, D1-298, D1-362 and E2-000, the aerogels were compressed and captured particles in the tracks were searched with an optical microscope.

Results and Discussion: The examined tracks on the Tanpopo aerogels were classified into 5 types, based on their morphologies in additions to the three types already identified by the Stardust mission. Type 1 (E2-000) is a track formed by a cosmic dust impact, where two pyroxene particles were identified at the tips of two tracks[7]. The track shape resembles the Stardust type B track although its entrance hole is wider than the typical Stardust tracks. Type 2 (D1-231) is somewhat similar to the Stardust type A track. Type 3 (E1-200 and E1-304) is a track having abundant cracks developed on the inner wall with a narrow entrance. Type 4 (F1-328 and F1-389) is exoriginorigintremely asymmetrical in its shape but has cracks similar to Type 3. Type 5 (D1-362 and F1-623) is a bowl-shaped track with a large entrance, also known as a "pit crater". The relationship between L_t and Dm of these tracks were almost identical as that of the Stardust tracks, except for Type 5. However, their specific shapes of Types 2, 3 and 4 are significantly different from the Stardust tracks. The cracks of these tracks are similar to those seen at the end of Stardust type A and B tracks, indicating that they might be formed by a relatively low-speed impact. Similar tracks to Type 5 or pit craters were also reported in the aerogel exposed on the Mir Space Station[8]. DET results showed that most of fine particles in the tracks do not contain any Fe and Ni. Low values of their X-ray linear absorption coeffi-cients are smaller than that of cosmic dust. They should have been formed by impact of weakly-adhered aggregates that were broken into very small pieces during the track excavation and mixed with the condensed aerogel. Two particles that were confirmed by an optical microscope after compressing in D1-231 and D1-362 have relatively high linear absorption coefficient. Type 1 must be the track with cosmic dust origin since pyroxene grains are present within the track[7]. By considering the 3D-shape features of the tracks and their DET results, Types 2, 3 and 4 might not be tracks with cosmic dust origins, such as secondary impact products since few orbital debris can impact the space pointing face of the ISS Kibo Exposed Facility. Type 5 may be due to high-speed impacts of weakly-adhered aggregates[8].

References: [1] Yamagishi A. et al. (2012) Space Utilization Research 28:220-223. [2] Chyba C. & Sagan C. (1992) Nature 355:125-132. [3] Brownlee D. et al. (2006) Science 314:1711-1716. [4] Hörz et al. (2006) Science 314:1716-1719. [5] Tsuchiyama A. et al. (2009) Meteoritics & Planetary Science 44:1203-1224. [6] Tsuchiyama A. (2013) Geochimica et Cosmochimica Acta 116:5-16. [7] Noguchi T. (2018) Personal communication. [8] Hörz and Zolensky. (2000) Icarus 147:559-579.

NORTHWEST AFRICA 11708 AND 12252: TWO NEW UNEQUILIBRATED CHONDRITES FROM SAHARA.

V.Moggi Cecchi[1], G.Pratesi[2], A.Franza[2], I.A.Franchi[4], R.C.Greenwood[4], [1]Museo di Storia Naturale, Università di Firenze, Via G. La Pira 4, I-50121, Firenze, Italy, [2]Dipartimento di Scienze della Terra, Università di Firenze, Via G. La Pira 4, I-50121, Firenze, Italy, e-mail: vanni.moggicecchi@unifi.it, [4]Planetary and Space Sciences, The Open University, Milton Keynes, MK7 6AA United Kingdom.

Introduction: Two meteorites were found by anonymous finders in Western Sahara. One was purchased in 2016 at the Erfoud market by Hichame Mimaghador and the other one was purchased by Nicola Castellano at the Genova Mineral Fair in May 2017 from a Moroccan dealer. The main masses, weighing 1104 and 752 g, respectively, are markedly different from each since the first one is almost completely covered by black fusion crust and show cracks on the outer surface and the second instead has only small traces of fusion crust. The sawn surface of both show a chondritic texture, the first one almost without metal, the second with several metal spots. Both meteorites have been approved by the Nomenclature Committee of the Meteoritical Society with the names Northwest Africa 11708 and Northwest Africa 12252, respectively [1]. Both the main masses are with owners. The type specimens, weighing 24 and 41 g, respectively, and one thin section are on deposit at the Museo di Storia Naturale dell'Università di Firenze.

Instruments and methods: Optical microscopy was undertaken at the laboratories of the Dipartimento di Scienze della Terra, Università di Firenze, Italy, using an Axioplan-2 polarizing optical microscope equipped with Axiocam-HR camera. SEM-SE images have been performed at the MEMA center of the Università degli Studi di Firenze laboratories by means of a ZEISS EVO MA 15 SEM. EMPA-WDS analyses have been performed at the Firenze laboratories of the IGG – CNR (National Council of Research) with a Jeol Microbeam microprobe. Oxygen isotope analysis of NWA 11708 was undertaken at the Open University.

Experimental results: Both meteorites were investigated by means of optical microscopy, SEM and EMPA techniques. A thin section of each sample was analyzed. The thin section of the first one (NWA 11708) shows a texture composed of separated, well-formed chondrules (ranging in diameter from 300 to 600 µm) of different types, in a fine-grained matrix consisting of Fe-rich olivine, coarse grained Fe-rich olivine fragments and scattered opaque phases. Chondrule types are mainly PO, with minor POP and PP types. Main minerals are olivine, orthopyroxene, Ca-rich plagioclase and clinopyroxene. Opaques mainly consist of troilite and magnetite, with minor altered kamacite. The thin secton of the second meteorite (NWA 12252) shows a chondritic texture, with scattered GO, GOP, PO and POP chondrules, ranging in size from 400 to 800 µm, in a fine grained matrix. GOP chondrules are poikilitic, with olivine grains embedded in twinned clinopyroxene. POP chondrules display olivine grains and elongated pyroxene grains in a glassy mesostasis. Plagioclase is Na and K-rich. Opaque phases consist of Fe,Ni alloys and troilite as individual grains scattered in the matrix or rimming chondrules. An armoured chondrule is visible.

EMPA analyses of selected grains were performed in order to determine the general minerochemical features of the matrix and of chondrules for classification purposes. As concerns NWA 11708, olivine in PO and POP chondrules is remarkably forsteritic ($Fa_{1.7\pm0.2}$, Fe/Mn = 11.4±1.1, N = 6), while olivine in mineral fragments is fayalitic ($Fa_{38.9\pm5.3}$, Fe/Mn = 101.7±10.1, N = 10);   orthopyroxene in chondrules is enstatitic ($Fs_{2.5\pm0.2}Wo_{2.1\pm0.1}$, Fe/Mn = 11.5±1.2, N = 15), while a fassaite-rich fragment has been observed ($Fs_{4.4\pm0.4}En_{56.6\pm0.3}Wo_{39.0\pm0.9}$, Al_2O_3 = 6.0 Wt.%, N = 5). Feldspar is anorthitic ($An_{95.7}Or_{0.1}$). For NWA 12252 olivine is homogeneous both in chondrules and in the matrix ($Fa_{17.4\pm6.2}Fo_{82.7\pm5.9}$; Fe/Mn = 41.2, n=25); orthopyroxene in chondrules is inhomogeneous, with a core-rim variability ($Fs_{18.3\pm0.5}En_{79.9\pm0.5}Wo_{1.8\pm0.1}$, in chondrules' grains rims and in matrix Fe/Mn = 24.1, n=13); low-Ca px in grains cores ($Fs_{7.9\pm4.2}En_{91.6\pm3.9}Wo_{0.5\pm0.1}$, Fe/Mn = 15.1, n=7), high-Ca pyroxene ($Fs_{2.1\pm2.0}En_{52.4\pm5.3}Wo_{45.5\pm4.5}$, n=7); plagioclase is Na and K-rich ($An_{33.7}Or_{33.4}$). Weathering is moderate for NWA 11708 and high for NWA 12252 (W4). Shock stage is low for the second one.

Oxygen isotope analyses performed on NWA 11708 provided the following results: $\delta^{17}O$ = - 4.75 ‰, $\delta^{18}O$ = -1.14 ‰, $\Delta^{17}O$ = -4.15 ‰.
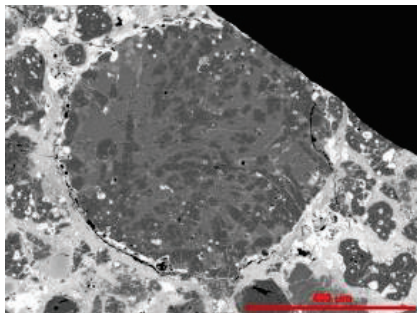

Figure 1: SEM-BSE image of a PO chondrule of NWA 11708; pale gray is olivine; white areas are iron oxides
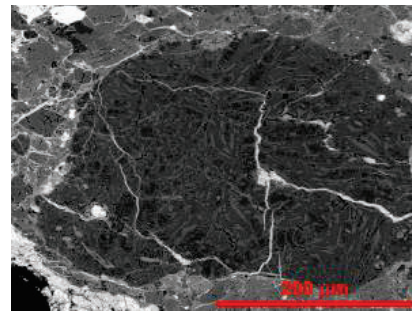

Figure 2: SEM-BSE image of a POP chondrule of NWA 12252; pale grey is olivine; dark grey is orthopyroxene;

Discussion and conclusions:

The textural and minerochemical data are distinctive and point to a classification as CK3 for NWA 11708 and as H3.6 for NWA 12252 [1,2]. Oxygen isotope data confirm this hypothesis for NWA 11708 [3].

References: [1] Gattacceca J., et al. (2019) Meteorit. Planet. Sci. 54 in press.; [2] Grady M. et al. (2014), *Atlas of Meteorites*, 1st ed., CUP, Cambridge, pp.350; [3] Greenwood R.C. et al. (2010). Geochim. Cosmochim. Acta 74, 1684-1705.

DETERMINING COSMOGENIC CONTRIBUTIONS IN APOLLO SAMPLES WITH NOBLE GAS MEASUREMENTS.

P. Morino[1], H. Busemann[1], C. Maden[1] and M. Schönbächler[1]
[1]Instute of Geochemistry and Petrology, ETH Zürich, 8092 Zürich, Switzerland. precillia.morino@erdw.ethz.ch

Introduction: It is generally accepted that the Moon formed as a result of the collision between proto Earth and a potentially Mars-sized impactor, Theia [e.g., 1]. The origin and composition of Theia can be constrained by comparing isotope variations in lunar samples to terrestrial and meteorite data. Previous studies showed a striking similarity in O, Si, Ti and Zr isotopes between the Earth's mantle and the Moon [2-5]. Based on these observations, two hypotheses can be advanced: the Moon mainly formed from the Earth's mantle or Theia originated from the inner solar system and was isotopically similar to the Earth [5-8]. Genetic relationships between solar system objects can be traced by using nucleosynthetic isotope variations. For example, ^{54}Cr variations have a nucleosynthetic origin, while ^{53}Cr is also produced by the decay of the short-lived radionuclide ^{53}Mn. Both types of variations are well characterised in solar system materials [9]. Therefore, high precision Cr isotope data have the potential to further tighten the constraints on the moon-forming scenario [5]. However, the lunar surface is exposed to galactic cosmic rays (GCR) that cause cosmogenic reactions, which can strongly affect the Cr isotope composition of lunar samples. These effects need to be corrected [10]. All four Cr isotopes can be affected by spallogenic reactions on Fe and Ni isotopes, in addition to spallation and neutron capture reactions on Cr itself. The dominant GCR-induced reaction is still debated [11-13], but likely depends on several factors such as chemical composition of the rock, shielding conditions, and the duration of exposure. Thus, knowledge of the different cosmogenic contributions is essential to precisely determine the Cr isotope composition of the Moon. Noble gases are sensitive to cosmogenic reactions and can be a useful tool to constrain these contributions; ^{3}He, ^{21}Ne and ^{38}Ar are easily detectable products of spallation, while additional excesses in ^{80,82}Kr and ^{128}Xe can be produced by neutron capture on ^{79,81}Br and ^{128}I [14]. Previous noble gas studies of Apollo samples rarely report a complete dataset of all He to Xe isotopes. Moreover, the cosmic ray exposure (CRE) ages, if published, are calculated using various analytical techniques, variable and potentially outdated production rates and/or different isotopic systems. To address these shortcomings, we performed a systematic high-sensitivity study of noble gas compositions (He to Xe) in lunar samples with the goal to quantify the GCR effects. Based on the results, we will quantify the different cosmogenic noble gas components and select the least affected samples as best candidates to determine the nucleosynthetic Cr isotope compositions of the Moon.

Samples and Method: We analysed 18 Apollo samples including 14 basalts, two anorthosites, one norite and one sample of lunar orange soil. Noble gas compositions were measured on an in-house-built mass spectrometer ("Albatros") at ETH Zürich. Noble gases were extracted from 1 to 10 mg bulk samples wrapped in commercial Al-foil, in one heating step at ~1700°C. All noble gases (He to Xe) were separated and analysed following the method of [15]. We verified total degassing of the samples by occasional measurements of a "re-extraction" at ~1750°C, which were found to be comparable to blank measurements. Instrumental mass fractionation and sensitivity were monitored using various well-known calibration gases (He-Ne, Ar and Kr-Xe mixtures) and corrected.

Results: The samples yielded ^{21}Ne/^{22}Ne ratios ranging from 0.05 to 0.90 and ^{20}Ne/^{22}Ne ratios from 0.81 to 12.14. Out of 18 analysed samples, 8 show a trapped Ne-Solar Wind (SW) component in addition to cosmogenic Ne. After deconvolution of these two components and calculating the amount of cosmogenic ^{21,22}Ne and ^{3}He, all samples define a positive correlation between ^{3}He/^{21}Ne and ^{22}Ne/^{21}Ne. Furthermore, for 12 samples, the determined cosmogenic ^{3}He concentrations correlate with published exposure ages, mostly calculated based on Ne, Ar and Xe. Both correlations indicate no ^{3}He loss by diffusion [16]. Thus, the new He and Ne data can and will be used for the calculation of new CRE ages. The measured ^{36}Ar/^{38}Ar ratios range from 0.65 to 4.95, while the accepted cosmogenic ^{36}Ar/^{38}Ar ratio in meteorites is ≈ 0.65 [17,18]. In total 9 samples show noticeable amounts of trapped Ar. After deconvolution, all samples yield cosmogenic ^{38}Ar that roughly positively correlates with cosmogenic ^{3}He and ^{21}Ne. This indicates that, for at least noble gases, the neutron capture contribution is negligible.

References: [1] Canup, R. M. (2004) *Icarus* 168:433–456. [2] Wiechert, U. et al. (2001) *Science* 294:345–348. [3] Fitoussi, C. & Bourdon, B. (2012) *Science* 335:1477-1480. [4] Zhang, J. et al. (2012) *Nature Geosci.* 5:251–255. [5] Akram, W. & Schönbächler, M. (2016) *Earth Planet. Sci. Lett.* 449:302–310. [6] Canup, R. M. (2012) *Science* 338: 1052-1055. [7] Dauphas N. et al. (2014) *Philos. Trans. Royal Soc. A* 372:20130244. [8] Meier M. M. M. et al. (2014). *Icarus* 242:316–328. [9] Qin L. *et al* .(2010) *Geochim. Cosmochim. Acta* 74:1122-1145. [10] Leya I. et al. (2001) *Meteorit. Planet. Sci.* 36:1547–1561. [11] Leya I. et al. (2003) *Geochim. Cosmochim. Acta* 67:529–541. [12] Mougel B. et al. (2018) *Earth Planet. Sci. Lett.* 481:1-8. [13] Liu J. et al. (2019) *Geochim. Cosmochim. Acta* 251:73-86. [14] Marti K. et al. (1966) *ZNaturforschung* 21a:398-413. [15] Riebe M. E. I. et al. (2017) *Meteorit. Planet. Sci.* 52:2353-2374. [16] Eugster O. (1988) *Geochim. Cosmochim. Acta* 52:1649-1662. [17] Wieler, R. (2002) *Reviews in Mineralogy and Geochemistry* 47:125-170. [18] Leya I. & Masarik J. (2009) *Meteorit. Planet. Sci* 44:1061-1086.

U-Pb Dating of Baddeleyite in Zagami by NanoSIMS Imaging Analysis

T. Morita[1], Y. Sano[1], N. Takahata[1], K. Misawa[2], S. Sakata[3] and K. Terada[4], [1]Atmosphere and Ocean Research Institute, University of Tokyo (5-1-5 Kashiwa-noha, Kashiwa, Chiba 277-8564, Japan, Corresponding author, E-mail: ysano@aori.u-tokyo.ac.jp), [2]National Institute of Polar Research (10-3 Midorimachi, Tachikawa, Tokyo 190-0014, Japan), [3]Department of Chemistry, Gakushuin University (1-5-1 Mejiro, Toshimaku, Tokyo 171-0031, Japan), [4]Department of Earth and Space Science, Osaka University (1-1 Machikaneyama, Toyonaka, Oasaka 560-0043, Japan)

Introduction: Shergottites is a group of Martian meteorites, which shows relatively young formation ages [1] and important for investigating history of Martian volcanic activity. There are several reports of U-Pb dating for phosphate grains using an ion microprobe method [2,3]. Baddeleyite is a candidate of dating target because it is uranium bearing mineral [4]. However, their grains are significantly small to obtain the precise age by ion microprobe method. We have developed a new method, "imaging analysis", in which larger area than a target mineral is scanned, and the counting data are extracted from the sample grain using a data-processing program after measurements [5]. In this study, we describe a method of imaging analysis and show the U-Pb age of baddeleyites in Zagami, a basaltic shergottite with enriched geochemical signature.

Experiment: Thick section of Zagami with a basaltic lithology [6] was polished carefully by lapping films and carbon coated. Zr mapping was conducted by an electron microprobe (JXA-8900) to locate baddeleyite grains in the section. Twenty baddeleyite grains were identified where we selected seven grains larger than 3 μm. The U-Pb imaging analysis was conducted using an ion microprobe (NanoSIMS 50). $^{16}O^-$ ion was used as a primary beam with a current of 200 pA and a spot diameter of <1 μm. The raster area of primary beam was set to 3×3 μm where 32×32 pixels data were obtained. The intensities of $^{30}Si^+$, $^{90}Zr^+$, $^{204}Pb^+$, $^{206}Pb^+$, ^{207}Pb, $^{238}UO^+$ and $^{238}UO_2^+$ were measured by a multi-ion counter system with magnetic field scanning. These data were calibrated against those of our baddeleyite standard derived from the Phalaborwa Igneous Complex in the lowveld plains of Northern Transvaal, South America [7]. When the sample grains were significantly small, parts of pixel data among 32×32 pixels were selected based on $^{90}Zr^+$ counts and used for U-Pb dating.

Results and Discussion: Observed $^{238}U/^{206}Pb$ ratios of sample grains were calibrated against the ratio of Phalaborwa standard based on the relationship between UO_2/UO and $^{206}Pb/UO$ ratios. The $^{207}Pb/^{206}Pb$ ratios were corrected by the measurement of glass standard, SRM610 under the assumption that matrix effect on lead isotopes is negligibly small. Observed and then corrected $^{238}U/^{206}Pb$, $^{207}Pb/^{206}Pb$ and $^{204}Pb/^{206}Pb$ ratios of seven grains are plotted in 3-D diagram, where data points are linearly aligned within experimental error. Intersect of the regression line on the Tera-Wassurburg Concordia curve gives the U-Pb age of 194±28Ma, which is consistent with the age of 182.7±6.9 Ma in a literature [8]. Common lead component is estimated as $^{206}Pb/^{204}Pb$=12.5±1.6 and $^{207}Pb/^{204}Pb$=11.7±1.7 by the intercept of $^{207}Pb/^{206}Pb$-$^{204}Pb/^{206}Pb$ plane. These values are consistent with evolution curve of terrestrial lead at approximately 3.7 Ga [9], suggesting similar U-Pb systematics.

References: [1] Nyquist et al. (2001) *Chronology and evolution of Mars* 96:105-164, Kluwer Academic Publishers. [2] Sano et al. (2000) *Meteoritics and Planetary Sciences* 35:341-346. [3] Terada et al. (2003) *Meteoritics and Planetary Sciences* 38:1697-1703. [4] Herd et al. (2017) In *Microstructural Geochronology*: Planetary Records Down to Atom Scale, Geophysical Monograph 232:137-166. [5] Terada et al. (2018) *Scientific Reports* 8:11806. [6] McCoy et al. (1992) *Geochimica et Cosmochimica Acta,* 56: 3571-3582. [7] Reischmann, T. (1995) *South African Journal of Geology*, 98: 1-4. [8] Zhou et al. (2013) *Earth and Planetary Science Letters,* 374: 156-163. [9] Stacey and Kramers (1975) *Earth and Planetary Science Letters,* 26: 207-221.

URANIUM-LEAD SYSTEMATICS OF LUNAR BASALTIC METEORITE NORTHWEST AFRICA 2977

N. Moromoto[1], Y. Kawai[1, 2], S. Yokota[1, 2], K. Terada[1, 2], M. Miyahara[3], N. Takahata[4] and Y. Sano[4]

[1]Department of Earth and Space Science, Graduate School of Science, Osaka University, Osaka, 560-0043, Japan (ykawai@ess.sci.osaka-u.ac.jp), [2]Project Research Center for Fundamental Sciences, Graduate School of Science, Osaka University, Osaka, 560-0043, Japan, [3]Department of Earth and Planetary Systems Science, Graduate School of Science, Hiroshima University, Higashi-Hiroshima, 739-8526, Japan, [4]Atmosphere and Ocean Research Institute, The University of Tokyo, Kashiwa, 277-8564, Japan

Introduction: Northwest Africa 2977 (NWA 2977) is a lunar basaltic meteorite found in 2005 [1], which mainly consists of olivine, pigeonite, augite, and plagioclase with accessory minerals including K-feldspar, chromite, ilmenite, phosphate, baddeleyite, troilite and Fe-Ni metal [2]. From this mineral composition, NWA 2977 is classified as an olivine cumulate gabbro, and its origin is a Mare area of the Moon. As a remarkable texture, there is a shock-induced melt vein structure in the investigated sample. For a better understanding of the thermal history recorded in NWA 2977, we have conducted *in-situ* U-Pb isotopic measurement of phosphate grains using an ion microprobe.

Analytical Methods: Initially, in order to identify the location and mineralogy of the phosphate phases from a polished thin section of NWA 2977, the elemental composition measurement was conducted using SEM-EDS. Then, the isotope analysis was carried out with the NanoSIMS at the Atmosphere and Ocean Research Institute (AORI), The University of Tokyo [3]. The primary ion beam (O$^-$) of 0.3 nA was focused to sputter an area 4 μm in diameter on the phosphates, and the positive secondary ions, $^{238}UO^+$, $^{238}UO_2^+$, $^{206}Pb^+$, $^{204}Pb^+$ and $^{207}Pb^+$, were collected from 15 phosphates found in the shock melt vein (SMV) and host-rock of NWA 2977. From the empirical relationship of the standard apatite, PRAP [4], the isotope ratios, $^{238}U/^{206}Pb$, $^{207}Pb/^{206}Pb$, $^{204}Pb/^{206}Pb$, were obtained.

Results and Discussion: The data from 15 phosphate grains in NWA 2977 are well expressed by linear regression and are not scattered on the plane in the $^{238}U/^{206}Pb$, $^{207}Pb/^{206}Pb$, $^{204}Pb/^{206}Pb$ three-dimensional space, which means that the disturbance of the U-Pb systems did not occur in this meteorite. The resultant concordia age was 3.13 ± 0.10 Ga, which is consistent with the previous studies obtained from the whole-rocks and minerals (Nd-Sm age of 3.10 ± 0.05 Ga, Rb-Sr age of 3.10 ± 0.05 Ga, and Pb-Pb baddeleyite isochron age of 3.12 ± 0.01 Ga) [5,6]. There is no clear difference in the isotopic compositions between the phosphates found in the SMV and host-rock, while the shape and size of the grains and the Raman spectra show the evidence of intense shock metamorphism. Based on this finding, the cooling rate of phosphate was calculated to be very fast, constrained to be larger than 140 K/s.

The U-Pb systematics of NWA 2977, shows an extremely low μ-value ($^{238}U/^{204}Pb$ ratio) compared with those of Apollo samples ranging from several hundreds to several thousands [7]. The extremely low μ-value and the young crystallization age of 3.10 Ga of NWA 2977 suggest that the origin of magma source of this meteorite might be different from those of the explored region of the Moon surface.

[1] Connolly H. C. et al. (2006) *Meteorit. Planet Sci.* 41:1383–1418. [2] Bunch T. et al. (2006). *LPS XXXVII*, Abstract #1375. [3] Sano Y. et al. (2006) *Geochem. J.* 40:597-608. [4] Sano Y. et al. (1999) *Chem. Geol.* 153:249-258. [5] Nyquist L. et al. (2009) *Meteorit. Planet. Sci.* 44 (Issue S7):A15–A229, Abstract #5347. [6] Zhang A. (2010) *Meteorit Planet Sci.* 45:1929-1947. [7] Snape J. F. et al. (2016) *Earth Planet. Sci. Lett.* 451:14-158.

MID-INFRARED MICROSPECTROSCOPIC STUDY OF DIFFERENT STRUCTURES OF TSAREV METEORITE AFTER SHOCK-WAVE LOADING

R.F. Muftakhetdinova[1], N. A. Kruglikov[1,2,3], and V. I. Grokhovsky[1], [1]Ural Federal University, [2]Institute of Metal Physics of Ural Branch of RAS,[3]Ural State University of Economics, Ekaterinburg, Russian Federation, e-mail: nick@imp.uran.ru

Introduction: Comparison of the reflection spectra of meteoritic substances obtained in the laboratory after impact, with the results of remote observation of asteroids is of great importance and allows us to judge the composition and surface properties of the atmosphereless bodies of the Solar System [1].The aim of the work is to investigate the spectral properties of Tsarev L5 ordinary chondrite after model experiments on shock-wave loading.

Samples and Methods: After the shock-wave loading in the ball, three visually distinguishable zones were formed: 1) the central part corresponds to the complete remelting of the chondrite substance; 2) the black ring corresponds to the effect of a partial change in the initial chondritic structure. The temperatures reached in this zone as a result of shock loading cause the metal and troilite to melt while maintaining the original texture of the silicate part of the substance; 3) the slightly modified part practically corresponds to the initial structure.

Spectra of three different zones of the ball were obtained using a SIMEX FT801 Fourier spectrometer with a Micran-2 infrared microscope.

Results and Discussion: Measurements were taken on a diametric section of sphere samples obtained from the Tsarev meteorite fragments. We used the same technology for measurements and averaging as before [2]. The main feature of the Tsarev after shock-wave loading is shifting of the olivine 886 and pyroxene 1065 peaks of different structures (Fig. 1).
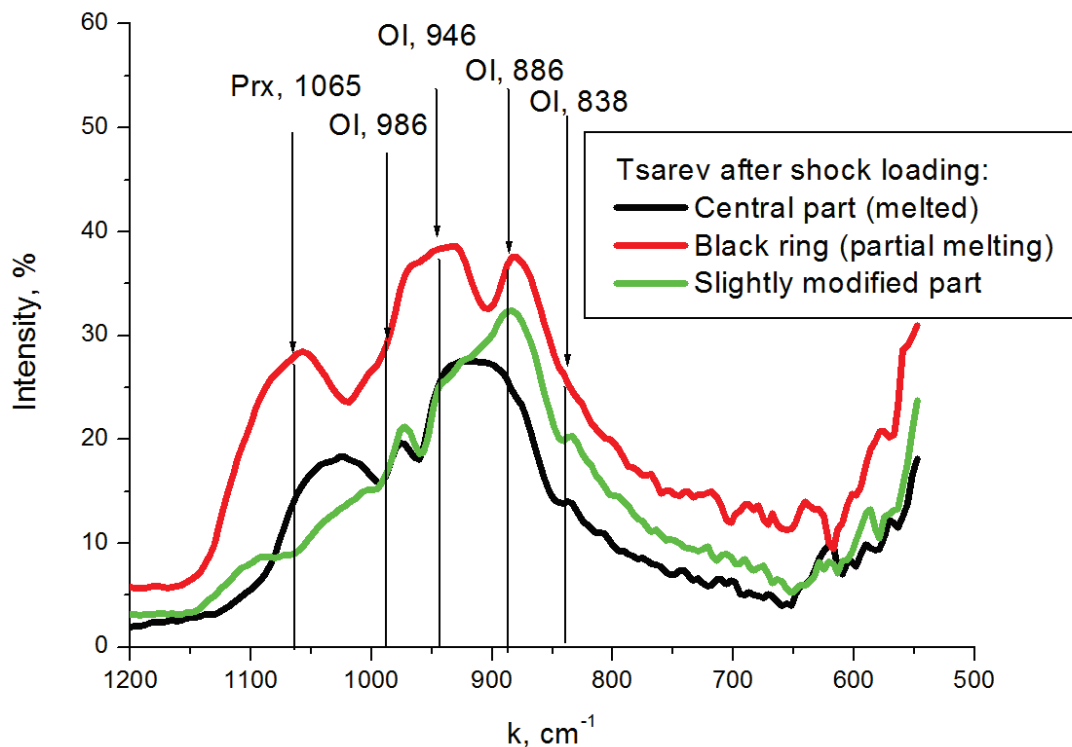

Fig.1. Mid-infrared spectra of different structures of the Tsarev meteorite after shock-wave loading.

References:[1] Busarev V.V., et.al. (2015) *Icarus* 262: 44-57. [2] Kruglikov N.A., Grokhovsky V.I. (2017) *Meteoritics & Planetary Science* 52: 6356.

STRUCTURAL FEATURES OF THE IMPACT MELT OF THE ORDINARY CHONDRITE OZERKI L6: PRELIMINARY DATA.

R. F. Muftakhetdinova, A.Yu. Pastukhovich , G. A. Yakovlev, V. I. Grokhovsky. Institute of Physics and Technology, Ural Federal University, Ekaterinburg, Russian Federation, e-mail: gizrozka91@bk.ru.

Introduction: The fall of the Ozerki meteorite shower occurred on June 21, 2018 (at 01:16:20 UT) in the Lipetsk region, Russia. The meteorite was classified as ordinary chondrite L6, S4/5, W0. Most fragments represent samples of light lithology, several fragments of dark lithology (shock-melted substance) have also been found. This work presents the results of the study of the structural features in the shock-melted sample.

Samples and Methods: Fragment with a shock-modified structure (15.4 g, density 3.7 g/cm^3) was the object of this research. This sample was found on August 12, 2018. The coordinates of the finding are 52°47.956'N, 38°10.508'E. Part of the sample was prepared for microscopic analysis by standard metallographic procedures: grinding, polishing, and etching with 2% nital. The meteoritic microstructure was examined using a Zeiss Axiovert 40 MAT inverted microscope and FE-SEM ∑IGMA VP equipped with EBSD and EDS units.

Results and Discussion: The sample under study has two visually distinct zones (two lithologies). The first zone is gray in color, this area correspond to complete remelting of the chondrite substance followed by recrystallization. In this structure, new olivine grains, metal-sulfide globules with an eutectic structure and impact veins are observed. The second zone is black, this lithology is an intermediate between the initial light substance and complete remelting. The structure of the black lithology contains relict chondrules in a silicate matrix, which consists of large grains of olivine and pyroxenes. The grain boundaries in the matrix are filled with a metal-troilite melt. Chromite, albite, and apatite grains are also observed. The metal is present in the form of kamacite, taenite, and martensite. In the zone with black lithology, several grains with the structure of lenticular martensite are founded. Troilite grains have a porous, spongy-like structure. High-nickel nanoscale grains were found in veins and globules. The phase composition in the metal-sulfide components varies greatly. Chemical mapping shows the background enrichment of various elements of the platinum group in different metal grains, metal-sulfide veinlets and globules. If in troilite it is Pl-Os-Ir, then in apatite it is Ru and Rh. Earlier in [1, 2], phases with PGE in a meteoritic substance were described. It is believed that the metal in the LL and L chondrites is more enriched in PGE than the metal in the H-chondrites [3]. At the border of two lithologies, there is a massive metallic inclusion, which contains martensite, kamacite, and taenite. Precipitation of pure copper has been found on the border of kamacite and martensite.

In this sample, there is a small amount of fusion crust. The fusion crust contains dendrites of magnetite and olivine in a silicate matrix, as well as a large number of gas bubbles.

Conclusions: On grounds of the shock-metamorphosed structure of gray lithology and the newly formed olivine grains it can be concluded that the pressure exceeded 45 GPa and the temperature reached 1400°C. This corresponds to the shock stage S5. In intermediate lithology, the pressure did not exceed 35 GPa, the degree of metamorphism corresponding to this zone – S4. A higher density than the original substance (the density of light lithology is 3.3 g/cm^3) may be due to a large number of metal-sulfide inclusions, as well as the presence of PGE.

References: [1] Palme H. (2008) *Elements* 4:233-238. [2] Rambaldi E.R. (1977) *Earth & Planetary Science Letters* 36:347–358. [3] Kargel J.S. (1994) *Journal of Geophysical Research* 90:21,129–21,141.

GLOBAL DATASETS OF THE GEOPHYSICAL FIELDS AS AN INSTRUMENT FOR IMPACT STRUCTURES DISCOVERY

L. A. Muravyev[1,2], [1]Institute of Geophysics Ural Branch of RAS, 620016, Amundsen st. 100, Ekaterinburg, Russia, mlev@igeoph.net, [2]Ural Federal University 620002, Myra st.19, Ekaterinburg, Russia, l.a.muravyev@urfu.ru.

Introduction: Imprints of shock processes, which the Earth's crust keeps till the present time, contain important information about the geological past of the lithosphere and the processes of impact metamorphism in rocks. Therefore, the study of impact structures is an important part of planetary science and the systematic identification of such structures on Earth is being conducted. Earth impact database [1] now contains 190 records of reliably confirmed structures, and many of them have the status of uncertain. The problem is also that some geological structures of a ring shape are exclusively terrestrial in origin. Now the remote sensing of the Earth is one of the most perspective methods for detecting new impact structures. Geological structures can be reflected in the geopotential fields (magnetic, gravitational), the present relief, and be visible in modern highly detailed satellite images. Of course, the geophysical criterion and the criterion of form cannot be the only method for identifying impact structures and irrefutable proof of their cosmic origin, but a focused study of modern datasources can lead to finding new objects and direct further ground-based geological research. A detailed study of the anomalous magnetic field of impact structures was performed [2] using the magnetic field database WDMAM ver. 1. But the quantity, quality, spatial resolution of modern global geophysical databases are increasing every year, keeping the relevance of analyzing and comparing these sources among themselves for solving the problem of identifying new geological structures of cosmic origin.

Methods. We explored modern global databases of magnetic, gravitational fields and relief. At 2003 the International Association of Geomagnetism and Aeronomy started work on creating a global map of magnetic anomalies of the Earth, which was finished in 2007 by the publication of the first version of the World Digital Magnetic Anomaly Map (WDMAM). Now available the second version of the WDMAM database [3] with spatial resolution 0.05 arc degrees. The corresponding altitude of the data is 5 km for terrain and sea level for marine model data. During this work, Maus et al. presented their own map, named EMAG2. The difference in the models is in different methods of processing of almost the same sets of source data. EMAG2 version 3 has the 2 arc min spatial resolution, and the height reduced to 4 km above the geoid [4].

There are several global databases of gravitational field anomalies, obtained by a number of scientific groups by merging terrestrial, altimetry-derived, and airborne gravity data and results of satellite projects Grace and GOCE. In these models the gravitational field described as a truncated series of spherical harmonics with maximum degree 2190, which corresponds to a spatial resolution of no worse than 10 km. The first of the most detailed models of global gravity is EGM2008, also we have reviewed newer models GECO and EIGEN-6C4, available for calculation on the website ICGEM and model WGM2012 [5], which available as 2 arc min grid.

We can use data from the SRTM project, implemented in 2000 and covering the territory from 56° S to 60° N, as a source of high-precision relief data. The CGIAR-CSI version 4 provides the best global coverage full resolution SRTM dataset [6]. Later this project was generalized and combined with ocean bathymetry data, but the spatial resolution of these data is significantly lower. The SRTM alternative has even better spatial resolution and greater coverage - the ASTER GDEM project, but this data contains many errors, outliers and voids.

Results and discussion. For the analysis, we selected the 20 largest confirmed impact structures according to the Earth impact database [1]. The smallest structures included in the analysis have a diameter of 40 km (Araguainha, Chesapeake Bay, Mjølnir, Puchezh-Katunki, Saint Martin, Woodleigh). This test set includes both ground and underwater structures. We have constructed maps of the databases listed above for the territories around them. The results of the comparison of different databases among themselves are given in the report. It was concluded that even large impact structures are reflected differently in geopotential fields. For some of them, the anomalies are weak and blurred, indistinguishable from the anomalies of other features of the geological structure, which were formed in subsequent periods. Interestingly, for some locations, the shapes of the anomalies are significantly different for different models due to deficiencies in the source data. However, the global databases of geophysical field anomalies, available online, can be a reliable tool for discovering new impact structures and modern computational resources and technology can automate this process. In addition to global databases, it is necessary to systematize the primary data of local digital field databases available for particular regions and countries and include into the processing procedure.

References: [1] Earth Impact Database, http://www.passc.net/EarthImpactDatabase/New%20website_05-2018/Index.html. [2] Anca Isac et al. (2016) *Advances in Space Research* **57**, 477–492. [3] Lesur, V. et.al. (2016) *Earth, Planets and Space,* **68**(1), 27. DOI:10.1186/s40623-016-0404-6. [4] Meyer B. et.al. (2017) EMAG2 Version 3. DOI:10.7289/V5H70CVX. [5] Balmino, G., Vales, N., Bonvalot, S. Briais, A. (2012) *Journal of Geodesy,* **86**(7), 499-520 [6] SRTM 90m DEM Digital Elevation Database, http://srtm.csi.cgiar.org/

The Chrono List of Bad Meteorites

L. A. Muravyev[1,2] and V. I. Grokhovsky[1]

[1]Ural Federal University 620002, Myra st.19, Ekaterinburg, Russia, grokh47@mail.ru;

[2]Institute of Geophysics Ural Branch of RAS, 620016, Amundsen st. 100, Ekaterinburg, Russia, mlev@igeoph.net

Introduction: Since the formation of the Solar System, each planet has been exposed to interplanetary matter. Planets with solid surfaces as well as their satellites and even asteroids keep traces of meteorite bombardment, and their surfaces are dotted with impact craters of various sizes. The Earth was also subject to these effects, but the presence of soil, vegetation, erosion led to the disappearance of most craters.

The problems of asteroid-comet hazard have been much discussed lately. The result of the Earth's collision with a huge meteorite or comet can affect the climatic conditions on the planet. But these events occur infrequently. The last time such a phenomenon probably led to the dinosaur's extinction and a sharp cooling. Falls of small meteorites occur much more often. Most of them fall into the ocean, seas, deserts, dense forests and other sparsely populated areas, however, the probability of a meteorite entering the area of human activity is still non-zero.

Methods: We have systematized the available official information on cases of damage to property or human health by an extraterrestrial substance, in order to assess whether this threat is significant to humanity.

For the first recorded incident of damage by a meteorite, we take a record of a Franciscan monk killed by a meteorite in 1654 (according to the British Museum meteorite catalog [1]). This catalog was taken as the basis for the search and verification of information about the fall of "bad" meteorites before 1966. Later data were checked for regular releases of the official Meteoritical Bulletin, available online [2].

We selected reports of direct damage to buildings (for example, a roof was punched), or property (for example, a car), or damage caused to persons or animals. It should be mentioned about many cases when a meteorite fell directly near a person (up to 1 meter, as for the Thika meteorite in Kenya, 2011), but since there was no harm, these messages are not included in the table. Also not included are reports of meteorites falling on agricultural fields, edges of roads, football fields, etc. Also, the table does not include the Tunguska cosmic phenomenon, due to the absence of the detected meteoric substance.

Results and discussion: Systematized information about these events was published in Russian in 2008. It was concluded that for the entire time of registration of meteorite falls only a few dozen cases of cosmic substances penetrating the human environment were recorded. There are several unreliable cases of a meteorite hitting a person, but most often meteorites fall into the rooftops, causing local damage of different buildings.

The fall of the Chelyabinsk meteorite significantly changed the picture at that time. Unprecedented destruction occurred as a result of the shock wave. A lot of windows were broken in the regional center Chelyabinsk and nearby settlements. People were injured by glass fragments. According to media reports, a total of 1,613 people came to the hospitals of the Chelyabinsk region with wounds, of which 69 were hospitalized. The roof is damaged and the brick wall of the warehouse of the zinc plant is destroyed. The damage described was not the result of exposure to a meteorite directly, but is relates to its flight in the atmosphere. So Chelyabinsk meteorite should certainly be included in the list, and work on the list of "bad" meteorites should be continued.

On the poster, we present a table containing information on such cases to date. In compiling the table, we took as a basis the information provided by the electronic and printed Meteoritical Bulletin. To date (April 2019), 123 bad meteorites have been recorded in meteoritic catalogs, there are 6 cases of a meteorite killing animals, 6 cases of a meteorite hitting humans, 3 of which are fatal, 7 meteorites damaged cars. If we take the total number of recorded meteorite falls over 1300 (falls, not including finds), then in about every tenth visible fall, the meteoritic substance directly affects a person and his property.

References: [1] Hey M.H. Catalogue of meteorites (3d Edition) //British Museum, London,1966.

[2] The Meteoritical Bulletin, [electronic resource] https://www.lpi.usra.edu/meteor/.

GENETIC RELATIONSHIP BETWEEN MARTIAN CHASSIGNITES AND NAKHLITES REVEALED FROM NOBLE GASES. K. Nagao[1], J. Park[2,3,4], J. Choi[1], J. M. Baek[1], M. K. Haba[5], T. Mikouchi[6], M. E. Zolensky[7], G. F. Herzog[3], C. Park[1], J. I. Lee[1], and M. J. Lee[1], [1]Korea Polar Res. Inst. (KOPRI), Yeonsu-gu, Incheon 21990, Rep. of Korea (nagao@kopri.re.kr), [2]Kingsborough Comm. Coll., Brooklyn, NY 11235, USA, [3]Dept. Chem. & Chem. Biol., Rutgers Univ. of Piscataway, NJ 08854, USA, [4]Amer. Muse. of Natural History (AMNH), NY 10024, USA, [5]Dept. of Earth & Planet. Sci., Tokyo Inst. of Technology, Meguro-ku, Tokyo 152-8551, Japan, [6]Univ. Museum, Univ. of Tokyo, Tokyo 113-0033, Japan, [7]ARES, NASA Johnson Space Center, Houston, TX 77058, USA.

Introduction: The group called Martian meteorites comprises shergottites, nakhlites, chassignites, ALH 84001 orthopyroxenite, and NWA 7034 and its pairs. They are thought to come from Mars. The nakhlites and chassignites show similar cosmic-ray exposure (CRE) ages of 11-12 Ma, although their petrologic characteristics are very different. Both nakhlites and chassignites indicate similar cooling rates, and would have cooled in identical scale of igneous bodies [e.g., 1, 2]. However, relationship between nakhlites and chassignites is still unclear: They might have been ejected at the same time by coincidental impacts that occurred at different places on Mars or by a single impact that excavated both nakhlites and chassignites from a relatively small area. Based on noble gas data obtained in our laboratory we propose that the chassignites and nakhlites were located within a relatively narrow area from which launch took place. If both chassignites and nakhlites were ejected by a single impact, they provide a geological/petrological profile in the area where both pyroxene-rich lava (nakhlites) and dunite-rich rocks (chassignites) are located close to Martian surface.

Samples: Three chassignites (Chassigny, NWA 2737, NWA 8694), Nakhla, and four MIL nakhlites were analyzed either as total melts (TM) or by heating in n steps (nSH): Chassigny (49.1 mg 8SH), NWA 2737 (109.3 mg 6SH; 221.9 mg 13SH; 210.7 mg 16SH; 27.9 mg TM; 26.3 mg TM), NWA 8694 (31.47 mg 9SH; 5.44 mg TM), Nakhla (126.4 mg 8SH; 13.6 mg TM), MIL 03346 (87.5 mg 15SH; 35.2 mg TM), MIL 090030 (43.7 mg 9SH; 4.75 mg 16SH), MIL 090032 (44.3 mg 9SH; 5.18 mg 17SH), and MIL 090136 (49.0 mg 9SH; 5.16 mg 17SH).

Results and Discussion: Average CRE ages based on cosmogenic ^{3}He, ^{21}Ne and ^{38}Ar for nakhlites and chassignites calculated following the methods by [3, 4] are 11.5 ± 0.7 and 12.3 ± 3.6 Ma, respectively. The older age range with larger uncertainties for chassignites is mainly due to higher and lower ages yielded from ^{3}He and ^{38}Ar, respectively. It was already reported that ^{3}He yields consistently higher ages for Chassigny [5]. Both ages for nakhlites and chassignites, however, overlap within experimental uncertainties, and also with most of ages reported [e.g., 5, 6, 7, 8]. In plot of ^{129}Xe/^{132}Xe versus ^{84}Kr/^{132}Xe (see figure) Martian meteorites are shown to contain several noble gas components of different origins, i.e., Martian interior (Chassigny), Martian atmosphere (Impact glasses in shergottites), elementally fractionated Martian atmosphere (aqueously altered minerals such as iddingsite), and elementally fractionated Earth atmospheric contamination [e.g., 5, 9, 10, 11]. The three chassignites show wide variation, different from each other. Data for NWA 2737 plot along a mixing line between Martian interior and atmosphere, suggesting a presence of shock-implanted Martian atmosphere, consistent with the heavily shocked nature of this meteorite. The third chassignite NWA 8694, however, shows important trend suggesting a presence of both Chassigny-like and MIL-nakhlite-like noble gases. The characteristic trend for MIL, heavier fractionation than that for iddingsite, is different from those for other nakhlites [12, 13, 14]. The similar trends observed for NWA 8694 and MIL nakhlites suggest that both rocks were affected by aqueous alteration while exposed to surface fluids containing extremely fractionated Martian atmospheric noble gases.

The identical CRE ages and characteristic noble gas compositions observed for both MIL nakhlites and NWA 8694 chassignite strongly support that both nakhlites and chassignites are launch-paired Martian meteorites.

References: [1] Mikouchi T. et al. (2017) *Ann. Meeting Meteorit. Soc.* Abst. #6109. [2] Mikouchi et al. (2006) *LPS XXXVII* Abst. #1865. [3] Eugster O. and Michel Th. (1995) *GCA* 59:177–199. [4] Welten K. et al. (1997) *Meteorit. Planet. Sci.* 32:891–902. [5] Ott U. (1988) *GCA* 52:1937–1948. [6] Okazaki R. et al. (2003) *Antarct. Meteorite Res. NIPR* 16:58–79. [7] Marty B. et al. (2006) *Meteorit. Planet. Sci.* 41:739–748. [8] Eugster O. et al. (1997) *GCA* 61:2749–2757. [9] Bogard D. D. and Johnson P. (1983) *Science* 221:651–654. [10] Mohapatra R. K. et al. (2009) *GCA* 73:1505–1522. Swindle T. D. et al. (2000) *Meteorit. Planet. Sci.* 35:107–115. [12] Murty S. V. S. et al. (2005) *LPS XXXVI* Abstract #1280. [13] Nagao K. and Park J. (2008) *LPS XXXIX* Abstract #1614. [14] Nagao K. et al. (2016) *Ann. Meeting Meteorit. Soc.* Abst. #6109.
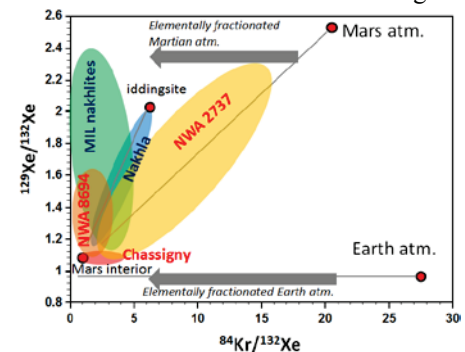
ABUNDANT ^{16}O-RICH OLIVINES IN CHONDRULES FROM ORDINARY CHONDRITES: IMPLICATIONS TO OUTWARD TRANSPORT OF DUST IN THE PROTOPLANETARY DISK.

K. Nagashima[1], G. Libourel[2], D. L. Schrader[3], and A. N. Krot[1], [1]HIGP, University of Hawai'i, 1680 East-West Road, POST 602, Honolulu, HI 96822, USA (kazu@higp.hawaii.edu), [2]Observatoire de la Côte d'Azur, Nice, France, [3]CMS, SESE, Arizona State University, Tempe, AZ 85287, USA.

Introduction: Ca, Al-rich inclusions (CAIs) and amoeboid olivine aggregates (AOAs) are thought to have formed in a gas of ~solar composition in a hot innermost region of the protoplanetary disk at the birth of the solar system. The presence of these objects in chondrites and 81P/Wild 2 comet suggests CAIs and AOAs were subsequently transported outward from this region and dispersed throughout the disk. The exact mechanism of this transport, however, is not understood: radial transport by disk wind and by disk expansion and turbulent diffusion are being discussed [e.g., 1–3]. We have recently described abundant relict ^{16}O-rich olivine grains, most likely related to AOAs, in agglomeratic olivine chondrules and igneous rims around chondrules; both types of objects experienced melting to a very minor degree [4–7]. In CR chondrules, the abundance of ^{16}O-rich relict grains is several % [6]. Because chondrules in different chondrite groups formed in different disk regions, the abundances of ^{16}O-rich relict grains in chondrules could potentially provide important constraints on the efficiency of radial transport of refractory solids. Here, we report on distribution of ^{16}O-rich olivines in chondrules from the least metamorphosed unequilibrated ordinary chondrites (UOCs).

Results and Discussion: Three chondrules from Semarkona (LL3.01) and MET 00452 (L/LL3.05) chondrites were investigated. Two of them are composed of fine-grained (largely <20 µm) FeO-rich olivine, Na-bearing feldspathic glass, and rare low-Ca pyroxenes, and are texturally similar to agglomeratic olivine objects [7–8]. Some relatively large olivine grains have MgO-rich cores. One microporphyritic/agglomeratic olivine chondrule from Semarkona has a layered structure with a type I chondrule host surrounded by a type II chondrule-like igneous rim. Two to four δ^{18}O isotope maps per chondrule were obtained using the Isotope Microscope system [5]. All δ^{18}O maps revealed ^{16}O-rich (δ^{18}O ~ −40‰) olivine grains (Fig. 1). These are typically from MgO-rich cores in olivine crystals. This result clearly indicates AOA-like olivines were a common precursor of chondrules in UOCs.

The 2D disk model [9] show µm-sized grains can be efficiently transported outward by turbulent diffusion. The recent models of protoplanetary disk evolution, including formation of a gap due to an early accretion (0.6 Myr after CAIs) of a proto Jupiter [10], and radial transport of CAIs by disk expansion and turbulent diffusion along the disk midplane suggest CAIs initially transported throughout the disk would have been subsequently removed from the disk inside Jupiter's orbit by aerodynamic drag and thus could explain the virtual absence of CAIs in ordinary and enstatite chondrites [3]. The model of [3] predicts abundant CAIs (~1–5 vol%) in the inner disk region within 1 Myr, which would have accreted to early formed asteroids such as the HED parent asteroid. However, these achondrites do not show stable isotope anomalies that CAIs often carry (e.g., ^{50}Ti, ^{95}Mo). The nearly complete absence of refractory inclusions with ^{16}O-rich µm-sized olivine grains in UOCs may suggest two different mechanisms for outward transport of refractory solids: small ^{16}O-rich olvines were transported throughout the disk mid-plane by disk expansion and turbulent diffusion, while larger CAIs were transported beyond Jupiter by the disk wind.

References: [1] Hansen B. M. S. (2013) *Mon. Not. R. Astron. Soc.* 440:3545–3556. [2] Yang L. and Ciesla F. J. (2012) *MAPS* 47:99–119. [3] Desch S. J. et al. (2018) *ApJS.* 238:11. [4] Nagashima K. et al. (2013) *LPS 44*, Abstract #1780. [5] Nagashima K. et al. (2015) *GCA* 151:49–67. [6] Nagashima K. et al. (2016) *Goldschmidt* Abstract #2210. [7] Schrader D. L. et al. (2018) *GCA* 223: 405–421. [8] Ruzicka A. et al. (2012) *GCA* 76:103–124. [9] Taillifet E. et al. (2014) *LPS 45*, Abstract #2086. [10] Nanne J. A. M. et al. (2019) *EPSL* 511:44–54.
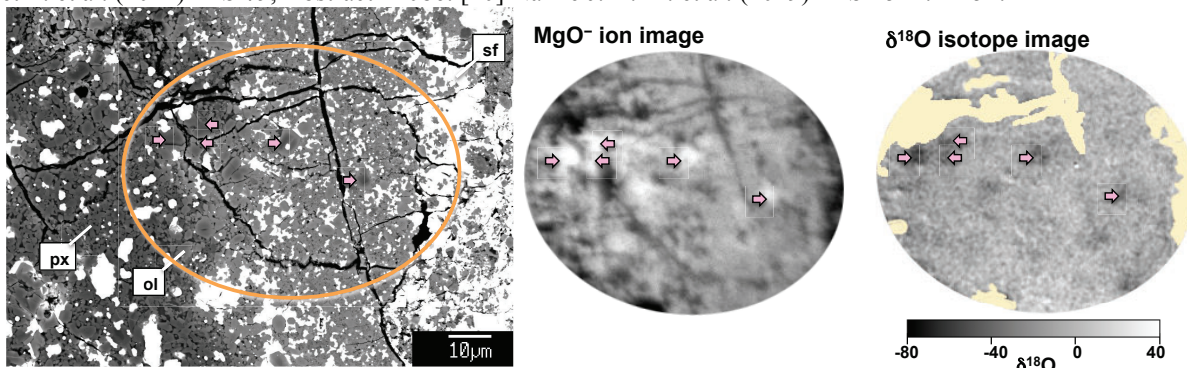

Figure 1. BSE and isotope images (MgO and δ^{18}O) in AO#1 chondrule from Semarkona (UNM312). Pink arrows indicate ^{16}O-rich olivine grains. Yellow regions in δ^{18}O map are masked due to unstable/low oxygen signals.

EXPLOSIVE CRATER EXPERIMENTS OF POROUS GYPSUM TARGETS.

A. M. Nakamura[1], K. Ogawa[1], Y. Murakami[1], Y. Yamasaki[1], Y. Nagaashi[1], K. Nomura[1], T. Kadono[2], R. Suetsugu[2], N. Kawai[3], S. Tanaka[3], and T. Okamoto[4], [1]Department of Planetology, Kobe University (1-1 Rokkodai-cho, Nada-ku, Kobe, 657-8501, Japan), [2]School of Medicine, University of Occupational and Environmental Health (1-1 Isei-gaoka, Yahata, Kitakyusyu, 807-8555, Japan), [3]Institute of Pulsed Power Science, Kumamoto University (2-39-1, Kurokami, Chuo-ku, Kumamoto City, 860-8555, Japan), [4]The Institute of Space and Astronautical Science, Japan Aerospace Exploration Agency (3-1-1 Yoshinodai, Chuo-ku, Sagamihara, Kanagawa, 252-5210, Japan).

Introduction: Crater size on the surface of a planetary body generally depends on the gravity acceleration and target properties such as density and mechanical strength [1]. Crater size on porous meteorite parent bodies is determined by material strength as well as porosity when an impact excavates the solid interior of the body under the regolith on the surface. Laboratory impact experiments have shown that the cratering efficiency decreases as the bulk porosity of the target increases. On the other hand, explosive events were considered to be effective for simulating large craters that are impossible in impact experiments. In the development of crater scaling relationship in the gravity regime, data of explosive events were used in addition to those of the impact events[2]. We performed explosive crater experiments using porous gypsum targets to examine the similarity between the outcomes of explosive events and impact events on porous targets.

Experiments: We prepared twenty-seven cylindrical gypsum targets with diameter of 15–40 cm, height of 7–33 cm, and density of $1.0–1.1 \times 10^3$ kg/m^3 (porosity of 52–57%). We used a detonator (No. 6 electric detonator produced by Kayaku Japan Co., Ltd.) and a SEP explosive (Kayaku Japan Co., Ltd.), density of 1.3×10^3 kg/m^3, detonation velocity of 6.97 km/s, and mass of 0–6 g. The explosives were buried at a depth between 0 and 4.5 cm from the top of the cylinder. The energy density of the SEP explosive is 4.158×10^6 J/kg. This value of energy density is equivalent to the kinetic energy of an impactor with the same mass as the SEP explosive and with 2.9 km/s in velocity. The explosion was monitored by a high-speed imaging camera at 6400 fps.

Results: Targets were engulfed to form a circular crater. Targets with small diameter were partially destructed with the bottom surface of the target was essentially unbroken, or totally destructed. The degree of destruction depended on the diameter of the target, the amount of explosives, and the depth of burial of the explosives or the detonator. The deeper the explosives were buried, the more damage and the larger the crater volume tended to be. We reconstructed the partially destructed targets. The crater had a spherical deep depression (pit) in the center of the larger shallow depression (spall). Pit diameter, spall diameter, and crater depth were measured. The volume of the crater was measured by pouring glass beads into the crater cavity. The ratio of the spall diameter to the pit diameter was approximately 1.5, which corresponds to the lower limit of values for craters formed in impact experiments using a two-stage light-gas gun [3]. We will discuss a detailed comparison with the literature data of laboratory impact crater experiments on gypsum targets [4, 5].

References: [1] Holsapple K. (1980) *Proc. Lunar Planet. Sci. Conf.* 11, 2379-2401. [2] Holsapple K. (1993) *Annual review of earth and planetary sciences* 21, 333-373. [3] Nakamura A. M. 2017. *Planetary and Space Science* 149:5-13. [4] Yasui M. et al. (2012) *Icarus* 221, 646-657. [5] Okamoto T. and Nakamura A. (2017) *Icarus* 292, 234-244.

EXPERIMENTAL REPRODUCTION OF SPACE WEATHERING OF C-TYPE ASTEROIDS BY HE EXPOSURE TO SHOCKED AND PARTIALLY DEHYDRATED CARBONACEOUS CHONDRITES.

T. Nakamura[1], C. Lantz[2], S. Kobayashi[1], Y. Nakauchi[3], K. Amano[1], R. Brunetto[2], M. Matsumoto[1], M. Takahashi[1], M. Matsuoka[3], T. Noguchi[4], T. Matsumoto[4], A. Miyake [5], A. Tsuchiyama[6], M. E. Zolensky[7], [1]Division of Earth and Planetary Materials Science, Graduate School of Science, Tohoku University, Aoba, Sendai, Miyagi 980-8578, Japan, [2]Institut d'Astrophysique Spatiale, CNRS, Université Paris-Saclay, Orsay, France, [3]JAXA/ISAS, Sagamihara, Japan, [4]Faculty of Arts and Science, Kyushu University,Fukuoka 819-0395, Japan, [5]Division of Earth and Planetary Sciences, Graduate School of Science, Kyoto University, [6]Ritsumeikan University, Kusatsu, Shiga, 525-8577, Japan, [7]NASA/JSC, Houston, TX 77058, USA. (email: tomoki@m.tohoku.ac.jp)

Introduction: Hayabusa2 onboard spectrometers showed that C-type asteroid 162173 Ryugu is very dark object where the reflectance is (1.60 ± 0.15) % at 0.55μm (standard-measurement condition [1, 2]) and showed a small 2.7μm absorption band indicative of phyllosilicates [3]. All spectroscopic observations suggest that the closest meteorite analogue is hydrated carbonaceous chondrites that experienced heating and/or shock impacts and partial dehydration [1-3]. Ryugu's surface shows color variations, especially in the slope of b-band (0.48 µm) to x-band, (0.86 µm) [2]. Bluer spectral slopes are observed at both poles and on the equatorial ridge, both of which are topographic highs and thus may be flesh material exposed by gradual erosion [2]. On the other hand, many locations conducive to deposition, such as crater floors, exhibit redder and darker colors [2]. These observations suggest that a surface-correlated process is responsible for the color variation, most probably from blue to red, but the mechanism for the change is not yet identified. Space weathering is one of possible mechanism, although the spectral changes of C-type asteroids from space weathering are far from being fully understood. Recent experimental studies using hydrous carbonaceous chondrites show that He exposure (simulating solar wind irradiation) changes spectra to bluer and brighter [4], while laser exposure (simulating micrometeorite bombardments) changes spectra to bluer and darker [5]. In this study, we performed further He exposure experiments using the same experimental procedure applied in [4] using the most appropriate analogue meteorites for asteroid Ryugu. In addition, to explore the effects of physical properties on the spectral changes, we prepared a chip and a powder from the same meteorite.

He exposure experiment and spectra measurement: 20-keV He irradiation with a dose rate of $\sim 10^{13}$ ions/(sec cm^2) was performed at CSNSM-IAS Orsay, France until total dose reached 1, 3, and 6 x10^{16} ions/cm^2. Shocked CM chondrite MET01072 and partially dehydrated CI chondrite Y 980115, both of which show reflectance spectra similar to Ryugu [2, 3], were used. A 1-cm sized chip with a flat surface with roughness made by a #400 polishing disk was prepared from each meteorite. In addition, a powder of Y 980115 with grain size < 155µm was pressed to 5 tons to make a pellet with a very flat surface, which is the same procedure used in [4]. Reflectance spectra of the same portions of samples were made before and after exposure in the wavelength range from 0.45 to 11.5µm in France. The spectra of the same area of unexposed and exposed (only samples with 6 x10^{16} ions/cm^2) were also measured at wavelengths from 0.4 to 15µm in Japan, which perfectly matched the results of the measurements in France. TEM observations will now be performed on FIB thin sections of all exposed samples.

Results and discussion: Y 980115 shows completely different spectral changes between chip and pellet. Unexposed samples of both chip and pellet show almost featureless spectra in the wavelength range 0.4 to 1.0µm with 6-7% reflectance at 0.55µm. With increasing total dose of He exposure, the pellet shows bluing and brightening. On the other hand, the chip shows only slight reddening of spectra with no significant brightening. This clearly indicates that spectral changes are completely different depending on the physical properties of the C chondrite samples and suggests complex spectral changes occur during space weathering of C-type asteroids. The chip seems to be more porous than the pellet, which is consistent with slightly redder spectra of the unexposed chip than the unexposed pellet. Other interesting spectral changes are observed from the chip of MET01072. This meteorite was compressed by an impact, but retains phyllosilicates [6]. The unexposed MET01072 chip shows featureless and flat spectra in the wavelength range 0.4 to 1.0µm, similar to Y 980115. With increasing He total dose, the MET01072 chip shows bluing and brightening, similar to the Y 980115 pellet, but different from the Y 980115 chip. This indicates that chip samples of hydrous C chondrites responded differently to He exposure, likely due to different physical properties. The same behavior between the MET01072 chip and the Y 980115 pellet could be explained by similar compressed properties of the two samples. Another noteworthy spectral change, although it cannot be explained, is that with increasing total dose, reddening occurs after bluing at < 0.65µm wavelength, in case for the MET01072 chip and the Y 980115 pellet.

References: [1] Watanabe S. et al. (2019) *Science* 364, 10.1126/science.aav8032. [2] Sugita S. et al. (2019) *Science* 364, 10.1126/science.aaw0422. [3] Kitazato et al. (2019) *Science* 364, 10.1126/science.aav7432. [4] Lantz, C. et al. (2017) *Icarus* 285, 43–57. [5] Matsuoka et al. (2015) *Icarus* 254, 135-143. [6] Nakamura et al. (2016) *Goldschmidt Conf.* abstract 2228.

HAYABUSA2: CURRENT SUMMARY.

T. Nakamura[1], S. Watanabe[2,3], M. Hirabayashi[4], N. Hirata[5], N. Hirata[6], R. Noguchi[3], Y. Shimaki[3], H. Ikeda[7], E. Tatsumi[8], M. Yoshikawa[3], S. Kikuchi[3], H. Yabuta[9], S. Tachibana[8,2], Y. Ishihara[3†], T. Morota[2], K. Kitazato[5], N. Sakatani[3], K. Matsumoto[10,11], K. Wada[12], H. Senshu[12], C. Honda[5], T. Michikami[13], H. Takeuchi[3], T. Kouyama[14], R. Honda[15], S. Kameda[16], T. Fuse[17], H. Miyamoto[8], G. Komatsu[18,12], S. Sugita[8], T. Okada[3], N. Namiki[10,11], M. Arakawa[6], M. Ishiguro[19], M. Abe[3], R. Gaskell[20], E. Palmer[20], O. S. Barnouin[21], P. Michel[22], A. S. French[23], J. W. McMahon[23], D. J. Scheeres[23], P. A. Abell[24], Y. Yamamoto[3], S. Tanaka[3], K. Shirai[3], M. Matsuoka[3], M. Yamada,[12] Y. Yokota,[3] H. Suzuki,[25] K. Yoshioka,[8] Y. Cho,[8] S. Tanaka,[6] N. Nishikawa[6], T. Sugiyama[5], H. Kikuchi[8], R. Hemmi[8], T. Yamaguchi[3††], N. Ogawa[3], G. Ono[7], Y. Mimasu[3], K. Yoshikawa[7], T. Takahashi[3], Y. Takei[3], A. Fujii[3], C. Hirose[7], T. Iwata[3,11], M. Hayakawa[3], S. Hosoda[3], O. Mori[3], H. Sawada[3], T. Shimada[3], S. Soldini[3], H. Yano[3], R. Tsukizaki[3], M. Ozaki[3,11], Y. Iijima[3‡], K. Ogawa[6], M. Fujimoto[3], T.-M. Ho[26], A. Moussi[27], R. Jaumann[28], J.-P. Bibring[29], C. Krause[30], F. Terui[3], T. Saiki[3], S. Nakazawa[3], Y. Tsuda[3], [1]Tohoku University, Sendai 980-8578, Japan, [2]Nagoya University, Nagoya 464-8601, Japan, (seicoro@eps.nagoya-u.ac.jp), [3]Institute of Space and Astronautical Science, JAXA, Japan, [4]Auburn University, Auburn, AL 36849, USA, [5]University of Aizu, Aizu-Wakamatsu 965-8580, Japan, [6]Kobe University, Kobe 657-8501, Japan, [7]Research and Development Directorate, JAXA, Sagamihara 252-5210, Japan, [8]University of Tokyo, Tokyo 113-0033, Japan, [9]Hiroshima University, Higashi-Hiroshima 739-8526, Japan, [10]National Astronomical Observatory of Japan, Mitaka 181-8588, Japan, [11]SOKENDAI (The Graduate University for Advanced Studies), Hayama 240-0193, Japan, [12]Chiba Institute of Technology, Narashino 275-0016, Japan, [13]Kindai University, Higashi-Hiroshima 739-2116, Japan, [14]National Institute of Advanced Industrial Science and Technology, Tokyo 135-0064 Japan, [15]Kochi University, Kochi 780-8520, Japan, [16]Rikkyo University, Tokyo 171-8501, Japan, [17]National Institute of Information and Communications Technology, Kashima 314-8501, Japan, [18]Università d'Annunzio, 65127 Pescara, Italy, [19]Seoul National University, Seoul 08826, Korea, [20]Planetary Science Institute, Tucson, AZ 85710, USA, [21]Johns Hopkins University Applied Physics Laboratory, Laurel, MD 20723, USA, [22]Université Côte d'Azur, Observatoire de la Côte d'Azur, CNRS, Laboratoire Lagrange, 06304 Nice, France, [23]University of Colorado, Boulder, CO 80309, USA, [24]NASA Johnson Space Center, Houston, TX 77058, USA, [25]Meiji University, Kawasaki 214-8571, Japan, [26]DLR (German Aerospace Center), Institute of Space Systems, 28359 Bremen, Germany. [27]CNES (Centre National d'Etudes Spatiales), 31401 Toulouse, France, [28]DLR, Institute of Planetary Research, 12489 Berlin-Adlershof, Germany, [29]Institute d'Astrophysique Spatiale, 91405 Orsay, France, [30]DLR, Microgravity User Support Center, 51147 Cologne, Germany. †Current affiliation: National Institute for Environmental Studies, Tsukuba 305-8506, Japan, ††Current affiliation: Mitsubishi Electric Corporation, Kamakura 247-8520, Japan, ‡Deceased. (email: tomoki@m.tohoku.ac.jp)

Hayabusa2 is the 2nd Japanese sample return mission from C-type asteroid 162173 Ryugu. The purpose of the mission is to uncover the early solar system evolution and to obtain crusial information for the origin of life and water in the solar system. So far (till 2019 April), the science operations of the spacecraft went very well: we succeeded spectroscopic, morphological, and geological observation of an entire region of the asteroid for global mapping from Box-A (20km high) and -C (5-7km high), first touchdown on a part of the equatrial ridge after several time rehearsals, deployment of the small landers such as MASCOT, and injection of a metallic Cu plate (Small Carry-on Impactor) onto the asteroid surface. Chracteristic spinning-top shape and very low density (1.2 g/cc) indicate that Ryugu is a rubble pile asteroid formed by a catastrophic impact and deformed by high spin rates sometime after the impact [1]. Spectroscopic observation shows that Ryugu is very dark object (< 2% reflectance at 0.55μm with standard-measurement condition [1, 2]) and has a small 2.7μm (~10% absorption) band suggestive of a global distribution of phyllosilicates [3]. The closest analogue would be partially-dehydrated carbonaceous chondrites or C-rich interplanetary dust particles [2,3]. Ryugu's surface shows slight color variations: bluer areas are located at regions such as equatorial ridge and poles [2], although we do not fully understand what is resonsible for the colar variation. On the day of Feb 22th 7:29am (JST), HY2 spacecraft succceded to touchdown on the surface area of L08-E1 that is very close to the planned touchdown point (deviation is ~1m), suggesting that the spacecraft was very wel controlled. A metallic projectile was fired when the sample horn touched the surface and numerous rock fragments were despersed from the surface and came to the horn, which we observed by CAM-H camera. Therefore, it is expected to some rock fragments to reach a catcher in the spacecraft. The sample recovery cupsule will be coming back to the Earth in December 2020 and the initial analysis of the returned samples will start from spring 2021.

References: [1] Watanabe S. et al. (2019) *Science* 364, 10.1126/science.aav8032. [2] Sugita S. et al. (2019) *Science* 364, 10.1126/science.aaw0422. [3] Kitazato et al. (2019) *Science* 364, 10.1126/science.aav7432.

THE OSIRIS-REx SCIENCE VALUE MAP OF ASTEROID BENNU.

K. Nakamura-Messenger[1], H. C. Connolly Jr.[2,3], D. S. Lauretta[3], S. Messenger[1], and the OSIRIS-REx team, [1]Robert M Walker Laboratory for Space Science, ARES/EISD, NASA JSC, 2101 NASA Parkway, Houston, TX, USA, keiko.nakamura-1@nasa.gov, [2]Dept. of Geology, Rowan University, Glassboro, NJ, USA, [3]Lunar and Planetary Laboratory, University of Arizona, Tucson, AZ, USA.

Introduction: The OSIRIS-REx mission is carrying out an intensive remote sensing campaign at asteroid Bennu in preparation for surface sample acquisition in July 2020 [1]. Sample site selection will be guided by four maps of the asteroid surface: the Safety Map, Deliverability Map, Sampleability Map, and Science Value Map (SVM) [2]. The SVM is a quantitative measure of the suitability of sampleable surface regolith for addressing the science goals of the mission [2].

Science Value. A primary goal of the OSIRIS-REx mission is to test hypotheses on the origin, geological history, and dynamical evolution of Bennu through analyses of the returned sample [2]. The best scientific value area for sample collection would encompass the diversity of chemistry, mineralogy, and geology of Bennu, allowing for tests of these hypotheses. Remote optical imaging and spectral mapping by the OVIRS and OTES instruments are yielding dozens of maps that are being used to assess science value. Of particular interest will be surface regions showing evidence of organics, hydrated minerals, chemical and mineralogical diversity, and the presence of freshly exposed materials and volatiles.

Here we present the early observations of Bennu that are being used to assess the relative science value of candidate sampling sites. At this writing, the Detailed Survey phase of the mission has just begun. Results of these observations will be discussed at the Meteoritical Society Meeting.

SVM visualization: Owing to the mission's tight operational schedule, these diverse data products need to be combined quickly in a simple and flexible manner. We developed a visualization tool that combines spectral and geological remote sensing maps into an integrated SVM and projects the SVM onto the Bennu 3D shape model and global image mosaic. Each remote sensing map is converted to a score map, where values of each facet on the shape model are assigned a value from 0 to 1, based on confidence of detection of that map element. The science value score is determined by selection and weighting of inputs to the SVM and is user-adjustable.

Early observations: Global-scale imaging and spectral observations confirmed that Bennu is hydrated and volatile-rich [3]. However, the surface is more rugged than expected and shows large albedo variations that are not yet understood. Observations of impact craters suggest that the surface is on the order of 100–1,000 million years old, and smaller craters have been erased by mass movement [4]. Unexpected observations of particle ejection events in the Orbital A phase show that Bennu remains geologically active, although the cause of these events has not yet been determined.

Geology science value. With Bennu's old age, most of the surface regolith has probably undergone extensive space weathering. Small craters are thought to be younger; thus fresher, scientifically valuable subsurface material should be found within them. Particle ejections *may* be volatile driven, and if so, source areas would be of high science value. The abundant boulders on Bennu show diversity in morphology that may relate to both intrinsic properties and geological history on the surface. Both rounded and angular boulders are observed, showing various types of fracturing and layering. Collecting fragments from a variety of rock types would be of high science value.

Mineralogy science value. Hydrated minerals are a priority target for collection and appear to be abundant on Bennu [4]. Early observations further suggest the presence of magnetite [1], a common byproduct of aqueous alteration in meteorites. So far, the spectra suggest an affinity to CM carbonaceous chondrites. Collection of material having such diagnostic minerals is a key goal of the mission because it allows for testing of hypotheses, such whether Bennu is analogous to carbonaceous chondrite meteorites.

Chemistry science value. The chemistry science value is primarily related to the abundance and type of organic matter. Spectra acquired during the Detailed Survey phase are expected to have sufficient sensitivity to detect organic features. Any positive spectral detection of organics would mark a potential sample site as having high science value.

Sample site selection: The top candidate sample sites are now being evaluated, with refinements made as new observations and compositional maps are made available. The early observations of Bennu show a fascinating body that has scientifically valuable material everywhere on its surface.

References: [1] Lauretta D. S. et al. (2019) *Nature* 568:55–60. [2] Lauretta, D. S., et al. (2017) *Space Science Reviews* 212: 925-984. [3] Hamilton V. E. (2019) *Nature Astronomy* 3:332–340. [4] Walsh K. J. et al. (2019) *Nature Geoscience* 12:242–246.

Oyxgen isotope systematics of porphyritic chondrules and their fragments in CH and CB chondrites.

D. Nakashima[1,2], M. Kimura[3,4], K. Yamada[4], T. Noguchi[4,5], T. Ushikubo[2,6], and N.T. Kita[2], [1]Tohoku University, Sendai, Japan (dnaka@tohoku.ac.jp), [2]WiscSIMS, University of Wisconsin-Madison, USA, [3]NIPR, Tokyo, Japan, [4]Ibaraki University, Mito, Japan, [5]Kyushu University, Fukuoka, Japan, [6]JAMSTEC, Kochi, Japan.

Introduction: Chondrules in carbonaceous chondrites including non-porphyritic chondrules in CH and CB chondrites show systematic trends that the $\Delta^{17}O$ (= $\delta^{17}O – 0.52 \times \delta^{18}O$) values increase with decreasing Mg# (= mol.% MgO/[MgO+FeO]) [e.g., 1-2], which are explained by an addition of ^{16}O-poor water ice as an oxidant to the ^{16}O-rich anhydrous precursors [e.g., 3]. In contrast, porphyritic chondrules in CH and CB chondrites show no systematic difference in the $\Delta^{17}O$ values between type I and II chondrules (–4.7‰ to +4.1‰ vs. –2.1‰ to +2.7‰; [2,4]), though the detailed relationship with Mg# is unclear. Here we report new SIMS oxygen isotope analyses of olivine and pyroxene fragments in the Asuka-881020 CH chondrite (15μm Cs$^+$ primary beam, WiscSIMS). We further discuss the $\Delta^{17}O$-Mg# systematics of the porphyritic chondrules in CH and CB chondrites.

Results and discussion: Thirteen of 20 fragments are FeO-poor with Mg# of 90.7 – 99.3 and others are FeO-rich with Mg# of 50.5 – 80.0. The oxygen isotope ratios plot along with the primitive chondrule mineral (PCM) line [1] with $\Delta^{17}O$ values from –5.0‰ to +3.2‰. These data are compared to the average $\Delta^{17}O$ values of the individual porphyritic chondrules (excluding relict grains; [2,4]) in $\Delta^{17}O$ versus Mg# plot in Fig. 1a. The $\Delta^{17}O$ ranges of FeO-poor and -rich fragments overlap those of the type I and II chondrules in CH and CB chondrites, respectively, suggesting that the olivine and pyroxene fragments are fragments of the porphyritic chondrules. Skeletal olivine-pyroxene chondrules may not be a source of the fragments, as they have a narrow range of $\Delta^{17}O$ values of –2.6 ± 1.4‰ [5].

The $\Delta^{17}O$ values of the type I chondrules and FeO-poor fragments increase with increasing Mg#, while those of the type II chondrules and FeO-rich fragments show no correlation with Mg# (Fig. 1a). Similarly, type II chondrules in CR and Tagish Lake-type chondrites have $\Delta^{17}O$ variations from ~ –3‰ to +2‰ with no correlation with Mg# [6-7], which are are explained by an addition of ^{16}O-poor water ice to the ^{16}O-rich precursors [e.g., 3]. However, the positive $\Delta^{17}O$-Mg# correlation for chondrules and fragments with Mg# > 96 cannot be explained by this process, but may be explained by addition of ^{16}O-poor reductant to the ^{16}O-rich precursors or addition of ^{16}O-rich oxidant (water ice) to the ^{16}O-poor precursors. The latter case is less likely, as chondrules with Mg# of ~ 99 and $\Delta^{17}O$ of ~ +4‰ are not observed in other chondrites and oxides that inherited oxygen isotope ratios of water ice are ^{16}O-poor [e.g., 8]. In the former case, chondrules with Mg# of ~ 96 and $\Delta^{17}O$ of ~ –4‰, which are the lower end of the positive $\Delta^{17}O$-Mg# correlation, may correspond to the ^{16}O-rich precursors. Such chondrules are rarely observed in Acfer 094 (ungr. C3.0) and CR chondrites [1,9]. The ^{16}O-poor reductant may be carbon-rich organics, given the two observations; ^{16}O-poor organics in primitive chondrites [10] and heating experiments that produced Fo$_{99}$ olivine from Fo$_{94}$ olivine and graphite or diamond [11]. Heating experiments produced chondrules with $\delta^{18}O$ of +5.6‰ from type I chondrules with $\delta^{18}O$ of +6.5‰ and 5 wt% graphite [12], indicating oxygen isotope mass fractionation between the chondrules and oxidized carbon (CO or CO$_2$). Fig. 1b shows the deviation of $\delta^{18}O$ values from the PCM lines ($\Delta^{18}O_{PCM}$) for the type I chondrules and FeO-poor fragments along with the $\Delta^{17}O$ values. The chondrules and fragments with high $\Delta^{17}O$ values have negative $\Delta^{18}O_{PCM}$ values. This suggests the oxygen isotope mass fractionation during the reduction and supports the view of addition of ^{16}O-poor carbon-rich organics to ^{16}O-rich precursors.
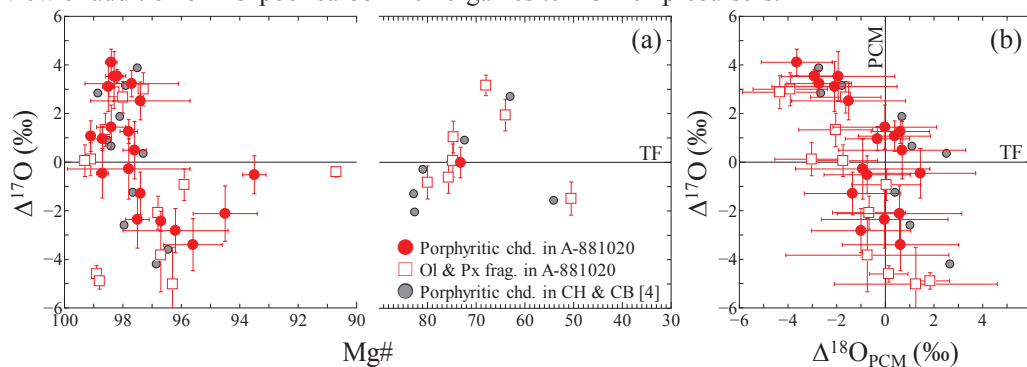

Fig. 1: (a) $\Delta^{17}O$ vs. Mg# of porphyritic chondrules and olivine and pyroxene fragments in CH and CB chondrites and (b) $\Delta^{17}O$ vs. $\Delta^{18}O_{PCM}$ of type I porphyritic chondrules and FeO-poor fragments in CH and CB chondrites.

Legend: ● Porphyritic chd. in A-881020 ☐ Ol & Px frag. in A-881020 ● Porphyritic chd. in CH & CB [4]

References: [1] Ushikubo T. et al. (2012) *GCA* 90:242-264. [2] Nakashima D. et al. (2010) *M&PS* 47:A148. [3] Tenner T.J. et al. (2015) *GCA* 148: 228-250. [4] Krot A.N. et al. (2010) *GCA* 74:2190-2211. [5] Krot A.N. and Nagashima K. (2017) *GJ* 51:45-68. [6] Connolly Jr. H.C. and Huss G.R. (2010) GCA 74:2473-2483. [7] Yamanobe M. et al. (2018) *Polar Sci.* 15:29-38. [8] Sakamoto N. et al. (2007) *Science* 317:231-233. [9] Schrader D.L. et al. (2013) *GCA* 101:302-327. [10] Hashizume K. et al. (2011) *Nature Geosci.* 4:165-168. [11] Connolly Jr. H.C. et al. (1994) *Nature* 371:136-139. [12] Ash R.D. et al. (1998) *M&PS* 33:A11.

THERMAL HISTORY OF CARBONACEOUS CHONDRITE PECORA ESCARPMENT 02012.

A. Nakato[1], A.J. Brearley[2], T. Nakamura[3], T. Noguchi[4], Y. Kebukawa[5], J.I. Lee[6], M. Matsuoka[1], S. Sasaki[7], and N. Shirai[8], [1] Inst. Space Astronaut. Sci., Japan Aerosp. Explor. Agency (JAXA), 3-1-1 Yoshinodai, Chuo, Sagamihara, Kanagawa 252-5210, Japan (nakato@planeta.sci.isas.jaxa.jp), [2]University of New Mexico. Albuquerque, New Mexico 87131, USA, [3]Tohoku University, Miyagi, 980-8578, Japan, [4] Kyushu Univ., Fukuoka 819-0395, Japan, [5]Yokohama National University, Yokohama 240-8501, Japan, [6]Korean Polar Research Institute, Incheon, 406-840, Korea, [7]Osaka University, Osaka 560-0043, Japan, [8]Tokyo Metropolitan Univ., Tokyo 192-0397, Japan

Introduction: Thermally metamorphosed carbonaceous chondrites (TMCCs) are plausible candidate for Ryugu surface materials based on the spectroscopic observation [1]. Based on the previous studies, not only Ryugu but also several C-complex main-belt asteroids show similar VIR spectra with the TMCCs [e.g., 2]. Constraints on metamorphic processes that affected these asteroids may come from the study of a significant number of TMCCs [e. g., 3, 4, 5]. Studies of TMCCs indicate that the conditions of thermal metamorphism experienced by these meteorites may have been quite variable, suggesting that metamorphism of the TMCCs was complex [e.g., 6, 7]. We have investigated the Antarctic find, Pecora Escarpment (PCA) 02012 as a unique TMCC [8, 9]. Here we report additional information on the petrology, mineralogy, and organic structure and estimate the thermal history of PCA02012.

Results and Discussion: Studies of PCA 02012 show that it is one of the strongly TMCCs, like B-7904 [8, 9]. In addition, its bulk oxygen isotope composition suggests that PCA 02012 might have been a CM2 chondrite before thermal metamorphism [8]. However, the constituent minerals of the matrix are quite different from the other CMs and TMCCs. The matrix mainly consists of Fe-rich olivine, pyroxene, plagioclase (Ab15-78) and Fe-sulfide. Fe-Ni metal and Fe-rich spinel were also found as minor phases. Based on TEM observations, any phyllosilicates and their pseudomorphs are not observed even though they are observed in experimentally heated Murchison at 900 ℃ for 96 hours.

FEGSEM observation shows that chondrule rims and matrix consist of a mixture of three texture: granoblastic, coarse-grained, and fine-grained (Fig. 1). The granoblastic texture is especially dominant in matrix rather than the rim (Fig.1b). The granoblastic texture in PCA 02012 is similar to amoeboid olivine aggregates (AOAs) in C2 - C3 chondrites, but is much finer grained (100 nm c.f. microns to 10s of microns in AOAs). Annealed textures similar to those in AOAs have been reproduced by heating experiments on anorthite and San Carlos olivine at various temperature for 3 - 100 h [10]. The texture consisting of silicate grains ~10 μm in size formed after 3 h at 1288 ºC. TEM observation of PCA 02012 revealed that this characteristic texture formed with olivine, pyroxene, and plagioclase is the same as the other fine- and coarse-grained textures in the matrix. Therefore, coexistence of these three textures consisting of the same materials suggests that PCA 02012 has suffered thermal metamorphism heterogeneously.

The structural changes of organic material during heating carry important clues to understand the thermal history of PCA 02012. We performed STXM-XANES analyses at the carbon edgeof PCA 02012 matrix and compared of the results to Allende (CV3) and experimentallyheated Murchison. PCA 02012 and heated Murchison show the absence of the graphene feature (~291.6 eV) that corresponds to a 1s-σ* exciton [11] for carbon. In contrast, Allende which suffered long duration thermal metamorphism induced by short-lived radio nuclide decay shows a clear peak of graphene. This result indicatesthat PCA 02012 experienced relatively short duration heating that was too rapid to drive graphitization of the organic material.
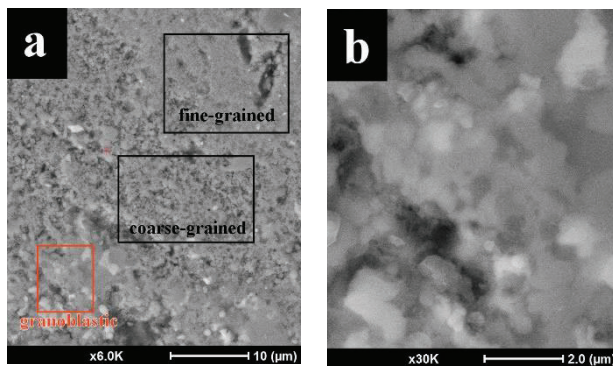

Figure 1. BSE images of PCA 02012. (a) A matrix image. Three textures: granoblastic, fine-grained, coarse-grained, coexist in the matrix. (b) An enlarged-view of granoblastic area in (a).

References: [1] Kitazato K. et al. (2019) *Science* 10.1126/science.aav7432. [2] Hiroi et al., 1993. *Science* 261:1016-1081. [3] Kimura, M. and Ikeda Y. (1992) *Proc. NIPR Symp. on Ant. Met.*, 5, 74-119. [4] Tomeoka K. (1989) *Proc. NIPR Symp. on Ant. Met.*, 2, 55-74. [5] Ivanova M. A. et al. (2010) *Meteoritics&Planetaly Science* 1-16. [6] Nakamura T. (2005) *J. of Min. and Pet. Sci.*, 100, 260-272. [7] Nakato A. et al. (2009) *72nd Met. Soc.*, #5336. [8] Nakato A. et al. (2013) *44th Lunar & Planetary Science Conference*, #2708. [9] Nakato A. et al. (2013) *76th Met. Soc.*, #5282. [10] Komatsu M. et al. (2009) *Polar Science,* 3, 31-55. 2708. [11] Cody G.D. et al. (2008) *Earth and Planetary Science Letters* 272:446–455.

SOLUBLE ORGANIC MATTER (SOM) ANALYSIS PLAN OF THE HAYABUSA2-RETURNED SAMPLES

H. Naraoka[1], Y. Takano[2], J. P. Dworkin[3], and SOM analysis team, [1]Department of Earth and Planetary Sciences and Research Center for Planetary Trace Organic Compounds, Kyushu University, 744 Motooka, Nishi-ku, Fukuoka 819-0395; [2]Japan Agency for Marine-Earth Science Technology (JAMASTEC), 2-15 Natsushima, Yokosuka 237-0061, Japan; [3]NASA Goddard Space Flight Center, Greenbelt, Maryland 20771, USA.

Introduction: The Hayabusa2 spacecraft successfully performed the first touch and go sampling of the surface materials of asteroid 162173 Ryugu on 22nd February, 2019. The collected surface materials of Ryugu will be delivered to Earth in late 2020. Because Ryugu has the surface of C-type reflectance spectra with a low abundance hydrous minerals [1], the asteroid surface appears composed of materials similar to that of carbonaceous chondrites. Such primitive meteorites are expected to yield various soluble organic matter (SOM) including amino acid, carboxylic acid, etc. The occurrence of SOM in Ryugu will provide clues to the formation pathways of organic compounds as well as prebiotic molecules with respect to origins of life in the primitive solar system. In order to investigate the organic evolution of Ryugu, an international team consisting of 24 members currently is organized for the initial SOM analysis for the Hayabusa2-returned samples. In this study, we propose the comprehensive SOM analyses using high-sensitive and high-resolution analytical methods.

Methods: We have been developing the advanced techniques to analyze the trace amounts of soluble organic compounds in very small extraterrestrial materials, because the sampling amount is expected to be >100 mg [2]. The analytical procedures must be performed under clean conditions to avoid terrestrial contaminations. Meteoritic SOM usually occurs as a complex mixture consisting of various types of organic compounds with very small concentrations at each compound, therefore, high resolution analyses are required under high sensitivity. Currently we are planning to perform four techniques. 1) High-resolution mass spectroscopy (HRMS) of various solvent extracts coupled with or without nano-liquid chromatography by electrospray ionization (ESI) using Fourier Transform-Ion Cyclotron Resonance/Mass Spectrometry (FT-ICR/MS) [3] and/or Orbitrap MS [4]. 2) Chiral amino acid analysis using multi-dimensional (2D or 3D) high-performance liquid chromatography with high-sensitive fluorescence detection (FD) coupled with HRMS [5, 6]. 3) *In situ* organic compound analysis and molecular imaging using desorption electrospray ionization (DESI) equipped with HRMS [7, 8]. 4) Spatial resolution imaging of organic compounds using time of flight-secondary ion mass spectrometry (ToF-SIMS) [9]. If the sample is available, we will also perform 5) compound-specific isotope analysis using gas chromatography/combustion or pyrolysis /isotope ratio mass spectrometry (GC/C or pyrolysis/IRMS). In addition, we plan to measure bulk chemical and isotopic compositions of organic matter (C, H, N, O and S) using nanoEA-IRMS and/or laser-tunable FT-IR spectroscopy. The returned samples will be extracted sequentially with non-polar (e.g. hexane) to polar (H_2O) solvents and/or polar to non-polar solvents in a clean bench (ISO Class 5) set inside of a clean room (ISO Class 6). The extracts will be delivered to some research institutes for the detailed analyses. In addition, grain-level minimally-destructive analysis will be performed by nanoLC/Orbitrap MS and DESI/HRMS.

Results and Discussion: The preliminary result of one grain analysis of the Murchison meteorite (~ a few tens μg) demonstrated the organic compound identification by nanoLC/Orbitrap MS. The predominance of CHN compounds in the methanol extract of Murchison is similar between the two analytical methods (nanoLC *vs*. HPLC). The nanoLC coupled with nanoESI could enhance the sensitivity of detection by three magnitudes compared to that of conventional HPLC with ESI. The 2D-HPLC/FD analysis clarified the enantiomer distribution of amino acids using ~μg fragments of Murchison. The result suggests heterogeneous distribution of amino acid enantiomers in the meteorite, which is consistent with previous studies. [10]

We will further conduct preliminary tests of the sequential analysis for various types of SOM using 30 mg, 10 mg, and 1 mg samples of the carbonaceous meteorites and baked serpentine (as a blank). After the sequential extraction of samples, the residues will be used for the analysis of insoluble organic matter (IOM).

References: [1] Kitazato K. et al. (2019) *Science* 364:272-275. [2] Tachibana S. (2014) *Geochem. J.* 48:571–587. [3] Schmitt-Kopplin P. et al. (2010) *Proc. Natl. Acad. Sci. USA* 107:2763-2768. [4] Naraoka H. et al. (2017) *ACS Earth & Space Chem.* 1:540-550. [5] Glavin D. P. et al. (2011) *Meteoritics & Planetary Science* 45:1848-1972. [6] Hamase K. et al. (2014) *Chromatography* 35:103-110. [7] Naraoka H. & Hashiguchi M. (2018) *Rapid Commun. Mass Spectrom.* 32:959-964. [8] Hashiguchi M. & Naraoka H. (2019) *Meteoritics & Planetary Science* 54:452-468. [9] Naraoka H. et al. (2015) *Earth, Planets & Space* 67:67. [10] Pizzarello et al. (2003) *Geochim. Cosmochim. Acta* 67:1589-1595.

THERMAL ALTERATION OF METEORITE PARENT BODY AS RECORDED BY INSOLUBLE ORGANIC MATTER: XANES AND RAMAN STUDY

N. Shreeya[1] and K.K Marhas[2], [1]Indian Institute of Space Science and Technology, Thiruvananthapuram , Kerala-695547(shreeyaniyer@gmail.com) , [2]Physical Research Laboratory, Ahmedabad, Gujarat-380009.

Introduction: Meteorites, especially chondrites accreted 0.1-5wt% of carbon in both organic and inorganic forms. A large amount of this organic carbon (>60-70%) is the acid Insoluble organic material (IOM) and the remaining is the Soluble organic material (SOM). These organic constituents within the meteorites are tell tales of their journey through the interstellar space and into the formation of the solar system in a molecular cloud in which low temperature radiation-driven chemistry and isotopic fractionation could occur in both the gas phase and on ice and mineral grain surfaces[1-2]. Additional changes in organics could have taken place after incorporation into planetesimals, including asteroids and comets. Furthermore the radiogenic decay of short-lived radionuclides (e.g., 60Fe and 26Al), impact shocks and other processes could heat the planetesimals[3-4] thereby forming a long and diverse range of thermal metamorphism and aqueous alteration conditions affecting the formation , destruction and transformation of the organic content within.

A correlation between petrographic type and molecular structure of IOM have been shown in various studies. In the present study, we analyzed the IOM extracted from recently fallen Carbonaceous Chondrite, Mukundpura, along with 34 other meteorite samples with varying groups and petrological types (1-6). The IOM extraction was carried out using CsF method [5]. The insoluble organic contents were then subjected to various analytical techniques starting with Field Emission Scanning Electron Microscopy (FE-SEM) , Carbon X-ray Absorption Near Edge Structure (C-XANES) spectroscopy and laser RAMAN to obtain the temperatures of thermal metamorphism of different samples using the exciton intensity (1s-σ*) and Raman band parameters , Γ_D and Γ_G [6-7] and to understand the effects of petrologic grade on them.

Results and Discussions: The effective alteration temperatures derived from XANES analysis and the Raman parameters of meteoritic IOM are as shown in the figure. The calculated temperatures for our samples is within range predicted form various mineralogical studies [8-9].The peak width Γ_D and Γ_G generally decrease with increasing metamorphism[7]. Sharp and wide D and G band for Mukundpura indicates very low thermal alterations which compliments the least effective temperatures calculate using exciton intensity. Low temperatures of Mukundpura is also consistent with the mineral based petrological study of the meteorite [10]. This study also favours the thermometric calculations from XANES and Raman as described in[6-7].
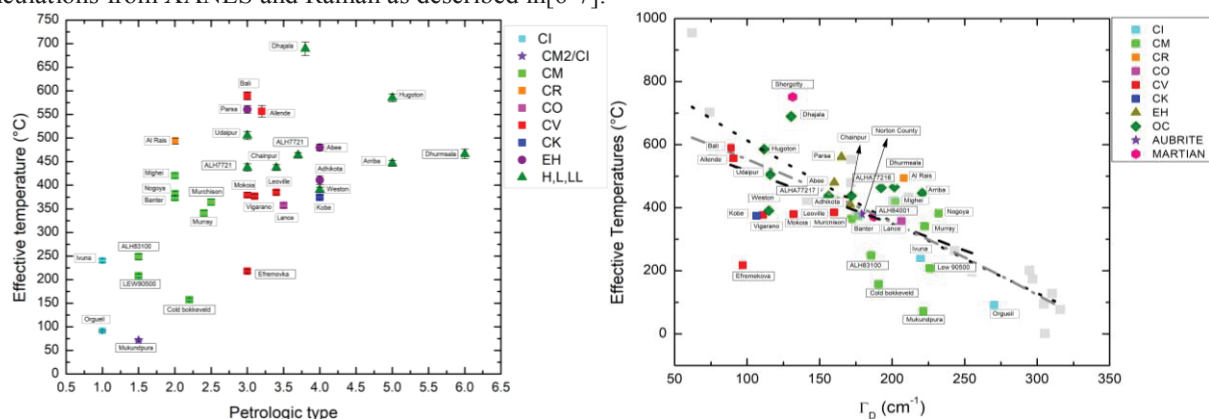

Figure : a)Correlation between T_{EFF} obtained from XANES analysis of IOM and their petrological type. b) The correlation between Raman width parameters and the exciton derived T_{EFF} estimates. The bold dashed line shows the best linear fit through the data ; the dotted line represents the fit through literature data [6] and the gray line represents the fit for all data combined

References: [1] Albertsson, T. et al. (2014) *The Astrophysical Journal. 784, 39.*[2] Ehrenfreund P. and Charnley S.B. (2000). *Annual review of Astronomy and Astrophysics. 38, 427-483* [3] Dyl K.A. Bischoff. et al. (2012). *Proceedings of the National Academy of Sciences. 109, 18306-18311.*[4] Weiss B.P. and Elkins-Tanton L.T. (2013). *Annual Review of Earth Planet Sciences 41, 529-560.*[5] Cody G.D et al.(2002) *Geochimica et Cosmochimica Acta 66, 1851–1865.*[6] Cody G.D et al. (2008) *Earth and Planetary Science Letters. 272. 446-455.*[7] Busemann H. et al. (2007). *Meteoritics and Planetary Sciences 42, 1387–1416.*[8]Huss, G.R et. al. (2006) *Meteorites & the Early Solar system II,pp,567-586.*[9]Brearley, A.J., (2006). *Meteorites & the Early Solar system II,pp,584-624.*[10] D. Ray. et.al (2018). *Planetary and Space Science.*

CRYOVOLCANIC LABORATORY EXPERIMENTS ON CARBONACEOUS CHONDRITES

J. Nava[1], A. Maturilli[2], F. Zambon[3], C.Carli[3], G. Alemanno[2], J. Helbert[2], S. Genovesi[4] and M. Massironi[1], [1]University of Padova, Department of Geosciences, Via G.Gradenigo 6, 35131 Padova, Italy (jacopo.nava@phd.unipd.it), [2]Institute of Planetary Research, German Aerospace Center (DLR), Berlin, Germany, [3]IAPS-INAF, Istituto Nazionale di Astrofisica e Planetologia Spaziali, Roma, Italy, [4]Università degli Studi di Bologna, Dipartimento di Geologia, Bologna, Italy.

Introduction: Cryovolcanism is a process that affected many different planetary bodies such as asteroids, satellites and TNOs like Ceres [1], Europa and Enceladus [2-3] and Charon [4]. Although prerequisites for cryovocanicm have been delineated by [5], cryovolcanic processes and related products are still not well understood. For this reason we made some experiments in laboratory with Carbonaceous Chondrites (CCs) and ices to try to recreate a cryovolcanic process.

Methods: Experiments were carried out at the DLR PEL laboratory in Berlin. We powdered 3 CCs: FRO90006, FRO99040 and MCY14014. We mixed FRO99040 with deionized water and FRO90006 and MCY14014 with ammoniated water (mixtures were around 20-30% water and 80-70% meteorite). We put the mixtures in the dryer for around 30 minutes to avoid the formation of atmospheric frost and then we froze them at -80°C. Once frozen the mixtures were put in a cup with liquid nitrogen to preserve the temperature and then transferred into a vacuum chamber equipped with plates capable of heating up the samples. Samples were heated from around -100°C (due to liquid nitrogen) up to 100°C in few minutes. Once the experiments finished we acquired reflectance spectra in the NIR range and compared them with spectra of the original samples acquired before the experiment.

Petrography: FRO99040 and FRO90006 are CO3 chondrites while MCY14014 is a CM2. FRO99040 and FRO90006 are mainly made of olivine and pyroxene, metal is abundant (~10%) and also CAIs containing fassaite, garnets, spinel and melilite are found. MCY14014 is mainly composed of olivine, widespread phyllosilicates, minor calcite crystals often associated to troilite, FeNi alloys are generally rare.

Results: During the heating process the samples started to outgas fine particles at T~ -20°C. Between around -5°C and 0°C FRO99040 and MCY14014 also experienced a violent episode, after which outgassing of fine particle ceased. This outburst was not observed during FRO90006 heating, which gradually stopped outgassing particles. The ejected outgassed powders of FRO90006 and FRO99040 always show absorption bands around 3.4-3.5 µm while previous of the degassing process and on the powders that remained in the sample holder this feature is not seen. Ejceted outgassed powders of MCY14014 still show the absorptions at 3.4-3.5 µm, but less prominently.

Discussion: The 3.4-3.5 µm absorption bands may thus be tracers for hydrothermal-cryovolcanic processes. This band is usually attributed to organic compound [6]. This experiment also gives information on the temperature and pressure range over which cryovolcanism and hydrothermal activity may be active on an icy body. In fact, outgassing of particles started at T~20°C with an explosive event around 0°C. Considering that on bodies like Ceres brines and salts are also involved in cryovolcanism [1], these temperatures may be even lower. Pressure in the evacuated chamber was ~ 10^{-4} Bar. Furthermore the shallow 3.4-3.5 µm bands in the MCY14014 sample compared to the prominent ones in FRO99040 and FRO90006 suggest that the primary mineralogies play an important role on the formation of cryovolcanic material and rule out laboratory contaminations of the samples. On the contrary the composition of the fluid (deionized water versus ammoniated water) doesn't seem to strongly affect the products characteristics.

References: [1] Ruesch O. et al. 2016. *Science* 353:6303. [2] Quick L.C. et al. 2017. *Icarus* 284:77-488. [3] Postberg F. et al. 2009. *Nature* 459:1098-1101. [4] Desch S.J. and Neveu M. 2016. *Icarus*, *287*:175-186. [5] Neveu M. et al. 2015. *Icarus* 246:48-64. [6] De Sanctis M.C. et al. 2017. *Science* 355:719-722.

Hydrothermal activity on the CV parent body:
new perspectives from the unique CV-like TAM5.29 micrometeorite

J. Nava[1], M.D. Suttle[2], R. Spiess[1], L. Folco[2], J. Najorka[3] C.Carli[4] and M. Massironi[1], [1]University of Padova, Department of Geosciences, Via G.Gradenigo 6, 35131 Padova, Italy (jacopo.nava@phd.unipd.it), [2]Dipartimento di Scienze della Terra, Università di Pisa, 56126 Pisa, Italy, [3]Core research laboratories, Department of Earth Science, The Natural History Museum, Cromwell Rd, London, UK, [4]IAPS-INAF, Istituto Nazionale di Astrofisica e Planetologia Spaziali, Roma, Italy

Introduction: Unmelted micrometeorites (MMs) from anhydrous CC groups are relatively rare, in contrast ,up to the 50% cosmic spherules have oxygen isotopic compositions related to the CO/CV/CK population [1]. Among MM collections only two particles have been recognized as CV-like [2-3], although neither were the subject of a detailed investigation and their classification as CV-like revealed some issues. Here we provide a detailed characterisation of the first well-documented unambiguous CV-like MM, expanding knowledge in the compositional range of MMs as well as investigating the thermal metamorphism and hydrothermal history of the CV parent body-(ies). Furthermore, given that MMs originate from the asteroid belt [4] and cometary sources [5], the study of this sample can be a useful support to recent and upcoming space missions to C-type asteroids and comets

Methods: We collected Raman, EBSD and EMPA analyses at the University of Padova. FE-SEM-EDS analyses were made at the University of Pisa and µXRD at the Natural History Museum in London. Reflectance spectra were take with FT-IR at the IAPS-INAF laboratories in Rome.

Petrography: TAM5.29 is dominated by an Fe-rich matrix composed of orientated fayalitic olivines ($Fa_{42.5}$ to $Fa_{92.3}$). Inclusions of andradite surrounded by diopside-jarosite mantles are also present as well as minor fibrous phyllosilicates – chondrules are absent. Micron-sized spinels co-occur with metal-oxides dispersed within the matrix. Pyroxenes – within the inclusions - have variable compositions ($Fs_{1.8-60}$ $Wo_{0.7-48}$), meanwhile, portions of the olivine groundmass have been altered resulting in a mixture of fine-grained hydrated Mg-Fe-sulphur-rich minerals, that we identify as iddingsite. The particle bulk composition is similar to that of CCs and unmelted micrometeorites. However, TAM5.29 demonstrates enrichment in Fe and depletion in Mg compared to the CCs. The Al content of TAM5.29 is similar to that of CVs, however, Ca and Ti are depleted compared to CVs. Strong enrichment in K in TAM5.29 is also detected compared to both CVs and other UMM. Raman analyses identified ubiquitous carbon and the presence of OH, S-H and C-H functional groups. Another important observation is a linear feature that cross-cuts the fayalitic groundmass showing a displacement of primary features. This feature is composed of a nanocrystalline or glassy matrix and hosting anhedral rounded olivine crystallites and minor Fe-Ni oxides. We interpret the linear feature as a shock melt vein, evidence of impact processing.

Discussion: TAM5.29 mineralogy lies in between the CV_{oxA} and CV_{oxB} being rich in andradite, magnetite and FeNiS, like CV_{oxA}, but also containing hydrated minerals as seen in the CV_{oxB} group. CV_{oxB} also contains almost pure fayalite, which is rare in TAM5.29. TAM5.29 mineralogy is dominated by thermal metamorphism products formed at ~275-250°C within the presence of Fe-alkali-halogens-rich fluids [6] and under highly oxidizing conditions resulting in significant Fe enrichment. This may represent a newly described alteration environment on the CV parent body: higher oxidizing conditions, heterogeneous thermal metamorphism (different degrees of alteration within TAM5.29 micrometeorite were detected) and a different secondary alteration history enabled by a particular impact history. This is the proof of an even more heterogeneous CV parent body(-ies) thus adding a unique sample to the known CV lithologies. We suggest a multistage formation of TAM5.29: 1) metasomatism at ~275-250°C with Fe-alkali-halogens-rich fluids occurred on the parent body. 2) The particle was involved in an impact that terminated the metamorphic event resulting in a unequilibrated composition with cryptocrystalline and amorphous phases and generating a preferred orientation of olivine. 3) Formation of iddingsite at lower temperatures (<100°C), possibly from fluid released by hydrated minerals during the impact. Furthermore IR reflectance spectra of TAM5.29 is very similar to the spectra of C-type asteroids (e.g. Ceres, 52 Europa) thereby acting as analogue samples, giving possible insights into their composition and geological evolution.

References: [1] Suavet C. et al. 2010. Earth & Planetary Science Letters 293:313-320. [2] Genge M.J. 2010. Meteoritics & Planetary Science Supplement 73. [3] van Ginneken M. et al. 2012. Meteoritics & Planetary Science 47:228-247. [4] Genge M.J. et al. 2008. Meteoritics & Planetary Science 43:497-515. [5] Noguchi T. et al. 2015. Earth & Planetary Science Letters 410:1-11. [6] Krot A.N. et al. 1998. Meteoritics & Planetary Science 33:1065-1085.

THE ISODENSITY ANALYSIS OF THE COMETS

Y. A. Nefedyev[1], A. O. Andreev[1]
[1]Kazan Federal University, Russia, Kazan, Kremlyovskaya st., 18. E-mail: star1955@mail.ru

Introduction: Comet nuclei are remnants of the primary matter of the Solar System that formed the protoplanetary disc. Their study therefore allows building up an evolutionary picture of the formation of planets. Structures and physical properties of cometary atmospheres are mainly investigated using the observations of bright near-Earth comets. However, the modern studies of near-Earth comets and the ones at significant heliocentric distances have shown a considerable difference in their activity [1]. The analysis of structural features of various comets will allow building a more accurate theory of their evolutionary parameters [2].

Methods: The isodensity analysis was applied to produce equidensites with the difference that for isophotes of the second stage was used not the isophote of the first stage, but its contact negative obtained on the same photographs as equidensites of the first stage. This was done to enhance the contrast and produce narrower and closer isophotes. This allowed selecting isophotes that were rather close to each other. Isodensity models were constructed for Bennett, 45P/Honda, and Arend-Roland comets.

Results: Simulation of isophotes for Bennett comet allowed producing the structure of the brightest part of the nucleus and coma. Two isophotes have the form of circles. The rest of isophotes have ledges in the same direction, which obviously corresponds to the ejection from the comet nucleus. Luminance rays are clearly seen. The optical center is located asymmetrically. The map of isophotes was produced with a 17.85 times magnification. The isophotes are tightly arranged. The mean difference between isophotes is 0.06 stellar magnitude. The total fall in brightness from the first isophote to the last one is 3.40 stellar magnitude. The comet tail is clearly observed at a significant distance from the head as well as its radiant structure. When simulating isophotes for 45P/Honda the accuracy of the method appeared to be 0.045^m. This accuracy is also confirmed by the fact that in some cases are observed the isophotes differing by 0.02, 0.025, and 0.03 of the relative magnitude. For all the isophotes, the consistent change in the form of isophotes is observed from the center to the periphery. Near the nucleus, isophotes resemble circles. Closer to the edge appear ledges in the direction of the comet tail. In the periphery areas, particularly closer to the tail, isophotes have the form of wide stripes, while in the central areas, closer to the comet nucleus, they represent narrow lines. For Arend-Roland it was managed to detect rather narrow and close isophotes using the contact negatives with isophotes. This method was applied for producing isophotes of the second and third stages. Isophotes differeing by 0.03 stellar magnitude and 0.02^m difference in densities were revealed. The reproducibility of isophotes using this method is 0.02 stellar magnitude.

Discussion: The isodensity method allows comparing isophotes for various comets, and on the basis on data collected also allows conducting a comparative analysis of cometary activity. Depending on the results of this analysis, it is possible to estimate the evolutionary parameters of cometary bodies, dynamical evolution, and processes in the Solar Nebula more accurately [3]. Generally speaking, some comets may have come to our Solar System from the interstellar space and this fact should therefore be considered when drawing final conclusions [4].

Conclusions: Comets are the time capsules. They contain the information on the time when the Sun was young and the Earth was just being born [5]. Comet nuclei conserve the initial matter from which the Solar System was formed 4,5 billion years ago. Comets accumulated ice, frozen gases, solid particles. Even the amino acid glycine, which is essential for all living creatures, has been found in the comet [6]. Modern theories consider the process of converting asteroids into comets [7, 8]. The study of the genetic relationships of comets with meteorites is impotant for the theory of planetary evolution [9]. The determination of structural, physical, and chemical cometary parameters is therefore very important to comprehend dynamical evolution and processes in the Solar Nebula [10].

References: [1] Janna M. Dlugach, et al. (2018) *Journal of Quantitative Spectroscopy & Radiative Transfer* 205: 80–90. [2] Micla Pennetta (2018) *Geosciences* 8: 235. [3] Sokolova M., et al. (2016) *Advances in Space Research* 58/4: 541-544. [4] Sokolova M.G., et al. (2018) *Advances in Space Research* 62/8: 2355-2363. [5] Usanin V. (2017) *Advances in Space Research* 60/5: 1101–1107. [6] Usanin V. et al. (2016) *Advances in Space Research* 58/11: 2400–2406. [7] Sokolova M.G., et al. (2014) *Advances in Space Research* 54/ 11: 2415-2418. [8] Sergienko M. V. et al. (2018) *Meteoritics & Planetary Science* 53/S1: 6162. [9] Andreev A.O. , et al. (2018) *Meteoritics & Planetary Science* 53/S1: 6157. [10] Nefedyev Y.A. , et al. (2018) *Meteoritics & Planetary Science* 53/S1: 6192.

THE METHOD OF ANALYZING THE COMPLEX OF SPORADIC METEOROIDS

Y. A. Nefedyev[1], A. O. Andreev[1], R. Hudec[2], O. I. Belkovich[1], N. Y. Demina[1]
[1]Kazan Federal University, Russia, Kazan, Kremlyovskaya st., 18. E-mail: star1955@mail.ru
[2]Czech Technical University, Prague 6, Czech Republic

Introduction: Currently, much attention is paid to the study of systems of sporadic meteoroids [1, 2]. One of the most important tasks of meteor astronomy is the construction of a model of sporadic meteor bodies (SMB) complex in the neighborhood of the Earth's orbit [3]. The practical value of such a model is defined by the possibility to use it in geophysical and space researches and meteor radio communication [4]. From the theoretical point of view, the importance of this model is that it serves as a basis for establishing the distribution of SMB in the Solar System [5]. The reasons for the construction of the model are the results in ground-based observations of meteors using photographic and radio methods as most accurate and statistically supported ones, the achievements in physics of meteor phenomena in the Earth's atmosphere, and methodological developments [6].

Methods: One of the possible methods of simulating the stationary SMB complex at heliocentric distance r with a mass m greater than some given mass m_0 is the determination of parameters of meteor bodies flux density over the celestial sphere. It is well known that there is no method of recording meteor phenomena that could allow simulating the flux of meteor bodies with a mass greater than minimum recorded value [7]. The parameters such as brightness and amplitude of a reflected signal higher than a certain level may be determined from observations of meteor flux [8]. Accounting the influence of Earth's movement and attraction on SMB flux density [9] provides the distribution of flux density in the heliocentric coordinate system. Thus, the method of simulating SMB complex developed in this paper presents a system of heliocentric radiants and velocities distribution according to the analytical dependencies.

Results: As a result, for the distribution function of heliocentric velocity $f(v)$ and its variance $d(f)$, the analytical dependencies on the angle of heliocentric elongation as well as the dependence of heliocentric radiants on elongation and azimuth angle are determined. The problem of constructing a model of sporadic meteor bodies complex may be considered as solved. To assess the approximation adequacy, the model velocity distributions are compared with the ones produced on the basis of observations. Besides, the dependencies of heliocentric velocity and the variance of this velocity distribution on elongation angles are compared in 2 ways: with the ones produced from observations and with the developed model. As one of the conditions, this work considers meteor bodies distribution model in the narrow mass range. As a rule, such meteoroids generate meteors recorded using a single observation method.

Discussion: The disadvantage of the specified simulation method considering the whole SMB complex as unified is the impossibility to simulate multi-modal conditional distributions of heliocentric velocities. This multimodality is caused by the complicated structure of SMB complex which in its turn is determined by the distribution of probable parental bodies, comets, and asteroids. The disadvantage may be overcome by dividing, based on some assumptions, the whole SMB complex into groups, applying the above-mentioned scheme to each group separately, and superposition of the models with corresponding weighting functions.

Conclusions: Another interesting problem is finding the dependence between averaged distributions of heliocentric velocities on elongation. As the value $f(v)$ is by definition an inverse value of the Earth's major semi-axis, the analysis of distribution of this value for comets and asteroids may provide some information both to solve this problem and to determine new parameters of the dependence of radiant distribution on heliocentric distance, which is very important for the construction of the SMB complex for the whole Solar System and the study of large-scale material mixing at the early stages of the Solar System [10].

References: [1] Moorhead A.V., et al. (2017) *MNRAS* 472/4: 3833-3841. [2] Andreev V.V., et al. (1994) *Planetary and Space Science* 42/9: 785-790. [3] Sokolova M., et al. (2016) *Advances in Space Research* 58/4: 541-544. [4] Golubaev A.V. (2015) *Solar System Research* 49/4: 226-236. [5] Sokolova M.G., et al. (2018) *Advances in Space Research* 62/8: 2355-2363. [6] Sokolova M.G., et al. (2014) *Advances in Space Research* 54/ 11: 2415-2418. [7] Sergienko M. V. et al. (2018) *Meteoritics & Planetary Science* 53/S1: 6162. [8] Sokolova M., et al. (2016) *Advances in Space Research* 58/4: 541-544. [9] Sokolova M.G., et al. (2018) *Advances in Space Research* 62/8: 2355-2363. [10] Vojáček V., et al. (2019) *Astronomy and Astrophysics* 621: A68.

An In-Situ Organic Molecular Study of the Matrices of a Primitive CR2 Chondrite Meteorite Hills 00426

N. D. Nevill[1], S. J. Clemett[2], S. Messenger[3], K. L. Thomas-Keprta[4], P. A. Bland[1], N. E. Timms[1] & L.V. Forman[1], [1]School of Earth and Planetary Sciences, Curtin University, GPO Box U1987, Perth, Western Australia, 6845, [2]ERC Inc. / [3]Robert M Walker Laboratory for Space Science, ARES, NASA Johnson Space Center, Houston, TX, 77058, USA, [4]Barrios, Engineering Science Contract Group (ESCG), 2224 Bay Area Blvd, Houston, TX, 77058, USA.

Introduction: Carbonaceous chondrites (CC) retain organic matter of varying formation environments i.e. the interstellar media; solar nebula; parent body processing. These molecules retain unique records of their origins and subsequent evolutionary journey's [1-4]. CR chondrites are of particular value in recent years, retaining rare organics of extreme isotopic enrichments pertained to formation within cold molecular clouds and/or the outer protoplanetary disk (Nanoglobules) [5]. Meteorite Hills (MET) 00426 underwent significantly less aqueous alteration than other members of its group like Queen Alexandra Range (QUE) 99177, retaining a higher degree of O-bearing pre-solar grains, ferromagnesium silicates, isotopically anomalous pre-solar signatures and amino acids than typically recorded in CC [1, 7-9]. MET 00426's carbonaceous material also exhibits a low degree of crystallinity indicating low thermal processing [6, 8]. These studies suggest a very primitive matrix, retaining signatures of early nebula processing [1-8].

Previous studies have focused on defining organic morphologies, textural and contextual relationships within MET 00426 matrix through in-situ analyses predominately using the transmission electron microscope (TEM) [7-8, 10]. These studies identified relationships with carbon rich material and nanoglobules in association with phyllosilicates, oxysulphide and in rare cases tochilinite grains [7-10]. A recent study by Le Guillou and Brearely (2014) suggested MET 00426's spatial distribution relationships between carbon rich regions and hydrated inorganics supports a current interstellar theory which suggests nanoglobules become trapped within ice on IDP's and/or other pre solar carriers. These materials later become incorporated into meteorites. The ice melts, mobilizing these organic materials into cracks and boundaries. Understanding this relationship and refining our primitive organic evolutionary knowledge requires an understanding of insoluble and soluble organic spatial distribution. Preliminary geochemical studies on MET 00426 have used Raman and Auger probe spectroscopy [11-12], however no study thus far has chemically classified distinct molecular speciation spatial relationships or produced a comprehensive organic molecular classification of MET 00426's insoluble and soluble organic material due to technical limitations.

Experimental and Results: We carried out in-situ chemical, isotopic and contextual analyses of ~20-50 μm matrix regions pressed into Au foil utilizing an optically flat sapphire window. These regions were randomly selected across whole rock to reduce the effect of bias results. No chemical treatments i.e. epoxy, were utilized during the prep process, enhancing the chemical classification of our primitive sample.

Samples were then initially characterized with non-destructive ultraviolet (UV) microscopy, showing spatial distribution of IOM. We then chemically mapped and obtained spectral data of whole and intact molecular species at the ~2 μm scale using the two-step laser mass spectrometry (μL^2MS) at Johnson Space Centre. This provided spatial distribution relationships of whole insoluble and soluble organic species across the matrix regions studied.

Subsequent study measures isotopic images at high spatial resolution (<200 nm pixel dimension) for ^{12}C, ^{13}C, ^{16}O, $^{12}C^{14}N$, $^{12}C^{15}N$ & ^{28}Si using the NanoSIMS 50 with a focused 16 keV Cs^+ primary ion beam. Due to the primitive nature of the sample, this provided speciation relationships with chemical information aiding to refine our understanding of the primitive relationships of organic species.

Finally, samples are coated with 2 nm of Pt to reduced surface charging for contextual mineralogical analysis utilizing energy dispersive x-ray spectroscopy (EDX) to correlate chemical species with carbonaceous textural relationships previously discussed in literature.

Discussion: A significant enrichment of nanoglobules were observed, indicating primitive organic origins as supported through previous literature [9, 13]. Associated isotopic signatures presented results observed in our previous study of QUE99177 [13], exhibiting rare anomalies consistent with outer regions of the protosolar disk and/or within pre-solar molecular clouds [5]. Primitive O-enriched organic species were observed in association with MET 00426′s nanoglobules, consistent with primitive chemistries. Our study has produced a comprehensive chemical classification of MET 00426′s organic molecular species and their contextual spatial distribution relationships within the matrix.

References: [1] Abreu N. M. and Brearley A. J. (2010) *GCA, 74,* 1146. [2] Alexander C. M. O'D., et al., (2017) *Chemie der Erde – Geochem., 77(2),* 227. [3] Sephton M. A. (2002) *Nat. Prod. Rep., 19(3),* 292. [4] Greenwood et al. (2010) *GCA, 74(5),* 1684. [5] Nakamura-Messenger et al. (2006) *Science, 314, 1439.* [6] Floss C. and Stadermann F. J. (2008) *MetSoc, 71st,* #5008. [7] Abreu N. M. and Brearley A. J. (2006) *LPSC, 37,* #2395. [8] Le Guillou C. and Brearely A. (2014) *GCA, 131,* 344. [9] Le Guillou et. al. (2011) *LPSC, 42,* #1455. [10] Abreu N. M. and Brearley A. J. (2010) *MetSoc, 73rd,* #5334. [11] Floss C. and Stadermann F. (2009) *GCA, 73,* 2415. [12] Starkely et. al. (2013) *Met. Planet. Sci., 48,* 1800. [13] Nevill N. et al. (2018) *LPSC, 49,* #1007.

PETROGENESIS ON MILLER RANGE 090032: COMPARISON WITH OTHER MARTIAN METEORITES

T. Niihara[1,2] and K. Misawa[3], [1]Department of Systems Innovation, School of Engineering, University of Tokyo. 7-3-1 Hongo, Bunkyo-ku, Tokyo 113-8656, Japan (niihara@sys.t.u-tokyo.ac.jp), [2]University Museum, University of To-kyo. 7-3-1 Hongo, Bunkyo-ku, Tokyo 113-0033, Japan, [3]National Institute of Polar Research, 10-3 Midori-cho, Tachikawa, Tokyo 190-8518, Japan.

Introduction: Evidences of aqueous alteration such as iddingsite veins on olivine grains are reported on nakhlite group Martian meteorites [1-3]. Such secondary altered veins are also found in Miller Range (MIL) 090032 nakhlite [4]. Hallis et al. [4] conducted detailed transmission electron microscopic works and suggested that the veins were formed either under Mars (iddingsite, Fe-smectite phyllosilicate) and terrestrial (jarosite, gypsum, amorphous sili-cates, Fe-oxides and hydroxides) conditions. Terrestrial alteration products occurred at the edge of meteorite block and exposed to terrestrial condition. Therefore, alteration products on nakhlite and surrounding materials are im-portant to understand the petrogenesis of nakhlites. Here we report comparison of MIL 090032 and other martian meteorite (shergottites) and discuss petrogenesis of martian meteorites.

Sample and method: A thin section of MIL 090032 allocated from the Meteorite Working Group was observed under an optical microscope. Scanning electron microscope observation has conducted at the Chiba Institute of Tech-nology using a JEOL JSM-6510LA. Electron microprobe analyses were performed on a JEOL JXA-8900 at the Uni-versity of Tokyo.

Results: MIL 090032 consists of orthopyroxene, olivine, fine-grained mesostasis include dendritic minerals and glassy materials. Shock feature is minor and found small shock vein. Pyroxene grains show euhedral shape with size of 300 μm to over 1mm and remain igneous chemical zoning, core of the grains is homogeneous and rich in Mg ($En_{38}Fs_{21}Wo_{41}$) relative to Fe-rich rim ($En_{10}Fs_{58}Wo_{32}$). Olivine grains show subhedral to anhedral shape with size of over 1mm. Olivine grains also remain chemical zoning, core of the grains is homogeneous with Mg-rich composi-tion ($Fo_{44}Fa_{56}$) relative to Fe-rich rim ($Fo_{16}Fa_{84}$). Mesostasis of the rock composed of dendritic spinel, SiO_2-rich ma-terial, and glassy materials. Round-shape, SiO_2-rich material could be relict of primary mineral.

Alteration veins are ubiquitous in olivine grains. Some veins show two-layer structure; an outer layer is enriched in Cl than the inner layer (Fig.1). These veins are cross cutting olivine grain, but do not continue to be surrounding other minerals such as pyroxene.

Discussion and summary: Zoning trends in pyroxene and olivine grains are consistent with normal igneous pro-cess and could be a two-stage magmatism, residence in a deep magma chamber and following rapid cooling. We did not observe a reverse zoning trend in MIL 090032. Zagami and Larkman Nunatak 12011 shergottites [5-7] show a reverse zoning, possibly indicating a magma mixing or crustal assimilation. Rim of pyroxene grains in MIL 090032 have Fe- and Ca-rich compositions which close to hedembergite. This trend also indicates that MIL 090032 solidified rapidly. The texture is similar to that of Olivine-rich lithology of Zagami which intruded into Normal Zagami. The difference is that Zagami contains more evolved materials such as fayalite (Fa_{97}) [5]. MIL 090032 does not show any intrusive structure or chemical zoning trend, suggesting magma mixing or crustal assimilation is less plausible. MIL 090032 experienced minor aqueous alteration interact with volatile-rich (Cl) fluid after crystallization.

[1] Gooding J.L. et al. (1991) *Meteoritics & Planetary Science* 26, 135-143. [2] White L.M. et al. (2014) *Astrobi-ology* **14**, 170. [3] Lee M.R. et al. (2015) *Geochim. Cosmochim. Acta* 154, 49-65. [4] Hallis L.J. et al. (2014) *Geochim. Cosmochim. Acta* 134, 275-288. [5] Niihara T. et al. (2012) *Meteoritics & Planetary Science* 47: A5075. [6] Niihara T. and Misawa K.(2018).*LPS XLIX*, Abstract #2652. [7] Niihara T. and Misawa K.(2019).*LPS L*, Abstract #2242.
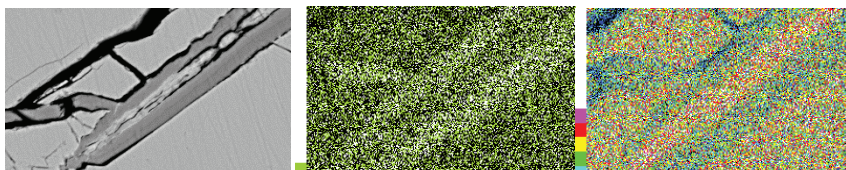
Figure 1. Alteration veins in olivine grain. Outer layer contains Cl and is poor in Fe. (left backscatter electron image, middle, Cl distribution, right: Iron distribution.

FIFTY YEARS OF COSMOGENIC NUCLIDE STUDIES IN LUNAR SAMPLES: WHAT WE HAVE LEARNED AND WHAT WE WOULD LIKE TO KNOW.

K. Nishiizumi, Space Sciences Laboratory, University of California, Berkeley, CA 94720-7450, USA. (E-mail: kuni@berkeley.edu).

Introduction: The Moon has virtually no atmosphere and a relatively weak magnetic field, so in addition to galactic cosmic ray (GCR) irradiation and meteorite bombardment, the lunar surface is subjected to solar wind implantation, solar cosmic ray (SCR) irradiation, and micrometeorite bombardment. When the surface of the Moon is bombarded by cosmic rays, a wide range of radioactive and stable nuclides is produced by nuclear interactions. Immediately upon return from the Moon, and receipt at the Lunar Receiving Laboratory, cosmogenic radionuclides were measured by various investigators. Some of the highlights of these measurements are itemized below.

SCR: SCRs have lower energy but a much higher flux compared to GCRs, SCR-produced cosmogenic nuclides dominant the inventory in the upper few g/cm^2 of a surface [1]. In meteorites it is rare to find SCR-produced nuclides; surface ablation during atmospheric entry removes the upper few cm of material. On the other hand, SCR-produced nuclides are observed in nearly all lunar surface materials and the abundance of the SCR-produced nuclides provides key information to the evolutional histories of lunar surface materials, such as erosion of rock and regolith gardening. Detailed measurements of depth profiles of SCR-produced nuclides in lunar rocks provide a ground-truth archive of past solar activities. The difficulty of the measurements and the lack of ideal samples resulted in only several rock samples being studied extensively. Recently, we measured cosmogenic nuclides in the glass-coated ilmenite basalt 12054, a sample that was studied as part of a consortium [2] in 1977! Based on preliminary results, 12054 has complex exposure history and is not a good rock sample for SCR studies.

Erosion Rate: The surfaces of lunar rocks are continuously bombarded by micrometeorites, which erode the surface. This erosion can be obtained by measuring of SCR-produced ^{53}Mn and ^{26}Al depth profiles, as well as by measurements of the track density or micrometeorite impact pits. We obtained an erosion rate from ~0.5 mm/Myr for the glass coated basalt 64455 [3] to 3 - 4 mm/Myr for the breccia 68815 [4]. These represent the only direct measurements of erosion rates of a planetary surface outside of Earth.

Regolith Gardening: Lunar regolith gardening is caused by overturning of regolith materials caused by impact crater formation. This gardening process affects the maturity of the regolith – by bringing to the surface relatively immature regolith - and also excavates rocks and boulders from deeper in the regolith. Continuous impacts by meteorites and micrometeorites are considered to be the dominant cause of mixing processes on the lunar surface [5]. Twenty-one single or double drive tubes and 3 deep drill cores were collected by six Apollo missions. We have measured cosmogenic radionuclides in 16 out of the 24 cores. Gault et al. [6] estimated a turnover rate of 10^7 yr for 1 cm and 10^9 yr for 10 cm based on meteorite influx rate and laboratory impact experiment. Arnold [7] calculated a gardening rate of 10^6 yr for 1 cm and 4×10^7 yr for 10 cm using a Monte Carlo model. Recently, Speyerer et al. [8] predicted a regolith overturn rate of 8.1×10^4 yr for 2 cm and 1.0×10^7 yr for 20 cm using the contemporary production rate of small craters with Lunar Reconnaissance Orbiter Camera (LROC) temporal imaging. These rates, based on LROC imaging, are considerably faster than the earlier estimates. Cosmogenic SCR-produced ^{26}Al and ^{53}Mn, on the other hand, indicate turnover rates of ~2 cm/Myr for small craters over the last several million years [e.g., 9, 10]. These direct measurements by cosmogenic nuclides have provided the ground truth for lunar regolith formation and mixing models.

Pebbles vs. Bulk Soils: The work done to date on lunar pebbles and soils have noted several outstanding, and surprising features [e.g., 11, 12]: (1) most pebbles have a different depositional history than the bulk soil; (2) most pebbles contain lower cosmogenic radionuclide concentrations or lower neutron fluences than bulk soils located at the same depth; and (3) basaltic or crystalline type pebbles show these differences in exposure history, but soil breccia type pebbles do not show clear difference from bulk soils. We are investigating this unsolved problem of lunar surface processing.

References: [1] Reedy R. C. and Arnold J. R. (1972) *Journal of Geophysical Research* 77:537-555. [2] Hartung J. B. et al. (1978) *Proceedings of Lunar Science Conference* 9th:2507-2537. [3] Nishiizumi K. et al. (2009) *Geochimica et Cosmochimica Acta* 73:2163-2176. [4] Kohl C. P. et al. (1978) *Proceedings of the Lunar and Planetary Science Conference* 9th:2299-2310. [5] Langevin Y. and Arnold J. R. (1977) *Annual Review of Earth and Planetary Sciences* 5:449-489. [6] Gault D. E. et al. (1974) *Proceedings of the Lunar Science Conference* 5th:2365-2386. [7] Arnold J. R. (1975) *The Moon* 2:157-170. [8] Speyerer E. J. et al. (2016) *Nature* 538:215. [9] Fruchter J. S. et al. (1978) *Proceedings of the Lunar and Planetary Science Conference* 9th:2019-2032. [10] Nishiizumi K. et al. (1979) *Earth and Planetary Science Letters* 44:409-419. [11] Curtis D. B. and Wasserburg G. J. (1977) *Proceedings of the Lunar Science Conference* 8th:3575-3593. [12] Nishiizumi K. et al. (1980) *Lunar and Planetary Science* XI:818-820.

LUNAR SURFACE REGOLITH PROCESSES: THE COSMOGENIC NUCLIDE RECORD IN 15008.

K. Nishiizumi[1] and M. W. Caffee[2], [1]Space Sciences Laboratory, University of California, Berkeley, CA 94720-7450, USA. (E-mail: kuni@berkeley.edu). [2]Department of Physics and Astronomy, Purdue University, West Lafayette, IN 47907-1396, USA. (E-mail: mcaffee@purdue.edu).

Introduction: Lunar regolith soils are formed by repetitive meteorite and micrometeorite impact fragmentation of local rocks. The lunar regolith is continuously overturned by frequent meteorite and micrometeorite impacts but mixing processes are extremely slow [e.g., 1]. Quantifying the long-time morphological changes of soils on the Moon, and other solar system bodies, requires an understanding of how these soils are altered and mixed by impacts of various sizes. Lunar surface modification can be studied by two different methods: remote sensing and direct laboratory measurements of lunar surface materials. Visible observations provide essential information regarding the surface topography, impact crater count/size, and thickness of the regolith. Careful laboratory characterization of the physical properties of lunar samples and measurements of cosmogenic radioactive and stable nuclides, nuclear tracks, solar wind components, abundances of agglutinates, and the maturity index, I_s/FeO, provide a completely independent source of about lunar surface processes. Twenty-one single or double drive tubes and 3 deep drill cores were collected by six Apollo missions. Cosmogenic radionuclides were measured in 16 out of the 24 cores; the number of nuclides measured in each core varied from 1 to more than 8. The cosmogenic nuclide depth profiles in each core are distinct, especially those produced by solar cosmic ray (SCR) produced ^{26}Al and ^{53}Mn, but all show surface gardening processes occurring over a million-year time scale. Among the 16 cores, 15008 is the least disturbed so it is an ideal core and serves as a calibration of gardening process of other lunar cores.

15008: The Apollo 15 core 15008 is an upper portion of 15008/7 double drive tube. It was collected at station 2 on the flank of St. George crater near the base of the Apennine Front. It was drilled in the continuous ejecta blanket on the rim of a 10 m diameter shallow crater [2]. The core is 23.1 cm in length and has a density of 1.65 g/cm^3 after extrusion. Based on ^{26}Al measurements Fruchter et al. [3] concluded that the core's surface is undistorbed, unique among lunar cores. Likewise, ^{36}Cl [4] and ^{14}C [5] show a nearly undisturbed depth profile. Manganese-53, which has a longer half-life, shows slightly undersaturated profile [6].

New Measurements: To expand the use of this core as a calibration point, we measured ^{10}Be, ^{26}Al, and ^{41}Ca depth profiles from 15008/7. Beryllium, Al, and Ca were separated from same solution of previous ^{36}Cl and ^{53}Mn measurements [4, 6] and purified for AMS measurements. Beryllium-10 and ^{26}Al measurements were performed at CAMS, Lawrence Livermore National Laboratory [7] and ^{41}Ca measurements were performed at PRIME lab, Purdue University [8]. Results are shown in Fig. 1 along with previous ^{26}Al measurements [3].

As predicted, SCR-produced ^{10}Be is less than 1 dpm/kg at the surface (left). Our ^{26}Al results (middle) are in excellent agreement with previous measurements [3] but have lower uncertainties. The SCR-produced ^{41}Ca (right) produced in the near surface (< 3 g/cm^2) is minimal. This SCR-contribution is similar to that of 74275 [9]. Increasing ^{41}Ca concentration with increasing depth below 3 g/cm^2 is due to the ^{40}Ca(n,γ)^{41}Ca reaction by secondary low energy neutrons. The higher sampling frequency for this core compared to that of Apollo 15 drill core makes that the depth profiles of this core are ideal for calibration at depth of ≤ 50 g/cm^2.
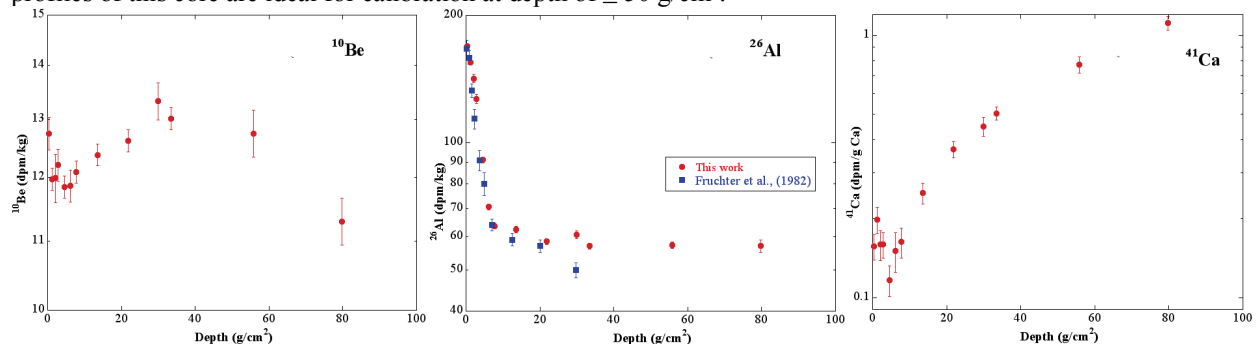
Fig. 1. Depth profiles for ^{10}Be (left), ^{26}Al (middle), and ^{41}Ca (right) of 15008/7 double drive tube.

References: [1] Langevin Y. and Arnold J. R. (1977) *Annual Review of Earth and Planetary Sciences* 5:449-489. [2] Apollo P. E. T. (1972) *Science* 175:363-375. [3] Fruchter J. C. et al. (1982) *LPS* XIII:243-244. [4] Nishiizumi K. et al. (1989) *Proceedings of the Nineteenth Lunar and Planetary Science Conference* 19:305-312. [5] Jull A. J. T. et al. (1998) *Geochimica et Cosmochimica Acta* 62:3025-3036. [6] Nishiizumi K. et al. (1990) *LPS* XXI:895-896. [7] Davis J. C. et al. (1990) *Nuclear Instruments and Methods in Physics Research* B52:269-272. [8] Sharma P. et al. (2000) *Nuclear Instruments and Methods in Physics Research* B172:112-123. [9] Fink D. et al. (1998) *Geochimica et Cosmochimica Acta* 62:2389-2402.

ISOTOPIC IMPRINTS OF SUPER-AGB STARS AND THEIR SUPERNOVAE IN THE SOLAR SYSTEM.

L. R. Nittler, Dept. of Terrestrial Magnetism, Carnegie Institution of Washington, 5241 Broad Branch Rd NW, Washington DC 20015, USA (lnittler@ciw.edu)

Introduction: In studies of the origin of presolar grains and bulk nucleosynthetic isotopic anomalies in meteorites, little attention has been paid to the potential importance of stars in the mass range of ~8-10 solar masses. These stars lie in a middle-ground between low- and intermediate mass asymptotic giant branch (AGB) stars that end their lives as white dwarfs and massive stars whose cores burn all the way to Fe before collapsing and exploding as supernovae (SNII), leaving behind neutron stars or black holes. They evolve through a "super-AGB" phase, undergoing thousands of thermal pulses and losing most of their mass in strong winds [1]. However, their final fates (*e.g.,* as white dwarfs versus neutron stars following core-collapse supernovae) depend on highly uncertain physics and diagnostic observable signatures of both super-AGB stars and their possible supernovae are controversial [1, 2]. Here we discuss possible ways super-AGB stars and their supernovae may have left nucleosynthetic imprints in the solar system.

Super-AGB stars: Although most presolar SiC, silicate and oxide stardust grains are inferred to have originated in AGB stars [3], the isotopic signatures largely point to relatively low-mass (~1-3 $M_\odot$) progenitors. Until recently, intermediate-mass (4-8$M_\odot$) AGB stars have largely been ruled out as parent stars because their predicted O isotopic ratios are not observed. However, re-measurement of a key reaction rate has made such an origin plausible for Group 2 (^{18}O-depleted) presolar grains [4], albeit with the requirement of some mixing of the pure AGB component with isotopically normal material, perhaps from a binary companion. More recently, large ^{25}Mg excesses have been found in some Group 1 presolar silicates [5, 6], inconsistent with the low-mass AGB origin implied by these grains' O isotopes. Leitner and Hoppe [5] favored an origin for these grains in SNII undergoing explosive H-burning. However, hot bottom burning in super-AGB stars, especially those of lower-than-solar metallicity, also produces large ^{25}Mg/^{24}Mg ratios [7] and mixing of their ejecta with more normal material from a binary companion can quantitatively explain the isotopic data for such grains, similar to that proposed for Group 2 grains, providing an alternative possible origin.

Electron Capture Supernovae: ECSN may occur when the electron-degenerate ONeMg white dwarf core of a super-AGB star reaches a Chandrasekhar mass, and undergoes electron-captures on ^{20}Ne that lead ultimately to a thermonuclear runaway. Most studies have found that the nuclear burning results in the WD core collapsing to a neutron star, while ejecting newly synthesized neutron-rich isotopes. Several studies of nucleosynthesis in such core collapse (cc-)ECSN have found that n-rich isotopes of relevance to meteorite studies, including ^{48}Ca, ^{50}Ti, ^{54}Cr, ^{60}Fe, and light r-process isotopes may be produced [8-11]. Nittler et al. [12] suggested either high-density Type Ia supernovae [13] or ccECSN as a source of extreme ^{54}Cr and ^{50}Ti-enriched nano-sized presolar oxide grains from the Orgueil meteorite, as well as of the putative presolar carriers of ^{48}Ca anomalies. More recent studies have begun to investigate the possible existence of thermonuclear (t-)ECSN in which the nuclear energy generation occurs rapidly enough for the entire core to explode [2]. Jones et al. [14] recently showed that nucleosynthesis in a tECSN is similar to that previously found for high-density Type Ia SNe [13] and in fact, this work suggested that tECSN *are* the hypothesized high-density SNIa, for which hitherto there has been no astrophysical origin identified. The calculated tECSN nucleosynthesis provides an excellent match to the most extreme ^{54}Cr-rich grain of [12], as well as producing many other n-rich isotopes and important short-lived nuclides like ^{26}Al, ^{53}Mn, and ^{60}Fe. One advantage of tECSN over ccECSN for explaining the meteoritic data is they eject copious amounts of ^{16}O, facilitating the formation of oxide dust without requiring mixing with unburnt core material [15]. In any case, the lifetimes of super-AGB stars (15-25 Myr) is comparable to that of molecular clouds, suggesting the possibility of direct interaction between the ejecta of such stars (both during super-AGB winds and/or ECSN explosions) and the forming solar system, with potentially important implications for understanding the isotopic diversity of meteoritic materials and early solar system evolution.

References: [1] Doherty C. L., et al. (2017) *Publications of Astronomical Society of Australia, 34.* [2] Jones S., et al. (2016) *Astronomy and Astrophysics, 593.* [3] Zinner E., in: A.M. Davis (Ed.), Meteorites and Cosmochemical Processes (Vol. 1), Treatise on Geochemistry (Second Edition, eds: H. D. Holland and K. K. Turekian), Elsevier-Pergamon, Oxford, 2014, pp. 181–213. [4] Lugaro M., et al. (2017) *Nature Astronomy, 1,* 0027.. [5] Leitner J. and Hoppe P. (2018) *LPS 49,* Abstract #1858. [6] Verdier-Paoletti M. J., et al. (2019) *This meeting.* [7] Doherty C. L., et al. (2014) *Monthly Notices of the Royal Astronomical Society, 437,* 195-214. [8] Wanajo S., et al. (2013) *Astrophysical Journal Letters, 767.* [9] Wanajo S., et al. (2013) *Astrophysical Journal Letters, 774.* [10] Wanajo S., et al. (2011) *Astrophysical Journal Letters, 726,* L15. [11] Wanajo S., et al. (2009) *Astrophysical Journal, 695,* 208-220. [12] Nittler L. R., et al. (2018) *Astrophysical Journal Letters, 856,* L24. [13] Woosley S. E. (1997) *Astrophysical Journal, 476,* 801-810.[14] Jones S., et al. (2018) *Astronomy and Astrophysics, in press.* [15] Yu T., et al. (2014) *LPS 45,* Abstract #2247.

RELATIONSHIP BETWEEN Fe^{3+} CONTENTS IN SERPENTINE AND DEGREES OF AQUEOUS ALTERATION AMONG CM CHONDRITES: A COMBINED MÖSSBAUER, XANES, AND EPMA STUDY.

T. Noguchi[1], R. Sagae[2], H. Ishibashi[3], S. Odake[4], H. Kagi[5], M. Akasaka[6], M. Kimura[7], and A. Yamaguchi[7], [1]Kyushu University, Fukuoka 819-0395, Japan (tnoguchi@artsci.kyushu-u.ac.jp), [2]JASCO Co. Ltd., 2967-5 Ishikawa-cho, Hachioji, Tokyo 192-8537, Japan, [3]Shizuoka University, 836 Ohya, Suruga-ku, Shizuoka 422-8529, Japan, [4]Gemological Institute of America Inc., 4-19-9 Taito, Tokyo 110-0016, Japan, [5]University of Tokyo, 7-3-1 Hongo, Bunkyo-ku, Tokyo 113-0033, Japan, Shimane University, 1060 Nishikawazu-cho, Matsue, Shimane 690-8504, Japan, [7]National Institute of Polar Research, 10-3 Midori-cho, Tachikawa, Tokyo 190-8518, Japan.

Introduction: In CM chondrites, anhydrous phases such as olivine and pyroxene, Fe-Ni metal, Fe-Ni sulfide, and chondrules glass are replaced by hydrous phases, serpentine and tochilinite (e.g. [1] and references therein). Temperatures during aqueous alteration have been estimated to be from ~0 ^{o}C to <170 ^{o}C [2]. $Fe^{3+}/\Sigma Fe$ ratio of cronstedtite $(Fe^{2+}_{4}Fe^{3+}_{2})(Fe^{3+}_{2}Si_{2})O_{10}(OH)_{8}$ in matrix and chondrule rims were measured by TEM-EELS [3]. Two Fe Kα XANES studies measured $Fe^{3+}/\Sigma Fe$ ratios of matrices and serpentine in CM chondrites, respectively [4, 5]. However, two among three studies [4, 6] suggest that there is no correlation between the $Fe^{3+}/\Sigma Fe$ ratios and the degrees of aqueous alteration but another [5] suggests that there is a positive correlation between them. We performed a combined study of Fe Kα XANES and ^{57}Fe Mössbauer spectroscopy to estimate $Fe^{3+}/\Sigma Fe$ ratios of serpentine-group minerals in CM chondrites quantitatively. Based on these data, we revisited the relationships between the $Fe^{3+}/\Sigma Fe$ ratios and the degrees of aqueous alteration.

Samples and methods: We used cronstedtite from two different localities (Aude, France and Bohemia, Czech). ^{57}Fe Mössbauer spectroscopy was measured in room temperature by using 370 MBq ^{57}Co in Pd as a source at Shimane University. About 20 mg aliquots of the samples were used as absorbers. Thin sections of LEW 85311, Murchison, Murray, Mighei, Y-75293, Bells, Nogoya, Cold Bokkeveld, Essebi, Y-82042, and Sayama were used for this study. To determine the degrees of aqueous alteration according to [6], we observed texture and mineralogy by using both an optical microscope and a SEM at Ibaraki University. Chemical compositions of the serpentine-group minerals in chondrules were measured by an electron microprobe at National Institute of Polar Research, Japan. Fe Kα XANES was measured at Beamline 4A, KEK-PF. Electron microprobe analysis of serpentine and ferromagnesian silicates in chondrules in the CM chondrites were performed at National Institute of Polar Research. Accelerating voltage and probe current are 15 kV and 9 nA, respectively.

Results and discussion: It has been expected that Mg content in phyllosilicates increases as aqueous alteration proceeds [7, 8]. The average $Fe^{*}/(Mg+Fe^{*})$ ratio of serpentine in Sayama CM 2.1 was 0.35 and that of LEW 85311 CM 2.1 was 0.73 ($Fe^{*}=Fe^{2+}+Fe^{3+}$). There is a positive correlation ($R^{2}=0.8757$) between average $Fe^{*}/(Mg+Fe^{*})$ ratios and average $Fe^{3+}/\Sigma Fe$ ratios of serpentine-group minerals. Both average ratios tend to be smaller in CM chondrites experienced heavier aqueous alteration except for Essebi and Bells. The standard deviation of the $Fe^{3+}/\Sigma Fe$ ratio of each meteorite is considerably large in comparison with the corresponding average value, which may reflect the fact that most CM chondrites are breccias containing clasts with different extent of aqueous alteration. Comparison between $Fe^{*}/(Mg+Fe^{*})$ and $(Fe^{3+}+Al)/[(Fe^{3+}+Al)+(Si+Mg+Fe^{2+})]$ ratios in serpentine revealed that Fe^{3+} and Al^{3+} cations in serpentine that replaced mesostasis of chondrules decreased as aqueous alteration proceeded. In contrast, Fe^{2+} and Mg^{2+} in the serpentine increased. This result supports the reaction of replacing elements proposed by [8]. Fe^{2+} and Mg^{2+} were probably supplied from phenocrysts in chondrules that replaced by serpentine. There is a negative correlation between $Fe^{3+}/\Sigma Fe$ ratios of serpentine and modal abundance of magnetite determined by [9], which indicates that more Fe^{3+} ions were expelled from serpentine as aqueous alteration proceeded and that the expelled Fe^{3+} ions were consumed to form magnetite.

References: [1] Brearley A. D., Jones R. (1998) *Reviews in Mineralogy* 38, Chap. 3. [2] Keil K. (2000) *Planetary and Space Science* 48: 887-903. [3] Zega T. J. (2003) *American Mineralogist* 88: 1169-1172. [4] Beck P. et al. (2012) *Geochimica et Cosmochimica Acta* 99: 305-316. [5] Mikouchi T. et al. (2012) *LPSC 43*, Abstract #1496. [6] Rubin A. et al. (2008) *Geochimica et Cosmochimica Acta* 71: 2361-2382. [7] Zolensky M. E. et al. (1989) *Icarus* 78: 411-425. [8] Browning L. B. et al. (1996) *Geochimica et Cosmochimica Acta* 60: 2621-2633. [9] Howard K. T. et al. (2009) *Geochimica et Cosmochimica Acta* 73: 4576-4589.

HOW UNIQUE IS ALMAHATA SITTA AND HOW RELEVANT IS IT TO BENNU?

J. O. Nolau[1], T. D. Swindle[2], H. Campins[1], and H. C. Connolly Jr.[3],[1]University of Central Florida, Department of Physics, 4000 Central Florida Blvd. Orlando, FL 32816, USA,[2]University of Arizona, Lunar and Planetary Laboratory, 1629 E. University Blvd. Tucson, AZ 85721, USA, [3]Rowan University, Department of Geology, 201 Mullica Hill Rd. Glassboro, NJ 08028, USA. Corresponding author. Email: jnolau@knights.ucf.edu

Introduction: The albedo diversity on the surface of asteroid 101955 Bennu is the largest observed in any asteroid. The geometric albedo ranges from 3.5% to >20% and the surface features detected so far range from centimeters to decameters in diameter. To date, similar albedo diversity among meteorites have been reported for Almahata Sitta and Kaidun; however for Kaidun the different lithologies were present within one meteorite, but the sample size was too small be used as an analog for the surface of Bennu [5]. Using a larger-scale event for comparison, Almahata Sitta was an observed fall (in 2008) that contained different lithologies within its strewn field including: ureilites, enstatites, two types of ordinary chondrites (H and L), and carbonaceous chondrites [2,4], which were linked to Almahata Sitta by their exposure histories. How rare is it to observe meteoritic falls that contain different classifications within its strewn field? We aim to make the comparison of the uniqueness seen in Almahata Sitta with the intriguing feature diversity seen on 101955 Bennu. This comparison is motivated in part by the likelihood that both Bennu and Almahata Sitta originated from the same region of the asteroid belt and may have been affected by similar processes [1,3].

Methods: We analyzed strewn fields of low albedo material in order to determine if there are xenoliths of high albedo material present among them, as is the case for Almahata Sitta. We determined the location and size of the six carbonaceous chondrite strewn fields listed in the Meteoritical Bulletin Database: Allende (CV3, fell in Mexico, 1969), Moss (CO3, Norway, 2006), Murchison (CM2, Australia, 1969), Sutter's Mill (CM2, United States, 2012), Orgueil (CI1, France, 1864), and Tagish Lake (C2 ungrouped, Canada, 2000). The meteorite candidates were mapped and narrowed down by geographic location, placement relative to each strewn field, and year of find to determine their likelihood of being a potential member of the original body.

Results: There are eight high albedo finds (ordinary chondrites, H and L) within the Allende strewn field that postdate the recorded fall. The finds have a placement that is consistent with being possible members of the Allende strewn field, although weathering of finds and exposure ages are still to be studied. No other recorded finds have been reported within the other strewn fields.

Discussion: Further investigation of the exposure ages (both the cosmic-ray exposure ages and the terrestrial exposure ages) of the individual finds within the Allende strewn field would provide valuable information to evaluate whether they could be part of the Allende fall. The fact that a large number of high-albedo meteorites have been found within the Allende strewn field, and none have been found in the other strewn fields, is consistent with the possibility that the incorporation of foreign lithologies into a carbon-rich meteoroid may not be as uncommon as previously estimated. If correct, the data would suggest that the Allende parent body was composed of multiple lithologies, similar to that of the Almahata Sitta parent body (2008 TC3), and possibly Bennu.

References: [1] Campins H. and Morbidelli A. et al. (2010) *The Astrophysical Journal Letters* 721: L53-L57. [2] Bischoff A. and Horstmann M. et al. (2010) *Meteoritics & Planetary Science* 45: I10-11: 1638-1656. [3] Goodrich C. A. and Hartmann W. K. et al. (2014) *Meteoritics & Planetary Science* 50: 782-809. [4] Jenniskens P. and Vaubaillon J. et al. (2010) *Meteoritics & Planetary Science* 45: I10-11: 1590-1617. [5] Zolensky M. E. and Ivanov A. V. et al. (1996) *Meteoritics & Planetary Science* 31: I4: 484-493. [6] Jenniskens P. and Shaddad M. H. et al. (2009) *Nature* 458: I7237: 485-488. [7] Gayon-Markt J. and Delbo M. et al. (2012) *Monthly Notices of the Royal Astronomical Society* 424: I1, I21: 508-518.

DO WE NEED A NEW DEFINITION FOR A COMET?

J. A. Nuth[1], N. M. Abreu[2], B. Clark[3], N. M. Johnson[4], D. P. Glavin[1] [1]NASA-GSFC, Code 690, Greenbelt MD 20771 USA (joseph.a.nuth@nasa.gov), [2]The Pennsylvania State University, DuBois, PA, USA, [3]Space Science Institute, Boulder, CO 80301, USA. [4]NASA-GSFC, Code 690, Greenbelt MD 20771 USA

Introduction: Scott et al. [1] have demonstrated distinct isotopic differences between carbonaceous and ordinary chondrites that are consistent with the formation of the carbonaceous chondrite parent bodies outside of the orbit of Jupiter. Active asteroids in the Main Belt have been observed to form comae and tails near perihelion that are probably driven by subliming water vapor (among other mechanisms). Some B- and C-type asteroids are sources for meteor streams while some B-type asteroids were first discovered as comets, then were later re-discovered as asteroids [2,3] such as Comet Wilson-Harrington. The distinction between comets and asteroids is not always clear.

Order in the Primitive Solar System: In the very early solar system, there are reasons to believe that small bodies formed a roughly continuous sequence from dry asteroids near the Sun, through increasingly water-rich bodies beyond the giant planet region [4]. However, there is evidence that this orderly progression was then thoroughly mixed due to tidal interactions between the giant planets and the nebular disk [5-10] that threw dry bodies into the outer nebula and drove water-rich bodies into the inner solar system. This mixing plays havoc with many distinctions previously used to differentiate between comets and asteroids and, in particular, makes a dynamic definition of a comet problematic. For example, many parent bodies formed in the inner solar system were thrown out to the Kuiper Belt and into the Oort Cloud. If a dry, Eros-like, asteroid were to fall into the inner solar system from the Oort Cloud following a typical cometary trajectory, would this be a comet? If a body of similar composition is captured into a Jupiter Family orbit, is this a JFC? In the same manner, if a small body formed well beyond the orbit of Jupiter but were deflected into the inner solar system, and spent the majority of the last 4.5 billion years in the Main Asteroid Belt, is such a body a comet?

Survival in the Inner Solar System: A simple rule of thumb is that an active comet survives for about one thousand perihelion passages before activity ceases. So for an active, long-period comet such as Halley, its active lifetime is on the order of 100,000 years while for a Jupiter Family comet like Churyumov-Gerasimenko its active lifetime might be as short as 5000 years. On the other hand, a comet is stable in the inner solar system for approximately 200,000 – 500,000 years [11] before it gets thrown out of the solar system or into the Sun. This implies that there are 10 – 100 times more dormant comets than active comets in the solar system. Are such dormant comets now asteroids? If this asteroid class undergoes a major collision that exposes deeply buried volatiles producing a coma or tail, is the asteroid now a comet again? Is there a particular class of asteroid that is most likely a dormant comet?

Type-B Asteroids are Dormant Comets: As a comet evolves from active to dormant by losing volatiles and/or growing an insulating crust over its surface [12], traces of its former activity could remain. Some asteroid class members might be discovered as a barely active comet, lost, then re-discovered as an asteroid [2,3]. Some could be the source of meteor streams [13]. Some class members could still emit particles near perihelion driven by subliming volatiles [14], though there are other mechanisms that could potentially drive such emissions at other locations over the orbit. As a class, B-type asteroids fulfill each of these criterion and we suggest that such asteroids are the first stage of cometary dormancy.

What is a comet? Loss of volatiles over time or through closer approaches to the Sun results in the formation of B- and probably other (C, P, D?) asteroid types. Metamorphism of a comet's surface resulting from relatively rapid passages close to the Sun could result in a similar surface spectrum to a volatile-rich body that slowly metamorphoses while residing in the Main Belt. A dynamical definition (above) of a comet also makes little sense. *We suggest that any small body that completed its formation outside the Snow Line in the primitive solar nebula should be considered a comet based on its high water/rock ratio regardless of its subsequent dynamic evolution.*

References: [1] Scott, E.R.D., Krot, A.N., Sanders, I., 2017. In 80th MetSoc., Abstr. #6395. [2] Fernandez, Y.R., McFadden, L.A., Lisse, C.M., Helin, E.F., Chamberlin, A.B., 1997. Icarus 128, 114-126. [3] Ishiguro, M., Ham, J.-B., Tholen, D.J., Elliott, G.T., Micheli, M., et al., 2011. Ap.J. 726. [4] Nuth, J.A., McCoy, T., Johnson. N.M. & Abreu, **Primitive Meteorites and Asteroids** (Elsevier Inc., 2018) pp.409-439. [5] Gomes;, R.; H. F. Levison; K. Tsiganis; A. Morbidelli (2005). Nature. **435** 466–9. [6] Tsiganis, K.; Gomes; R.; Morbidelli, A.; F. Levison, H. (2005). Nature. **435** 459–461.[7] Morbidelli, A.; Levison, H.F.; Tsiganis, K.; Gomes, R. 2005 Nature. **435** 462–465. [8] Walsh, Kevin J.; Morbidelli, Alessandro; Raymond, Sean N.; O'Brien, David P.; Mandell, Avi M. 2011 Nature **475**, 206–209.[9] Morbidelli, Alessandro; Crida, Aurélien 2007. Icarus. 191, 158–171. [10] Brasser, R.; Matsumura, S.; Ida, S.; Mojzsis, S. J.; Werner, S. C. 2016 Ap.J. 821: 75.[11] Levison, H. & Duncan, M. J., 1994, Icarus 108, 18-36.[12] Storrs, A.D., Fanale, F.P., Saunders, R.S., Stephens, J.B., 1988. Icarus 76, 493-512.[13] Whipple, F. L. (October 25, 1983). Marsden, B. G. (ed.) IAU Circular. 3881.[14] H. H. Hsieh, D. C. Jewitt, and Y. R. Fernandez, 2004, 127, 2997–3017.

PAST SOLAR WIND FLUXES AT THE LOCATIONS OF GAS-RICH METEORITE PARENT BODIES BASED ON NOBLE GAS STUDIES: IMPLICATIONS TO THE PAST HELIOCENTRIC DISTANCES.

T. Obase[1] and D. Nakashima[1], [1]Division of Earth and Planetary Materials Science, Graduate School of Science, Tohoku University, Sendai, Miyagi 980-8578, Japan. E-mail: tomoya.obase.s3@dc.tohoku.ac.jp

Introduction: To understand the evolutions of asteroid orbits, past heliocentric distances (HDs) of asteroids are critical information, which can be provided by solar wind (SW) fluxes recorded on old regolith in the asteroids, as the SW flux is inversely related to the square of the HD. Several studies attempted to obtain the past HDs of meteorite parent bodies by comparing SW noble gas concentrations in gas-rich meteorites with those in the lunar samples [e.g. 1-4] but with a problem that the different properties between the lunar and asteroid regolith such as maturities, gardening processes and effect of the Earth's magnetosphere are not considered. Regolith breccias have experienced exposures to SW and galactic cosmic rays on the surface of the parent bodies [5] and acquired SW noble gases and cosmogenic ones. The past SW flux on the meteorite parent body can be calculated from a correlation between these noble gas abundances in the regolith breccia. Here we describe a new method to estimate past SW fluxes at the locations of meteorite parent bodies and calculate and recalculate the HDs of the parent bodies of several meteorites. For the calculations, the problem shown above is avoided by directly comparing the estimated SW fluxes with the 1 AU SW flux obtained by the Genesis mission without obstruction by the Earth's magnetosphere [6].

Methods: Gas-rich meteorites listed in Table 1 were analyzed for noble gases in previous studies. More than 18 samples from gas-rich portions show positive correlations of concentrations between SW-^{36}Ar (^{36}Ar$_S$) and cosmogenic-^{21}Ne (^{21}Ne$_C$) for the respective meteorites. Assuming that the surface regolith on a meteorite parent body is continuously well-mixed due to a repeated impact gardening, the concentrations of ^{36}Ar$_S$ and ^{21}Ne$_C$ in the regolith increase in a ratio of the ^{36}Ar$_S$ flux to the production rate of ^{21}Ne$_C$ (P_{21}) per unit area. Then, the slope of the correlation line corresponds to the ratio of the ^{36}Ar$_S$ flux to the P_{21} per unit area. The past ^{36}Ar$_S$ flux (F_{36}) at the HD of the parent body is obtained by the following equation; $F_{36} = \pi a P_{21}$, where a is the slope of the correlation line and π is a correction factor to take into account the rotation of the parent body. The P_{21} is calculated from a physical model [7].

Results & Discussion: The past ^{36}Ar$_S$ flux at the location of the parent body of the howardite Kapoeta is 53 ± 9 atoms cm^{-2} s^{-1}. Assuming that the Kapoeta's parent body is asteroid 4 Vesta and its HD (2.4 AU) has never changed significantly, the past ^{36}Ar$_S$ flux at 1 AU is calculated as 310 ± 50 atoms cm^{-2} s^{-1}, which is similar to the current ^{36}Ar$_S$ flux obtained by the Genesis mission ([6]; Table 1). Assuming the past SW flux is similar to the current one, the past HDs of the meteorite parent bodies are given by comparing the estimated SW flux at the locations of the parent bodies (Table 1) with the SW flux at 1AU obtained by the Genesis mission. In Table 1 we summarized the calculated and recalculated HDs of the meteorite parent bodies with their classifications. The past HDs of the parent bodies of enstatite and rumuruti chondrites are close to the Sun compared to those of H chondrite parent bodies. Recent astrophysical model predicts the formation regions of enstatite, H and rumuruti chondrites as 1.9 - 2.1 AU, 2.43 AU, and 2.6 AU, respectively [8]. This is roughly in agreement with our estimations except for PRE 95410 (R3). The high SW flux on the PRE 95410 parent body may suggest inner migration from the formation region or several times higher SW flux than the current SW flux when the regolith was exposed to the SW. Dating the antiquities of the exposures are highly desirable for further constraints on the past HDs and the SW flux evolution in the history of the solar system.

References: [1] Obase T. et al. (2015) *JPGU meeting 2015*, Abstract PPS22-08. [2] Nakashima D. et al. (2006) *M&PS* 41:851-862. [3] Wieler R. et al. (1989) *GCA* 53:1441-1448. [4] Nakashima D. et al. (2002) *AMR* 15:97-113. [5] Bischoff A. et al. (2002) *MESSII*, pp. 679-712. [6] Meshik A. et al. (2014) *GCA* 127:326-347. [7] Leya I. et al. (2001) *M&PS* 36:1547-1561. [8] Desch S. J. et al. (2018) *ApJ* 238:11. [9] Schultz L. and Franke L. (2004) *M&PS* 39:1889-1890. [10] Pedroni A. (1989) Ph.D. dissertation, ETH Zurich.

	PRE 95410	ALH 85119	MAC 88136	Fayette-ville	Tsukuba	Acfer 111	Kapoeta	Genesis data [6]
^{36}Ar$_S$ flux	221±64	<210	<138	86±21	46±17	41±6	53±9	371±5
Past heliocentric distance	1.3±0.2	>1.3	>1.6	2.1±0.3	2.8±0.5	3.0±0.2	2.6±0.2	-
Classification	R3	EL3	EL3	H4	H5-6	H3-6	Howardite	-
Noble gas data	[1]	[2]	[2]	[3]	[4]	[9]	[10]	-

Table 1. The past solar wind ^{36}Ar flux (atoms cm^{-2} s^{-1}) at the heliocentric distances of meteorite parent bodies with the current solar wind ^{36}Ar flux at 1 AU obtained by the Genesis mission [6] and the calculated and recalculated past heliocentric distances (AU) of the meteorite parent bodies.

ISOTOPIC MEASUREMENTS OF <100 ng CARBON AND NITROGEN THROUGH EA/IRMS AND ITS APPLICATION TO EXTRATERRESTRIAL MATERIALS.

N.O. Ogawa[1*], Y. Kebukawa[2], M. Zolensky[3], Y. Takano[1], and N. Ohkouchi[1]. [1]JAMSTEC (2-15 Natsushimacho, Yokosuka, Kanagawa, 237-0045, Japan. *nanaogawa@jamstec.go.jp) [2]Yokohama National University (Yokohama, Kanagawa, 240-8501, Japan), [3]NASA Johnson Space Center (Houston, TX 77058, USA)

Introduction: Carbon and nitrogen abundance and their isotopic compositions in the extraterrestrial materials provide crucial information for its origin and history. Furthermore, they have stimulated our discussion on the origin of life. To precisely measure these chemical properties with a small sample amount, we have improved the commercial system of continuous-flow elemental analyzer/isotope-ratio mass spectrometer (EA/IRMS) system, and applied it to various extraterrestrial samples. In this presentation, we introduce the instrument and some applications of this sensitivity-improved nano-scale EA/IRMS [1].

Nano-scale EA/IRMS: We have modified automated EA/IRMS system (Thermo Flash EA1112-Conflo III-Delta Plus) to improve the sensitivity for the precise determination of quantity and the stable isotopic compositions of carbon and nitrogen from very small amount of samples [1]. The usefulness of the EA/IRMS is by its wide analytical capability over carbon and nitrogen characteristics (Figure 1). The commercial EA/IRMS system usually requires more than 50 μg of carbon or nitrogen to obtain reliable results, which is often limits the sample kind. For example, meteorites generally contain trivial amount of organic matter with less combustible form, which is often beyond oxidation capacity of the commercial EA/IRMS system. However, by improving the EA/IRMS to reduce its required sample amount to <100 ng as carbon or nitrogen, it becomes possible to obtain reliable quantity and isotopes of carbon and nitrogen from very tiny amount of meteorites (generally, <0.1 to 3 mg) with keeping the quality of the data (Figure 2). Furthermore, with the combination of isolation/purification of target compounds by HPLC, and its high-temperature oxidation method (Ox-flash combustion) of EA, the nano-scale EA/IRMS is able to determine the quantity and isotopic compositions of organic matters with wide ranges of polarity and molecular weight (Figure 1). This is a strong contrast to the GC/IRMS (gas chromatograph-combustion/reduction-IRMS) whose application is practically limited to relatively low polarity, low molecular weight (~600 Da) organic compounds. We are planning to apply this technique to analyze organic matter in the samples recovered from asteroid Ryugu through Hayabusa 2 project [4].
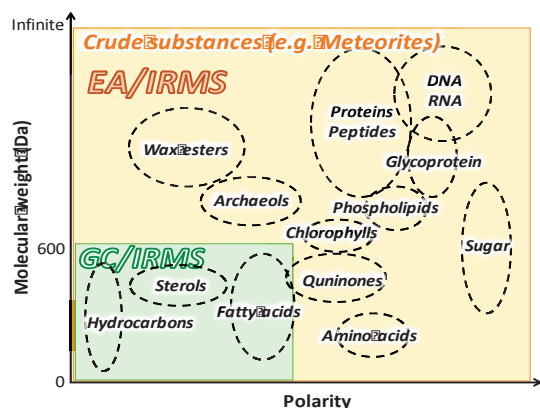

Figure 1 Schematic illustration of organic substances and the type of IRMS analysis. Having an EA as a sample preparation system to IRMS, EA/IRMS has broader analytical capability.
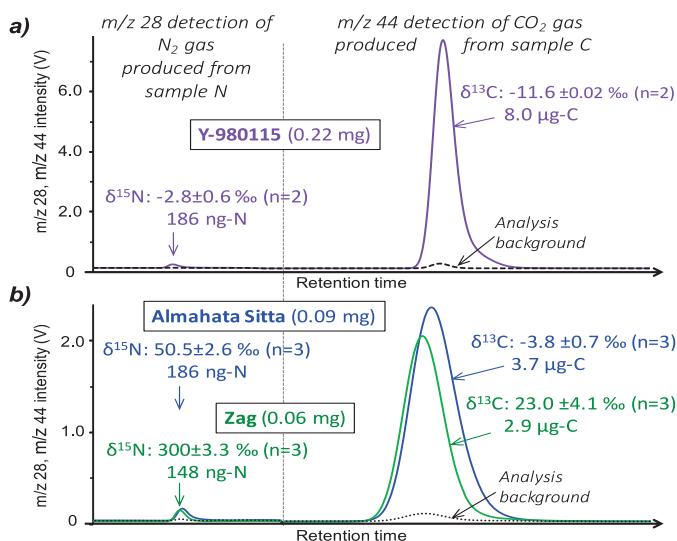

Figure 2 The IRMS chromatograms from nano-scale EA/IRMS analysis of meteorites. a) 0.22 mg of the CI chondrite Y-980115 [2], b) 0.093 mg of chondrite Almahata Sitta 671 and 0.055 mg of carbonaceous clast in the Zag meteorite [3]. Numbers indicate C and N quantities and their isotopic compositions determined by this method.

References:
[1] Ogawa N. O. et al. (2010) in *Earth, Life, and Isotopes* (eds N. Ohkouchi, I. Tayasu, & K. Koba) 339–353 (Kyoto University Press). [2] Chan M. S. et al. (2016) *Earth, Planets and Space* 68:7. [3] Kebukawa Y. et al. (2019) *JpGU2019*, Abstract #PPS07-05. [4] Naraoka et al. (2019) *JpGU2019*, Abstract #PPS03-P14.

ACQUISITION AND DISPLAY OF ULTRA HIGH-RESOLUTION BACKSCATTERED ELECTRON IMAGES OF METEORITE SECTIONS

R. C. Ogliore, Washington University in St. Louis (rogliore@physics.wustl.edu)

Introduction: Backscattered electron (BSE) imaging in a scanning electron microscope (SEM), where image contrast mainly depends on atomic number, is used to understand the mineralogy and petrology of a polished meteorite thin/thick section. Mineralogic heterogeneity in a 1-inch round meteorite section can be on the scale of nanometers to centimeters. A BSE image covering the entire $\sim 2 \times 2$ cm sample, at a resolution of ~ 50 nm per pixel, could be used understand the small- and large-scale mineralogy of the meteorite sample. A catalog of digital BSE images of entire meteorite thin sections could be used by researchers to choose a sample that best suits their project. Additionally, this would save time, money, and beam damage to the sample (especially critical for fragile or volatile-containing samples) as each researcher would not have to reacquire BSE images. Much of the reconnaissance work to find certain interesting mineral phases could be done remotely. However, acquisition and digital on-line display of such a large BSE image is challenging for the following reasons: 1) Variation of the sample height across the thin section is much larger than the SEM depth-of-field (<50 μm) under normal operating conditions. 2) BSE contrast must be kept constant over the entire sample. 3) Stitching $\sim 40,000$ images together using commercial software is very challenging. 4) The size of the final panorama is 10–150 gigapixels, which consumes up to 50 gigabytes of memory (3 bytes/pixel). Here we describe software algorithms to acquire and display large BSE images of meteorite sections, and show an example of a large BSE image from the ungrouped carbonaceous chondrite Acfer 094.

Methods: The meteorite section is mounted on an SEM stub with clips to ensure the sample does not move during the long BSE acquisition. The SEM is tuned for optimal BSE image acquisition at high magnification. First, we acquire a "focus map" before the high-resolution BSE acquisition. The sample is scanned over a coarse grid ($\sim 50 \times 50$ images) using the Image Snapper software on a Tescan Mira3 FEG-SEM with the SEM's auto-working-distance function enabled. The optimal working distance for each image (recorded in a header file) are used to build a focus map that is sampled at each position in the coarse grid. Outliers are removed, then the remaining points are fit to a two-dimensional, second-order polynomial (to account for curvature of the sample from polishing). The x, y and working distance values are then calculated for the full-resolution BSE scan from this polynomial (including a user-defined overlap fraction, $\sim 20\%$). These coordinates are fed into a Matlab function that writes an Image Snapper acquisition file for collection of the high-resolution BSE scan. Images are only acquired over the actual sample (defined as the perimeter of points that the user defined in the focus map), minimizing wasted acquisition time. Next we optimize the BSE brightness and contrast for the sample we are analyzing. With auto-working-distance and auto-brightness-contrast disabled, we acquire BSE images over the entire sample using Image Snapper and the acquisition file written in the previous step (acquisition takes ~ 3 days). After acquisition, images are renamed to their locations in the scan grid.

Individual images are then assembled using a combination of Matlab for feature matching and pyvips for stitching. In Matlab, we find identifying features in the overlap regions of each image using the function detectFASTFeatures. The position of each image in the final stitched panorama is calculated from matching features and computing the geometric transform between overlapping images. Each image is assigned an affine transform matrix which encodes its position in the final panorama. The computation time for this process is ~ 2-3 hrs. The affine transform and image list is then fed into a Python function which uses the vips affine transform function and logical image overlay with a transparency mask to assemble these images into the final BSE panorama. The final panorama (at the same nm/pixel as the original acquisition) is written as a deep zoom format image using dzsave in pyvips.

The assembled BSE panorama in deep zoom format is displayed on a website using the OpenSeadragon open-source, web-based viewer. Various tools are added to the web display of the image, including a scale bar. Each field-of-view has a unique url so the positions of interesting features can be recorded.

Results: An example BSE mosaic image of Acfer 094 is available on our lab's website https://presolar.physics.wustl.edu. The code used in this project is freely available at https://github.com/ogliore/DeepZoomSEM.

Future Work: Future improvements include display of 16-bit images with user-defined maximum, minimum, and gamma parameters, simultaneous acquisition and display of different SEM imaging modalities (e.g. secondary electrons, cathodoluminescence, X-ray) and annotation capabilities.

OXYGEN AND HYDROGEN ISOTOPIC COMPOSITION OF ZAG WATER MEASURED BY CAVITY RING-DOWN SPECTROSCOPY

R. C. Ogliore[1], G. Dominguez[2], L. Tafla[2], [1] Washington University in St. Louis (rogliore@physics.wustl.edu), [2] California State University, San Marcos

Introduction: Fluid inclusions in halite found in Zag (H3–6 regolith breccia) are one of the only samples of extraterrestrial liquid water available for laboratory study. The precise H and O isotopic composition of asteroidal water is important for determining the origin of water on the terrestrial planets. The isotopic compositions of individual fluid inclusions in Zag and Monahans (1998) were measured using SIMS with a cryogenic sample holder by [1]. In recent years, cavity ring-down spectroscopy (CRDS) has matured into a high-precision technique to measure O and H isotopes in small amounts ($\sim$1 μL) of liquid water [2]. Here we report CRDS H and O isotope measurements of water liberated by crushing a whole stone of Zag.

Samples and Methods: We built a device to crush whole stones (up to $\sim$5 cm in size) under vacuum. Solenoid coils, controlled with a timer, drive a steel piston into a steel chamber containing the sample. Liberated water vapor (and other volatiles) from the crushed rock leaves the chamber via a dust-guarded feed-through into stainless steel vacuum line connected to the input of a Picarro-L2120-i CRDS.

We crushed a $\sim$3$\times$2$\times$1 cm whole stone of Zag with a near-complete fusion crust (chosen to minimize the loss of halite due to terrestrial weathering), as follows. After loading and pumping on the sample using the vacuum line until the pressure and apparent leak rate (as determined using a vacuum gauge) was below an acceptable level to minimize background contamination over the expected duration of the crushing experiment, water vapor, and possibly other volatile compounds, liberated from crushing, was cold trapped in a stainless steel U-trap built into the vacuum line. This U-trap allows us to concentrate small water samples to a small volume before being thawed and carried into the CRDS using Ultra-High-Purity nitrogen gas for isotopic analysis. We measured the O an H isotopic composition of released water vapor after five different $\sim$30 min crushing episodes (we heated the outside of the crushing chamber to 50–60° C with a heat gun after the second episode). We bracketed these samples with water standards (GISP) to monitor the response of the CRDS instrument over the duration of the experiment.

Results: The H and O isotopic composition of water released from Zag during five crushing episodes is shown in Figure 1. Each measurements contained 2–3$\times$10^4 ppmv of water vapor under flow conditions as measured by the CRDS. We are currently calibrating the CRDS under similar conditions to determine the amount of water in each measurement.
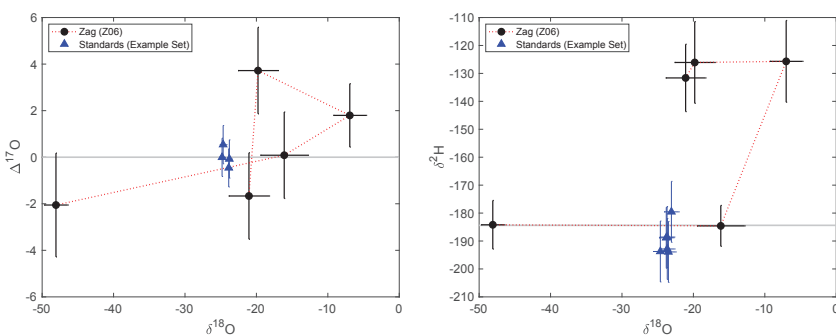

Figure 1: Left) Δ^{17}O vs. δ^{18}O for Zag (black circles) and a representative set of four standard analyses (blue triangles). Red dotted line shows the order of measurements from the five crushing episodes. Right) δ^2H vs. δ^{18}O for the same samples.

Discussion: The first two measurements showed contamination from adsorbed terrestrial water. The fourth measurement showed the largest Δ^{17}O anomaly: 3.7 $\pm$ 1.9‰ (2σ), and is likely the highest fidelity measurement of the isotopic composition of Zag water. The H composition of the fourth sample was measured to be δ^2H$=-126 \pm 15$‰ (δ^2H in samples 3–5 were consistent). However, fractionation of H isotopes during the measurement (δ^2H in samples 1–2) may be significant and will be investigated. Our measured Δ^{17}O is consistent with one Zag inclusion measured by [1] (3.5$\pm$10.0) but lower than three others (20.4, 25.4, 27.0).

Conclusions: Our CRDS measurements of water released from a crushed Zag stone yield higher precision H and O isotope ratios but lack the *in-situ* capability of SIMS measurements made by [1]. CRDS and SIMS can serve as complementary techniques to measure the isotopic composition of asteroidal liquid water in meteorite fluid inclusions.

References: [1] Yurimoto, H. et al. 2014. *Geochemical Journal* 48.6:549 [2] Salvo, C. et al. 2013. *Analytica chimica acta* 804:176.

NANOSTRUCTURES OF ALTERED LOW-CA PYROXENE IN THE ALLENDE CV3 CHONDRITE: AN INVESTIGATION BY ABERRATION CORRECTED SCANNING TRANSMISSION ELECTRON MICRSCOPY.

I. Ohnishi[1], M. Kadoi[1] and K. Tomeoka[2], [1]JEOL Ltd., 3-1-2 Musashino, Akishima, Tokyo 196-8558, JAPAN (ionishi@jeol.co.jp), [2]Faculty of Science, Kobe Univestiy.

Introduction: Low-Ca pyroxene is one of the major constituents of chondrules in chondritic meteorite. In oxidized CV3 chondrites, low-Ca pyroxene has been commonly altered by Fe-rich olivine to various extents [e.g., 1]. Although a number of studies have been conducted on alteration of low-Ca pyroxene in CV3 chondrites, much still remains to be known as to process and condition of the alteration. We here present the results of a mineralogical study of altered low-Ca pyroxene in a chondrule of the Allende CV3 chondrite using an aberration corrected scanning transmission electron microscope (STEM) with a highly sensitive energy dispersive X-ray spectrometer. Our purpose is to provide new insight into alteration of low-Ca pyroxene by observing its texture at atomic-level resolution.

Material and Methods: After ordinary petrographic observations of a polished thin section of Allende, ultrathin sections from the specific areas of the sample were made using a focused ion beam instrument (JEOL JIB-4501). The ultrathin sections were studied using an aberration corrected 300 kV STEM (JEOL JEM-ARM300F) equipped with a cold field emission electron gun and two windowless silicon drift detectors, whose sensor areas are 158 mm^2 and total X-ray collection solid angle is 2.21 sr [2].

Results: The low-Ca pyroxene studied here occurs as a phenocryst of a porphyritic olivine-pyroxene chondrule. The pyroxene phenocryst has been partially replaced by Fe-rich olivine and has many extremely thin (< 1 μm in thick) veins, whose thickness is less than the spatial resolution of conventional scanning electron microscopes. Our STEM observations reveal that the veins are filled with polycrystalline aggregates of small grains (< 50 - 300 nm in size) of Fe-rich olivine with minor amounts of magnetite and Fe-Ni sulfide. The aggregates also contain rectangular to irregular shaped voids (< 50 - 200 nm). Individual olivine grains in the aggregates contain even smaller grains (< 20 nm) of Fe-Ni sulfide and Al, Cr-rich phase, probably spinel and voids (< 20 - 50 nm). High-Ca pyroxene occurs as isolated grains (< 10 - 300 nm) near the veins and also as thin (< 3 nm thick) layers along the boundaries between veins and low-Ca pyroxene. The isolated high-Ca pyroxene grains have a specific relationship of crystal orientation with the low-Ca pyroxene; i.e., all crystallographic axes of both pyroxenes are almost completely parallel. In addition, the high-Ca pyroxene contains many planar defects and narrow double- and triple-chain lamellae oriented parallel to (010). Those multiple-chain lamellae terminate at the boundaries between high-Ca and low-Ca pyroxenes.

Discussion: Our study revealed the presence of high-Ca pyroxene grains inside a low-Ca pyroxene phenocryst in an Allende chondrule. The occurrence of high-Ca pyroxene is limited only in areas close to the veins filled with Fe-rich olivine. The high-Ca pyroxene is crystallographically closely related to the low-Ca pyroxene. These observations suggest that the high-Ca pyroxene formed by topotactic replacement of the low-Ca pyroxene in a process associated with the formation of veins. We also found that the high-Ca pyroxene contains multiple-chain lamellae parallel to (010). Those lamellae are very similar to the hydrous biopyribole found previously from low-Ca pyroxene in an Allende chondrules [3]. If we can assume that the multiple-chain lamellae are biopyriboles, then the presence of them in the chondrule studied here imply that the chondrule has experienced a hydration process. However, in the present study, the multiple-chain lamellae were found only in high-Ca pyroxene, not in low-Ca pyroxene. The results of both previous and present studies suggest that chondrules in Allende have experienced aqueous alteration, but the condition and process of alteration differed considerably among chondrules and the alteration reactions within individual chondrules were much more complicated than previous thought.

References: [1] Krot A.N. et al. (1995) *Meteoritics* **30**:748–775. [2] Ohnishi I. et al. (2018) *e-J. Surf. Sci. Nanotech* **16**:286-288. [3] Brearley A.J. (1997) *Science* **276**:1103-1105.

THERMAL INERTIA OF C-TYPE NEAR-EARTH ASTEROID 162173 RYUGU DETERMINED FROM THE DAWN SIDE OBSERVATIONS BY THERMAL INFRARED IMAGER

T. Okada[1,2] , T. Fukuhara[3], S. Tanaka[1], M. Taguchi[3], T. Arai[4], N. Sakatani[1], Y. Shimaki[1], H. Senshu[5], H. Demura[6], Y. Ogawa[6], K. Suko[6], T. Sekiguchi[7], T. Kouyama[8], J. Helbert[9], T. G. Mueller[10], A. Hagermann[11], J. Biele[9], M. Grott[9], M. Hamm[9], M. Delbo[12], and The Hayabusa2 TIR Team[1], [1]AInstitute of Space and Astronautical Science, Japan Aerospace Exploration Agency, Sagamihara, Japan, okada@planeta.sci.isas.jaxa.jp, [2]University of Tokyo, Tokyo, Japan, [3]Rikkyo University, Tokyo, Japan, [4]Ashikaga University, Tochigi, Japan, [5]Chiba Institute of Technology, Narashino, Japan, [6]University of Aizu, Aizu-Wakamatsu, Japan, [7]Hokkaido University of Education, Asahikawa, Japan, [8]National Institute of Advanced Industrial Science and Technology, Tokyo, [9]German Aerospace Center (DLR), Germany, [10]Max Planck Institute for Extraterrestrial Physics, Garching, Germany, [11]University of Stirling, Stirling, UK, [12] Code d'Azur Observatory, Nice, France.

Introduction: Thermal inertia is a fundamental thermophysical property of materials on planetary bodies, which is derived as the response of temperature change in a day-night cycle. It informs on the surface physical state such as grain size, porosity, or small-scale roughness, even if the planetary surface is not observed directly from the near range nor measured by spatially resolved observations. It is already evidently found that the surface of Ryugu, the target asteroid of Hayabusa2, are not covered with fine regolith, but rocks and boulders with several centimeter or larger size [1], [2]. There is a difficulty in determining thermal inertia of such rough surface, since a diurnal temperature profile using a simple thermal model is not well fit to the observations [3].

Ryugu is a C-type Near-Earth asteroid and its average density is 1199 ± 20 kg m^{-3}, with more than 50 % of porosity assuming the typical CI and CM chondrite meteorites [4]. The materials on Ryugu, even those of the large boulders, might have very porous structure under the low gravity condition [5]. The lower thermal inertia should be expected for the surface Ryugu compared with that of the typical value of CI or CM chondrites, and it needs a hard task to derive the quantitative TI value for such a rough surface.

Thermal Inertia Estimate by TIR: There are several ways to derive the thermal inertia of Ryugu: 1) peak temperature, 2) delay of peak temperature , 3) fitting the diurnal temperature curves, 4) cooling rate after sunset, 5) warming rate after sunrise, 6) lowest temperatures just before sunrise. There needs a proper thermal model for the rough surface, considering the self-heating between the facing facets, shadowing and shading the surface structures, and small-scale roughness within a node. Here we take lowest temperature just before sunrise during the dawn side observations, because it is most simple case where no solar radiation inputs to the surface, and the heat exchange is minimum at the low temperature.

A meaningful data of the dawn side becomes available after conjunction and the Sun-Probe-Earth (SPE) angle is larger than 20° so that the several pixels in the nighttime get imaged. TIR has performed to take thermal images during one rotation (~7.63 hours) at the step of every 6° or 3°. On 13 March 2019, for example, a one-rotation set of TIR images was taken at the solar distance of 1.38 au, at the SPE angle of 18.4°, and from the Box-A (20 km from the asteroid) and showed that the temperature just before sunrise is below 200 K almost all the surfaces. This result indicates the thermal inertia of 250 [J m^{-2} K^{-1} s$^{-0.5}$: hereafter, tiu] or lower considering simple thermal model. This value of thermal inertia is consistent with the thermal inertia of 300 ± 100 tiu derived from the daytime data of TIR [6], and with *in situ* measurements of a single boulder by MARA radiometer on MASCOT [7], and also with the prediction by the ground observations of 150 to 300 tiu [8]. This result is still preliminary but concludes that the surface of Ryugu has much lower thermal inertia compared with that of a typical CI or CM chondrite meteorites.

Asteroid thermal model considering the surface roughness should be updated to explain the flat diurnal profiles which were observed on Ryugu, and other comets 9P/Tempel 1 and 103P/Hartley [9], and to explain the dawn and dusk profiles more completely.

References:
[1] Okada T, et al. (2019) LPSC 50th, Abstract #1457. [2] Schröder S.E. et al. (2019) LPSC 50th, Abstract #2450. [3] Shimaki Y. et al. (2019) LPSC 50th, Abstract #1724. [4] Watanabe S. et al. (2019) Science 264, 268-272. [5] Sugita S. et al. (2019) Science 264, 252, [6] Okada T. et al., (2019) in preparation. [7] Grott M. et al. (2019) LPSC 50th, Abstract #1267. [8] Mueller T.G. et al. (2017) A&A 559, A103. [9] Groussin O. et al. (2013) Icarus 222, 580-594.

IN-SITU K-AR DATING OF ROCK SAMPLES BY A COMBINATION OF LASER-INDUCED BREAKDOWN SPECTROSCOPY (LIBS) AND NOBLE-GAS MASS SPECTROMETRY.

R. Okazaki[1], M. Harada[1,2], and K. Yogata[1,3], [1]Dept. Earth Planet. Sci., Facult. Sci., Kyushu Univ., W1 Building A-506, 744 Motooka, Nishi-ku, Fukuoka 819-0395, Japan (okazaki.ryuji.703@m.kyushu-u.ac.jp), [2]Mitsubishi Material Corp., [3]Inst. Space Astronaut. Sci., Japan Aerosp. Explor. Agency (JAXA).

Introduction: Radiometric dating using a combination of K and Ar is one of the common method for rock samples. In order to date a specific microscopic portion, it is necessary to determine K and Ar simultaneously. Ar-Ar method is the best solution for this, but it is not easy because handling of neutron-irradiated materials is restricted to controlled areas. In this study, we have developed a measurement system combining a laser-extraction noble gas analysis with an elemental analysis using plasma emission spectroscopy (LIBS). We have applied the system to determine K-Ar ages of lithic clasts in a brecciated H-chondrite [1], Willard (b). Chondrules and matrix of the host chondrite have also been analyzed. Here we present the analysis system and report the in-situ K-Ar ages obtained.

Experimental: The system consists of an Nd: YAG pulse laser (wavelength: 1064 nm; pulse width: 7-8 nsec; original beam diameter: 5 mm), a visible light spectrometer (spectral resolution: ~0.5 nm), and a noble gas mass spectrometer. Polished sections (about 100 μm in thickness) were prepared from mineral standards and Willard (b). Laser ablation was carried out by focusing the beam with energy of 0.1 uJ to a diameter of 20 μm on the polished samples. Typical ablated mass is about 1 μg (10 holes with 20 μm diameter and 100 μm thickness). The K concentration with the LIBS was calculated based on the area ratio of emission lines of K (767 nm) and oxygen (777 nm). Mineral standards were orthoclase (K_2O = 15.226 wt%), albite (K_2O = 0.255 wt%), and wollastonite (K_2O = 0.466 wt%). The noble gas extraction efficiency was corrected based on the orthoclase analysis using the K concentration determined by EPMA and the K-Ar age of 461 Ma [2-3]. The sensitivity correction of the noble gas mass spectrometer was performed with a known amount of the earth atmosphere.

Results and Discussion: Reproducibility of the LIBS analysis for the standard minerals was obtained by using the above condition of laser ablation. The detection limit for K was estimated to be about 1000 ppm for 1 μg samples based on the result for the albite standard sample, and is similar to the typical chondritic values. Hence, we should apply our system to K-rich phases at this stage. Our SEM/EPMA observation revealed that most lithic clasts in Willard (b) have CI-like mineralogy and contain K of ~1000-3000 ppm, which is higher than the typical CI chondrite value of 550 ppm [4].

The K concentrations determined by the LIBS analysis for two CI-like clasts, W2CLT2 and W2CLT3, are 2950 and 1880 ppm, respectively. The ^{40}Ar concentrations for the clasts are 8.6 and 4.9 × 10^{-5} cm^{3}STP/g, respectively. Based on these K and Ar concentrations for the clasts, we obtained K-Ar ages of 3.0 and 2.8 Ga. These values are longer than CI chondrites and in the range of CM chondrites [5]. Isotopic ratios of He and Ne for the clasts and matrix portions are indicative of the presence of solar wind gases. Higher concentrations of ^{4}He and ^{20}Ne are consistent with this interpretation. The light noble gas compositions suggest that Willard (b) and also the lithic clasts have not experienced any heating event after lithification of the regolith material of the Willard (b) parent body. The younger K-Ar age for the lithic clasts are due to either the recent heating before arrival to the Willard (b) regolith layer, or due to ^{40}Ar loss caused by recoil [6] and low gas retentivity of phyllosilicate that is the major component of the clasts. In the case of the former, the timing of the lithification of the regolith material should be later than 2.8 Ga.

For chondrules and matrix of Willard (b), concentrations of K are typically lower than 1000 ppm, which is difficult to determine quantity with our LIBS system. Based ^{40}Ar concentrations of two bulk samples (6.36 and 6.57 × 10^{-5} cm^{3}STP/g) determined using pyrolysis extraction method and the typical K content of 782 ppm [4], the K-Ar age of Willard (b) is calculated to be 4.6 Ga. The laser extraction analysis revealed that ^{40}Ar concentrations in the chondrules vary from 0.5 to 7 × 10^{-5} cm^{3}STP/g. Higher concentrations of ^{40}Ar (6-10 × 10^{-5} cm^{3}STP/g) were determined uniformly in matrix, suggesting heterogeneous distribution of K-rich phases in the matrix. However, it is difficult currently to calculate K concentrations in most of the matrix and chondrules based on the LIBS spectrum. In the case of K concentration lower than 1000 ppm, the uncertainty of the multi-function fitting calculation exceeds 100%. In the future, we will improve the limit of quantification by reviewing the measurement conditions of the LIBS system and improving the accuracy of background correction and function fitting of LIBS spectrum.

References: [1] Grossman J. N. (1997) *Meteoritics & Planetary Science* 32:A159-A166. [2] Wartho J. A. et al. (1999) Earth Planet. Sci. Lett. 170:141-153. [3] Nägler T. F. and Villa I. M. (2000) Chemical Geology 169:5-16. [4] Lodders K. and Fegley Jr. B. (1998) The Planetary Scientist's Companion, Oxford Univ, Press. [5] Turrin B. et al. (2014) *LPS XXXXV*, Abstract #2485. [6] Szczerba M. et al. (2015) Geochim Cosmochim Acta 159:162-176.

TRIDYMITE POLYMORPH IN CUMULATE EUCRITES INDICATING THEIR THERMAL HISTORIES

H. Ono[1, 2], A. Takenouchi[3], T. Mikouchi[1, 2] and A. Yamaguchi[3], [1]Department of Earth and Planetary Science, The University of Tokyo, 7-3-1 Hongo, Bunkyo-ku, Tokyo 113-0033, Japan (o-haruka@eps.s.u-tokyo.ac.jp), [2]The University Museum, The University of Tokyo, 7-3-1 Hongo, Bunkyo-ku, Tokyo 113-0033, Japan, [3]National Institute of Polar Research (NIPR), 10-3 Midori-cho, Tachikawa, Tokyo 190-8518, Japan.

Introduction: Eucrites are one of achondrite meteorite groups and probably came from asteroid 4 Vesta's crust [1]. Eucrites are divided into two subgroups: cumulate and non-cumulate. Since pyroxenes in cumulate eucrites exhibit thick exsolution textures due to slow cooling and their cooling rates are estimated by a width of exsolution lamellae to discuss formation of the Vesta's crust [e.g., 2]. However, pyroxene lamellae can clarify thermal histories only at high-temperature (600-1000 °C) [3]. In order to reveal low-temperature (<600 °C) thermal histories, we have focused on silica minerals in cumulate eucrites. Silica minerals are present in eucrites (about 10 vol.%) [4] and have many polymorphs under various P-T conditions including very low-temperature (<400 °C) range [e.g., 5]. Specifically, tridymite is useful to reveal low-temperature thermal histories because tridymite is known to have six polymorphs below 400 °C [5]. Each tridymite polymorph is mainly classified into four distinct crystal structures, hexagonal, monoclinic, orthorhombic and pseudo-orthorhombic [5]. Transformation processes of tridymite are complicated; for example, monoclinic tridymite is transformed from hexagonal tridymite via orthorhombic tridymite below 400 °C [5]. In this study, we try to estimate thermal histories of cumulate eucrites using tridymite polymorphs.

Samples: We stuided polished thin sections of Moore County, Moama and Yamato (Y) 980433 cumulate eucrites. Moore County is particularly studied and is considered to have experienced at least two-stage cooling processes [3]. The first process occurred with 0.00016 °C/yr cooling during accumulation, and subsequently, the second one happened with 0.3 °C/yr cooling due to an impact event [2]. On the other hand, Moama is estimated to have cooled slower than 0.0004 °C/yr [6]. Although Y 980433 has no report of its cooling rate, it is suggested that the cooling rate of Y 980433 is similar to Serra de Mage cumulate eucrite (0.00018 °C/yr [7]) [8]. Although we have reported observations of silica minerals in these three samples, we add new results and further discussions in this study.

Methods: We analyzed EBSD patterns and Raman spectra to identify silica phases using FE-SEM (JEOL JSM-7100F) and micro-Raman spectrometer (JASCO NRS-1000), respectively, both at NIPR. We also performed quantitative chemical analyses and elemental mapping by electron microprobe (JEOL JXA-8530F) at University of Tokyo.

Results: We previously observed silica minerals in three cumulate eucrites [9]. Although all cumulate eucrites contained monoclinic tridymite, only Moama has lamella-shaped orthorhombic tridymite (width: <26 μm). In Moama, monoclinic tridymite was commonly found as a host phase, and orthorhombic tridymite occurred as lamellae parallel to a particular crystallographic direction. Orthorhombic tridymite contains abundant cracks, while monoclinic one is unfractured. According to electron microprobe analysis, chemical compositions of monoclinic and orthorhombic tridymite are indistinguishable from each other even in minor elements.

Discussions: Since monoclinic tridymite is reported to be stable at room temperature, orthorhombic tridymite transforms to monoclinic tridymite during cooling under an equilibrium condition [5]. Therefore, we consider that the presence of orthorhombic tridymite indicates more rapid cooling than samples not containing orthorhombic tridymite. In this study, Moore County and Y 980433 have only monoclinic tridymite, and Moama has both of monoclinic and orthorhombic tridymite, and therefore we inferred that Moama cooled more rapidly than the others at least below 400 °C. Although Moama has much slower pyroxene cooling rate (<0.0004 °C /yr) than that of Moore County (>0.3 °C /yr) [2], we imply that their cooling rates were reversed during cooling by/below 400 °C. Therefore, we consider that Moama was located at a shallower place compared with Moore County and Y 980433 within the Vesta's crust.

Conclusions: We found monoclinic tridymite in three cumulate eucrites and orthorhombic tridymite lamellae only in Moama. The presence of orthorhombic tridymite in Moama indicates that Moama cooled more rapidly than the other two samples at low temperatures (below 400 °C). This result is different from the slower cooling rate of Moama (<0.0004 °C/yr) than that of Moore County (>0.3 °C/yr, after the shock event) at high temperatures (~900-1000 °C) estimated by the width of pyroxene exsolution lamellae [2]. The difference of the cooling rates may reflect geologic setting after impact excavation from the deep crust. Silica polymorphs are useful to infer thermal histories of meteorites as well as pyroxene and plagioclase.

References: [1] Binzel R. P. and Xu S. (1993) *Science* 260: 186-191. [2] Miyamoto M. and Takeda H. (1994) *Earth and Planetary Science Letters* 122:343-349. [3] Lindsley D. H. (1983) *American Mineralogist* 68:477-493. [4] Delaney J. S. et al. (1984) *Journal of Geophysical Research* 89:C251-C288. [5] Graetsch H. and Flörke O. W. (1991) *Zeitschrift für Kristallographie* 195:31-48. [6] Harlow G. E. et al. (1979) *Earth and Planetary Science Letters* 43:173-181. [7] Miyamoto M. and Takeda H. (1994) *Meteoritics* 29:505-506. [8] Takeda H. et al. (2011) 34th Symposium on Antarctic Meteorites. [9] Ono H. et al. (2016) *LPS XLVII,* Abstract # 1903.

GEOCHEMICAL AND PETROLOGICAL CHARACTERIZATION OF FOUR NEW SHERGOTTITES

K.J. Orr[1], L.V. Forman[1] and G.K. Benedix[1]
[1]Space Science and Technology Centre (SSTC), School of Earth and Planetary Sciences, Curtin University, Perth, Australia.
Email: kenneth.orr@postgrad.curtin.edu.au

Introduction: Martian meteorites represent the only suite of geological samples from Mars that we have on Earth. They are extremely rare, comprising < 0.5% of the total number of confirmed meteorites. Thus, new additions to this suite of meteorites represent an important and significant opportunity to expand our understanding of the geology of Mars. Northwest Africa (NWA) 10441, 10818, 11043, 12335 were all found within the last 5 years, and classified as Martian shergottites (MetBull issues 104-107). Shergottites are the most abundant and diverse type of Martian meteorite. Classified into six textural sub-groups, they represent a wide variety of magmatic, geochemical and impact related processes. This makes them a powerful tool for unraveling the geological history of Mars. NWA 10818 and 11043 were provisionally classified as poikilitic, while NWA 10441 and 12335 were classified as diabasic. Here we report new geochemical and petrological data to confirm the shergottites initial classification and then to further characterize their mineralogical and petrological relationships.

Methods: Thin-sections of each meteorite were made from ~0.6 g chips of the samples that we acquired from UNM. These were analyzed using a Tescan Integrated Mineral Analyzer (TIMA) which produces high-resolution mineral maps and calculates modal mineralogy of each sample. NWA 11043 was also analyzed using Energy Dispersive X-Ray Spectroscopy (EDS) with a MIRA3 scanning electron microscope (SEM) to determine preliminary mineral compositions. Further EDS and other e-probe (EPMA and EBSD) analysis will be carried out on all samples.

Results and Discussion: The diabasic shergottites, NWA 10441 and 12335, are primarily composed of pyroxene; ~52% and ~68%, respectively. Pyroxene generally has low-Ca pigeonite cores, with high-Ca augite rims. Both samples contain ~27% and ~36% maskelynite (shocked plagioclase), respectively. They also contain accessory phases of apatite, ilmenite, pyrrhotite, magnetite and a Si-rich mineral. The average grain sizes range from 1-2mm with NWA 12335 exhibiting a slightly coarser texture. The poikilitic shergottites, NWA 10818 and 11043, are primarily composed of pyroxene (~52% and ~37%) and olivine (~41% and ~51%). Maskelynite is also present at ~2% and ~6%, respectively. Accessory phases include apatite, pyrrhotite, Cr-spinel, magnetite and a Si-rich mineral. Both sections display areas of poikilitic and non-poikilitic texture. The pyroxene oikocrysts (low-Ca pigeonite with high-Ca augite rims) enclose olivine chadacrysts. Preliminary analysis of pyroxenes in NWA 11043 have compositions of pigeonite, $En_{38-47} Wo_{5-19} Fs_{43-50}$ and augite, $En_{30-35} Wo_{29-45} Fs_{25-36}$. NWA 10818, 11043 and 12335 have Ca-rich minerals, possibly carbonate, occurring as veins throughout the sample, most likely due to terrestrial weathering [1].

We confirm the initial classification of NWA 10818 and 11043 as poikilitic shergottites and NWA 10441 and 12335 as diabasic shergottites. The diabasic shergottites display very similar textures to other diabasic shergottites, such as Los Angeles and NWA 8657 [2,3]. The primary difference is the lack of olivine (Fig 1). The poikilitic shergottites display similar textures to other poikilitic shergottites, such as RBT 04262 and NWA 4797 [4,5]. Further petrological and geochemical characterization will be presented at the meeting.

References: [1] Crozaz G. and Wadhwa M. (2001) *Geochimica et Cosmochimica Acta* 65: 971-978. [2] Rubin A.E. et al. 2000. *Geology* 28: 1011-1014. [3] Howarth G.H. et al. 2018. *Meteoritics & Planetary Science* 53: 249-267. [4] Usui T. et al. 2010. *Geochimica et Cosmochimica Acta* 74: 7283-7306. [5] Walton E.L. et al. 2012. *Meteoritics & Planetary Science* 47: 1449-1474. [6] Roszjar J. et al. 2012. *LPS XLIII,* Abstract #1780. [7] Hui H. et al. 2011. *Meteoritics & Planetary Science* 46: 1313-1328. [8] Mikouchi T. (2001) *Antarctic Meteorite Research* 14: 1-20. [9] Stöffler D. et al. 1986. *Geochimica et Cosmochimica Acta* 50: 889-903. [10] Mikouchi T. et al. 1996. *LPS XXVII,* Abstract #879. [11] Walton E.L. et al. 2009. *LPS XL* Abstract #1464. [12] Treiman A.H. et al. 1994. *Meteoritics* 29: 581-592. [13] Lin Y. et al. 2005. *Meteoritics & Planetary Science* 40 (Suppl.):5154.
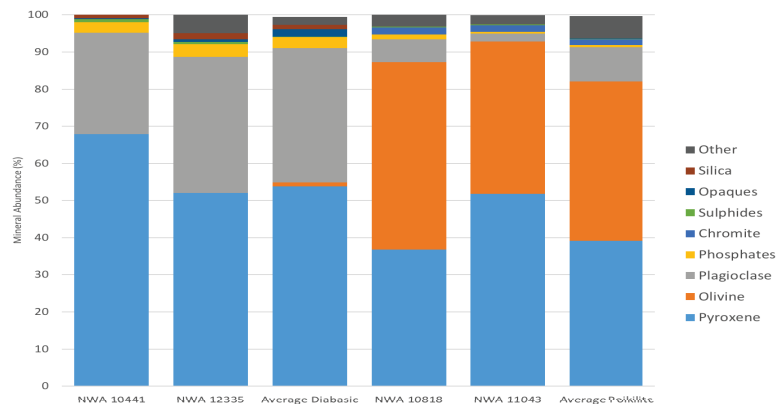
Figure 1. Mineral modal abundances of the four new shergottites compared to diabasic and poikilitic shergottite averages [3,4,5,6,7,8,9,10,11,12,13].

COMPARISON OF MOLECULAR COMPLEXITY BETWEEN CHONDRITES, MARTIAN METEORITE AND LUNAR SOILS.

F.-R. Orthous-Daunay[1], C. Wolters[1], L. Flandinet[1], V. Vuitton[1], P. Beck[1], L. Bonal[1], J. Isa[1], F. Moynier[2], D. Voisin[3], S. Moran[4], S. Horst[4], G. Danger[5], V. Vinogradoff[5], L. Piani[6], D. V. Bekaert[6], L. Tissandier[6], Y. Isono[7], S. Tachibana[8], H. Naraoka[9], L. Remusat[10] and R. Thissen[11]

[1]IPAG CS 40700 38058 Grenoble Cedex 9, France, frod@univ-grenoble-alpes.fr [2]IPGP, 1 Rue Jussieu, 75005 Paris [3]IGE,CS 40700 38 058 Grenoble Cedex 9 [4]JHU, 3400 N. Charles St.Baltimore, MD 21218 [5]PIIM, Avenue Escadrille Normandie-Niémen 13397 Marseille cedex 20 [6]CRPG, Université de Lorraine, 15 rue Notre Dame des Pauvres, BP 20, 54501 Vandoeuvre-lès-Nancy [7]Hokkaido University, N10 W8, Sapporo 060-0810, Japan [8]University of Tokyo 7-3-1 Hongo, Tokyo 113-0033, Japan [9]Kyushu University, 744 Motooka, Nishi-ku, Fukuoka 819-0395 Japan 10 MNHN, 57 Rue Cuvier 75231 Paris Cedex 05, France [11]LCP, 310 Rue Michel Magat, 91400 Orsay

Introduction: Meteorites and comets bear organic molecules ranging in size from one single to an arbitrarily large number of carbon atoms. This contrasts with the limited size of free molecules detected in space environments[1]. Understanding the organic matter cycle in the solar system requires to identify the time and place where the molecules were formed and destroyed.

The High Resolution Mass Spectrometry technique has been used for almost a decade to characterize extraterrestrial material[2]. The technique only accesses the soluble part of the samples and is used both with and without liquid chromatography for molecular identification[3]. Several scenarios have been proposed for the of soluble organic matter in extraterrestrial samples, with for instance aqueous alteration being invoked to explain the growth of N-bearing molecules[4] detected in Murchison.

During the last years, the IPAG group has developed a tool dedicated to the interpretation of the polymerization degree of any kind of organic sample. We highlighted a peculiar pattern in meteorite extracts that can be only reproduced by highly reducing gas phase polymerization experiments[5]. This is interpreted as a piece of evidence for protoplanetary disk origin. The work presented here is a comparison between the typical protosolar pattern and the features found or not in Martian meteorites and lunar soils.

Method: We extracted the organic mixtures from 4 lunar soils and from the NWA7533 "black beauty" Martian meteorite[6] by maceration in Toluene and Methanol for 1 week at room temperature. We did the same for several carbonaceous chondrites including Orgueil, Murchison, 4 CR type samples. Laboratory experiment residues produced from ionized gas[7, 8], photon irradiated ices [9, 10] or reactive liquids[11, 12] were also analyzed to provide comparison to well constrained synthesis environments. Mass spectra were acquired with a Thermo LTQ Orbitrap XL at its highest resolving power, coupled with Electrospay ionization (ESI) source. Anions and cations in the following mass range 150 to 800 u were analized on a 4 decades dynamic range.

Results: The Orbitrap mass spectrometry provides the mass distribution of mixtures with resolution and precision high enough to undoubtfully identify polymeric patterns. In every sample, CH_2 patterns are detected. A CH_2 family has only molecules with R-$(CH_2)_n$ formula. From each CH_2 family, the free parameters of the Wesslau model [13] for polymerization can be adjusted to match the distribution. Each sample has from 3 to 15 CH_2 families with up to 30 members. In the synthetic samples, the parameters depend mainly on the precursor mixtures. The meteorites exhibit larger variations of the polymerization parameters than synthetic samples. We discuss the relevance of the various candidates for the emergence of molecular diversity in asteroids. Polymeric patterns in the NWA7533 involve C, H and O. Only CH_2, C_2H_2 and C_2H_4O patterns seem to be responsible of the molecular complexity. Heteroatomic (O-bearing) pattern is the major difference between chondritic and Martian organics. Another major difference is the absence of nitrogen in any observed cation whereas it was a key feature in Murchison. The patterns in lunar soils are highly variable. Some soils exhibit very little polymerization patterns, if any. One has a pattern comparable to the asteroidal one and one has a peculiar mass distribution that doesn't match any other extraterrestrial sample. The latter is the most exposed to solar wind and the mass range of its mixture is the most extended. We discuss such features in terms of origin and possible evolution of the organic matter delivered to the moon.

References: [1]Caselli P. and Ceccarelli C. (2012) *Astron. Astrophys. Rev.*, *20*, 1 p. 56.[2]Schmitt-Kopplin P. et al. (2010) *Proc. Natl. Acad. Sci.*, *107*, 7 pp. 2763–2768.[3]Yamashita Y. and Naraoka H. (2014) *Geochem. J.*, *48*, 6 pp. 519–525.[4]Naraoka H. et al. (2017) *ACS Earth Sp. Chem.*, *1*, 9 pp. 540–550.[5]Bekaert D. V. et al. (2018) *Astrophys. J.*, *859*, 2 p. 142.[6]Humayun M. et al. (2013) *Nature*, *503*, 7477 pp. 513–516.[7]Hörst S. M. and Tolbert M. A. (2013) *Astrophys. J. Lett.*, *770*, 1 p. L10.[8]Kuga M. et al. (2015) *Proc. Natl. Acad. Sci.*, *112*, 23 pp. 7129–7134.[9]Danger G. et al. (2016) *Geochim. Cosmochim. Acta*, *189* pp. 184–196.[10]Piani L. et al. (2017) *Astrophys. J.*, *837*, 1 p. 35.[11]Renard P. et al. (2013) *Atmos. Chem. Phys.*, *13*, 13 pp. 6473–6491.[12]Vinogradoff V. et al. (2017) *Icarus*, *305* pp. 358–370.[13]Weßlau V. H. (1956) *Die Makromol. Chemie*, *20*, 1 pp. 111–142.

STUDY OF THE FUSION CRUST IN CHELYABINSK LL5 FRAGMENTS USING X-RAY DIFFRACTION AND MÖSSBAUER SPECTROSCOPY.

M. I. Oshtrakh[1], A. A. Maksimova[1], A. V. Chukin[1] and E. V. Petrova[1], [1] Institute of Physics and Technology, Ural Federal University, Ekaterinburg, 620002, Russian Federation (oshtrakh@gmail.com).

Introduction: The fusion crust formation after meteorite entrance into the Earth atmosphere shows how the internal matter combustion can occur. It is possible that different time of meteorite fragments fall can be a reason of some variations in the fusion crust. Therefore, we studied two fragments of Chelyabinsk LL5 meteorite which have the fusion crust by means of X-ray diffraction (XRD) and Mössbauer spectroscopy in comparison with those studies of their internal matter.

Materials and Methods: The powdered samples of the fusion crust and internal matter from two fragments of Chelyabinsk LL5 meteorite with different lithologies (fragment No 1a with light lithology and fragment No 2a with mixed light and dark lithologies) were prepared for XRD and Mössbauer studies. The XRD patterns were measured with the XRD–7000 powder diffractometer (Shimadzu). The ^{57}Fe Mössbauer spectra were measured at 295 K using SM-2201 spectrometer with a high velocity resolution.

Results and Discussion: The results of the fusion crust XRD patterns analysis showed the presence of the main phases such as olivine, orthopyroxene, troilite and magnesioferrite ($MgFe_2O_4$) as the ferric compound. However, the content of these phases in fragments No 1a and No 2a was slightly different: ~56 wt.% (olivine), ~22 wt.% (orthopyroxene), ~8 wt.% (troilite) and ~8 wt.% (magnesioferrite) in fragment No 1a and ~62 wt.% (olivine), ~20 wt.% (orthopyroxene), ~7.5 wt.% (troilite) and ~3 wt.% (magnesioferrite) in fragment No 2a. Earlier, the presence of magnesioferrite in the fusion crust was found in one meteorite only [1]. Mössbauer spectra of the fusion crust demonstrate also the presence of magnesioferrite (this spinel has a formula $(Mg_{1-x}Fe_x)_A[Mg_yFe_{2-y}]_BO_4$ with 8 metal cations occupied tetrahedral A sites and 16 metal cations occupied octahedral B sites). Other spectral components were related to the M1 and M2 sites in olivine and orthopyroxene, troilite, chromite, residual Fe-Ni-Co alloy and unknown ferrous compound. The relative areas of these spectral components, which can roughly correspond to the relative iron content in these phases, were: (i) ~42 % (olivine), ~9 % (orthopyroxene), ~5 % (troilite), ~4 % (Fe-Ni-Co alloy), ~4 % (chromite), ~3 % (ferrous compound) and ~33 % (magnesioferrite) in fragment No 1a; (ii) ~53 % (olivine), ~9 % (orthopyroxene), ~6 % (troilite), ~3 % (Fe-Ni-Co alloy), ~1 % (chromite), ~6 % (ferrous compound) and ~22 % (magnesioferrite) in fragment No 2a. These results showed a smaller content of magnesioferrite in the fusion crust from fragment No 2a in comparison with fragment No 1a. Further, these results were compared with those of Mössbauer spectroscopy of the internal matter from these fragments. It was found that formation of the fusion crust led to different decrease in the initial content of the same phases in fragments No 1a and No 2a: ~74 % and ~45 % for troilite, ~25 % and ~14 % for olivine and ~39 % and ~52 % for orthopyroxene, respectively (Fig. 1). These differences and different content of magnesioferrite in fragments No 1a and No 2a can be explained as a result of different time of fragments fall in the atmosphere and combustion. We can suppose that fragment No 1a with light lithology was close to the suface of Chelyabinsk meteoroid while fragment No 2a with mixed light and dark lithologies was deeper inside meteoroid and released later than fragment No 1a. Therefore, the latter fragment fell relatively longer time with formation of a larger amount of magnesioferrite than fragment No 2a (see details in [2]).
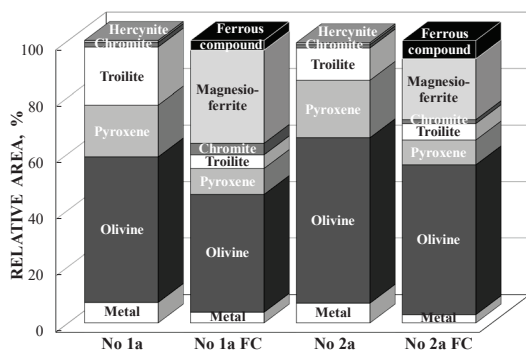

Fig. 1. Comparison of the differences in the total relative areas for the Mössbauer spectral components corresponding to the iron-bearing phases (roughly equivalent to the relative iron content in these phases) in the internal matter and in the fusion crust (FC) in Chelyabinsk LL5 meteorite fragments No 1a with light lithology and No 2a with mixed light and dark lithologies.

References:

[1] Rubin A. E. (1997) *Meteoritics & Planetary Science* 32:231–247. [2] Oshtrakh M. I. et al. (2019) *Spectrochimica Acta, Part A: Molecular and Biomolecular Spectroscopy*, in press (DOI: 10.1016/j.saa.2019.03.036).

THERMAL EMISSIVITIES' RELATIONSHIP TO METEOR ABLATION.

D. R. Ostrowski[1,2] and J. B. Haskins[1,3], [1]NASA Ames Research Center, Moffett Field, CA, USA.,
E-mail: daniel.r.ostrowski@nasa.gov. [2]Bay Area Environmental Research Institute, Moffett Field, CA, USA,
[3]Analytical Mechanics Associates, Moffett Field, CA, USA

Introduction: Most meteors bombarding Earth are small and burning up in the atmosphere. A few are large enough to survive entry and cause notable damage. The combination of ablation and fracturing means most meteorites lose greater than 80% of their mass during entry [1]. Ablation rate models require a meteorites emissivity as an input [2,3,4], which has a direct input in the time it takes for a surface material to reach melt conditions. If a material has a lower emissivity at high temperatures it will increase the surface temperature and thus increase the ablation rate [5]. The nonmetals in the meteorites are poor thermal conductors with high emissivity, as temperature increases the thermal conductivity tends to increase and emissivity decrease [5].

Experimental: Thermal emissivity is measured over a broad wavelength range of 8 to 14 μm from 20°C to 1000°C. Emissivity is measured by dual laser infrared thermometers. Emissivity values for up to atmospheric entry temperatures are needed for modeling material response of meteor entry. Surface temperature simulations are performed with the Icarus material response solver, which is a fully implicit, parallel finite volume code, and a 1D grid that represents the stagnation point on the surface of a large meteoroid. Surface is treated with an aerothermal boundary condition using the typical assumption of radiative equilibrium.

Results: Elevated temperatures cause a fluctuation in the emissivity of the different meteorite classes [6]. As temperature increases to 100°C the emissivity decreases then rebounds and stabilizes for the next 100° C. Lowest emissivity for all stony meteorites is between 300-350°C, values below 0.90. Average heated chondrites range in emissivity between 0.85-0.95 between 100°C to 1000°C temperature range. Iron meteorites have a drastically different emissivity profile as a function of temperature with a rapid 0.5 drop in the emissivity in the first 100°C and not rebounding till after 300°C. This different profile is caused by the phase transitions in kamacite as heated.

Material response simulations of surface heating during entry may be performed. To evaluate the influence of the temperature-dependent, solid optical properties on entry, the preheating stage of the meteor is evaluated. In the iron meteorite (Fig. 1A) simulation using heritage values result in the surface temperature reaching the melting point within 0.2 s of entry, while the present work values leads to the time to surface melted being cut in half. The reduction in the time to melt is a result of the 0.5 increase in emissivity of the Sikhote-Alin sample above 300°C. The simulation for Tamdakht (H5) (Fig. 1B) reaches melted surface within 0.02s from heritage dataset and 0.018s for present work. Both heritage and present work for Jbilet Winselwan (CM) (Fig. 1C) time to surface melted in 0.02s.

Conclusion: The emissivity profile of stony meteorites as temperature increases is similar up to 600°C, after that CM chondrites emissivity decreases while other stony meteorites remain flat. Iron meteorites have a different emissivity profile caused by the phase changes in kamacite. Simulation results show time to meteor surface melt conditions has minimal dependence on ordinary and carbonaceous chondrite. Changing thermal emissivity has a major affect on time to surface being melted for iron meteors by cutting time in half to 0.1 second. Time to melt is slower for iron meteorites compared to chondrites because of iron meteorites higher thermal conductivity, which leads to rapid transport of heat from surface into interior.

References: [1] Sears D.W. et al. (2016) *Planetary and Space Science*, 124:105-117. [2] Flynn G.J. (1989) *Icarus*, 77:287–310. [3] Lyne et al. (1996) *JGR*, 101:23,207-23,212. [4] Campbell-Brown M.D. et al. (2013) *Astronomy and Astrophysics*, 557:A41:1-13. [5] Loehle S. et al. (2017) *Meteoritics & Planetary Science*, 52:197-205. [6] Ostrowski D.R. and Haskins J.B. (2019) *LPSC* L, Abstract #2761.
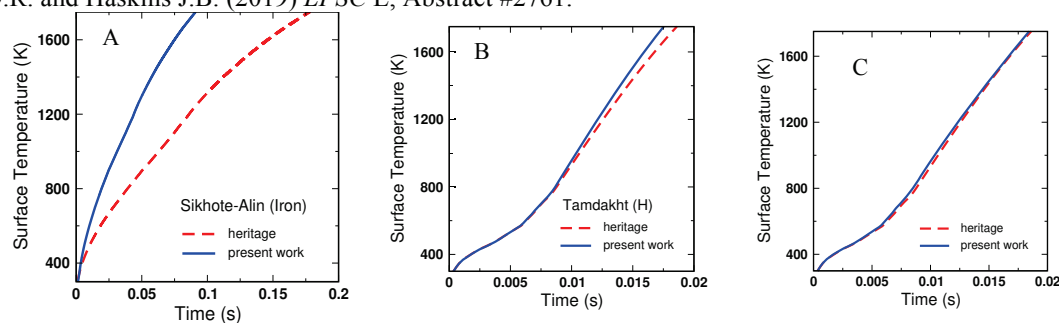

Figure 1: Material response modeling of the surface temperature of (A) Sikhote-Alin (IIAB), (B) Tamdakht (H5), and (C) Jbilet Winselwan (CM). Heritage results based on class average optical properties evaluated at 20° C tem-peratures. Present work takes into account fluctuating emissivity as temperature increases.

MELT INCLUSION ANALYSES TO CONSTRAIN PARENTAL MAGMA COMPOSITIONS OF THE NAKHLITE METEORITES.

A. M. Ostwald[1], A. Udry[1], and J. Gross[2], [1]University of Nevada, Las Vegas, 4505 Maryland Pkwy, Las Vegas, NV 89154; ostwald@unlv.nevada.edu, [2]Rutgers University, 610 Taylor Road, Piscataway, NJ 08854; jgross@eps.rutgers.edu.

Introduction: Nakhlite meteorites originate from a single location on Mars, and the 22 unpaired samples represent the largest suite of igneous rocks from another planet [1]. Despite geochemical evidence for heterogeneity in parental magma compositions [1,2], only three nakhlites (Nakhla, Governador Valadares, and Miller Range [MIL] 03346) have established parental melt compositions [e.g., 3,4,5]. We are conducting a study on the melt inclusions (pockets of trapped parental melt) present in a comprehensive suite of nakhlites to possibly constrain their parental melt compositions as well as distinguish metasomatic alteration or crustal contamination. Identifying the parental melt composition(s) of the nakhlite meteorites will help to constrain geochemical heterogeneities present in the martian mantle and crust. We present here initial findings on the parental melt compositions present in both the olivine- and pyroxene-hosted inclusions of four nakhlites: Governador Valadares, MIL 090030, MIL 090032, and a new find; Northwest Africa (NWA) 10645.

Methods: We measured major and minor elemental compositions of the different minerals and glasses present in the melt inclusions of each sample through electron microprobe analysis using methods found in [6]. Melt inclusions continue to exchange divalent cations (Mg, Fe) with their host crystals in the subsolidus, typically resulting in a net Fe-loss [7]. We corrected olivine-hosted melt compositions for the effects of rehomogenization with *Petrolog3*, which requires an estimated initial FeO_T and the known Fo# of the host mineral. We selected FeO_T values from two proposed parental melt compositions, both using *in situ* microanalytical techniques without experimental rehomogenization. Reference [3] found a FeO_T of 28.9 wt.% in the olivine-hosted inclusions of Nakhla, whereas [5] calculates an FeO_T of 22.2 wt.% in the augite-hosted inclusions of MIL 03346. Corrections for cation exchange between pyroxene and melt were made in Rhyolite_MELTS [8]. The modal contribution of pyroxene in the trapped liquid compositions was adjusted until pyroxene was in equilibrium, and the resultant liquid composition was then inferred to be the parental trapped liquid composition.

Results: Texturally, olivine-hosted inclusions are complex and frequently contain pyroxene microlites in high-Si glassy phases in addition to olivine and oxides. Pyroxene inclusions are simple glass surrounded by wall augite, and they occasionally contain large Ti oxides. Calculated parental trapped liquids in olivine-hosted melt inclusions contain 0.5-1.0 wt.% K_2O and 1.4-2.0 wt.% Na_2O, while pyroxene-hosted inclusion compositions contain 0.7-3.0 wt.% K_2O and 0.6-2.4 wt.% Na_2O. Olivine-hosted inclusions have P2O5 concentrations ranging from 0.5-1.1 wt.%, contrasted with 0.1-0.4 wt.% in pyroxene-hosted inclusions. Pyroxene-hosted inclusions are also more siliceous, containing an average of 53.1 wt.% SiO_2 compared to an average of 48.8 wt.% SiO_2 in olivine-hosted inclusions. Olivine-hosted MgO values range from 1.3-3.6 wt.%, while pyroxene-hosted MgO is 5.8 wt.%. Aluminum oxide in olivine-hosted inclusions averages at 8.4 wt.% against 5.4 wt.% in pyroxene-hosted ones. Melt inclusions hosted in olivine show a distinct evolutionary trend when alkali elements (Na_2O and K_2O) are compared to silica, and are primarily basaltic in composition; melt inclusions hosted in pyroxene, however, show no evolutionary trends and are andesitic basalt.

Discussion: There is significant major and minor element variation in the trapped liquids hosted by olivine and pyroxene (the two primary cumulus phases present in nakhlites), as well as textural dissimilarities between the two types of inclusions. Cumulus pyroxene is possibly a late-stage phase enclosing a more evolved melt composition than the melt entrapped in earlier-crystallizing olivine, resulting in a relative K enrichment. Olivine-hosted inclusions in the four nakhlites reveal distinct compositional evolution that may originate from a single source composition. Significant chemical differences between olivine- and pyroxene-hosted inclusions may result from fractional crystallization (the removal of primitive solid phases), or from the presence of xenocrystic olivine from a distinct parental magma. In light of these findings, a larger study encompassing more samples is warranted.

References: [1] Udry, A., and Day, J.M.D. (2018) *GCA, 238,* 292-315. [2] Righter, M., et al. (2016) *LPSC XLVII*, Abstract #2780. [3] Goodrich, C.A. et al. (2013) *Meteoritics & Planet. Sci., 48,* 2371-2405. [4] Harvey, R.P., and McSween, H.Y. (1992) *Earth & Planet. Sci., 111,* 467-482. [5] Imae, N., and Ikeda, Y. (2007) *Meteoritics & Planet. Sci., 47,* 171-184. [6] Sonzogni, Y. and Treiman, A. (2015) *Meteoritics & Planet. Sci.*, 50, 1880-1895. [7] Danyushevsky, L.V. and Plechov, P. (2011) *Geochem Geophys Geosys, 12, No. 7.* [8] Gualda, G.A.R., et al. (2012) *Journal of Petrology*, 53, 875-890.

CHEMICAL CONTENT OF THE DIDIM AND KEMER METEORITES.

B. Ozdemir[1], M. E. Ozel[2], M. Yesiltas[3], M. G. Yalcin[1] [1]Department of Geology Engineering, Akdeniz University, Antalya, Turkey 07070 (s.busraozdemirr@gmail.com) , [2]Fatih Sultan Mehmet University, Istanbul, Turkey 34445, [3]Faculty of Aeronautics and Space Sciences, Kirklareli University, Kirklareli, Turkey 39100.

Introduction: Until today, a total of 16 meteorites fell in Turkey, two of which are Didim and Kemer meteorites. Didim fell in 2007 in Aydin, and Kemer fell in 2009 in Kemer. Both events are observed falls. Didim is an H3-5 ordinary chondrite, it contains H5 clasts in a H3 host [1]. Opaque phases are also present in Didim, and were investigated previously [2]. There are multiple lithologies in the Didim meteorite, such as white, gray, and dark lithologies. Initial characterization indicates an homogeneous composition for olivine and pyroxene in the white lithology (Fa_{19-20}, Fs_{17-19}), however a variable composition in the darker lithology [1]. Kemer is an L4 ordinary chondrite with an homogeneous composition for olivine and pyroxene [3]. Thus far, there is no detailed information on the molecular composition of these meteorites. We studied multiple stones of the Didim and Kemer meteorites in order to obtain detailed chemical and molecular compositional information from various phases and lithologies. This information may help us constrain their parent body processes.

Samples: Multiple stones of Didim and Kemer meteorites were acquired from the main mass holders. Thin slabs of both meteorites were cut and separated using a saw and then they were prepared as polished thin sections for our microspectroscopic investigation. We also studied bulk and unpolished fragments of both meteorites using the same techniques to assess the sample preparation effects on the collected data.

Methods: Micro-Raman spectroscopy experiments were conducted at Science and Technology Application and Research Center of Canakkale Onsekiz Mart University. The setup consists of a commercial WiTec alpha300 R (WiTec GmbH) confocal Raman imaging system, equipped with a 532-nm Nd:YAG laser, spectrometer with a CCD camera and 50X objective (NA = 0.8). The laser power was between 0.2 and 2.4 mW. We collected two-dimensional chemical distribution maps and individual spectra from various phases present in the samples. Additionally, we collected X-ray fluorescence (XRF) spectra of Didim and Kemer at Department of Geology Engineering of Akdeniz University. Using a commercial Rigaku NEX CG (Rigaku GmbH) XRF system, we were able to obtain elemental composition of the studied samples.

Results: Raman spectra from multiple regions/lithologies have been collected from the surface of Didim as part of our initial study. These spectra indicate presence of magnetite (evident from Raman peaks at 160, 318, 517, and 660 cm^{-1}), olivine (evident from a doublet with peaks at 826 and 852 cm^{-1}), pyroxene (with major peaks at 677 and 1015 cm^{-1}), iron oxides such as hematite (prominent peaks at 224, 288, 405, 494, 613, and 660 cm^{-1}), sulfides such as violarite (with a strong peaks at 320 and a weak peak 376 cm^{-1}) and arzakite (with peaks at 215, 275, 384, and 576 cm^{-1}). Raman spectra of Kemer show that it contains olivine, pyroxene, magnetite, and sulfides as well. Our initial XRF analyses that consist of multi-element $K\alpha$ values indicate that Didim and Kemer appear to be consistent with the ordinary chondrite classification. More experiments are certainly needed to understand chemical constituents of Didim and Kemer.

References: [1] Weisberg, M. K. et al. (2008) The Meteoritical Bulletin, No. 94. *Meteoritics & Planetary Science,* 43, 1551-1584. [2] Komorowski et al. (2009) *Meteoritics & Planetary Science* 44,A112,5. [3] Garvie, L. A. J. (2002) The Meteoritical Bulletin, No. 99. *Meteoritics & Planetary Science,* 47, E1-E52.

Merrilite Rim around the Phyllosilicate clast in Mukundpura Carbonecous Chondrite (CM2) Meteorite

D. K. Panda, D. Ray and A.D. Shukla. Physical Research Laboratory, Ahmedabad 380 009, India
(pdipak@prl.res.in).

Introduction: The CM2 type of meteorites have been investigated for understanding the asteroidal aqueous alteration processes. The alteration processes induce formation of secondary and hydrous minerals like phyllosilicates, calcites, poorly charachterized phases and phosphates [1,2]. The occurrences of phosphate minerals has been generally postulated due to fluid assisted metasomatism on the parent body[3]. Earlier studies introduced that the Mukundpura carbonaceous chondritehas been classified as CM2 chondrite and its alteration records are primarily discussed based on nature and abundance of phyllosilicates and carbonates in matrix [4,5] . In this study, we discuss the mineralogy, formation process of phosphate mineral phases, uniquely occurred within a phyllosilicate clast, with an aim to understand aqueous alteration history in Mukundpura CM2, the recent meteorite fall in India.

Analytical Techniques: Mineral compositions and X-ray mapping were carried out using three epoxy mounted thick sections . For imaging and semiquantitave (EDS) and quantitative (WDS) analyses, a JEOL IT300 scanning electron microscope with an OXFORD EDS operated at 20 keV 500pA and a Cameca SX 100 electron microprobe with operation biasing voltage of 15 kV, 15nA with 2 μm beam diameter have been used .

Results: In the studied thick sections, all the chondrule and the matrix of the meteorite are highly altered except a few isolated chondrule appears to be survived as a relict clast and fayalitic in composition. The matrix includes mainly clast of phyllosilicates or poorly crystallised phases(PCP) along with presence of minor calcite, dolomite (rare) . Interstingly, one of the studied sections hosts an altered chondrule ~100 μm size and is surrounded by Ca-P rich fine-grained rim. The rim width also varies from 4 to 10 μm in size. Under X-ray mapping, it appears that the Ca-P layer is not homogeneous in nature. The EPMA elemental analysis shows CaO 50-42 % & P_2O_5 30-25.6%. Na_2O 1.8 to 3.2 %, MgO 1.5-4.4%, FeO 4-7 % and MnO 0.19 to 0.37%, SO_2 ~1 %, Cr_2O_3 600 -1000 ppm. The phyllosilicates and calcite are common near the fracture zone of the rim. The elemental analysis within the fracture zone shows CaO 28-38 % & P_2O_5 16-24%, Na_2O 1.5 to 2.2 %, MgO 6-10%, SiO_2 9-16% . FeO 7-14 %, MnO 0.2 to 0.3% and SO_2 ~1-3 %. The matrix is predominantly Fe (2-14% FeO), Mn rich merrilite (0.3 -2.6% MnO). The chondrule at the interior is altered and compositionally akin to Cr- rich phyllosilicates. The EPMA analysis also shows that phyllosilicates in the matrix are phosphorus rich (upto 7.5 % of P_2O_5), while the PCP are relatively depleted in P_2O_5 (0.1-0.2 %). The calcite is also occasionally foundenriched with phosphorus (P_2O_5 0.4-1.1 %).

Discussion: Based on SEM study, it appears that Mukundpura is depleted in CAI (Calcium-Aluminium-Inclusion) , clast-rich CM2 with a highly altered matrix rich chondrite. The occurrences of phosphorus phases in terms of phosphate at reaction rim clearly suggests the migration of P and Ca from some Fe-Ni and CAI bearing phases. The X-ray maping and EPMA analysis show the presence of Na, Mg, Fe in phosphate, whereas Cl and F are apparently absent. Based on the chemical analysis, the rim formation the phosphate mineral resembles merrilite in composition. The phosphate mineral are secondary product which can be formed due to interaction of fluid which led to migration of elements and formation, thereafter. Apart from this the phosphate mineral also can be formed by fluid assisted metamorphism. In our studied sections of the Mukundpura the concentric inward growth texture of hydrous clast can be also considered as an additional evidence for migration of fluids or testifies substantial aqueous activities. The width of the rim is very small size (4-10 μm) and attributed to be formed by metamorphic process[6]. Based on chemical anlysis and textural characters, it can be postulated that during the alteration process Ca, P, Na migrated to form the fine-grained Ca-P rich rim [7] . The Ca-P mineral phases are associated with $CaCO_3$ grains outside the Ca-P rim. It is to be noted that the concentration of P and S increased in the phyllosilicates which may be due to the fluid interaction processes of Fe-Ni-S-P with the matrix

Conclusion: Our study suggests that Mukundpura experienced complex aqueous alteration processes. The presence of phosphate (Merrilite) mineral is formed due to the low temperature alteration processes .

References: [1] Rubin et al. (2007) GCA 71, 2361 [2] Rubin and Grossman (1985) Meteorites, 20, 479 [3] Ebihara and Honda (1987) Meteorites, 22, 179 [4] Ray D. and Shukla A.D. (2018). *Planet. Space Sci* [5] Panda et al. (2018) 2007, [6] Hauss et al. (1981), GCA, 45, 33. [7] Brearley and Chizmadia (2005), 46th LPSC 2171

CONSTRAINTS ON THE COOLING RATE FROM ^{16}O-RICH PEROVSKITE IN A COMPACT TYPE A CAI FROM ALLENDE.

C. Park[1], N. Sakamoto[2], S. Wakaki[3], S. Kobayashi[3], N. Kawasaki[4], and H. Yurimoto[2,4,5]
[1]Division of Earth-System Sciences, Korea Polar Research Institute, Republic of Korea (changkun@kopri.re.kr), [2]Isotope Imaging Laboratory, Hokkaido University, [3]Kochi Institute for Core Sample Research, JAMSTEC, [4]Natural History Sciences, Hokkaido University, [4]Institute of Space and Astronautical Science, JAXA, Japan.

Introduction: Coarse-grained type A Ca-Al-rich inclusions (CAIs) in CV3 chondrites consist of mostly melilite and minor amount of spinel, perovskite, Al-Ti-diopside, and hibonite. Oxygen isotopes of the CAI minerals except perovskite have been extensively studied; those of spinel and hibonite are uniformly ^{16}O-enriched ($\sim$−24‰ in $\Delta^{17}O$), whereas those of melilite and Al-Ti-diopside are relatively ^{16}O-depleted [1]. Only few studies reported ^{16}O-depleted compositions for perovskite grains in compact type A CAIs from CV chondrites [2-4]. Several mechanisms have been proposed to explain O-isotopic variation among and within the individual minerals: 1) gas-melt interaction in the ^{16}O-depleted nebula gas [e.g., 5, 6], 2) diffusive exchange between CAI minerals and ^{16}O-poor nebular gas by multiple reheating events [7], postcrystallization O-isotope exchange during fluid-rock interaction on the parent body [8, 9]. Since perovskite is a common primary phase in most CAI varieties, further investigation on O-isotopic compositions for perovskite may shed a light on the O-isotope evolution of CAI minerals.

Experimental: A compact type A CAI (*ON01*) from Allende was studied for mineral chemistry and oxygen isotopes. Spot analyses and quantitative imaging for oxygen isotopes of perovskite and enclosing melilite carried out with the Hokudai isotope microscope system consisted of the Cameca ims-1270 and a stacked CMOS-type active pixel sensor (SCAPS) ion imager. The analytical procedure is described in the previous study [10].

Results and Discussion: Perovskite are small (generally <20 μm in diameter) and enclosed by large (mostly 300 – 500 μm) melilite. Quantitative O-isotope imaging and spot analyses on the individual perovskite inclusions clearly shows that O-isotopes become heavier from the crystal core towards rim. The O-isotopic compositions of perovskite vary from −22‰ to −1‰ in $\Delta^{17}O$, whereas those of enclosing melilite are homogeneously ^{16}O-depleted ($\Delta^{17}O \geq$ −5‰). The O-isotope dichotomy between perovskite and melilite can constrain their origin. If fluid-assisted thermal metamorphism on the CV parent body resulted in almost complete O-isotope exchange of melilite with ^{16}O-depleted fluid [9], O-isotopes of perovskite is also expected to have changed to ^{16}O-depleted, based on its much smaller grain size and much faster O-isotope diffusivity relative to melilite [11-14]; thus it may not be the case in spite of the lack of experimental data on O-isotope diffusion under wet condition. If multiple reheating events in the ^{16}O-depleted gaseous reservoir [7] changed O-isotopes of entire melilite crystals, O-isotopic compositions of perovskite enclosed by the melilite should have also become ^{16}O-depleted; thus it is also not the case. The most plausible scenario to explain the ^{16}O-enriched perovskite enclosed by ^{16}O-depleted melilite is that the perovskite is relic as already mentioned by previous study [15] and the melilite has crystallized from the melt that exchanged its O-isotopes with surrounding ^{16}O-depleted gas. O-isotope diffusive exchange between melilite and relic perovskite likely resulted in O-isotope variation within the perovskite, and thus can constrain the cooling rate of the CAI. The estimated cooling rate of the CAI by numerical modeling is 1000 – 5000 K/hr at peak temperature of ~1600K, the melting temperature of perovskite in compact type A CAI composition [15]. Such fast cooling rate of the CAI is comparable with <3000 K/hr estimated by the cooling experiment on perovskite reproducing (101) twins that is commonly observed in type A CAIs from CV chondrites [16, 17]. It is worthy to note that relatively slow cooling rate for type B CAI melts (0.5 – 50 K/hr [18]) mostly relied on the crystallization of euhedral anorthite.

References: [1] Yurimoto, H. et al. (2008) *Reviews in Mineralogy and Geochemistry* 68: 141-186. [2] Kim, G. L. et al. (2002) *Journal of Mineralogical and Petrological Sciences* 97: 161-167. [3] Ito, M. et al. (2004) *Geochimica et Cosmochimica Acta* 68: 2905-2923. [4] Fintor, K. et al. (2014) *Meteoritics & Planetary Science* 49: 812-823. [5] Yurimoto, H. et al. (1998) *Science* 282: 1874-1877. [6] Aleon, J. et al. (2007) *Earth and Planetary Science Letters* 263: 114-127. [7] Simon, J. I. et al. (2011) *Science* 331: 1175–1777. [8] Wasson, J. T. et al. (2001) *Geochimica et Cosmochimica Acta* 65: 4539-4549. [9] Krot, A. N. et al. (2019) *Geochimica et Cosmochimica Acta* 246: 419-435. [10] Park, C. et al. (2012) *Meteoritics & Planetary Science* 47: 2070-2083. [11] Gautason, B. and K. Muehlenbachs (1993) *Science* 260: 518-521. [12] Sakaguchi, I. and H. Haneda (1996) *Journal of Solid State Chemistry* 124: 195-197. [13] Yurimoto, H. et al. (1989) *Geochimica et Cosmochimica Acta* 53: 2387-2394. [14] Ryerson, F. J. and K. D. McKeegan (1994) *Geochimica et Cosmochimica Acta* 58: 3713-3734. [15] Beckett, J. (1986) The University of Chicago. Ph.D thesis. [16] Keller, L. P. and P. R. Buseck (1994) *American Mineralogist* 79: 73-79. [17] Greshake, A., et al. (1998) *Meteoritics & Planetary Science* 33: 75-87. [18] Stolper, E. and J. M. Paque (1986) *Geochimica et Cosmochimica Acta* 50: 1785-1806.

NOBLE GAS SUTIDES ON NORTHWEST AFRICA (NWA) 8785 EL3 AND NWA 8789 EH3 CHONDRITES.

J. Park[1,2,3,4], M. K. Weisberg[1,2,5], K. Nagao[4], G. F. Herzog[3], L. E. Nyquist[6], D. S. Ebel[2,5], R. Okazaki[7], J. Choi[4], J. M. Baek[4], C. Park[4], M. J. Lee[4], and J. I. Lee[4]. [1]Kingsborough Community College (KCC), Brooklyn, New York 11235, USA (jisun.park@kbcc.cuny.edu), [2]American Museum of Natural History (AMNH), NY, NY 10024, USA, [3]Dept. Chem. & Chem. Biol., Rutgers University, Piscataway, NJ 08904, USA, [4]Korea Polar Research Institute (KOPRI), Incheon 21990, Korea, [5]Dept. Earth and Environmental Sci., Graduate Center, City University New York, New York, USA, [6]XI/NASA Johnson Space Center, Houston, TX 77058, USA, [7]Dept. Earth Planet. Sci., Kyushu University, 744 Motooka, Nishi-ku, Fukuoka 819-0395, Japan.

Introduction: We present noble gas analyses of the recent finds Northwest Africa (NWA) 8785 (EL3) and 8789 (EH3). Both were found in 2014 in Rissani, Morocco. NWA 8785 is an unusual EL3 in having a high abundance of matrix which is FeO-rich and contains secondary minerals [1]. Additionally, a refractory inclusion in NWA 8785 contains sodalite [1], a common alteration mineral in refractory inclusions in some CV chondrites (e.g., [2]). Our main interest in NWA 8785 is to see if there is a signature of aqueous processes in the noble gas abundances. While most enstatite chondrites are dry, lacking any evidence of alteration minerals, the presence of FeO-rich matrix and sodalite in NWA 8785 is an important clue of secondary alteration.

In laboratory experiments, disaggregated samples of Allende (CV) chondrite showed losses of noble gases after hydrothermal treatment (T=200°C; P(H$_2$O)=15 atm; t=1 week) [3]. Similarly, powdered samples of the Ningqiang (C3) kept in deionized water at 200°C for periods of 10 and 20 days, also lost noble gases. The latter authors [4] interpreted the losses as due to the removal of noble gas components from amorphous coatings of fine grained olivine and pyroxene. Nebular water might have been present during accretion of enstatite chondrites, thereby accounting for the presence of sodalite in NWA 8785, and providing the potential for loss of noble gas components. Earlier noble gas studies on some carbonaceous chondrites [4-8] suggested losses of primordial Ar, Kr, and Xe and some loss of He and Ne under a light HF-HCl etching conditions. The authors commented that the majority of the noble gases other than Q in this inclusion were located in very acid-sensitive material.

Methods: Six bulk samples with masses between 24 and 36 mg were preheated at 150 °C for 24 h and then degassed stepwise at temperatures of 500, 800, 1000, 1300 and 1800 °C for 30 minutes in order to search for signatures of aqueous alteration in the noble gas data. Noble gas concentrations and isotopic compositions of He, Ne, Ar, Kr, and Xe were measured with a mass spectrometer, modified-VG5400 at Korea Polar Research Institute (KOPRI) [9]. Sensitivities and mass discrimination correction factors were determined by measuring aliquots of atmospheric He, Ne, Ar, Kr, and Xe, and separately standardized mixtures of ^{3}He and ^{4}He to determine mass discrimination correction factor for ^{3}He/^{4}He.

Results and discussion: Generally most of the ^{3}He, radiogenic ^{4}He and ^{40}Ar (largely radiogenic) are released at low temperatures (500–1000 °C) during stepped-heating analyses. Cosmogenic Ne typically is released between the temperatures of 1000 and 1800 °C, while much of the trapped ^{20}Ne compoents are released below 1000 °C. For NWA 8785, 54 % of the trapped ^{20}Ne content was released in the 800 °C step, possibly from trapped components of P3 [10]. Possibly it is because of the matrix rich in NWA 8785 [1]. Judging from their neon isotope ratios, and like most other E3 chondrites, NWA 8785 (EL3) and NWA 8789 (EH3) contain little or no solar wind (^{20}Ne/^{22}Ne of ~12 for some enstatite chondrites with trapped solar wind [11]). ^{40}Ar (radiogenic)/^{36}Ar(trapped) in NWA 8785 is higher than in NWA 8789. ^{36}Ar, ^{84}Kr and ^{132}Xe enrichments in NWA 8785 are observed compared to those in NWA 8789 by a factor of 2. ^{36}Ar/^{132}Xe ratios are rather constant near the Q-value throughout the stepped heating; ^{84}Kr/^{132}Xe ratios trend from Q towards higher values for both meteorites. So far we are unable to identify alteration signatures from the bulk noble gas data. More analyses of specific mineral phases will be necessary.

For further work, we plan (1) isotope analyses of the matrix materials in NWA 8785 and (2) ^{40}Ar/^{39}Ar dating to define the timing of any alteration, either on the E chondrite parent body, or on a secondary body after breakup and ejection. (3) TEM and XRD to identify the matrix mineralogy and determine effects of alteration.

References: [1] Weisberg M. K. et al. (2019) *This conference*. [2] Ganino C. & Libourel G (2017) *Nature Comm., 8*, DOI: 10.1038/s41467-017-00293-1. [3] Nakasyo E. et al. (2000) *Antarctic Meteorite Research* 13:135-144. [4] Yamamoto Y. et al. (2006) *Meteoritics & Planetary Science* 41:541-551. [5] Nakamura T. et al. (2003) *Meteoritics & Planetary Science* 38:243-250. [6] Riebe M. E. et al. (2016) Annual Meeting of *Meteoritical Society* 79:A6211. [7] Weimer D. et al. (2017) Annual Meeting of *Meteoritical Society* 80:A6300. [8] Okazaki R. and Nagao K. (2017) *Meteoritics & Planetary Science* 52:669-689. [9] Nagao K. *et al.* (2016) Annual Meeting of *Meteoritical Society* 79:A6109. [10] Ott U. (2014) *Chemie der Erde* 74, 519-544. [11] Schultz L. and Franke L. (2004) *Meteoritics & Planetary Science* 39:1889-1890.

Probing the Oxygen Environments in Melilite Melts using ^{17}O NMR: Implication for Variable Oxygen Isotopic Compositions of Melilite in Type A CAIs

S. Y. Park[1], C. Park[1], H. N. Kim[2], S. Y. Lee[3], and S. K. Lee[3]. [1]Dept. of Earth-System Sciences, Korea Polar Research Institute, Incheon (sunyoung@kopri.re.kr), [2]Dept. of Earth Environmental Sciences, Kongju National University, Gongju, [3]School of Earth and Environmental Sciences, Seoul National University, Republic of Korea

Ca-Al-rich inclusions (CAIs) are known to be the oldest objects in the Solar System [1], thus probing the formation process of CAI provides insight into understanding the early evolution of our Solar System. Melilite is a primary and major phase in type A CAIs together with spinel. The crystallization sequence for type A CAI melt inferred from experimental study is spinel followed by melilite [2]. Oxygen isotopic compositions of spinel in type A CAIs are uniformly ^{16}O-rich, whereas those of melilite are relatively ^{16}O-poor and variable [3]. In some igneous type A CAIs, melilite shows oxygen isotopic variation in a single crystal, which has been explained by oxygen isotope exchange either between gas and melt in the solar nebula, [e.g., 4, 5] or between melilite crystal and aqueous fluid on the CV parent body [6]. The objective of this study is to explain the origin of oxygen isotopic variations among and within type A CAI minerals with respect to the isotope diffusion rate in the melts. The structures (coordination number and network connectivity) of melts have implications for the macroscopic properties (e.g., viscosity and diffusivity) [7, 8]. Here, we report experimental results on the effects of composition on the structure of melilite glasses and melts [åkermanite ($Ca_2MgSi_2O_7$) and gehlenite ($Ca_2Al_2SiO_7$) join] with varying åkermanite content using high-resolution solid-state nuclear magnetic resonance (NMR).

The ^{17}O 3QMAS NMR spectra of melilite glasses show that three types of bridging oxygens (BOs, Si–O–Si, Al–O–Al, and Si–O–Al) and three types of non-bridging oxygens (NBOs, Ca–O–Si, Ca-O-Al, and mixed {Ca, Mg}–NBO) are partially resolved. The fraction of NBO in melilite glasses increases with increasing åkermanite content. The observed structural changes in the melilite glasses can provide an improved understanding of their structure–property relationships. The observed increase in NBO fraction with increasing åkermanite content indicates an obvious decrease in melt viscosity toward an åkermanite endmember [9]. The diffusion of oxygen is also affected by the melt polymerization because the activation energy required for diffusion increases with increasing melt polymerization [10]. It is predicted that as Mg (i.e., åkermanite content) in the melts increases, the oxygen isotope diffusion rate will increase due to decreasing melt polymerization [10].

If the precursor materials of type A CAIs formed in the ^{16}O-rich nebular gas and experienced melting in the ^{16}O-poor gas, spinel can retain its ^{16}O-rich composition because it is the first phase crystallized from the melt and its oxygen diffusivity is quite sluggish [11] or spinel could be just relict. Oxygen isotopic change from ^{16}O-rich to ^{16}O-poor compositions with increasing åkermanite content in melilite [5] can be explained by changing oxygen diffusivity of the melt during fractional crystallization. While the gehlenitic melilite, which is formed in the early stage, may have a similar isotopic composition to that of spinel (^{16}O-rich), the melilite with higher åkermanite content may show ^{16}O-poor composition similar to the surrounding gas composition, as the diffusion rate in melts increased.
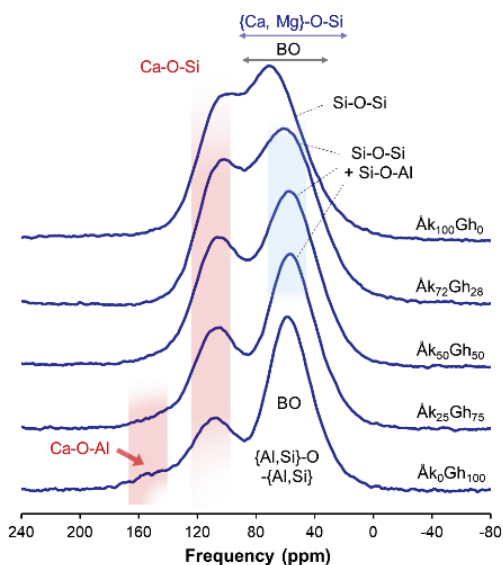

Figure 1. ^{17}O MAS NMR spectra for melilite glasses with varying åkermanite content at 9.4 T. The fraction of non-bridging oxygen increases with increasing åkermanite content.

References:
[1] Connelly, J. N. et al. (2012) *Science* 338: 651-655. [2] Stolper, E. (1982) *Geochimica et Cosmochimica Acta* 46: 2159-2180. [3] Yurimoto, H. et al. (2008) *Reviews in Mineralogy and Geochemistry* 68:141-186. [4] Yurimoto, H., et al. (1998) *Science* 282: 1874-1877. [5] Aleon, J. et al. (2007) *Earth and Planetary Science Letters* 263: 114-127. [6] Krot, A. N., et al. (2019) *Geochimica et Cosmochimica Acta* 246: 419-435. [7] Lee, S. K. (2011) *Proceedings of the National Academy of Sciences of the United States of America* 108: 6847-6852. [8] Mysen, B. O. and Richet, P. (2005) Elsevier: Amsterdam, 259-290. [9] Giordano, D. et al. (2009) *Geochimica et Cosmochimica Acta* 73: 6613-6630. [10] Lesher, C. E. (2010) *Reviews in Mineralogy and Geochemistry* 72: 269-309. [11] Ryerson, F. J. and K. D. McKeegan (1994) *Geochimica et Cosmochimica Acta* 58: 3713-3734.

AMINO ACIDS IN ANTARCTIC MICROMETEORITES

E. T. Parker[1], C. Engrand[2], J. P. Dworkin[1] and D. P. Glavin[1]
[1]Solar System Exploration Division, NASA Goddard Space Flight Center, Greenbelt, MD 20771 U.S.A.
[2]CSNSM, CNRS/Univ. Paris Sud, Université Paris-Saclay, France

Introduction: Deposition of organics to Earth from asteroids and comets, and their fragments, could have contributed to the origin of life on Earth. *In situ* studies of the coma of comet 67P/Churyumov-Gerasimenko [1] and laboratory analyses of meteorites suggest amino acids are present on asteroids and comets [2]. Amino acids are important target analytes when investigating extraterrestrial samples because the abundances, distributions, and enantiomeric and isotopic compositions of amino acids can infer information regarding parent body processing [2].

Meteorite organics have been heavily studied, yet, organics in micrometeorites (MMs) are poorly understood [3-6]. Responsible for $\sim 30 \times 10^6$ kg/yr [7-8], MMs are the primary contributor of extraterrestrial material to Earth [7,9]. To illustrate, 100 – 250 µm MMs deposit $\sim 1000 \times$ more mass than other sources of extraterrestrial material [10].

Large (100 – 400 µm) Antarctic MMs (AMMs) have been recovered from the South Pole Water Well (SPWW), Cap Prud'homme (CP), Dome Fuji, and Dome C (Concordia Station), Antarctica. Groups of dozens of AMMs from SPWW and CP have been analyzed, leading to the detection of α-aminoisobutyric acid (α-AIB), a non-protein extraterrestrial amino acid [3,6]. Yet, it is unknown if MMs possess a broader distribution of extraterrestrial amino acids, which would provide insight into parent body processes and potential MM amino acid contributions to early Earth.

Experimental: In this work, 6 AMM grains (~ 7 µg total mass) from the Concordia collection [11] have been analyzed for amino acids. The particles were subjected to pre-column derivatization using *o*-pthaldialdehyde/*N*-acetyl-L-cysteine [12] to enhance instrumental sensitivity to, and specificity for, primary amino groups, and to provide chromatographic separation of chiral amino groups. Subsequent to derivatization, sample analyses were executed with ultra performance liquid chromatography with fluorescence detection and time-of-flight mass spectrometry.

Results and Discussion: The present work detected numerous extraterrestrial amino acids, and used $\sim 1000 \times$ less material than previous MM studies [6]. The amino acids detected possessed a distribution of abundant achiral, straight-chained *n*-ω-amino acids (Figure 1). Thermally altered CV3 and CO3 chondrites also contain elevated abundances of *n*-ω-amino acids. Interestingly, such a distribution is disproportionately not observed in the analyses of low temperature, aqueously altered CR, CI, and CM chondrites [13]. Based on the observed amino acid distribution, it is plausible that the MMs analyzed in this study originated from a thermally altered parent body. However, we cannot rule out the possibility that the amino acids were affected by atmospheric entry heating, which warrants further investigation.
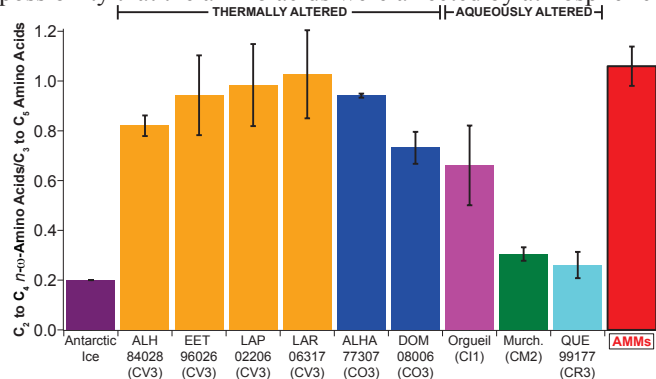

Figure 1. C_2 to C_4 *n*-ω-amino acids relative to C_3 to C_5 amino acids of **Antarctic ice**, thermally altered **CV3** and **CO3** chondrites [13], and low temperature aqueously altered **CI1**, **CM2**, and **CR3** chondrites [14], compared to the present analysis of 6 **AMM grains**.

Implications: This work provides the first evidence of extraterrestrial *n*-ω-amino acids in MMs, suggesting these compounds were formed at elevated temperatures. Additionally, while it was previously thought that the only indigenous extraterrestrial amino acid in MM grains was α-AIB [3,6], our new results indicate that MMs may have delivered a much broader range of amino acids to the primordial Earth than suggested by prior research in the field.

References: [1] Altwegg K. et al. (2016) *Science Advances* 2:e1600285. [2] Burton A. S. and Berger E. L. (2018) *Life* 8:doi:10.3390/life8020014. [3] Brinton, K. L. F. et al. (1998) *Origins of Life and Evolution of the Biosphere* 28:413-424. [4] Clemett S. J. et al. (1998) *Origins of Life and Evolution of the Biosphere* 28:425-448. [5] Glavin D. P. et al. (2004) *Advances in Space Research* 33:106-113. [6] Matrajt G. et al. (2004) *Meteoritics & Planetary Science* 39:1849-1858. [7] Love S. G. and Brownlee D. E. (1993) *Science* 262:550-553. [8] Taylor S. et al. (1998) *Nature* 392;899-903. [9] Chyba C. and Sagan C. (1992) *Nature* 355:125-132. [10] Love S. G. and Brownlee D. E. (1991) *Icarus* 89:26-43. [11] Duprat, J. et al. (2007) Advances in Space Research 39:605-611. [12] Glavin D. P. et al. (2006) *Meteoritics & Planetary Science* 41:889-902. [13] Burton A. S. et al. (2012) *Meteoritics & Planetary Science* 47:374-386. [14] Glavin, D. P. et al. (2010) *Meteoritics & Planetary Science* 45:1948-1972.

NEW UNIQUE BRACHINITE-LIKE ACHONDRITE CALAMA 029.

A. Iu. Pastukhovich[1], S. V. Berzin[2], K. A. Dugushkina[2], , V. I. Grokhovsky[1], M. V. Chervyakovskaya[2],
[1]Ural Federal University, 19 Mira st., Ekaterinburg, 620002 Russia, a.iu.pastukhovich@urfu,
[2]A.N. Zavaritsky Institute of Geology and Geochemistry UB RAS, 15 Academic Vonsovsky st.,
Ekaterinburg, 620016, Russia, sbersin@ya.ru .

Introduction: Meteorite Calama 029 was found in 2017 by URFU Meteorite Expedition to the Atacama desert in Antofagasta province (Chili). As a result of research meteorite Calama 029 is a unique achondrite that has no analogues among any known meteorites. In this study we make assumptions about the mechanisms of formation and the parent body of the meteorite Calama 029.

Materials and Methode: We studied two polished section of the meteorite Calama 029 by optical microscope in transmitted and reflected lights, by SEM JSM 6390LV (Jeol) with EDS X-max 80 in Common Use Center "Geoanalyst" IGG UB RAS. Cu isotope composition was measured by TIMS TRITONE PLUS in "Geoanalyst" IGG UB RAS.

Results: Petrographic observation of a polished section shows a fine-graned recrystallized poikilitic texture. Achondrite consist of olivine Fa31 (N=15) 65%, orthopyroxene En73Fs25Wo2 (N=12) 15%, clinopyroxene En45Fs11Wo44 (N=9) 5-7%, plagioclase An20 (N=9) 10%, chromite 2-3%, troilite 3-4%, Fe-Ni-metal < 0,5%, accessory apatite and ilmenite. Olivine grains are 50-300 μm in size, however we observed large olivine grains up to 800 μm in size. Such olivine grains contains plagioclase, troilite and metal inclusion. One relict bared olivine (BO) chondrule was found in thin section of the achondrite. This chondrule has a recrystallized boundaries and contains enstatite and clinopyroxene inclusion. This apparently indicates intense recrystallizaton of the initial chondrule.

Olivine contains MnO 0.4 wt.%. Clinopyroxene has slight variations in composition. Plagioclase contains K_2O 0.6-1.3 wt.%. The average composition of chromite (N=8): SiO_2 0.6%, TiO_2 3.6%, Al_2O_3 5.1%, Cr_2O_3 54.6%, FeO 32.1%, MnO 0.6%, MgO 1.6%, V_2O_3 1.0%, ZnO 0.3%. The average composition of FeNi-metal (N=13): Fe 49.0%, Ni 47.8%, Co 2.5%. Meteorite Calama 029 has high $\delta^{65}Cu/^{63}Cu$ 4.19‰.

Optical features (sharp extinction of olivine) indicate that the sample is very weakly or not shocked (S1). Heavy oxidation of metal and troilite, beginning alteration of mafic silicates. Weathering grade is W3.

Discusion: Definitely, the meteorite Calama 029 is a primitive achondrite. This is indicated by the content of the rare relict chondrule and the fine-graned recrystallized texture of the meteorite.

Composition of olivine, orthopyroxene, clinopyroxene and plagioclase in this meteorite is similar to mineral composition of brachinites. However, this meteorite has small content of olivine 65% and has fine-graned poikilitic texture. Orthopyroxene predominate to clinopyroxene in this meteorite. While brachinite is dunitic to wherlitic rocks with granoblastic to protogranular medium to coarse-grained texture. Brachinite content of olivine 75-95% and characterized by majority of clinopyroxene to orthopyroxene. The meteorite texture are similar to an acapulcoite. However the meteorite contains more ferroan olivine and more ferroan pyroxene unlike the acapulcoites. We offer to classified this meteorite us the unique brachinite like achondrite.

Many researchers identifies the formation of brachinites with magmatic processes on parent asteroids [1-4]. Meteorite Calama 029 has not igneous structure and obviously formed by metamor-phism of the chondrite. We suppose the meteorite Calama 029 is an unmelted primitive precursor for brachinite meteorites.

References: [1]Keil K. (2014) Chemie der Erde - Geochemistry 74:311–329. [2] Hasegawa H.et al.(2019) Meteoritics & Planetary Science 54:752–767.[3] Mittlefehldt D.W.et al. (2003) Meteoritics & Planetary Science 38:1601–1625.[4] Swindle TD et al. (1998) Meteoritics & Planetary Science 33: 31–48.

RUSSIAN-MONGOLIAN METEORITE EXPEDITION TO THE GOBI DESERT

A. Iu. Pastukhovich[1], S. Demberel[2], V. I. Grokhovsky[1], R. N. Kolunin[1], M. Y. Larionov[1], L. A. Muravyev[1,3], T. Nasan-Ochir[2], E. V. Petrova[1] and G. A. Yakovlev[1]
[1]Ural Federal University 620002, Mira st.19, Ekaterinburg, Russia, a.iu.pastukhovich@urfu.ru;
[2]Institute of Astronomy and Geophysics of MAS, Ulaanbaatar, Mongolia, demberel@iag.ac.mn
[3]Institute of Geophysics Ural Branch of RAS, 620016, Amundsen st. 100, Ekaterinburg, Russia, mlev@igeoph.net

Introduction: The arid climate of hot deserts make them ideal for the accumulation and preservation of extraterrestrial matter. Deserts located in Oman, Chile and North-West Africa feature numerous dense collection areas (DCA) of meteorite specimens. The Gobi Desert in Mongolia is the third largest hot desert covers the area of 1,300,000 km². However, the Meteoritical Bulletin Database currently contains only 10 records of meteorites found in Mongolia. In addition, no DCA has thus far been found in the Gobi Desert. In 2018, the first Russian-Mongolian expedition to the Gobi Desert was undertaken with the purpose of searching for meteorites and studying the mechanisms of their accumulation.

Methods: To the best of our knowledge, the only large-scale targeted expedition to search for meteorites and study the Tabun-Khara-Obo crater was organized in 1993 by Addi Bishoff [1]. However, due to an abnormally rainy period preceding Bishoff's expedition, the search for meteoritic matter yielded no results. When preparing for the expedition, we relied on our own experience of organizing search works in hot [2,3,4] and cold [5] deserts.

Our research team consisted of six Ural Federal University employees (Russia) and one Institute of Astronomy and Geophysics, MAS, employee (Mongolia). Two off-road vehicles were used to search for meteorites across different zones of the desert. Fieldwork was carried out from 23rd August to 6th September, 2018. The total length of the expedition route was about 3000 km.

A visual search was carried out both on foot and from the vehicles at a speed of 10-15 km/h with stops to inspect specimens resembling meteorites. A visual search on foot was performed either across plateau areas or elevations of light shades or in places with difficult topography. The key criteria for selecting the material were a black or dark brown colour (as a possible indication of rust traces), the presence of fusion crusts and magnetic properties. The presence of magnetic properties was verified with the help of permanent magnets attached to telescopic holders, which were used by each member of the expedition. The search was hampered by a large amount of vegetation, which had appeared as a result of extreme precipitation in the first half of August, 2018.

Results and discussion: The expedition yielded 5 meteorite samples with a total weight of about 1.5 kg. A fragment of a stone meteorite weighing 800 g was found 50 km east of the Noion somon in a mountain stony desert area consisted mainly of sedimentary rocks of a white or light-gray colour (1500 m above sea level). The second group of finds comprised fragments of meteorite rain having disintegrated in the atmosphere. This is evi-denced by the similarity of the fragments found 10 km north-west of the Shinejinst somon at a distance of 100-500 meters from each other. The terrain was characterized by sloping hills covered with scattered stones of light shades. Some fragments fitted together perfectly at chipped sides. It should be noted that not all the fragments of this mete-orite were found.

According to their cleavage structure and magnetic susceptibility parameters, the discovered fragments correspond to chondrites. The meteorites exhibit various degrees of weathering, which is likely to be determined both by their different terrestrial age and different environmental conditions during their terrestrial residency.

Unfortunately, we have failed to find any DCA in this large desert, which maintains the urgency of organizing new expeditions to the Gobi Desert.

References: [1] Gerel O. et al, (1995) In Workshop on Meteorites from Cold and Hot Deserts, (LPI) pp.32-33. [2] Muravyev L.A. and Grokhovsky V.I (2018) Meteoritics & Planetary Science 53 SI: 6280. [3] Pastukhovich A.Yu. et al (2017) Meteoritics & Planetary Science 52 SI: A265. [4] Pastukhovich A.Yu.et al (2018) Meteoritics & Planetary Science 53 SI: 6071. [5] Larionov M.Yu. et al (2016) Meteoritics & Planetary Science 51 SI: A400.

INVESTIGATING SHOCK DEFORMATION WITH LAUNCH-PAIRED MARTIAN SHERGOTTITES

R. P. Patel[1], G. Benedix[1], L. Forman[1], and N. Timms[1]. [1]School of Earth and Planetary Sciences, Faculty of Science and Engineering, Curtin University, Bentley, Western Australia, 6102

Introduction: In recent decades, the study of Martian meteorites has significantly impacted the planetary science community and has helped to build a greater understanding of the surface geology and processing on Mars [1]. Currently, there are ~60,000 known meteorites on Earth, with only ~200 known to have originated on Mars. Shergottites (~80% of Martian meteorites) are mafic to ultramafic achondritic meteorites with basaltic to lherzolitic compositions and are moderately to highly shocked, with substantially higher shock levels than most other meteorites [2]. Shock manifests itself in the deformation of minerals within the meteorites. Levels of shock have been qualitatively defined using experimental data and past literature, whilst referring to a new shock classification system proposed by Stöffler et al. (2018) [3]. We have examined 4 shergottites that have the same cosmic ray exposure age and span different shergottite classes to investigate the shock features of meteorites that likely sample from the same ejection event on Mars.

Samples and Methods: Thin and thick sections of RBT 04262, ALHA 77005, Los Angeles and LAR 06319/12011 were examined optically and with electron backscatter diffraction (EBSD) techniques on the TESCAN Mira 3 instrument located within the John De Laeter Centre, Curtin University. All these samples have a published preferred cosmic ray exposure age of ~3.1 Ma [2,4,5]. They are classified as poikilitic (RBT/ALHA), olivine-phyric (LAR), and diabasic (LA) and all have depleted rare earth element (REE) patterns, apart from ALHA 77005, which has an intermediate REE pattern. EBSD data was obtained, processed and reduced using integrated Oxford Instruments software: AZtecHKL (Aztec 3.3 SP1) and HKLChannel5 (HKLTango). Grain reference orientation deviation maps (GROD – the angle of deviation from the average orientation of a grain is determined for each pixel within that grain, for all grains within the mapped area); grain orientation spread maps (GOS – the angle of deviation from the average orientation of a grain for each pixel within that grain is averaged, for all grains within the mapped area – i.e. average of all GROD values within a grain); and maximum orientation spread maps (MOS – the maximum angle of deviation from the average orientation of all pixels within that grain – i.e. maximum GROD value within a grain) were constructed. Statistics on GOS and MOS values for each individual grain (minimum grain area of 3 pixels) in each map were compiled and analysed.

Results and Discussion: Recent advances in EBSD data reduction allow us to visualise deformation in crystals in thin/thick section [6]. We analysed a number of regions of interest on each thin/thick section using EBSD. Figure 1 shows a MOS map of Los Angeles,P10075 representing the maximum angle of deviation from the average orientation of all pixels within a number of pyroxene grains. For pyroxenes in all samples, the maximum MOS and GOS values range from 22.93° to 33.10° and 6.51° to 10.47° respectively, with the highest maximum for both found in Los Angeles. For olivines in all samples, the maximum MOS and GOS values range from 4.95° to 35.41° and 3.44° to 9.93° respectively, with the highest maximum for both found in RBT 04262. For opaque minerals in all samples, the maximum MOS and GOS values range from 12.18° to 17.30° and 5.15° to 6.37° respectively, with the highest maximum for both found in ALHA 77005. The findings of this project are significant as we can potentially differentiate between multiple lava flows (or a singular lava flow that has differentiated) and shock impacts in a specific volcanic region on Mars, and significantly enhance our knowledge of shock impact processes on Mars, and by extension such processes on Earth.

Figure 1: Maximum orientation spread (MOS) map of Los Angeles,P10075

References: [1] Collinet, M., Charlier, B., Namur, O., Oeser, M., Médard, E., & Weyer, S. (2017). Crystallization history of enriched shergottites from Fe and Mg isotope fractionation in olivine megacrysts. Geochimica et Cosmochimica Acta, 207, 277-297. doi:https://doi.org/10.1016/j.gca.2017.03.029. [2] Nyquist, L. E., Bogard, D. D., Shih, C. Y., Greshake, A., Stöffler, D., & Eugster, O. (2001). Ages and Geologic Histories of Martian Meteorites. Space Science Reviews, 96(1), 105-164. doi:10.1023/A:1011993105172. [3] Stöffler, D., Hamann, C., & Metzler, K. (2018). Shock metamorphism of planetary silicate rocks and sediments: Proposal for an updated classification system. Meteoritics & Planetary Science, 53(1), 5-49. doi:10.1111/maps.12912. [4] Nishiizumi, K., & Caffee, M. (2010). A tale of two shergottites: RBT 04261 and RBT 04262. [5] Nagao, K. (2008). Noble Gases and Cosmic-Ray Exposure Ages of Two Martian Shergottites, RBT 04262 and LAR 06319, Recovered in Antarctica (Vol. 43). [6] Forman, L. V., Benedix, G. K., Timms, N. E., Bland, P. A., Healy, D., & Reddy, S. (2018). Exploring the effects of crystallographic orientation on the generation of shock deformation features in Martian Shergottites.
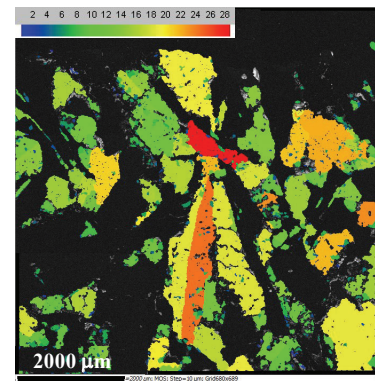
CHROMIUM ISOTOPES AND TRACE ELEMENT CONCENTRATION OF XENOLITHIC C1 CLASTS IN BRECCIATED CHONDRITES AND ACHONDRITES.

M. Patzek[1], Y. Kadlag[2], A. Bischoff[1], R. Visser[2], H. Becker[2], and T. John[2], [1]Institut für Planetologie, University of Münster, Wilhelm-Klemm-Str. 10, D-48149 Münster, Germany. [2]Freie Universität Berlin, Institut für Geologische Wissenschaften, Malteserstr. 74-100, 12249 Berlin, Germany. E-Mail: markus.patzek@uni-muenster.de.

Introduction: CI- and CM-like clasts have been identified based on petrographic criteria in various chondrite and achondrite breccias including CR and OC chondrites as well as ureilites and HEDs [1-4]. Despite their similar mineralogy, CI-like clasts from different host meteorites and CI chondrites exhibit different H and O isotope signatures as well as different S isotopic distributions of their sulfide grains [5-7]. Altogether, these clasts are better referred to as C1 clasts rather than CI-like. In this study, Cr isotope data and trace element concentrations of one C1 clast from the DaG 1064 ureilite (C1a) and one from the CR chondrite Acfer 311 (C1b) will be discussed. Additional data on a CM-like clast from the polymict eucrite NWA 7542 will be presented.

Samples and Methods: Cr isotopic compositions as well as previously obtained O isotopic compositions have been investigated for three extracted clasts: Dar al Gani (DaG) 1064-C (C1a), Acfer 311-C (C1b), and Northwest Africa (NWA) 7542-G (CM-like). A three-step ion exchange chromatography (anion and cation resin) was used to separate Cr from the matrix. The isotopic compositions were analyzed using a Thermo Scientific Triton Plus TIMS at the Freie Universität Berlin. The Rare Earth Element (REE) abundances are analyzed on an Element XR ICP-MS.
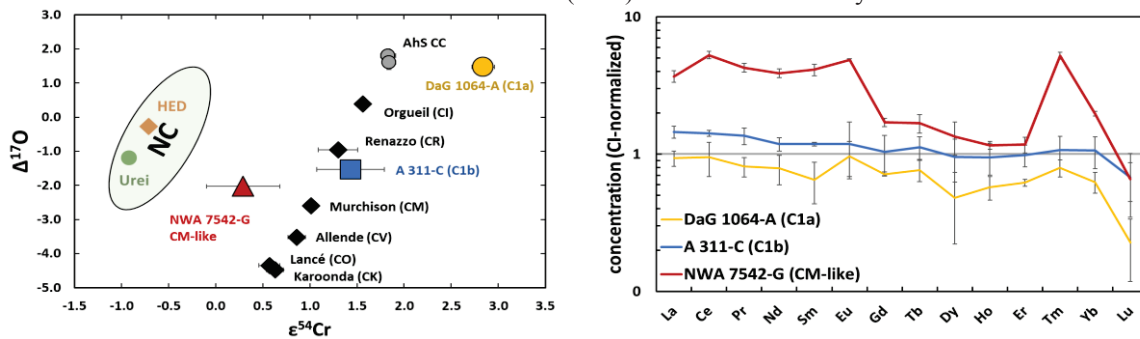

Fig 1: (a) ε^{54}Cr vs. Δ^{17}O plot showing data that define the carbonaceous (CC) and non-carbonaceous (NC) meteorite reservoirs and data of individual clasts (this study) from different meteorites (colored). Literature data from [8-9 and references therein]. (b) REE abundances of the studied clasts normalized to average CI chondrite values [11].

Results and Discussion: DaG 1064-A (C1a) yielded ε^{54}Cr of 2.84 ± 0.12 and ε^{53}Cr of 0.66 ± 0. The high ^{54}Cr excess for DaG 1064-A is remarkable since similar material from Almahata Sitta (AhS CC) exhibits lower excesses (Fig. 1a; [8]). This high excess might have been caused by a heterogeneous distribution of ^{54}Cr excess in the carrier phases within the sample, since our aliquot is smaller compared to those of [8-10]. Acfer 311-C (C1b) shows a less pronounced excess in ^{54}Cr and ^{53}Cr with ε^{54}Cr of +1.43 ± 0.36 and ε^{53}Cr = 0.39 ± 0.11, respectively. The similarity in its ^{54}Cr excess as well as in H and O isotopes [6] compared to CR chondrites favors a genetic relation between the clast and the host CR chondrite (Fig. 1a). CM-like clast NWA 7542G exhibits only minor (if any) excesses in ^{54}Cr and ^{53}Cr with ε^{54}Cr = 0.29 ± 0.39 and ε^{53}Cr = 0.29 ± 0.05, respectively, maybe due to contamination with HED material during separation. REE concentrations of clasts A311-C and DaG1064-A are roughly chondritic showing a slightly decreasing trend from La to Lu (Fig. 1b). The REE data of CM-like clast NWA 7542-G show a pattern similar to those of group II Ca,Al-rich inclusions, which may dominate the pattern in the analyzed aliquot (Fig. 1b).

Take Home Messages: *C1a clasts* in ureilites are enriched in ^{54}Cr and they show chondritic REE concentrations. Together with O and H isotope data [5,6] it is clear that this material is of very primitive nature. The *C1b clast* in the CR chondrite shows an excess in ^{54}Cr similar to the data of CR chondrites. The O and H isotope data of the same clast also indicate a genetic relationship between the clast and the host. *CM-like clasts* in HEDs are clearly related to "common" CM chondrites considering petrology, O, H, and partly their Cr isotopes.

References: [1] Bischoff A. et al. (1993) *Geochimica et Cosmochimica Acta* 57:2631-2648. [2] Buchanan P. et al. (1993) *Meteoritics & Planetary Science* 28:659-669. [3] Zolensky M.E. et al. (1996) *Meteoritics & Planetary Science* 31:518-537. [4] Patzek M. et al. (2017) *Meteoritics & Planetary Science* 53:2519-2540. [5] Patzek M. et al. (2017) *Meteoritics & Planetary Science* 53 #6254. [6] Patzek M. et al. (2019) *LPS L, Abstract 1779*. [7] Visser R. et al. (2017) *Meteoritics & Planetary Science* 53, #6190. [8] Goodrich et al. (2019) *LPS L, Abstract 1312*. [9] Trinquier et al. (2007) *The Astrophysical Journal* 655:1179-1185. [10] Petitat et al. (2010) *The Astrophysical Journal* 736:23. [11] Lodders (2003) *The Astrophysical Journal* 591:1220-1247.

ON THE PROBLEM OF GALACTIC DUST DISCOVERING

N. I. Perov[1,2] and V. E. Pakhomycheva[2], [1]Cultural and Educational Center named after V.V. Tereshkova. Ul. Chaikovskogo, 3, Yaroslavl-150000, Russian Federation. E-mail: perov@yarplaneta.ru, [2]State Pedagogical University named after K.D. Ushinskii. Ul. Respublikanskaya, 108, Yaroslavl-150000, Russian Federation. E-mail: pahomycheva.vika@mail.ru.

Introduction: Particles arrived in the Solar System from interstellar medium are found but their nature is not cleared [1, 2]. Discovering of such particle fluxes and working out the criteria of galactic meteors identification is a problem of the modern astronomy [2]. Below light pressure and effect of Pointing-Robertson as well as gravitational force acting on the particle from the Sun are taken into account.

The based equations: The model equation of particle motion we put in the form (1) [3]

$$d^2\mathbf{r}/dt^2 = -GM'\mathbf{r}/r^3 - 2b'v\cos(u)\mathbf{e}_r/r^2 - b'v\sin(u)\mathbf{e}_t/r^2 \tag{1}$$

Here, v is velocity of the considered particle, u is an angle between the vector of the velocity $\mathbf{v}$ and the heliocentric radius-vector $\mathbf{r}$ of the particle, $\mathbf{e}_r$ and $\mathbf{e}_t$ are units' orts of radial and tangent directions of the particle vector acceleration, $b' = \pi R^2 q r_{SE}^2/(Mc^2)$, $M' = M_S - \pi R^2 q r_{SE}^2/(GMc)$, G is the gravitational constant, c is the velocity of light, R is a radius of the particle, q is the solar constant, M' is reduced mass of the Sun, M_S is the mass of the Sun, M is mass of the particle, r_{SE} is the averaged distance between the Earth and the Sun. Using the density ρ of the spherical black particle we have $M = \frac{4}{3}\pi R^3 \rho$, $b' = (3/4)q r_{SE}^2/(\rho R c^2)$, $M' = M_S - (3/4)q r_{SE}^2/(\rho R G c)$.

If the particle moves along the straight line in the gravitational field of the Sun (light pressure and effect of Pointing-Robertson are also taken into account), then equation (1) is simplified ($u=\pi$) and after integrating (1)

$$\frac{v - v_0}{2b'} + \frac{GM'}{(2b')^2} \cdot \ln\left(\frac{2b'v - GM'}{2b'v_0 - GM'}\right) = \frac{1}{r_0} - \frac{1}{r}. \tag{2}$$

Where v_0 is the initial velocity of the particle, r_0 is the initial positions of the particle, the final distance of the particle from the Sun is equal to $r=r_{SE}$.

Example: Graph of v (v_0, $\rho \cdot R$) functions, presented in figure (Fig.1), are plotted for values: $q=1360$ Wt. $/m^2$, $r_{SE}=1.49597 \cdot 10^{11}$ m, $M_S = 2 \cdot 10^{30}$ kg, $r_0 = 100000$ AU, $G=6.672 \cdot 10^{-11}$ $m^3/$ $(kg \cdot s^2)$, $c=3 \cdot 10^8$ m/s; $0<v_0<100000$ m/s, $0<\rho \cdot R<1000$ kg/m^2.
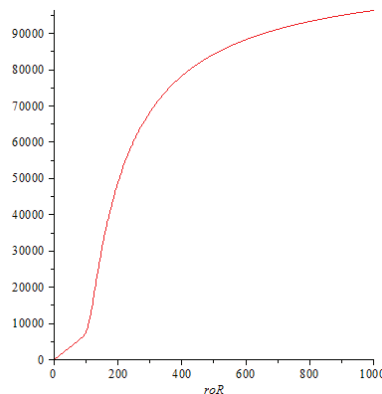

Fig.1. Dependence of v near the Earth's orbit on $\rho \cdot R$ for $v_0=100000$ m/s

Conclusion: The small values of the radii R and the low density ρ of the particles make the velocities of interstellar meteoroids near the Earth's orbit tend to zero even for the large initial velocities of these meteoroids (Fig.1). So, the interstellar meteoroids in some cases have almost zero velocities near the Earth's orbit and majority of them may be lost for their searching in accordance with the method [4], using only the criterion of high velocities of interstellar meteoroids.

References: [1] Hajdukov'a M., Paulech Jr. and Paulech T. (2007) *Contrib. Astron. Obs. Skalnat'e Pleso.* V. 37. P. 18-30. (http://www.ta3.sk/caosp/Eedition/FullTexts/vol37no1/pp18-30.pdf). [2] Kramer E.N. and Smirnov V.A. (1999) *Solar System Research.* V. 33. P.77. [3] Radzievskii V.V. (2003) *Photogravitational Celestial Mechanics.* Nijnii Novgorod: Editor Chief Yu. A. Nikolayev. 196 pp. (In Russian). [4] Slivinskii A.P., Bushuev F.I., Kalyujnyi N.A. and Shulga A.V. (2013). *NTR.* V. 92. N 2. P. 28-34.

FTIR quantification of the functional C groups in coals and extraterrestrial kerogens: a calibration procedure

Van T.H. Phan[1], Eric Quirico[1], Pierre Beck[1], Nathalie Carrasco[2], Thomas Gautier[2], Lora Jovanovic[2], Jesus Raya[3], Yann Le Brech[4], Corentin Le Guillou[5]

[1]IPAG, UGA, 38400, France (thi-hai-van.phan@univ-grenoble-alpes.fr; beck.pierre@univ-grenoble-alpes.fr; eric.quirico@univ-grenoble-alpes.fr)
[2]CNRS/INSU, LATMOS-IPSL, Guyancourt F-78280, France (nathalie.carrasco@latmos.ipsl.fr; lora.jovanovic@latmos.ipsl.fr; thomas.gautier@latmos.ipsl.fr)
[3]ICN, CNRS, Université de Strasbourg, BP 296 R8 670008 Strasbourg (jraya@unistra.fr)
[4]LRGP, CNRS, Université de Lorraine, 1 rue Grandville 54000 Nancy, France (yann.le-brech@unive-lorraine.fr)
[5]Unité Matériaux et Transformations, UMET, UMR-CNRS 8207, Université de Lille, France (corentin.san@gmail.com)

Introduction: Kerogens and coals are complex polyaromatic carbonaceous solids that formed in Earth sediments from the thermal maturation and preservation of living organisms [1]. Kerogen-like polyaromatic materials are also present in primitive meteorites, presumably formed in the proto-solar disk through thermal and/or radiolytic reactions and were further processed in their parent bodies [2]. Though decades of analytical investigations, the composition and chemical structure of those materials remain not fully elucidated. FTIR (Fourier-Transform Infrared Spectroscopy) has been proved to be a powerful technique for characterizing coals, peats, terrestrial and meteoritic kerogens [2]–[4]. However, the quantification of functional C groups by calculating of the integrated cross-section of each functional C groups is hampered by the lack of precise knowledge of their integrated cross-sections.

Our present work aims to investigate the infrared spectra using the different standards as known polymers [5] and synthetic polyaromatic materials (e.g. tholin), produced by thermal degradations of a ^{13}C-substituted precursor. It was synthesized in a cold plasma reactor (PAMPRE, Latmos, Guyancourt) from a ^{13}CH$_4$: ^{13}CO = 7: 3 gas mixture with 90% of Ar [6]. Characterization of known molecular polymer and the carbonized tholin were performed and Nuclear Magnetic Resonance (NMR) measurements were then run, providing estimates of the integrated cross-sections ratio of the aromatic, C=C, C=O and CH$_x$ groups. The carbonization process can increase the polyaromatic character in the tholin composition toward a structure similar to that observed in these terrestrial and extraterrestrial materials.

We will present the whole calibration procedure and applications to the quantification of the above-mentioned functional groups for coal and meteoritic kerogen samples. A series of coals with different vitrinite reflectances and some FTIR data of IOM samples from chondrites will be re-calculated to compare with the previous data to see the contribution of the relative abundance of carbon atoms regrading to the C=C, C=O, CH$_3$, CH$_2$ and aromatic groups.

References:
[1]   A. Hutton, S. Nharato, and T. Robl (1994), *Energy and Fuels*, 8: 1478–1488.
[2]   G. D. Cody *et al.* (2011), *Proc. Natl. Acad. Sci.,* 108(48): 19171–19176.
[3]   Y. Chen, M. Mastalerz, and A. Schimmelmann (2012), *Int. J. Coal Geol.*, 104: 22–33.
[4]   P. Beck *et al.* (2010), *Geochim. Cosmochim. Acta*, 74(16): 4881–4892.
[5]   C. Le Guillou et al. (2018), *Anal. Chem.*, 90(14): 8379–8386.
[6]   C. Szopa et al. (2006), *Planet. Space Sci.*, 54: 394–404.

HYDROGEN ISOTOPIC COMPOSITION OF WATER IN HYDRATED CHONDRITES

L. Piani[1], Y. Marrocchi[1], L.G. Vacher[1], M. Piralla[1], M. Bizzarro[2], C.M.O'D. Alexander[3] and, K.T. Howard[4]. [1]CRPG - UMR7358, Université de Lorraine, 15 rue Notre Dame des Pauvres, Vandoeuvre-les-Nancy, France. (Laurette.piani@univ-lorraine.fr). [2]Centre for Star and Planet Formation and Natural History Museum of Denmark, University of Copenhagen, DK-1350 Copenhagen, Denmark. [3]Department of Terrestrial Magnetism, Carnegie Institution for Science, Washington, DC 20015, USA. [4]Physical Sciences Department, Kingsborough Community College, City University of New York, 2001 Oriental Blvd., Brooklyn, New York, NY 11235, USA.

Introduction: Hydrogen is the most abundant element in the solar system. The hydrogen isotopic composition of water (expressed as the D/H ratio) in planetary objects [1] is generally thought to increase from very low values close to the Sun (D/H ≈ 20×10^{-6}), to intermediate D/H ratios in inner solar system objects (e.g., Earth's ocean D/H ≈ 156×10^{-6}), to high D-enrichments in outer solar system objects such as comets (up to 530×10^{-6} in comet 67P/Churyumov-Gerasimenko; [2]).

Chondrites are rocky fragments of asteroids that could have formed at heliocentric distances from ∼ 2 to more than 15 AU in the early solar system (e.g., [3]). Most of chondrite groups contain water-bearing minerals attesting that efficient water-rock interactions occurred on asteroids. Nonetheless, the hydrogen isotopic composition of water in the different chondrite groups remains poorly constrained (e.g., [4]). This is because hydrated minerals cannot be easily separated from organic matter, the other main H-bearing phase in chondrites, intertwinned at the submicrometer scale with minerals in the matrix [5]. Bulk chondrite hydrogen isotopic compositions are thus complex mixtures of these two H-bearing phases. Direct estimates of the chondritic water D/H ratios cannot be obtained easily due to the difficulty in estimating the organic matter contribution to the whole H budget.

Method and previous results: We developed a method based on in-situ measurements of the C/H and D/H ratios of hydrated chondrite matrices by Secondary Ion Mass Spectrometer (SIMS) IMS 1280-HR [6]. This protocol allows the D/H ratios of hydrous chondritic minerals to be determined without hindrance from hydrogen in adjacent organic materials. Depending on the position of the SIMS primary beam on the matrix, the D/H and C/H ratios vary as a function of the relative amount of hydrated minerals to organics. Since the D/H ratio is higher for organics than for hydrated minerals in carbonaceous chondrites, correlations between the D/H and C/H ratios can be obtained and used to estimate the D/H ratio of water [6]. Using this method, we determined the D/H ratios of hydrated minerals in carbonaceous chondrites from different groups and petrological types. Results on six CM-type and three CV-type carbonaceous chondrites have been reported in [6] and [7], respectively. We recently obtained data for four new CM-type carbonaceous chondrites (Mukundpura, Jbilet Winselwan, Lonewolf Nunataks 94101 and Maribo), one CR chondrite (Renazzo), one CI chondrite (Orgueil) and two anomalous carbonaceous chondrites (Essebi and Bells).

Results: The isotope signature of the water component of most of the CM-type carbonaceous chondrites is D-poor (D/H = $[101 \pm 6] \times 10^{-6}$) [6]. This D-poor value indicates that water in CM chondrites is not inherited from the outer solar system contrary to water in comets [1], but has been equilibrated with H_2 in the inner disk before CM parent body accretion. On the least altered CM chondrites (Paris and to a lesser extent Maribo and LON 94101), the D/H ratio of water is less depleted in D. The D/H signtaure of hydrated phases present in the CM protolith before parent body alteration might have been partially preserved in these meteorites.

Water in CV-type carbonaceous chondrites (CV_{oxB}) shows less depletion in deuterium (D/H ≈ 144×10^{-6}) than CM chondrite water. CV chondrites might have partially accreted D-rich water ice grains from the outer solar system or the water D/H ratio in CV chondrite could have been modified by exchange with D-rich organics [7].

For Orgueil, Renazzo and in the ungrouped carbonaceous chondrites Bells and Essebi, the water D/H ratio is significantly higher than that of CM-type chondrite water (D/H ≈ 130 to 350×10^{-6}).

The hydrogen isotopic compositions of the different groups and types of chondrites will be compared to previous estimation of water in carbonaceous and ordinary chondrites and in other solar system objects [1, 8-10], and used to discuss the isotopic distribution of water in the proto-planetary disk at the time and place of the carbonaceous asteroid formation.

References: [1] Ceccarelli et al., (2014), in Protostars and Planets VI (University of Arizona Press). [2] Altwegg et al. (2015), *Science* **347**, 2–5. [3] Desch et al. (2018), *Astrophys. J. Suppl.* **238**, 11. [4] Alexander, C. M. O'D. (2017), *Philos. Trans. R. Soc. A Math. Phys. Eng. Sci.* **375**. [5] Le Guillou et al. (2014) *Geochim. Cosmochim. Acta.* **131**, 368–392. [6] Piani et al. (2018) *Nat. Astron.* **2**, 317–323. [7] Piani, L. & Marrocchi, Y. *Earth Planet. Sci. Lett.* **504**, 64–71 (2018) [8] Alexander et al., (2012) *Science* 337, 721–723. [9] Piani et al. (2015) *Earth Planet. Sci. Lett.* **415**, 154–164. [10] van Kooten et al., (2018) *Geochim. Cosmochim. Acta*. **237**, 79–102.

CARBONATES WITHIN LAFAYETTE.

J. D. Piercy[1], J. C. Bridges[1] and L. J. Hicks[1]. [1]Space Research Centre, University of Leicester, UK, LE1 7RH. Email: jdp32@leicester.ac.uk.

Introduction: The martian nakhlites contain a unique carbonate-bearing hydrothermal alteration assemblage. Lafayette hosts the most extensive secondary minerals, showing veins containing Ca-rich siderite, ferric saponite, Al-rich ferric serpentine, smectitic amorphous gel and minor ferric oxide [1, 2, 3]. The remaining 10 nakhlites display a variation in their secondary phases, this correlates with the nakhlite depth of formation model [4]. Studying these important alteration minerals is vital in preparation for missions like Mars2020. For instance, Jezero Crater shows carbonate-bearing outcrops [5]. Studying Lafayette carbonates as an analog will help optimise *in situ* measurements and analyses.

The Ca-siderite contained within Lafayette's olivine and mesostasis hosted assemblages display textures indicative of corrosion and replacement by saponite and serpentine respectively. This dissolution contributes to the evolving nature of the fluid just as the dissolution of olivine and mesostasis plagioclase does in the first stages of alteration. Interpretation of these carbonates informs us about the fluid history of the parent rock and thus the habitability of the associated environment. Since the source of CO_2 is ultimately the ancient martian atmosphere, carbonate minerals also allows us to help constrain past pCO_2 models of the martian atmosphere [6]. Here we report on the carbonate dissolution within Lafayette and the effect that has on the nakhlite fluid.

Methods: The thin section USNM 7849 was characterised using an FEI Quanta 650 FEG-SEM. Wafers suitable for Scanning Transmission Electron Microscopy (STEM) imagery were extracted using Focused Ion Beam (FIB) milling on a FEI Quanta 200 3D Dual FIB-SEM. STEM imagery was performed using a JEOL 7200 FEG-SEM. Fe-K X-ray Absorption Spectroscopy (XAS) was carried out using the I-18 microfocus and I-14 nanofocus spectroscopy beamlines at the *Diamond* synchrotron, UK.

Mineralogy and Textures: The thin section studied here contains the largest abundance, ~4 %, of martian meteorite carbonate yet reported. Two textural sites for carbonate show evidence of partial replacement by ferric phyllosilicates.

Mesostasis-hosted carbonate comprises ~3.2 vol% of the thin section and is found in interstitial areas. These areas display a texturally variable assemblage of carbonate and radial phyllosilicate (Fig. 1). The compositions of this carbonate $Mg_0Cc_{21-42.3}Sd_{57.7-78.9}Rh_{0-4.5}$ are metastable (Fig. 2). This range of compositions reflects a varying fluid composition where cations could be exchanged more readily than in the olivine fractures. The carbonate grains show veining within them where the evolving fluid has partially replaced it with saponite (Fig. 1; arrows).

Olivine-hosted carbonates are situated at the margins of sawtooth-shaped fractures. They compromise ~0.8 % of the thin section and up to ~6% of the olivine, the alteration phases can take up ~20 % of the olivine. The compositions of olivine carbonate are $Mg_0Cc_{27.3-28.8}Sd_{46.9-53.4}Rh_{19.2-24.2}$ and again metastable (Fig. 1). Identical replacement textures as seen in the mesostasis carbonate are present.

STEM Imagery: Dark Field (DF) imagery of a TEM wafer, taken from an olivine alteration vein, shows the boundary between the carbonate and saponite phases (Fig. 3), highlighting the saponite replacement of carbonate.

X-ray Absorption Analysis: Fe-K XANES analysis showed that the iron in the saponite and serpentine contains significant Fe^{3+} while olivine has an undetectable amount. Measurements of the carbonate also showed some ferric iron, consistent with partial dissolution and replacement by saponite.

Discussion: Our results show that as the nakhlite fluid cooled the carbonate precipitated in the mesostasis and olivine fractures. Once all HCO_3^- had been exhausted the carbonate formation stopped, the ferric fluid dissolved a significant proportion of the existing Ca-siderite, and saponite was precipitated.

The large carbonate content of 4 % observed within this Lafayette section, initially higher prior to the partial replacement by saponite and serpentine, if taken as an upper estimate on the possible average throughout the martian crust, equates to 2200 mbar pCO_2. Considering the thick ancient atmosphere model predicts ~400 mbar pCO_2 trapped as carbonate on current day Mars [8], this new upper limit is consistent with thick pCO_2 models for ancient Mars.

References: [1] Changela H. and Bridges J. (2011) *Meteoritics 45, 1847-1867.* [2] Hicks L. et al. (2014) *Geochimica et Cosmochimica Acta* 136, 194-210. [3] Bridges J. C. and Schwenzer S. (2012) *Earth and Planetary Science Letters* 359-360, 117-123. [4] Mikouchi, T. et al (2012) *LPSC XLIII*, Abstract #2363. [5] Ehlmann B. et al. (2008) *Science* 322, 1828-1832. [6] Bridges J. C. et al. (2019) *Volatiles on Mars,* Elsevier. 426pp. [7] Anovitz L. and Essene E. (1987) *Journal of Petrology* 28, 389-414. [8] Manning C. et al. (2006) *Icarus* 180, 38-59.
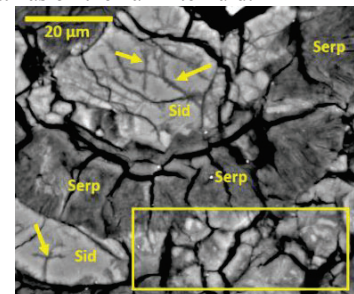

Figure 1 - BSE image of mesostasis assemblage showing siderite and serpentine. Dissolution and replacement textures (arrows and box) are shown.
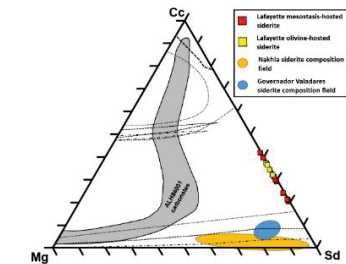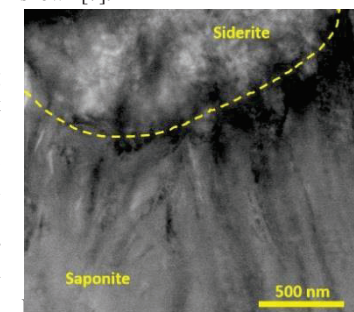

Figure 2 - Magnesite (Mg), Calcite (Cc), Siderite (Sd) ternary showing the compositions of Lafayette carbonates. ALH84001, Nakhla and Governador Valadares carbonate compositions are from [6]. Calculated stability fields for formation at 400 °C (dash-dot), 550 °C (dashed) and 700 °C (dotted) are also shown [7].

and saponite boundary (dashed line) from an olivine secondary assemblage.

OLIVINE ALTERATION IN SHERGOTTITE NORTHWEST AFRICA 10416.

J. D. Piercy[1], J. C. Bridges[1], L. J. Hicks[1], J. L. MacArthur[1], R. C. Greenwood[2] and I. A. Franchi[2], [1]Space Research Centre, University of Leicester, UK, LE1 7RH. Email: jdp32@leicester.ac.uk. [2]Planetary and Space Sciences, School of Physical Sciences, The Open University, Walton Hall, Milton Keynes MK7 6AA, United Kingdom.

Introduction: Secondary alteration phases in martian meteorites allow us to study martian hydrous processes and potential habitability, but first, it is crucial to discover the origin of any secondary alteration phases, martian or terrestrial. Here we report on the petrology and alteration history of the olivine-phyric shergottite, Northwest Africa (NWA) 10416, paying particular attention to the origin of the extensive aqueous alteration products identified in this meteorite.

Methods: A thin section was characterised using a FEI Quanta 650 FEG-SEM. A JEOL JXA-8200 Electron Microprobe was also used for EPMA-WDS analysis at the University of Nottingham. Wafers suitable for Transmission Electron Microscopy (TEM) were extracted using Focused Ion Beam (FIB) Milling on a FEI Quanta 200 3D Dual FIB-SEM and TEM was performed using a JEOL 2100+ at the University of Nottingham. Fe-K X-ray Absorption Spectroscopy (XAS) was carried out using the 2.5μm I-18 microfocus spectroscopy beamline at the *Diamond* synchrotron, UK. Oxygen isotopic analysis of NWA 10416 was performed using the infrared laser-assisted fluorination system at the Open University [1].

Olivine: Occurs in two forms, the ~1 mm, megacrysts bearing a distinctive zoned colouration, and smaller, ~400 μm, groundmass grains. The megacrysts display amber-coloured cores, brown mantle zones and clear rims (Fig. 1). We identified a gradual compositional trend across the grains that is consistent with relict igneous zonation, showing amber-coloured Mg-rich cores and clear rims of almost equal MgO and FeO content, Fo_{52}. Notably, the groundmass olivine shows no signs of zonation and has a large compositional range, Fo_{39-58}, which overlaps with the megacryst clear rims. EPMA-WDS analysis reveals that only the groundmass grains and megacryst clear rims are stoichiometric olivine, the coloured zones of olivine have low WDS totals, consistent with alteration and partial replacement.
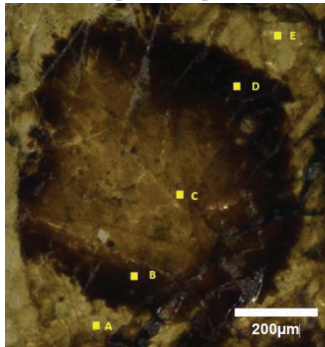

Figure 1 - *Optical image of olivine megacryst, labelled A to E are the locations corresponding to XAS data in Figure 2.*
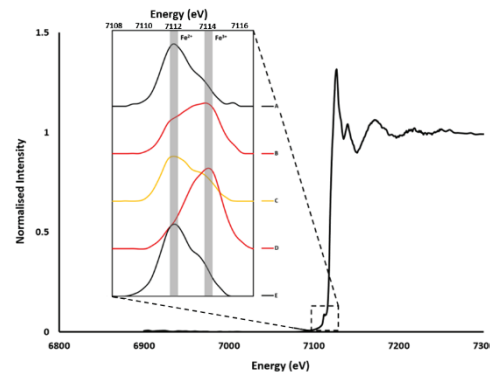

Figure 2 - *XAS data of Fe K XANES region. Lines A to E correspond to XAS sites shown in Figure 1.*
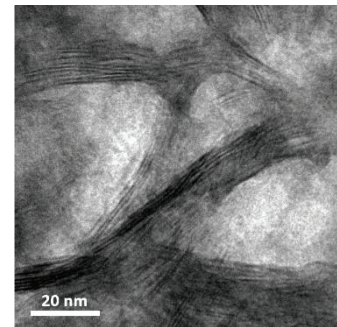

Figure 3 - *HRTEM image of alteration features seen in a shock-melt olivine grain. Image taken at ×150k magnification.*

X-ray Absorption Spectroscopy: was performed across a megacryst (Fig. 1) in order to gather information about the oxidation state of the different coloured zones. The results (Fig. 2) revealed that the coloured olivine has an increase in ferric iron compared to the clear rim (clear rim, $Fe^{3+}/\Sigma Fe = 0.03$; brown mantle zone, $Fe^{3+}/\Sigma Fe = 0.77$; amber core, $Fe^{3+}/\Sigma Fe = 0.24$).

TEM Analysis: A TEM wafer was taken from an olivine within a shock-melt vein in order to investigate the origin of the alteration. The hypothesis being that if fluid alteration features overprint the shock features then it is more probable that the water-rock interaction took place after the shock event and most likely on Earth. During analysis we did identify sporadic curved *d*-spacings (Fig. 3), characteristic of a flexible phyllosilicate structure, that were unaffected by any type of shock feature. The d-spacings were of a trioctahedral nature and were measured as 0.95 nm, consistent with dehydrated saponite. This presence of clay features, without disturbance by any shock features, suggests that the fluid alteration postdates the shock event and is therefore terrestrial in origin.

Oxygen Isotope Analysis: Bulk meteorite is $\delta^{17}O = +2.98$ ‰, $\delta^{18}O = +5.13$ ‰, and $\Delta^{17}O = +0.309$ ‰; and amber-coloured relict olivine, $\delta^{17}O = +2.68$ ‰, $\delta^{18}O = +4.63$ ‰, and $\Delta^{17}O = +0.272$ ‰. The bulk material essentially plots on the Martian Fractionation Line (=0.307 ‰) [2]. Amber-coloured olivine, average $\Delta^{17}O = 0.271 \pm 0.002$ (2σ) ‰, lies slightly closer to the TFL, consistent with some terrestrial fluid contamination from the NWA desert find locality.

Discussion: Mg-olivine is more susceptible to alteration than its Fe counterpart under oxidizing conditions [3,4] like those shown through our XAS analysis, when exposed to low T fluids. This could explain why the alteration is only within the Mg-rich megacryst cores. Shock effects caused veins and fracturing of the compositionally zoned olivines, and finally, during its time in NW Africa, groundwater exploited the fractures and altered the olivine in a way that was controlled by the pre-existing, igneous compositional zonation.

References: [1] Greenwood R. C. (2017) *Chemie der Erde - Geochemistry,* 77(1): 1-43. [2] Franchi I. A. et al. (1999) *Meteoritics & Planetary Science,* 34: 657-661. [3] Hausrath E. M. and Brantley S. L. (2010) *Journal of Geophysical Research, 115,* 2156–2202. [4] Wogelius R. A. and Walther J. (1992) *Chemical Geology,* 97(1-2): 101-112.

THE SHOCKING GROUND TRUTH OF LUNAR SAMPLES.

C. M. Pieters[1], T. Hiroi[1], G. Osinski[2] [1]Brown University, Dept. Earth, Environmental, and Planetary Sciences, Providence, RI, 02912 USA (Carle_Pieters@brown.edu), [2] Centre for Planetary Science and Exploration, University of Western Ontario, Canada

Introduction: Spectroscopic measurement of the Moon with remote sensors have been key in constraining the global properties of the lunar crust. Samples of lunar anorthosite returned during Apollo exhibit a well-defined diagnostic absorption near 1.25 µm due to trace amounts of ferrous iron in the crystal structure. It wasn't until spectroscopic instruments were flown to the Moon onboard Kaguya and Chandrayaan-1 that lunar surface areas of pure anorthosite were identified using this diagnostic signature. Previously, high albedo lunar areas that exhibit no absorptions from mafic minerals were interpreted to be anorthositic. The logic was that highly shocked feldspar loses its crystal structure becoming isotropic or so-called diiaplectic glass. This solid state non-crystalline form of plagioclase, called maskelynite, would thus not exhibit the crystalline plagioclase ferrous feature near 1.25 µm (and would of course also exhibit no absorption features from mafic minerals). This hypothesis describing 'featureless plagioclase' could unfortunately not be confirmed with samples. Only one clean sample of lunar maskelynite was obtained from a mineral separate of the highly shocked lunar gabbroic meteorite A881757. This natural maskelynite sample was not featureless; it exhibited distinct ferrous glass absorptions near 1 and 1.9 µm. Since 'featureless' lunar spectra acquired remotely from orbit exhibit a red-sloped continuum, other models that involve space weathering products were also proposed as possibe explanations (Lucey 2002, GRL; Yamamoto et al., 2015, JGRP).

Laboratory spectra of lunar anorthosite samples that exhibit extensive shock features petrographicaly (along with abundant maskelynite) were nevertheless shown to exhibit a clear crystalline 1.25 µm anorthosite diagnostic feature in the near-infrared (see examples in Figure 1). The one possible exception (61016,538) turned out to be a possible mixture (saw fines) from 61016, the large 'Big Muley' aluminous impact melt rock with a 'cap' of shocked anorthosite (e.g., Pieters et al., 2018, LPSC49 #1698). Additional samples of *only* the anorthositic cap of 61016 were requested and a new spectrum of coarse (1-3 mm) vitreous chips (61016,538) is also shown in Figure 1. Although the presence of trace amounts of pyroxene cannot be excluded yet, our initial interpretation is that this specific lunar sample is essentially pure maskelynite, which would make it only the second one recognized.

Work underway. We were allocated a special sample (,546) from the upper surface of the 61016 anorthosite cap (Figure 2). The small chip (443 mg) includes part of the exposed surface (exhibiting a patina) on one side and unexposed (shocked) anorthosite on the other. This sample is currently being measured in the RELAB. We have also obtained grain mounts coordinated with the particulate samples of Figure 1 to petrographically document and provide insight into their shock history in order to integrate and (we hope) clarify the shocked anorthosite story, and what it can tell us about lunar crustal evolution.
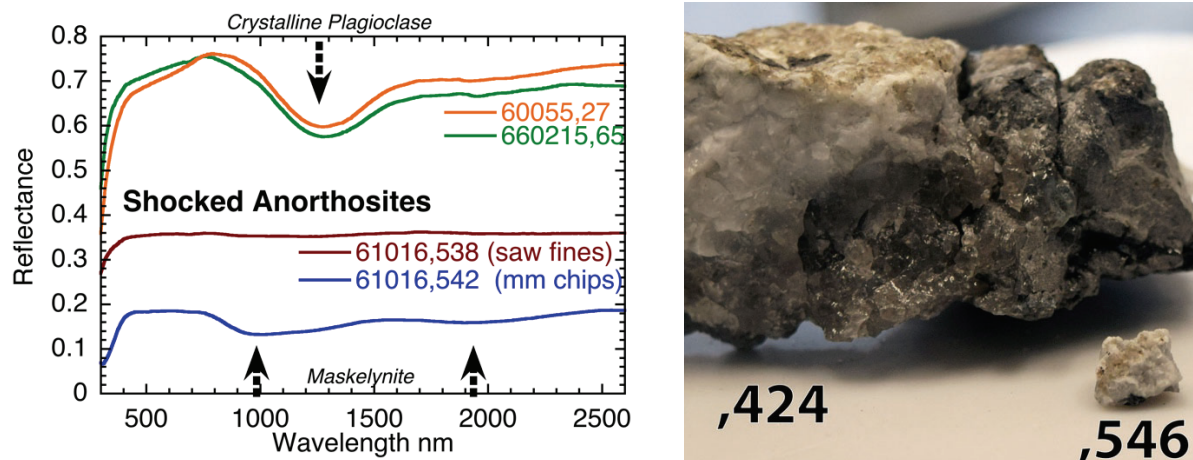

Figure 1 (left) Bidirectional reflectance spectra of particulate samples of lunar anorthosites that have been described as exhibiting extensive shock features. Diagnostic absorption bands of crystalline plagioclase (~1.25µm) and maskelynite (~1 and 1.9 µm) are indicated.

Figure 2 (right) Image of the 6 mm chip 61016,546 obtained from the upper surface of the anorthositic 'cap' of the large 61016 'Big-Muley' Apollo 16 sample.

PROTOSOLAR CLOUD COLLAPSE AND REDISTRIBUTION OF [26]AL

F.C. Pignatale[1,2], , E. Jacquet[2], M. Chaussidon[1], S. Charnoz[1]
[1]Université de Paris, Institut de Physique du Globe de Paris, CNRS, 1 rue Jussieu, 75005 Paris, FRANCE
[2]Muséum national d'Histoire naturelle, Institut de Minéralogie, Physique des Matériaux et de Cosmochimie, Département Origines et Evolution, UMR 7590, CP52, 57 rue Cuvier, 75005, Paris, FRANCE

Introduction: Ca-Al-rich inclusions (CAIs), chondrules and matrix in individual chondrites are diverse in thermal history and isotopic compositions [1]. Isotopic analysis, in particular Al-Mg systematics, suggests a short interval of formation for CAIs, in the order of ~150 kyr, from precursor condensates that may have formed in an even shorter interval of time [2-4]. The retrieved timescales are comparable with those of the collapse of a cloud parental to a protoplanetary disk [5] and suggests that the oldest chondrite components formed during that epoch. Following the work of [6,7], [8] studied the distribution and thermal alteration of dust (of different chemical compositions) during their transport from the collapsing cloud to the forming disk, and found extensive evaporation of infalling matter, recondensing in condensates, many of which were advected toward the outer disk and mixed with unprocessed dust, in agreement with the compositional gradient for major families of chondrites [1] and the old age of CAIs. However, the widely used Al-Mg chronology [4] is predicated on the uniformity of the $^{26}Al/^{27}Al$ ratio, which is called into question by apparently old yet ^{26}Al-poor CAIs such as FUN CAIs [9]. This suggests that the parental cloud was itself heterogeneous in ^{26}Al, hence the importance of investigating the distribution of different reservoirs of ^{26}Al within the cloud and the transport and incorporation of ^{26}Al in the Solar System solids that populate the forming disk.

Method: We [10] use the model presented in [8], and study how different ^{26}Al-distributions within the collapsing cloud are redistributed in different refractory dust components (CAIs and bulk material) in the forming disk. In terms of the $^{26}Al/^{27}Al$ ratio, we considered both a monotonic zoning (with a plateau) and a spike profile, both reaching a maximum around $t = 80$ kyr consistent with the timescale of CAI production [8]. Our 1D disk model includes several processes such as gas and dust condensation/evaporation, dust growth/fragmentation, radiative and viscous heating, dead zone and cloud infall in the form of a source term [8].

Results: We find that CAIs essentially inherit the $^{26}Al/^{27}Al$ ratio of the matter infalling at the time of their formation, so that variations of $^{26}Al/^{27}Al$ among FUN and normal CAIs can be accounted for, without requiring any supercanonical reservoir anywhere. The prevalence of a canonical ratio among normal CAIs, the fact that bulk chondrites show a near-canonical $^{26}Al/^{27}Al$ ratio, and the ^{26}Al level required for the differentiation of the first planetesimals suggest a scenario where ^{26}Al sharply rose relatively close to the center of the protosolar cloud and essentially remained at a high level outward (rather than having decreased since). As the ^{26}Al abundance would be relatively homogeneous after cessation of infall, this would warrant the use of the ^{26}Al-^{26}Mg chronometer from the formation of normal CAIs onward, to chondrules and chondrite accretion.

References: [1] Scott, E.R.D., 2007, Annual Review of Earth and Planetary Sciences, 35, 577. [2] Connelly, J. N., Bizzarro, M., Krot, A. N., et al. 2012, Science, 338, 651. [3] Jacobsen, B., Yin, Q.-z., Moynier, F., et al. 2008, Earth and Planetary Science Letters, 272, 353. [4] Mishra, R. K., & Chaussidon, M. 2014, Earth and Planetary Science Letters, 390, 318. [5] Williams, J. P., & Cieza, L. A. 2011, ARA&A, 49, 67. [6] Hueso, R., & Guillot, T. 2005, A&A, 442, 703. [7] Yang, L., & Ciesla, F. J. 2012, Meteoritics and Planetary Science, 47, 99. [8] Pignatale F. C. et al. (2018). ApJL, 867:L23. [9] MacPherson, G.J., Davis, A.M., Zinner, E.K.,1995, Meteoritics, 30, 365. [10] Pignatale F. C. et al., submitted to ApJ.

PRIMORDIAL WATER AND DUST OF THE SOLAR SYSTEM: INSIGHTS FROM *IN-SITU* OXYGEN MEASUREMENTS OF CI CHONDRITES

M. Piralla[1], Y. Marrocchi[1], M. J. Verdier-Paoletti[2,3], L. G. Vacher[1,4], J. Villeneuve[1], L. Piani[1], D. V. Bekaert[1] and M. Gounelle[2], [1]CRPG, CNRS, Université de Lorraine, UMR 7358, Vandoeuvre-lès-Nancy, 54501, France (maxime.piralla5@etu.univ-lorraine.fr), [2]IMPMC, CNRS & Muséum national d'Histoire naturelle, UMR 7590, CP52, 57 rue Cuvier, 75005 Paris, France, [3]DTM, Carnegie Institution for Science, Washington, DC, 20015, USA, [4]Department of Physics, Washington University in St. Louis, St. Louis, MO, USA

Introduction: CI chondrites are fundamental meteorites, as their chemical compositions closely resemble to that of the Sun's photosphere [1]. Measuring their oxygen isotopic compositions is fundamental to constrain the origin and dynamics of dust and water ice grains in the protoplanetary disk [e.g., 2-3]. However, subsequent parent body fluid circulation processes make difficult straightforward estimation of the primordial isotope composition of CI chondritic water and anhydrous minerals.

Materiel and methods: We determined the oxygen isotopic composition of mechanically-isolated olivine and carbonate grains from the Orgueil CI chondrite with a SIMS CAMECA 1270 E7. $^{16}O^-$, $^{17}O^-$, and $^{18}O^-$ ions produced by a Cs^+ primary ion beam (~15 μm, ~4 nA) were measured in multi-collection mode using three Faraday cups.

Results: Our results show that orgueil olivine grains are Mg-rich with Fo88-95 and show low abundances of trace elements such as CaO ($\leq$ 0.2 wt%). All olivine grains but one show Earth-like O-isotopic compositions ($\Delta^{17}O$ = 0 ‰) plotting at the intersection of the TFL and PCM, the other standing on the latter. Ca-carbonates (calcite and dolomite) define a trend with $\delta^{17}O = 0.50$ ($\pm$ 0.05) $\times$ $\delta^{18}O + 0.9$ ($\pm$ 1.4) that is indistinguishable from TFL.

Discussion: The CI chondrites are the only subgroup of chondrites that do not contain chondrules, even pseudomorphosed. It has been proposed that mafic minerals from CIs correspond to (i) chondrule fragments or (ii) grains formed by condensation processes. Our petrographic and isotopic results demonstrate that (i) chondrules likely represent a significant constituent of CIs before the onset of aqueous alteration, (ii) the proportion of iron-rich olivine grains was significantly higher in CIs than in other carbonaceous chondrites (CCs) and (iii) cometary materials could have sampled mafic minerals with similar features than those observed in CI chondrites.

The Ca-carbonates trend is statistically different from mass-independent fractionation lines defined by secondary phases in other CCs [e.g., 4-5]. At the exception of magnetite, all other secondary phases point toward a CI primordial water characterized by terrestrial-like isotopic composition as also inferred from pyrolysis [6] and clumped-isotope thermometry of CO_2 (Δ^{47}; [7]).

All together, the O-isotopic composition of CI water does not show significant $^{17,18}O$ enrichments as expected if the CI parent body had formed in regions of the Solar System where self-shielding of UV light by ^{16}O-rich nebular CO would have produced a ^{16}O-poor water [8]. Instead, CI water is characterized by near-Earth O-isotope compositions. If CCs were accreted beyond the orbit of Jupiter as suggested by Mo and Ni isotopic systems [9-10], this suggests that the oxygen isotope composition of water in the outer Solar System was not as ^{16}O-depleted with respect to the inner Solar System. In addition, CI anhydrous silicates show terrestrial values ($\Delta^{17}O \sim 0$), implying that the different constituents of CI chondrites all had near-Earth isotopic compositions. Although CI chondrites are slightly depleted in oxygen relative the Sun's photosphere, our data, however, define a fundamental paradox where CIs are chemically solar but isotopically terrestrial. Such results can be taken as a strong argument in favor of a scenario where the primordial dust of the Solar System would be ^{16}O-poor, with $\Delta^{17}O \sim 0$, relative to the ^{16}O-rich nebular gas [11]. In this scenario, ^{16}O-rich and ^{16}O-poor reservoirs could have co-existed in the protoplanetary disk with the nebular regions characterized by enhanced dust/gas ratio being ^{16}O-poor relative to solar due to the overabundance of ^{16}O-poor solids. Our data show that CI chondrites have Earth-like O-isotopic compositions, confirming that primordial dust of the Solar System could correspond to CI-like material, characterized by a ^{16}O-poor isotopic composition.

References: [1] Lodders K. (2003) *The Astrophysical Journal* 591:1220–1247. [2] Vacher L. G. et al. (2016) *The Astrophysical Journal Letters* 827:1–6. [3] Marrocchi Y. et al. (2018) *Earth and Planetary Science Letters* 496:132-141. [4] Vacher L. G. et al. (2017) *Geochimica et Cosmochimica Acta* 213:271–290. [5] Verdier-Paoletti M. J. et al. (2017) *Earth and Planetary Science Letters* 458:273–281. [6] Baker L. et al. (2002) *Meteoritics & Planetary Science* 37:977–985. [7] Guo W. and Eiler J. M. (2007) *Geochimica et Cosmochimica Acta* 71:5565–5575. [8] Clayton R. N. (2002) *Nature* 415:860–861. [9] Kruijer T. S. et al. (2017) *Proceedings of the National Academy of Sciences* 114:6712-6716. [10] Nanne J. A. M. et al. (2019) *Earth and Planetary Science Letters* 511:44–54 [11] Krot A. N et al. (2010) *The Astrophysical Journal* 713:1159–1166.

TWINNING AND AMORPHIZATION IN NATURALLY SHOCKED PLAGIOCLASE: AN EBSD STUDY.

L. Pittarello[1], L. Daly[2], L. Ferrière[3], P. Chung[2], A. E. Pickersgill[2], and M. R. Lee[2], [1]Department of Lithospheric Research, University of Vienna, Austria (lidia.pittarello@univie.ac.at), [2]School of Geographical and Earth Sciences, University of Glasgow, United Kingdom, [3]Natural History Museum, Vienna, Austria.

Introduction: Even though plagioclase is one of the most common minerals in the crust of terrestrial planetary bodies, its response to shock metamorphism is not yet fully constrained. In particular, the occurrence of planar deformation features (PDFs) in plagioclase has been almost exclusively described in shocked rocks from terrestrial impact structures, rarely in meteorites and very rarely reproduced in experiments (e.g., [1-3]). In this work, we focus on a shatter cone sample from the central uplift of the Manicouagan impact structure, Canada (e.g., [4]), which contains shocked plagioclase, characterized by extensive micro-twinning (e.g., [5]) and planar features that were reported as optically consistent with PDFs [6-8] or as possible PDFs [9]. Electron back-scatter diffraction (EBSD) was used to determine the crystallographic orientation and the crystallinity of shocked plagioclase grains, and to quantitatively describe the progression of shock amorphization in plagioclase.

Methods: A petrographic thin section from sample WMM-102A-64C1 was prepared for EBSD after a preliminary survey by optical microscopy. EBSD data were collected using a Zeiss Sigma variable pressure field emission scanning electron microscope (VP-FEG-SEM) equipped with an Oxford Instruments NordlysMax[2] EBSD detector at the ISSAC microscopy facility (University of Glasgow). Plagioclase crystals that were observed to contain shock microstructures in optical microscopy images were mapped. Crystallographic information was extracted from the EBSD data using the Channel 5 software package and noise reduced using a wildspike and 6 point nearest neighbor correction. Finally, the orientation of twins was graphically related to rational crystallographic orientations, according to the more common twinning rules and to the occurrence of PDFs in plagioclase as reported in the literature.

Results: Sample WMM-102A-64C1 is a garnet-bearing metagranite comprised of plagioclase, garnet, biotite, quartz, and accessory phases. Shock metamorphic effects in plagioclase include general decrease in birefringence and development of fine-grained twins, which locally might be optically (mis)interpreted as PDFs. These pseudo-PDFs are organized in crosscutting, multiple sets, with <10 μm spacing and thicknesses of 1-2 μm, consisting of amorphous material, as highlighted by EBSD analysis. The most common amorphous set is oriented along {010}, with further amorphous sets oriented along {100} or {1-20} that contain patches of crystalline material with a twin relationship to the host mineral. Correlated energy dispersive X-ray spectroscopy element maps indicate that concentrations of Na, Ca, and K do not differ between twins and within the same crystal.

Discussion and conclusions: In quartz, PDFs are straight and narrow (<200 nm), closely spaced (< 1μm), parallel amorphous lamellae, which develop along rational crystallographic planes (e.g., [10-11]). Even though they have been extensively studied in the last decades, their formation mechanism is still debated. For comparison, optically isotropic sets of lamellae in shocked plagioclase with similar characteristics to PDFs in quartz are generally described as PDFs, without further investigation. Our observations suggest that in the sample WMM-102A-64C1, amorphous lamellae in plagioclase all follow known twin relationships and have formed as shock-induced (compressional stage) micro-twins in plagioclase, commonly nucleating at grain boundaries. The incomplete or selective amorphization (due to shock decompression) of these twins supports the fact that shock amorphization is controlled by the crystallographic orientation, as already suggested by [1]. All these sets are oriented along the most common orientations attributed to PDFs [1], but are also consistent with plagioclase twin rules. Optically, the amorphous twins might be easily mistaken for PDFs and we cannot exclude that in the literature based on optical observations alone they were described as PDFs. The orientation of each twin or whole crystal relative to the local shock wave scattering determines the shock response of the crystal. This effect may be weakened or strengthened due to the nature of the surrounding phases with different impedance, such as other plagioclase crystals but with a different orientation or other minerals (quartz, garnet). Amorphization in plagioclase is initiated along microtwins that are oriented favorably with respect to the local shock wave propagation direction. Observations limited to optical microscopy might lead to the interpretation of such microtwins as PDFs. Whether these features can be considered PDFs and whether PDFs in quartz might also form initially as twins remain open questions that require further investigations.

References: [1] Stöffler D. (1967) *Contrib Mineral Petr* 16:51-83. [2] Ostertag R. (1983) *J Geophys Res* 88:B364-B376. [3] Huffman A.R. et al. (1993) *J Geophys Res* 98:22171-22197. [4] Spray J.G. et al. (2010) *Planet Space Sci* 58:538-551. [5] Pickersgill A.E. (2015) *Meteorit Planet Sci* 50:1546-1561. [6] Dworak U. (1969) *Contrib Mineral Petr* 24:306-347. [7] Dressler B. (1990) *Tectonophysics* 171:229-245. [8] White J.C. (1993) *Contrib Mineral Petr* 113:524-532. [9] Ferrière L. and Osinski G. R. 2013. In: *Shock metamorphism. In Impact cratering: Processes and products* (G.R. Osinski and E. Pierazzo E. Eds.) Wiley-Blackwell, Chichester. pp. 106–124. [10] Engelhardt W.v. and Bertsch W. (1969) *Contrib Mineral Petr* 20:203-234. [11] Stöffler D. and Langenhorst F. (1994) *Meteorit Planet Sci* 29:155-181.

COMPARISON OF DIFFERENT SPECTROSCOPIC TECHNIQUES IN INVESTIGATING SHOCKED PLAGIOCLASE.

L. Pittarello[1] J. Fritz[2], J. Roszjar[3], C. Lenz[4], C. Chanmuang N.[4], and C. Koeberl[1,3], [1]Department of Lithospheric Research, University of Vienna, Austria (lidia.pittarello@univie.ac.at), [2]Saalbau Weltraum Projekt, Heppenheim, Germany, [3]Natural History Museum, Vienna, Austria, [4]Institute of Mineralogy and Crystallography, University of Vienna, Austria.

Introduction: Shock metamorphism is important in the history of the Solar System. The transformation of plagioclase, one of the most abundant minerals on the surface of terrestrial planetary bodies, into diaplectic glass [1] (often referred to as maskelynite for plagioclase composition [2-4]) is commonly used together with shock effects in olivine to evaluate the degree of shock metamorphism in meteorites (e.g., [5-6]). Amorphization of plagioclase is generally identified with measurement of its refractive index with the optical microscope ([7-8] and references therein). However, this technique has been progressively supplemented by more rapid methods based on X-ray diffraction (e.g., [9,10]) and visible/near-infrared spectroscopy [11]. Raman spectroscopy (e.g., [12] and cathodoluminescence (CL) [13-16] are further spectroscopic techniques that have been proposed to characterize shock effects in plagioclase. Here, we apply several spectroscopic techniques, including micro-Raman spectroscopy, cathodoluminescence, and photoluminescence (PL; e.g., [17]), combined with optical and electron microscopy, to characterize the degree of amorphization in experimentally shocked plagioclase.

Methods: A circular slab (15 mm in diameter and 0.6 mm thick) of troctolite (sample B59- 36-A) was shocked using the reverberation technique at 28 GPa, after pre-cooling to 77 K, at the Ernst Mach Institute for High-Speed Dynamics in Freiburg, Germany [18]. Hand-picked plagioclase-bearing clasts, mounted and polished for petrographic studies, were investigated by micro-Raman spectroscopy and PL (Institute of Mineralogy and Crystallography, University of Vienna), optical CL (Department of Lithospheric Research, University of Vienna), and scanning electron microscope (SEM)-CL and spectral CL (Natural History Museum, Vienna). Major and minor element composition of the selected grains was additionally analyzed with a CAMECA SFive field-emission electron microprobe (Department of Lithospheric Research, University of Vienna).

Results: Three plagioclase clasts out of the eight selected from the investigated sample, all with composition $An_{55\pm1}$ and lacking of chemical zoning, exhibit remaining patchy crystallinity, whereas the others are completely isotropic. Amorphous domains are characterized by substantial peak broadening as observed for the major Raman modes of plagioclase via confocal Raman spectroscopy and for crystal-field split PL emissions of Nd^{3+}. Optical and panchromatic CL highlight the presence of abundant luminescence centers, which do not correspond to visible inclusions, in domains with remaining optical birefringence. The isotropic domains show a dark blue luminescence. SEM-CL spectra of the birefringent plagioclase display emission bands, which can be assigned to Mn and Fe substitutions. These bands are progressively broadened and finally disappear in optically isotropic domains, even though the related trace element abundances do not show any variation.

Discussion and conclusions: The observed heterogeneous distribution of amorphous domains within single, shocked grains further supports the importance to evaluate shock effects on a statistically meaningful number of grains using a variety of techniques. Whereas optical microscopy allows a first approximation of the amorphization of plagioclase and with contribution from the whole thickness (30-40 μm) of the thin section, spectroscopic techniques provide structural information down to a few μm from the surface. The comparably high spatial resolution may be favored among the classical application of optical microscopy to highlight local effects. Furthermore, Raman, PL and CL spectroscopy is not restricted to petrographic thin-sections, but allows the application to grains or polished samples to evaluate shock effects in valuable rocks, without requiring the preparation of a thin section.

References: [1] v. Engelhardt W. et al. (1967) *Contrib Mineral Petr* 15:93-102. [2] Tschermak G. (1872) LXV *B. der Sitzb. der k. Akad. der Wissenschaft* 1:1-29. [3] Binns R.A. (1967) *Nature* 213:1111-1112. [4] Ferriere L. and Brandstätter F. (2015) 78th Annual Meeting of the Meteoritical Society, Abs. #5184. [5] Stöffler D. et al. (1991) *Geochim Cosmochim Ac* 55: 3845-3867. [6] Fritz J. et al. (2017) *Meteorit Planet Sci* 52:1216-1232. [7] Stöffler D. (1967) *Contrib Mineral Petr* 16:51-83. [8] Gibbson R.V. and Ahrens T.J. (1977) *Phys Chem Miner* 1:95-107 [9] Hörz F. and Quaide W.L. (1973) *Moon* 6:45-82. [10] Sims M. et al. (2019) *Earth Planet Sc Lett* 507:166-174. [11] Johnson J.R. et al. (2003) *Am Mineral* 88:1575-1582. [12] Fritz J. et al. (2005) *Antarctic Meteor Res* 18:96-116. [13] Kaus A. and Bischoff A. (2000) *Meteorit Planet Sci* 35:A86. [14] Götte T. (2009), pp. 45-60, and [15] Götze J. (2009), pp. 87-110, In: *Cathodoluminescence and its application in the planetary sciences*, Gucsik A. Ed. Heidelberg: Springer-Verlag. [16] Kayama M. et al. (2018) *Meteorit Planet Sci* 53:1476-1488. [17] Lenz C. et al. (2019) *Front Chem* doi:10.3389/fchem.2019.00013. [18] Fritz J. et al. 2019 *Meteorit Planet Sci* doi:10.1111/maps.13289.

A SURVEY OF ZIRCON MICROTEXTURES IN THE ROCHECHOUART IMPACTITES

A. Plan[1], P. Lindgren[1], P. Lambert[2]. [1]Lunds University, Department of Geology, *Sölvegatan 12, 223 62, Lund, Sweden, email: anders.plan@geol.lu.se* [2]CIRIR - Center for international Research and Restitution on Impacts and on Rochechouart, *87600 Rochechouart, France, email: lambertbdx@gmail.com*

Introduction: The Rochechouart impact structure recently dated at 207 Ma [1], is emplaced in a granitic-gneissic crystalline basement at the western margin of the Hercynian Massif Central in France. Impact deposits are still preserved in a 12 km zone, filling the central depression of an eroded complex crater interpreted as a peak ring structure that initially reached 50 km in diameter or more [2]. It contains a variety of impactites ranging from lithic breccias to melt-bearing breccias and coherent melts [3,4] and has lately been the target of an international scientific drilling campaign under the scope of the *Center for international Research and Restitution on Impacts and on Rochechouart* (CIRIR) [5]. This ongoing study is part of the CIRIR team effort and has focussed on the survey of zircon microtextures in various impact lithologies from Rochechouart.

Samples and Methods: Impactite surface samples – ranging from lithic breccias to coherent melt – were collected at seven localities within the Rochechouart impact structure, and an unshocked gneiss was sampled below the crater floor. From these samples, thin sections were manufactured, and zircon was separated via conventional Wilfley-table techniques. For each investigated rough sample, grains were divided into either translucid or stained, based on their appearance under binocular microscope. So far, SEM-BSE studies have been made on rough surface zircon separates from four lithologies: (i) unshocked gneiss from Moulin la Brousse used as a control sample, (ii) a clast of shocked gneiss included in melt bearing breccia from Puy de Chiraud, (iii) melt-bearing impact breccia from Chassenon, and (iv) impact-melt from Babaudus. Also, zircons in three Chassenon (iii) thin sections have been studied under SEM-BSE.

Result: All impactites (ii-iv) display shock features under petrographic microscope e.g. planar deformation features (PDFs), ballen- and mosaicism texture in quartz, whereas the 'control sample' (i) displays no shocked features, and will be utilized as a guideline for comparing unshocked- and shocked zircons. Zircons separates in the unshocked gneiss are mainly subhedral with sizes ranging from c. 60-150 µm. The stained populations have more rugged surfaces which may be remnant imprints from accessory phases e.g. apatite. No impact-related textures are distinguishable. Contrarily, the shocked gneiss generally displays a variety of textures, distinguished as impact signatures. Grains are mainly subhedral and ovoid, with sizes ranging from c. 50-160 µm. Both the translucid- and stained populations have similar textural characteristics but are more distinct in the latter: Single- or traversed curviplanar to planar fractures (PFs), oriented c. 40°-90° and/or c. 120° perpendicular to the c-axis. Granularization occurs at various degrees, commonly propagating from structural weaknesses i.e. PFs and lattice termination. In rough surface imagery, only a few grains in the stained population from the melt-bearing impact breccia (iii) exhibits faint traversed PFs. Grains have ovoid and oblong irregular shapes, with sizes between c. 50-120 µm. Their appearances are similar to the stained zircons from the unshocked gneiss. However, in thin section imagery, zircons affiliated with lithic clast are euhedral with sharp crystal boundaries or with shattered irregular shapes, both display well-defined to faint PFs. Further, skeletal zircons with spongey textures and granular zircons occurs in association with the groundmass i.e. impact melt. The Babaudus zircons (iv) have sizes ranging from c. 50-230 µm, with mainly subhedral and oblong morphologies. All grains in the stained population displays granular textures i.e. the crystals surface are entirely covered by a myriad of disorderly arranged cryptocrystalline aggregates, consisting of neoblastic zircon crystallites (<1-2 µm). About 40% of these zircons are to various degrees encased within a quartzofeldspathic microcrystalline mass, similar to the Babaudus groundmass. The translucid population is scarce in comparison, lacks granular texture, and overall has a smooth but rugged surface. Rough surface features on one grain consist of needle-shaped (acicular) ornaments, which can either resemble angular- or irregular lattice engravings.

Future work: The granular zircons in Chassenon (iii) and Babaudus (iv) will be the focus of future electron backscatter diffraction (EBSD) analyses to distinguish whether they are so called FRIGN (former reidite in granular neoblastic) zircons [6]. It is important to determine the behaviour and response to shock in zircon since this mineral is a candidate for impact age determination via the U-Pb system, e.g. see recent work on shocked zircons in the Babaudus melt from Rochechouart [7].

References: [1] Cohen B.E. et al. 2017. *Meteoritics & Planetary Science* 52:1600-1611. [2] Lambert P. et al. 2019 *50th LPSC*, Abstract#2005. [3] Lambert P. (2010) *GSA* 465:509-541. [4] Sapers H. M. et al. 2014 *Meteoritics & Planetary Science* 49:2152-2168. [5] Lambert P. et al 2017 *48th LPSC*, Abstract#1936. [6] Cavosie A. J. et al. 2018 *49th LPSC,* Abstract#1816 [7] Rasmussen R. and Stockli D. F. (2019) *50th LPSC*, Abstract#2820.

INVESTIGATION OF THE HYDRATION FEATURES OF ASTEROIDS WITH CARBONACEOUS CHONDRITES: EXPERIMENTAL ANALYSIS AND COMPARISON WITH ASTRONOMICAL OBSERVATIONS.

S. Potin[1], P. Beck[1,2], L. Bonal[1], F. Usui[3], P. Vernazza[4], B. Schmitt[1], [1]Institut de Planétologie et d'Astrophysique de Grenoble (IPAG), 414 rue de la Piscine, 38400 Saint-Martind'Hères, France (sandra.potin@univ-grenoble-alpes.fr). [2]Institut Universitaire de France. [3]Center for Planetary Science, Graduate School of Science, Kobe University, 7-1-48 Minatojima-Minamimachi, Chuo-Ku, Kobe 650-0047, Japan. [4]Laboratoire d'Astrophysique de Marseille (LAM), 38 rue Frédéric Joliot Curie, 13013 Marseille, France.

Introduction: C-complex asteroids make for 2/3 of the total mass of the Main Belt Asteroids (MBAs) and their low reflectance value suggest a primitive composition, rich in carbon and volatiles elements [1].Two space missions are currently orbiting C-complex Near-Earth Asteroids (NEAs): OSIRIS-REx around (101955) Bennu [2] and Hayabusa2 around (162173) Ryugu [3]. While 50% of C-complex MBAs show signs of hydration features in their reflectance spectra [4], such hydration bands are detected on only a few percents of NEAs [5]. All small Solar System bodies have experienced heating in their lifetime [6] and temperature on the surface of NEAs is generally higher than MBAs because of their closer distance to the Sun [7]. We focus here on laboratory investigation of the effect of heating on the reflectance spectra of carbonaceous chondrites. Our results will be compared to telescopic observations of C-complex MBAs and NEAs.

Samples and methods: 13 carbonaceous chondrites (10 CM, 1 CR, 1 CV and 1 CI) have been selected for the experiment given their type and petrographic grade. After manual powdering, each sample is set in an environmental chamber and put under secondary vacuum to remove the adsorbed molecular atmospheric water. Reflectance spectra from the visible to near-infrared [8] are acquired inside the cell under vacuum and at room temperature, before and after having heated the sample up to 250°C for 1.5 hour.

Results: It is observed that heating results in *(i)* reducing iron-related bands at 0.7 and 0.9µm, *(ii)* modifying the spectral slope, and *(iii)* reducing the amplitude and broadness of the -OH 2.7µm signature. The shape of the -OH band is also modified, changing from round to sharp. Interestingly, the most acqueously altered chondrites show the smallest variations of the 2.7µm band along heating. Spectral fitting is performed to separate the different components of the hydration band: -OH groups in hydrated minerals like phyllosilicates, and/or molecular water adsorbed and/or strongly trapped in minerals [9]. The model shows that the varying shape of the 2.7 µm band is due to the removal of the free and coordinated water, leaving the sharp unaltered phyllosilicates component to appear. A deepening of the organics feature around 3.4µm is also observed along heating of each considered chondrite. Raman spectroscopy of the initial and heated samples testifies of a reorganization of the polyaromatic carbonaceous matter with heating.

Comparison with telescopic observations: The 2.7µm bands obtained on the heated carbonaceous chondrites are compared to astronomical observations of C-complex asteroids from the Main Belt with the AKARI space telescope [10]. Reflectance spectra of the two NEAs Ryugu and Bennu are also compared to our measurements. The band center and amplitude are consistent between the measured meteorites spectra and the observations, but differences are found when comparing the broadness and sharpness of the 2.7µm band. This effect could be assigned to the short heating time imposed by our experiment, and effects of long-term heating are currently under study.

Conclusion: Hydration features on the reflectance spectra of laboratory thermally altered carbonaceous chondrites are consistent with astronomical observation of MBAs and NEAs, though the effect of long-term heating is still to be studied in the laboratory. The procedure of spectral fitting used on the meteorites spectra is currently being applied to asteroids observations, with the objective to distinguish the type of hydration on the surface of the small bodies.

References: [1] Vilas, F. and Smith, B. (1985) *Icarus* 64:503-516. [2] Kitazato, K. et al. (2019) *Science* 10.1126/science.aav7432. [3] Hamilton, V.E. et al. (2019) *Nature Astronomy* 3:332-340. [4] Fornasier, S. et al. (2014) *Icarus* 233:163-178. [5] Rivkin, A.S. and DeMeo, F.E. (2019) *Journal of Geophysical Research: Planets* 124:128-142. [6] Keil, K. (2000) *Planetary and Space Science* 48:887-903. [7] Marchi, S. et al. (2009) *Monthly Notices of the Royal Astronomical Society* 400:147-153. [8] Potin, S. et al. (2018) *Applied Optics* 57:8279-8296. [9] Frost, R. L. et al. (2000) *Thermochimica Acta* 346:63-72. [10] Usui, F. et al. (2019) *Publications of the Astronomical Society of Japan* 71:1-41.

THE EFFECTS OF TERRESTRIAL WEATHERING ON SAMARIUM-NEODYMIUM ISOTOPIC COMPOSITION OF CHONDRITES

H. Pourkhorsamdi*[1,2], V. Debaille[1], R. M. G. Armytage[1,3], M. van Ginneken[4], P. Rochette[2] and J. Gattacceca[2]
[1]Laboratoire G-Time, Université Libre de Bruxelles, Brussels, Belgium. [2]Aix-Marseille Univ, CNRS, IRD, Coll France, INRA, CEREGE, Aix-en-Provence, France. [3]Jacobs/JETS, NASA Johnson Space Center, Houston, USA. [4]RBINS, Brussels, Belgium.
*E-mail: hamed.pourkhorsandi@ulb.ac.be

Introduction: Following their fall to Earth, meteorites experience weathering. During this process, their mineralogy and chemical composition can be deeply modified [e.g. 1]. Most studies about meteorite weathering have dealt with mineralogy and major elements geochemistry. Fewer studies also have focused on particular trace elements such as Ba, Sr, and REE [2, 3]. The number of the studies is even more limited when it comes to isotopic investigations. However, paucity of information in this topic does not correlate with its importance.

The systematics of rare earth elements (REE) and Sm-Nd isotopic pairs are the basis for petrogenetic and radiometric dating studies of terrestrial and extra-terrestrial rocks. As a result of their slightly different nuclear and chemical properties, the REE respond to common petrological processes, such as partial melting and partial evaporation, by developing fractionated light-REE (from La to Sm) or heavy-REE (from Eu to Lu) enriched elemental patterns [e.g. 4]. Despite their importance in cosmochemical studies, REE and especially Sm-Nd isotopic system have been rarely studied in a systematic manner to track meteorite weathering effects on their composition.

In this study we aim to systematically evaluate REE composition of ordinary chondrites from the Antarctic cold desert and Atacama (Chile) and Lut (Iran) hot deserts. We also analyzed the Sm-Nd isotopic systematics of the meteorites with heavily affected REE compositions.

Results: In comparison to the Antarctic meteorites, hot desert samples show greater disturbances and REE fractionation relative to the average fall values. Similar to Antarctic samples, ΣREE contents in the hot deserts meteorites is lower than the average fall values. Our Sm-Nd isotopic data show that $^{147}Sm/^{144}Nd$ ratios in the hot desert meteorites are showing significant deviations from the chondritic isochron and the values reported for ordinary chondrite falls. The $^{147}Sm/^{144}Nd$ in the measured hot desert chondrite ranges from 0.0777 to 0.1973. These ratios are generally lower than the average of 0.1958 reported for falls [5]. The average $^{147}Sm/^{144}Nd$ for the Atacama and Lut samples is 0.1433 $\pm$ 0.0287 (n=10) and 0.1876 $\pm$ 0.0080 (n=7), respectively. This indicates a higher variation and lower values of $^{147}Sm/^{144}Nd$ for the Atacama samples than those from the Lut desert. The εNd values range from -2.20 to 1.61, which is wider than the -1.07 to 0.64 range for falls [5]. The average εNd value for the Atacama and Lut desert samples are -1.05 and -0.58, respectively.

Discussion and Conclusions: Our data reveals that terrestrial weathering of meteorites both in Antarctica and hot deserts changes their trace element (Sr, Ba, REE, Hf, Th, and U) concentrations. In addition, Sm-Nd isotopic measurements of ordinary chondrites from the Atacama and Lut hot deserts show significant effects of terrestrial weathering as manifested by their non-CHUR $^{147}Sm/^{144}Nd$ and $^{143}Nd/^{144}Nd$ ratios. Disturbance of Sm/Nd ratio is responsible for lower $^{147}Sm/^{144}Nd$ ratio which is more evident in the Atacama samples as they have more fractionated REE patterns. Lower Sm/Nd ratios show the effects of mixing with a terrestrial component. The majority of the Atacama meteorites regardless of their weathering degrees (at least W$\geq$2) are indeed contaminated.

Both $^{147}Sm/^{144}Nd$ ratio and εNd values do not show a straightforward relationship with the weathering degrees. However in both cases, the samples with the highest negative isotopic disturbances are H chondrites from the Atacama and Lut deserts.

More studies such as in situ analysis will be needed to find the main factors controlling contamination of Sm-Nd isotopic composition of hot desert meteorites. Care must be taken account while dealing samples collected from hot deserts, even if they look fresh, and including the Atacama desert which is shown to be an extraordinary region hosting high population of meteorites, including unique samples [6,7].

References: [1] Bland, P. A. et al. (2006) *Meteorites and the early solar system II*:853–867. [2] Crozaz G. et al. (2003) *Geochimica et Cosmochimical Acta* 67:4727-4741. [3] Pourkhorsandi H. et al. (2017) *Meteoritics & Planetary Science* 52:1843-1858. [4] Davis A. M. and Richter F. M. (2014) *Treatise on Geochemistry* 1:335-360. [5] Bouvier A. et al. (2008) *Earth and Planetary Science Letters* 273:48-57. [6] Gattacceca J. et al. (2011) *Meteoritics & Planetary Science* 46:1276-1287. [7] Pourkhorsandi H. et al. (2017) *Geochimica et Cosmochimical Acta* 218:98-113.

ALUMINIUM-26 IN MARTIAN AND LUNAR METEORITES: A COMPARISON OF COSMIC-RAY EXPOSURE AGES.

P. P. Povinec[1], I. Sýkora[1], A. J. T. Jull[2,3], L. Kornoš[1], R. J. Macke[4], V. Porubčan[1,5] and J. Tóth[1], [1]Faculty of Mathematics Physics and Informatics, Comenius University, 84248 Bratislava, Slovakia, (pavel.povinec@uniba.sk), [2]Dept. of Geosciences, University of Arizona, Tucson, AZ 85721, USA, [3]ICER, Institute for Nuclear Research, Hungarian Academy of Sciences, 4026 Debrecen, Hungary, [4]Vatican Observatory, V-00120 Vatican City-State, [5]Institute of Astronomy, Slovak Academy of Sciences, 84228 Bratislava, Slovakia.

Introduction: From more than 61,000 meteorites currently known, only over 300 (total mass of about 190 kg) are meteorites from the Moon and over 220 (total mass of about 120 kg) are of Mars origin. Many of the stones are paired fragments of the same meteoroid. They were produced by impacts of asteroids or comets on the Moon or on the Mars planet, orbiting then for the order of 10^4-10^7 years around the Sun (or the Earth in the case of some lunar meteorites), and afterwards they finally landed on the Earth. A meteorite to be released from the Moon needs to overcome the velocity of 2.38 km/s, which is only possible to attain after an impact of a large asteroid, which will form on the planet a crater of several hundred meters in diameter and up to several tens meter deep. In the case of Mars the required velocity is 5.4 km/s and the impact crater diameter can be several kilometers in diameter and up to several hundred meters deep. Lunar and Martian meteorites represent therefore important extraterrestrial samples carrying information on the composition and characteristics of the Moon and Mars surface and subsurface depending of the crystallization and ejection depth. They are unique samples, as there are currently no other possibilities to investigate the subsurface of Moon and Mars at depths several tens or hundred meters, respectively. In contrast to APOLLO samples, the lunar meteorites are random samples of the Moon providing a more representative sampling of the lunar surface, including sampling from the farside of the Moon [1,2].

Samples and methods: One fragment of the Lunar meteorite – NWA 482 (13.10 g, obtained from private collection), and two meteorites of Martian origin - Chassigny (15.79 g) and Nakhla (153.67 g, obtained from the Vatican Observatory) were analysed non-destructively in the Low-level gamma-spectrometry laboratory of the Department of Nuclear Physics and Biophysics of the Comenius University in Bratislava. The gamma-spectrometer consisted of a large volume lead-iron-polyethylene-copper passive shield where HPGe detector (70% relative efficiency), NaITl and plastic scintillations detectors for coincidence-anticoincidence measurements were installed [3,4,5]. **Results:** As short lived cosmogenic radionuclides have already decayed, only long-lived ^{26}Al (half-life of 0.717 Myr) has been found in all analyzed samples. The obtained values were 39.6±3.6 dpm/kg for Chassigny, 61.8±4.8 dpm/kg for Nakhla and 61.4±7.8 dpm/kg for NWA 482. The Chassigny value is in very good agreement with recently measured ^{26}Al levels in the Tissint meteorite (the average value from analysis of two Tissint fragments was 36.9±3.1 dpm/kg) [6]. The measured low ^{26}Al activities in the Chassigny meteorite may be explained, similarly as in the case of the Tissint meteorite, by an unsaturated production of ^{26}Al, which could be caused either by short cosmic-ray exposure (CRE) ages and/or by small dimensions of the meteoroids which prevented development of higher (saturated) ^{26}Al levels, and/or by long terrestrial ages (not the case for Chassigny – fall in 1815, and Nakhla – fall in 1911). The Tissint meteorite (fall in 2011) has short CRE age (0.9±0.3 Myr [7]), which is not the case for Chassigny and Nakhla meteorites (having CRE ages of 10-11 Myr [8]). Therefore, the reason for unsaturated production of ^{26}Al in Chassigny could be in its small pre-atmospheric radius (about 10 cm (for comparison <20 cm in the Tissint case). For the lunar NWA 482 the measured ^{26}Al activity is probably higher due to contributions from solar protons as for the CRE age of about 0.3 Myr and the measured terrestrial age of 8.6 kyr [9], the pre-atmospheric radius could be <10 cm. The activities of the primordial radionuclides measured in the Chassigny meteorite (460±90 dpm/kg for ^{40}K, 97±13 dpm/kg for ^{226}Ra, and 17±9 dpm/kg for ^{232}Th) are much higher than in the Tissint meteorite.

References: [1] Eugster O. et al. (2006) Irradiation records, cosmic ray exposure ages, and transfer time of meteorites. In Lauretta D. and McSween H.Y.Jr. (eds.) *Meteorites and the Early Solar System II*, University of Arizona Press, pp. 829– 851. [2] Herzog G.F. (2005) Cosmic-ray exposure ages of meteorites. In Davis A.M. (ed.) *Meteorites, Planets, and Comets.* Elsevier, p 347–380. [3] Povinec PP et al. (2009) *Journal of Radioanalytical and Nuclear Chemistry* 282:805–808. [4] Kováčik A et al. (2013) *Journal of Radioanalytical and Nuclear Chemistry* 298:665–672. [5] Povinec P.P et al. (2015) *Meteoritics & Planetary Science* 50:880-892. [6] Povinec et al.. (2016) *Journal of Radioanalytical and Nuclear Chemistry* 307:2403-2407 [7] Povinec P.P et al. (2018) *Meteoritics & Planetary Science* #6182. [8] Korochantseva E.V. et al. (2011) *Meteoritics & Planetary Science* 46: 1397–1417. [9] Jull A.J.T. Terrestrial ages of meteorites. In Lauretta D. and McSween H.Y.Jr. (eds.) *Meteorites and the Early Solar System II*, University of Arizona Press, pp. 889–905.

IODINE-XENON RECORD OF THE EARLY SHOCK EVENTS ON THE CHELYABINSK LL5 CHONDRITE PARENT BODY.

O. Pravdivtseva[1], A. Meshik[1], V. Grokhovsky[2], [1]McDonnell Center for the Space Sciences and Physics Department, CB 1105, Washington University, Saint Louis, MO 63130, USA(olga@physics.wustl.edu); [2]Institute of Physics and Technology, Ural Federal University, Ekaterinburg 620002, Russia.

Introduction: The Chelyabinsk LL meteorite consists of three distinct lithologies [1,2], indicative of genomict breccia. A light-colored lithology is LL5 material that has experienced thermal metamorphism and subsequent shock at levels near S4. The second lithology is a shock darkened LL5 material in which the darkening is caused by melt and metal-troilite veins along grain boundaries. The third lithology is an impact melt breccia that formed at ~1600°C. The U-Pb [3,4], Pb-Pb [5], Rb-Sr [6,7], Sm-Nd [1,7,8], Ar-Ar [7,9,10] and K-Ar [7] data for Chelyabinsk indicate a complex history of impacts and heating events. Here we present results of the I-Xe study of Chelyabinsk.

Results: The Xe isotopic composition was measured by step-wise pyrolysis in a fragment of Chelyabinsk chondrule, and in the light (Ch-L) and dark (Ch-D) Chelyabinsk lithology samples, neutron-irradiated for I-Xe dating alongside the absolute age standard Shallowater aubrite.

Table 1. Concentrations of Xe components in the Chelyabinsk samples (tr – trapped; fis – U-fission; * – I-derived).

Sample	mg	$^iXe\times10^{-10}$, cm^3 STP/g			
		$^{132}Xe_{tr}$	$^{132}Xe_{fis}$	$^{129*}Xe$	$^{128*}Xe$
Ch-L	17.4	0.10	0.02	0.25	0.92
Ch-D	28.6	0.80	0.05	0.22	0.89
chondr.	6.8	0.89	0.04	0.33	1.20

I-Xe system in all Chelyabinsk samples exhibits effects of shock-induced disturbance, resulting in the I-Xe isochrones and subsequent relative ages that are defined with high uncertainties. Release profiles of radiogenic ^{128,129}Xe in Ch-L indicate presence of two distinct iodine carrier phases characterized by simultaneous closure of the I-Xe system at 4557.1 ± 0.8 Ma (relative to Shallowater age of 4562.4 ± 0.2 Ma [11]), consistent with shock resetting rather than slow cooling after the early metamorphism on the parent body (Fig.1a). Release profiles of ^{128,129*}Xe in the Chelyabinsk chondrule also suggest two iodine-carrier phases, although the low-temperature one is disturbed up to 1250°C (Fig.1c). I-Xe ages of Ch-L and chondrule agree within the uncertainties. The I-Xe system in these two samples was most probably reset by the same event, but it affected them to a different degree, possibly due to the smaller grain sizes in the Chelyabinsk chondrules compared to the grain sizes in its matrix. The I-Xe system in Ch-D was reset ~ 11.6 Ma later by a higher energy shock event resulting in the redistribution of radiogenic Xe from the low temperature carrier phase and in influx of trapped Xe component. I-Xe systematics in Chelyabinsk are compatible with previously reported data for the dark and light lithologies from the LL6 St Séverin chondrite [12], suggesting common parent body origin.

Figure 1. Release profiles of ^{128*,129*}Xe in the Chelyabinsk samples. Absolute I-Xe ages are calculated relative to Shallowater [11].

References: [1] Galimov E.M. et al. (2013) *Geochemica International* 51:522–539. [2] Meteoritical Bulletin #102 (2013). [3] Popova O. et al. (2013) *Science* 342:1069–1073. [4] Lapen T.J. et al. (2014) *LPS XLV*, Abstract #2561. [5] Bouvier A. (2013) *LPI Contributions* 1737:3087. [6] Nakamura E. et al. (2015) *LPS XLVI*, Abstract #1865. [7] Righter K. et al. (2015) *Meteoritics & Planetary Science* 50:1790–1819. [8] Bogomolova E.S. et al. (2013) *Doklady Earth Sciences* 452:1034–1038. [9] Beard S.P. et al. (2014) *LPS XLV*, Abstract #1807. [10] Korochantseva E.V. et al. (2015) *LPI Contributions* 1856:5268. [11] Pravdivtseva O. et al. (2016) *Geochimica et Cosmochimica Acta* 201:320–330. [12] Hohenberg C.M. et al. (1981) *Geochimica et Cosmochimica Acta* 45:535–546.
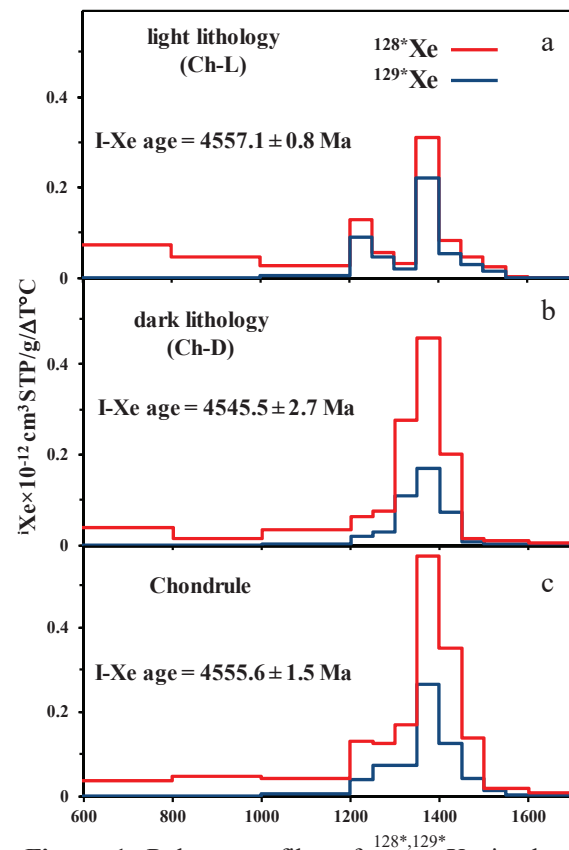
Redox controlled planetary Cr isotopic fractionation.

L. Qin and J. Shen, CAS Key Laboratory of Crust-Mantle Materials and Environment & CAS Center for Excellence in Comparative Planetology, University of Science and Technology of China, 96 Jinzhai RD., Hefei, Anhui, 230026, China (lpqin@ustc.edu.cn).

Introduction: Recently stable Cr isotopes have been employed to constrain the formation and differentiation of Earth and Moon and other planetary bodies [1-5]. Stable chromium (Cr) isotopes were documented to be fractionated during magmatic differentiation of lunar basalts [2]. The slightly lighter Cr isotopic composition of the lunar samples than Earth was attributed to volatile loss of CrO_2 following cooling and accretion of the Moon[5]. Chromium is a redox sensitive element and its isotopic composition may be subjected to change under varying redox conditions. Moon is much more reduced than Earth (IW-2 to IW-1vs IW+2 to IW+6), and it has not been yet to evaluated whether magmatic differentiation fractionates Cr isotopes in terrestrial samples. In this study, we present a quantitative model that relates the Cr isotope compositions of basalts from Earth, the Moon and Vesta, to the fractional crystallizing assemblage, the degree of fractional crystallization and partial melting, and the $Cr^{2+}/\Sigma Cr$ ratios in co-existing minerals and melts, which can be related to the oxygen fugacities. Our model was further assessed with measurements of terrestrial basalts, lunar samples and HEDs.

Methods: The ionic model on the equilibrium isotopic fractionation between two phases was initially developed in [6] to explain Fe isotopic fractionations and was further adopted for Cr isotopes [7]. In this study basically the same scheme was used to calculate the equilibrium Cr isotopic fractionation factor between the melt and mineral assemblage using the average force constant of the Cr-O bounding between the two phases, with the latter being a function of the valence state and the coordination number of Cr. Chromium stable isotopic composition was measured on a Thermo Finnegan Triton TIMS using double-spike method following the procedure described in [8]. Within each analytical session, a double-spiked NIST SRM 979 standard was loaded on two filaments and was run at least three times. The resulting 2 standard deviation for these standard measurements is usually $0.02 \sim 0.03‰$ on $\delta^{53}Cr$. The internal errors (2s.e.) for individual sample analyses were usually slightly larger than this ($0.02 \sim 0.06‰$). The long-term reproducibility of NIST SRM 979 standard over a period of one year is 0.035‰.

Results and conclusions: As in the cases of both Kilauea Iki lava lake basalts and mare basalts, the crysalization assemblage is chromite+olivine, we calculated the the Cr fractionation factors between spinel and melt and between olive and melt and found both increase with decreasing oxygen fagacity. As a result, the expected Cr isotope fractionation during mare magma differentiation is larger than that for Kilauea Iki magma. The correlations between $\delta^{53}Cr$ and MgO content found for both Kilauea Iki basalts and for mare basalts are mainly controled by crystallization of chromite as the latter is the dominant Cr host phase. We further speculate that the lunar mantle has a relatively homogeneous BSE-like isotope composition (-0.17‰ to -0.10‰). The observations of the isotopically lighter lunar basalts is a result of redox-dominated fractional crystallization and accumulation processes, as well as different melting degrees of the primitive lunar mantle. This work presents an alternative interpretation for the observations of the lunar rocks with $\delta^{53}Cr$ slightly lower than BSE. Further, according to our model, the evolved eucrites can also be interpreted by fractional crystallization of isotopically heavier olivine + clinopyroxenes + chromite from a terrestrial mantle-like magma source under IW-1 to IW buffer conditions, while the diogenites represent the accumulations of isotopically heavy mineral phases (*e.g.* orthopyroxene and spinel). Combining with previous results on the variations in Cr valence states and concentrations in silicate melts and minerals associated with changing redox conditions, Cr concentration and isotopic composition can serve as an useful oxybarometer for understanding the redox conditions of planetary differentiation and magmatic evolution.

References: [1] Bonnand, P. and Halliday, A. (2018) *Nature Geoscience* 11:401. [2] Bonnand, P., et al. (2016) *Geochimica Cosmochimica Acta* 175:208-221. [3] Qin, L. et al. (2015). *LPS XLVI,* Abstract #1832. [4] Schoenberg, R. et al. (2016). *Geochimica et Cosmochimica Acta* 183:14-30. [5] Sossi, P.A., et al. (2018). *Proceedings of the National Academy of Sciences* 115:10920-10925. [6] Young, E. D. et al. (2015) *Chemical Geology* 395:176-195. [7] Shen, J., et al. (2018). *Earth and Planetary Science Letters* 499:278-290. [8] Xia, J. et al. (2017) *Earth and Planetary Science Letters* 464:103-115.

SUCCESS AND FAILURE OF SCHOCK RECOVERY EXPERIMENTS FOR SIMULATING SHORT DURATION PARENT BODY HEATING

E. Quirico[1], H. Yabuta[2], P. Beck[1], L. Bonal[1], A. Bardyn[3], L. Nittler[3], C.M.O'D. Alexander[3], N. Carrasco[4], C. Szopa[4]. [1]UGA/CNRS IPAG Grenoble France, [2]Hiroshima University, Japan. [3]DTM, Carnegie Institution USA. [4]CNRS/INSU LATMOS-IPSL, Guyancourt France

Introduction: Short duration heating is a post-accretional process that has effected the chondrite parent bodies to varying degrees, and that might be involved in the formation of Ultra Carbonaceous Antaric Micro-Meteorites (UCAMMs)[1,2]. Hypervelocity impacts are a plausible source of heating, owing to the fact that the chondrites were excavated from their parent bodies by collisions. Here, we report shock recovery experiments that are dedicated to simulating these short duration heating processes. Three samples were studied: Murchison (CM2), EET 90628 (LL/3.0) and a tholin sample as a presumed analog precursor of some N-rich UCAMMs [3].

Experiments: Shock recovery experiments were conducted at Tokyo Institute of Technology (Japan) during four sessions between 2010 and 2016. A 5-50 GPa peak pressure range in the recovery capsule was achieved by combining different flyers with different velocities. The shocked state in the sample was assumed to equilibrate with that of the capsule through multiple reflections at the capsule boundaries. Peak pressures were calculated with the impedance match method, using the Hugoniot curves of iron and of the flyer plate material. Samples were characterized by FTIR and Raman spectroscopy (IPAG Grenoble and LGL Lyon, France) and SIMS (Carnegie Institute, Washington USA). Tholin samples were produced with a cold plasma reactor (LATMOS, France).

Results and discussion:

Murchison. The IOM composition is very sensitive to shocks, even at low peak pressure (5 GPa). Thanks to FTIR analysis, we observe an increase of the CH_2/CH_3 ratio (estimated from the peak intensity ratio of the antisymmetric stretching modes at 2925 and 2955 cm^{-1}), a decrease of the carbonyl C=O group (~1700 cm^{-1}), a decrease of the aliphatic (CH, CH_2, CH_3) abundance (except at 50 GPa, for which a large increase is observed), and the development of a new narrow band centered at ~ 1650 cm^{-1}. At high shock pressure, large chemical variations are observed within the IOM, pointing to strong spatial heterogeneities of pressure and temperature in the capsule. Overall, these variations are consistent with those measured in heated chondrites. A high CH_2/CH_3 ratio is always associated evidence for thermal events in type 2 and 3 chondrites, as well as the decrease of the aliphatic abundance. Note, however, the exception of the CM QUE 93005 that shows a dramatic increase of aliphatic groups that might be consistent with the 50 GPa experiment. The band at ~ 1650 cm^{-1} has never been detected in C1, C2 or type 3 chondrites. This feature is possibly due to the formation of quinones, perhaps as a result of oxidation during the shock event. The gun is maintained under a primary vacuum, possibly favouring oxidation reactions that might not happen in natural conditions. The carbon structure probed by Raman spectroscopy (514 nm) displays moderate variations, which are more significant at 40 and 50 GPa. The data account for stage II heated chondrites, but not for III/IV stages [4]. In this respect, our shock experiments do not properly mimic the highest degrees of the heating process, possibly because the reverberation process to reach the peak pressure in the experiment releases less heat than a single shock process that happens in natural conditions [5]. SIMS measurements report a dramatic effect on the D/H composition of the IOM. At 5 GPa, the D/H ratio is drastically reduced, and at 40 GPa the IOM is isotopically normal. These findings are basically consistent with IOM compositions from heated C2 chondrites [6].

EET 90628. The Raman data of EET 90628 IOM display co-variations of the FWHM-D and I_D/I_G parameters pointing to a structural grade that is more consistent with a ~ 3.1 petrologic type. At the same time, we observe an increase of FWHM-G and a decrease of ω_G. These results show that some primitive type 3 chondrites may have been perturbed by shock processes, and are also consistent with the fact that FWHM-G and ω_G are not reliable tracers of thermal metamorphism.

Tholin 97:3. Shock experiments on a 97:3 tholin show major effects on the composition, and the development of a polyaromatic structure at 20 GPa and beyond. However, even at 40 GPa, the degree of structural order remains lower than that measured in N-rich UCAMMs. We may expect that shocks under natural conditions should lead to more mature carbonaceous materials. However, the D/H sensitivity to thermal processing is inconsistent with hypervelocity impact involvement in UCAMM formation (provided that D carriers are similar in Murchison and UCAMMs).

References: [1] Tonui E. et al. (2014) *Geochimica Cosmochimica Acta* 126:284–306. [2] Augé B. et al. (2016) *A&A* 592:A99. [3] Bonnet J-Y et al. (2015) Icarus 250: 53-63. [4] Quirico E. et al. (2018) *Geochimica Cosmochimica Acta* 126:284–306 241:17-37. [5] Tomeoka K. et al. (1999) *Geochimica Cosmochimica Acta* 63:3683-3703. [6] Alexander C.M.O'D et al. (2010) *Geochimica Cosmochimica Acta* 74:4417-4437

FORMATION AND EMPLACEMENT OF MARTIAN POIKILITIC SHERGOTTITES

R. R. Rahib[1], A. Udry[1], G. H. Howarth[2], J. Gross[3], M. Paquet[4], L. M. Combs[1], D. L. Laczniak[5], and J. M. D. Day[5], [1]Department of Geosciences, University of Nevada Las Vegas, 4505 S. Maryland Pkwy, Las Vegas, NV 890154 (rahibr@unlv.nevada.edu; arya.udry@unlv.edu), [2]Department of Geological Sciences, University of Cape Town, Rondebosch 7701, South Africa, [3]Department of Earth and Planetary Sciences, Rutgers University, Piscataway NJ 08854, [4]Scripps Institution of Oceanography, University of California San Diego, La Jolla CA 92093-0244, [5]Department of Earth, Atmospheric, and Planetary Sciences, Purdue University, West Lafayette, IN 47907.

Poikilitic shergottites: Poikilitic shergottites make up >20% of the current martian meteorite collection, with a total of 27 samples. These meteorites are intrusive gabbroic and lherzolitic rocks and represent igneous materials recording important processes in the martian crust. Poikilitic shergottites originate from enriched [high bulk $(La/Yb)_{CI}$ ratios, high $^{87}Sr/^{86}Sr$ and $^{187}Os/^{188}Os$, and low εNd and εHf] [e.g., 1-10] to intermediate [moderate bulk $(La/Yb)_{CI}$ ratios, $^{87}Sr/^{86}Sr$, $^{187}Os/^{188}Os$, εNd, and εHf compared with martian shergottites as a whole] sources [e.g., 1-9]. No depleted poikilitic shergottites have been identified yet. Poikilitic shergottites show a characteristic bimodal texture representing polybaric crystallization from the crust/mantle boundary (early stage) to hypabyssal (late stage) depths, which allows examination of parental magma evolution from the interior of Mars to the surface [9]. Here we present a comprehensive study of the largest suite of poikilitic shergottites to date to better constrain their formation, emplacement, and links with the other shergottites. We measured bulk rock major and trace element compositions, mineral major element compositions, oxygen fugacity (fO₂) values, crystallization temperatures, and quantitative textural analyses on eleven samples (Northwest Africa – NWA – 7755, NWA 7397, NWA 4468, NWA 10169, Allan Hills – ALHA – 77005, Lewis Cliff – LEW – 88516, Roberts Massif – RBT – 04261/2, and four newly recovered samples: NWA 11065, NWA 11043, NWA 10961, and NWA 10618).

Results and discussions:

Source of poikilitic shergottites. Bulk rock $(La/Yb)_{CI}$ allows determination of shergottite source compositions, with enriched shergottites distinguished by $(La/Yb)_{CI}$ values ≥0.8 and intermediate shergottites $(La/Yb)_{CI}$ values between 0.30–0.50 [e.g., 2, 3, 8–12]. Northwest Africa 11043 originated from a light rare earth element (LREE)-enriched mantle source (the greatest $(La/Yb)_{CI}$ value of our samples = 1.54), whereas the newly recovered NWA 10961 and NWA 11065 sampled an intermediate source. The bulk Zr/Y-Nb/Y and $^{187}Os/^{188}Os$ composition of NWA 11043 falls within the fields of intermediate shergottites [13, 14].

Oxygen fugacities. We calculated fO₂ for the different poikilitic shergottites using the olivine-pyroxene-spinel oxybarometer and we observe consistent increases in fO₂ from early-stage to late-stage textures ranging from 1.2 to 2.0 log units below the Quartz-Fayalite-Magnetite (QFM) buffer for enriched poikilitic shergottites, and 2.0 to 2.9 log units for intermediate poikilitic shergottites. The fO₂ increase indicates that degassing was likely an important process in the formation of poikilitic shergottites, similar to olivine-phyric shergottites [15]. In addition, we do not observe correlation between fO₂ and LREE enrichment, although it was previously suggested to represent different shergottite reservoirs [16]. Thus, fO₂ is not a reliable tool to distinguish shergottite sources.

Emplacement of poikilitic shergottites. Crystal size distribution (CSD) analyses of the olivine population show similar patterns for all poikilitic shergottites, including olivine accumulation, indicating similar emplacement processes for all of these rocks. Using a combination of geochemical, mineralogical, and quantitative textural data, we suggest that the enriched poikilitic shergottites were emplaced in various shallow sills and at different geographical locations compared with of intermediate poikilitic shergottites. In addition, the Ti/Al of poikilitic pyroxenes are relatively similar for all poikilitic shergottites, suggesting that early mineral assemblages formed at the crust/mantle boundary of Mars. Thus, the presence of at least two magmatic chambers at these depths on Mars, possibly resulting in formation of the different enriched and intermediate shergottites, is likely [15].

References: [1] Lin (2013) *Meteoritics & Planet. Sci.* 48:1572–1589. [2] Lodders (1998) *Meteoritics & Planet. Sci.* 33. [3] McSween et al. (2015) *Am. Min.* 100:2380–2395. [4] Mikouchi and Kurihara (2008) *Polar Science* 2: 175–194. [5] Lin et al. (2005) *Meteorit. Planet. Sci.* 40:1599–1619. [6] Usui (2010) *GCA* 74:7283–7306. [7] Walton et al. (2012) *Meteorit. Planet. Sci.* 47:1449–1474. [8] Combs et al. (2018) *LPSC XLIX*, Abstract #2083. [9] Howarth et al. (2014) *Meteorit. Planet. Sci.* 49:812–830. [10] Tait and Day (2018) *EPSL* 494:99-108. [11] Barrat et al. (2002a) *Meteorit. Planet. Sci.* 37:487–499. [12] Filiberto et al. (2012) *Meteorit. Planet. Sci.* 47:1256–1273. [13] Day et al. (2018) *Nat. Comm.* 9:4799. [14] Paquet et al. (2019) *LPSC L*, Abstract #1456. [15] Herd (2019) *LPSC L*, Abstract #2746. [16] Castle and Herd (2018) *Meteorit. Planet. Sci.* 53:1341–1363.

NOBLE GAS COMPONENTS IN THE LUNAR METEORITE NORTHWEST AFRICA 10203

P. M. Ranjith[1], H. He[1], T. M. Smith[1], F. Su[1], Y. Lin[2], R. Zhu[1]. [1]State Key Laboratory of Lithospheric Evolution, Institute of Geology and Geophysics, Chinese Academy of Sciences, Beijing 100029, China, [2]Key Laboratory of Earth and Planetary Physics, Institute of Geology and Geophysics, Chinese Academy of Sciences, Beijing, 100029, China
Email: ranjith@mail.iggcas.ac.cn

Introduction: Northwest Africa (NWA) 10203 is a feldspathic regolith breccia with numerous fragmental light and dark clasts with mineral fragments connected through a glassy matrix. We expect the presence of trapped solar noble gases in this meteorite, in addition to cosmogenic gases. Helium, neon and argon were measured in clast and matrix samples of this meteorite with two key objectives. First to characterize trapped solar gases and second to estimate the cosmic ray exposure age of the meteorite.

Experimental Procedures: We have extracted He, Ne and Ar from two clast and three matrix samples from a slice of NWA 10203 by stepwise heating using a CO_2 laser, to characterize the gas release properties of different clast and matrix components. Laser power was increased in steps such as 10, 20, 40, 65 (in %), until complete gas extraction. Extracted gases were purified and processed following standard procedures as detailed in [1].

Results and discussions: Measured He is a mixture of cosmogenic, radiogenic and trapped components with $^4He/^3He$ varying from ~ 8-20. This shows severe He loss in NWA 10203 compared to most of lunar meteorites [2]. Neon and Ar were resolved into cosmogenic and trapped components. Based on a Ne-three isotope diagram, trapped Ne is fractionated solar wind (SW) with an inferred $^{20}Ne/^{22}Ne$ ratio of 12.17±0.16. Cosmogenic $^{22}Ne/^{21}Ne$ is in the range ~ 1.4-1.7, consistent with the feldspathic composition, based on the recent Lunar meteorite data compilation [2]. Measured $^{40}Ar/^{36}Ar$ is in the range 1.9-6.0 and $^{36}Ar/^{38}Ar$ is ~5.2, mostly representing trapped Ar as in most lunar meteorites. The elemental ratio of trapped $^{20}Ne/^{36}Ar$ is in the range ~0.02 to 0.16, which is even lower than the terrestrial atmospheric value, indicating diffusive gas loss. The $^{40}Ar/^{36}Ar$ ratios are higher for low-T steps than for high- T steps. This indicates that Ar from the first releases is from K-rich mineral like plagioclase.

Trapped gas release: Trapped Ne and Ar are clearly observed in all the clast and matrix samples. For example, in one clast sample, at 10% laser power, trapped ^{20}Ne ($^{20}Ne_{trap}$) represents only 1.4% of the total ^{20}Ne of this step whereas cosmogenic Ne ($^{21}Ne_{cos}$) represents 52% of the total ^{21}Ne of this step. At a higher laser power of 40%, $^{20}Ne_{trap}$ is 50% whereas $^{21}Ne_{cos}$ is only 19%. This trend is observed in all the samples. Therefore, cosmogenic Ne tends to be released earlier than trapped SW-Ne. As the SW is surface sited, one would expect the release of SW components to occur earlier than that of the volume sited cosmogenic gases. This may indicate that all the trapped gases in low retentive mineral like plagioclase may have been lost due to the brecciation process, but cosmogenic gases are still present and got released at lower temperature. Like Ne, trapped Ar was also released at high temperature, possibly from the highly retentive minerals. In addition, release patterns of both cosmogenic and trapped Ar are similar. This could be due to trapped solar gases originally surface correlated having migrated to grain volumes later. This may also indicate the regolith reworking due to brecciation or micrometeorite bombardment.

Cosmogenic components: Cosmogenic light noble gases ^3He, ^{21}Ne, ^{38}Ar are used to derive cosmic ray exposure ages (CREAs) T_3, T_{21} and T_{38} respectively. This CREA represents combined irradiation record on the lunar surface and during Moon–Earth transit. Production rates of ^3He, ^{21}Ne and ^{38}Ar are estimated based on [3] and [4]. The CREAs for two clast samples are estimated as T_3 = (9-14 Ma), T_{21} = (23-29 Ma) and T_{38} = (66-70 Ma). T_3 and T_{21} are clearly lower than T_{38}, which indicates depletion in lighter noble gases He and Ne. This may be caused due to degassing activated by the ejection processes from the Moon. Reults from more clast samples from NWA 10203 will be presented during the meeting.

References: [1] Ranjith, P. M et al. (2017).Planetary and Space Science, 146: 20-29. [2] Meszaros et al. (2018). Meteoritics & Planetary Science, 53(5),1104-1107. [3] Hohenberg C. M et al. (1978). In LPSC Proceedings (Vol. 9, pp. 2311-2344) [4] Chen J et al. (2017). Meteoritics & Planetary Science, 52(4), pp.646-655

IRON ISOTOPE COMPOSITIONS OF Si-BEARING METAL NODULES FROM THE MOUNT EGERTON AUBRITE

S. Ray[1], M. Wadhwa[1,2], V. K. Rai[1], L. A. J. Garvie[1,2], [1]School of Earth and Space Exploration and [2]Center for Meteorite Studies, Arizona State University,Tempe, AZ 85287-6004. Soumya.Ray@asu.edu

Introduction: Aubrites are enstatite achondrites that are dominated by nearly Fe-free enstatite, with variable amounts of Fe-free diopside and forsterite, Si-bearing Fe-Ni metal, plagioclase, troilite and a range of accessory minerals [1]. Their mineralogy is indicative of the highly reduced conditions under which they formed [1]. We showed that the Fe isotope compositions of 18 metal nodules from several aubrites belonging to the main aubrite and Shallowater parent bodies, are correlated with their Si contents and structure [2-6]. The majority of aubrite metals, except from Shallowater which is unbrecciated, derive from either regolith or fragmental breccias [1]. Based on our results, we suggested that the Si-poor metal nodules were exogenous, and thus distinct from the Si-bearing nodules [2,4,6]. The Si-bearing metals are proposed to have a "residual" origin (i.e., represent equilibration with silicates) and likely were formed during igneous processes on the parent body. We also observed an anti-correlation between the Si content and δ^{56}Fe of Si-bearing metal nodules fom several aubrites [6]. As a follow-up to these investigations, here we report the Fe isotope compositions of metal nodules from the Mount Egerton aubrite. Mount Egerton is an unbrecciated, anomalous aubrite with 21 wt. % of Si-bearing metal [1].

Analytical Method: Sample preparation and column chemistry were carried out under clean laboratory conditions in the Isotope Cosmochemistry and Geochronolgy Laboratory (ICGL) at Arizona State University (ASU). Four metal nodules (ME1 to 4 ranging from 11 to 18 mm in diameter) from the Mount Egerton aubrite were cut in half: one half was mounted in epoxy and then characterized using the CAMECA SX100 electron microprobe in the Michael J. Drake Electron Microprobe Laboratory at University of Arizona using methods similar to [5]. A clean, interior piece (weighing about ~6 mg) of the other half of each nodule was ultrasonicated in ethanol, and then dissolved in concentrated HCl. Iron was purified using standard anion exchange column chemistry techniques [7]. Iron isotopes were measured on a Thermo Neptune multicollector inductively coupled plasma mass spectrometer in medium-resolution mode and instrument mass bias was corrected using both Cu-doping and sample-standard bracketing (using IRMM-014 as the standard). The accuracy and precision of our analyses were assessed using repeated analyses of BCR-2, AGV-1, BHVO-1 terrestrial rock standards as well as a homogenized bulk sample of the Allende CV3 chondrite during each analytical session.

Results and Discussion: The metal nodules ME1 to 4 have similar Si contents, i.e., 2.00±0.04 to 2.07±0.04 wt% (2SD errors are ±5%) and Fe isotope compositions (δ^{56}Fe) of 0.015±0.043‰ to 0.026±0.021‰ (2SD). These values are similar, within errors, to the composition of Mount Egerton metal (average δ^{56}Fe =0.002±0.024‰, 2SD) [8]. Our δ^{56}Fe data are similar to those of the Si-bearing Norton County metal nodules with similar Si content (e.g., NC9, which has Si ~2 wt. % and δ^{56}Fe = (0.03±0.01‰) [6]). This study of the correlated measurements of Fe isotopes and Si content of metal nodules from the Mount Egerton aubrite is consistent with our previous study of metal nodules in the brecciated aubrites, and supports the anti-correlation between Si content and δ^{56}Fe in Si-bearing metal nodules [6]. This further suggests that the Si-bearing metal nodules in brecciated and unbrecciated aubrites (from the main group or other anomalous groups) equilibrated with silicates at either different temperatures or redox conditions on their parent bodies.

References: [1] Keil K. (2010) *Chemie der Erde, 70,* 295–317. [2] Ray S. et al. (2017) *MetSoc Meeting, Abstract* #6400. [3] Garvie L. A. J. et al. (2017) *MetSoc Meeting, Abstract* #6384. [4] Ray S. et al. (2018) *49th LPSC, Abstract* #2140. [5] Garvie L. A. J. (2018) *49th LPSC, Abstract* #2104. [6] Ray S. et al. (2019) *50th LPSC, Abstract* #1960. [7] Arnold G. L. et al. (2007) *Analytical Chemistry*, 76, 322-327. [8] Jordan M. K. et al. (2019) *GCA, 246,* 461-477.

PETROLOGY, GEOCHEMISTRY AND PB-PB AGE OF A LARGE IGNEOUS INCLUSION FROM THE ORDINARY CHONDRITE PAPOSO 004

P. M. Reger[1], S. B. Simon[2], A. M. Gannoun[3], J. M. Gibson[4], R. C. Greenwood[4], A. Bouvier[1,5]. [1]University of Western Ontario, Department of Earth Sciences, Canada (preger@uwo.ca). [2]University of New Mexico, Institute of Meteoritics, USA, [3]Université Clermont Auvergne, Laboratoire Magmas et Volcans, France, [4]The Open University, Planetary and Space Sciences, UK, [5]Universität Bayreuth, Bayerisches Geoinstitut, Germany

Introduction: Large igneous inclusions are relatively rare and enigmatic components of ordinary chondrites, as they are only found in about 4% of this class of meteorites [1]. They can range up to several cm in diameter and are generally low in metal and sulfides. It has been suggested that individual large igneous inclusions could have formed by a range of mechanisms: some may have formed as unusually large chondrules [e.g. 1], others as impact melts [e.g. 1,2], igneous differentiates, or nebular melts formed at high-temperature via evaporation or condensation [e.g. 1,3]. Recently, O isotope analysis has demonstrated that some inclusions formed in distinct reservoirs before being incorporated into their host chondrites. This indicates that nebular or collisional mixing occurred prior to complete accretion of ordinary chondrite parent bodies [4].

Here, we report the petrology, geochemistry, triple O isotopic composition, and Pb-Pb whole-rock age of a large igneous inclusion found in the L3.1 ordinary chondrite Paposo 004. This inclusion may provide further insights into the origin and accretion mechanisms of planetary bodies.

Sample and Methods: The melt inclusion, named Pap-I1, was ca. 16 mm by 8 mm at the surface of the slab of its host chondrite Paposo 004 (L3.1). A section of the inclusion was prepared for SEM imaging and electron microprobe analysis at UNM and Western. One whole-rock (WR) fraction (~30 mg) was crushed and dissolved for major and trace element analysis by quadrupole ICP-MS iCAP Q at Western, while another WR fraction (~220 mg) was taken for an 8-step dissolution procedure for Pb isotopic analysis. This procedure follows the protocol of [5] where terrestrial and common Pb-rich components are first removed before radiogenic Pb is progressively leached out. Lead separation from the leachate and residue matrices was achieved using ion-exchange chromatography [5]. Total procedural blanks were 1.4±1.0 pg, while sample-to-blank ratios for the leachates and residues range from 180 to 5348. Lead isotopic analyses were carried out using a Neptune Plus MC-ICP-MS at UCA. Instrumental mass fractionation was corrected using the Tl-doping and NBS 981 standard-bracketing method, and NBS 983 was used as a secondary isotopic standard. The Pb-Pb age was calculated using $^{238}U/^{235}U = 137.786 \pm 0.011$ [6]. For O isotopes, an approximately 10 mg whole-rock chip was crushed and homogenised and ~2 mg aliquots of this powder were then loaded for O isotope analysis by infrared laser-assisted fluorination at the OU [7].

Results: *Petrography*. The inclusion is dominated by microporphyritic olivine grains (<100 μm) with some larger phenocrysts (>250 μm), a barred olivine relict chondrule with low-Ca pyroxene ($Fs_{22.1\pm4.9}$, $Wo_{1.5\pm1.3}$), glass (sodic plagioclase: $Na_2O = 8.8\pm3.0$ wt%) and troilite, kamacite and taenite. The smaller olivine grains are more Fe-rich than the phenocrysts, with $Fa_{29.4\pm6.8}$ and $Fa_{14.5\pm2.3}$, respectively. The Fe/Mn ratios in olivine (46.2±9.4) resemble those of L chondrites (43.0±5.8 [4]). *Geochemistry*. The bulk chemistry of Pap-I1 indicates that it did not experience any fractionation process, based on lithophile elements, with only Ca being significantly depleted compared to CI chondrites. Bulk REE abundances are slightly enriched by 30 to 50% compared to CI chondrites, but show no significant signs of fractionation between REE. *Pb-Pb age*. Blank-corrected $^{206}Pb/^{204}Pb$ ratios range from 12.3 to 37.4. Plotting the last 5 leachates and residue fractions in an "inverse" $^{204}Pb/^{206}Pb$ vs. $^{207}Pb/^{206}Pb$ diagram results in a Pb-Pb errorchron age of 4534±11 Ma (MSWD = 103). *O isotopes*. The mean of the two replicates of Pap-I1 gave the following composition: $\delta^{17}O = 3.492 \pm 0.238$‰, $\delta^{18}O = 4.595 \pm 0.219$‰, $\Delta^{17}O = 1.103 \pm 0.124$‰ and plots in the L chondrite field [8].

Discussion: The Pb-Pb age of Pap-I1, while imprecise due to its unradiogenic composition, is nonetheless within the range of formation ages obtained for other inclusions in ordinary chondrites, with I-Xe and Hf-W model ages found between 0.5 to 50 Ma after CAI formation [9,10,11]. These relatively young ages of inclusions, along with their unfractionated chemistry and texture, are best explained as products of impact melting. The presence of Pap-I1 within an unbrecciated ordinary chondrite indicates a protracted accretion history for the L ordinary chondrite parent body.

References: [1] Bridges, J. C. & Hutchison, R. (1997) *Meteorit. Planet. Sci.* 32, 389–394. [2] Ruzicka, A. M. et al. (1998) *Geochim. Cosmochim. Acta* 62, 1419–1442. [3] Ruzicka et al. (2012) *Meteorit. Planet. Sci.* 47, 1809–1829. [4] Ruzicka et al. (2019) *Geochim. Cosmochim. Acta* (in press). [5] Bouvier, A. & Wadhwa, M. (2010) *Nat. Geosci.* 3, 637–641. [6] Connelly et al. (2017) *Geochim. Cosmochim. Acta* 201, 345–363. [7] Greenwood et al. (2017) *Chemie der Erde* 77, 1-43. [8] Clayton et al. (1991) *Geochim. Cosmochim. Acta* 55, 2317-2337. [9] Ruzicka et al. (2018) *LPS XLIX*, Abstract #1714. [10] Crowther et al. (2018) *EPSL* 481, 372-386. [11] Crowther et al. (2019) *LPSC L*, Abstract #2629.

MOLECULAR AND ISOTOPIC EVOLUTION OF INSOLUBLE ORGANIC MATTER OF THE ORGUEIL METEORITE UPON HEATING.

L. Remusat[1], J.-Y. Bonnet[2], S. Bernard[1], A. Buch[3] and E. Quirico[4]
[1]IMPMC, UMR CNRS 7590, Sorbonne Université, MNHN, Paris, France (laurent.remusat@mnhn.fr),
[2]LATMOS-IPSL, Université Versailles St-Quentin, Sorbonne Université, CNRS UMR 8190, Guyancourt, France,
[3]LGPM, Centrale Supelec, Gif-sur-Yvette, France,
[4]IPAG, UMR CNRS 5274, Université Grenoble Alpes, Grenoble, France.

Introduction: Understanding the origin of organic compounds in carbonaceous chondrites is crucial to assess how organic matter synthesis happened in the solar system, in protoplanetary disk and on the asteroids. It may also improve our knowledge of the emergence of life on Earth or in other places of the solar system. Insoluble organic matter (IOM) is the largest organic component recovered in carbonaceous chondrites, representing more than 75 wt. % of the total organic matter recovered from these meteorites. Despites a significant aqueous alteration on its parent body, the Orgueil meteorite contains an IOM that shows a significant enrichment in heavy isotopes of H and N. In particular, the D/H ratio it about 6 times higher than the protosolar value and shows variations at the micron and the molecular scales that point to a complex of origin [1,2]. This IOM is likely the assemblage of several components that have experienced different conditions in the protoplanetary disk, or even before in the parent molecular cloud, before being subjected to secondary aqueous alteration on the parent body [3]. In the meantime, its molecular properties relate to a rather condensed macromolecule made of small aromatic units with a high degree of cross linking, containing about 3 wt% of N [4]. The thermal behavior of the Orgueil IOM was investigated to improve the understanding of its isotope reservoirs and its molecular constituents.

Methods: We have subjected the Orgueil IOM to heating at 300°C and 500°C, for one hour, under an Ar flow [5]. The evolutions of structural and molecular properties were assessed by Raman, infrared and XANES spectroscopies, the H- and N-isotopic compositions by NanoSIMS.

Results: Upon heating, the IOM structure undergoes significant modifications that results in a depletion in aliphatic carbons and the development of larger aromatic units, with concomitant loss of carboxylic and alcohol groups. This is consistent with the sharp decrease in H/C elemental ratio, starting at 300°C, whereas N/C ratio remains constant within error bars, even after heating at 500°C. This indicates that N is likely involved in aromatic groups less prone to thermal decomposition. The structure of the residual IOM is not subjected to severe carbonization process as indicated by the persistence of quite broad G and D-bands of comparable intensities, even at 500°C, although the structural ordering increases as the result of aromatic unit growth.

NanoSIMS imaging shows contrasted evolution of H and N isotope distributions. The abundant D-rich hotspots contained in the Orgueil IOM are destroyed after heating at 500°C. Meanwhile, ^{15}N-rich hotspots, also commonly observed in this IOM, are much less affected by heating, at both 300 and 500°C. Hence, D and ^{15}N-rich organic reservoirs have different behavior toward increasing temperature. In the Orgueil IOM, D-rich moieties are related to aliphatic carbon and thermally labile whereas ^{15}N-rich moieties are recalcitrant. The H and N isotope compositions are decoupled, showing that the Orgueil IOM contains organic components formed in various environments of the protoplanetary disk or the parent molecular cloud.

Discussion: The evolution of Orgueil IOM upon heating echoes with observations on IDPs [6]. The organic matter in these objects tends to loose quickly its D-rich component as a consequence of heating during the atmospheric entry, whereas the ^{15}N enrichments are poorly affected. That would indicate that the D-rich and ^{15}N-rich organic components are similar in IDPs and carbonaceous chondrites. The evolution we observe is also similar to the evolution observed when comparing the IOM of several fragments of the Tagish Lake meteorite showing increasing degrees of parent body processing [7]. H/C and D/H decrease with increasing hydrothermal alteration, whereas both N/C and ^{15}N/^{14}N remain constant. That could indicate that temperature increase during the hydrothermal alteration on the Tagish Lake parent body has controlled the evolution of its IOM.

Our experiment, may bring constrains on the heating experienced by organic matter in the gas phase prior accretion on parent bodies. Orgueil IOM derives from micron sized organic grains formed in cold environments that could have been thermally reprocessed on their route to the location of the parent body accretion closer to the sun; we can estimate that they were not exposed to higher temperature than 300°C for more than 1 hour, in order to preserve D-enrichments; ^{15}N-rich precursors may have experienced up to 500°C.

References: [1] Remusat L. et al. (2005) *Earth and Planetary Science Letters* 243, 15-25. [2] Remusat L. et al. (2009) *The Astrophysical Journal* 698, 2087-2092. [3] Remusat L. et al. (2010) *The Astrophysical Journal* 713, 1048-1058. [4] Derenne S. and Robert F (2010) *Meteoritics & Planetary Science* 45, 1461-1475. [5] Remusat L. et al. (2019) *Geochimica et Cosmochimica Acta* Under revision. [6] Keller et al. (2004) *Geochimica et Cosmochimica Acta* 68, 2577-2589. [7] Alexander C. M. O'D. et al. (2014) *Meteoritics & Planetary Science* 49, 503-525.

Overview of carbonaceous chondrites in the US Antarctic meteorite collection: implications for understanding Bennu and Ryugu.

K. Righter[1] [1]NASA Johnson Space Center, Mailcode XI2, 2101 NASA Pkwy., Houston, TX 77058; kevin,righter-1@nasa.gov.

Introduction: Spectral studies of the target asteroids of the OSIRIS-REx and Hayabusa2 missions - Bennu and Ryugu - have included comparisons to several samples from the US Antarctic meteorite collection including MET 00639 (CM2), MET 01072 (CM2), ALH 83100 (CM1/2), and LAP 02277 (CM1)[1-3]. The fact that these four samples provide insight into understanding these asteroids leads one to wonder what carbonaceous chondrites (CCs) are represented in the US collection and are there others that might also be helpful for comparison? Here is an overview of the CCs in the collection (n=930) and a demonstration of the great diversity of samples available as a resource to these missions.

CM chondrites: There are 344 CM chondrites in the US Antarctic meteorite collection, including large pairing groups from the ALH, EET, LEW, LAP, MET, MIL, and QUE dense collection areas. Several areas have been visited over the course of numerous seasons and/or over a decade, thus making pairing a challenge as the groups emerge over long periods of time. We are examining pairing in a number of groups with small masses, to preserve as much material as possible, while also making material as widely available as possible. CM2 chondrites are the most common of the CCs in the US collection; their mineralogy is fine grained and difficult to study using standard optical microscopy, but x-ray diffraction studies indicate their major mineralogy is cronstedtite, olivine, pyroxene, calcite, magnetite, and sulfide [4,5]. CM1 chondrites are more rare in the collection, typically of small size (<10 g), and have Mg-rich serpentine forming at higher degrees of aqueous alteration. There are transitional CM1/2 that represent intermediate degrees of aqueous alteration. An excellent example is ALH83100, which is comprised of ~50 pieces paired together in the field for a total of 3.019 kg. Because this sample is readily available, it has been relatively easy to allocate as part of many studies. The MET pairing group of CM chondrites has visible layering or foliation that resembles layering observed on some boulders on Bennu [6].

CR chondrites: There are 80 CR chondrites in the collection, including a large EET pairing group (50), small and scientifically precious QUE 99177, LAP 02342, GRA 95229, MET 00426, and more recent and larger MIL 15328, LAR 12247, and GRO 17063/64 samples. CRs share some spectral features with Bennu in that it has regions of higher reflectivity [1], which is a characteristic of the CRs [7]. Aqueously altered CR1s are rare in our collection, but include GRO 95577, a focus of many studies of hydrated CRs.

CM ungrouped or anomalous chondrites: Some CM anomalous or ungrouped chondrites share spectral features with Ryugu, which has a small hydration peak [3]. This peak is argued to be due to hydrated minerals left after either heating or shock in carbonaceous chondrites. PCA 91008, WIS 91600, QUE 99038, and LEW 85311 are all anomalous CCs that have experienced heating from shock or metamorphism [8]. These samples may hold clues to understanding the mineralogy of Ryugu, or interpretations of its spectral properties.

CK chondrites: There are 117 CK chondrites in the collection – these represent the only major group of carbonaceous chondrites that has experienced metamorphic temperatures analogous to the ordinary chondrite groups. Although magnetite is common in CM chondrites (see above), it is also present in significant modal percentage in CK chondrites. Magnetite has been observed in both the general [2] and local [9] spectra of Bennu. Thus, consideration of CK chondrites in interpretation of the diverse lithologies present on Bennu and Ryugu may be prudent. Large CK chondrite pairing groups have been recovered in the LAR, QUE, and EET areas; the CK group was initially established with heavy reliance on US Antarctic finds [10]. CKs may be worth characterizing in more detail to set a baseline for magnetite-bearing or magnetite-rich samples, and to better understand the distinction between magnetite features in CM and CK chondrites.

Other C chondrites: CO (248), CV(115), CB(11), and CH (8) chondrites are all robust groups in the collection, but these samples do not share much in common with the spectra from Bennu or Ryugu. There are no CI chondrites in the US collection.

Summary: The diversity of textures, mineralogy and composition represented within the CM, CR, CK, and C ungrouped meteorites within the US Antarctic meteorite collection should serve as a very useful resource in interpreting spectral data, comparing to returned samples, and ultimately to allow stronger connections between meteorites and asteroids.

References: [1] Lauretta, D.S. et al. (2019) *Nature* 568, 55-60; [2] Hamilton, V.E. et al. (2019) *Nature Astronomy* 3, 332-340; [3] Kitazato, K. et al. (2019) *Science* 364, 272-275; [4] Howard, K. et al. (2011) *GCA* 75, 2735-2751; [5] Howard, K. et al. (2015) *GCA* 149, 206-222 [6] Antarctic Meteorite Newsletter, volume 24, number 2; MET 00431; [7] Garenne, A. et al. (2016) *Icarus* 264, 172–183; [8] Choe, W.H. et al. (2010) *MaPS* 45, 531–554; [9] Jawin, E. et al. (2019) *50th LPSC*, abstract #1577; [10] Kallemeyn, G.W. et al. (1991) *GCA* 55, 881-892.

Pairing Relations of the CO3 chondrites recovered at the Dominion Range, Transantarctic Mountains.

K. Righter[1], J. Schutt[2], R.P. Harvey[2], J. Karner[3], K. Pando[4], and C. Satterwhite[4], [1] NASA Johnson Space Center, Mailcode XI2, 2101 NASA Pkwy., Houston, 77058; kevin.righter-1@nasa.gov, [2] EEPS, Case Western University, Cleveland, OH 44106. [3] Geology & Geophysics, University of Utah, Salt Lake City UT 84112. [4] Jacobs-JETS, NASA Johnson Space Center, Mailcode XI2, 2101 NASA Pkwy., Houston, 77058.

Introduction: Fourteen CO3 chondrites have been recovered in the Dominion Range (DOM) dense collection area of the Transantarctic Mtns by ANSMET teams during the 2008-09, 2010-11, and 2014-15 seasons [1-3]. DOM 08006, one of the largest masses, has been studied extensively and is recognized to be a very primitive unmetamorphosed sample of great value to planetary science [4]. Studies of pre-solar grains, organics, chondrules, inclusions, and matrix have revealed a rich scientific treasure helping to constrain the conditions in the early solar system (e.g., [4-8]). Many of the masses paired with this sample are significant, yet the pairing has been called into question due to the finding that DOM 08004 seems less primitive than DOM 08006 [5]. Because of the significant masses involved, and the great scientific value of DOM 08006, we have undertaken a detailed assessment of the pairing using field relations, macroscopic observations, petrography, and olivine compositions.

Samples and approach: We examined NASA-JSC library thin sections of DOM 08004, DOM 08006, DOM 08139, DOM 08351, DOM 10101, DOM 10104, DOM 10121, DOM 10299, DOM 10847, 10900, DOM 14019, DOM 14127, DOM 14305, and DOM 14359. Using the approach of [9] we measured the Cr content of olivine in type II FeO-rich chondrules. In addition to the olivine analyses, we also examined the field photos, labs photos for macroscopic appearance, and modal mineralogy in thin section.

Methods: Electron microprobe analyses were obtained using the Cameca SX100 electron microprobe at NASA Johnson Space Center. Standards employed were Marjalahti pallasite olivine, chromite, fayalite, diopside, oligoclase, and rhodonite. Analytical conditions include 15 kV accelerating voltage and 20 nA sample current. Because such chondrules are relatively rare in CO3 chondrites, we examined both full chondrules and individual olivine grains or fragments that are related to the FeO-rich chondrules, to increase the number of samples analyzed and thus the population statistics for the measurements. Standard deviation in Cr contents of as many olivine grains as possible were calculated and used to assess petrologic type (3.0, 3.1, 3.2, etc.) for each DOM sample [9].

Results: These samples all fall along the trend of Cr_2O_3 versus σ-Cr_2O_3 defined by previous studies of CO chondrites [9,10]. Many of the masses examined have primitive characteristics like DOM 08006 - DOM 08351, DOM 10104, DOM 10847, DOM 10900, and DOM 14359 all have high average Cr contents and relatively low σ-Cr_2O_3, and represent a total of 1.4 kg of material. On the other hand, DOM 08004, DOM 08139, DOM 10101, DOM 10121, DOM 10299, DOM14019, DOM 14127, and DOM 14305 all have higher σ-Cr_2O_3, and fall on the trend of more thermally altered, perhaps as 3.1 or 3.15. In addition, our measurements of magnetic susceptibility show that all of the least metamorphosed samples have $\log\chi$ values from 4.8 to 5.0, whereas the more metamorphosed samples have $\log\chi$ < 4.8. Such trends have also been observed for other CO3 where metamorphic grade correlates with Raman parameters [11], $\log\chi$ [12], and thermal luminescence [13]; our data support these trends and suggest that unmetamorphosed CO3 have $\log\chi$ near 4.95.

Given the heterogeneity in olivine composition from this group, as well as suggestions from thermal luminescence that there is more than one pairing group [13], it seems likely that these samples might be part of at least two distinct groups. There could be two groups – one primitive (3.0 to 3.05) and one more thermally metamorphosed (3.1 to 3.2). Alternatively, the DOM CO3 chondrites could be from the same fall, perhaps similar in mass and size to the Sutter's Mill and Tagish Lake strewnfields [14,15] - 1.7 kg of material recovered over a length of ~6 km. In that case there would be an inherent heterogeneity and a range of metamorphic grades represented within the members of the group. Perhaps cosmic ray exposure and terrestrial age studies can help to resolve this issue.

References: [1-3] Antarctic Meteorite Newsletter, vol. 32, no. 2; [2] Antarctic Meteorite Newsletter, vol. 34, no. 2; [3] Antarctic Meteorite Newsletter, vol. 37, no. 1; [4] Nittler L.R. et al. (2013) 44th LPSC #2367; [5] Alexander, C.M.O'D. et al. (2018) GCA 221, 406–420; [6] Simon, S.B. and Grossman, L. (2015) MaPS 50, 1032-1049; [7] Simon, S.B. et al. (2019) *GCA 246*, 109-122; [8] Haenecour, P. et al. (2018) *GCA* 221, 379-405; [9] Grossman, J.N. and Brearley, A. (2005) MaPS *40*, 87-122; [10] Davidson J. et al. (2014) 45th LPSC, #1384; [11] Bonal, L. et al. (2007) GCA 71, 1605-1623; [12] Rochette, P. et al. (2008) MaPS 43, 959-980; [13] Sears, D.W.G. (2016) GCA 188, 106-124; [14] Jenniskens, P. et al. (2012) *Science* 338, 1583-1587; [15] Brown, P. G. et al. (2000) *Science* 290, 320-325.

SM-ND, LU-HF AND U-PB SYSTEMATICS OF NORTHWEST AFRICA 11509 SHERGOTTITE.

M. Righter[1], T. J. Lapen[1], A. J. Irving[2] and B. Hoefnagels, [1]Dept. of Earth & Atmospheric Sciences, University of Houston, TX, USA (mrighter@uh.edu), [2]Dept. of Earth & Space Sciences, Univ. of Washington, Seattle, WA, USA.

Introduction: Northwest Africa (NWA) 11509, a fresh 500 gram stone found in Mali, is a relatively coarse grained olivine gabbroic shergottite containing shock-melted intercumulus zones [1]. It consists of relatively equant grains of clinopyroxene (51 vol.%) and olivine (17 vol.%) with vesicular, plagioclase-rich interstitial regions. NWA 11509 exhibits unique shock features including the complete melting and recrystallization of plagioclase as well as olivine grains that are recrystallized into aggregates of fine-grained polygonal subgrains [1]. Among the 134 unpaired Martian meteorites now recognized, only a few (e.g. NWA 6342 [2]) exhibit such extreme shock features. In addition to these unique shock features, NWA 11509 shows unique isotopic/geochemical characteristics. The rare earth element abundances of NWA 11509 are similar to those for intermediate shergottites. However, the measured bulk Nd and Hf isotopic compositions show that NWA 11509 falls in between the established fields for intermediate and enriched shergottites. Here we present preliminary results of Sm-Nd and Lu-Hf isotopic analyses, plus phosphate U-Pb systematics, and place these new data in the context of existing data for shergottites with the aim of identifying similarities and potential source affinities.

Samples and analytical procedures: Clean, representative dust produced by cutting a sample portion on an IsoMet saw using a Cu alloy plated stainless steel blade was used to conduct whole rock analysis. An intact interior fragment of NWA 11509 (~0.1 g) was also analyzed. A ~2.4 g aliquot of NWA 11509 was crushed in an aluminum oxide mortar and pestle, and pyroxene grains were hand-picked under a microscope. Both "whole rock" fractions and the pyroxene fraction were spiked for Lu-Hf and Sm-Nd analyses. All chemical separation procedures were carried out in clean laboratory facilities at the University of Houston (UH), and Sm, Nd, Lu and Hf isotope analyses were conducted using the Nu Instruments *Nu Plasma II* MC-ICP-MS at UH.

In situ U-Pb isotopic analysis on a polished thick section was carried out with a Photon Machines Excite coupled to a Varian 810 quadrupole ICPMS at UH. Each spot analysis was conducted with $85\,\mu m$ in diameter laser bean at 15 Hz repetition rate, a fluence of 4 J/cm², 20s on-peak blank, 30s ablation time. Operating conditions for the samples and standards were exactly matched for each analysis. Yates Mine and Madagascar phosphates were used as the external calibration standards and Bear Lake phosphate as the internal standard.

Results: The Sm-Nd analyses of NWA 11509 whole rock (*dust*) gave a measured $^{147}Sm/^{144}Nd = 0.2651$ and a present-day $\varepsilon^{143}Nd = +6.67$, which plots between the established fields for intermediate and enriched shergottites. The handpicked pyroxene fraction yielded a present-day $\varepsilon^{143}Nd = +6.63$, which is essentially the same as the value for WR-dust. The Lu-Hf analyses of whole rock (*dust)* gave a present-day $\varepsilon^{176}Hf = +3.60$ and a measured $^{176}Lu/^{177}Hf = 0.01742$. The other whole rock (*chunk*) gave a present-day $\varepsilon^{176}Hf = +5.77$ and a measured $^{176}Lu/^{177}Hf = 0.01669$. The whole rock (*dust*) and the pyroxene define a slope corresponding to a Lu-Hf age of 820 ± 84 Ma for $\lambda(^{176}Lu) = 1.865$ x 10^{-11} yr^{-1} with an initial $^{176}Hf/^{177}Hf$ value of 0.283542 ± 0.000031 using the Isoplot regression program [3]. The whole rock (*chunk*) and the pyroxene define a slope corresponding to a Lu-Hf age of 518 ± 88 Ma. The modeled source $^{176}Lu/^{177}Hf$ and $^{147}Sm/^{144}Nd$ isotope ratios were calculated using a two-stage model, assuming a differentiation age of 4.513 Ga [4] and the CHUR parameters of [5] for both 820 Ma and 518 Ma. The calculated source $^{176}Lu/^{177}Hf$ and $^{147}Sm/^{144}Nd$ compositions are 0.03797 and 0.1957 for 820 Ma, 0.03727 and 0.2008 for 518 Ma, respectively. These calculated source compositions are in good agreement in spite of the apparent age differences. The source compositions of NWA 11509 suggest that it is derived from Martian mantle mixtures that are somewhat similar to those that produced other known intermediate shergottites, but further extend the observed range in intermediate source compositions for both Lu/Hf and Sm/Nd isotopic systems.

Eight phosphate grains were analyzed for U-Pb systematics by LA-ICP-MS. All results plot on discordia between common Pb compositions and values for very recent materials (within about 12 Ma). These very young U-Pb ages of phosphates, as well as the existence of completely recrystallized plagioclase observed throughout NWA 11509, suggest that this shergottite experienced relatively high levels of shock metamorphism in comparison to other shergottites to recrystallize plagioclase and phosphates after extensive melting, likely caused during the recent (3 Ma ago [1]) energetic ejection of this specimen from Mars.

References: [1] Irving A. J. et al. (2018) *LPS* XLIX, Abstract #2279. [2] Kizovski T. V. et. al. (2019) *Meteoritics & Planetary Science* 54, 768-784. [3] Ludwig K. R. (2003) *Berkeley Geochronology Center Spec. Pub.* 1a, 59. [4] Borg L. E. et al. (2003) *GCA* 67, 3519−3536. [5] Bouvier A. et. al. (2008) *Earth Planet. Sci. Lett.* 280, 285−295.

MAPPING THE IRON DISTRIBUTION AND VALENCE STATE IN PRIMITIVE METEORITES BY SYNCHROTRON MOSSBAUER SPECTROSCOPY.

M. Roskosz[1], P. Beck[2], J. Zhao[3], W. Bi[3,4], E.E. Alp[3], [1]IMPMC, MNHN-Sorbonne Université- UMR CNRS 7590- 61 rue Buffon. 75005 Paris. France. IPAG, Université Grenoble Alpes, CNRS (Grenoble - France). [3] Advanced Photon Source, Argonne National Laboratory, USA. [4]University of Illinois at Urbana-Champaign, USA.

Introduction: Chondritic meteorites contain, at the micron-scale, heterogeneous iron-bearing phases with the 3 oxidation states, that are thus not in thermodynamical equilibrium. The ubiquity of iron makes it a tracer of initial condensation, recrystallization. Furthermore, during and after their accretion, thermal metamorphism and aqueous alteration triggered a partial textural and chemical reequilibration. As a consequence the initial state of the different components are poorly known. In this context, the study of the Fe valence state and mineralogy is of crucial importance. First because the valence state is very sensitive to the redox conditions that prevailed during the formation of iron-bearing phases and second because aqueous alteration efficiently changes this valence state. But if a detailed mineralogy of iron is the key to understand the formation and evolution of small bodies, the origin of its heterogeneity is highly debated and lacks from a comprehensive mapping at the sample scale. Here, we use the unique Synchrotron Mossbauer Spectroscopy (SMS) developed at the Advanced Photon Source to produce these maps. This development will be crucial to analyze returned samples from the next space missions (Hayabusa 2 and Osiris Rex).

Analytical methods: The issue with iron as a chemical proxy is analytical in essence. First, chemical analysis of minerals hardly provides a quantification of the valence state because a fraction of silicates are amorphous or poorly crystallized and also because some of these minerals can accept both divalent and trivalent iron cations. Second, other spectroscopic methods such as XANES and STXM may in principle be used to image the valence state of iron at the nanoscale. However, these methods require complicated cross calibration and are poorly adapted to quantify and characterize metallic phases.

In this context, Synchrotron-based Nuclear Resonant Scattering techniques, such as SMS are much more relevant but were hardly available until recently. These methods involve nuclear resonant transitions of Mössbauer nuclei excited by a synchrotron radiation. These techniques are sensitive to the chemical environment of Mössbauer isotopes. The Mössbauer microscopy developped at Sector 3ID allows imaging samples at the micrometer spatial resolution. This microscopy collects coherent nuclear resonant scattering signal and yields information based on hyperfine interactions of the nuclei in the solid. It leads to quantitative and absolute information about the magnetic, valence and spin state of the system, and local atomic symmetry for all the possible valence state of iron. In other words, this microscopy alleviates all the caveats of other available methods. Some proof-of-principle experiments were carried out employing the instruments at beamline 3-ID at the Advanced Photon Source (APS). Excellent signal-to-noise ratio was achieved, a resolution to 5 microns has been achieved, and sub-micrometer is envisioned.

Results: In an effort to develop this method to characterize meteorite samples, we mapped six samples of well-known carbonaceous chondrites (Orgueil, CI; Paris, CM3.0; Murchison, CM2.5; QUE 97990, CM2.0; PCA 91008, heated CM). The area scanned are as large as a millimeter square, consisting of 40000 data points. Maps of Fe distribution were first collected and then local analyses were performed. This spatial mapping enables to locate region of interest for further analysis. In the case of PCA 91008, it was possible to distinguish matrix silicates (Fig. 1, green spectra) from a large oxide grain with probable hyperfine splitting (Fig. 1, blue spectra). When comparing measurement obtained on matrix area from the series of CM, similarities are found among CM chondrites (Murchison, QUE 97990, Paris). The SMS spectra of PCA91008 matrix seems distinct (counts minima at 50 and 80 ns), possibly related to the thermal process experienced by this sample. Overall all SMS spectra obtained on these suite of CM are in agreement with silicates (including phyllosilicates) being the major host of iron. On the contrary, the spectra of Orgueil is clearly different with a lot of structure in agreement with Fe being majorly present within magnetite. Detailed fitting of this data is underprocess and should reveal the fine crystallographic environment of iron in this suite of samples.
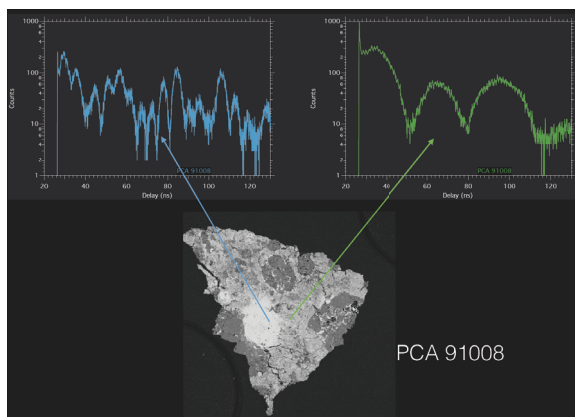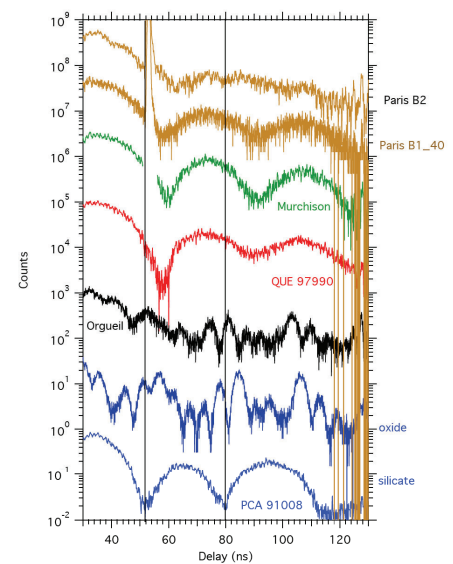

Figure 1 (left): Typical SMS spectra of olivine (green), and magnetite, (blue).

Figure 2 (right): Typical SMS spectra of the matrices of studied meteorites with some reference spectra of single minerals. The spectral variations reflects the relative proportions of iron-bearing minerals in these matrices.

SECONDARY ALTERATION OF THE SERRA PELADA EUCRITE.

J. Roszjar[1], [1]Natural History Museum (NHM) Vienna, Burgring 7, 1010 Vienna, Austria (julia.walterroszjar@nhm-wien.ac.at).

Introduction: In this study, the petrology of the observed meteorite fall Serra Pelada from Brazil has been investigated with a focus on secondary alteration features of this meteorite that form by shock- and thermal-metamorphic reactions and probably even fluid-rock interactions. Such complex crustal processes on rocky asteroidal bodies in the inner Solar System are abundant but yet not well understood. As the Serra Pelada meteorite exhibit a variety of secondary alteration features, this sample has been selected for this case study.

Results and Discussion: The Serra Pelada meteorite fell on June 29th 2017, weighing 12 kg total and has been classified as a monomict eucrite. Here, two polished sections (O336 and O338, inventory NHM Vienna) were investigated using the optical and electron microscope facility at the NHM Vienna, Austria. Results confirm that Serra Pelada is a moderately shocked monomict basaltic eucrite. This sample displays a brecciated texture composed of various lithic clast types embedded in a fine-grained silicate matrix, mainly consisting of pyroxene and plagioclase. The lithic clasts are typically ophitic to subophitic, and some exhibit evidence of recrystallization. In addition, some rounded clasts occur as inclusions in large orthopyroxene mineral fragments.

Shock features include undulatory extinction and mosaicism of silicates, the occurrence of melt pockets and impact melt veins cross-cutting the sample, and the absence of maskelynite, confirming the moderate degree of shock metamorphism. In addition to rock-forming silicates, accessory minerals are present in Serra Pelada, as typically found in other basaltic eucrites, including: silica, ilmenite, chromite, troilite, and (low Ni-) Fe-metal. In addition, F-apatite, merrillite, zircon and baddeleyite, and (secondary) Fe-rich olivine veinlets within larger pyroxene grains are present. The Ca-phosphates are often fractured and occur interstitial to plagioclase, low- and high-Ca-pyroxenes and often in mineral assemblages with troilite, chromite and ilmenite. Some Ca-phosphate grains are located within lithic clasts and here often in association with silica and rare zircon. Replacement reactions of merrillite and F-apatite are observed, again indicative of a thermal-metamorphic reaction affecting the host rock. Zircon grains are subrounded and up to 20 µm in size, often fractured, and typically enclosed in or exsolved from ilmenite and in association with merrillite. This petrological finding can be assigned to thermal metamorphism, and has been used together with radioisotope analysis to constraint the timing of a global crustal metamorphic event on the eucrite parent body(ies) [e.g., 1]. A lithic clast of ~60 µm in size and composed of silica, plagioclase and orthopyroxene, located at the margin of a large ~500 µm ilmenite grain, is surrounded by a ~5 µm zircon rim. This rim is composed of aligned individual zircon grains that likely formed by a thermal-metamorphic reaction in the Serra Pelada eucrite.

In addition, chromite and ilmenite grains are often intergrown, which seems typical for highly metamorphosed (type 5 and 6) eucrites [2], and which is petrologically consistent with the presence of coarse augite exsolution lamellae within pigeonite hosts and extensive replacement of pigeonite by augite. Two lithic clasts with a fine-grained, recrystallized texture, mainly composed of Ca-pyroxene and silica grains of <20 µm each, also contain larger chromite and ilmenite grains of up to 200 µm in size, which are located along the margins. Within these two clasts finely dispersed troilite, F-apatite and chromite grains of <10 µm are present in addition that likely crystallized upon intense thermal metamorphism.

The Fe-rich olivine veinlets are always associated with coarse pyroxene grains in the silicate matrix or large pyroxene grains within lithic clasts (i.e., absent in plagioclase). They formed as a trail of individual olivine grains, which are accompanied by anorthitic plagioclase, chromite and troilite grains. The finding of such Fe-rich olivine veinlets is interpret to form during secondary alteration processes, either related to metasomatic, shock- or thermal-metamorphic origin and/or a combination of those processes. These petrologic features were discovered and discussed in a limited number of eucrite and howardite samples so far, e.g. [3-7].

Conclusions: The moderately shocked, monomict basaltic eucrite Serra Pelada is characterized by the occurrence of lithic clasts with various textures and a series of shock- and thermal-metamorphic and probably even metasomatic features. Observed secondary alteration processes not only affect the rock-forming silicate textures, but are prominently recorded in the petrology of accessory phases, such as in spinels, zircon and Ca-phosphates grains in particular, further supporting their relevance for the interpretation of large-scale metamorphic processes on meteorite parent bodies.

References: [1] Iizuka T. et al. (2015) *Earth and Planetary Science Letters* 409:182-192. [2] Yamaguchi A. (2000) *Meteoritics & Planetary Science* 35:A174. [3] Barrat J.-A. et al. (2011) *Geochimica et Cosmochimica Acta* 75:3839-3852. [4] Warren P. (2002) *LPS XXXIII*, Abstract #1147. [5] Roszjar J. et al. (2011) *Meteoritics & Planetary Science* 46:1754-1773. [6] Pang R. et al. (2017) *Meteoritics & Planetary Science* 52:2113-2131. [7] Patzer A. and McSween H. Y. (2018) *Meteoritics & Planetary Science* 53:1131-1149.

THE PETROLOGY AND GEOCHEMISTRY OF CY CHONDRITES: A STUDY OF YAMATO 82162 AND YAMATO 980115

S. S. Russell[1], J. Spratt[2] and A. J. King[1]. [1]Planetary Materials Group, Department of Earth Sciences, Natural History Musuem, Cromwell Road, London SW7 5BD, UK. [2]Core Research Laboratories, Natural History Musuem, Cromwell Road, London SW7 5BD, UK. Email: sarr@nhm.ac.uk

Introduction: Three unusual carbonaceous chondrites – Yamato 82162, Yamato 86720, and Belgica 7904 - were studied by a consortium in 1992 [1]. Along with several meteorites found since then (e.g. Yamato 86789, Yamato 86029, Yamato 980115, Dhofar 1988 and Dhofar 2066), these aqueously altered and dehydrated meteorites have bulk oxygen isotope compositions heavier than any other carbonaceous chondrite group (typical $\delta^{18}O$ ~22 ‰ [2]) and an unusual mineralogy [3]. Although they experienced later thermal metamorphism, this cannot explain their distinct compositions [4]. Thus, while they are often linked to the CI or CM chondrites, it has been suggested they represent a new group of meteorites, the CYs [1, 4]. These meteorites are of particular interest as their extremely dark colour may suggest a relationship to the Hayabusa2 target Ryugu [5]. Here, we have studied the mineralogy, geochemistry and petrology of two of these meteorites, Yamato 980115 (Y-980115) and Yamato 82162 (Y-82162).

Methods: Thin sections of Y-82162 and Y-980115 were characterized using an FEI Quanta 650 FEG-SEM. The bulk composition of matrix phyllosilicates was determined using a Cameca SX100 electron microprobe, defocused to a beam size of 20 microns. More detailed element maps and focused spot analyses at a resolution of ~1 micron were made using a JEOL JXA-8530F Hyper-Probe EPMA.

Results: Y-82162 and Y-980115 are fine-grained brecciated meteorites containing abundant clasts of sulphides, magnetite, periclase and phosphate. Unlike the CI chondrites, they have relict chondrule-shaped features (typical size 10-50μm) consisting of phyllosilicates, magnetite, sulphides, carbonates and Mg-Ca-Fe bearing phases, consistent with a high degree of aqueous alteration. Figure 1 compares the matrix composition of Y-980115 with a CI1 and CM1 chondrite. The CI has a phyllosilicate composition that lies between serpentine and saponite, in keeping with TEM observations suggesting that the two are finely intermixed in CI matrix [6], whereas the CM1 has a composition closer to serpentine. In contrast, Y-980115 contains at least two distinct compositions; a Mg-rich serpentine and a component similar in composition to the CI.

Discussion: The two meteorites studied here, like most CYs, are petrological type 1, although B-7904 contains unaltered chondrules and is a CY2. The intial presence of chondrules in Y-82162 and Y-980115 is clear, but they have been fully altered. Other researchers have suggested the rare presence of altered CAIs in Y-980115 [7] and in B-7904 [8,9]. These meteorites are petrographically, geochemically and isotopically distinct from other groups and we support naming them "CY" chondrites.

References: [1] Ikeda Y. (1992) *Proc. NIPR Symp. Antarct. Meteorites* **5**, 49–73. [2] Clayton R. N. & Mayeda T. K. (1999) *GCA* **63**, 2089–2104. [3] King A. J. et al. (2015) *GCA* **165**, 148–160. [4] King A. J. & Russell S. S. (2019) *LPSC* abstract #1386. [5] Kitazato et al. (2019) *Science* **364**, 272–275. [6] Tomeoka K. & Buseck P. (1988) *GCA* **52**, 1627–1640. [7] Fujiya et al. (2011) *Meteoritical Society Abtract* #5240. [8] Bischoff A. and Metzler K. (1991) *Proc NIPR Symp. Antarct. Meteorites*, **4**, 226-246 [9] Harries D. and Langenhorst F. (2013) *MAPS* **48** 879-903.
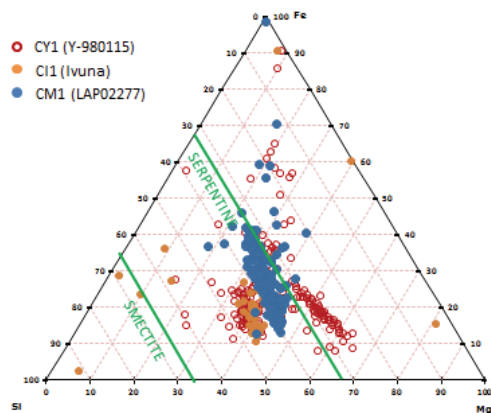
Figure 1. Matrix compositions of a CM1, CI1 and CY1 meteorite compared.

MALOTAS: A NEW VIEW OF AN OLD FALL FROM ARGENTINA

M. E. Saavedra[1], J. Roszjar[2], M. Humayun[3], R. Tanaka[4], M. E. Varela[1] and R. Lira[5]

[1]ICATE-CONICET, Av. España 1512 Sur, San Juan J5402DSP, Argentina (m.saavedra@conicet.gov.ar); [2]Natural History Museum Vienna, Burgring 7,1010 Vienna, Austria; [3]Florida State University, Tallahassee, FL 32310, USA; [4]Institute for Planetary Materials, Okayama University, 827 Yamada, Misasa, Tottori, 682-0193, Japan; [5]Museo de Mineralogía y Geología Dr. Alfred Stelzner, FCEFyN-UNC, CONICET, Av. Vélez Sársfield 249, X5000JJC, Córdoba, Argentina.

Introduction: In the morning of June 22nd, 1931, a meteorite fall was reported in the province of Santiago del Estero, Argentina. MALOTAS is the official name given to the type H5 ordinary chondrite as the registered fall 1931, which we have re-investigated with surprising results.

Historical aspects: In 1931 collected rock samples of this recent meteorite fall were given to Professor Juan A. Olsacher from Córdoba University who decided to inspect the fall locality and collect some further pieces. His report [1] indicates that the fall covered an area of 5 x 2.5 km with the main axis having a NE to SE direction in the vicinity of the Dulce River. Therefore many of the individual pieces were likely lost. As the area was covered by a dense forest he was able to collect three pieces only. His studies showed that "*the meteorite is made up of fragments that correspond to two different types based on their composition and structure: one is chondritic, composed by olivine and pyroxene with abundant metallic minerals; the second one is feldspar-rich with scarce presence of the previous components and with an ophitic texture" [1].* During a visit of the small meteorite collection of the Museo de Mineralogía y Geología Dr. Alfred Stelzner in 2015, one of us (MEV) found that two different stones (a chondrite and an achondrite) were exhibited in the showcase, labeled as "*Malotas, 1931*". After further investigation of the achondritic fragment, the meteorite turned out to be a basaltic eucrite. Below is a description of both rocks.

The eucrite: is an individual, fully encrusted piece weighing 62.4 g. The interior is very fresh covered by a very shiny black fusion crust. Optical and electron microscopic investigations reveal that the sample is a basaltic monomict breccia, mainly consisting of coarse- and fine–grained silicate domains. There are few shock features record by crystals with only some faint undulatory extinction and one melt vein cross-cutting the sample. Microprobe examination of two polished sections reveal very similar silicate compositions for the coarse- and fine-grained lithologies: Low-Ca pyroxene $Fs_{62.5\pm0.8}Wo_{2.23\pm0.9}$, Ca-rich pyroxene $Fs_{26.9\pm0.9}Wo_{43.9\pm1}$, and plagioclase $An_{82.1\pm3.4}$, with minor, secondary anorthitic plagioclase with $An_{95.71\pm2.7}$. Spinel composition is $Chr_{0.74}$-$Her_{0.18}$. Since the Ti contents of spinels in basaltic eucrites seems to be diagnostic of its thermal metamorphic grade [2], variations in the Cr, Al and Ti contents allow a classification as to metamorphic type 4. Trace element compositions of the coarse- and fined-grained lithologies are similar, with REE ($\sim20 \times CI$), characterized by a flat pattern with a negative Eu anomaly ($\sim15 \times CI$). This characteristic together with the bulk rock FeO/MgO ratio and La and Sc concentrations, indicate that this meteorite belongs to the group of Stannern-trend eucrites. Replicate analyses of stable oxygen isotopes (in ‰), obtained by laser fluorination revealed values of: $\delta^{17}O$ of 1.785 and 1.775; $\delta^{18}O$ of 3.779 and 3.787; $\Delta^{17}O$ of -0.208 and -0.222. MALOTAS (b) is the official name given to this basaltic eucrite (approved: 4 July, 2018), because this meteorite might be connected to the 1931 fall event according to [1]. However, as there are still some doubts on the pairing of the individual rock fragments, it was approved as a 'find, doubtful fall".

The chondrite: exhibited in the showcase of the museum as Malotas 1931, is an ordinary chondrite with a total mass of 79.4 g. A petrographic study of two thin sections revealed the occurrence of relict fragments and chondrules. Among the latter, barred olivine, radiating pyroxene and porphyritic olivine pyroxene chondrules are the most abundant. The rock has minimal shock features, e.g., faint undulatory extinction and absence of planar fractures. Major element analysis of the main mineral phases are: olivine ($Fa_{24.56}$) and pyroxene ($Fs_{21.17}$; $Wo_{1.47}$), consistent with an L-type classification. This is in conflict with the officially accepted classification of MALOTAS with a chemical composition of olivine Fa_{19}, [3], Co concentration of 1100 μg/g [4], and a magnetic susceptibility of 5.40, consistent with an H-type. Since the main mass of MALOTAS (4712 g) is in the E. Jawerbaum private collection (Buenos Aires), further studies are on the way to compare fragments of MALOTAS to those of the chondrite in the Museo de Mineralogía y Geología of Cordoba. The discovery of these new fragments, provides the opportunity to (re)evaluate the 1931 fall under a different view: Was it a polymict fall?.

Refernces: [1] Olsacher (1931) Imprenta de la Universidad, Cordoba, 1-18; [2] Yamaguchi (2000) *Meteoritics and Planetary Science,* **35**, Suppl. A174; [3] Mason (1963) *Geochimica et Cosmochimica Acta,* **27**, 1011-1023; [4] Ligner et al., (1987) *Geochimica et Cosmochimica Acta,* **51**, 727-739.

^{176}LU–^{176}HF AND ^{87}RB–^{87}SR SYSTEMATICS AND RARE EARTH ELEMENT ABUNDANCES OF DIOGENITES: EVIDENCE FOR THEIR CRYSTALLIZATION FROM PARTIAL MELTS OF THE VESTAN MANTLE.

T. Saito[1], H. Hidaka[1], and S.-G. Lee[2], [1]Depatment of Earth and Planetary Sciences, Nagoya University, Nagoya 464-8601, Japan (saito.takaharu@f.mbox.nagoya-u.ac.jp), [2]Geological Research Division, Korea Institute of Geoscience and Mineral Resources, Daejeon 34132, Republic of Korea.

Introduction: The asteroid 4 Vesta is one of the differentiated rocky bodies in the solar system. Vesta is a distinctively informative object for investigating the scale dependence of the evolution of rocky planets. Furthermore, since Vesta is probably a remnant protoplanet [1], its physical property and internal structure possibly provide fundamental and unique information about the accretion processes in the early solar system. Howardite–eucrite–diogenite (HED) meteorites, which are believed to be surface materials from Vesta [2], offer clues for the differentiation processes of the Vestan crust. However, despite geochemical, mineralogical, and petrological studies of HED meteorites over several decades, the differentiation processes of the Vestan crust are still controversial. In this study, we focus on the relationship between crystallization timings of eucrites and diogenites, which are geochemically and petrologically distinct subgroups of HED meteorites. Although this relationship may put strong constraints on the differentiation processes of HED meteorites, it is still in debate mainly due to lack of chronological data of diogenites. On the one hand, the pioneering study on the ^{87}Rb–^{87}Sr systematics and the recent study on the short-lived ^{26}Al–^{26}Mg chronometry of diogenites suggested the later crystallization of diogenites than that of eucrites [3,4]. On the other hand, some other studies found that ^{53}Mn–^{53}Cr and ^{60}Fe–^{60}Ni isotopic data of diogenites define isochron regressions together with the eucrite data [5–7], suggesting approximately synchronous crystallization of these two meteorite classes. Although, at present, the reason for the discrepancy among these diogenite chronologies is not obvious, thermal disturbances associated with the heavy bombardment on Vesta [8] might contributed to it. Furthermore, since the previous studies mentioned above analyzed only two or three diogenite samples, their results are not necessarily representative to all diogenites. Here, we present the ^{176}Lu–^{176}Hf systematics of nine diogenites, which is characterized by considerably high closure temperature [9], together with the ^{87}Rb–^{87}Sr systematics and the rare earth element (REE) abundances and discuss about their differentiation processes.

Samples and Experiments: Three fall diogenites (Bilanga, Johnstown, and Tatahouine), one desert-find diogenite (NWA 5480), three Antarctic diogenites (Y-74013, Y-74097, and Y-002875), and two provisional diogenites were used in this study. After an acid-leaching treatment using 5 mL of hot (100°C) 0.5 M HCl to remove the terrestrial contaminants, the acid-residue of each powdered sample (~1 g) was completely digested by concentrated HF–HClO$_4$ mixture. A minor portion (~10% of the total) of the sample solution was used for the determination of elemental abundances by ICP-MS (Agilent 7700x), while the major portion (~90%) was used for the isotopic a work. Sr and Hf were purified from the sample solution through a two-step column chemistry using Ln-spec and Sr-spec resin respectively. Isotopic analyses were performed by TIMS (VG Sector 54-30) for Sr and MC-ICP-MS (Neptune Plus) for Hf.

Results and Discussion: The ^{176}Lu–^{176}Hf age of 4.40 ± 0.38 Ga with the initial ^{176}Hf/^{177}Hf ratio of 0.2820 ± 0.0013 are calculated from the ^{176}Lu–^{176}Hf data set of the nine diogenites. This initial ^{176}Hf/^{177}Hf ratio is significantly higher than the reference eucrite value (0.27977 ± 0.00008 [10]), while the ^{176}Lu–^{176}Hf age is identical to that of eucrites (4.59 ± 0.15 Ga [10]) within the error range. The high initial ^{176}Hf/^{177}Hf ratio of the diogenites indicates their differentiation from the source material characterized by superchondritic Lu/Hf ratio. An olivine-rich mantle crystallized from a planetary-scale magma ocean on Vesta [11] is probably the source material of diogenites, because it should be extremely enriched in Lu relative to Hf based on experimentally obtained olivine/melt partitioning coefficients [12]. The heavier REE abundances of the diogenites show significant variation, indicating their crystallization from compositionally diverse parental melts. A combination of the ^{176}Lu–^{176}Hf and REE data of the diogenites suggests their crystallization from partial melts of the Vestan mantle. The variation of the REE abundances can be explained by the variation of the degree of partial melting. In contrast to the ^{176}Lu–^{176}Hf systematics, the ^{87}Rb–^{87}Sr systematics of the diogenites are totally disturbed probably due to intense impacts on the Vestan surface.

References: [1] Russell C. T. et al. (2012) *Science* 336: 684–686. [2] Binzel R. P. and Xu S. (1993) *Science* 260: 186–191. [3] Takahashi K. and Masuda A. (1990) *Nature* 343: 540–542. [4] Hublet G. et al. (2017) *Geochimica et Cosmochimica Acta* 218: 73–97. [5] Trinquier A. et al. (2008) *Geochimica et Cosmochimica Acta* 72: 5146–5163. [6] Day J. M. D. et al. (2012) *Nature Geoscience* 5: 614–617. [7] Tang H. and Dauphas N. (2012) *Earth and Planetary Science Letters* 359–340: 248–263. [8] Bogard D. D. and Garrison D. H. (2003) *Meteoritics & Planetary Science* 38: 669–710. [9] Anczkiewicz R. et al. (2007) *Lithos* 95: 363–380. [10] Bouvier A. et al. (2015) *Meteoritics & Planetary Science* 50: 1896–1911. [11] Righter K. and Drake M. J. (1997) *Meteoritics & Planetary Science* 32: 929–944. [12] Kennedy A. K. et al. (1993) *Earth and Planetary Science Letters* 115: 177–195.

EXTREME ^{16}O-RICH REFRACTORY INCLUSIONS IN THE ISHEYEVO CHONDRITE.

N. Sakamoto and N. Kawasaki, Hokkaido University, Sapporo 001-0021 Japan (naoya@ep.sci.hokudai.ac.jp)

Introduction: The oxygen three-isotope diagram shows fractionation and mixing of materials having different origins. Whole-rock oxygen isotopic compositions of chondrite groups plotted on the diagram provide mixing lines with different slopes (e.g. CO-CM 0.70, CR-CH 0.59) as a consequence of the interaction of primordial isotopic reservoirs in the solar system [1]. CV chondrites lie close to the carbonaceous chondrite anhydrous mineral line (CCAM, slope 0.941) defined by separated minerals from Allende refractory inclusions (CAI), implying that their isotopic compositions were determined by an exchange interaction between two reservoirs, one ^{16}O-rich and the other ^{16}O-poor [2]. An ^{16}O-poor end member (Δ^{17}O = +85‰) was found from cosmic symplectites composed of magnetite and iron sulfide, interpreted that the ^{16}O-poor reservoir is H_2O water [3]. Although several candidates were reported for the ^{16}O-rich reservoir from a chondrule named a006 (Δ^{17}O = -37‰) [4], 4 refractory inclusions (Δ^{17}O = -37 to -32‰) [5,6] from CH chondrites and the Sun (Δ^{17}O = -28‰) [7] enriched in ^{16}O relative to common CAIs (Δ^{17}O = -23‰) [e.g. 8], the nature of the primordial ^{16}O-rich reservoir is poorly understood. In this study, we surveyed extremely ^{16}O-enriched refractory inclusions in the Isheyevo CH/CB carbonaceous chondrite.

Experimental: Thirteen thick sections of the Isheyevo chondrite were newly prepared. Al and/or Ca rich inclusions were picked up from combined X-ray elemental maps of the whole sections obtained by FE-SEM equipped with a X-Max^N 150 EDS detector. Oxygen isotope analysis were performed by ims-1280 and ims-1280HR SIMS instruments at Hokkaido University.

Results and Discussion: Oxygen isotopic compositions of 263 refractory inclusions were measured and 4 extreme ^{16}O-rich inclusions were found. The extreme ^{16}O-rich inclusions are composed of grossite core rimmed by thin layers of spinel, melilite and/or Ti-rich diopside. Although the grossite cores show heterogeneous oxygen isotopic composition ranging from Δ^{17}O = -32 to -36‰, high precision isotopograph clearly revealed that the grossite can be isotopically altered and the inclusions are enriched in ^{16}O relative to common CAIs including the thin layers. On the other hand, the spinel grains in the thin layer have uniform ^{16}O-rich composition (Δ^{17}O = -37‰) and fall on somewhat lower than the CCAM line. In order to confirm the characteristic oxygen isotopic composition of the extremely ^{16}O-rich material, the oxygen isotopic composition of olivine grains in the shell of the a006 chondrule were measured with high precision condition using three Faraday cups. The oxygen isotopic composition of the olivine grains in a006 chondrule (δ^{17}O = -77.26‰, δ^{18}O = -75.15‰, Δ^{17}O = -38.18‰) was plotted close to the spinel data of the Isheyevo inclusions and makes a regression line with olivine grains of a porphyritic olivine chondrule δ^{17}O = (0.9882±0.0051) × δ^{18}O – (3.00±0.25). Cosmic symplectites are located at the terminal of the line passing through the chondrules [9]. The extreme ^{16}O-rich materials also located on the extension of the lower limit of the standard deviation of the recommended group averages (area A, B, C and F) with a mass dependent fractionation line from the average of Genesis data [7]. If the extreme ^{16}O-rich end member simply formed a line mixed with the primordial ^{16}O-poor water, CAIs in CV chondrites (Δ^{17}O = -24‰) formed in a distinct oxygen reservoir slightly fractionated from the Solar System line.

References: [1] Clayton and Mayeda (1999) *Geochimica et Cosmochimica Acta* 63:2089-2104. [2] Clayton et al. (1977) *Earth & Planetary Science Letters* 34:209-224. [3] Sakamoto et al. (2007) *Science* 317:231-233. [4] Kobayashi et al. (2003) *Geochemical Journal* 37:663–669. [5] Gounelle et al. (2009) *Astrophysical Journal* 698:L18-L22. [6] Krot et al. (2017) *Geochimica et Cosmochimica Acta* 201:185-223. [7] McKeegan et al. (2011) *Science* 332:1528-1532. [8] Kawasaki et al. (2018) *Geochimica et Cosmochimica Acta* 221:318-341. [9] Ushikubo et al. (2012) *Geochimica et Cosmochimica Acta* 90:242-264.

BA ISOTOPIC HETEROGENEITY IN CM CHONDRITES

K. Sakuma[1], H. Hidaka[1] and S. Yoneda[2], [1]Department of Earth and Planetary Sciences, Nagoya Uniersity (Furo-cho D2-2 (510), Chikusa-ku, Nagoya 464-8601, Japan. E-mail: sakuma.keisuke@j.mbox.nagoya-u.ac.jp, hida-ka@eps.nagoya-u.ac.jp), [2]Department of Science and Engineering, National Museum of Nature and Science (Ama-kubo 4-1-1, Tsukuba 305-0005, Japan. E-mail: yoneda@kahaku.go.jp).

Introduction: Ba has seven stable isotopes and consists of s-, r- and p-process nucleosynthetic components. In addition, isotopic abundance of ^{135}Ba may be affected by radiogenic components decayed from the presently extinct ^{135}Cs ($t_{1/2}$ = 2.3 Ma). Therefore, Ba isotopic studies in primitive planetary materials provide information of the presences of several additional nucleosynthetic components in the early solar system and the chronological application using ^{135}Cs-^{135}Ba decay system [1, 2, 3, 4]. The Ba isotopic data of primitive planetary materials are important to understand the evolution processes of the early solar system. In this study, isotopic analysis of Ba and quantitative analyses of Rb, Sr, Cs, Ba and REE abundances from the acid leachates of four CM2 chondrites, Cold Bokkeveld, Murray, Nogoya and NWA 4428, were performed to discuss the origin of Ba isotopic variations.

Sample and Experiment: Each powdered sample (600~900 mg) was leached using 10 mL of 0.1M acetic acid-ammonium acetate, 0.1M HCl, 2M HCl and aqua regia, successively. The acid residue was finally decomposed by HF-HClO$_4$ about 150°C for 5 days. Separately from the above leaching treatment, about 100 mg of powdered sample was decomposed by HF–HClO$_4$, and treated as a whole rock for analysis. Each solution was divided into two portions; a major portion for Ba isotopic analysis by TIMS and another minor portion for the determination of Rb, Sr, Cs, Ba and REE abundances by ICP-MS. For the isotopic analysis, each major portion was treated with conventional resin chemistry to purify the Sr and Ba fractions. The sample solution was loaded onto cation exchange resin packed column (AG50WX8, 200–400 mesh, H$^+$ form, 50 mm length × 4.0 mm diameter). The column was washed with 3.5 mL of 2 M HCl for the elution of major elements, and then it was washed with 3.5 mL of 2 M HCl for the elution of the Sr fraction. Finally, the column was washed with 3 mL of 2 M HNO$_3$ for the elution of the Ba fraction. For further purification, Ba fraction was loaded onto a Sr resin packed column (Eichrom, Sr resin, particle size of 100–150 μm, 50 mm length × 4.0 mm diameter). The column was washed with 3.5 mL of 3 M HNO$_3$, and was washed with 6.5 mL of 7.5 M HNO$_3$ for the elution of Ba.

Results and Discussion: The Ba isotopic data of the whole rock show small (-0.58 < ε < 0.24) or no isotopic variations within the analytical errors. On the other hand, the Ba isotopic data from most of the acid leachates show variable isotopic excesses of ^{135}Ba, ^{137}Ba and ^{138}Ba. Furthermore, the Ba isotopic data of the acid residues show variable isotopic deficits of ^{130}Ba, ^{132}Ba, ^{135}Ba, ^{137}Ba and ^{138}Ba. These isotopic data set suggest a heterogeneous distribution of s- and r- process nucleosynthetic components of Ba isotopes in the early solar system. In previous studies [2, 3, 4], the Ba isotopic data of the acid residue in CI and CM chondrites and Tagish Lake (C2-ungrouped) meteorite showed large isotopic anomalies because of the enrichment of a carrier of s-process isotopes such as presolar SiC grains [5, 6]. However, some Ba isotopic data cannot be explained only from the contribution of s- and r-process nucleosynthetic components. As one of the possibilities, there is a contribution of X-type SiC grains, which are thought to come from type II supernovae (n-process components) [7, 8]. Assuming that the isotopic compositions of s-, r- and n-process nucleosynthetic components in individual samples are constant, we propse a model to estimate the ^{135}Cs isotopic abundances from the subtraction of the additional components.

References: [1] Hidaka H. et al. (2001) *Earth Planet. Sci. Lett* 193: 459-466. [2] Sakuma K. et al. (2018) *The Astrophysical Jounal* 853: 92. [3] Hidaka H. et al. (2003) *Earth Planet. Sci. Lett* 214: 455-466. [4] Hidaka H. and Yoneda S. (2011) *Geochimca et Cosmochimica Acta* 75: 3687-3697. [5] Ott U. and Begemann F. (1990) *The Astrophysical Jounal* 353: L57-L60. [6] Prombo C. A. et al. (1993) *The Astrophysical Jounal* 410: 393-399. [7] Pellin M. J. et al. (2000) *LPS* 31: 1934. [8] Stephan T. et al. (2018) *Geochimca et Cosmochimica Acta* 221: 109-126.

ISOTOPIC COMPOSITIONS OF W AND Mo IN ALLENDE'S CAIs, CHONDRULES AND MATRIX: POSSIBLE LEGACY OF AQUEOUS REDISTRIBUTION OF W AND Mo FROM PRESOLAR GRAINS?

I. S. Sanders[1] and E. R. D. Scott[2], [1]Department of Geology, Trinity College, Dublin 2, Ireland; isanders@tcd.ie, [2]Hawai'i Institute of Geophysics & Planetology, University of Hawai'i at Manoa, Honolulu, HI 96822, USA.

Puzzling isotopic signatures in fine-grained CAIs: The most recent Hf-W isochron for calcium-aluminium-rich inclusions (CAIs) [1] is based almost entirely on 8 coarse-grained (c-g) CAIs and 6 fine-grained (f-g) CAIs from the Allende (CV3) chondrite. The isochron is tightly constrained but to get the f-g CAIs to plot on the line their measured ε^{182}W first had to be corrected to remove *variable* nucleosynthetic ε^{182}W that correlates with ε^{183}W. The origin of this nucleosynthetic ε^{182}W, which is almost negligible in the c-g CAIs, is puzzling. It was attributed by [1] to 'initial heterogeneities in the primitive solar nebula ... at the scale of individual CAI'. We find this explanation unattractive because it seems to suggest a separate (local?) reservoir of hot nebular gas for each f-g CAI. Aware that Allende was extensively altered hydrothermally, [1] also considered, but dismissed, parent body alteration as a cause of the W isotope variation in f-g CAIs, claiming that mobilization of W would have disturbed the Hf-W isochron.

Brennecka et al. [2,3] measured Mo isotopes in the same CAIs that were analysed by [1] for W isotopes. They found that the f-g CAIs plot on the 'carbonaceous' (CC) 'outer solar system' line on the ε^{94}Mo v ε^{95}Mo diagram of [4], with ε^{94}Mo varying enormously, from -20 ε units (enriched in s-process Mo) to +15 ε units (depleted in s-process Mo); the c-g CAIs all plot together above the CC line due to enrichment of r-process Mo. To account for these observations they, like [1], invoked nebular heterogeneity. Since we find this hard to envisage, we ask why else the Mo and W isotopic compositions of the f-g CAIs might differ from those of the c-g CAIs, and why the f-g CAIs plot far apart along the CC line on the ε^{94}Mo v ε^{95}Mo diagram. We appeal here to hydrothermal alteration.

A possible solution: Brennecka et al. [2,3] noted that Mo isotopes in leachates from Murchison (CM2), obtained by [5] using increasingly aggressive acids, also spread widely (from -40 to +25 in ε^{94}Mo) along the CC line. We suggest that if acid leaching of a CM chondrite in the laboratory can yield Mo extracts that spread far along the CC line, then similar leaching might have happened naturally in the Allende parent body where, instead of acids, there would have been a succession of aqueous metamorphic fluids, released as the temperature rose. We imagine that Mo in the first warm flush of fluid came from the more-easily dissolved presolar grains, depleted in s-process Mo, and that later on, hotter fluid scavenged Mo from less-soluble s-process-enriched presolar carriers like SiC. Successive flushes of fluid would have transferred their Mo solute to separate f-g CAIs to account for the diverse ε^{94}Mo values of the latter. We do not know how the process might have worked, but suspect it was linked to disequilibrium metamorphic changes in Allende, involving dehydration and rehydration. We suggest that the c-g CAIs kept their original Mo, perhaps in refractory metal nuggets (RMNs) [2], and escaped significant alteration because of their grain size. We suggest that the f-g CAIs were isotopically identical to the c-g CAIs to begin with but, having few, if any, RMNs [2], they had little initial Mo, so their Mo isotopes became dominated by Mo that arrived later in solution.

We suggest that W was transferred like Mo from presolar carriers into the f-g CAIs. The Hf-W isochron was undisturbed, we think, because the empirical correction made by [1] for nucleosynthetic ε^{182}W effectively removed the ε^{182}W that travelled with correlated ε^{183}W from the presolar carriers (like W in the Murchison leachates of [5]), while radiogenic ^{182}W was safely sealed within unaltered silicate grains where its lithophile parent, ^{182}Hf, decayed.

Our suggestions appear to be consistent with the facts (1) that Mo is a mobile element, as is seen, for example, in its behaviour in CM chondrites [6], and (2) that most elements whose isotopes have been measured in CAIs (for example Ti, Sr and Ba [2]) are isotopically similar in both c-g and f-g CAIs, whereas W and Mo stand out as being isotopically different in the two [2]. Also, (3) some c-g CAIs (including one of those analysed by [1]) are perhaps thermally modified f-g CAIs because they have the distinctive Group II REE pattern which is typical of f-g CAIs.

Chondrules and matrix: Budde et al. [4,7] found that chondrules in Allende are depleted, and matrix is enriched, in s-process W and Mo relative to the bulk meteorite. They presented this 'nucleosynthetic isotopic complementarity' as a key constraint for chondrule formation. However, the constraint is puzzling because it seems hard to reconcile it with any chondrule-forming model [see 8], though we tried to accommodate it with our splashing model [9]. We propose here that the complementary isotopic relationship of Allende's chondrules and matrix has no bearing on chondrule formation because it arose later, during hydrothermal alteration, when s-process-depleted W and Mo were leached from presolar grains in the matrix and transferred into the chondrules.

References: [1] Kruijer T. S. et al. (2014) *EPSL* 403:317-327. [2] Brennecka G. A. et al. (2017) *LPSC* abstract #1619. [3] Brennecka G. A. et al. (2018) *LPSC* abstract #2429. [4] Budde G. et al. (2016) *EPSL* 454:293-303. [5] Burkhardt C. et al. (2012) *EPSL* 357/8:298-307. [6] Friedrich J. M. et al. (2018) *GCA* 237:1-17. [7] Budde G. et al. (2016) *PNAS* 113:2886-2891. [8] Zanda B. et al. (2018) 81st Meteoritical Society Meeting abstract #6171. [9] Sanders I. S. and Scott E. R. D. (2018) Chapter 14 in *Chondrules*, Cambridge University Press.

SUGARS AND RELATED COMPOUNDS: COMPARISONS BETWEEN METEORITES AND THE RESIDUES PRODUCED FROM THE UV IRRADIATION OF ASTROPHYSICAL ICE ANALOGS.

S. A. Sandford[1], M. Nuevo[1,2], and G. Cooper[1], [1]NASA Ames Research Center, MS 245-6, Moffett Field, CA 94035, USA, [2]BAER Institute, 625 2nd St., Ste. 209, Petaluma, CA 94952, USA (E-mails: Scott.A.Sandford@nasa.gov; Michel.Nuevo-1@nasa.gov; George.W.Cooper@nasa.gov)

Introduction: Murchison as well as other carbonaceous chondrites contain a large variety of organics, which include amino acids [1,2], amphiphiles [3,4], nucleobases [5,6], functionalized polycyclic aromatic hydrocarbons [7,8], and sugar derivatives [9]. The presence of these compounds of prebiotic significance in meteorites suggests that molecules essential to life can form abiotically under astrophysical conditions. Among the sugar derivatives found in Murchison and Murray [9], one sugar (dihydroxyacetone) and a large variety of sugar derivatives containing up to 6 carbon atoms have been identified.

Laboratory studies in the last two decades have routinely shown that complex organics are formed when simulated astrophysical ice mixtures consisting of H_2O, CO, CO_2, CH_3OH, CH_4, NH_3, etc., are irradiated with ultraviolet (UV) light at low temperature. The organic residues recovered at room temperature in these experiments have been shown to contain many similar organics to those found in meteorites [10–17]. However, the formation of sugars and their derivatives in such residues has only been studied very recently [18-20].

Results: We have performed a large number of experiments in which ice mixtures containing H_2O, CH_3OH, CO, CO_2, and/or NH_3 were UV irradiated at 10 K, and carried out a systematic search for sugars and sugar derivatives in the resulting organic residues. Results confirm the presence of a wide variety of sugar alcohols, sugars, and sugar acids with up to 6 carbon atoms, including ribose. This work also shows the presence of several deoxy variants of sugar derivatives that have not been reported in previous studies, including 2-deoxyribose (the sugar of DNA) and several deoxysugar alcohols [21] (Table 1), and compares them with pre-existing and new meteoritic data [9,21].

Table 1 Deoxysugar derivatives identified in the ice photolysis residues (regular and ^{13}C-labeled)

Compounds[a]	Formulas	R_t (min)[b]	Abundances in residues[c] (pmol)	Detected in meteorites?
Deoxysugars				
2-Deoxyribose	$C_5H_{10}O_4$	61.2, 61.4	217–3855	Undetermined[k]
2-Deoxyxylose[d]	$C_5H_{10}O_4$	57.0, 57.3	373-3636[e]	Undetermined[k]
Deoxysugar alcohols				
1,2-Propanediol[f]	$C_3H_8O_2$	9.9	≥8–375	Yes[l,m]
1,3-Propanediol[f,g]	$C_3H_8O_2$	36.9	≥19–27	No
2-Methyl-1,3-propanediol[g,h]	$C_4H_{10}O_2$	38.7	≤1038-3354[h]	No
2-(Hydroxymethyl)-1,3-propanediol	$C_4H_{10}O_3$	30.9	n.d.	Yes[l]
1,2,3-Butanetriol	$C_4H_{10}O_3$	14.5	6–39	No
1,2,4-Butanetriol	$C_4H_{10}O_3$	32.2	35–50	Yes[l]
Deoxysugar acids				
3,4-Dihydroxybutyric acid[i,j]	$C_4H_8O_4$	16.5	—	Yes[n]
Sugars				
Ribose	$C_5H_{10}O_5$	64.7, 65.0	237-2467	No

n.d., Not detected
[a]Compounds were detected using the (+)-2-butanol/TFAA derivatization method, unless otherwise stated
[b]Retention times (R_t) correspond to average values in the GC-MS chromatograms of the residues, or to standard chromatograms if compounds were not detected in the residues. Chiral compounds whose enantiomers are separated have two retention times
[c]Abundances for chiral compounds correspond to the sum for both enantiomers
[d]Tentatively identified by comparison of its mass spectrum with that of the 2-deoxyribose standard
[e]Abundances estimated based on the GC-MS detector response for the 2-deoxyribose standard
[f]Volatile compounds that may have been partially lost during the warm-up phase and/or the sample preparation. Abundances given thus correspond to lower limits
[g]Detected in samples derivatized with the MTBSTFA method
[h]Elutes with another unidentified compound with similar mass fragments, so abundances given are upper limits
[i]Tentatively identified by comparison with the NIST mass spectrometry library in samples derivatized with the BSTFA method
[j]May be present in its dimer form
[k]The presence of these compounds in meteorites is uncertain, and further analyses are required
[l]Detected in Murchison
[m]Detected in GRA 06100
[n]Detected in Murchison and Murray

Adapted from Nuevo M. et al. (2018). *Nat. Commun.*, *9*, 5276.200

References: [1] Kvenvolden K. et al. (1970) *Nature*, *228*, 923–926. [2] Cronin J. R. and Pizzarello S. (1997) *Science*, *275*, 951–955. [3] Deamer D. W. (1985) *Nature*, *317*, 792–794. [4] Deamer D. W. and Pashley R. M. (1989) *OLEB*, *19*, 21–38. [5] Folsome C. E. et al. (1971) *Nature*, *232*, 108–109. [6] Stoks P. G. and Schwartz A. W. (1979) *Nature*, *282*, 709–710. [7] Bernstein M. P. Et al. (1999) *Science*, *283*, 1135–1138. [8] Ashbourn, S. F. M. et al. (2007) *Meteor. Planet. Sci.*, *42*, 2035–2041. [9] Cooper G. et al. (2001) *Nature*, *414*, 879–883. [10] Bernstein M. P. et al. (2002) *Nature*, *416*, 401–403. [11] Muñoz Caro G. M. (2002) *Nature*, *416*, 403–406. [12] Nuevo M. et al. (2008) *OLEB*, *38*, 37–56. [13] Dworkin J. P. et al. (2001) *PNAS*, *98*, 815–819. [14] Nuevo M. et al. (2009) *Astrobiol.*, *9*, 683–695. [15] Nuevo M. et al. (2012) *Astrobiol.*, *12*, 295–314. [16] Materese C. K. et al. (2013) *Astrobiol.*, *13*, 948–962. [17] Nuevo M. et al. (2014) *ApJ*, *793*, 125 (7 pp.). [18] Nuevo M. et al. (2015) AbSciCon 2015, Abstract No. 7132 [19] Nuevo M. et al. (2015) ACS Fall Meeting 2015, Abstract No. PHYS 272 [20] Meinert C. et al. (2016) *Science*, *352*, 208–212. [21] Nuevo M. et al. (2018). *Nat. Commun., 9*, 5276.200

UV EXCITED LUMINESCENCE OF CHELYABINSK LL5 CHONDRITE SILICATES
IN 7 – 340 K TEMPERATURE RANGE

S. S. Savchenko, A. S. Vokhmintsev and I. A. Weinstein
Ural Federal University, Mira street 19, Yekaterinburg, Russia, 620002, s.s.savchenko@urfu.ru

Introduction: It was previously shown that fragments of the Chelyabinsk meteorite with light lithology dominating have various luminescence phase composition from the olivine and the group of multicomponent pyroxenes [1, 2]. The variety of silicates, their quantitative composition, radiation history, numerous structural and other transformations significantly effects photo- and thermally stimulated processes for different fragments of the same meteorite [1 – 4]. Thus, the selective study of the luminescent properties of individual silicate grains is a relevant material science challenge. At the same time, the analysis of optical processes at cryogenic temperatures for individual phases is of fundamental interest, when non-radiative transitions in most silicates are frozen-in. In this case, the estimation of microparameters for different interacting optically active centers is more reliable and is not distorted by electron-phonon effects. In this regard, the work aimed at studying the spectral and temperature features of the photoluminescence behavior of individual silicate grains from Chelyabinsk chondrite in the range of 7 – 340 K.

Samples and Technique: A fragment of Chelyabinsk LL5 chondrite predominantly characterized by light-colored lithology was selected. A core of the meteorite was separated from fusion crust and crushed into micropowder. Individual grains of silicates ∼ 10 μm in size were isolated from the obtained powder. Optical and PL images of the samples under study were obtained by means of an Axio CSM 700 confocal optical microscope (Carl Zeiss, Inc.) and a LUMAM I3 luminescence microscope (LOMO, Inc.) with an EOS 650D digital SLR camera (Canon, Inc.), respectively. A DTL-389QT solid-state laser (Laser-Export, LLC) with a wavelength of λ = 263 nm was used to excite luminescence response. PL signal was registered via a Shamrock SR-303i-B (Andor, Inc.) and a cooled Newton^{EM} DU970P-BV-602 CCD matrix (Andor, Inc.). The sample temperature was varied using a CCS-100/204N closed loop helium cryostat (Janis Research Company, LLC) equipped with a DT-670B-CU sensor, HC-4E compressor and Model 335 controller (Lake Shore Cryotronics, Inc.). PL spectra measurements were performed in 350 – 900 nm range at the following temperatures (T): 7 K, in 10 – 100 K range with a step of 10 K and from 100 to 340 K incremented by 20 K.

Results and Discussion: The investigated silicate grains are found to exhibit blue-white (BW) and white (W) luminescence. The PL curves of BW grains are characterized by two wide structureless bands with maxima at ≈ 2.5 eV (490 nm) and ≈ 1.8 eV (680 nm) in the spectral range under study at T = 300 K. The emission of W grains also reveals two components peaked at ≈ 2.3 eV (540 nm) and ≈ 1.8 eV (690 nm). Moreover, BW and W grains have a different intensity ratio of the detected bands. The emission in the 2.5 eV band dominates in the BW grains, while for the W grains the 1.8 eV band prevails. Ratio of maximum intensities of the observed emission bands has a complex temperature dependence. The obtained results for BW grains are in reasonable agreement with our preceding PL studies of individual fragments and powder of the Chelyabinsk meteorite in 7 – 300 K temperature range [1, 5]. W grains are found to exhibit the following PL spectra peculiarities in the studied temperature range. As T decreases, the luminescence intensity and area under the curve drops by a factor of 2 in the 2.3 eV band and increase by a factor of 4 in the 1.8 eV band. In this case, the position of the 2.3 eV band is not changed, and in the 1.8 eV band the 0.06 eV red shift occurs as T varies from 340 to 7 K. It was shown that all experimental PL spectra in the 1.8 eV band are satisfactorily approximated (the determination coefficient R^2> 0.995) by a single Gaussian peak. The nature of the recorded PL bands is discussed in comparison with independent data for the studied chondrite and the Tsarev meteorite [6, 7]. The analysis of the temperature dependences of the maximum PL intensity in the bands under study for various grains was carried out within the framework of the Mott-Seitz luminescence model with one and two non-radiative channels [8, 9]. W grains reveals two non-radiative relaxation pathways with the activation energies of E_q = 70 ± 10 meV and 5 ± 1 meV at T = 70 – 340 and 7 – 70 K ranges, respectively. The possible PL quenching mechanisms and origin of related optically active centres are discussed.

References: [1] Popova O.P. et al. 2013. *Science* 342: 1069–1073. [2] Kohout T. et al. 2014 *Icarus* 228: 78–85. [3] Weinstein I.A. et al. 2014. *Meteoritics & Planetary Science* 49: A428. [4] Vokhmintsev A.S. and Weinstein I.A. 2017. *Meteoritics & Planetary Science* 52: A371. [5] Vokhmintsev A.S. and Weinstein I.A. 2018. *Meteoritics & Planetary Science* 53: 6304. [6] Vokhmintsev A.S. et al. 2015. *Meteoritics & Planetary Science* 50: A5200 [7] Weinstein I.A. et al. 2018. *Meteoritics & Planetary Science* 53: 6319. [8] Weinstein I.A. et al. 2006. *Tech. Phys. Letters* 32: 58–60. [9] Vokhmintsev A.S. et al. 2019. *Radiation Measurements* 124: 35–39.

IRON ISOTOPE EVIDENCE FOR VERY RAPID ACCRETION AND DIFFERENTIATION OF THE PROTO-EARTH.

M. Schiller[1], M. Bizzarro[1] and J. Siebert[2,3], [1]Centre for Star and Planet Formation, University of Copenhagen, Øster Voldgade 5–7, DK-1350, Denmark (schiller@ign.ku.dk), [2]Institut de Physique du Globe de Paris, Université Sorbonne Paris Cité, 75005, Paris, France, [3]Institut Universitaire de France, France.

Introduction: Terrestrial planet formation is thought to proceed in stages, where the final assembly of the terrestrial planets occurred over several tens of millions of years via large collisions between embryos [1], many of which will have differentiated into metal cores and silicate mantles. In these models, oxidised solids and volatile elements such as water are inferred to have been delivered to the Earth towards the end of accretion, possibly by volatile-rich, outer Solar System bodies scattered inward by the outward migration of Jupiter [2]. However, a recent study of the isotope composition of the siderophile element ruthenium in Solar System objects, including Earth and the parent bodies of chondrite meteorites, suggest that Earth's volatile element budget may have been acquired much earlier [3], perhaps during its main accretion phase. Moreover, new planet formation models based on the rapid accretion of pebbles onto asteroidal seeds suggest that Earth's main accretion phase may have been completed within the ~5 Myr lifetime of the protoplanetary disk [4]. Here, we take advantage of nucleosynthetic iron (Fe) isotope variability amongst early Solar System objects to distinguish between rapid and protracted terrestrial planet growth to elucidate the timescales of Earth's accretion. Iron is a redox-sensitive, siderophile major element whose partitioning between mantle and core on rocky planets is a proxy of the overall oxidation state of a planet. More importantly, iron readily oxidises in the presence of water, significantly lowering its partitioning into the metal core. Therefore, if Earth became more oxidised during accretion and core formation, the mass-independent Fe isotope composition of Earth's mantle is predicted to be dominated by that of the late (volatile-rich) accreting material. The existence of nucleosynthetic Fe isotope variability in Solar System objects can thus provide a powerful tool to fingerprint the source of the material responsible for the delivery of water and oxidised solids to the Earth and the subsequent oxidation of Earth's mantle.

Methods: In order to establish the presence of nucleosynthetic Fe isotope variability, we analysed the Fe isotope composition of dissolution steps of the CI chondrite Ivuna that have been previously measured for their strontium, chromium, magnesium and calcium isotope signatures [5-7]. In addition, we measured whole rock samples from chondritic and achondritic solar reservoirs. Iron was separated from the matrix following published methods [8] and measured by MC-ICP-MS at the Natural History Museum of Denmark relative to the IRMM-014 Fe isotope standard. We report our data in the μ^{54}Fe-notation, which refers to the deviation of the ^{54}Fe/^{56}Fe ratio from the terrestrial value in parts per million (p.p.m.) when corrected for kinetic mass fractionation using a ^{57}Fe/^{56}Fe ratio of 0.023261 [9].

Results and Discussion: The step wise dissolution experiment reveals that labile phases dissolved in the early dissolution steps exhibit elevated μ^{54}Fe values of around +46 p.p.m., whereas later dissolution steps contain both negative as well as positive μ^{54}Fe values. In particular, the dissolution step that exhibits a large ^{84}Sr deficit linked to the dissolution of presolar silicon carbide (SiC) grains [5] is also characterized by the highest μ^{54}Fe value. This signature can be understood when considering that SiC grains are also known to have large ^{57}Fe overabundances [10]. As such, variable presence of these presolar carriers of nucleosynthetic Fe isotope heterogeneity can impart variability in disk solids. Apart from bulk CI chondrites, which have a μ^{54}Fe identical to Earth's mantle, all analysed achondrites, chondrites and individual chondrules are characterized by resolvable excesses in μ^{54}Fe ranging from +5.4 to +28.8 p.p.m. As such, our data establish the presence of disk wide nucleosynthetic iron isotope variability, where apart from CI chondrites, none of the meteorites analysed here, including all main chondrite groups, match the terrestrial mantle composition. A single reservoir origin (CI chondrites) of the Earth's mantle iron is difficult to reconcile with stochastic collisional accretion models of the Earth. Instead, the iron isotope signature of the mantle is consistent with a very rapid main accretion and differentiation of the Earth that occurred during the ~5 Myr disk lifetime. During this stage volatile-rich CI-like material is accreting onto the proto-Sun via the inner disk, thereby delivering CI-like solids to the accretion region of the Earth. As such, our findings support the recent suggestion that changes in the nucleosynthetic signatures of bulk planets track the progressive admixing of pristine CI-like dust to an initially thermally processed inner protoplanetary disk [11].

References: [1] Walsh, K.J. et al. (2011) *Nature* 475:206–209. [2] O'Brien et al. (2018) *Space Science Reviews* 214:47. [3] Fischer-Gödde, M. and Kleine, T. (2017) *Nature* 541:525–527. [4] Johansen, A. et al., 2015. *Science Advances* 1:e1500109. [5] Paton, C. et al. (2013) *The Astrophysical Journal Letters* 763:L40. [6] Schiller, M. et al. (2014) *Journal of Analytical Atomic Spectrometry* 29:1406–1416. [7] Schiller, M. et al. (2015) *Geochimica et Cosmochimica acta* 149:88–102. [8] Dauphas, N. et al. (2004) *Analytical Chemistry* 76:5855–5863. [9] Völkening, J. and Papanastassiou, D.A. (1989) *The Astrophysical Journal* 347:L43–L46. [10] Marhas, K.K. et al. (2008) *The Astrophysical Journal* 689:622. [11] Schiller, M., et al. (2018) *Nature* 555:507–510.

RE-INVESTIGATION OF SPECIFIC IMPACTOR COMPOSITIONS FROM TERRESTRIAL IMPACT CRATERS BY THE DIAGNOSTIC ELEMENT RATIOS RU/RH AND IR/RH

G. Schmidt, Institute of Earth Sciences, Heidelberg University, D-69120 Heidelberg, Germany,
Gerhard.Schmidt@geow.uni-heidelberg.de

Introduction: Studying the nature of impactors is crucial to understand the characteristics and origin of the material delivered to planets. To date, there are 190 confirmed impact structures on Earth. Utility elements to identify specific impactor compositions in melts from impact craters are refractory elements Os, Ru, Ir, Rh (PGE) and Ni. PGE are abundant in most meteorites but depleted in crustal rocks. For Ir and Os, there is a difference of four orders of magnitude, and Rh three orders of magnitude between their meteoritic and crustal abundances. Cr for example is only 30times more abundant in meteorites compared to Earth's upper crust. The determination of PGE in melt samples is a difficult challenge because of low contents in the pg/g to ng/g range. There are still few data on Rh in impact melt samples, mainly because of difficulties with analysis. Mass element ratios on Ru/Rh and Ir/Rh from iron meteorites show that re-investigation on specific impactor compositions shed light in controversial identifications.

Clearwater East, Brent, Wanapitei Impact Craters, Canada: Clearwater East has highest PGE contents in melt samples from any terrestrial impact crater. Since the earlier studies by Palme and co-workers 1978 a chondrite has been suggested as impactor based on PGE, Ni, Cr [1-6] and Cr isotopes [7]. However, LA-ICP-MS data on PGE including Ni from iron meteorites [8] allows comparing these data with ICP-MS [4] and neutron activation data from Clearwater East melt samples [5]. Surprisingly, element ratios of iron meteorite IVA Gibeon (see figures) agree with Clearwater East samples. The authors [1-6] reached their conclusions without the benefit of Rh from iron meteorites. Up to ~1.2 wt.% of a IVA
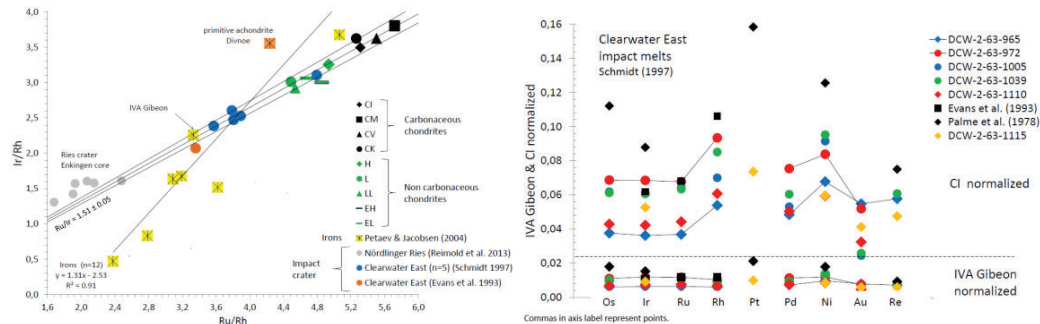
Gibeon-like component could be contained in the melt samples. However, a member of an unidentified chondrite group as projectile type, which is not known from meteorite collections, could also be possible (Palme 2019, pers. communication) - similar problem with excess mantle PGE. Possibly ε^{100}Ru data could solve the mystery in the future. For Brent and Wanapitei craters [4], iron bolides (e.g., IA, IVA, IIC) were identified by Ru/Rh and Ir/Rh ratios.

Rochechouart, France: Rochechouart samples [9] and melt rocks from Apollo 16 landing site[10] match Ru/Rh and Ir/Rh from IA, IIC and IVA irons. An ordinary chondrite is favoured by [7] based on Cr isotopic composition.

Hiawatha, Greenland: A "highly fractionated iron asteroid" has been suggested for the 31-kilometer-wide, circular bedrock depression beneath Hiawatha Glacier in northwest Greenland [11]. Diagnostic element ratios of a mixture of upper crust and an iron meteorite would not match element ratios determined in glaciofluvial sediments.

Popigai, Siberia: [12] reported "…Ru/Rh vs. Pt/Pd or Ru/Rh vs. Pd/Ir, the Popigai impactor is clearly identified as an ordinary chondrite and most likely L-chondrite". However, EL chondrites or even iron meteorites match diagnostic Ru/Rh and Ir/Rh ratios from the late Eocene Popigai impact structure.

Conclusion: Most diagnostic element ratios for specific impactor compositions are Ir/Rh, Ru/Rh and Os/Ir [13]. High quality data especially of Rh might answer fundamental questions of cosmochemistry [14] and contribute to our understanding of processes involved in the formation and unique composition of planetary bodies.

References: [1] Palme H. et al. (1978) *Geochimica et Cosmochimica Acta* 42:313–323. [2] Palme H. et al. (1979) *Proceedings Lunar Planetary Science Conference* 10th:2465–2492. [3] Grieve R. A. F. et al. (1981) *Contributions to Mineralogy and Petrology* 75:187-198. [4] Evans N. J. et al. (1993) *Geochimica et Cosmochimica Acta* 57:3737-3748. [5] Schmidt G. (1997) *Meteoritics & Planetary Science* 32:761-767. [6] McDonald I. (2002) *Meteoritics & Planetary Science* 37:459-464. [7] Koeberl C. et al. (2007) *Earth and Planetary Science Letters* 256:534–546. [8] Petaev M. I. & Jacobsen S. B. (2004) *Meteoritics & Planetary Science* 39:1685-1697. [9] Tagle R. et al. (2009) *Geochimica et Cosmochimica Acta* 73:4891-4906. [10] Fischer-Gödde M. and Becker H. (2012) *Geochimica et Cosmochimica Acta* 77:135-156. [11] Kjær K. H. et al. (2018) *Science Advances* 4:1-11. [12] Tagle R. & Claeys P. (2005) *Geochimica et Cosmochimica Acta* 69:2877–2889. [13] Schmidt G. (2009) *72nd Annual Meteoritical Society Meeting*, Abstract #5001. [14] Schmidt G. (2019) *16th Rußbach School on Nuclear Astrophysics*, Austria. https://indico.ph.tum.de/event/4158/contributions/3380/

OUTSTANDING NATURAL OCCURRENCE OF TiO2–II AT THE CHICXULUB CRATER – ANATOMY OF A SHOCK-PRODUCED HIGH-PRESSURE POLYMORPH

Martin Schmieder[1,2], Timmons M. Erickson[3,4], Zia Rahman[3,4], Lindsay P. Keller[3], David A. Kring[1,2], and the IODP–ICDP Expedition 364 Science Party,
[1]Lunar and Planetary Institute – USRA, Houston, TX 77058 USA (martin@suevite.com), [2]NASA – SSERVI, [3]NASA Johnson Space Center, Houston, TX 77058 USA, [4]Jacobs JETS, NASA/JSC, Houston, TX 77058 USA.

Introduction and Background: Scientific drilling of the end-Cretaceous, ~180 km-diameter Chicxulub crater (Yucatán Peninsula, Mexico) during IODP–ICDP Expedition 364 has provided new insights into the formation, shock metamorphism, structural evolution, and thermal history of peak rings in large complex impact craters [1–6]. An outstanding feature in uplifted granitoid rocks of the Chicxulub peak ring is the preservation of TiO2–II, an orthorhombic high-pressure polymorph of TiO_2 with an α-PbO_2 structure [7,8], produced during the impact from rutile and/or anatase at shock pressures of ~12.5–17.5 GPa [4]. Unlike other mostly micro- and cryptocrystalline occurrences of TiO2–II at terrestrial impact sites, ejecta deposits ([9,10] and references therein), and in rare ultra-high pressure metamorphic rocks [11], TiO2–II at Chicxulub occurs as abundant euhedral crystals ≤70 μm in size within aggregates of altered magmatic titanite. This mode of occurrence provides an excellent opportunity to investigate the crystallography and transformation kinetics of the shock-produced high-pressure polymorph using scanning electron microscopic, micro-Raman, electron backscatter diffraction (EBSD) [9,10], focused ion beam (FIB), as well as transmission-EBSD and transmission electron microscopic (TEM) techniques. Here we present refined microstructural and new crystallographic results for TiO2–II at the Chicxulub crater.

Sample and Analysis: TiO_2 in shocked granitoid rock sample 174–2–19–20 (core depth 949 m below seafloor [1,2,9,10]) from the Chicxulub peak ring was analyzed using a 7600f JEOL field emission gun scanning electron microscope (FEG-SEM) with an Oxford Instruments Symmetry EBSD detector for phase and orientation mapping and transmission-EBSD; a Quanta 3D FEG for FIB sectioning; and a JEOL 2500 field-emission scanning-transmission electron microscope (FE-STEM) for diffraction pattern analysis, indexing, and the determination of unit cell parameters at the NASA Johnson Space Center.

Results and Interpretation: High-resolution EBSD mapping of TiO_2 crystals (Fig. 1A) reveals a complex arrangement of lamellar and granular crystal domains. TiO2–II, which commonly forms larger, coherent, lamellar subdomains (Fig. 1B), is the dominant mineral phase. Rutile occurs as microcrystalline granules and lamellae that locally overprint shock-produced TiO2–II and is, thus, interpreted as a post-shock reversion product. Individual TiO2–II lamellae are related to one another by rational twin orientations (Fig. 1C), indicating twinning occurred during the solid-state transformation to minimize intracrystalline strain energy. Three dominant twin orientations are observed with a disorientation axis of 87°/<010>, 55°/<010>, and 85°/<100>. Moreover, TiO2–II and neoblastic rutile are systematically misoriented from one another, suggesting the solid-state TiO2–II-to-rutile reversion is crystallographically controlled. High-resolution transmission-EBSD and TEM analyses were carried out to further characterize the nanostructure and unit cell parameters in natural, shock-produced TiO2–II. Results from TEM electron diffraction analysis and indexing are consistent with the unit cell parameters of experimentally produced TiO2–II [12]. These results underline the outstanding natural occurrence of TiO2–II at the Chicxulub impact crater, which may be an appropriate type locality for this high-pressure polymorph.
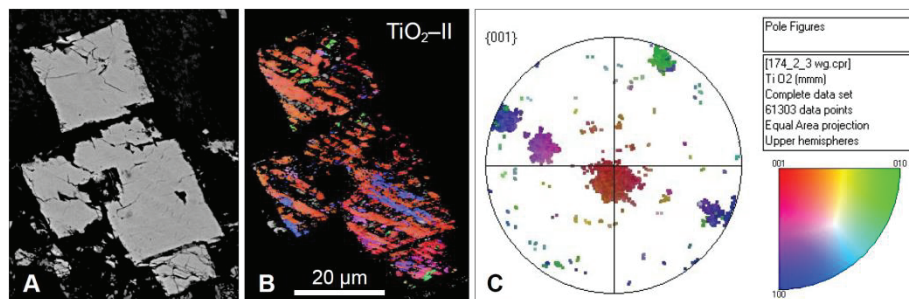

Fig. 1: TiO2–II in shocked granitoid rock from the Chicxulub peak ring (sample 174–2–19–20). **A:** Back-scattered electron image of TiO_2 crystals. **B:** EBSD inverted pole figure map of TiO2–II. **C:** Pole figure corresponding to map shown in B (IPF-z).

References: [1] Morgan J. V. et al. (2016) *Science*, 354, 878–882. [2] Gulick S. P. S. et al. (2017) Exp. 364 Prelim. Rep., IODP, 38 pp. [3] Kring D. A. et al. (2017) *GSA Today*, 27, 5 pp. [4] Rae A. S. P. et al. (2017) *LPS XLVIII*, abstr. #1934. [5] Kring D. A. et al. (2017) *LPS XLVIII*, abstr. #1212. [6] Kring D. A. et al. (2016) *Nature Comm.*, 7, 13161. [7] Linde R. K. and DeCarli P. S. (1969) *J. Chem. Phys.*, 50, 319–325. [8] El Goresy A. et al. (2001) *EPSL*, 192, 485–495. [9] Schmieder M. et al. (2017) 80th MetSoc, abstr. #6134. [10] Schmieder M. et al. (2019) *LPS XLIX*, abstr. #1658. [11] Shen P. et al. (2001) *Int. Geol. Rev.*, 43, 366–378. [12] Gerward, L. and Staun Olsen, J. (1997) *J. Appl. Cryst.*, 30, 259–264.

Topics: Organic Matter in Extraterrestrial Materials

(ULTRA)HIGH RESOLUTION ORGANIC SPECTROSCOPY ANALYSIS OF SOLUBLE ORGANIC MATTER IN METEORITES

P. Schmitt-Kopplin[1,2], J. Hertzog[1,2], M. Mazka[1], N. Hertkorn[1], M. Harir[1], [1]Analytical BioGeoChemistry, Helmholtz Zentrum Muenchen, Munich, Germany, schmitt-kopplin@helmholtz-muenchen.de, [2]Analytical Food Chemistry, Technische Universität München, Munich, Germany,

Observations such as astrochemistry (telescopic observations) and laboratory wet chemical analysis of return objects such as meteorites enables us to understand the origin and evolution of organic matter. The molecular composition and diversity of non-terrestrial organic matter in carbonaceous chondrites can be studied by means of both, targeted [1] and non-targeted [2,3] chemical analytical approaches, leading to new insights/histories on the studies samples. Targeted chemical analyses as followed with mass spectrometry coupled to gas or liquid chromatography are hypothesis-driven and are largely focused on molecules of biological/prebiotic interest; these can be amino acids, sugars, nucleotides, fatty acids. In the non-targeted approach using rather higher resolution type of instrumentations such as nuclear magnetic resonance spectroscopy (NMR) or (ultra)high resolution mass spectrometry (FTICR-MS), all analytes are globally profiled within the limits of the analytical possibilities and without biased or constrained hypothesis in order to gain comprehensive information.

Both approachs enabled insights into the holistic complex compositional space to tens of thousands of different molecular compositions and functional groups having in total millions of diverse structures. Solvent extractions of pristine carbonaceous meteorits could show this in the last decade [2, 3], and suggests that interstellar chemistry is extremely active and rich.

In this presentation we give a state of the art on the chemical description of the soluble organics of meteorites by non-targeted approach. We described to date that heteroatomic organic molecules play an important role in the description of non-terrestrial chemical evolution. The thermally and shock-stressed Chelyabinsk (LL5) [4] showed high number of nitrogen counts within CHNO molecular formulas, especially in the melt region. This match of the organic molecular profile with the petrologic character could be also observed for Novato (L6) [5], Braunschweig (L6) and the latest German fall Stubenberg (LL6) [6]. Recently novel falls such as Hamburg (L4), Renchen (L5-6) and Ejby (H5-6) and the thermals affected CM2 Diepenveen confirmed these findings. The resulted extreme richness in chemical diversity offers information on the meteoritic parent body history and help in expanding our knowledge or astrochemistry towards higher molecular masses and complex molecular structures.

In mass spectrometry all the performed studies involve electrospray ionization (ESI) sources in both negative and positive-ion modes that is known to be appropriate for the ionization of species over a wide mass and polarity range. DESI is a surface analysis that was recently used and which is based on the ESI-process as well [7]. The less polar and oxygen depleted species are not necessarily detected by this method and thus the chemical description of the material can not be the most exhaustive. using an atmospheric pressure photoionisation source (APPI) coupled to a high resolution Fourier transform ion cyclotron resonance mass spectrometer (FT-ICR MS). This method is well known to ionize the less polar to nonpolar species such as the polyaromatic hydrocarbons (PAH) or unsaturated heteroatom compounds. The contribution of APPI, to a better understanding the chemical composition of the meteorite, will be discussed by comparing the elemental compositions achieved by positive- and negative-ion ESI FT-ICR MS. In the light of the forthcoming return missions we feel important to adapt modern analytical tools for a wider observation of chemical classes in minimal amount of sample use.

References:
[1] Pizzarello, S. et al. PNAS, 110(39):15614–15619. [2] Schmitt-Kopplin, P. et al. 2010 PNAS 107(7):2763–2768. [3] Hertkorn, N. et al. 2015. Magnetic Resonance in Chemistry, 53(9):754–768. [4] Popova, O.P. et al. 2013 Science, 342(6162): 1069–1073. [5] Jenniskens, P. et al. 2014. Meteoritics & Planetary Science, 49(8): 1388–1425. [6] Bischoff, A. 2017 Meteoritics & Planetary Science, 52(8):1683–1703. [7] Naraoka et al. 2018 Rapid Com. Mass Spec. 32, 959-994.

DETERMINING THE GEOTHERMOMETRY OF A HAYABUSA-RETURNED SULFIDE PARTICLE.

D. L. Schrader[1] and T. J. Zega[2], [1]Center for Meteorite Studies, School of Earth and Space Exploration, Arizona State University, Tempe, AZ 85287, USA (devin.schrader@asu.edu), [2]Lunar and Planetary Laboratory, University of Arizona, Tucson, Arizona 85721, USA (tzega@lpl.arizona.edu).

Introduction: Geothermometry of pyrrhotite-pentlandite intergrowths in meteorites, using compositional data from quantitative electron probe microanalysis (EPMA), shows that most of them formed during primary cooling from high temperature (i.e., during chondrule formation) or after thermal metamorphism [e.g., 1–5]. Sulfides in LL4 to LL6 chondrites equilibrated <600°C [2], likely <250°C [4], consistent with formation during cooling after thermal metamorphism [2,4]. However, geothermometry of pyrrhotite-pentlandite intergrowths from an LL5–6 impact melt-breccia indicated that the sulfides were annealed at ≤230°C, likely after an impact event [1]. In comparison, analyses of silicate-bearing Hayabusa-returned particles have identified asteroid 25143 Itokawa as LL4 to LL6 chondrite material (~10% LL4 and ~90% LL5 to LL6) [e.g., 6–9] that was thermally metamorphosed between ~780 and 840°C [6]. Sulfides in Hayabusa particles [e.g., 6,10,11] record additional and/or complementary information on the formation conditions of Itokawa [e.g., 12], however their pyrrhotite-pentlandite intergrowths are too small to analyze via EPMA [12]. Our goal is to further constrain the formation and alteration conditions of asteroid Itokawa by determining the geothermometry of sulfide-bearing Hayabusa-returned particles via quantitative energy-dispersive x-ray spectroscopy (EDS) using a transmission electron microscope (TEM).

Samples and Analytical Procedures: We identified pyrrhotite-pentlandite intergrowths in the sulfide-bearing Itokawa sample RB-CV-0234 and Saint-Séverin USNM2608-3 (LL6). We have described pyrrhotite-pentlandite intergrowths in sections from RB-CV-0234 [12] and Saint-Séverin [13] extracted with the FEI Helios NanoLab 660 focused-ion-beam-scanning electron microscope (FIB-SEM) at the University of Arizona (UAz), and analyzed using the 200 keV aberration-corrected Hitachi HF5000 scanning TEM at UAz. Prior to FIB-TEM, the pyrrhotite-pentlandite intergrowth in Saint-Séverin region of interest (ROI)A was analyzed for its elemental compositions via EPMA [2,13]. We obtained quantitative EDS data from FIB sections of both samples via TEM following [14].

Results: The compositions of RB-CV-0234 via quantitative EDS [14] are 35.2 wt.% S and 64.8 wt.% Fe for pyrrhotite, and 32.4 wt.% S, 49.4 wt.% Fe, and 18.2 wt.% Ni for pentlandite. The compositions of Saint-Séverin ROIA via quantitative EDS are 37.9 wt.% S and 62.1 wt.% Fe for pyrrhotite, and 35.7 wt.% S, 45.6 wt.% Fe, and 18.7 wt.% Ni for pentlandite. The compositions via EPMA of Saint-Séverin ROIA prior to FIB extraction are 36.8 wt.% S and 63.7 wt.% Fe for pyrrhotite, and 33.6 wt.% S, 43.9 wt.% Fe, and 21.0 wt.% Ni for pentlandite.

Discussion: The compositions of both pyrrhotite and pentlandite in Saint-Séverin ROIA determined by EDS are within ~1 to 2 wt.%, for Fe, Ni, and S, of the values determined by EPMA. These compositional differences could: (1) be due to EPMA analyzing the sample surface, whereas EDS measurements of the FIB section sample the subsurface; or (2) imply that the uncertainty in the EDS measurements relative to EPMA analyses is ~1 to 2 wt.%.

In [12] we showed that the pyrrhotite-pentlandite intergrowth in RB-CV-0234 is most similar to that found in Saint-Séverin (LL6, S2), indicating that RB-CV-0234 might be from LL6, ≤S2 chondrite material. However, the higher Fe-content of pentlandite in RB-CV-0234 compared to that in Saint-Séverin ROIA indicates they had different parent-body thermal histories. The chemical compositions of pyrrhotite and pentlandite in Saint-Séverin ROIA are most consistent with equilibrating <400°C, perhaps ~300°C (using phase diagrams in [15,16]). The compositions of pyrrhotite and pentlandite in RB-CV-0234 determined via EDS are consistent with equilibrating <300°C, perhaps as low as ~230°C. These temperatures are most similar to the closure temperatures of ≤230°C and <250°C for pyrrhotite-pentlandite intergrowths from NWA 4859 (LL5–6 impact melt-breccia) [1] and Stubenberg (LL6, S3) [4], respectively. This indicates that RB-CV-0234 is likely from LL6 chondrite material.

References: [1] Jamsja N. and Ruzicka A. (2010) *Meteorit. Planet. Sci.* 45:828. [2] Schrader D. L. et al. (2016) *Geochim. Cosmochim. Acta* 189:359. [3] Schrader D. L. et al. (2015) *Meteorit. Planet. Sci.* 50:15. [4] Bischoff A. et al. (2017) *Meteorit. Planet. Sci.* 52:1683. [5] Schrader D. L. et al. (2018) *Earth Planet. Sci. Lett.* 504:30. [6] Nakamura T. et al. (2011) *Science* 333:1113. [7] Noguchi T. et al. (2014) *Earth Planets Space* 66:124. [8] Tsuchiyama A. et al. (2011) *Science* 333:1125. [9] Tsuchiyama A. et al. (2014) *Meteorit. Planet. Sci.* 49:172. [10] Berger E. L. and Keller L. P. (2015) *Microscopy Today* 23:18. [11] Harries D. and Langenhorst F. (2014) *Earth Planets Space* 66:163. [12] Schrader D. L and Zega T. J. (2019) *LPS L*, Abstract #2009. [13] Schrader D. L. and Zega T. J. (2017) *80th MetSoc.* Abstract #6347. [14] Zega T. J. et al. (2018) *Microsc. Microanal. 24*, Abstract #2084. [15] Misra K. and Fleet M. E. (1973) *Econ. Geo.* 68:518. [16] Raghavan V. (2004) *J. Phase Equilib.* 25:373.

EVOLVING STRAIN PATTERNS DURING IMPACT IN THE WORLD'S LARGEST CENTRAL UPLIFT – EVIDENCE FOR DECLINING STRAIN RATE AND STRAIN LOCALISATION WITHIN MINUTES

S. Selkirk[1], R.L. Gibson[1] and A. Tshibubudze[1]
School of Geosciences, University of the Witwatersrand, Private Bag 3, P.O. Wits 2050, Johannesburg, South Africa.

The formation of central uplifts in complex impact craters remains one of the most enigmatic aspects of cratering mechanics. Numerical modelling is able to explain the gross evolving strain patterns within central uplifts but, as yet, cannot resolve the smaller scale patterns responsible for structures at the outcrop scale or in heterogeneous targets layered at scales up to tens to hundreds of metres.

The Vredefort Dome is the 90 km wide, deeply exhumed (~10 km of erosion [1]), central uplift of one of the world's largest complex impact structures (D ~320 km [1]). The dome comprises a 40-km-wide crystalline basement core that is surrounded by a 25 km wide collar of layered supracrustal and intrusive rocks that show complex macroscopic deformation features. The dome presents a unique opportunity to study impact-related deformation in the deep levels of a giant impact structure that may be inaccessible below younger impact structures. The layered metasedimentary rocks of the Witwatersrand Supergroup in the collar, in particular, provide planar markers on scales ranging from millimeters to hundreds of meters. This allows for elucidation of fault displacemnets, kinematics, block rotations and fold patterns, as well as strain patterns.

This study examines the geometry and sequence of formation of complex structural deformation features induced by the impact in a quartzite-metapelite-ironstone succession located at a radial distance of ~22 km from the centre of the dome in the northwestern collar. The following sequence of impact-related strain features have been identified: (1) A pair of pervasive, mm- to cm-spaced, orthogonal "shatter cleavages" [2]. The shatter cleavages are attributed to passage of the shock wave. Restoration of the strata to the time of impact (horizontal orientation) produces an intersection lineation that can be projected to the point of impact (located ~10 km above the centre of the dome); (2) Horsetail fractures, branching off a preferred shatter cleavage are shown to terminate in the direction of shock wave propagation; (3) Shatter cones, restoration of the master shatter cone axis, to the time of impact, produces an lineation that can be projected to the point of impact; (4) Polyphase folding: F1 folds have upright axial planes, trending oblique to the strike of the collar, with moderately inwardly plunging hinges, ~100 m wavelengths and decametre amplitudes, showing no vergence; F2 folds are on a scale of hundreds of metres and comprise of overturned, centrifugally-verging folds, with moderately steeply centripetally-dipping axial planes and horizontal tangential hinges. F2 fold hinges are commonly cut by thrust faults; (5) A network of pseudotachylite-bearing faults with oblique- to normal-slip displacements of up to a few tens of metres that are oriented oblique to the strike of the collar and show some preferred orientation parallel to the F1 folds, and ; (6) Extensional faults, that cross-cut pseudotachylite veins.

After palinpastic restoration, these deformational features can be classified into 4 main phases:
1) Shock Deformation — shatter cleavages, horsetail fractures, and shatter cones forming during the contact and compression phase.
2) Ductile Deformation — F1 radially-trending, centripetally-plunging folds, associated withconstrictional during the early phases of the modification stage - central peak formation.
3) Brittle-Ductile Deformation — F2 folds, associated with radial and tangential extension during the mid-modification phase - central peak collapse.
4) Brittle Deformation — faulting and frictional melting with associated pseudotachylite emplacement, and extensional faulting that post dates pseudotachylite emplacement. Late modification phase - central peak collapse and stabilisation.

These results suggest that detailed structural mapping of layered target rocks in central uplifts can help discriminate between different strain patterns associated with various stages in the formation of central uplifts. The results indicate that at depth vertical movements associated with uplift and collapse are more significant, as opposed to near surface features that preserve more significant lateral displacements.

References:
[1] Gibson, R.L., Reimold, W.U. and Stevens, G., (1998). *Geology*, 26, 787–790.[2] Milton, D.J., (1977) *In: Impact and Explosion Cratering: Planetary and Terrestrial Implications*, 703–714.

MINERALOGY OF NORTHWEST AFRICA 6963 DETERMINED BY RAMAN SPECTROSCOPY

M. Serbestoglu[1], M. Yesiltas[2], M. Gurhan Yalcin[1]. [1] Department of Geological Engineering, Akdeniz University, Antalya, Turkey, 07058 (merveserb@gmail.com), [2]Faculty of Aeronautics and Space Sciences, Kırklareli University, Kırklareli, Turkey, 39100.

Introduction: Martian meteorites are important samples for understanding the present and past of Mars. They contain information about Martian geological evolution and physical and chemical characteristics [1]. The Martian meteorites are divided into three main groups: Shergottites, Nakhlites and Chassignites [2]. The shergottites are the most abundant among them and are also the most diverse of the Martian meteorite subgroups. They are divided into two types: basaltic and lherzolitic [3]. Northwest Africa (NWA) 6963 is a basaltic shergottite that was found in Morocco in 2011[4]. Previously studies show that NWA 6963 exhibits a range of textures with coarse mineralogy in a fine matrix [5]. Pyroxene, maskelynite are the dominant components in NWA 6963, ulvöspinel, merrillite, chlorapatite and pyrrhotite exist in minor amounts [6]. We are investigating NWA 6963 using multiple micro-spectroscopic techniques with the goal of revealing molecular composition of NWA 6963 in detail. These data will potentially allow us to understand processes that might be taking place on the surface of Mars.

Samples and Methods: We prepared a polished thin section from a thick slab of NWA 6963 at Istanbul Technical University, Department of Geological Engineering. Subsequently, micro-Raman imaging and spectral data on this sample was acquired at Canakkale Onsekiz Mart University, Science and Technology Application and Research Center. We used a WiTec alpha300 R (WiTec GmbH) confocal Raman imaging system equipped with a 532-nm Nd:YAG laser and a spectrometer with a CCD camera (cooled to -60 °C), and a 50X objective (NA = 0.8). Laser power was around 1- 3 mW. Integration time 0.2-0.5 s for two dimensional chemical distribution maps, and 1 second for individual spectra, for which 30-60 accumulations were collected. The collected data was analyzed using a commercial software package Project FOUR. First, cosmic ray lines were removed from the data and a background correction was applied. Second, various molecular phases were identified using their Raman band positions. These positions were then used to create two dimensional chemical distribution maps of respective phases.

Results: Raman spectra and chemical maps of NWA 6963 were collected from multiple locations on the surface of the sample. Collected data indicate that the studied sample is dominated by silicates and shock phases. Specifically, NWA 6963 contains abundance of pyroxene with multiple endmembers, evident from varying peak positions and spectral profiles. For instance, spectral profile of pyroxene bands between 280-428 cm^{-1} vary based on the chemical composition of the endmember. Additional Raman peaks for pyroxene appear at 667 and 1001 cm^{-1}. Maskelynite is also abundant in NWA 6963, it is evident from the broad Raman peak centered around 1065 cm^{-1}. Olivine presents a doublet near 840 cm^{-1}. Hematite presents multiple peaks, they appear at 224, 290, 404, 612, and 656 cm^{-1}. In addition to Raman, we have plans to collect infrared and electron microscope data on NWA 6963 to study its mineralogy and chemistry in detail.

References:
[1] do Nascimento-Dias et al. (2018). *X-Ray Spectrometry*, *47*(1), 86-91. [2] Davis, A. M. (Ed.). (2005). *Meteorites, Comets, and Planets: Treatise on Geochemistry* (Vol. 1). Elsevier. [3] Meado, A. L.et al. (2017). Crystallization history of gabbroic shergottite NWA 6963 as revealed by pyroxene zoning. [4] Filiberto, J. et al. (2018). *Journal of Geophysical Research: Planets*, *123*(7), 1823-1841. [5] McSween, H. Y., & Treiman, A. H. (1998). *Planetary Materials, Reviews in Mineralogy*, *36*, 6-1. [6] Ruzicka, A. et al. (2014). *Meteoritics & Planetary Science*, *49*(8), E1-E101.

ANALYSIS OF THE GENETIC CONNECTIONS BETWEEN NEAR-EARTH OBJECTS AND DELTA CANCRIDS METEOROIDS

M. V. Sergienko[1], M. G. Sokolova[1], A. O. Andreev[1], Y. A. Nefedyev[1],
[1]Kazan Federal University, Russia, Kazan, Kremlyovskaya st., 18. E-mail: maria_sergienko@mail.ru

Introduction: The Delta Cancrids (DCA) relates to unconfirmed small meteor showers, has 2 branches – the Northern (NCC) and the Southern (SCC) Delta Cancrids, and is observed between January, 1 and January, 31. According to IAU, the Northern Delta Cancrids (NCC) is allegedly related to the 1991 AQ? asteroid, while the Southern Delta Cancrids is related to 2001 YB5? (the symbol "?" indicates the status of hypothesis, date of the application is August 18, 2018). The purpose of the paper is to study the activity of the poorly investigated Delta Cancrids and to search for close orbits among NEOs.

Methods: To study the structure of the Delta Cancrids we used the visual observations provided by the International Meteor Organization (http://www.imo.net/data/visual) which has the data on the observations of the Delta Cancrids taken between 1987 and 2006 without separating NCC from SCC. Using the method [1], about 5000 observations of meteors were processed in order to determine the number of meteors and to distribute them for stellar magnitude. We also used meteor orbits of the NCC and SCC branches of the Delta Cancrids presented in television catalogues by Japanese Meteor Network SonatoCo and Croatian Meteor Network CMN (Croatian Meteor Society, http://cmn.rgn.hr/downloads/downloads.html#orbitcat), the total number of orbits was 178. The search for a parental body (PB) was performed among 17800 asteroid orbits (http://ssd.jpl.nasa.gov/sbdb_query.cgi). The study of the shower's connections with asteroids from the Apollo, Aten, Amor, and Atira groups was conducted using the D-criterion by J.D. Drummond [2] and metrics by K.V. Kholshevnikov [3] as functions of the distance between the orbits as well as Tisserand's parameter and 2 quasi-dynamic parameters of the restricted three-body problem [4]. The upper values of the criteria under which the hypothesis of the orbits' identity was accepted or declined were defined by calculating mean orbits of the shower in each catalogue taking into account variance and catalogue observation errors.

Results: For meteors with the minimum recorded magnitude of $+3^m$ or higher the maximum of activity (8.6 ± 2 meteors an hour) is observed at the ecliptic longitude of the Sun of $298.5°\pm1.2°$. The maximum of activity for smaller meteoroids is recorded $1.4°$ later. The descending and ascending branches of the activity profile are gently sloping, the shower's width at half of the maximum activity is $5°$. The calculations of spatial density for the Delta Cancrids shows that at the shower's maximum activity 1 particle heavier than 1 g is observed at a cube with an edge of 1000 km. When searching for a parental body, the following asteroids from the Apollo group are marked out with the highest probability of more than 0.7: for NCC – 85182 (1991AQ) and 2015PC, for SCC – 2212 Hephaistos (1978SB), 2011SR12, and 2014RS17. For the Delta Cancrids in general the asteroids 2014RS17, 2011SR12, 2003RW11, 2001BO6 from the Apollo group are marked out with the probability higher than 0.6. Almost all the selected asteroids move along asteroid types of orbit (Tisserand's parameter > 3). The modern positions of orbit nodes for the asteroids 2001YB5 and 2010QD2 selected for SCC with the probability of 0.6 coincide with the position of DCA maximum activity within 2°. The search for close orbits in the Aten, Atira, and Amor groups has not given any results.

Discussion: The Delta Cancrids is a poorly studied meteor shower, there are almost no articles concerning the search for a parental body. The asteroid 2001YB5 presented by IAU as a hypothetical parental body for DCA is selected by us with the high probability of 0.7, while for the southern and northern branches – with the probability of 0.6 and 0.5 respectively. Potentially hazardous objects among the selected ones are 2014BX2, 2001YB5, and 2014RS17 with 0.004 AU at the closest approach.

Conclusions: The observation of the shower's maximum activity at the Sun's longitude of 298,5° suggests that the orbit of a potentially parental body of the Delta Cancrids during the period of the shower's formation had node longitude between 298° and 299°. The involvement of the shower's structure at identifying it with NEOs is important to clarify the shower's origin.

References: [1] Sokolova M., et al. (2016) *Advances in Space Research* 58/4: 541-544. [2] Drummond J. D. (1981) *Icarus* 45: 545-553. [3] Kholshevnikov K.V., et al. (2016) *MNRA* 462/2: 2275–2283. [4] Kramer E. N. and Shestaka I. S. (1987) *Sol. Syst. Res.* 21/1: 75–83.

THE KAPPA CYGNIDS METEOROID SHOWER AND ITS CONNECTION WITH NEAR-EARTH ASTEROIDS

M. V. Sergienko[1], M. G. Sokolova[1], A. O. Andreev[1], Y. A. Nefedyev[1],
[1]Kazan Federal University, Russia, Kazan, Kremlyovskaya st., 18. E-mail: maria_sergienko@mail.ru

Introduction: The purpose of the research is to study the Kappa Cygnids meteoroid shower's connections with various groups of asteroids crossing the Earth's orbit on the basis of the meteor shower's structure observed and the complex approach of assessing the distance between the orbits of the 2 celestial bodies. The Kappa Cygnids meteor shower (KCG) is observed from 3 to 25 August and relates to showers with low activity. The size of its mean orbit is 3.2 AU, geocentric velocity is 24 km/s. There is no parent body (PB) found for the meteor shower among comets. The meteor shower's connections with asteroids, as probable PB of the shower, are being actively studied; some of them are listed on the IAU MDC website.

Methods: To study the structural features of the Kappa Cygnids meteor shower the long-term statistically supported set of visual observations of meteors by The International Meteor Organization (http://www.imo.net/data/visual) and television observations taken by the Mini-Mega TORTORA (MMT) of Kazan Federal University (Russia) between 2013 and 2016 are used. The source database for the search for the PB consisted of 17800 orbits (http://ssd.jpl.nasa.gov/sbdb_query.cgi). The television orbit catalogues by Japan Meteor Network (http://sonotaco.jp/doc/SNM/index.htm) and Croatian Meteor Network CMN (http://cmn.rgn.hr/downloads/downloads.html#orbitcat) as well as photographic one by IAU MDC (containing 700 orbits of Kappa Cygnids meteors were used. The study of connections between the shower and asteroids from the Apollo, Aten, Amor, and Atira groups was carried out using D-criterion by J.D. Drummond [1] and metrics by K.V. Kholshevnikov [2] as functions of the distance between orbits as well as Tisserand's parameter and 2 parameters (dynamic criteria) of the restricted three-body problem [3]. The critical upper values of D-criterion and the dynamic parameters, under which a hypothesis of the orbits' identity was accepted or declined, were determined by calculating mean orbits of the shower in each catalogue, taking into account their variance and catalogues' observation errors. The probability of the orbits proximity was defined as the full probability of the occurrence of joint events with a given level of significance.

Results: The investigation of Kappa Cygnids structure was performed with the method described in [4]. Using the visual observations of the number and magnitude of the meteors higher than $+3^m$ for the period between 1996 and 2011 it has been found that the increased shower activity is observed from August, 13 and remains at the level of 11 to 14 meteors an hour until August, 19 (the interval of the ecliptic longitude of the Sun is 140°–146°). The highest ratio of large components to small ones is recorded at 142.8° longitude of the Sun. This suggests that a potential parental body for Kappa Cygnids during the formation of the shower might have had an orbit with node longitude of about 142.8°. For the meteors' magnitude range observed between -5^m and $+3^m$ there is a decrease in semimajor axes of 0.8 AU and in eccentricities of 0.04 for the orbits of Kappa Cygnids depending on the meteors' magnitude. When searching for the parental body of Kappa Cygnids among the Apollo group, there are 2 asteroids 2001MG1 and 2002LV marked out with the probability of 0.7. Besides, there are the asteroids from the Amor group 2002GJ8, 2010QA5, and 2012QH49 marked out with the probability of 0.6. In the Aten and Atira groups the probability of identifying asteroids with the orbits of Kappa Cygnids does not exceed 0.2.

Discussion: The asteroids from the Apollo group 2001MG1 and 2002LV are also mentioned by other authors as potentially related to Kappa Cygnids. The asteroids 2004LA12 2008ED69 having the probability of 0.4 are considered as well. As for the asteroids of the Amor group, there are no connections with Kappa Cygnids found. It should be noted that 2002GJ8, 2010QA5, and 2012QH49 from the Amor group have the Tisserand's parameter in relation to Jupiter of 2.6, 2.7, 2.8 respectively, which relates them to the objects of cometary type.

Conclusions: Although the Kappa Cygnids is well studied (unlike other small meteor showers), its parental body is still unidentified. The development of an unbiased method for selection of asteroids with close orbits is of particular importance. The studies of the structure of meteor showers with unknown parental bodies provides additional criteria to clarify the question of their origins [5].

References: [1] Drummond J.D. (1981) *Icarus* 45: 545-553. [2] Kholshevnikov K.V., et al. (2016) *MNRA* 462/2: 2275–2283. [3] Kramer E.N. (1987) *Astronomical Vestnik* 21/1: 75–83. [4] Sokolova M., et al. (2016) *Advances in Space Research* 58/4: 541-544. [5] Sokolova M.G., et al. (2018) *Advances in Space Research* 62/8: 2355-2363.

SHOCK VEINS IN METEORITES: WHAT THEY TELL US ABOUT SHOCK CONDITIONS.

T. G. Sharp[1] and J. Hu[2], [1]School of Earth and Space Exploration, Arizona State University, Tempe AZ, 85287-1404, USA. Tom.sharp@aus.edu, [2]Division of Geological and Planetary Sciences, California Institute of Technology, Pasadena, California 91125, USA, jinping@caltech.edu.

Introduction: The goal of classifying the shock metamorphic features in meteorites is to estimate the corresponding shock pressure conditions [1]. However, the temperature variability of shock metamorphism is equally important and can result in diverse shock features in samples with equilibrated pressures. Shock-melt veins and melt pockets correspond to the highest temperatures in shock meteorites and they are the location of high-pressure (HP) minerals [2]. The usefulness of shock veins for interpreting shock conditions is debated. Stoeffler et al [3] suggest that shock veins do not provide useful estimates of shock pressure because they represent large deviations from average shock effects. However, these features provide an important mineralogical and chemical record of shock history [4]. Fritz et al. [5] claim that shock veins and HP minerals only record peak shock pressure in the isobaric zone for low-velocity (~ 2km/s) impacts, such as that recorded in L chondrites. Although other shocked materials may not sample the isobaric zone, their crystallization history is still useful for understanding the shock history. Here we calculate shock-temperatures and quench paths to semi-quantitatively evaluate the relationship between shock-melt crystallization and shock pressure.

Shock Temperatures and Shock-Melt Quench: Shock temperatures for a variety of rocks were calculated using the integral approximation along their Hugoniots [6]. The release *P-V-T* correlations are constructed by assuming an isentropic release adiabat and using a Mie-Grüneisen EOS. The bulk shock temperature of an L chondrite remains ~ 1000° cooler than the solidus up to 50 GPa. Shock-melt veins and pockets represent local temperature peaks that are caused by pore collapse, shear heating and complex peak-pressure variations during compression. For melting to occur during shock, these hot zones must reach temperatures in excess of 2200 K at 20 GPa and nearly 3000 K at 50 GPa. Small volumes of melt, as in S6 shock veins, are quenched primarily by heat transfer to the relatively cool surrounding rock. Adiabatic decompression of a shock melt, without heat transfer to a cooler host rock, would not crystallize HP minerals, but would result in crystallization at ambient pressure.

Constraints from Shock Vein Assemblages: Shock stage S6 is restricted to melt zones in chondrites with bulk shock stages of S4 to S5 [1]. S6 shock veins in L chondrites generally contain crystallization assemblages of majoritic garnet with oxide, ringwoodite or wadsleyite. Samples, such as Tenham and Acfer 004, have higher pressure assemblages with bridgmanite and akimotoite. Many of these shock veins have assemblages that reflect a relatively narrow range of crystallization pressure, suggesting crystallization in the isobaric zone of the impact [5]. However, L6 impact-melt rocks, such as Chico and NWA 091, which show pervasive melting and darkening but no high-pressure minerals, indicate shock pressures higher than S6. Shocked Martian meteorites show a distinctly different crystallization history. Some have olivine disproportionation reactions that indicate higher pressures than those recorded in L6 chondrites. In addition, the shock-melt quench products vary significantly depending on the size of the melt zone. In Tissint, for example [7], μm-scale veins crystallized high-pressure assemblages whereas, mm-scale melt pockets remained liquid until after pressure release. This is because the shock duration, from a relatively small impactor, was shorter than the cooling time for the thick veins. The Martian augite basalt, NWA 8159 [8], has mm-scale shock veins contain majoritic garnets throughout, indicating a narrow range of crystallization pressure and a relatively long shock pulse. The crystallization assemblage preserved in shock meteorite is dependent on both the shock pressure and the local thermal history of the sample. Calculated shock-temperature heterogeneities and resulting melt-quench paths constrain the possible relationships between peak shock pressure and crystallization pressure in shocked meteorites. We show that detailed characterization of shock melt can help construct a comprehensive *P-T* history of shock, including the peak shock pressure. Shock veins in meteorites should not be ignored.

References: [1] D. Stöffler, et al. (1991). *Geochimica et Cosmochimica Acta* 55: 3845–3867. [2] T. G. Sharp and P. DeCarli (2006). *In Meteorites and the early solar system II. The University of Arizona Press*. 653–677. [3] D. Stoeffler et al (2018) *Meteoritics & Planetary Science* 1, 5-49. [4] J. Hu and T. G. Sharp (2017) *Geochimica et Cosmochimica Acta,* 215, 277-294. [5] J. Fritz et al. (2017) *Meteoritics & Planetary Science 52*, 1216–1232. [6] R. G. McQueen (1989) *In High-pressure equations of state: Theory and Applications. Elsevier*. 101-216. [7] E. L. Walton et al. (2014) *Geochimica et Cosmochimica Acta* 140 (2014) 334–348. [8] T.G. Sharp et al (2019) *Geochimica et Cosmochimica Acta* 246, 197–212.

NICKEL-RICH METAL-SULFIDE GLOBULES IN FUSION CRUST OF CHELYABINSK METEORITE

V. V. Sharygin[1,2,3], [1]V.S.Sobolev Institute of Geology and Mineralogy, SB RAS, Novosibirsk, 630090, Russia; [2]Novosibirsk State University, Novosibirsk, 630090, Russia; [3]ExtraTerra Consortium, Institute of Physics and Technology, Ural Federal University, Ekaterinburg 620002, Russia; E-mail: sharygin@igm.nsc.ru.

Introduction: Fusion crust (product of melting in the Earth's atmosphere) is common of all fragments of the Chelyabinsk LL5 chondrite. Its thickness does not exceed 600 μm. Temperature of melting may be estimated in the 1800-2270°C interval. The composition and structure of the fusion crust does not depend on size of meteorite fragments and lithological type, which was involved in melting event (initial chondrite, impact melt, impact veins). In general, it contains numerous gas vesicles and is zoned in structure.The outer zone is cryptocrystalline and contains skeletal new-formed crystals of zoned olivine and magnetite (up to 5 μm) and mafic glass (commonly devitrified). The inner zone consists of larger crystals of olivine, glass and minor magnetite. Both zones also contain relics of initial chromite (rarely olivine) and new-formed Ni-rich metal-sulfide globules (5-50 μm). Chemical and phase composition of such globules drastically differs from metal-sulfide assemblages in other lithologies of the Chelyabinsk meteorite [1-6].

Experimental: Polished samples with fusion crust (Chelyabinsk meteorite) were examined using optical microscope Olympus BX51, scanning microscope TESCAN MIRA 3MLU SEM (EDS) and electron microprobe JEOL JXA-8100 (WDS).

Results and Discussion: The following phases have been observed in metal-sulfide globules: two heazlewoodite solid solutions (Hzss1 - $(Ni,Fe)_{3\pm x}S_2$, Hzss2 – $(Ni,Fe)_{4\pm x}S_3$), godlevskite solid solution (Gdss – $(Ni,Fe)_{7\pm x}S_6$), nickel, awaruite, pentlandite $(Fe,Ni)_9S_8$, tetrataenite, rarely kamacite, taenite and unidentified Os-Ir-Pt-rich phase. Wüstite or bunsenite may appear as thin rim around some globules (Fig. 1). In general, the phase composition of globules strongly varies depending on location in the individual zone of fusion crust. The association of Hzss1 + nickel (or awaruite) ± Os-Ir-Pt phase is dominant for globules from the outer zone, whereas Hzss2, Gdss, pentlandite and other Ni-poorer phases are common for globules located in the inner zone. Unfortunately, it is unclear, whether melting event led to the appearance of one melt (with further separation into metal-sulfide and silicate components) or two individual melt existed independantly.In any case, the interaction of new-formed melts with atmospheric oxygen is a main reason in the appearance of such Ni-rich metal-sulfide paragenesises in the fusion crust of the Chelyabinsk meteorite. As a result, during melting and further crystallization metal-sulfide melt was getting richer in Ni and poorer in Fe than silicate liquid. The platinum-group elements were concentrated in metal-sulfide component with formation of individual phase (mainly as inclusions in Ni-rich metal, Fig. 1) despite of high rate of melting and further crystallization. It is not excluded that part of sulfur evaporated during melting. Such process of melting in the Earth's atmosphere with formation of the fusion crust seems to be common for all chondrites.

References: [1] Anfilogov V. N. et al. 2013. *Litosfera* 13(3):118-129. [2] Sharygin V. V. et al. 2013. *Mineralogical Magazine* 77(5):2189-2189. [3] Sharygin V. V. et al. 2014. *Conference "Meteorite Chelyabinsk – one year on the Earth", Chelyabinsk*:654-666. [4] Andronikov A. V. et al. 2015. *Planetary and Space Science* 118:54-78. [5] Sharygin V. V. et al. 2015. *Meteoritics and Planetary Science* 50(SI1):5274.pdf. [6] Sharygin V. V. et al. 2016. *Meteoritics and Planetary Science* 51(SI1):A567-A567.
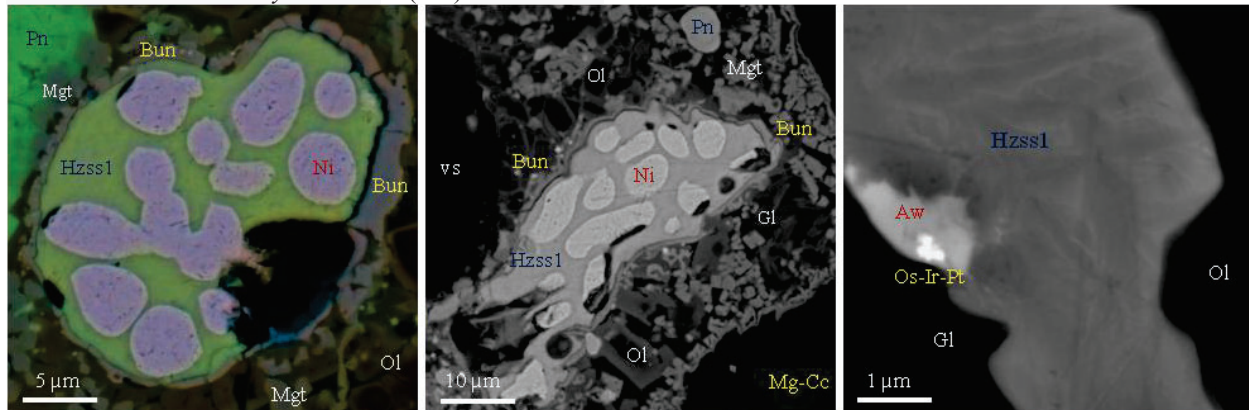

Figure 1. BSE images of some metal-sulfide globules from fusion crust of the Chelyabinsk chondrite. Symbols: Mgt – magnetite; Ol – olivine; Hzss1 – heazlewoodite solid solution $(Ni,Fe)_{3\pm x}S_2$; Ni – nickel; Bun – bunsenite; Pn – pentlandite; Gl – silicate glass; vs – gas vesicle; Aw – awaruite; Mg-Cc – Mg-rich calcite; Os-Ir-Pt - Os-Ir-Pt-rich Fe-Ni-alloy.

SODIUM-RICH PHOSPHATE AND SILICATE INCLUSIONS IN TROILITE NODULE IN DARINSKOE IRON METEORITE (IIC)

V. V. Sharygin[1,2,3], [1]V.S.Sobolev Institute of Geology and Mineralogy, SB RAS, Novosibirsk, 630090, Russia; [2]Novosibirsk State University, Novosibirsk, 630090, Russia; [3]ExtraTerra Consortium, Institute of Physics and Technology, Ural Federal University, Ekaterinburg 620002, Russia; E-mail: sharygin@igm.nsc.ru.

Introduction: Meteorite Darinskoe (1 sample, 11.2 kg) was found in 1984 in Ural'sk district of Kazakhstan. It is plessitic octachedrite (IIC group) [1], which contains two troilite nodules (up to 3 cm). In addition to large troilite nodules and plessite aggregate the Darinskoe iron consists of small troilite isolations (up to 1 mm), kamacite, chromite, schreibersite (rhabdite), pentlandite and cobaltpentlandite. The terrestrial alteration phases are represented by goethite, Cl-bearing Fe-hydroxides (akaganeite, droninoite) and siderite. According to LA-ICP-MS data [2] the bulk composition of the Darinskoe meteorite is: Ni – 11.4 wt.%; Co – 0.59 wt.%; Cu - 147; Ga – 44; Ge – 90; As - 5.6; Mo - 18.3; Ru – 25.1; Rh – 1.6; Pd – 2.9; Ir – 12.8; Pt – 13.5; Au – 0.6, Re – 1; W – 3.3 ppm.

Experimental: Polished samples of the Darinskoe meteorite were examined using optical microscope Olympus BX51, scanning microscope TESCAN MIRA 3MLU SEM with EDS/WDS system and LabRAM HR 800 mm spectrometer.

Results and Discussion: The studied troilite nodule (2.5 cm) contains rounded chromite grains (50-100 μm), euhedral schreibersite (10-100 μm), phosphate and silicate inclusions (10-30 μm) (Fig. 1). Sulfides (Cl-free djerfisherite, pentlandite, chalcopyrite, cubanite) and unidentified micron-sized Ni-Te-phase (Ni - >16, Te - >32 wt.%) sometimes associated with the inclusions. Host troilite is rich in Cr (0.4-1.0 wt.%). Average composition of djerfisherite is (n=15, in wt.%): Fe – 44.48; Ni – 9.31; Co - 0.15; Cu – 3.04; K – 8.90, S – 34.01; Cl - 0.00. Phosphate inclusions are mainly composed by hydrated Ca-Mn-Fe phosphates (supported by Raman), which seems to be alteration products of initial alkali-rich anhydrous phosphates in the terrestrial conditions. Only buchwaldite $NaCa(PO_4)$ has been found as a primary phase in some phosphate inclusions. Its composition is (n=6, in wt.%): Na_2O – 19.50; K_2O – 0.16; CaO – 35.57; FeO – 1.26; P_2O_5 – 43.75; SO_3 – 0.32. It is very closy to buchwaldite observed in troilite nodules of another iron meteorites [3]. The silicate inclusions have very specific and variable composition (range in wt.%): SiO_2 – 60.7-72.6; TiO_2 – 3.5-11.2; Cr_2O_3 – 2.1-3.4; Al_2O_3 – 0.05-0.15; FeO – 2.3-2.4; MgO – 0.3-0.4; CaO – 0.3-0.4; Na_2O – 11.5-12.9; K_2O - 2.4-4.0; P_2O_5 – 0.51; SO_3 – 0.4-0.5. We did not find any similar compositions among known mineral species and thus suggest that it maybe a Na-rich silicate glass.

References: [1] Wlotzka F. 1995. *Meteoritics* 30:792-796. [2] Chernonozhkin S. M. et al. 2014. *Journal of Analytical Atomic Spectrometry* 29:1001-1016. [3] Olsen E. et al. 1977. *American Mineralogist* 62: 362-364.
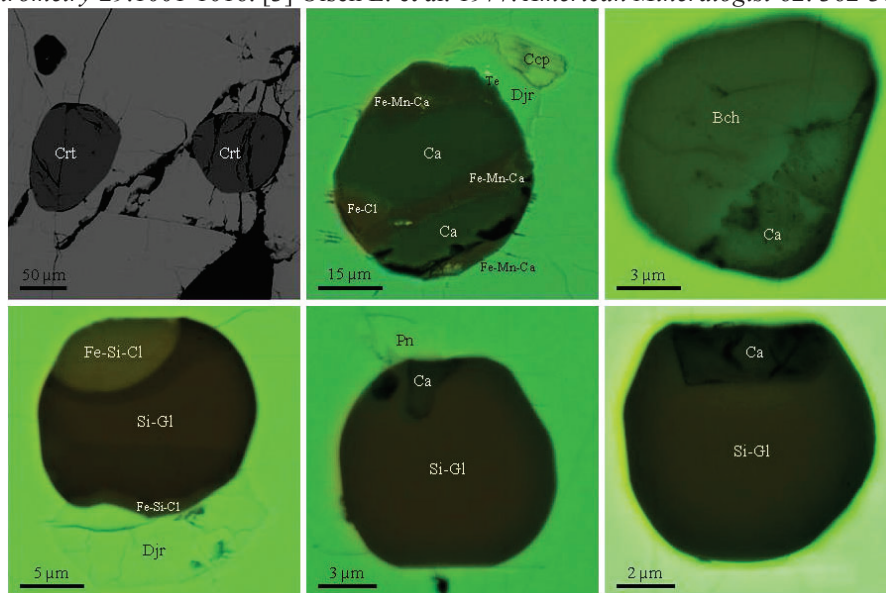

Figure 1. BSE images of chromite, phosphate and silicate inclusions in troilite nodule of the Darinskoe iron meteorite. Symbols: Crt – chromite; Ccp - chalcopyrite; Djr – Cl-free djerfisherite; Te – Te-Ni-rich phase; Bch – buchwaldite; Pn – pentlandite; Ca - hydrated Ca-phosphate after buchwaldite; Fe-Mn-Ca, Fe-Cl – hydrated phosphates after alkali-rich anhydrous phosphates; Si-Gl – Na-Ti-rich silicate glass ?; Fe-Si-Cl – Fe-Cl-rich silicate ?.

HEATING EXPERIMENTS OF MASKELYNITE IN ZAGAMI AND ELEPHANT MORAINE A79001: IMPLICATIONS FOR THEIR RELATIVE SHOCK DEGREES.

R. Shikina[1,2] and T. Mikouchi[1,2], [1]Dept. Earth & Planet. Sci., University of Tokyo, Hongo, Tokyo 113-0033, Japan (r-shikina@um.u-tokyo.ac.jp), [2]University Museum, University of Tokyo, Hongo, Tokyo 113-0033, Japan

Introduction: Maskelynite is understood as a diaplectic plagioclase glass that has been transformed from plagioclase in solid-state transformation by strong impact and is commonly found in martian meteorites [e.g., 1]. The shock pressure of martian meteorites has been quantitatively estimated from the refractive index of plagioclase by comparing with the recovered shocked plagioclase by dynamic high-pressure experiments [1]. However, the time scale of the impact is significantly different between natural events and laboratory experiments [2-3], and it has been pointed out that the shock pressure may be overestimated [4]. In this study, we performed heating experiments of maskelynite in martian meteorites because it is known that maskelynite is easily converted to crystalline plagioclase by reheating and the degree of recrystallization depends upon shock pressure [5]. We tried to evaluate the shock pressures of two shergottites (Zagami and EETA 79001) because they are reported to have experienced different degrees of shock [1].

Experiments: Small slices (~5 mm in size) of Zagami and EETA 79001 were heated at 900 °C (1, 8, 24 and 168 hours) and 1000 °C (1 hour) in a CO_2-H_2 gas mixing furnace at the oxygen fugacity of two log units above the iron-wüstite buffer ($\log fO_2$=IW+2). The heated samples were observed with an optical microscope to estimate the degree of plagioclase recrystallization and mineral compositions were analyzed by electron microprobe (JEOL JXA 8530F and JXA 8900L at Univ. of Tokyo).

Results: As reported in [6], Zagami did not show clear evidence of recrystallization in the experiment heated at 900 °C for 1 hour, but fibrous crystalline plagioclase was observed in the experiments heated at 900 °C for 8, 24, and 168 hours. Zagami maskelynites heated at 900 °C for 24 and 168 hours were almost completely converted to polycrystalline plagioclase. In maskelynites heated at 900 °C for 8 hours and heated at 1000 °C for 1 hour, fibrous crystalline plagioclase was observed only along the cracks and edges of the original grains. Although maskelynites appear to have a smooth surface through optical microscopy, the recrystallised plagioclase shows a dirty devitrified texture. Electron microprobe analysis revealed that Na and K are reduced, but Ca is enriched in the recrystallized plagioclase of the samples showing partial recrystallization (900 °C for 8 and 24 hours and 1000 °C for 1 hour). In the maskelynite grains heated at 900 °C for 168 hours, small glass regions enriched in Na and K are present (Na_2O: 6.5 wt%, K_2O: 2.5 wt%), suggesting that Na and K concentrate in areas where recrystallization did not start yet.

Similar to Zagami, EETA 79001 did not show clear evidence of recrystallization in the experiment heated at 900 °C for 1 hour, but fibrous crystalline plagioclase was observed in samples heated at 900 °C for 8, 24, and 168 hours. Maskelynites heated at 1000 °C for 1 hour also showed fibrous crystalline plagioclase. The sample heated at 900 °C for 24 hours shows concentration of Na and K in glass areas (Na_2O: ~5.0 wt%, K_2O: ~ 2.0 wt%), which resembles Zagami maskelynites heated at 900 °C for 24 and 168 hours.

In EETA 79001 maskelynites heated at 900 °C for 24 hours and at 1000 °C for 1 hour, the degree of recrystallization in one grain was similar compared to the samples under the same heating conditions of Zagami. However, there was a difference that EETA 79001 had lower volumes of the recrystallized regions compared to Zagami. This is probably because the grain size of maskelynites in EETA 79001 are smaller (~300 μm) compared to those of maskelynites in Zagami (500-800 μm).

Discussion and Conclusion: The degree of recrystallization of maskelynite is reported to be related to the original shock degree of plagioclase as experimentally demonstrated [5]. The results of [5] showed that the higher the degree of impact, the lower the recrystallization rate, as compared for the samples with the same heating time. The shock pressure of Zagami and EETA 79001 are estimated to be 29.5 ± 0.5 GPa and 36 ± 5 GPa, respectively [1]. Comparing our Zagami experiments with those of EETA 79001, in the heating experiments at 900 °C and 1000°C, the degree of recrystallization was similar, but EETA 79001 samples showed smaller volumes of recrystallization areas because of there differences in grain sizes. Therefore, we consider our experimental results are consistent with the higher shock degree of EETA 79001 than Zagami.

References: [1] Fritz J. et al. (2011) Meteoritics and Planetary Science 40:1393-1411. [2] Xie X. et al. (2001) European Journal of Mineralogy 13:1177-1190. [3] Ohtani E. et al. (2004) Earth and Planetary Science Letters 227:505-515. [4] Tomioka N. et al. (2010) Geophys. Res. Lett. 37:L21301. [5] Ostertag R. and Stöffler D. (1982) Proceedings of 13th Lunar and Planetary Science Conference:A457-A463. [6] Mikouchi T. et al. (2002) Meteoritics and Planetary Science 37:Suppl. A100.

HYDROGEN ABUNDANCES AND ISOTOPE COMPOSITIONS OF CHONDRULES IN CARBONACEOUS AND ORDIANARY CHONDRITES.

K. Shimizu[1], C. M. O'D. Alexander[1], E. H. Hauri[1], A. R. Sarafian[2], L. R. Nittler[1], J. Wang[1], S. D. Jacobsen[3], and R. A. Mendybaev[4]. [1]Department of Terrestrial Magnetism, Carnegie Institution for Science, Washington, DC, [2]Science and Technology Division, Corning Incorporated, Corning, NY, [3]Department of Earth and Planetary Sciences, Northwestern University, Evanston, IL, [4]Department of Geophysical Sciences, University of Chicago, Chicago, IL.

Introduction: It may be possible to constrain the partial pressure of H_2/H_2O and its isotopic composition during chondrule formation using the H abundances and isotopic compositions in chondrules. If H_2 from nebula gas dominated during chondrule formation, it should have imparted low H contents and δD in chondrules. In contrast, if chondrules formed by planetesimal collisions [e.g., 1], one migh expect high H contents and δD values similar to those of the bulk chondrites, particularly the water-rich carbonaceous chondrites (CCs). For ordinary chondrite (OC) chondrules, this could help constrain the timing of migration of outer Solar System objects into the inner Solar System [e.g., 2, 3].

Due to the expected low H concentrations generated during chondrule formation, as well as the potential parent body overprinting, the measurement of primary H isotopic compositions in chondrules is challenging. Highly variable concentrations and isotopic compositions have been reported in previous in situ measurements of H in chondrites [e.g. 2, 4, 5, 6]. In situ studies of nominally anhydrous minerals (NAMS) in chondrules have reported high H contents [4, 6], which, if taken at face value, may require unreasonably high pressure environments during chondrule formation. Therefore, the high H contents reported in chondrule NAMS could instead imply parent body alterations at lower temperatures. We have undertaken an initial study to measure H abundances and isotopic compositions in chondrules of the least altered/metamorphosed primitive meteorites that are available.

Samples and Methods: The meteorites selected for this study are: QUE 97008, (L3.05), Semarkona (LL3.0), ALH 77307 (CO3.0), and Kaba (CV3.1). The majority of our analyses so far have been carried out on a section of QUE 97008 and most recently on a section of Semarkona for which the measurements are still ongoing. We have also analyzed chondrule NAM (olivine and orthopyroxene) grains that were picked from powdered meteorite samples that were then mounted in indium. The major element compositions of the mesostases and olivines were measured by EPMA. The volatile (H, C, P, S, F, Cl) concentrations H isotopic compositions were measured with the Cameca NanoSIMS 50L following the technique of [7, 8].

Results and Discussions: After background correction, the H_2O concentrations in the chondrule mesostases and NAMs in QUE 97008, ALH 77307, and Kaba range from 10 to 118 ppm and 9 to 17 ppm, respectively. These are significantly lower than previously reported values for mesostases (1000 to several wt.%) and NAMs (76–2100 ppm, [4, 6]). The measured H_2O concentrations are, however, significantly higher compared to the concurrently determined background of H_2O concentration using Suprasil glass (2–4 ppm).

The H isotopic compositions of the chondrule mesostases glass in QUE 97008, ALH 77307, and Kaba range from ~800 ‰ to 15,000 ‰. In particular, the mesostases glass in the QUE 97008 section have high average D/H ratios of 12,000±2,800 ‰. While these D-enrichments in mesostases glass may have been inherited from water ice that formed in the presolar molecular cloud [2, 4], this would require that the inner Solar System OCs accreted proportionately more interstellar water than the outer Solar System CCs and even all comets (maximum cometary D/H ≈ 3,000±1,000 ‰ observed on C/2012 F6 Lemmon). Alternatively, the mesostases may have approached isotopic equilibrium with D-rich water generated through an isotopic Rayleigh distillation process during oxidation of Fe by water and loss of D-poor H_2 [9, 10]. Diffusion lengthscales for H_2O in chondrule glass estimated from diffusion coefficients in relevant glass compositions [11] and relevant conditions (300ºC [12]) are at least ~350 μm in 1 Ma, suggesting the possibility of isotopic equilibration between D-rich fluids and chondrule through diffusion of D-rich H_2O into the mesostases. In contrast to the homogeneously D-rich chondrule mesostases of the QUE 97008 section, the recently conducted measurements of chondrule mesostases in the Semarkona section have found variable D/H ratios of ~200 ‰ to 11,000 ‰ (H_2O concentration = ~10 to 4,000 ppm) that do not seem to be associated with variable contamination via surface features (e.g., correlate with Cl and C associated with epoxy). The measurements on the Semarkona section are still ongoing, and the implications of these observations will be discussed at the meeting.

References: [1] Fedkin A. V. and Grossman L. (2013) *GCA, 112,* 226–250. [2] Deloue E. and Robert F. (1995) *GCA, 59,* 4695–4706. [3] Alexander C. M. O'D. et al. (2012) *Science, 337,* 721–723. [4] Deloue E. et al. (1998) *GCA, 62,* 3367–3378. [5] Bonal L. et al. (2013) *GCA, 106,* 111–133. [6] Stephant A. et al. *GCA, 199,* 75–90. [7] Hauri E. H. et al. (2002) *Chem. Geol. 182*, 99–114. [8] Hauri E. H. et al. (2006) *Chem. Geol. 235*, 352–365. [9] Alexander C. M. O'D. et al. (2007) *GCA, 71,* 4380–4403. [10] Alexander C. M. O'D. et al. (2010) *GCA, 74,* 4417–4437. [11] Zhang et al. (2010) *Rev. Mineral. Geochem. Vol 72*, 311–408. [12] Busemann et al. (2007) *MAPS. 42*, 1387–1416.

SIDEROPHIELE ELEMENT FRACTIONATION IN IMPACT GLASS FROM THE WABAR IMPACT CRATER.

N. Shirai[1] and M. Ebihara[2]
[1]Departmento fo Chemistry, Graduate School of Science, Tokyo Metropolitan Univeristy, Tokyo, 192-0397 Japan (shirai-naoki@tmu.ac.jp), [2]Department of Earth Sciences, School of Education and Integrated Arts and Sciences, Waseda University, Tokyo, 169-8050 Japan

Introduction: Siderophile elements such as Co, Ni and PGE are depleted in crustal materails because these elements are strongly partitioned into core. In contrast, these element abundances of extraterrestrial materials such as chondrites and iron meteorites are several orders of magnitude higher than those for crustal materials. Therefore, the elevated siderophile element abundances in implact-related rock samples are due to the incorporation of meteoritic components into crustal materaials. Individual chondrites and iron meteorites have characteristic absolute and relative abundances of siderophile elements. Thus, siderophile elements have been used for the detection and identification of projectile materials [e.g., 1]. Recent studies indicated that there is a possibility of elemental fractionation during impact events [e.g., 2-4]. However, processes of elemental fractionation and interaction between projectile and target materials during impact events are poorly understood. Thus, elemental fractionation lead to a difficulty in indentifying projectile metarials. Both projectiles and impact-related materials were collected from small and young craters such as Kamil Crater of Egypt [5] and Wabar crater of Saudi Aravia [6]. In this study, elemental abundances of impact glass from Wabar cater were determined by using instrumental neutron activation analysis (INAA) and instrumental photon activation analysis (IPAA) in order to constrain the processes of elemental fractionation during impact event.

Experiments: Impact glass from Wabar crater was received from NIPR and roughly ground into small pieces. Black and white melts were separated by using tweezers and analyzed by using INAA and IPAA. INAA and IPAA were performed at Institute for Integrated Radiation and Nuclear Science, Kyoto University for the determination of elemental abundances of impact glass. For INAA, sample was irradiated for 10 sec and 4 hrs at the pn-3 and pn-2, respectively. For IPAA, the irradiation was carried out using the linear accelerator operated at 20 MeV electron beam energy and 102 μA current for 36 hrs.

Results and Discussion: Our analytical results of black and white melts are consistent with the previous studies [2,6,7]. As observed by [7], black melt has higher abundances of Co, Ni, Ir and Au than those of white melt. Black melt contains 300 ppm for Co, 3710 ppm for Ni, 336 ppb for Ir and 5.72 ppb for Au. Mass fractions of Wabar iron in the black melt analyzed in this study were estimated to be 4 to 6% based on Co, Ni and Ir abundances for Wabar iron [2] and black melt [this study]. Assuming that target material has similar siderophile element abundances to those of upper continental crust, impact-related material having 4 to 6% mass fraction of projectile has similar chemical characteristics of siderophile elements. Figure compares siderophile elements abundances of black melt with those of bulk Wabar iron. Siderophile element abundances were normalized to Ni and those for bulk Wabar iron. Black melt has higher Co/Ni ratio and lower Ir/Ni and Au/Ni ratios compared with those of bulk Wabar iron. For comparison, siderophile element abundances of kamacite and taenite from Wabar iron are shown in Fig. Ir/Ni ratio of black melt fall in the range between those of kamacite and taenite. However, Au in black melt are highly depleted compared with kamacite and taenite. Based on our analytical results of INAA and IPAA, projectile could not be simply incorporated into target material. Other siderophile elements abundances such as Ru, Rh, Pd and Pt will be determined and the detailed fractionation among siderophile elements will be discussed.
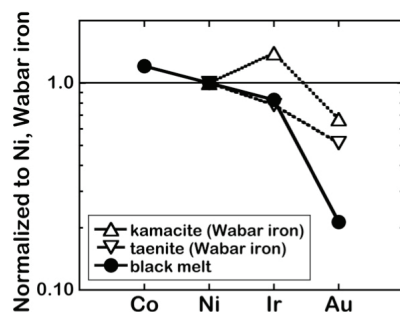

Fig. Siderophile elements of black melt (this work) and kamacite and taenite from Wabar iron (Mullane et al. [8]).

References: [1] Tagle R. and Berlin J. 2008. *Meteoritics & Planetary Science* 43:541-559. [2] Mittlefehldt D. W. et al. 1992. *Meteoritics* 27:361-370. [3] Jonásová S. et al. 2016. *Geochimica et Cosmochimica Acta* 190:239-264. [4] Goderis S. et al. 2017. *Geochimica et Cosmochimica Acta* 217:28-50. [5] Fazio A. et al. 2014. *Meteoritics & Planetary Science* 49:2175-2200. [6] Gnos E. et al. 2013. *Meteoritics & Planetary Science* 48:2000-2014. [7] Hörz F. et al. 1989. *Procedings of the 19th Lunar and Planetary Science Conference* 697-709. [8] Mullane E. et al. 2004. *Chemical Geology* 208:5-28.

MASS SPECTROMETRIC STUDY OF PEROVSKITE EVAPORATION FROM KNUDSEN CELL

S. I. Shornikov and O. I. Yakovlev, Vernadsky Institute of Geochemistry & Analytical Chemistry of RAS, Kosygin st. 19, Moscow 119991, Russia, e-mail: sergey.shornikov@gmail.com, yakovlev@geokhi.ru

Introduction: Calcium titanate $CaTiO_3$ (perovskite) is of particular interest for cosmochemical studies as a mineral that is part of the substance of refractory Ca–Al–inclusions (CAIs) and is the earliest object of the Solar system with unusual isotopic characteristics [1]. It is believed that perovskite is a polygenic material that combines a relict substance formed in the inner shells of supernova stars, and a condensation product from a high-temperature gas, and a crystallization product of a silicate melt [2, 3]. In this regard, experimental information on evaporation processes and thermodynamic properties of perovskite is of particular importance for understanding of their formation in CAIs.

Results and discussion: We studied evaporation of perovskite in the temperature range 1791–2241 K and the CaO–TiO_2 melts in the temperature range 2241–2441 K from the Knudsen molybdenum effusion cell by the mass spectrometric method. The established molecular composition of the gas phase over perovskite and over the CaO–TiO_2 melts shows to evaporation according to reactions typical for the evaporation of individual oxides. The $(CaTiO_3)$ presence in minor amounts in the gas phase testified to the occurrence of the following heterogeneous reactions $[CaTiO_3] = (CaTiO_3)$. The values of partial pressures of vapor species (p_i) over perovskite (Fig. 1) and over the CaO–TiO_2 melts were determined by the Hertz-Knudsen equation. The CaO, TiO_2 and $CaTiO_3$ activities (a_i) were calculated from the partial pressures values (Fig. 2). They allowed to determine the values of mixing energy, as well as the enthalpy and entropy of perovskite formation equal to -39.88 ± 0.54 kJ/mol and 3.15 ± 0.28 J/(mol×K), respectively, and the melting enthalpy of perovskite at 2241 ± 10 K, equal to 47.61 ± 1.84 kJ/mol (per 1 mol compound) [4].
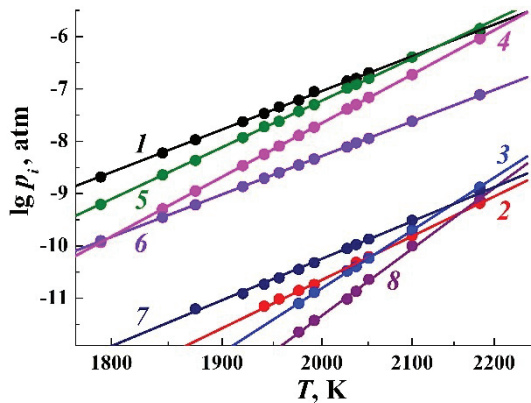

Fig. 1. The partial pressure values of vapor species over perovskite: Ca (*1*), CaO (*2*), Ti (*3*), TiO (*4*), TiO₂ (*5*), O (*6*), O₂ (*7*), CaTiO₃ (*8*).
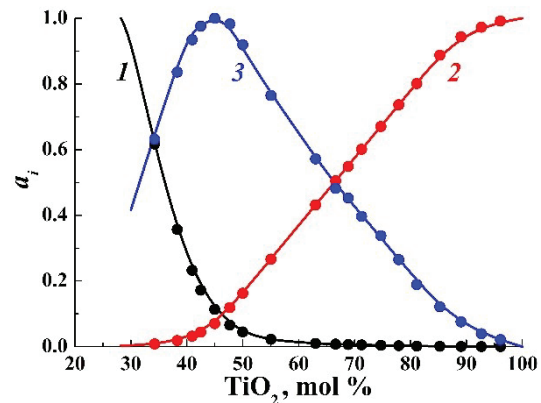
Fig. 2. The activities of CaO (*1*), TiO₂ (*2*) and CaTiO₃ (*3*) in the CaO–TiO₂ system, determined at the present study at 2250 K.

According to the rules established earlier in [5] the change in the composition of the gas phase over perovskite in the temperature region 1700–2400 K (Table 1), calculated from the values of the oxide activity, shows an increase in the $(CaTiO_3)$ content in the vapor by 10^4 times. It should be taken into account when considering the perovskite fractionation during evaporation [1].

Table 1. The composition of the gas phase over perovskite (mol %).

T, K	O	O_2	Ca	CaO	Ti	TiO	TiO_2	Ti_2O_3	Ti_2O_4	$CaTiO_3$
1700	34	1.3	35	8.0×10^{-3}	3.4×10^{-5}	0.96	29	4.7×10^{-3}	2.5×10^{-3}	3.9×10^{-5}
2241	16	1.2	10	3.4×10^{-2}	2.8×10^{-3}	8.2	64	0.13	0.11	6.6×10^{-2}
2400	17	1.4	8.6	5.1×10^{-2}	6.0×10^{-3}	11	62	0.15	0.12	0.39

References: [1] Zhang J. et al. (2014) *GCA*, *140*, 365–380. [2] Nazarov M. A. et al. (1984) *Meteoritika*, *43*, 49–65 (in Russian). [3] Goswami J. N. et al. (1991) *Met. Planet. Sci.*, *26*, 339. [4] Shornikov S. I. (2019) *Materials Processing Fundamentals*. *The Minerals, Metals & Materials Ser.*, doi: 10.1007/978-3-030-05728-2_23, 253–263. [5] Shornikov S. I. and Yakovlev O. I. (2015) *Geochem. Int.*, *53*, 690–699.

ANALYSIS OF THE INFRASOUND DATA ASSOCIATED WITH THE ANNAMA FIREBALL (19 APRIL 2014).

E. A. Silber[1] and M. Gritsevich[2,3,4]
[1]Department of Earth, Environmental and Planetary Science, Brown University, Providence, RI, USA, 06912 (e-mail: elizabeth_silber@brown.edu), [2]Finnish Fireball Network, Helsinki, Finland, [3]Department of Physics, University of Helsinki, Gustaf Hällströmin katu 2a, P.O. Box 64, FI-00014 Helsinki, Finland (maria.gritsevich@helsinki.fi), [4]Institute of Physics and Technology, Ural Federal University, Mira str. 19. 620002 Ekaterinburg, Russia.

Introduction: Infrasound is low frequency sound, lying below the human hearing range. Among many sources of infrasound, are the meteoroids larger than a few centimeters. As a meteoroid interacts with the Earth's atmosphere during its hypersonic flight, it produces a shock wave, which decays to low frequency infrasonic waves that propagate over great distances [1]. Infrasound is a valuable tool in estimating energy release by meteoric events and validation of existing models (e.g. [2]). Here we study the infrasound data associated with the meteorite-producing fireball Annama observed by the Finnish Firebal Network on April 19, 2014 [3-7].

Methodology: The waveform data from IMS network [8] of the Comprehensive Nuclear-Test-Ban Treaty Organization (CTBTO) within 5000 km of the event were examined for possible infrasound signals. To search and identify probable infrasonic signals emanating from the fireball, we used two software packages: the Progressive Multi-Channel Correlation (PMCC) algorithm, and MatSeis 1.7. PMCC is optimized for locating signals with low signal-to-noise ratio. It employs element pair-wise correlation algorithm to search for detections based on signal coherency and common back azimuth, identifying return "families" in time and frequency. Details about relative advantages of these two software packages and references can be found in [9].

Summary: A coherent airwave, consistent with the back azimuth and timing of the fireball, was identified at IS43RU (56.72°N, 37.22°E), 1359 km from the point of origin. Other IMS stations did not show evidence of infrasound signals. The infrasonic wave arrived in two stratospherically ducted packets (phases), with the overall frequency content of approximately 1 Hz. The first arrival was recorded at 23:26:36 UTC, with the primary phase persisting for 174 seconds. The measured back azimuth of 348.9° is in excellent agreement with the theoretical back azimuth of 348.6°. The second arrival occurred shortly thereafter, at 23:30:09 UTC, in a burst lasting only 44 s.

The dominant signal period was measured in two ways; first, by measuring the zero crossings at maximum peak-to-peak amplitude (maximum Hilbert envelope), and second, by finding the inverse of the signal frequency, with the noise subtracted, at the maximum signal power density (PSD). The dominant signal period, tabulated from the frequency at maximum PSD, is 1.83 s, which is consistent, within the measurement uncertainty, with the period measured at the maximum amplitude. Using the empirical period-energy AFTAC relation [10], the signal period corresponds to energy release of approximately 30 t of TNT equivalent (1 TNT = $1.184 \cdot 10^9$ J).

References: [1] Silber E. A. et al. (2018) *Adv. Sp. Res.*, 62, 489-532. [2] Moreno-Ibáñez M. et al. (2018) *The Astrophysical Journal* 863(2), 174. [3] Gritsevich M. et al. (2014) *Meteoritics and Planetary Science*, 49, A143. [4] Trigo-Rodríguez J. M. et al. (2015) *MNRAS*, 449(2), 2119-2127. [5] Dmitriev V. et al. (2015) *Planetary and Space Science*, 117, 223–235. [6] Lyytinen E. and Gritsevich M. (2016) *Planetary and Space Science*, 120, 35-42. [7] Kohout et al. (2017) *Meteoritics and Planetary Science*, 52, 1525–1541. [8] Christie D. R. and Campus P. (2010) "The IMS Infrasound Network: Design and Establishment of Infrasound Stations", In: A. Le Pichon, E. Blanc and A. Hauchecorne (Eds.), *Infrasound Monitoring for Atmospheric Studies*, Springer, New York, pp. 29-75. [9] Silber E. A. and Brown P. G. 2014. Optical Observations of Meteors Generating Infrasound – I: Acoustic Signal Identification and Phenomenology, *JASTP*, 119, 116-128. [10] ReVelle D. O. (1997) "Historical Detection of Atmospheric Impacts by Large Bolides using Acoustic-Gravity Waves", Annals of the New York Academy of Sciences, Near-Earth Objects - The United Nations International Conference (Ed. J. L. Remo), 822, 284-302.

EVALUATING FIDELITY OF EMPIRICAL ENERGY RELATIONS FOR DETERMINING BOLIDE ENERGY DEPOSITION AND IMPLICATIONS FOR IMPACT HAZARD.

E. A. Silber[1], M. Moreno-Ibáñez[2], M. Gritsevich[3,4], J. M. Trigo-Rodríguez[5,6] and R. E. Silber[7]
[1]Department of Earth, Environmental and Planetary Science, Brown University, Providence, RI, USA, 06912 (e-mail: elizabeth_silber@brown.edu), [2]Aistech Space S.L., Rua das Pontes 3, 36350, Nigrán, Galicia, Spain (manuel.moreno-ibanez@gmail.com), [3]Department of Physics, University of Helsinki, Gustaf Hällströmin katu 2a, P.O. Box 64, FI-00014 Helsinki, Finland (maria.gritsevich@helsinki.fi), [4]Institute of Physics and Technology, Ural Federal University, Mira str. 19. 620002 Ekaterinburg, Russia, [5]Institute of Space Sciences (ICE, CSIC), Meteorites, Minor Bodies and Planetary Science Group, Campus UAB, Carrer de Can Magrans, s/n E-08193 Cerdanyola del Vallés, Barcelona, Catalonia, Spain (trigo@ice.csic.es), [6]Institut d'Estudis Espacials de Catalunya (IEEC), C/ Gran Capitá, 2-4, Ed. Nexus, desp. 201, E-08034 Barcelona, Catalonia, Spain, [7]Department of Geology and Geophysics, Yale University, New Haven, USA, 06511 (reynold.silber@yale.edu).

Introduction: Meteoroids in the size range of up to several tens of meters in diameter are one of the least constrained populations in the Near-Earth environment. This is because these objects are not abundant enough, and too small to be readily detected via optical means. However, meteoroids in this size range may present a significant hazard if they impact the atmosphere [1], as exemplified by the spectacular breakup of the Chelyabinsk bolide over Russia in 2013 [2]. These objects deposit tremendous amounts of energy during their passage through the atmosphere and during the catastrophic breakup, also known as airburst [3]. Therefore, it is important to study energy deposition and destructive potential of these objects. The estimates of energy deposition of bolides is typically obtained through observations of light emissions (e.g. from space [4] and ground), and from infrasound (low frequency acoustic wave) records. Infrasound is a product of shock waves generated by meteoroids as they interact with the atmosphere [3,5,6]. Most empirical energy relations relying on infrasound records were originally developed for estimating yield of nuclear and chemical explosions, and later adopted for bolide energy estimates [6-7]. However, the recurring issue is that various relations produce very different results, making accurate predictions of energy deposition difficult. We evaluate the fidelity and consistency of various energy relations based on infrasound records, with the goal to better understand how these vary and what the implications are for our current knowledge of bolide properties.

Methods: In our systematic and detailed study, we use well-documented and well-characterized published bolide records, and apply various energy relations developed over the years [7] to compare and evaluate the outcomes, and establish the implications for impact hazard. We perform additional analyses to quantify the potential damage, which will be presented in more detail through a future publication. We also compare our results to energy deposition estimates determined through space based sensor data to better constrain the validity of various energy relations and evaluate the applicability to observations where only infrasound records might be available.

Summary: When a large extra-terrestrial object enters the Earth's atmosphere at hypervelocity, it produces a shock wave. The shock induced phenomena can cause damage on the ground to both life and infrastructure. Oftentimes, infrasound observations of bolides might be the only means of detections (e.g. daylight events and events over remote regions) [7,8], and determining the object properties (such as size) might be obtainable only through such records. However, applying various empirical energy relations might lead to contradicting results, making it difficult to constrain bolide properties and accurately evaluate energy deposition. Thus far, to the best of our knowledge, no study has compared all known energy relations in the context of bolide class impacts in order to better constrain how these relations might affect our present knowledge of energy estimates and impact hazard.

References: [1] Gritsevich M.I. et al. (2012) *Cosmic Research*, 50(1), 56–64. [2] Brown P. G. et al. (2013) *Nature*, 503, 238-241. [3] Silber E. A. et al. (2018) *Adv. Sp. Res.*, 62, 489-532. [4] Bouquet A. et al. (2014) *Planet. and Space Sci.*, 103, 238-249. [5] Moreno-Ibáñez M. et al. (2018) *The Astrophysical Journal* 863(2), 174. [6] Tapia M. and Trigo-Rodríguez J.M. (2017) In *Assessment and Mitigation of Asteroid Impact Hazards*, Trigo-Rodríguez J. M., Gritsevich M., Palme H., Eds., Astrophysics and Space Science Proceedings, 46. Springer, Switzerland, 199 p. [7] Silber E. A. and Brown P. G. (2019) in *Infrasound Monitoring for Atmospheric Studies*, Ch 31, 939-986. [8] Silber E. A. (2011) *GRL*, 38, L12201.

NON MASS-DEPENDENT CALCIUM ISOTOPE EFFECTS IN AND AMONG PLANETARY MATERIALS

J. I. Simon[1], R. M. G. Armytage[1,2], and M. J. Tappa[1,2,3], [1]Center for Isotope Cosmochemistry and Geochronology, Astromaterials Research and Exploration Sciences, NASA Johnson Space Center, Houston, TX 77058, USA (Justin.I.Simon@NASA.gov), [2]Jacobs/JETS, NASA Johnson Space Center, Mail Code XI3, Houston, TX 77058 USA, [3]Now at Department of Earth and Environmental Sciences, Boston College, Chestnut Hill, MA, USA.

Introduction: Here we report Ca isotope measurements acquired with a refined thermal ionization mass spectrometry (TIMS) method that can be used to simultaneously measure ^{40}Ca radiogenic and ^{43,46,48}Ca stable isotope effects in primitive materials. This method builds upon the those developed at Caltech, UC Berkeley, Univ. Chicago-Caltech-JPL, and NASA JSC [1-5]. Primitive meteorites often contain small radiogenic ^{40}Ca excesses in addition to rare epsilon level stable isotope anomalies that are near the analytical resolution of current mass spectrometry techniques. Calcium-Aluminum-rich inclusions (CAIs) may have larger ^{40}Ca and more resolvable ^{43,46,48}Ca isotope effects. The relative abundances of isotopic anomalies in ^{48}Ca and ^{50}Ti are believed to be correlated among some early solar system materials [e.g., 4], but the carrier of these nucleosynthetic signatures remains unknown. Measuring refractory elements that both have neutron-rich isotopes that are believed to be produced by the same nucleosynthetic process potentially provide useful constraints on their stellar origins (i.e., their correlation indicates contributions from a type Ia supernovae, [6]). Additionally, the degree to which isotopic heterogeneity exists within and among planetary materials can be used to understand the dynamics and evolution of the protoplanetary disk. Non mass-dependent calcium isotope compositions of bulk planetary materials, chondrites, and chondrite components (CAIs and chondrules) some that were measured for their ^{50}Ti isotopic anomalies by [7] are the focus of this ongoing work.

Methods: Digested materials are passed through a single-stage 2 ml TODGA resin vacuum column, which effectively separates Ti from all other major elements. This is an important step due to potential isobaric interferences between ^{46,48}Ca and ^{46,48}Ti. Following Ti separation, Ca is purified using a second TODGA column. This procedure, previously detailed in [8] has been documented to be effective for a range of sample compositions. Calcium isotope measurements are made using the Thermo Scientific TRITON mass spectrometer housed in the Center for Cosmochemistry and Geochronology (CICG) at NASA JSC. Purified Ca is dissolved in dilute HCl and loaded in 2-3 µg aliquots with dilute H_3PO_4 on outgassed Re filaments. A Parafilm dam is applied to the filament prior to loading the sample in an effort to reduce spreading and improve the consistency of loading. Filaments are slowly heated to evaporate loading acid and residual Parafilm. Calcium is analyzed using a multi-dynamic method, which is preferred to a static approach because it allows us to monitor the unavoidable cup degradation effects of large ion beams. One standard (SRM 915a) is run for ~ every 2 unknowns; normally 3 standards per barrel. A single run consists of 9 blocks of 15 ratios through four cup settings. Virtual amplifier rotation and baseline calibration are preformed preceding each block. The ^{40}Ca beam intensity is usually between 20-30 V using a 10^{11} Ω resistor. Instrumental mass fractionation is corrected using an exponential law and a ^{42}Ca/^{44}Ca value of 0.31221 [1]. Isobaric interfering elements are monitored on ^{39}K and ^{47}Ti during the analysis.

Summary of Results: Significant column and mass spectrometry calibration was required to re-establish the CICG labs for calcium isotope measurements after major renovations (>3-years). In addition to the analysis of standards used for Ca analysis (SRM 915a, terrestrial basalt BCR-2, and the Harvard peridotite TP-12), bulk dissolutions of the meteorites Allende and Sioux County have been measured. Analysis of the rock standards demonstrate comparable uncertainties to both [5] for ε^{40}Ca (~0.4, 2σ) and [4] for ε^{43}Ca (~0.4, 2σ), ε^{46}Ca (~15, 2σ), and ε^{48}Ca (~0.8, 2σ) in one instrumental setup. As seen previously, the basaltic rocks have ε^{40}Ca values that are ~0.8 e-units lower than SRM 915a [2,3,5,9]. No resolvable ε^{43}Ca, ε^{46}Ca, ε^{48}Ca isotopic anomalies were observed in Allende as previously reported by [2,3] despite resolvable effects reported in some other chondrites [4]. A ε^{48}Ca value of ~ -2 e-units for the Sioux County eucrite similar to that reported by [4] was found. Further analytical work is needed to evaluate the extent of Ca isotopic heterogeneity in and among early formed solids and bulk meteorites to address the existence of distinct reservoirs in the protoplanetary disk and the degree to which refractory inclusions and other early-formed solids were mixed during planetary accretion.

References: [1] Niederer F.R. and Papanastassiou D.A. (1984) *GCA* 48: 1279-1293, [2] Simon J.I. et al. (2009) *ApJ* 702: 707-715, [3] Moynier F. et al. (2010) *ApJL* 718: L7-L13, [4] Dauphas N. et al. (2014) *EPSL* 407: 96-108, [5] Mills R.D. et al. (2018) *EPSL* 495: 242-250, [6] Meyer B.S. et al. (1996) *ApJ* 462: 825-838, [7] Simon J.I. et al. (2017) *EPSL* 472: 277-288, [8] Righter K. et al. (2015) *MAPS* 50: 1790-1819, [9] Yokoyama T. et al. (2017) *EPSL* 458: 233-240.

CHONDRULE FORMATION THROUGH COLLISIONS BETWEEN PLANETESIMALS CONTAINING VOLATILE MATERIALS

S. Sirono[1] and D. Turrini[2], [1] Graduate School of Earth and Environmental Sciences, Nagoya University, Nagoya, Japan (sirono@eps.nagoya-u.ac.jp) , [2]Institute for Space Astrophysics and Planetary Science INAF-IAPS, Rome, Italy.

Introduction: From a physical point of view, the two most important quantities of chondrules still to be understood are size and cooling rate. Although many models have been proposed, consistent explanation of these two quantities is still lacking. The collision of molten planetesimals [1,2] is a promising candidate mechanism for chondrule formation. However, the nebula gas is too rarefied to break the silicate melt ejected by the collision down to chondrule size (0.1 – 2 mm [3]). Here we propose that collisions of low temperature planetesimals containing volatile material naturally explain the size and cooling rate of chondrules, since the rapidly heated volatile material quickly expands and break up the silicate melt down to the required small sizes.

Numerical Simulations: To verify this idea, we performed three sets of simulations: 1: Orbital evolution of a swarm of planetesimals in the solar nebula undergoing the dynamical excitation induced by Jupiter's formation with the Mercury-Arχes n-body code [4,5]. From these simulations, the impact probability and collision velocity distributions are determined. 2: Collision of planetesimals. We performed iSALE [6] hydrocode simulations of collisions between planetesimals with sizes of 100 and 400 km and determined the amount of silicate melt produced during a collision. 3: 1-D hydrodynamical simulations of gas-melt mixture expansion. A layer of gas-melt mixture expands due to the volatile materials contained in a planetesimal. Size of melt droplets and their cooling rates are determined.

Numerical Results: From simulation 1, we found that about 5% of collisions has impact velocity higher than 4 km/s when planetesimals are embedded in a gaseous protoplanetary nebula. The high velocity collisions continue 1 Myr after Jupiter formation. From simulation 2, we obtained that the amount of melt exceeds 50% of the projectile volume if the collision velocity is higher than 4 km/s. From simulations 1 and 2, we could estimate that the total amount of silicate melt is about 10% of the total volume of planetesimals. In simulation 3, there are three key parameters: initial temperature, thickness of mixture, and gas (volatile) mass fraction. We determined the evolution of cooling rate and size (Fig. 1) for various sets of parameters. The size and cooling rate fall within 0.26-1.6 mm and 20-2000 K/h, respectively, consistently with measured values of chondrules.

Conclusions: Collisions of planetesimals containing volatile materials consistently explain both the size and the cooling rate of chondrules. The beginning of the formation period of chondrules coincides with Jupiter's formation and the resulting dynamical excitation of planetesimals.
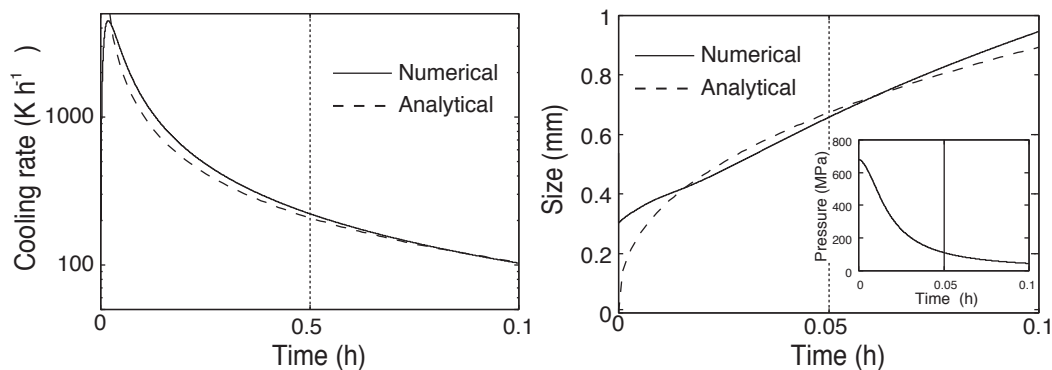

Fig. 1. Evolution of cooling rate (left) and size (right) of silicate melt. Initial temperature is 1800 K, thickness of mixture is 10 km, gas mass fraction is 10%. Solid and dashed curves are simulation results and analytical formula, respectively. Right inset: evolution of gas pressure.

References: [1] Asphaug E. et al. (2011) *EPSL.* 308, 369-379. [2] Sandars I. S. & Scott E. (2012) *Meteo. Planet. Sci.* 47, 2170-2192. [3] Friedrich J. M. (2015) *Chemie der Erde* 75:419–443. [4] Chambers J. E. (1999), *MNRAS,* 304, 793 [5] Turrini D., et al. (2019), ApJ, in press, https://arxiv.org/abs/1802.04361 [6] Collins G. S. et al. 2016. *iSALE-Dellen manual* https://doi.org/10.6084/m9.figshare.3473690.v2.

TERRESTRIAL AGES OF THE SHIŞR 015 METEORITE STREWN FIELD FROM THE SULTANATE OF OMAN, DETERMINED USING MEASURED IN SITU ^{14}C and [10]Be

M. U. Sliz[1,2], R. Braucher[3], C. Espic[4], J. Gattacceca[3], B. A. Hofmann[2], I. Leya[1], S. Szidat[4], ASTER Team[3]
[1]Space Research and Planetary Sciences, University of Bern, Sidlerstrasse 5, Bern 3012, Switzerland (malgorzata.sliz@space.unibe.ch), [2]Natural History Museum Bern, Bernstrasse 15, Bern 3005, Switzerland, [3]CNRS, Aix Marseille Univ, IRD, Coll France, INRA, CEREGE, Aix-en-Provence, France, [4]Department of Chemistry and Biochemistry & Oeschger Center for Climate Change Research, University of Bern, Freiestrasste 3, Bern 3012, Switzerland.

Introduction: Terrestrial age determination via ^{14}C analysis of purified silicate fractions from meteorites is now routinely done at the University of Bern. The extraction system has undergone several changes and optimizations in the past year, and we are now able to perform numerous measurements (approx. 30-40) whilst maintaining the system closed, i.e. not breaking the vacuum. Our current aim is to measure several meteorite strewn fields from the Sultanate of Oman to *i*) extend the database of meteorite terrestrial ages, *ii*) to study the meteorite flux over time, and *iii*) to better understand and quantify the parameters affecting weathering. So far, we measured three fragments of the L5 meteorite strewn field Shişr 015 (purified silicate fractions). The successfully extracted CO_2 gas has been sent to the Accelerator Mass Spectrometry (AMS) MICADAS system [1] at the University of Berne for ^{14}C/^{12}C measurements. The [10]Be concentrations for the silicate fractions of the Shişr 015 fragments were already determined at the ASTER (Accélérateur pour les Sciences de la Terre) Accelerator Mass Spectrometry (AMS) facility at CEREGE in Aix-en-Provence, France [2], and are used together with the ^{14}C data to determine ^{14}C/[10]Be terrestrial ages, which are less dependent on shielding and are therefore more reliable than ages determined using ^{14}C only. In the next step we might combine the ^{14}C/[10]Be ages with the shielding indicator [22]Ne/[21]Ne to further improve the ages (if necessary).

Experimental Setup: Several changes and improvements were applied to the ^{14}C extraction line since the first description of the setup [3,4]. In the current version, the extraction unit consists of a high frequency generator (RF) and a quartz glass crucible with an inner platinum (Pt) crucible. Platinum was the material of choice because it withstands oxidation even at high temperatures and at oxygen partial pressures. In addition, Platinum is conductive and can efficiently be heated using RF heating. Therefore, samples are heated and oxidized via the Pt crucible, eliminating the need to add iron or steel to the sample to promote heating. As before, quartz granulate fills the bottom of the quartz glass crucible, preventing contact between the Pt and the outer crucible. In addition, to prevent the Pt crucible from tilting and damaging the outer crucible walls, three U-shaped pieces of tungsten wire are placed between the top of the Pt crucible and the wall of the quartz crucible. Pre-heating of samples still takes place in UHP O_2 flow for 1 h at ~500°C with continuous pumping, and the extraction of ^{14}C is performed in 15-30 mbar O_2 partial pressure at ~1600°C for only 10 mins, instead of 40 mins in the earlier setup.

Tests to establish the correct pre-heating and extraction temperatures, i.e., currents of the RF generator, were performed using the previously measured and well-studied JaH 073 strewn field. Note that the temperature of the Pt crucible cannot be measured directly but is determined indirectly by the color of the crucible. As a first quality check we can also compare the extracted CO_2 pressure with the CO_2 pressures for earlier measurements (system blank, procedural blank, sample). However, the most reliable proof for the reliability of the current setup comes from the AMS data. In addition, melting of samples is often clearly indicated by a sudden considerable drop of the O_2 partial pressure in the crucible (>10 mbar in 1-5 minutes, instead of 2-3 mbar in 5 mins). Reproducibility tests, also using the JaH 073 strewn field, indicated good results which are also comparable to literature data [4,5].

Results and Discussion: Three individuals of the L5 meteorite strewn field Shişr 015 were measured, with two replicates per individual. Consisting of 43 stones, Shişr 015 has a combined weight of 23.7 kg. The strewn field has an E-W orientation and measures 21.1 km in length. The weathering grade of the strewn field ranges between 3 and 4, with majority of the individuals of grade 4.

Aliquots of 0.05 g of purified powdered silicates (125-250 μm grain size) were used. We measured ^{14}C activities between 0.86±0.02 and 1.33±0.04 dpm/kg, and by using a ^{14}C saturation activity of 51.1±1.0 dpm/kg we calculate a ^{14}C terrestrial age between 30.0±1.0 and 33.6±1.1 kyr. The data therefore indicate only a small variation among the different individuals of the strewn field. The measured [10]Be activities of the same fragments range from 14.3 to 16.4 dpm/kg. If combined with the ^{14}C data we calculate ^{14}C/[10]Be ages of 27.7±0.2, 28.1±0.4, and 29.9±0.2 kyr for the three measured individuals. The average ^{14}C/[10]Be terrestrial age is 28.6±0.6 kyr.

References: [1] Szidat S. et al. (2014) *Radiocarbon*, 56:561-566. [2] Arnold M. et al. (2010) *Nuclear Instruments and Methods in Physics Research*, 238:1954-1959. [3] Sliz M. et al. (2018) *Meteoritics and Planetary Science*, Abstract #6297. [4] Meszaros M. et al. (2017) *Radiocarbon*, 60:601-615. [5] Gnos E. et al. (2009) *Meteoritics and Planetary Science*, 44:375-87.

EARLY CORE FORMATION OF THE ASTEROID VESTA REVEALED BY HSE CONCENTRATIONS IN EUCRITES.

N. Slotte[1,2], V. Debaille[1], A.N. Wainwright[1], S. Goderis[2], A. Luguet[3]
[1]Laboratoire G-Time, Université Libre de Bruxelles, Brussels, Belgium (nslotte@ulb.ac.be); [2]AMGC, Vrije Universiteit Brussel, Brussels, Belgium ; [3]Universität Bonn, Bonn, Germany.

Highly siderophile elements (HSE: Os, Ir, Ru, Rh, Pt, Pd, Re, Au) are characterized by a strong affinity for iron with respect to silicate materials [1,2].

These elements have been partitioned into the metallic core of planetary bodies during early differentiation, leaving their silicate portions stripped of HSE [3]. Thus, the HSE concentrations in the silicate mantle and crust mainly depends on the HSE metal-silicate partition coefficients but also the replenishment during and after core formation by the accretion of chondritic materials [3].

We analyzed five unbrecciated eucrites previously dated by Al-Mg systematics [4] for their HSE systematics. These eucrites can be divided in two distinct populations based on their chondrite-relative HSE abundances. We suggest that the discrepancies in HSE depletion reflect the progressive decrease of core segregation intensity in favor of the intake of HSE by chondritic accretion in the vestan mantle within 1 million years. The HSE concentrations in the silicate crust of Vesta thus capture the competition of both HSE depletion and enrichment by core formation and chondritic intake, respectively. Our results highlight that core segregation was an efficient and progressive process that can be tracked down by using HSE.

[1] J.M.D. Day, A.D. Brandon, R.J. Walker, Reviews in Mineralogy and Geochemistry 81 (2016) 161–238. [2] U. Mann, D.J. Frost, D.C. Rubie, H. Becker, A. Audétat, Geochimica et Cosmochimica Acta 84 (2012) 593–613. [3] C.W. Dale, K.W. Burton, R.C. Greenwood, A. Gannoun, J. Wade, B.J. Wood, D.G. Pearson, Science 336 (2012) 72–75. [4] G. Hublet, V. Debaille, J. Wimpenny, Q.-Z. Yin, Geochimica et Cosmochimica Acta 218 (2017) 73–97.

THE EUROPEAN SPACE AGENCY EXPLORATION SAMPLE ANALOGUE COLLECTION (ESA[2]C) AND CURATION FACILITY – UPDATE.

C. L. Smith[1], D. Martin[2], S-J Gill[1], K. Manick[1], C. G. Miller[1], C. Jones[1], M. S. Rumsey[1], L. Duvet[2]. [1]The Natural History Museum, Cromwell Road, London, U.K., SW7 5BD (C.L.Smith@nhm.ac.uk), [2]Human Spaceflight and Robotic Exploration Programmes Directorate, European Space Agency ECSAT, Fermi Avenue, Harwell Campus, Didcot, Oxfordshire, U.K., OX11 0FD (Dayl.Martin@esa.int)

Introduction: Since 2014, the Natural History Museum (NHM) has been the prime contractor to the European Space Agency (ESA) for defining and initiating the development of an Exploration Sample Analogue Collection (ESA[2]C) and Sample Analogue Curation Facility (SACF) in support of the Human & Robotic Exploration mission preparation programme. The ESA[2]C and SACF will support the ongoing and future technology development activities that are required for human and robotic exploration of Mars, the Moon, Phobos, Deimos and C-Type Asteroids. The long-term goal of this work is to produce a useful and useable resource for scientists and engineers developing technologies for ESA missions and for appropriately qualified international users as well.

Sample Analogue Collection: The complex mission architectures and diverse target bodies of interest means that a variety of different analogue materials are required to test all systems that come into contact with or remotely analyse the target body, whether these be part of the spacecraft system, such as landing and/or roving systems (e.g. wheels), sample collection systems (e.g. drills or scoops) or scientific payload. The analogue materials must replicate as far as possible the expected 'geological' environment of the target body in terms of both physical/mechanical properties and chemical/mineralogical properties. Samples selected include a variety of aggregates from the olivine-rich basalts from the Antrim Lava Group of Northern Ireland and clay samples from Cyprus, Spain and Senegal. Detailed characterisation of the analogue samples' physical and chemical properties has been carried out [1,2,3]: *Chemical properties:* Whole-rock chemistry – major, minor and trace element analyses. Mineralogy – analytical SEM, EPMA and XRD (whole-rock). *Physical and mechanical properties:* Particle Size Distribution (PSD) (aggregate and granular samples). Grain Size and Morphology – SEM, X-ray micro-CT and visual inspection. Density and porosity (all samples) – mass-volume measurement and helium pycnometry, X-ray micro-CT. Shear strength (aggregate, granular and powder samples) – shear box apparatus. Compressive and tensile strength (rock samples) – UCS testing and Brazilian indirect tensile method. As part of ongoing work, further samples have been acquired for the ESA[2]C – including anorthosite (Norway), basaltic sand and basaltic/ hyaloclastite (Askja Region, Iceland), volcaniclastic/sedimentary/clay masonry unit (CMU) analogues that will be used for system level testing of the ExoMars crushing station, and other commercially available analogues such as the Zybek NU-LHT-2M, USGS NU-LHT-2M and EAC-1 lunar analogues, and carbonaceous chondrite simulants (CI, CM, and CR).

ESA Sample Analogue Curation Facility: This unique venture will build on ESA's Human & Robotic Exploration mission preparation programme by establishing methodologies and protocols/procedures for curating the ESA[2]C, as well as defining and validating the distribution mechanisms and information exchange protocols for the analogue materials. The overarching role of the SACF is to:- *Curate ESA[2]C samples and associated data pertaining to those samples; make samples available for study and provide access to relevant data pertaining to those samples; carry out fundamental physical and chemical properties testing in the SACF (or testing via appropriately qualified external laboratories).* All analogues in the ESA[2]C will undergo *fundamental properties characterisation* using procured (or outsourced) equipment in the SACF laboratory, which include the following: *Mineralogical and Chemical Properties:* X-ray diffraction (XRD) – bulk mineralogy; SEM – mineral chemistry by point analysis of dominant phases; X-ray fluorescence (XRF) – minor and trace element identification and quantification; fourier-transform infrared (FTIR) and raman – chemical/molecular bonding and fingerprinting. *Physical and mechanical properties:* soil PSD – sieving and laser particle analysis; soil grain size and morphology – SEM and visual inspection; soil bulk density and rock dry density – mass-volume measurements; rock and soil particle density (for porosity) – gas pycnometry; soil shear strength– direct shearbox; rock UCS – uniaxial/unconfined compression.

Future Opportunities: The facility formally opened on the Harwell campus (UK) in January 2019. Specimens from the ESA[2]C are being used by engineers and scientists in the United Kingdom, Hungary, Germany, Italy, Australia, and the US to support planetary research, related technology developments and testing activities for a variety of missions and mission architectures. The analogue materials in the ESA[2]C, which have been well characterised, i.e. have known fundamental physical/mechanical and chemical/mineralogical properties, provide a unique resource for scientists and engineers to carry out comparative and collaborative investigations into the vast sector of space exploration. The ESA Sample Analogue Curation Facility hopes to spearhead and centralise access to these resources for many years to come.

References: [1] Manick K. et al. (2017) *LPSC XLVIII*, Abstract #1220. [2] Manick K. et al. (2017) *LPSC XLVIII*, Abstract #1222. [3] Manick, K. et al. (2018) *LPSC XLIX*, Abstract #1411.

TEMPORAL VARIABILITY IN CARBON MONOXIDE ABUNDANCES IN YOUNG STELLAR OBJECTS AND IMPLICATIONS FOR THE EARLY SOLAR SYSTEM.

R. L. Smith[1,2,3], G. A. Blake[4], K. M. Pontoppidan[5], A. C. A. Boogert[6,7]
[1]North Carolina Museum of Natural Sciences (rachel.smith@naturalsciences.org), [2]Appalachian State University, Department of Physics & Astronomy, [3]UNC Chapel Hill, [4]California Institute of Technology, Division of Geological and Planetary Sciences, [5]Space Telescope Science Institute, [6]Infrared Telescope Facility, [7]Institute for Astronomy, University of Hawaii.

Introduction: Observations of young stellar objects (YSOs) provide a unique window into protoplanetary chemistry. In particular, high-resolution near-infrared observations of carbon monoxide (CO) gas toward YSOs and evaluation of carbon and oxygen isotopes have yielded valuable insights into protoplanetary processes with implications for the early solar nebula [1-7]. While each spectral observation is a snapshot in a several-million-years timescale, YSOs have interestingly been observed to vary in several important parameters over timescales of months to a few years. For example, observations of late-stage solar-type disks reveal up to 50% variability in infrared (IR) fluxes, possibly due to the stellar companions or magnetic fields [8], and 70% of Class I and II YSOs studied in Orion show IR variability in amplitude, possibly due to gas extinction or warps in disk geometry [9]. Significant light-curve variations have further been found in YSOs of the Lynds 1688 region, attributed to possible structural changes in the inner disk [10], and IR photometric variability in nearly 100 YSOs in Cygnus observed over a few years could be due to changes in disk dynamics [11]. Here we present our intial variability analysis of gas-phase CO observations toward a range of solar-type and massive YSOs, with separations in observations of each YSO target ranging from months to a few years. This study is centered on exploring how key molecular reservoirs may vary in the very short-term in evolving systems, and how these variations may differ between solar-type and massive YSOs.

Observations and Methods: Our data set includes CO rovibrational bands observed with Keck-NIRSPEC in high-resolution mode (R~25,000, ~12 km/s) for three massive, luminous YSOs each observed 2 to 3 years apart, and six low-mass, solar-type YSOs observed with VLT-CRIRES at very high resolution (R~95,000, ~3.2 km/s), from a few months to 1 year apart. Fundamental ($\upsilon=1-0$, 4.7 μm) bands were obtained for all targets, probing optically thin $^{13}C^{16}O$, $^{12}C^{18}O$ and $^{12}C^{17}O$ isotopologue lines. First-overtone ($\upsilon=2-0$, 2.3 μm) spectra, probing optically thin $^{12}C^{16}O$, were obtained for two of the massive YSOs, enabling $^{12}C/^{13}C$ comparisons between epochs. Column densities were measured using equivalent widths and a curve-of-growth analysis (NIRSPEC data), or Gaussian fits to measure the optical depths and line widths directly from the line profiles (CRIRES data). Total molecular column denstities and gas temperatures were computed using a Boltzmann distribution in a rotational analysis for each data set.

Results: Initial findings for the massive YSOs show that in the span of two years, total $^{12}C^{16}O$ and $^{13}C^{16}O$ column densities increased by as much as ~17% and ~33% respectively, while gas temperatures changed by ~10%. Column densities for $^{12}C^{18}O$ varied by ~8%, and [^{12}CO]/[^{13}CO] varied by ~12%. An example of significant spectral variability is shown in **Fig. 1** for massive YSO, W3IRS5. We find that low-mass YSOs thus far show less variability in CO column densities, with $^{13}C^{16}O$ and $^{12}C^{18}O$ changing by only ~3% in observations separated by 1 year, gas temperatures varying by 15% or less, and [$^{13}C^{16}O$]/[$^{12}C^{18}O$] remaining constant.

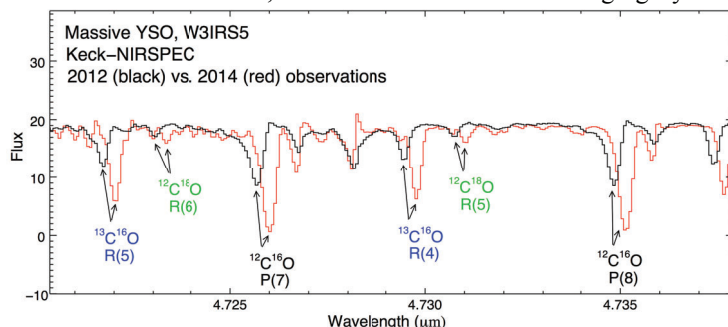*Figure 1. Portion of the 4.7 μm spectra obtained with Keck-NIRSPEC for YSO, W3IRS5, clearly showing the variability in line depths between 2012 and 2014. CO isotopologue lines are marked.*

Conclusions: Our initial results suggest that massive YSOs may be more prone to column density variability as compared to low-mass YSOs, which may be due to their significant wind and/or radiation field variations. Low-mass YSOs could be less prone to significant molecular abundance changes even with short-term IR flux or disk variations. This ongoing exploration of molecular variability in a range of YSO environments is relevant to the formation of planetary systems in high radiation fields, and to solar system models that explore molecular reservoirs parameterized with disk physics and nebular processes. We aim to supplement our data with near-future observations at the Infrared Telescope Facilty and/or Keck telescopes.

References: [1] Brittain S.D. et al. (2005) *ApJ* 626: 283-291. [2] Pontoppidan K. M. (2006) *A&A* 453: L47-L50. [3] Smith R.L. et al. (2009) *ApJ* 701: 163-179. [4] Young E.D. et al. (2011) *ApJ* 729: 43-53. [5] Smith R.L. et al. (2015) *ApJ* 813: 120-135. [6] Smith R.L. et al. (2018) 81st Metsoc, #2067. [7] Boogert A.C.A. et al. (2000) A&A *353*: 349-362. [8] Flaherty et al. (2012) *ApJ 748*: 71-99. [9] Morales et al. (2011) *ApJ 733*: 50-58. [10] Gunthe et al. (2014) *ApJ 148*: 122-141. [11] Wolk et al. (2013) *ApJ 773*: 145-164.

COSMIC-RAY EXPOSURE AGE AND PREATMOSPHERIC SIZE OF THREE RECENT FALLS (L6)

T. M. Smith[1], S. Li[2], P. M. Ranjith[1], F. Su[1], J. Gattacceca[3], ASTER Team[4], and H. He[1] [1]State Key Laboratory of Lithospheric Evolution, Institute of Geology and Geophysics, Chinese Academy of Sciences, Beijing 100029, China, [2]Center for Lunar and Planetary Sciences, Institute of Geochemistry, Chinese Academy of Sciences, Guiyang 550081, China, [3]Centre Européen de Recherche et d'Enseignement de Géosciences de l'Environnement (CEREGE), UM 34 CNRS-IRD, Aix-Marseille Université, Technopôle de l'Environnement Arbois-Méditerranée, 13545 Aix-en-Provence, France, [4]G. Aumaître, D. L. Bourlès, and K. Keddadouche.

Introduction: Over the past months, three L6 chondrites falls have been observed; Mangui from China, Ozerki in Russia, and Viñales in Cuba. The Mangui meteorite fell in the Yunnan Province, China at 9:43 pm on June 1st, 2018 [1]. Based on recent calculations, the meteorite entered Earth's atmosphere with an angle of 55.3±2.5°, from southeast to northwest, resulting in a strewn field of ~12 km long [2]. Up to now, more than 1000 individuals or fragments have been identified, with masses ranging from 0.04 g to ~1280 g, the total mass being ~50 kg. Mangui has been classified as a L6 ordinary chondrite, with a shock stage S4-S5 [1,2]. The Ozerki meteorite (L6, shock stage S4-S5) fell in Russia on June 21, 2018, 20 days after Mangui. Based on models, the total number of specimens has been estimated to be ~100 individuals, for a total mass of ~7 kg. Search campaigns are still ongoing, and more masses are expected to be found. Finally, the Viñales meteorite (L6, schock stage S3) fell in Cuba on February 1st, 2019. In the following days, several hundred of individuals have been collected by locals. Here we study the cosmic-ray exposure (CRE) history of two individual samples of Mangui, Ozerki, and Viñales by measuring cosmogenic radionuclides and noble gases, produced in space by galactic cosmic rays (GCRs). We are especially interested in the CRE age and the preatmospheric size of the meteoroid, the latter could help to better understand the disruption mechanisms during the atmospheric entry. Based on the short time interval between the different observed falls, similar petrographic types, and the similar shock characteristics, we expect these three meteorites to have a similar exposure history and therefore to be paired.

Experimental methods: The cosmogenic noble gas concentrations (^{3,4}He, ^{20,21,22}Ne, and ^{36,38,40}Ar) and isotopic ratios in the meteorite samples have been measured by pyrolysis, using a NOBLESSE © noble gas mass spectrometer at the noble gas laboratory of the Institute of Geology and Geophysics, Chinese Academy of Sciences (IGGCAS). In addition, targets for the cosmogenic radionuclides ^{10}Be, ^{26}Al, ^{36}Cl, and ^{41}Ca have been prepared for two Mangui samples and will be measured at the Centre d'Enseignement et de Recherche Européen des Géosciences de l'Environnement (CEREGE), Aix-en-Provence (France), host of the French national 5MV Accelerator Mass Spectrometry ASTER facility [3].

Results: Here we present only the results obtained on Mangui; Ozerki and Viñales could not be measured at the time of the abstract deadline. First, the preatmospheric size of Mangui has been determined using the measured cosmogenic (^{22}Ne/^{21}Ne)$_c$ ratios and the calculated cosmogenic ^{3}He$_c$, ^{21}Ne$_c$, and ^{38}Ar$_c$ production rates, as described in [4]. Based on this, we estimate the preatmospheric radius to be in the range of ~30-35 cm. Second, we calculated the preatmospheric mass using the empirical relation given in [5]. We calculated a preatmospheric mass of ~109 kg, which, when considering an average bulk density of 3.29 g/cm^3 gives a preatmospheric radius of ~20 cm; this is relatively consistent with the ~50 kg mass so far recovered. The CRE age has been calculated using the concentrations in cosmogenic ^{21}Ne$_c$, and ^{38}Ar$_c$, later labelled T_{21} and T_{38}, as described in e.g. [6]. The CRE ages vary between ~0.5-0.9 Ma, in agreement with the ^{26}Al-^{21}Ne CRE ages. We observe the common trend $T_{21}<T_{38}$; the T_3 age is much lower, and consistent with significant He diffusive losses, thus suggesting Mangui might have suffered severe heating after the breakup from its parent body and during its travel to Earth. We estimate the diffusive losses to be ~54-75%. In addition, we will compare the calculated CRE ages with the ^{36}Cl-^{36}Ar and ^{10}Be-^{21}Ne dating schemes [7], ^{36}Cl and ^{10}Be being not yet available at the time of the abstract submission. Finally, the gas retention age was determined using both radiogenic ^{4}He$_r$ (T_4) and ^{40}Ar$_r$ (T_{40}). The calculated T_4 and T_{40} retention ages range between ~4-12 Ma and ~88-108 Ma, respectively, suggesting a severe thermal and impact history. The CRE history of Ozerki and Viñales will be presented at the conference.

References: [1] Ji, J. et al. (2018). *Chinese Science Bulletin* 64:579-587. [2] Li, S. et al. (2019). *Acta Mineralogica Sinica*. [3] Braucher, R. et al. (2018). *Nuclear Instruments and Methods in Physics Research Section B* 420:40-45. [4] Dalcher, N. et al. (2013). *Meteoritics & Planetary Science* 48:1841-1862. [5] Bhandari, N. et al. (1980). *Nuclear Tracks* 4:213-262. [6] Li, S. et al. (2017). *Meteoritics & Planetary Science* 52:937-948. [7] Lavielle, B. et al. (1999). *Earth and Planetary Science Letters* 170:93-104.

DEVELOPMENT OF LOW-COST MICROMANIPULATION SYSTEMS FOR SMALL EXTRATERRESTRIAL SAMPLES.

C. J. Snead[1,2], T. R. Cowden[1], and F. M. McCubbin[3] [1]JETS, NASA Johnson Space Center, Houston TX 77058, USA, [2]Texas State University, San Marcos, 601 University Dr., San Marcos, TX 78666. [3] NASA Johnson Space Center, Mailcode XI2, 2101 NASA Parkway, Houston, TX 77058, USA

Introduction: The analysis of microscale to mm-scale astromaterials often involves the transfer of samples from storage or collection substrates to analytical substrates. These transfers are accomplished by hand (via tweezers or fine-tipped needles) or by utilizing micromanipulation instruments. Freehand manipulation of small particles is extremely challenging due to involuntary hand tremors on the order of 100μm [1] and due to the triboelectric charging [2] induced by frequent contact between the manipulation tool and the support substrate. Months or years of practice may be required before an investigator develops the necessary experience to confidently transfer a 10-20μm particle in this manner. Handling even mm-sized particles with fine-tipped tweezers can be challenging, due to the inability to precisely control the force with which grains are being held. Mechanical, hydraulic, and motorized/electrical micromanipulators enable the precise handling of microscale samples and are often utilized in laboratories where frequent small sample preparation is required. However, the price of such instruments (~ $10,000 to $100,000) makes them cost-prohibitive for some institutions. Graduate students or early-career scientists interested in conducting research on interplanetary dust particles, Itokawa particles returned by Hayabusa, or future samples returned by OSIRIS-REx [3] or Hayabusa2 [4] may experience difficulty in justifying the expense of a micromanipulator to their advisors or principle investigators. Johnson Space Center's Astromaterials Acquisition and Curation Office and the Lunar and Planetary Institute conduct annual training for early career scientists and for investigators that require experience with handling of small extraterrestrial samples. In support of this training, we have been developing low-cost mechanical alternatives to expensive micromanipulators that training participants can implement in their respective facilities.

Manipulation System Development: We have modified two microscope systems to manipulate small particles: the Nikon SMZ800N stereo zoom microscope and the Leica EZ4W stereo zoom microscope with integrated camera and WiFi. The modifications are easily reversible for both systems. The Nikon SMZ800N was equipped with a geared Nikon (P-SXY) XY stage. We clamped a test indicator holder (designed to attach to milling machine spindles) to the microscope focus mount; a glass needle held by a pin vise with a 4mm shaft diameter was inserted to the end of the indicator holder. The adjustable nature of the indicator holder allowed us to position the needle at the focal point of the microscope objective at high magnification. With this configuration, it was possible to transfer microparticles between substrates by moving the XY stage and by using the focus as a Z-axis positioner. This method has the disadvantage that the particle cannot be viewed in sharp focus until it is almost at the same position as the needle. Despite this limitation, we were routinely able to transfer 10-20μm particles into custom SEM mounts for characterization and imaging.

Our Leica EZ4W manipulation system utilized an inexpensive (~$100) geared XY stage fixed to a custom aluminum extrusion frame. A mounting bar was attached to the side of the microscope via pre-existing M3 screw hole ports intended for securing the microscope casing. We mounted a MicroSupport tweezer actuation system to this bar, and fixed the actuation control knob to the XY stage frame. As with the Nikon system, tweezers were manually positioned until the tips were at the focal plane of the microscope. Manipulation of samples as small as 0.3mm were achieved by moving the XY stage, focusing in Z to bring the tweezers to the target grain, and closing the tweezers via the manual control knob. The lack of fine Z focusing adjustments precluded the transfer of particles smaller than 0.3mm on the Leica system; however, the system achieves the goal of making manipulation of grains >300μm accessible to novices, and was tested by attendees of the 50th Lunar and Planetary Science Conference earlier this year.

Next Steps: A significant shortcoming of the Leica manipulation system is the use of the proprietary tweezer actuation system, which at ~$3000, exceeds the combined cost of all other system components (including the microscope). We are currently working to develop a low-cost tweezer actuation system that can be constructed with commercially available (or 3D-printed) components. We are also developing fine-positioning mechanisms using commercialy available equipment that will facilitate the alignment of the needle (for the Nikon sytem) or tweezer tips (for the Leica system) in the microscope focal planes.

References: [1] Barer R. (1951) *Journal of Scientific Instruments*. [2] Matsusaka S. et al. (2010) *Chemical Engineering Sci., 65,* 5871-5807. [3] Lauretta D. S. (2017) *Space Science Reviews 212,* 925-984. [4] Minamino H. et al. (2012) *Asteroids, Comets, Meteors,* Abstract #6188.

MICROTEKTITES FROM THE SØR RONDANE MOUNTAINS, EAST ANTARCTICA: TOWARDS AN EXTENSION OF THE AUSTRALASIAN STREWN FIELD?

B. Soens[1*], M. van Ginneken[1,2,3], V. Debaille[3], F. Vanhaecke[4], Ph. Claeys[1] and S. Goderis[1] ([*]e-mail: Bastien.Soens@vub.be), [1]AMGC, Vrije Universiteit Brussel, Pleinlaan 2, 1050 Brussels, Belgium; [2]Royal Belgian Institute of Natural Sciences, Rue Vautier 29, 1000 Brussels, Belgium; [3]Laboratoire G-Time, Université Libre de Bruxelles, Franklin Rooseveltlaan 50, 1050 Brussels, Belgium; [4]Department of Chemistry, Ghent University, Krijgslaan 281, S12, 9000 Ghent, Belgium.

Introduction: The Australasian (micro)tektites constitute one of the four major strewn fields currently known on Earth, next to the North-American, Ivory Coast and Central-European tektite fields. While the Australasian strewn field (ASF) is the most recent (ca. 0.78 Ma) of these large asteroid/cometary impacts on Earth, the location of its impact crater currently remains elusive. Based on the distribution of (micro)tektites, their respective sizes and compositions, several studies have suggested that the hypothetical source crater is located on the northern or central parts of the Indochina peninsula [1-6]. A detailed investigation of their moderately (e.g., Ni, Co, Cr) and highly siderophile elements (e.g., PGEs) clearly indicates that their geochemistry is consistent with mixed contributions from upper continental crust and chondrite-like material [7-9]. More recently, Australasian microtektites have been discovered in sediment traps on nunataks and glacial moraines in the Transantarctic Mountains (TAM) [10-12]. Major and trace element geochemistry of the TAM microtektites are consistent with the ASF. Volatile element contents, which record a strong degree of vaporization, are compatible with large-scale translation from the source crater [5,12]. Fission track dating has reported similar ages (ca. 0.85 ± 0.17 Ma) that match the Australasian impact event [13], extending the central lobe of the AST approximately 3000 km southward. Here we report the discovery of ca. 30 microtektite-like particles from sediment traps in the Sør Rondane Mountains (SRM - Dronning Maud Land, East Antarctica), located 2500 km from the TAM at the opposite side of the Antarctic continent. We present preliminary major and trace element concentrations to demonstrate their similarity with a subpopulation of Australasian microtektites from the TAM.

Methodology: Potential microtektites were extracted from non-magnetic sediment fractions (i.e., 800-400 µm and 400-200 µm) in the Widerøfjellet 18 Mt #01 deposit. Seven microtektite candidates ranging between 400-250 µm were embedded in epoxy resin and polished for SEM-EDS at the Vrije Universiteit Brussel. Major and trace elements were subsequently determined using a Teledyne Cetac Technologies Analyte G2 excimer-based laser ablation system coupled to a Thermo Scientific Element XR double-focusing sector field ICP-mass spectrometer at the Department of Chemistry (Ghent University). Three replicate analyses with a beam size of 35 µm were performed on each sample.

Results and Discussion: The newly discovered microtektite-like particles display a characteristic yellow and transparent appearance similar to 'normal-type' Australasian microtektites found in e.g., ODP cores from the Indian Ocean and the TAM. The abundance of potential microtektites from the SRM is relatively low (<1-2 per 100 g sediment) in comparison with the TAM (<1-30 per 100 g sediment). Particles do not display chemical alteration, but are often slightly abraded at the surface. Their major element chemistry is identical to that of the 'normal-type' microtektites reported in the TAM [10-11]. Surprisingly, no Mg-, Ni- or Al- rich varieties have been recovered from the SRM so far. Volatile element contents are consistent with large-scale atmospheric transportation and vaporization, intermediate between the values observed at Miller Butte and Larkman Nunatak in the TAM, but are systematically higher compared to the TAM microtektites. Trace element concentrations and patterns largely resemble those of the upper continental crust, except for the aforementioned volatile element components. Furthermore, trace element concentrations fall within the range defined by the 'normal-type' TAM microtektites and therefore strongly support the microtektite nature of the particles discovered in the SRM, and their relationship to the AST. These observations suggest that the SRM microtektites represent an individual cluster that possibly extends the western-most lobe of the AST approximately 4000-4500 km southwestward.

Conclusions: About thirty microtektite-like particles were discovered in sediment traps from the SRM and strongly resemble the appearance, size and geochemistry of 'normal-type' microtektites from the TAM. Their pristine condition, along with their relatively low abundance, lack of other Australasian microtektite types, and slight but systematic enrichment in volatile element components in comparison with the TAM microtektites, indicate that the SRM microtektites likely extend the western-most lobe of the AST ca. 4000-4500 km southwestward. These preliminary conclusions will be further investigated using Sr and Nd isotope systematics and ^{40}Ar-^{39}Ar dating.

References: [1] Barnes (1964). *GCA* 28, 893-913. [2] Lee and Wei (2000). *MAPS* 35, 1151-1155. [3] Ma et al. (2004). *GCA* 68, 3883-3896. [4] Folco et al. (2010a). *EPSL* 293, 135-139. [5] Folco et al. (2010b). *Geology* 38, 211-214. [6] Whymark (2013). In *Lunar and Planetary Science XLIV, Lunar and Planetary Institute, Houston, #1077 (abstract)*. [7] Goderis et al. (2017). *GCA* 217, 28-50. [8] Ackerman et al. (2018). *GCA* 252, 179-189. [9] Folco et al. (2018). *GCA* 222, 550-568. [10] Folco et al. (2008). *Geology*, 36, 291-294. [11] Folco et al. (2009). *GCA* 73, 3694-3722. [12] Van Ginneken et al. (2018). *GCA* 228, 81-94. [13] Folco et al. (2011). *GCA* 75, 2356-2360.

ACHONDRITIC COSMIC SPHERULES FROM THE SØR RONDANE MOUNTAINS, EAST ANTARCTICA: PROBING THE ASTEROID BELT BEYOND THE METEORITE INVENTORY

B. Soens[1*], J. Villeneuve[2], M. van Ginneken[1,3,4], V. Debaille[4], F. Vanhaecke[5], Ph. Claeys[1] and S. Goderis[1] ([*]e-mail: Bastien.Soens@vub.be), [1]AMGC, Vrije Universiteit Brussel, Pleinlaan 2, 1050 Brussels, Belgium; [2]CRPG, 15 Rue Notre Dame des Pauvres, 54500 Vandoeuvre-lès-Nancy, France; [3]Royal Belgian Institute of Natural Sciences, Rue Vautier 29, 1000 Brussels, Belgium; [4]Laboratoire G-Time, Université Libre de Bruxelles, Franklin Rooseveltlaan 50, 1050 Brussels, Belgium; [5]Department of Chemistry, Ghent University, Krijgslaan 281, S12, 9000 Ghent, Belgium.

Introduction: Achondritic micrometeorites represent a rare subpopulation (<1 to 1.6%) of the cosmic dust flux to Earth [1-2]. They commonly display vitreous textures due to their lower Mg content, facilitating the melting process of precursor particles during atmospheric entry. As unmelted achondritic micrometeorites are exceptionally rare [3-5], the majority of achondritic micrometeorites will not retain its primary textural, chemical and isotopic properties. However, achondritic materials systematically display higher Fe/Mg ratios (for similar Fe/Mn ratios) relative to chondritic materials [1-2, 6-8]. This can be attributed to a range of planetary differentiation processes (e.g., development of crust, core-mantle segregation) taking place on achondritic parent bodies. Achondritic cosmic spherules (i.e., fully molten micrometeorites) are furthermore characterized by elevated CaO and Al_2O_3 contents (up to 11.6 wt% and 12.4 wt%, respectively), enriched REE contents (up to 11.6x CI chondrites), variable REE patterns and siderophile element contents (e.g., Ni: 0.17-131 ppm and Co: 1.3-68.1 ppm), reflecting their precursor mineralogy [2,7]. Based on their triple-oxygen isotopic compositions, the majority of achondritic cosmic spherules is related to Vesta-like parent bodies [2]. Here, we present new data for five vitreous, achondritic cosmic spherules from the Sør Rondane Mountains (Dronning Maud Land, East Antarctica) with unique major, trace element and triple-oxygen isotopic compositions, possibly expanding the diversity of planetary bodies in the Solar System.

Methodology: Hundreds of vitreous cosmic spherules were extracted from non-magnetic sediment fractions in the Widerøfjellet 18 Mt #01 deposit. Particles were placed on a double-sided sticky-tape and analyzed with SEM-EDS at the Vrije Universiteit Brussel. The achondritic parentage of 5 cosmic spherules (i.e., AC#01-05 representing <1% of the cosmic spherules found) could be determined based on their distribution in the Fe/Mg versus Fe/Mn diagram [6]. The achondritic spherules were embedded in epoxy resin and polished prior to major and trace element analysis. Three replicate analyses with a spot size of 35 μm were performed using a Teledyne Cetac Technologies Analyte G2 excimer-based laser ablation system coupled to a Thermo Scientific Element XR double-focusing sector field ICP-mass spectrometer at the Department of Chemistry (Ghent University). Triple-oxygen isotopic compositions were determined with a Cameca IMS 1270 E7 ion microprobe at the CRPG in Nancy (CNRS - Université de Lorraine) with a spot size of ca. 15 μm. Typical analytical uncertainties are ca. 0.5‰ (2σ) for ^{17}O, ca. 0.5‰ (2σ) for ^{18}O, and ca. 0.6‰ for $\Delta^{17}O$.

Results and Discussion: The five achondritic spherules range between 526-341 μm and display a homogenous, vitreous texture that often contains a dissolution rim due to terrestrial alteration. Four particles are closely positioned near the 4-Vesta/Mars line (Fe/Mn ≈ 32), while one particle (AC#02) is positioned next to the Lunar line (Fe/Mn ≈ 70) in the Fe/Mg versus Fe/Mn diagram. The CaO and Al_2O_3 contents range between 2.7-15.2 wt% and 0.98-25.5 wt%, respectively. Average REE contents are clearly enriched and range between 8.7-20.1x CI chondrite values. The REE patterns are generally flat, except for a positive Eu-anomaly in particle AC#04, a negative Eu-anomaly in particle AC#03, and negative Ce-anomalies in particles AC#02, AC#03 and AC#04. The latter are attributed to the volatile behavior of Ce during atmospheric entry of the precursor particle [9]. The concentrations of Ni and Co range from 6.1 to 75.2 ppm and from 0.85 to 18.7 ppm, respectively, compatible with metal-poor precursor bodies. Triple-oxygen isotopic compositions for particles AC#01 ($\delta^{18}O$: 17.99‰ and $\Delta^{17}O$: -0.47‰) and AC#03 ($\delta^{18}O$: 12.09‰ and $\Delta^{17}O$: -0.53‰) are similar to HED-like spherules found in the Transantarctic Mountains [2]. Particles AC#02 ($\delta^{18}O$: 21.85‰ and $\Delta^{17}O$: -0.39‰), AC#04 ($\delta^{18}O$: 24.38‰ and $\Delta^{17}O$: -0.76‰) and AC#05 ($\delta^{18}O$: 43.44‰ and $\Delta^{17}O$: -0.65‰) display more ambiguous triple-oxygen isotopic compositions and cannot readily be assigned to a specific achondritic parent body. The latter particles may thus sample planetary bodies currently not represented in the meteorite inventory. However, to verify this hypothesis, an accurate assessment of atmospheric reprocessing effects will be required.

Conclusions: Five achondritic spherules were discovered in sediment traps from the Sør Rondane Mountains displaying unique major, trace element and oxygen isotopic compositions, possibly representing new planetary materials. These results will be complemented with stable Fe isotope systematics to determine the extent of atmospheric alteration processes on the precursor particles, allowing a more refined assessment of their parent bodies.

References: [1] Taylor et al. (2007). *MAPS* 42, 223-233. [2] Cordier et al. (2012). *GCA* 77, 515-529. [3] Gounelle et al. (2005). *MAPS* 40, 917-932. [4] Gounelle et al. (2009). *PNAS* 106, 17, 6904-6909. [5] Badjukov et al. (2010). *MAPS* 45, 1502-1512. [6] Goodrich and Delaney (2000). *GCA* 64, 149-160. [7] Cordier et al. (2011*). GCA* 75, 1199-1215. [8] Papike et al. (2003). *Am. Mineral.* 88, 469-472. [9] Cordier et al. (2011). *GCA* 75, 5203-5218.

THE RADIANTS DISTRIBUTION OF THE DELTA CANCRIDS METEOROIDS

M. G. Sokolova[1], M. V. Sergienko[1], A. O. Andreev[1], Y. A. Nefedyev[1]
[1]Kazan Federal University, Russia, Kazan, Kremlyovskaya st., 18. E-mail: star1955@yandex.ru

Introduction: The aim of this paper is to refine the coordinates of the Delta Canrcids' (DCA) branches and their drift motion and to study features of radiants distribution and orbit elements for DCA using television observations. The DCA complex is an unconfirmed small meteor shower with 2 branches – Northern (NCC) and Southern (SCC) ones. The shower is observed between January, 1 and January, 31 and its radiant is in the constellation of Cancer. The maximum of activity for the meteors with the minimum registered magnitude of $+3^m$ or higher is 8.6±2 meteors an hour at the solar ecliptic longitude of 298.5°±1.2°. The calculations of spatial density for DCA shows that at the maximum of the shower's activity there is 1 particle heavier than 1 g for a cube with an edge of about 1000 km. For DCA there is no parental body found among comets, and its genetic connections with asteroids are therefore being studied. The observations of DCA were produced using radar and television methods.

Methods: The meteoroid orbits of NCC and SCC branches of DCA complex presented in the television catalogues SonatoCo [2] and CMN [3] were used. In the SonatoCo catalogue 111 and 59 meteor orbits for NCC and SCC respectively are presented using the observations taken between 2007 and 2015. The minimum registered magnitude for the meteors was $+3.5^m$, the error of determining geocentric speed was about 1 km/s. The coordinates of the radiant and their diurnal variations for each branch were determined using both the individual radiants' coordinates of the registered meteors and the coordinates averaged on 1° of the solar longitude. For the study of radiants distribution and orbit elements methods of robust analysis were applied.

Results: The values of geocentric radiants' coordinates at solar longitude of 298° were obtained: for NCC right ascension = 130.0°±3.1° with diurnal variation = +0.22°, declination 19.8°±2.8° with diurnal variation = −0.03°; for SCC right ascension = 128.2°±6.0° with diurnal variation = +0.11°, declination = 13.3°±2.0° with diurnal variation = −0.06°. For NCC and SCC radiation areas are 7°× 6° and 4°× 3° respectively. For NCC diurnal radiant drift is more reliably determined than for SCC due to the presence of a larger statistical base for its orbits. The study of the dependence of major semi-axes and eccentricities on a meteor's magnitude in the range from $−5^m$ to $+3^m$ has shown that at NCC for weaker meteors the values of major semi-axes and eccentricities decrease by 0.2 AU and 0.01 respectively. For SCC this dependence is poorly expressed.

Discussion: The NCC and SCC branches are observed on the same dates, geocentric velocities of the branches' meteoroids almost coincide, but radiants are clearly localized both by right ascension and declination. The meteors' radiants of each branch are distributed evenly with no subradiants detected, and the coordinates dependence on meteors' magnitude is not revealed either. At the same time, the orbits of meteoroids are decreased, in particular for NCC, depending on their mass, which might be caused by the non-gravitational Poynting–Robertson effect due to significant age of the shower. The comparison of orbits produced using television and radar methods and given at [1] also confirms the results obtained by us. The DCA meteoroids have orbital period of about 4 years and are exposed to strong gravitational perturbations from Jupiter. For SCC in the zone of strong resonances 1:1 and 2:1 meteoroids with resonant orbits are not recorded, the NCC meteoroids are not observed only at 1:1 resonance.

Conclusions: The radiants for the Delta Cancrids that are consistent with few data obtained by other authors are produced [4]. The values of diurnal variation for radiants are refined, radiation areas are derived [5, 6]. For NCC in magnitude range between $−5^m$ to $+3^m$ there is a decrease in major semi-axes and orbit eccentricities depending on meteors' magnitude [7, 8]. As the radiation area for SCC is smaller than for NCC and the dependence of orbits' size on their mass has not been revealed, one may suggest there are different formation mechanisms for NCC and SCC branches (e.g. secondary disintegration of a parental body) [9].

References: [1] Jenniskens P. 2006 Cambridge, UK: Cambridge University Press. 790. [2] The SonotaCo network (SoNotaco) http://sonotaco.jp/doc/SNM/index.html); Croatian Meteor Network (CMN), http://cmn.rgn.hr/downloads/downloads.html#orbitcat. [3] MMO (IMO, http://www.imo.net/data/visual). [4] Sokolova M., et al. (2016) *Advances in Space Research* 58/4: 541-544. [5] Sokolova M.G., et al. (2018) *Advances in Space Research* 62/8: 2355-2363. [6] Sokolova M.G., et al. 2014. *Advances in Space Research*. 54/ 11: 2415-2418. [7] Sokolova M.G., et al. 2013. *Advances in Space Research*. Vol. 52/7: 1217-1220. [8] Sergienko M. V. et al. (2018) *Meteoritics & Planetary Science* 53/S1: 6162. [9] Sergienko M. V., et al. (2018) *Meteoritics & Planetary Science* 53/S1: 6165.

DYNAMIC EVOLUTION OF THE ORBITS OF 2001YB5 AND (356394) 2010QD2 ASTEROIDS

M. G. Sokolova[1], M. V. Sergienko[1], Y. A. Nefedyev[1], A. O. Andreev[1]
[1]Kazan Federal University, Russia, Kazan, Kremlyovskaya st., 18. E-mail: star1955@yandex.ru

Introduction: The aim of this paper is to analyze the changes in orbital elements of 2001YB5 and 2010QD2 asteroids over a long-term period and to identify them with the Delta Cancrids (DCA) meteor shower. DCA is a confirmed meteor shower with 2 branches – northern (NCC) and southern (SCC) ones observed between January, 1 and January, 31. For DCA there is no parental body found among comets, and the meteor shower's potential connections with the asteroids crossing the Earth's orbit (Atira, Aten, Apollo, and Amor) are therefore being investigated. Using the D-criterion by J.D. Drummond [1] and the metrics by K.V. Kholshevnikov [2] as functions of the distance between 2 orbits in the orbital phase space as well as Tisserand's parameter and 2 quasidynamic parameters of the restricted three-body problem [3], 9 Apollo asteroids for NCC and 9 Apollo asteroids for SCC were revealed. The modern positions of the asteroids' 2001YB5 and 2010QD2 orbit nodes selected only for the southern branch (SCC) are coinciding within 2° with the position of the shower's maximum activity of 8.6±2 an hour for the meteors with the minimum recorded magnitude of $+3^m$ or higher which is recorded at the ecliptic longitude of the Sun of 298.5°±1.2°. The purpose of the work is therefore to analyze the orbital elements of 2001YB5 and 2010QD2 asteroids over a long-term period. In this paper, the orbits of meteoroids belonging to NCC and SCC branches (178 orbits) produced on the basis of television [4] and visual [5] observations were used to determine the activity profile for the Delta Cancrids.

Methods: To determine orbit elements at the given moment of time, HORIZONS integrator that takes into account perturbations from all the planets was used. The integration of orbits was carried out over a period of 1000 years starting from 1550 to 2550 (500 years backward and 500 years forward).

Results: The character of the asteroids' 2001YB5 and 2010QD2 orbital evolution significantly differs. The secular variations of eccentricity, perihelion distance, and angular elements at 2001YB5 are of periodic character. The full period of changes in angular elements is about 3000 years with the orbit node changing from 0° to 224°, the inclination angle varies within 14° over the entire period. The dynamics of 2001YB5 is influenced by Jupiter's orbital resonances resulting in fluctuations of the increase in eccentricity and perihelion distance (up to 0.01 AU) with a period of 3 Jupiter's ones. Unlike 2001YB5, the changes in orbital elements of the asteroid 2010QD2 demonstrate an unvarying character with short-period changes in eccentricity and perihelion distance but multidirectional and smaller oscillations amplitude. At a long-term period, the values of node longitude, inclination, and orbit eccentricity for 2010QD2 decrease over time, while perihelion distance increases.

Discussion: The asteroids 2001YB5 and 2010QD2 have significantly elongated orbits with eccentricities close to 0.8, perihelia are within the Earth's orbit, aphelia are about 4 AU, the asteroids' sizes are up to 1 km. The values of Tisserand's parameter significantly differ: for 2001YB5 it is 2.89, which relates its orbit to a cometary type; for 2010QD2 it is 3.34 with its orbit corresponding to the asteroid type. The calculations of the values of D-criterion [2] and metrics [3] for the elements of the asteroids' 2001YB5 and 2010QD2 osculating orbits and the elements of mean orbit of DCA, NCC, and SCC over the period of 1000 years have shown that only for 2010QD2 is there a monotone decrease in the value of D during the integration of the asteroid's orbit back in time.

Conclusions: The retrograde analysis of the asteroids' 2001YB5 and 2010QD2 orbit elements selected with the probability of 0.6 for the southern branch (SCC) of the Delta Cancrids leads to a conclusion that only the orbital evolution of 2010QD2 demonstrates a possible connection with the meteor shower in the past [6, 7]. The results of the work will find their application when performing research of the genetic links of meteoroids [8], [9], [10].

References: [1] Drummond J. D. (1981) *Icarus* 45: 545-553. [2] Kholshevnikov K.V., et al. (2016) *MNRA* 462/2: 2275–2283. [3] Kramer, E. N. and Shestaka, I. S. (1987) *Sol. Syst. Res.* 21/1: 75–83. [4] The SonotaCo network (SoNotaco) http://sonotaco.jp/doc/SNM/index.html); Croatian Meteor Network (CMN), http://cmn.rgn.hr/downloads/downloads.html#orbitcat). [5] MMO (IMO, http://www.imo.net/data/visual). [6] Sokolova M.G., et al. (2018) *Advances in Space Research* 62/8: 2355-2363. [7] Sokolova M., et al. (2016) *Advances in Space Research* 58/4: 541-544. [8] Nefedyev Y. A. (2018) *Meteoritics & Planetary Science* 53/S1: 6188. [9] Andreev, A. O., (2018) *Meteoritics & Planetary Science* 53/S1: 6157. [10] Nefedyev Y. A. (2018) *Meteoritics & Planetary Science* 53/S1: 6192.

DEGASSING AND VOLATILE CONTENT OF L3 CHONDRITE ABA PANU

A. V. Stennikov*, V.S. Fedulov, N.V. Dushenko, S. G. Naimushin and S. A. Voropaev
Institute of Geochemistry and Analytical Chemistry RAS, Moscow; *e-mail: ya_email@mail.ru

Introduction: Planetesimals and meteorites contain volatile components within to be released later during accretion, differentiation, magmatic or impact processes. These gases make up the most part of early (secondary) atmosphere of terrestrial planets [1]. Content and proportion of these volatiles are usually derived from thermodynamic modeling [2], while experimental results are not seen often [3,4]. We have analyzed oridinary chondrites different types as a primitive material conserved from the solar nebula. Chondrites are generally believed to be the building blocks of the Earth and other rocky asteroids, planets and satellites. The chondrites are undifferentiated (i.e., unmelted) stony meteorite containing metal+sulfide+silicate. The ordinary (H, L, LL) chondrites constitute about 97% of all chondrites. Here we present the initial results on experimental degassing during annealing of L3 S4 W0 ordinary chondrite Aba Panu. The meteor is a fall, which detonation was observed over the Nigerian state of Oyo in April, 2018.

Methods: To conduct the experiments, a special instrument was designed at the Institute of Geochemistry and Analytical Chemistry RAS. The apparatus consist of system of quartz tubes filled with hydrogen, insulated chamber and control panel. Sample annealing was done as a series of experiments with set temperature between 200 and 800°C with 100°C step between them; after temperature was settled the volatile content in reactor was assessed by gas chromatography every 15 minutes for 1,5 hours. More detailed description of the experiment is presented in [5].

Results and discussion: The following volatile constituents were identified: H_2O, N_2, CO_2, CO, CH_4, H_2, and H_2S. The substances can be conditionally divided into macro- and microcomponents. H_2O, N_2, and CO_2 belong to the first group, their concentration varies in the range of 3–120 µg/g of sample; the remained ones are in the second group (the concentration varies within 0.1–0.9 µg/g).

Combining all profiles at different temperatures for individual volatile results in time-temperature-concentration diagram, presented as a heat contour (fig. 1).
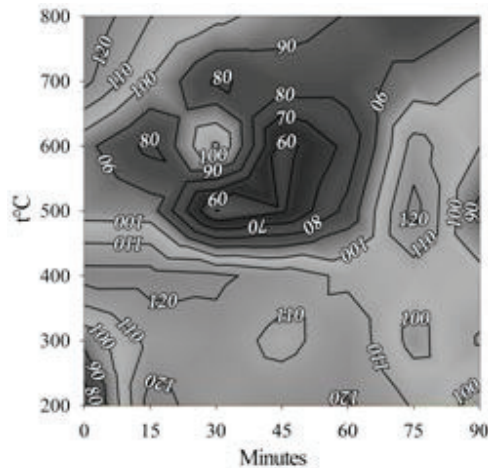

Figure 1. Heat contour of H_2O concentration (mg/g sample) versus time-temperature from degassing of Aba Panu

Observed change in concentration indicates chemical behaviour and possible form of accumulation within meteorite matrix. The following conclusions can be made: the main products of thermal meteorite outgassing are CO_2, N_2, and H_2O, where the first two behave rather inertly. However, with an increase in temperature and H_2 content, products of reducing reactions, such as CO, CH_4, and H_2S, also begin to form.

References:
[1] Massol H. et al. (2016) *Space Science Reviews* 205: 153–211. [2] Shaefer L. and Fehley B. Jr. (2007) *Icarus* 186: 462-483. [3] Gooding J.L. and Muenow D.W. (1977) *Meteoritics* 12: 401-408. [4] Muenow D.W. et al. (1995) *Meteoritics* 30: 639-645. [5] Stennikov A.V. et al. (2019) *Solar system research* 53: 199-207.

MOLYBDENUM IN PRESOLAR SILICON CARBIDE GRAINS REVEAL DETAILS OF *s-*, *r-*, AND *p-*PROCESS NUCLEOSYNTHESIS.

T. Stephan[1,2] and A. M. Davis[1,2,3], [1]Department of the Geophysical Sciences, The University of Chicago, Chicago, IL 60637, USA, [2]Chicago Center for Cosmochemistry, [3]The Enrico Fermi Institute, The University of Chicago, Chicago, IL 60637, USA, E-mail: tstephan@uchicago.edu.

Introduction: The isotopic information stored in presolar grains, which formed around dying stars, reflects a combination of three distinct sources: (1) the initial abundances in the parent stars of the grains, providing compositional snapshots of the times and locations where the stars formed; (2) matter newly synthesized by nuclear reactions within those stars; and (3) matter with solar isotopic composition from the protosolar cloud, the host meteorite's parent body, or contamination in the laboratory. Solar System material is itself a complex, and often slightly variable, mixture of matter formed in various nucleosynthetic processes.

Molybdenum is a favorable element for studying nucleosynthesis, because of the variety of sources represented in solar composition and in presolar grains, and, from an experimental perspective, because all of its stable isotopes have the same solar abundances within a factor of less than three, which makes measurements easier. Molybdenum has seven stable isotopes: *p*-process ^{92}Mo and ^{94}Mo; mixed *s*- and *r*-process ^{95}Mo, ^{97}Mo, and ^{98}Mo; *s*-process-only ^{96}Mo; and *r*-process-only ^{100}Mo.

Methods: Recent studies with RIMS (resonance ionization mass spectrometry) using CHILI (the Chicago Instrument for Laser Ionization) [1] provided high-precision Mo isotope data for single presolar mainstream [2,3] and types AB1 [4], AB2 [2,3], Y [5], and Z [5] SiC grains. Others have used MC-ICPMS (multicollector inductively coupled plasma mass spectrometry) to analyze Mo in bulk samples and leachates of primitive meteorites [6–10].

Results: RIMS data of presolar SiC mainstream grains show mixing lines in three-isotope plots of ^{i}Mo/^{96}Mo vs. ^{92}Mo/^{96}Mo between two endmember compositions, one indistinguishable from solar, the other pointing towards pure *s*-process Mo. These measurements provide the best estimate to date for *s*-process Mo made in low-mass AGB (asymptotic giant branch) stars [2]. Variability in individual grain data reflects variability of conditions (neutron density, temperature, timescale) during *s*-process nucleosynthesis in the grains' parent stars [2]. Other presolar SiC grain types including AB1, AB2, Y, and Z show trends in Mo isotopes that are all consistent with mainstream grain three-isotope plot mixing lines [2–5]. Furthermore, these mixing lines are also consistent with MC-ICPMS data for bulk samples and leachates of primitive meteorites showing depletions in *s*-process Mo isotopes relative to solar [6–10].

Discussion: Presolar mainstream, Y, and Z SiC grains, which all come from low-mass AGB stars, should show mixtures of *s*-process Mo produced in those stars with Mo from the unprocessed stellar envelopes and perhaps from solar contributions. In order to explain the linear mixing lines in Mo three-isotope plots for such grains as a result of three-component mixing, unprocessed Mo from each of the grains' parent stars must itself plot along those mixing lines defined by *s*-process and solar. This suggests that the ratio between *p*- and *r*-process Mo in presolar SiC from many low-mass AGB stars is $Mo_p/Mo_r = 0.767$ [2], a value that was inferred for the Solar System from *s*-process and solar endmembers of the mixing lines. The same is true for AB1 and AB2 grains, whose stellar origins are still a matter of debate and include J-type carbon stars, born-again AGB stars, and Type II supernovae.

It is important to emphasize that a constant Mo_s/Mo_{r+p} ratio is not required to explain the mixing lines observed for presolar SiC grains, as changing this ratio would move data points only along those lines. Depletions in *s*-process Mo as observed in bulk samples and leachates of primitive meteorites, which are consistent with $Mo_p/Mo_r = 0.767$, reflect some heterogeneity of Mo_s/Mo_{r+p} in the early Solar System. However, the carriers of the *s*-process-depleted Mo have not been identified so far. Presolar SiC X grains, which are attributed to Type II supernovae, could not be that carrier. Although they show indeed enrichments of mixed *s*- and *r*-process isotopes ^{95}Mo and ^{97}Mo, equivalent enrichment in *r*-process-only ^{100}Mo and in *p*-process isotopes have not been observed [11]. Also, a dichotomy, as observed between carbonaceous and noncarbonaceous meteorites [9], was not detected in SiC.

Conclusions: The constant ratio between *p*- and *r*-process Mo in presolar SiC, primitive meteorites, and the Solar System shows that *r*- and *p*-processes must be strongly correlated over time and perhaps space in the Galaxy.

References: [1] Stephan T. et al. (2016) *International Journal of Mass Spectrometry* 407:1–15. [2] Stephan T. et al. (2019) *The Astrophysical Journal,* in press. [3] Liu N. et al. (2017) *The Astrophysical Journal Letters* 844:L12. [4] Liu N. et al. (2018) *The Astrophysical Journal* 855:144. [5] Liu N. et al. (2019) *The Astrophysical Journal,* submitted. [6] Dauphas N. et al. (2002) *The Astrophysical Journal Letters* 569:L139–L142. [7] Burkhardt C. et al. (2011) *Earth and Planetary Science Letters* 312:390–400. [8] Burkhardt C. et al. (2012) *Earth and Planetary Science Letters* 357–358:298–307. [9] Budde G. et al. (2016) *Earth and Planetary Science Letters* 454:293–303. [10] Budde G. et al. (2018) *Geochimica et Cosmochimica Acta* 222:284–304. [11] Pellin M. J. et al. (2006) *LPS XXXVII*, Abstract #2041.

METEORITES OF THE NULLARBOR PLAIN; RECENT RECOVERY & CLASSIFICATION EFFORTS

N. R. Stephen[1], H. E.Brand[2] & A. Tomkins[3], [1]Plymouth Electron Microscopy Centre, University of Plymouth, Drake Circus, Plymouth, Devon, PL4 8AA, United Kingdom (natasha.stephen@plymouth.ac.uk), [2]Australian Synchrotron, ANSTO, 800 Blackburn Rd., Clayton, VIC 3168 Australia. [3]School of Earth, Atmosphere and the Environment, Monash University, Melbourne, Victoria, 3800, Australia

Introduction: The Nullarbor Plain in Southern Australia provides opportune conditions for meteorite preservation; largely arid, the Nullarbor has been known to preserve meteorites for thousands of years. These meteorites are located either through use of 'fireball' cameras such as the *desert fireball network*, which has found four meteorites to date [1], or by manual search & recovery expeditions. Each year, a team from Monash University and the University of Plymouth manually explore a previously uncovered region of the Nullarbor in order to retrieve new meteorite specimens. Since 2008, this team have recovered more than 200 new meteorites, with 78 officially classified so far.

A recent study provided insight into a small sample of the more recent Nullarbor recoveries using synchrotron powder X-ray diffraction (XRD), aiming to inform a full classification of each specimen [2], upon which this study will build prior to submission to the Meteoritical Bulletin.

Samples & Analytical Techniques: Nine chondrite meteorites were used in this study, as polished thin sections or homogenized powders. The meteorites are not yet officially classified and have therefore been named for the date they were found (DDMMYY), then alphabetically for the order. *Scanning Electron Microscopy (SEM):* Large area, whole section backscattered electron (BSE) images and energy dispersive spectroscopy (EDS) maps were generated for each thin-section, using a JEOL 7001F FEG-SEM with an accelerating voltage of 15 kV, unless otherwise indicated. Layered X-ray element maps combined with spot analyses to determine mineral composition were generated using an Oxford Instruments X-Max 80 mm^2 EDS detector with AZtec software, and calibrated using a cobalt reference standard and MAC rock-forming minerals block. *X-Ray Diffraction:* Samples were crushed, hand ground and mixed with a ZnO internal standard before being loaded into capillaries on the PD beamline at the Australian synchrotron. Data were analysed using Topas V6 (Bruker).
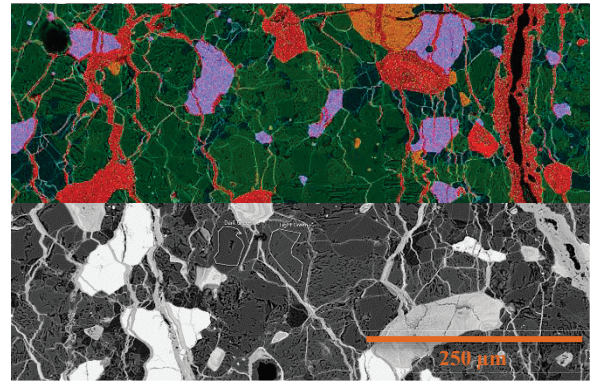

Figure 1: Layered EDS (top) and BSE (bottom) image showing the typical weathered texture observed in Nullarbor chondrites (sample 24417G), with Fe-oxide phases identified within pervasive veining. Red - Fe-oxide weathering products; orange - chromite; purple - sulfides; green - pyroxene; dark green - feldspar.

Results: Modal analyses by XRD and SEM-EDS were generated for each of the samples, allowing for a direct comparison between the two methods. However, the SEM-EDS also allowed comparisons to be made across the suite of chondrites with respect to chondrule size, type, degree of weathering and amount of metal. Most of the samples have chondrules between 100 µm and 1.2 mm diameter of varied composition, with 24417G indicating the most severe weathering. Major phases within chondrules and matrix included pyroxene, olivine and feldspar, whilst goethite, pyrrhotite and troilite were all observed as veins or within matrix (see figure 1). Minor phases across all samples analysed included chromite, apatite and chlor-apatite (<6.5 wt% Cl).

Discrepancies were observed within the initial modal data obtained via XRD vs SEM-EDS owing to several minor phases (i.e. apatite) sitting below the detection limit of the XRD technique. In addition, a lower proportion of some phases (i.e. goethite) were observed within XRD analyses, and others (i.e. sulfides & feldspar) were missing from XRD datasets (table 1) entirely. However, we are confident that the phases are correct owing to SEM-EDS analyses, and the varied compositions observed as a result (figure 1). Several of the phases determined using SEM-EDS are not represented in the XRD data due to sample preparation bias; this is being addressed through a separate study. It is hoped that this combination of SEM-EDS & XRD will enable the backlog of Nullarbor meteorites to now be classified.

	Goethite & Fe-oxides	Chromite	Sulfides	Apatite	Pyroxene	Feldspar
XRD	8.00	3.00	Not seen	Below limit	89.00	Not seen
SEM-EDS	19.57	1.04	4.35	0.92	65.10	9.03

Table 1: Modal mineralogy for sample 24417G, determined via XRD [3] or SEM-EDS.

References: [1] Benedix, G. K. et al. (2017) *Met. Soc.* Abstract #6229. [2] Brand, H.E. et al. (2019) *LPS L*, Abstract #1361.

APPEARANCE OF THE IMPACT FLASH IN METEORITE DISRUPTION EXPERIMENTS.

M. M. Strait[1], G. J. Flynn[2], D. D. Durda[3], M. J. Molesky[1], B. A. May[1], S. N. Congram[1], C. L. Loftus[1], J. R. Reagan[1], [1]Alma College, Alma, MI 48801 (straitm@alma.edu), [2] SUNY-Plattsburgh, 101 Broad St., Plattsburgh, NY 12901, [3] Southwest Research Institute, 1050 Walnut Street, Suite 300, Boulder, CO 80302.

Introduction: Studies of the optical flash that occurs in a hypervelocity impact have been done for some time [1, 2, 3], however, most of these have concentrated on results applying to space debris or missile defense. Our lab has observed the flash and occasionally made casual observations, but have done no concentrated studies on this flash. Herein we report on a preliminary examination of the flash as impacts are made into a variety of geological materials.

Experimental Setup: Terrestrial and meteoritic materials have been impacted for a number of years using the NASA Ames Vertical Gun Range. We have reported on other aspects of these experiments, including the energy of impact [4] and the -requency distribution of the ejecta [5]. The impacts have been imaged using high speed photography. Using this imagery we have made observations on a range of materials under a variety of impact conditions. The samples are hung from a nylon line in a near vacuum and then impacted with 1/16" or 1/8" Al- projectiles moving between 4 and 5.5 km/sec. Although various angles were imaged, a consistent view from above was used to study the impact flash. Imagery was done at a frame rate of ~70,000 fps. To characterize the flash, observations were done on color, shape and duration of the flash, and the size of the flash relative to the size of the sample.

Results and Discussion: A combination of terrestrial hydrated samples and various classes of meteorites, including artificially hydrated CI simulant materials, were measured. In general, it was observed that the initial flash for hydrated materials was smaller and more confined in shape, and that the entire flash sequence was shorter than for nonhydrated materials. Smaller flashes tended to be shaded with yellow or pink, while bigger flashes were haloed with blue. There did not seem to be a correlation with impactor size or speed, or whether the resulting impact resulted in disruption of the sample or not. There is a concern about the timing of the flash with the video timing. This is more of a concern in earlier years when the frame rate was lower. The results were relatively consistent across multiple impacts on different samples of the same material.

Table I. Summary of Observations on Impact Flash

| Sample	Impact Speed (km/sec)	Impactor Size (inch)	Flash to Sample Size Ratio	Flash Shape	Flash Color
Carbonate	4.56	1/16	0.35	Ball with flare	White/pink
Montmorillonite	4.57	1/16	0.03	Small ball	White/yellow
Serpentine	4.21	1/16	0.23	Small jet	Pink/white
Hydrated NWA 4502	4.93	1/16	0.19	Flare	White
Hydrated NWA 869	5.08	1/16	0.25	Ball	Yellow/white
NWA 4502	4.5	1/16	2.14	Ball with flare	Blue/white
NWA 869	4.31	1/16	0.11	Flare	Blue/white
Saratov	4.18	1/16	1.66	Flare	Blue/white
Gibeon	4.47	1/16	5.23	Flash	Blue/white
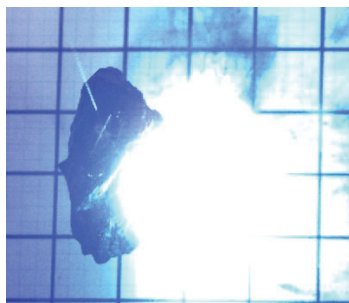
Figure 1. Initial impact for NWA 4502 (CV3) showing large blue-white flash. The grid in the background is a 1-inch grid used for impact recoil measurements.

Figure 2. Initial impact for a sample of montmorillonite against the same background as in Figure 1.

References: [1] Eichorn, G. (1975) *Planet. Space Sci.* 23:1519-1525. [2] Lawrence, R.J. et al. (2006) *Intl. J. Imp. Engr.* 33:353-363. [3] Goel, A. et al. (2015) *Intl. J. Imp. Engr.* 84:54-63. [4] Flynn, G.J. et al. (2017) *Planet. Space Sci.* 164:91-105. [5] Flynn, G.J. et al. (2009) *Planet. Space Sci.* 57:119-126.

STRUCTURAL AND ELEMENTAL TRANSFORMATION OF METEORITIC NANODIAMONDS DURING IN SITU HEATING IN A UHV SCANNING TRANSMISSION ELECTRON MICROSCOPE

R. M. Stroud[1], [1] US Naval Research Laboratory, 4555 Overlook Ave. SW, Washington, DC 20375.

Introduction: Nanodiamond isolates from meteorites carry nucleosynthetic anomalies indicative of a presolar supernova origin [1]. however the major element (C, N) isotope compositions of the bulk isolates are consistent with solar system values. Thus, the origins of meteoritic nanodiamonds remain enigmatic. Possible origins include formation in by condensation in the dusty outflows of supernova and AGB stars, or by shock and radiation processing of carbonaceous matter in the interstellar medium or the solar nebula. If the nucleosynthetic anomalies were distributed uniformly in the nanodiamond isolates, up to 1 in 10 nanodiamonds might retain a signature of a presolar origin. However, in addition to diamond, the isolates also contain varying amounts sp^2 carbon, presolar SiC, and refractory metal nuggets, which may also be carriers. The temperature release patterns of noble gases from the isolates identify multiple noble gas components with different cosmochemical histories, e.g., the P3 planetary gases, which reflect early solar system processes, and "HL" gases that are indicative of the supernova component, released at low and high temperature, respectively [2]. By performing heating stage experiments on the nanodiamond isolates *in situ* in a UHV STEM we aim to identify structural and elemental changes that correlate with the noble gas release patterns, in order to constrain the specific carriers.

Methods: An aqueous suspension of Allende DM nanodiamond was pipetted onto holey carbon film on heating stage supports compatible with the Protochips Fusion heating holder. The nanodiamond samples were subsequently analyzed with the Nion UltraSTEM 200-X aberration-corrected scanning transmission electron microscope at the Naval Research Lab, equipped with a Bruker Xflash 100 energy dispersive X-ray (EDX) spectrometer, and Gatan Enfinium HR electron energy loss (EEL) spectrometer. The Nion was operated at 60 kV, with a nominal 0.15 nm, 50-100 pA probe. Heating stage experiments to observe the transformation of the isolates were performed in the Nion with a Protochips Fusion system. The temperature was raised in 50°C increments at a rate of 1°C per second, and an EEL spectrum and dark-field images were recorded at each temperature step, up to a maximum of 1200°C.

Results: The as-deposited sample showed the characteristic C-K edge EEL fine-structure of diamond, along with a small π^* peak at 284.3 eV, indicative of the sp^2 component common to nanodiamonds. In addition, there was a small peak at ~282.4 eV, reported to be associated with N impurities in diamond (N-V center) [3], or with partially H-passivated surface defects [4]. Based on our earlier EDX analysis of Allende DM nanodiamond aliquots, the N content is ~ 0.1 to 0.3 at%.

On heating to between 400°C and 600°C, the N defect peak in the EELS spectrum dramatically decreased in intensity. This rules out the possibility of attributing this feature to surface H, which would be desorbed under the electron beam at much lower temperature. Continued heating of the sample to 1200°C under UHV conditions resulted in a gradual increase in graphitization, demonstrated by the relative intensity increase of the π^* peak, a shift the centroid to 285.3 eV, and changes in the extended structure at higher energies. The most dramatic changes occurred above 900°C, including increased porosity and formation of linear channels, consistent with the onset of the release of HL components in pyrolysis experiments. By 1200°C, the sample consisted of at least 50% graphitic carbon, and remained that way on cooling back to room temperature.

Discussion: The direct observation in the STEM of the low temperature release (400°C to 600°C) of N is important because published stepped combustion studies show the low temperature N release to be the least isotopically anomalous. However, the stepped combustion data could not provide definitive evidence that the N was carried by the diamond, rather than sp^2 carbon or other components in the isolates. Our preliminary data show direct evidence that the low-temperature-released N is intrinsic to the diamond, and thus these N-bearing diamonds are most likely formed in the solar system. Additional heating studies *in situ* in the Nion STEM, and ex situ in air, are planned in order to provide new context for interpreting nanodiamond pyrolysis and stepped combustion experiments, and to offer new constraints as to the nanodiamond formation histories.

References:
[1] Lewis R. et al. *Nature* (1987) 326:162-165. [2] Ott U. et al. (2012) *Publications of the Astronomical Society of Australia* 29:90-97. [3] S. L. Y. Chang et al. (2016) *Nanoscale* 8:10548-10552. [4] Garvie L. A. J. (2006) *Meteoritics & Planetary Science* 41:667-672.

RYUGU'S PARENT-BODY PROCESSES ESTIMATED FROM HAYABUSA2 MULTI-BAND OPTICAL OBSERVATIONS

S. Sugita[1,7], R. Honda[2], T. Morota[3], S. Kameda[4], E. Tatsumi[1], C. Honda[5], Y. Yokota[6], M. Yamada[7], T. Kouyama[8], N. Sakatani[6], H. Suzuki[9], K. Yoshioka[1], Y. Cho[1], M. Matsuoka[6], K. Ogawa[10], D. Domingue[11], H. Miyamoto[1], O. S. Barnouin[12], P. Michel[13], C. M. Ernst[12], T. Hiroi[14], T. Nakamura[15], H. Sawada[6], M. Hayakawa[6], N. Hirata[5], N. Hirata[10], H. Kikuchi[1], R. Hemmi[1], T. Michikami[16], Eric Palmer[11], R. Gaskell[11], M. Hirabayashi[17], R. Jaumann[18], K. Otto[18], N. Schmitz[18], S. E. Schröder[18], G. Komatsu[19], S. Tanaka[6], K. Shirai[6], M. Yoshikawa[6], S. Watanabe[3], Y. Tsuda[6], [1]Univ. of Tokyo (Tokyo, Japan, sugita@eps.s.u-tokyo.ac.jp), [2]Kochi Univ., [3]Nagoya Univ., [4]Rikkyo Univ., [5]Univ. of Aizu, [6]JAXA/ISAS, [7]PERC CIT, [8]AIST, [9]Meiji Univ., [10]Kobe Univ., [11]Planetetary Science Institute, [12]APL, Johns Hopkins University, [13]Observatoire de la Cote d'Azur, [14]Brown Univ., [15]Tohoku Univ. [16]Kindai Univ. [17]Auburn Univ., [18]DLR, [19]Univ. d'Annunzio

Introduction: JAXA's Hayabusa2 spacecraft arrived at asteroid 162173 Ryugu on June 27, 2018 and conducted global observations (~2 m/pix) from 20 km of altitude first and subsequently conducted a number of high-resolution regional and local observations (down to ~1mm/pix) during low-altitude descents including touch-down operation for sampling on Feb. 22, 2019 [1,2]. In this study, we summarize optical imaging observation results obtained from these wide range of spatial resolutions, focusing on the constraints they provide on Ryugu's parent body.

Spectroscopic Properties: The global observations have revealed many important properties of Ryugu [3]. Ryugu's average spectrum is consistent with Cb type and does not exhibit a strong 0.7-µm absorption band. It has a very low 0.55-µm geometric albedo of 0.045 ± 0.002, among the lowest in the solar system. Its crater retention age for small craters ($\geq$ 10m) is very young (< a few Myr), strongly suggesting a high surface rejuvenation rate.

Ryugu's Parent Body: The observed spectral characteristics of Ryugu is consistent with the dynamically most probable source asteroid families for Ryugu: Eulalia and Polana families in the inner main belt [4]. This agreement between the prediction from dynamic calculations and spectral observations suggests that one of the two asteroids is likely Ryugu's parent body. These families are among the most widely dispersed C-complex families in the inner main belt, allowing to deliver family members at very high flux rate to the resonance zones (ν_6 and 3:1) at both inner and outer boundaries of the inner main belt, which are the dominant source of near-Earth objects (NEO's).

Boulders on Unconsolidated Surface: Furthermore, very high abundance (about twice Itokawa) of boulders is seen on Ryugu. Many lines of evidence for mass wasting observed on Ryugu's surface indicate that its surface is mechanically unconsolidated, allowing surface boulders to move easily. The morphologies (e.g., raised rims and wall slumping) of impact craters on Ryugu are consistent with low internal cohesion of materials, leading to production of large ejecta masses. These suggest that large mass of boulders and pebbles can be ejected from Ryugu to space over time.

Meteoritic Counterparts: Thus, a large number of macroscopic objects of Ryugu-like materials may enter Earth's atmosphere, implying that there should be counterparts in our meteorite collection. One of such candidates is moderately dehydrated carbonaceous chondrites, which exhibit very low albedo and flat spectra. They are also found with high abundance in Antarctica, which has sampled the long-term average flux of infalling meteorites on Earth [5]. Another is interplanetary dust particles (IDPs), which also exhibit low albedos and account for large influx of extraterrestrial material to Earth. Although a decisive conclusion may not be obtained before the analysis of Ryugu samples returned to Earth, currently available observational evidence, such as high boulder abundance on Ryugu, favors that its composition may be similar to moderately dehydrated carbonaceous chondrites. This would further suggest that Ryugu's relatively low abundance of hydrated minerals [6] may be due to partial dehydration on Ryugu's parent body.

References: [1] Watanabe et al. (2019) *Science*, *363,* 268-272. [2] Yabuta et al. (2019) *Nature Astron.*, *3*, 287-288. [3] Sugita et al. (2019) *Science*. dx.doi.org/10.1126/science.aaw0422. [4] Bottke et al. (2015) *Icarus 247*, 191. [5] Tonui et al. (2014) *GCA*, 126, 284. [6] Kitazato et al. (2019) *Science*, *363,* 272-275. Acknowledgements: This study was supported by JSPS Core-to-Core program "International Network of Planetary Sciences", CNES, and Univ. Côte d'Azur.

NORTHWEST AFRICA 4747, AN UNIQUE MESOSIDERITE.

N. Sugiura [1], T.Arai [1] and T. Matsui [1], [1]Planetary Exploration Research Center, Chiba Institute of Technology (Narashino, Chiba, Japan, NWA1878@gmail.com)

Introduction: Origin of mesosiderites is not yet well understood. In particular, the heat source for their reheating is not known. Therefore, petrographic observation concerning their reheating and subsequent cooling is important. Here we report petrographic features of a polished section of the Northwest Africa 4747 (NWA 4747) mesosiderite. The observation was made with a SEM (JEOL JSM6510) and elemental compositions were measured with EDS.

Observation and interpretation: Metal nodules up to 3 mm in size are present. In contrast to most metal nodules in other mesosiderites, those in NWA 4747 do not contain silicate inclusions. They contain small spheroidal FeS grains near the center of nodules. It is possible that the nodules grew in situ from smaller metal grains by partial melting and sintering. The FeS abundance in NWA 4747 is estimated 7.9 +/- 2.7 (1 sigma) wt.% based on the sulfur X-ray maps for an area of ~11.6 mm^2. FeS abundances are variable in mesosiderites, ranging from less than 1 wt.% to more than 12 wt. % [1], and the formation mechanism is not well understood. FeS in NWA 4747 is more abundant in silicate-rich areas than in metal-rich areas. Taenite is often observed in the FeS-rich areas. Fine-grained FeS + pyroxene mixture, replacing olivine, similar to that reported by [2] is observed, but it is minor in abundance. Most FeS seems to have formed by sulfidation of Fe-Ni metal. All together, we think that sulfur was introduced as S_2 gas, and sulfidation proceeded efficiently in silicate-rich permeable areas. Occasionally, chromite is found in metal nodules and Cr diffusion profiles are observed over ~10 μm in the surrounding kamacite. This suggests that the reheating event was short-lived and the subsequent cooling was rapid. Olivine clasts are not rare and are Fe-rich and Mn-rich. Many olivines show Fe/Mg > 0.6 and Fe/Mn < 30. In contrast, most olivines in mesosiderites are Fe/Mg < 0.6 and Fe/Mn ~ 40 [1]. The high Fe contents suggests oxidizing conditions. Phosphide and rutile are absent in NWA 4747, also suggesting oxidizing conditions. Phosphate exists as tiny grains in the matrix, suggesting formation from a silicate melt. This is in contrast to phosphate in other mesosiderites where it is mostly attached to metal surface. The phosphate occurrence suggests that the reheating occurred at least twice. This is because P was initially in metal and stays in metal at high (>1100C) temperatures and phosphate forms only at <1100C during cooling [3]. A second heating is needed to dissolve the phosphate into a silicate melt. There are interesting varieties of Ni profiles in metal grains. Isolated taenites show M-shape Ni profiles. But the central Ni vs. size plot does not follow the trend expected for mesosiderites [4]. In composite grains consisting of kamacite and taenite, Ni profiles in taenite are nearly flat at ~50% Ni. Therefore, a metallographic cooling rate cannot be determined from taenite. However, Ni in kamacite shows gradients due to the Agrell effect and the gradients are similar to those reported for mesosiderites by [4]. Therefore, there is no doubt that NWA 4747 cooled very slowly and therefore it is a mesosiderite in spite of various unique features. It should be emphasized that phosphide is not detected in the metal in NWA 4747. It is well known that Ni diffusion rates in P-poor kamacite and taenite are much lower than those in P-saturated metals of most mesosiderites [4]. The apparently similar Ni gradients in NWA 4747 kamacite to those in P-saturated metals in other mesosiderites might mean that NWA 4747 cooled more slowly than other mesosiderites.

Summary: Sulfidation of NWA 4747 occurred early. Sulfur fugacity was high at the peak reheating temperature. Either abundant FeS was present before the main reheating event, or sulfur was introduced during the main reheating event that was caused by an impact. A difficulty of the impact heating model is that mesosiderites do not show textures of shock. Since metals in mesosiderites are contiguous, induction heating could be efficient on the mesosiderite parent body. Induction heating is brief and repetitive, which is attractive attribute for explaining the petrologic features of NWA 4747. NWA 4747 is probably the first mesosiderite that does not contain phosphide. Source materials for mesosiderite silicates was more variable in terms of redox conditions than hitherto considered.

References:

[1] Mittlefehldt D.W. et al. (1998) Chapter 4. In *Planetary Materials* ed. Papike J.J. [2] Zhang A-C. et al. (2018) *Geochimica Cosmochimica Acta* 220: 125-145. [3] Harlow G.E. et al. (1982) *Geochimica Cosmochimica Acta* 46: 339-348. [4] Hopfe W.D. and Goldstein J.I. (2001) *Meteoritics & Planetary Science* 36:135-154.

GEOCHEMICAL AND MINERALOGICAL FEATURES OF CHONDRULE AND MATRIX OLIVINE FROM THE BUSCHHOF ORDINARY CHONDRITE

K.G. Sukhanova[1,2], S.G. Skublov[1,2], O.L. Galankina[1], E.V. Obolonskaya[2], E.L. Kotova[2], [1]Institute of Precambrian Geology and Geochronology, Russian Academy of Sciences (IPGG RAS) (2, Makarova emb., St. Petersburg, Russian Federation), [2]Saint-Peterburg Mining University (2, 21st Line, St. Petersburg, Russian Federation).

Introduction: Buschhof meteorite is L6 ordinary chondrite. Substance of the meteorite for research was provided by Mining museum (Saint-Petersburg Mining University), where it was stored since 1920's as part as Edward Kupffer meteoritical collection [1]. In this research we are measured major and trace elements contents for understanding formation differences between chondrule and matrix in ordinary chondrites. Olivine is the common mineral in chondules and matrix of ordinary chondrites and also stable in impact metamorphism conditions. Trace elements, including REE, are well known as sensitive indicators of geochemical processes.

Major elements content was detected by SEM-EDS method on JEOL JSM-6510 LA electron microscope in IPGG RAS. Content of trace elements in olivine was determined by the SIMS method on a Cameca IMS-4f ion microprobe in VALIEV IPT RAS using the procedure described in [2] .

Chondrules in Buschhof meteorite are different by mineral composition, size and morphology and occupy around 20% of meteoritical volume. The largest chondrule is around 2 mm, GOP type and has troilite and chromite rim. In meteorite also occurs small barred and radial chondrules (no more than 0.5 mm) without any rim and with indistinct character of chondrules border. The matrix is consist of finegrained silicate minerals (olivine, pyroxene, plagioclase) with large (to1mm) tanite, kamacite, troilite and chromite grains.

In Buschhof meteorite were identified: olivine, Ca-rich pyroxene, Ca-low pyroxene, plagioclase, apatite, merrillite, chromite, troilite, tetratenite, kamacite and taenite. Ca-rich pyroxene, apatite, merrillite and tetrataenite were diagnosed for the first time in Buschhof meteorite.

Results: Olivine (Fo 74-76) in Buschhof meteorite is located in structurally different chondrules and in the matrix. In the GOP chondrule isometric rounded olivine grains vary greatly in size from 20 to 200 mkm. The BO chondrule is represented by a single skeletal crystal of olivine, the intercrystalline space of which is filled with pyroxene and plagioclase. Size of the RP chondrule is 0.5 mm. In the matrix olivine has a coarse-grained short-prismatic shape (300-700 mkm).

There is no noticed relation between contents of the major elements in olivine and its location in chondrule. It can be caused either real absence of variation of contents of major elements or insufficient accuracy of the analysis method SEM-EDS.

Olivine from the center of GOP chondrule is enriched by HFSE Zr (the average content 0.56 ppm) and Nb (0.31 ppm) regarding olivine from the chondrule rim (0.20 и 0.11 ppm, respectively) and the matrix of meteorite (0.05 и 0.12 ppm). Hf behavior does not demonstrate reliable patterns, but in the chondrule center Hf contents in olivine above detection level and below detection level in the chondrule rim.

Content of the LILE Ba (the average content 2.21 ppm) and Sr (3.72 ppm) goes down in olivine from the chondrule center to the chondrule rim (0.36 и 0.24 ppm, respectively) as well and further to meteoritical matrix (0.11 и 0.14 ppm).
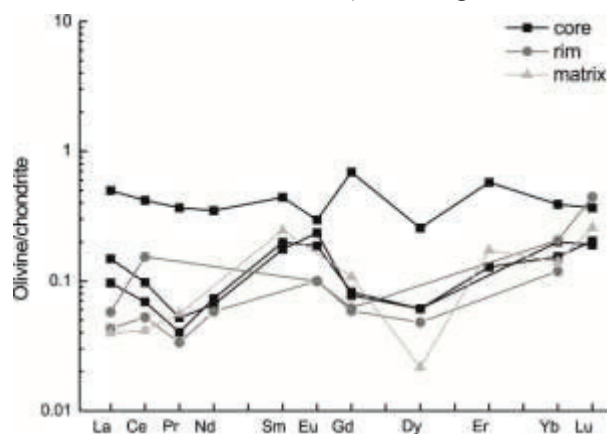
Maximum amount of Cr (the average content 538 ppm) is contained in olivine from the chondrule center compared to the chondrule rim (456 ppm) and meteoritical matrix (349 ppm). Ni behavior in olivine is more complicated – Ni abundance is greatly reduced from the chondrule center to the rim (avg from 158 to 26.2 ppm) and then a little bit increases in matrix (avg to 44.8 ppm).

Olivine is generally deplete in REE (Fig. 1), total content does not exceed about 1 ppm. On average, olivine from the central part of the chondrule contains 0.50 ppm REE with excess of LREE over HREE, in chondrule rim and matrix abundance of REE reduced to 0.15-0.16 ppm. The REE spectra are practically not differentiated.

Fig. 1. The REE spectra in olivine from Buschhof meteorite

References: [1] Obolonskaya E.V., Popova E.E. (2014). Meteorite Chelyabinsk - a year on Earth, 355-363, [2] Sobolev, A.T., Batanova, V.G. (1995). Petrology, 3(5), 440-448.

COSMIC MICROSPHERES AT BOUNDARY OF THE KUNGURIAN STAGE

R.Kh. Sungatullin[1], G.M. Sungatullina[1], Yu.P. Balabanov[1], M.S. Glukhov[1], L.R. Kosareva[1], A.I. Bakhtin[1],
A.V. Gusev[1], D.M. Kuzina[1]
[1]Kazan Federal University, Institute of Geology and Petroleum Technologies, Russia, Kazan, Kremlyevskaya st., 18.
E-mail: Rafael.Sungatullin@kpfu.ru

Introduction: At present, the comparison of different facies sections based on traditional biostratigraphic, lithological, and geochemical methods is very difficult. One of the new additional methods of their correlation is the study of cosmic particles, which in ancient times were deposited on the Earth's surface [1]. Some researchers [2–4] associate with such objects the possibilities of distinguishing event-related stratigraphic levels of a global, regional, and local scale. Our study is devoted to the study of magnetic microspheres from the Mechetlino section, located in the Southern Urals, Russia. This geological section is a candidate GSSP (Global Boundary Stratotype Section and Point) for the lower boundary of the Kungurian Stage (~ 283.5 million years ago) of the International Stratigraphic Time Scale.

Methods: We carried out magnetic separation of 22 samples taken from the sedimentary rocks of the Kungurian-Artinskian boundary of the Mechetlino section (thickness of 20 meters) using a neodymium magnet. Microspheres were studied using a Phoenix V | tome | X S 240 x-ray microtomograph and a Phillips XL-30 electron microscope with an energy dispersive spectrometer. For rocks samples of section, measurements of the volume magnetic susceptibility were carried out using the Bartington MS2 instrument and differential thermomagnetic analysis.

Results: In the Artinskian deposits of the Mechetlino section (16 samples) microspheres were not found, and in Kungurian deposits in the layers 12, 15 and 17 iron oxide (wustite) and intermetallic (Fe-Cr) microspheres were found. The diameter of the particles is 5-300 μm, they have an ideal spherical shape (Fig. 1), a strong metallic luster with a characteristic dendrite and tabular surface. In rare cases, microspheres of native iron were encountered. In addition, a large number of Fe-Cr intermetallic compounds in the form of irregular particles are found in magnetic fraction from Kungurian deposits.

Discussion: According to petromagnetic data, the magnitude of the induced magnetization of rocks varies from 0.13×10^{-3} to 6.08×10^{-3} A/m, and magnetic susceptibility ranges from -0.3×10^{-5} to 8.0×10^{-5} units SI. The content of magnetic minerals is very small, and changes of petromagnetic parameters are not enough for distinguishing different conditions of sedimentation in section. Findings of the microspheres are very useful tool for the dismemberment of this section. The chemical and mineral (wustite, native iron, Fe–Cr intermetallic compounds) composition of the studied objects are close to the microspheres, which appeared during the ablation of meteorites and falling out of cosmic dust [1, 2].

Conclusions: In the future, objects of cosmic origin can significantly increase the accuracy of dismemberment and improve the system of global correlation of geological sections on Earth.

References: [1] Korchagin O.A. 2010. Doklady Earth Sciences, 431, 6: 783-787. [2] Sungatullin R.Kh. et al. 2017. Meteoritics & Planetary Science, 52, Is.: A336. [3] Sungatullin R.Kh. et al. 2017. Russian Geology and Geophysics, 58: 59-69. [4] Sungatullin R.Kh. et al. 2018. Meteoritics & Planetary Science 53: A6291.
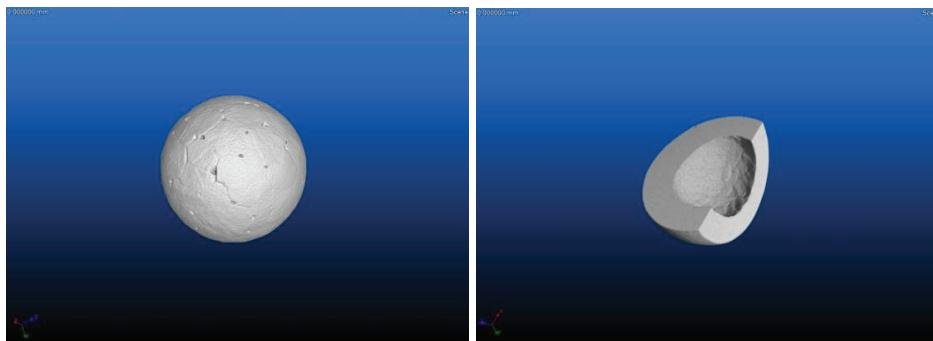

Fig. 1. Tomographic (3D) images of the microsphere. Mechetlino section. Layer 12. Diameter of microsphere 300μm

SPACE EVENTS AND EVOLUTION OF THE CONODONTS

G.M. Sungatullina[1], R.Kh. Sungatullin[1], M.S. Glukhov[1], A.I. Bakhtin[1], A.V. Gusev[1], D.M. Kuzina[1]
[1]Kazan Federal University, Institute of Geology and Petroleum Technologies, Russia, Kazan, Kremlyevskaya st., 18.
E-mail: Guzel.Sungatullina@kpfu.ru

Introduction: Geologists drew attention to cosmic dust particles in connection with the study of degree for cosmic processes influence on biotic events in geological history and the prospects of conducting correlations for different facies stratum. Our study is devoted to the possible influence of cosmic events on the evolution of conodonts - the most important group of fauna for the Paleozoic Era. The object of research is the Usolka section, located in the Southern Urals, Russia. We have previously studied here the distribution of cosmic microsphere [1, 2] from the sediments of the Pennsylvanian Series Carboniferous System (302-310 million years ago). The importance of joint study of cosmic and biotic events is due to the fact that the Usolka section is a candidate of the Global Boundary Stratotype Section and Points (GSSP) of the lower boundary of the Kasimovian and Gzhelian Stages.

Methods: The microparticles were analyzed on the field emission scanning electron microscope "Merlin" Carl Zeiss equipped with an energy-dispersive spectrometer "AZTEC" X-MAX Oxford Instruments and using differential thermomagnetic analysis. Studies of the chemical and isotopic composition of rocks were carried out on the X-ray fluorescence wave dispersion spectrometer S8 Tiger of the company Bruker, isotopic mass spectrometer DeltaVPlus (Thermo Fisher Scientific, Germany) with the prefix FlashHT. All analyzes were performed in laboratories of Kazan Federal University.

Results: In Usolka section, there are negative carbon anomalies ($\delta^{13}C_{V\text{-}PDB}$ = -4 – -9 ‰), positive yttrium anomalies (up to 400 ppm) and a sharp increase in the number of microspheres in separate intervals (Fig. 1).

Discussion: A joint analysis of paleontological data, distribution of chemical elements and magnetic microspheres showed that the intervals of increasing the number of microspheres in the Usolka section coincide with the Stages of renewal of the species composition of conodonts in the Moscovian – Kasimovian boundary and at the base of the Gzhelian Stage.

Conclusions: The development of conodonts is considered for the first time in connection with the amount of space dust entering the Earth. These processes can lead to significant climate changes (cooling, the development of anoxic, lowering the temperature of ocean waters, etc.), which can affect the development of marine organisms. These factors acted simultaneously or closely on a geological time scale.

References: [1] Sungatullin R.Kh. et al. 2017. Meteoritics & Planetary Science, 52, Is.: A336. [2] Sungatullin R.Kh. et al. 2017. Russian Geology and Geophysics, 58: 59-69.
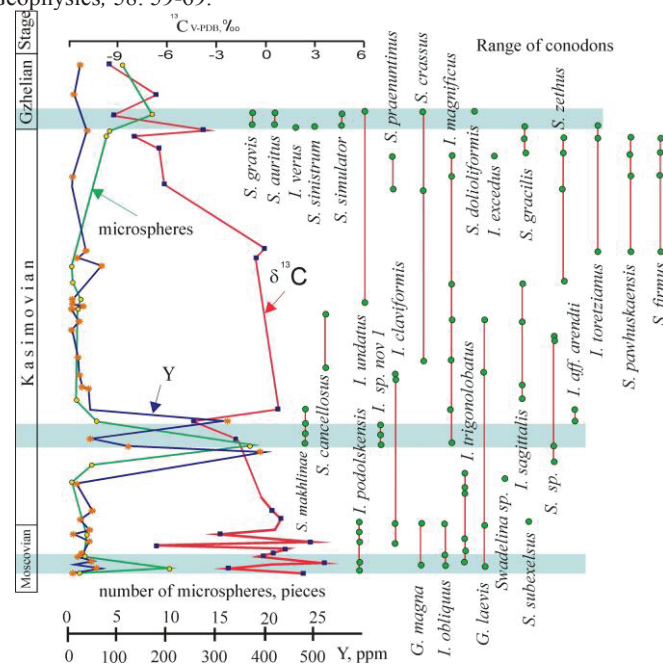
Fig. 1. Distribution of conodonts, geochemical anomalies and cosmic microspheres in the Usolka section

PSEUDOMORPHIC CHONDRULES IN HYDRATED FINE-GRAINED MICROMETEORITES –AND THE IDENTIFICATION OF A NEW HYDRATED PARENT BODY

Suttle, M.D.[1], Folco, L[1], [1] Dipartimento di Scienze della Terra, Università di Pisa, 56126 Pisa, Italy (martindavid.suttle@dst.unipi.it).

Introduction: Hydrated fine-grained micrometeorites are the most abundant subtype of cosmic dust across the entire size range of the flux (50-3000μm)[1,2,3]. They are chondritic particles dominated by Fe-Mg phyllosilicates and may contain as minor components: partially replaced anhydrous silicates (forsterite, enstatite and augite), magnetite, Fe-sulfides and refractory spinels. Despite these significant atmospheric entry overprints, parent body textures are commonly preserved and identifiable[4]. Recently we demonstrated the ability to identify relict coarse-grained components, including pseudomorphic chondrules and altered CAIs. This required that some fine-grained micrometeorites have experienced intense aqueous alteration on their parent bodies[5].

Here we provide the first rigorous statistical analysis of chondrule properties among the fine-grained micrometeorite population. We analyze 42 chondrules within 25 giant (>400μm) micrometeorites using a combination of SEM-BSE, EDX/EMPA and μCT. In addition, we investigate a single micrometeorite (TAM19B-7) containing multiple replaced chondrules in further detail using O-isotope systematics (collected by laser fluorination mass spectrometry at the Open University, UK).

Results: Chondrules in fine-grained micrometeorites are predominantly pseudomorphic (47.6%), with partially altered (11.9%) and unaltered (40.9%) types also identified. They range in size from 24-384μm diameter with a mean average of 148μm and a median average of 130μm. Fine-grained rims are present in just 29% of chondrules and have thicknesses of <107μm and a median average thickness of just 13μm. Among the intact chondrules only POP and PO varieties are recognized.

TAM19B-7: We investigated a single particle (TAM19B-7) further owing to its exceptionally large size (2017μm [avg. diameter]) and the presence of three pseudomorphed, squashed chondrules with notable fine-grained rims. Chondrules in this particle appear to be POP varieties which vary in size from 143-183μm and have homogenous rims (<20μm thick). These chondrules have aspect ratios of 1.1-1.3 (oblate shapes), while the matrix phyllosilicates demonstrate a clear petrofabric, consistent with the direction of chondrule alignment[6]. Bulk triple O-isotope data yielded the following values: $\delta17O=1.094$, $\delta18O=1.126$ and $\Delta17O=0.508$. This particle therefore plots above the terrestrial fractionation line (TFL) and far from the fields of established hydrated chondrite groups (CM, CR, CI), including prominent ungrouped representatives such as C2 Tagish Lake. Although TAM19B-7 is intensely weathered, resulting in partial equilibration with Antarctic water, which lowers its pre-atmospheric $\delta18O$ value, weathering cannot draw the O-isotope signature above the TFL. TAM19B-7, therefore does not appear to be associated with any known hydrated chondrite group.

Discussion: Recognizable chondrules in fine-grained micrometeorites are exclusively small (<400μm). Their average size best matches the CO group (150μm) while values also extend towards the average diameter of CM chondrites (300μm)[7]. Large chondrules, consistent with the average size in CR chondrites (~700μm)[7] are not observed. However, O-isotope and geochemical data have previously identified CM/CR representatives[8,9], therefore, sampling biases and fragmentation dynamics clearly play a significant role removing the largest chondrules, which will instead appear among the flux as coarse-grained micrometeorites.

Despite these effects, this study clearly demonstrates two factors: (1) that fine-grained micrometeorites contain abundant small chondrules, including microchondrule representatives (<40μm diameter) and that (2) where present these chondrules tend to be heavily affected by alteration replacement (in 59.5% of cases). These findings extend the conclusions of our previous study - based on 5 giant micrometeorites[5]. Here we argue, based on a significantly larger population that that much of the fine-grained micrometeorite flux originates from intensely altered C-type asteroids.

In addition, data from TAM19B-7 provides strong evidence that fine-grained micrometeorites sample a range of parent bodies, including those not present among meteorite collections. This new group is characterized by extreme aqueous alteration, equivalent to the C1 petrologic subtype combined with a prominent petrofrabric, implying impact events were the source of heat energy driving aqueous alteration on this asteroid.

References: [1] Taylor et al., 2012 MAPS, doi:10.1111/j.1945-5100.2011.01292.x [2] Badyukov et al., 2018. Geochemistry International, doi:10.1134/S0016702918110022 [3] Cordier and Folco 2014. GCA, doi:10.1016/j.gca.2014.09.038 [4] Suttle, et al., 2017. GCA, doi:10.1016/j.gca.2017.03.002 [5] Suttle et al., 2019. GCA, doi:10.1016/j.gca.2018.11.019. [6] Suttle et al., 2017. MAPS, doi:10.1111/maps.12927 [7] Jones, 2012, MAPS, doi:10.1111/j.1945-5100.2011.01327.x [8] Genge et al., 1997. GCA, doi:10.1016/S0016-7037(97)00308-6 [9] Cordier and Folco, 2014, doi:10.1016/j.gca.2014.09.038

PETROGRAPHIC STUDY OF A COMPACT TYPE A CAI WITH PARTIAL MELTING PROCESS

A. Suzumura[1], Y. Seto[2] and S. Itoh[1], [1] Department of Earth and Planetary Science, Kyoto University. (suzumura.akimasa.83z@st.kyoto-u.ac.jp), [2] Department of Planetology, Kobe University (seto@crystal.kobe-u.ac.jp).

Introduction: Compact type A CAIs (CTAs) are expected to be formed in the earliest stage of the solar nebula and experienced a partial melting at least once (e.g., [1]). Thus, it is important to constrain the formation process of CTAs to understand the thermal processes in the early solar system. But, chemical compositions and isotopic compositions in CTAs, which are important indicators for estimating the formation process, may change due to partial melting. Therefore, it is necessary to interpret chemical compositions and isotopic compositions in consideration of partial melting. However, there are only a few studies referring to the formation processes of CTAs from the perspective of crystal growth in partial melting states (e.g., [2]).

Generally, spinel in CTAs is poikilitically enclosed in melilite or fassaite, and estimated to be an initially crystallized mineral from CAI melt [3]. Namely, spinel in CTAs is expected to preserve valuable information about the thermal histories such as partial melting processes. However, there are few studies of partial melting research focusing on spinel. Since spinel has a high melting point, focusing on spinel is expected to provide new insights on the higher temperature thermal processes. Therefore, we focus on the relationship between spinel grains and the surrounding minerals in CTAs.

Methods: The CTA (KU-N) is included in a polished thin section of Northwest Africa 7865 reduced CV3 carbonaceous chondrite. The preliminary study concluded that they experienced multiple partial melting process. We have undertaken petrographic and mineralogical investigations of the CTA (KU-N-02) focusing on the microtextures resulting from partial melting (local compositional zoning, grain morphology and relationships of crystallographic orientation), using a polarizing microscope, scanning electron microscope (SEM), transmission electron microscope (TEM) and electron back-scattered diffraction (EBSD).

Results & Discussion: In the KU-N-02 CTA, spinel crystals are enclosed in melilite or fassaite. The former (up to 50 μm in size) in melilite is substantially euhedral with rounded edges, while the latter (about 10 - 100 μm in size) in fassaite is almost euhedral with sharp edges.

In interior KU-N-02 CAI, single crystal melilite with spinel inclusions exhibits monotonic decrease of Al and increase of Mg from core to rim. This melilite crystal has a "normal" compositional zoning, whereas the area of about 10 μm wide around the spinel surfaces has Åk-rich composition in comparison. Small Al-Ti-diopside grains occurs as rims on spinel and between spinel grains enclosed in Åk-rich melilite area. By the EBSD analyses, both crystal orientations of Åk-rich melilite and Åk-poor melilite are same. As results, it is difficult to explain how Åk-rich part surrounding spinel in a melilite crystal crystallized by a single stage cooling. Åk-rich melilite part (~10μm) surrounding spinel is crystallized after Åk-poor host single melilite crystal. FIB sections were cut from KU-N-02 to observe the boundaries between spinel and melilite, in order to examine the formation process of Åk-rich melilite with TEM analysis. FIB sections mainly consist of spinel with small Al-Ti-diopside, Åk-rich melilite and perovskite. The grain boundaries in spinel grains show the significant curvature (concave inward), indicating that surfaces on the spinel had experienced partial melting.

Melilite forms eutectic system with both spinel and Al-Ti-diopside. The boundary area between spinel with Al-Ti-diopside and melilite had eutectically melted at a high temperature by some heating process, and then Mg/Al contents had been redistributed to melilite, spinel, and Al-Ti-diopside. This partial melting probably resulted in the unique morphology of the spinel enclosed in melilite and local composition zoning of the melilite. The rounded shape of spinel and Åk-rich zoning surrounding spinel in melilite could be an indicator of partial melting.

References: [1] S. B. Simon et al. (1999) Geochimica et Cosmochimica Acta 63:1233–1248. [2] N. Kawasaki et al., (2017) Geochimica et Cosmochimica Acta 201:83-102. [3] Stolper E. (1982) Geochimica et Cosmochimica Acta 46:2159-2180.

RELATIONSHIP BETWEEN MEAN ATOMIC WEIGHT AND IRON TO SILICON RATIO FOR LUNAR MATERIALS.

M. Szurgot, Lodz University of Technology, Center of Mathematics and Physics, Al. Politechniki 11, 90 924 Lodz, Poland (mszurgot@p.lodz.pl).

Introduction: Mean atomic weight is important to characterize minerals, rocks, planets, moons and asteroids, and is important to classify meteorites. Recenty interrelationships between mean atomic weight *(Amean),* grain density *(dgrain),* and iron to silicon ratio *(Fe/Si)* for planetary materials have been revealed and applied for predicting and verifying mean atomic weight, *Fe/Si* atomic ratio, and grain density of ordinary and enstatite chondrites, Earth, Venus, Mars, Mercury, Vesta, and Moon [1-6]. It has been shown that lunar surface materials have their own *dgrain(Amean)* and *dgrain(Fe/Si)* relationships which can be applied for predicting and verifying grain density of lunar meteorites and Apollo samples [6]. For ordinary chondrites relationship between mean atomic weight and *Fe/Si* atomic ratio has been discovered by Szurgot in 2015 [2].

The aim of the paper was to reveal relationship between mean atomic weight and iron to silicon ratio for lunar surface materials and to predict and verify *Amean* values for lunar meteorites and Apollo samples.

Literature data on chemical composition of lunar meteorites and Apollo samples [7-13] were used to calculate *Amean* and *Fe/Si* values and to establish new *Amean(Fe/Si)* relationship. Various lunar meteorites and Apollo samples representing various groups of lunar crust materials were analyzed.

Results and discussion: Collected data indicate that a new empirical *Amean(Fe/Si) d*ependence describing lunar surface materials can be expressed by the equation:

$$Amean(Fe/Si) = 4.96 \cdot Fe/Si + 21.20, \tag{1}$$

for which $R^2 = 0.98$, and RMSE = 0.16. Equation (1) predicts mean values: for highland crust: *Amean(Fe/Si) =* 21.59 *(Fe/Si* = 0.078), for intermediate crust: *Amean(Fe/Si)* = 22.20 *(Fe/Si* = 0.202), and for mare crust: *Amean(Fe/Si)* = 23.09 *(Fe/Si* = 0.382), and for mean global Moon's crust: *Amean(Fe/Si)* = 21.79 *(Fe/Si* = 0.119 [14]). Bulk composition data [9] indicate average values of mean atomic weight: for highland crust: *Amean* = 21.62, for intermediate crust: *Amean* = 22.13, for mare crust: *Amean* = 23.15, and for global Moon's crust: *Amean* = 21.7 [1,6]. Ranges of *Fe/Si,* and [*Amean(Fe/Si)*] values have been established: for anarthositic group of rocks: 0.01-0.15 [21.2-21.9], for intermediate, basaltic-anarthositic group: 0.15-0.25 [21.9-22.4], for basaltic group: 0.31-0.49 [22.7-23.6], and for global Moon's crust: 0.01-0.49 [21.2-23.6].

For individual lunar meteorites the following *Fe/Si* ratios, and values of *Amean* are predicted by eq. (1): Dhofar 733: *Fe/Si* = 0.057, *Amean(Fe/Si) =* 21.48 *(*21.46), Dar al Gani 400: *Fe/Si* = 0.068, *Amean(Fe/Si)* = 21.54 *(*21.63), Allan Hills A81005: *Fe/Si* = 0.099, *Amean(Fe/Si) =* 21.69 (21.65), Yamato 791197: *Fe/Si* = 0.116, *Amean(Fe/Si) =* 21.78 (21.74), Northwest Africa 4932: *Fe/Si* = 0.155, *Amean(Fe/Si) =* 21.97 (21.83), Calcalong Creek: *Fe/Si* = 0.193, *Amean(Fe/Si) =* 22.16 (22.25), Northwest Africa 773: *Fe/Si* = 0.352, *Amean(Fe/Si) =* 22.95 (22.57), Northwest Africa 4898: *Fe/Si* = 0.314, *Amean(Fe/Si) =* 22.76 (22.82), LaPaz Icefield 02205: *Fe/Si* = 0.362, *Amean(Fe/Si)* = 23.00 (23.18), Northwest Africa 4734: *Fe/Si* = 0.484, *Amean(Fe/Si) =* 23.60 (23.23), Yamato 793169: *Fe/Si* = 0.422, *Amean(Fe/Si) =* 23.29 (23.40), Asuka 881757: *Fe/Si* = 0.422, *Amean(Fe/Si) =* 23.29 (23.41). *Amean* values of lunar materials shown in parentheses were determined by bulk composition [6].

For Apollo returned samples the following values of *Fe/Si* ratio, *Amean(Fe/Si),* and (*Amean)* are predicted: 60025: *Fe/Si* = 0.0094, *Amean(Fe/Si) =* 21.25 (21.41), 15418: *Fe/Si* = 0.116, *Amean(Fe/Si) =* 21.78 (21.77), 14303 (matrix): *Fe/Si* = 0.188, *Amean(Fe/Si) =* 22.13 (21.99), 14321(matrix): *Fe/Si* = 0.199, *Amean(Fe/Si) =* 22.19 (22.14), 15545: *Fe/Si* = 0.417, *Amean(Fe/Si) =* 23.27 (23.01), 12009: *Fe/Si* = 0.392, *Amean(Fe/Si) =* 23.14 (23.10), 15555: *Fe/Si* = 0.423, *Amean(Fe/Si) =* 23.30 (23.23), 12051: *Fe/Si* = 0.373, *Amean(Fe/Si) =* 23.05 (23.25), 12063: *Fe/Si* = 0.408, *Amean(Fe/Si) =* 23.22 (23.33), and 70215: *Fe/Si* = 0.429, *Amean(Fe/Si) =* 23.33 (23.69).

Conclusion: *Amean(Fe/Si)* relationship was revealed for lunar surface materials which can be applied for predicting and verifying mean atomic weight of lunar meteorites and Apollo samples.

References: [1] Szurgot M. (2015) *LPSC 46*, Abstract #1536. [2] Szurgot M. (2015) *Annual Meeting of the Meteoritical Society 78*, Abstract #5013. [3] Szurgot M. (2017) *Annual Meeting of the Meteoritical Society 80*, Abstract #6008. [4] Szurgot M. (2017) *Modern Analytical Methods II*, Abstract #6007. [5] Szurgot M. (2018) *Annual Meeting of the Meteoritical Society 81*, Abstract #6001. [6] Szurgot M. (2019) *LPSC 50*, Abstract #1165. [7] Papike J.J. et al. (1998) *Reviews in Mineralogy* 36:1-234. [8] Korotev R.L. (2005) *Chemie der Erde* 65:297-346. [9] Demidova S.I. et al. (2007) *Petrology* 15:386-407. [10] Taylor S.R. and McLennan S.M. (2009) *Planetary crusts: Their composition, origin,* and evolution, Cambridge. [11] Meyer C. (2008) *Lunar sample compendium.* [12] Righter K. (2010) *Lunar meteorite compendium.* [13] Warren P.H. and Taylor G.J. (2014) *The Moon*, in: *Treatise on Geochemistry* 2:213-250. [14] Kuskov O.L. (1998) *Advanced Mineralogy* 3:39-46.

MEAN ATOMIC WEIGHT AND THERMOPHYSICAL PROPERTIES OF SARIÇIÇEK HOWARDITE.

M. Szurgot[1], R. A. Wach[2], O. Unsalan[3] and C. Altunayar-Unsalan[4], [1]Lodz University of Technology, Center of Mathematics and Physics, Al. Politechniki 11, 90 924 Lodz, Poland (mszurgot@p.lodz.pl), [2]Lodz University of Technology, Institute of Applied Radiation Chemistry, Wróblewskiego 15, 93-590 Lodz, Poland (wach@mitr.p.lodz.pl), [3]Ege University, Faculty of Science, Department of Physics, 35100, Bornova, Izmir, Turkey (physicistozan@gmail.com), [4]Ege University, Central Research Testing and Analysis Laboratory Research and Application Center, 35100, Bornova, Izmir, Turkey (cisemaltunayar@gmail.com).

Introduction: Mean atomic weight and thermophysical properties are important to characterize minerals, rocks, planets, moons and asteroids, and are important to classify meteorites. Recenty interrelationships between mean atomic weight *(Amean)*, grain density*,* and iron to silicon ratio for planetary materials were revealed and applied for predicting and verifying mean atomic weight, *Fe/Si* atomic ratio, and grain density of ordinary and enstatite chondrites, Earth, Venus, Mars, Mercury, Moon, and Vesta [1-5]. The aim of the paper was to determine mean atomic weight and to predict heat capacity, thermal conductivity, and thermal diffusivity of Sariçiçek howardite. Sariçiçek meteorite fell on September 2, 2015 in Turkey, and have been classified as an eucrite-rich howardite [6].

Literature data on chemical composition of Sariçiçek howardite [6] and composition of various HED meteorites [7] were used to calculate *Amean* and *Fe/Si* values and to establish *Amean(Fe/Si)* relationship for howardites. Relationship between specific heat and bulk density (*Cp(dbulk)*) [8] was used to predict specific heat capacity, and relationship between thermal conductivity and porosity (*K(porosity)*) [9] was used to predict *K* values.

Results and discussion: Collected data indicate that there exists empirical *Amean(Fe/Si) d*ependence describing howardite matter expressed by the equation:

$$Amean(Fe/Si) = 7.67 \cdot Fe/Si + 20.08, \tag{1}$$

for which $R^2 = 0.74$, and RMSE = 0.14. Iron to silicon atomic ratio for the Sariçiçek *Fe/Si* = 0.30 ± 0.01 is close to the mean value of *Fe/Si* for howardites (0.33, range: 0.26-0.39). Equation (1) predicts for Sariçiçek *Amean(Fe/Si)* = 22.37 ± 0.14 ≈ 22.4 ± 0.1, and predicts the average value for howardites *Amean(Fe/Si)Howardites* = 22.61 ± 0.14 ≈ 22.6 ± 0.1. Equation (1) predicts for Frankfort (stone) howardite *Amean(Fe/Si)* value: 22.22 ± 0.14 ≈ 22.2 ± 0.1 (*Fe/Si* = 0.28), and bulk composition of this howardite reveals the value: *Amean* = 22.2 [7].

Bulk elemental composition [6] leads to *Amean* = 22.56 ± 0.13 ≈ 22.6 ± 0.1 for the Sariçiçek meteorite, and bulk elemental composition of seventy howardites [7] to the average value of *Amean* = 22.4 ± 0.2, and to the *Amean* range: 22.0 - 22.8 [7] for most howardites. Diogenites bulk composition reveals *Amean* range: 21.4-22.3, and average *Amean* = 21.8, and eucrites bulk composition reveals *Amean* range: 22.1-23.3, and average *Amean* = 22.7 [7]. Average *Amean* values follow the inequality:

$$AmeanDiogenites(21.8){<}AmeanHowardites(22.4){<}AmeanSariçiçek\mathbf{(}22.6){<}AmeanEucrites(22.7). \tag{2}$$

Presented data confirm classification of Sariçiçek as an eucrite-rich howardite [6]. These new *Amean* data for HED meteorites and protoplanet Vesta indicate that: *AmeanHEDs(21.8-22.7) < AmeanVESTA(24.2* [2]), which supports the presence and contribution of metallic core to the global mean atomic weight of Vesta [2].

Cp(dbulk) dependence [8] leads to the value of specific heat capacity of Sariçiçek: *Cp* = 756 J(/kg·K) at room temperature (300 K) (*dbulk* = 2.91 g/cm^3 [6]). The volumetric heat capacity of Sariçiçek *Cvolumetric* = 2.2·10^6 J/(m^3·K) at RT, and is close to RT value characteristic of stony meteorites: 2.5·10^6 J/(m^3·K) [8]. Mean atomic heat (*Amean·Cp*) of Sariçiçek is: 17.0±0.2 kJ/(mol·K) at room temperature.

Thermal conductivity of Sariçiçek predicted by *K(Porosity)* dependence [9] (*P* = 9.4±0.9% [6]) is equal to: 1.1±0.2 W m^{-1} K^{-1} at 200 K, and estimated by *K(T)* dependence: 1.3±0.2 W m^{-1}K^{-1} at 300 K. For comparison: thermal conductivity measured for Frankfort (stone) howardite: 1.3 W m^{-1}K^{-1} at 200 K, and 1.6 W m^{-1}K^{-1} at 300 K [10]. Thermal diffusivity of Sariçiçek predicted by *D(Cp,K,dbulk)* dependence is 0.6±0.2·10^{-6} m^2/s at 300 K, and 0.8±0.2·10^{-6} m^2/s at 200 K.

Conclusion: Mean atomic weight of Sariçiçek meteorite confirms its classification as an eucrite-rich howardite.

References: [1] Szurgot M. (2015) *LPSC 46*, Abstract #1536. [2] Szurgot M. (2015) *Comparative Tectonics and Geodynamics*, Abstract #5001. [3] Szurgot M. (2016) *Annual Meeting of the Meteoritical Society 79*, Abstract #6005. [4] Szurgot M. (2019) *Acta Societatis Metheoriticae Polonorum* 10:140-159. [5] Szurgot M. (2019) *LPSC 50*, Abstract #1165. [6] Unsalan O. et al. (2019) *Meteoritics & Planetary Science* doi: 10.1111/maps.13258. [7] Beck A. W. et al. (2015) *Meteoritics & Planetary Science* 50:1311–1337. [8] Szurgot M. (2011) *LPSC 42*, Abstract #1150. [9] Flynn G. J. et al. (2018) *Chemie der Erde* 78:269-298. [10] Opeil C. P. et. al. (2012) *Meteoritics & Planetary Science* 47:319–329.

SPATIAL DISTRIBUTION OF ALUMINUM MONOXIDE MOLECULES IN A HIGH MASS PROTOSTAR CANDIDATE ORION SOURCE I.

S. Tachibana[1,2], T. Kamizuka[3], T. Hirota[4,5], N. Sakai[6], Y. Oya[7], A. Takigawa[8], and S. Yamamoto[7]
[1]UTokyo Organization for Planetary and Space Science, The University of Tokyo, 7-3-1 Hongo, Tokyo 113-0033, Japan (tachi@eps.s.u-tokyo.ac.jp), [2]Institute of Space and Astronautical Science, JAXA, [3]Institute of Astronomy, The University of Tokyo, [4]Mizusawa VLBI Observatory, National Astronomical Observatory of Japan, [5]Department of Astronomical Sciences, SOKENDAI (The Graduate University for Advanced Studies), [6]RIKEN Cluster for Pioneering Research (CPR), [7]Department of Physics, The University of Tokyo, [8]The Hakubi Center for Advanced Research/Division of Earth and Planetary Sciences, Kyoto University.

Introduction: Aluminum monoxide (AlO) is a refractory molecule that can be present as vapor at high temperature. It is a key molecule to form most refractory solids and could thus be a good tracer of kinematics in high-temperature regions around young stellar objects (YSOs). In extended atmospheres of oxygen-rich AGB stars, AlO forms aluminum oxide including corundum (α-Al_2O_3) as the first dust [e.g., 1–3]. The spatial distribution of AlO around an evolved star was observed by ALMA [4]. In circumstellar environments around YSOs, AlO can form refractory minerals within Ca- and Al-rich inclusions (CAIs) in chondrites. The chemistry, mineralogy, and petrology of CAIs strongly suggest their high-temperature origin in the very early stage of disk evolution, but it has been under debate where and how CAIs formed in the early Solar System. The observation of AlO around YSOs should provide a new insight into the formation of refractory components in the early Solar System. There has been no definitive detection of AlO in the star forming regions except for tentative detection of AlO emissions at 229.7 and 344.4 GHz in Orion Source I, a candidate of high-mass YSO in the Orion Kleimann-Low (KL) region [5]. In this study, we analyzed the ALMA observation data for Orion Source I to search for AlO molecules [6].

Data Reduction: The ALMA observation data of Orion Source I obtained in Cycle 1 (2012.1.00123.S) and Cycle 2 projects (2013.1.00048.S) were used in this study. The Band 8 data in the Cycle 2 observation and the Band 9 data in the Cycle 1 observation were used for investigating AlO emissions at 497 and 650 GHz, respectively. The data were reduced following the procedure described in [7]. The reduction was processed with the Common Astronomy Software Applications (CASA) software.

Results: We found broad emission features at 497 and 650 GHz, consistent with AlO (N=13–12 and 17–16) lines with hyperfine structures. The peaks at 497 and 650 GHz can be well reproduced with the line-of-sight velocities of 3.6 ± 0.3 and 4.6 ± 0.1 km s^{-1} and the velocity widths (FWHM) of 24.1 ± 0.9 and 20.0 ± 0.4 km s^{-1} for the Gaussian dispersion, respectively. The obtained line-of-sight velocities are consistent with those of other molecules (e.g., SO, SO_2, SiS, SiO, H_2O, and alkali halides) observed for Orion Source I [e.g., 5, 7]. The integrated flux maps of the two emission features show that they are localized in the launching point of outflow from the circumstellar rotating disk of Orion Source I.

Discussion: The upper state energies of AlO lines at 497 and 650 GHz are ~167 and ~281 K, respectively. Detection of AlO emissions is expected in the wide range of the outflow from the disk if it is in the gas phase. However, the distribution of AlO is limited to the base of the rotating outflow from the disk, which indicates that AlO molecules are not present in the gas phase most likely due to its refractory nature. Aluminum monoxide may thus not be present in the gas phase in the expanding outflow due to recondensation of refractory dust as discussed for alkali halides [5], while SiO molecules sublimated from silicate dust are present in the gas phase in the outflow [7]. The hot nature of the disk around the embedded massive protostar suggests that CAI-like solid objects enriched in refractory elements could form in the disk. Further observations of high-temperature metal-bearing gas molecules in the disk around YSOs could link the high-temperature CAI formation event occurred in the early Solar System to the star formation and subsequent planetary formation processes.

References: [1] Takigawa A. et al. (2014) *Geochim. Cosmochim. Acta* 124:309–327. [2] Takigawa A. et al. (2015) *Astrophys. J. Suppl.* 218:2 (16 pp). [3] Takigawa A. et al. (2018) *Astrophys. J. Lett.* 862, L13 (6 pp). [4] Takigawa A. et al. (2017) *Science Advances* 3:eaao2149 (5 pp). [5] Ginsburg A. et al. (2019) *Astrophys. J.* 872:54 (16 pp). [6] Tachibana S. et al. (2019) *Astrophys. J. Lett.* 875:L29 (4 pp). [7] Hirota T. et al. (2017) *Nature Astronomy* 1:0146 (5 pp).

HIGH-TEMPERATURE HYDROTHERMAL ALTERATION RECORDED IN A DARK INCLUSION IN THE NWA 2900 CK CARBONACEOUS CHONDRITE

M. Takahashi[1], T. Nakamura[1], T. Shibuya[2], and M. E. Zolensky[3],
[1]Department of Earth Science, Graduate School of Science, Tohoku University, Sendai, Miyagi 980-8578, JAPAN, (miki.takahashi.p4@dc.tohoku.ac.jp), [2]Japan Agency for Marine-Earth Science and Technology (JAMSTEC), Yokohama, Kanagawa 236-0001, JAPAN, [3]Astromaterials Research and Exploration Science, NASA Johnson Space Center, Houston, TX 77058, USA.

Introduction: Dark inclusions are rock fragments with low visible reflectance and have mineralogical and petrological features different from the host meteorites. They show a variety of mineralogy and petrology: some contain chondrules [e. g., 1-3], while the others have no chondrules [e. g., 4, 5]. The former shows mineralogy similar to hydrous carbonaceous chondrites such as the CM type. The latter consists entirely of fine-grained materials with/without chondrules that are complete replacement by phyllosilicates. In this study, we performed a mineralogical study of a dark inclusion in the NWA 2900 CK3.5-3.7 carbonaceous chondrite and found many large diopside veins in the inclusion. Such large veins have not been previously reported from any carbonaceous chondrite. We constrained the formation temperature of the dark inclusion thermodynamically, based on the mineralogy and the bulk chemical composition of the inclusion.

Results: The dark inclusion is 1.0×2.5 cm in size and consists mainly of dark and fine-grained material (typically <20µm but occasionally 100µm in grain size). It does not contain chondrules, but contains many bright veins. The fine-grained material consists mainly of olivine ($Fa_{34.8\pm0.52}$), magnetite, plagioclase ($Ab_{63.6\pm7.1}$, $An_{35.8\pm7.3}$), Cr spinel crystals, and a small amount of tiny pentlandite. On the other hand, the bright veins (~1cm long and ~100µm width) cross-cut an entire region of the dark inclusion, connecting with other veins, forming a network structure. Besides the long veins, many small veinlets (~100µm long) also occur. The veins and veinlets consist mainly of crystalline diopside with high Wo contents (Wo>40), some variations of Mg/(Mg+Fe+Ca) ratio (51.9>En>31.1), and low concentrations of minor elements such as Al, Na, Mn, Cr, and Ti. The relative abundance of the major five minerals, normalized to 100wt%, in the dark inclusion, is estimated to be olivine 61.8wt%, diopside 16.8wt% magnetite 14.8wt%, plagioclase 4.0wt%, and spinel 2.6wt%.

Discussion: The diopside compositional features, such as high Wo and En contents, and low minor-element concentrations and the absence of phyllosilicate in the inclusion are consistent with a high-temperature hydrothermal origin of the dark inclusion and the diopside veins [e. g., 6-10]. Within the veins, thin and long drain-like structures of Fe-bearing diopside are present within Mg-rich diopside, suggesting step-by-step formation of the veins during cooling of the high temperature fluids. The dark inclusion is embedded in an unbrecciated host CK chondrite, which suggests that the inclusion accreted in the early solar nebula together with chondrules and CAIs to form the CK chondrite parent asteroid. Since the diopside veins occur only in the dark inclusion and terminate at its edge, it is probable that the dark inclusion was formed by high-temperature aqueous alteration in a different (previous) asteroid, excavated by a subsequent impact, and later arrived to the accreting, host CK parent asteroid.

Thermodynamic calculations were performed with conditions that a rock with the bulk chemical composition of the dark inclusion equilibrated with water at various temperatures up to 900°C and water/rock ratios of 0.25, 1, 2.6, and 4 (oxygen mol). The equilibrated mineral combination and the relative mineral abundance were obtained and then compared with those of the dark inclusion. The results indicate that the dark inclusion formed at a temperature higher than 800°C. No carbonaceous chondrites are known to have experienced aqueous alteration at such a high temperature. Assuming that the heat source was ^{26}Al, the dark-inclusion is likely to have formed before chondrule formation. The timing of formation depends on the water/rock ratio (water-rich asteroids are difficult to heat and thus are required to form earlier). Because water-free asteroids need have formed at 2.2 Myr after CAIs to reach the peak temperature of 800°C [11], the dark inclusion must have formed before this time. This early formation date is consistent with the observation that chondrules are absent in the dark inclusion and that the host CK chondrite is an accretionary breccia.

References: [1] Weisberg and Prinz, 1998. *Meteoritics & Planetary Science* 33:1087-1099. [2] Tomeoka and Kojima, 1998. *Meteoritics & Planetary Science* 33:519-525. [3] Greenwood et al. 2015. *LPSC 2015* :2975. [4] Kojima and Tomeoka, 1993. *Meteoritics & Planetary Science* 28:649- 658. [5] Zolensky et al. 2003. *Meteoritics & Planetary Science* 38:305–322. [6] Bird et al. 1984. *Economic Geology* 79:671-965. [7] Manning and Bird, 1986. *Contrib Mineral Petrol* 92:437-447. [8] Robinson et al. 2002. *Proceedings of the Ocean Drilling Program, Scientific Results* 176. [9] Python et al. 2007. *EPSL* 255:289-305. [10]Alt et al. 2010. *Geochemistry Geophysics Geosystems* 11:1525-2027. [11] Wakita et al. 2014. *Meteoritics & Planetary Science* 49:228-236.

ANALYTICAL DEVELOPMENT OF UNDERIVATIZED AMINO ACIDS AND SHORT-CHAIN PEPTIDE MOLECULES

Y. Takano, S. Furota, N. O. Ogawa, and N. Ohkouchi,
Japan Agency Marine-Earth Science & Technology (JAMSTEC)
(*E-mail: takano@jamstec.go.jp*)

Introduction: The chromatographic separations of short-chain peptide molecules are basically two ways; one is gas chromatographic separation with an appropriate derivatization procedure to form volatile chemical formula, the other is a liquid chromatographic separation with or without a derivatization procedure. Among those we chemical procedure, it is important to care about the natural hydrolysis as a potential artifact. Dipeptides are the smallest peptides consisting of two amino acids, hence, for example theoretically 400 dipeptides are possible combinations in the protein type amino acids. In addition, we should take into consideration including non-protein type amin acid combination in the natural samples.

For further evaluation of the original molecular information through an accurate analytical procedure, we have developed the method as underivatized short-chain peptide formula, likewise a analytical process of amino acids [1,2]. For the chromatographic separation of underivatized dipeptides, we used an improved method using an ion-pairing liquid chromatography / electrospray ionization mass spectrometry (LC/ESI-MS) and/or a corona charged aerosol detector system (LC/CAD). The advantage of determination of underivatized formulas are high-through put and high-recovery of the analytical procedure without derivatization.

Analytical development: At first, we confirmed the baseline resolution with the correlations between amino compounds and aliphatic elongations (Fig.1) ; the extracted ion chromatogram showed the baseline resolution of underivatized dipeptide molecules on LC/ESI-MS (as $[M+H]^+$ on positive mode). For C_3-carbon skelton of primary AAs, α-alanyl-X and β-alanyl-X dimer combinations (*e.g.,* α-alanylglycine, α-alanylalanine, and α-alanylvaline in α-alanyl-series) are potentially abundant alanyl series dipeptides. We also observed the chromatographic separation of cyclic anhydrite dimers (e.g., glycylclycine anhydrite, alanylalanine anhydrite) and some oligo-peptide molecules in the present method.

Secondly, the pretreatment prior to LC/ESI-MS is important to assure the analytical accuracy. To eliminate the inorganic and organic matrix effect on the practical analysis, we also validated the purification procedure for dipeptide fraction using the cation-exchange chromatography ([3]; *cf.* nitrogen isotopic fractionation through the wet procedure, *i.e.,* $\Delta^{15}N_{amino\ acids} = \delta^{15}N_{before} - \delta^{15}N_{before} = \sim 0$ ‰). The recovery of dipeptide isolation showed better than 95.0 ± 3.5 % (ave., $n = 10$) using the mix solution of Glycyl-X series (*i.e.,* -Gly, -Ser, -Pro, -Glu, -Leu, -Met, -His, -Arg, -Phe, -Trp, as model compounds). Therefore, the present method is applicable to the sample of complex organic molecules containing aliphatic, cyclic, heterocyclic amino- /imino- structures [4,5]. This work was partly supported by a Grant-in-Aid for Scientific Research on Innovative Areas (No. 25108006) from the JSPS grant.
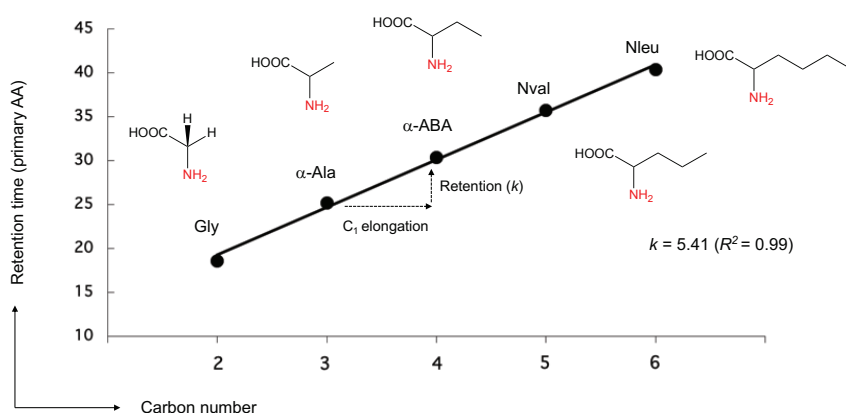

Figure 1. Retention factor on the LC for primary amino acid monomers with the carbon elongation, e.g., neutral AA series of glycine (C_2), α-alanine (C_3), α-aminobutyric acid (C_4), norvaline (C_5), norleucine (C_6).

References: [1] Takano Y. *et al.* (2015) *International Journal of Mass Spectrometry,* 379, 16-25. [2] Furota S. et al. (2018) *Journal of Chromatography B*, 1095, 191-197. [3] Takano Y. *et al.* (2010) *Rapid Communications in Mass Spectrometry*, 24, 2317-2323. [4] Oba Y. *et al.* (2016) *Astrophysical Journal Letters,* 827, L18.; Oba, Y. *et al.,* (2019) Detection of nucleobases and dipeptides in organic residues formed by photochemical reactions in interstellar ice analogs. *Goldschmidt 2019* abstract. [5] Naraoka *et al.* (2019) *JpGU 2019*, abstract #PPS03-P14.

Ar-Ar, I-Xe ages and shock textures of Northwest Africa 2139 LL6 chondrite: Implications for shock history of LL chondrite parent body

A. Takenouchi[1,2], H. Sumino[2], K. Shimodate[2], K. Nagao[2] and A. Yamaguchi[1] [1]National Institute of Polar Research (NIPR) (10-3, Midori-cho, Tachikawa, Tokyo, Japan. email: takenouchi.atsushi@nipr.ac.jp), [2]The University of Tokyo (3-8-1, Komaba, Meguro-ku, Tokyo, Japan).

Introduction: Since collisional records in meteorites reflect ancient asteroidal movement, we expect to describe asteroidal moving histories by revealing how and when collisional events occurred. Relations between shock features and pressure-temperature-time (P-T-t) path have been investigated from the 1960s [e.g., 1]. Shock chronology commonly adopted Ar-Ar technique because a high diffusion rate of Ar easily leads to lose radiogenic Ar during moderate shock heating [e.g., 2]. However, the number of studies combining detailed shock petrology and chronology is still limited [3-6]. Therefore, we need to conduct shock petrological-chronological studies on various types of meteorites. In this study, we reported both shock features and chronological data of the Northwest Africa (NWA) 2139 LL6 chondrite and discussed collisional histories of the ordinary chondrite parent body(ies).

Sample and Methods: NWA 2139 consists of two portions, visually light and dark parts. We prepared two thin sections from each portion for petrological observation by FE-SEM (JEOL JSM-7100F). Noble gases were analyzed using a noble gas mass spectrometer (modified-VG3600) [7]. For Ar-Ar and I-Xe analysis, aliquots from each portion were irradiated by neutron at the Institute for Integrated Radiation and Nuclear Science, Kyoto University. The Hb3gr hornblende and synthesized CaF_2 and K_2SO_4 were simultaneously irradiated to monitor neutron flux and correct neutron-produced Ar interferences, respectively [8]. The Shallowater (aubrite) was also irradiated as an anchor of I-Xe age (4562.7±0.3 Ma) [9].

Results: Light portion is mainly composed of chemically homogeneous olivine, orthopyroxene, Fe-Ni metal, troilite and a small amount of albite. We cannot readily recognize chondrules and matrices indicating high-degree of thermal metamorphism. Constituent minerals such as albite, commonly show wavy extinction (not vitrified). Two types of shock veins were observed; one is thick (~400 μm) cataclastic vein containing fragments of mineral and matrices. The matrices display a fine-grained (~3 μm) granular texture accompanied by voids along grain boundaries. The fragments and surrounding minerals contain healed cracks. The other vein is thin (<10 μm) and composed of finer-grained or glassy matrices without voids. These thin veins sharply cut the other thick ones. Dark portion consists of fine-grained olivine-pyroxene fragments with scattered Fe-Ni metal and troilite, resulting from a brecciating process. Thin shock veins are texturally similar to the thin one in the light portion and cut the brecciated regions. Albite in dark parts also shows wavy extinction. We cannot find any high-pressure phases so far in this meteorite.

In Ar-Ar analysis, we cannot define "plateau ages" in neither light nor dark portions. In particular, Ar-Ar spectra from the dark portion are highly disturbed showing unrealistically old ages, which may be caused by recoil effect due to fine-grained (brecciated) texture. In the light portion, each Ar fraction indicates gas retention ages of 3.8-4.4 Ga. I-Xe analysis results in 4515.9±11.7 Ma and 4494.9±8.5 Ma for light and dark portions, respectively.

Discussion: Petrological observation revealed that the light portion in NWA 2139 experienced at least two shock events. The first and second shock events induced the thick and thin veins, respectively. The first shock may be intense and reset the I-Xe age at 4515.9±11.7 Ma. After the first shock, thermal modification by post-shock heating may have occurred, which resulted in healing cracks, annealing vein matrices and possibly devitrifying maskelynite. The Ar-Ar ages in high-temperature fractions (~4.4 Ga) may record this thermal event. The second shock occurred at 3.8 Ga or later inducing partial or no resetting of Ar-Ar ages. Brecciation may have happened between the thermal modification and the second shock event because both light and dark portions showed similar thin veins overwritten on brecciated texture and dark portion contains mineral fragments with healed cracks within less annealed matrices. This study indicates that the thermal modification after intense shock event may occur in the early stage of the LL chondrite parent body(ies) as pointed out by [6]. Since such thermal activity may erase shock features of hypervelocity impact, high-pressure phases could not survive even if they formed by the initial shock event at around 4.5 Ga. Since L chondrite which experienced a severe shock at ~0.5 Ga [3, 5, 10] commonly contains high-pressure phases indicating weak modification by post-shock heating, collisional conditions, such as impactor/target size ratios, should be different between early and late stage shock events on ordinary chondrite parent bodies.

References:
[1]. Stöffler D. et al. (2018) *Meteoritics & Planetary Science*, 53, 5-49. [2] Bogard D. D. (2011) *Chem. der Erde*, 71, 207-226. [3] Bogard D. D. (1995) *GCA*, 59, 1383-1399. [4] Weirich J. R. et al. (2011) *Meteoritics & Planetary Science*, 45, 1868-1888. [5] Metzler K. et al. (2011) *Meteoritics & Planetary Science*, 46, 652-680. [6] Rubin A. *GCA*, 68, 673-689. [7] Ebisawa N. et al. (2004) *J. Mass Spectrom. Soc. Jpn., 52*, 219-229. [8] Roddick J. C. (1983) *GCA*, *47*, 887-898. [9] Gilmour J. D. and Crowther S. A. (2017) *Geochemical Journal*, 51, 69-80. [10] Swindle T. D. et al. (2014) *Geological Society of London*, 378, 333-347.

H^+ ION IRRADIATION EXPERIMENTS OF ENSTATITE: SPACE WEATHERING BY SOLAR WIND.

A. Takigawa[1,2], Y. Asada[1], Y. Nakauchi[3], T. Matsumoto[4], A. Tsuchiyama[5,6], M. Abe[3], N. Watanabe[7] [1] Division of Earth and Planetary Sciences, Kyoto University (takigawa@kueps.kyoto-u.ac.jp), [2]The Hakubi Center for Advanced Research, Kyoto University, [3]Institute of Space and Astronautical Science, Japan Aerospace Exploration Agency, [4]Faculty of Arts and Science, Kyushu University, [5]Research Organization of Science and Technology, Ritsumeikan University, [6]Gunazhou Institute of Geochemistry, [7]Institute of Low Temperature Science, Hokkaido University.

Introduction: Space weathering occurred on air-less bodies such as asteroids is caused by micrometeorite bombardment and irradiation of solar wind and/or cosmic ray [1-3]. The analysis of the regolith particles returned from an S-type asteroid Itokawa shows evidences of the space weathering on Itokawa, such as vesicle structures (blisters) in partially amorphous layers called space-weathered rims [4-6]. It has been proposed that the blisters and space-weathered rims might have formed mainly by solar wind irradiation rather than by micrometeorite bombardment [4].

The solar wind consists of typically 1 keV H^+ ions (95.41 %) and 4 keV He^{++} ions (4.57 %) [7]. Irradiation experiments of 1 keV H^+ ions and 4 keV He^+ ions to minerals consisting of the Itokawa regolith are important in order to evaluate the influence of solar-wind irradiation on the formation of blisters and space-weathered rims on the Itokawa regolith. Many irradiation experiments of 4 keV He^+ ions have been already performed [e.g., 8], but the structural changes by irradiation of 1 keV H^+ ions have been poorly understood. In this study, we performed irradiation experiments of 1 keV H^+ to orthoenstatite, which are the major minerals consisting of ordinary chondrites.

Experiments: As targets for irradiation experiments, we prepared rectangular samples of orthoenstatite (En_{99}, Tanzania). The sample size is 3 mm x 5 mm x 0.5 mm. We mechanically polished (until 0.25 μm roughness) and performed the chemical polishing with colloidal silica to remove the damage layer of the surface.The low-energy ion irradiation equipment developed in ISAS/JAXA was used in the experiments. The polished enstatite samples were irradiated with 1 keV H^+ ions with dose of 10^{16}, 10^{17}, 3×10^{17}, and 10^{18} ions/cm^2. The surface structures of irradiated samples were observed with an FE-SEM (JEOL JSM 7001F). Focused ion beam (FIB) lift-out sections were prepared with an FE-FIB (FEI Helios NanoLab 3G CX) and observed with a field-emission transmission electron microscope (FE-TEM; JEOL JEM 2100F).

Results and discussion: No change of the surface structure was observed on the irradiated enstatite with dose of 10^{16} ions/cm^2. Blisters of 60–110 nm in diameter and partially amorphous layers of ~30 nm in thickness were observed on the surface of the enstatite samples irradiated with dose of higher than 10^{17} ions/cm^2. This indicates that the threshold dose of blistering and amorphization is ~0.5×10^{17} ions/cm^2. The blisters grew with dose from 1×10^{17} to 3×10^{17} ions/cm^2 but shrank after irradiation of 10^{18} ions/cm^2. The blister size change with dose may be caused by change of the crystal structure due to ion implantation.The implanted hydrogen diffuses within the enstatite and the internal gas pressure increases to form blisters [9]. Further irradiation destroyed the crystal structure, increased the diffusion rate of a hydrogen gas, and reduced the retention of gas.

The thickness of the amorphous layer of the irradiated enstatite is less than Itokawa enstatite particles (30–60 nm). The thicker amorphous layers on the Itokawa particles may be due to deeper implantation depth of 4 keV He^+ ions than 1 keV H^+ ions [4,10]. The blisters formed by irradiaton with dose of 10^{18} ions/cm^2 locate immediately beneath the surface, and their size is tens nm (Fig. 1), which are clearly different from irradiated enstatite by higher energy hydrogen ions [10] and very similar to Itokawa particles [4-6]. These results indicate that the blisters on the surface of Itokawa particles mainly formed by implantation of the solar wind 1 keV H^+ ions, whereas the thickness of the amorphous layer is explained by irradiation of the solar wind 4 keV He^{++} ions.

Fig. 1: TEM image of an irradiated enstatite surface (10^{18} ions/cm^2). Arrows indicate bubbles/blisters near the surface.

References: [1] Pieters C. T. et al. (2000) *MAPS* **35**, 1101. [2] Hapke B. (2001) *J. Geophys. Res.* **106**, 10039. [3] Clark B. E. et al. (2002) in *Asteroid Space Weathering and Regolith Evolution, Asteroids III*., 585. [4] Noguchi T. et al. (2014) *MAPS*. 49, 188-214. [5] Matsumoto T. et al. (2015) *Icarus* 257, 230-238. [6] Matsumoto T. et al. (2016) *GCA*. **187,** 195. [7] Reisenfeld D. B. et al. (2007) *Space Sci.* **130**, 79. [8] Demyk K. et al. (2001) *A&A* **368**, L38. [9] Muto, S. and Enomoto, N. (2005) *Materials trans.* **46**, 2117. [10] Uchida H. et al. (2017) *JpGU*, abstract PPS10-01. [11] Ziegler J. F. et al. (2008) *The stopping and range of ions in matters*.
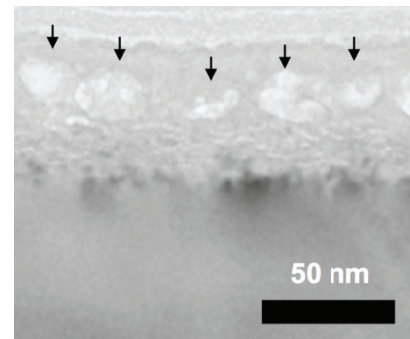
FORMATION OF METASTABLE ALUMINA DUST AROUND AGB STARS: CONDENSATION EXPERIMENTS USING INDUCTION THERMAL PLASMA SYSTEMS.

A. Takigawa[1,2], T.-H. Kim[3], Y. Igami[4], T. Umemoto[1], A. Tsuchiyama[5,6], C. Koike[7], J. Matsuno[1], T. Watabnabe[8] [1]Division of Earth and Planetary Sci., Kyoto Univ. (takigawa@kueps.kyoto-u.ac.jp), [2]The Hakubi Center for Advanced Research, Kyoto Univ., [3]Inst. Nuclear Science and Technology, Jeju National Univ., [4]Inst. Materials and Systems for Sustainability, Nagoya Univ., [5]Research Organization of Science and Technology, Ritsumeikan Univ., [6]Gunazhou Inst. Geochemistry, [7]Dept. Physics, Ritsumeikan Univ., [8]Dept. Chemical Engineering, Kyushu Univ.

Introduction: Presolar grains identified in primitive meteorites and cometary dust are survivals of the circumstellar dust of evolved stars formed prior to the birth of the solar system. Mid-infrared spectroscopic observations of evolved stars provide complementary information on circumstellar dust. Many of oxygen-rich asymptotic giant branch (AGB) stars display a broad dust feature at ~11–12 μm [1]. Chemically synthesized amorphous alumina (Al_2O_3) is widely accepted as the source of this emission, whereas few presolar amorphous alumina was reported previously [2]. Moreover, it is not obvious that amorphous alumina can condense in circumstellar conditions. There are more than eight transition aluminas, which are metastable alumina phases with different crystal structures, other than the stable phase of Al_2O_3, corundum (α-alumina). Even from gases undergoing very high cooling, metastable transition alumina, rather than amorphous alumina, might condense [3, 4]. Alumina that forms under strong disequilibrium might contain other abundant elements in their structures, such as Mg or Si.

Experiments: An induction thermal plasma (ITP) system provides ultrahigh-temperature plasma to vaporize refractory materials and a high cooling rate for gases with a sharp temperature gradient where nanoparticles condense [5]. We performed condensation experiments of Al–Si–O, Al–Si–Mg–O, and Mg–Al–O gases using ITP systems. The crystal structures of the condensed particles are examined with X-ray powder diffraction (XRD; Rigaku SmartLab) and a field-emission transmission electron microscope (FE-TEM; JEOL JEM-2100F). Their MIR spectra are then measured with a Fourier transform infrared spectroscopy (FT-IR; JASCO MFT-680 and Thermo Nicolet iS5) and compared with the dust emission of the alumina-rich star T Cephei [6].

Results and discussion: The condensed nanoparticles from the Al and O gases were neither amorphous nor corundum but transition aluminas based on face centered cubic (fcc) packed oxygen (δ- and λ-alumina, and an unknown phase; Fig. 1). Sharp peaks of their FT-IR spectra are not observed from circumstellar dust. The fcc oxygen frameworks were maintained in many of the condensed alumina grains containing small amounts of Mg and Si. Condensates from Al-rich gases containing a few percent of Mg had δ- and γ-alumina structures. The condensed transition alumina containing ~10% Si had λ- and γ-alumina structures and showed similar MIR spectral shapes to the observed dust emission from alumina-rich AGB stars (Fig. 2). Based on the present results, it is reasonable that the source of 11–12 μm broad emission of alumina-rich stars is not amorphous alumina but is transition alumina containing ~10% Si.

No presolar transition alumina grain containing Si was reported previously. This is probably because of the sample selection for isotopic analysis. Most of the presolar alumina were identified from acid residues of meteorites [e.g., 2, 7-9]. Corundum is acid resistant but amorphous and transition alumina are easily dissolved into HF and $HClO_4$ [9]. Even if presolar metastable alumina were present in primitive meteorites, they had been lost during acid processing, which also explains the rarity of amorphous presolar alumina. Careful studies both on the chemical composition and crystal structure of individual presolar alumina grains without chemical treatment and prior to the destructive isotopic measurements are needed to conclude the presence of presolar Si-containing transition alumina grains in chondrites.
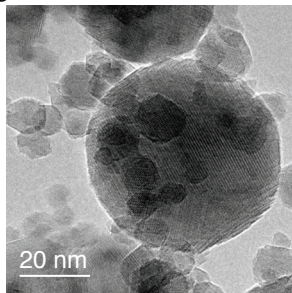

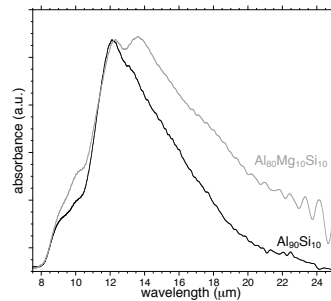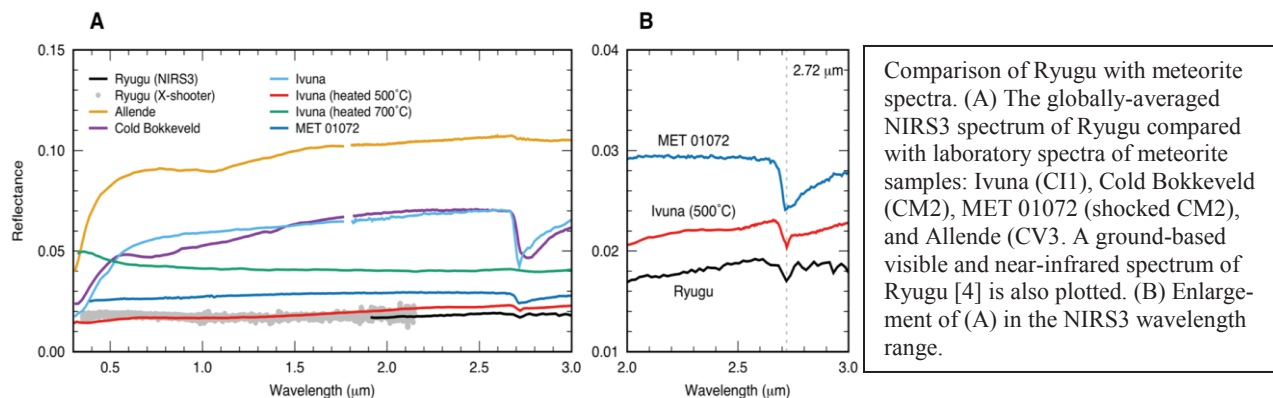Fig. 1: TEM image of condensed δ-alumina (Al_2O_3 composition).

Fig. 2: FT-IR spectra of condensed alumina containing ~10% of Si. Gray and black curves compare the difference in Al:Mg:Si ratio.

References: [1] Sloan, G. C. et al. (2003), *ApJS*, **147**, 379. [2] Stroud, R. M. et al. (2004), *Science*, **305**, 1455. [3] Tavakoli, A. H. et al. (2013), J. *Phy. Chem. C*, **117**, 17123. [4] Ishizuka, S. et al. (2016), *Chemistry of Materials*, **28**, 8732. [5] Shigeta, M., & Watanabe, T. (2011), *Journal of Materials Research*, **20**, 2801. [6] Takigawa A. et al. (2019) *ApJL*, under revision. [7] Choi, B. 1998, *Science*, **282**, 1284. [8] Nittler, L. et al. (1994), *Nature*, **370**, 443. [9] Takigawa, A. et al. (2014), *GCA*, **124**, 309.

SPECTRAL CHARACTERISTICS OF ASTEROID (162173) RYUGU WITH HAYABUSA2 NIRS3

D. Takir[1] (driss.takir@nasa.gov), K. Kitazato[2], R. E. Milliken[3], T. Iwata[4,5], M. Abe[4,5], M. Ohtake[4,5], S. Matsuura[6], T. Arai[7], Y. Nakauchi[4], T. Nakamura[8], M. Matsuoka[4], H. Senshu[9], N. Hirata[2], T. Hiroi[3], C. Pilorget[10], R. Brunetto[10], F. Poulet[10], L. Riu[4], J.-P. Bibring[10], D. L. Domingue[11], F. Vilas[11], M. A. Barucci[12], D. Perna[12,11], E. Palomba[14], A. Galiano[14], K. Tsumura[8,15], T. Osawa[16], M. Komatsu[5], A. Nakato[4], T. Arai[9], N. Takato[17,5], T. Matsunaga[18], Y. Takagi[19], K. Matsumoto[16,5], T. Kouyama[20], Y. Yokota[4,21], E. Tatsumi[22], N. Sakatani[4], Y. Yamamoto[4,5], T. Okada[4,22], S. Sugita[22], R. Honda[21], T. Morota[23], S. Kameda[24], H. Sawada[4], C. Honda[2], M. Yamada[9], H. Suzuki[25], K. Yoshioka[22], M. Hayakawa[4], K. Ogawa[26], Y. Cho[22], K. Shirai[4], Y. Shimaki[4], N. Hirata[26], A. Yamaguchi[27,4], N. Ogawa[4], F. Terui[4], T. Yamaguchi[28], Y. Takei[4], T. Saiki[4], S. Nakazawa[4], S. Tanaka[4,5], M. Yoshikawa[4,5], S. Watanabe[23,4], Y. Tsuda[4,5]. [1]Jacobs, Astromaterials Research and Exploration Science, NASA Johnson Space Center, Houston, TX, USA. [2]The University of Aizu, Fukushima, Japan. [3]Brown University, Providence, RI, USA. [4]Institute of Space and Astronautical Science (ISAS), Japan Aerospace Exploration Agency (JAXA), Sagamihara, Japan. [5]The Graduate University for Advanced Studies (SOKENDAI), Kanagawa, Japan. [6]Kwansei Gakuin University, Hyogo, Japan.[7]Ashikaga University, Tochigi, Japan. [8]Tohoku University, Sendai, Japan. [9]Chiba Institute of Technology, Chiba, Japan. [10]Institut d'Astrophysique Spatial, Université Paris-Sud, Orsay, France.[11]Planetary Science Institute, Tucson, AZ, USA. [12]Laboratoire d'Etudes Spatiales et d'Instrumentation en Astrophysique (LESIA), Observatoire de Paris, Meudon, France. [13]Osservatorio Astronomico di Roma, Istituto Nazionale di Astrofisica (INAF), Monte Porzio Catone, Italy. [14]Istituto di Astrofisica e Planetologia Spaziali, INAF, Roma, Italy. [15]Tokyo City University, Tokyo, Japan. [16]Japan Atomic Energy Agency, Ibaraki, Japan. [17]National Astronomical Observatory of Japan, Tokyo, Japan. [18]National Institute for Environmental Studies, Ibaraki, Japan. [19]Aichi Toho University, Nagoya, Japan. [20]National Institute of Advanced Industrial Science and Technology, Tokyo, Japan. [21]Kochi University, Kochi, Japan. [22]The University of Tokyo, Tokyo, Japan. [23]Nagoya University, Nagoya, Japan. [24]Rikkyo University, Tokyo, Japan. [25]Meiji University, Tokyo, Japan. [26]Kobe University, Kobe, Japan. [27]National Institute of Polar Research, Tokyo, Japan. [28]Mitsubishi Electric Corporation, Kanagawa, Japan.

The Japanese Aerospace Exploration Agency (JAXA) spacecraft and sample return mission Hayabusa2 has arrived at the near-Earth asteroid 162173 Ryugu, which is classified a primitive carbonaceous object [1]. Here we report recent results of near-infrared spectrometer (NIRS3) on the Hayabusa2 spacecraft. NIRS3 is a point spectrometer with a 0.1° FOV that acquire continuous point target spectra over effective wavelength range 1.9-3.2 µm [2]. These observations provide direct measurements of the surface composition of Ryugu and context for the returned samples. NIRS3 has detected a weak and narrow absorption feature centered at 2.72 µm across entire observed surface. This absorption feature is attributed to the presence of hydroxyl (OH)-bearing minerals [3]. The NIRS3 observations also revealed that Ryugu is the darkest object to be observed up-close by a visiting spacecraft. The intensity of the OH feature and low albedo are consistent with thermally-and/or shock-metamorphosed, and/or carbon-rich space-weathered primitive and hydrated carbonaceous chondrites [3].

Comparison of Ryugu with meteorite spectra. (A) The globally-averaged NIRS3 spectrum of Ryugu compared with laboratory spectra of meteorite samples: Ivuna (CI1), Cold Bokkeveld (CM2), MET 01072 (shocked CM2), and Allende (CV3. A ground-based visible and near-infrared spectrum of Ryugu [4] is also plotted. (B) Enlargement of (A) in the NIRS3 wavelength range.

References: [1] Watanable S. et al. 2019. *Science* 10.1126/science.aav8032 (2019). [2] Iwata T. et al. 2017. *Space Sci. Rev.* 208, 317–337. [3] Kitazato et al. 2019. *Science* 10.1126/science.aav7432 (2019). [4] Perna D. et al. 2017. Astron. Astrophys. 599, L1.

DEVELOPMENT OF U-PB SIMS ANALYSIS OF APATITE IN ORDINARY CHONDRITES

M. Telus[1], A. T. Hertwig[2], and M.-C. Liu[2] [1]University of California Santa Cruz (1156 High St, Santa Cruz, CA 95064), [2]University of California Los Angeles (595 Charles Young Drive E. Los Angeles, CA 90095).

Introduction: Chronological constraints on the evolution of ordinary chondrite parent bodies are primarily derived from bulk U-Pb analyses of phosphates, such as apatite and whitlockite. Bulk analyses require a significant portion of a meteorite to be crushed before apatite grains can be separated out and analyzed for their ages; therefore, only ~10 H chondrites have been analyzed for their ages using bulk techniques [e.g., 1], despite these samples being crucial for our understanding of chondrite parent bodies [e.g., 2]. We seek to significantly increase the number of U-Pb age constraints for ordinary chondrites by further developing *in situ* U-Pb techniques for analyzing individual phosphate grains within polished slices of meteorites. Although *in situ* analysis is associated with larger analytical uncertainties (>10 Ma) than the bulk methods (± 0.1 Ma), it allows for preservation of the petrographic context of each grain. *In situ* U-Pb analyses have been performed for dating terrestrial apatites by laser ablation ICP-MS [e.g., 3, 4] and SIMS [e.g., 5, 6], but only a few *in situ* analyses of chondrite apatite have been reported so far [7]. Here, we present our current ion microprobe analysis protocol, preliminary results, and plans for the future method development.

Samples: A suite of terrestrial apatite standards from McClure Mountain (MMAP, ~524 Ma, [4]), Durango (DUR, ~32 Ma, [4]) and Madagascar apatite (MAD, ~487 Ma, [4]) were mounted in epoxy alongside the apatite samples separated from LL5/6 Cherokee Springs (~4540 Ma, [8]). The samples were cleaned with soapy DI water and methanol and oven dried prior to gold coating.

SIMS Technique: *In situ* analyses of U-Pb systematics were carried out using the Cameca IMS-1290 ion microprobe at UCLA. The primary O_2^- beam (~ 3 nA) produced by a Hyperion-II RF oxygen ion source [9] rastered over the sample surface (25×25 μm^2) for 90 s to clean the analysis area before data collection. Data acquisition was done using a smaller 15×15 μm^2 raster square. The mass resolving power was set to ~7500 (10% peak height) to resolve interferences from REE oxides. Secondary $^{40}Ca_2P^{16}O_4^+$, $^{204}Pb^+$, $^{206}Pb^+$, $^{207}Pb^+$, $^{208}Pb^+$, $^{232}Th^+$, $^{238}U^+$, $^{238}U^{16}O^+$, and $^{238}U^{16}O_2^+$ ions were collected over 20 cycles using the axial electron multiplier in mono-collection mode, and the total analysis time for one measurement was ~50 min. Before each analysis, magnetic field centering was performed by referencing all the Pb peaks to $^{40}Ca_2P^{16}O_4^+$ and U-related peaks to $^{232}Th^+$.

Data analyses: After correcting for the deadtime in the counting system, raw isotope ratios were determined by dividing the mean count rates of the respective isotopes. At this point, uncertainties in the ratios are estimated based on counting statistics. For the terrestrial standards, we apply a ^{207}Pb-based common lead correction scheme. MMAP analyses were used to calibrate the relative sensitivity factor (RSF) of Pb/U using raw UO^+/U^+. Due to the preliminary nature of error analysis, we report an unweighted mean of the $^{206}Pb/^{238}U$ dates of a sample; the spread in dates is shown as 1SD.

Results: Our *in situ* U-Pb analyses of terrestrial apatite yield dates consistent with those determined from the bulk and LA ICP-MS measurements. Using MMAP as our calibration standard, we obtain 508 Ma ± 15 Ma (n=23) and 32 Ma ± 3 Ma (n=3) for Madagascar apatite and Durango apatite, respectively; within uncertainties, these values are consistent with 486.58 ± 0.85 Ma (ID-TIMS U-Pb, 95% conf, [4]) and 32.2 ± 5.3 Ma (LA ICP-MS, concordia age, 2s, [4]). Apatite analyses of LL5/6 Cherokee Springs are uncorrected for non-radiogenic lead, because of unknown isotopic composition of the common lead component. $^{206}Pb/^{238}U$ dates of 9 analyses range from ~3-5 Ga, which is consistent with the distribution derived from bulk U-Pb analyses [8].

Discussion: SIMS U-Pb ages of apatite in chondrites can be improved by (1) identifying terrestrial standards that cover a broader range in UO^+/U^+ for a more accurate RSF calibration; (2) constraining the common Pb for each sample, possibly by analyzing appropriate minerals in each sample; (3) reducing surface contamination, which may be more difficult with thin sections compared to mineral separates. Although uncertainties in SIMS U-Pb ages are significantly larger than for bulk analyses, this technique deserves more attention as it has the potential to provide constraints on samples that may be out of reach for bulk analyses due to low quantities of material (e.g., from sample return missions).

References:
[1] Gopel C. et al. (1994) *Earth and Planetary Science Letters 121*, 153–171. [2] Trieloff M. et al. (2003) *Nature 422*, 502–506. [3] Chew, D.M. et al. (2011) *Chemical Geology 280*, 200–216. [4] Thomson S.N. et al. (2012) *G³ 13,* Q0AA21. [5] Sano, Y. et al. (1999) *Chemical Geology 153*, 249–258. [6] Terada, K. & Sano, Y. (2003) *Applied Surface Science 203–204*, 810–813. [7] Terada, K. & Sano, Y. (2002) *Geophysical Research Letters 29*. [8] Edwards G., et al., *in preparation*. [9] Liu M.-C. et al. (2018) *International Journal of Mass Spectrometry 424*, 1-9.

DEVELOPMENT ON NON-DESTRUCTIVE MUONIC X-RAY ANALYSIS OF CARBONACEOUS CHONDRITES: FEASIBILITY TEST FOR RETURNED SAMPLES FROM C-TYPE ASTEROIDS.

K. Terada[1], A. Sato[1], K. Ninomiya[1], Y. Kawashima[1], K. Shimomura[1,2], D. Tomono[1], Y. Kawai[1], T. Osawa[3] and S. Tachibana[4], [1]Osaka University (include full mailing address and terada@ess.sci.osaka-u.ac.jp), [2]High Energy Accelerator Research Organization, [3]Japan Atomic Energy Agency and [4]The University of Tokyo.

Introduction: The muon is a lepton with a mass of 105.7 MeV/c^2, approximately 200 times heavier than the electron. So far, electron-induced characteristic X-ray analysis has been widely used to determine chemical compositions of materials in Earth and Planetary Science. In recent years, analysis of characteristic X-rays from muonic atoms, in which a muon is captured, has attracted attention because both a muon beam and a muon-induced characteristic X-ray have high transmission abilities, of which energies are about 200 times higher (e.g., muonic carbon-Kα is 75keV, whereas electron-induced carbon-Kα is 0.3 keV). From these features, a muonic X-ray analysis has great advantages in several ways; (1) non-destructive elemental analysis from light to heavy elements, (2) depth profile analysis, (3) isotopic measurement for heavy elements and (4) investigation of chemical condition (redox-state). Such a non-destructive muonic X-ray analysis has a great potential to characterize precious extraterrestrial samples returned by spacecraft such as Hayabusa2 and OSIRIS-REx in 2020's, before the sophisticated "destructive" analysis such as combustion, acid decomposition, polish, and sputtering so on.

Results and Discussion: We carried out the depth profile analysis of the four-layered sample that consists of SiO$_2$, C (graphite), BN (boron nitride) and SiO$_2$ using the D2 beam line at J-PARC MUSE. The negative muon beam was collimated to approximately 2.7 cm diameter and focus on the 50 mm × 75 mm × 4 mm sample that was oriented at 45 degree to the beam. Changing the Muon's momentum from 32.5 to 57.5 MeV/c, the generated high energy X-rays were measured by two Ge detectors. We also measured the Muonic X-rays from the Allende and Muchison meteorites. We also detected significant Mg and Fe signals from powered Murchison meteorite sealed in glass tube of which thickness is 1 mm.

Following our successful detection of muonic X-ray spectra from carbonaceous chondrites with intense pulsed Muon beam at J-PARC [1], we have developed on muonic X-ray analysis at the MuSIC (MuSIC; MUon Science Innovative Channel at Osaka University), and obtained the fundamental data for quantitative analysis of planetary materials. Using one of the world-leading intense direct current muon beam source, we successfully detected characteristic muonic X-rays of Mg, Si, Fe, O, S and C from Jbilet Winselwan CM chondrite, of which carbon content is about 2 wt%, and the obtained elemental abundance pattern was consistent with that of CM chondrites [2]. We also checked Muon irradiation damage of pellets of mixed organic chemical reagents (alanine, glucose, paraformaldehyde, phenanthrene, and stearic acid) after 3–12 hour exposure to check the irradiation damage, and confirmed that they do not show any systematic changes with either the exposure time or the depth, and are not different from those of non-exposed samples within the variation of initial reagent mixtures. We also performed the muonic X-ray analysis of terrestrial PbS (Galena) for Pb isotopes measurement [3] and iron meteorite to check the feasibility of chemical condition (redox-state) measurement. At the conference, we will report on our recent progress of muonic X-ray analysis and discuss on a future prospect for applications for Earth and planetary science.

References:
[1] Terada K. et al. (2014) *Sci. Rep.* 4: 5072. [2] Terada K. et al. (2017) *Sci. Rep.* 7: 15478. [3] Ninomiya K. et al. (2019) J Radioanal Nucl Chem. https://doi.org/10.1007/s10967-019-06506-9

KREEP and Mg-suite investigations through Northwest Africa 6950

M.M. Thiemens*,[1,2], P. Sprung[1,3], V. Debaille[2], and C. Münker[1], *Maxwellmt@gmail.com, [1]University of Cologne, Germany, [2]Laboratoire G-Time, Université Libre de Bruxelles, Brussels, Belgium, [3]Paul Scherrer Institute (PSI), Switzerland .

Introduction: The Moon represents a convenient, relatively pristine source of information on planetary formation. The model of lunar formation is derived from the limited samples we have available, wherein the Moon accretes from the residue of an impact (or impacts) with the early Earth [1]. The formation of KREEP, the incompatible residue from the crystallizing Moon, provides a timeline for the ending of solidifaction. The KREEP-rich Apollo samples cluster in age around 3.8 ± 0.1 Ga, a potential consequence of the proximity of their sample sites.

Meteorites avoid this sampling bias. The Northwest Africa (NWA) 773 family of meteorites (which includes NWA 6950, 2977, 2700, 2727, and 3333) comprise rare lunar gabbros and bear geochemical signatures akin to KREEP but distinctly less trace element enriched at extremely low Ti contents. Of this family, NWA 6950 is a magnesian gabbro bearing veins of shock-induced melt [2].

This study: A sample of NWA 6950 was crushed, and minerals density separated and picked for purity, in order to avoid the shock melt. Samples were analyzed on the University of Cologne's Neptune plus. Creating a Lu-Hf isochron from the picked mineral separates, we find an age of 3.103 ± 0.039 Ga which significantly overlaps with the baddeleyite ^{207}Pb-^{206}Pb age of 3.108 ± 0.020 Ga for NWA 6950 reported by [2], from which we infer the Lu-Hf age to represent a pristine crystallization age. The initial εHf of NWA 6950 (-12.46 ± 0.64) can now greatly expand a perfectly defined array in εHf vs. age space of older KREEP-rich breccias [3] and KREEP-basalts [4] to much younger ages. In contrast, Mg-suite samples, i.e., some of the earliest magmatic lunar rocks, plot above this array. This implies that Mg-suite samples represent a different mantle source(s) than KREEP-dominated rocks, whose source gave rise to magmatism for well over 1 Gyr and which might have been established within the first 50 Myrs of the solar system, consistent with recent Hf-W evidence [5].

References: (1) Snyder *et al.* GCA 56, 3809-3823 (1992) (2) Shaulis *et al.* (2017) GCA 213, 435-456, (3) Sprung *et al.* (2013) EPSL 380, 77-87, (4) Gaffney and Borg (2014) GCA 140, 227-240, (5) Thiemens *et al.*, under review

INVESTIGATING THE EFFECTS OF SIMULATED MICROMETEORITE IMPACTS ON A CARBONACEOUS CHONDRITE THROUGH COORDINATED ANALYSIS.

M. S. Thompson[1], M. J. Loeffler[2], R. V. Morris[3], S. J. Clemett[4], D. Trang[5], L. P. Keller[3], R. Christoffersen[4], and D. G. Agresti[6]. [1]Department of Earth, Atmospheric, and Planetary Sciences, Purdue University, West Lafayette, IN 47907, mthompson@purdue.edu, [2]Department of Physics and Astronomy, Northern Arizona University, Flagstaff, AZ 86011, [3]ARES, NASA Johnson Space Center, Houston, TX 77058, [4]Jacobs, NASA Johnson Space Center, Houston, TX 77058, [5]Hawai'i Institute of Geophysics and Planetology, University of Hawai'i at Mānoa, Honolulu, HI 96822, [6]University of Alabama at Birmingham, Department of Physics, Birmingham, AL 35294

Introduction: Space weathering modifies the surfaces of airless bodies via micrometeorite impacts and solar wind irradiation. Together, these processes alter the microstructure, chemical composition, and reflectance properties of surface material [1]. While considerable work has been done to understand the effects of space weathering on lunar and ordinary chondritic materials, e.g., [2,3], there are fewer constraints on how hydrated, organic-rich materials respond to these processes. With ongoing sample return missions OSIRIS-REx and Hayabusa2 to carbonaceous asteroids Bennu and Ryugu, respectively, it is important to understand how space weathering affects surface materials on these asteroids, especially in the context of early results, e.g., [4,5]. In advance of sample return, we can investigate the effects of space weathering on carbonaceous materials by performing experiments in the laboratory, e.g., [6,7]. Here we present coordinated analytical results of pulsed laser irradiation experiments designed to simulate the progressive space weathering of a carbonaceous chondrite by micrometeorite impact processes.

Samples and Methods: We rastered an Nd-YAG pulsed laser (λ=1064 nm, ~6 ns pulse duration, energy 48 mJ/pulse) over the surface of three dry-cut rock chips of the CM2 Murchison meteorite, 1x, 3x, and 5x, respectively. We collected reflectance spectra from both the raw and irradiated regions over the wavelength range of 0.35-2.5 µm using an ASD FieldSpec 3 Spectrometer. We analyzed organic functional group chemistry using the µL^{2}MS instrument at Johnson Space Center (JSC). We prepared electron-transparent thin sections of multiple phases from the meteorite using the FEI Quanta 3D focused ion beam (FIB) for analysis in the JEOL 2500 transmission electron microscope (TEM) at JSC. Finally, we used a radiative transfer model to investigate the spectral effects of submicroscopic Fe-bearing nanoparticles embedded in and on silicate grains, enabling us to correlate microstructural and chemical features observed in the irradiated samples to measured reflectance data.

Results and Discussion: Spectral analyses show that the irradiated regions are darker and bluer than the raw material, but become progressively brighter with each laser raster. We see the progressive weakening of most absorption features with irradiation, e.g., the 0.7 µm feature associated with phyllosilicates. Organic spectral maps spanning the raw and irradiated regions of the 1x and 5x lasered samples both show an increase in the concentration of aromatic species in the surface (Fig. 1). Results from the TEM analyses of sulfide, olivine, and matrix phases reveal the presence of amorphous surface layers consistent with melting and vaporization processes and abundant nanoparticles (5-50 nm in size) of varying compositions. High resolution TEM and energy dispersive x-ray spectroscopy (EDS) chemical maps indicate the nanoparticle compositions include metallic Fe, Fe_3O_4 (magnetite), Fe-S (troilite), and Fe-Ni-sulfide (pentlandite). The results of our radiative transfer models predict that nanophase (<40 nm) magnetite particles enclosed in silicate hosts cause overall samples darkening, with the effect becoming more pronounced for microphase (>40 nm) particles. Both nano- and micro-phase magnetite nanoparticles cause bluing of the reflectance spectrum. Similarly, both nano- and microphase inclusions of troilite cause darkening, but nanophase troilite causes reddening, whereas microphase particles cause bluing.

These results demonstrate the complexity of space weathering on carbonaceous surfaces. Our radiative transfer modeling shows that particle size and composition play a significant role in the observed spectral effects. Evolving populations of these particles offers an explanation for the inconsistency in spectral results among laboratory experiments. The development of nanophase magnetite may be relevant to the detection of this phase on Bennu [4].

Figure 1: µL^{2}MS maps of the raw and irradiated regions of the 1x lasered sample. The color bar represents organic concentration from low (blue) to high (red).

References: [1] Pieters C.M. and Noble S.K. (2016) J. Geophys. Res-Planet. 121: 1865-1884. [2] Keller L.P. and McKay D.S. (1993) Science, 261, 1305-1307. [3] Noguchi T. et al. (2011) Science 333: 1121-1125. [4] Lauretta, D.S. et al. (2019) *Nature*. [5] Kitazato, K., et al. (2019) Science 364: 272-275. [6] Matsuoka M. et al. (2015) Icarus 254: 135-143. [7] Gillis-Davis J.J. et al. (2017) Icarus 286: 1-14.
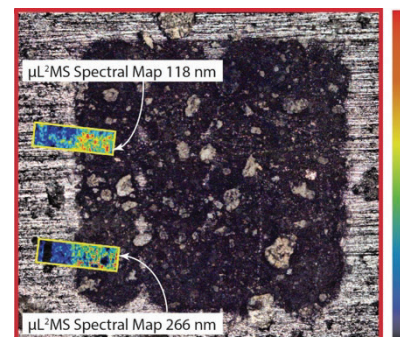
HYDROGEN MOBILITY DURING SHOCK DEFORMATION IN OLIVINE

J. Tielke[1,2], A.H. Peslier[3], R. Christoffersen[3], T. Erickson[3], M.J. Cintala[2], R.V. Morris[2], R. Montes[3], and C.J. Cline[3], [1]Lunar and Planetary Institute, 3600 Bay Area Blvd, Houston, TX 77058, USA, jacob.a.tielke@nasa.gov, [2]ARES, Mail Code XI3, NASA-Johnson Space Center, Houston, TX 77058, USA, [3]Jacobs, NASA Johnson Space Center (JSC), Mail Code XI3, Houston, TX 77058, USA.

Introduction: Understanding how shock modifies the storage and transport of hydrogen in minerals is central to understanding the evolution of water in the solar system. During shock, crystals are exposed to extreme stress, pressure, and temperature conditions, resulting in the development of a range of defects [1]. Importantly, shock results in an increase in line-defects (dislocations) in crystals [2], which may act as short-circuit diffusive pathways for hydrogen [3]. Enhanced diffusion rates and modification of hydrogen content resulting from increased dislocation densities during shock may complicate interpretations of hydrogen concentrations and isotopic measurements in meteorites and other planetary samples. To investigate the influence of shock on hydrogen mobility, we carried out a series of shock experiments on olivine, which is one of the most common minerals found in the solar system.

Methods: Olivine single crystals were oriented, cored, and sliced parallel to the (010) plane into discs 6.35 mm in diameter and 0.8 mm thick. Some of the olivine discs were dehydrated prior to shock by heating at 1300°C in a one-atmosphere gas-mixing furnace with oxygen fugacity controlled at the FMQ buffer. The olivine discs were shocked under vacuum conditions in tungsten alloy capsules at peak pressures ranging from 22 to 42 GPa in a flat plate accelerator (Figure 1a) at the Experimental Impact Laboratory at NASA's Johnson Space Center. The crystals were analyzed prior to and after shock using Fourier Transform Infrared Spectroscopy (FTIR), Electron Backscatter Diffraction (EBSD), Electron-probe microanalyses (EPMA), Mössbauer spectroscopy, and Raman spectroscopy.

Results: FTIR analyses of the olivine discs prior to and after shock reveal absorbance peaks at wavenumbers indicative of the presence of OH incorporated into the crystal lattice. Prior to impact, the olivine discs contained 60 to 100 ppm H_2O by weight, with the largest concentration in the center of the discs and the lowest at the edges, providing a chemical potential gradient for hydrogen diffusion during shock. Extensive fracturing is observed in the shocked crystals (Figure 1b). Post-shock FTIR analyses of dehydrated olivine reveal no detectable OH absorbance, indicating that no atmospheric water was added during shock. Post-shock FTIR analyses for natural olivine reveal minor variation in the position of peaks of OH-stretching bands compared to those of the starting material. EBSD analyses reveal the development of orientation gradients in the shocked crystals and that the density of geometrically necessary dislocations (GNDs) increases systematically with shock pressure but is independent of hydrogen content.

Discussion: The results presented above are consistent with a small influence of shock on the diffusivity of hydrogen in olivine for the studied conditions. Calculations of diffusion distances of hydrogen in olivine that incorporate published hydrogen diffusion coefficients [4, 5, 6] for olivine with the measured density of GNDs reveal that pipe-diffusion is the dominant hydrogen diffusion process during shock. However, diffusion distances of hydrogen during shock experiments are less than 5 μm. Therefore, large olivine crystals are likely to retain their original hydrogen content during shock over the investigated range of conditions, but minor migration of hydrogen is evidenced by changes in the observed position of absorbance peaks associated with intrinsic H in the FTIR spectra.

References: [1] Stöffler et al. (1988) in *Meteorites and the Early Solar System* 165-202. [2] Ashworth & Barber (1975) EPSL *27*, 43-50. [3] Tien et al. (1976) *Metallurgical Transactions A* 7.6 821-829. [4] Mackwell & Kohlstedt (1990) *JGR Solid Earth* 95 5079-5088. [5] Demouchy & Mackwell (2006) *PCM* 33.5 347-355. [6] Demouchy (2010) *EPSL* 295 305-313.
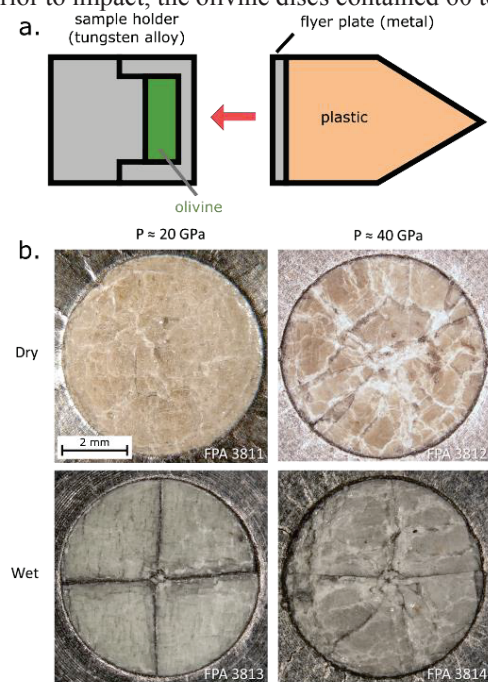

Figure 1: a. Simplified diagram (not to scale) illustrating the geometry of shock experiments using the flat plate accelerator. Shock is induced by the impact of the flyer plate on the capsule containing the olivine crystal. b. Optical micrographs of shocked olivine crystals in this study.

TOPOTAXIAL INTERGROWTHS OF EPSILON-(MG,FE)$_2$SIO$_4$ IN WADSLEYITE AND RINGWOODITE IN SHOCKED CHONDRITES.

N. Tomioka[1], T. Okuchi[2], M. Miyahara[3], T. Iitaka[4], N. Purevjav[2], R. Tani[1,3] and Y. Kodama[5], [1]Kochi Institute for Core Sample Research, JAMSTEC (200 Monobe Otsu, Nankoku, Kochi 783-8502, Japan, email: tomioka@jamstec.go.jp), [2]Institute for Planetary Materials, Okayama University (827 Yamada, Misasa, Tottori 682-0193, Japan), [3]Department of Earth and Planetary Systems Science, Graduate School of Science, Hiroshima University (Kagami-yama 1-3-1, Higashihiroshima, Hiroshima 739-8526, Japan), [4]Computational Engineering Applications Unit, RIKEN ISC (2-1 Hirosawa, Wako, Saitama 351-0198, Japan), [5]Marine Works Japan (3-54-1, Oppamahigasi, Yokosuka 237-0063, Japan)

Introduction: Phase equilibria studies have demonstrated that olivine transforms into a spinelloid phase (wadsleyite) and then into a spinel phase (ringwoodite) with increasing pressure. Natural ringwoodite and wadsleyite were first discovered in heavily shocked ordinary chondrites [1, 2]. The defect structures in these olivine polymorphs were repeatedly characterized by transmission electron microscopy [e.g. 3–4]. Based on occurrences of stacking faults in these phases, shear-promoted diffusionless mechanisms were proposed in transformations among olivine, wadsleyite, and ringwoodite [4]. The transformation models also predicted the possible occurrence of an intermediate phase, named 'ε-phase', exhibiting the smallest unit cell among all spinel/spinelloid structures [4]. Although the ε-phase had been discovered neither in high-pressure syntheses products nor in natural samples, we recently found the phase in ringwoodite grains in the shocked chondrite Tenham [5]. In the present study, we present further characterization of the ε-phase based on transmission electron microscopy of meteoritic samples and the first principles calculations.

Experimental methods: Polished thin sections of Tenham (L6) and Miami chondrites (H5) were used in the present study. Aggregates of ringwoodite and wadsleyite in shock veins were extracted and processed into thin foils by Ar-ion milling (Gatan DuoMill model 600) and focused ion milling (Hitachi SMI-4050). The thin foil samples were examined using a transmission electron microscope (JEOL JEM-ARM200F). Crystal structure and stability of the ε-phase were evaluated by the first principles calculations based on the initial model of the ε-phase proposed by previous topological study [4]. The first-principles calculations were performed with *Quantum Espresso* codes [6] based on plane wave basis set, pseudopotentials, and a generalized gradient approximation [7] of density functional theory.

Results and Discussion: Tenham and Miami chondrites have shock veins containing the host rock olivine fragments that partially or totally transformed into its high-pressure phases. In Tenham, we examined submicron-sized ringwoodite grains occurring as polycrystalline aggregates in shock veins. These ringwoodite grains are crystallographically randomly oriented and exhibit pervasive planar defects on {110}. Despite the typical microtexture [4], the detailed analysis of the respective grains revealed novel crystallographical features. SAED patterns from most of the ringwoodite grains show weak extra diffraction spots corresponding to a new spinelloid structure theoretically predicted as 'ε-phase' in Mg$_2$SiO$_4$ [4]. In addition, the SAED patterns of ringwoodite with ε-phase lamellae show that both phases have a topotaxial relationship: a_ε, b_ε//$<110>_{Rwd}$ and c_ε//c_{Rwd}. In Miami, wadsleyite also shows a similar occurrence to ringwoodite in Tenham. Many of the wadsleyite grains exhibit planar defects on (010). The wadsleyite with the ε-phase lamellae shows the following topotaxy: a_ε//a_{Wds}, b_ε//b_{Wds}, and c_ε//c_{Wds}. The first principle calculations clarified all the atomic positions in the ε-phase structure is slightly displaced along c-axis from those in the ideal one. All the lattice vibrations of the ε-phase have real numbers in their phonon frequencies. This suggests dynamic stability of the ε-phase, although its *P-T* conditions of formation have yet to be understood. The above crystallographic relationships between ε-phase and ringwoodite/wadsleyite can be explained in terms of periodic arrangements of a basic unit of spinel and spinelloid structures. Olivine in the host rock of Tenham and Miami entrapped in the shock veins initially transformed into polycrystalline ringwoodite and wadsleyite through a nucleation and growth mechanism during shock compression. The ε-phase would have been produced by shear transformation from the ringwoodite and wadsleyite during the shock compression or subsequent shock pressure release.

References: [1] Binns R. A. et al. (1969) *Nature* 221:943–944. [2] Price G. D. et al. (1983) *Canadian Mineralogist* 21:29–53. [3] Price G. D. (1983) *Physics of the Earth and Planetary Interiors* 33:137–147. [4] Madon M. and Poirier J. P. (1983) *Physics of the Earth and Planetary Interiors* 33:31–44. [5] Tomioka N. and Okuchi T. (2017) *Scientific Reports* 7:17351. [6] Giannozzi P. et al. (2009) *Journal of Physics: Condensed. Matter* 21:395502 (2009) [7] Perdew J. P., Burke K. and Ernzerhof M. (1996) *Physical Review Letters* 77:3865.

MYSTERIOUSLY MISSING MARTIAN MIF-S.

A. G. Tomkins[1] , S. L. Alkemade[1] and S. Nutku[1], [1]School of Earth, Atmosphere and Environment, Monash University, Melbourne, Victoria, Australia. [1]Corresponding author: Andy.Tomkins@monash.edu

Introduction: The Martian atmosphere is often compared to the Archean Earth's as both are dominated by CO_2-rich and O_2-poor chemistries. Archean Earth rocks preserve mass-independently fractionated sulfur isotopes (MIF-S; non-zero $\Delta^{33}S$), originating from photochemistry in an anoxic atmosphere [1]. Thus, Martian crustal rocks might be expected to preserve non-zero $\Delta^{33}S$. Studies of NWA 7034 (and pairs) – a Martian basaltic breccia – have revealed an anomalous atmospheric MIF-O ($\Delta^{17}O$) signature in metamict zircon, indicating that this regolith sample interacted with the Martian atmosphere-surface environment at 1.5 Ga (middle Amazonian) [2]. This meteorite and its pairs also contain metasomatic pyrite that likely formed in a near-surface regolith setting [3], and thus offers an ideal opportunity to investigate the atmospheric chemistry of Mars through its MIF-S signature.

Methods: We have investigated the sulfide petrogenesis in two pairs of NWA 7034 (NWA 8171 and 11220) and 19 additional Martian meteorites using optical and electron probe-based petrography. SIMS was used to investigate variations in $\Delta^{33}S$ in several of these including NWA 8171. We also conducted LA-ICP-MS on sulfides and chromite in several meteorites to examine their PGE concentrations.

Results: As found previously [3], the basaltic breccia samples contain abundant fine-grained pyrite and almost no pyrrhotite. Amongst the remainder, sulfides (mainly pyrrhotite, minor pentlandite) are most abundant in olivine-phyric, followed by basaltic and poikilitic shergottites. Nakhlites NWA 10720 and MIL 03346 contain ~5 times fewer sulfides than the shergottites. Chassignite NWA 2737 has slightly more abundant sulfides than the nakhlites. In the olivine-phyric shergottites, pyrrhotite is dominantly interstitial. Basaltic shergottites contain pyrrhotite up to 200μm diameter, mainly hosted in the crystal interstices; rare pyrrhotite inclusions in olivine occur in Zagami.

The LA-ICP-MS analyses found that sulfide grains contain insufficient IPGE to be detectable, and very low concentrations of Pd were found in most sulfide grains, and occasionally Pt, Rh and Ru were barely detectable. Of the basaltic shergottites, low PPGE concentrations were only found in NWA 8656.

In basaltic breccia NWA 8171, $\Delta^{33}S$ values for pyrite measured by SIMS range from -0.22 to 0.07 ‰ with an average $\Delta^{33}S$ = -0.12 ± 0.27 ‰, $\delta^{34}S$ values range from -2.34 to 1.02 ‰ with an average of $\delta^{34}S$ = -1.41 ± 0.38 ‰, and $\Delta^{36}S$ values range between -1.46 to +0.40 ‰. Amongst the shergottites NWA 7320, 7397, 8656 and 8716, the calculated averages are $\delta^{34}S$ = -0.31 ± 0.29 ‰ and $\Delta^{33}S$ = -0.02 ± 0.14 ‰.

Discussion: Amongst the shergottites, the basaltic shergottites are the most important for understanding MIF-S because these likely represent lavas that physically interacted with the surface where atmosphere-moderated sulfur-bearing minerals reside. In all basaltic shergottites examined, sulfides are paragenetically late and contain very low PGE indicating low R factor (and thus minimal sulfide-silicate melt interaction), which is consistent with late sulfide saturation. This implies that the lavas did not assimilate surface sulfur, and thus could not inherit a MIF-S signature.

Our S isotope results for basaltic brecca NWA 8171 indicate that it contains no resolvable mass-independent fractionation of S at the 2-sigma level. At first glance this appears to be a surprising result, given that the pyrite clearly formed within the regolith setting from relatively sulfur-rich fluids. But no Martian meteorite yet has yielded a MIF-S signature akin to the large deviations seen on Earth (Fig. 1). We have identified several reasons in addition to that given for the shergottites, why a large MIF-S signature should not be expected on Mars.
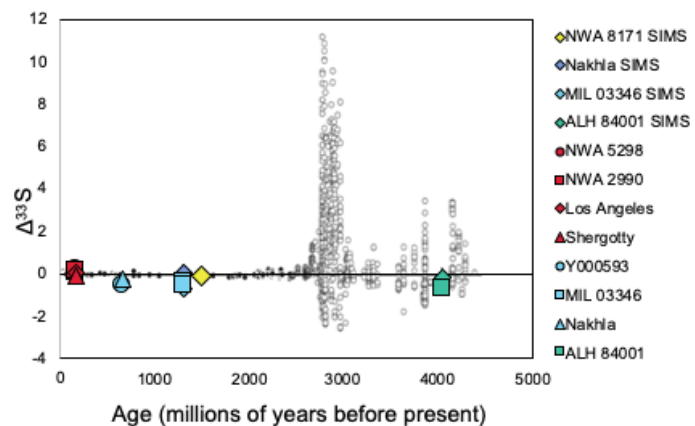

Fig. 1. NWA 8171 (yellow diamond, this study) and anomalous Martian MIF-S analyses (coloured, [1] [4]) compared with the Earth MIF-S record (greyscale points [5]).

References: [1] Farquhar J. et al. (2000) *Nature* 404:50-52. [2] Nemchin A. A. et al. (2014) *Nature Geoscience* 7:638-642. [3] Lorand, J.P. et al. (2015) *Meteoritics & Planetary Science* 50:2099-2120. [4] Franz H. B. et al. (2014) *Nature* 508:364-368. [5] Domagal-Goldman, S.D. et al. (2008) *Earth & Planetary Science Letters* 269:29-40.

CHROMIUM ISOTOPE COMPOSITIONS OF REFRACTORY INCLUSIONS: IMPLICATIONS FOR ISOTOPIC VARIABILITY IN THE EARLY SOLAR SYSTEM.

Z. A. Torrano[1], V. K. Rai[1], and M. Wadhwa[1], [1]Center for Meteorite Studies, School of Earth and Space Exploration, Arizona State University, Tempe, AZ, USA (ztorrano@asu.edu)

Introduction: Calcium-aluminum-rich inclusions (CAIs) in chondrites are the first solids formed in the early Solar System and preserve a record of the earliest processes and conditions in the solar nebula [1]. CAIs exhibit mass-independent anomalies in a variety of isotope systems, and these anomalies are thought to represent formation in an isotopically distinct reservoir when compared to chondrite parent bodies and terrestrial planets ([2] and references therein). Previous studies of Cr isotopic anomalies in CAIs have focused exclusively on inclusions from CV3 chondrites Allende (n ≈ 25) and Vigarano (n = 4) [3-9]. This present study is part of a larger, ongoing project to determine the mass-independent Cr and Ti isotope compositions of a diverse group of CAIs from other chondrites and chondrite groups, with the goal of providing a more rigorous assessment of the isotopic composition and variability of the broader CAI-forming region in the early Solar System [10-15]. We have previously reported the Cr isotope composition of 11 CAIs from several CV3 and CK3 chondrites and here we report the Cr isotopic compositions of an additional 5 relatively pristine CAIs from 4 CV3 chondrites: "Saguaro" from NWA 5508, "ZT6" from NWA 2900, "ZT10" from NWA 6991, and "ZT13" and "ZT14" from Axtell. The Ti isotope compositions of these CAIs have been reported in our earlier work [11-12, 14-15].

Analytical Methods: All sample handling and chemical processing was conducted under clean laboratory conditions in the Isotope Cosmochemistry and Geochronology Laboratory (ICGL) at Arizona State University (ASU). Each CAI was carefully extracted from the meteorite slab and subsequently digested in an $HF:HNO_3$ mix in a Parr bomb. A 5% aliquot was reserved for measurement of elemental abundances (including the REEs) on the iCAP-Q quadrupole inductively coupled plasma mass spectrometer (ICPMS) in the Keck Laboratory at ASU. A portion of the remainder of each sample solution was processed for the separation of elements of interest, and Cr was purified using procedures adapted from [16]. Purified Cr samples and standards were analyzed on the Thermo Neptune multicollector ICPMS in the ICGL using methods similar to those described previously [10]. Samples and standards (800 ppb concentration) were introduced using an Elemental Scientific Apex-Q desolvating nebulizer with a 100 μL/min flow rate. Measurements were done in high resolution mode to avoid polyatomic interferences [17]. The intensities of ^{50}Cr, ^{52}Cr, ^{53}Cr, and ^{54}Cr were measured, along with ^{49}Ti, ^{51}V, and ^{56}Fe to monitor and correct for isobaric interferences. The Cr isotopic data are reported relative to the NBS 979 Cr standard after internal normalization to $^{50}Cr/^{52}Cr$ (=0.051859; [18]).

Results and Discussion: The 16 CAIs in this sample suite (5 of which are reported here for the first time) represent diverse petrologic and geochemical types. This sample set includes CAIs with Group I REE patterns (Lisa, ZT1, ZT6, ZT7, ZT13, Saguaro), Group II patterns (Homer, ZT2, ZT3, ZT5, ZT9, ZT10, ZT14), and Group III patterns (Marge, Bart, ZT8). These 16 CAIs make up a single population of $\varepsilon^{54}Cr$ values that range from 3.16 ± 0.30 to 7.28 ± 0.22 (3.50 ± 0.22 to 6.15 ± 0.31 in the 5 new CAIs reported here). The $\varepsilon^{54}Cr$ values for CAIs from the various CV3 chondrites included in this study fall within the range of $\varepsilon^{54}Cr$ values of previously measured CAIs from the CV3 chondrites Allende and Vigarano [3-9]; the previously reported $\varepsilon^{54}Cr$ values of the two CAIs from CK3 chondrites fall within this same range [10]. This supports the previous assertion (based on Ti isotope compositions) that CAIs from CV and CK chondrites originated in a common nebular reservoir [15, 19]. As was also reported previously for $\varepsilon^{50}Ti$ values in CAIs [15, 20], there appears to be no correlation between REE patterns and $\varepsilon^{54}Cr$ in the 16 CAI samples that we have studied thus far. The resolvable variation in $\varepsilon^{54}Cr$ is consistent with the variation in $\varepsilon^{50}Ti$ in these same CAIs [11-12, 14-15] and indicates that the CAI-forming reservoir preserved isotopic variability in multiple elements.

References: [1] MacPherson G. J. (2014), *Treatise on Geochemistry (2nd Ed.)*, 139–179. [2] Dauphas N. and Schauble E. A. (2016), *Annual Review of Earth and Planetary Science* 44, 709–783. [3] Birck J. -L. and Allègre C. J. (1984) *Geophysical Research Letters* 11, 943–946. [4] Birck J. -L. and Allègre C. J. (1985) *Geophysical Research Letters* 12, 745–748. [5] Papanastassiou D. A. (1986) *The Astrophysical Journal* 308, 27–30. [6] Birck J. L. and Lugmair G. W. (1988) *Earth and Planetary Science Letters* 90, 131–143. [7] Loss R. D. et al. (1994) *The Astrophysical Journal* 436, L193–L196. [8] Bogdanovski O. et al. (2002) *LPSC XXXIII,* Abstract #1802. [9] Mercer C. M. et al. (2015) *LPSC XLVI*, Abstract #2920. [10] Mane P. et al. (2016) *LPSC XLVII*, Abstract #2778. [11] Torrano Z. A. et al. (2017) *LPSC XLVIII*, Abstract #3045. [12] Torrano Z. A. et al. (2017) *MetSoc 80*, Abstract #6318. [13] Torrano Z. A. et al. (2018) *LPSC XLIX*, Abstract #2405. [14] Torrano Z. A. et al. (2019) *LPSC L*, Abstract #1501. [15] Torrano Z. A. et al. (in review) *Geochimica et Cosmochimica Acta*. [16] Yamakawa A. et al. (2009) *Analytical Chemistry* 81, No. 23, p. 9787–9794. [17] Schoenberg R. et al. (2008) *Chemical Geology*, 249, 294–306. [18] Shields W. R. et al. (1966) *Journal of Research of the National Bureau of Standards*, 70A, No. 2, 193–197. [19] Ebert S. et al. (2018) *Earth and Planetary Science Letters* 498, 257–265. [20] Davis A. M. et al. (2018) *Geochimica et Cosmochimica Acta,* 221, 275–295.

SYNCHROTRON RADIATION-BASED NANO-TOMOGRAPHY FOR EXTRATERRESTRIAL MATERIALS.

A. Tsuchiyama[1,2], A. Miyake[3], K. Uesugi[4], A. Takeuchi[4], T. Nakano[5], J. Matsuno[2], [1]Research Organization of Science and Technology, Ritsumeikan University (1-1-1 Nojihigashi, Kusatsu, 525-8577, Japan, tsuchiyama.akira.4x@kyoto-u.jp), [2]Guangzhou Institute of Geochemistry, [3]Graduate School of Science, Kyoto University, [4]JASRI/SPring-8, [5]AIST/Geological Survey of Japan.

Introduction: X-ray computed tomography (CT) is a non-destructive method for obtaining the 3D internal structure of an object with quantitative size information (e.g., length and volume) usually by using X-ray absorption. This method was originally developed for medical diagnostics [1] and are used in a variety of research fileds including earth and planetary science. In addition to X-ray absorption, a variety of information of X-rays such as phase diference, diffraction, fluorescence and XAFS can be used particularly if we use synchrotron radiation (SR) X-rays, which has high coherency and are easily monochromatized. Monochromatized X-rays make it possible to obtain quantitative information about absorption and phase contrasts with high S/N ratio and high spatial resolution. If we use parallel X-ray beam, the spatial resolution is limitted to the wave length of visual light because the X-ray is converted to visual light to obtain projection images (micro-tomography) [2]. If we use imaging optical system with a Fresnel zone plate (FZP), nanometer-scale resolution (~30 nm) can be obtained (nano-tomography). Nano-tomography developed at SPring-8, SR facility in Japan, and its application to returned samples are introduced.

Absorption tomography and dual-energy tomography (DET): Refractive index of X-ray is expressed by $n=1-\delta+i\beta$. The imaginary part, β, is the extinction coefficient, which is related to the liner attenuation coefficient (LAC), $\mu = \rho\Sigma\tau_j(E)w_j$. ρ is the material density, $\tau_j(E)$ is the mass attenuation coefficient (MAC) of element-j, which is a function of the X-ray energy, E, and w_j is the weight fraction of element-j. Thus, absorption contrast images (spatial distributions of μ) have inforamtion on the chemical compositions of objects. Elemental images can be obtained by the difference between images measured just below and above the absorption edge energy of the element (subtrtaction tomography) [3]. However, the concentration cannot be obtained without the date of ρ.

It is sometimes diffuicult to discreminate between minerals from its LAC value alone. We can discreminate many minerals by using the LAC values below and above the absorption edge energy of a specific element (dual-energy microtomography: DET) [4]. If we use the Fe K-edge energy (7.11 keV), we can discreminate Fe-poor and Fe-rich minerals as well as minerals with light and heavy elements and mineral distribution in 3D can be obtained. However, we cannot discriminate between void, organics and water because their LAC values are similar.

Phase tomography and scanning-imaging X-ray micropscopy (SIXM): The real part in the equation of n, $1-\delta$, is the refractive index. δ is the deviation from unity (refractive index decrement; RID) and nearly proportional to ρ. Thus, phase contrast images (spatial distributions of δ) correspond to distribution of ρ, and we can discriminate between void and organics (or water). Phase and absorption contrast images can be simultaneously obtained in 3D by using scanning-imaging X-ray microscopy (SIXM) [5]. By combining DET and SIXM, more detailed information on the 3D distribution of minerals, organic s (or water) and voids can be obtained (three-color tomography) [6].

Application to returned samples and related materials: SR-based absorption tomography has been applied to Stardust samples. Particles collected from impact tracks of comet Wild-2 dust were imaged by nano-tomography and particles selected by CT were further examined by SEM, TEM and nano-SIMS, and chondrule-like materials were found [7]. The 3D track shapes were also obtained by micro-tomography [8] and dust size and density were estimated [9]. Absorption nano-tomography was systematically used in the initial analysis of Hayabusa samples [10]. Mineral discrimination was successively made by DET and impact origin of the regolith particles were proposed from the 3D shapes [11]. By combining with FIB micro-sampling from a thin section, we can obtain 3D structures for regions of interest [12]. SIXM was applied to search fluid inclusions in carbonate grains in carbonaceous chondrites [13]. By using combined DET-SIXM, ultra-porous lithology as fossil of ice in chondrite was found in Acfer 094 meteorite [14]. We are now preparing for the initial analysis of Hayabusa2 samples collected from C-type Asteroid Ryugu, which will be returned to Earth in December 2020.

References: [1] Hounsfield G. N. (1973) *British Journal of Radiography* 46: 1016-1022. [2] Uesugi M. (2019) this workshop. [3] Thompson A. C. et al. (1984) *Nuclear Instruments and Methods in Physics Research* 222: 319−323. [4] Tsuchiyama A. et al. (2013) *Geochimica et Cosmochimica Acta* 116: 5-16. [5] Takeuchi A. et al. (2013) *Journal of Synchrotron Radiation* 20: 793-800. [6] Tsuchiyama A. et al. (2017) *LPS XLVIII*, Abstract #2680. [7] Nakamura T. et al. (2008) *Science* 321: 1664-1667. [8] Iida Y. (2010) *Meteoritics & Planetary Science* 45: 1302-1319. [9] Niimi R. et al. (2012) *The Astrophysical Journal* 744:18. [10] Nakamura T. et al. (2011) *Science* 333: 1113-1116. [11] Tsuchiyama A. et al. (2011) *Science* 333: 1125-1128. [12] Miyake A. et al. (2014) *Microscopy* 63: i24-25. [13] Tsuchiyama A. (2018) *Meteoritics & Planetary Science* 6187.pdf. [14] Matsumoto M. et al. (2019) *This MetSoc Meeting*.

POSSIBLE ORIGIN OF PRIMITIVE AMORPHOUS SILICATES IN CARBONACEOUS CHONDRITES.

A. Tsuchiyama[1,2], A. Takigawa[3,4], T. Hirose[3], H. Kawano[3], Y. Imura[3], S. Enju[3], Y. Igami[5], [1]Research Organization of Science and Technology, Ritsumeikan University (atsuchi@fc.ritsunei.ac.jp), [2]Guangzhou Institute of Geochemistry, [3]Graduate School of Science, Kyoto University, [4]The Hakubi Center for Advanced Research, Kyoto University. [5]Institute of Materials and Systems for Sustainability, Nagoya University.

Introduction: Less-altered carbonaceous chondrites (CCs) called primitive CCs have fine-grained matrix of amorphous silicate, silicate mineral grains, complex organic compounds, and relatively abundant presolar grains. The amorphous silicates more or less resemble glass with embedded metal and sulfides (GEMS) observed in chondritic porous interplanetary dust particles (CP-IDPs) (e.g., [1]). Such GEMS-like materials in primitive CCs are considered to represent the building blocks of the solar system [2-4] as well as GEMS and micrometeorites (e.g., [5]). Primitive CCs are present in various CC groups (CM, CR, CO, and C-ungrouped) (e.g., [2-4,6-8]). GEMS-like materials are more or less aqueously altered and show chemical and textural diversity, which is explained by different degrees of aqueous alteration of GEMS or related materials (e.g., [2]) In this paper, a possible process of the formation and alteration of GEMS-like materials in primitive CC matrix is proposed based on the observation of GEMS-like materials and condensation [9,10] and aqueous alteration experiments [11] conducted so far.

Diversity of GEMS-like materials: Some of GEMS-like materials are spherical objects like GEMS and observed in porous regions of Paris (CM) [2] and Acfer 094 (C-ungrouped) [4] and organics-rich regions of MIL 090657 (CR) [12] and LAP 02342 (CR) [3]. The majority of the GEMS-like materials seem to be aggregates of such spherical objects [4]. In contrast to GEMS, abundant Fe(-Ni) sulfide nanograins are observed in GEMS-like materials, and Fe-Ni metal is mostly absent. Some of them contain Fe oxide nanograins (unknown phase in Paris [2], magnetite and goethite in MIL 090657 [12]) and metal nanograins in LAP 02342 [3], DOM 08006 (CO). Amorphous silicates are relatively rich in Fe (Fe^{2+} and Fe^{3+}) and more or less hydrated (e.g., [4,13]). The electron diffraction of amorphous silicate usually has rings, indicating poorly crystallized feature [2,4], which correspond to magnesium silicate hydrate (MSH) [4]. Layered hydrous silicates are also observed (e.g., [7]).

Condensation and aqueous alteration experiments: Condensation experiments were performed using gases of the GEMS mean composition in the system Mg-Fe-Si-O-S [9] and those of CI composition in the system Mg-Fe-Si-Al-Ca-Ni-O-S [10] under various redox conditions. In these experiments, fine particles of amorphous silicate with Fe-bearing nanograins, which resemble GEMS and GEMS-like materials, were produced. In oxidizing conditions, abundant FeS nanograins are in Fe-rich amorphous silicates and metal is absent or rare. Monosulfide solid solution (MSS: (Fe,Ni)S) also formed in the Ni-bearing system. In intermediate redox conditions, FeS and Fe or α-(Fe,Ni) nanograins are in Fe-poor amorphous silicates. In reducing conditions, Fe_3Si instead of metal, FeS and MgS nanograins are in almost Fe-free amorphous silicates. Only a small amount of S is included in amorphous silicates.

In in-situ aqueous alteration experiments, amorphous $MgSi_2O_4$ and $MgSiO_3$ immersed in pure water at room temperature were observed under TEM or in-situ measured by X-ray diffraction [11]. The amorphous silicates are hydrated first. Then, Mg is selectively dissolved into water and MSH forms from the Mg-rich solution. Layered hydrous silicates particularly mixed layer silicates may form from further alteration of MSH.

Formation and alteration of GEMS-like materials: The above features of the GEMS-like materials strongly suggest that they have experienced aqueous alteration in different degrees. However, aqueous alteration of GEMS ((Fe,Ni), FeS nanograins in amorphous silicate) cannot simply explain the diversity of the GEMS-like materials. For example, abundant Fe(-Ni) sulfide nanograins without metal in the GEMS-like materials requires sulfidation of metal (e.g., [5]), but there is no sufficient source of S for the sulfidation. In addition, Fe-rich amorphous silicate does not easily form via aqueous alteration because it requires dissolution of amorphous silicate and re-precipitation of Fe-bearing MSH. Fe-rich amorphous silicates with FeS (and probably MSS) formed in relatively oxidizing condition are most likely original materials of some GEMS-like materials. We should distinguish between original material and later aqueous alteration features. If this is the case, GEMS and GEMS-like materials were formed by condensation probably in different locations of the primitive solar nebula, and CP-IDPs and the primitive matrix in CCs may represent samples of the building blocks of the solar system in different locations.

References: [1] Keller L. P. and Messenger S. (2011) *Geochimica et Cosmochimica Acta* 75: 5336–5365. [2] Leroux H. et al. (2015) *Geochimica et Cosmochimica Acta* 170: 247–265. [3] Nittler L. R. (2019) *Nature Astronomy* https://doi.org/10.1038/s41550-019-0737-8. [4] Matsumoto M. et al. (2019) *This meeting*. [5] Noguchi T. (2017) *Geochimica et Cosmochimica Acta* 208: 119–144. [6] Greshake A. (1977) *Geochimica et Cosmochimica Acta* 61: 437-452. [7] Abreu N. M. and Brearley A. J. (2010) *Geochimica et Cosmochimica Acta* 74: 1146-1171. [8] Nittler L. R. (2018) *Geochimica et Cosmochimica Acta* 226: 107-131. [9] Enju S. et al. (2019) *This meeting*. [10] Imura Y. et al. (2019) *Japan Geoscience Union Meeting 2019* Abstract PCG23-P03. [11] Igami Y. (2019) *Goldschmidt2019* Abstract. [12] Tsuchiyama A. et al. (2018) *Japan Geoscience Union Meeting 2018* Abstract PPS06-01. [13] Le Guillou C et al. (2015) *Earth and Planetary Science Letters* 420: 162-173.

RELATIONSHIP BETWEEN THE MATUYAMA-BRUNHES REVERSAL AND INDOCHINITES

H. Ucar[1] and G. Kletetshka[2, 3, 4], [1]Dept. of Geophysical Engineering, Faculty of Engineering, Istanbul University-Cerrahpasa, 34320, Avcilar, Istanbul, Turkey (hakanucar1993@hotmail.com), [2]Institute of Geology, Czech Academy of Sciences, Rozvojova 269, Prague, Czech Republic, [3]Department of Applied Geophysics, Charles Univ, Albertov 6, Prague, Czech Republic, [4]Geophysical Institute, University of Alaska Fairbanks, 903 N Koyukuk Drive, Fairbanks, AK, USA, (gunther.kletetschka@natur.cuni.cz).

Introduction: Indochinites are a sort of tektite which forms as a result of cosmic impacts. Several studies [1, 2, 3, 4, 5] showed that Australasian tektite fall could change magneto-hydrodynamic motions of the Earth's core. In this study, the relationship between Matuyama-Brunhes magnetic reversal and indochinites is discussed.

Methods and results: A study [4] suggested that the effect of a large cosmic impact on Earth can create a geomagnetic reversal. According to that, the dust from impact crater may trigger an ice age. Rotational speed of the crust and mantle is changed by redistribution of the water near the equator to ice. When the sea level change is larger than 10 meters and within a few hundred years, the speed change in the liquid outer core may disturb the convective cells making the dynamo effect. This new convective cells then reduce the dipole component while increasing the energy in the multipole components. Finally, a dipole is rebuilt by reestablished dynamo action and a geomagnetic reversal occurs. The estimated mass of indochinites in Australasian strewnfield is 100 million tons [1] and the area includes 10% of the earth's surface [3].

It was situated that the deposition date of Australasian indochinites is close to the beginning of the Matuyama-Brunhes magnetic reversal [6]. In fact the inclination of the magnetic field starts rapidly fluctuate at about the same time as the deposition of the indochinites. The glacial age following the tektite deposition [4] and disappearance or formation of some marine radiolarian and foraminiferal micro-organisms support this idea [3, 7]. Furthermore, a 30-50 cm thick ocean sediment layer including Australasian microtektites was thought to be related to Matuyama-Brunhes magnetic reversal [2].

On the other hand, it is known that all large impact events associated with magnetic reversals did not produce tektites [3]. Ivory Coast tektites deposited just after the Jaramilo magnetic reversal [5, 8, 9]. In Cretaceous-Tertiary boundary, a tektite fall occured much time (0.2 my) before the Chron C29R reversal [5, 10, 11]. Furthermore, 105 magnetic reversals occured in the last 35 million years [3, 12], but the number of craters, which are larger than 10 km and thought to be related to a magnetic reversal, is 10 [3, 13]. It's much less than the number of reversals. However, some craters may not be visible because they are in water or covered by sedimentation and other events [3].

Discussion and conclusions: In the light of this informations, we try to combine the relationship between indochinites and Matuyama-Brunhes magnetic reversal from a cave sediment data. Australasian tektite strewnfield, and Moravian cave sediments occur simultaneously. We provide a new model to explain how the impact event responsible for tectites could lead to magnetic reversal recorded in Moravian cave sediments..

References: [1] Glass B. P. and Heezen B. C. (1967) *Nature* 214.5086:372. [2] Cassidy W. A. et al. (1969) *Journal of Geophysical Research* 74.4:1008-1025. [3] Glass B. P. et al. (1979) *Lunar and Planetary Science Conference Proceedings* 10:2535-2545. [4] Muller R. A. and Morris, D. E. (1986) *Geophysical Research Letters* 13.11:1177-1180. [5] Schneider D. A. et al. (1992) *Earth and Planetary Science Letters* 111.2-4:395-405. [6] Gentner W. et al. (1967) *Earth and Planetary Science Letters* 2.2: 83-86. [7] Keany J. and Kennett J.P. (1972) *Deep Sea Research and Oceanographic Abstracts* 19.8:529-548 [8] Glass B. P. et al. (1991) *Earth and Planetary Science Letters* 107.1:182-196. [9] Schneider D.A. and Kent D.V. (1990) *Geophysical Research Letters* 17.2:163-166. [10] Sigurdsson H. et al. (1991) *Nature* 349.6309:482. [11] Preisinger A. et al. (1986) *Nature* 322.6082:794. [12] Heirtzler J.R. et al. (1968) *Journal of Geophysical Research* 73.6:2119-2136. [13] Grieve R.A.F. and Robertson, P.B. (1979) *Icarus* 38.2:212-229.

1. **INTEGRATED SYNCHROTRON RADIATION COMPUTED TOMOGRAPHY SYSTEM FOR THE ANALYSIS OF EXTRATERRESTRIAL MATERIALS**

M. Uesugi[1]
[1]Japan synchrotron radiation research institute (JASRI/Spring-8)
uesugi@spring8.or.jp

Synchrotron radiation (SR) computed tomography (CT) is one of the important tools for the analysis of extraterrestrial materials [e.g. 1], especially returned samples by spacecraft missions [2,3,4], because of its non-destructive feature. X-ray with high photon flux density, high energy and high coherent enables us to investigate mm-sized sample with micron to sub-micron of spatial resolution, three dimensionally. However, there are several problems in the CT observation of those extraterrestrial materials. Higher spatial resolution makes narrower field of view (FOV). Thus, if we intend to observe whole structure of large sample by X-ray CT, we should apply CT system with lower spatial resolution. In other words, we should break the sample into small pieces if we want to observe the sample with higher spatial resolution. In addition of those problems, we can not determine the materials inside the unknown samples only by the CT. We can observe the internal texture, which shows difference of X-ray linear absorption coefficient (LAC) [4,5,6] in the material by CT. However, the value of LAC for mineral phases inside the extraterrestrial material significantly overlaps each other. Thus it is difficult to distinguish the mineral phases uniquely only by the LAC and texture.

Recently, those problems are gradually resolved by multi-mode and multi-scale tomography technique. In BL20XU/SPring-8, we constructed an integrated CT system, which consists of three X-ray beam monitors those having different spatial resolution and FOV, and several optical elements, such as Fresnel zone plate (FZP). By changing X-ray beam monitors and optical elements with repeatability error much less than the spatial resolution of the system, we can measure a sample with multiple SR-CT methods. Currently, normal absorption contrast CT with two different resolution, Wide FOV and Low spatial resolution mode (WL mode) and Narrow FOV and High spatial resolution mode (NH mode), scanning x-ray diffraction (SXRD), X-ray diffraction CT (XRD-CT) and differential phase contrast CT (DP-CT) are available in the integrated CT system. X-ray energy used in this system is 30 keV, which is enough to penetrate extraterrestrial samples around 5 mm in diameter [5]. We can choose the set of pixel size of WL mode and NH mode. For the setup of larger samples, pixel size and FOV are 3 μm and 6 mm for WL mode and 0.25 μm and 0.5 mm for NH mode. For setup of smaller samples, pixel size and FOV become 0.5 μm and 1 mm for WL mode and 50 nm and 60 μm for NH mode. In SXRD mode, X-ray was focused into 1 μm spot. Samples are scanned by the focused X-ray beam, and diffraction image was obtained for each scanning point by the X-ray beam monitor with pixel size of 20 μm and FOV of 40 mm. Then mineral composition of each position can be obtained. If we scan a sample horizontally by the focused X-ray with rotating the sample using the SXRD setup, we can obtain the texture of the mineral phases in a horizontal plane by XRD-CT. DP-CT is under the development, but we can obtain CT images with high sensitivity for the materials consist of light elements, such as carbon, with pixel size around 0.1 μm.

We can obtain information of samples with the system from several aspects without breaking it. The system can provide an important start point for the analysis of extraterrestrial samples, expecially samples returned by spacecraft missions, such as Hayabusa2, OSIRIS-REx and MMX.

References: [1] Ebel D. S. and Rivers. M. (2007) *Meteoritics & Planetary Science* 42:1627 [2] Nakamura T. et al. (2008) *Science* 321:1664. [3] Tsuchiyama A. et al. (2011) *Science* 333:1121 [4] Tsuchiyama A. et al. (2013) *Geochim. Cosmochim. Acta*, 116:5. [5] Uesugi M. et al. (2010) *Earh Planet. Sci. Lett.* 299:259. [6] Uesugi M. et al. (2013) *Geochim. Cosmochim. Acta*, 116:17.

PREPARATION FOR THE ANALYSIS OF HAYABUSA2 RETURNED SAMPLES.

M. Uesugi[1], K. Uesugi[1], M. Ito[2], N. Tomioka[2], T. Ohigashi[3], A. Yamaguchi[4], N. Imae[4], Y. Karouji[5], N. Shirai[6], T. Yada[7], M. Abe[7], K. Hirahara[8], Y. Kodama[9] and I. Sakurai[10]
[1] Japan Synchrotron radiation Research Institute (JASRI/SPring-8) (uesugi@spring8.or.jp), [2]Kochi Institute for Core Sample Research, JAMSTEC, [3]Institute for Molecular Science, [4]National Institute Polar Research, [5]JSEC/JAXA, [6]Tokyo Metropolitan University, [7]ISAS/JAXA, [8]Osaka University, [9]Marine Works Japan, [10]Nagoya Univestiy.

Extraterrestrial Sample Curation Center at JAXA (ESCuC/JAXA) organized a team for development of techniques and devices for the handling, transfer and analysis of the Hayabusa2-returned samples from 2015, with the members of the ESCuC/JAXA, Kochi Institute for Core Sample Research, JAMSTEC (Kochi), JASRI/SPring-8, UVSOR Synchrotron/ Institute for Molecular Science, National Institute of Polar Research (NIPR) and Tokyo Metropolitan University. The team consists of specialists of analytical methods of diverse scientific fields, to gather the knowledge and experience of the state-of-art analytical methods. The team was authorized as the Phase 2 curation team KOCHI at 2017, which is one of the activities of ESCuC for describing the Hayabusa2-returned samples in detail, using even destructive methods [1]. Thus, major purpose of the team is to construct comprehensive methods for the handling and analysis of the returned samples of future missions, and to describe Hayabusa2-returned samples in detail.

In the activities of the team, Facility to Facility Transfer Container (FFTC) was developed for the inter-facility and inter-instruments transfer of samples [2]. The container includes several options, according to sample size and conditions, such as a quartz (Qz) glass holder for the unprocessed grains from 10 μm to several milli-meters, a rod holder for samples fixed on a tip of fiber or rods, and processed sample holders such for ultra-thin sections of Transmission Electron Microscopy (TEM). It is confirmed that the FFTC can keep positive pressure as well as vacuumed condition (lower than) more than 1 month. Thus it can also be used for temporary storage of samples. An universal sample holder using Vertically-Aligned Carbon NanoTube (VACNT) was developed for the holder of unprocessed samples for the non-destructive analyses such as Synchrotron Radiation (SR) Computed Tomography (CT), X-ray Diffraction (XRD), and Field Emission Scanning Electron Microscopy (FE-SEM) [3]. During the SR experiments, the holder was sealed by polyimide tube. The VACNT holder is also applicable to the Secondary Ion Mass Spectrometry (SIMS) and fabrication of samples by Focused Ion Beam (FIB). Because the Qz glass holder of FFTC, VACNT and polyimide tube will contact unprocessed samples directly, cleanness of them should be examined before application. The cleanness of the Qz glass, VACNT holder and polyimide tube was evaluated using Instrumental Photon Activation Analysis (IPAA) and Instrumental Neutron Activation Analysis (INAA) [4]. It is confirmed that elemental contamination transferred from those materials are considerably small. An universal holder for ultra-thin sections, called KOCHI grid is also developed, for the safe handling of ultra-thin sections in the glovebox, and linkage of high spatial resolution analysis using ultra-thin section. [5] The grid can be installed into TEM, Scanning Transmition X-ray Microscopy with using Near Edge X-ray Absorption Fine Structure analysis (STXM-NEXAFS) and NanoSIMS. When installing the KOCHI grid into STXM-NEXAFS system, the grid was fixed into new sample cell, OKAZAKI cell. The OKAZAKI cell can be installed into FFTC as the option for ultra-thin section transfer. We are also developing sample handling tools, such as a tool for pressing sample onto metal film for the analysis of organic matters, glovebox system for the sample handling, atmosphere shielded loading system of samples to instruments, and cutting method for the samples with low sample damage, as well as techniques for the curatorial works and sequential analysis.

Using those devices and systems, Antarctic micrometeorites (AMMs) showing similar characteristics to carbonaceous chondrites and four Antarctic meteorites, Y-791198 (CM2.4), Y-980115 (CI1), Y-793495 (CR2.8) and A-881595 (CR2), were investigated as the rehearsals of the analysis of Hayabusa2-returned samples. They were investigated by SR-CT, XRD and FE-SEM to characterize their internal structure and mineral compositions, and to select region of interest (ROI). After that, ultra-thin sections were extracted using FIB from ROI. The section was investigated by STXM-NEXAFS, TEM and NanoSIMS, focusing mainly on characteristics of organic materials. For the case of Antarctic meteorites, Field-Emission Electron Probe MicroAnalyzer (FE-EPMA) and Laser Ablation Inductively Coupled Plasma Mass Spectrometry (LA-ICP-MS) will be applied for the detailed analysis of chemical compositions of each hydrous and un-hydrous phase. Through the rehearsals, sample damage and problems of analytical flow are evaluated, along with constructing database for the comparison of returned samples. Analytical flow of the sample will be improved based on the result of a series of rehearsals. In the actual analysis of Hayabusa2 returned samples, the flow will be modified according to the characteristics of the samples flexibly.

References: [1] Ito et al. (2019) *MAPS* abstract, submitted. [2] Uesugi K. et al. (2019) *in prep.* [3] Uesugi M. et al. (2019) *in prep.* [4] Shirai N. et al. (2019) *in prep.* [5] Ohigashi T. et al. (2019) *in prep.*

Development for in-situ Volatile Element Abundances, and Hydrogen and Sulfur 2-Isotope Analyses of Silicate Glasses by SIMS.

T. Ushikubo[1] and K. Shimizu[1], [1]Kochi Institute for Core Sample Research, JAMSTEC, 200 Monobe-otsu, Nankoku, Kochi 783-8502 Japan (ushikubot@jamstec.go.jp).

Introduction: Enrichment or depletion of water and other volatile elements significantly affect igneous processes occurred in the protoplanetary disk and the interior of planets/planetesimals, resulting diversity of inclusions in chondrites and the surface and internal evolution of planets. Due to high mobility and reactivity of volatile elements, however, it is difficult to correctly trace abundances of volatile elements in source materials and their behavior in igneous processes. Glass is one of major phases to contain volatile elements. Since glass is highly susceptible to later aqueous and/or thermal processes, it is important to measure volatile elements in pristine glasses such as a melt inclusion encapsulated in robust minerals. We developed in-situ analysis techniques of volatile element abundances (CO_2, H_2O, F, Cl, S, and P_2O_5) of silicate glasses, and hydrogen (D/H) and sulfur 2-isotope ($^{34}S/^{32}S$) analyses for silicate glasses with abundant water (≥ 0.2 wt.%) and sulfur (≥ 500 ppm) contents.

Analytical procedures and results: In-situ analyses were performed with an ion microprobe, CAMECA IMS 1280-HR at Kochi Institute, JAMSTEC. For accurate measurements of volatile element abundances, we established homogeneous standard glasses (EPR-G3, IND-G1, IND-G2, FJ-G2, and MRN-G1) [1]. We also used several synthetic glasses for calibration and the ranges of volatile elemental abundances measured standard glasses are 97 - 9400 ppm for CO_2, 0.020 – 4.8 wt% for H_2O, 55 - 2957 ppm for F, 51 - 1372 ppm for S, 55 - 2833 ppm for Cl, and 0.084 - 0.41 wt% for P_2O_5, respectively [1]. the synthetic quartz glass, HERALUX-E-LA, was used to check back ground signals. The samples were polished using alumina lapping films (down to #10000; 0.5μm) and were pressed onto the indium metal loaded in a 1-inch diameter Al-metal cup.

Figure 1: Calibration lines for H_2O content in basaltic glasses determined in 5 separate measurement sessions. (from [1])

Volatile abundances were measured using a 20 kV Cs^+ ion primary beam (300 to 500 pA and ~10 μm in diameter). Secondary ions ($^{12}C^-$, $^{16}OH^-$, $^{19}F^-$, $^{31}P^-$, $^{32}S^-$, $^{35}Cl^-$, and $^{30}Si^-$) were accelerated at -10 kV and detected by an axial electron multiplier (EM) detector using a magnetic peak switching method. To reduce contribution of surface contamination, we set the field aperture at 5×5 μm of the field of view and cut ion signals from the edge of the primary beam. Mass resolving power (MRP, M/ΔM) was set at 6000. Volatile element signals were normalized to the $^{30}Si^-$ signal. We performed multiple sessions to obtain the calibration lines. We applied a power-law regression for the CO_2 calibration and a linear-law regression for other volatile elements. The range of session-to-session variation of slopes of calibration lines is about 10% for 4 years (e.g., Figure 1). Reproducibility of the standard glass (EPR-G3) measurements in each measurement session is typically 1-2% for all volatile elements. It should be noted that sufficient pre-pumping (>12 hours before measurement) in the high-vacuum storage chamber and complete removal of epoxy are desirable for accurate H_2O content and hydrogen isotope analyses.

Figure 2: The image of a melt inclusion in olivine with volatile (V), hydrogen isotope (H), and sulfur isotope (S) measurement pits. (modified from [2])

For hydrogen and sulfur 2-isotope analyses, we employed a FC-EM detector setting to achieve quick and accurate analyses for H_2O- and/or S-rich samples. Primary Cs^+ beam conditions are ~5 nA and ~15 μm in diameter for hydrogen isotope analysis, and ~0.5 nA and ~10μm in diameter for sulfur 2-isotope analysis, respectively. Details in analytical conditions were described in [2]. Hydrogen isotope ratios were determined by simultaneously detected $^{16}OH^-$ (FC, MRP~5000) and $^{16}OD^-$ (Axial EM, MRP~10000) signals. Although the instrumental fractionation was large (~+600‰), we could achieve the spot-to-spot reproducibility (2 SD) of ~±6‰ for basaltic glasses with >1 wt% H_2O and ~±12‰ for natural abyssal basaltic glasses with ~0.2 wt% H_2O [2]. Sulfur 2-isotope ratios were determined by simultaneously detected $^{32}S^-$ (FC, MRP~2200) and $^{34}S^-$ (Axial EM, MRP~5000). The spot-to-spot reproducibility (2 SD) of the standard glass (EPR-G3, [S]=1269 ppm) was ~±0.7‰ [2]. Combined with these analytical techniques, we can measure volatile element abundances, hydrogen, and sulfur isotope ratios of melt inclusions as small as 30 μm in size (Figure 2). By employing an EM-EM detector setting, we expect to extend our techniques for studies on extraterrestrial samples with much lower volatile contents (e.g. [3]).

References: [1] Shimizu K. et al. (2017) *Geochemical Journal* 51:299-313. [2] Shimizu K. et al. (2019) *Geochemical Journal*: in press. [3] Hauri E. H. et al. (2011) *Science* 333:213-215.
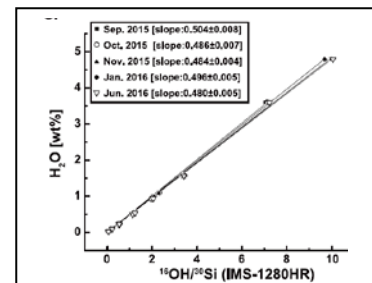
NANOSIMS O & S-ISOTOPE ANALYSES OF COSMIC SYMPLECTITE IN THE PRIMITIVE CHONDRITE ACFER 094

L. G. Vacher[1], R. C. Ogliore[1], N. Liu[1] and J. B. Lewis[1], [1]Department of Physics, Washington University in St. Louis, St. Louis, MO, USA (lvacher@wustl.edu).

Introduction: Cosmic Symplectite (COS) are anomalous ^{17,18}O-rich magnetite-sulfide grains (Δ^{17}O = ~90‰) found in the ungrouped carbonaceous chondrite Acfer 094 [1, 2]. They are thought to have formed from sulfidation and oxidation of Fe,Ni metal by H_2S and isotopically heavy water vapor. This ^{17,18}O-rich water possibly originated from isotopic mass-independent fractionation (MIF) from CO photochemical self-shielding in the protoplanetary disk [3, 4].

Like for the O-isotopes, S-isotopes (Δ^{33}S) may undergo MIF by UV photodissociation processes [5], but the magnitude of fractionation is smaller than for O-isotopes (only few per mil). Because COS has large O isotope MIF and contains ≈10 wt.% S [2], it is an important phase to investigate S-MIF in the early Solar System. Here we report petrographic and O-isotopic searches for COS in Acfer 094 and present preliminary results of S isotope measurements.

Methodology: COS candidates were identified from petrographic observations and SEM-EDS analyses using a Tescan Mira3 FEG-SEM (Fig. 1A). Oxygen isotope measurements on COS candidates were then performed with the Wash U NanoSIMS using a ~2 pA primary beam focused to ~100 nm. We acquired 10x10 µm scanning ion images of ^{16}O$^-$, ^{17}O$^-$, and ^{18}O$^-$ using EMs. O isotope ratios of COS were normalized to their surrounding matrix, assumed to have the same composition as reported in [1]. 2σ errors were estimated to be ≈10‰ on δ^{18}O, ≈23‰ on δ^{17}O. Finally, we performed S-isotope (^{32}S, ^{33}S and ^{34}S) on these COS grains under similar analytical conditions as O isotopes. Because sulfide grains in CM-CI chondrites fall along a mass-dependent fractionation (MDF) line [6], we corrected the Δ^{33}S values of COS with micrometer sulfide grains located in the matrix that show reproductible Δ^{33}S values (σ ≈ 2‰), assumed to fall along a MDF line (i.e., $\Delta^{33}S_{sulfide}$ = 0‰). 2σ errors were estimated to be ≈5‰ on Δ^{33}S.

Results and discussion: The O-isotopic compositions of the three COS candidates reveal that these grains have anomalous O-isotopic signature compared to their surrounding matrix (δ^{17}O ≈ δ^{18}O ≈ 130-160‰; Fig. 1B), confirming their nature as cosmic symplectite [1, 7]. The S isotopic compositions of two COS grains are consistent with zero and one COS showed a

Fig. 1 – (A) BSE image of a COS grain in Acfer 094. (B) δ^{18}O vs δ^{17}O showing the O-isotopic composition of the COS from this study and from [1]. Other data from [8] and references therein. (C) Δ^{33}S plot showing Δ^{33}S measurements in COS (this study) and in chondrites (Bulk CM: [9]; CM2 Pyrrhotite/Pentlandite: [6]; Organics: [10]). Errors are given as 2σ.

hint of S-MIF anomaly at the 2σ level: $\Delta^{33}S_{COS}$ ≈ 6 ± 5‰ (Fig. 1C). If the COS S-MIF can be confirmed with a higher precision measurement, then this result suggests that a MIF process, e.g. UV photodissociation, for both O & S were recorded for some COS grains. The analytical uncertainties of our S isotope measurements by NanoSIMS ion imaging are too high (and dominated by systematics) to detect small mass-independent fractionation as expected for S-isotopes (only S-MIF > 5‰ can be ruled out). Future S isotope analyses of a selection of identified COS using a Cameca ims 1280 are planned.

References: [1] Sakamoto N. et al. (2007) *Science* 317:231–233. [2] Abe K. et al. (2017). *Geochemical Journal* 51:3-15. [3] Yurimoto H. & Kuramoto K. (2004) *Science* 305:1763–1766. [4] Lyons J. R. & Young E. D. (2004) *Nature* 435:317–320. [5] Chakraborty S. et al. (2013) *PNAS* 110:17650–17655. [6] Bullock E. S. et al. (2010) *MAPS* 45:885–898. [7] Nittler L. et al. (2015) 46th *LPSC* Abstract #2097. [8] McKeegan K. D. et al. (2011) *Science* 332:1528-1532. [10] Cooper G. W. et al. (1997) *Science* 277:1072-1074.
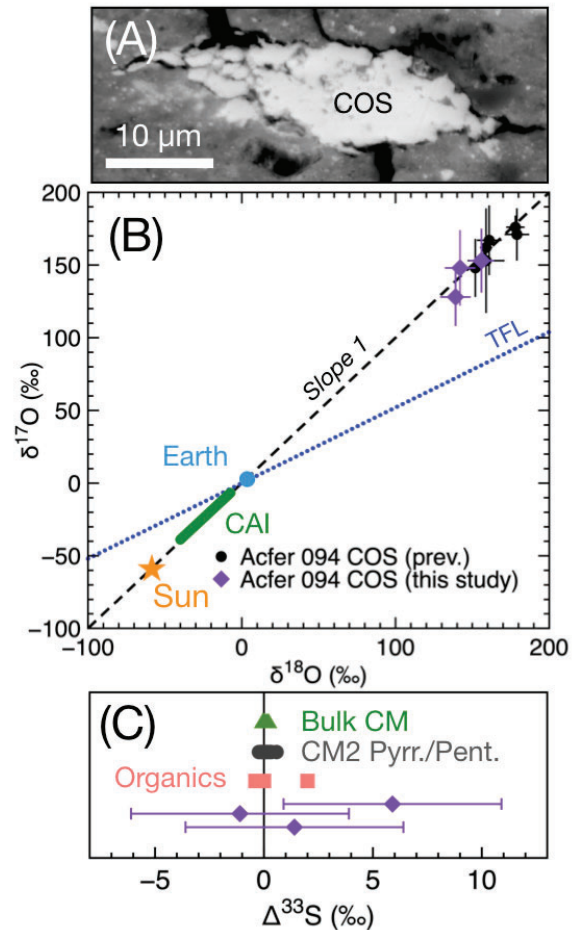
DUNITE BRECCIAS NORTHWEST AFRICA 12217, 12562: POSSIBLE PLANETESIMAL MANTLES

Z. Vaci[1], C. B. Agee[1], and K. Ziegler[1]. [1]Institute of Meteoritics, Department of Earth and Planetary Science, University of New Mexico, Albuquerque, NM.

Introduction: We report here the discovery of two new ungrouped achondrites, Northwest Africa (NWA) 12217 and 12562. NWA 12217 was purchased by Jay Piatek in 2015 from a Moroccan meteorite dealer. The specimen is a single 148 g stone partially covered with black fusion crust. NWA 12562, reportedly found in Algeria in 2017, was purchased by Zuokai Ke in 2018. The specimen is a single 3930 g stone with a small patch of fusion crust. Both samples appear brecciated in hand sample and contain cream-colored to pale green fragmental grains up to 1 cm in size. Discoloration from weathering on some clasts is apparent on both samples.

Mineralogy and Petrology: Polished mounts and a thin section of NWA 12217 show a dunite composed of approximately 93% olivine, 4% low and high-Ca pyroxene, and minor chromite, Fe-sulfide, FeNi metal, andesine plagioclase, alkali feldspar, merrillite, and silica. A polished mount of NWA 12562 shows a similar dunite with approximately 87% olivine, 9% pyroxene, and minor chromite, Fe-sulfide, FeNi metal, and plagioclase. Both meteorites also contain vermicular symplectites composed of chromite and both low and high-Ca pyroxene. Both also appear moderately shocked, with planar fracturing evident in olivine grains. Olivine grains in NWA 12217 display undulose extinction and heavy mosaicism, consistent with shock deformation. Lamellar inclusions composed of chromite, Fe-sulfide, and high-Ca pyroxene cut across olivine grains in NWA 12217. Fractures displace both these and the symplectites, suggesting that these secondary features preceded a shock event.

Major Element Chemistry: The mineralogy of NWA 12217 and 12562 appears equilibrated, as major phases show uniform, unzoned compositions. The variety in these compositions suggests that both meteorites are polymict fragmental breccias, with NWA 12562 displaying a larger amount of variance. Microprobe analyses, NWA 12217: olivine Fa9.1±2.3, Fe/Mn=36±2, n=90; low-Ca pyroxene Fs19.0±1.2 Wo2.7±0.5, Fe/Mn=25±2, n=9; high-Ca pyroxene Fs4.7±1.5 Wo39.6±3.9, Fe/Mn=21±10, n=5; plagioclase Ab62.5±8.8 An35.6±9.2, n=11; alkali feldspar Ab41.6±9.5 An2.6±7, n=9; chromite (in wt%) Al_2O_3=10.1±6.8 Cr_2O_3=59.8±5.1 MgO=10.2±2.9 MnO=0.6±0.1 FeO=17.2±3.1, n=9; kamacite (in mol%) Fe=93.1±0.1 Ni=6.8±0.1, n=8; taenite (in mol%) Fe=82.8±5.1 Ni=17.1±5.1. Microprobe analyses, NWA 12562: olivine Fa14.7±5.0, Fe/Mn=40±3, n=60; low-Ca pyroxene Fs28.8±11.6 Wo3.1±1.0, Fe/Mn=28±2, n=17; high-Ca pyroxene Fs32.3±13.9 Wo21.9±14.9, Fe/Mn=26±3, n=13; chromite (in wt%) Al_2O_3=7.2±4.8 Cr_2O_3=54.4±6.0 MgO=5.0±1.1 MnO=0.7±0.1 FeO=25.7±2.1, n=6.

Oxygen Isotopes: Laser fluorination analyses of three acid-washed fragments from each meteorite show the following oxygen isotopic values. NWA 12217: $\delta^{18}O$ = 3.723, 3.869, 3.660; $\delta^{17}O$ = 1.793, 1.884, 1.796; $\Delta^{17}O$ = -0.173, -0.159, -0.136; weighted average $\delta^{18}O$ = 1.836; $\delta^{17}O$ = 3.776; $\Delta^{17}O$ = -0.158. NWA 12562: $\delta^{18}O$ = 3.477, 3.795, 3.492; $\delta^{17}O$ = 1.609, 1.788, 1.619; $\Delta^{17}O$ = -0.227, -0.216, -0.225; weighted average $\delta^{18}O$ = 1.671; $\delta^{17}O$ = 3.586; $\Delta^{17}O$ = -0.222 (linearized, all per mil, TFL slope = 0.528). The oxygen isotopic composition of the two meteorites is almost indistinguishable, and their values plot in the vicinity of the HED meteorites, angrites, and brachinites in triple-oxygen space. Their $\Delta^{17}O$ values plot between the eucrite and angrite fractionation lines [1].

Discussion: Both NWA 12217 and 12562 exhibit petrological and geochemical characteristics that preclude their designation in any achondrite group. While the brachinites have similar dunitic mineralogy, their olivine composition is much more forsteritic (~Fa27-36 [2]). The brachinite-like achondrites contain more forsteritic olivines (~Fa20-30 [3]), but they exhibit reverse zoning and rims of orthopyroxene and opaques due to sulfidization [3]. The ureilites contain forsteritic olivine (~Fa5-25 [3]), but their diversity in oxygen isotopic composition, high CaO and Cr_2O_3 in their olivines, wt% levels of interstitial C, and olivine reduction rims [3] suggest NWA 12217 and 12562 are not associated with ureilites. The oxygen isotopic composition of these new meteorites could imply affinity with the HED meteorites such as the dunitic diogenites Miller Range (MIL) 03443 or NWA 2968 [4]. However, the presence of albitic plagioclase and alkali feldspar argues against this, as HEDs generally contain anorthitic plagioclase [5]. The symplectites identified in NWA 12217 and 12562 closely resemble similar inclusions found in lunar rocks [6], although those are associated with plagioclase. They also resemble symplectites found in the ungrouped achondrite Queen Alexandria Range (QUE) 93148 [7]. Olivines in brachinites, ureilites, and other primitive achondrites show near-constant chondritic Mn/Mg ratios, suggesting that they are residues of low degrees of partial melting [3,7]. The olivines in NWA 12217 and 12562 show constant Fe/Mn and variable Fe/Mg, suggestive of cumulates formed by large degrees of igneous differentiation and fractional crystallization, potentially within a planetesimal mantle.

References: [1] Greenwood et al. (2005) *Nature* 435:916-918. [2] Krot et al. (2007) *Treatise on Geochemistry*, 1:1-52. [3] Goodrich et al. 2017. *Meteoritics & Planetary Science* 52#5:949-978. [4] Beck et al. 2011. *Meteoritics & Planetary Science* 48#8:1133-1151. [5] Mittlefehldt (2015) *Chemie der Erde* 75:155-183. [6] Elardo et al. (2012) *Geochimic et Cosmochimica Acta* 87:154-177. [7] Goodrich and Righter 2000. *Meteoritics & Planetary Science* 35:521-535.

METEORITIC ABLATION DEBRIS FROM THE SØR RONDANE MOUNTAINS, ANTARCTICA.

M. Van Ginneken[1,2,3,*], N. Artemieva[4,5], P. Claeys[2], V. Debaille[3], S. Decrée[1], L. Hecht[6], S. Yang[7], F. Kaufmann[6], B. Soens[2], F. van Maldeghem[2], M. Humayun[7] and S. Goderis[2] ([*]e-mail: mvanginneken@naturalsciences.be), [1]BGS, Royal Belgian Institute of Natural Sciences, 1000 Brussels, Belgium, [2]AMGC, Vrije Universiteit Brussel, Brussels, Belgium, [3]Laboratoire G-Time, Université Libre de Bruxelles, Brussels, Belgium, [4]PSI, Tucson, Arizona 85719, USA, [5]IDG, Russian Academy of Sciences, Moscow 119334, Russian Federation. [6]. LIEB, Museum für Naturkunde, Berlin, Germany. [7]National High Magnetic Field Laboratory, Tallahassee, FL 32310, USA.

Introduction: Impactors several tens up to 200 m in size are likely to suffer complete disruption and to produce airbursts, similarly to the Tunguska and Chelyabinsk events over Russia in 1908 and 2013, respectively [e.g., 1]. Observations and numerical modeling of medium sized impacts producing airbursts have shown that such impacts represent a significant fraction of extraterrestrial matter accretion to Earth, with Tunguska-like events occurring every 100 to 10,000 years, which is significantly more frequent than crater-forming impact events. However, little is known about occurrences of such airburst events in the geological past, principally due to the lack of easily observable evidences such as impact craters. Finding residues of such events is thus critical to understand the full impact history of the Earth. Here we present the recovery of extraterrestrial particles in the Sør Rondane Mountains, Queen Maud Land, Antarctica, showing characteristic features of airburst impact residues.

Results and discussion: Igneous particles were recovered from glacial sediment collected during the 2017-2018 BELAM (Belgian Antarctic Meteorites) expedition that took place in the Sør Rondane Mountains, Queen Maud Land, Antarctica. Glacial sediment was sampled from a flat eroded summit and a glacial moraine in the Walnumfjellet area. [10]Be exposure age of nearby summits suggest that the first sampled area has been continuously exposed over the last 1-2 Ma [2]. The particles are black, subrounded to perfectly spherical. About half the particles are compound spherules consisting of two or more spherules fused together. Twenty particles were embedded in Epoxy resin and subsequently sectioned. Petrography and mineralogy of the particles were determined using a FEI Quanta 200 environmental scanning electron microscope at the Royal Belgian Institute of Natural Sciences of Brussels, Belgium. Their major element compositions were determined using a JEOL JXA-8500F electron microprobe at Museum für Naturkunde of Berlin, Germany. Oxygen isotopic compositions were determined by means of secondary ion mass spectrometry using a Cameca IMS 1270 at the CRPG of Nancy, France. The mineralogy of the particles consists of olivine and spinel, with minor interstitial glass. On the basis on their internal textures and spinel content, we identify three groups of particles: 1/ the spinel-rich particles (SR; N = 9) ($\geq$19% vol. spinel); 2/ Porphyritic olivine (PO; N = 5) characterized by large euhedral crystals of olivine with minor spinel content (<10% vol.); 3/ Barred olivine (BO; N = 3), which are indistinguishable from barred olivine cosmic spherules on a textural level, containing minor spinel content (<10% vol.).

The bulk major element compositions of the particles are chondritic, pointing to a meteoritic origin. Spinel chemistry in SR particles is characterized by high NiO and MgO contents (3.28-4.84 wt% and 8.12-12.26 wt%, respectively) and Fe^{3+}/Fe_{tot} = 72-89. In porphyritic olivine particles, NiO and MgO contents (0.73-1.16 wt% and 1.77-1.99 wt%, respectively) and ferric iron content (Fe^{3+}/Fe_{tot} = 60-62) are lower, suggesting less oxidizing conditions. Olivine composition is iron poor in SR particles ($Fa_{10\pm3}$) and iron-rich in PO and BO particles (i.e. $Fa_{22\pm4}$ and $Fa_{21\pm5}$, respectively). Nickel content in olivine is always high in all particle types (NiO = 2.78 ± 0.46 wt%), confirming overall highly oxidizing formation conditions. Bulk, spinel and olivine chemical compositions are consistent with meteoritic ablation spheres (MAS), as opposed to cosmic and impact spherules [3]. Furthermore, on a petrological and chemical level, our MAS match extraterrestrial dust particles found as layers in EPICA Dome C and Dome Fuji and dated at ~430 ka ago (i.e. L1 and DF2641, respectively) [4; 5], suggesting a continental distribution. A likely scenario is the disruption of a large (i.e. at least 150 m in size) chondritic asteroid over Antarctica ~430 ka ago. Oxygen isotopic signatures of our MAS are characterized by a highly negative $\delta^{18}O$, ranging from -35 to -52‰, and $\Delta^{17}O$ ranging from -0.5 to -1.2‰, consistent with oxygen isotopic compositions of MAS from the L1 and DF2621 layers. This suggests interaction of the impact plume with Antarctic inland ice (i.e. $\delta^{18}O$ ranging from −55 to −59‰) [6].

Conclusion: We report the discovery of meteoritic ablation spheres from the Sør Rondane Mountains. Their chondritic chemistry, coupled with characteristic spinel and olivine chemical compositions show that they formed in the lower atmosphere during a large airburst event. Oxygen isotopic signatures suggest important interaction with the ice sheet during plume formation. Combining chemical and isotopic composition with a numerical model will help understanding the complex formation processes occurring during this unique airbust event over Antarctic ~430 ka ago.

References: [1] Artemieva N. A. and Shuvalov V. V. (2016) *Annu. Rev. Earth Planet. Sci.* 44: 37–56. [2] Suganuma Y. et al. (2014) *Quat. Sc. Rev.* 97: 102-120. [3] Van Ginneken M. et al. (2010) *Earth Planet. Sci. Lett.* 293: 104–113. [3] Narcisi B. et al. (2007) *Geophys. Res. Lett.* 34: (2007) [4] Misawa K. et al. (2010) *Earth Planet. Sci. Lett.* 289: 287–297. [5] H. Motoyama (2007) *Eos Trans. AGU 88*, abs. #C51A-0076.

SILICA-RICH OBJECTS IN ACFER 182: A NEW VIEW

M. E. Varela[1]

[1]ICATE-CONICET, Av. España 1512 Sur, San Juan, Argentina (eugeniavarela@conicet. gov.ar)

Introduction: Acfer 182 is a member of the CH carbonaceous chondrite group [1], and provides direct information concerning the early solar nebula processes. The CH chondrites [2] are a member of the "CR chondrite Clan" [3, 1] that also includes two other chondrite groups: the CR and CB, subdivided in CBa, and CBb [4-5]. These chondrites are very rich in small chondrules (<90 μm) and chondrule fragments (70 vol. %) [e.g., 2]. A few of these objects have very high SiO_2 contents [6, 7]. These silica-rich objects (SRO) are very rare in carbonaceous chondrites [6, 7]. I report the results of major and trace element studies of some SRO in Acfer 182 (PTS M6013, NHM, Vienna) and compared them with previous studies of SRO, Mg-rich cryptocrystalline (CC) and radiating pyroxene (RP) chondrules in CH chondrites [e.g., 7-12].

Results and Discussion: The studied chondrules (Ch III, VI and XV) with apparent diameters ~90 μm, have amoeboid textures (referred as amoeboid–type objects, from here on) made of silica glass (nearly pure SiO_2) within a silicate (hypersthene normative) matrix. They have bulk abundances of Ca, Al and Mg varying from 0.4 to 0.8 x CI with Cr, Mn, Na and Fe contents that decrease with decreasing volatility. Normalized trace element patterns are flat for the ultra-refractory (Zr, Sc,Nb) and REE elements (with abundances ~ 1-3 x CI), with decreasing and increasing abundances of the moderately volatile (V, Cr, Mn) and volatile elements (Rb, K), respectively. Other SRO from Acfer 182 have emulsion-like textures (referred as emulsion–type objects, from here on) dominated by silicate globules in a silica matrix [e.g., 7, 11]. They exhibit low contents of the ultra-refractory and REE elements (~ 0.01-0.1 x CI) with variable abundances of moderately volatile and volatile elements [11]. The texture of amoeboid- and emulsion-type objects points to co-existence of pyroxene- and silica-normative liquids. Their bulk silica-rich composition (from 74.6 to 86.7 wt% SiO_2) indicate that they formed from a highly-fractionated nebular gas (Si/Mg >1) in which a cosmochemical process was involved, as supported by their Yb and La abundances spreading around the solar ratio. Previous studies of several SRO, in addition to amoeboid- and emulsion-type objects, foresee their formation by liquid immiscibility at high temperatures, above 1968 K, with subsequent fast cooling [7]. However, temperatures ~2000 K would cause grains around 0,2 mm in radius to be fully vaporized [12] as well as extremely low REE contents in those that escaped vaporization. The large variation (one/two orders of magnitude) in trace element abundances revealed by amoeboid-and emulsion-type SRO, signals two chondrule forming regions. Similarly to what has been envisaged for the formation of Mg-rich CC and RP chondrules in Acfer 182 [12]. These chondrule forming regions require a sufficiently high dust/gas ratio to allow formation of stable silicate liquids. Full equilibrium condensation calculations show that it is theoretically possible to have enstatite as the stable liquidus phase in an 800×Cl dust-enriched nebular gas at a p^{tot} of 10^{-3} atm, if about 72% of the original Mg is removed (as forsterite?) from the system [13]. Because pyroxene-dominated chondrules need "dust-enriched" regions with similar dust/gas ratios (>500 x CI) as those needed to form BO chondrules (~700 x CI) [14], both objects could have shared the same nebular region. Therefore, formation in the CH chondrule forming region of barred and skeletal olivine (BO, SO) chondrules, as well as Mg-rich CC and RP ones will progressively deplete the gas in Mg and trace element contents, and increase its SiO_2 content. Cooling of such dust-enriched regions, from which Mg and trace elements are gradually removed, might end in the formation of liquids rich in Si and poor in refractory elements (e.g., the SRO precursors).

References: [1] Krot et al., (2002) *Meteoritics and Planetary Science* **37,** 1451–1490; [2] (Bischoff et al., (1993) *Geochimica et Cosmochimica Acta* **57,** 2631–2648; [3] Weisberg et al., (1995) *Proc. Natl. Inst. Polar Res.: Symp. Antarct. Meteorites* **8**, 11–32; [4] Weisberg et al., (1993) *Geochimica et Cosmochimica Acta*, **57**, 1567-1586; [5] Weisberg et al., (2001) *Meteoritics and Planetary Science* **36**, 401–418; [6] Petaev et al., (2001) *LPSC 32, #* 1450; [7] Hezel et al., (2003) *Meteoritics and Planetary Science*, **38**, 1199–1215; [8] Krot et al., (2001) *Science* **291**, 1776–1779; [9] Russell et al., (2000) *Meteoritics and Planetary Science* **35**, Supp. A139; [10] Hezel et al., (2004) *Workshop on Chondrites and Protoplanetary Disk*, # 9095; [11] Varela and Zinner (2012) LPSC 43 # 1405; [12] Varela (2019) Geochimica et Cosmochimica Acta (in press); [12] Horányl et al., (1995) *Icarus*, **114**, 174-185; [13] Engler et al., (2007) *Icarus* **192**, 248–286; [14] Varela et al., (2006) *Icarus,* **184**, 344–364.

High-resolution measurements of Mg, Si, Fe and Ni isotopes of O-rich presolar grains.

M. J. Verdier-Paoletti[1], L. R. Nittler[1], and J. Wang[1], [1] DTM, Carnegie Institution for Science, Washington, DC, 20015, USA (mverdier@carnegiescience.edu)

Introduction: Presolar grains, hosted within the matrix of primitive meteorites, are windows into the nucleosynthesis of stars. Presolar O-rich grains, such as silicates and oxides, have been divided into partially distinct groups on the basis of their large O-isotope anomalies [1]. Group 1 encompasses the largest fraction of grains (~70%), and likely formed in outflows of low-mass AGB stars (1.2-2.2 $M_\odot$) and an AGB origin is also probable for the highly ^{18}O-depleted Group 2 grains [1]. Aside from possible radioactive decay products (*e.g.*, ^{26}Mg from ^{26}Al), nucleosynthesis in these stars is not expected to significantly modify Mg, Si, Fe or Ni isotopes [2,3,4,5]. As a consequence, the isotopic compositions of Group 1 presolar grains in those elements is thought to represent those of the parent stars, thus reflecting galactic chemical evolution (GCE). Mg isotopes have been extensively studied in presolar oxides [3,6,7] but very little in presolar silicates [2], the latter often having large errors owing to technical limitations [2,3]. These limitations were recently removed with the new Hyperion II RF plasma O primary ion source for the NanoSIMS that has already enabled high-resolution studies of Mg and Si isotopes in presolar silicates [5,8,9]. Here we report additional isotope measurements of those elements along with Fe and Ni isotopes in several presolar silicates and oxides from the Acfer 094 (ungrouped C3) meteorite.

Methods: Presolar grains were identified in Acfer 094 by O isotopic mapping (with a Cs^+ primary beam) in the Carnegie NanoSIMS 50L and analyzed for additional elements with the Hyperion II RF plasma O^- source. 18 presolar silicates and 3 oxides (19 group 1, 2 group 2) were measured for $^{24,25,26}Mg$, ^{27}Al, and $^{28,29,30}Si$ isotopes in multicollection mode with a 0.5pA primary beam (~80nm resolution) over a $2\times2\mu m^2$ raster. Each measurement was normalized to its surrounding matrix. 11 grains were re-measured in a second session for ^{52}Cr, $^{54,56,57}Fe$ and $^{58,60,61,62}Ni$ isotopes in combined analysis mode with similar beam conditions over a $3\times3\mu m^2$ raster. Metal globules of the meteorite and the 519-4-1 glass were used as standards. We corrected for possible ^{54}Cr contributions to ^{54}Fe assuming a solar composition of Cr and ^{58}Fe contribution to ^{58}Ni in the same way.

Results & Discussion: Si-isotopic measurements of our grains are consistent with previous studies, *i.e.* roughly lining along the SiC Mainstream-line with $\delta^{29}Si$ and $\delta^{30}Si$ ranging between -35 to 204‰ and -14 to 176‰ respectively. Fig. 1 shows the large range of Mg-isotopes compositions recorded in O-rich presolar grains. We found fewer grains with close to solar composition and a larger scatter from the GCE trend than observed in previous studies. A few grains cluster around a ^{25}Mg-enriched composition close to 200‰ with solar to slightly enriched ^{26}Mg. In addition, a significant fraction of our grains depart from the GCE trend toward more ^{25}Mg-depleted compositions for $\delta^{26}Mg$ values close to 100‰. The isotope maps also revealed four grains with Mg and/or Si isotopic anomalies that were not identified on the basis of O isotopes; all have Mg and Si isotope compositions falling within the range of presolar silicates and oxides attesting to their presolar origin. One exhibits high enrichments in both ^{25}Mg and ^{26}Mg, falling close to the GCE trend (Fig. 1a). One Group 2 silicate grain has the highest enrichment in ^{25}Mg ever recorded with a $\delta^{25}Mg$ value of ~2000‰. It is unlikely that this composition can be reached in an intermediate-mass AGB star or novae. A supernova experiencing explosive H burning may explain this grain [9], but we suggest instead that a super-AGB star origin may be more likely [10]. Out of eleven grains measured, six exhibited Fe and possible Ni anomalies but data are still being processed.

Figure 1 – Mg isotopes compositions of presolar grains in this study. Red circles represent Mg-anomalous grains of which no O-isotopic composition was acquired. Error bars are 1σ. Dashed line depict the solar composition. Solid line has a slope 1 and roughly represents the GCE trend.

References: [1] Nittler L. R. & Ciesla F.(2016), *ARAA, 54*, 53-93. [2] Kodolanyi J., et al. (2014), *GCA, 140*, 577-605. [3] Nguyen A. N. & Messenger S. (2014), *ApJ*, 784 :149. [4] Trappitsch R., et al. (2018), *GCA, 221*, 87-108. [5] Hoppe P., et al. (2018), *ApJ*, 869:47. [6] Nittler L. R., et al. (2005), *ApJ*, 682:150-1478. [7] Gyngard F., et al. (2010), *ApJ*, 717:107-120. [8] Leitner J., et al. (2019) *LPS 50th*, Abstract #2090. [9] Leitner J. & Hoppe P. (2018) *LPS 49th*, Abstract #1858. [10] Doherty L. C., et al. (2014), *MNRAS*, 437, 195-214.
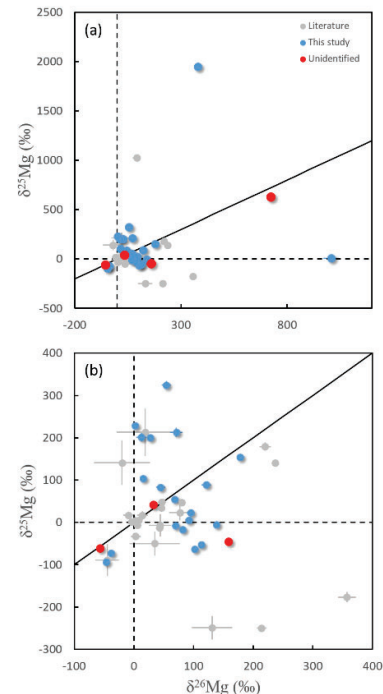
A NANOSCALE ANALYTICAL STEM STUDY OF THE PARIS METEORITE

K. L. Villalon[1,2,], J. P. Bradley[3], H. A. Ishii[3], K. K. Ohtaki[3], A. M. Davis[1,2,4], and T. Stephan[1,2]. [1]Department of the Geophysical Sciences, The University of Chicago, Chicago, IL, USA, [2]Chicago Center for Cosmochemistry, [3]Hawaiʻi Institute of Geophysics & Planetology, University of Hawaiʻi at Mānoa, Honolulu, HI, USA. [4]Enrico Fermi Institute, The University of Chicago, Chicago, IL, USA. E-mail: kvillalon@uchicago.edu

Introduction: Paris is considered to be the least altered CM chondrite [1]. It is a breccia with evidence of heterogeneous aqueous alteration, containing both metal-rich lithologies with abundant amorphous silicates as well as metal-poor lithologies with abundant phyllosilicates. In the least altered lithologies, Paris has been found to preserve material closely resembling GEMS (glass with embedded metal and sulfides) from interplanetary dust particles (IDPs) [2]. If the GEMS-like material in Paris can be confirmed to be related to IDP GEMS, it may uniquely demonstrate the progression of silicates from the interstellar medium and/or early solar nebula to incorporation into a growing planetesimal and subsequent alteration. If the GEMS-like material in Paris is unrelated to IDP GEMS, it may represent a significant yet altogether unexplored class of objects in primitive meteorites.

GEMS grains have yet to be unambiguously identified in meteorites. While the GEMS-like material in Paris has textural similarities to IDP GEMS as well as comparable average chemical compositions as measured by energy-dispersive X-ray spectroscopy (EDS), the ubiquity of nanophase components throughout the GEMS-like material makes comparisons difficult and necessitates more detailed scrutiny before definitive identifications can be asserted. The same is true for GEMS-like material that has recently been observed in the CR chondrite LaPaz Icefield 02342 [3] and whose nanophase components also await definitive mineral identification. Inclusions in GEMS and GEMS-like objects are ~1–30 nm in size, smaller than the thinnest TEM sections. Nanodiffraction [4] is able to obtain diffraction patterns from regions <1 nm. Unlike with EDS, it is more easily discerned when multiple phases are contributing to an electron diffraction pattern, and it is possible to remove the contribution from unwanted phases. Nanodiffraction can therefore provide essential mineralogical information on the often-neglected smallest class of objects in meteorites.

Samples and Methods: Section 2010-1 of the Paris meteorite was provided by the Muséum National d'Histoire Naturelle. Nine electron-transparent lamellae were lifted out with a TESCAN LYRA3 FIB-SEM at the University of Chicago and thinned and polished with an FEI Helios NanoLab 660 Dual Beam FIB at the Hawaiʻi Institute of Geophysics & Planetology (HIGP). Areas of interest were chosen from a range of petrologic settings with possibly different formation histories and varying degrees of aqueous alteration. The final size of each lamella was <100 nm × ~15 μm × 7–8 μm with a ~5 μm protective strap. The sections were examined using a FEI Titan3 G2 scanning transmission electron microscope (STEM) equipped with a Genesis 4000 Si(Li) solid-state X-ray energy-dispersive spectrometer (EDAX Inc.) at HIGP. The sections were imaged using both conventional bright-field and high-angle annular dark-field (HAADF) modes. Elemental compositions were measured by EDS, while crystallographic information was acquired by electron diffraction—either nanodiffraction for nanoscale phases or SAED (selected area electron diffraction) for larger phases. In some cases, high-magnification lattice-fringe images were also taken.

Results: Preliminary EDS and diffraction analyses indicate compositional and mineralogical differences between the nanophase inclusions in IDP GEMS and Paris GEMS-like material. Notably, nanophase FeNi metal grains have yet to be identified in Paris. Grains with EDS spectra suggestive of FeNi metal have diffraction patterns inconsistent with metal and, instead, are identified as carbides or oxides, demonstrating the problem with relying on EDS spectra alone in identifying nanoscale phases. The nano-inclusions are predominantly pyrrhotite and pentlandite. Nanophase pentlandite appears to be more prevalent in more highly altered matrix material but is also found in the least altered matrix material of Paris. Pentlandite is not found as inclusions within IDP GEMS and is usually considered to be evidence of hydration when present in IDPs [5]. Other mineral phases identified in our Paris sections include low-iron, Mn-enriched (LIME, $Mn/FeO \geq 1$) silicates, an enstatite platelet, and two forsterite whiskers.

Discussion and Conclusions: While the matrices of Paris and other primitive chondrites contain material with textural and elemental similarities to GEMS from cometary IDPs, nanodiffraction reveals mineralogical differences between the respective nano-inclusion populations. At this time, it is unclear if the differences between IDP GEMS and the GEMS-like material of Paris require an independent origin, or if the differences are solely the result of alteration. The presence of LIME silicates, enstatite platelets, and forsterite whiskers confirms the incorporation of vapor phase condensates into the CM parent body and may suggest a relationship between the Paris matrix and cometary material, but more studies are needed to verify such a relationship.

References: [1] Hewins R. H. et al. (2014) *Geochimica et Cosmochimica Acta* 124:190–222. [2] Leroux H. et al. (2015) *Geochimica et Cosmochimica Acta* 170:247–265. [3] Nittler L. R. et al. (2019) *Nature Astronomy,* https://doi.org/10.1038/s41550-019-0737-8. [4] Cowley J. M. (1999) *Microscopy Research & Technique* 46:75–97. [5] Zolensky M. E and Thomas K. L. (1995) *Geochimica et Cosmochimica Acta* 59:1407–1412.

ORIGIN AND EVOLUTION OF THE OXYGEN ISOTOPIC COMPOSITIONS OF CHONDRULES

J. Villeneuve[1] and Y. Marrocchi[1]

[1]CRPG, CNRS, Université de Lorraine, UMR 7358, Vandoeuvre-lès-Nancy, 54501, France (johanv@crpg.cnrs-nancy.fr)

Introduction: Chondrules, sub-millimeter-size silicate spheroids comprising olivine ($[Mg,Fe]_2SiO_4$) and low-Ca pyroxene ($[Mg,Fe]SiO_3$) crystals embedded in glassy mesostasis, constitute the main high-temperature component of chondrites. They formed by the solidification of melt droplets, though the mechanism(s) that produced those droplets remain(s) elusive. A key clue to their origin would be the identification of the precursor material that was melted to form chondrules [1]. In this effort, cosmochemists may find help in the incomplete melting of most chondrules, as evidenced by their widespread porphyritic texture.

Method & Results: A new analytical approach based on high-current X-ray maps, high-current quantitative eletron microprobe analyses and oxygen isotopic analyses via secondary ion mass spectrometry has revealed previously unrecognized internal structures within type I chondrules of Northwest Africa 5958 (C2-ung) and Kaba (CV3). Indeed, studied chondrules displayed Ca-Al-Ti-poor olivine cores surrounded by Ca-Al-Ti-richer olivine overgrowths often showing oscillatory zoning toward the edge of the chondrules [2-3]. Considering that relict grains are those with $\Delta^{17}O$ beyond 3σ of the host value [4], oxygen isotopic measurements demonstrated that many of these core grains are isotopically distinct from host olivine and therefore must be relict. Apart for one chondrule in NWA 5958, all of the relict olivine grains are enriched in ^{16}O compared to their host. They yield a wide range of $\Delta^{17}O$, ranging overall from -23‰ to 0.5‰, even within a single chondrule [2-3]. In contrary, hosts olivine show a single discrete $\Delta^{17}O$ within each chondrule [2-3].

Discussion: This study allowed the first the chemical characterization of relict olivine grains in type I chondrules. The Ca-Al-Ti-poor and ^{16}O-rich nature of most relicts indicate chemical and isotopic similarities with AOAs-like condensates. It is also worth to note that the analyzed relict olivine grains define a $\delta^{17}O$–$\delta^{18}O$ correlation described by $\delta^{17}O = (1.04\pm0.06) \times \delta^{18}O – (2.78\pm0.60)$ that is indistinguishable within errors from the primary chondrule minerals (PCM) line defined by SIMS measurements in chondrules (i.e., amalgamated host and relict data) from different carbonaceous chondrites [4]. The PCM line may thus have been already established in the chondrule precursors rather than being a result of chondrule formation, although some of the relicts (presumably among those in the range of host compositions) may be recycled chondrule debris. Overall, chondrules are complex objects formed by (i) recycling of a previous generation of solids in all likelihood formed in the solar protoplanetary disk, as demonstrated by relict olivine grains, and (ii) *in situ* host minerals crystallization with significant gas-melt interactions in the chondrule-forming region(s) [2-3, 5-6]. In conjunction with literature data [7-8], we used our results to (i) define the chemical and oxygen isotopic composition of relict and host olivine grains in type I chondrules and (ii) discuss the origin and the evolution of the oxygen isotopic composition of chondrules.

References:
[1] Jacquet E. & Marrocchi Y. (2017) *Meteoritics & Planetary Science* 52: 2672-2694. [2] Marrocchi Y. et al. (2018) *Earth and Planetary Science Letters* 496:132-141. [3] Marrocchi Y. et al. (2019) *Geochimica and Cosmochimica Acta* 247:121-141. [4] Ushikubo T. et al. (2012) *Geochimica and Cosmochimica Acta* 90:242-264. [5] Piani L. et al., (2016) *Geochimica and Cosmochimica Acta* 195: 84-99. [6] Marrocchi Y. & Libourel G. (2013) *Geochimica and Cosmochimica Acta* 119:117-136. [7] Hertwig A.T. et al. (2018) *Geochimica and Cosmochimica Acta* 224:116-131. [8] Chaumard N. et al. (2018) *Geochimica and Cosmochimica Acta* 228:220-242.

MANGANESE-CHROMIUM AGES OF CARBONATES IN AQUEOUSLY-ALTERED CARBONACEOUS CHONDRITES AND CLASTS.

R. Visser[1], T. John[1], M. Patzek[2], A. Bischoff[2], and M. J. Whitehouse[3].

[1] Freie Universität Berlin, Institut für Geologische Wissenschaften Berlin, Malteserstr. 74-100, 12249, Berlin, Germany (correspondence: robbin.visser@fu-berlin.de). [2] Institut für Planetologie, University of Münster, Wilhelm-Klemm-Str. 10, D-48149 Münster, Germany. [3] Swedish Museum of Natural History, Box 50007, 104 05, Stockholm, Sweden.

Introduction: Recent studies show great improvements in the understanding of xenolithic material that can be found in various achondrites (HED, ureilites) and chondrites (ordinary chondrites, CR, CB, CH chondrites) [1,2]. This xenolithic material shares similarities with CI and CM chondrites but might represent material that has not yet been identified as bulk meteorites. So far, previous work shows that C1 clasts (previously referred to as CI-like) and CM-like have a very similar mineralogy to CI and CM chondrites [e.g., 1]. Apart from the mineralogy, peak temperatures experienced by clasts and chondrites are also coherent with each other [3]. However, recent isotope studies [4,5] show evidence for differences between C1 clasts and CI chondrites. Isotope signatures of CM clasts and CM chondrites overlap. The differences in isotopic compositions between C1 clasts and CI chondrites might have been caused by sampling spatially different reservoirs or a difference in timing of parent body formation resulting in sampling of differently evolved reservoirs. To evaluate whether the timing of formation is a factor that might have caused sampling of different isotopic reservoirs, the Mn/Cr system is used. Its short half-life (3.7 Ma [6]) makes it suitable to date processes active at the early stages of the solar system evolution [e.g., 7, 8]. In this study, Mn/Cr ages of carbonates in CI and CM chondrites as well as those in CM-like and C1 clasts are determined, to investigate the timing of the aqueous alteration forming these carbonates.

Methods: Mn/Cr ages of calcite and dolomite in 7 carbonaceous chondrites; Ivuna, Alais, Orgueil (all CI), Murchison, Murray, LON94101 (all CM), Essebi ($C2_{ung}$) and ~10 xenolitic clasts (C1 and CM-like) in Kaidun, DaG 319, Sahara 98465, NWA 7542, PRA 04401, PRA 04402 were obtained using an ims1280 secondary ion mass spectrometer at NORDSIMS, Stockholm. The analytical methods used in this study are similar to those of [9] and a San Carlos olivine as well as a synthetic calcite standard (produced by P. Donohue from the Hawai'i Institute of Geophysics and Planetology) were used to correct for instrumental mass fractionation (IMF) and to determine the relative sensitivity factor (RSF). All analyses were anchored to the D'Orbigny angrite (4563.4 ± 0.27 Ma; [10]) to obtain the absolute ages.

Results and Discussion: Mn/Cr ages of carbonates in CM2 chondrites [11], CI chondrites [12], and CR chondrites [9] have been constrained in literature. Preliminary results of this study show that Mn/Cr ages for dolomites in Ivuna ($4562.8^{+0.8}_{-1.1}$) and Orgueil ($4563.4^{+1.3}_{-1.7}$) are coherent to ages previously determined [12]. A newly constrained Mn/Cr age of dolomites in Alais appears to be within the same range ($4564.2^{+0.8}_{-1.0}$). Mn/Cr ages of carbonates of C1 volatile-rich clasts in DaG 319 and Sahara 98465 however, could not be constrained even though compositional analyses show similar Mn and Cr concentrations to dolomites analysed in the CI chondrites. Possibly, the carbonates were formed after the extinction of the short-lived ^{53}Mn meaning that the aqueous alteration happened at least 15 Ma after that of CI chondrites. Alternatively, the carbonates could also have formed due to terrestrial weathering on Earth. Both possibilities will be investigated as well discussing Mn/Cr ages of carbonates in CM-like clasts and different CM and C1 lithologies in Kaidun. Ultimately, we are trying to resolve any differences between the Mn/Cr ages of carbonates in CI chondrites and C1 clasts.

Conclusion: Mn/Cr ages of carbonates in aqueously-altered carbonaceous chondrites agree well with previously published ages. Extending the dataset with more Mn/Cr ages of carbonates in CI clasts could potentially resolve the question of whether there is an actual difference in timing of the aqueous alteration event between the parent bodies of CI chondrites and C1 clasts.

References: [1] Patzek M. et al. (2018) *Meteoritics and Planetary Science* 53:2519-2540. [2] Zolensky M.E. et al. (1996) *Meteoritics & Planetary Science* 31:518-537. [3] Visser R. et al. (2018) *Geochimica et Cosmochimica Acta* 241:38-55. [4] Patzek M. et al. (2019) *LPS L,* Abstract 1779. [5] Visser R. et al. (2017) *Meteoritics and Planetary Science* 53:#6190 [6] Honda M. and Imamura M. (1971) *physical review C* 4:1182. [7] Lugmair G. W. and Shukolyukov A. (1998) *Geochimica et Cosmochimica Acta* 62:2863-2886. [8] Endress M. et al. (1993) *Nature* 379:701 [9] Jilly-Rehak C. et al. (2017) *Geochimica et Cosmochimica Acta* 201:224-244. [10] McKibbin S. J. et al. (2015) *Geochimica et Cosmochimica Acta* 110:216-228. [11] Fujiya W. et al. (2011) *Nature communications* 3:627 [12] Fujiya W. et al. (2013) *Earth and Planetary Science Letters* 362:130-142.

MICROPHOTOLUMINESCENCE STUDY OF CHELYABINSK LL5 CHONDRITE

A. S. Vokhmintsev, S. S. Savchenko, N. A. Martemyanov and I. A. Weinstein
Ural Federal University, Mira street 19, Yekaterinburg, Russia, 620002, a.s.vokhmintsev@urfu.ru

Introduction: It was previously found that fragments of the Chelyabinsk meteorite with light and dark lithology have different physicochemical properties [1, 2]. Photo- and thermally stimulated recombination processes occur more intensively in light lithology samples due to the presence of various chain silicates from the olivine and group of multicomponent pyroxenes. Moreover, the kinetic and spectral characteristics of the observed mechanisms depend not only on the phase composition, but also on the radiation history, numerous structural and other transformations in the studied chondrite [3–6]. This work deals with the investigation of photoluminescence properties of the Chelyabinsk chondrite with microscale spatial resolution and comparative analysis of the data obtained with the results of scanning electron microscopy study.

Samples and Technique: Fragments of the Chelyabinsk LL5 chondrite with the dominance of light lithology were examined. Optical images of the samples under study (see Fig. 1, *a*) was obtained using an Axio CSM 700 confocal optical microscope (Carl Zeiss, Inc.). Microphotoluminescence (µPL) spectra were studied by means of LUMAM I3 microscope (LOMO, Inc.). The µPL signal was recorded in the 400–700 nm spectral region under excitation by filtered light of a DRSh-250 mercury lamp in the 300–380 nm range. The surface images of the samples in the luminescence mode were obtained using an EOS 650D digital SLR camera (Canon, Inc.) (see Fig. 1, *b*). To achieve high spectral resolution, the images were transferred through an A2873 quartz fiber (Hamamatsu Inc.) to Shamrock SR-303i-B spectrograph (Andor, Inc.). This dispersed signal was measured using Newton[EM] DU970P-BV-602 CCD matrix (Andor, Inc.) cooled down to 193 K. A quantitative chemical analysis and mapping of elements distribution were carried out via a SIGMA VP electron microscope (Carl Zeiss, Inc.) fitted with an X-Max energy dispersive spectrometer (Oxford Instruments, Inc.).

Results and Discussion: Fig. 1 shows that the sample surface luminesces in different spectral ranges. Blue-white and brown emission originating from the areas of about 10 µm dominates. Luminescence in the blue spectral region is also observed in several spatial domains with dimensions of ≤ 1 µm. Additionally, there are some few spots ≤ 1 µm in size of green and yellow colors.
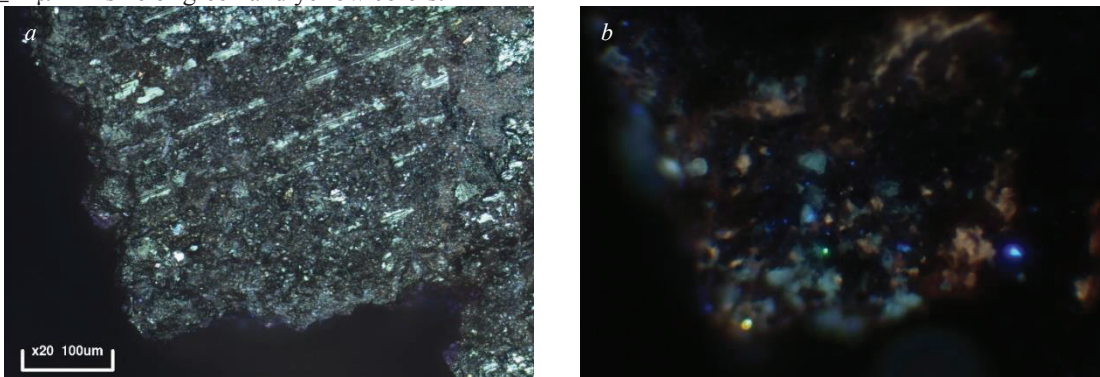
Fig. 1. Photo (*a*) and µPL image (*b*) of the Chelyabinsk LL5 chondrite with the same scale bar.

The study presents µPL spectra measurements of the regions identified by different emission color. Wide structureless bands are observed and positions of spectral maxima are shifted upon the color change of the luminescent region. The obtained results are in reasonable agreement with our preceding PL studies both of individual fragments and powder of the Chelyabinsk meteorite without spatial resolution [1]. The following chemical elements were found at the area demonstrated in Fig. 1: O (61.0 at. %), Si (13.5 at. %), Mg (13.2 at. %), Fe (6.3 at. %), Al (1.8 at. %), Ca (1.4 at. %), Na (1.1 at. %), S (0.9 at. %), Cr (0.4 at. %), P (0.2 at. %) and K (0.2 at. %). Comparison of the µPL image with the elements distribution maps was carried out. It was concluded that olivine and Mg-Fe pyroxenes prevail in the samples of LL5 chondrite along with the presence of lower concentrations of other pyroxenes.

References: [1] Popova O.P. et al. 2013. Science 342: 1069–1073. [2] Kohout T. et al. 2014 Icarus 228: 78–85. [3] Weinstein I.A. et al. 2014. Meteoritics & Planetary Science 49: A428. [4] Weinstein I.A. et al. 2015. Meteoritics & Planetary Science 50: 5175. [5] Vokhmintsev A.S. and Weinstein I.A. 2017. Meteoritics & Planetary Science 52: A371. [6] Vokhmintsev A.S. and Weinstein I.A. 2018. Meteoritics & Planetary Science 53: 6304.

EXPERIMENTAL STUDY OF NORTHWEST AFRICA 12370 METEORITE'S MECHANICAL PROPERTIES.

Voropaev S.A.[1], Nugmanov I.I.[2], Dushenko N.V.[1]
[1]V.I. Vernadsky Institute of Geochemistry and Analytical Chemistry RAS, Kosygina 19, Moscow; [2]Kazan Federal University, 420008, Kazan, Russia. E-mail: voropaev@geokhi.ru

Introduction: Usually, pre-entry 10-100 meter scale interplanetary meteoroids are typically highly fractured and can break up under tensile stresses of 0.03 + 1 MPa [1]. The exception is the fall (September 15, 2007) of the Carancas stony meteorite in Peru that caused the formation of a 13 m wide impact crater. It was classified as an ordinary chondrite H4-5 W0 S3 with an estimated initial size ~ 0.9 + 1.7 m, a compressive strength ~ 20 + 40 MPa and a tensile strength ~ 1.2 + 2.4 MPa, depending of the trajectory [2]. So, the Carancas meteorite is a rare example of a monolithic meteoroid that was almost free of internal cracks. Such meteorites are the most dangerous to the Earth and we have tried to study their mechanical properties more fully with the help of the most appropriate analogue. The very similar meteorite, Norhtwest Africa 12370, was purchased at the mineralogical exhibition (Mineralientage München, Germany) in October 25, 2018 from the Mr. Ait Ha Lahcen from Erfoud, Morocco (see table 1 for theirs comparison). It was classified by Lorenz C.A., Vernadsky Institute, as H5 W1 S2 [3].

Table 1. Mineral compositions

Meteorite, name	Classification	Fayalite (mol %)	Ferrosilite (mol %)	Wollastonite (mol %)	Oxygen isostopes (‰)
Carancas	H4-5 W0 S3	18.4±0.5	16.1±0.2	No data	$\Delta^{17}O = 3.017$; $\delta^{18}O = 4.519$; $\Delta^{17}O = 0.667$
NWA 12370	H5 W1 S2	19.3±0.6	16.1±0.3	1.5±0.9	No data

Methods: The study of mechanical properties of the meteorite sample was performed in accordance with the following regulatory documents: ASTM D2845-08 Standard Test Method for Laboratory Determination of Pulse Velocities and Ultrasonic Elastic Constants of Rock.The testing was carried out at the Institute of Geology and Petroleum Technologies, Kazan Federal University. Measurement of the velocity of the longitudinal and transverse ultrasonic wave is performed at the PEAK-ULTRASONIC-EP installation. The system consists of two ultrasonic sensors, a signal source, an oscilloscope, an RLC and a relay systems. The source generates a signal with a frequency of 1 MHz. The signal is received by one of the sensors, which excites the pulses of S and P waves. The waves pass through the sample installed in the core holder and are detected by a second ultrasonic measurement sensor.

Results and Discussion: The calculation of the dynamic elastic moduli (Young's and Poisson's ratio) were carried out according to the formula (1)

$$R = V_p/V_s = \sqrt{2}(1-\mu)/(1-2\mu), \quad E = V_p^2 \rho (1+\mu)(1-2\mu)/(1-\mu), \tag{1}$$

where R - ratio of longitudinal and transverse waves, Vp - velocity of longitudinal waves, Vs - velocity of transverse waves, μ - dynamic Poisson's ratio, E - dynamic Young's modulus, ρ - density of rocks. Cylindrical sample of NWA 12370 with length 41.74 mm and diameter 29.55 mm had a density $\rho = 3.518$ g/cm^3.

Table 2. Results of determining the velocity and dynamic elastic parameters of NWA 12370

Pressure, MPa	Vs, km/s	Vp, km/s	E (dyn), GPa	Poisson ratio (dyn)
1	3.413	5.471	95.97	0.1814
10	3.441	5.773	101.12	0.2245
30	3.528	5.773	104.35	0.2019

Dynamic parameters and values obtained by static load of meteorites [4] may differ significantly. Full consideration will be given in the following article.

References:
[1] Popova O. et al. 2011. Meteoritics and Planetary Science, **46**(10): 1525-1550.[2] Connolly H. C. et al. 2008. The Meteoritical Bulletin, No. 93. Meteoritics and Planetary Science, **43**: 571-632. [3] Lorenz C.A. et al. 2019. The Meteoritical Bulletin, No. 108 (in preparation). [4] Voropaev S., Nugmanov I., Dushenko N. et al. 2017. Doklady Astronomy&Physics, 62(10): 486-489.

SPECIFIC HEAT, MEAN ATOMIC WEIGHT AND RELICT TEMPERAURES OF BURSA L6 CHONDRITE.

R. A. Wach[1], M. Szurgot[2], O. Unsalan[3] and C. Altunayar-Unsalan[4], [1]Lodz University of Technology, Institute of Applied Radiation Chemistry, Wróblewskiego 15, 93 590 Lodz, Poland (wach@mitr.p.lodz.pl), [2]Lodz University of Technology, Center of Mathematics and Physics, Al. Politechniki 11, 90 924 Lodz, Poland (mszurgot@p.lodz.pl), [3]Ege University, Faculty of Science, Department of Physics, 35100, Bornova, Izmir, Turkey (physicistozan@gmail.com), [4]Ege University, Central Research Testing and Analysis Laboratory Research and Application Center, 35100, Bornova, Izmir, Turkey (cisemaltunayar@gmail.com).

Introduction: Thermophysical properties and mean atomic weight are important for characterization of extraterrestrial rocks and their parent bodies: asteroids and planets. Differential scanning calorimetry (DSC) is widely used for measuring specific heat capacity of extraterrestrial matter, temperature of phase transformations, and enthalpy changes in terrestrial and meteoritic minerals. The aim of the paper was to measure specific heat capacity of Bursa meteorite at various temperatures, to measure grain density, determine relict temperatures, troilite content, mean atomic weight, and mean atomic heat of this chondrite. Bursa meteorite fell in 1946, in Turkey, and have been classified as a L6 chondrite.

Methods: Specific heat capacity Cp of crushed samples (c.a. 20 mg) were determined by a DSC Q200 (TA Instruments, USA) in the temperature range between 223 and 623 K. Literature data on chemical composition of Bursa chondrite [1] were used to calculate $Amean$ and Fe/Si values. Apart from the bulk composition, also Fe/Si ratio and measured grain density $dgrain$ were used to predict $Amean$ values using $Amean(Fe/Si)$, and $Amean(dgrain)$, relationships, established by Szurgot (e.g. [2-4]). Relict temperatures and troilite content were determined using DSC technique and troilite thermometry (e.g. [5,6]).

Results and discussion: It was established that the mean specific heat of four Bursa interior samples in temperature range between 223 and 623 K increases from 603 to 971 J/(kg·K). Cp values of individual samples exhibit significant differences. Specific heat capacity of sample 1, for example, is between 571 and 1038 J/(kg·K), and of sample 2 is between 630 and 978 J/(kg·K), at temperatures 223 K and 623 K, respectively. The mean values of Cp vary with the temperature and are equal to: 603±33 J/(kg·K) at 223 K, 772±32 J/(kg·K) at 323 K, 837±36 J/(kg·K) at 373 K, 896±48 J/(kg·K) at 473 K, and 934±35 J/(kg·K) at 573 K.

Measurements of specific heats of individual Bursa interior samples at room temperature (300 K) exhibited the following values: 686, 711, 737, 747, 748, 760, and 788 J/(kg·K) (mean:740±33 J/(kg·K), range: 686-788 J/(kg·K)). Mean atomic heat ($Amean·Cp$) of Bursa chondrite: 17.5±0.9 kJ/(mol·K) at room temperature.

Room temperature values of specific heat of Bursa meteorite are close to Cp of other ordinary chondrites: L chondrites: 742 J/(kg·K) [7], H chondrites: 714 [7], Braunschweig L6 chondrite: 727±32 J/(kg·K) [6], Soltmany L6 chondrite: 728±35 J/(kg·K) [5], Jilin H5: 726±13 J/(kg·K) [8], and Gao-Guenie H5: 732±7, 740 ±27 J/(kg·K) [8].

Bursa Fe/Si atomic ratio (0.563) is close to the average for L6 falls: 0.60 ± 0.04, and is within the L6 range: 0.53-0.65 [3]. Mean atomic weight of Bursa: $Amean$ = 23.61±0.17 (average of $Amean(Bulk\ composition)$ = 23.41, $Amean(Fe/Si))$ = 23.71, and $Amean(dgrain)$ = 23.70) is close to the mean atomic weight of L6 chondrite falls (average: 24.06 ± 0.16, range: 23.6-24.4, [3]). Average values of $Amean's$ and Fe/Si for OC's follow the inequalities [4]: $AmeanLL(22.90)<AmeanL/LL(23.34)<AmeanBursa(23.61)≈AmeanL(23.67)<AmeanH/L(24.32)<AmeanH(24.63)$, $Fe/SiLL(0.52) < Fe/SiL/LL(0.54) < Fe/SiBursa(0.56) < Fe/SiL(0.59) < Fe/SiH/L(0.73) < Fe/SiH(0.81)$.

Measured grain density of Bursa meteorite $dgrain$ = 3.52±0.02 g/cm^3, and predicted by $dgrain(Amean)$ relationship [2,3,9,10] $dgrain(Amean)$ = 3.51±0.02 g/cm^3, and $dgrain(Fe/Si)$ relationship [10] reveals grain densities: 3.54±0.02 g/cm^3 for the Bursa whole rock.

Relict temperature of interior Bursa samples measured by troilite thermometry reveal range: 55-77 °C, and crust sample reveals relict temperature: 222±30 °C. Troilite content in Bursa meteorite determined by DSC measurements of troilite α/β solid transition is: 5.6±0.2 wt.%., and resulting from ICP-MS data on sulfur content is: 5.5±0.2 wt%.

Conclusions: Mean atomic weight, and Fe/Si ratio indicate that Bursa belongs to L6 chondrites, as previously established. $Amean$ and Fe/Si ratio satisfactorily predict grain density of Bursa meteorite. Specific heat capacity of Bursa meteorite is comparable with measured Cp values of various ordinary chondrites.

References: [1] Kaygisiz E. et al. (2019) *72nd Geological Congress of Turkey,* Abstracts:399-400. [2] Szurgot M. (2015) *LPSC 46,* Abstract #1536. [3] Szurgot M. (2015) *Acta Societatis Metheoriticae Polonorum* 6:107-128. [4] Szurgot M. (2016) *LPSC 47,* Abstract #2180. [5] Szurgot M. et al. 2012. *Meteorites* 2:53-65. [6] Bartoschewitz R. et al. 2017. *Chemie der Erde* 77:207-224. [7] Yomogida K. and Matsui T. 1983. *Journal of Geophysical Research* 88:9513-9533. [8] Beech M. et al. 2009. *Planetary and Space Science* 57:764–770. [9] Szurgot M. (2018) *LPSC 49,* Abstract #1039. [10] Szurgot M. (2018) *LPI Contribution No.2067,* Abstract #6001.

OXYGEN AND AL–MG ISOTOPE SYSTEMATICS OF A HIBONITE-MELILITE-RICH FINE-GRAINED CAI IN THE REDUCED CV CHONDRITE NORTHWEST AFRICA 8613.

Sohei Wada[1], Noriyuki Kawasaki[1] and Hisayoshi Yurimoto[1,2]
[1]Natural History Sciences, Hokkaido university (sohei@ep.sci.hokudai.ac.jp), [2]ISAS/JAXA.

Introduction: Ca–Al-rich inclusions (CAIs) in meteorites are composed of high-temperature condensates from the solar nebular gas [1]. CAIs in CV chondrites are petrographically divided into the coarse-grained CAIs and fine-grained CAIs (FGIs). Complex layer structures of constituent minerals [2, 3] and volatility-fractionated trace-element patterns [4, 5] of FGIs indicate they are condensates from the solar nebular gas. Igneous CAIs that experienced melting and crystallization have been extensively studied for their formation processes, oxygen isotope compositions of minerals, and formation ages [e.g. 6, 7]. On the other hand, such systematic investigations for the formation of FGIs have been poorly conducted. We investigated oxygen and Al−Mg isotope systematics of a hibonite-melilite-rich FGI from the reduced CV chondrite Northwest Africa 8613 (NWA 8613) as well as detailed petrographic observations, in order to decipher its formation processes, surrounding nebular environment, and formation age.

Experimental: Petrographic observations were conducted using a FE-SEM-EDS-EBSD system (JEOL JSM-7000F + Oxford X-Max 150 + Oxford HKL) at Hokkaido University. Oxygen and Al−Mg isotopic compositions of minerals in the FGI were measured using Cameca ims-1270 and ims-1280HR SIMS instruments at Hokkaido University. The full analytical procedures are reported in [7, 8].

Results and Discussion: The FGI from NWA 8613 named HKD01 has an irregular shape with a size of approximately 10×12 mm and composed mainly of melilite, hibonite, and spinel with their crystal sizes of less than ~20 μm. The FGI is petrographically divided into hibonite-rich core, spinel-rich core, melilite-rich inner-mantle, and hibonite-spinel-rich outer mantle. Each petrographic domain contains melilite, hibonite, and spinel with variable proportions of those minerals. The FGI is rimmed by thin spinel and diopside layers. Although hibonite crystals distribute entire the FGI, crystallization experimental work [9] indicate that hibonite cannot be crystallized from a melt with the bulk chemical composition of the FGI HKD01, being consistent with the inferred condensation origin of FGIs [e.g. 3].

Oxygen isotope compositions of the constituent minerals plot along the CCAM line, ranging between $\Delta^{17}O \sim$ −23‰ and 0‰. Melilite crystals in the core exhibit normal chemical zoning and oxygen isotope compositions from $\Delta^{17}O \sim$ −23‰ to −10‰ with increasing Åk composition. The melilite crystals in the inner-mantle show chemically complex, oscillatory zoning patterns, but are uniformly ^{16}O-poor ($\Delta^{17}O \sim$ 0‰) despite their chemical variations (Åk2−14). Melilite crystals in the outer-mantle exhibit normal chemical zoning and variable oxygen isotope compositions from $\Delta^{17}O \sim$ −17‰ to 0‰ with increasing Åk composition. The spinel and hibonite grains in the FGI are uniformly ^{16}O-rich ($\Delta^{17}O \sim$ −23‰). On the $^{26}Al–^{26}Mg$ evolutionary diagram, Al−Mg isotope data of the constituent minerals plot on a single straight line within error despite the petrographic structures; the Al−Mg mineral isochron is defined to give an initial $^{26}Al/^{27}Al$ value of $(4.50 \pm 0.09) \times 10^{-5}$.

Petrography and bulk chemistry suggest that the constituent minerals formed by condensation and were accumulated to form the FGI HKD01. These formation processes occurred within 20 Kyr as inferred from the error of the initial $^{26}Al/^{27}Al$ ratio. The crystal growth sequences with oxygen isotope variations of the minerals imply that the nebular gas changed its oxygen isotopic composition, at least, from ^{16}O-rich ($\Delta^{17}O \sim$ −23‰) to ^{16}O-poor ($\Delta^{17}O \sim$ 0‰), and back to ^{16}O-rich ($\Delta^{17}O \sim$ −17‰) during the condensation formation. The $^{26}Al–^{26}Mg$ systematics of the FGI indicate that these formation events occurred at 0.16 ± 0.02 Myr after the formation of so-called canonical CAIs [10, 11], if ^{26}Al was homogeneously distributed. Our combined data infer the presence of the solar nebular gas with variable oxygen isotope compositions 0.16 ± 0.02 Myr after the formation of canonical CAIs. This nebular chemical system is consistent with the observations of coarse-grained CAIs showing the nebular gas with variable oxygen isotope compositions during the first ~0.2 Myr of the Solar System formation [7, 8, 12].

References: [1] Grossman (1972) *GCA* 36, 597–619. [2] Wark and Lovering (1977) In: Proc. of the 8th LPSC, pp 95–112. [3] Krot et al. (2004) *MaPS* 39, 1517−1553. [4] Boynton (1975) *GCA* 39, 569–584. [5] Davis and Grossman (1979) *GCA* 43, 1611–1632. [6] Yurimoto et al. (1998) *Science* 282, 1874–1877. [7] Kawasaki et al. (2018) *GCA* 221, 318–341. [8] Kawasaki et al. (2017) *GCA* 201, 83−102. [9] Beckett and Stolper (1994) *MaPS* 29, 41–65. [10] Jacobsen et al. (2008) *EPSL* 272, 353−364. [11] Larsen et al. (2011) *ApJL* 735, L37–L43. [12] Kawasaki et al. (2019) *EPSL* 511, 25–35.

SPATIALLY CORRELATED ANALYSES OF HYDROGEN ISOTOPE COMPOSITIONS AND IRON VALENCE IN DISH HILL KAERSUTITES: IMPLICATIONS FOR MARTIAN IGENOUS SAMPLES.

M. Wadhwa[1], A. Stephant[2], S. Sutton[3] and D. Bell[4], [1]School of Earth and Space Exploration, Arizona State University, Tempe, AZ 85287, [2] Department of Physical Sciences, The Open University, Walton Hall, Milton Keynes, MK7 6AA, UK, [3]Department of the Geophysical Sciences and Center for Advanced Radiation Sources, University of Chicago, Chicago IL 60637, [4]Nelson Mandela University, Port Elizabeth, 6031 South Africa.

Introduction: We are investigating microscale variations in D/H ratios, water abundances and Fe valence in carefully characterized terrestrial igneous samples with the goal of understanding the variability in hydrogen isotope compositions and redox within and among the martian meteorites. A large suite of kaersutite megacrysts was collected from the Dish Hill alkali basalt volcano in southeastern California; of these, 17 have been well characterized with the electron microprobe [1]. These megacrysts span a range in Mg# with systematically correlated minor and trace element abundances. Bulk water contents and D/H ratios were previously determined for these 17 kaersutites by vacuum line manometry and gas source IRMS [1].

Analytical Methods: In this study, we selected a subset of the well-characterized Dish Hill kaersutites (DSH 34, 40, 41, 53, 54 and 55) for co-located microscale analyses of hydrogen isotope systematics and iron valence. Secondary ion mass spectrometry (SIMS) measurements of D/H ratios and H_2O concentrations in these kaersutites were performed on the Cameca IMS-6f at Arizona State University. A Cs^+ primary beam of ~10 nA was rastered on a 30×30 μm^2 surface area. A field aperture set the analyzed area to 15 μm diameter, which reduced background associated with hydrogen adsorbed to the sample surface at the edge of the sputtered crater. Presputtering was performed for ~5 min prior to analyses. Each measurement comprised of 50 cycles of measuring H^- and D^- ions with counting times of 1s and 10s, respectively. At the end of each measurement, $^{16}O^-$ was measured. The H_2O contents were determined using a $H^-/^{16}O^-$ vs. H_2O calibration based on three terrestrial amphiboles: Kipawa, Bamble and Mont Emma (Deloule et al., 1991). The instrumental mass fractionation (IMF) factor was calculated based on analyses of these same amphibole standards. The background for H_2O concentrations was determined using the $H^-/^{16}O^-$ ratio measured in San Carlos olivine and was subtracted from the H_2O concentration estimated for each kaersutite measurement.

The Fe K XANES spectra were collected on spots adjacent to the SIMS pits on each of the Dish Hill kaersutites studied here using the GSECARS X-ray microprobe at the Advanced Photon Source at Argonne National Lab. Analysis spots (~ 1 μm) were ~ 30 μm from the edge of the SIMS pit and spectra were collected with the kaersutite grain at four different orientations, accomplished by rotating the sample mount through 90 degree increments. Three different valence determination methods were applied to each spectrum [2]. The "Centroid" method used the centroid energy of the pre-edge multiplet and was calibrated using amphibole spectra collected using the X26A X-ray microprobe at NSLS-I (Brookhaven Nat. Lab.) on 44 amphibole samples which were also analyzed by Mössbauer. The "PLS" (partial least squares) method used a comparison of the full spectrum with those standards. The "Lasso" (least absolute shrinkage and selection operator) method is an ordinary least squares regression model using only those energies in the standard spectra that are most sensitive to valence. For each spot and each method, valence was determined for the spectrum from each of the 4 orientations and those were averaged. The average valences for the three methods were in good agreement. The results using the Lasso method produced the smallest standard deviations for the different orientations and those values are reported here.

Results and Discussion: The water (H_2O) abundances measured via SIMS in the DSH kaersutites range from 0.7 to 1.8 wt.% while the δD values vary from -168 ± 84 ‰ to +538 ± 155 ‰ and are anti-correlated. The Fe valence, defined as "2 + ($Fe^{3+}/\Sigma Fe$)", in most kaersutites analyzed here (DSH 40, 41, 54 and 55) is identical (2.43 ± 0.02; 2SD), so the variation in water content and δD in these samples may be attributed largely to subsolidus diffusion and loss of H_2O. However, the Fe valence in DSH 34 is higher (2.52 ± 0.04), while that in DSH 53 is on average still higher and shows resolvable variation (2.50 ± 0.01 to 2.58 ± 0.02). Petrologic and geochemical evidence suggests that the higher Fe valence in DSH 34 may be from wall-rock assimilation. In contrast, the Fe valence in DSH 53 is anti-correlated with H_2O content and correlated with δD, indicative of dehydrogenation of its parent magma. These results suggest that combined H_2O-δD-$Fe^{3+}/\Sigma Fe$ systematics are likely to provide valuable insights into the petrogenesis of the martian meteorites, some of which may also have experienced similar processes (e.g., assimilation, dehydrogenation, and subsolidus diffusion) on Mars.

References: [1] Bell, D. R. and Hoering, T.C. (1994) *Conference on Deep Earth and planetary volatiles,* Pasadena, CA, LPI Contribution: p.4. [2] Dyar, M.D., Speicher, E.A., Gunter, M.E., Lanzirotti, A., Tucker, J.M., Carey, CJ, Peel, S.A., Brown, E.B., Oberti, R., and Delaney, J.S. (2016) *Amer. Mineral.,* 101, 1171-1189.

HUOYANSHAN IRON METEORITE: BULK CHAMICAL COMPOSITION AND CLASSIFICATION.

G. Q. Wang [1,2] and Y. T. Lin[3], [1]State Key Laboratory of Isotope Geochemistry, Guangzhou Institute of Geochemistry, CAS, Guangzhou 510640, China, E-mail: guiqinwang@gig.ac.cn.; [2]CAS Center for Excellence in Comparative Planetology, China; [3]Key Laboratory of Earth and Planetary Physics, Institute of Geology and Geophysics, CAS, Beijing 100029, China.

Introduction: The first piece of iron meteorite Huoyanshan was found on Oct. 6, 2016, by Mr. Yanzheng Wang, et al. at 15 km NE of the Mountain Huoyanshan. It was approved by the Meteorite Nomenclature Committee and published in MB106 [1]. And now, it is estimated that thousands pieces with a total mass more than ~700 kg have been collected with a piece weigh from100 g up to 8.9 kg.

Experiments: All trace elements are measured by a X Series 2 ICP-MS instrument (Thermofisher Scientific, USA). Major elements of Fe and Ni were measured using a VISTA-PRO, CCD simultaneous inductively coupled plasma-optical emission spectroscopy (ICP-OES, Varian Inc., USA). Details on interference corrections and the analyzing procedure were same as Wang et al.(2016) [2]. All chemical procedures and instruments were performed at the State Key Laboratory of Isotope Geochemistry, Guangzhou Institute of Geochemistry, Chinese Academy of Sciences (GIG, CAS). Major chemical compositions of minerals were analyzed using a JXA8230 electron probe microanalyzer (EPMS) at the Institute of Geology and Geophysics, CAS. The beam current was 20 nA, and the accelerating voltage was 15 kV.

Petrology and minerals: It is a finest octahedrite, with Widmanstätten pattern consisting of kamacite (band width of <0.035 mm) and taenite. Kamacite contains 4.6-7.0 wt% Ni. Taenite shows a typical M-type zoning with Ni content decreasing from 36.7 wt% at the rims to 25.7 wt% at the cores. Minor schreibersite ($\sim$47.8 wt% Ni, $\sim$ 15.1 wt% P) usually occurs within kamacite.

Bulk chemical composition: The Nantan is a IAB-MG iron which have a large recovery mass and have been analyzed many times by different researchers. To verify the accuracy of the data, two duplicate pieces of Nantan iron meteorite were measured in this study. The results show that the data are consistent on two duplicate samples and with published data. Therefore, the acurrancy is well in this study. The bulk chemical compositions of Huoyanshan are listed in Table 1.

Table 1. The chemical composition of Huoyanshan.

Name	Type	wt %		ppm														
		Ni	Co	P	Cr	Ga	Ge	As	Ru	Rh	Pd	Sn	W	Re	Os	Ir	Pt	Au
Nantan-1	IAB-MG	7.8	0.44	0.12	8.2	74	281	12	4.2	1.2	3.1	4.6	1.1	0.15	0.71	1.7	4.8	1.5
Nantan-2	IAB-MG	7.8	0.43	0.13	12	71	265	12	4.1	1.1	3.1	4.4	0.66	0.15	0.95	1.6	4.6	1.5
HYS	IAB-sLH	22	0.62	0.11	9.1	1.1	1.7	30	0.07	0.06	8.8	10	1.1	0.002	0.04	0.02	0.04	2.0

Note: Ni and Co were measured by a ICP-OES, trace elements were measured by ICP-MS. HYS – Huoyanshan iron meteorite.

Classification: The bulk chemical compositions of Ni (22, wt%) and Ir (0.02), Ga (1.1), and Ge (1.7 ppm) were ploted on log-log plots of Ga-Ni, Ir-Ni, and Ge-Ni, which were usually used as iron meteorite classification [3]. All of them were in the IIICD areas which have been grouped in IAB-complex [4] at present. Subsequently, the values of Ni, Co (0.62 wt%), As (30 ppm), Ga and Au (2.0 ppm) were ploted on log-log plots of Ni, Co, As, Ga vs. Au [4], and all of them were in areas of a subgroup of sLH. Worsham et al, (2016) [5] measured PGEs and Re-Os isotopes of 3 sLH iron. The characteristics of Huoyanshan PGEs are agree with those data from Worsham et al, (2016) [5].

Conclusions: Huoyanshan iron meteorite is an typical IAB-sLH. Until now, there are only 10 IAB-sLH iron were approved by the Meteorite Nomenclature Committee including Huoyanshan iron. Huoyanshan iron meteorite is significant to provid more information on research of IAB-sLH.

References: [1] Gattacceca J. et al. (2019). *Meteorites and the early solar system* 54:469-471. [2] Wang G. et al. (2016). *Rapid Communications in Mass Spectrometry* 30:543-551. [3] Hutchison R. (2004). *Meorites* P.357. [4] Wasson J. T. and Kallemeyn G. W. (2002). *Geochimica et Cosmochimica Acta* 66:2445-2473. [5] Worsham E. A. et al. (2016). *Geochimica et Cosmochimica Acta* 188:261-283.

INFRARED SPECTROSCOPIC CHARACTERISTICS OF ZIRCON IN LUNAR METEORITES NORTHWEST AFRICA 2995 AND 4485

N. Wang[1], R. Tartèse[2], K. H. Joy[2], J. F. Pernet-Fisher[2], Y. T. Lin[1], [1]Institute of Geology and Geophysics, Chinese Academy of Sciences, Beijing 100029, China. Email: wangnian@mail.iggcas.ac.cn, [2]School of Earth and Environmental Sciences, The University of Manchester, Manchester M13 9PL, UK.

Introduction: Zircon is commonly used when investigating the geochronology of the Moon, because it can provide both U-Pb and Pb/Pb isotopic dates, and is resistant to isotopic resetting up to fairly high temperatures. However, it is not impervious in all environments, especially at extreme pressure and temperature conditions, and when its crystalline structure has been damaged by radioactive decay of radionuclides like U and Th [1-6]. Extreme impact shock pressure can cause metamorphism and affect the mineral structure to transform zircon into its high-pressure polymorph reidite [3]. Both radiation damage and high-T metamorphism could thus result in metamictization and amorphization of zircon [4-6]. These processes can be accompanied by diffusion of Pb and result in discordant U-Pb dates [1-7]. Identifying these processes and constraining the extent to which they affected studied samples are essential for accurately interpreting U-Pb and Pb/Pb isotopic data and derive accurate ages for lunar sample [7].

Methods: Infrared spectroscopic analysis is a useful method to investigate the effects of radiation damage and high shock pressure on zircon [3,5]. To elucidate their provenance and provide context for interpreting measured U-Pb dates, we have investigated infrared spectra features of zircon from lunar meteorites Northwest Africa (NWA) 4485 and NWA 2995. Fourier-transform infrared spectroscopy (FTIR) analysis was carried out on polished sections of NWA 2995, NWA 4485, and a set of terrestrial crystalline zircon standards with a Perkin-Elmer Spotlight-400 instrument. Mid-infrared reflectance spectra were collected between 4000 cm^{-1} to 650 cm^{-1} (~2.5 µm to 15.4 µm) at 4 cm^{-1} spectral resolution, with an instrument aperture size of 25×25 µm.

Results： *FTIR features of terrestrial zircon standards.* We analyzed four different zircon standards (91500, Penglai, Qinghu and Mud Tank) for comparison with lunar samples. Two main spectral types were obtained: type 1 displays a broad peak from 900-1015 cm^{-1}, and a smaller peak at ~1100 cm^{-1}; type 2 displays a main peak band at 995-1015 cm^{-1}, and two smaller peak bands at 900-925 cm^{-1} and 1050-1080 cm^{-1} (Fig. 1). These features are consistent with the 'untreated' zircon results in [3,5]. All analyses of standard 91500 (2 large grains) are of type 1, while the other three standards (many small separate grains) all show types 1 and 2 features, with a few grains showing intermediate features, which we interpret as reflecting different crystal orientations.

The shift of the Christiansen Feature (CF) position. The CF position (point of lowest reflectance [8]) of the zircon standards has a small range of variation between 1120 cm^{-1}-1160 cm^{-1}. The CF positions obtained in lunar zircon grains show a much wider range from ~1100 cm^{-1} to 1260 cm^{-1}. Additionally, the CF position seems to be related to variations of the intensity of two peaks at 928 cm^{-1} and 1080 cm^{-1}, shifting towards higher wavenumbers when the 928 cm^{-1} peak intensity decreases.

Metamorphism effects. Lunar zircon grains have different spectral profiles compared to the terrestrial standards. The intensity of the 928 cm^{-1} and 1080 cm^{-1} peaks can vary widely within a single zircon grain and between different zircon grains. For example, Figure 1 shows that for grain 1, an increase of the 1080 cm^{-1} peak intensity is related to a decrease of the 928 cm^{-1} peak intensity from CL-active area to CL-inactive area (both are identified as amorphous phases in Raman spectra), which

Figure 1: FTIR spectra of terrestrial zircon standards (left) and in lunar meteorite NWA 4485 and 2995 (right).

likely implies different degrees of metamictization. The FTIR profile for grain 2 is different to those for grain 1, but consistent with that of type 2 terrestrial zircon standards (Fig. 1), This may indicate that grain 2 suffered lower shock pressure than grain 1, which is also consistent with Raman data.

In summary, zircon grains in NWA 2995 and 4485 show that shock-induced metamorphism and metamictization result in different FTIR spectra characteristics, and that intensities and shapes of peaks at 928 cm^{-1} and 1080 cm^{-1} are good indicators for different degrees of metamictization in both terrestrial [3] and lunar zircon.

References: [1] Timms N. E. et al. (2017) *Earth-Science Reviews* 165:185-202. [2] Reimold W. U. et al. (2002) *European Journal of Mineralogy* 14:859-868. [3] Gucsik A. et al. (2004) *Mineralogical Magazine* 68:801-811. [4] Zhang M. et al. (2000) *Journal of Physics: Condensed Matter* 12.8:1915-1925. [5] Zhang M. and Salje E. K. H. (2001) *Journal of Physics: Condensed Matter* 13.13:3057-3071. [6] Zhang M. et al. (2002) *Journal of Physics: Condensed Matter* 14.12: 3333-3352. [7] Hoskin P. W. O. (2000) *Journal of Metamorphic Geology* 18:423-439.
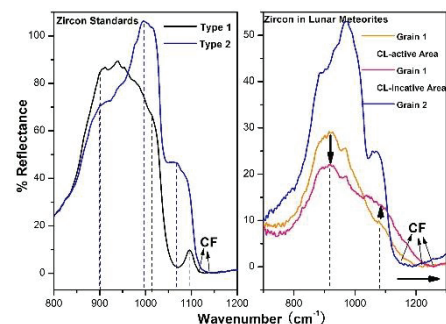
PETROLOGY AND IN SITU GEOCHRONOLOGY OF THE YOUXI MESOSIDERITE.

Y. Wang[1] and W. Hsu[1,2], [1]CAS Center for Excellence in Comparative Planetology, Purple Mountain Observatory, Nanjing 210034 (y_wang@pmo.ac.cn), [2]The State Key Laboratory of Lunar and Planetary Science/Space Science Institute, Macau University of Science and Technology, Taipa, Macau.

Introduction: Mesosiderites are roughly composed of equal mass proportions of metals and silicates, and have been widely regarded as mixtures of the core and crust materials of differentiated asteroids[1]. However, the timing and mechanism of the metal-silicate mixing remain enigmatic despite long and extensive debates. In order to unravel the formation age and origin of mesosiderites, we carried out petrologic, mineralogic, and geochronological studies of the Youxi mesosiderite.

Results and Discussion: Youxi was found in Youxi City, Fujian Province of China in 2006. It is composed of ~70 vol% of silicates and ~30 vol% of metals. Numerous well-defined lithic clasts exhibit diverse lithologies from basaltic to gabbroic, orthopyroxenitic, and rare peridotitic, silica-rich, and phosphate-rich ones. Mineral clasts are mostly orthopyroxene and plagioclase. Metal phases are mainly kamacite with minor taenite, troilite, and accessory schreibersite. The silicate part of Youxi has bulk REE compositions [$(1.3-4.0)\times$ CI; $(La/Lu)_{CI}$: 0.90; Eu/Eu*: 1.89] similar to HED meteorites. Mineral compositions of pyroxene ($En_{66.0\pm2.3}Wo_{2.5\pm0.6}$), plagioclase ($An_{92.7\pm2.4}Ab_{7.2\pm2.4}$), and olivine ($Fo_{61.5-77.8}$) are roughly consistent with those in HEDs. The petrographic, bulk and mineral chemical affinities of Youxi with those of HEDs indicate that the silicate part of Youxi might be genetically related with the parent body of HEDs.

Merrillite is ubiquitous (~2 vol%) in Youxi. Most are anhedral coarse grains (>100 μm) closely associated with Fe,Ni-metals. Different from the REE-enriched merrillite (La: $7600-25000 \times$ CI) in eucrite[2], merrillite in Youxi has significantly lower REE abundances (~$20-500 \times$ CI; Fig. 1). Therefore, unlike the magmatic origin of eucritic merrillite, the phosphate in Youxi probably formed from oxidation of P in metallic phases during the metal-silicate mixing. In situ Pb-Pb dating was carried out on 53 merrillite crystals using the Cameca ims 1280 ion microprobe at the IGGCAS in Beijing. Our analyses yielded a $^{207}Pb/^{206}Pb$ age of 3950 ± 80 (2σ) Ma, which is close to the Ar-Ar age (~3.9 Ga) of mesosiderites[4] but distinctly younger than the ~4.5 Ga ages in literatures[e.g., 5].

Considering the cooling history of mesosiderites[1,6,7] (~5×10^3 to 2×10^6 °C/Myr at 1150-600 °C and ≤ 1 °C/Myr at ~500-350 °C), the diffusion of Pb isotopes in merrillite (T_c>450 °C)[8] should have come to closure within ~50 Myr after its formation. In addition, the secondary thermal and shock metamorphism of Youxi is minimal. Therefore, the $^{207}Pb/^{206}Pb$ age of 3950 ± 80 Ma represents the formation time of merrillite, and accordingly the time of metal-silicate mixing that had produced the Youxi mesosiderite.

References: [1] Mittlefehldt D. W. et al. (1998). In *Planetary Materials* (ed. J.J. Papike) pp. 4-140-4-160. [2] Hsu W. and Crozaz G. (1996) *Geochimica et Cosmochimica Acta* 60: 4571-4591. [3] Ward D. et al. (2017) *American Mineralogist* 102: 1856-1880. [4] Bogard D. D. & Garrison D. H. (1998) *Geochimica et Cosmochimica Acta* 62, 1459-1468. [5] Haba M. K. et al. (2017) *Geochimica et Cosmochimica Acta* 215, 76-91. [6] Ganguly J. et al. (1994) *Geochimica et Cosmochimica Acta* 58: 2711-2723. [7] Haack H. et al. (1996) *Geochimica et Cosmochimica Acta* 60: 2609-2619. [8] Cherniak D. J. et al. (1991) *Geochimica et Cosmochimica Acta* 55:1663-1673.
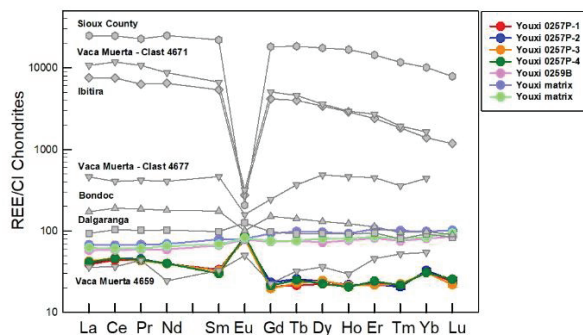
Fig. 1 CI-normalized REE abundances of merrillite in Youxi, compared with those of eucrites and other mesosiderites[2-3].
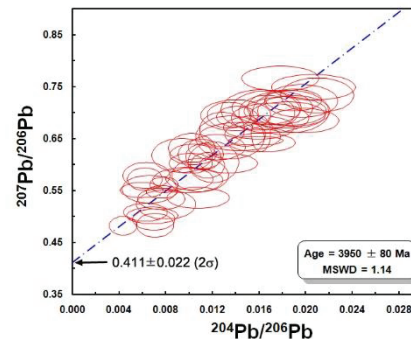

Fig.2 $^{207}Pb/^{206}Pb$ vs. $^{204}Pb/^{206}Pb$ plot of merrillites in Youxi. The intercept on Y-axis (0.411 ± 0.022, 2σ) corresponds to a Pb/Pb age of 3950 ± 80 (2σ) Ma.

PETROLOGY AND MINERALOGY OF THE NORTHWEST AFRICA 11005 MESOSIDERITE.

Y. Wang[1], A. Mei[1,3], and W. Hsu[1,2], [1]CAS Center for Excellence in Comparative Planetology, Purple Mountain Observatory, Chinese Academy of Sciences, Nanjing 210034 (y_wang@pmo.ac.cn), [2]The State Key Laboratory of Lunar and Planetary Science/Space Science Institute, Macau University of Science and Technology, Taipa, Macau, [3]School of Astronomy and Space Sciences, University of Science and Technology of China, Hefei 230026.

Introduction: Mesosiderite is one of the two subtypes of stony-iron meteorites, the other being pallasite. Compared with pallasite, mesosiderite has more complicated texture, composition, and petrogenesis[1]. Mesosiderites are polymict breccias composed of roughly equal proportions of metals and silicates. The formation processes of mesosiderites include early differentiation of chondritic asteroids and subsequent magmatism, brecciation of silicates, metal-silicate mixing, and secondary alterations. Lines of evidence have shown that the silicate part of mesosiderites is genetically related to HED meteorites, and the metallic part has similar compositions to IIIAB irons[1-3]. However, when and how the metal-silicate mixing had occurred are still under debate[1-4]. To understand the time and mechanism of metal-silicate mixing that produced mesosiderites, we carried out petrologic and mineralogic studies of the NWA 11005 mesosiderite. Here reported are preliminary results.

Results and Discussion: NWA 11005 was found in Morocco in 2016. The whole rock weighs 1.5 kg and is partially covered by a fusion crust. Modal analyses show that NWA 11005 is composed of ~55 vol% of silicates and ~45 vol% of metals. Micron- to centimeter-sized lithic and mineral clasts are embedded in a matrix composed of fine-grained metal-silicate intergrowths (Fig. 1). Most lithic clasts are basaltic and gabbroic with angular and sharp boundaries. Mineral clasts are dominated by pyroxene and plagioclase. Accessory minerals include olivine, chromite, ilmenite, silica, merrillite, rutile, and baddeleyite. Metal phases are mostly kamacite and taenite, with minor troilite and schreibersite. Metal oxide veins are present along mineral fractures, indicating a moderate degree of terrestrial weathering. Considering the relatively high modal abundance of plagioclase (~40 vol%) and the partially recrystallized texture of matrix, NWA 11005 is classified as a type 2A mesosiderite[1].

Minerals in NWA 11005 have similar chemical compositions to those in other mesosiderites. Pyroxene is mostly orthopyroxene ($Fs_{15.6-59.9}Wo_{1.2-4.8}$), with minor pigeonite ($Fs_{27.2-56.9}Wo_{5.4-14.5}$) and augite ($Fs_{25.8-33.6}Wo_{38.6-40.3}$). Subsolidus exsolution of augite and orthopyroxene lamellae is ubiquitous in gabbroic clasts. Compositions of plagioclase ($An_{80.5-95.4}$) and olivine ($Fo_{45.5-87.1}$) vary among different clasts and matrix. The lithology and mineral chemistry of the silicate part of NWA 11005 exhibit high affinities with those of HEDs, consistent with a genetic link between mesosiderites and HEDs[1-2].

We have found numerous merrillite (>100 μm) and baddeleyite (~20 μm) grains in NWA 11005 (Fig. 2), which are good candidates for U-Pb dating. To constrain the formation time of NWA 11005, chronological works are underway.

References: [1] Mittlefehldt D. W. et al. (1998) In *Planetary Materials* (ed. J.J. Papike) pp. 4-140-4-160. [2] Greenwood R. C. et al. (2006) *Science* 313: 1763-1765. [3] Hassanzadeh J. et al. (1990) *Geochimica et Cosmochimica Acta* 54: 3197-3208. [4] Quitté G. et al. (2005) *Geochimica et Cosmochimica Acta* 69: 1321-1332.
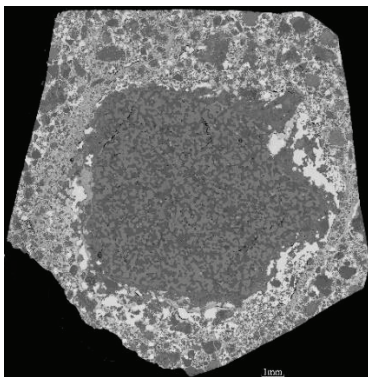
Fig. 1 A BSE image of a polished section of NWA 11005. Note the gabbroic clast (~13×14 mm) in the center.
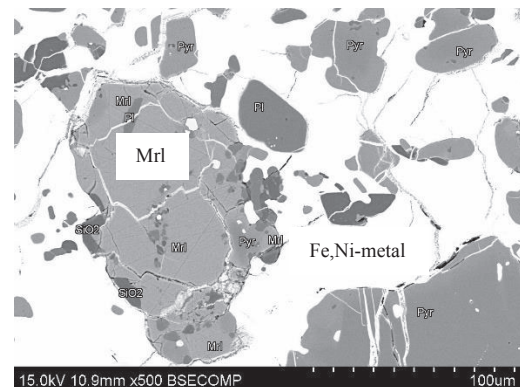

Fig.2 A BSE image of a merrillite (Mrl) grain in the matrix of NWA 11005.

TWO UNBRECCIATED, VESICULAR, POSSIBLY PAIRED EUCRITES, BOTH TOTALLY UNMETAMORPHOSED AND EXTRAORDINARILY SODIUM-RICH: NORTHWEST AFRICA 7035 AND NORTHWEST AFRICA 8661.

Paul H. Warren[1], [1]Earth, Planetary & Space Sciences, UCLA, Los Angeles, CA 90095, USA, pwarren@ucla.edu.

Only a small minority of the more than one thousand known eucrites are unbrecciated [1]. Only a tiny minority (now perhaps 5?) are conspicuously vesicular [2]. The proportion that have escaped even mild thermal metamorphism is not much bigger than that. It is also rare, especially among the majority noncumulate type of eucrites, to encounter deviation from a narrow range of composition-space. In this work I characterize two Northwest Africa eucrites, NWA 7035 and NWA 8661, that display similar exceptionalism in all of these ways. Despite a mild disparity in measured oxygen-isotopic compositions (reported in their *Met. Bull.* entries), I suspect these two may be paired.

Both NWA 7035 and NWA 8661 are mildly, but among eucrites very exceptionally, vesicular, with the vesicles typically irregular-elongate (seldom round) in shape, and mostly associated with mesostasis. Vesicles constitute about 3.5 vol% of NWA 7035 and 3.7 vol% of NWA 8661. The nearest precedent is Ibitira, a highly metamorphosed and generally odd [3] (non-Vestan?) eucrite with about 3 vol% preponderantly near-spherical vesicles [2]. A considerable portion of the vesicularity in both of the subject eucrites occurs as small cavities within plagioclase. It has been inferred from the expectation of extremely feeble pressure in surface flows on any asteroid that the rare vesicular eucrites must have originally crystallized several km deep in the crust [2]. If so they would be unlikely to fully avoid thermal metamorphism [cf. 1]. However, the vesicles in NWA 7035 and NWA 8661 may have formed late enough in a near-surface igneous crystallization process to become trapped.

Fig. 1. Pyroxene compositions of two unmodified-igneous eucrites, and for comparison one typically metamorphosed eucrite. Data from NWA 7035, not shown, are virtually identical to NWA 8661.
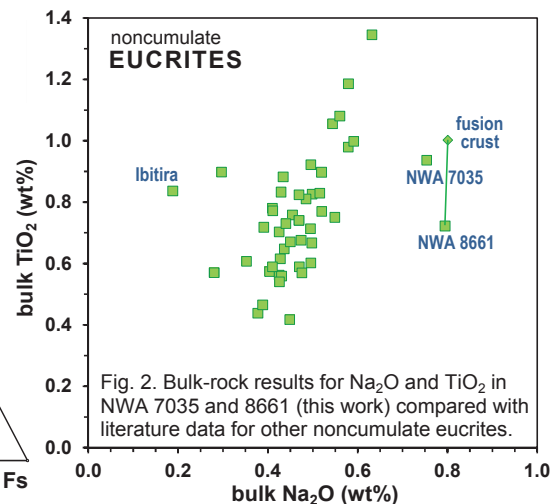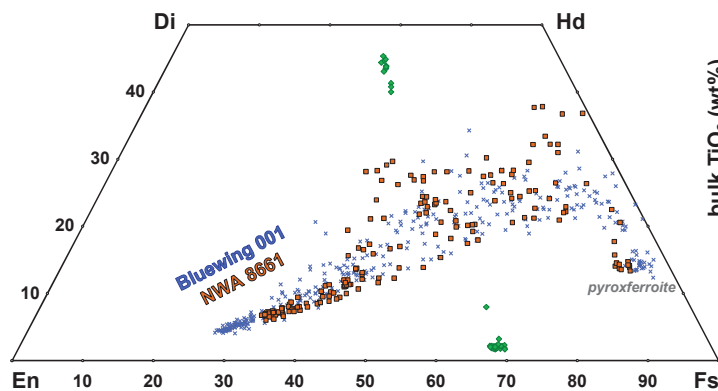

Fig. 2. Bulk-rock results for Na_2O and TiO_2 in NWA 7035 and 8661 (this work) compared with literature data for other noncumulate eucrites.

The total avoidance of thermal metamorphism in both NWA 7035 and NWA 8661 is manifested, inter alia, by exquisite preservation of minute-scale igneous textures, and by extensive zonation within the pyroxenes (Fig. 1) along a trend that begins in both cases at precisely the same, distinctively ferroan (in this context), composition. Textural similarity between the two extends to mildly ophitic enclosure of many of the smaller plagioclase grains within some of the larger pyroxenes. As noted by [4], this texture, too, is rare among eucrites. Also, both feature distinctive late-igneous veins of evolved (high Na, low Mg) composition scattered within cores of some pyroxenes.

Both NWA 7035 and NWA 8661 are also distinctly enriched in sodium compared to other noncumulate eucrites (Fig. 2). The data for NWA 8661 are from both microprobe fused-bead analysis (MFBA) and INAA [cf. 5]; backed up by microprobe data for a small region of the fusion crust. Data for NWA 7035 are as-yet only from MFBA, but from long experience we know that MFBA and INAA are both highly accurate for sodium in eucrites. The degree to which the sodium-rich composition is related to the distinctive textural and low-metamorphism characteristics of this duo will become clearer as more and more eucrites are characterized in coming years.

References: [1] Mayne R. G. et al. (2009) *Geochim. Cosmoch. Acta* 73, 794-819. [2] McCoy T. J. et al. (2006) *Earth Planet. Sci. Lett.* 246, 102-108. [3] Mittlefehldt D. W. (2005) *Meteor. Planet. Sci.* 40, 665-677. [4] Irving A. and Kuehner S. (2012) *Met. Bull.* entry for NWA 7035. [5] Warren P. H. et al. (2009) *Geochim. Cosmoch. Acta* 73, 5918-5943.

FURTHER (PETROGRAPHIC) EVIDENCE THAT CV CAIS HAD A PRESOLAR ORIGIN

J. T. Wasson, University of California, Los Angeles, CA 90095-1567.

Introduction: Isotopic compositions of several elements in CAIs are so different from those in the chondrite groups and in the Earth Moon and Mars that it seems impossible to devise a scenario that allows formation of CAIs from any of these materials; the simplest explanation seems to be that they formed in the nebula around another star, perhaps one formed in the same large (~10^3 stars) protostar cluster as the Sun [1}. Time scales for mixing molecular clouds are too long to expect all stars in the cluster to have a uniform composition. If this formation scenario is correct, it has strong implications for solar system chronology and the cosmochemical formation of the meteorites and inner planets.

Isotopic evidence. As shown in Fig. 1, isotopic compositions of elements that record non-mass-dependent fractionations (e.g., O, Cr, Ti) are so different in CAIs than those in carbonaceous, ordinary and enstatite chondrites that it is not possible for simple fractionation processes to produce CAIs from chondritic starting compositions. Note that evaporation should make O have a heavier composition whereas it is lighter in CAIs.

Petrographic approach: We have focused our petrographic considerations on the coarse-grained type-B CAIs; we assume that all 16-O-rich CAIs originated under similar conditions and that the differences among the different types mainly reflect differences in physical conditions related to the details of local conditioins.

The type-B CAI formed igneously, perhaps by the evaporation of precursors that were chondrite-like in terms of their mix of minerals. Because isotopes of elements such as Mg record isotopic compositions similar to those of chondrites we can be sure that fractional distillation did not occur. Thus, the melting and evaporation must have occurred rapidly, with too little time to allow the mixing of the residual liquid while the process was occurring. Although some workers suggest that CAIs formed by condensaton, equilibirum condensation cannot produce liquids at plausible nebular pressures [3].

Late arrival of CAIs at the CV formation location: Many (about 50% of) CV chondrules are surrounded by igneous rims, and many have surfaces made irregular due to collisions [2]. These show that energetic processes were continuing throughout the chondrule forming period. In contrast, type-B CAIs do not host igneous rims, and most show relatively intact surfaces. This is strong evidence that these were the last materials added to the CV region before planetesimal formation, and is consistent ithe the conclusion that these were only accreted to the solar nebula very late. This strongly supports the idea that they are foreign materials arriving from another stellar system.

Conclusions: Chaotic accretion of the solar nebula: As the number of isotopic studies of elements such as Cr and Ti that show non-mass dependent fractions (i.e., in ε^{54}Cr and ε^{50}Ti) increases it becomes increasingly clear that the solar nebula was never well mixed, and that it continued to accrete throughout the period within which chondrites were forming. We have known for decades that tiny presolar grains can have isotopic compositions unlike thos in the common elements in chondrites. It simplifies many aspects of planetary formation if CAIs are large presolar grains which obtained their compositions in another stellar system.

References: [1] Wasson J. T. (2017) *Meteoritics Planet. Sci* Santa Fe abstract,. [2] Rubin A. E. *Geochim. Cosmochim. Acta* 48, 1779 [3] Grossman L. and Clark S. P. (1973) *Geochim. Cosmochim. Acta* 37, 635.
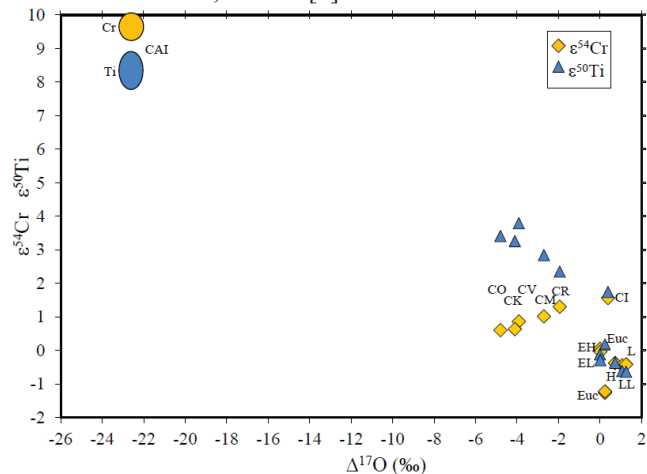

Fig. 1 Distribution of non-mass dependent Δ^{17}O, ε^{54}C and ε^{50}Ti.

NORTHWEST AFRICA (NWA) 8785, AN EL3 CHONDRITE WITH FEO-RICH MATRIX.

M. K. Weisberg[1,2,3] M. E. Zolensky[4] M. Kimura[5,6], K. T. Howard[1,2,3], D. S. Ebel[2, 3] and Y. Bolega[7] [1]Dept. Physical Sci., Kingsborough College CUNY, Brooklyn, NY 11235. (mweisberg@kbcc.cuny.edu) [2]Dept. Earth and Environmental Sci., CUNY Graduate Center, New York, NY 10016. [3]Dept. Earth and Planetary Sci., American Museum of Natural History, New York, NY 10024., [4]ARES, NASA Johnson Space Center, Houston, TX 77058. [5]Natinal Institute of Polar Research, Tokyo, Japan. [6]Ibaraki University, Mito, Japan. [7]Earth and Atmospheric Sciences, [7]City College, New York, NY 10031.

Introduction: The enstatite (E) chondrites are enigmatic but important for understanding the evolution of the terrestrial planets. They have highly reduced mineral assemblages in which enstatite (near pure in composition) is the dominant silicate, metal is abundant and has >2.5 wt. % Si in some EH3s, elements that are generally lithophile in most chondrites occur as sulfide and some E3s contain nitrides and carbides [1,2,3]. Notably, stable isotope compositions are similar to the Earth-Moon [4,5,6]. Aside from E chondrite clasts in the Kaidun breccia [7,8], the enstatite chondrites are dry, lacking evidence of hydrous minerals, distinguishing them from most other chondrite groups and suggesting they formed relatively close to the sun, inside of the snow line. Compared to other chondrite groups, the E3s are also matrix-poor, with EH3s having ~4-12 vol. % and EL3s ≤5 vol % matrix [9,10]. Here we present a study of NWA 8785, a remarkable new EL3 chondrite with abundant, potentially altered FeO-rich, fine-grained matrix. Our goals are to understand E chondrite matrix and the evolution and alteration history of the EL3 parent body.

Results: NWA 8785 was studied in polished sections. It contains (in vol. %) sharply bound chondrules (45.9%), metal/sulfide-rich nodules (9.8%), mineral and lithic fragments (10.6%) and rare refractory inclusions all surrounded by a fine-grained FeO-rich matrix (33.7%) (Fig. 1a); the highest matrix abundance known among EL3 chondrites. Chondrules range in size up to 2mm with most 500-700μm, close to the mean EL3 chondrule size of 520μm [11]. All chondrule textures are present but are dominantly pyroxene-rich (PP and RP) varieties. The metal-rich nodules in NWA 8785, common in all EL3s [12, 13], are unlike those in other EL3 chondrites. They contain enstatite, silica, graphite and sulfides as in other EL3s but are texturally, and in some cases mineralogically, different; intergrowths of enstatite laths characteristic of nodules in other EL3s are less common, suggesting a different origin for the NWA 8785 nodules. Matrix, much more abundant than in other EL3s, is littered with mineral (enstatite, Na-rich plagioclase, FeS and FeNi) and lithic (chondrule) fragments up to 50μm in size surrounded by a fine grained (submicrometer) FeO-rich mixture (Fig. 1b, c) showing variable amounts of SiO_2, MgO and FeO, likely a product of alteration. This contrasts sharply with matrix in other E3s which is composed of silica and enstatite as major components, with metal and sulfides. (TEM and XRD are underway to decipher the mineralogy of the fine-grained matrix component in NWA 8785.) Additionally, in one matrix area, a 30μm spinel-rich inclusion was found, consisting of $MgAl_2O_4$ spinel surrounded by sodalite, a common alteration product in refractory inclusions in CV chondrites.

Discussion: NWA 8785 is an unusual EL3 chondrite with an FeO-rich, fine-grained matrix unlike matrix found in other E3 chondrite, except for the E3 clasts in the Kaidun breccia which show various degrees of aqueous alteration [8]. The NWA 8785 matrix, more abundant than in other EL3s, may have been the carrier of ices that accreted to the parent body, resulting in alteration. Further study of this altered material and alteration fluids may advance our understanding of the proposed E chondrite - Earth-Moon relationship.

References: [1] Keil K. (1968) *Jour. Geophys. Res. 73,* 6945-6076. [2] Weisberg M. K. and Kimura M. (2012) *Chemie der Erde 72,* 101–115. [3] Jacquet E. et al. (2018) *in Chondrules and the Protoplanetary Disk*, editors S. Russel, H. C. Connolly and A. N. Krot. Cambridge Press. [4] Javoy M. (1995) *Geophys. Res. Lett., 22,* 2219-2222 [5] Warren P. (2011) *Earth Planet. Sci. Lett., 311,* 93-100. [6] Paniello R. C. (2012) *Nature, 490,* 376-379. [7] Zolensky M. E. and Ivanov A. (2004) *Chemie der Erde 63,* 185-246. [8] Higashi K. et al. (2019) *Lunar Planet. Sci. Conf. 50th,* 2344. [9] Rubin A. E. et al. (2009). *Meteorit. Planet. Sci 44,* 589-601. [10] Weisberg M. K. et al. (2014) *Lunar Planet. Sci. Conf. 45th,* 1551. [11] Rubin A. E. (2000) *Earth Sci. Rev. 50,* 3-27. [12] Van Niekirk D. and Keil K. (2011) *Meteor. Planet. Sci., 46,* 1487–1494. [13] Weisberg et al. (1997) *Lunar Planet. Sci. Conf. 28th,* 1523-1524.
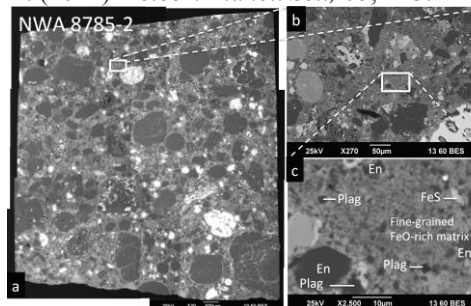

Fig. 1. Backscattered electron images of section NWA 8785-2 (a) whole PTS showing chondrules dominated by enstatite (dark grey), metal-rich nodules (white) and the fine-grained FeO-rich matrix (medium grey). (b) Enlargement of the area outlined in (a) showing the matrix which is littered with mineral and lithic fragments up to 50 μm in size. (c) Enlargement of the area outlined in (b) showing the FeO-rich fine-grained matrix with enstatite (En), Na-rich plagioclase (plag), FeS grains ranging from about 1-10 μm in the size. The fine-grained areas shows variable amounts of FeO, SiO_2, MgO.

POTENTIAL ALTERTION PRODUCTS OF ORGANIC MATERIALS BY X-RAY COMPUTED TOMOGRAPHY OF MARS RETURNED SAMPLES

L.C.Welzenbach[1], M.D. Fries[2], M.M. Grady[1,3], R.C. Greenwood[1], F.M. McCubbin[2], C.L. Smith[3,4], A. Steele[5], R.A. Zeigler[2], [1]The Open University, Milton Keynes, UK (lwelzenbach@rice.edu), [2]NASA-Johnson Space Center, Houston TX, [3]The Natural History Museum, London UK,[4]The University of Glasgow, UK,[5]Geophysical Laboratory,Carnegie Institution of Washington DC

Introduction: The Mars 2020 rover mission will collect and cache samples from the martian surface for possible retrieval and subsequent return to Earth. Mars Returned Samples may provide definitive information about the presence of organic compounds that could shed light on the existence of past or present life on Mars. Post-mission analyses will depend on the development of a set of reliable sample handling and analysis procedures that cover the full range of materials which may or may not contain evidence of past or present martian life [1].

MSR Curation Protocol- Preliminary Examination by XCT: As part of planning for the initial characterization and subsequent distribution to the scientific community, samples would be analyzed while still sealed in their containers using non-destructive, non-invasive techniques. Studies [1,2] suggest that X-ray Computed Tomography (XCT) may minimally alter samples for most subsequent techniques including organic analyses. Both [1,2] also point out that the effects of increased radiation on the organics in samples would need to be evaluated, especially for what is expected to be a small native organic signal [3] that would be difficult to detect.
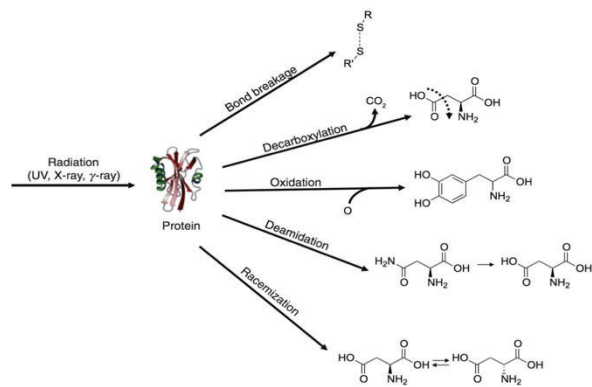
Figure 1: Examples of the types of alteration that organic compounds may experience as a result of primary and secondary effects following X-ray exposure. Image from [6]

Evidence for alteration of organics from XCT. Several studies show no alteration of organics (in meteorites) following exposure to monochromatic synchrotron radiation [4,5]. Others [5,6] show that work is needed to quantify the effects of polychromatic laboratory laboratory XCT radiation, especially at fluences and energies that will allow in situ examination through the Mars 2020 cache tube. X-rays, transmitted to samples through X-ray tomography, X-ray diffraction, and/or X-ray fluorescence interact with sample materials, potentially producing ionizing radiation. Bertrand et al. [6] suggest that organic rich materials experience a wide range of alteration by both primary and secondary radiation effects from photon energies that approach the carbon absorption edge (Fig. 1). Other additional indirect effects may include the creation of chemically reactive by-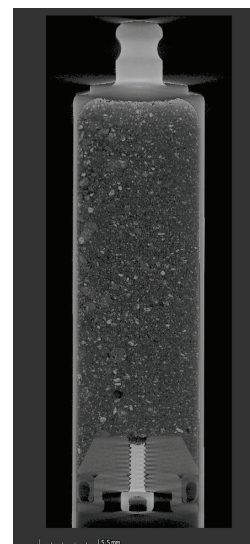products, which can react with the original atoms or molecules (e.g. formation of OH radicals or the production of free radicals from macromolecular carbon (MMC) [5]). This combination of effects is the principal mechanism of concern for X-ray alteration of organic-bearing returned samples.

Types and products of organic alteration. An example set of the Tier I analytes selected for this work [7]; were mixed with simulant and loaded into two analogue Mars 2020 cache tubes. One tube served as a control and was not exposed while the other was imaged for 545 minutes at 180 kV and 150 μA using a 1 mm Cu filter to test the instrument's ability to adequately penetrate the cache analogue tube (Fig. 2). Taking into account the variety of potential alteration effects for the given suite of organic analytes we will provide a list of the potential by-products produced during XCT exposure to be tested in individual exposure experiments and analyzed by GCMS. Preliminary examination of the supernatant fluid extracted from the XCT exposed sample suggests that some type of visually identifiable change occurred in the simulant material.

References: [1] Kminek, G. et al. (2014) Report of the workshop for life detection in samples from Mars *Life Sciences in Space Research* 2: p. 1-5. [2] Hanna, R. et al. (2017) *Chemie de Erde* 77, #4, p. 547-572 [3] Summons R. E., et al. (2014) *Astrobiology* 14.12 : p. 969-1027. [4] Glavin, D.P. et al. (2017) *LPSC XLVIII* abstract #1070 [5] Friedrich, J. M. et al. (2016) *Meteoritics & Planetary Science* **51**: p. 429-437 [6] Bertrand, L. et al., (2015) *Trends in Analytical Chemistry* 66: p. 128-145. [7] Welzenbach, L. C. et al., (2017). *80th METSOC*, Abstract #6253.

Figure 2: XCT image of a Mars 2020 analogue cache tube, with Mars simulant (<1mm to 4mm fragments) and organic compounds inside.

COLD CURATION TECHNIQUES: X-RAY COMPUTED TOMOGRAPHY OF THE HAMBURG METEORITE

L. C. Welzenbach[1], Z. E. Wilbur[2], M. D. Fries[3], [1]The Open University, Milton Keynes, UK, lwf2@rice.edu, [2]Jacobs [3]NASA/Johnson Space Center, Houston TX, [3]NASA Johnson Space Center, Houston, TX.

Introduction: The Hamburg meteorite fell on 17 January 2018 near the town of Hamburg, outside Detroit, MI [1]. Meteorites were recovered from frozen lake surfaces almost immediately following the fall. One stone in particular was collected by the Sloan*Longway Museum and Planetarium for the purpose of a Cold Curation study (Fries et al, abstract this meeting). An early step in the cold curation analytical sequence is to conduct a non-destructive scan of the meteorite with X-Ray Computed tomography (XCT).

Cold XCT of planetary materials: XCT is a well-established non-destructive tool for curating planetary materials [2], but at the time of this writing has never been completed with cold astromaterials. XCT of cold samples has been accomplished in both the oil and gas exploration industry and the medical fields [3,4], with the latter likely providing the best applications of cryo-scanning using laboratory XCT instrumentation. As part of this Preliminary Examination process for a Cold Curation sample, we have fabricated a simple sample holder for cold measurement and to establish instrument parameters for generating high resolution 3D imagery of the meteorite. Key factors include maintaining low temperatures for the duration of a high resolution scan, and removing interferences caused by cold containment hardware.

Sample Handling Procedure: For this effort, the Nikon XT H 320 LC at NASA's Johnson Space Center was used to conduct the scan. Large cabinet instruments such as this are capable of handling large samples on a free standing sample stage that can rotate 360 degrees. The sample stage currently does not have cooling capability, so a stand alone sample container that can maintain cold temperatures would need to be created. The metal-free, commercially available thermally insulated container was obtained and modified to hold the sample, rated to maintain both hot and cold temperatures for up to 3 hours. To ensure the coldest temperatures could be maintained as rated and potentially for longer during a high resolution scan, dry ice would be used inside the sample container. The interior was modified to house a centrally situated separate sample holder that would stabilize the sample and isolate it from contact with the dry ice. One of the chief concerns beyond sample contamination was stability of the sample and container during the duration of the scan with specific regard to devolatilization of the dry ice. For this reason, the dry ice was pulverized and packed into the space between the central sample chamber and the interior walls of the thermal container.
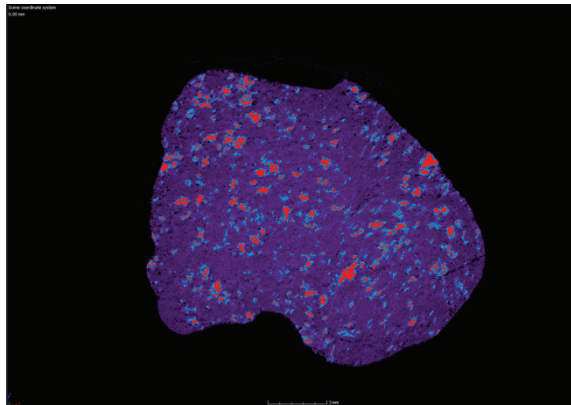

Figure 1- False color image slice of the Hamburg meteorite. Red and blue are metal and sulfide phases, purple undifferentiated silicate phases. Image by Z. Wilbur, NASA-JSC.

XCT of Hamburg: Parameters for scanning the Hamburg meteorite were established from a series of tests with three different proxy samples. Starting with a sample at room temperature, we identified the parameters needed for a scan of sufficient resolution, using the same sample materials that currently enclose the Hamburg meteorite. Follow up tests using dry ice provided information about the stability of dry ice during several subsequent scans before conducting a final scan with the Hamburg meteorite. While the proxy scans provided the best method of loading the sample and dry ice, the Hamburg sample enclosing materials may have shifted during the scan, leading to minor distortion of the scan. The scan parameters of 130 kV at 109 uA, 1250 frames at a resolution of 15 microns were sufficient to penetrate all materials and provide good contrast of silicates and metal phases. Total time from sample loading to its return to the freezer was 3.5 hours. The temperature of the interior sample chamber when the sample was loaded was below the detection limit of the laser thermometer (-40 degrees Celsius) and the final reading of the interior of the sample chamber was -30 degrees Celsius with half the dry ice remaining.

References: [1] Hanna, R.M et al. (2017) *Chemie de Erde* 77(4)pp. 547-572. [2] Kampschulte, M., et al. (2015) *Scanning*, 37(1), pp.63-72 [3] Vasilescu, D.M., (2016) *Journal of Applied Physiology*, 122(1), pp.161-169 [4] Greer, J. et al. (2019) *LPSC XV*, Abstract #1638.

PETROLOGIC CHARACTERIZATION AND IN-SITU ^{60}Fe-^{60}Ni SYSTEMATICS OF CO3 CHONDRITES.

T. D. Wickland[1], M. Telus[1] and M.-C. Liu[2] [1]Earth and Planetary Sciences, University of California Santa Cruz (1156 High St, Santa Cruz, CA 95064), [2]University of California Los Angeles (595 Charles Young Drive E. Los Angeles, CA 90095).

Introduction: The presence of ^{60}Fe ($t_{1/2}$= 2.6 Ma) in the early solar system, inferred by excesses in ^{60}Ni found in meteorites, could potentially help constrain the timing and environmental conditions of the early forming solar system [1, 2]. Live ^{60}Fe in the early solar system cannot be a product of particle irradiation in the solar protoplanetary disk, therefore, its presence above galactic background levels would imply addition from a stellar source (e.g. supernova) [3]. Previous estimates on the inferred initial ratio from bulk and SIMS analyses have given conflicting results [4, 5]. Bulk analyses indicate initial ^{60}Fe/^{56}Fe consistent with background, while initial ratios inferred from SIMS are consistently higher [2]. Another major concern is that UOC chondrites show chemical alterations and significant remobilization of Fe and Ni, plaguing analyses in UOCs even at low petrologic types [6]. However, CO3.0 chondrites appear to be more pristine than UOCs based on presolar grain abundances [7], potentially providing a better sample set for constraining the initial ^{60}Fe/^{56}Fe of the solar system. Here, we discuss petrographic analyses of primitive CO3.0 samples and in situ Fe-Ni systematics using secondary ion mass spectrometry (SIMS).

Methods: We characterized a large suite of CO3.0 chondrites for this study using Raman spectroscopy. Raman analysis characterizes the degree of defects in matrix carbon which correlates with the metamorphic grade. This technique is especially sensitive to thermal alteration of low petrologic types (< 3.2) [8]. CO3.0 chondrites analyzed for this study were DOM 08006, DOM 10104, DOM 14359, DOM 14305, DOM 14019, DOM 14127, MIL 11213, MIL 090785, MIL 090480, MIL 090038, NWA 7892, and NWA 8737.

Following characterization, we then measured Ni isotopes in magnetite from DOM 14305 (type 3.1 based on our Raman analyses) using the Hyperion II ^{16}O^{-} beam on the Cameca 1290 ion microprobe at UCLA. We used monocollection mode with a 3-5 nA beam current and a 10 μm spot size. Ni isotopes counted during analysis are summed and isotope ratios were calculated. Excess ^{60}Ni was calculated by applying a linear mass fractionation correction to Δ^{60}Ni, then converting Δ^{60}Ni back to ratios using terrestrial reference values [2]. Isochrons are generated by weighted linear regressions of Δ^{60}Ni and Fe/Ni ratios normalized using both ^{61}Ni and ^{62}Ni to check for consistency.

Results: Raman spectroscopy confirmed that these samples are petrologic type 3.0 and relatively unaltered. DOM 14305 was particularly interesting because it showed some of the least alteration, second only to DOM 08006, the least altered CO3.0 as of now [7]. Because radiogenic ^{60}Ni is scarce relative to natural ^{60}Ni, samples chosen need to have high Fe/Ni ratios and low Ni concentrations. CO3.0 chondrites rarely contained low Ni and high Fe silicate minerals so we decided to focus on magnetite for SIMS analysis as it has the highest Fe/Ni ratios and suitable grain sizes for Fe-Ni measurements. Even then, there were only few magnetite grains suitable for these analyses. We analyzed two magnetites from DOM 14305 and two from UOC Semarkona for comparison. Both do not show any resolvable excess ^{60}Ni. Given our conservative estimate of errors for excess ^{60}Ni and ^{56}Fe/^{62}Ni ratios of up to 16 million, we constrain initial ratios to < 9.6 x10^{-8}.

Discussion: There appears to be no observable amount of excess ^{60}Ni in magnetite grains in CO3.0 chondrites. Magnetite is not an ideal mineral to analyze because the timing of its formation is poorly understood. There are several reasons why magnetite does not show excess ^{60}Ni could including 1) Formation after the decay of ^{60}Fe, given that the ages are not well-constrained. 2) Secondary alteration and mobilization of Fe and/or Ni [6], but this is unlikely because of the high abundance of pre-solar grains in CO3.0 chondrites [7]. 3) Excess ^{60}Ni exists below our detection limits and is constrained by the upper limit of the initial ratio of 9.6 x 10^{-8}. Troilite was analyzed in this study but had large discrepancies in Fe/Ni ratios between SIMS and electron microprobe analysis for reasons that are unclear but may be related to the presence of an oxide layer. Although Fe-rich silicates are rare in CO3.0 chondrites, they do occur and would be good targets for future resonance ion mass spectrometry (RIMS) analysis that could potentially better constrain excess ^{60}Ni [9].

References: [1] Mishra R. K. and Goswami J. N. (2014) *Geochimica et Cosmochimica Acta* 132:440–457. [2] Telus M. et al. (2018) *Geochimica et Cosmochimica Acta* 221:342–357. [3] Huss G. R. et al. (2009) *Geochimica et Cosmochimica Acta* 73:4922–4945. [4] Kita N. T. et al. (2000) *Geochimica et Cosmochimica Acta* 64:3913–3922. [5] Tachibana S. and Huss G.R. (2003) *The Astrophysical Journal Letters* 588:41:44. [6] Telus M. et al. (2016) *Geochimica et Cosmochimica Acta* 178:87–105. [7] Floss C. and Haenecour P. (2016) *Geochemical Journal* 50:3-25. [8] Bonal L. et al. (2007) *Geochimica et Cosmochimica Acta* 71:1605–1623. [9] Trappistch et al. (2018) *The Astrophysical Journal Letters* 857:15-21.

INVESTIGATING THE HISTORY OF AUBRITES USING X-RAY COMPUTED TOMOGRAPHY AND BULK PARTITION COEFFICIENTS.

Z. E. Wilbur[1], A. Udry[2], F. M. McCubbin[3], K. E. Vander Kaaden[1], R. A. Zeigler[3], K. Ziegler[4], and C. DeFelice[2]. Jacobs-JETS Contract, NASA Johnson Space Center, Houston, TX, USA. [2]University of Nevada, Las Vegas, Las Vegas, NV, USA. [3]NASA Johnson Space Center, Houston, TX, USA. [4]Institute of Meteoritics, Dept. of Earth and Planetary Sciences, University of New Mexico, Albuquerque, NM, USA.

Introduction: The aubrites are a unique group of differentiated meteorites that formed on parent bodies with oxygen fugacities (fO$_2$) from ~2 to ~6 log units below the iron-wüstite buffer [1-2]. At these highly reduced conditions, elements deviate from the geochemical behavior exhibited at terrestrial fO$_2$, and may form FeO-poor silicates, Si-bearing metals, and exotic sulfides [1-3]. Geochemical examinations of aubrites, such as mineral major-element compositions, bulk-rock compositions, O isotopes, and crystallization ages, are crucial to understand their formation and evolution at extreme fO$_2$ conditions. In this study, we determine partitioning relationships of elements between bulk silicate, sulfide, and metal phases within aubrites, and compare the results to partition coefficients determined from petrologic experiments run under mercurian conditions [4]. While previous studies have described the petrology and 2D modal abundances of aubrites, this work provides the first 3D view of aubritic mineralogies, which are compared to the available 2D data. Constraints of 3D modal abundances will increase the accuracy of computed bulk distribution coefficients; therefore, 3D scans of aubrite samples are imperative. We utilize X-ray computed tomography (XCT) to non-destructively analyze the distribution and abundances of mineral phases in aubrites and locate composite clasts of sulfide grains for future analysis.

Samples: We investigate a large representative suite of aubrites (n = 14): Allan Hills (ALH) 78113, ALH 84007, Bishopville, Cumberland Falls, Khor Temiki, Larkman Nunatak (LAR) 04316, LaPaz Icefield (LAP) 02233, Miller Range (MIL) 07008, MIL 13004, Mount Egerton, Northwest Africa (NWA) 8396, Norton County, Peña Blanca Spring, and Shallowater. These samples have varying degrees of brecciation and originate from two or more parent bodies [1-2]. Miller Range 07008, MIL 13004, and NWA 8396 have not been previously studied in detail aside from their initial classification.

Results: While we have analyzed bulk rock and oxygen isotopic compositions, XCT and bulk partition coefficient results will be highlighted here.

XCT Modal Mineralogy and Textures. The Cumberland Falls, Mount Egerton, Norton County, Peña Blanca Spring, and Shallowater aubrites were scanned using a Nikon XTH 320 micro-XCT at NASA Johnson Space Center. The results of the XCT data have enabled the determination of abundances of silicate groundmass (i.e., enstatite, forsterite, albite, and diopside), sulfides (i.e. troilite [FeS], alabandite [MnS] and daubréelite [FeCr$_2$S$_4$]), and Fe,Ni metal by segmenting a density histogram in Volume Graphics Studio software. The discernable phases are within ~5% of the linear attenuation coefficients (LAC) [5]. Surprisingly, the Mt. Egerton sample contains vesicles and fractures with a preferred orientation along long axes. This may give insight into the temperature and pressure conditions on its parent body, as Mt. Egerton is considered anomalous and may not have formed on the main aubrite parent body, which had been subjected to pyroclastic volcanism [6].

Bulk Distribution Coefficients. The geochemical behavior of elements change as a function of fO$_2$ [3]. Bulk distribution coefficient calculations are underway for the studied aubrites. We use the formula $D_i = c_i^{X}/c_i^{Y}$, where c is the concentration of element i in phase X and Y (metal, sulfide, or silicate), and include modal abundances of silicate, sulfide, and metal phases and mineral major element data. Similar to the experimental mercurian D_i interpretations in [4], the aubrite D_i calculations show that Fe, Cr, and Mn should preferentially incorporate into sulfides over other chalcophile elements. If the combined abundances of Fe, Cr, and Mn are insufficient relative to the available sulfide component, then Ti, K, Ca, and Mg are expected to partition into sulfide phases.

Discussion: The aubrite bulk distribution coefficients from this study have important implications for understanding reduced magmatism on other bodies in our Solar System, such as Mercury [7]. The 3D modal mineralogical results in this study give similar volume percentages as 2D modal results. However, we have located composite clasts of metal and sulfide grains for future analytical study. The use of XCT is a powerful tool to nondestructively observe the internal composition of precious meteoritic material.

References: [1] Keil K. (1968) JGR, 73, 6945–6976. [2] Keil K. (2010) Chemie de Erde, 70, 295-317. [3] Kaufman S. V. (2016) LPS XXVII, Abstract #2743. [4] Vander Kaaden K. E. and McCubbin F. M. (2016) GCA, 173, 246-263. [5] Tsuchiyama A. et al. (2005) Am. Min., 90, 132-142. [6] Benedix et al. GCA, 72, 2417-2428. [7] McCoy T. J. and Bullock E. S. (2017) Planetesimals, 71-91.

REGOLITH HISTORY OF SIX LUNAR REGOLITH BRECCIAS
DERIVED FROM NOBLE GAS ELEMENTAL AND ISOTOPIC ABUNDANCES.

P. Will, H. Busemann, M. E. I. Riebe and C. Maden
Institute of Geochemistry and Petrology, ETH Zürich, 8092 Zürich, Switzerland. patrizia.will@erdw.ethz.ch.

Introduction: The Moon offers an invaluable archive of planetary formation, magmatic, impact and regolith processing of our solar system [1]. Processes such as large impacts producing craters to erosion by particles producing sub-micron-sized pits are recorded in the lunar surface over billions of years, while solar wind and cosmic-ray particles produce effects at the atomic scale [2]. The nearside of the Moon was sampled by the Apollo and Luna missions [3], while samples from the farside are currently only available by meteorites. The evolution of the lunar regolith can probably best be studied by noble gases. The noble gas isotopic and elemental composition reveals for instance the composition and (potential) evolution of the solar wind, monitors the exposure to galactic cosmic rays, records impact events, and finally allows us to assess the transport history to Earth. Here we present noble gas data on six Antarctic and Northwest African lunar regolith breccias of different lithologies not studied for noble gases elsewhere so far [initial results given in 4], and discuss their lunar surface history and processes, possible pairing, and ejection events.

Samples: Northwest Africa (NWA) 10404 is classified as feldspathic regolith breccia and exhibits a mostly vitric and vesicular matrix [5,6]. NWA 11237 is a feldspathic breccia with mineral clasts and some sparse glass fragments in a finer-grained vesicular matrix [7]. Similarly, NWA 11273 is a feldspathic breccia composed of mineral and rare basaltic clasts in a finer-grained vesicular matrix [7]. Meteorite Hills (MET) 01210 represents a polymict regolith breccia containing mostly coarse-grained, low-Ti mare basalt and minor anorthositic highland clasts [8,9]. Mount DeWitt (DEW) 12007 is a polymict regolith breccia predominantly composed of glassy impact-melt breccia particles, gabbroic and feldspathic clasts in a fine-grained matrix and contains vesicular shock-induced glass veins [10]. Pecora Escarpment (PCA) 02007 is a polymict, dominantly feldspathic regolith breccia with some basaltic clasts, agglutinates and impact glasses in a fine-grained partially glassy matrix [9].

Methods: Noble gas analyses were carried out on interior sample splits. Fragments with weights of 1 to 100 mg were degassed at 100 °C in the UHV storage system for several days. The noble gases were extracted by melting to ~1700 °C for 30 minutes. Gas purification, separation and measurements followed the procedure described by [11]. Re-extractions at ~1750 °C confirmed complete degassing. Blank contributions were negligible.

Results: PCA, MET, NWA 10404 and DEW contain large amounts of solar wind (SW) He-Xe and are thus true regolith samples. PCA is the most mature regolith in terms of SW accumulation when compared to the regolith noble gas data reported so far [cf. 12] and contains extremely high abundances of e.g. $^{20}Ne_{SW}$ (1.5×10^{-3} cm^3 STP/g) and $^{132}Xe_{SW}$ (4.0×10^{-8} cm^3 STP/g). MET, DEW and NWA 10404 are less gas-rich (0.9 to 3.7×10^{-4} cm^3 STP/g $^{20}Ne_{SW}$, 3.3 to 17.3×10^{-9} cm^3 STP/g $^{132}Xe_{SW}$) and contain higher concentrations of cosmogenic nuclides relative to the trapped gases for instance evident in the Ne, Ar and Kr isotopic compositions. These breccias exhibit shorter surface regolith exposure to the solar wind. The $^4He/^{36}Ar$ and $^{20}Ne/^{36}Ar$ ratios in DEW, MET and NWA 10404 are lower than in PCA and mean Apollo, Luna 16 and Luna 20 samples [13] suggesting gas loss during regolith gardening [14]. Glassy clasts in NWA 10404 were indeed interpreted as impact spherules deformed by reheating of the regolith breccia [6].

NWA 11273 contains very low amounts of SW (2.8×10^{-6} cm^3 STP/g ^{20}Ne) and its Ne isotopes plot between Ne-SW and cosmogenic Ne. NWA 11237 does not contain any SW. Small cosmogenic noble gas contents in NWA 11237 and 11273 suggest short exposure to cosmic rays. However, low $^4He/^{36}Ar$ ratios of 0.05 to 0.07, $^{20}Ne/^{36}Ar$ ratios of 0.196 to 0.218 and very low ^4He concentrations (4.2 to 8.3×10^{-7} cm^3 STP/g) indicate that NWA 11237 and 11273 experienced strong and late He and Ne losses, which might have disturbed the radiogenic ^4He and cosmogenic noble gas inventory. Atmospheric contamination, neutron capture in halogens (^{80}Kr, ^{82}Kr and ^{128}Xe) and fission excesses are absent in all studied regolith samples. Regolith processing, averaged shielding depths, cosmic-ray exposure ages and possible pairing will be discussed at the meeting.

References: [1] Barboni M. et al. (2017) *Sci. Adv.* 3:e1602365. [2] Taylor S. R. (1982) Planetary science: A lunar perspective. LPI, Houston. pp. 390. [3] Taylor S. R. (1975) Lunar science: A post-Apollo view. pp. 390. [4] Will P. et al. (2016) *Meteorit. Planet. Sci.* 51:A664. [5] Kuehner S. M. et al. (2016) *LPS XLVII*, Abstract #2246. [6] Wittmann A. et al. (2016) *Meteorit. Planet. Sci.* 51:A667. [7] Gattacceca J. et al. (2019) *Meteorit. Planet. Sci.* 54:469-471. [8] Arai T. et al. (2010) *Geochim. Cosmochim. Acta* 74:2231-2248. [9] Day J. M. D. et al. (2006) *Geochim. Cosmochim. Acta* 70(24):5957-5989. [10] Collareta A. et al. (2016) *Meteorit. Planet. Sci.* 51:351-371. [11] Riebe M. E. I. et al. (2017) *Meteorit. Planet. Sci.* 52:2353-2374. [12] Mészáros M. et al. (2018) *Meteorit. Planet. Sci.* 53:1-4. [13] Fegley B. and Swindle T. Resources of near-Earth space. University Arizona Press, Tucson, pp. 977. [14] Bogard D. D. and Hirsch W. C. (1975) *Proc. 6th Lunar Sci. Conf.*:2057-2083.

LIQUID CHROMATOGRAPHY ORBITRAP MASS SPECTROMETRY STUDY OF SYNTHETIC AND CHONDRITIC ORGANIC MIXTURES.

C. Wolters[1], V. Vuitton[1], F.-R. Orthous-Daunay[1], L. Flandinet[1], Chao He[2], Sarah Moran[2], Sarah Horst[2], D. V. Bekaert[3], L. Tissandier[3], B. Marty[3], L. Piani[3]
[1]Univ. Grenoble Alpes, CNRS, CNES, IPAG, 38000 Grenoble, France (cedric.wolters@univ-grenoble-alpes.fr), [2]Department of Earth and Planetary Sciences, Johns Hopkins University, Baltimore, MD, USA, [3]Centre de Recherches Pétrographiques et Géochimiques, UMR 7358 CNRS - Université de Lorraine, 15 rue Notre Dame des Pauvres, BP 20, 54501 Vandoeuvre-lès-Nancy, France.

Introduction: Meteorites show a high level of complexity of their organic matter content[1]. To try to understand its origin, an experimental approach consists in conducting laboratory synthesis experiments in well-constrained environments and compare the products with natural samples. Any feature of the final mixture shared with an extraterrestrial material will designate its synthesis conditions to be comparable to those at the origin of the extraterrestrial sample.

We postulate that the molecular complexity is a good indicator at the whole sample level. We highlight a method that uses the stoichiometry and functional complexity of the samples to propose an origin for natural samples. Liquid chromatography coupled to Orbitrap mass spectrometry is a technique of choice to describe both stoichiometries - thanks to the high mass resolution - and functionality - thanks to the time separation due to chemical interactions[2-3].

Methods: We evaluate here the differences between molecules produced in the laboratory by plasma irradiation in the gas phase[4,5] and those present in the carbonaceous chondrite soluble organic matter extracts[6]. The gas phase experiments aim at reproducing the protosolar nebula environment that is supposed to be at the origin of the extraterrestrial organic matter. A starting material of around 1mg is enough to perform all the described analyses.

The proposed analysis workflow is based on two analytical instruments and a home-made data-treatment software. A direct infusion (without chromatographic separation) measurement with an ESI-LTQ-Orbitrap™ mass spectrometer (Thermo Scientific) is performed to obtain mass spectra of the samples in both positive and negative mode, from m/z 50 to 300u and from 150 to 500u. The double polarity acquisition mitigates an ESI-Orbitrap bias that would discriminate some acido-basic functions in one mode over the other.

Along with the direct infusion, samples are analyzed by HPLC with Orbitrap™ detection (m/z from 50 to 350) with a ZIC-pHILIC column (Merck Millipore) where the retention is based on a hybrid behavior with both hydrophilic partitioning, ionic and hydrogen bonding interaction. The elution gradient is adapted from a metabolomic method[7] and consists in an acetonitrile/carbonate buffer (20mmol/L, pH 9.2) starting from 80/20 (%vol) to 60/40 in 10 minutes, followed by a plateau during 30 minutes, and then washing and equilibration of the column for a total run of 80 minutes. The home-made HPLC data-analysis starts from raw data of mass vs. time and generates an 'Ion Map' that is a 2D representation of mass vs. time with intensity color code. This allows us to do peak isolations and mathematical modelisations to extract for each chromatographic peak a couple of mass and retention time. This couple of values can then be attributed and compared to standard compounds or even predicted retention times[7].

Results: In direct infusion mass spectrometry, meteorites and analogues show a large amount of CHNO-bearing molecules, with a specific distribution based on carbon chain families[8]. Even if these samples present some differences, the stoichiometry only cannot discriminate them. The chromatographic analysis reveals that analogue samples present some mass and time correlation whereas extraterrestrial samples do not present this correlation. This indicates that the molecules' polarity inside extraterrestrial samples presents an homogeneous distribution compared to the discrete and separable polarity distribution that can be seen in synthetic samples.

References: [1] Schmitt-Kopplin P, et al. (2010) *Proceedings of the National Academy of Sciences* 107(7):2763–2768. [2] Yamashita Y, Naraoka H (2014) *Geochemical journal* 48(6):519–525. [3] Naraoka H, et al. (2017). *ACS Earth and Space Chemistry* 1(9):540–550. [4] Bekaert DV, et al. (2018) *The Astrophysical Journal* 859(2):142. [5] Hörst SM, et al. (2018) *Nature Astronomy* 2(4):303–306. [6] Orthous-Daunay F-R, et al. (2019) *Geochemical Journal* 53(1):21–32. [7] Creek DJ, et al. (2011) *Analytical Chemistry* 83(22):8703–8710. [8] Orthous-Daunay F-R, et al. (2019). this conference

THE CURIOUS CASE OF MARS' FORMATION

J. M. Y. Woo[1], R. Brasser[1], S. Matsumura[2], S. J. Mojzsis[3,4], S. Ida[1]

[1]Earth Life Science Institute, Tokyo Institute of Technology, Tokyo, Japan; woo.m.aa@m.titech.ac.jp; brasser@elsi.jp), [2]Division of Physics, University of Dundee, [3]Department of Geological Sciences, University of Colorado, [4]Institute for Geological and Geochemical Research, Research Center for Astronomy and Earth Sciences, Hungarian Academy of Sciences

Introduction: Recent data from terrestrial samples and martian meteorites suggest that Mars' isotopic and thus bulk composition is distinct from that of Earth, and therefore it likely grew further from the Sun [1]. Mars shows distinct signatures in the nucleosynthetic isotopes $\Delta^{17}O$, $\varepsilon^{48}Ca$, $\varepsilon^{50}Ti$, $\varepsilon^{54}Cr$, $\varepsilon^{62}Ni$ and $\varepsilon^{92}Mo$ [2,3,4,5]. This compositional difference has been attributed to Mars accreting a higher fraction of material akin to ordinary chondrite than Earth, which is thought to have formed mostly from material akin to enstatite chondrite [6], though this is still actively debated. Nevertheless these distinct isotopic signatures should be reproduced with modern N-body planet formation models.

Method and results: We ran 672 N-body simulations in total with two different planet formation models: the Classical model, in which Jupiter and Saturn are kept on their current orbits, and the Grand Tack model, wherein Jupiter and Saturn migrate through the primordial asteroid belt inward and then outward. Our results show that both models tend to yield Earth and Mars analogues with overlapping accretion zones. We also estimate the average percentage of primitive chondrite assembled into Earth and Mars by assuming that the initial solid disk consists of only enstatite chondrite in the inner region, and ordinary chondrite in the outer region. Our results show that a change in composition of the initial disk could have occurred near 1.3 AU. We further report that the Classical model fares better than the Grand Tack model for forming Mars with its documented compositions (29–68% enstatite chondrite plus 32–67% ordinary chondrite [7]) though the Mars analogues are generally too massive in the Classical case. We further calculate the predicted isotopic composition of ^{17}O, ^{50}Ti, ^{54}Cr, ^{142}Nd, ^{64}Ni and ^{92}Mo in the martian mantle from the Grand Tack simulations. We find that it is possible to match the measured isotopic composition of all the elements, but the resulting uncertainities are too large to place restriction on the dynamical evolution and birth place of Mars.

Future prospect: Our results show that increasing the resolution of dynamical simulation and higher precision isotopic measurements from the martian meteorites, especially for modrate and highly siderophile elements, are required to solve the mystery of Mars' formation. Combining planetary dynamics and cosmochemistry should be the future in tackling problems related to planet formation.

References: :[1] Brasser et al. (2017) EPSL, 468, 85 [2] Lodders & Fegley (1997) Icarus, 126, 373 [3] Sanloup et al (1999) Phys. Earth Planet In. 112, 43 [4] Tang & Dauphas (2014) EPSL, 390, 264 [5] Warren (2011) EPSL, 311, 93 [6] Javoy et al. (2010) EPSL, 293, 259 [7] Brasser et al. (2018) GRL, 45, 5908-5917.

TRACE ELEMENT GEOCHEMISTRY AND U-PB CHRONOLOGY OF THE BASALTIC SHERGOTTITE NORTHWEST AFRICA 8653.

Y. Wu[1] and W.Hsu[1,2], [1]CAS Center for Excellence in Comparative Planetology, Purple Mountain Observatory, Nanjing, China, yhwu@pmo.ac.cn, [2]The State Key Laboratory of Lunar and Planetary Science, Macau University of Science and Technology, Taipa, Macau, wbxu@pmo.ac.cn.

Introduction: Northwest Africa (NWA) 8653 is a basaltic shergottite mainly composed of pyroxene, maskelynite, and other minor phases [1]. The crystallization age of shergottites is highly controversial as whole-rock and non-radiogenic mineral Pb-Pb isochrons imply ancient ages [2], while mineral isochrons and *in situ* U-Pb analyses reveal much younger ages [3-4]. Detailed geochemical and chronological analyses are carried out in this study to set additional constraints on the formation of NWA 8653 shergottite.

Analytical Methods: Rare earth element (REE) concentrations of individual minerals and feldspathic intergrowths were analyzed *in situ* with an LA-ICP-MS at the State Key Laboratory of Geological Processes and Mineral Resources, China University of Geosciences, Wuhan. *In situ* U-Pb and Pb-Pb analyses of fine baddeleyite grains ($\geq$ 5*5 μm) were conducted using the Cameca IMS-1280HR secondary ion mass spectrometer at the Institute of Geology and Geophysics, Chinese Academy of Sciences, Beijing. *In situ* Pb-Pb analyses of phosphate, feldspathic intergrowth and maskelynite were also conducted using the SHRIMP at the Beijing SHRIMP Center, Chinese Academy of Geological Sciences.

Rare Earth Elements: Pyroxene exhibits an LREE-depleted pattern with La varying from 0.1 to 2.1×CI, and Lu from 1.6 to 9.1×CI. Maskelynite exhibits a positive Eu anomaly (Eu=~11×CI) with HREE ranges from below detection limits to ~0.6×CI. Merrillite is rich in REEs (La=~780×CI) with a subtle negative Eu anomaly (Eu/Eu*=0.7). And HREEs gradually decrease from Gd (~840×CI) to Lu (~410×CI). Apatite has a similar REE pattern to that of merrillite at a much lower level (La=~40×CI). The calculated bulk REEs from the average REE concentrations of individual minerals and their modal abundances are consistent with those of enriched shergottites with a $(La/Yb)_{CI}$ value around 1.1 [5].

The feldspathic intergrowths also displays a positive Eu anomaly, but the concentrations are varying. The analyzed intergrowth with lower SiO_2 (65.3 wt %) and higher CaO (6.79 wt %) exhibits a similar REE pattern to that of maskelynite, while others (SiO_2 73.3-78.6 wt %, CaO 1.0-4.42 wt %) have slightly higher LREEs and HREEs with variable Eu. The correlation of REEs and major element contents is not obvious. Overall, the average REE contents of intergrowth areas are slightly higher than maskelynite.

Chronology: U concentrations of baddeleyite varies from 25 to 207 ppm with an average of ~ 72 ppm. The majority has a $^{206}Pb/^{204}Pb$ ratio below 500 and about half of them are below 100. Only one grain has a $^{206}Pb/^{204}Pb$ ratio above 1000. The Pb-Pb isotopic composition of baddeleyite concides with the 0.2 Ga isochron. The uncorrected $^{207}Pb/^{206}Pb$ and $^{238}U/^{206}Pb$ plotted on a Tera-Wasserburg diagram reveals a young age of 190.5 ± 6.4 Ma (MSWD = 1.7). The Raman spectra reveals characteristic for monoclinic baddeleyite [1]. Thus, the age is likely to represent the crystallization age of NWA 8653. This is consistent with young crystallization ages of some other shergottites in previous studies [3-4].

The uncorrected Pb-Pb isotopic composition of phosphate, feldspathic intergrowth and maskelynite exhibits overlaps lying near the 4.1 Ga isochron while maskelynite leans towards the most primitive value of shergottite as suggested in [6]. The common Pb level of these phases is significantly higher than that of baddeleyite with measured $^{206}Pb/^{204}Pb$ ratios below 20, which may result from mixing of modern terrestrial Pb and primitive Martian Pb [6].

Conclusion: NWA 8653 is a young enriched basaltic shergottite. The feldspathic intergrowth presenting within maskelynite represents an evolved end with slightly elevated REEs and minor Fe-rich minerals such as fayalite and ilmenite. *In situ* Pb-Pb analyses suggest that both phosphate and maskelynite (including feldspathic intergrowth) may provide misleading chronological information. Unshocked baddeleyite grains with less common Pb is more likely to record the crystallization age.

References: [1] Hsu W. and Wu Y. 2016. *Meteoritics& Planetary Science* 51:A342. [2] Bouvier A. et al. (2008) *Earth and Planetary Science Letters* 266:105-124. [3] Nyquist L. E. et al. (2001) *Chronology and Evolution of Mars* 96: 105-164. [4] Darling J. R. et al. (2016) *Earth and Planetary Science Letters* 444:1-12.[5] Papike J. J. et al. (2009) *Geochimica et Cosmochimica Acta* 73: 7443-7485. [6] Moser D. E. et al. (2013) *Nature* 499: 454-457.

The spatial density of in-situ Australasian tektites in Southern China

Z. Xiao[1], Y. Ma[1], P. Yan[1], J. Pu[1], T. Kenkmann[2], G. Wulf[2], and J. Cui[3], [1]Planetary Science Institute, School of Earth Sciences, China University of Geosciences (Wuhan), zyxiao@cug.edu.cn, [2]Albert-Ludwigs-Universität Freiburg, Institut für Geo-und Umweltnaturwissenschaften, [3]School of Atmospheric Sciences, Sun Yat-sen University.

Introduction: The source crater of the Australasian strewn of tektites and microtektites has not been found. Most studies agree that the source crater should be somewhere around 17ºN and 107ºE [1]. The distribution of various forms of tektites (i.e., splash-form, ablated splash-form and Muong Nong tektites), the spatial density of microtektites collected from deep ocean sedimentary cores, the possible trend of devolatilization observed in microtektites all suggest that the source crater should be located somewhere in the southeast Asia [cf. 2]. Among the multiple lines of evidence, the spatial density of microtektites is the most important one, as the density generally decreases with larger distances from the southeast Asia, although the data points are rather scattered [1]. However, a potential caveat of the method is that although dozens of cores have recovered microtektites from this strewn field, the combined area of the cores is less than 1 m^2 [3], while the entire strewn field covers >20% of the Earth surface [4]. Therefore, whether or not the observed density variations of microtektites represent the actual situation should be regarded as an open question. A fundamental reason supporting this argument is that the transportation process of microtektites is not resolved at all, since the trajectory is heavily intertwined with the impact-disturbed atmosphere [5].

Tektites are at least two-orders of magnitude larger than micro-tektites, so that the transportation of tektites should be less affected by the atmosphere and their trajectories are more akin to ballistic trajectory. An investigation of the spatial density of tektites should be informative to both the spatial distribution of microtektites and possible location of source crater. However, there has been no such study for tektites. This is because except for 5 locations that have discovered possible in-situ tektites (i.e., tektites that have not been mobilized after the initial deposition; [6]), so far, the collected tektites have uniformly been transported after deposition.

Stratigraphy of tektites in the southern China: The current northern boundary of the Australasian strewn field is located at Baise, Guangxi Province [7]. It is well known at the southern China, tektites typically occur right at the boundary between the two sections of the Beihai Formation, although the majority of tektites in southern China are also transported ones [8]. During the past three years, we have done a systematical field investigation over a 2º×2º areas in the Guangdong, Hainan, and Guangxi Provinces to study the stratigraphic positions of tektites. We found 25 outcrops that probably contain in-situ tektites. Three pieces of evidence support the scenario of in-situ occurrence: (1) the discovered tektites are uniformly located between the upper sandstone and lower conglomerate sections of the Beihai Formation, and this boundary has the same stratigraphic ages with the tektites ([10]Be age is under investigation); (2) the discovered tektites are little eroded and they are larger than the grain size of the sandstone and conglomerate above and below their occurrences, so that they are unlikely to have been transported. Before [10]Be age for the boundary is successfully derived, we have to face at least one extreme possibility that may negate this scenario: the tektites might have been transported for short distances after deposition, e.g., under the effect of micro-topography (10s-m scale).

Spatial density: During the field trip, we have measured the line density for these in-situ tektites, assuming that the spatial density of tektites at a given location is uniform so a line density can be representative of the general density. The measured profiles have gentle dips, and those with complicated attitudes are avoided considering that small-scale transportation might have inevitably occurred. A more strict method should wholly reveal the boundary and carefully collect the number of tektites within a given area. We notice the following spatial density: (1) at each given location, the line density of tektites can be varied by >10 folds, which is consistent with that of microtektites [1]; (2) the southernmost Hainan Province and the Lei Zhou peninsula do not have uniformly larger line densities of tektites than the areas to the north, which is inconsistent with that of the general spatial densities of microtektites reported by [2] and [3].

References: [1] Glass B. P. and Koeberl C. (2006). *Meteoritics & Planetary Science*. 41: 305-326. [2] Glass B. P. and Simonson B. M. (2013) Distal impact ejecta layers: A record of large impacts in sedimentary deposits. Springer. [3] Prasad M. S. et al. *Journal of Geophysical Research* 112:E06007. [4] Van Ginneken et al. (2018) *Geochimica et Cosmochimica Acta* 228, 81–94. [5] Goldin T. J. and H. J. Melosh (2009) *Geology*, 37(12), 1135–1138. [6] McColl D. (2017) Australia's little space travelers. Springer. [7] Hou Y. et al. (2000) *Science* 287, 1622–1625. [8] Yuan B. and Ye. L. (1978) *Science Bulletin* 6, 271–273.

Focused Ion Beam (FIB) and Microtome Combined Ultrathin Slice Preparation for Transmission Electron Microscopy (TEM) Observation

Yuchen Xu[1,2], Lixin Gu[2], Yang Li[3], Bing Mo[3], Yangting Lin[2]
[1]State Key Laboratory of Space Weather, National Space Science Center, Chinese Academy of Sciences (CAS), Beijing 100190, China. [2]Key Laboratory of Earth and Planetary Physics, Institute of Geology and Geophysics, CAS, Beijing 100029, China. [3]Center for Lunar and Planetary Sciences, Institute of Geochemistry, CAS, Guiyang 550081, China

Introduction: With the advances of microbeam analytical techniques, integrated analyses have been performed on a single micron-sized sample to understand its formation and evolution history. Especially, crystallographic information combined with morphological, chemical, isotopic measurements are crucially beneficial to constrain the geological or cosmochemical processes of the sample. Therefore, it is important to develop technology to prepare the transmission electron microscopy (TEM) slices ($\leq$100 nm) from a specific micron-sized grain on a polished section or deposited on surface of a sample mount. Focused ion beam (FIB) is good at precisely lifting out. Microtome is applicable to prepare several ultrathin slices. Here, we combide the FIB and microtome techniques. Take an identified micron-sized presolar graphite for example, it is surrounded by amorphous carbonaceous residue with solar isotopes [1].

Samples: The carbon-rich residue of Qingzhen (EH3) meteorite has been separated by acid etching [2], which was dispersed on a high pure gold foil mount. Presolar graphite grains were identified based on anomalous C-isotopic compositions by NanoSIMS measurements [1]. The spherical presolar graphite selected has cauliflower-onion morphology, glassy-type with D/G = 1.13 in Raman spectra, and relatively high in ^{12}C (^{12}C/^{13}C = 99 $\pm$ 2) and ^{29}Si (δ^{29}Si/^{30}Si = 172 $\pm$ 36‰).

Experiments and Results: The TEM slices preparation process included two main steps. (1) Sample transfer with FIB. A carbon fiber was picked up and shaped via FIB, and an epoxy resin mount was trimmed with a black-face and Au-coated. The selected graphite spherule was attached to the top of the carbon fiber and moved to the top of the resin base together. The carbon fiber was cut free finally. (2) Sections slicing with the microtome. The sample was embedded in the resin drop, with the aid of a micromanipulator under an optical microscope. After curing, the sample was sliced with the microtome, and ultrathin sections were located on the holey-C-coated Cu TEM grids for TEM observations.

Under TEM, the graphite slice was found on one end of the carbon fiber, divided by the deposited Pt. The spherule has poor crystallization with turbostratic layering of contorted lattice planes and short-range layer continuity, which is consistent with its Raman signature. But no other submicron-sized inclusions were seen with diffraction contrast imaging and EDS measurements.

Advantages: First, several ultrathin sections can be obtained from a micron-sized grain. Second, reducing the risk of grain loss caused by static charge with the help of FIB. Third, carbon fiber served as a fiducial marker would be benefit for grain relocating.

Implications: Such FIB-microtome technique can be used to prepare TEM sections of micron-sized grains. Furthermore, the samples returned by future mission, either Lunar or small bodies, contain abundant micron-sized [3]. This technique can be a critical experimental method for theses retuned samples. In addition, it is also can be applied to tiny high pressure mineral, porous specimens, and other rare and unique micron-sized grains of terrestrial rocks and meteorites.

References: [1] Xu Y. et al., 2016. *The Astrophysical Journal* 825, 111-122. [2] Lin Y. et al., 2002. *The Astrophysical Journal* 575, 257-263. [3] Nakamura T. et al., 2011. *Science* 333, 1113-1116.

82nd Annual Meeting of The Meteoritical Society 2019 (LPI Contrib. No. 2157)

6337.pdf

Relationship between visible reflectance at 550 nm and carbon contents in carbonaceous chondrites: Attempt to estimate the bulk carbon contents of asteroid Ryugu's surface.

H. Yabuta[1], M. Ikehara[2], E. Tatsumi[3], S. Sugita[3], S. Yamashita[4], K. Mogi[4], K. Amano[4], M. Matsuoka[5], S. Kobayashi[4] and T. Nakamura[4], [1]Department of Earth and Planetary Systems Science, Hiroshima University (Kagamiyama 1-3-1, Higashi-Hiroshima 739-8526, Japan. E-mail: hyabuta@hiroshima-u.ac.jp). [2]The Center for Advance Marine Core Research, Kochi University, [3]Department of Earth and Planetary Science, University of Tokyo, [4]Division of Earth and Planetary Materials Science, Tohoku University, [5]ISAS/JAXA.

Introduction: Remote sensing observations of asteroid Ryugu by Hayabusa2 mission has revealed that Ryugu is one of the darkest bodies in the Solar System [1-3]. It is of great interest to identify the darkening agent of Ryugu's surface. In the preliminary investigation by Hiroi and Sugita, it was reported that there was a correlation between the reflectance at 550 nm of primitive carbonaceous chondrites and the insoluble organic matter (IOM) contents of the meteorites. Their result suggests that the bulk carbon contents of asteroid Ryugu are potentially estimated by the visible reflecntance acquired by optical navigation camera (ONC), an onboard scientific instrument of Hayabusa2 spacecraft. On the other hand, it is challenging to estimate IOM contents from meteorites, due to the mass loss during the purification process by the repetitive acid treatment and/or due to its static electricity. In this regard, total carbon contents can be estimated more accurately rather than IOM contents. Therefore, in this study, the reflectance spectra and total carbon contents (i.e., sum of IOM, SOM, and carbonates) of the same meteorite samples were measured in this study for increasing the accuracy of correlation.

Samples and Methods: As the samples, three primitive carbonaceous CM/CI chondrites (Murchison, Murray, and Yamato 980115), five thermally metamorphosed CM/CI chondrites (Jbilet Winselwan, Yamato 982086, Yamato 793321, Belgica 7904, and Yamato 86720), and three carbonaceous chondrites (Murchison, LAP 04721, and Tagish Lake) experimentally heated at different temperatures (300, 400, 500, 600 and 900°C) for 50 hours, and a simulant of Phobos were used. Their grain sizes and/or porosity were made constant. Reflectance spectra of the meteorites were analyzed by VERTEX 70v, Bruker (Tohoku Universty). Total carbon contents of the meteorites were analyzed by a CHN elemental analyzer (Flash EA1112, Thermo/Finnigan) (Kochi University).

Results and discussion: For the primitive CM/CI chondrites and thermally metamorphosed CM/CI chondrites, roughly linear correlations were observed between total carbon contents and reflectance at 550 nm (R(550)) and 390 nm (R(390)). Thus, the meteorites with higher carbon contents show lower reflectance. However, some meteorites (Murchison, Murray, Y-982086, Jbilet Winselwan, Y-793321) with similar carbon contents showed variations in reflectance. This is probably due to the difference in chemical compositions between primitive CM/CI chondrites and thermally metamorphosed CM/CI chondrites. The thermally metamorphosed CM/CI chondrites containing IOM with higher aromaticity [4] show lower reflectance compared to the primitive CM/CI chondrites. Based on the relationship, asteroid Ryugu, whose mean R(550) is 0.019, may contain higher than 3% of carbon.

In the correlation plots between total carbon contents and R(550) and R(390) for the experimentally heated carbonaceous chondrites, overall, meteorites with higher carbon contents show lower reflectance. However, individual meteorites showed different behaviors during heating. For instance, the reflectance values of Murchison were lowered while the total carbon contents of Murchison did not change during heating up to 400°C. During heating at 500 - 600°C, the reflectance values of Murchison were raised again while the total carbon contents of Murchison decreased only slightly. At 900°C, the total carbon contents of Murchison suddenly decreased with increasing reflectance. These variations in reflectance are related to not only total carbon contents but also chemical change of IOM with increasing temperature, such as aromatization, pyrolytic degradation, and gasification. LAP 04721 and Tagish Lake showed similar trends, but their variations in reflectance differed depending on their original carbon contents and compositions (including carbonates). Based on the relationship, R(550) of Ryugu is the most similar to those of the heated Tagish Lake at 400-600°C or heated Murchison at 400°C. The result appears to be consistent with the conclusion obtained by the near infrared spectral pattern of the surface of Ryugu [3]. However, further investigation will be necessary by consideration of other possible effects of grain sizes, porosity, space weathering degree, and inorganic compounds (e.g., magnetite, sulfide) on low reflectance of Ryugu's surface.

References: [1] Watanabe S. et al. (2019) *Science* 364: 268-272. [2] Sugita S. et al. (2019) *Science* 364: eaaw0422. [3] Kitazato K. et al. (2019) *Science* 364: 272-275. [4] Yabuta H. et al. (2005) *MAPS* 40: 779–787.

PREPARATION FOR CURATING SAMPLES RECOVERED FROM C-TYPE ASTEROID RYUGU BY HAYABUSA2 AND PRESENT STATUS OF CURATION OF SAMPLES RETURNED FROM S-TYPE ASTEROID ITOKAWA BY HAYABUSA.

T. Yada[1], M. Abe[1], A. Nakato[1], K. Yogata[1], K. Sakamoto[1], M. Nishimura[1], T. Okada[1], M. Yoshitake[1], K. Kumagai[2], A. Iwamae[2], S. Furuya[1], T. Hayashi[1], D. Yamamoto[1], S. Tachibana[1,3] and H. Yurimoto[1,4], [1]Inst. Space Astronaut. Sci., Japan Aer-osp. Explor. Agency (JAXA), 3-1-1 Yoshinodai, Chuo, Sagamihara, Kanagawa 252-5210, Japan (yada@planeta.sci.isas.jaxa.jp), [2]Marine Works Japan Ltd., 3-54-1 Oppamahigashi, Yokosuka 237-0063 Japan, [3]UTOPS, Grad. Sch. Sci., Univ. Tokyo, 7-3-1 Hongo, Bunkyo, Tokyo 113-0033, Japan, [4]Dept. Earth Planet. Sci., Grad. Sch. Sci., Hokkaido Univ., Kita 8, Nishi 5, Kita, Sapporo, Hokkaido 060-0808, Japan

Introduction: Hayabusa2 spacecraft successfully performed the touchdown sampling onto the surface of its target C-type asteroid Ryugu on Feb 22, 2019 [1]. A series of images shot by its onboard cameras indicate that it should have recovered the surface regolith grains into its sample catcher successfully. Additionally, Ryugu's reflectance spectra taken by the Near Infrared Spectrometer (NIRS3) show a weak but clear global adsorption feature at 2.72 μm, which indicates the presence of OH-bearing minerals [2]. Together with its low albedo, surface materials of Ryugu are similar either to thermally- and/or shock-metamorphosed carbonaceous chondrites or to materials with weak aqueous alteration [3]. The Ryugu samples will be returned to the Earth at the end of 2020. We Astromaterial Science Research Group (ASRG) are now preparing for handling and curating them in the Extraterrestrial Sample Curation Center (ESCuC) at JAXA Sagamihara campus.

Curation Plan for Returned Ryugu Samples: Due to the plausible volatile-containing property of Ryugu, contamination of volatiles, such as H_2O and organics, should be minimal. The samples will thus be enclosed into a sample container using a metal sealing mechanism [4, 5]. Volatile components released inside the sample container will be collected via a gas extraction line, prior to the container opening, at the quick-look facility near the landing site of the reentry capsule. The container will be then carried into the cleanroom of the ESCuC and introduced into the clean chambers (CCs) for sample handling after a series of cleaning and disassembling process [6]. The CCs for Ryugu samples are composed of five components; CC3-1 for opening of the container to extract the sample catcher in vacuum, CC3-2 for removal of the cover of catcher and picking up of a certain amount of samples from the catcher for storage in vacuum, CC3-3 for change of the environment from vacuum to purified nitrogen atmosphre, CC4-1 and CC4-2 for disassembly of the sample catcher, catcher handling and description. The initial description of the samples in CCs 4-1 and 4-2 is planned to include weighing by a microbalance, observing by an optical microscope and spectroscopic analysis by the FT-IR. A infrared spectral imager, equivalent to MicrOmega on board the MASCOT lander, will be equipped to CC3-3 for non-destructive sample description [7].

Some fractions of the samples will be distributed to initial analyses and phase 2 curation team after 6 month from the capsule recovery. Ten percent will be distributed to NASA after a year from the capsule recovery based on the MOU between JAXA and NASA. The Ryugu samples will be available to the community through the international announcement of opportunity (AO) after one and a half years from the capsule recovery.

Curation of Returned Itokawa Samples: ASRG has continuing description of Itokawa samples since their return in 2010. The number of those initially described reaches more than 650. More than 100 of Itokawa particles whose size range from 11 to 238 μm were newly described in 2018. Their details including SEM images and EDS spectra are available at the ASRG website (https://curation.isas.jaxa.jp/curation/hayabusa/index.html). Research proposals for Itokawa particles can be submitted anytime through the website (https://curation.isas.jaxa.jp/ao/index.html).

References: [1] Watanabe S. et al. (2019) *LPS L*: abstract #1265. [2] Kitazato K. et al. (2019) *Science* 364:272. [3] Sugita S. et al. (2019) *Science* 364:252. [4] Okazaki R. et al. (2017) *Space Sci. Rev. 208,* 107. [5] Sawada T. et al. (2017) *Space Sci. Rev. 208,* 81. [6] Yada T. et al. (2019) *LPS L*: abstract #1795. [7] Bibring J. -P. et al. (2019) *this meeting*.

JAPANESE ANTARCITC METEORITES: PAST, CURRENT, AND FUTURE.

A. Yamaguchi[1], N. Imae[1], M. Kimura[1], and T. Noguchi[1,2], [1]National Institute of Polar Research, Tokyo 190-8158, Japan (yamaguch@nipr.ac.jp), [2]Kyushu University, Fukuoka 819-0395, Japan

In December, 1969, an inland survey team of the 10th Japanese Antarctic Research Expedition (JARE-10) found a total of nine meteorites with at least five distinct types (E, H, L, CK chondrites, a diogenite) in the bare ice fields near the Yamato Mountains [1]. The discovery of Yamato meteorites led to systematic searches for meteorites in Antarctica that resulted in the recovery of a large number of meteorites. The success of meteorite expeditions stimulated the international community. By 2019, more than 38,000 Antarctic meteorites have been collected, comprising ~64% of world collections. The recovery of Antarctic meteorites led to expanding our understanding of the early Solar System and geologic history of the Moon and Mars. In addition, micrometeorites are collected from moraines and snow. These micrometeorites contain a large number of pristine types including possible cometary dust. Therefore, Antarctica is a treasure trove of extraterrestrial materials.

Although several sample-return missions are planned or on-going, meteorite studies are still important for planetary sciences. Meteorites represent the most diverse materials from the Solar System which provide the information of chemical and isotopic heterogeneity of the early Solar System. Secondary, meteorite collection has also provided material to complementary to sample-return missions. Centimeter scale samples provide a hint to understand lithologic types of small samples collected by missions (e.g., Hayabusa2). Finally, Antarctic meteorites were kept at low-temperature conditions on ice, collected by scientific teams and curated in institutions, which is especially important for organic chemistry.

JAREs comprising 24 parties, collected over 17,000 meteorites. About 11,600 meteorites have been classified so far. Recently, we published 6 issues of Meteorite Newsletter (Vol. 21-26) from 2012 to 2018 [2-7]. The total number of classified meteorites is 4,936. They include Yamato, Asuka, and Belgica meteorites collected by JARE as well as the Japan-Belgium joint expeditions (Asuka 09, 10, and 12 meteorites). Meteorites in Newsletters 21-26 include 53 carbonaceous chondrites (CM, CO, CV, CR, CH, CK, and ungrouped), 4 enstatite chondrites (EH and EL), 7 R chondrites, 196 HED meteorites, 7 ureilites, 10 primitive achondrites (acapulcoites, lodranites, and winonaite), 2 mesosiderites (A 09545 and A 10143 [3]), 1 angrite (A 12209 [5]), and 3 martian meteorites (shergottites) (Y 002192 and Y 002712 [4], and A 12325 [6]). We also published the bulk chemical compositions of 1,162 meteorites, including chondrites, HEDs, martian meteorites, and others, analyzed by the wet chemical method [8]. We are going to publish an issue Meteorite Newsletter including several hundred meteorites including some iron meteorites.

We attempt to continue the search for meteorites and micrometeorites in Antarctica for the next several years. Expedition to Nansen icefield for Asuka meteorites is planned. Expeditions to Yamato mountains will be difficult because of logistical and financial problems. We are going to make a proposal for the Yamato expeditions in Phase X (2022-2027). Micrometeorites are recovered from fresh snows in other areas (e.g., Dome Fuji) in Phase IX of JARE planned from 2016 to 2021 (JARE 58-63).

References: [1] Yosida M. (2010) *Polar Science* 3:272-284. [2] Yamaguchi A. et al. (2012) *Meteorite Newsletter* Vol 21, 33 pp. [3] Yamaguchi A. et al. (2013) *Meteorite Newsletter* Vol 22, 32 pp. [4] Yamaguchi A. et al. (2014) *Meteorite Newsletter* Vol 23, 16 pp. [5] Yamaguchi A. et al. (2015) *Meteorite Newsletter* Vol 24, 20 pp. [6] Yamaguchi A. et al. (2016) *Meteorite Newsletter* Vol 25, 25 pp. [7] Yamaguchi A. et al. (2018) *Meteorite Newsletter* Vol 26, 29 pp. [8] Kimura M. et al. (2018) *Polar Science* 15:24-28.

OXYGEN ISOTOPE EXCHANGE BETWEEN CAI MELT AND WATER VAPOR: AN EXPERIMENTAL STUDY.

D. Yamamoto[1], S. Tachibana[1,2], N. Kawasaki[3], M. Kamibayashi[2] and H. Yurimoto[1,3], [1]Institute of Space and Astronautical Science, Japan Aerospace Exploration Agency (daiki@planeta.jaxa.isas.ac.jp), [2]UTokyo Organization for Planetary Spece Science, The Univesity of Tokyo, [3]Department of Natural History Sciences, Hokkaido University.

Introduction: Coarse-grained calcium-aluminum-rich refractory inclusions (CAIs) are known as the oldest high temperature mineral assemblages with sizes up to ca. 1 centimeter in the Solar System, and exhibit mass-independent oxygen isotope variation among constituent minerals [e.g. 1–3]. A possible explanation of oxygen isotope variation in CAIs is the partial melting and associated gas-melt oxygen isotope exchange during reheating events [e.g. 3, 4]. However, oxygen isotope exchange mechanism and kinetics between CAI melt and disk gas have been poorly understood. In this study, we conducted oxygen isotope exchange experiments between synthetic CAI melt and water vapor under a disk-like low water vapor pressure (P_{H2O}) to constrain the thermal history of CAIs in the early Solar System.

Experiments: The starting material was prepared by mixing SiO_2, TiO_2, Al_2O_3, MgO and $CaCO_3$ powder with a mixing ratio close to the average type B CAI-like composition (CAIB) [5, 6]. The oxygen isotope exchange experiments between the synthetic CAIB melt and ^{18}O-enriched water vapor with P_{H2O} of 5×10^{-2} Pa were carried out at 1390°C for 3–24 hours using a high temperature vacuum furnace equipped with a gas flow system for water vapor. The spherical CAIB droplet (spinel and glass mixture) was hung in the furnace using a Pt wire loop technique. Low pressure-water vapor was supplied from ^{18}O-enriched water ice (97-atom% ^{18}O) in a freezer [7, 8]. The experimental temperature of 1390°C is 10 K higher than the melilite liquidus temperature (1380°C) of CAIB. Run products were analyzed with FE-SEM-EDS (JEOL JSM-7000F) for observation and chemical analysis, and oxygen isotopic compositions of samples were measured with SIMS (Cameca ims-1280HR) at Hokkaido University.

Results and discussion: The heated spherical samples were composed of glass and spinel. The ^{18}O fraction in the melt increased toward the surface of the sphere, and that at the surface increased with time, suggesting that the surface oxygen isotope exchange and the self-diffusion of oxygen into melt interior simultaneously occurred. Obtained oxygen isotope profiles were explained by a three-dimensional spherical diffusion equation with a time-dependent surface concentration [9], yielding the oxygen self-diffusion coefficient D of 1.87×10^{-7} cm^2 sec^{-1} and the surface oxygen isotope exchange efficiency of ~0.27 for colliding water vapor. The obtained D in the CAIB melt is consistent with that estimated in basaltic melt at 1390°C [10, 11]. This is likely because the diffusivity of oxygen would be related to the degree of melt polymerization (NBO/T) [12] and the CAIB melt has a similar NBO/T as that of basaltic melt.

Melilite is the first phase crystallizing from spinel-bearing CAI melt with type B CAI composition [5, 6]. Melilite in natural type B CAIs shows typically ^{16}O-poor oxygen isotopic compositions with a limited isotope variation [e.g. 4, 13]. If the precursors of CAIs have ^{16}O-rich isotopic compositions close to that of spinel, those observations indicate melilite crystallized from the melt that was isotopically equilibrated with surrounding disk gas with ^{16}O-poor isotopic compositions above the melilite liquidus temperature [3]. Therefore, based on obtained kinetic data, we evaluated a timescale required for 1 cm-sized CAI droplet to isotopically equilibrate with ambient water vapor as a function of P_{H2O} at 1390°C. The timescale is dependent of P_{H2O} at low P_{H2O} ($<\sim 10^{-6}$ bar), where the supply of water vapor is a rate-limiting step. On the other hand, it is independent of P_{H2O} at higher P_{H2O} because the reaction is controlled by oxygen diffusion in the melt. At temperatures above the melilite liquidus and plausible range of P_{H2O} in the protosolar disk ($10^{-9} < P_{H2O}$ (bar) $<10^{-6}$) [14], oxygen isotope exchange reaction between CAI melt (<1 cm) and water vapor would be mainly controlled by the supply of water vapor, and the timescale for isotope equilibration is at least a dozen days for 1 cm-sized CAI melt. Homogeneous ^{16}O-poor oxygen isotopic compositions of melilite in most natural type B CAIs suggest that type B CAIs would be heated for at least a dozen days in a ^{16}O-poor environment during the reheating processes in the early Solar System.

[1] Clayton R. N. et al. (1973) *Science* 182:485–488. [2] Connelly J. N. et al. (2012) *Science* 338:651–655. [3] Yurimoto H. et al., (1998) *Science*, 282:1874–1877. [4] Kawasaki N. et al. (2018) *Geochemica et Cosmocochemica Acta* 221:318–341. [5] Stolper E. (1982) *Geochemica et Cosmochemica Acta* 46:2159–2180 [6] Stolper E. & Paque J. M. (1986) *Geochemica et Cosmochemica Acta* 50:1785–1806. [7] Yamamoto D. & Tachibana S. (2018) *ACS Earth and Space Chemistry* 2:778–786. [8] Yamamoto D. et al. (2018) *The Astrophysical Journal* 865:98 (14pp). [9] Crank J. (1975) *The Mathematics of diffusion*. 2nd edition Oxford:Oxford University Press. [10] Canil D. & Muehlenbachs K. (1990) *Geochemica et Cosmochemica Acta* 54:2947–2951. [11] Lesher C. E. et al. (1996) *Geochemica et Cosmochemica Acta* 60:405–413. [12] Liang et al. (1996) *Geochemica et Cosmochemica Acta* 60:4353–4367. [13] Yurimoto H. et al. (2008) *Reviews in Mineralogy & Geochemistry* 68:141–186. [14] Wood J. A. & Morfill G. E. (1988) In *Meteorites and the Early Solar System*, Tucson, AZ: University of Arizona Press.

THE PETROGENESIS OF VERY LOW-TI MARE BASALTIC CLASTS IN LUNAR METEORITE DHOFAR 1442.

J. Yang[1,2] , Y. T. Lin[2], K. H. Joy[3], and B. Chen[1], [1]Department of Earth and Space Sciences, Southern University of Science and Techonology, Shenzhen, China, [2]Key Laboratory of Earth and Planetary Physics, Chinese Academy of Sciences, Beijing, China, [3]School of Earth and Environmental Sciences, University of Manchester, Oxford Road, Manchester, UK.
Email: yangj37@sustech.edu.cn.

Introduction: Lunar meteorite Dhofar (Dho) 1442 is a clast-rich regolith breccia with a glassy and vesicular matrix [1-2]. The lithic clast content includes basalts, mafic breccias, gabbros, norites, anorthosites, impact spherules and evolved lithologies-granophyres [1-4]. Dho 1442's bulk composition is the 2nd most incompatibly trace element rich sample to date [1, 5], after the impact melt clast component of Sayh al Uhaymir (SaU) 169 [6]. The provenance of Dho 1442 is almost certainly within the Procellarum KREEP Terrane (PKT) [2]. In the present work, in order to clarify the petrogenesis of basaltic clasts in Dho 1442, we conducted a detailed study on the petrography, mineralogy and geochemistry of basaltic clasts using *in-situ* electron microprobe and LA-ICP-MS techniques.

Results: Six mare basaltic clasts were identified in the meteorite section we studied. They exhibit a range of textures from subophitic to porphyritic. There are no apatite or merrillite or zircon found within the Dho 1442 basaltic clasts. Using the Apollo mare basalt classification scheme of Neal and Taylor [7], three of these basaltic clasts (named Ba1, Ba3, Ba5) can be classified as very low-Ti (VLT), high-Al (15-18 wt%) basalts, and two clasts (Ba2, Ba4) are VLT (0.5-1 wt%), low-Al (6-8 wt%) basalts, and one (Ba6) can be classified as a low-Ti (2.5 wt%), high-Al (18.5 wt%) basalt. These basaltic clasts all have low incompatible element (ITE) concentrations. Both Ba1 and Ba4 show positive Eu-anomalies (Ba1 = 1.6 Eu/Eu*; Ba4 = 3.0 Eu/Eu*, where $Eu/Eu* = Eu_{cn}/\sqrt{[Sm_{cn}*Gd_{cn}]}$), which is not typical of the majority of Apollo mare basalts.

Discussion: Although these clasts are small (150-500 μm), they can potentially provide new insights to lunar volcanism and the processes that caused magma production at different times in the Moon's past.

What were the source regions of basaltic clasts in Dho 1442? The high Al_2O_3 and CaO content (15.3 and 11.1 wt%, respectively) of Ba1 suggest that its source region was predominately composed of plagioclase and pyroxene. Thus, the parent magma of Ba1 may have been derived from decompression-driven partial melting of a leuconoritic crustal lithology. Alternatively, the generation of Ba1 might be from melting of a hybridized source consisting of a mixture of early- and late-stage lunar magma ocean cumulates (orthopyroxene+olivine and clinopyroxene+plagioclase, respectively). Ba4 in Dho 1442 is an unusual VLT mare basalt. With the exception of Ba4, other VLT mare basalts in lunar meteorites and returned samples exhibiting positive Eu-anomalies contain >11 wt% Al_2O_3 [e.g., 8-9] and are classified as high-Al basalts. In contrast, the bulk Al_2O_3 content of Ba4 is only 7.8 wt%. As Al_2O_3 is an incompatible oxide, the Al_2O_3 content in the basaltic partial melt should be enriched relative to the content in the source region. In other words, the Al_2O_3 content of Ba4 source region might be lower than ~4 wt% (assuming ~50% degree of melting), ruling out the possibility of partial melting of a plagioclase-rich lithology. If the source region of Ba4 was dominated by orthopyroxene, its Al_2O_3 and CaO content were ~3 wt% and ~2 wt% respectively based on the Al and Ca partition coefficients of orthopyroxene-basalt [10-11]. Both the calculated Al_2O_3 and CaO content of Ba4 source region are consistent with the composition of lunar orthopyroxene [e.g., 12-13], indicating origin from partial melting of a mantle region dominated by early orthopyroxene cumulates of the magma ocean.

What was the role of KREEP? Although the bulk rock composition of the Dho 1442 meteorite suggests it originated within the nearside PKT region, compared with high-Ti and low-Ti mare basalts, low concentrations of ITEs in Dho 1442 basaltic clasts indicate that the parent magmas of these basalts was not from urKREEP-rich portions of the mantle, and that during ascent the magmas did not mixed with any KREEPy crustal rocks or KREEPy impact melt components. Thus, the basalts may represent mantle melting that was not driven by KREEP induced heating.

References: [1] Korotev R. L. et al. (2009) *Meteoritics & Planetary Science* 44:1287-1322. [2] Zeigler R. A. et al. (2011) *LPS XLII*, Abstract #1012. [3] Weisberg M. K. et al. (2009) *Meteoritics & Planetary Science* 44:429-462. [4] Demidova S. I. et al. (2014) *Petrology* 22:1-16. [5] Korotev R. L. (2012) *Meteoritics & Planetary Science* 47:1365-1402. [6] Zeigler R. A. et al. (2006) *LPS XXXVII*, Abstract #2366. [7] Neal C. R. and Taylor L. A. (1992) *Geochimica et Cosmochimica Acta* 56:2177-2211. [8] Sokol A. K. et al. (2008) *Geochimica et Cosmochimica Acta* 72:4845-4873. [9] Snape J. F. et al. (2011) *Meteoritics & Planetary Science* 46:1288-1312. [10] Shearer C. K. et al. (2006) *Reviews in Mineralogy and Geochemistry* 60:365-518. [11] Adam J. and Green T. (2006) *Contributions to Mineralogy and Petrology* 152:1-17. [12] Robinson K. L. et al. (2012) *Meteoritics & Planetary Science* 47:387-399. [13] Shaulis B. J. et al. (2017) *Geochimica et Cosmochimica Acta*. 213:435-456.

NOTICE ON THE EBSD ANALYSIS OF OLIVINE IN METEORITES.

M. Yasutake[1], A. Miyake[2], T. Mikouchi[3], A. Tsuchiyama[1,4], [1] Research Organization of Science and Technology, Ritsumeikan University, [2]Kyoto University, [3]The University of Tokyo, [4]Guangzhou Institute of Geochemistry.

Introduction: Olivine is one of the most common constituent minerals in meteorites. It occurs in most of the meteorites including chondrites, primitive achondrites, achondrites, stony-iron meteorites, and silicate inclusion in iron-meteorites [e.g., 1 and reference therein]. Such a wide-spread occurrence of olivine in meteorites makes it a good indicator to understand the origin and evolutionary history of meteorites and their parent bodies [e.g., 2-3].

The recent advance of SEM-EBSD techniques enables us to understand easily and rapidly the crystallographic features of constituent minerals in meteorites. EBSD data helps us to understand the formation history of meteorites and their parent bodies such as accumulation processes, igneous processes, and shock metamorphism [e.g., 4-6]. However, we found that there are some points that we should pay attention to the procedure of EBSD analysis of olivine. Here we make short notices on this matter with basic crystallographic information of forsterite.

Crystallographic Data of Olivine: Olivine is a group of orthorhombic silicate mineral with the formula of M_2SiO_4. Forsterite is an Mg-endmember of the olivine (Mg_2SiO_4) and the most common mineral in meteorites. Therefore, we discussed the crystallography of forsterite. The cell length of forsterite and corresponding crystallographic axes and optical indicatrix are shown in Table 1. Laue group of forsterite is *mmm* and conventionally *Pbnm* space

Table 1. Crystallographic parameter and optical indicatrix of forsterite.

Cell length	*Pbnm*	*Pnma*	*Opt. Ind.*
4.75 Å	*a*	*c*	*Z*
10.20 Å	*b*	*a*	*X*
5.98 Å	*c*	*b*	*Y*

group is used among mineralogical and petrological studies. On the other hand, *Pnma* space group is also used for minerals with *mmm* Laue group [7], and some mineralogical studies used *Pnma* space group [e.g., 8]. The correspondence of crystallographic axes in *Pbnm* and *Pnma* space groups is the following: $a_{Pbnm} = c_{Pnma}$, $b_{Pbnm} = a_{Pnma}$, and $c_{Pbnm} = b_{Pnma}$ as shown in Table 1.

We investigated the crystallographic database of olivine in the latest default database in SEM-EBSD systems. In the dataset of Oxford Instrument software, most indices are based on *Pnma* space group and two indices are based on *Pbnm*. In the dataset of EDAX software, the index is based on the *Pbnm* space group. If the EBSD data was analyzed using the default dataset of Oxford Instruments, it might be based on the *Pnma* space group. Therefore, we should be careful to choose the index of olivine to construct EBSD data. If the obtained crystallographic data mismatches other data such as grain shape, estimated crystal facets, and/or lineation texture, it could be because of the mismatch of the space group. We suggest that EBSD data analyzed based on the *Pnma* space group is needed to replace by the *Pbnm* space group and suggest noting the space group and cell parameter used on the investigation to avoid the confusion.

Recent studies found developed olivine fabrics implying ductile solid-state deformation [e.g., 9-10]. Then, the olivine fabric of meteorites is the topic of arousing interest. Although the recent studies used SEM-EBSD system to investigate the fabric, most of the previous fabric analyses used optical microscope techniques with the universal stage [e.g., 11]. Correspondence of crystallographic axes by the *Pbnm* space group and optical indicatrix is following: $a = Z$, $b = X$, and $c = Y$. Therefore, we also should be careful when comparing the crystallographic orientation data obtained by the optical microscope technique and SEM-EBSD technique.

At the last, we notice the mismatch between the crystallographic data obtained by SEM-EBSD and the SEM image [12]. It depends on the setting of SEM used for EBSD analysis, and so we do not describe in detail this topic here. The detailed procedure to confirm and correct the mismatch is described on our webpage: "http://www.kueps.kyoto-u.ac.jp/~web-min/SEM-EBSD/JpGU2016_SMP-P05_e.pdf".

References: [1] Papike J. J. (Ed.). (2018). *Planetary Materials* (Vol. 36). Walter de Gruyter GmbH & Co KG.. [2] Stöffler D. et al. (1991) *Geochimica et Cosmochimica Acta* 55:3845-3867. [3] Wlotzka F. (2005) *Meteoritics & Planetary Science* 40:1673-1702. [4] Bland P. A. et al. (2011) *Nature Geoscience* 4:244. [5] Ruzicka A. M. et al. (2017) *Meteoritics & Planetary Science* 52:1963-1990. [6] Hasegawa, H. et al. (2019) *Meteoritics & Planetary Science* 54:752-767. [7] Hahn T. et al. (Eds.). (1983) *International Tables for Crystallography*, Vol. 1. [8] Brodholt J. (1997) *American Mineralogist* 82:1049-1053. [9] Tkalcec B. et al. (2013) *Nature Geoscience* 6:93-97. [10] Yasutake M. et al. (2019) *50th LPSC*, Abstract #1796. [11] Berkley J. et al. (1976) *Geochimica et Cosmochimica Acta* 40:1429-1437. [12] Miyake A. et al. (2016) *Japan Geoscience Union Meeting 2016*, Abstract SMP43-P05.

3D OBSERVATION OF POROUS MATRICES IN PRIMITIVE CM-CO CHONDRITES BASED ON SR-NANO-XCT IMAGING.

M. Yasutake[1], E. Vacarro[2], K. Uesugi[3], A. Takeuchi[3], T. Nakano[4], A. Takigawa[5], A. Tsuchiyama[1,6], [1]Research Organization of Science and Technology, Ritsumeikan University (yasutakemasahiro.meteo@gmail.com), [2]The Natural History Museum, London, [3]JASRI/SPring-8, [4]Geological Survey of Japan, AIST, [5]Kyoto University, [6]Guangzhou Institute of Geochemistry.

Introduction: Carbonaceous chondrites are well-known samples that preserve primitive and pristine features of the solar system. Especially, primitive carbonaceous chondrites (PCC) are thought to experience little alteration and metamorphic processes. Matrix is one of the dominant components of chondrites. Recent studies revealed that matrices in PCC contain unique components resembles CP-IDPs that is one of the most primitive materials [e.g. 1,2]. However, their origin of matrices is still controversial. It is well known that carbonaceous chondrite matrix (CCM) has fine, complex and heterogeneous texture from the 2D investigation. 3D observation based on X-ray CT is a very strong tool to understand such complex material. Furthermore, the recent advance of synchrotron radiation nano-scale X-ray CT (SR-nanoXCT) enables us to investigate fine structures such as CCM. Here, we show the 3D structure of matrices in primitive carbonaceous chondrites based on SR-nanoXCT and discuss their formation history.

Samples and Methods: We investigated matrices of four PCC classified CM-CO clan; Paris (CM3), ALH 77307 (CO3), DOM 08006 (CO3), and MIL 07687 (CO3). The surface of the matrix was investigated by SEM-EDS. Relatively porous matrices were chosen to investigate. Micro-sized CT samples ($\sim25 \times 25 \times 25$ µm) were picked up with a FIB/FE-SEM system (FEI Helios nanolab G3). CT data were obtained at beamline BL47XU, SPring-8, SR facility in Japan. CT images were acquired at X-ray energies of 7 keV and 7.35 keV. X-ray linear attenuation coefficients (LAC) were obtained and mineral phases were estimated using a dual-energy tomography (DET) method [3].

Results and discussion: We classified matrices into 3 types based on the observed constituent material and texture. *Type1:* The observed matrices in ALHA 77307 and DOM 08006, and one of the matrices in Paris (M1) mainly consisted of amorphous silicates including submicron-sized Fe-rich phases (Fig. 1a). Fine pores were uniformly distributed in the matrices. Notably, fibrous material was abundant in the matrix. It is hard to estimate the mineral phases of most fibrous material because of their small sizes, but one largest material in Paris was estimated to be olivine or low-Ca pyroxene (Fig. 1b). It is probably enstatite whisker as the case of some carbonaceous chondrites [e.g. 1]. The type 1 matrix is likely to be the most primitive in this study.

Type2: The observed matrix in MIL 07687 mainly consisted of amorphous silicate with Fe,Ni-metal as type 1 (Fig. 1c). On the other hand, this matrix contained many large lathes of serpentine. Pores were uniformly distributed in the matrix. There were unique components with a spherical structure; a layered structure composed of a serpentine shell, Fe,Ni-metal core, and a dark mantle in CT-images possibly consisting of organic materials. Coexistence of amorphous silicates, Fe,Ni-metal, and well-grown serpentine indicates that matrix had suffered very local alteration, or it is a mechanical mixture of primitive matrices like type1 and pre-accretionary altered products.

Type3: Another matrix in Paris (M2) mainly consists of relatively large olivine grains ($\sim$0.5–2.0 µm). It contains minor sulfide and Fe-rich oxide/hydroxide, which is an alteration product of Fe,Ni-metal (Fig. 1d). Pores are distributed among olivine grains. The 3D observation certifies that this is not an artifact product during sample preparation such as plucking of the mineral grains at the surface. Olivine is one of the well-known materials that crystallize during condensation in the gas nebular [e.g. 4]. It might be formed by condensation processes.

Conclusion: 3D observation based on SR-nanoXCT reveals the presence of whisker-like materials, wide-spreading pores, and unique spherical components in matrices of PCC. These features are hard to be distinguished from the 2D investigation. Further mineralogical investigation using TEM will help us to better understand the building blocks in the early solar system.

References: [1] Vacarro E. (2017) PhD thesis, The Open University. [2] Leroux H. et al. (2015) *Geochimica et Cosmochimica Acta*, 170:247-265. [3] Tsuchiyama A. et al. (2013) *GCA*, 116:5-16. [4] Ebel D. S. (2006). *Meteorites and the early solar system II*, 1:253-277.
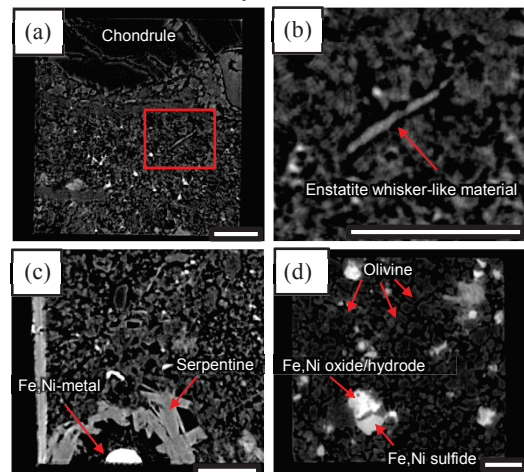

Fig. 1. CT images at 7.35 keV of (a) type 1 matrix in Paris (M1), (b) enlarged image in (a) showing a whisker-like material, (c) type 2 matrix in MIL 07678, and (d) type 3 matrix in Paris (M2). Silicates are shown in dark grey, pores in black, and Fe-rich materials in light grey to white. Scale bar = 5 µm.

OLIVINE CHEMICAL FEATURES AND O-Cr-Ti ISOTOPIC COMPOSITIONS OF NORTHWEST AFRICA 7312 UNIQUE DIFFERENTIATED METEORITE: COMPARING TO OTHER METEORITE GROUPS.

M. Yasutake[1], A. Yamaguchi[2], R. C. Greenwood[3], Y. Hibiya[4,5], T. Iizuka[5], I. A. Franchi[3], [1]Ritsumeikan University, [2]NIPR, Japan, [3]The Open University, UK, [4]JAMSTEC, [5]University of Tokyo.

Introduction: Differentiated meteorites enable us to better understand the early evolution of molten asteroids. NWA 7312 is an ultramafic differentiated meteorite consisting of Mg-rich silicates (olivine: Fo_{96}, ~40 vol%; orthopyroxene: En_{95}, ~60 vol%), with a well-developed petrofabric that implies ductile solid-state deformation in the parent body [1]. While the petrological features of NWA 7312 resemble lodranites, its O-isotopic composition is outside the range of the acapulcoite-lodranite clan, but within the range of CR chondrites. These results raise the possibility that NWA 7312 is derived from an unknown body. The minor element composition of olivine also provides a good indicator of formation history and relationship to other meteorite groups. O-Cr-Ti isotope systematics should help to demonstrate whether NWA 7312 is a carbonaceous or non-carbonaceous chondrite-related meteorite. We have investigated these features of NWA 7312 and compare the results with known meteorite groups.

Sample and Methods: We prepared three polished thin/thick sections for mineralogical study. The mineral chemical composition was obtained using an EPMA at NIPR. Cr isotope analyses were performed using a TIMS at the National Museum of Nature and Science, Japan. Ti isotope analyses were carried out using an MC-ICP-MS at the University of Tokyo. The Cr-Ti isotope analyses were performed following the procedures of [2, 3]. Oxygen isotope analysis of NWA 7312 was carried out by laser fluorination at the Open University following the procedures of [4].

Results and Discussion: The Fe/Mg-Fe/Mn systematics of olivine can be used to reveal formation processes and redox conditions [5]. Fe/Mg-Fe/Mn values for NWA 7312 fall within the subchondritic range (Fig. 1) and differ from chondrites and primitive achondrites that are within the chondritic range. These values also differ from all other known achondrites. We interpret NWA 7312 as a residual lithology that underwent more extensive melting than other primitive achondrites under reducing condition. This suggestion is consistent with the petrologic features of NWA 7312, which is a coarse-grained ultramafic rock. Alternatively, it could be a result of a metasomatic process that does not cause simple Fe loss/addition, although this process is poorly understood.

The CaO and Cr_2O_3 contents of olivine are distinguishable from those of ureilites, brachinites, and other achondrites, including lodranites. The olivine in NWA 7312 contains minor CaO (0.12-0.15 wt%) and Cr_2O_3 (0.18-0.29 wt%). The CaO and Cr_2O_3 contents of olivine in NWA 7312 are intermediate between ureilites and most other achondrites. These minor element contents are outside the range of any known meteorite group.

Ti and Cr isotopic compositions are shown in Fig. 2. NWA 7312 plots in the non-carbonaceous group. The composition of NWA 7312 resembles that of the ureilites and differs from the CR chondrites. NWA 7312 and the ureilites have distinct O-isotope compositions (Fig. 2).

Based on the mineralogical and isotopic evidence, we conclude that NWA 7312 is derived from an unknown differentiated asteroid that experienced extensive melting and later ductile solid-state deformation.

References: [1] Yasutake M. et al. (2019) *50th LPSC*, Abstract #1796. [2] Hibiya Y. et al. (2019) *Geostandards and Geoanalytical Research*, 43:133-145 [3] Hibiya Y. et al. (2019) *Geochimica et Cosmochimica Acta* 245:597-627. [4] Greenwood R. C. et al. (2017) *Chemie der Erde*, 77:1-43. [5] Goodrich C. A. and Delaney. et al. (2000) *Geochimica et Cosmochimica Acta,* 64:149-160. [6] Goodrich C. A. and Righter K. (2000) *Meteoritics & Planetary Science*, 35:521-535.
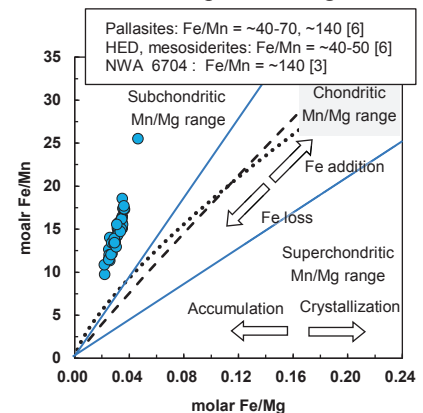

Fig. 1. Plot of molar Fe/Mg vs. molar Fe/Mn in olivine comparing NWA 7312 with regression curves for ureilites (broken curve) and lodranites (dotted curve) by [6].
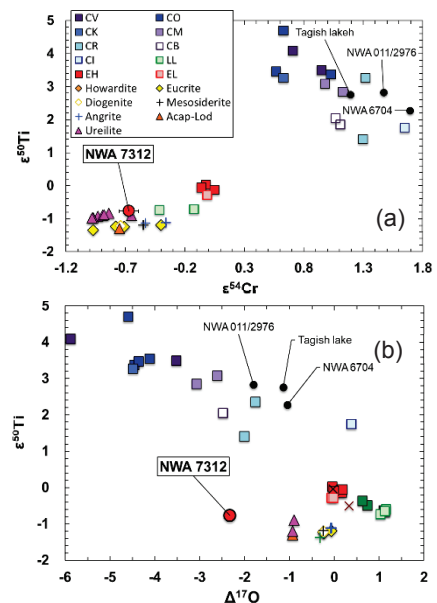

Fig. 2. Plots of $\varepsilon^{54}Cr$ vs. $\varepsilon^{50}Ti$ (a) and $\varepsilon^{50}Ti$ vs. $\Delta^{17}O$ (b) of NWA 7312. The data for other meteorite groups and some ungrouped meteorite are shown for comparison. The reference data of NWA 6704 is from [3] and other references therein. The errors of $\varepsilon^{50}Ti$ and $\Delta^{17}O$ are within the symbol.

SPECTROSCOPY OF CARBONACEOUS MATTER IN THE SARICICEK METEORITE.

M. Yesiltas[1], T. D. Glotch[2], S. Jaret[3], A. B. Verchovsky[4], R. C. Greenwood[4], [1]Faculty of Aeronautics and Space Sciences, Kirklareli University, Kirklareli, Turkey 39100 myesiltas@knights.ucf.edu, [2]Department of Geosciences, Stony Brook University, Stony Brook, NY, USA 11794, [3]Department of Earth and Planetary Sciences, American Museum of Natural History, New York, New York 10024, [4]Planetary and Space Sciences, Open University, Walton Hall, Milton Keynes MK7 6AA, U.K.

Introduction: On the late night of September 2, 2015, the Sariçiçek (SC) meteorite fell in the village of Sariçiçek, Bingöl, Turkey. The fall of SC was captured by several cameras in the region, which enabled the recovery of many fragments. Thus far, more than 340 pieces of the meteorite have been recovered from the streets and fields in the Sariçiçek village, totaling to a mass of ~15.24 kg. As of today, this meteorite is the newest howardite and the only confirmed fall among the 17 known howardites. In this work, we investigated the molecular constituents of the SC meteorite samples. We present, in addition to O and C isotopic data, mineralogy and carbonaceous content of the SC fragments with three different sets of infrared data and one set of Raman data.

Carbonaceous matter on 4-Vesta is foreign material, perhaps delivered through impacts by micrometeorites or larger objects. The dark material on Vesta may indicate the presence of impact melts and exogenous carbonaceous material [1]. Therefore, carbonaceous phases present in the SC samples might provide clues regarding the impactor material (e.g. carbonaceous chondrites).

Samples and Methods: Various pieces of the SC meteorite were prepared in the form of powder as well as thin sections, which were then studied using (i) synchrotron-based FTIR spectroscopy, (ii) micro-FTIR spectroscopy spanning mid- and far-infrared regions, (iii) micro-Raman imaging spectroscopy. The collected data provide spectral and spatial information on the chemical constituents and various phases present in the studied fragments. C- and O-isotopic composition of the samples have also been investigated.

Results and Discussion: The $\Delta^{17}O$ values for the SC fragments are all close to each other, being -0.235 ‰, -0.242 ‰, and -0.235 ‰ for SC15, SC21, and SC183, respectively (Fig. 1). The mean $\Delta^{17}O$ value for the three SC fragments is -0.237 ‰, which is within error of the mean value for eucrite and cumulate eucrite falls and finds of -0.240 ± 0.018 (2σ) obtained by [2]. This indicates that the SC meteorite is a normal member of the HED suite and that any carbonaceous chondrite-related component that may be present has had a negligible effect on its oxygen isotope composition. Infrared spectra of the three SC samples display a set of prominent silicate peaks that are mostly due to pyroxene (clinopyroxene and orthopyroxene), with some contribution from Mg-rich olivine. The IR maps show locations of forsterite, fayalite, ilmenite, plagioclase, and enstatite. Raman spectra show that the samples are dominated by augite, diopside, enstatite, kanoite, rhodonite, and ferrosilite, with minor contribution from olivine, plagioclase feldspars anorthite and labradorite. C-isotopic measurements show that there is indigeneous carbon in the SC fragments studied here. Raman peaks of carbon (D- and G-bands) indicate heterogeneously distributed graphitic domains in the sample. Comparison of Raman spectral characteristics of our data with other meteorites indicate that the carbon in SC seem to fall near that of type 2-3 chondrites reported by [3] and [4]. Although we note that these comparisons are only qualitative and by no means unambiguous.

References: [1] Reddy V. et al. (2012) *Science* 336:700-704. [2] Greenwood R. C. et al. (2017) *Chemie Der Erde-Geochemistry* 77:1-43. [3] Bonal L. et al. (2016) *Geochimica et Cosmochimica Acta* 189: 312-337. [4] Quirico E. et al. (2014) *Geochimica and Cosmochimica Acta* 136: 80-99.
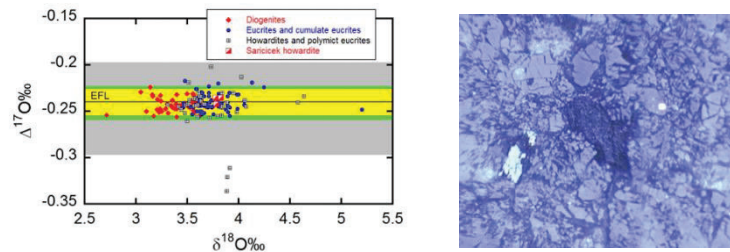

Fig. 1. Left: O-isotopic data of SC samples compared with other HED meteorites. Right: Visible micrograph of a carbonaceous phase in one of the SC fragments.

THE FIRST TURKISH ANTARCTIC METEORITE SEARCH EXPEDITION.

M. Yesiltas[1], M. Zolensky[2], T. D. Glotch[3], [1]Faculty of Aeronautics and Space Sciences, Kirklareli University, Kirklareli, Turkey 39100 (myesiltas@knights.ucf.edu), [2]NASA Johnson Space Center, Houston TX, USA 77058, [3]Department of Geosciences, Stony Brook University, Stony Brook, NY, USA 11794.

Introduction: Antarctica provides the best conditions for meteorites. Samples are protected and preserved in a cold environment with less weathering [1]. Recovered meteorites provide invaluable information and insights towards understanding the formation of our solar system. Blue ice fields of East Antarctica have been searched for meteorites in the past (e.g., Japanese Antarctic Research Expedition JARE, Belgian expedition SAMBA, etc…) and many samples have been recovered. As part of the Turkish Antarctic Expedition TAEIII and with the logistical support of Belgium's Princess Elisabeth Antarctica (PEA) Station, the first Turkish Antarctic Meteorite Search Expedition (TAMSE1) took place in East Antarctica during the 2018-2019 season. Through this expedition, reconnaissance visits to several places within the Sør Rondane Mountains were organized in an effort to plan for future meteorite search expeditions. During the season, a daily trip to the Nansen blue ice fields (~120 km away from the PEA station) was also organized, which resulted in the recovery of 3 meteorites.

Descriptions and Findings: TAMSE1 was meant as an observational preliminary trip to East Antarctica. Several blue ice fields, mountains, and moraines were visited to finalize our meteorite search and recovery protocols for future expeditions. Nevertheless, a total of 3 meteorites were recovered during our preliminary search in the 2018-2019 Antarctic season near the Nansen blue ice field. Upon recovery, they were given preliminary identification numbers of 190109286, 190109287, and 190109288. Their weights are 7.52 g, 50.68 g, and 6.24 g, respectively. Out of the recovered meteorites, one is a whole stone (190109287) with several cracks on the surface and rusty edges. The other two meteorites are broken samples with missing parts up to 50%, revealing their interior to atmospheric conditions. As a result, the interior of the broken samples was rusted and degraded until the recovery. The three meteorites found are currently undergoing initial investigations at NASA's Johnson Space Center for classification and characterization. Once classified, they will be given permanent names and will be assigned an official name and number according to the guidelines set by the Nomenclature Committee of the Meteoritical Society. The Turkish Meteorite Working Group has established a protocol to store and curate the recovered meteorites upon request after their necessary investigations.

References: Apostolopoulos, D. S., Wagner, M. D., Shamah, B. N., Pedersen, L., Shillcutt, K., & Whittaker, W. L. (2000). Technology and Field Demonstration of Robotic Search for Antarctic Meteorites. The International Journal of Robotics Research, 19(11), 1015–1032.

A TEM INVESTIGATION OF FORMATION PROCESS OF COESITE FROM THE XIUYAN IMPACT CRATER.

Feng Yin[1,2], Ming Chen[2], Thomas Sharp[3], [1]Department of Geology, Hunan University of Science and Technology, Xiangtan, China 411201 (yinfeng@hnust.cn), [2]Guangdong Provincial Key Laboratory of Mineral Physics and Materials, Guangzhou Institute of Geochemistry, Chinese Academy of Sciences, Guangzhou, China 510640, [3]School of Earth and Space Exploration, Arizona State University, Tempe AZ, USA 85287-1404.

Introduction: Coesite is widely distributed in metamorphic rocks, meteorites, and impact craters. It was firstly found in Meteor crater by Chao et al. [1] and was explained to be formed via a polymorphic transformation of quartz. Coesite had been reported in more than 30 impact craters and is considered to be a result of solid-state transformation of amorphous silica [2] or crystallize from silica melt [3]. Coesite is common in silica glasses of the suevite from the Xiuyan crater. Chen et al. [4] proved these coesite crystallized from silica melt based on the morphology and occurrence of coesite. Here, we summarize the further investigations of the microtextures of coesites with different occurrences in the Xiuyan crater.

Results: The suevite consists of fragments of gneiss, amphibolite, silicate glass and fine-grained matrix. Gneiss clasts are strongly shocked and are composed of silica glass, vesicular feldspar glass, and opaque black material. Most of the silica glasses have the same morphology as primary quartz, and some silica glass fragments are rounded. Coesite grains embedded in the silica glasses occur in stringer and granular morphologies.

The stringer coesites are polycrystalline aggregates of coesite nanocrystals (a). Coesite crystals along the edge are large, fractured and deformed (c), whereas coesite crystals in the center are small, randomly distributed single crystals (b).The granular coesite are polycrystalline aggregates of coesite nanocrystals (d). Most crystals display twinning and a slight shape-preferred orientation (nearly horizontal) (e).
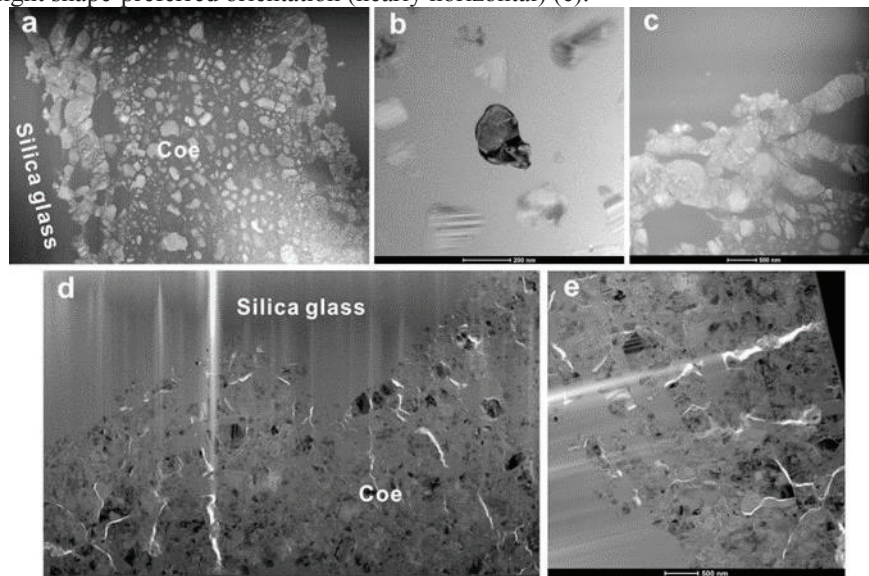
Disscussion: The vesicular feldspar glass and silica glass in the gneiss clast indicate the shock pressure is > 45 GPa [5]. The two occurrences of coesite are from one gneiss clast in the shock breccia, and therefore both of them definitely underwent the same shock pressure. Similar stringer coesites have been observed in Ries crater. Fazio et al. [3] concluded that the coesite crystallites at the rim and at the core of stringer formed by heterogeneous nuclea-tion and homogeneous nucleation from silica melt, respectively. In this study, TEM images reveal that the micro-textures of granular coesites are same as the coesite aggregates at the rim of stringer, e.g. fractured and a slight preferred orientation of the crystals. This suggests that they formed by heterogeneous nucleation on the edge of a silica melt. The randomly distributed coesite in the core of stringer formed by homogeneous nucleation from silica melt. Coesite crystallized at 4.5-13 GPa during pressure release [6].

References: [1] Chao E.C.T. et al. (1960) *Science* 132:220-222. [2] Stähle V. et al. (2008) *Contributions to Mineralogy and Petrology* 155:457-472. [3] Fazio A. et al. (2017) *Meteoritics & Planetary Science* 52:1437-1448. [4] Chen M. et al. (2010) *Earth & Planetary Science Letter* 297:306-314. [5] Stöffler et al. (2018) *Meteoritics & Planetary Science* 53:5-49. [6] Zhang J. et al. (1996) *Physics and Chemistry of Minerals* 23:1-10.

PETROGRAPHY AND U-Pb CHRONOLOGY OF ANOMALOUS EUCRITE SERRA PELADA.

Q. Z. Yin[1], Q. Zhou[2], M. E. Sanborn[1], K. Ziegler[3], Q. L. Li[4], Y. Liu[4] and C. L. Li[2], [1]University of California, Davis, One Shields Avenue, Davis, CA 95616, USA (qyin@ucdavis.edu), [2]National Astronomical Observatories, Chinese Academy of Sciences, Beijing, 100012, China (zhouq@bao.ac.cn), [3]Institute of Meteoritics, University of New Mexico, Albuquerque, NM 87131, USA, [4]Institute of Geology and Geophysics, Chinese Academy of Sciences, Beijing, 100029, China.

Introduction: Serra Pelada is a brecciated eucrite observed to fall in the State of Pará, northern Brazil on June 29th 2017. There are very few published studies on this new meteorite [1]. The latest petrography studies have described this meteorite as a monomict eucritic breccia, which samples a single basaltic lithology [1]. Here we report the petrography and zircon U-Pb dating results for this new meteorite.

Experiment: Two polished thin sections were examined using a Carl Zeiss SUPRA-55 field-emission scanning electron microscope equipped with energy dispersive spectrometer (EDS) at the National Astronomical Observatories (NAO), Chinese Academy of Sciences (CAS) in Beijing. Cr and O isotope data were obtained at UC Davis and UNM respectively. In-situ U-Pb isotopic analysis for zircon grains was performed on a Cameca IMS-1280 ion microprobe at the Institute of Geology and Geophysics, CAS. Due to the small size of zircon grains in Serra Pelada, the analytical spot size was reduced to 5μm. The details of U-Pb experimental procedure are as described in [2-4].

Results: Serra Pelada is a clast-rich breccia containing a variety of minerals and lithic clasts in a fine-medium grained matrix. The clasts and matrix are dominated by pyroxene and plagioclase, with minor to trace amounts of ilmenite, silica, chromite, FeNi metal, troilite, phosphate and zircon. The lithic clasts are also observed, including basalts, gabbros and impact melt clasts. The medium grained basaltic clasts typically have needles of plagioclase with subophitic texture. The gabbroic clasts are coarse grained with variable texture from subophitic to equigranular. Serra Pelada also contains minor impact melt clasts which have mineral and lithic clasts set in a fine grained matrix. Cr and O isotope compositions suggest that Serra Pelada is an anomalous eucrite, similar to NWA 8671. Therefore it is unlikely associated with asteroid 4 Vesta, contrary to the common assumption for other normal eucrites [5], but instead must be coming from a different parent body.

Eighteen analyses of U-Pb isotopic compositions were performed on two zircon grains in Serra Pelada. Both of these zircon grains are irregular in shape. One zircon grain encloses ilmenite as inclusions (Fig.1a), and the other zircon grain is associated with plagioclase (Fig.1b). Uranium and thorium concentrations are variable from 26-110 ppm, and 4-37 ppm, respectively. The Th/U ratios range from 0.14 to 0.72.

The U-Pb data give a concordia age of 4554 ± 14 Ma (Fig.2a). There was no significant Pb-loss from the zircon grains, with a corresponding $^{207}Pb/^{206}Pb$ age of 4556.0 ± 6.1 Ma (Fig.2b), indicating that the U-Pb system of Serra Pelada zircon was not disturbed during the late impact or thermal events. We therefore infer that the $^{207}Pb/^{206}Pb$ date of zircons records the primary crystallization age.

Eucrites represent the remnants of the early magmatic activies of the Solar System. Previous studies have obtained U-Pb zircon age for eucrite [4, 6-8], which indicated a peak of basaltic magmatism at 4552 ± 7 Ma [4]. Compared to the literature data, the $^{207}Pb/^{206}Pb$ age of Serra Pelada is also consistent with the other eucrites (Fig.3).

References:
[1] Zucolotto M. E. et al. (2018) *Anais da Academia Brasiliera de Ciências* 90:3-16. [2] Li Q. L. et al. (2010) *JAAS,* 25:1107-1113. [3] Liu Y. et al. (2011) *JAAS.* 26:845-851. [4] Zhou Q. et al. (2013) *GCA* 110:152-175. [5] Binzel R.P. and Xu S. (1993) *Science* 260:186-191. [6] Misawa K. et al. (2005) *GCA,* 69:5847-5861. [7] Ireland T.R. and Wlotzka F. (1992) *EPSL,* 109:1-10. [8] Ireland T.R. and Bukavanská M. (2003) *GCA,* 67:4849-4856.
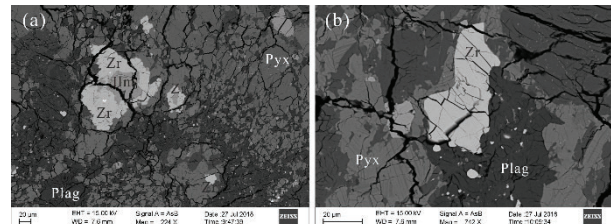

Fig. 1. Backscattered electron images of Serra Pelada, containing pyroxene (Pyx), plagioclase (Plag), ilmenite (Ilm) and zircon (Zr).
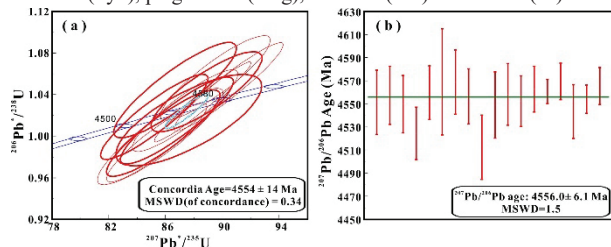

Fig. 2. U-Pb Concordia age and the weighted average of $^{207}Pb/^{206}Pb$ age are determined in Serra Pelada zircon. Uncertainties are 2σ.

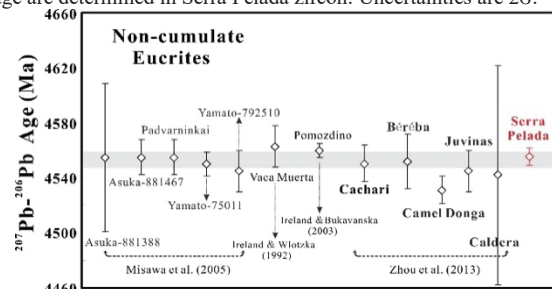Fig. 3. The $^{207}Pb/^{206}Pb$ age of Serra Pelada (red symbol) is consistent with the other non-cumulate eucrites.

DETERMINATION OF PETROLOGIC SUBTYPES OF CV3 CHONDRITES BY RAMAN SPECTROSCOPY

S. T. Yokoyama[1, 2], K. T. Tait[1, 2], V. E. Di Cecco[2], B. C. Hyde[2, 3] [1]Department of Earth Sciences (University of Toronto, 22 Russell St., Toronto, ON, Canada M5S 3B1 sean.yokoyama@utoronto.ca, ktait@rom.on.ca), [2]Department of Natural History (Royal Ontario Museum, 100 Queens Park, Toronto, ON, Canada M5S 2C6 syoko-yama@rom.on.ca, ktait@rom.on.ca, vdicecco@rom.on.ca), [3]Department of Earth Sciences (Western University, Biological & Geological Sciences Building, Room 1026, 1151 Richmond St. N. London, ON Canada N6A 5B7 bhyde@uwo.ca).
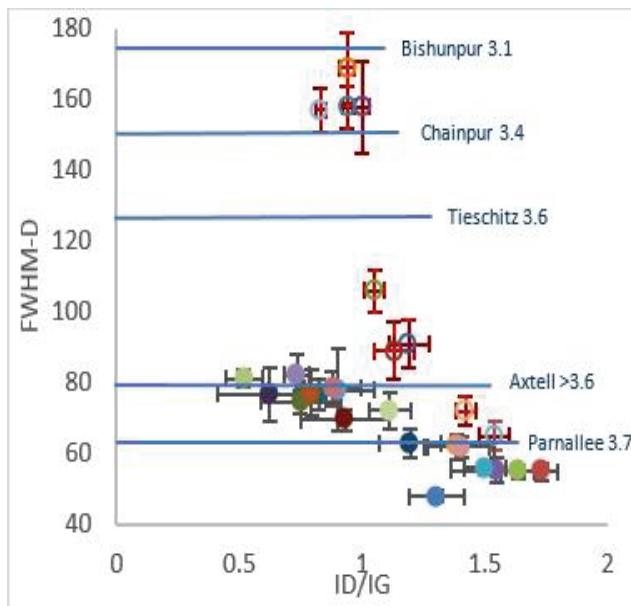

Figure shows the relationship between the FWHM-D and I_D/I_G of the CV chondrites. The filled in plots with black error bars represent samples from our study while plots with red error bars represent CV chondrites from [3].

Introduction: Meteorites come from a wide variety of rocky bodies throughout the solar system. To characterize these meteorites and to understand the parent body processes that produced them, we use classification schemes that include petrologic type and shock classification [1, 2]. Petrologic type for chondritic meteorites range from type 1 to 6; 1 being the most aqueously altered and 6 being the most thermally metamorphosed [1]. Meteorites of petrologic type 3 are the most pristine [1]. Type 3 chondrites can then be further divided into subtypes (e.g. 3.x) [3]. The current classification scheme for chondrites assigns a petrologic type of 3.0 to meteorites that do not possess any signs of thermal metamorphism and 3.1 or higher for those that show increasing, but limited, metamorphic features [4]. A Raman spectroscopy study of unequilibrated ordinary and carbonaceous chondrites by [3] observed that the Full Width Half Maxima of the D band (FWHM-D) of carbon found in the matrix decreases with increasing petrologic subtype as well as the increasing height ratio between the D band and the G band (I_D/I_G). The most common petrologically pristine group of chondrites is the CV group carbonaceous chondrites. Here we introduce new type 3 CV chondrites and determine their petrologic subtypes with the classification scheme of [3] using Raman spectroscopy.

Experimental: A suite of 17 CV group carbonaceous chondrites was analyzed for the FWHM-D and I_D/I_G of carbon in the matrix using a Horiba LabRAM Aramis micro-Raman spectrometer at the Royal Ontario Museum (ROM). A 532 nm, 50 mW laser was used, filtered down to a power of 171.9 µW to prevent carbon alteration in the sample. An 1800 gr/mm grating and 100 µm slit were used during collection. A Kr reference lamp was used for calibration. The spectra were collected for 90 s, measured 10 times and then averaged. Ten spots were analyzed for each sample. A 50x long-working-distance objective was used with a spot size of 0.865 µm. Five of the samples belong to the ROM (Toronto, Canada): NWA 10395, NWA 4838, NWA 11554, NWA 12565, Allende and Dhofar 2037. Eleven others were loaned by the National Institute of Polar Research (NIPR) in Tokyo, Japan: Asuka 87344, Asuka 880835, Asuka 881317, Asuka 12373, Yamato 86009, Yamato 86751, Yamato 86752, Yamato 980010, Yamato 980145, Yamato 980146, Yamato 981208.

Results: The Raman spectra of the Allende CV group carbonaceous chondrite shows petrologic subtype of >3.7 that closely resembles the subtype of previous studies [3]. The subtype of the remaining samples were also determined based on the same study [3]. The samples all plot on a trend similar to that of [3].

Discussion: We support the usage of Raman spectroscopy as a non-destructive tool for determining the petrologic subtype of CV chondrites. We have incorporated these analyses into our typing procedures and four untyped meteorites from the ROM collection have now been analyzed. Future work will consist of plotting the ratio between FWHM-D/(I_D/I_G) to the elemental abundance acquired by the LA-ICP-MS.

References: [1] Brearley & Jones (1998) Chapter 3 in *Planetary Materials* (Papike, Ed.); [2] Stöffler & Keil (1991) *GCA 55*, 3845-3867; [3] Bonal et al. (2016) *GCA 189*, 312-337; [4] Sears et al. (1980) *Nature 287*, 791;

THE KOMAKI METEORITE: A NEW FALL IN JAPAN.

S. Yoneda[1], A. Yamaguchi[2], T. Ojima[2], M. Kimura[2], and R. Okazaki[3]. [1]National Museum of Nature and Science, 4-1-1 Amakubo, Tsukuba 305-0005, Japan (s-yoneda@kahaku.go.jp), [2]National Institute of Polar Research, Midoricho 10-3, Tachikawa, Tokyo 190-8518, Japan, [3]Kyushu University, 744 Motooka, Nishi-ku, Fukuoka 819-0395, Japan.

Introduction: We report a new L6 chondrite fall in Japan. The Komaki meteorite (Fig.1) fell at Komaki-city, Aichi-prefecture, Japan on September 26, 2018 and was brought to the National Museum of Nature and Science (NMNS), Tokyo, where it was recognized as a meteorite [1]. It weighs more than 650g in total and is almost entirely covered by the fusion crust.

Circumstances of Fall and Recovery: Around 22:30 on September 26, 2018, a detonating sound was heard at a private house in Komatsuji, Komaki city, Aichi prefecture, Japan. No fireball was, however, observed because of the cloudy weather with intermittent rain. Next morning, several fragments including 81g and 23g were found on the roof and in the garden. A 550g mass was also found at the next-door house. The meteorite apparently hit the roof (Fig. 2) and bounced to the next house, and penetrated the roof of the carport and hit the roof of the car, and finally came to rest in front of the entrance door. The meteorite was brought to NMNS on October 6, where cosmogenic Na-22 and Al-26 gamma rays were detected by the pure Ge detector.

Physical characteristics and Textures: The 550g mass is rounded disk shape and one side is fully covered by the fusion crust and the other side is about half covered. The 81g and 23g fragments are fit together with the 550g mass, hence the meteorite was one mass that fragmented due to the impact on the roof. A polished thin section and a polished mount were made from a 1g fragment at the National Institute of Polar Research (NIPR). Olivine compositions are Fa 23.9-25.5 (mean=24.7, N=31), and low-Ca pyroxene compositions are Fs 20.0-21.3 (mean=20.7, N=19), indicative of L chondrite. The presence of plagioclase $>50\,\mu$ m indicates that the petrologic type is 6. The presence of mottled extinction and planar fractures in olivine indicates that the shock stage is S3.

Noble Gas analyses: Using a 50mg fragment, noble gas analyses were made at the Kyushu University. The Ne-21 cosmic-ray exposure age is 25.1 ± 0.6 Ma, and the K-Ar gas retention age is 4.4 ± 0.2 Ga.

References: [1] Press release: http://www.kahaku.go.jp/procedure/press/pdf/326013.pdf (in Japanese)

Fig. 1 The Komaki meteorite (3 large fragments fit together)   Fig. 2 The roof where the meteorite hit

PRELIMINARY RESULTS OF SAMPLE PREPARATION OF ULTRA-THIN FILM BY USING FOCUSED ION BEAM TECHNIQUE FOR EXTRATERRESTRIAL MATERIALS IN JAXA

M. Yoshitake[1], I. Ohnishi[2], A. Nakato[1] and H. Yurimoto[1,3], [1]Astromaterials Science Research Group, Extraterrestrial Sample Curation Center, Inst. Space Astronautical Sci., Japan Aerosp. Explor. Agency, 3-1-1 Yoshino-dai, Chuo-ku, Sagamihara, Kanagawa 252-5210, JAPAN (e-mail: yoshitake@planeta.sci.isas.jaxa.jp), [2]JEOL Ltd., 3-1-2 Musashino, Akishima, Tokyo 196-8558, JAPAN, [3]Natural History Sci., Hokkaido Univ., Sapporo 060-0810, JAPAN

Introduction: Sample return mission is an useful project for planetary material sciences, because it gives us opportunities for direct handling of extraterrestrial materials known of their astronomical/geological occurrence such as in comets and asteroids. However, the returned samples are often limited in mass and volume. For instance, the nominal mass returned are expected to be 0.1 g for JAXA Hayabusa2 and 1 g for NASA OSIRIS-Rex. Transmission electron microscopy (TEM) does not need large volume of a sample and it is very effective to analyze small sample at micro- to nano-meter level. However, conventional ion milling methods using Ar^+ ion could lose large amount of sample to make ultra-thin film for TEM. Then, ultramicrotomy was widely used in sample preparation of ultra-thin film for micrometeorites [1]. Recently, a focused ion beam (FIB) method using Ga^+ ion has been utilized for sample preparation of ultra-thin film from extraterrestrial materials such as meteorites and cosmic dusts [e.g., 2]. The method can precisely make ultra-thin film from any interested area in a sample with spatial resolution of micrometer to submicrometer. In 2018, we installed a FIB instrument at Extraterrestrial Sample Curation Center (ESCuC) of JAXA and started to construct the procedure of ultra-thin film sample preparation of extraterrestrial materials for TEM. We present here the detail of procedure and preliminary results of evaluation of ultra-thin film made with the FIB.

Material and Methods: In this study, ultra-thin films were made from a Ca, Al-rich inclusion (CAI) in thin section of the Allende CV3 chondrite using triple beam FIB instrument (HITACHI NX2000) at ESCuC, equipped with a variety of detectors such as secondary and backscattered electron detectors and silicon drift X-ray detector (Oxford X-Max 80). The petrological and mineralogical studies were conducted using the function of scanning electron microscope in the FIB before ion thinning. The CAI studied here was classified to fluffy type A inclusion and its primary minerals such as anorthite and diopside have been significantly altered by the secondary minerals including nepheline, hedenbergite and so on. Ultra-thin films were extracted from the altered area in the CAI. After rough thinning with Ga^+ ion at 30 kV and 5kV, fine thinning with Ar^+ ion at 1 kV was performed to reduce amorphous layer at the surface of films. The films were studied using conventional 120 kV TEM (JEOL JEM-1400) at ESCuC and an aberration corrected 300 kV STEM (JEOL JEM-ARM300F) at JEOL R&D factory.

Results & Discussion: Our conventional TEM observations indicate that all the ultra-thin films made in this study are very thin enough for electron beam to transmit even at 120 kV of accelerating voltage. Although a variety of minerals, which have different etc

hing rates of Ga^+ ion each other, coexisted in the films, the surface of films seems to be homogenously flat. In addition, re-deposition of sample seems to be negligible. The results suggest that the fine thinning with Ar^+ ion after rough thinning with Ga^+ ion is very effective to remove damage layers and contamination from the surface of films. Because all the ultra-thin films made in this study are enough thin, they are also use to observe atomic resolution images as shown in Figure 1.

References: [1] Bradley J.P. and Brownlee D.E. (1986) *Science* **231**:1542–1544. [2] Lee M.R. et al. (2003) *Mineralogical Magazine* **67**:581-592.
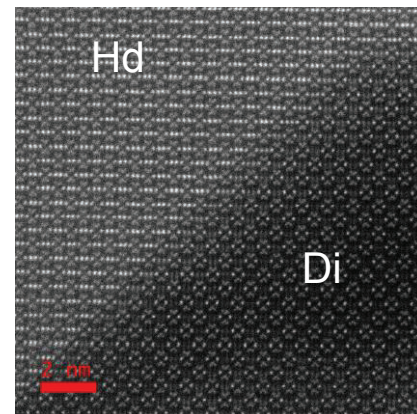
Figure 1: Atomic resolution STEM high angle annular dark field image showing the boundary between diopside (Di) and hedenbergite (Hd) in an ultra-thin section from altered CAI. The image was obtained with JEM-ARM300F at 300 kV.

ACCRETION OF DUST TO MAKE FINE-GRAINED RIMS ON STILL COOLING CHONDRULES

P.-M. Zanetta[1,2], C. Le Guillou[1], H. Leroux[1], B. Zanda[2,3,4].
[1]Univ. Lille, CNRS, INRA, ENSCL, UMR 8207 - UMET - Unité Matériaux et Transformations, F-59000 Lille, France, [2]IMPMC, Sorbonne Université, MNHN, UPMC Paris 06, UMR CNRS 7590, 75005 Paris, France. [3]EPS, Rutgers Univ., Piscataway, NJ 08854, USA. [4]Observatoire de Paris, IMCCE, 75014 Paris, France.
(Pierre.marie.zanetta@gmail.com)

Introduction: Primitive chondrites are samples of the asteroids formed in the early solar system [1]. Understanding their accretion in term of temporality, mechanisms and physical conditions is fundamental. Located at the interface between the high temperature components and the fine-grained matrix (mostly formed at low temperature) fine-grained rims (FGRs) most likely hold valuable information about the dust accretion process. However, most primitive chondrites (and their FGRs) are affected by secondary hydrothermal modifications that have obscured their original nature to various degrees. In addition, FGRs are difficult to analyze since they consist of a heterogeneous nanometer-sized phase assemblage. To address these problems, we conducted a systematic survey of FGRs in three of the least altered chondrites from different chondrite groups (Semarkona, DOM 08006, QUE 99177, following previous work on Paris [2]) using the ACADEMY methodology [3] at the SEM and TEM scales. The objective is to study how chondrules could have interacted with the fine-grained dust of the nebula.

Method: For each sample, we selected a set of representative rimmed chondrules showing minimal traces of alteration. Using the ACADEMY methodology, we did high resolution SEM mapping coupled with EPMA analysis, to obtain phase abundances, a density map and the bulk composition of the analyzed area. Four FIB sections were then extracted from each meteorite (12 in total), in the rims and their adjacent matrix for quantitative TEM analysis.

Results: At the SEM scale, texture, modal abundances and compositions differ between FGRs and their adjacent matrix. The amorphous silicate is always more abundant in the rim (mean ~93±7%) than the matrix (mean~80±6%), while anhydrous silicates and sulfides are less abundant (4±0.05% vs. 10±0.1% and 0.5±0.004 % vs. 2±0.01% respectively) and smaller (<few microns) in the rim, yielding distinctive compositions for rims and matrix.

At the TEM scale, the matrices of DOM 08006 and Semarkona show domains of amorphous silicate associated with randomly distributed crystalline nano-phases (sulfides, Fe-Ni metal, anhydrous silicates) and an abundant porosity (~8 % and 20% respectively). The associated rims in Semarkona and DOM 08006 (and Paris) exhibit more compact textures (~2.6% and 5.8%) in which crystalline phases are not randomly dispersed anymore but are grouped in specific regions (clumps) and embedded in an amorphous/poorly crystallized silicate. In Semarkona, one rim shows a progressive, radial microstructure evolution. Starting from the same crystalline clumps + amorphous microstructure but getting closer to the chondrule, the abundance of the poorly crystallized silicates decreases while the abundance and grain size of the anhydrous silicates and Fe-sulfides increases. Inversely, in QUE 99177 no textural difference is observed and the porosity is low both in the matrix and the rims (~4%). Despite these textural differences, the compositions in major elements of the amorphous regions are similar for the rim and the matrix within a given chondrite (but differ between chondrite).

Discussion: Pristine chondrites reveal systematic differences between matrices and FGRs while the composition of the amorphous silicate is similar in both areas. It suggests that matrix and FGRs accreted similar type of dust but were subsequently affected afterwards by different physical processes [4]. (1) Matrix appears to have accreted a higher amount of crystalline phases in comparison to the rim, leading to a slightly different global composition. This could be explained either by the addition of chondrules fragments after rim formed [5], or represent an independent reservoir enriched in crystalline phases. (2) FGRs: in all groups, when they texturally differ from their adjacent matrix, appear to evolve toward the same micro-texture (compact amorphous + clumps of crystalline phases). Assuming that the matrix preserved the initial texture, FGRs in all groups must have been affected by a similar process to pass from the initial texture to the observed one. Aqueous alteration is unlikely to account for this feature, given the elevated abundance of amorphous silicate and the absence of secondary alteration phases in FGRs [6]. As an alternative, we propose that FGRs accreted on chondrule rapidly after their formation, while they were not entirely cooled, whereas matrix accreted later in a cooler environment. Accretion on a "hot" particles could induce a mild annealing and explain their more compacted nature. If, for each chondrite group, dusts accreted on chondrules at a different temperature, it might have led to different degrees of compaction/annealing of the sub-domains that could possibly explain the second order textural differences observed between the rims in different groups.

References: [1] Scott, E. and Krot, A. (2005) Treatise on Geochemistry 1, 143-200. [2] Zanetta, P. M., et al. (2018). 81st Metsoc, abstract #2067. [3] Zanetta, P. M., et al. (2019). Chemical Geology 514, 27-41. [4] Chizmadia, L. J., & Brearley, A. J. (2008). Geochimica et Cosmochimica Acta, 72(2), 602-625. [5] Metzler, K., Bischoff, A., & Stöffler, D. (1992). Geochimica et Cosmochimica Acta, 56(7), 2873-2897. [6] Tomeoka, K., & Tanimura, I. (2000). Geochimica et Cosmochimica Acta, 64(11), 1971-1988.

THE APOLLO SAMPLE COLLECTION: 50 YEARS OF SOLAR SYSTEM INSIGHT.

R. A. Zeigler, Astromaterials Acquisition and Curation Office, NASA Johnson Space Center, 2101 NASA Parkway, Mail Code XI2, Houston, TX, 77058 USA. ryan.a.zeigler@nasa.gov.

Introduction: The Apollo program was the seminal moment in modern human history and the crowning technological achievement of the 20th century. Scientific results from the Apollo samples have had a lasting impact on a range of scientific fields, particularly planetary science and cosmochemistry. Studies of Apollo samples continue to make significant insights into planetary bodies throughout the solar system. Here we will discuss the history of Apollo samples collection, curation, and study, and also look forward to expected new developments in the coming years.

Apollo Samples: From 1969 to 1972, the Apollo astronauts collected 382 kg of rock, regolith, and core samples from six geologically diverse locations on the Moon. The Apollo samples span an incredible range of sample types, including: large rock samples, multiple rocks chipped from large boulders, bulk surface, trenched, and shaded lunar soils , multiple 30-60 cm drive tubes, deep drill cores samples up to ~3 meters in depth, and several different types of special vacuum-sealed regolith and drive tube samples. There have been 3158 unique lunar sample requests from >500 different Principal Investigators from over 15 different countries in the past 50 years and the total number of samples allocated is >50,000 individual subsamples. Currently 145 active lunar PIs are studying >8,000 samples.

Discussion: Studies of the Apollo samples, both early and more recent, continue to yield significant insights into the formation, evolution, and maturation of the Earth-Moon system, as well as many other planetary bodies in both the inner and outer solar system. Listed below are a subset of results that highlight the wide-ranging, long-lasting, and diverse nature of studies of Apollo samples: (1) The Moon formed from the debris of a giant impact between the proto-Earth and a large bolide early in the solar system history [1]. (2) The Moon had a Lunar Magma Ocean, and evolved akin to a global (though asymmetric) layered-mafic intrusion [2]. (3) A prevalence of ~3.9 Ga ages of lunar impact melts suggests that there might have been a "Lunar Cataclysm" at that time, which would have affected all of the inner solar system [3]. (4) The potential prevalence of impacts ~600 Ma after solar system formation (i.e., the "Lunar Cataclysm") was one of the factors leading to new dynamical models for the evolution of the entire solar system, e.g., the Nice Model [4]. (5) By tying the ages of Apollo basalts to the crater densities in the regions of the Apollo landing sites, relative crater counting ages can be given absolute ages on the Moon, as well as elsewhere in the inner solar system [5]. (6) Despite decades of null results for volatiles in lunar samples (e.g., H_2O), recent results [e.g., 6,7] have shown that the Moon is not "bone dry" and these volatile abundances inform the models for lunar formation. (7) The composition of Apollo samples have directly contributed to the interpretation of remotely sensed data sets, including their use as ground truth for both Clementine and Lunar Prospector global geochemical maps [8].

Future Apollo Studies: NASA recently solicited proposals as part of the Apollo Next Generation Sample Analysis (ANGSA) program [9]. The ANGSA program includes previously unopened, vacuum-sealed drive tubes and bulk soil samples, cold-curated samples (-20°C), and samples only handled in a He-purged environment. Furthermore, JSC Curation can now scan samples using X-ray Computed Tomography (XCT); XCT scans of polymict breccias are expected to identify "new" lithic clasts for PIs to study. Similarly, there are 10,000s of small particles in the >110 kg of bulk lunar regolith, and a portion of these will also be classified and made available to PIs after a retroactive preliminary examination process utilizing XCT, micro X-ray Fluorescence, and Imaging micro-Raman Spectroscopy. Additionally, a new searchable database for lunar geochemical data called MoonDB has been brought online [10].

Conclusions 50 years of study of Apollo samples yielding important insights into a wide-variety of topics and planetary bodies has shown that sample return missions are "the gift that keeps on giving." Many of the results highlighted in this abstract were not yet conceived of (or the instruments not yet invented) when the samples were first brought back. However, because the samples have remained available, and been maintained in a pristine manner, future generations of scientists continue to extract greater and increasingly novel value beyond the initial studies. Despite the costs, complexity, and risk (real or perceived) associated with sample return missions, the long-lasting legacy of scientific return for sample-return missions more than offsets these mitigating factors. This is not to say that sample-return missions and sample-related studies are the only type of planetary science that should be pursued, but rather that they are a key component of a holistic way of studying the solar system, combined with remote-sensing and *in-situ* missions, as well as modelling-based and experimental-based studies on Earth.

References: [4] Canup R. M. and Asphaug E. (2001) *Nature,* **412**, 708-12. [2] Wood J. A. (1975) *PLSC,* **6**, 1087-1102. [3] Marchi S. et al. (2012) *EPSL,* **325-36**, 27-38. [4] Morbidelli A. et al., (2007) *The Astronomical J.,* **135**, #5. [5] Hiesinger H. et al., (2012) *JGR Planets,* https://doi.org/10.1029/2011JE003935. [6] Hauri E. H. et al. (2011) *Science,* **333**, 213-15. [7] McCubbin F. M. et al. (2010) *PNAS, https://doi.org/-10.1073/pnas.1006677107.* [8] Lawrence D. J. et al., (2002) *JGR Planets,* **107**, 13-1-13-26. [9] Specially Curated Apollo Samples – Programmatic Information Package. [10] Lehnert, K. et al., (2018) 50th LPSC, Abstract #2996.

USING X-RAY COMPUTED TOMOGRAPHY AS A TOOL FOR PRELIMINARY EXAMINATION TOOL OF CURRENT AND FUTURE EXTRATERRESTRIAL SAMPLE RETURN MISSIONS

R.A. Zeigler[1] and Z. E. Wilbur[2], [1]Astromaterials Acquisition and Curation Office, NASA Johnson Space Center, 2101 NASA Parkway, Mail Code XI2, Houston, TX, 77058 USA. ryan.a.zeigler@nasa.gov. [2]Jacobs-JETS Contract, NASA Johnson Space Center, Houston, TX, USA.

Introduction: The Astromaterials Acquisition and Curation Office at the Johnson Space Center is the past, present, and future home of all of NASA's astromaterials sample collections. The primary goals of the curation office are to maintain the long-term integrity of the samples and ensure that the samples are distributed for scientific study in a fair, timely, and responsible manner, thus maximizing the return on each sample.

Advanced Curation Studies: Part of the curation process is planning for the future. To this end, we perform fundamental research in advanced curation initiatives to better prepared for future sample return missions. Advanced Curation is tasked with developing procedures, technology, and data sets necessary for curating new sample collections, or getting new results from existing sample collections.

X-ray Computed Tomography Laboratory: As part of these advanced curation efforts, we have installed and are operating a Nikon XTH 320 X-ray Computed Tomography(XCT) system in the JSC curation office with four interchangeable X-ray sources, a large-area detector, and a heavy-duty stage. These instrument characteristics allow us exceptional flexibility to analyze a wide range of sample sizes, from sub-mm soil particles to rocks >10 cm in diameter. The penetrative nature of the XCT scans allows for astromaterials samples to be analyzed within sealed low-density containers (e.g., Teflon bags), preserving the pristinity of the samples. We have begun scanning of the Apollo and Antarctic Meteorite sample suites in order to non-destructively map out lithic clasts (and other features) within the samples. The data from these scans will be made available to scientists via the JSC curation website and the Astromaterials Curation Newsletter. We anticipate sample requests from these "new" lithic clasts identified in these "old" samples. We also anticipate that XCT analyses like these would be useful for future sample return missions, like the OSIRIS REx mission, as well as future sample return missions.
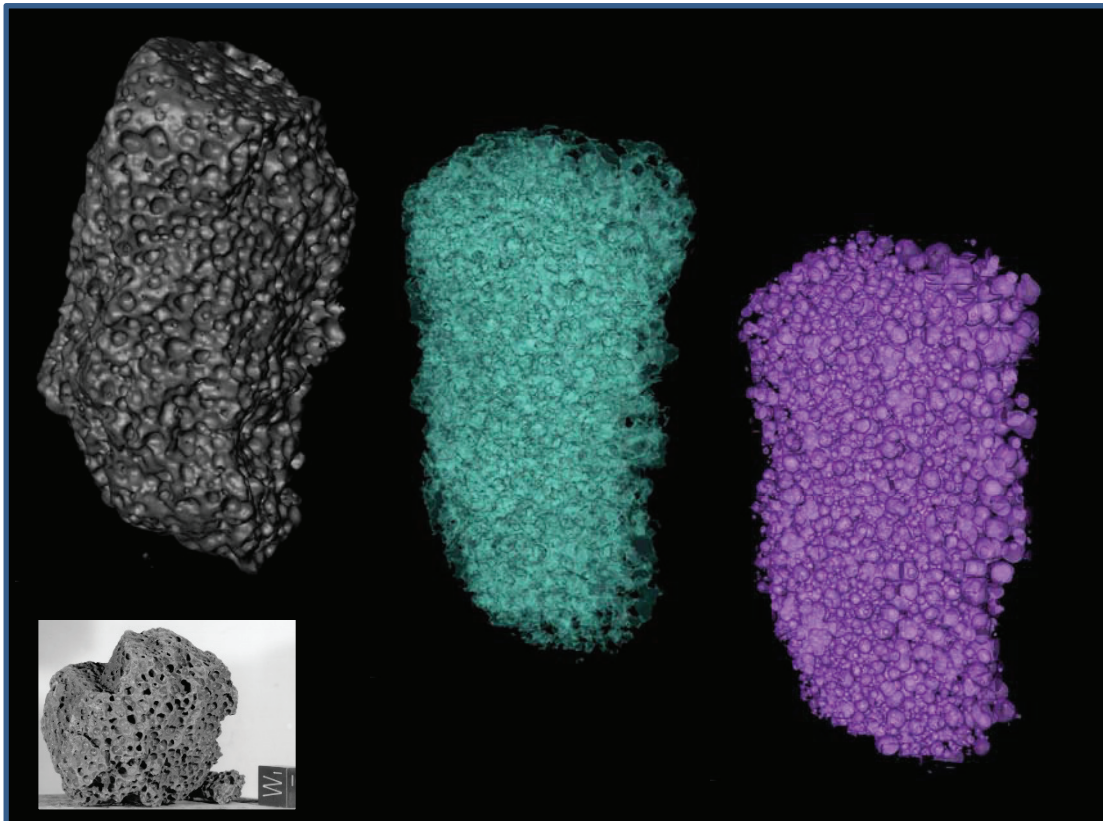

Figure 1: XCT image of Apollo sample 15556 showing, from left to right, the exterior surface, the solid materials inside the sample, and the vesicles within the sample.

OCCURRENCE AND IMPLICATIONS OF SECONDARY OLIVINE VEINLETS IN LUNAR HIGHLAND BRECCIA NORTHWEST AFRICA 11273

X. Zeng[1], S. Li[1], K. Joy[2], X. Li[1], Y. Li[1], R. Li[1], and S. Wang[1] [1]Institute of Geochemistry, Chinese Academy of Sciences, Guiyang, China; [2]School of Earth and Environmental Sciences, University of Manchester, Manchester, UK

Introduction: During the past few decades, secondary olivine veinlets (i.e., the olivine veinlets crossing cut pyroxene grains) have been discovered in a series of HED meteorites [e.g., 1–3]. Similar secondary olivine veinlets have also been observed in a few lunar basaltic samples, e.g., Apollo 14 mare basalts 14072 [4]. Warren et al. (2018) suggested that the olivine veinlets in Apollo basalt 14072 are likely deposited by a water-bearing fluid. However, the formation mechanism of lunar olivine veinlets and their geological records on the Moon are still poorly understood. Recently, five olivine veinle-bearing clasts have been recognized in Northwest Africa (NWA) 11273. This finding could help expand our understanding of the secondary olivine veinlets from a new geographic region on the Moon.
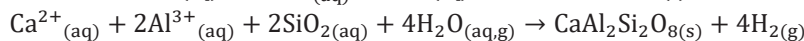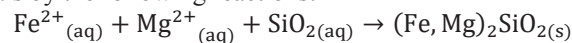
Sample and Methods: Polished thick sections of NWA 11273 have been characterized by a suite of different analytical techniques, including FE-SEM, EMPA, Raman spectrometer, and STEM. Bulk major and trace elements compositon of this meteorite were measured using ICP-OES and ICP–MS, respectively.

Results and Discussion:

Petrography and mineralogy of olivine veinlet-bearing clasts. In NWA 11273, we have recognized the secondary olivine veinlets cutting across pyroxene grains in five lithic clasts (i.e., clasts V1–V5; see Fig. 1). These olivine veinlets exhibit similar mineralogy mainly composed of olivine with a few accessory mineral grains of chromite, pyroxene, and plagioclase. Compared with other olivine grains ($Fa_{54.3-83.1}$) in lithic clasts and matrix of NWA 11273, the olivine veinlets in clasts V1–V5 are relatively fayalitic ($Fo_{41.4-51.9}$).

Bulk-rock meteorite composition. NWA 11273 has high bulk Al_2O_3 of 25.1 wt% and relatively low incompatible trace elements (e.g., Sm = 0.49 ppm and Th = 0.17 ppm). Such geochemical composition indicates that NWA 11273 is most likely ejected from the lunar FHT [5].

Origin and geological records of olivine veinlets on the Moon. Multiple formation mechanisms have been proposed to account for veinlets in HED meteorites and lunar mare basalts [1, 2, 3, 6]. In the case of secondary olivine veinlets in NWA 11273. Our studies shown that the fluid deposition processes seems the most plausible mechanism for interpreting the formation of secondary olivine veinlets in NWA 11273. Specifically, the fluid agent (water-bearing?) could transport the olivine/Ca-plagioclase cations (e.g., Fe^{2+}, Mg^{2+}, Si^{4+}, Ca^{2+}, and Al^{3+}) and then direct deposited the secondary minerals by the following reactions:

$$Fe^{2+}_{(aq)} + Mg^{2+}_{(aq)} + SiO_{2(aq)} \rightarrow (Fe, Mg)_2SiO_{2(s)}$$

$$Ca^{2+}_{(aq)} + 2Al^{3+}_{(aq)} + 2SiO_{2(aq)} + 4H_2O_{(aq,g)} \rightarrow CaAl_2Si_2O_{8(s)} + 4H_{2(g)}$$

Where aq = aqueous (water-bearing), g = gas, and s = solid. The specific details and mineral chemistry of products are controlled by temperature, fluid partial pressure, oxygen fugacity etc.

The studied secondary olivine veinlets in NWA 11273 may be evidence of fluid deposition at or close to the lunar surface. On the basis of the currently available data, we propose that such fluid was likely S,P-poor and was from an endogenic origin on the Moon.

Further works: To better understand the formation mechanism of secondary olivine veinlets on the Moon, more olivine veinlet-bearing lunar clasts are need to be examined and comparative studies of olivine veinlets between lunar samples (such as those that will be collected by the upcoming Chang'e-5 mission) and HED meteorites are also necessary. In addition, the systematic studies of *in situ* oxygen isotope and trace elements, in the future, would allow for greater revealing the geological records of such secondary olivine veinlets in lunar samples.

References: [1] Barrat J. A. et al. (2011) *Geochimica et Cosmochimica Acta* 75, 3839–3852. [2] Roszjar J. et al. (2011) *Meteoritics & Planetary Science* 46, 1754-1773. [3] Warren P. H. et al. (2014) *Geochimica et Cosmochimica Acta* 141, 199–227. [4] Warren P. H. et al. (2018) *LPSC* abstrct #2747. [5] Korotev R. L. (2005) *Chemie der Erde*, 65, 297–346. [6] Pang R. L. et al. (2017) *Geochimica et Cosmochimica Acta* 141:199–227.
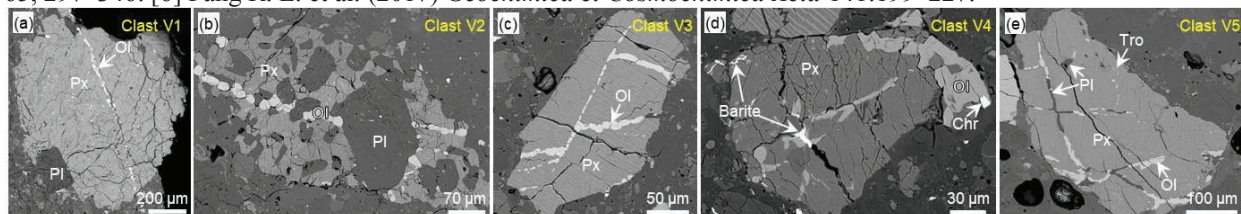

Figure 1. Back-scattered electron (BSE) images of the olivine veinlets bearing lithic clasts in NWA 11273. The mineral phases are labeled: Px = pyroxene, Ol = olivine, Pl = plagioclase, Chr = chromite, Tro = troilite.

FUSION CRUSTS OF RECENT MOROCCAN FALLS: TOWARDS THE IDENTIFICATION OF ABLATION SPHERULES AMONG COSMIC SPHERULES.

L. Zennouri[1,2], H. Chennaoui Aoudjehane[1]
[1]GAIA Laboratory, Faculty of sciences Ain Chock, Hassan II University of Casablanca
[2] Department of Earth Sciences, University of Pisa

Introduction: The earth intercepts more than 30'000 tons of extraterrestrial material every year [1]. Most of this consists of interplanetary dust produced by collision and evaporation of rocky and icy bodies in the solar system. A fraction of this dust is collected on the surface of the Earth in the form of microscopic particles (typically< 2 mm) termed Micrometeorites (MMs). They range from unmelted particles that retain most of their original mineralogy to totally melted cosmic spherules (CSs). The accumulation of micrometeorites on Earth is an important process in the history of Earth formation. Understanding their origins and formation mechanisms is fundamental.

Fusion Crusts form in all meteorites during their passage through the atmosphere. Their thickness, color brightness, and composition is closly related to the meteorite class as well as the parent size of the meteoroid, his velocity and angle of entry in Earth atmosphere. In this work, we aim to explore the relationship between the micrometeorites and meteorites fusion crusts, focusing on recent ordinary chondrite falls in Morocco.

Methods: We performed mineralogical and petrographic analysis of fusion crusts of some recent Moroccan ordinary chondrite falls, in order to establish criteria to understand the fusion crusts formation process, taking account the difference in fusion crust characteristics from the front and rear in the case of oriented meteorites. Selected meteorites include: Tamdakht which is one of the main focus of our research, Tinajdad, Benguerir, Mahbas Arraid and Sidi Ali ou Azza. Meteorites fusion crusts and One hundred Cosmic spherules where studied by "optical microscope, SEM, EMPA and µRaman comparing their texture, compositions and the mineralogy. Cosmic spherules are from the Transantarctic Mountains micrometeorite collection [2].

Results: There is a large difference between the fusion crust of Tamdakht and other samples, especially concerning the thickness, which is very important in some areas and may be millimetric in Tamdakht, whereas, it is less than one millimeter for other samples [3]. They contain vesicles, their size is also larger in Tamdakht compared to the other samples. We also show the presence of layers and the limit of fusion crust with the meteorite. In Tamdakht we can distinguish clear boundaries between three layers. In Tinajdad sample it's very difficult to determine the limit between the melting crust and the meteorite. Concerning the mineralogical composition, most fusion crusts are heterogeneous and consist mainly on melted substrate elements losing volatile elements and converting metal to magnetite, except Tamdakht fusion crust that shows an important iron oxide layer, comparing to other samples.

Cosmic spherules show considerable diversity in texture, composition and mineralogy and are sub-divided into several chemical and textural groups. The basic chemical types of CSs, which are also reflected in their mineralogy, are the iron-rich spherules (I-type), a glass with magnetite (G-type) group and silicate-type (S-type) [4,5].

Conclusion: According to our studies on ordinary chondrites and cosmic spherules, we have found that there is a similarity at the textural and chemical composition level. For example, the outermost layer of the Tamdakht melting crust, which consists of magnetite and or wustite, has the same composition and texture found in the cosmic spherules (type I) which are dominated by Fe oxides, magnetite and wustite [5], also data from melted crust suggest that meteorite ablation spheres have similar compositions to silicate dominated cosmic spherules [6]. There are even several similarities between the various layers of fusion crusts and other types of cosmic spherules. In order to investigate further relationships between the cosmic spherules and the fusion crusts of meteorites, we will extend our work the fusion crusts of achondrites.

References:
[1] Love, S. G., & Brownlee, D. E. (1991). Heating and thermal transformation of micrometeoroids entering the Earth's atmosphere. Icarus, 89(1), 26–43.
[2] Rochette, P., Folco, L., Suavet, C., van Ginneken, M., Gattacceca, J., Perchiazzi, N., … Harvey, R. P. (2008). Micrometeoites from the Transantarctic Mountains. Proceedings of the National Academy of Sciences, 105(47), 18206–18211.
[3] Chennaoui Aoudjehane H. et al. (2017), Meteoritics & Planetary Science 48, abstract #6140.
[4] Blanchard, M.B., Brownlee, D.E., Bunch, T.E., Hodge, P.W. and Kyte, F.T. (1980) Meteoroid ablation spheres from deep-sea sediments. Earth and Planetary Science Letters, 46, 178–190.
[5] Genge, M. J. (2008). Micrometeorites and their implications for meteors. Advances in Meteoroid and Meteor Science, (November 2007), 525–535.
[6] Genge, M. J., & Grady, M. M. (1999). The fusion crusts of stony meteorites: Implications for the atmospheric reprocessing of extraterrestrial materials. Meteoritics and Planetary Science, 34(3), 341–356.

SHOCK METAMORPHISM OF THE NEW BASALTIC LUNAR METEORITE NORTHWEST AFRICA 12008.

A. C. Zhang[1,2], V. Assis Fernandes[3,4] and B. Hoefnagels[5]　[1]School of Earth Sciences and Engineering, Nanjing University, China (aczhang@nju.edu.cn), [2]CAS Center for Excellence in Comparative Planetology, China, [3]School of Earth and Environmental Sciences, University of Manchester, UK, [4]Museum für Naturkunde, Leibniz Institut für Biodiversität und Evoltionsforschung, Invalidenstr. 43, 10115 Berlin, Germany (veraafernandes@yahoo.com), [5]BigBangMeteorites, The Hague, The Netherlands (Ben@citygis.nl).

Introduction: Basaltic lunar meteorites are usually used to constrain the composition of the lunar mantle and the magmatic history of the Moon. In the meteorite collection, only 11 basaltic lunar meteorites have been recovered up to date. Northwest Africa (NWA) 12008 is the latest basaltic lunar meteorite. Previous investigations suggested that NWA 12008 is unique and not paired with other basaltic lunar meteorites [1,2]. Shock metamorphism is an important dynamic process that may affect the interpretation of geochronological data. Therefore, we studied the shock-induced feature in NWA 12008 to constrain its shock metamorphism.

Results: A polished section of NWA 12008 is used in this study. It shows an ophitic texture with minor phenocrysts of olivine and pyroxene. Plagioclase occurs as elongated laths with interstitial regions mainly filled by fine-grained pyroxene. Almost all plagioclase grains have transformed into glass, probably maskelynite. In olivine and pyroxene phenocrysts, irregular fractures are common. However, parallel fractures, which are perpendicular to the **c** axis of pyroxene, are common in relatively fine pyroxene grains. In olivine phenocrysts, radiating fractures surrounding melt inclusions are observed. A few thin shock melt veins (<20 μm in width) are observed in our sample. The shock melt veins are composed mainly of tiny Al-rich pyroxene grains (<1 μm in size). Aggregates of stishovite and silica glass (up to 13 μm in size) and pyroxene fragments with a smooth outline are also observed in the shock melt veins. The presence of stishovite is confirmed by its EBSD pattern. No high-pressure polymorphs were observed for olivine and pyroxene grains that are directly adjacent to the shock melt veins.

Discussion: High-pressure minerals are important clues to constrain the shock pressure. In this study, stishovite is such a mineral to constrain the lower limit of shock pressure. Based on the phase diagram of SiO_2 [3], stishovite is stable at a pressure of >8 GPa. This indicates that the shock pressure NWA 12008 has experienced is at least 8 GPa. Based on a recent study of [4], the complete transformation from plagioclase to maskelynite suggests that the sample experienced a shock pressure of at least 24 GPa. This inferred pressure is much higher than the pressure that was expected for the transformation (>15 GPa) from olivine to ringwoodite. However, ringwoodite was absent in this study. This might suggest a very short shock duration. This inference is consistent with the scale of the widths of shock melt veins in NWA 12008. Based on the typical width of the shock melt veins, the shock duration might be very short (<0.1 ms, [5]). Such a short duration can also account fo the absence of coesite in NWA 12008. In shocked eucrites with similar shock degree but relatively long shock durations, coesite is present as a rim surrounding stishovite+silica glass aggregates [6,7]. In summary, NWA 12008 has experienced a shock metamorphism up to 24 GPa with a short shock duration.

References: [1] Cohen M. E. et al. (2019) *LPSC 50*, abstract #2508. [2] Webb S. et al. (2019) *LPSC 50*, abstract #2686. [3] Presnall D. C. (1995) *Mineral Physics and Crystallography, A Handbook of Physical Constrains* 248-268. [4] Fritz J. et al. (2019) *Meteoritics & Planetary Science* 54 (in press). [5] Langenhorst F. and Poirier J. P. (2000) *Earth and Planetary Science Letters* 184:37-55. [6] Pang R. L. et al. (2016) *Scientific Reports* 6:26063. [7] Chen D. L. et al. (2019) *Meteoritics & Planetary Science* 54 (in press).

UNIQUE ANGRITE-LIKE FRAGMENTS IN A CH3 CHONDRITE REVEAL A NEW BASALTIC PLANETESIMAL.

A. C. Zhang[1,2], N. Kawasaki[3], M. Kuroda[3], Y. Li[1], H. Wang[4], X. N. Bai[5], N. Sakamoto[6], Q. Z. Yin[7], H. Yurimoto[3,6,8], [1]School of Earth Sciences and Engineering, Nanjing University, China (aczhang@nju.edu.cn), [2]CAS Center for Excellence in Comparative Planetology, China, [3]Department of Natural History Sciences, Hokkaido University, [4]School of Earth Sciences, Chinese University of Geosciences (Wuhan), China, [5]Institute for Advanced Study and Tsinghua Center for Astrophysics, Tsinghua University, China, [6]IIL, Creative Research Institution, Hokkaido University, Japan, [7]Department of Earth and Planetary Sciences, University of California Davis, USA, [8]Institute of Space and Astronautical Science, Japan Aerospace Exploration Agency, Japan.

Introduction: Meteorites are believed to be chips from planetesimals. Planetesimals are the building blocks of our planetary system. They can be used to constrain the chemical evolution and dynamic history of the early Solar System. Angrites are a group of volcanic and plutonic meteorites that have unique chemical feature and mineral assemblage [1]. Here, we report the discovery of angrite-like material enclosed in a primitive CH3 chondrite Sayh al Uhaymir (SaU) 290 and discuss its significance for understanding the dynamic evolution of the early Solar System.

Results: Petrography and mineralogy of SaU 290 have been reported in our previous investigations [2–3]. In this study, two oval-shaped fragments (ALF-1 and ALF-2) are observed consisting mainly of Ca,Fe-rich olivine and Al,Ti-rich augite with minor other phases. The olivine grains in the two fragments are Ca,Fe-enriched to various degrees but their Ca-Mg-Fe variation trends are similar to that of olivine in volcanic angrites [4]. The fragment ALF-1 has a Mn,Cr-rich zone along the margin (>20 μm). However, the interior olivine in ALF-1 and olivine in ALF-2 have Fe/Mn values consistent with that of olivine in angrites. In the interior of ALF-1, the Al,Ti-rich augite grains have two groups of compositions in FeO, MgO, and Al_2O_3. Both fragments contain chromite and spinel and the chormite grains in ALF-2 show irregular micro-scale heterogeneity in BSE images. The fragment ALF-1 has a thin rim (~2 μm in width) composed of low-Ca pyroxene with minor high-Ca pyroxene and FeNi metal. High-precision SIMS measurements reveal that the olivine in the two fragments is ^{16}O-poor with an average $\Delta^{17}O$ value of 0.91 ±0.18‰ (2σ).

Discussion: The presence of Ca,Fe-rich olivine and Al,Ti-rich augite in the two fragments is the key feature similar to those in angrites [1]. The Fe/Mn values of olivine are largely consistent with that of olivine in angrites [5]. These two features indicate that the parent body of the fragments may have major-element bulk composition, oxygen fugacity, and differentiation similar to that of volcanic angrites. However, the oxygen isotope compositions of the fragments in this study are distinctly different from that of angrites [5], indicating they have been derived from different parent bodies.

Although the chemical composition of olivine can be interpreted with simple fractional crystallization, many of other textural and composition features in the two fragments imply that the fragments have experienced complex thermal events after their initial crystallization. They include (1) absence of igneous texture; (2) coexistence of two groups of augite; (3) Mn,Cr-rich zone along the margin; (4) a rim of pyroxene + FeNi metal; and coexistence of spinel and chromite. Among these features, the Mn,Cr-rich zone along the margin and the rim of pyroxene +FeNi metal can be best, if not uniquely, explained with thermal events in nebular settings, probably similar to chondrule-forming environments. This implies that the parent body of the two fragments might have formed prior to the complete dissipation of the solar nebular gas. Given the Fe/Mn value in basaltic meteorites as a proxy of heliocentric distance [4], the parent bodies of the two fragments and angrites represent two generations of differentiated planetesimals at similar heliocentric distances. The parent body of the two fragments was formed within the solar nebula; whereas the angrite parent body was formed afterwards. Following the hypothesis and classification scheme of meteorites of Warren [6], angrites and CH chondrites belong to non-carbonaceous and carbonaceous meteorites and were formed in the inner solar system and the outer solar system, respectively. Thus, the presence of the two fragments enclosed in the SaU 290 CH chondrite indicates a large-scale migration and mixing between the inner and the outer solar system materials.

References: [1] Keil K. (2012) *Chemie der Erde* 72:191–218. [2] Zhang A. C. and Hsu W. B. (2009) *Meteoritics & Planetary Science* 44:787-804. [3] Zhang A. C. et al. (2015) *Geochimica et Cosmochimica Acta* 163:27–39. [4] Papike J. J. et al. (2017) *American Mineralogist* 102:1759–1762. [5] Greenwood R. C. et al. (2017) *Chemie der Erde* 77:1–43. [6] Warren P. H. (2011) *Earth and Planetary Science Letters* 311:93–100.

PB-PB CHRONOMETRY OF IMPACT MELTS FROM LUNAR METEORITE OUED AWLITIS 001

B. ZHANG[1], P. M. REGER[1], A. GANNOUN[2], M. BOYET[2], D. L. SCHRADER[3], M. WADHWA[3], L. FERRIÈRE[4], A. BOUVIER[1,5]

[1]University of Western Ontario, Department of Earth Sciences, Centre for Planetary Science and Exploration, London, Ontario N6A 3K7, Canada (bzhan262@uwo.ca), [2]Laboratoire Magmas et Volcans, Université Clermont Auvergne, 63178 Aubière Cedex, France, [3]Center for Meteorite Studies, School of Earth and Space Exploration, Arizona State University, Tempe, Arizona 85287, USA, [4]Natural History Museum, Burgring 7, A-1010 Vienna, Austria, [5]Universität Bayreuth, Bayerisches Geoinstitut, Bayreuth 95447, Germany

Introduction: Oued Awlitis (OA) 001 meteorite was classified as a lunar clast-rich melt rock [1]. It was proposed to have been launched from the Pierazzo crater (9.3 km diameter) that resides on the ejecta blanket of Orientale basin, based on its petrography and remote-sensing data [2]. In this case, OA 001 would have formed during the Orientale-basin-forming event and its formation age may then be used to constrain the age of this basin. The only age reported so far for OA 001 is an Ar-Ar age earlier than 3555 ± 34 Ma [3]. Here we present Pb-Pb isotopic analyses of a fragment of crystallized impact melt from OA 001 that places further constraints on the Orientale-basin-formation age.

Sample: OA 001 contains 89 vol% of plagioclase ($An_{88-97}Ab_{3-12}Or_{0-0.3}$), and other mineral phases are olivine (Fa_{30-44}), pigeonite ($En_{48-59}Fs_{26-40}Wo_{6-19}$), and augite ($En_{64-70}Fs_{20-24}Wo_{25-34}$) [2]. The oikocrystic olivine and pyroxene are within a phenocrystic plagioclase groundmass [2]. It has minor phases like troilite, ilmenite, and spinel [2], and we also identified apatites. The plagioclase has strong undulose extinction, planar deformation features, and is partially transformed to diaplectic glass. The shock stage of OA 001 was estimated to be S4 (20–24 GPa) [3]. The selected chip was documented using back-scattered electron microscopy and did not contain any clasts.

Methods: About 125 mg of the impact melt-rich chip from OA 001 was ground to fine powder in an agate mortar. The powder was leached sequentially as follows: ultrasonicated for 15 min each in 0.5 M HBr (acid wash named W1), H_2O (W2), and 0.5 M HNO_3 (W3); in 6 M HCl (W4), 7 M HNO_3 (W5) and 7 M HNO_3 (W6) at 120°C for one hour each; then ultrasonicated for 1 hour in 1 M HF (W7) and fluxed at 90°C for 12 hours in 1M HF (W8). For sample digestion, we used a 29 M HF and 16 M HNO_3 mixture (at 120°C for 48 hours); the sample and all leachates were then treated with 16 M HNO_3 (at 120°C), and 6 M HCl (at 120°C); finally, all the samples were dissolved in 1.5 M HBr (at 120°C). For Pb chromatography, we followed the HBr-HNO_3 method [4]. The procedural blank (included leaching, digesting, and column passing) was on average 1.4 ± 0.3 pg. A Thermo-Finnigan Neptune Plus MC-ICPMS was used to analyze Pb isotope ratios at UCA. Tl-doping and standard (NBS 981) bracketing methods were used to correct for instrumental mass bias [5], and NBS 983 was used as a secondary isotopic standard.

Results and Discussion: In total, we analyzed 8 leachates and 1 residue of an impact melt-rich chip from OA 001. Only the most radiogenic leachates (W4, W6–8) were used to calculate the Pb-Pb age. An isochron age of 3902.2 ± 4.8 Ma (MSWD=2.0) was defined by these 4 leachates (Fig. 1) using $^{238}U/^{235}U=137.79$.

If OA 001 was launched 0.3 My ago from the Pierazzo crater located on the ejecta blanket of the Orientale basin [2], the crystallization age of OA 001 impact melt would point to the age of the Orientale-basin-forming event. The Orientale event has been previously proposed to have an age of 3.72–3.85 Ga based on crater counting in [6]. This period is significantly later than the Pb-Pb age reported here; as such, OA 001 would not be related to the Orientale ejecta blanket. However, using new crater imagery from the Lunar Reconnaissance Orbiter Camera, the Orientale formation age is defined at $3.89^{+0.06}_{-0.1}$ Ga [7],

Figure 1. Pb-Pb isochron age of OA 001

which is in very good agreement with our Pb-Pb age. This suggests that the formation age of the OA 001 impact melt constrains the Orientale event more precisely at 3902.2 ± 4.8 Ma. Regardless of the potential connection between OA 001 impact melt and the formation of the Orientale basin, our data suggest that an impact melt-forming impact event may have occurred on the lunar far side [2] at ~3.9 Ga, slightly later than near-side basin-formation events such as Imbrium (proposed at 3.92–3.94 Ga) [8].

References: [1] Ruzicka A. et al. (2017) *Meteorit. Planet. Sci.* 52. [2] Wittmann A. (2019) *Meteorit. Planet. Sci.* doi.org/10.1111/maps.13218. [3] Ferrière L. et al. (2017) *LPS XLVIII, Abstract* #1621. [4] Bouvier A. et al. (2011) *Geochim. Cosmochim. Acta* 75: 5310–5323. [5] Bouvier A. et al. (2007) *Geochim. Cosmochim. Acta* 71: 1583–1604. [6] Stöffler D. et al. (2006) *Rev. Mineral. Geochem.* 60: 519–596. [7] Povilaitis R. Z. et al. (2018) *Planet. Space. Sci.* 162: 41–51. [8] Bottke W. F. & Norman M. D. (2017) *Annu. Rev. Earth Planet. Sci.* 45: 619–647.
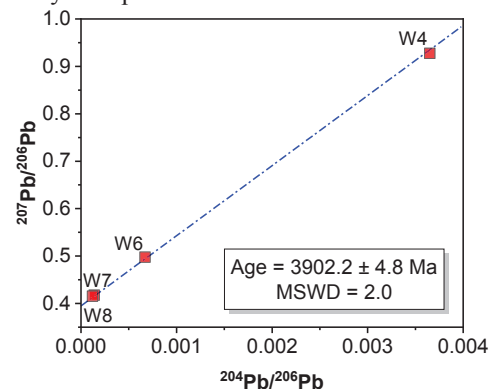
FORMATION OF THE FLOWED CORE IN A LEOVILLE TYPE B CAI: PLASTIC DEFORMATION OR HOT ACCRETION?

Mingming Zhang[1], Yangting Lin[1], Guoqiang Tang[1], and Ingo Leya[2], [1]Institute of Geology and Geophysics, Chinese Acadmy of Sciences (IGGCAS), No.19, Beituchengxi Road, Chaoyang District, 100029, Beijing, China, zhang-mingming113@mails.ucas.ac.cn, [2]Physical Institute, Space Sciences and Planetology, University of Bern, 3012 Bern, Switerland, ingo.leya@space.unibe.ch.

Introduction: Calcium-aluminum-rich inclusions (CAIs) from the highly shocked (S3) reduced-type CV3 chondrite Leoville are typically elongated and deformed (Cain et al., 1986; Scott et al., 1992). Caillet et al. (1993) described a flattened (L/W > 6) Leoville Type B inclusion (3537-1) with two distinct petrologic units, one exhibits poikiloblastic texture, which anorthite blades enclose numerous round crystals of Al-Ti-diopside and melilite; another is relict island of coarse-grained Al-Ti-diopside, melilite, anorthite, and spinel. ^{26}Al-^{26}Mg isotope systematics showed that the poikiloblastic unit contains little or no excess ^{26}Mg, while the relict island unit has typical initial $^{26}Al/^{27}Al$ of ~ 4.6×10^{-5}. To explain its unique petrologic and isotopic characteristics, Caillet et al. (1993) proposed that this inclusion was accreted onto the Leoville parent body while still very hot, and deformed into its elongate shape at the instant it impacted. Here we present a petrology and oxygen isotope study of a Leoville Type B CAI, which may also indicate a hot accretion process.

Results: BBL2-1 is slightly flattened (~9.5×4.5 mm^2; L/W~ 2) Type B1 CAIs with a blurred core-mantle structure. Its mantle is mostly intact and consists predominantly of melilite with minor intergranular anorthite and Al-Ti-diopside. Its core, identified by the coarse-grained (up to 0.8 mm in length) anorthite and Al-Ti-diopside as well as aggregates of large spinel crystals (up to 80 μm), is highly flattened and flowed, especially for the Al-Ti-diopsides and anorthites. It starts from the middle left of this inclusion to the entire center part and finally arrives the middle right with a shape like a "bird". Nearly 80% of the inclusion is surrounded by a Wark-Lovering (WL) rim composed of spinel + perovskite, melilite, spinel, Al-Ti-diopside, diopside + forsterite (from innermost to outermost). The middle left part of the inclusion is lack of WL rim. Noteworthy, the WL rim material and chondrite matrix were involved with the "bird-flowed core" into the interior of the inclusion. Round clasts of CAI materials, including melilite and Al-Ti-diopside with/without the WL rim, are present in the nearby chondrite matrix. The matrix was melted with olivines nucleated at high angles to the clast surface, and also contains tiny globules of metal and sulfide.

The mantle Al-Ti-diopside and anorthite are homogeneously ^{16}O-enriched with an average $\Delta^{17}O$=-23.3 ± 1.4‰ (2sd). In the core, those euhedral Al-Ti-diopsides and anorthites remain ^{16}O-enriched ($\Delta^{17}O$=-23.3 ± 1.3‰, 2sd), while those flowed counterparts have relatively fluctuant oxygen isotopic compositions with $\Delta^{17}O$ range from -23.5‰ to -14.6‰. Similarly, those diopsides of WL rim that existed in the interior of the inclusion have a relatively wide range of oxygen isotopic compositions ($\Delta^{17}O$: -24.1‰ to -12.7‰). In contrast, melilites from both the core and mantle are significantly ^{16}O-depleted with $\Delta^{17}O$ range from -3.87‰ to 0‰ (average: -1.94 ± 1.6‰, 2sd). Furthermore, the melilite from the WL rim and the CAI clasts in the nearby matrix are slightly less ^{16}O-depleted with $\Delta^{17}O$ range from -12.1 ‰ to -2.6‰, and from -8.2 ‰ to -1.8‰, respectively.

Discussions: (1) How the WL material and the chondrule matrix involved into the interior of the inclusion? Since the middle left part of the inclusion, where the core flow starts, is absent of WL rim, we believe that the WL rim material, as well as the chondrite matrix, was conveyed into the CAI interior by the flowed core minerals; (2) Which process triggered the flow of core minerals? Solid-state plastic deformation during shock event would be capable, but no signs of plastic deformation of anorthite and Al-Ti-diopside were observed in previous transmission electron microscope studies on Leoville chondrules and matrix (Cain et al., 1986; Nakamura et al., 1992), though we cannot rule out this possibility based on this. On the contrary, hot accretion would be possible. If the CAI was incompletely solidified, trace amount of residual melt would be flowed and transported the crystallized core minerals, broken WL rim materials, and the chondrite matrix inside the inclusion during the impact event that happened immediately after it accretion. To explain the relatively homogeneous ^{16}O-enriched compositions of anorthite and the ^{16}O-depleted compositions of melilite, which are decoupled from each other, the temperature would be higher than 800℃ and lasted for some time after it buried in the parent body. While the melilites at the WL rim or the chondrite matrix were less affected and been more ^{16}O-enriched. More discussions will be made at the conference.

References: [1] Caillet, C., MacPherson, G. J. and Zinner, E. K. (1993) Petrologic and Al-Mg isotopic clues to the accretion of two refractory inclusions onto the Leoville parent body: One was hot, the other wasn't. *Geochimica et Cosmochimica Acta* **57**, 4725-4743. [2]Cain, P. M., McSween Jr, H. Y. and Woodward, N. B. (1986) Structural deformation of the Leoville chondrite. *Earth and Planetary Science Letters* **77**, 165-175. [3] Nakamura, T., Tomeoka, K. and Takeda, H. (1992) Shock effects of the Leoville CV carbonaceous chondrite: a transmission electron microscope study. *Earth and Planetary Science Letters* **114**, 159-170. [4] Scott, E. R. D., Keil, K. and Stöffler, D. (1992) Shock metamorphism of carbonaceous chondrites. *Geochimica et Cosmochimica Acta* **56**, 4281-4293.

CALCIUM ISOTOPIC COMPOSITION OF THE KREEPS

Z. F. Zhang[1], W. Wu[1.2], X. Li[1] and Y. J. An[1], [1]State Key Laboratory of Isotope Geochemistry, Guangzhou Institute of Geochemistry, Chinese Academy of Sciences, Guangzhou 510640, China, [2]School of Earth and Planetary Science, University of Chinese Academy of Sciences, Beijing 100049, China.

Introduction: The difference of calcium isotopic compositions of the Bulk Silicate Moon (BSM) and the Bulk Silicate Earth (BSE) is one of the key factors to understand the formation of the Earth-Moon system. The calcium isotopic composition of BSE could be constrained by investigating the calcium isotopic compositions of the Earth mantle because it contains about 99% of the Earth calcium. However, unlike the BSE, the calcium isotopic composition of BSM is not well constrained mainly because calcium budget in lunar crust and KREEPs should not be ignored. That means, just like the lunar crust, KREEPs (potassium, rare-earth element, phosphor-rich), as the product of the last stage of the lunar magma ocean and an important record of the magma activity on the Moon (e.g. [1], [2]), also contains a certain amount of the lunar calcium. Thus, the calcium isotopic compositions of the KREEPs should be an important part to be considered to estimate the composition of the BSM. Here we attempted to reveal that by detailed work on a lunar meteorite NWA 5000. NWA 5000 is a KREEP basalt with obvious presence of KREEP-bearing materials and is further confirmed by its unusually high REE concentration and negative Eu anomaly.

Experiments: Both the chemical and instrumental analyses were performed in the State Key Laboratory of Isotope Geochemistry, Guangzhou Institute of Geochemistry, Chinese Academy of Sciences (GIG, CAS), following the procedure described in Zhu et al. (2016)[3]. The sample was grounded to 200 mesh before a certain amount of the powder was weighted into a Teflon beaker and digested in a mixture of conc. HF and conc. HNO_3. All chemical analyses were done from a single mother solution of the sample digest. The trace elements of NWA 5000 are measured on an iCAP Qc ICP-MS instrument (Thermofisher Scientific, USA), Calcium isotopes are measured on a Triton TIMS (Thermofisher Scientific, USA) for 6 times and precision was given based on these 6 measurement. The obtained $\delta^{44/40}Ca$ (relatively to SRM915a) of NIST SRM 915a, IAPSO seawater, BHVO-2 and BCR-2 ran in the same period as the sample are 0.02±0.02‰ (2SE, n=26), 1.82±0.03‰ (2SE, n=17), 0.76±0.02‰ (2SE, n=19) and 0.80±0.02‰ (2SE, n=18) respectively, well agreed with document.

Conclusions: Our recent practices indicated that NWA 5000 shares a similar $\delta^{44/40}Ca$ (0.78± 0.04‰, 2SE, n=6) with feldspar breccia [4]. This implies that KREEPs and the feldspar breccia may have similar calcium isotopic composition. Alternatively, the proportion of KREEPs in NWA 5000 has little effect on modifying the bulk rock calcium isotopic compositions. Based on the average concentrations of Th (0.37ppm) and K_2O (0.027 wt.%) in the lunar crust [5] and those in KREEP (Th, 12.4ppm; K_2O, 0.5 wt.%; [6] [7]), we estimated that NWA 5000 contains approximately 30~50% KREEPs, the CaO content in KREEPs could be 7-12% and the calcium isotopic composition of the KREEP is about 0.82-0.86‰. This indicates that the Ca isotopic composition of the KREEPs is indistinguishable from that of the lunar crust under the current analytic techniques.

References: [1] Taylor S. R. (1982) *Lunar and Planetary Institute, Houston*, Abstract #502. [2] Jolliff B. L. et al. (2006) *Mineralogical Society of America.* [3] Zhu et al. (2016) *Geostandards and Geoanalytical Research* 40:185-194. [4] Schiller M. et al. (2018) *Nature* 555:507-510. [5] Korotev R. L. et al. (2003) *Geochim. Cosmochim. Acta* 67:4895-4923. [6] Neal C.R. and Taylor L.A. (1992) *Geochim Cosmochim Acta* 56:2177-2211. [7] Hess P.C. and Parmentier E.M. (2001) *Journal of Geophysical Research:Planets*, 106, #11.

Chromium isotopic constraints on the origin the ureilite parent body.

K. Zhu (朱柯)[1*], F. Moynier[1,2], M. Schiller[3], D. Wielandt[3], K. K. Larsen[3], E. M. M. E. van Kooten[1] and M. Bizzarro[3]

[1]Institut de Physique du Globe de Paris, Université de Paris, CNRS, 1 rue Jussieu, Paris 75005, France (*zhu@ipgp.fr), [2]Institut Universitaire de France, 103 boulevard Saint-Michel, Paris 75005, France, [3]Centre for Star and Planet Formation and Natural History Museum of Denmark, University of Copenhagen, Øster Voldgade 5–7, Copenhagen DK-1350, Denmark

Introduction: Ureilites are primitive achondrites that represent the mantle of a now disrupted partially differentiated parent body (UPB), and some primitive geochemical information have survived from isotopic homogenization (e.g. during a magma ocean stage) in ureilites [1, 2]. Therefore, the geochemical signatures of ureilite meteorites can provide valuable information about not only the origin of the UPB but also early evolution of the Solar System. For instance, individual ureilite meteorites cover a range of Fe/Mn ratios and $\Delta^{17}O$ values which further correlate with the Mg# of their olivine cores. However, the origin of these co-variations is highly debated [1-4], and the heterogeneous $\Delta^{17}O$ features contradict to their homogenous $\varepsilon^{54}Cr$ [5, 6]. Moreover, the formation time for UPB is also poorly constrained, due to the low-radiogenic Pb (decay from U), Nd (decay from Sm) and Sr (decay from Rb) content in monomict ureilites (mantle restites) and lack of variation for Hf/W, Al/Mg and Mn/Cr among them. In order to better constrain the timescale of differentiation using volatile-sensitive ^{53}Mn-^{53}Cr system ($T_{1/2}$ = 3.7 Myrs) [7, 8, 10] and the degree of Cr isotopic heterogeneity of the UPB [8, 10], a larger variety of ureilite samples must be studied. Here, we report high precision Cr isotope data for eleven monomict ureilites and one ureilitic trachyandesite clast (ALM-A [9]) which has a complementary crustal composition.

Analytical methods: Around 10 mg of ureilite samples were well dissolved using Teflon bombs and an *Analab EvapoClean*, which is the same as [10]. Chromium was purified from 50% aliquots based on a procedure involving a three-step chromatographic ion-exchange purification protocol described in [11], and the total yield ranges from from 84% to 98%. The mass-independent Cr isotopic compositions of all the samples except for ALM-A were determined using the Neptune Plus located at the StarPlan, University of Copenhagen. Detailed analytical and data reduction method are described in [12]. ALM-A was measured on Triton TIMS here alongside the samples reported in [10] and the related methods have been described in detail in previous studies [13, 16].

Results: The $\varepsilon^{54}Cr$ values of all the monomict ureilites, vary from -1.06 ± 0.04 to -0.78 ± 0.05 with an average value of -0.91 ± 0.15 (2SD, N =18, including the data in [5]). A regression of the monomict ureilite $\varepsilon^{53}Cr$ values with their respective $^{55}Mn/^{52}Cr$ ratios calculated by *IsoplotR*, yields a slope of 0.569 ± 0.094 and an intercept of -0.28 ± 0.07 (MSWD = 2.0). The ALM-A clast investigated in this study has the highest $^{55}Mn/^{52}Cr$ ratio (1.35), $\varepsilon^{53}Cr$ (0.45 ± 0.05) and $\varepsilon^{54}Cr$ values (-0.68 ± 0.09). Notably the $\varepsilon^{53}Cr$ ($^{55}Mn/^{52}Cr$) and $\varepsilon^{54}Cr$ values appear to correlate. Also, the Cr isotope variation correlates with Mg# and Fe/Mn in olivine cores.

Discussion: These $\varepsilon^{54}Cr$ variations among monomict ureilites reflect primitive mantle heterogeneity of the UPB, which therefore did not experience a global-scale magma ocean. Furthermore, the $\varepsilon^{54}Cr$ values, Mn/Cr ratios, C isotopic composition [14], Mg# and Fe/Mn ratio in the olivine cores for the ureilites are correlated with each other, confirming that the UPB represent the the mixing of least two chemically and isotopically distinct reservoirs, rather than resulting from smelting process [3] or ice melting [4]. All the monomict ureilite fall on a well-defined ^{53}Mn-^{53}Cr isochron corresponding to a $^{53}Mn/^{55}Mn$ ratio of $(6.45 \pm 1.07) \times 10^{-6}$. This represents the first external Mn-Cr isochron obtained for the UPB, which can be translated to 4567.1 ± 1.0 Ma (within 1 Ma after CAIs), when anchored to U-corrected D'Orbigny angrite. We argue that this age represents the formation of the ureilite precursors (ureilite planetesimals). There is a ~4 Ma age discrepancy between the external isochron in this study and internal isochron ages for the polymict ureilites (e.g. [5, 9, 15, 16]), likely reflect the early impact history of the UPB.

References: [1] Goodrich C.A. et al. (2015) *Meteoritics & planetary science* 50: 782-809. [2] Goodrich C.A. et al. (2004) *Chemie der Erde-Geochemistry* 64: 283-327. [3] Goodrich C.A. et al. (2007) *Geochimica et Cosmochimica Acta* 71: 2876-2895. [4] Sanders I.S. et al. (2017) *Meteoritics & Planetary Science* 52: 690-708. [5] Yamakawa, A. et al. (2010) *The Astrophysical Journal* 720: 150. [6] Qin L. et al. (2010) *Meteoritics & Planetary Science* 45: 1771-1777. [7] Zhu K. et al. (2019) *Geochimica et Cosmochimica Acta*, under review. [8] Zhu K. et al. (2019) *The Astrophysical Journal* 873: 82. [9] Bischoff A. et al. (2014) *Proceedings of the National Academy of Sciences* 111: 12689-12692. [10] Zhu K. et al. (2019) *The Astrophysical Journal Letters*, under review. [11] Larsen K.K. et al. (2018) *Journal of Analytical Atomic Spectrometry* 33: 613-628. [12] Schiller M. et al. (2014) *Journal of analytical atomic spectrometry* 29: 1406-1416. [13] Van Kooten E.M.M.E. et al. (2016) *Proceedings of the National Academy of Sciences* 113: 2011-2016. [14] Barrat J.-A. et al. (2017) *Earth and Planetary Science Letters* 478: 143-149. [15] Goodrich C.A. et al. (2010) *Earth and Planetary Science Letters* 295: 531-540. [16] van Kooten, E.M.M.E. et al. (2017) *Geochimica et Cosmochimica Acta* 208: 1-23.

UNUSUAL TINY OBJECTS IN YOUR HED.

M. Zolensky[1], P. Buchanan[2], L. Le[3], D.K. Ross[3], J. Martinez[3]. [1]NASA Johnson Space Center, Houston, TX 77058, USA (michael.e.zolensky@nasa.gov); [2]Kilgore College, Kilgore, TX 75662, USA; [3]Jacobs Technology, Houston, TX 77058, USA.

Introduction: Thirty years ago we studied carbonaceous chondrite clasts in HED meteorites [1]. At that time our major conclusion was that the bulk of these lithologies, both in size and total volume, consisted of CM2 material which had been thermally metamorphosed to varying degree during impact onto the HED parent asteroid, widely held to be Vesta. However, some of the smaller clasts of C chondrite material in these same HEDs proved to be more enigmatic. These largely consisted of phyllosilicates but with varying amounts of loose crystals and aggregates olivine and low-Ca pyroxene, lacked chondrules or CAI, and contained significant quantities of magnetite – often framboids and spherulites. We suggested that these lithologies were most similar to the matrix of CR chondrites and CI chondrites, but we could form no firm conclusion as to their true nature. Gounelle et al. [2] even suggested a possible connection to chondritic micrometeorites. In light of our recent discoveries of vaguely similar lithologies in ordinary chondrites [3,4] and ureilites [5], and the march of analytical techniques to finer scales, we have begun to reexamine these HEDs.

Techniques: The samples were imaged and analyzed using a JEOL 7600-FE scanning electron microscope, and JEOL 8530-FE electron microprobe at the E-beam laboratory of the Astromaterials Research and Exploration Science (ARES) section of JSC. Between abstract and meeting time we plan to perform some electron back-scattered diffraction analyses.

Results: Thus far we have reexamined the small, phyllosilicate and magnetite-bearing lithologies in the Jodzie and Y-793497 howardites. Each meteorite contains numerous tiny target clasts, with different mineralogies. Thus our first main result is that these objects are not all the same lithology.

Y-793497: We have examined six tiny (<1mm) clasts in a single section of Y-793497. Three of the clasts are obviously CM2 material. Clasts 3 and 6 are predominantly phyllosilicate with scattered olivine (Fo_{90-72}), high and low-Ca pyroxene ($En_{71}Wo_1$ – a single analysis) and magnetite crystals (placquettes and framboids). Fe-Ni sulfides are only present as micron-sized and smaller crystals embedded in phyllosilicates. EPMA analyses of the matrix phyllosilicates indicate compositions nearer to being pure saponite than seen in any other chondritic material we have examined (i.e. CI, CR, CM), save Kaidun. Thus far we have not observed carbonates in these two clasts.

Jodzie: We examined 18 sub-mm clasts in two sections of Jodzie. 14 of these are CM lithologies, heated to varying degree (based on EPMA totals and phyllosilicate textures). Clasts 4 and 12 consist of a phyllosilicate matrix with scattered crystals and aggregates of forsterite (Fo_{100-99}), low-Ca pyroxene ($En_{69}Wo_3$ – a single analysis), Ca carbonate, coarse- to fine-grained pyrrhotite and pentlandite, and magnetite (plaquettes, framboids and euhedral crystals). The matrix phyllosilicates are a mixture of saponite and serpentine-type phases with a bulk composition most similar to those observed in CI chondrites. Clasts III-4 and III-5 are very strange. We only have space to describe III-4 briefly here. This lithology consists mainly of matrix-supported, flattened olivine crystals and aggregates (Fo_{98-45}), low-Ca pyroxene ($En_{99-37}Wo_{1-5}$), and Fe-Ni sulfides. These define a foliation. Sulfides have textures indicating flash heating. The matrix is almost entirely fine-grained, equidimensional crystals of Fe-rich olivine and pyroxene (Fo and En 70s to 40s) – these textures do not resemble heated phyllosilicates we have previously encountered. There are two "veins" of heated phyllosilicates (high EPMA totals) and possible tochilinite. This clast could be a shock-heated CM2, with a texture we have not previously observed.

Preliminary conclusion: With the exception of the obvious CM chips, these tiny objects are not pieces of CR or CI chondrites, but rather appear to be mineralogically distinct.

References: [1] Zolensky et al. (1996) Meteoritics and Planetary Science **31**, 518-537; [2] Gounelle et al. (2003) Geochimica et Cosmochimica Acta **67**:507–527; [3] Chan et al. (2018) *Science Advances* **4**, eaao3521; [4] Kebukawa et al. (2019) *Nature Scientific Reports* **9**, article number: 3169; [5] Goodrich et al. (2019) *50th Lunar and Planetary Science Conference Abstracts*.